

# ANALYSIS OF ELECTRIC MACHINERY AND DRIVE SYSTEMS

**IEEE Press**  
445 Hoes Lane  
Piscataway, NJ 08854

**IEEE Press Editorial Board 2013**

John Anderson, *Editor in Chief*

Linda Shafer  
George W. Arnold  
Ekram Hossain  
Om P. Malik

Saeid Nahavandi  
David Jacobson  
Mary Lanzerotti

George Zobrist  
Tariq Samad  
Dmitry Goldgof

Kenneth Moore, *Director of IEEE Book and Information Services (BIS)*

A complete list of titles in the IEEE Press Series on Power Engineering  
appears at the end of this book.

---

# ANALYSIS OF ELECTRIC MACHINERY AND DRIVE SYSTEMS

---

THIRD EDITION

---

Paul Krause  
Oleg Wasynczuk  
Scott Sudhoff  
Steven Pekarek



Mohamed E. El-Hawary, *Series Editor*

 **IEEE**  
IEEE PRESS

**WILEY**

Copyright © 2013 by Institute of Electrical and Electronics Engineers, Inc. All rights reserved.

Published by John Wiley & Sons, Inc., Hoboken, New Jersey.  
Published simultaneously in Canada.

No part of this publication may be reproduced, stored in a retrieval system, or transmitted in any form or by any means, electronic, mechanical, photocopying, recording, scanning, or otherwise, except as permitted under Section 107 or 108 of the 1976 United States Copyright Act, without either the prior written permission of the Publisher, or authorization through payment of the appropriate per-copy fee to the Copyright Clearance Center, Inc., 222 Rosewood Drive, Danvers, MA 01923, (978) 750-8400, fax (978) 750-4470, or on the web at [www.copyright.com](http://www.copyright.com). Requests to the Publisher for permission should be addressed to the Permissions Department, John Wiley & Sons, Inc., 111 River Street, Hoboken, NJ 07030, (201) 748-6011, fax (201) 748-6008, or online at <http://www.wiley.com/go/permissions>.

**Limit of Liability/Disclaimer of Warranty:** While the publisher and author have used their best efforts in preparing this book, they make no representations or warranties with respect to the accuracy or completeness of the contents of this book and specifically disclaim any implied warranties of merchantability or fitness for a particular purpose. No warranty may be created or extended by sales representatives or written sales materials. The advice and strategies contained herein may not be suitable for your situation. You should consult with a professional where appropriate. Neither the publisher nor author shall be liable for any loss of profit or any other commercial damages, including but not limited to special, incidental, consequential, or other damages.

For general information on our other products and services or for technical support, please contact our Customer Care Department within the United States at (800) 762-2974, outside the United States at (317) 572-3993 or fax (317) 572-4002.

Wiley also publishes its books in a variety of electronic formats. Some content that appears in print may not be available in electronic formats. For more information about Wiley products, visit our web site at [www.wiley.com](http://www.wiley.com).

***Library of Congress Cataloging-in-Publication Data:***

Krause, Paul C.

Analysis of electric machinery and drive systems / Paul Krause, Oleg Wasynczuk, Scott Sudhoff, Steven Pekarek. – Third edition.

pages cm

“Institute of Electrical and Electronics Engineers.”

Includes bibliographical references and index.

ISBN 978-1-118-02429-4 (cloth)

1. Electric machinery. 2. Electric driving. I. Wasynczuk, Oleg. II. Sudhoff, Scott D. III. Pekarek, Steven. IV. Institute of Electrical and Electronics Engineers. V. Title.

TK2181.K72 2013

621.31'042–dc23

2012050394

Printed in the United States of America.

10 9 8 7 6 5 4 3 2 1

---

# CONTENTS

---

<b>Preface</b>	<b>xiii</b>
<b>1 THEORY OF ELECTROMECHANICAL ENERGY CONVERSION</b>	<b>1</b>
1.1. Introduction	1
1.2. Magnetically Coupled Circuits	1
1.3. Electromechanical Energy Conversion	12
1.4. Elementary ac Machines	35
Reference	44
Problems	44
<b>2 DISTRIBUTED WINDINGS IN AC MACHINERY</b>	<b>53</b>
2.1. Introduction	53
2.2. Describing Distributed Windings	54
2.3. Winding Functions	64
2.4. Air-Gap Magnetomotive Force	67
2.5. Rotating MMF	71
2.6. Flux Linkage and Inductance	73
2.7. Resistance	76
2.8. Voltage and Flux Linkage Equations for Distributed Winding Machines	77
Reference	83
Problems	84
<b>3 REFERENCE-FRAME THEORY</b>	<b>86</b>
3.1. Introduction	86
3.2. Background	87
3.3. Equations of Transformation: Change of Variables	88
3.4. Stationary Circuit Variables Transformed to the Arbitrary Reference Frame	90
3.5. Commonly Used Reference Frames	97

3.6. Transformation of a Balanced Set	98
3.7. Balanced Steady-State Phasor Relationships	99
3.8. Balanced Steady-State Voltage Equations	102
3.9. Variables Observed from Several Frames of Reference	105
3.10. Transformation Between Reference Frames	110
3.11. Specialty Transformations	111
3.12. Space-Phasor Notation	113
References	115
Problems	115
<b>4 PERMANENT-MAGNET AC MACHINES</b>	<b>121</b>
4.1. Introduction	121
4.2. Voltage and Torque Equations in Machine Variables	122
4.3. Voltage and Torque Equations in Rotor Reference-Frame Variables	125
4.4. Analysis of Steady-State Operation	127
4.5. Brushless dc Motor	129
4.6. Phase Shifting of Applied Voltages of a Permanent-Magnet ac Machine	134
4.7. Control of Stator Currents	138
References	140
Problems	140
<b>5 SYNCHRONOUS MACHINES</b>	<b>142</b>
5.1. Introduction	142
5.2. Voltage Equations in Machine Variables	143
5.3. Torque Equation in Machine Variables	149
5.4. Stator Voltage Equations in Arbitrary Reference-Frame Variables	149
5.5. Voltage Equations in Rotor Reference-Frame Variables	151
5.6. Torque Equations in Substitute Variables	157
5.7. Rotor Angle and Angle Between Rotors	158
5.8. Per Unit System	159
5.9. Analysis of Steady-State Operation	160
5.10. Stator Currents Positive Out of Machine: Synchronous Generator Operation	171
5.11. Computer Simulation	201
References	210
Problems	210

<b>6 SYMMETRICAL INDUCTION MACHINES</b>	<b>215</b>
6.1. Introduction	215
6.2. Voltage Equations in Machine Variables	216
6.3. Torque Equation in Machine Variables	220
6.4. Equations of Transformation for Rotor Circuits	222
6.5. Voltage Equations in Arbitrary Reference-Frame Variables	224
6.6. Torque Equation in Arbitrary Reference-Frame Variables	229
6.7. Commonly Used Reference Frames	232
6.8. Per Unit System	233
6.9. Analysis of Steady-State Operation	235
6.10. Free Acceleration Characteristics	244
6.11. Free Acceleration Characteristics Viewed from Various Reference Frames	251
6.12. Dynamic Performance During Sudden Changes in Load Torque	257
6.13. Dynamic Performance During a Three-Phase Fault at the Machine Terminals	260
6.14. Computer Simulation in the Arbitrary Reference Frame	261
References	266
Problems	267
<b>7 MACHINE EQUATIONS IN OPERATIONAL IMPEDANCES AND TIME CONSTANTS</b>	<b>271</b>
7.1. Introduction	271
7.2. Park's Equations in Operational Form	272
7.3. Operational Impedances and $G(p)$ for a Synchronous Machine with Four Rotor Windings	273
7.4. Standard Synchronous Machine Reactances	276
7.5. Standard Synchronous Machine Time Constants	278
7.6. Derived Synchronous Machine Time Constants	278
7.7. Parameters from Short-Circuit Characteristics	283
7.8. Parameters from Frequency-Response Characteristics	290
References	295
Problems	297
<b>8 ALTERNATIVE FORMS OF MACHINE EQUATIONS</b>	<b>299</b>
8.1. Introduction	299
8.2. Machine Equations to Be Linearized	300
8.3. Linearization of Machine Equations	302

8.4. Small-Displacement Stability: Eigenvalues	308
8.5. Eigenvalues of Typical Induction Machines	309
8.6. Eigenvalues of Typical Synchronous Machines	312
8.7. Neglecting Electric Transients of Stator Voltage Equations	313
8.8. Induction Machine Performance Predicted with Stator Electric Transients Neglected	318
8.9. Synchronous Machine Performance Predicted with Stator Electric Transients Neglected	322
8.10. Detailed Voltage Behind Reactance Model	325
8.11. Reduced Order Voltage Behind Reactance Model	332
References	333
Problems	335
<b>9 UNBALANCED OPERATION AND SINGLE-PHASE INDUCTION MACHINES</b>	<b>336</b>
9.1. Introduction	336
9.2. Symmetrical Component Theory	337
9.3. Symmetrical Component Analysis of Induction Machines	338
9.4. Unbalanced Stator Conditions of Induction Machines: Reference-Frame Analysis	339
9.5. Typical Unbalanced Stator Conditions of Induction Machines	346
9.6. Unbalanced Rotor Conditions of Induction Machines	351
9.7. Unbalanced Rotor Resistors	354
9.8. Single-Phase Induction Machines	358
9.9. Asynchronous and Unbalanced Operation of Synchronous Machines	368
References	375
Problems	375
<b>10 DC MACHINES AND DRIVES</b>	<b>377</b>
10.1. Introduction	377
10.2. Elementary dc Machine	377
10.3. Voltage and Torque Equations	384
10.4. Basic Types of dc Machines	386
10.5. Time-Domain Block Diagrams and State Equations	394
10.6. Solid-State Converters for dc Drive Systems	398
10.7. One-Quadrant dc/dc Converter Drive	400
10.8. Two-Quadrant dc/dc Converter Drive	418
10.9. Four-Quadrant dc/dc Converter Drive	421

10.10. Machine Control with Voltage-Controlled dc/dc Converter	423
10.11. Machine Control with Current-Controlled dc/dc Converter	426
References	431
Problems	431
<b>11 SEMI-CONTROLLED BRIDGE CONVERTERS</b>	<b>434</b>
11.1. Introduction	434
11.2. Single-Phase Load Commutated Converter	434
11.3. Three-Phase Load Commutated Converter	445
11.4. Conclusions and Extensions	456
References	458
Problems	458
<b>12 FULLY CONTROLLED THREE-PHASE BRIDGE CONVERTERS</b>	<b>460</b>
12.1. Introduction	460
12.2. The Three-Phase Bridge Converter	460
12.3. Six-Step Operation	466
12.4. Six-Step Modulation	474
12.5. Sine-Triangle Modulation	477
12.6. Extended Sine-Triangle Modulation	483
12.7. Space-Vector Modulation	485
12.8. Hysteresis Modulation	489
12.9. Delta Modulation	492
12.10. Open-Loop Voltage and Current Regulation	493
12.11. Closed-Loop Voltage and Current Regulation	495
References	499
Problems	500
<b>13 INDUCTION MOTOR DRIVES</b>	<b>503</b>
13.1. Introduction	503
13.2. Volts-per-Hertz Control	504
13.3. Constant Slip Current Control	510
13.4. Field-Oriented Control	517
13.5. Direct Field-Oriented Control	521
13.6. Robust Direct Field-Oriented Control	523
13.7. Indirect Rotor Field-Oriented Control	528
13.8. Direct Torque Control	532
13.9. Slip Energy Recovery Drives	535

13.10. Conclusions	538
References	538
Problems	539
<b>14 PERMANENT-MAGNET AC MOTOR DRIVES</b>	<b>541</b>
14.1. Introduction	541
14.2. Voltage-Source Inverter Drives	542
14.3. Equivalence of Voltage-Source Inverters to an Idealized Source	543
14.4. Average-Value Analysis of Voltage-Source Inverter Drives	552
14.5. Steady-State Performance of Voltage-Source Inverter Drives	555
14.6. Transient and Dynamic Performance of Voltage-Source Inverter Drives	557
14.7. Case Study: Voltage-Source Inverter-Based Speed Control	562
14.8. Current-Regulated Inverter Drives	567
14.9. Voltage Limitations of Current-Regulated Inverter Drives	571
14.10. Current Command Synthesis	572
14.11. Average-Value Modeling of Current-Regulated Inverter Drives	576
14.12. Case Study: Current-Regulated Inverter-Based Speed Controller	578
References	581
Problems	581
<b>15 INTRODUCTION TO THE DESIGN OF ELECTRIC MACHINERY</b>	<b>583</b>
15.1. Introduction	583
15.2. Machine Geometry	585
15.3. Stator Windings	590
15.4. Material Parameters	593
15.5. Stator Currents and Control Philosophy	596
15.6. Radial Field Analysis	597
15.7. Lumped Parameters	602
15.8. Ferromagnetic Field Analysis	603
15.9. Formulation of Design Problem	609
15.10. Case Study	614
15.11. Extensions	618
Acknowledgments	619
References	620
Problems	621

<b>Appendix A Trigonometric Relations, Constants and Conversion Factors, and Abbreviations</b>	<b>623</b>
A.1. Basic Trigonometric Relations	623
A.2. Three-Phase Trigonometric Relations	624
A.3. Constants and Conversion Factors	624
A.4. Abbreviations	625
<b>Appendix B Carter's Coefficient</b>	<b>626</b>
<b>Appendix C Leakage Inductance</b>	<b>629</b>
References	635
<b>Index</b>	<b>636</b>



---

# PREFACE

---

Those familiar with previous editions of this book will find that this edition has been expanded and modified to help meet the needs of the electric machinery, electric drives, and electric power industries.

Like previous editions, reference-frame theory is at the core of this book. However, new material has been introduced that sets the stage for machine design. In particular, in Chapter 2, the winding function approach is used to establish the rotating air-gap magnetomotive force and machine inductances, including end-turn winding effects. In addition, an introduction to machine design is set forth in Chapter 15. These two new chapters, combined with reference-frame theory-based machine analysis, add a significant dimension not found in other texts.

Another major change is set forth in Chapter 8, wherein the standard linear and reduced-order machine equations are derived and a section has been added on the method of analysis referred to as *voltage behind reactance*. This new formulation of the machine equations is especially useful in the analysis and modeling of electric machines that are coupled to power electronic circuits. Consequently, this technique has become a useful tool in the electric power and electric drives industries.

There are other, less major, changes and additions in this edition that warrant mentioning. In Chapter 1, the electromagnetic force (torque) equations are derived without the need of numerous, involved summations that have plagued the previous approach. This straightforward approach is made possible by the identification of a second energy balance relationship. Also, the chapter on reference-frame theory has been augmented with transformations that apply when the three-phase currents, currents, and flux linkages sum to zero. Although this is not the case if a third harmonic is present, it is quite common, and the transformations are helpful in cases where the neutral is not accessible, and only the line-to-line voltages are available.

Calculation of operational impedances is given in Chapter 7. Added to this material is a generalized approach of determining machine parameters from machine measurements. An interesting combination of Park's approach to the derivation of the torque relationship and reference-frame theory is set forth in Chapter 6.

In the previous editions the synchronous machine was analyzed assuming positive current out of the machine, convenient for the power system engineer. Unfortunately, this approach is somewhat frustrating to the electric drives engineer. The chapter on synchronous machines has been modified in an attempt to accommodate both drive and power system engineers. In particular, the analysis is first carried out with positive currents into the machine and then with the current direction reversed.

However, whenever power system operation or system fault studies are considered, positive current is assumed out of the machine consistent with power system convention. The remaining chapters, including the chapters on electric drives, as well as the chapters on converters, have been updated to include recent advances in analysis and converter control. Also, the analysis of unbalanced operation covered in the first edition but not in the second, has been simplified and is presented in Chapter 9.

We have spent a major part of our professional careers dealing with electric machines and drives. We are not only coauthors but colleagues and good friends. With the close working relationship that existed during the preparation of this manuscript, an ordering of the coauthors based on contribution would be difficult if not impossible; instead, the ordering is by age only.

PAUL KRAUSE  
OLEG WASYNCZUK  
SCOTT SUDHOFF  
STEVEN PEKAREK  
*West Lafayette, Indiana*  
*May 2013*

---

# THEORY OF ELECTROMECHANICAL ENERGY CONVERSION

---

## 1.1. INTRODUCTION

The theory of electromechanical energy conversion allows us to establish expressions for torque in terms of machine electrical variables, generally the currents, and the displacement of the mechanical system. This theory, as well as the derivation of equivalent circuit representations of magnetically coupled circuits, is established in this chapter. In Chapter 2, we will discover that some of the inductances of the electric machine are functions of the rotor position. This establishes an awareness of the complexity of these voltage equations and sets the stage for the change of variables (Chapter 3) that reduces the complexity of the voltage equations by eliminating the rotor position dependent inductances and provides a more direct approach to establishing the expression for torque when we consider the individual electric machines.

## 1.2. MAGNETICALLY COUPLED CIRCUITS

Magnetically coupled electric circuits are central to the operation of transformers and electric machines. In the case of transformers, stationary circuits are magnetically

---

*Analysis of Electric Machinery and Drive Systems*, Third Edition. Paul Krause, Oleg Wasyczuk, Scott Sudhoff, and Steven Pekarek.

© 2013 Institute of Electrical and Electronics Engineers, Inc. Published 2013 by John Wiley & Sons, Inc.

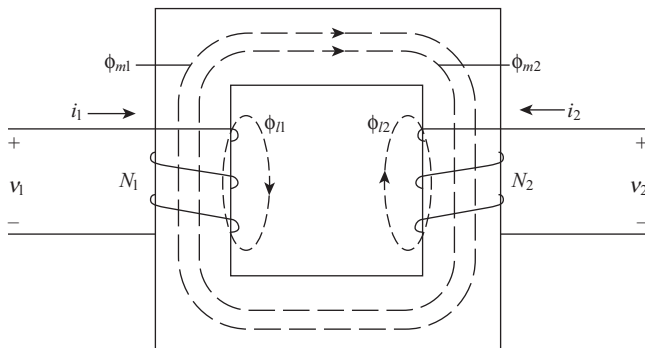


Figure 1.2-1. Magnetically coupled circuits.

coupled for the purpose of changing the voltage and current levels. In the case of electric machines, circuits in relative motion are magnetically coupled for the purpose of transferring energy between mechanical and electrical systems. Since magnetically coupled circuits play such an important role in power transmission and conversion, it is important to establish the equations that describe their behavior and to express these equations in a form convenient for analysis. These goals may be achieved by starting with two stationary electric circuits that are magnetically coupled as shown in Figure 1.2-1. The two coils consist of turns  $N_1$  and  $N_2$ , respectively, and they are wound on a common core that is generally a ferromagnetic material with permeability large relative to that of air. The permeability of free space,  $\mu_0$ , is  $4\pi \times 10^{-7}$  H/m. The permeability of other materials is expressed as  $\mu = \mu_r \mu_0$ , where  $\mu_r$  is the relative permeability. In the case of transformer steel, the relative permeability may be as high as 2000–4000.

In general, the flux produced by each coil can be separated into two components. A leakage component is denoted with an  $l$  subscript and a magnetizing component is denoted by an  $m$  subscript. Each of these components is depicted by a single streamline with the positive direction determined by applying the right-hand rule to the direction of current flow in the coil. Often, in transformer analysis,  $i_2$  is selected positive out of the top of coil 2 and a dot placed at that terminal.

The flux linking each coil may be expressed

$$\Phi_1 = \Phi_{l1} + \Phi_{m1} + \Phi_{m2} \quad (1.2-1)$$

$$\Phi_2 = \Phi_{l2} + \Phi_{m2} + \Phi_{m1} \quad (1.2-2)$$

The leakage flux  $\Phi_{l1}$  is produced by current flowing in coil 1, and it links only the turns of coil 1. Likewise, the leakage flux  $\Phi_{l2}$  is produced by current flowing in coil 2, and it links only the turns of coil 2. The magnetizing flux  $\Phi_{m1}$  is produced by current flowing in coil 1, and it links all turns of coils 1 and 2. Similarly, the magnetizing flux  $\Phi_{m2}$  is produced by current flowing in coil 2, and it also links all turns of coils 1 and 2. With the selected positive direction of current flow and the manner in that the coils are wound (Fig. 1.2-1), magnetizing flux produced by positive current in one coil adds to the

magnetizing flux produced by positive current in the other coil. In other words, if both currents are flowing in the same direction, the magnetizing fluxes produced by each coil are in the same direction, making the total magnetizing flux or the total core flux the sum of the instantaneous magnitudes of the individual magnetizing fluxes. If the currents are in opposite directions, the magnetizing fluxes are in opposite directions. In this case, one coil is said to be magnetizing the core, the other demagnetizing.

Before proceeding, it is appropriate to point out that this is an idealization of the actual magnetic system. Clearly, all of the leakage flux may not link all the turns of the coil producing it. Likewise, all of the magnetizing flux of one coil may not link all of the turns of the other coil. To acknowledge this practical aspect of the magnetic system, the number of turns is considered to be an equivalent number rather than the actual number. This fact should cause us little concern since the inductances of the electric circuit resulting from the magnetic coupling are generally determined from tests.

The voltage equations may be expressed in matrix form as

$$\mathbf{v} = \mathbf{ri} + \frac{d\lambda}{dt} \quad (1.2-3)$$

where  $\mathbf{r} = \text{diag}[r_1 \ r_2]$ , is a diagonal matrix and

$$(\mathbf{f})^T = [f_1 \ f_2] \quad (1.2-4)$$

where  $f$  represents voltage, current, or flux linkage. The resistances  $r_1$  and  $r_2$  and the flux linkages  $\lambda_1$  and  $\lambda_2$  are related to coils 1 and 2, respectively. Since it is assumed that  $\Phi_1$  links the equivalent turns of coil 1 and  $\Phi_2$  links the equivalent turns of coil 2, the flux linkages may be written

$$\lambda_1 = N_1 \Phi_1 \quad (1.2-5)$$

$$\lambda_2 = N_2 \Phi_2 \quad (1.2-6)$$

where  $\Phi_1$  and  $\Phi_2$  are given by (1.2-1) and (1.2-2), respectively.

## Linear Magnetic System

If saturation is neglected, the system is linear and the fluxes may be expressed as

$$\Phi_{l1} = \frac{N_1 i_1}{\mathcal{R}_{l1}} \quad (1.2-7)$$

$$\Phi_{m1} = \frac{N_1 i_1}{\mathcal{R}_m} \quad (1.2-8)$$

$$\Phi_{l2} = \frac{N_2 i_2}{\mathcal{R}_{l2}} \quad (1.2-9)$$

$$\Phi_{m2} = \frac{N_2 i_2}{\mathcal{R}_m} \quad (1.2-10)$$

where  $\mathcal{R}_{l1}$  and  $\mathcal{R}_{l2}$  are the reluctances of the leakage paths and  $\mathcal{R}_m$  is the reluctance of the path of the magnetizing fluxes. The product of  $N$  times  $i$  (ampere-turns) is the magnetomotive force (MMF), which is determined by the application of Ampere's law. The reluctance of the leakage paths is difficult to express and measure. A unique determination of the inductances associated with the leakage flux is typically either calculated or approximated from design considerations. The reluctance of the magnetizing path of the core shown in Figure 1.2-1 may be computed with sufficient accuracy from the well-known relationship

$$\mathcal{R} = \frac{l}{\mu A} \quad (1.2-11)$$

where  $l$  is the mean or equivalent length of the magnetic path,  $A$  the cross-section area, and  $\mu$  the permeability.

Substituting (1.2-7)–(1.2-10) into (1.2-1) and (1.2-2) yields

$$\Phi_1 = \frac{N_1 i_1}{\mathcal{R}_{l1}} + \frac{N_1 i_1}{\mathcal{R}_m} + \frac{N_2 i_2}{\mathcal{R}_m} \quad (1.2-12)$$

$$\Phi_2 = \frac{N_2 i_2}{\mathcal{R}_{l2}} + \frac{N_2 i_2}{\mathcal{R}_m} + \frac{N_1 i_1}{\mathcal{R}_m} \quad (1.2-13)$$

Substituting (1.2-12) and (1.2-13) into (1.2-5) and (1.2-6) yields

$$\lambda_1 = \frac{N_1^2}{\mathcal{R}_{l1}} i_1 + \frac{N_1^2}{\mathcal{R}_m} i_1 + \frac{N_1 N_2}{\mathcal{R}_m} i_2 \quad (1.2-14)$$

$$\lambda_2 = \frac{N_2^2}{\mathcal{R}_{l2}} i_2 + \frac{N_2^2}{\mathcal{R}_m} i_2 + \frac{N_2 N_1}{\mathcal{R}_m} i_1 \quad (1.2-15)$$

When the magnetic system is linear, the flux linkages are generally expressed in terms of inductances and currents. We see that the coefficients of the first two terms on the right-hand side of (1.2-14) depend upon the turns of coil 1 and the reluctance of the magnetic system, independent of the existence of coil 2. An analogous statement may be made regarding (1.2-15). Hence, the self-inductances are defined as

$$\begin{aligned} L_{11} &= \frac{N_1^2}{\mathcal{R}_{l1}} + \frac{N_1^2}{\mathcal{R}_m} \\ &= L_{l1} + L_{m1} \end{aligned} \quad (1.2-16)$$

$$\begin{aligned} L_{22} &= \frac{N_2^2}{\mathcal{R}_{l2}} + \frac{N_2^2}{\mathcal{R}_m} \\ &= L_{l2} + L_{m2} \end{aligned} \quad (1.2-17)$$

where  $L_{l1}$  and  $L_{l2}$  are the leakage inductances and  $L_{m1}$  and  $L_{m2}$  the magnetizing inductances of coils 1 and 2, respectively. From (1.2-16) and (1.2-17), it follows that the magnetizing inductances may be related as

$$\frac{L_{m2}}{N_2^2} = \frac{L_{m1}}{N_1^2} \quad (1.2-18)$$

The mutual inductances are defined as the coefficient of the third term of (1.2-14) and (1.2-15).

$$L_{12} = \frac{N_1 N_2}{\mathcal{R}_m} \quad (1.2-19)$$

$$L_{21} = \frac{N_2 N_1}{\mathcal{R}_m} \quad (1.2-20)$$

Obviously,  $L_{12} = L_{21}$ . The mutual inductances may be related to the magnetizing inductances. In particular,

$$\begin{aligned} L_{12} &= \frac{N_2}{N_1} L_{m1} \\ &= \frac{N_1}{N_2} L_{m2} \end{aligned} \quad (1.2-21)$$

The flux linkages may now be written as

$$\lambda = \mathbf{Li}, \quad (1.2-22)$$

where

$$\mathbf{L} = \begin{bmatrix} L_{11} & L_{12} \\ L_{21} & L_{22} \end{bmatrix} = \begin{bmatrix} L_{l1} + L_{m1} & \frac{N_2}{N_1} L_{m1} \\ \frac{N_1}{N_2} L_{m2} & L_{l2} + L_{m2} \end{bmatrix} \quad (1.2-23)$$

Although the voltage equations with the inductance matrix  $\mathbf{L}$  incorporated may be used for purposes of analysis, it is customary to perform a change of variables that yields the well-known equivalent T circuit of two magnetically coupled coils. To set the stage for this derivation, let us express the flux linkages from (1.2-22) as

$$\lambda_1 = L_{l1}i_1 + L_{m1}\left(i_1 + \frac{N_2}{N_1}i_2\right) \quad (1.2-24)$$

$$\lambda_2 = L_{l2}i_2 + L_{m2}\left(\frac{N_1}{N_2}i_1 + i_2\right) \quad (1.2-25)$$

Now we have two choices. We can use a substitute variable for  $(N_2/N_1)i_2$  or for  $(N_1/N_2)i_1$ . Let us consider the first of these choices

$$N_1i_2' = N_2i_2 \quad (1.2-26)$$

whereupon we are using the substitute variable  $i_2'$  that, when flowing through coil 1, produces the same MMF as the actual  $i_2$  flowing through coil 2. This is said to be referring the current in coil 2 to coil 1, whereupon coil 1 becomes the reference coil. On the other hand, if we use the second choice, then

$$N_2i_1' = N_1i_1 \quad (1.2-27)$$

Here,  $i_1'$  is the substitute variable that produces the same MMF when flowing through coil 2 as  $i_1$  does when flowing in coil 1. This change of variables is said to refer the current of coil 1 to coil 2.

We will derive the equivalent T circuit by referring the current of coil 2 to coil 1; thus from (1.2-26)

$$i_2' = \frac{N_2}{N_1}i_2 \quad (1.2-28)$$

Power is to be unchanged by this substitution of variables. Therefore,

$$v_2' = \frac{N_1}{N_2}v_2 \quad (1.2-29)$$

whereupon  $v_2i_2 = v_2'i_2'$ . Flux linkages, which have the units of volt-second, are related to the substitute flux linkages in the same way as voltages. In particular,

$$\lambda_2' = \frac{N_1}{N_2}\lambda_2 \quad (1.2-30)$$

Substituting (1.2-28) into (1.2-24) and (1.2-25) and then multiplying (1.2-25) by  $N_1/N_2$  to obtain  $\lambda_2'$ , and if we further substitute  $(N_2^2/N_1^2)L_{m1}$  for  $L_{m2}$  into (1.2-25), then

$$\lambda_1 = L_{l1}i_1 + L_{m1}(i_1 + i_2') \quad (1.2-31)$$

$$\lambda_2' = L_{l2}'i_2' + L_{m1}(i_1 + i_2') \quad (1.2-32)$$

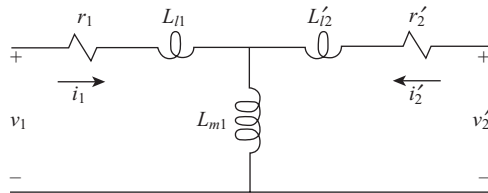


Figure 1.2-2. Equivalent circuit with coil 1 selected as reference coil.

where

$$L'_{l2} = \left( \frac{N_1}{N_2} \right)^2 L_{l2} \quad (1.2-33)$$

The voltage equations become

$$v_1 = r_1 i_1 + \frac{d\lambda_1}{dt} \quad (1.2-34)$$

$$v'_2 = r'_2 i'_2 + \frac{d\lambda'_2}{dt} \quad (1.2-35)$$

where

$$r'_2 = \left( \frac{N_1}{N_2} \right)^2 r_2 \quad (1.2-36)$$

The above voltage equations suggest the T equivalent circuit shown in Figure 1.2-2. It is apparent that this method may be extended to include any number of coils wound on the same core.

**EXAMPLE 1A** It is instructive to illustrate the method of deriving an equivalent T circuit from open- and short-circuit measurements. For this purpose, let us assume that when coil 2 of the transformer shown in Figure 1.2-1 is open-circuited, the power input to coil 2 is 12 W when the applied voltage is 110 V (rms) at 60 Hz and the current is 1 A (rms). When coil 2 is short-circuited, the current flowing in coil 1 is 1 A when the applied voltage is 30 V at 60 Hz. The power during this test is 22 W. If we assume  $L_{l1} = L'_{l2}$ , an approximate equivalent T circuit can be determined from these measurements with coil 1 selected as the reference coil.

The power may be expressed as

$$P_1 = |\tilde{V}_1| |\tilde{I}_1| \cos \phi \quad (1A-1)$$

where  $\tilde{V}$  and  $\tilde{I}$  are phasors, and  $\phi$  is the phase angle between  $\tilde{V}_1$  and  $\tilde{I}_1$  (power factor angle). Solving for  $\phi$  during the open-circuit test, we have

$$\begin{aligned}
 \phi &= \cos^{-1} \frac{P_1}{|\tilde{V}_1||\tilde{I}_1|} \\
 &= \cos^{-1} \frac{12}{110 \times 1} \\
 &= 83.7^\circ
 \end{aligned} \tag{1A-2}$$

With  $\tilde{V}_1$  as the reference phasor and assuming an inductive circuit where  $\tilde{I}_1$  lags  $\tilde{V}_1$ ,

$$\begin{aligned}
 Z &= \frac{\tilde{V}_1}{\tilde{I}_1} \\
 &= \frac{110/0^\circ}{1/-83.7^\circ} \\
 &= 12 + j109.3 \Omega
 \end{aligned} \tag{1A-3}$$

If we neglect hysteresis (core) losses, then  $r_1 = 12 \Omega$ . We also know from the above calculation that  $X_{l1} + X_{m1} = 109.3 \Omega$ .

For the short-circuit test, we will assume that  $i_1 = -i_2'$ , since transformers are designed so that  $X_{m1} \gg |r_2' + jX_{l2}'|$ . Hence, using (1A-1) again

$$\begin{aligned}
 \phi &= \cos^{-1} \frac{22}{30 \times 1} \\
 &= 42.8^\circ
 \end{aligned} \tag{1A-4}$$

In this case, the input impedance is  $(r_1 + r_2') + j(X_{l1} + X_{l2}')$ . This may be determined as follows:

$$\begin{aligned}
 Z &= \frac{30/0^\circ}{1/-42.8^\circ} \\
 &= 22 + j20.4 \Omega
 \end{aligned} \tag{1A-5}$$

Hence,  $r_2' = 10 \Omega$  and, since it is assumed that  $X_{l1} = X_{l2}'$ , both are  $10.2 \Omega$ . Therefore,  $X_{m1} = 109.3 - 10.2 = 99.1 \Omega$ . In summary

$$\begin{aligned}
 r_1 &= 12 \Omega & L_{m1} &= 262.9 \text{ mH} & r_2' &= 10 \Omega \\
 L_{l1} &= 27.1 \text{ mH} & & & L_{l2}' &= 27.1 \text{ mH}
 \end{aligned}$$

## Nonlinear Magnetic System

Although the analysis of transformers and electric machines is generally performed assuming a linear magnetic system, economics dictate that in the practical design of many of these devices, some saturation occurs and that heating of the magnetic material exists due to hysteresis loss. The magnetization characteristics of transformer or machine materials are given in the form of the magnitude of flux density versus

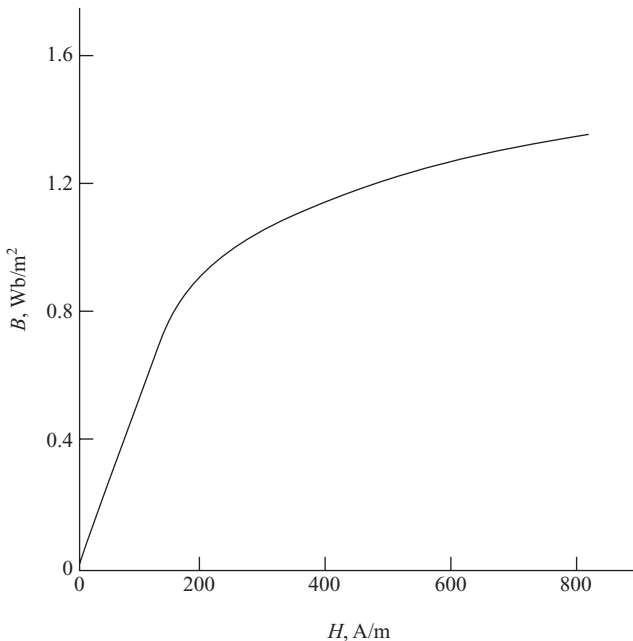


Figure 1.2-3.  $B$ – $H$  curve for typical silicon steel used in transformers.

magnitude of field strength ( $B$ – $H$  curve) as shown in Figure 1.2-3. If it is assumed that the magnetic flux is uniform through most of the core, then  $B$  is proportional to  $\Phi$  and  $H$  is proportional to MMF. Hence, a plot of flux versus current is of the same shape as the  $B$ – $H$  curve. A transformer is generally designed so that some saturation occurs during normal operation. Electric machines are also designed similarly in that a machine generally operates slightly in the saturated region during normal, rated operating conditions. Since saturation causes coefficients of the differential equations describing the behavior of an electromagnetic device to be functions of the coil currents, a transient analysis is difficult without the aid of a computer. Our purpose here is not to set forth methods of analyzing nonlinear magnetic systems. A method of incorporating the effects of saturation into a computer representation is of interest.

Formulating the voltage equations of stationary coupled coils appropriate for computer simulation is straightforward, and yet this technique is fundamental to the computer simulation of ac machines. Therefore, it is to our advantage to consider this method here. For this purpose, let us first write (1.2-31) and (1.2-32) as

$$\lambda_1 = L_{l1}i_1 + \lambda_m \quad (1.2-37)$$

$$\lambda'_2 = L'_{l2}i'_2 + \lambda_m \quad (1.2-38)$$

where

$$\lambda_m = L_{m1}(i_1 + i'_2) \quad (1.2-39)$$

Solving (1.2-37) and (1.2-38) for the currents yields

$$i_1 = \frac{1}{L_{l1}}(\lambda_1 - \lambda_m) \quad (1.2-40)$$

$$i_2' = \frac{1}{L_{l2}'}(\lambda_2' - \lambda_m) \quad (1.2-41)$$

If (1.2-40) and (1.2-41) are substituted into the voltage equations (1.2-34) and (1.2-35), and if we solve the resulting equations for flux linkages, the following equations are obtained:

$$\lambda_1 = \int \left[ v_1 + \frac{r_1}{L_{l1}}(\lambda_m - \lambda_1) \right] dt \quad (1.2-42)$$

$$\lambda_2' = \int \left[ v_2' + \frac{r_2'}{L_{l2}'}(\lambda_m - \lambda_2') \right] dt \quad (1.2-43)$$

Substituting (1.2-40) and (1.2-41) into (1.2-39) yields

$$\lambda_m = L_a \left( \frac{\lambda_1}{L_{l1}} + \frac{\lambda_2'}{L_{l2}'} \right) \quad (1.2-44)$$

where

$$L_a = \left( \frac{1}{L_{m1}} + \frac{1}{L_{l1}} + \frac{1}{L_{l2}'} \right)^{-1} \quad (1.2-45)$$

We now have the equations expressed with  $\lambda_1$  and  $\lambda_2'$  as state variables. In the computer simulation, (1.2-42) and (1.2-43) are used to solve for  $\lambda_1$  and  $\lambda_2'$ , and (1.2-44) is used to solve for  $\lambda_m$ . The currents can then be obtained from (1.2-40) and (1.2-41). It is clear that (1.2-44) could be substituted into (1.2-40)–(1.2-43) and  $\lambda_m$  eliminated from the equations, whereupon it would not appear in the computer simulation. However, we will find  $\lambda_m$  (the magnetizing flux linkage) an important variable when we include the effects of saturation.

If the magnetization characteristics (magnetization curve) of the coupled coil are known, the effects of saturation of the mutual flux path may be incorporated into the computer simulation. Generally, the magnetization curve can be adequately determined from a test wherein one of the coils is open-circuited (coil 2, for example) and the input impedance of coil 1 is determined from measurements as the applied voltage is increased in magnitude from 0 to say 150% of the rated value. With information obtained from this type of test, we can plot  $\lambda_m$  versus  $(i_1' + i_2')$  as shown in Figure 1.2-4, wherein the slope of the linear portion of the curve is  $L_{m1}$ . From Figure 1.2-4, it is clear that in the region of saturation, we have

$$\lambda_m = L_{m1}(i_1' + i_2') - f(\lambda_m) \quad (1.2-46)$$

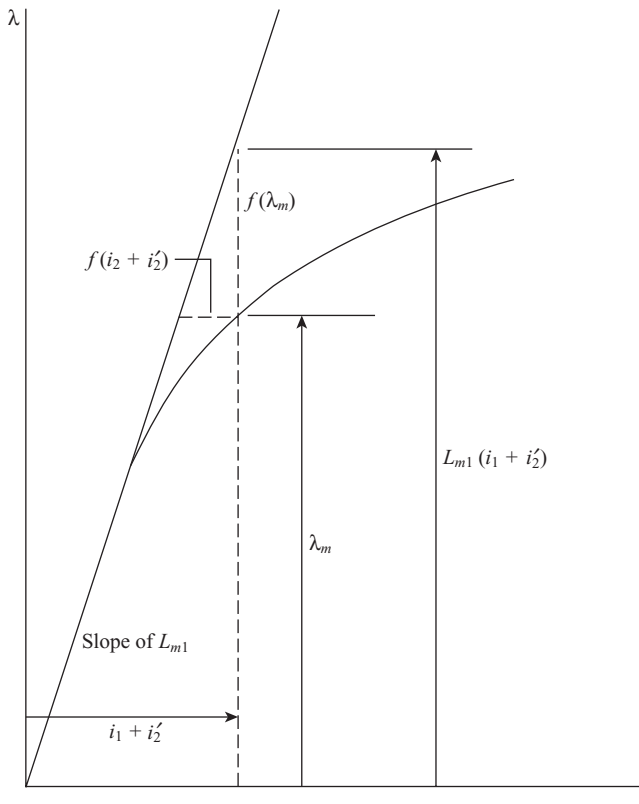


Figure 1.2-4. Magnetization curve.

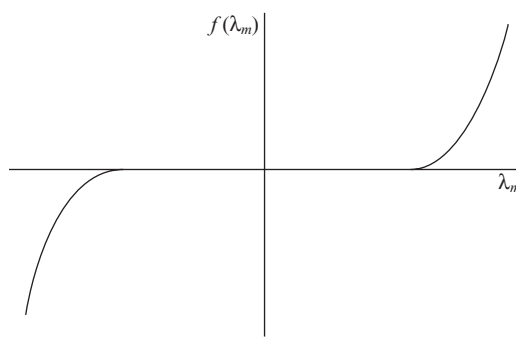


Figure 1.2-5.  $f(\lambda_m)$  versus  $\lambda_m$  from Figure 1.2-4.

where  $f(\lambda_m)$  may be determined from the magnetization curve for each value of  $\lambda_m$ . In particular,  $f(\lambda_m)$  is a function of  $\lambda_m$  as shown in Figure 1.2-5. Therefore, the effects of saturation of the mutual flux path may be taken into account by replacing (1.2-39) with (1.2-46) for  $\lambda_m$ . Substituting (1.2-40) and (1.2-41) for  $i_1$  and  $i_2'$ , respectively, into (1.2-46) yields the following equation for  $\lambda_m$

$$\lambda_m = L_a \left( \frac{\lambda_1}{L_{l1}} + \frac{\lambda'_2}{L'_{l2}} \right) - \frac{L_a}{L_{m1}} f(\lambda_m) \quad (1.2-47)$$

Hence, the computer simulation for including saturation involves replacing  $\lambda_m$  given by (1.2-44) with (1.2-47), where  $f(\lambda_m)$  is a generated function of  $\lambda_m$  determined from the plot shown in Figure 1.2-5.

### 1.3. ELECTROMECHANICAL ENERGY CONVERSION

Although electromechanical devices are used in some manner in a wide variety of systems, electric machines are by far the most common. It is desirable, however, to establish methods of analysis that may be applied to all electromechanical devices. Prior to proceeding, it is helpful to clarify that throughout the book, the words “winding” and “coil” are used to describe conductor arrangements. To distinguish, a winding consists of one or more coils connected in series or parallel.

#### Energy Relationships

Electromechanical systems are comprised of an electrical system, a mechanical system, and a means whereby the electrical and mechanical systems can interact. Interaction can take place through any and all electromagnetic and electrostatic fields that are common to both systems, and energy is transferred from one system to the other as a result of this interaction. Both electrostatic and electromagnetic coupling fields may exist simultaneously and the electromechanical system may have any number of electrical and mechanical systems. However, before considering an involved system, it is helpful to analyze the electromechanical system in a simplified form. An electromechanical system with one electrical system, one mechanical system, and with one coupling field is depicted in Figure 1.3-1. Electromagnetic radiation is neglected, and it is assumed that the electrical system operates at a frequency sufficiently low so that the electrical system may be considered as a lumped parameter system.

Losses occur in all components of the electromechanical system. Heat loss will occur in the mechanical system due to friction and the electrical system will dissipate heat due to the resistance of the current-carrying conductors. Eddy current and hysteresis losses occur in the ferromagnetic material of all magnetic fields while dielectric losses occur in all electric fields. If  $W_E$  is the total energy supplied by the electrical source and  $W_M$  the total energy supplied by the mechanical source, then the energy distribution could be expressed as

$$W_E = W_e + W_{eL} + W_{es} \quad (1.3-1)$$

$$W_M = W_m + W_{mL} + W_{ms} \quad (1.3-2)$$

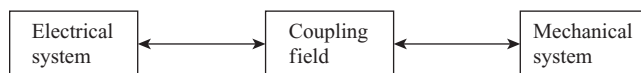


Figure 1.3-1. Block diagram of elementary electromechanical system.

In (1.3-1),  $W_{eS}$  is the energy stored in the electric or magnetic fields that are not coupled with the mechanical system. The energy  $W_{eL}$  is the heat losses associated with the electrical system. These losses occur due to the resistance of the current-carrying conductors, as well as the energy dissipated from these fields in the form of heat due to hysteresis, eddy currents, and dielectric losses. The energy  $W_e$  is the energy transferred to the coupling field by the electrical system. The energies common to the mechanical system may be defined in a similar manner. In (1.3-2),  $W_{mS}$  is the energy stored in the moving member and compliances of the mechanical system,  $W_{mL}$  is the energy losses of the mechanical system in the form of heat, and  $W_m$  is the energy transferred to the coupling field. It is important to note that with the convention adopted, the energy supplied by either source is considered positive. Therefore,  $W_E$  ( $W_M$ ) is negative when energy is supplied to the electrical source (mechanical source).

If  $W_F$  is defined as the total energy transferred to the coupling field, then

$$W_F = W_f + W_{fL} \quad (1.3-3)$$

where  $W_f$  is energy stored in the coupling field and  $W_{fL}$  is the energy dissipated in the form of heat due to losses within the coupling field (eddy current, hysteresis, or dielectric losses). The electromechanical system must obey the law of conservation of energy, thus

$$W_f + W_{fL} = (W_E - W_{eL} - W_{eS}) + (W_M - W_{mL} - W_{mS}) \quad (1.3-4)$$

which may be written as

$$W_f + W_{fL} = W_e + W_m \quad (1.3-5)$$

This energy relationship is shown schematically in Figure 1.3-2.

The actual process of converting electrical energy to mechanical energy (or vice versa) is independent of (1) the loss of energy in either the electrical or the mechanical systems ( $W_{eL}$  and  $W_{mL}$ ), (2) the energies stored in the electric or magnetic fields that are not common to both systems ( $W_{eS}$ ), or (3) the energies stored in the mechanical system ( $W_{mS}$ ). If the losses of the coupling field are neglected, then the field is conservative and (1.3-5) becomes [1]

$$W_f = W_e + W_m \quad (1.3-6)$$

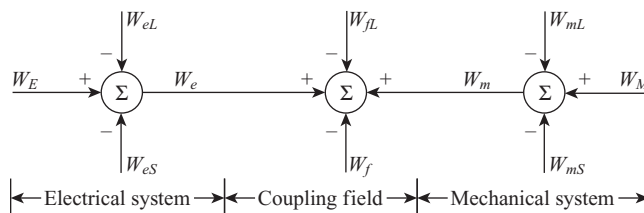


Figure 1.3-2. Energy balance.

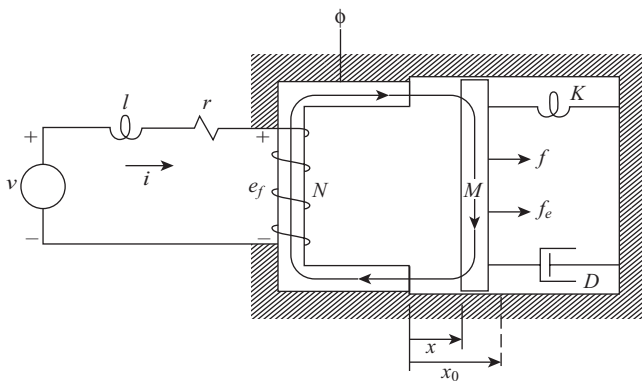


Figure 1.3-3. Electromechanical system with magnetic field.

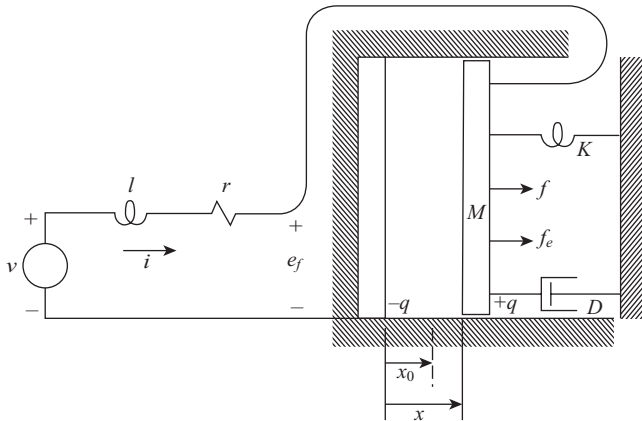


Figure 1.3-4. Electromechanical system with electric field.

Examples of elementary electromechanical systems are shown in Figure 1.3-3 and Figure 1.3-4. The system shown in Figure 1.3-3 has a magnetic coupling field, while the electromechanical system shown in Figure 1.3-4 employs an electric field as a means of transferring energy between the electrical and mechanical systems. In these systems,  $v$  is the voltage of the electric source and  $f$  is the external mechanical force applied to the mechanical system. The electromagnetic or electrostatic force is denoted by  $f_e$ . The resistance of the current-carrying conductors is denoted by  $r$ , and  $l$  denotes the inductance of a linear (conservative) electromagnetic system that does not couple the mechanical system. In the mechanical system,  $M$  is the mass of the movable member, while the linear compliance and damper are represented by a spring constant  $K$  and a damping coefficient  $D$ , respectively. The displacement  $x_0$  is the zero force or equilibrium position of the mechanical system that is the steady-state position of the mass with  $f_e$  and  $f$  equal to zero. A series or shunt capacitance may be included in the electrical system wherein energy would also be stored in an electric field external to the electromechanical process.

The voltage equation that describes both electrical systems may be written as

$$v = ri + l \frac{di}{dt} + e_f \quad (1.3-7)$$

where  $e_f$  is the voltage drop across the coupling field. The dynamic behavior of the translational mechanical systems may be expressed by employing Newton's law of motion. Thus,

$$f = M \frac{d^2x}{dt^2} + D \frac{dx}{dt} + K(x - x_0) - f_e \quad (1.3-8)$$

The total energy supplied by the electric source is

$$W_E = \int v i dt \quad (1.3-9)$$

The total energy supplied by the mechanical source is

$$W_M = \int f dx \quad (1.3-10)$$

which may also be expressed as

$$W_M = \int f \frac{dx}{dt} dt \quad (1.3-11)$$

Substituting (1.3-7) into (1.3-9) yields

$$W_E = r \int i^2 dt + l \int i di + \int e_f i dt \quad (1.3-12)$$

The first term on the right-hand side of (1.3-12) represents the energy loss due to the resistance of the conductors ( $W_{el}$ ). The second term represents the energy stored in the linear electromagnetic field external to the coupling field ( $W_{eS}$ ). Therefore, the total energy transferred to the coupling field from the electrical system is

$$W_e = \int e_f i dt \quad (1.3-13)$$

Similarly, for the mechanical system, we have

$$W_M = M \int \frac{d^2x}{dt^2} dx + D \int \left( \frac{dx}{dt} \right)^2 dt + K \int (x - x_0) dx - \int f_e dx \quad (1.3-14)$$

Here, the first and third terms on the right-hand side of (1.3-14) represent the energy stored in the mass and spring, respectively ( $W_{mS}$ ). The second term is the heat loss due to friction ( $W_{mL}$ ). Thus, the total energy transferred to the coupling field from the mechanical system with one mechanical input is

$$W_m = - \int f_e dx \quad (1.3-15)$$

It is important to note that a positive force,  $f_e$ , is assumed to be in the same direction as a positive displacement,  $x$ . Substituting (1.3-13) and (1.3-15) into the energy balance relation, (1.3-6), yields

$$W_f = \int e_f i dt - \int f_e dx \quad (1.3-16)$$

The equations set forth may be readily extended to include an electromechanical system with any number of electrical inputs. Thus,

$$W_f = \sum_{j=1}^J W_{ej} + W_m \quad (1.3-17)$$

wherein  $J$  electrical inputs exist. The  $J$  here should not be confused with that used later for the inertia of rotational systems. The total energy supplied to the coupling field from the electrical inputs is

$$\sum_{j=1}^J W_{ej} = \int \sum_{j=1}^J e_{fj} i_j dt \quad (1.3-18)$$

The total energy supplied to the coupling field from the mechanical input is

$$W_m = - \int f_e dx \quad (1.3-19)$$

The energy balance equation becomes

$$W_f = \int \sum_{j=1}^J e_{fj} i_j dt - \int f_e dx \quad (1.3-20)$$

In differential form

$$dW_f = \sum_{j=1}^J e_{fj} i_j dt - f_e dx \quad (1.3-21)$$

## Energy in Coupling Fields

Before using (1.3-21) to obtain an expression for the electromagnetic force  $f_e$ , it is necessary to derive an expression for the energy stored in the coupling fields. Once we have an expression for  $W_f$ , we can take the total derivative to obtain  $dW_f$  that can then be substituted into (1.3-21). When expressing the energy in the coupling fields, it is

convenient to neglect all losses associated with the electric and magnetic fields, whereupon the fields are assumed to be conservative and the energy stored therein is a function of the state of the electrical and mechanical variables. Although the effects of the field losses may be functionally taken into account by appropriately introducing a resistance in the electric circuit, this refinement is generally not necessary since the ferromagnetic material is selected and arranged in laminations so as to minimize the hysteresis and eddy current losses. Moreover, nearly all of the energy stored in the coupling fields is stored in the air gaps of the electromechanical device. Since air is a conservative medium, all of the energy stored therein can be returned to the electrical or mechanical systems. Therefore, the assumption of lossless coupling fields is not as restrictive as it might first appear.

The energy stored in a conservative field is a function of the state of the system variables and not the manner in which the variables reached that state. It is convenient to take advantage of this feature when developing a mathematical expression for the field energy. In particular, it is convenient to fix mathematically the position of the mechanical systems associated with the coupling fields and then excite the electrical systems with the displacements of the mechanical systems held fixed. During the excitation of the electrical systems,  $W_m$  is zero, since  $dx$  is zero, even though electromagnetic or electrostatic forces occur. Therefore, with the displacements held fixed, the energy stored in the coupling fields during the excitation of the electrical systems is equal to the energy supplied to the coupling fields by the electrical systems. Thus, with  $W_m = 0$ , the energy supplied from the electrical system may be expressed from (1.3-20) as

$$W_f = \int \sum_{j=1}^J e_{fj} i_j dt \quad (1.3-22)$$

It is instructive to consider a single-excited electromagnetic system similar to that shown in Figure 1.3-3. In this case,  $e_f = d\lambda/dt$  and (1.3-22) becomes

$$W_f = \int i d\lambda \quad (1.3-23)$$

Here  $J = 1$ , however, the subscript is omitted for the sake of brevity. The area to the left of the  $\lambda-i$  relationship, shown in Figure 1.3-5, for a singly excited electromagnetic device is the area described by (1.3-23). In Figure 1.3-5, this area represents the energy stored in the field at the instant when  $\lambda = \lambda_a$  and  $i = i_a$ . The  $\lambda-i$  relationship need not be linear, it need only be single valued, a property that is characteristic to a conservative or lossless field. Moreover, since the coupling field is conservative, the energy stored in the field with  $\lambda = \lambda_a$  and  $i = i_a$  is independent of the excursion of the electrical and mechanical variables before reaching this state.

The area to the right of the  $\lambda-i$  curve is called the *coenergy*, and it is defined as

$$W_c = \int \lambda di \quad (1.3-24)$$

which may also be written as

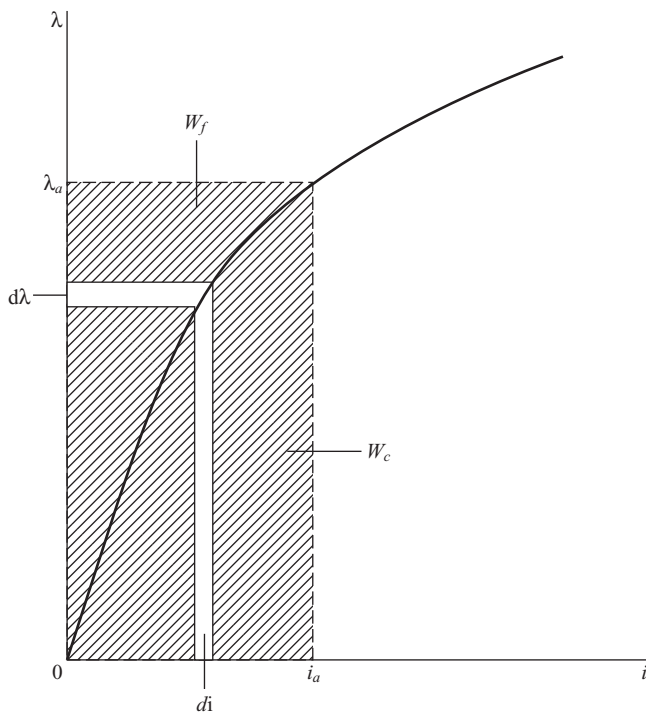


**Figure 1.3-5.** Stored energy and coenergy in a magnetic field of a singly excited electromagnetic device.

$$W_c = \lambda i - W_f \quad (1.3-25)$$

For multiple electrical inputs,  $\lambda i$  in (1.3-25) becomes  $\sum_{j=1}^J \lambda_j i_j$ . Although the coenergy has little or no physical significance, we will find it a convenient quantity for expressing the electromagnetic force. It should be clear that  $W_f = W_c$  for a linear magnetic system where the  $\lambda$ - $i$  plots are straight-line relationships.

The displacement  $x$  defines completely the influence of the mechanical system upon the coupling field; however, since  $\lambda$  and  $i$  are related, only one is needed in addition to  $x$  in order to describe the state of the electromechanical system. Therefore, either  $\lambda$  and  $x$  or  $i$  and  $x$  may be selected as independent variables. If  $i$  and  $x$  are selected as independent variables, it is convenient to express the field energy and the flux linkages as

$$W_f = W_f(i, x) \quad (1.3-26)$$

$$\lambda = \lambda(i, x) \quad (1.3-27)$$

With  $i$  and  $x$  as independent variables, we must express  $d\lambda$  in terms of  $di$  before substituting into (1.3-23). Thus, from (1.3-27)

$$d\lambda(i, x) = \frac{\partial \lambda(i, x)}{\partial i} di + \frac{\partial \lambda(i, x)}{\partial x} dx \quad (1.3-28)$$

In the derivation of an expression for the energy stored in the field,  $dx$  is set equal to zero. Hence, in the evaluation of field energy,  $d\lambda$  is equal to the first term on the right-hand side of (1.3-28). Substituting into (1.3-23) yields

$$W_f(i, x) = \int i \frac{\partial \lambda(i, x)}{\partial i} di = \int_0^i \xi \frac{\partial \lambda(\xi, x)}{\partial \xi} d\xi \quad (1.3-29)$$

where  $\xi$  is the dummy variable of integration. Evaluation of (1.3-29) gives the energy stored in the field of a singly excited system. The coenergy in terms of  $i$  and  $x$  may be evaluated from (1.3-24) as

$$W_c(i, x) = \int \lambda(i, x) di = \int_0^i \lambda(\xi, x) d\xi \quad (1.3-30)$$

With  $\lambda$  and  $x$  as independent variables

$$W_f = W_f(\lambda, x) \quad (1.3-31)$$

$$i = i(\lambda, x). \quad (1.3-32)$$

The field energy may be evaluated from (1.3-23) as

$$W_f(\lambda, x) = \int i(\lambda, x) d\lambda = \int_0^\lambda i(\xi, x) d\xi \quad (1.3-33)$$

In order to evaluate the coenergy with  $\lambda$  and  $x$  as independent variables, we need to express  $di$  in terms of  $d\lambda$ ; thus, from (1.3-32), we obtain

$$di(\lambda, x) = \frac{\partial i(\lambda, x)}{\partial \lambda} d\lambda + \frac{\partial i(\lambda, x)}{\partial x} dx \quad (1.3-34)$$

Since  $dx = 0$  in this evaluation, (1.3-24) becomes

$$W_c(\lambda, x) = \int \lambda \frac{\partial i(\lambda, x)}{\partial \lambda} d\lambda = \int_0^\lambda \xi \frac{\partial i(\xi, x)}{\partial \xi} d\xi \quad (1.3-35)$$

For a linear electromagnetic system, the  $\lambda$ - $i$  plots are straight-line relationships; thus, for the singly excited system, we have

$$\lambda(i, x) = L(x)i \quad (1.3-36)$$

or

$$i(\lambda, x) = \frac{\lambda}{L(x)} \quad (1.3-37)$$

Let us evaluate  $W_f(i, x)$ . From (1.3-28), with  $dx = 0$

$$d\lambda(i, x) = L(x)di \quad (1.3-38)$$

Hence, from (1.3-29)

$$W_f(i, x) = \int_0^i \xi L(x) d\xi = \frac{1}{2} L(x) i^2 \quad (1.3-39)$$

It is left to the reader to show that  $W_f(\lambda, x)$ ,  $W_c(i, x)$ , and  $W_e(\lambda, x)$  are equal to (1.3-39) for this magnetically linear system.

The field energy is a state function, and the expression describing the field energy in terms of system variables is valid regardless of the variations in the system variables. For example, (1.3-39) expresses the field energy regardless of the variations in  $L(x)$  and  $i$ . The fixing of the mechanical system so as to obtain an expression for the field energy is a mathematical convenience and not a restriction upon the result.

In the case of a multiexcited, electromagnetic system, an expression for the field energy may be obtained by evaluating the following relation with  $dx = 0$ :

$$W_f = \int \sum_{j=1}^J i_j d\lambda_j \quad (1.3-40)$$

Because the coupling fields are considered conservative, (1.3-40) may be evaluated independent of the order in which the flux linkages or currents are brought to their final values. To illustrate the evaluation of (1.3-40) for a multiexcited system, we will allow the currents to establish their final states one at a time while all other currents are mathematically fixed either in their final or unexcited state. This procedure may be illustrated by considering a doubly excited electric system. An electromechanical system of this type could be constructed by placing a second coil, supplied from a second electrical system, on either the stationary or movable member of the system shown in Figure 1.3-3. In this evaluation, it is convenient to use currents and displacement as the independent variables. Hence, for a doubly excited electric system

$$W_f(i_1, i_2, x) = \int [i_1 d\lambda_1(i_1, i_2, x) + i_2 d\lambda_2(i_1, i_2, x)] \quad (1.3-41)$$

In this determination of an expression for  $W_f$ , the mechanical displacement is held constant ( $dx = 0$ ); thus (1.3-41) becomes

$$\begin{aligned} W_f(i_1, i_2, x) &= \int i_1 \left[ \frac{\partial \lambda_1(i_1, i_2, x)}{\partial i_1} di_1 + \frac{\partial \lambda_1(i_1, i_2, x)}{\partial i_2} di_2 \right] \\ &\quad + i_2 \left[ \frac{\partial \lambda_2(i_1, i_2, x)}{\partial i_1} di_1 + \frac{\partial \lambda_2(i_1, i_2, x)}{\partial i_2} di_2 \right] \end{aligned} \quad (1.3-42)$$

We will evaluate the energy stored in the field by employing (1.3-42) twice. First, we will mathematically bring the current  $i_1$  to the desired value while holding  $i_2$  at zero.

Thus,  $i_1$  is the variable of integration and  $di_2 = 0$ . Energy is supplied to the coupling field from the source connected to coil 1. As the second evaluation of (1.3-42),  $i_2$  is brought to its desired current while holding  $i_1$  at its desired value. Hence,  $i_2$  is the variable of integration and  $di_1 = 0$ . During this time, energy is supplied from both sources to the coupling field since  $i_1 d\lambda_1$  is nonzero. The total energy stored in the coupling field is the sum of the two evaluations. Following this two-step procedure, the evaluation of (1.3-42) for the total field energy becomes

$$W_f(i_1, i_2, x) = \int_{i_1} \frac{\partial \lambda_1(i_1, i_2, x)}{\partial i_1} di_1 + \int \left[ i_1 \frac{\partial \lambda_1(i_1, i_2, x)}{\partial i_2} di_2 + i_2 \frac{\partial \lambda_2(i_1, i_2, x)}{\partial i_2} di_2 \right] \quad (1.3-43)$$

which should be written as

$$W_f(i_1, i_2, x) = \int_0^{i_1} \xi \frac{\partial \lambda_1(\xi, i_2, x)}{\partial \xi} d\xi + \int_0^{i_2} \left[ i_1 \frac{\partial \lambda_1(i_1, \xi, x)}{\partial \xi} d\xi + \xi \frac{\partial \lambda_2(i_1, \xi, x)}{\partial \xi} d\xi \right] \quad (1.3-44)$$

The first integral on the right-hand side of (1.3-43) or (1.3-44) results from the first step of the evaluation, with  $i_1$  as the variable of integration and with  $i_2 = 0$  and  $di_2 = 0$ . The second integral comes from the second step of the evaluation with  $i_1 = i_1$ ,  $di_1 = 0$ , and  $i_2$  as the variable of integration. It is clear that the order of allowing the currents to reach their final state is irrelevant; that is, as our first step, we could have made  $i_2$  the variable of integration while holding  $i_1$  at zero ( $di_1 = 0$ ) and then let  $i_1$  become the variable of integration while holding  $i_2$  at its final value. The result would be the same. It is also clear that for three electrical inputs, the evaluation procedure would require three steps, one for each current to be brought mathematically to its final state.

Let us now evaluate the energy stored in a magnetically linear electromechanical system with two electric inputs. For this, let

$$\lambda_1(i_1, i_2, x) = L_{11}(x)i_1 + L_{12}(x)i_2 \quad (1.3-45)$$

$$\lambda_2(i_1, i_2, x) = L_{21}(x)i_1 + L_{22}(x)i_2 \quad (1.3-46)$$

With that mechanical displacement held constant ( $dx = 0$ ),

$$d\lambda_1(i_1, i_2, x) = L_{11}(x)di_1 + L_{12}(x)di_2 \quad (1.3-47)$$

$$d\lambda_2(i_1, i_2, x) = L_{21}(x)di_1 + L_{22}(x)di_2. \quad (1.3-48)$$

It is clear that the coefficients on the right-hand side of (1.3-47) and (1.3-48) are the partial derivatives. For example,  $L_{11}(x)$  is the partial derivative of  $\lambda_1(i_1, i_2, x)$  with respect to  $i_1$ . Appropriate substitution into (1.3-44) gives

$$W_f(i_1, i_2, x) = \int_0^{i_1} \xi L_{11}(x) d\xi + \int_0^{i_2} [i_1 L_{12}(x) + \xi L_{21}(x)] d\xi \quad (1.3-49)$$

which yields

$$W_f(i_1, i_2, x) = \frac{1}{2} L_{11}(x) i_1^2 + L_{12}(x) i_1 i_2 + \frac{1}{2} L_{22}(x) i_2^2 \quad (1.3-50)$$

The extension to a linear electromagnetic system with  $J$  electrical inputs is straightforward, whereupon the following expression for the total field energy is obtained as

$$W_f(i_1, \dots, i_J, x) = \frac{1}{2} \sum_{p=1}^J \sum_{q=1}^J L_{pq} i_p i_q \quad (1.3-51)$$

It is left to the reader to show that the equivalent of (1.3-22) for a multiexcited electrostatic system is

$$W_f = \int \sum_{j=1}^J e_{fj} dq_j \quad (1.3-52)$$

### Graphical Interpretation of Energy Conversion

Before proceeding to the derivation of expressions for the electromagnetic force, it is instructive to consider briefly a graphical interpretation of the energy conversion process. For this purpose, let us again refer to the elementary system shown in Figure 1.3-3, and let us assume that as the movable member moves from  $x = x_a$  to  $x = x_b$ , where  $x_b < x_a$ , the  $\lambda$ - $i$  characteristics are given by Figure 1.3-6. Let us further assume that as the member moves from  $x_a$  to  $x_b$ , the  $\lambda$ - $i$  trajectory moves from point A to point B. It is clear that the exact trajectory from A to B is determined by the combined dynamics of the electrical and mechanical systems. Now, the area  $OACO$  represents the original energy stored in field; area  $OBDO$  represents the final energy stored in the field. Therefore, the change in field energy is

$$\Delta W_f = \text{area } OBDO - \text{area } OACO \quad (1.3-53)$$

The change in  $W_e$ , denoted as  $\Delta W_e$ , is

$$\Delta W_e = \int_{\lambda_A}^{\lambda_B} id\lambda = \text{area } CABDC \quad (1.3-54)$$

We know that

$$\Delta W_m = \Delta W_f - \Delta W_e \quad (1.3-55)$$

Hence,

$$\Delta W_m = \text{area } OBDO - \text{area } OACO - \text{area } CABDC = -\text{area } OABO \quad (1.3-56)$$

Here,  $\Delta W_m$  is negative; energy has been supplied to the mechanical system from the coupling field, part of which came from the energy stored in the field and part from the

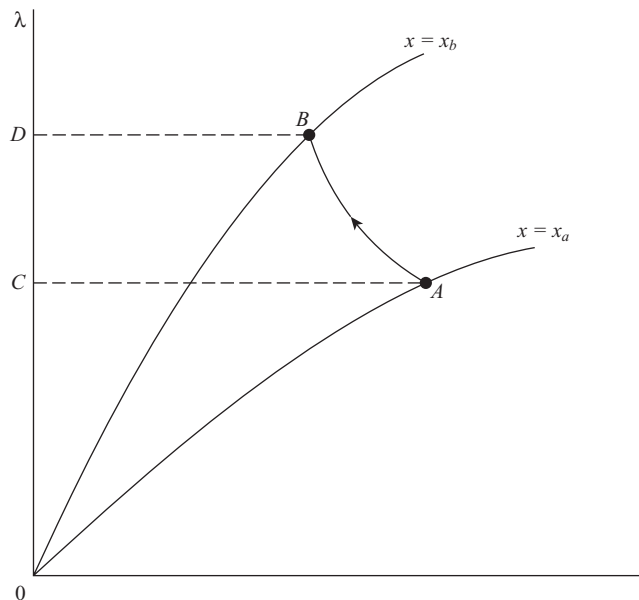


**Figure 1.3-6.** Graphical representation of electromechanical energy conversion for  $\lambda$ - $i$  path A to B.

electrical system. If the member is now moved back to  $x_a$ , the  $\lambda$ - $i$  trajectory may be as shown in Figure 1.3-7. Hence  $\Delta W_m$  is still area  $OABO$ , but it is now positive, which means that energy was supplied from the mechanical system to the coupling field, part of which is stored in the field and part of which is transferred to the electrical system. The net  $\Delta W_m$  for the cycle from A to B back to A is the shaded area shown in Figure 1.3-8. Since  $\Delta W_f$  is zero for this cycle

$$\Delta W_m = -\Delta W_e \quad (1.3-57)$$

For the cycle shown, the net  $\Delta W_e$  is negative, thus  $\Delta W_m$  is positive; we have generator action. If the trajectory had been in the counterclockwise direction, the net  $\Delta W_e$  would have been positive and the net  $\Delta W_m$  negative, which would represent motor action.

## Electromagnetic and Electrostatic Forces

The energy balance relationships given by (1.3-21) may be arranged as

$$f_e dx = \sum_{j=1}^J e_{fj} i_j dt - dW_f \quad (1.3-58)$$

In order to obtain an expression for  $f_e$ , it is necessary to first express  $W_f$  and then take its total derivative. One is tempted to substitute the integrand of (1.3-22) into (1.3-58)

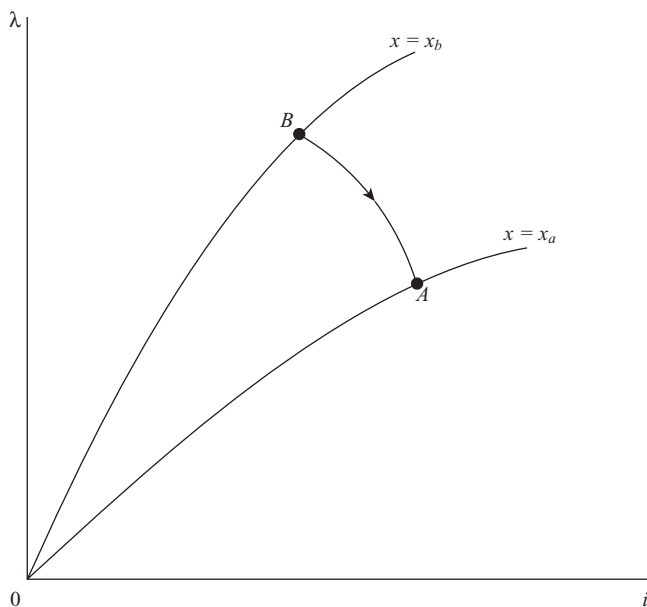


Figure 1.3-7. Graphical representation of electromechanical energy conversion for  $\lambda$ - $i$  path  $B$  to  $A$ .

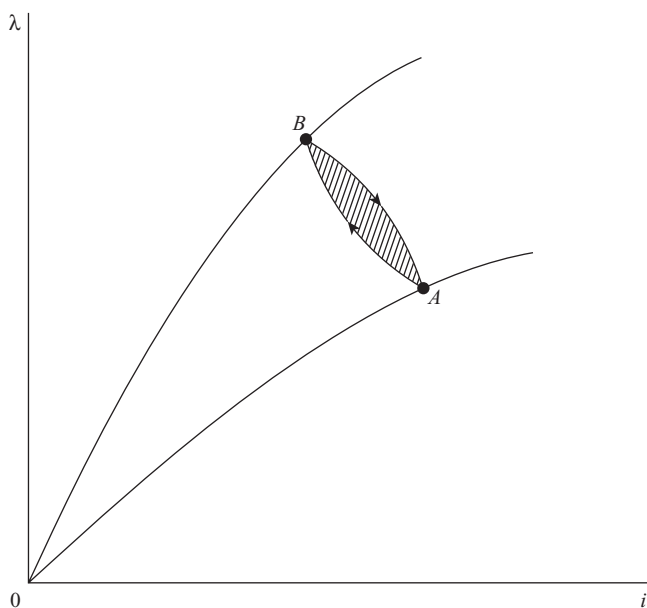


Figure 1.3-8. Graphical representation of electromechanical energy conversion for  $\lambda$ - $i$  path  $A$  to  $B$  to  $A$ .

for the infinitesimal change of field energy. This procedure is, of course, incorrect, since the integrand of (1.3-22) was obtained with the mechanical displacement held fixed ( $dx = 0$ ), where the total differential of the field energy is required in (1.3-58). In the following derivation, we will consider multiple electrical inputs; however, we will consider only one mechanical input, as we noted earlier in (1.3-15). Electromechanical systems with more than one mechanical input are not common; therefore, the additional notation necessary to include multiple mechanical inputs is not warranted. Moreover, the final results of the following derivation may be readily extended to include multiple mechanical inputs.

The force or torque in any electromechanical system may be evaluated by employing (1.3-58). In many respects, one gains a much better understanding of the energy conversion process of a particular system by starting the derivation of the force or torque expression with (1.3-58) rather than selecting a relationship from a table. However, for the sake of completeness, derivation of the force equations will be set forth and tabulated for electromechanical systems with one mechanical input and  $J$  electrical inputs.

For an electromagnetic system, (1.3-58) may be written as

$$f_e dx = \sum_{j=1}^J i_j d\lambda_j - dW_f \quad (1.3-59)$$

Although we will use (1.3-59), it is helpful to express it in an alternative form. For this purpose, let us first write (1.3-25) for multiple electrical inputs

$$\sum_{j=1}^J \lambda_j i_j = W_c + W_f \quad (1.3-60)$$

If we take the total derivative of (1.3-60), we obtain

$$\sum_{j=1}^J \lambda_j di_j + \sum_{j=1}^J i_j d\lambda_j = dW_c + dW_f \quad (1.3-61)$$

We realize that when we evaluate the force  $f_e$  we must select the independent variables; that is, either the flux linkages or the currents and the mechanical displacement  $x$ . The flux linkages and the currents cannot simultaneously be considered independent variables when evaluating the  $f_e$ . Nevertheless, (1.3-61), wherein both  $d\lambda_j$  and  $di_j$  appear, is valid in general, before a selection of independent variables is made to evaluate  $f_e$ . If we solve (1.3-61) for the total derivative of field energy,  $dW_f$ , and substitute the result into (1.3-59), we obtain

$$f_e dx = - \sum_{j=1}^J \lambda_j di_j + dW_c \quad (1.3-62)$$

Either (1.3-59) or (1.3-62) can be used to evaluate the electromagnetic force  $f_e$ . If flux linkages and  $x$  are selected as independent variables, (1.3-59) is the most direct, while (1.3-62) is the most direct if currents and  $x$  are selected.

With flux linkages and  $x$  as the independent variables, the currents are expressed functionally as

$$i_j(\lambda_1, \dots, \lambda_j, x) \quad (1.3-63)$$

For the purpose of compactness, we will denote  $(\lambda_1, \dots, \lambda_j, x)$  as  $(\lambda, x)$ , where  $\lambda$  is an abbreviation for the complete set of flux linkages associated with the  $J$  windings. Let us write (1.3-59) with flux linkages and  $x$  as independent variables

$$f_e(\lambda, x)dx = \sum_{j=1}^J i_j(\lambda, x)d\lambda_j - dW_f(\lambda, x) \quad (1.3-64)$$

If we take the total derivative of the field energy with respect to  $\lambda$  and  $x$ , and substitute that result into (1.3-64), we obtain

$$f_e(\lambda, x)dx = \sum_{j=1}^J i_j(\lambda, x)d\lambda_j - \sum_{j=1}^J \frac{\partial W_f(\lambda, x)}{\partial \lambda_j} d\lambda_j - \frac{\partial W_f(\lambda, x)}{\partial x} dx \quad (1.3-65)$$

Equating the coefficients of  $dx$  gives

$$f_e(\lambda, x) = -\frac{\partial W_f(\lambda, x)}{\partial x} \quad (1.3-66)$$

A second expression for  $f_e(\lambda, x)$  may be obtained by expressing (1.3-59) with flux linkages and  $x$  as independent variables, solving for  $W_f(\lambda, x)$  and then taking the partial derivative with respect to  $x$ . Thus,

$$f_e(\lambda, x) = -\sum_{j=1}^J \left[ \lambda_j \frac{\partial i_j(\lambda, x)}{\partial x} \right] + \frac{\partial W_c(\lambda, x)}{\partial x} \quad (1.3-67)$$

If we now select  $\mathbf{i}$  and  $x$  as independent variables, where  $\mathbf{i}$  is the abbreviated notation for  $(i_1, \dots, i_J, x)$ , then (1.3-62) can be written

$$f_e(\mathbf{i}, x)dx = -\sum_{j=1}^J \lambda_j(\mathbf{i}, x)di_j + dW_c(\mathbf{i}, x) \quad (1.3-68)$$

If we take the total derivative of  $W_c(\mathbf{i}, x)$  and substitute the result into (1.3-68), we obtain

TABLE 1.3-1. Electromagnetic Force at Mechanical Input

---

$f_e(\mathbf{i}, x) = \sum_{j=1}^J \left[ i_j \frac{\partial \lambda_j(\mathbf{i}, x)}{\partial x} \right] - \frac{\partial W_f(\mathbf{i}, x)}{\partial x}$
$f_e(\mathbf{i}, x) = \frac{\partial W_c(\mathbf{i}, x)}{\partial x}$
$f_e(\boldsymbol{\lambda}, x) = -\frac{\partial W_f(\boldsymbol{\lambda}, x)}{\partial x}$
$f_e(\boldsymbol{\lambda}, x) = -\sum_{j=1}^J \left[ \lambda_j \frac{\partial i_j(\boldsymbol{\lambda}, x)}{\partial x} \right] + \frac{\partial W_c(\boldsymbol{\lambda}, x)}{\partial x}$

---

Note: For rotational systems, replace  $f_e$  with  $T_e$  and  $x$  with  $\theta$ .

$$f_e(\mathbf{i}, x)dx = -\sum_{j=1}^J \lambda_j(\mathbf{i}, x)di_j + \sum_{j=1}^J \frac{\partial W_c(\mathbf{i}, x)}{\partial i_j} di_j + \frac{\partial W_c(\mathbf{i}, x)}{\partial x} dx \quad (1.3-69)$$

Equating coefficients of  $dx$  yields

$$f_e(\mathbf{i}, x) = \frac{\partial W_c(\mathbf{i}, x)}{\partial x} \quad (1.3-70)$$

We will make extensive use of this expression. If we now solve (1.3-60) for  $W_c(\mathbf{i}, x)$  and then take the partial derivative with respect to  $x$ , we can obtain a second expression for  $f_e(\mathbf{i}, x)$ . That is

$$f_e(\mathbf{i}, x) = \sum_{j=1}^J \left[ i_j \frac{\partial \lambda_j(\mathbf{i}, x)}{\partial x} \right] - \frac{\partial W_f(\mathbf{i}, x)}{\partial x} \quad (1.3-71)$$

We have derived four expressions for the electromagnetic force, which are summarized in Table 1.3-1. Since we will generally use currents and  $x$  as independent variables, the two expressions for  $f_e(\mathbf{i}, x)$  are listed first in Table 1.3-1.

Before proceeding to the next section, it is important to take a moment to look back. In order to obtain  $f_e(\boldsymbol{\lambda}, x)$ , we equated the coefficients of  $dx$  in (1.3-65). If, however, we equate the coefficients of  $d\lambda_j$  in (1.3-65), we obtain

$$\sum_{j=1}^J \frac{\partial W_f(\boldsymbol{\lambda}, x)}{\partial \lambda_j} = \sum_{j=1}^J i_j(\boldsymbol{\lambda}, x) \quad (1.3-72)$$

Similarly, if we equate the coefficients of  $di_j$  in (1.3-69), we obtain

$$\sum_{j=1}^J \frac{\partial W_c(\mathbf{i}, x)}{\partial i_j} = \sum_{j=1}^J \lambda_j(\mathbf{i}, x) \quad (1.3-73)$$

TABLE 1.3-2. Electrostatic Force at Mechanical Input

$$f_e(\mathbf{e}_f, x) = \sum_{j=1}^J \left[ e_{fj} \frac{\partial q_j(\mathbf{e}_f, x)}{\partial x} \right] - \frac{\partial W_f(\mathbf{e}_f, x)}{\partial x}$$

$$f_e(\mathbf{e}_f, x) = \frac{\partial W_c(\mathbf{e}_f, x)}{\partial x}$$

$$f_e(\mathbf{q}, x) = -\frac{\partial W_f(\mathbf{q}, x)}{\partial x}$$

$$f_e(\mathbf{q}, x) = -\sum_{j=1}^J \left[ q_j \frac{\partial e_{fj}(\mathbf{q}, x)}{\partial x} \right] + \frac{\partial W_c(\mathbf{q}, x)}{\partial x}$$

Note: For rotational systems, replace  $f_e$  with  $T_e$  and  $x$  with  $\theta$ .

Equations (1.3-72) and (1.3-73) are readily verified by recalling the definitions of  $W_f$  and  $W_c$  that were obtained by holding  $x$  fixed ( $dx = 0$ ).

In Table 1.3-1, the independent variables to be used are designated in each equation by the abbreviated functional notation. Although only translational mechanical systems have been considered, all force relationships developed herein may be modified for the purpose of evaluating the torque in rotational systems. In particular, when considering a rotational system,  $f_e$  is replaced with the electromagnetic torque  $T_e$  and  $x$  with the angular displacement  $\theta$ . These substitutions are justified since the change of mechanical energy in a rotational system is expressed as

$$dW_m = -T_e d\theta \quad (1.3-74)$$

The force equation for an electromechanical system with electric coupling fields may be derived by following a procedure similar to that used in the case of magnetic coupling fields. These relationships are given in Table 1.3-2 without explanation or proof.

It is instructive to derive the expression for the electromagnetic force of a singly excited electric system as shown in Figure 1.3-3. It is clear that the expressions given in Table 1.3-1 are valid for magnetically linear or nonlinear systems. If we assume the magnetic system is linear, then  $\lambda(i, x)$  is expressed by (1.3-36) and  $W_f(i, x)$  by (1.3-39), which is also equal to the coenergy. Hence, either the first or second entry of Table 1.3-1 can be used to express  $f_e$ . In particular

$$f_e(i, x) = \frac{\partial W_c(i, x)}{\partial x} = \frac{1}{2} i^2 \frac{dL(x)}{dx} \quad (1.3-75)$$

With the convention established, a positive electromagnetic force is assumed to act in the direction of increasing  $x$ . Thus, with (1.3-15) expressed in differential form as

$$dW_m = -f_e dx \quad (1.3-76)$$

we see that energy is supplied to the coupling field from the mechanical system when  $f_e$  and  $dx$  are opposite in sign, and energy is supplied to the mechanical system from the coupling field when  $f_e$  and  $dx$  are the same in sign.

From (1.3-75) it is apparent that when the change of  $L(x)$  with respect to  $x$  is negative,  $f_e$  is negative. In the electromechanical system shown in Figure 1.3-3, the change  $L(x)$  with respect to  $x$  is always negative, therefore, the electromagnetic force is in the direction so as to pull the movable member to the stationary member. In other words, an electromagnetic force is set up so as to maximize the inductance of the coupling system, or, since reluctance is inversely proportional to the inductance, the force tends to minimize the reluctance. Since  $f_e$  is always negative in the system shown in Figure 1.3-3, energy is supplied to the coupling field from the mechanical system (generator action) when  $dx$  is positive and from the coupling field to the mechanical system (motor action) when  $dx$  is negative.

### Steady-State and Dynamic Performance of an Electromechanical System

It is instructive to consider the steady-state and dynamic performance of the elementary electromagnetic system shown in Figure 1.3-3. The differential equations that describe this system are given by (1.3-7) for the electrical system and (1.3-8) for the mechanical system. The electromagnetic force  $f_e$  is expressed by (1.3-75). If the applied voltage,  $v$ , and the applied mechanical force,  $f$ , are constant, all derivatives with respect to time are zero during steady-state operation, and the behavior can be predicted by

$$v = ri \quad (1.3-77)$$

$$f = K(x - x_0) - f_e \quad (1.3-78)$$

Equation (1.3-78) may be written as

$$-f_e = f - K(x - x_0) \quad (1.3-79)$$

The magnetic core of the system in Figure 1.3-3 is generally constructed of ferromagnetic material with a relative permeability in the order of 2000–4000. In this case, the inductance  $L(x)$  can be adequately approximated by

$$L(x) = \frac{k}{x} \quad (1.3-80)$$

In the actual system, the inductance will be a large finite value rather than infinity, as predicted by (1.3-80), when  $x = 0$ . Nevertheless, (1.3-80) is quite sufficient to illustrate the action of the system for  $x > 0$ . Substituting (1.3-80) into (1.3-75) yields

$$f_e(i, x) = -\frac{ki^2}{2x^2} \quad (1.3-81)$$

A plot of (1.3-79), with  $f_e$  replaced by (1.3-81), is shown in Figure 1.3-9 for the following system parameters [1]:

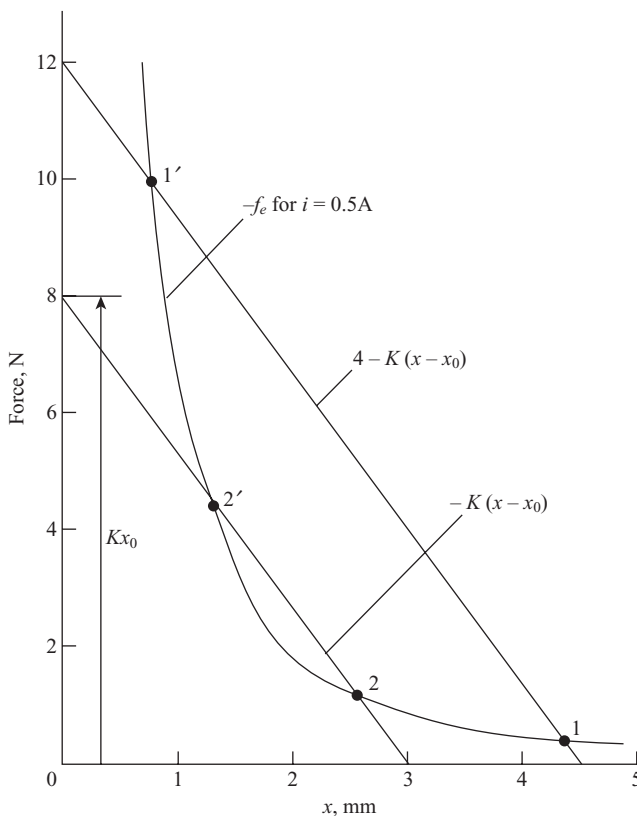


Figure 1.3-9. Steady state operation of electromechanical system shown in Figure 1.3-3.

$$r = 10 \Omega \quad x_0 = 3 \text{ mm}$$

$$K = 2667 \text{ N/m} \quad k = 6.293 \times 10^{-5} \text{ H} \cdot \text{m}$$

In Figure 1.3-9, the plot of the negative of the electromagnetic force is for an applied voltage of 5 V whereupon the steady-state current is 0.5 A. The straight lines represent the right-hand side of (1.3-79) with  $f=0$  (lower straight line) and  $f=4$  N (upper straight line). Both lines intersect the  $-f_e$  curve at two points. In particular, the upper line intersects the  $-f_e$  curve at 1 and 1'; the lower line intersects at 2 and 2'. Stable operation occurs at only points 1 and 2. The system will not operate stably at points 1' and 2'. This can be explained by assuming the system is operating at one of these points (1' and 2') and then show that any system disturbance whatsoever will cause the system to move away from these points. If, for example,  $x$  increases slightly from its value corresponding to point 1', the restraining force  $f - K(x - x_0)$  is larger in magnitude than  $-f_e$ , and  $x$  will continue to increase until the system reaches operating point 1. If  $x$  increases beyond its value corresponding to operating point 1, the restraining force is less than the electromagnetic force. Therefore, the system will establish steady-state operation at 1. If, on the other hand,  $x$  decreases from point 1', the electromagnetic

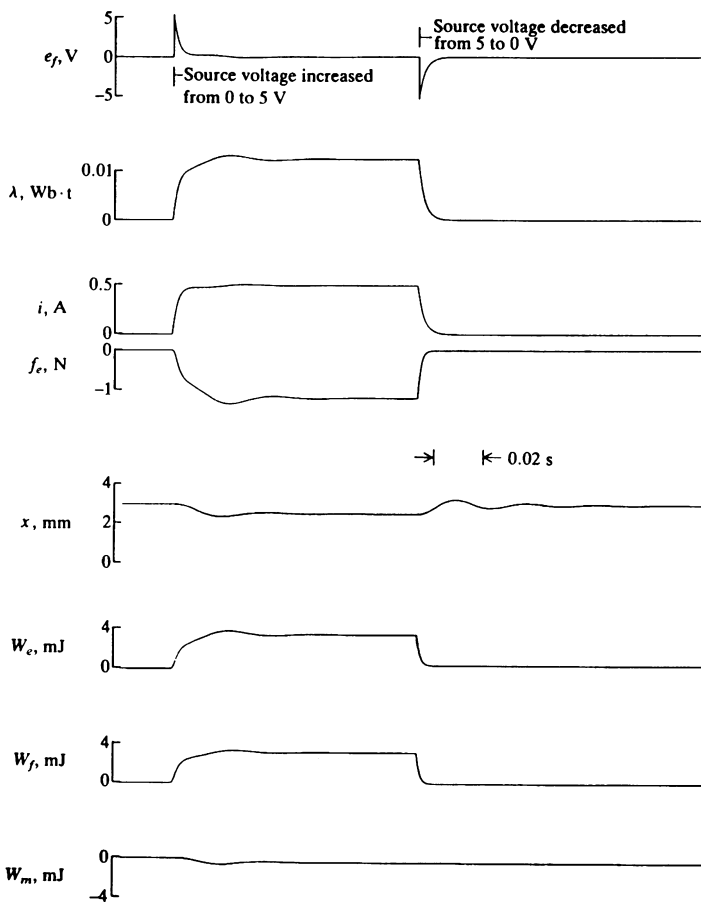


Figure 1.3-10. Dynamic performance of the electromechanical system shown in Figure 1.3-3 during step changes in the source voltage.

force is larger than the restraining force. Therefore, the movable member will move until it comes in contact with the stationary member ( $x = 0$ ). It is clear that the restraining force that yields a straight line below the  $-f_e$  curve will not permit stable operation with  $x > 0$ .

The dynamic behavior of the system during step changes in the source voltage  $v$  is shown in Figure 1.3-10, and in Figure 1.3-11 and Figure 1.3-12 for step changes in the applied force  $f$ . The following system parameters were used in addition to those given previously:

$$l = 0 \quad M = 0.055 \text{ kg} \quad D = 4 \text{ N} \cdot \text{s/m}$$

The computer traces shown in Figure 1.3-10 depict the dynamic performance of the example system when the applied voltage is stepped from 0 to 5 V and then back to 0 with the applied mechanical force held equal to 0. The following system variables:  $e_f$ ,  $\lambda$ ,  $i$ ,  $f_e$ ,  $x$ ,  $W_e$ ,  $W_f$ , and  $W_m$  are shown. The energies are plotted in millijoules (mJ). Initially, the

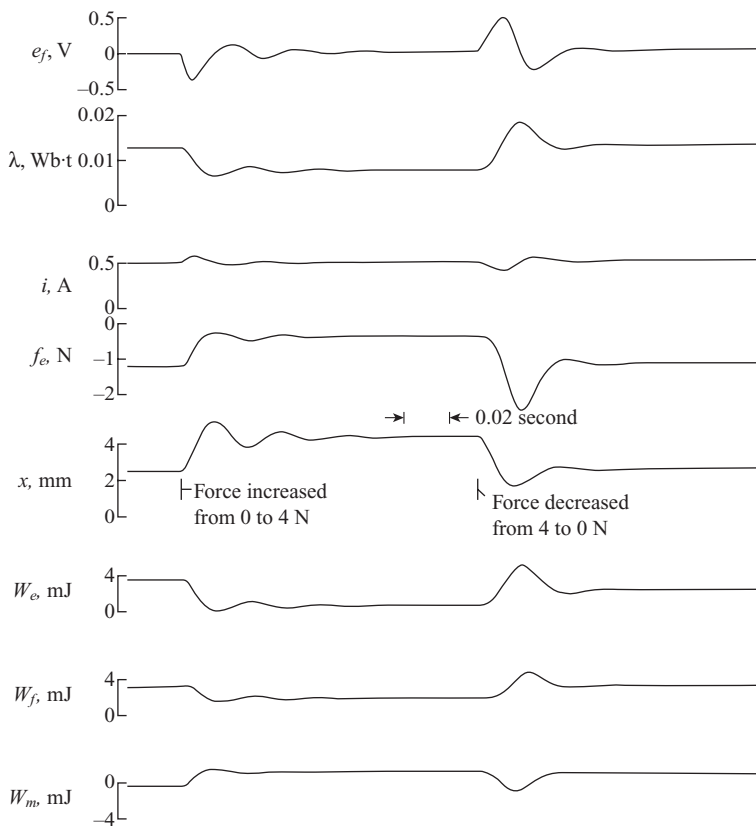


**Figure 1.3-11.** Dynamic performance of the electromechanical system shown in Figure 1.3-3 during step changes in the applied force.

mechanical system is at rest with  $x = x_0$  (3 mm). When the source voltage is applied,  $x$  decreases, and when steady-state operation is reestablished,  $x$  is approximately 2.5 mm. Energy enters the coupling field via  $W_e$ . The bulk of this energy is stored in the field ( $W_f$ ), with a smaller amount transferred to the mechanical system, some of which is dissipated in the damper during the transient period while the remainder is stored in the spring. When the applied voltage is removed, the electrical and mechanical systems return to their original states. The change in  $W_m$  is small, increasing only slightly. Hence, during the transient period, there is an interchange of energy between the spring and mass that is finally dissipated in the damper. The net change in  $W_f$  during the application and removal of the applied voltage is zero, hence the net change in  $W_e$  is positive and equal to the negative of the net change in  $W_m$ . The energy transferred to the mechanical system during this cycle is dissipated in the damper, since  $f$  is fixed at zero, and the mechanical system returns to its initial rest position with zero energy stored in the spring.

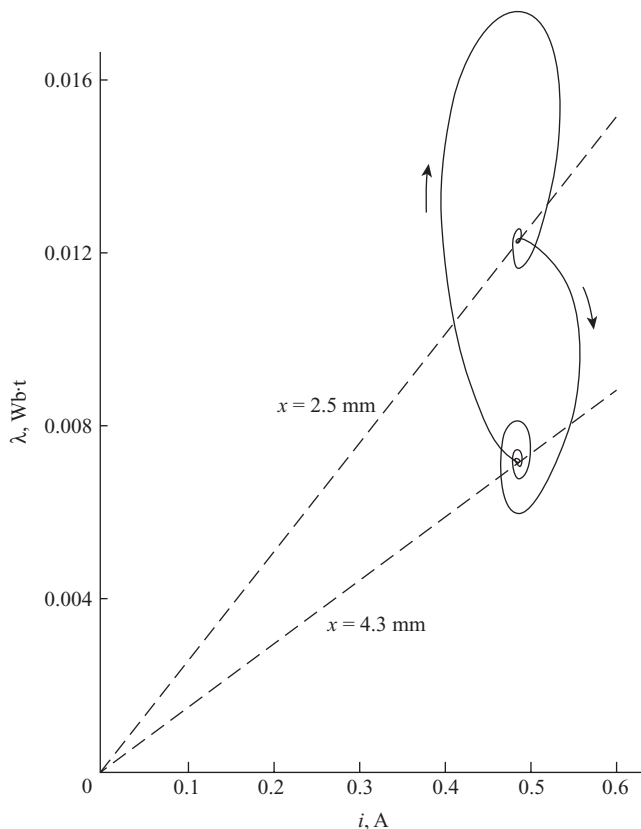
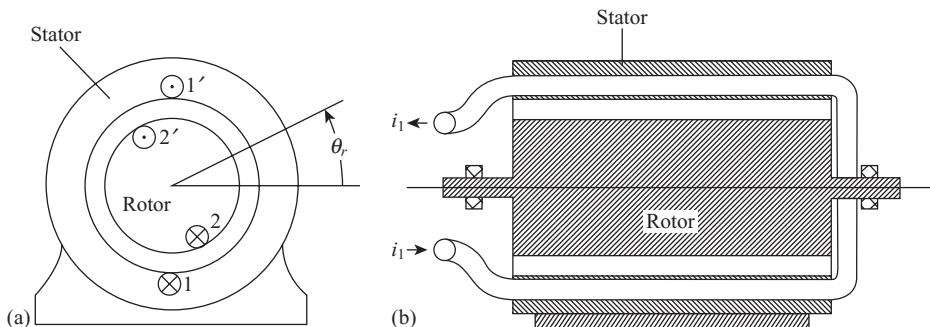


Figure 1.3-12. System response shown in Figure 1.3-3.

In Figure 1.3-11, the initial state is that shown in Figure 1.3-10, with 5 V applied to the electrical system. The mechanical force  $f$  is increased from zero to 4 N, whereupon energy enters the coupling field from the mechanical system. Energy is transferred from the coupling field to the electrical system, some coming from the mechanical system and some from the energy originally stored in the magnetic field. Next, the force is stepped back to zero from 4 N. The electrical and mechanical systems return to their original states. During the cycle, a net energy has been transferred from the mechanical system to the electrical system that is dissipated in the resistance. This cycle is depicted on the  $\lambda$ - $i$  plot shown in Figure 1.3-12.

**EXAMPLE 1B** It is helpful to formulate an expression for the electromagnetic torque of the elementary rotational device shown in Figure 1B-1. This device consists of two conductors. Conductor 1 is placed on the stationary member (stator); conductor 2 is fixed on the rotating member (rotor). The crossed lines inside a circle indicate that the assumed direction of positive current flow is into the paper (we are seeing the tail of the arrow), while a dot inside a circle indicates positive current flow is out of the paper



**Figure 1B-1.** Elementary rotational electromechanical device. (a) End view; (b) cross-sectional view.

(the point of the arrow). The length of the air gap between the stator and rotor is shown exaggerated relative to the inside diameter of the stator.

The voltage equations may be written as

$$v_1 = i_1 r_1 + \frac{d\lambda_1}{dt} \quad (1B-1)$$

$$v_2 = i_2 r_2 + \frac{d\lambda_2}{dt} \quad (1B-2)$$

where  $r_1$  and  $r_2$  are the resistances of conductor 1 and 2, respectively. The magnetic system is assumed linear; therefore the flux linkages may be expressed

$$\lambda_1 = L_{11}i_1 + L_{12}i_2 \quad (1B-3)$$

$$\lambda_2 = L_{21}i_1 + L_{22}i_2 \quad (1B-4)$$

The self-inductances  $L_{11}$  and  $L_{22}$  are constant. Let us assume that the mutual inductance may be approximated by

$$L_{12} = L_{21} = M \cos \theta_r \quad (1B-5)$$

where  $\theta_r$  is defined in Figure 1B-1. The reader should be able to justify the form of (1B-5) by considering the mutual coupling between the two conductors as  $\theta_r$  varies from 0 to  $2\pi$  rad.

$$T_e(i_1, i_2, \theta_r) = \frac{\partial W_c(i_1, i_2, \theta_r)}{\partial \theta_r} \quad (1B-6)$$

Because the magnetic system is assumed to be linear, we have

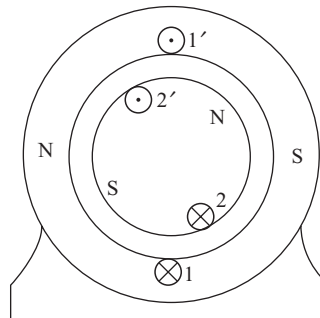


Figure 1B-2. Stator and rotor poles for constant currents.

$$W_c(i_1, i_2, \theta_r) = \frac{1}{2} L_{11} i_1^2 + L_{12} i_1 i_2 + \frac{1}{2} L_{22} i_2^2 \quad (1B-7)$$

Substituting into (1B-6) yields

$$T_e = -i_1 i_2 M \sin \theta_r \quad (1B-8)$$

Consider for a moment the form of the torque if  $i_1$  and  $i_2$  are both constant. For the positive direction of current shown, the torque is of the form

$$T_e = -K \sin \theta_r, \quad (1B-9)$$

where  $K$  is a positive constant. We can visualize the production of torque by considering the interaction of the magnetic poles produced by the current flowing in the conductors. If both  $i_1$  and  $i_2$  are positive, the poles produced are as shown in Figure 1B-2. One should recall that by definition flux issues from a north pole. Also, the stator and rotor each must be considered as separate electromagnetic systems. Thus, flux produced by the 1-1' winding issues from the north pole of the stator into the air gap. Similarly, the flux produced by the 2-2' winding enters the air gap from the north pole of the rotor. It is left to the reader to justify the fact that the range of  $\theta_r$  over which stable operation can occur for the expression of electromagnetic torque given by (1B-9) is  $-\pi/2 \leq \theta_r \leq \pi/2$ .

## 1.4. ELEMENTARY AC MACHINES

In Chapter 2, winding distributions, rotating air-gap magnetomotive force (MMF), and winding inductances common to several classes of electric machinery are derived in analytical detail. However, Example 1B has set the stage for us to take a preliminary look at what is coming in Chapter 2 from an elementary standpoint. For this purpose, let us consider a two-phase induction machine by adding two windings to Figure 1B-1; one on the stator and one on the rotor as shown in Figure 1.4-1. This device has two identical windings (same resistance and same number of turns) on the stator and two identical

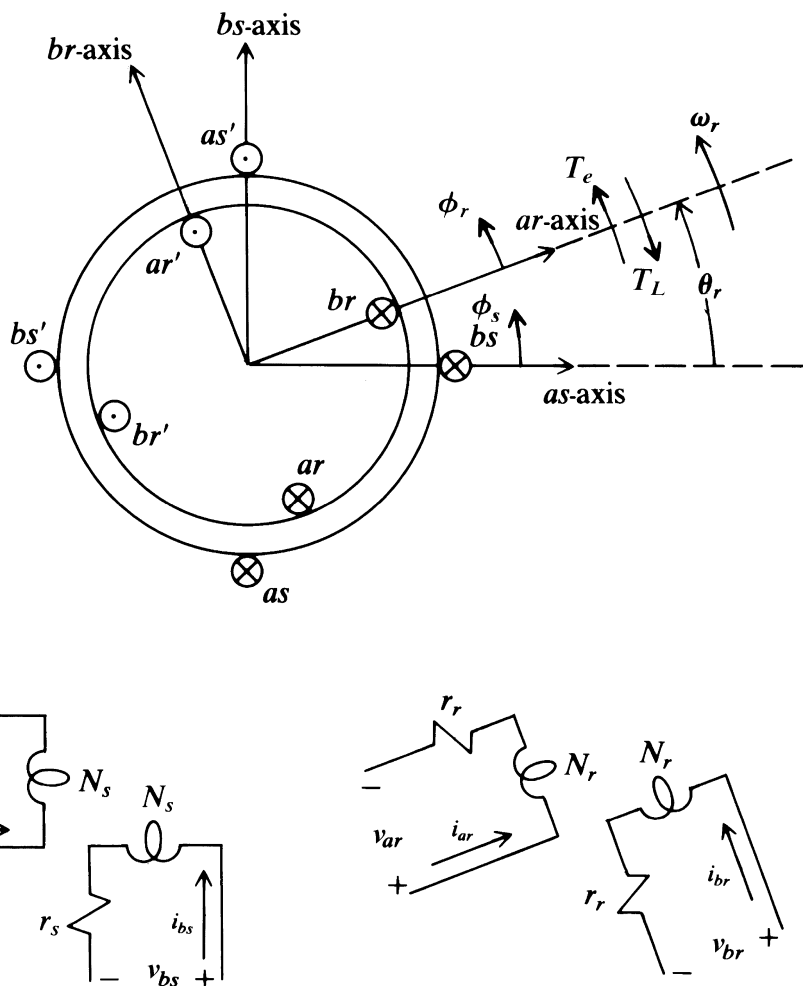


Figure 1.4-1. A two-pole, two-phase induction machine.

windings on the rotor. It is referred to as a symmetrical two-phase induction machine. We can write the flux linkage equations for the *as* and *ar* windings from our work in Example 1B. Following a similar procedure, we can write the flux linkage equations for all of the windings (assuming a linear magnetic system) as

$$\begin{bmatrix} \lambda_{as} \\ \lambda_{bs} \\ \lambda_{ar} \\ \lambda_{br} \end{bmatrix} = \begin{bmatrix} L_{asas} & 0 & L_{asar} & L_{asbr} \\ 0 & L_{bsbs} & L_{bsar} & L_{bsbr} \\ L_{aras} & L_{arbs} & L_{arar} & 0 \\ L_{bras} & L_{brbs} & 0 & L_{brbr} \end{bmatrix} \begin{bmatrix} i_{as} \\ i_{bs} \\ i_{ar} \\ i_{br} \end{bmatrix} \quad (1.4-1)$$

Because the stator (rotor) windings are identical and the air gap is uniform, the self-inductances  $L_{asas}$  and  $L_{bsbs}$  ( $L_{arar}$  and  $L_{brbr}$ ) are equal. It is clear that  $L_{asar} = L_{aras}$ ,  $L_{asbr} = L_{bras}$ , and so on. The self-inductances are constant, consisting of a leakage and a magnetizing inductance. The mutual inductances between stator and rotor phases are constant amplitude sinusoidal variations that are rotor position dependent. Thus, (1.4-1) can be written as

$$\begin{bmatrix} \lambda_{as} \\ \lambda_{bs} \\ \lambda_{ar} \\ \lambda_{br} \end{bmatrix} = \begin{bmatrix} L_{ls} + L_{ms} & 0 & L_{sr} \cos \theta_r & -L_{sr} \sin \theta_r \\ 0 & L_{ls} + L_{ms} & L_{sr} \sin \theta_r & L_{sr} \cos \theta_r \\ L_{sr} \cos \theta_r & L_{sr} \sin \theta_r & L_{lr} + L_{mr} & 0 \\ -L_{sr} \sin \theta_r & L_{sr} \cos \theta_r & 0 & L_{lr} + L_{mr} \end{bmatrix} \begin{bmatrix} i_{as} \\ i_{bs} \\ i_{ar} \\ i_{br} \end{bmatrix} \quad (1.4-2)$$

The stator self-inductances,  $L_{asas}$  and  $L_{asar} = L_{bsbs}$ , are generally expressed as  $L_{ss}$  or  $L_{ls} + L_{ms}$ , and the rotor self-inductance,  $L_{arar}$  and  $L_{brbr}$ , as  $L_{rr}$  or  $L_{lr} + L_{mr}$ . The inductance  $L_{sr}$  is the amplitude of the mutual inductances between the stator and rotor windings.

In order to take a preliminary look at a rotating air-gap MMF (rotating poles), let the stator currents be a balanced two-phase set expressed as

$$I_{as} = \sqrt{2}I_s \cos \omega_e t \quad (1.4-3)$$

$$I_{bs} = \sqrt{2}I_s \sin \omega_e t \quad (1.4-4)$$

At time zero, when  $I_{as}$  is  $\sqrt{2}I_s$  and  $I_{bs}$  is zero, the electromagnet system established by these currents is centered about the  $as$ -axis with the maximum air-gap MMF drop at the positive  $as$ -axis (to the right), which is a stator south pole, while the stator north pole is at the negative  $as$ -axis. As time progresses to where  $I_{as}$  is zero,  $I_{bs}$  is  $\sqrt{2}I_s$ , the magnetic field (poles) have rotated to where it is now centered about the  $bs$ -axis. Thus, as the electrical system “moved” or “rotated”  $(\pi/2)$  rad, the poles or air-gap MMF has moved  $(\pi/2)$  rad. Currents induced in the rotor windings create a magnetic system as well (rotor poles), and these will also rotate about the air-gap of the machine.

A four-pole, two-phase symmetrical induction machine is shown in Figure 1.4-2. In this case, the flux issuing along the  $as1$ -axis; one-half returns across the air-gap in the top half of the stator and one-half in the lower one-half. Similarly the flux issuing along the  $as2$ -axis; one-half returns across the air gap in the top one-half of the stator and one-half on the lower one-half.

It is interesting to note that when balanced two-phase currents flow in the stator windings, the air-gap MMF (poles) created by the stator currents rotate from the  $as1$ - and  $as2$ -axes to the  $bs1$ - and  $bs2$ -axes or  $(\pi/4)$  rad, while the electrical system has rotated  $(\pi/2)$  rad, as in the case of the two-pole system. In other words, the mechanical rotation of the air-gap MMF is determined by the number of poles created by the winding arrangement; however, the electrical system is unaware of the number of poles.

The flux linkage equations of the four-pole machine may be expressed as

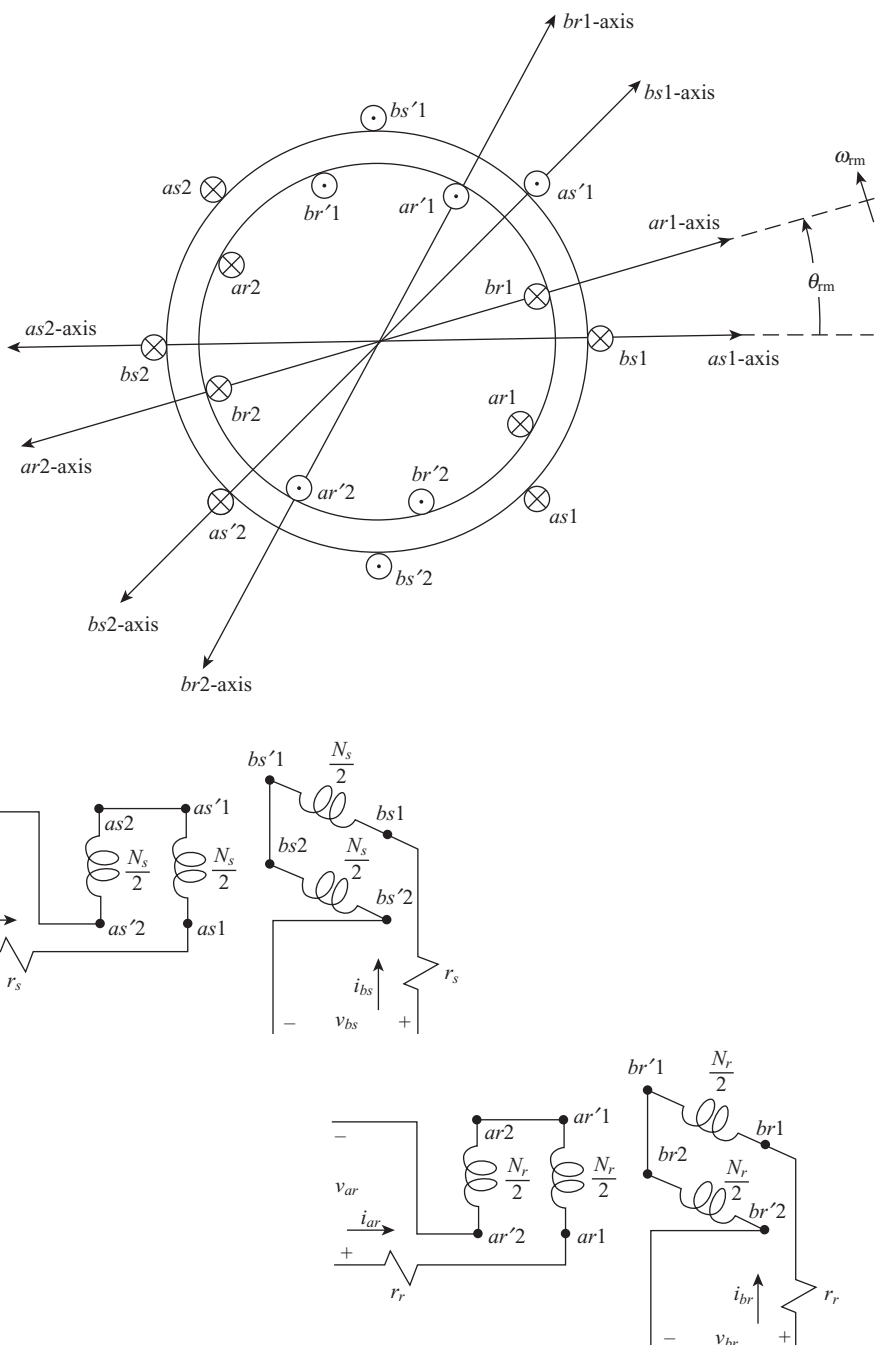


Figure 1.4-2. A four-pole, two-phase induction machine.

$$\begin{bmatrix} \lambda_{as} \\ \lambda_{bs} \\ \lambda_{ar} \\ \lambda_{br} \end{bmatrix} = \begin{bmatrix} L_{ls} + L_{ms} & 0 & L_{sr} \cos 2\theta_{rm} & -L_{sr} \sin 2\theta_{rm} \\ 0 & L_{ls} + L_{ms} & L_{sr} \sin 2\theta_{rm} & L_{sr} \cos 2\theta_{rm} \\ L_{sr} \cos 2\theta_{rm} & L_{sr} \sin 2\theta_{rm} & L_{lr} + L_{mr} & 0 \\ -L_{sr} \sin 2\theta_{rm} & L_{sr} \cos 2\theta_{rm} & 0 & L_{lr} + L_{mr} \end{bmatrix} \begin{bmatrix} i_{as} \\ i_{bs} \\ i_{ar} \\ i_{br} \end{bmatrix} \quad (1.4-5)$$

where  $\theta_{rm}$  is the mechanical displacement of the rotor. We will distinguish it from  $\theta_r$  presently.

It is important to note the difference between (1.4-2), the flux linkage equations for a two-pole machine, and (1.4-5) for a four-pole machine. Clearly, the inductances will generally be different in magnitude; however, the notable difference is that  $\theta_r$  is the angular displacement for the two-pole while  $\theta_{rm}$  is the displacement for the four-pole. In particular, we see from comparing (1.4-2) and (1.4-5) that if we substituted  $\theta_r$  for  $2\theta_{rm}$ , then the two equations would be identical in form. In general, we can define

$$\theta_r = \frac{P}{2} \theta_{rm} \quad (1.4-6)$$

This relation allows us to assume that all machines are two-pole machines, whereupon (1.4-2) will be the form of the flux linkage equations regardless of the number of poles. This appears reasonable in light of the previous discussion of the rotation of the magnetic poles produced by two-pole and four-pole machines. The displacement  $\theta_r$  is then referred to as the electrical angular displacement of the rotor. The actual angular rotor displacement can always be determined from (1.4-6). It follows that

$$\omega_r = \frac{P}{2} \omega_{rm} \quad (1.4-7)$$

where  $\omega_r$  is the electrical angular velocity of the rotor and  $\omega_{rm}$  is the actual angular velocity. We will find that we can consider all machines as two-pole devices and take the  $P/2$  factor into account when evaluating the torque.

An elementary two-pole, three-phase symmetrical induction machine is shown in Figure 1.4-3. Here, the flux linkage equations may be expressed as

$$\begin{bmatrix} \lambda_{abcs} \\ \lambda_{abcr} \end{bmatrix} = \begin{bmatrix} \mathbf{L}_s & \mathbf{L}_{sr} \\ (\mathbf{L}_{sr})^T & \mathbf{L}_r \end{bmatrix} \begin{bmatrix} \mathbf{i}_{abcs} \\ \mathbf{i}_{abcr} \end{bmatrix} \quad (1.4-8)$$

where

$$(\mathbf{f}_{abcs})^T = [f_{as} \ f_{bs} \ f_{cs}] \quad (1.4-9)$$

$$(\mathbf{f}_{abcr})^T = [f_{ar} \ f_{br} \ f_{cr}] \quad (1.4-10)$$

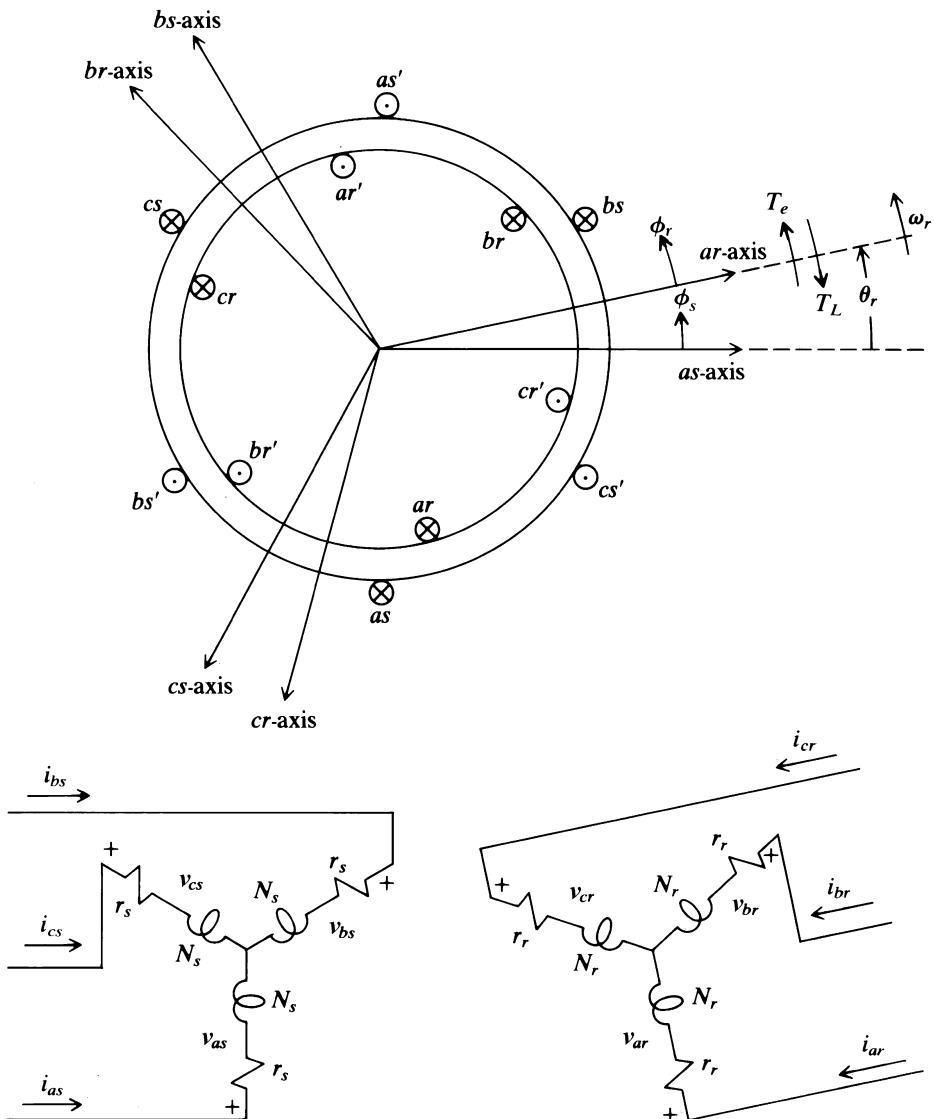


Figure 1.4-3. A two-pole, three-phase induction machine.

As a first approximation (a more detailed representation will be considered in Chapter 2),

$$\mathbf{L}_s = \begin{bmatrix} L_{ls} + L_{ms} & -\frac{1}{2}L_{ms} & -\frac{1}{2}L_{ms} \\ -\frac{1}{2}L_{ms} & L_{ls} + L_{ms} & -\frac{1}{2}L_{ms} \\ -\frac{1}{2}L_{ms} & -\frac{1}{2}L_{ms} & L_{ls} + L_{ms} \end{bmatrix} \quad (1.4-11)$$

$$\mathbf{L}_r = \begin{bmatrix} L_{lr} + L_{mr} & -\frac{1}{2}L_{mr} & -\frac{1}{2}L_{mr} \\ -\frac{1}{2}L_{mr} & L_{lr} + L_{mr} & -\frac{1}{2}L_{mr} \\ -\frac{1}{2}L_{mr} & -\frac{1}{2}L_{mr} & L_{lr} + L_{mr} \end{bmatrix} \quad (1.4-12)$$

$$\mathbf{L}_{sr} = L_{sr} \begin{bmatrix} \cos \theta_r & \cos\left(\theta_r + \frac{2\pi}{3}\right) & \cos\left(\theta_r - \frac{2\pi}{3}\right) \\ \cos\left(\theta_r - \frac{2\pi}{3}\right) & \cos \theta_r & \cos\left(\theta_r + \frac{2\pi}{3}\right) \\ \cos\left(\theta_r + \frac{2\pi}{3}\right) & \cos\left(\theta_r - \frac{2\pi}{3}\right) & \cos \theta_r \end{bmatrix} \quad (1.4-13)$$

We see that the three-phase stator (rotor) windings are coupled, unlike the two-phase machine (Fig. 1.4-1). The difference in coupling is also true for the four-pole, two-phase machine (Fig. 1.4-2). Why?

Although the above inductance matrices are rigorously derived in Chapter 2, we can get a “first look” from a simplistic consideration. We have previously defined the leakage, magnetizing, and mutual inductances; it is now the off-diagonal terms of  $\mathbf{L}_s$  and  $\mathbf{L}_r$  that are of concern. To explain these terms, let us first consider the coupling between the  $as$  and  $bs$  windings. They are displaced  $(2/3)\pi$  from each other. Let us assume that we can take the  $bs$ -winding and turn (twist) it clockwise through the stator iron for  $(2/3)\pi$  rad, whereupon it would be “on top” of the  $as$ -winding. In this case, the mutual inductance between the  $as$  and  $bs$  windings would be  $L_{ms}$ , neglecting any coupling of the leakage fluxes. Now let us turn the  $bs$ -winding counterclockwise back through the stator iron. The mutual inductance would vary as  $L_{ms}\cos\alpha$ , where  $\alpha$  is the angle measured counterclockwise from the  $as$ -axes; when we reach  $\alpha = (\pi/2)$ , there is no coupling between the two windings, just as in the case of the two-phase machine. When we have twisted the  $bs$ -winding back to its original position, the mutual inductance is  $L_{ms}\cos(2\pi/3)$  or  $-(1/2)L_{ms}$ . Following this type of simplistic reasoning, we can justify all of the off-diagonal terms of  $\mathbf{L}_s$  and  $\mathbf{L}_r$ .

In Chapter 2, we will derive the expressions for all inductances as functions of machine dimensions and the type of winding distribution; however, the resulting form of the inductance matrices are nearly the same as given in (1.4-11)–(1.4-13).

An elementary two-pole, two-phase synchronous machine is shown in Figure 1.4-4. The flux linkage equations may be expressed as

$$\begin{bmatrix} \lambda_{as} \\ \lambda_{bs} \\ \lambda_{fd} \end{bmatrix} = \begin{bmatrix} L_{ls} + L_A - L_B \cos 2\theta_r & -L_B \cos 2\theta_r & L_{sfd} \sin \theta_r \\ -L_B \cos 2\theta_r & L_{ls} + L_A + L_B \cos 2\theta_r & -L_{sfd} \cos \theta_r \\ L_{sfd} \sin \theta_r & -L_{sfd} \cos \theta_r & L_{bfd} + L_{mfd} \end{bmatrix} \begin{bmatrix} i_{as} \\ i_{bs} \\ i_{fd} \end{bmatrix} \quad (1.4-14)$$

The stator windings are identical in that they have the same resistance and the same number of turns.

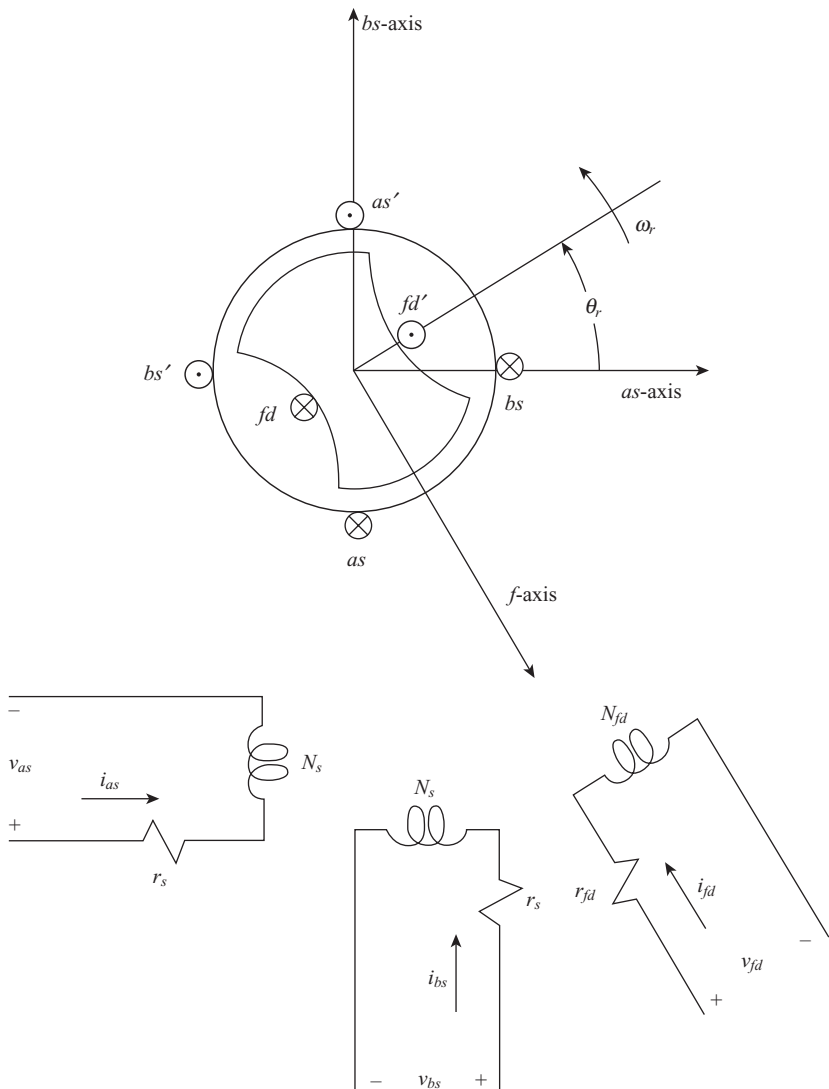


Figure 1.4-4. A two-pole, two-phase, salient-pole synchronous machine.

Due to the saliency of the rotor, the stator windings experience a change in self-inductance as the rotor rotates, which is here approximated as a double-angle variation about an average value. Moreover, the saliency of the rotor also causes a mutual coupling between the orthogonal stator windings. It is interesting that the  $L_B$  associated with the self-inductances is also the coefficient of the double-angle mutual inductance between stator phases. This is shown in Chapter 2. It is left to the reader to show that the mutual inductance between the stator phases is a negative with the direction of rotation and the current directions given in Figure 1.4-4.

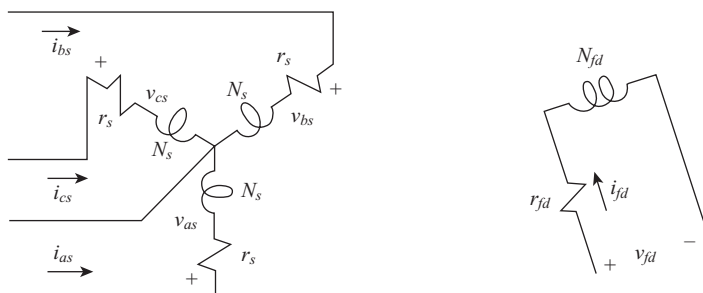
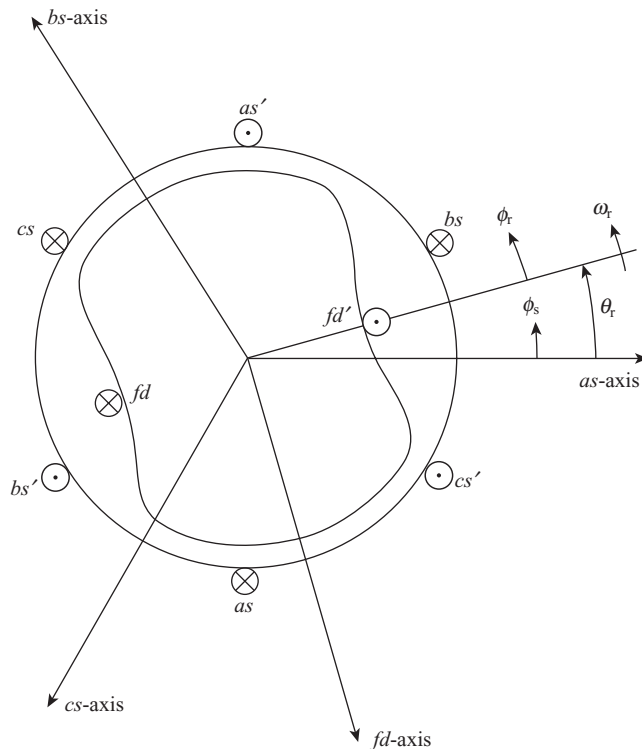


Figure 1.4-5. A two-pole, three-phase, salient-pole synchronous machine.

An elementary two-pole, three-phase synchronous machine is shown in Figure 1.4-5. The flux linkage equations may be written as

$$\begin{bmatrix} \lambda_{abcs} \\ \lambda_{fd} \end{bmatrix} = \begin{bmatrix} \mathbf{L}_s & L_{sfd} \sin \theta_r \\ \mathbf{L}_{sf} & L_{lfd} + L_{mfd} \end{bmatrix} \begin{bmatrix} \mathbf{i}_{abcs} \\ i_{fd} \end{bmatrix} \quad (1.4-15)$$

where

$$\mathbf{L}_s = \begin{bmatrix} L_{ls} + L_A - L_B \cos 2\theta_r & -\frac{1}{2}L_A - L_B \cos 2\left(\theta_r - \frac{\pi}{3}\right) & -\frac{1}{2}L_A - L_B \cos 2\left(\theta_r + \frac{\pi}{3}\right) \\ -\frac{1}{2}L_A - L_B \cos 2\left(\theta_r - \frac{\pi}{3}\right) & L_{ls} + L_A - L_B \cos 2\left(\theta_r - \frac{2\pi}{3}\right) & -\frac{1}{2}L_A - L_B \cos 2(\theta_r + \pi) \\ -\frac{1}{2}L_A - L_B \cos 2\left(\theta_r + \frac{\pi}{3}\right) & -\frac{1}{2}L_A - L_B \cos 2(\theta_r + \pi) & L_{ls} + L_A - L_B \cos 2\left(\theta_r + \frac{2\pi}{3}\right) \end{bmatrix} \quad (1.4-16)$$

where

$$\mathbf{L}_{sf} = \begin{bmatrix} L_{sfd} \sin \theta_r & L_{sfd} \sin \left(\theta_r - \frac{2\pi}{3}\right) & L_{sfd} \sin \left(\theta_r + \frac{2\pi}{3}\right) \end{bmatrix} \quad (1.4-17)$$

It is left to the reader to verify the stator mutual inductances. A practical synchronous machine is equipped with damper windings on the rotor that by induction motor action, damp low-frequency oscillations about a steady-state operating point. The inductances associated with these windings are incorporated in the performance analysis of synchronous machines in Chapter 5.

## REFERENCE

- [1] D.C. White and H.H. Woodson, Electromechanical Energy Conversion, John Wiley and Sons, New York, 1959.

## PROBLEMS

1. A two-winding, iron-core transformer is shown in Figure 1P-1.  $N_1 = 50$  turns,  $N_2 = 100$  turns, and  $\mu_R = 4000$ . Calculate  $L_{m1}$  and  $L_{m2}$ .
2. Repeat Problem 1 if the iron core has an air gap of 0.2 cm in length and is cut through the complete cross section. Assume that fringing (a curvature of the flux lines around the air gap) does not occur; that is, the flux lines follow a straight path through the air gap in which the effective cross-sectional area is 25 cm<sup>2</sup>.
3. Two coupled coils have the following parameters:

$$\begin{aligned} L_{11} &= 100 \text{ mH} & r_1 &= 10 \Omega \\ L_{22} &= 25 \text{ mH} & r_2 &= 2.5 \Omega \\ N_1 &= 1000 \text{ turns} & N_2 &= 500 \text{ turns} \\ L_{l1} &= 0.1L_{11} & L_{l2} &= 0.1L_{22} \end{aligned}$$

Develop an equivalent T circuit with coil 1 as the reference coil. Repeat with coil 2 as the reference coil.

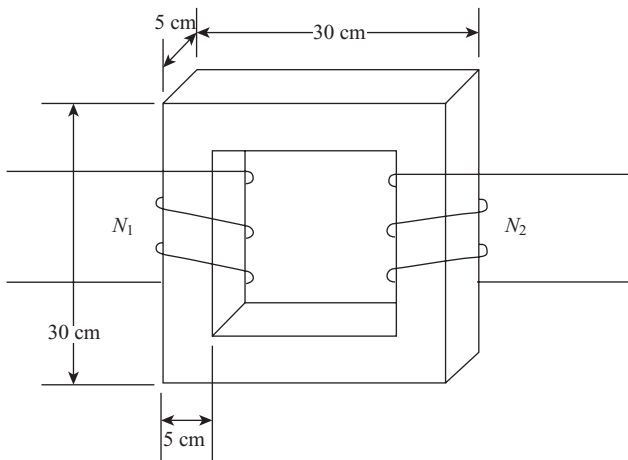


Figure 1P-1. Two-winding, iron-core transformer.

4. A system with two windings has a flux linkage versus current profile of

$$\lambda_1 = \left( 0.1 + \frac{0.03}{x} \right) i_1 - \frac{0.01}{x} i_2$$

$$\lambda_2 = \left( 0.0111 + \frac{0.03}{9x} \right) i_2 - \frac{0.01}{x} i_1$$

The resistance of the coils is  $r_1 = 1 \Omega$  and  $r_2 = 0.3 \Omega$ , respectively. The winding voltage equations can be expressed in a form (where  $p = d/dt$ ):

$$v_1 = r_1 i_1 + p\lambda_1$$

$$v_2 = r_2 i_2 + p\lambda_2$$

- (a) Derive the equivalent T circuit model for this system, assuming coil 1 as the reference. Show all component values. Label directions of all currents and voltages.
- (b) For this system, describe two conditions where you cannot make the common approximation that  $|\tilde{I}_1| \approx |\tilde{I}_2|$ .
5. A constant 10 V is suddenly applied to coil 1 of the coupled circuits given in Problem 3. Coil 2 is short-circuited. Calculate the transient and steady-state current flowing in each coil.
6. Determine the input impedance of the coupled circuits given in Problem 3 if the applied frequency to coil 1 is 60 Hz with coil 2 (a) open-circuited and (b) short-circuited. Repeat (b) with the current flowing in the magnetizing reactance neglected.
7. A third coil is wound on the ferromagnetic core shown in Figure 1.2-1. The resistance is  $r_3$  and the leakage and magnetizing inductances are  $L_{l3}$  and  $L_{m3}$ , respectively. The coil is wound so that positive current ( $i_3$ ) produces  $\Phi_{m3}$  in the same direction

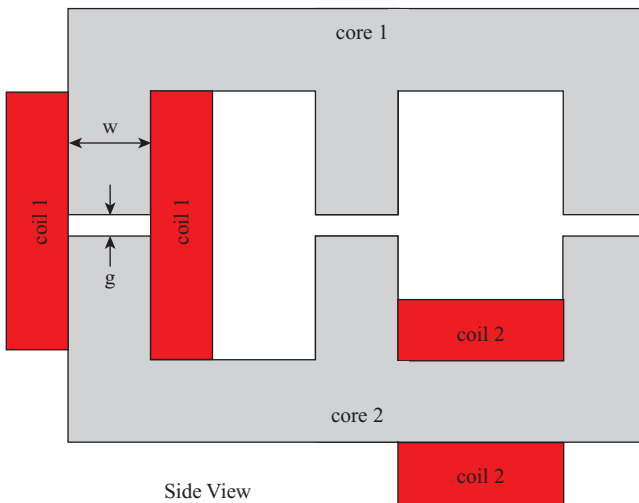


Figure 1P-2. EE iron-core transformer.

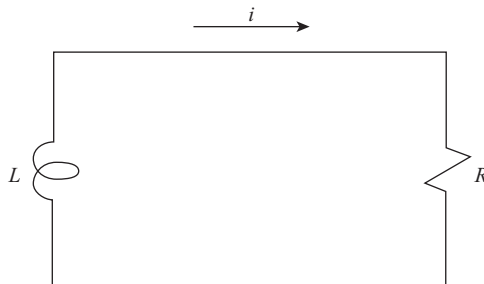


Figure 1P-3.  $R-L$  circuit.

as  $\Phi_{m1}$  and  $\Phi_{m2}$ . Derive the equivalent T circuit for this three-winding transformer. Actually, one should be able to develop the equivalent circuit without derivation.

8. Consider the magnetic device shown in Figure 1P-2, which is commonly referred to as an E-core. The permeability of the cores is infinite,  $g = \pi \text{ mm}$ ,  $w = 2.5 \text{ cm}$ , and the depth into the page is 10 cm. Coil 1 has  $I_1 = 10\cos 100t \text{ A}$ , 100 turns, and positive current causes the positive flux direction to be upward. Coil 2 has  $I_2 = 40\cos 100t \text{ A}$ , 100 turns, and positive current causes positive flux to travel to the left through the coil. The resistance of both coils, fringing around the gaps, and leakage fluxes are all negligible. Determine the voltage across coil 2 as a function of time.
9. Use  $\Sigma$  and  $1/p$  to denote summation and integration, respectively. Draw a time-domain block diagram for two coupled windings with saturation and (a) with leakage inductance and (b) without leakage inductance.
10. A resistor and an inductor are connected as shown in Figure 1P-3 with  $R = 15 \Omega$  and  $L = 250 \text{ mH}$ . Determine the energy stored in the inductor  $W_{eS}$  and the energy dissipated by the resistor  $W_{eL}$  for  $i > 0$  if  $i(0) = 10 \text{ A}$ .

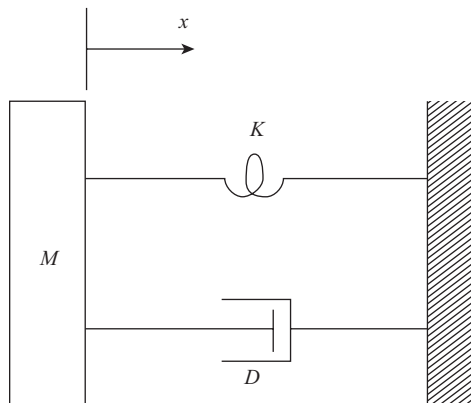


Figure 1P-4. Spring-mass-damper system.

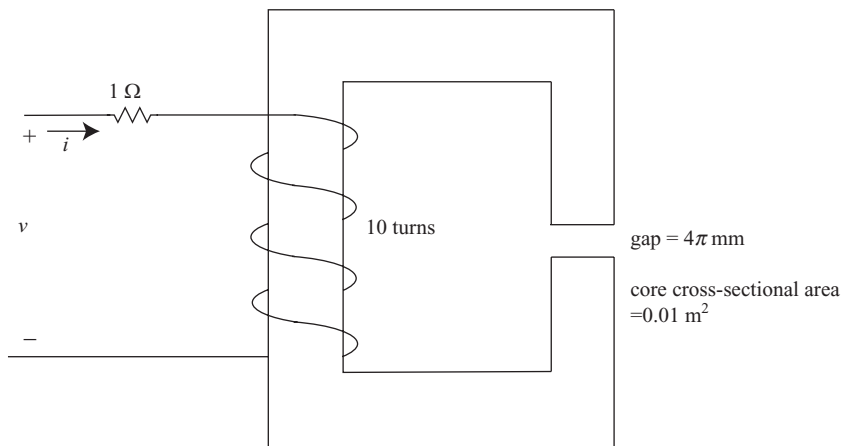


Figure 1P-5. C-core inductor.

11. Consider the spring-mass-damper system shown in Figure 1P-4. At  $t = 0$ ,  $x(0) = x_0$  (rest position) and  $dx/dt = 1.5$  m/s.  $M = 0.8$  kg,  $D = 10$  N·s/m and  $K = 120$  N·m. For  $t > 0$ , determine the energy stored in the spring  $W_{mS1}$ , the kinetic energy of the mass  $W_{mS2}$ , and the energy dissipated by the damper  $W_{mL}$ .
12. True/false: Magnetic hysteresis leads to a field that is nonconservative. Explain.
13. For the system shown in Figure 1P-5, which is often referred to as a “C-core,” determine the winding inductance if the leakage inductance is 1/10 the magnetizing inductance. If 10 V is applied to the winding at  $t = 0$  second, determine  $W_f$  and the force of attraction that acts to attempt to reduce the gap at  $t = 1$  second. Where is the energy of the coupling field stored in this system?
14. Given the UU-core transformer shown in Figure 1P-6. Assume leakage inductances and the MMF drop across the core is negligible. The cross-sectional area of the

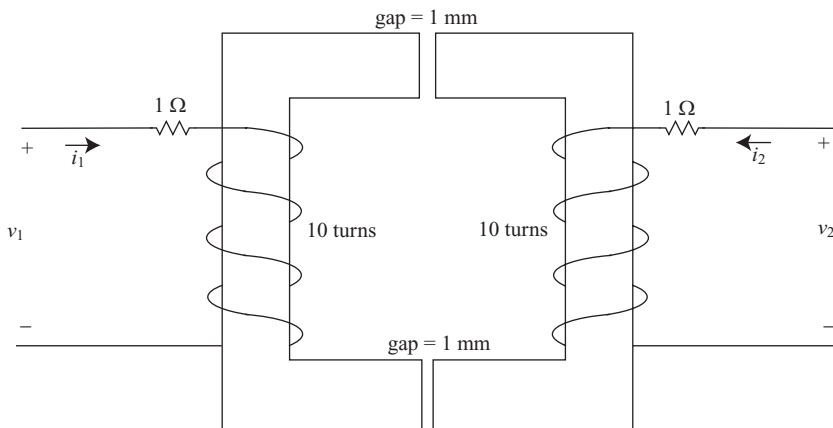


Figure 1P-6. UU-core transformer for Problem 14.

core is  $15.9154 \text{ m}^2$ . At  $t = 0$  second, an input voltage of  $v_1 = 10 \text{ V}$  is applied. The secondary is open-circuited. At  $t = 1$  second, the primary is open circuited and  $i_1$  goes from  $6.32 \text{ A}$  to  $0$  instantaneously. At the same instant, the secondary is short-circuited  $i_2$  goes from  $0$  to  $6.32 \text{ A}$  instantaneously. Determine  $W_E$ ,  $W_f$ ,  $W_{eL}$ , and  $W_m$  for  $t \geq 0$  second.

15. Express  $W_f(i, x)$  and  $W_c(i, x)$  for (a)  $\lambda(i, x) = i^{2/3}x^2$ ; (b)  $\lambda(i, x) = ki \sin(x/a)\pi - xi$ .
16. The energy stored in the coupling field of a magnetically linear system with two electrical inputs may be expressed as

$$W_f(\lambda_1, \lambda_2, x) = \frac{1}{2} B_{11}\lambda_1^2 + B_{12}\lambda_1\lambda_2 + \frac{1}{2} B_{22}\lambda_2^2$$

Express  $B_{11}$ ,  $B_{12}$ , and  $B_{22}$  in terms of inductances  $L_{11}$ ,  $L_{12}$ , and  $L_{22}$ .

17. An electromechanical system has two electrical inputs. The flux linkages may be expressed as

$$\lambda_1(i_1, i_2, x) = x^2 i_1^2 + xi_2$$

$$\lambda_2(i_1, i_2, x) = x^2 i_2^2 + xi_1$$

Express  $W_f(i_1, i_2, x)$  and  $W_c(i_1, i_2, x)$ .

18. Express  $f_e(i, x)$  for the electromechanical systems described by the relations given in Problem 15.
19. Express  $f_e(i_1, i_2, x)$  for the electromechanical system given in Problem 17.
20. The flux-linkage equations for a two-phase electromagnetic device are expressed as:

$$\lambda_{as} = 5i_{as} - 3\cos(2\theta_{rm})(i_{as} + i_{bs})^{1/2} + 2\cos(\theta_{rm})$$

$$\lambda_{bs} = 5i_{bs} - 3\cos(2\theta_{rm})(i_{as} + i_{bs})^{1/2} + 2\sin(\theta_{rm})$$

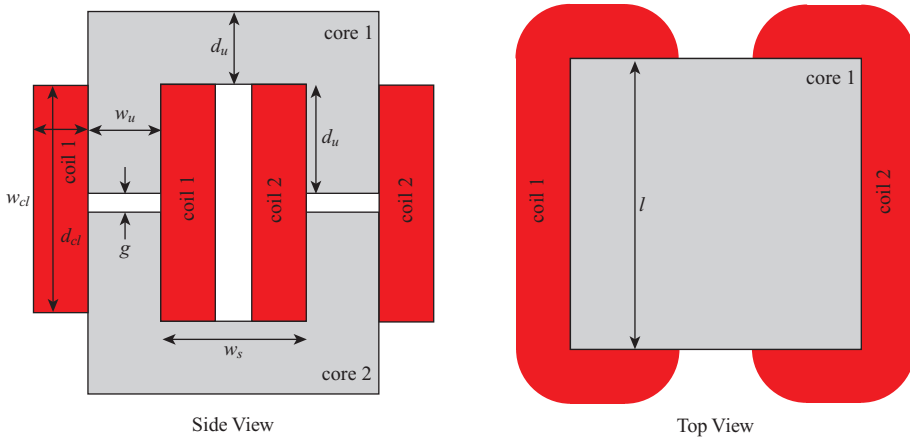


Figure 1P-7. UU-core transformer for Problem 21.

where  $\theta_m$  is the mechanical rotor position. Determine an expression for torque in terms of  $i_{as}$ ,  $i_{bs}$ , and  $\theta_m$ . Assume that both currents are greater than or equal to zero.

21. Consider the UU-core transformer shown in Figure 1P-7. Each coil is wound in a direction such that positive current will cause positive flux to flow in a clockwise direction. Neglecting leakage and fringing flux, derive an expression for the electromagnetic force of attraction between the cores in terms of the coil currents  $i_1$  and  $i_2$ , turns  $N_1$  and  $N_2$ ,  $\mu_0$ ,  $\mu_r$ , and the dimensions given in the figure.
22. Consider an electromechanical system whose flux-linkage equations given by

$$\lambda_1 = 5i_1 + 10\left(1 - \frac{1}{1+i_m}\right)\cos\theta_r$$

$$\lambda_2 = i_2 + 20\left(1 - \frac{1}{1+i_m}\right)\cos\theta_r$$

where  $i_1 \geq 0$ ,  $i_2 \geq 0$ ,  $i_m = i_1 + 2i_2$  and where  $\theta_r$  is the mechanical rotor position. Derive expressions for the coenergy and torque in terms of  $i_1$ ,  $i_2$ , and  $\theta_r$ .

23. Derive an expression for the forces  $f_{el}(\mathbf{i}, x_1, x_2)$  and  $f_{e2}(\mathbf{i}, x_1, x_2)$  in an electromechanical system with two degrees of mechanical motion.
24. For the multicore system shown in Figure 1P-8, assume the components are fixed with  $x_1 = x_2 = 1$  mm. The core cross-sectional area is  $0.05 \text{ m}^2$ ,  $I_1 = 10 \cos 377t \text{ A}$ ,  $I_2 = -20 \cos 377t \text{ A}$ . Determine the force acting on all components and  $W_c$  of the system at  $t = 1$  second. Neglect leakage flux.
25. Refer to Figure 1.3-6. As the system moves from  $x_a$  to  $x_b$ , the  $\lambda-i$  trajectory moves from  $A$  to  $B$  where both  $A$  and  $B$  are steady-state operating conditions. Does the voltage  $v$  increase or decrease? Does the applied force  $f$  increase or decrease? Explain.

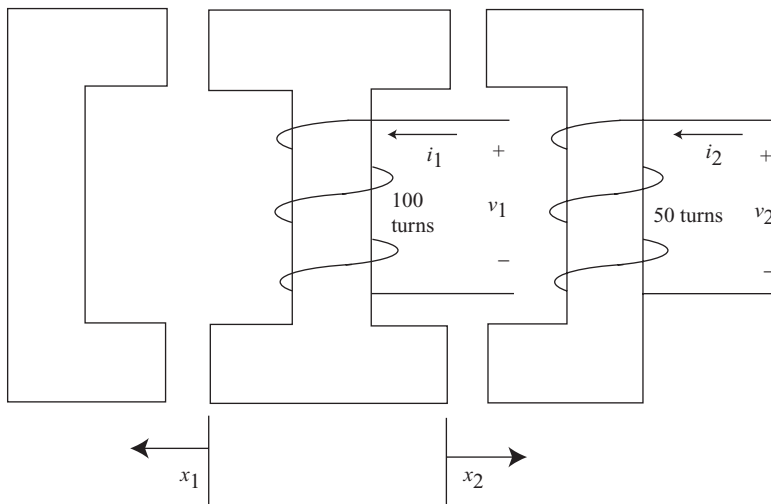


Figure 1P-8. Multicore system.

26. Refer to Figure 1.3-10. Following the system transients due to the application of the source voltage ( $v = 5$  V), the system assumes steady-state operation. For this steady-state operation, calculate  $W_{eS}$ ,  $W_f$ , and  $W_{mS}$ .
27. Refer to Figure 1.3-11. Repeat Problem 26 for steady-state operation following the application of  $f = 4N$ .
28. Refer to Figure 1.3-12. Identify the area corresponding to  $\Delta W_m$  when (a)  $x$  moves from 2.5 mm to 4.3 mm, and when (b)  $x$  moves from 4.3 to 2.5 mm.
29. Assume the steady-state currents flowing in the conductors of the device shown in Figure 1B-1 are

$$I_1 = I_{s1} \cos \omega_1 t$$

$$I_2 = I_{s2} \cos(\omega_2 t + \varphi_2)$$

Assume also that during steady-state operation the rotor speed is constant, thus

$$\theta_r = \omega_r t + \theta_r(0)$$

where  $\theta_r(0)$  is the rotor displacement at time zero. Determine the rotor speeds at which the device produces a nonzero average torque during steady-state operation if (a)  $\omega_1 = \omega_2 = 0$ ; (b)  $\omega_1 = \omega_2 \neq 0$ ; (c)  $\omega_2 = 0$ .

30. An elementary two-pole, two-phase, salient-pole synchronous machine is shown in Figure 1.4-4. The winding inductances may be expressed as

$$L_{asas} = L_{ls} + L_A - L_B \cos 2\theta_r$$

$$L_{bsbs} = L_{ls} + L_A + L_B \cos 2\theta_r$$

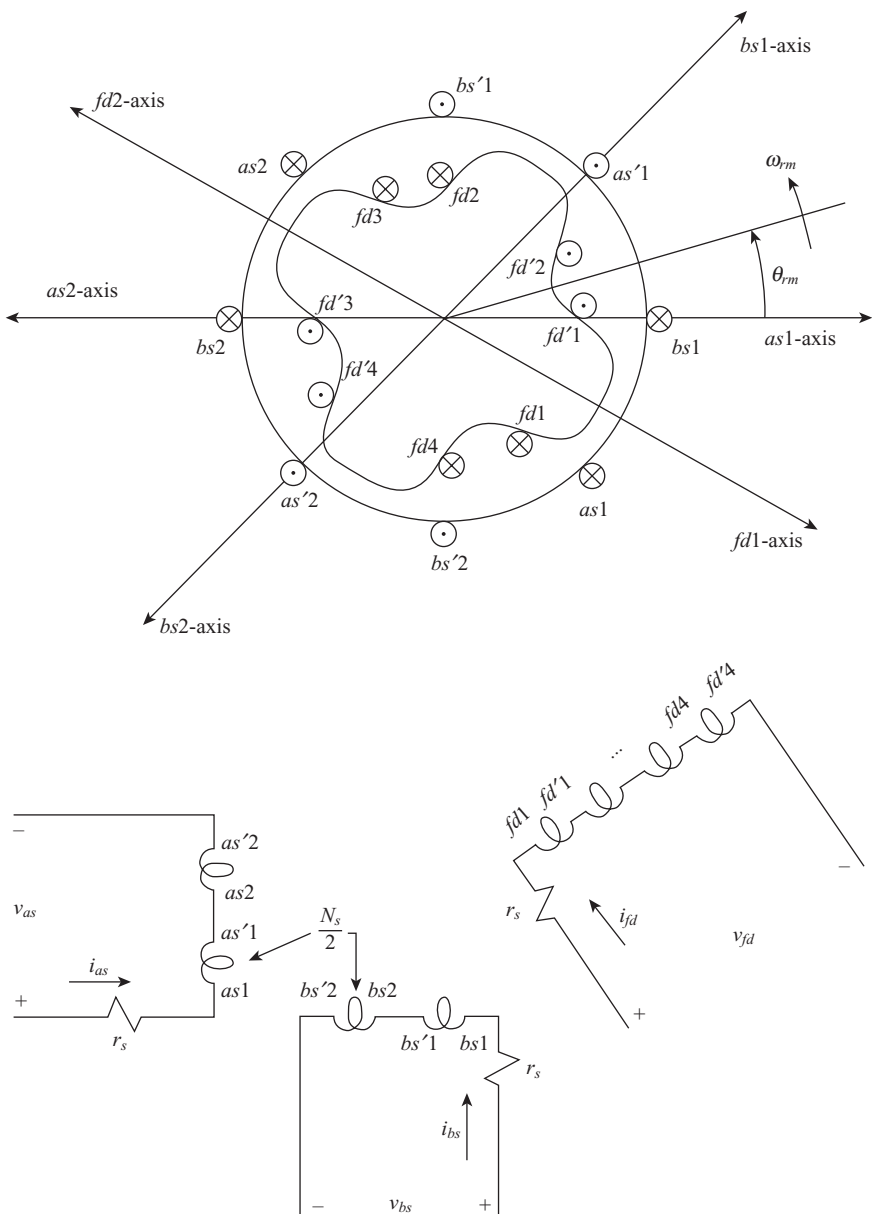


Figure 1P-9. Elementary four-pole, two-phase, salient-pole synchronous machine.

$$L_{asbs} = -L_B \sin 2\theta_r$$

$$L_{fdfd} = L_{lfd} + L_{mfd}$$

$$L_{asfd} = L_{sfd} \sin \theta_r$$

$$L_{bsfd} = -L_{sfd} \cos \theta_r$$

Modify these inductance relationships so that they will describe a two-phase, uniform air-gap synchronous machine.

31. Write the voltage equations for the elementary two-pole, two-phase, salient-pole synchronous machine shown in Figure 1.4-4 and derive the expression for  $T_e(i_{as}, i_{bs}, i_{fd}, \theta_r)$ .
32. An elementary four-pole, two-phase, salient-pole synchronous machine is shown in Figure 1P-9. Use this machine as a guide to derive expressions for the winding inductances of a  $P$ -pole synchronous machine. Show that these inductances are of the same form as those given in Problem 30 if  $(P/2)\theta_{rm}$  is replaced by  $\theta_r$ .
33. Derive an expression for the electromagnetic  $T_e(i_{as}, i_{bs}, i_{fd}, \theta_r)$ , for a  $P$ -pole, two-phase, salient-pole synchronous machine. This expression should be identical in form to that obtained in Problem 31 multiplied by  $P/2$ .
34. A reluctance machine has no field winding on the rotor. Modify the inductance relationships given in Problem 30 so as to describe the winding inductances of a two-pole, two-phase, reluctance machine. Write the voltage equations and derive an expression for  $T_e(i_{as}, i_{bs}, \theta_r)$ .
35. An elementary two-pole, two-phase, symmetrical induction machine is shown in Figure 1.4-1. If  $L_{asas} = L_{ls} + L_{ms}$ ,  $L_{arar} = L_{lr} + L_{mr}$ , and  $L_{asar} = L_{sr} \cos \theta_r$ , express the remaining self- and mutual inductances of all stator and rotor windings. Following the transformer derivation, refer the rotor quantities to the stator quantities. Express the stator and rotor flux linkages in terms of the referred variables.
36. Write the voltage equations for the induction machine shown in Figure 1.4-1 and derive an expression for the electromagnetic torque  $T_e(i_{as}, i_{bs}, i'_{ar}, i'_{br}, \theta_r)$  using the results obtained in Problem 35.
37. An elementary four-pole, two-phase, symmetrical induction machine is shown in Figure 1.4-2. Use this machine as a guide to derive expressions for the winding inductances of a  $P$ -pole induction machine. Show that these inductances are of the same form as those given in Problem 35 if  $(P/2)\theta_{rm}$  is replaced by  $\theta_r$ .

---

# DISTRIBUTED WINDINGS IN AC MACHINERY

---

## 2.1. INTRODUCTION

Many ac machines are designed based on the concept of a distributed winding. In these machines, the goal is to establish a continuously rotating set of north and south poles on the stator (the stationary part of the machine), which interact with an equal number of north and south poles on the rotor (the rotating part of the machine), to produce uniform torque. There are several concepts that are needed to study this type of electric machinery. These concepts include distributed windings, winding functions, rotating MMF waves, and inductances and resistances of distributed windings. These principles are presented in this chapter and used to develop the voltage and flux-linkage equations of synchronous and induction machines. The voltage and flux linkage equations for permanent magnet ac machines, which are also considered in this text, will be set forth in Chapter 4 and derived in Chapter 15. In each case, it will be shown that the flux-linkage equations of these machines are rather complicated because they contain rotor position-dependent terms. Recall from Chapter 1 that rotor position dependence is necessary if energy conversion is to take place. In Chapter 3, we will see that the complexity of the flux-linkage equations can be greatly reduced by introducing a change of variables that eliminates the rotor position-dependent terms.

---

*Analysis of Electric Machinery and Drive Systems*, Third Edition. Paul Krause, Oleg Wasenczuk, Scott Sudhoff, and Steven Pekarek.

© 2013 Institute of Electrical and Electronics Engineers, Inc. Published 2013 by John Wiley & Sons, Inc.

## 2.2. DESCRIBING DISTRIBUTED WINDINGS

A photograph of a stator of a 3.7-kW 1800-rpm induction motor is shown in Figure 2.2-1, where the stator core can be seen inside the stator housing. The core includes the stator slots in between the stator teeth. The slots are filled with slot conductors which, along with the end turns, form complete coils. The windings of the machine are termed distributed because they are not wound as simple coils, but are rather wound in a spatially distributed fashion.

To begin our development, consider Figure 2.2-2, which depicts a generic electrical machine. The stationary stator and rotating rotor are labeled, but details such as the stator slots, windings, and rotor construction are omitted. The stator reference axis may be considered to be mechanically attached to the stator, and the rotor reference axis to

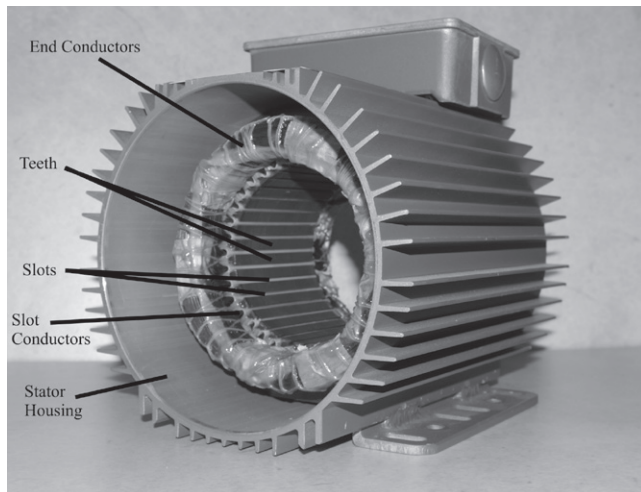


Figure 2.2-1. Distributed winding stator.

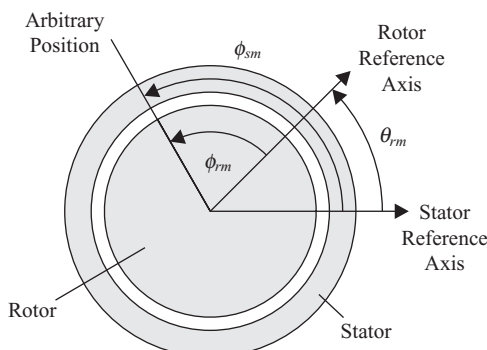


Figure 2.2-2. Definition of position measurements.

the rotor. Angles defined in Figure 2.2-2 include position measured relative to the stator, denoted by  $\phi_{sm}$ , position measured relative to the rotor, denoted by  $\phi_{rm}$ , and the position of the rotor relative to the stator, denoted by  $\theta_{rm}$ . The mechanical rotor speed is the time derivative of  $\theta_{rm}$  and is denoted by  $\omega_{rm}$ .

The position of a given feature can be described using either  $\phi_{sm}$  or  $\phi_{rm}$ ; however, if we are describing the same feature using both of these quantities, then these two measures of angular position are related by

$$\theta_{rm} + \phi_{rm} = \phi_{sm} \quad (2.2-1)$$

Much of our analysis may be expressed either in terms of  $\phi_{sm}$  or  $\phi_{rm}$ . As such, we will use  $\phi_m$  as a generic symbol to stand for either quantity, as appropriate.

The goal of a distributed winding is to create a set of uniformly rotating poles on the stator that interact with an equal number of poles on the rotor. The number of poles on the stator will be designated  $P$ , and must be an even number. The number of poles largely determines the relationship between the rotor speed and the ac electrical frequency. Figure 2.2-3 illustrates the operation of 2-, 4-, and 6-pole machines. Therein  $N_s$ ,  $S_s$ ,  $N_r$ , and  $S_r$  denote north stator, south stator, north rotor, and south rotor poles, respectively. A north pole is where positive flux leaves a magnetic material and a south pole is where flux enters a magnetic material. Electromagnetic torque production results from the interaction between the stator and rotor poles.

When analyzing machines with more than two poles, it is convenient to define equivalent “electrical” angles of the positions and speed. In particular, define

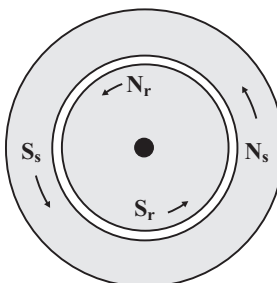
$$\phi_s \triangleq P\phi_{sm} / 2 \quad (2.2-2)$$

$$\phi_r \triangleq P\phi_{rm} / 2 \quad (2.2-3)$$

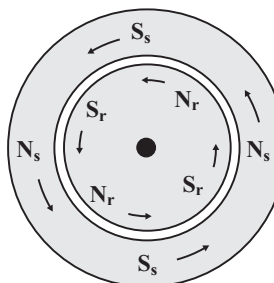
$$\theta_r \triangleq P\theta_{rm} / 2 \quad (2.2-4)$$

$$\omega_r \triangleq P\omega_{rm} / 2 \quad (2.2-5)$$

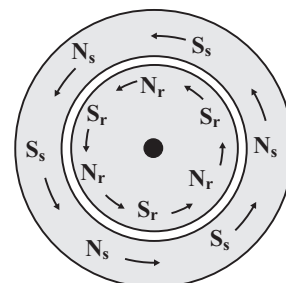
In terms of electrical position, (2.2-1) becomes



$$P = 2$$



$$P = 4$$



$$P = 6$$

Figure 2.2-3.  $P$ -pole machines.

$$\theta_r + \phi_r = \phi_s. \quad (2.2-6)$$

Finally, it is also useful to define a generic position as

$$\phi \triangleq P\phi_m / 2 \quad (2.2-7)$$

The reason for the introduction of these electrical angles is that it will allow our analysis to be expressed so that all machines mathematically appear to be two-pole machines, thereby providing considerable simplification.

## Discrete Description of Distributed Windings

Distributed windings, such as those shown in Figure 2.2-1, may be described using either a discrete or continuous formulation. The discrete description is based on the number of conductors in each slot; the continuous description is an abstraction based on an ideal distribution. A continuously distributed winding is desirable in order to achieve uniform torque. However, the conductors that make up the winding are not placed continuously around the stator, but are rather placed into slots in the machine's stator and rotor structures, thereby leaving room for the stator and rotor teeth, which are needed to conduct magnetic flux. Thus, a discrete winding distribution is used to approximate a continuous ideal winding. In reality, the situation is more subtle than this. Since the slots and conductors have physical size, all distributions are continuous when viewed with sufficient resolution. Thus, the primary difference between these two descriptions is one of how we describe the winding mathematically. We will find that both descriptions have advantages in different situations, and so we will consider both.

Figure 2.2-4 illustrates the stator of a machine in which the stator windings are located in eight slots. The notation  $N_{as,i}$  in Figure 2.2-4 indicates the number of conductors in the  $i$ 'th slot of the "as" stator winding. These conductors are shown as open circles, as conductors may be positive (coming out of the page or towards the front of the machine) or negative (going into the page or toward the back of the machine).

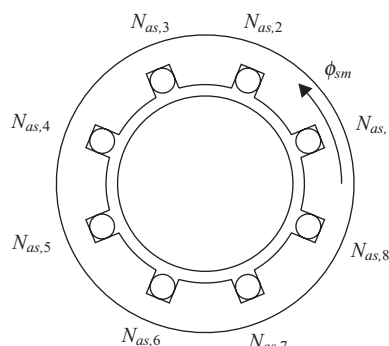


Figure 2.2-4. Slot structure.

Generalizing this notation,  $N_{x,i}$  is the number of conductors in slot  $i$  of winding (or phase)  $x$  coming out of the page (or towards the front of the machine). In this example,  $x = "as."$  Often, a slot will contain conductors from multiple windings (phases). It is important to note that  $N_{x,i}$  is a signed quantity—and that half the  $N_{as,i}$  values will be negative since for every conductor that comes out of the page, a conductor goes into the page.

The center of the  $i$ 'th slot and  $i$ 'th tooth are located at

$$\phi_{ys,i} = \pi(2i-2) / S_y + \phi_{ys,1} \quad (2.2-8)$$

$$\phi_{yt,i} = \pi(2i-3) / S_y + \phi_{ys,1} \quad (2.2-9)$$

respectively, where  $S_y$  is the number of slots, “y” = “s” for the stator (in which case  $\phi_{ys,i}$  and  $\phi_{yt,i}$  are relative to the stator) and “y” = “r” for the rotor (in which case  $\phi_{ys,i}$  and  $\phi_{yt,i}$  are relative to the rotor), and  $\phi_{ys,1}$  is the position of slot 1.

Since the number of conductors going into the page must be equal to the number of conductors out of the page (the conductor is formed into closed loops), we have that

$$\sum_{i=1}^{S_y} N_{x,i} = 0 \quad (2.2-10)$$

where “x” designates the winding (e.g., “as”). The total number of turns associated with the winding may be expressed

$$N_x = \sum_{i=1}^{S_y} N_{x,i} u(N_{x,i}) \quad (2.2-11)$$

where  $u(\cdot)$  is the unit step function, which is one if its argument is greater or equal to zero, and zero otherwise.

In (2.2-11) and throughout this work, we will use  $N_x$  to represent the total number of conductors associated with winding “x,”  $N_{x,i}$  to be the number of conductors in the  $i$ 'th slot, and  $\mathbf{N}_x$  to be a vector whose elements correspond to the number of conductors in each slot. In addition, if all the windings of stator or rotor have the same number of conductors, we will use the notation  $N_y$  to denote the number of conductors in the stator or rotor windings. For example, if  $N_{as} = N_{bs} = N_{cs}$ , then we will denote the number of conductors in these windings as  $N_s$ .

It is sometimes convenient to illustrate features of a machine using a developed diagram. In the developed diagram, spatial features (such as the location of the conductors) are depicted against a linear axis. In essence, the machine becomes “unrolled.” This process is best illustrated by example; Figure 2.2-5 is the developed diagram corresponding to Figure 2.2-4. Note the independent axis is directed to the left rather than to the right. This is a convention that has been traditionally adopted in order to avoid the need to “flip” the diagram in three-dimensions.

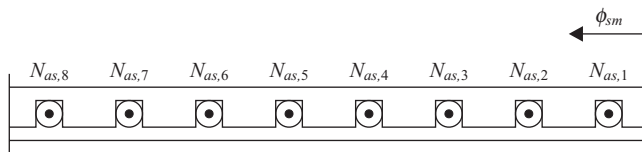


Figure 2.2-5. Developed diagram.

## Continuous Description of Distributed Windings

Machine windings are placed into slots in order to provide room for stator teeth and rotor teeth, which together form a low reluctance path for magnetic flux between the stator and rotor. The use of a large number of slots allows the winding to be distributed, albeit in a discretized fashion. The continuous description of the distributed winding describes the winding in terms of what it is desired to approximate—a truly distributed winding. The continuous description is based on conductor density, which is a measure of the number of conductors per radian as a function of position. As an example, we would describe winding “ $x$ ” of a machine with the turns density  $n_x(\phi_m)$ , where “ $x$ ” again denotes the winding (such as “as”). The conductor density may be positive or negative; positive conductors are considered herein to be out of the page (toward the front of the machine).

The conductor density is often a sinusoidal function of position. A common choice for the  $a$ -phase stator conductor density in three-phase ac machinery is

$$n_{as}(\phi_{sm}) = N_{s1} \sin(P\phi_{sm} / 2) - N_{s3} \sin(3P\phi_{sm} / 2) \quad (2.2-12)$$

In this function, the first term represents the desired distribution; the second term allows for more effective slot utilization. This is explored in Problem 6 at the end of the chapter.

It will often be of interest to determine the total number of conductors associated with a winding. This number is readily found by integrating the conductor density over all regions of positive conductors, so that the total number of conductors may be expressed

$$N_x = \int_0^{2\pi} n_x(\phi_m) u(n_x(\phi_m)) d\phi_m \quad (2.2-13)$$

## Symmetry Conditions on Conductor Distributions

Throughout this work, it is assumed that the conductor distribution obeys certain symmetry conditions. The first of these is that the distribution of conductors is periodic in a number of slots corresponding to the number of pole pairs. In particular, it is assumed that

$$N_{x,i+2s_y/P} = N_{x,i} \quad (2.2-14)$$

Second, it is assumed that the distribution of conductors is odd-half wave symmetric over a number of slots corresponding to one pole. This is to say

$$N_{x,i+S_y/P} = -N_{x,i} \quad (2.2-15)$$

While it is possible to construct an electric machine where these conditions are not met, the vast majority of electric machines satisfy these conditions. In the case of the continuous winding distribution, the conditions corresponding to (2.2-14) and (2.2-15) may be expressed as

$$n_x(\phi_m + 4\pi / P) = n_x(\phi_m) \quad (2.2-16)$$

$$n_x(\phi_m + 2\pi / P) = -n_x(\phi_m) \quad (2.2-17)$$

## Converting Between Discrete and Continuous Descriptions of Distributed Windings

Suppose that we have a discrete description of a winding consisting of the number of conductors of each phase in the slots. The conductor density could be expressed

$$n_x(\phi_m) = \sum_{i=1}^{S_y} N_{x,i} \delta(\phi_m - \phi_{ys,i}) \quad (2.2-18)$$

where  $\delta(\cdot)$  is the unit impulse function and  $\phi_m$  is relative to the stator or rotor reference axis for a stator or rotor winding, respectively.

Although (2.2-18) is in a sense a continuous description, normally we desire an idealized representation of the conductor distribution. To this end, we may represent the conductor distribution as a single-sided Fourier series of the form

$$n_x(\phi_m) = \sum_{j=1}^J a_j \cos(j\phi_m) + b_j \sin(j\phi_m) \quad (2.2-19)$$

where  $J$  is the number of terms used in the series, and where

$$a_j = \frac{1}{\pi} \int_0^{2\pi} n_x(\phi_m) \cos(j\phi_m) d\phi_m \quad (2.2-20)$$

$$b_j = \frac{1}{\pi} \int_0^{2\pi} n_x(\phi_m) \sin(j\phi_m) d\phi_m \quad (2.2-21)$$

Substitution of (2.2-18) into (2.2-20) and (2.2-21) yields

$$a_j = \frac{1}{\pi} \sum_{i=1}^{S_y} N_{x,i} \cos(j\phi_{ys,i}) \quad (2.2-22)$$

$$b_j = \frac{1}{\pi} \sum_{i=1}^{S_y} N_{x,i} \sin(j\phi_{ys,i}) \quad (2.2-23)$$

Thus (2.2-19), along with (2.2-22) and (2.2-23), can be used to convert a discrete winding description to a continuous one.

It is also possible to translate a continuous winding description to a discrete one. To this end, one approach is to lump all conductors into the closest slot. This entails adding (or integrating, since we are dealing with a continuous function) all conductors within  $\pi/S_y$  of the center of the  $i$ 'th slot and to consider them to be associated with the  $i$ 'th slot. This yields

$$N_{x,i} = \text{round} \left( \int_{\phi_{ys,i}-\pi/S_y}^{\phi_{ys,i}+\pi/S_y} n_x(\phi_m) d\phi_m \right) \quad (2.2-24)$$

where  $\text{round}(\ )$  denotes a function which rounds the result to the next nearest integer.

## End Conductors

The conductor segments that make up the windings of a machine can be broken into two classes—slot conductors and end conductors. These are shown in Figure 2.2-1. Normally, our focus in describing a winding is on the slot conductors, which are the portions of the conductors in the slots and which are oriented in the axial direction. The reason for this focus is that slot conductors establish the field in the machine and are involved in torque production. However, the portions of the conductors outside of the slots, referred to as end conductors, are also important, because they impact the winding resistance and inductance. Therefore, it is important to be able to describe the number of conductor segments on the front and back ends of the machine connecting the slot conductor segments together. In this section, we will consider the calculation of the number of end conductor segments.

Herein, we will focus our discussion on a discrete winding description. Consider Figure 2.2-6, which is a version of a developed diagram of the machine, except that instead of looking into the front of the machine, we are looking from the center of the machine outward in the radial direction. Therein,  $N_{x,i}$  denotes the number of winding  $x$  conductors in the  $i$ 'th slot. Variables  $L_{x,i}$  and  $R_{x,i}$  denote the number of positive end conductor in front of the  $i$ 'th tooth directed to the left or right, respectively. These variables are required to be greater than or equal to zero. The net number of conductors directed in the counterclockwise direction when viewed from the front of the  $i$ 'th tooth is denoted  $M_{x,i}$ . In particular

$$M_{x,i} = L_{x,i} - R_{x,i} \quad (2.2-25)$$

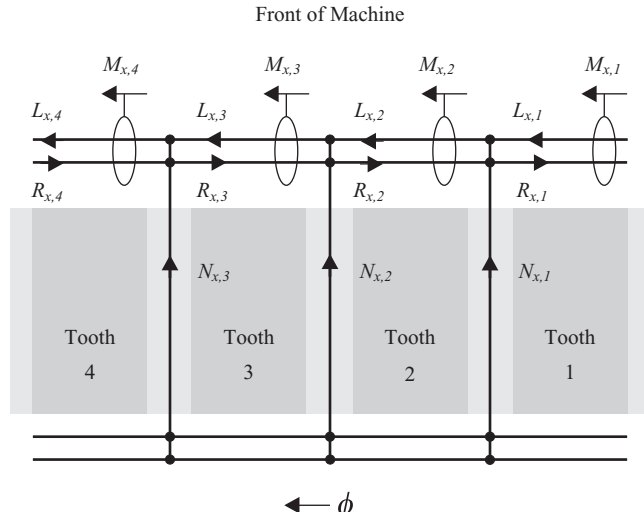


Figure 2.2-6. End conductors.

Unlike  $L_{x,i}$  and  $R_{x,i}$ ,  $M_{x,i}$  can be positive or negative. The number of canceled conductors in front of the  $i$ 'th tooth is denoted  $C_{x,i}$ . This quantity is defined as

$$C_{x,i} = \min(L_{x,i}, R_{x,i}) \quad (2.2-26)$$

Canceled conductors are undesirable in that they add to losses; however, some winding arrangements use them for manufacturing reasons.

It is possible to relate  $M_{x,i}$  to the number of conductors in the slots. From Figure 2.2-6, it is apparent that

$$M_{x,i} = M_{x,i-1} + N_{x,i-1} \quad (2.2-27)$$

where the index operations are ring mapped (i.e.,  $S_y + 1 \rightarrow 1, 1 - 1 \rightarrow S_y$ ). The total number of (unsigned) end conductors between slots  $i - 1$  and  $i$  is

$$E_{x,i} = |M_{x,i}| + 2C_{x,i} \quad (2.2-28)$$

The total number of end conductors is defined as

$$E_x = \sum_{i=1}^{S_y} E_{x,i} \quad (2.2-29)$$

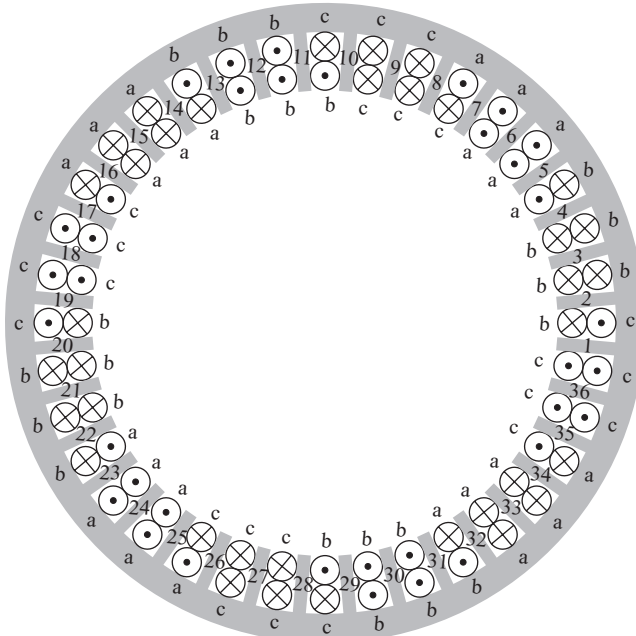


**Figure 2.2-7.** Stator winding for a four-pole 36-slot machine.

### Common Winding Arrangements

Before proceeding, it is convenient to consider a practical machine winding scheme. Consider the four-pole 3.7-kW 1800-rpm induction machine shown in Figure 2.2-1. As can be seen, the stator has 36 slots, which corresponds to three slots per pole per phase. Figure 2.2-7 illustrates a common winding pattern for such a machine. Therein, each conductor symbol represents  $N$  conductors, going in or coming out as indicated. This is a double layer winding, with each slot containing two groups of conductors. Both single- and double-layer winding arrangements are common in electric machinery. The number of  $a$ -phase conductors for the first 18 slots may be expressed as

$$N_{as}|_{1-18} = N[0\ 0\ 0\ 1\ 2\ 2\ 1\ 0\ 0\ 0\ 0\ -1\ -2\ -2\ -1\ 0\ 0]. \quad (2.2-30)$$

From (2.2-27)

$$\mathbf{M}_{as}|_{1-18} = \mathbf{M}_{as,36} + N[0\ 0\ 0\ 0\ 1\ 3\ 5\ 6\ 6\ 6\ 6\ 6\ 5\ 3\ 1\ 0\ 0]. \quad (2.2-31)$$

To proceed further, more details on the winding arrangement are needed.

Figure 2.2-8 illustrates some possible winding arrangements. In each case, the figure depicts the stator of a machine in an “unrolled” fashion similar to a developed diagram. However, the vantage point is that of an observer looking at the teeth from the center of the machine. Thus, each shaded area represents a tooth of the machine.

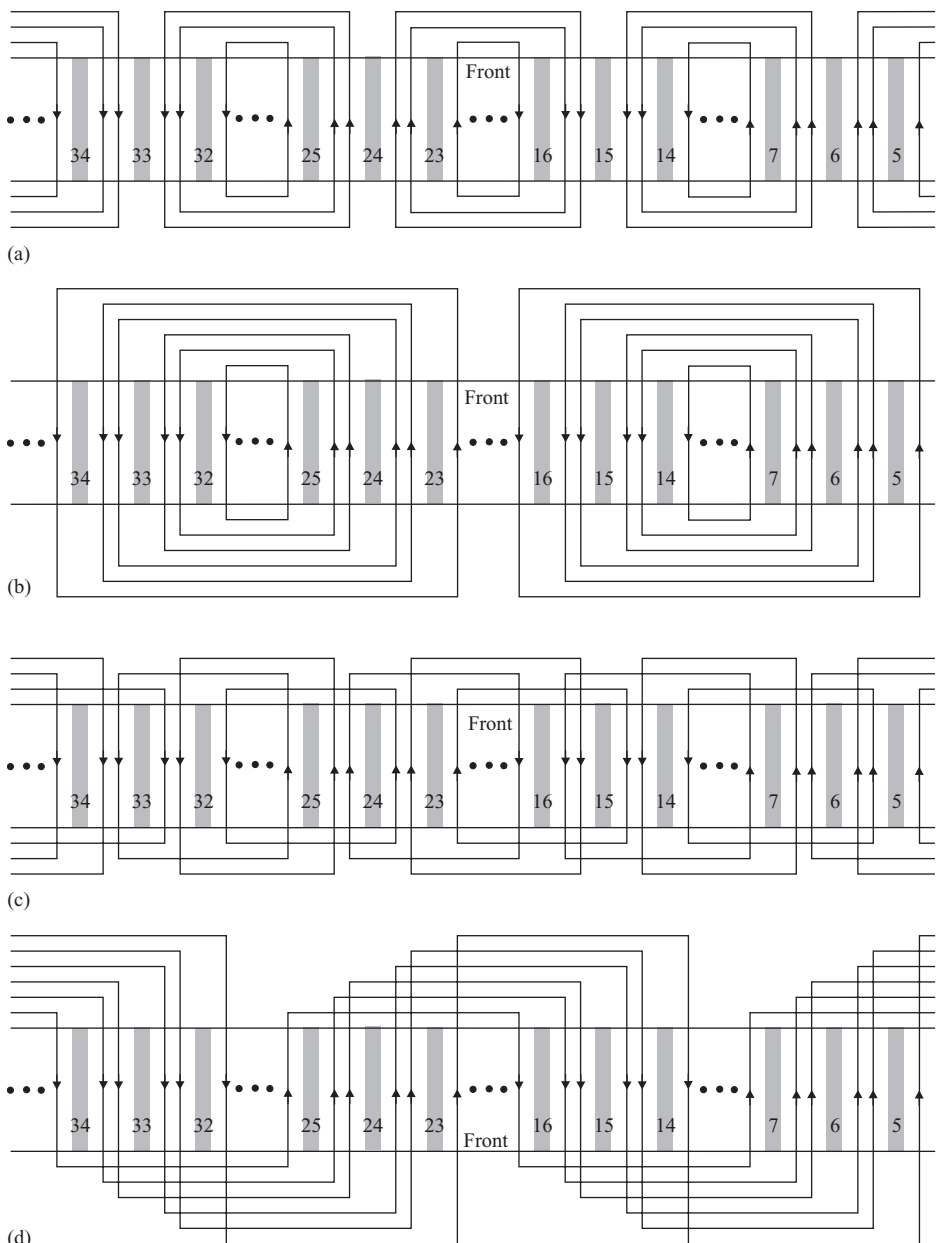


**Figure 2.2-8.** Winding arrangements. (a) Concentric winding arrangement; (b) consequent pole winding arrangement; (c) lap winding arrangement; (d) wave winding arrangement.

Figure 2.2-8a depicts a concentric winding arrangement wherein the  $a$ -phase conductors are organized in 12 coils, with three coils per set. Each coil is centered over a magnetic axis or pole associated with that phase. For this arrangement  $M_{as,36} = -3N$ ,  $C_{as,i} = 0 \forall i$ , and  $E_{as} = 88N$ .

In Figure 2.2-8b, a consequent pole winding arrangement is shown. In this arrangement, the windings are only wrapped around every other pole. From Figure 2.2-8b, we have  $M_{as,36} = 0$ ,  $C_{as,i} = 0 \forall i$ , and  $E_{as} = 108N$ . The increase in  $E_{as}$  will cause this arrangement to have a higher stator resistance than the concentric pole winding.

A lap winding is shown in Figure 2.2-8c. Each coil of this winding is identical. For this arrangement  $M_{as,36} = -3N$ , as in the case of the concentric winding. However, in this winding  $C_{as,6} = C_{as,15} = C_{as,24} = C_{as,34} = 2N$ , and all other  $C_{as,i} = 0$ . The total number of end turn segments is  $96N$ , which is better than the consequent pole winding, but not as good as the concentric winding.

Figure 2.2-8d depicts a wave winding, in which the winding is comprised of six coil groups. For this case,  $M_{as,36} = -6N$ ,  $C_{as,i} = 0$ , and  $E_{as} = 108N$ . Like the consequent pole winding, a relatively high stator resistance is expected; however, the reduced number of coil groups (and the use of identical groups) offers a certain manufacturing benefit.

### 2.3. WINDING FUNCTIONS

Our first goal for this chapter was to set forth methods to describe distributed windings. Our next goal is to begin to analyze distributed winding devices. To this end, a valuable concept is that of the winding function discussed in Reference 1. The winding function has three important uses. First, it will be useful in determining the MMF caused by distributed windings. Second, it will be used to determine how much flux links a winding. Third, the winding function will be instrumental in calculating winding inductances.

The winding function is a description of how many times a winding links flux density at any given position. It may be viewed as the number of turns associated with a distributed winding. However, unlike the number of turns in a simple coil, we will find that the number of turns associated with a distributed winding is a function of position. Using this notion will allow us to formulate the mathematical definition of the winding function.

Let us now consider the discrete description of the winding function. Figure 2.3-1 illustrates a portion of the developed diagram of a machine, wherein it is arbitrarily

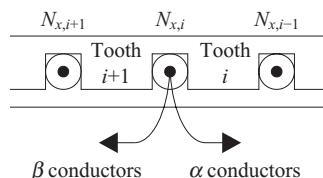


Figure 2.3-1. Calculation of the winding function.

assumed that the winding of interest is on the stator. Let  $W_{x,i}$  denote the number of times winding “ $x$ ” links flux traveling through the  $i$ ’th tooth, where the direction for positive flux and flux density is taken to be from the rotor to the stator.

Now, let us assume that we know  $W_{x,i}$  for some  $i$ . It can be shown that

$$W_{x,i+1} = W_{x,i} - N_{x,i} \quad (2.3-1)$$

To understand (2.3-1), suppose  $N_{x,i}$  is positive. Of the  $N_{x,i}$  conductors, suppose  $\alpha$  of these conductors go to the right (where they turn back into other slots), and  $\beta$  of these conductors go to the left (where again they turn back into other slots). The  $\alpha$  conductors form turns that link flux in tooth  $i$  but not flux in tooth  $i+1$  since they close the loop to the right. The  $\beta$  conductors form turns that are directed toward the left before closing the loop, and so do not link tooth  $i$ , but do link tooth  $i+1$ , albeit in the negative direction (which can be seen using the right hand rule and recalling that flux is considered positive from the rotor to the stator). Thus we have

$$W_{x,i+1} = W_{x,i} - \alpha - \beta \quad (2.3-2)$$

Since  $N_{x,i} = \alpha + \beta$ , (2.3-2) reduces to (2.3-1). Manipulation of (2.3-1) yields an expression for the winding function. In particular,

$$W_{x,i} = W_{x,1} - \sum_{j=1}^{i-1} N_{x,j} \quad (2.3-3)$$

In order to determine  $W_{x,1}$ , we will require that the winding function possess the symmetry conditions on the conductor distribution as stated in (2.2-14) and (2.2-15). In particular, we require

$$W_{x,i+S_y/P} = -W_{x,i} \quad (2.3-4)$$

where the indexing operations are ring-mapped with a modulus of  $S_y$ . Note that this requirement does not follow from (2.3-3); rather, it is part of our definition of the winding function. Manipulating (2.3-3) with  $i = 1 + S_y/P$  and using (2.3-4) yields

$$W_{x,1} = \frac{1}{2} \sum_{j=1}^{S_y/P} N_{x,j} \quad (2.3-5)$$

Using (2.3-5) and (2.3-1), the winding function can be computed for each tooth. It should be noted that it is assumed that  $S_y/P$  is an integer for the desired symmetry conditions to be met. In addition, for a three-phase machine to have electrically identical phases while ensuring symmetry of each winding, it is further required that  $S_y/(3P)$  is an integer.

Let us now consider the calculation of the winding function using a continuous description of the winding. In this case, instead of being a function of the tooth number,

the winding function is a continuous function of position, which can be position relative to the stator ( $\phi_m = \phi_{sm}$ ) for stator windings or position relative to the rotor ( $\phi_m = \phi_{rm}$ ) for rotor windings. Let us assume that we know the value of the winding function at position  $\phi_m$ , and desire to calculate the value of the winding function at position  $\phi_m + \Delta\phi_m$ . The number of conductors between these two positions is  $n_x(\phi_m)\Delta\phi_m$ , assuming  $\Delta\phi_m$  is small. Using arguments identical to the derivation of (2.3-1), we have that

$$w_x(\phi_m + \Delta\phi_m) = w_x(\phi_m) - n_x(\phi_m)\Delta\phi_m \quad (2.3-6)$$

Taking the limit as  $\Delta\phi_m \rightarrow 0$ ,

$$\frac{dw_x(\phi_m)}{d\phi_m} = -n_x(\phi_m) \quad (2.3-7)$$

Thus the winding function may be calculated as

$$w_x(\phi_m) = - \int_0^{\phi_m} n_x(\phi_m) d\phi_m + w_x(0) \quad (2.3-8)$$

In order to utilize (2.3-8), we must establish  $w_x(0)$ . As in the discrete case for computing  $W_{x,1}$ , we require that the winding function obeys the same symmetry conditions as the conductor distribution, namely (2.2-17). Thus

$$w_x(\phi_m + 2\pi/P) = -w_x(\phi_m) \quad (2.3-9)$$

Note that (2.3-9) does not follow from (2.3-8); rather, it is an additional part of the definition. Manipulating (2.3-8) with  $\phi_m = 2\pi/P$  and using (2.3-9)

$$w_x(0) = \frac{1}{2} \int_0^{2\pi/P} n_x(\phi_m) d\phi_m \quad (2.3-10)$$

Substitution of (2.3-10) into (2.3-8) yields

$$w_x(\phi_m) = \frac{1}{2} \int_0^{2\pi/P} n_x(\phi_m) d\phi_m - \int_0^{\phi_m} n_x(\phi_m) d\phi_m \quad (2.3-11)$$

In summary, (2.3-1), along with (2.3-5) and (2.3-11), provide a means to calculate the winding function for discrete and continuous winding descriptions, respectively. The winding function is a physical measure of the number of times a winding links the flux in a particular tooth (discrete winding description) or a particular position (continuous winding description). It is the number of turns going around a given tooth (discrete description) or given position (continuous description).

**EXAMPLE 2A** We will now consider the winding function for the machine shown in Figure 2.2-7. Recall that for this machine,  $P = 4$  and  $S_s = 36$ . From Figure 2.2-7, observe that the first slot is at  $\phi_{sm} = 0$ , hence  $\phi_{ss,1} = 0$ . The conductor distribution is given by (2.2-30), where  $N$  was the number of conductors in a group. Applying (2.3-5), we have  $W_{x,1} = 3N$ . Using (2.3-1), we obtain

$$W_{as}|_{1-18} = N[3\ 3\ 3\ 2\ 0\ -2\ -3\ -3\ -3\ -3\ -3\ -2\ 0\ 2\ 3\ 3\ 3] \quad (2A-1)$$

The winding function is only given for the first 18 slots since the pattern is repetitive.

In order to obtain the continuous winding function, let us apply (2.2-22) and (2.2-23) where the slot positions are given by (2.2-8). Truncating the series (2.2-19) after the first two nonzero harmonics yields

$$n_{as} = N(7.221\sin(2\phi_{sm}) - 4.4106\sin(6\phi_{sm})) \quad (2A-2)$$

Comparing (2A-2) with (2.2-12), we see that  $N_{s1} = 7.221N$  and  $N_{s3} = 4.4106N$ . From (2.3-8) we obtain

$$w_{as} = N\left(\frac{7.221}{2}\cos(2\phi_{sm}) - \frac{4.4106}{6}\cos(6\phi_{sm})\right) \quad (2A-3)$$

Figure 2A-1 depicts the conductor distributions and winding function for the winding. The discrete description of the winding function is shown as a series of arrows, suggesting a delta function representation. The corresponding continuous distribution (which is divided by 4) can be seen to have a relatively high peak. It is somewhat difficult to compare the discrete winding description to the continuous winding description since it is difficult to compare a delta function with a continuous function. The discrete representation of the winding function is shown as a set of horizontal lines spanning one tooth and one slot, and centered on the tooth. These lines are connected to form a contiguous trace. The continuous representation of the winding function can be seen to be very consistent with the discrete representation at the tooth locations. Had we chosen to include the next two harmonics, the error between the continuous winding function representation and the discrete winding function representation at the tooth centers would be further reduced.

The next step of this development will be the calculation of the MMF associated with a winding. As it turns out, this calculation is very straightforward using the winding function. The connection between the winding function and the MMF is explored in the next section.

## 2.4. AIR-GAP MAGNETOMOTIVE FORCE

In this section, we consider the air-gap magnetomotive force (MMF) and the relationship of this MMF to the stator currents. We will find that the winding function is

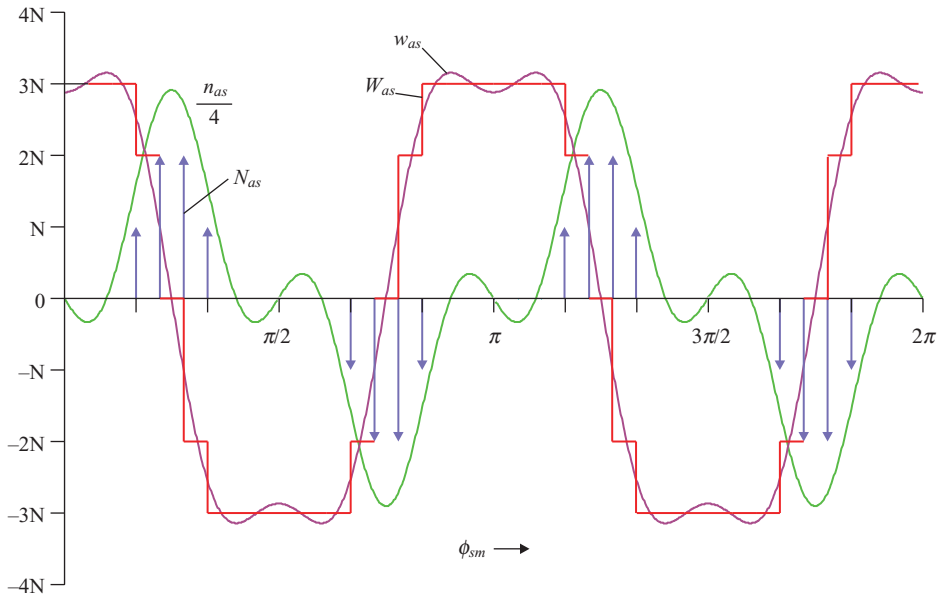


Figure 2A-1. Conductor distribution and winding functions.

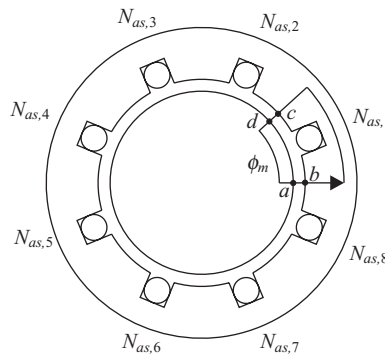


Figure 2.4-1. Path of integration.

instrumental in establishing this relationship. In doing this, we will concentrate our efforts on the continuous winding description.

Let us begin by applying Ampere's law to the path shown in Figure 2.4-1. In particular, we have

$$\oint_{abcd} \mathbf{H} \cdot d\mathbf{l} = i_{enc}(\phi_m) \quad (2.4-1)$$

where  $i_{enc}(\phi_m)$  is a function that describes the amount of current enclosed by the path. Expanding (2.4-1), we may write

$$\int_a^b \mathbf{H} \cdot d\mathbf{l} + \int_b^c \mathbf{H} \cdot d\mathbf{l} + \int_c^d \mathbf{H} \cdot d\mathbf{l} + \int_d^a \mathbf{H} \cdot d\mathbf{l} = i_{enc}(\phi_m). \quad (2.4-2)$$

The MMF across the air gap is defined as

$$\mathbb{F}_g(\phi_m) \triangleq \int_{\text{rotor}}^{\text{stator}} \mathbf{H}(\phi_m) \cdot d\mathbf{l} \quad (2.4-3)$$

where the path of integration is directed in the radial direction. Because of this, we may rewrite (2.4-3) as

$$\mathbb{F}_g(\phi_m) = \int_{\text{rotor}}^{\text{stator}} \mathbf{H}_r(\phi_m) \cdot d\mathbf{l} \quad (2.4-4)$$

where  $H_r(\phi_m)$  is the outwardly directed radial component of the air-gap field intensity.

The stator backiron of the machine is the iron region radially outward from the stator slots and teeth. It conducts flux in a predominantly circumferential direction. The rotor backiron is radially inward from any rotor slots or teeth, and again conducts flux predominantly in the circumferential direction. Referring to Figure 2.4-1, the MMF drops across the rotor and stator backiron are taken as

$$\mathbb{F}_{sb}(\phi_m) \triangleq \int_b^c \mathbf{H}(\phi_m) \cdot d\mathbf{l} \quad (2.4-5)$$

$$\mathbb{F}_{rb}(\phi_m) \triangleq \int_a^d \mathbf{H}(\phi_m) \cdot d\mathbf{l} \quad (2.4-6)$$

With these definitions, these MMF drops include a radial component in the teeth, but are both defined in a predominately counterclockwise circumferential direction. Later, it may be convenient to break the radial component out as a separate MMF drop, but the given definitions are adequate for present purposes.

Substituting the definitions (2.4-3)–(2.4-6) into (2.4-2) yields

$$\mathbb{F}_g(0) + \mathbb{F}_{sb}(\phi_m) - \mathbb{F}_g(\phi_m) - \mathbb{F}_{rb}(\phi_m) = i_{enc}(\phi_m) \quad (2.4-7)$$

To proceed further, we must develop an expression for the current enclosed by the path. This current may be expressed as

$$i_{enc}(\phi_m) = \sum_{x \in X} \int_0^{\phi_m} n_x(\phi_m) i_x d\phi_m \quad (2.4-8)$$

where  $X$  denotes the set of all windings. Rearranging (2.4-8)

$$i_{enc}(\phi_m) = \sum_{x \in X} \left( \int_0^{\phi_m} n_x(\phi_m) d\phi_m \right) i_x \quad (2.4-9)$$

From (2.3-8), it can be shown that

$$\int_0^{\phi_m} n_x(\phi_m) d\phi_m = w_x(0) - w_x(\phi_m) \quad (2.4-10)$$

Combining (2.4-7), (2.4-9), and (2.4-10),

$$\mathbb{F}_g(0) + \mathbb{F}_{sb}(\phi_m) - \mathbb{F}_g(\phi_m) - \mathbb{F}_{rb}(\phi_m) = \sum_{x \in X} (w_x(0) - w_x(\phi_m)) i_x \quad (2.4-11)$$

Replacing  $\phi_m$  by  $\phi_m + 2\pi/P$  in (2.4-11) yields

$$\begin{aligned} & \mathbb{F}_g(0) + \mathbb{F}_{sb}(\phi_m + 2\pi/P) - \mathbb{F}_g(\phi_m + 2\pi/P) - \mathbb{F}_{rb}(\phi_m + 2\pi/P) \\ &= \sum_{x \in X} (w_x(0) - w_x(\phi_m + 2\pi/P)) i_x \end{aligned} \quad (2.4-12)$$

Next, from the symmetry of the machine and the assumption on the winding distribution given by (2.3-9), all MMF terms are odd-half symmetric over a displacement of  $2\pi/P$ . Since the winding function has this property by definition, (2.4-12) may be written as

$$\mathbb{F}_g(0) - \mathbb{F}_{sb}(\phi_m) + \mathbb{F}_g(\phi_m) + \mathbb{F}_{rb}(\phi_m) = \sum_{x \in X} (w_x(0) + w_x(\phi_m)) i_x. \quad (2.4-13)$$

Subtracting (2.4-11) from (2.4-13) and manipulating yields

$$-\mathbb{F}_{sb}(\phi_m) + \mathbb{F}_g(\phi_m) + \mathbb{F}_{rb}(\phi_m) = \sum_{x \in X} w_x(\phi_m) i_x \quad (2.4-14)$$

The MMF source associated with the sum of the windings may be expressed as

$$\mathbb{F}_X(\phi_m) = \sum_{x \in X} w_x(\phi_m) i_x \quad (2.4-15)$$

Substitution of (2.4-15) into (2.4-14)

$$-\mathbb{F}_{sb}(\phi_m) + \mathbb{F}_g(\phi_m) + \mathbb{F}_{rb}(\phi_m) = \mathbb{F}_X(\phi_m) \quad (2.4-16)$$

The expression (2.4-15) is important in that it relates the sum of the backiron and air-gap MMFs to the net MMF source provided by the windings.

At times, it will be convenient to define the stator and rotor source MMFs as

$$\mathbb{F}_S(\phi_m) = \sum_{x \in X_S} w_x(\phi_m) i_x \quad (2.4-17)$$

$$\mathbb{F}_R(\phi_m) = \sum_{x \in X_R} w_x(\phi_m) i_x \quad (2.4-18)$$

where  $X_S$  is the set of stator windings and (e.g.,  $X_S = \{\text{"as," "bs," "cs"}\}$ ) and  $X_R$  is the set of rotor windings (e.g.,  $X_R = \{\text{"ar," "br," "cr"}\}$ ). Thus

$$\mathbb{F}_X(\phi_m) = \mathbb{F}_S(\phi_m) + \mathbb{F}_R(\phi_m) \quad (2.4-19)$$

It is often the case that the backiron MMF drops are neglected. This approximation comes about because if the flux density is finite, and the permeability is high, then the field intensity must be small relative to its value in the air gap and so  $\mathbb{F}_{rb}(\phi_m)$  and  $\mathbb{F}_{sb}(\phi_m)$  are small. In this case, from (2.4-16) and (2.4-19), the air-gap MMF may be readily expressed as

$$\mathbb{F}_g(\phi_m) = \mathbb{F}_S(\phi_m) + \mathbb{F}_R(\phi_m) \quad (2.4-20)$$

From the air-gap MMF drop, we may readily calculate the fields in the air gap. From (2.4-4), and assuming that the radial component of the field intensity is constant between the rotor and the stator, we have that

$$\mathbb{F}_g(\phi_m) = H_g(\phi_m) g(\phi_m) \quad (2.4-21)$$

whereupon the field intensity in the air gap may be expressed as

$$H_g(\phi_m) = \frac{\mathbb{F}_g(\phi_m)}{g(\phi_m)} \quad (2.4-22)$$

Since  $B = \mu_0 H$  in the air gap, flux density in the air gap may be expressed as

$$B_g(\phi_m) = \frac{\mu_0 \mathbb{F}_g(\phi_m)}{g(\phi_m)} \quad (2.4-23)$$

## 2.5. ROTATING MMF

A goal of this chapter is to establish methods that can be used to determine electrical circuit models of electromechanical systems. To this end, we have just discussed how to calculate the MMF due to a distributed winding. In the next section, we will use this information in the calculation of inductances of distributed windings. However, before

we proceed into that discussion, it will be interesting to pause for a moment, and consider our results thus far in regard to the operation of a machine.

Let us consider a three-phase stator winding. We will assume that the conductor distribution for the stator windings may be expressed as

$$n_{as}(\phi_{sm}) = N_{s1} \sin(P\phi_{sm} / 2) - N_{s3} \sin(3P\phi_{sm} / 2) \quad (2.5-1)$$

$$n_{bs}(\phi_{sm}) = N_{s1} \sin(P\phi_{sm} / 2 - 2\pi / 3) - N_{s3} \sin(3P\phi_{sm} / 2) \quad (2.5-2)$$

$$n_{cs}(\phi_{sm}) = N_{s1} \sin(P\phi_{sm} / 2 + 2\pi / 3) - N_{s3} \sin(3P\phi_{sm} / 2) \quad (2.5-3)$$

In (2.5-1)–(2.5-3), the second term to the right of the equal sign (the third harmonic term) is useful in achieving a more uniform slot fill.

In order to calculate the stator MMF for this system, we must first find the winding function. Using the methods of Section 2.3, the winding functions may be expressed as

$$w_{as}(\phi_{sm}) = \frac{2N_{s1}}{P} \cos(P\phi_{sm} / 2) - \frac{2N_{s3}}{3P} \cos(3P\phi_{sm} / 2) \quad (2.5-4)$$

$$w_{bs}(\phi_{sm}) = \frac{2N_{s1}}{P} \cos(P\phi_{sm} / 2 - 2\pi / 3) - \frac{2N_{s3}}{3P} \cos(3P\phi_{sm} / 2) \quad (2.5-5)$$

$$w_{cs}(\phi_{sm}) = \frac{2N_{s1}}{P} \cos(P\phi_{sm} / 2 + 2\pi / 3) - \frac{2N_{s3}}{3P} \cos(3P\phi_{sm} / 2) \quad (2.5-6)$$

From (2.4-17), the total stator MMF may be expressed as

$$\mathbb{F}_s(\phi_{sm}) = w_{as}(\phi_{sm})i_{as} + w_{bs}(\phi_{sm})i_{bs} + w_{cs}(\phi_{sm})i_{cs} \quad (2.5-7)$$

To proceed further, we need to inject currents into the system. Let us consider a balanced three-phase set of currents of the form

$$i_{as} = \sqrt{2}I_s \cos(\omega_e t + \phi_i) \quad (2.5-8)$$

$$i_{bs} = \sqrt{2}I_s \cos(\omega_e t + \phi_i - 2\pi / 3) \quad (2.5-9)$$

$$i_{cs} = \sqrt{2}I_s \cos(\omega_e t + \phi_i + 2\pi / 3) \quad (2.5-10)$$

where  $I_s$  is the rms magnitude of each phase current,  $\omega_e$  is the ac electrical frequency, and  $\phi_i$  is the phase of the a-phase current. Substitution of (2.5-4)–(2.5-6) and (2.5-8)–(2.5-10) into (2.5-7) and simplifying yields

$$\mathbb{F}_s = \frac{3\sqrt{2}N_{s1}I_s}{P} \cos(P\phi_{sm} / 2 - \omega_e t - \phi_i) \quad (2.5-11)$$

The result (2.5-11) is an important one. From (2.5-11), we can see that given a sinusoidal turns distribution and the appropriate currents we arrive at an MMF that is

sinusoidal in space ( $\phi_{sm}$ ) and sinusoidal in time ( $t$ ). It represents a wave equation. In other words, the resulting MMF is a moving wave. To see this, consider the peak of the wave, wherein the argument to the cosine term in (2.5-11) is zero. In particular, at the peak of the wave

$$P\phi_{sm} / 2 - \omega_e t - \phi_i = 0 \quad (2.5-12)$$

From (2.5-12), we have

$$\phi_{sm} = \frac{2}{P} \omega_e t + \frac{2}{P} \phi_i \quad (2.5-13)$$

Thus, the peak of the wave is moving at a speed of  $2\omega_e/P$ .

In synchronous machines, the rotor speed will be equal to the speed of the stator MMF wave in the steady state, so it is clear that the speed will vary with  $\omega_e$ . It can also be seen that as the number of poles is increased, the speed of the MMF wave (and hence the rotor) will decrease.

The creation of an MMF wave that travels in a single direction requires at least two currents and two windings. A single winding will produce an MMF with both forward and reverse traveling waves that significantly reduce the efficiency of the machine. Polyphase machines with unbalanced excitation also yields forward and reverse traveling waves. An example of this is explored in Problem 9.

## 2.6. FLUX LINKAGE AND INDUCTANCE

In the remaining sections of this chapter, we will start to fulfill the last of our goals for this chapter—that is the calculation of the electrical parameters (specifically inductance and resistance) of rotating electrical machines. To begin, it is convenient to view the flux linking any winding (winding  $x$ ) in terms of leakage flux linkage  $\lambda_{xl}$  and magnetizing flux linkage  $\lambda_{xm}$ . The total flux linkage of a winding is the sum of these two components. Thus,

$$\lambda_x = \lambda_{xl} + \lambda_{xm} \quad (2.6-1)$$

The distinction between leakage flux linkage and magnetizing flux linkage is not always precise. However, leakage flux is associated with flux that does not travel across the air gap or couple both the rotor and stator windings. Magnetizing flux linkage  $\lambda_{xm}$  is associated with radial flux flow across the air gap and links both the stator and rotor windings.

Associated with the concept of leakage and magnetizing flux are the concepts of leakage and magnetizing inductance, which relate their respective flux linkage components to current. In order to state these concepts mathematically, let  $x$  and  $y$  denote two windings (and will take on values of “as,” “bs,” “cs,” “ar,” “br,” and “cr,” etc.). Then the leakage and magnetizing inductance between two windings may be expressed as

$$L_{xyl} = \frac{\lambda_{xl}|_{\text{due to } i_y}}{i_y} \quad (2.6-2)$$

$$L_{xym} = \frac{\lambda_{xm}|_{\text{due to } i_y}}{i_y} \quad (2.6-3)$$

From our definition, the mutual leakage inductance between a stator winding and a rotor winding will be zero. However, there will be leakage inductances between different stator windings and between different rotor windings.

The total inductance of a winding is defined as

$$L_{xy} = \frac{\lambda_x|_{\text{due to } i_y}}{i_y} \quad (2.6-4)$$

From (2.6-1)–(2.6-4), it is clear that the total inductance is the sum of the leakage and magnetizing inductance, hence

$$L_{xy} = L_{xyl} + L_{xym} \quad (2.6-5)$$

The leakage inductance of a winding can be viewed as parasitic, and it is a strong function of the details of the winding. As such, the calculation of leakage inductance is deferred to Appendix C. We will instead concentrate our efforts on the calculation of the magnetizing inductance between two distributed windings. To this end, consider Figure 2.6-1, which shows a stator. Consider the incremental area along the inner surface of the stator, as shown. The radius of this incremental section is  $r$ , and its position is  $\phi_m$ . (Note that by this drawing,  $\phi_m$  is relative to the stator and could be designated as  $\phi_{sm}$ ; however, as an identical argument could be made using any reference point,  $\phi_m$  is used to denote position.) The length of the edge segment is  $rd\phi_m$ . If the axial length of the machine is  $l$ , it follows that the incremental area is  $lrd\phi_m$ . For small  $d\phi_m$ , the flux through this incremental area may be expressed as

$$\Phi(\phi_m) = B(\phi_m)lrd\phi_m \quad (2.6-6)$$

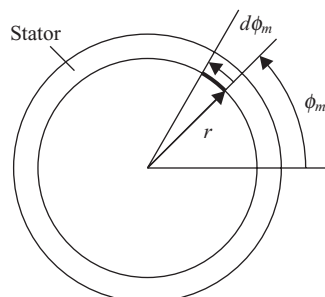


Figure 2.6-1. Calculation of flux linkage.

Now recall that the winding function  $w_x(\phi_m)$  describes the how many times a winding  $x$  links the flux at a position  $\phi_m$ . Thus, the contribution of the flux linking winding  $x$  through this incremental area may be expressed  $w_x(\phi_m)B(\phi_m)lrd\phi_m$ . Adding up all the incremental areas along the stator, we have

$$\lambda_{xm} = \int_0^{2\pi} B(\phi_m)w_x(\phi_m)lrd\phi_m \quad (2.6-7)$$

Now that we have a means to calculate the flux linkage given the flux density and winding function, recall from (2.4-23) (and using 2.4-17, 2.4-18, and 2.4-20) that the air-gap flux density due to winding  $y$  may be expressed as

$$B_{yg}(\phi_m) = \frac{\mu_0}{g(\phi_m)} w_y(\phi_m) i_y. \quad (2.6-8)$$

Substitution of (2.6-8) into (2.6-7) and manipulating, the flux in winding  $x$  due to the current in winding  $y$  is given by

$$\lambda_{sym} = \left( \mu_0 rl \int_0^{2\pi} \frac{w_x(\phi_m)w_y(\phi_m)}{g(\phi_m)} d\phi_m \right) i_y \quad (2.6-9)$$

From (2.6-9), it can be seen that the inductance between two windings may be expressed

$$\frac{\lambda_{sym}}{i_y} = L_{sym} = \mu_0 rl \int_0^{2\pi} \frac{w_x(\phi_m)w_y(\phi_m)}{g(\phi_m)} d\phi_m \quad (2.6-10)$$

This relationship is valid for both self- and mutual inductance. When using (2.6-10) to calculate self-inductance,  $y = x$ .

The expressions in (2.6-9) and (2.6-10) involve several approximations. First, they depend on an assumption made in (2.6-8) that the field is uniform across the air gap. In machines with large air gaps, or effectively large air gaps, it may be necessary to address the radial variation in the flux density. This is described in the context of a permanent magnet ac machine in Chapter 15. A second assumption associated with (2.6-9) and (2.6-10) is that they neglect the rather appreciable effect that slots may have on the magnetizing inductance. It is possible to derive a version of (2.6-9) and (2.6-10) that includes radial variation in flux density. Further, the effect of slots on the magnetizing inductance may be accounted for using Carter's method, which is described in Appendix B.

Before concluding this section, consider multipole machines wherein all position-dependent quantities are periodic, with a period of  $\pi P$ . Making use of the periodicity of field distribution, it is readily shown that (2.6-7) and (2.6-10) become

$$\lambda_{xm} = \int_0^{2\pi} B(\phi) w_x(\phi) l r d\phi \quad (2.6-11)$$

and

$$\frac{\lambda_{sym}}{i_y} = L_{sym} = \mu_0 r l \int_0^{2\pi} \frac{w_x(\phi) w_y(\phi)}{g(\phi)} d\phi \quad (2.6-12)$$

Note that while (2.6-11) and (2.6-12) appear identical to (2.6-7) and (2.6-10), in the former, all variables are periodic in  $2\pi$ , which makes the integral easier to evaluate in the presence of discontinuities, such as those arising from permanent magnets.

## 2.7. RESISTANCE

Besides inductance, another electrical characteristic of a coil is its resistance. In this section, we consider the problem of finding the resistance of a distributed winding. Our approach will utilize the discrete winding description, and begin by considering the spatial volume of the winding.

The volume of a winding can be broken down into two parts—the volume located in the slots, and the volume located in the end turns. The slot volume of winding  $x$  is denoted by  $V_{xs}$ , and is equal to the sum of the absolute value of the number of conductors in each slot times the volume of each conductor (which is, in turn, the length times the cross-sectional area). Thus

$$V_{xs} = (l + 2e)a_c \sum_{i=1}^{S_y} |N_{x,i}| \quad (2.7-1)$$

where  $a_c$  and  $e$  are the cross-sectional conductor area and axial distance from the end of the machine laminations to the center of the end-turn bundle, respectively.

The volume of conductor associated with the end turn region is denoted by  $V_{xe}$  and may be expressed as

$$V_{xe} = \frac{2\pi}{S_y} \bar{r}_x a_c E_x \quad (2.7-2)$$

In (2.7-2),  $2\pi/S_y$  is the angle of an end conductor sector and  $\bar{r}_x$  is the mean radius (from the center of the machine) to the end conductor bundle. The product of these two factors is the length of an end conductor sector. Multiplying the end conductor sector length times  $E_x$  and the cross-sectional area of the conductor,  $a_c$ , yields the end conductor volume for the winding. This volume is that of one (front or back) end.

Since there are two end turn regions, the total conductor volume,  $V_{xt}$ , associated with the winding may be expressed as

$$V_{xt} = V_{xs} + 2V_{xe} \quad (2.7-3)$$

The length of the conductor associated with the winding is then given by

$$l_x = V_{xt} / a_c \quad (2.7-4)$$

whereupon the phase resistance may be calculated as

$$r_x = \frac{l_x}{a_c \sigma_c} \quad (2.7-5)$$

where  $\sigma_c$  is the conductivity of the conductor used for winding  $x$ .

## 2.8. VOLTAGE AND FLUX LINKAGE EQUATIONS FOR DISTRIBUTED WINDING MACHINES

In this section, we will express the voltage equations and winding inductances for an elementary three-phase synchronous machine and a three-phase induction machine. Derivation of the voltage equations and winding inductances for a three-phase permanent magnet ac machine will be left for Chapter 15, wherein we will consider machine design.

### Stator Voltage Equations

It is convenient to begin this development with the stator voltage equations, which are common to the aforementioned classes of machines. Using Ohm's and Faraday's laws, the stator voltage equations are readily expressed

$$v_{as} = r_s i_{as} + p\lambda_{as} \quad (2.8-1)$$

$$v_{bs} = r_s i_{bs} + p\lambda_{bs} \quad (2.8-2)$$

$$v_{cs} = r_s i_{cs} + p\lambda_{cs} \quad (2.8-3)$$

where  $r_s = r_{as} = r_{bs} = r_{cs}$  is the stator winding resistance that may be calculated using the method of Section 2.7.

### Synchronous Machine

We will now consider an elementary synchronous machine. In this machine, in addition to the three-phase stator windings, there is a field winding on the rotor. In a practical machine, there would also be damper windings on the rotor; these will be considered

in Chapter 5, but will not be treated in this section. The expressions for the inductances of these additional windings can be readily ascertained from the work presented here.

It is convenient to begin with the voltage equation for the field winding. By Ohm's and Faraday's laws

$$v_{fd} = r_{fd}i_{fd} + p\lambda_{fd} \quad (2.8-4)$$

where  $r_{fd}$  is the resistance of the field winding.

Our next step will be to develop the flux linkage equations that relate the stator and field flux linkages to the stator and field currents. Assuming magnetic linearity, these can be readily expressed as

$$\lambda_{as} = L_{asas}i_{as} + L_{asbs}i_{bs} + L_{ascas}i_{cs} + L_{asfd}i_{fd} \quad (2.8-5)$$

$$\lambda_{bs} = L_{bsas}i_{as} + L_{bsbs}i_{bs} + L_{bscs}i_{cs} + L_{bsfd}i_{fd} \quad (2.8-6)$$

$$\lambda_{cs} = L_{csas}i_{as} + L_{csbs}i_{bs} + L_{cscs}i_{cs} + L_{csfd}i_{fd} \quad (2.8-7)$$

$$\lambda_{fd} = L_{fdas}i_{as} + L_{fdbas}i_{bs} + L_{fdcs}i_{cs} + L_{fdfd}i_{fd} \quad (2.8-8)$$

The next step in deriving a machine model is the rather more formidable step of determining expressions for these inductances.

To this end, we will assume a stator winding distribution as given by (2.5-1)–(2.5-3), and so the stator winding functions are given by (2.5-4)–(2.5-6). For simplicity, we will consider the case where the third harmonic term in the winding distribution is zero; hence  $N_{s3} = 0$ . Under this condition, using (2.2-13), the total number of conductors associated with each of the stator windings, herein denoted as  $N_s$  as it is the same for all stator windings, is found to be

$$N_s = 2N_{s1} \quad (2.8-9)$$

Thus, the winding function may be expressed in terms of electrical stator position as

$$w_{as}(\phi_s) = \frac{N_s}{P} \cos(\phi_s) \quad (2.8-10)$$

$$w_{bs}(\phi_s) = \frac{N_s}{P} \cos(\phi_s - 2\pi/3) \quad (2.8-11)$$

$$w_{cs}(\phi_s) = \frac{N_s}{P} \cos(\phi_s + 2\pi/3) \quad (2.8-12)$$

The conductor distribution for the field winding is assumed to be given by

$$n_{fd}(\phi_{rm}) = N_{fd1} \cos\left(\frac{P}{2}\phi_{rm}\right) \quad (2.8-13)$$

From (2.2-13), the total number of conductors associated with this winding is readily expressed as

$$N_{fd} = 2N_{fd1} \quad (2.8-14)$$

and, from (2.3-8), the corresponding winding function is

$$w_{fd}(\phi_{rm}) = -\frac{N_{fd}}{P} \sin\left(\frac{P}{2}\phi_{rm}\right) \quad (2.8-15)$$

In the case of the synchronous machine, the air gap is most conveniently expressed as a function of position relative to the rotor. Let us assume that the air gap may be expressed as

$$g(\phi_r) = \frac{1}{\alpha_1 - \alpha_2 \cos(2\phi_r)} \quad (2.8-16)$$

We now have all results needed in order to calculate the machine inductances. Let us first consider the self-inductance of the *a*-phase winding. From (2.6-5), this may be expressed as

$$L_{asas} = L_{lsp} + L_{asasm} \quad (2.8-17)$$

In (2.8-17),  $L_{lsp}$  is used as simpler notation for  $L_{asasl}$  since this leakage inductance will be common to all stator phases. Its calculation is discussed in Appendix C, wherein  $L_{lsp}$  is used as a generic symbol for either stator or rotor self-leakage inductance. Substitution of (2.8-10) and (2.8-16) into (2.6-12) with  $\phi = \phi_s$ , we have

$$L_{asasm} = \mu_0 r l \int_0^{2\pi} \left( \frac{N_s}{P} \cos(\phi_s) \right)^2 (\alpha_1 - \alpha_2 \cos(2\phi_r)) d\phi_s \quad (2.8-18)$$

We cannot evaluate (2.8-18) without taking into account that  $\phi_r$  is related to  $\phi_s$ . Using (2.2-6), (2.8-18) becomes

$$L_{asasm} = \mu_0 r l \int_0^{2\pi} \left( \frac{N_s}{P} \cos(\phi_s) \right)^2 (\alpha_1 - \alpha_2 \cos(2\phi_s - 2\theta_r)) d\phi_s \quad (2.8-19)$$

Evaluating (2.8-19) and substituting into (2.8-17), we obtain

$$L_{asas} = L_{lsp} + \pi \mu_0 r l \left( \frac{N_s}{P} \right)^2 \left( \alpha_1 - \frac{\alpha_2}{2} \cos 2\theta_r \right) \quad (2.8-20)$$

Applying this procedure to the other inductances, the inductance elements in (2.8-5)–(2.8-8) may be expressed as

$$L_{asas} = L_{lsp} + L_A - L_B \cos 2\theta_r \quad (2.8-21)$$

$$L_{bsbs} = L_{lsp} + L_A - L_B \cos 2(\theta_r - 2\pi/3) \quad (2.8-22)$$

$$L_{cscs} = L_{lsp} + L_A - L_B \cos 2(\theta_r + 2\pi/3) \quad (2.8-23)$$

$$L_{fdfd} = L_{lfd} + L_{mfd} \quad (2.8-24)$$

$$L_{asbs} = L_{lsm} - \frac{1}{2} L_A - L_B \cos 2(\theta_r - \pi/3) \quad (2.8-25)$$

$$L_{ascn} = L_{lsm} - \frac{1}{2} L_A - L_B \cos 2(\theta_r + \pi/3) \quad (2.8-26)$$

$$L_{bscs} = L_{lsm} - \frac{1}{2} L_A - L_B \cos 2(\theta_r + \pi) \quad (2.8-27)$$

$$L_{asfd} = L_{sfd} \sin \theta_r \quad (2.8-28)$$

$$L_{bsfd} = L_{sfd} \sin(\theta_r - 2\pi/3) \quad (2.8-29)$$

$$L_{csfd} = L_{sfd} \sin(\theta_r + 2\pi/3) \quad (2.8-30)$$

In (2.8-21)–(2.8-30),

$$L_A = \left( \frac{N_s}{P} \right)^2 \pi \mu_0 r l \alpha_1 \quad (2.8-31)$$

$$L_B = \frac{1}{2} \left( \frac{N_s}{P} \right)^2 \pi \mu_0 r l \alpha_2 \quad (2.8-32)$$

$$L_{sfd} = \left( \frac{N_s}{P} \right) \left( \frac{N_f}{P} \right) \pi \mu_0 r l (\alpha_1 + \alpha_2 / 2) \quad (2.8-33)$$

$$L_{mfd} = \left( \frac{N_f}{P} \right)^2 \pi \mu_0 r l (\alpha_1 + \alpha_2 / 2) \quad (2.8-34)$$

In (2.8-25)–(2.8-27),  $L_{lsm}$  denotes the mutual leakage inductance between stator phases. Its calculation is considered in Appendix C, wherein  $L_{lm}$  is used as a generic symbol for either stator or rotor mutual leakage inductance.

At this point, the complexity of machine model due to rotor position-dependent inductances is apparent. The transient solution of the voltage/flux linkage/inductance equations is involved, and can only be solved numerically. In Chapter 3, a change of variables will be used to eliminate the rotor position-dependent inductances and thereby markedly reduce the complexity of the machine model. However, the resulting differential equations are still nonlinear and require numerical solution for transient conditions.

## Induction Machine

An induction machine has the same winding arrangement as a synchronous machine and so the stator voltage equations are represented as in (2.8-1)–(2.8-3) and the stator winding functions are given by (2.8-10)–(2.8-12). The machine features a uniform air gap, and a set of rotor windings that may be implemented by a stator-like winding structure, a squirrel cage, or even a solid rotor. Herein, we will model the rotor winding by a three-phase set of windings. This may seem somewhat arbitrary for the later two cases; however, experience has shown the approach to yield reasonable results. Subject to this assumption, the voltage equations for the rotor circuits may be expressed as

$$v_{ar} = r_r i_{ar} + p\lambda_{ar} \quad (2.8-35)$$

$$v_{br} = r_r i_{br} + p\lambda_{br} \quad (2.8-36)$$

$$v_{cr} = r_r i_{cr} + p\lambda_{cr} \quad (2.8-37)$$

where  $r_r$  denotes the rotor resistance of the rotor windings.

Since there are six windings, the flux linkage equations have the form

$$\lambda_{as} = L_{asas}i_{as} + L_{asbs}i_{bs} + L_{asci}i_{cs} + L_{asar}i_{ar} + L_{asbr}i_{br} + L_{ascr}i_{cr} \quad (2.8-38)$$

$$\lambda_{bs} = L_{bsas}i_{as} + L_{bsbs}i_{bs} + L_{bsci}i_{cs} + L_{bsar}i_{ar} + L_{bsbr}i_{br} + L_{bscr}i_{cr} \quad (2.8-39)$$

$$\lambda_{cs} = L_{csas}i_{as} + L_{csbs}i_{bs} + L_{cscs}i_{cs} + L_{csar}i_{ar} + L_{csbr}i_{br} + L_{cscr}i_{cr} \quad (2.8-40)$$

$$\lambda_{ar} = L_{aras}i_{as} + L_{arbs}i_{bs} + L_{arci}i_{cs} + L_{arar}i_{ar} + L_{arbr}i_{br} + L_{arcr}i_{cr} \quad (2.8-41)$$

$$\lambda_{br} = L_{bras}i_{as} + L_{brbs}i_{bs} + L_{brci}i_{cs} + L_{brar}i_{ar} + L_{brbr}i_{br} + L_{brcr}i_{cr} \quad (2.8-42)$$

$$\lambda_{cr} = L_{cras}i_{as} + L_{crbs}i_{bs} + L_{crcs}i_{cs} + L_{crar}i_{ar} + L_{crbr}i_{br} + L_{crcr}i_{cr} \quad (2.8-43)$$

In order to compute the inductances, it is necessary to specify the winding distribution. We will assume a rotor winding conductor distribution given by

$$n_{ar}(\phi_{rm}) = N_r \sin(P\phi_{rm} / 2) \quad (2.8-44)$$

$$n_{br}(\phi_{rm}) = N_r \sin(P\phi_{rm} / 2 - 2\pi / 3) \quad (2.8-45)$$

$$n_{cr}(\phi_{rm}) = N_r \sin(P\phi_{rm} / 2 + 2\pi / 3), \quad (2.8-46)$$

for which, making use of the relation (2.3-11)

$$w_{ar}(\phi_r) = N_r \cos(\phi_r) / P \quad (2.8-47)$$

$$w_{br}(\phi_r) = N_r \cos(\phi_r - 2\pi / 3) / P \quad (2.8-48)$$

$$w_{cr}(\phi_r) = N_r \cos(\phi_r + 2\pi / 3) / P \quad (2.8-49)$$

where  $N_r$  is the total number of positive conductors associated with the winding, and is equal to  $2N_{r1}$ .

It is rather tedious to derive all the inductances in (2.8-38)–(2.8-43), so we will focus our attention on the computation of  $L_{asar}$ . Substitution of (2.8-10) and (2.8-47) into (2.6-12) and taking  $\phi = \phi_r$  and noting that the air gap is constant

$$L_{asar} = \frac{\mu_0 r l}{g} \int_0^{2\pi} \frac{N_s}{P} \cos \phi_s \frac{N_r}{P} \cos \phi_r d\phi_r \quad (2.8-50)$$

We cannot evaluate this expression directly since  $\phi_s$  and  $\phi_r$  are dependent; using (2.2-6), we obtain

$$L_{asar} = \frac{\mu_0 r l}{g} \int_0^{2\pi} \frac{N_s}{P} \cos(\phi_r + \theta_r) \frac{N_r}{P} \cos \phi_r d\phi_r \quad (2.8-51)$$

which reduces to

$$L_{asar} = \frac{N_s}{P} \frac{N_r}{P} \frac{\mu_0 r l \pi}{g} \cos(\theta_r) \quad (2.8-52)$$

Repeating this procedure for all the inductances, we obtain

$$\begin{bmatrix} L_{asas} & L_{asbs} & L_{ascr} \\ L_{bsas} & L_{bsbs} & L_{bscr} \\ L_{csas} & L_{csbs} & L_{cscr} \end{bmatrix} = \begin{bmatrix} L_{lsp} + L_{ms} & L_{lsm} - L_{ms} / 2 & L_{lsm} - L_{ms} / 2 \\ L_{lsm} - L_{ms} / 2 & L_{lsp} + L_{ms} & L_{lsm} - L_{ms} / 2 \\ L_{lsm} - L_{ms} / 2 & L_{lsm} - L_{ms} / 2 & L_{lsp} + L_{ms} \end{bmatrix} \quad (2.8-53)$$

$$\begin{bmatrix} L_{asar} & L_{asbr} & L_{ascr} \\ L_{bsar} & L_{bsbr} & L_{bscr} \\ L_{csar} & L_{csbr} & L_{cscr} \end{bmatrix} = L_{sr} \begin{bmatrix} \cos \theta_r & \cos(\theta_r + 2\pi/3) & \cos(\theta_r - 2\pi/3) \\ \cos(\theta_r - 2\pi/3) & \cos \theta_r & \cos(\theta_r + 2\pi/3) \\ \cos(\theta_r + 2\pi/3) & \cos(\theta_r - 2\pi/3) & \cos \theta_r \end{bmatrix} \quad (2.8-54)$$

$$\begin{bmatrix} L_{aras} & L_{arbs} & L_{arcr} \\ L_{brar} & L_{brbs} & L_{brcr} \\ L_{cras} & L_{crbs} & L_{crcr} \end{bmatrix}^T = L_{sr} \begin{bmatrix} \cos \theta_r & \cos(\theta_r + 2\pi/3) & \cos(\theta_r - 2\pi/3) \\ \cos(\theta_r - 2\pi/3) & \cos \theta_r & \cos(\theta_r + 2\pi/3) \\ \cos(\theta_r + 2\pi/3) & \cos(\theta_r - 2\pi/3) & \cos \theta_r \end{bmatrix} \quad (2.8-55)$$

$$\begin{bmatrix} L_{arar} & L_{arbr} & L_{arcr} \\ L_{brar} & L_{brbr} & L_{brcr} \\ L_{crar} & L_{crbr} & L_{crcr} \end{bmatrix} = \begin{bmatrix} L_{lsp} + L_{mr} & L_{lrm} - L_{mr} / 2 & L_{lrm} - L_{mr} / 2 \\ L_{lrm} - L_{mr} / 2 & L_{lsp} + L_{mr} & L_{lrm} - L_{mr} / 2 \\ L_{lrm} - L_{mr} / 2 & L_{lrm} - L_{mr} / 2 & L_{lsp} + L_{mr} \end{bmatrix} \quad (2.8-56)$$

where

$$L_{ms} = \left( \frac{N_s}{P} \right)^2 \frac{\pi \mu_0 r l}{g} \quad (2.8-57)$$

$$L_{mr} = \left( \frac{N_r}{P} \right)^2 \frac{\pi \mu_0 r l}{g} \quad (2.8-58)$$

$$L_{sr} = \frac{N_s}{P} \frac{N_r}{P} \frac{\pi \mu_0 r l}{g} \quad (2.8-59)$$

In (2.8-53),  $L_{lsp}$  and  $L_{lsm}$  denote the self-leakage inductance of a stator winding and the mutual leakage inductance between stator windings. Similarly, in (2.8-56),  $L_{lpr}$  and  $L_{lrm}$  denotes the self-leakage inductance of a rotor winding and the mutual leakage inductance between two rotor windings. The calculation of these leakage inductances is addressed in Appendix C using generic symbols  $L_{lp}$  and  $L_{lm}$  for self- and mutual leakage.

In nearly all motoring applications of induction machines, the stator windings are connected to a balanced three-phase source and the rotor windings are short-circuited. With balanced three-phase current flowing in the stator windings, an air-gap MMF that rotates at a speed determined by the frequency of the stator currents, and the number of poles is established. If the rotor speed is different from the speed of this rotating MMF, balanced three-phase currents will be induced (thus the name induction) in the short-circuited rotor windings. The frequency of the rotor currents corresponds to the difference in the speed of the rotating MMF due to the stator currents and the speed of the rotor. The induced rotor currents will in turn produce an air-gap MMF that rotates relative to the rotor at a speed corresponding to the radian frequency of the rotor currents divided by the number of pole pairs. The speed of the rotor air-gap MMF superimposed upon the rotor speed is the same speed as that of the air-gap MMF established by the currents flowing in the stator windings. These two air-gap MMFs rotating in unison may be thought of as two synchronously rotating sets of magnetic poles. Torque is produced due to an interaction of the two magnetic systems. It is clear, however, that torque is not produced when the rotor is running in synchronism with the air-gap MMF due to the stator currents since in this case currents are not induced into the short-circuited rotor windings.

Here again we see the complexity of the machine model due to the rotor position-dependent mutual inductances between stator and rotor circuits. We will see in Chapter 3 that a change of variables eliminates the rotor position-dependent inductances, resulting in a machine model that is still nonlinear but much more manageable.

## REFERENCE

- [1] N.L. Shmitz and D.W. Novotny, *Introductory Electromechanics*, Roland, New York, 1965.

## PROBLEMS

1. The number of conductors in each slot of the *a*-phase of the stator of the machine are as follows:

$$N_{as} = [10 \ 20 \ 20 \ 10 \ -10 \ -20 \ -20 \ -10 \ 10 \ 20 \ 20 \ 20 \ 10 \ -10 \ -20 \ -20 \ -10]^T$$

Compute and graph the winding function associated with this winding versus tooth number. Suppose the flux traveling from the rotor to the stator in each tooth is given by

$$\Phi_t = 10^{-3} \cdot [-2 \ -1 \ 1 \ 2 \ 2 \ 1 \ -1 \ -2 \ -2 \ -1 \ 1 \ 2 \ 2 \ 1 \ -1 \ -2]^T$$

How much flux is linking the winding?

2. Suppose the turns (conductor) density of a winding function is given by

$$n_{br} = 262 \cos(8\phi_{rm} - 2\pi/3)$$

Compute the rotor *b*-phase winding function in terms of position measured from the rotor.

3. Consider (2.2-22) and (2.2-23) of the text, which are used to convert a discrete winding description to a continuous one. Instead of treating the discrete winding description as a series of delta functions when converting it to a continuous one, derive analogous expressions if it is assumed that the conductors within each slot are uniformly distributed over the angle spanned by the slot (call this angle  $\Delta$ ).
4. The conductor distribution for the first 18 slots of a 36-slot machine is given by

$$N_{as}|_{1-18} = N[0 \ 0 \ 0 \ 1 \ 2 \ 2 \ 1 \ 0 \ 0 \ 0 \ 0 \ -1 \ -2 \ -2 \ -1 \ 0 \ 0]^T$$

Using the impulse function approach (2.2-22) and (2.2-23), plot the spectrum of the resulting winding function over the first 50 harmonics of the fundamental (the fundamental being at  $2\phi_{sm}$ ). Use a semi-log plot. On top of this, superimpose the results obtained using the results of Problem 3.

5. Consider the conductor density given by (2.2-12). Define the total conductor density as

$$n_t = |n_{as}| + |n_{bs}| + |n_{cs}|$$

Defining  $\alpha_3 = N_{s3}/N_{s1}$ , compute the value of  $\alpha_3$ , which minimizes the peak value of  $n_t(\phi_{sm})$ . A numerical answer is acceptable.

6. Consider Problem 5. Derive the value of  $\alpha_3$  which minimizes the total number of conductors. A numerical answer is acceptable.
7. The winding function of the *a*- and *b*-phase stator windings of a machine are given by  $w_{as} = 100\cos(4\phi_{sm})$  and  $w_{bs} = 250\sin(4\phi_{sm})$ . The *a*-phase current of the machine

is given by  $i_{as} = 10\cos(\omega_e t + \pi/8)$ . Determine the *b*-phase current and the air gap needed to achieve an air-gap flux density of  $B(\phi_{sm}, t) = 1.2\cos(\omega_e t + \pi/8 - 4\phi_{sm})$ .

8. The conductor turns density of a two-phase machine is given by

$$n_{as} = 100\cos 2\phi_{sm}$$

$$n_{bs} = -100\sin 2\phi_{sm}$$

The *a*- and *b*-phase currents are given by

$$i_{as} = 5\cos(400t)$$

$$i_{bs} = 5\sin(400t)$$

Express the total stator MMF. What is the speed and direction of the MMF?

9. The conductor turns density of a two-phase machine is given by

$$n_{as} = 100\cos 2\phi_{sm}$$

$$n_{bs} = -100\sin 2\phi_{sm}$$

The *a*- and *b*-phase currents are given by

$$i_{as} = 5\cos(400t)$$

$$i_{bs} = 4\sin(400t)$$

Express the total stator MMF as the sum of a forward and reverse traveling wave. This represents the situation in single-phase machines that have an auxiliary winding in series with a capacitor often used in residential applications.

# REFERENCE-FRAME THEORY

## 3.1. INTRODUCTION

We have found that some of the machine inductances are functions of rotor position, whereupon the coefficients of the differential equations (voltage equations) that describe the behavior of these machines are rotor position dependent. A change of variables is often used to reduce the complexity of these differential equations. There are several changes of variables that are used, and it was originally thought that each change of variables was unique and therefore they were treated separately [1–4]. It was later learned that all changes of variables used to transform actual variables are contained in one [5, 6]. This general transformation refers machine variables to a frame of reference that rotates at an arbitrary angular velocity. All known real transformations are obtained from this transformation by simply assigning the speed of the rotation of the reference frame.

In this chapter, this transformation is set forth and, since many of its properties can be studied without the complexities of the machine equations, it is applied to the equations that describe resistive, inductive, and capacitive circuit elements. Using this approach, many of the basic concepts and interpretations of this general transformation

are readily and concisely established. Extending the material presented in this chapter to the analysis of ac machines is straightforward, involving a minimum of trigonometric manipulations.

### 3.2. BACKGROUND

In the late 1920s, R.H. Park [1] introduced a new approach to electric machine analysis. He formulated a change of variables that in effect replaced the variables (voltages, currents, and flux linkages) associated with the stator windings of a synchronous machine with variables associated with fictitious windings rotating at the electrical angular velocity of the rotor. This change of variables is often described as transforming or referring the stator variables to a frame of reference fixed in the rotor. Park's transformation, which revolutionized electric machine analysis, has the unique property of eliminating all rotor position-dependent inductances from the voltage equations of the synchronous machine that occur due to (1) electric circuits in relative motion and (2) electric circuits with varying magnetic reluctance.

In the late 1930s, H.C. Stanley [2] employed a change of variables in the analysis of induction machines. He showed that the varying mutual inductances in the voltage equations of an induction machine due to electric circuits in relative motion could be eliminated by transforming the variables associated with the rotor windings (rotor variables) to variables associated with fictitious stationary windings. In this case, the rotor variables are transformed to a frame of reference fixed in the stator.

G. Kron [3] introduced a change of variables that eliminated the position-dependent mutual inductances of a symmetrical induction machine by transforming both the stator variables and the rotor variables to a reference frame rotating in synchronism with the fundamental angular velocity of the stator variables. This reference frame is commonly referred to as the synchronously rotating reference frame.

D.S. Brereton et al. [4] employed a change of variables that also eliminated the varying mutual inductances of a symmetrical induction machine by transforming the stator variables to a reference frame rotating at the electrical angular velocity of the rotor. This is essentially Park's transformation applied to induction machines.

Park, Stanley, Kron, and Brereton et al. developed changes of variables, each of which appeared to be uniquely suited for a particular application. Consequently, each transformation was derived and treated separately in literature until it was noted in 1965 [5] that all known real transformations used in induction machine analysis are contained in one general transformation that eliminates all rotor position-dependent mutual inductances by referring the stator and the rotor variables to a frame of reference that may rotate at any angular velocity or remain stationary. All known real transformations may then be obtained by simply assigning the appropriate speed of rotation, which may in fact be zero, to this so-called *arbitrary reference frame*. Later, it was noted that the stator variables of a synchronous machine could also be referred to the arbitrary reference frame [6]. However, we will find that the varying inductances of a synchronous machine are eliminated only if the reference frame is rotating at the electrical angular velocity of the rotor (Park's transformation); consequently, the arbitrary reference frame

does not offer the advantages in the analysis of the synchronous machines that it does in the case of induction machines.

### 3.3. EQUATIONS OF TRANSFORMATION: CHANGE OF VARIABLES

Although changes of variables are used in the analysis of ac machines to eliminate time-varying inductances, changes of variables are also employed in the analysis of various static, constant-parameter power-system components and control systems associated with electric drives. For example, in many of the computer programs used for transient and dynamic stability studies of large power systems, the variables of all power system components, except for the synchronous machines, are represented in a reference frame rotating at synchronous speed, wherein the electric transients are often neglected. Hence, the variables associated with the transformers, transmission lines, loads, capacitor banks, and static var units, for example, must be transformed to the synchronous rotating reference frame by a change of variables. Similarly, the “average value” of the variables associated with the conversion process in electric drive systems and in high-voltage ac–dc systems are often expressed in the synchronously rotating reference frame.

Fortunately, all known real transformations for these components and controls are also contained in the transformation to the arbitrary reference frame, the same transformation used for the stator variables of the induction and synchronous machines and for the rotor variables of induction machines. Although we could formulate one transformation to the arbitrary reference frame that could be applied to all variables, it is preferable to consider only the variables associated with stationary circuits in this chapter and then modify this analysis for the variables associated with the rotor windings of the induction machine at the time it is analyzed.

A change of variables that formulates a transformation of the three-phase variables of stationary circuit elements to the arbitrary reference frame may be expressed as

$$\mathbf{f}_{qd0s} = \mathbf{K}_s \mathbf{f}_{abcs} \quad (3.3-1)$$

where

$$(\mathbf{f}_{qd0s})^T = [f_{qs} \quad f_{ds} \quad f_{0s}] \quad (3.3-2)$$

$$(\mathbf{f}_{abcs})^T = [f_{as} \quad f_{bs} \quad f_{cs}] \quad (3.3-3)$$

$$\mathbf{K}_s = \frac{2}{3} \begin{bmatrix} \cos \theta & \cos\left(\theta - \frac{2\pi}{3}\right) & \cos\left(\theta + \frac{2\pi}{3}\right) \\ \sin \theta & \sin\left(\theta - \frac{2\pi}{3}\right) & \sin\left(\theta + \frac{2\pi}{3}\right) \\ \frac{1}{2} & \frac{1}{2} & \frac{1}{2} \end{bmatrix} \quad (3.3-4)$$

where the angular position and velocity of the arbitrary reference frame are related as

$$\frac{d\theta}{dt} = \omega \quad (3.3-5)$$

It can be shown that the inverse transformation is

$$(\mathbf{K}_s)^{-1} = \begin{bmatrix} \cos \theta & \sin \theta & 1 \\ \cos\left(\theta - \frac{2\pi}{3}\right) & \sin\left(\theta - \frac{2\pi}{3}\right) & 1 \\ \cos\left(\theta + \frac{2\pi}{3}\right) & \sin\left(\theta + \frac{2\pi}{3}\right) & 1 \end{bmatrix} \quad (3.3-6)$$

In the above equations,  $f$  can represent either voltage, current, flux linkage, or electric charge. The superscript  $T$  denotes the transpose of a matrix. The  $s$  subscript indicates the variables, parameters, and transformation associated with stationary circuits. The angular displacement  $\theta$  must be continuous; however, the angular velocity associated with the change of variables is unspecified. The frame of reference may rotate at any constant or varying angular velocity, or it may remain stationary. The connotation of arbitrary stems from the fact that the angular velocity of the transformation is unspecified and can be selected arbitrarily to expedite the solution of the system equations or to satisfy the system constraints. The change of variables may be applied to variables of any waveform and time sequence; however, we will find that, for a three-phase electrical system, the transformation given above is particularly appropriate for an  $abc$  sequence.

Although the transformation to the arbitrary reference frame is a change of variables and needs no physical connotation, it is often convenient to visualize the transformation equations as trigonometric relationships between variables as shown in Figure 3.3-1. In particular, the equations of transformation may be thought of as if the  $f_{qs}$  and  $f_{ds}$  variables are “directed” along paths orthogonal to each other and rotating at an angular velocity of  $\omega$ , whereupon  $f_{as}$ ,  $f_{bs}$ , and  $f_{cs}$  may be considered as variables directed along stationary paths each displaced by  $120^\circ$ . If  $f_{as}$ ,  $f_{bs}$ , and  $f_{cs}$  are resolved into  $f_{qs}$ , the first row of (3.3-1) is obtained, and if  $f_{as}$ ,  $f_{bs}$ , and  $f_{cs}$  are resolved into  $f_{ds}$ , the second row is obtained. It is important to note that  $f_0$  variables are not associated with the arbitrary reference frame. Instead, the zero variables are related arithmetically to the  $abc$  variables, independent of  $\omega$  and  $\theta$ . Portraying the transformation as shown in Figure 3.3-1 is particularly convenient when applying it to ac machines where the direction of  $f_{as}$ ,  $f_{bs}$ , and  $f_{cs}$  may also be thought of as the direction of the magnetic axes of the stator windings. We will find that the direction of  $f_{qs}$  and  $f_{ds}$  can be considered as the direction of the magnetic axes of the “new” windings created by the change of variables. It is also important not to confuse  $f_{as}$ ,  $f_{bs}$ , and  $f_{cs}$  or  $f_{qs}$  and  $f_{ds}$  with phasors.

The total instantaneous power of a three-phase system may be expressed in  $abc$  variables as

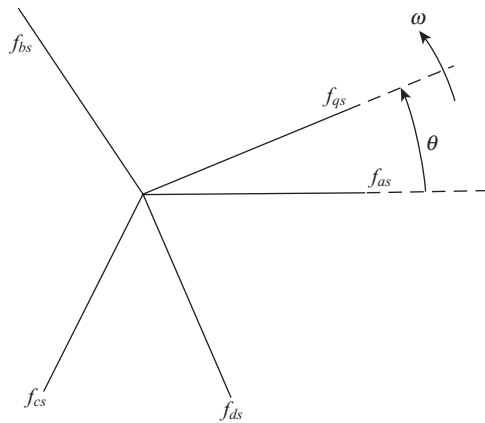


Figure 3.3-1. Transformation for stationary circuits portrayed by trigonometric relationships.

$$P_{abcs} = v_{as}i_{as} + v_{bs}i_{bs} + v_{cs}i_{cs} \quad (3.3-7)$$

The total power expressed in the  $qd0$  variables must equal the total power expressed in the  $abc$  variables, hence using (3.3-1) to replace actual currents and voltages in (3.3-7) yields

$$\begin{aligned} P_{qd0s} &= P_{abcs} \\ &= \frac{3}{2}(v_{qs}i_{qs} + v_{ds}i_{ds} + 2v_{0s}i_{0s}) \end{aligned} \quad (3.3-8)$$

The  $3/2$  factor comes about due to the choice of the constant used in the transformation. Although the waveforms of the  $qs$  and  $ds$  voltages, currents, flux linkages, and electric charges are dependent upon the angular velocity of the frame of reference, the waveform of total power is independent of the frame of reference. In other words, the waveform of the total power is the same regardless of the reference frame in which it is evaluated.

### 3.4. STATIONARY CIRCUIT VARIABLES TRANSFORMED TO THE ARBITRARY REFERENCE FRAME

It is convenient to treat resistive, inductive, and capacitive circuit elements separately.

#### Resistive Elements

For a three-phase resistive circuit

$$\mathbf{v}_{abcs} = \mathbf{r}_s \mathbf{i}_{abcs} \quad (3.4-1)$$

From (3.3-1)

$$\mathbf{v}_{qd0s} = \mathbf{K}_s \mathbf{r}_s (\mathbf{K}_s)^{-1} \mathbf{i}_{qd0s} \quad (3.4-2)$$

It is necessary to specify the resistance matrix  $\mathbf{r}_s$  before proceeding. All stator phase windings of either a synchronous or a symmetrical induction machine are designed to have the same resistance. Similarly, transformers, capacitor banks, transmission lines and, in fact, all power-system components are designed so that all phases have equal or near-equal resistances. Even power-system loads are distributed between phases so that all phases are loaded nearly equal. If the nonzero elements of the diagonal matrix  $\mathbf{r}_s$  are equal, then

$$\mathbf{K}_s \mathbf{r}_s (\mathbf{K}_s)^{-1} = \mathbf{r}_s \quad (3.4-3)$$

Thus, the resistance matrix associated with the arbitrary reference variables ( $f_{qs}$ ,  $f_{ds}$ , and  $f_{0s}$ ) is equal to the resistance matrix associated with the actual variables if each phase of the actual circuit has the same resistance. If the phase resistances are unequal (unbalanced or unsymmetrical), then the resistance matrix associated with the arbitrary reference-frame variables contains sinusoidal functions of  $\theta$  except when  $\omega = 0$ , whereupon  $\mathbf{K}_s$  is algebraic. In other words, if the phase resistances are unbalanced, the transformation yields constant resistances only if the reference frame is fixed where the unbalance physically exists. This feature is quite easily illustrated by substituting  $\mathbf{r}_s = \text{diag}[r_{as} \ r_{bs} \ r_{cs}]$  into  $\mathbf{K}_s \mathbf{r}_s (\mathbf{K}_s)^{-1}$ .

## Inductive Elements

For a three-phase inductive circuit, we have

$$\mathbf{v}_{abcs} = p \boldsymbol{\lambda}_{abcs} \quad (3.4-4)$$

where  $p$  is the operator  $d/dt$ . In the case of the magnetically linear system, it has been customary to express the flux linkages as a product of inductance and current matrices before performing a change of variables. However, the transformation is valid for flux linkages and an extensive amount of work can be avoided by transforming the flux linkages directly. This is especially true in the analysis of ac machines, where the inductance matrix is a function of rotor position. Thus, in terms of the substitute variables, (3.4-4) becomes

$$\mathbf{v}_{qd0s} = \mathbf{K}_s p [(\mathbf{K}_s)^{-1} \boldsymbol{\lambda}_{qd0s}] \quad (3.4-5)$$

which can be written as

$$\mathbf{v}_{qd0s} = \mathbf{K}_s p [(\mathbf{K}_s)^{-1}] \boldsymbol{\lambda}_{qd0s} + \mathbf{K}_s (\mathbf{K}_s)^{-1} p \boldsymbol{\lambda}_{qd0s} \quad (3.4-6)$$

It is easy to show that

$$p[(\mathbf{K}_s)^{-1}] = \omega \begin{bmatrix} -\sin \theta & \cos \theta & 0 \\ -\sin\left(\theta - \frac{2\pi}{3}\right) & \cos\left(\theta - \frac{2\pi}{3}\right) & 0 \\ -\sin\left(\theta + \frac{2\pi}{3}\right) & \cos\left(\theta + \frac{2\pi}{3}\right) & 0 \end{bmatrix} \quad (3.4-7)$$

Therefore,

$$\mathbf{K}_s p[(\mathbf{K}_s)^{-1}] = \omega \begin{bmatrix} 0 & 1 & 0 \\ -1 & 0 & 0 \\ 0 & 0 & 0 \end{bmatrix} \quad (3.4-8)$$

Trigonometric identities given in Appendix A are helpful in obtaining (3.4-8). Equation (3.4-6) may now be expressed as

$$\mathbf{v}_{qd0s} = \omega \boldsymbol{\lambda}_{dqs} + p \boldsymbol{\lambda}_{qd0s} \quad (3.4-9)$$

where

$$(\boldsymbol{\lambda}_{dqs})^T = [\lambda_{ds} \quad -\lambda_{qs} \quad 0] \quad (3.4-10)$$

Equation (3.4-6) is often written in expanded form as

$$v_{qs} = \omega \lambda_{ds} + p \lambda_{qs} \quad (3.4-11)$$

$$v_{ds} = -\omega \lambda_{qs} + p \lambda_{ds} \quad (3.4-12)$$

$$v_{0s} = p \lambda_{0s} \quad (3.4-13)$$

The first term on the right side of (3.4-11) or (3.4-12) is referred to as a "speed voltage," with the speed being the angular velocity of the arbitrary reference frame. It is clear that the speed voltage terms are zero if  $\omega$  is zero, which, of course, is when the reference frame is stationary. Clearly, the voltage equations for the three-phase inductive circuit become the familiar time rate of change of flux linkages if the reference frame is fixed where the circuit physically exists. Also, since (3.4-4) is valid in general, it follows that (3.4-11)–(3.4-13) are valid regardless if the system is magnetically linear or nonlinear and regardless of the form of the inductance matrix if the system is magnetically linear.

For a linear system, the flux linkages may be expressed

$$\boldsymbol{\lambda}_{abcs} = \mathbf{L}_s \mathbf{i}_{abcs} \quad (3.4-14)$$

Whereupon, the flux linkages in the arbitrary reference frame may be written as

$$\boldsymbol{\lambda}_{qd0s} = \mathbf{K}_s \mathbf{L}_s (\mathbf{K}_s)^{-1} \mathbf{i}_{qd0s} \quad (3.4-15)$$

As is the case of the resistive circuit, it is necessary to specify the inductance matrix before proceeding with the evaluation of (3.4-15). However, once the inductance matrix is specified, the procedure for expressing any three-phase inductive circuit in the arbitrary reference frame reduces to one of evaluating (3.4-15) and substituting the resulting  $\lambda_{qs}$ ,  $\lambda_{ds}$ , and  $\lambda_{0s}$  into the voltage equations (3.4-11)–(3.4-13). This procedure is straightforward, with a minimum of matrix manipulations compared with the work involved if, for a linear system, the flux linkage matrix  $\lambda_{abcs}$  is replaced by  $\mathbf{L}_s \mathbf{i}_{abcs}$  before performing the transformation.

If, for example,  $\mathbf{L}_s$  is a diagonal matrix with all nonzero terms equal, then

$$\mathbf{K}_s \mathbf{L}_s (\mathbf{K}_s)^{-1} = \mathbf{L}_s \quad (3.4-16)$$

A matrix of this form could describe the inductance of a balanced three-phase inductive load, a three-phase set of line reactors used in high-voltage transmission systems or any symmetrical three-phase inductive network without coupling between phases. It is clear that the comments regarding unbalanced or unsymmetrical phase resistances also apply in the case of unsymmetrical inductances.

An inductance matrix that is common is of the form

$$\mathbf{L}_s = \begin{bmatrix} L_s & M & M \\ M & L_s & M \\ M & M & L_s \end{bmatrix} \quad (3.4-17)$$

where  $L_s$  is a self inductance and  $M$  is a mutual inductance. This general form can be used to describe the stator self- and mutual inductance relationships of the stator phases of symmetrical induction machines, and round-rotor synchronous machines with arbitrary winding arrangement, including double-layer and integer and noninteger slot/pole/phase windings. From our work in Chapter 2, we realize that this inductance matrix is of a form that describes the self- and mutual inductances relationships of the stator phases of a symmetrical induction machine and the stator phases of a round-rotor synchronous machine with or without mutual leakage paths between stator windings. It can also describe the coupling of a symmetrical transmission line. Example diagrams that portray such coupling are shown in Figure 3.4-1. It is left to the reader to show that for  $\mathbf{L}_s$  given by (3.4-17)

$$\mathbf{K}_s \mathbf{L}_s (\mathbf{K}_s)^{-1} = \begin{bmatrix} L_s - M & 0 & 0 \\ 0 & L_s - M & 0 \\ 0 & 0 & L_s + 2M \end{bmatrix} \quad (3.4-18)$$

Linear three-phase coupled systems are magnetically symmetrical if the diagonal elements are equal and all off-diagonal elements of the inductance matrix are also equal. Equation (3.4-17) is of this form. We see from (3.4-18) that, for a symmetrical system,  $\mathbf{K}_s \mathbf{L}_s (\mathbf{K}_s)^{-1}$  yields a diagonal matrix that, in effect, magnetically decouples the substitute variables in all reference frames. This is a very important feature of the transformation.

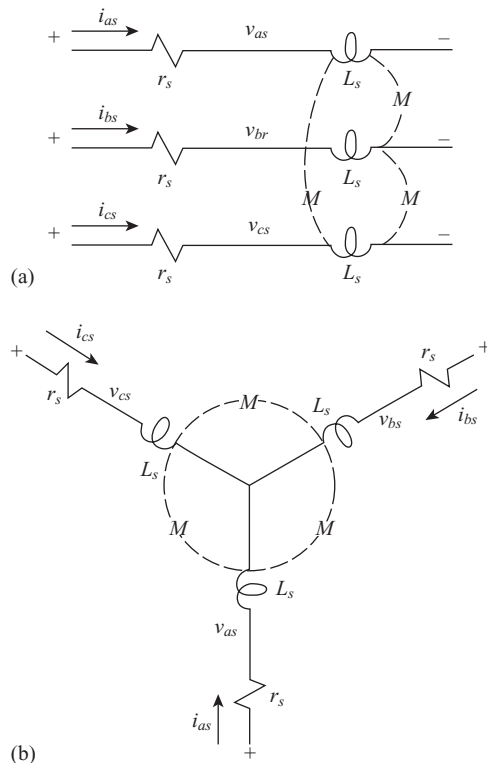


Figure 3.4-1. Three-phase RL circuit. (a) Symmetrical transmission line; (b) wye connection.

On the other hand, we have seen in Section 1.4 and Chapter 2 that the self- and mutual inductances between the stator phases of the salient-pole synchronous machine form a magnetically unsymmetrical system. It will be shown that for this case, there is only one reference frame, the reference frame rotating at the electrical angular velocity of the rotor, wherein the substitute variables are not magnetically coupled.

## Capacitive Elements

For a three-phase capacitive circuit, we have

$$\mathbf{i}_{abcs} = p\mathbf{q}_{abcs} \quad (3.4-19)$$

Incorporating the substitute variables yields

$$\mathbf{i}_{qd0s} = \mathbf{K}_s p[(\mathbf{K}_s)^{-1} \mathbf{q}_{qd0s}] \quad (3.4-20)$$

that can be written as

$$\mathbf{i}_{qd0s} = \mathbf{K}_s p[(\mathbf{K}_s)^{-1}] \mathbf{q}_{qd0s} + \mathbf{K}_s (\mathbf{K}_s)^{-1} p \mathbf{q}_{qd0s} \quad (3.4-21)$$

Utilizing (3.4-8) yields

$$\mathbf{i}_{qd0s} = \omega \mathbf{q}_{dqs} + p \mathbf{q}_{qd0s} \quad (3.4-22)$$

where

$$(\mathbf{q}_{dqs})^T = [q_{ds} \quad -q_{qs} \quad 0] \quad (3.4-23)$$

In expanded form, we have

$$i_{qs} = \omega q_{ds} + p q_{qs} \quad (3.4-24)$$

$$i_{ds} = -\omega q_{qs} + p q_{ds} \quad (3.4-25)$$

$$i_{0s} = p q_{0s} \quad (3.4-26)$$

Considering the terminology of “speed voltages” as used in the case of inductive circuits, it would seem appropriate to refer to the first term on the right side of either (3.4-24) or (3.4-25) as “speed currents.” Also, as in the case of inductive circuits, the equations revert to the familiar form in the stationary reference frame ( $\omega = 0$ ).

Equations (3.4-24)–(3.4-26) are valid regardless of the relationship between charge and voltage. For a linear capacitive system, we have

$$\mathbf{q}_{abcs} = \mathbf{C}_s \mathbf{v}_{abcs} \quad (3.4-27)$$

Thus, in the arbitrary reference frame we have

$$\mathbf{q}_{qd0s} = \mathbf{K}_s \mathbf{C}_s (\mathbf{K}_s)^{-1} \mathbf{v}_{qd0s} \quad (3.4-28)$$

Once the capacitance matrix is specified,  $q_{qs}$ ,  $q_{ds}$ , and  $q_{0s}$  can be determined and substituted into (3.4-24)–(3.4-26). The procedure and limitations are analogous to those in the case of the inductive circuits. A diagonal capacitance matrix with equal nonzero elements describes, for example, a three-phase capacitor bank used for power factor correction and the series capacitance used for transmission line compensation or any three-phase electrostatic system without coupling between phases. A three-phase transmission system is often approximated as a symmetrical system, whereupon the inductance and capacitance matrices may be written in a form similar to (3.4-17).

**EXAMPLE 3A** For the purpose of demonstrating the transformation of variables to the arbitrary reference frame, let us consider a three-phase RL circuit defined by

$$\mathbf{r}_s = \text{diag}[r_s \quad r_s \quad r_s] \quad (3A-1)$$

$$\mathbf{L}_s = \begin{bmatrix} L_{ls} + L_{ms} & -\frac{1}{2}L_{ms} & -\frac{1}{2}L_{ms} \\ -\frac{1}{2}L_{ms} & L_{ls} + L_{ms} & -\frac{1}{2}L_{ms} \\ -\frac{1}{2}L_{ms} & -\frac{1}{2}L_{ms} & L_{ls} + L_{ms} \end{bmatrix} \quad (3A-2)$$

Here we have broken up the self-inductance into a leakage,  $L_{ls}$ , and magnetizing inductance,  $L_{ms}$ . Also, the mutual inductance  $M$  is equal to  $-(1/2)L_{ms}$ . The voltage equations in the arbitrary reference frame can be written from (3.4-2) and (3.4-9), in expanded form as

$$v_{qs} = r_s i_{qs} + \omega \lambda_{ds} + p \lambda_{qs} \quad (3A-3)$$

$$v_{ds} = r_s i_{ds} - \omega \lambda_{qs} + p \lambda_{ds} \quad (3A-4)$$

$$v_{0s} = r_s i_{0s} + p \lambda_{0s} \quad (3A-5)$$

Since the example inductance matrix given by (3A-2) is in the same form as (3.4-17), we can use (3.4-18) as a guide to evaluate  $\mathbf{K}_s \mathbf{L}_s (\mathbf{K}_s)^{-1}$ . Thus

$$\mathbf{K}_s \mathbf{L}_s (\mathbf{K}_s)^{-1} = \begin{bmatrix} L_{ls} + \frac{3}{2}L_{ms} & 0 & 0 \\ 0 & L_{ls} + \frac{3}{2}L_{ms} & 0 \\ 0 & 0 & L_{ls} \end{bmatrix} \quad (3A-6)$$

Thus  $\lambda_{qs}$ ,  $\lambda_{ds}$ , and  $\lambda_{0s}$  in (3A-3)–(3A-5) become

$$\lambda_{qs} = \left( L_{ls} + \frac{3}{2}L_{ms} \right) i_{qs} \quad (3A-7)$$

$$\lambda_{ds} = \left( L_{ls} + \frac{3}{2}L_{ms} \right) i_{ds} \quad (3A-8)$$

$$\lambda_{0s} = L_{ls} i_{0s} \quad (3A-9)$$

The equivalent circuit that portrays the voltage equations (3A-3)–(3A-5) with flux linkages of (3A-7)–(3A-9) is given in Figure 3A-1.

In this chapter, we have chosen to introduce the transformation to the arbitrary reference frame by considering only stationary circuits. The complexities of the position-dependent inductances are purposely omitted. Although the transformation diagonalizes the inductance matrix and thus uncouples the phases, one cannot see the advantages of transforming to any reference frame other than the stationary reference frame since it tends to complicate the voltage equations of the static circuits. In other words, the above voltage equations are most easily solved with  $\omega = 0$ . However, our purpose is to set forth the basic concepts and the interpretations of this general transformation; its advantages in machine analysis will be demonstrated in later chapters.

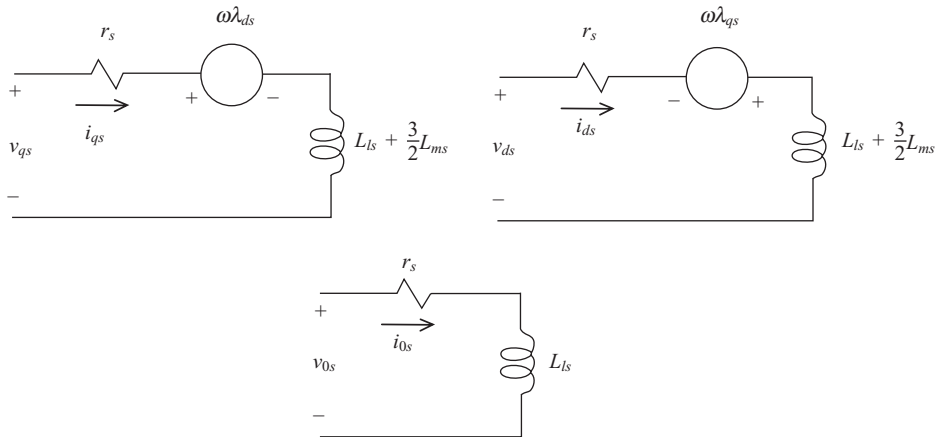


**Figure 3A-1.** Arbitrary reference-frame equivalent circuits for three-phase RL circuit described in Example 3A.

### 3.5. COMMONLY USED REFERENCE FRAMES

It is instructive to take a preliminary look at the reference frames commonly used in the analysis of electric machines and power system components; namely, the arbitrary, stationary, rotor, and synchronous reference frames. Information regarding each of these reference frames as applied to stationary circuits is given in the following table.

For purposes at hand, it is sufficient for us to define the synchronously rotating or the synchronous reference frame as the reference frame rotating at the electrical angular velocity corresponding to the fundamental frequency of the variables associated with stationary circuits, herein denoted as  $\omega_e$ . In the case of ac machines,  $\omega_e$  is the electrical angular velocity of the air-gap rotating magnetic field established by stator currents of fundamental frequency.

Reference-Frame Speed	Interpretation	Notation	
		Variables	Transformation
$\omega$ (unspecified)	Stationary circuit variables referred to an arbitrary reference frame	$\mathbf{f}_{qd0s}$ or $f_{qs}, f_{ds}, f_{0s}$	$\mathbf{K}_s$
0	Stationary circuit variables referred to a stationary reference frame	$\mathbf{f}_{qd0s}^s$ or $f_{qs}^s, f_{ds}^s, f_{0s}$	$\mathbf{K}_s^s$
$\omega_r$	Stationary circuit variables referred to a reference frame fixed in the rotor	$\mathbf{f}_{qd0s}^r$ or $f_{qs}^r, f_{ds}^r, f_{0s}$	$\mathbf{K}_s^r$
$\omega_e$	Stationary circuit variables referred to a synchronously rotating reference frame	$\mathbf{f}_{qd0s}^e$ or $f_{qs}^e, f_{ds}^e, f_{0s}$	$\mathbf{K}_s^e$

The notation requires some explanation. We have previously established that the  $s$  subscript denotes variables and transformations associated with circuits that are stationary

in “real life” as opposed to rotor circuits that are free to rotate. Later, when considering the induction machine, we will use the subscript  $r$  to denote variables and the transformation associated with rotor circuits. The raised index is used to denote the  $qs$  and  $ds$  variables and transformation associated with a specific reference frame except in the case of the arbitrary reference frame that does not have a raised index. Since the  $0s$  variables are not associated with a reference frame, a raised index is not assigned to  $f_{0s}$ . The transformation of stationary circuits to a stationary reference frame was developed by E. Clarke [7], who used the notation  $f_a$ ,  $f_b$ , and  $f_0$  rather than  $f_{qs}^s$ ,  $f_{ds}^s$ ,  $f_{0s}$ . In Park’s transformation to the rotor reference frame, he denoted the variables  $f_q$ ,  $f_d$ , and  $f_0$  rather than  $f_{qs}^r$ ,  $f_{ds}^r$ , and  $f_{0s}$ . There appears to be no established notation for the variables in the synchronously rotating reference frame. We will use the  $e$  superscript as indicated in the table. As mentioned previously, the voltage equations for all reference frames may be obtained from those in the arbitrary reference frame by assigning the speed of the desired reference frame to  $\omega$ .

### 3.6. TRANSFORMATION OF A BALANCED SET

Although the transformation equations are valid regardless of the waveform of the variables, it is instructive to consider the characteristics of the transformation when the three-phase system is symmetrical and the voltages and currents form a balanced three-phase set of  $abc$  sequence as given by (3.6-1)–(3.6-4). A balanced three-phase set is generally defined as a set of equal-amplitude sinusoidal quantities that are displaced by  $120^\circ$ . Since the sum of this set is zero, the  $0s$  variables are zero.

$$f_{as} = \sqrt{2} f_s \cos \theta_{ef} \quad (3.6-1)$$

$$f_{bs} = \sqrt{2} f_s \cos \left( \theta_{ef} - \frac{2\pi}{3} \right) \quad (3.6-2)$$

$$f_{cs} = \sqrt{2} f_s \cos \left( \theta_{ef} + \frac{2\pi}{3} \right) \quad (3.6-3)$$

where  $f_s$  may be a function of time and

$$\frac{d\theta_{ef}}{dt} = \omega_e \quad (3.6-4)$$

Substituting (3.6-1)–(3.6-3) into the transformation to the arbitrary reference frame (3.3-1) yields

$$f_{qs} = \sqrt{2} f_s \cos(\theta_{ef} - \theta) \quad (3.6-5)$$

$$f_{ds} = -\sqrt{2} f_s \sin(\theta_{ef} - \theta) \quad (3.6-6)$$

$$f_{0s} = 0 \quad (3.6-7)$$

With the three-phase variables as given in (3.6-1)–(3.6-3), the  $qs$  and  $ds$  variables form a balanced two-phase set in all reference frames except when  $\omega = \omega_e$ . In this, the synchronously rotating reference frame, the  $qs$  and  $ds$  quantities become

$$f_{qs}^e = \sqrt{2}f_s \cos(\theta_{ef} - \theta_e) \quad (3.6-8)$$

$$f_{ds}^e = -\sqrt{2}f_s \sin(\theta_{ef} - \theta_e) \quad (3.6-9)$$

where  $\theta_e$  is the angular position of the synchronously rotating reference frame. It is important to note that  $\theta_e$  and  $\theta_{ef}$  both have an angular velocity of  $\omega_e$ . Hence,  $\theta_{ef} - \theta_e$  is a constant depending upon the initial values of the variable being transformed,  $\theta_{ef}(0)$ , and the initial position of the synchronously rotating reference frame,  $\theta_e(0)$ . Equations (3.6-8) and (3.6-9) reveal a property that is noteworthy; there is one reference frame where a balanced set will appear as constants if the amplitude  $f_s$  is constant. In other words, if a constant amplitude balanced set appears in any reference frame, then there is another reference frame where this balanced set appears as constants. Obviously, the converse is true.

### 3.7. BALANCED STEADY-STATE PHASOR RELATIONSHIPS

For balanced steady-state conditions, the amplitude and frequency are constants and  $\theta_{ef}$  becomes  $\omega_e t + \theta_{ef}(0)$ , whereupon (3.6-1)–(3.6-3) may be expressed as

$$\begin{aligned} F_{as} &= \sqrt{2}F_s \cos[\omega_e t + \theta_{ef}(0)] \\ &= \text{Re}[\sqrt{2}F_s e^{j\theta_{ef}(0)} e^{j\omega_e t}] \end{aligned} \quad (3.7-1)$$

$$\begin{aligned} F_{bs} &= \sqrt{2}F_s \cos\left[\omega_e t + \theta_{ef}(0) - \frac{2\pi}{3}\right] \\ &= \text{Re}[\sqrt{2}F_s e^{j[\theta_{ef}(0) - 2\pi/3]} e^{j\omega_e t}] \end{aligned} \quad (3.7-2)$$

$$\begin{aligned} F_{cs} &= \sqrt{2}F_s \cos\left[\omega_e t + \theta_{ef}(0) + \frac{2\pi}{3}\right] \\ &= \text{Re}[\sqrt{2}F_s e^{j[\theta_{ef}(0) + 2\pi/3]} e^{j\omega_e t}] \end{aligned} \quad (3.7-3)$$

where  $\theta_{ef}(0)$  corresponds to the time-zero value of the three-phase variables. The upper-case are used to denote steady-state quantities. If the speed of the arbitrary reference frame is an unspecified constant, then  $\theta = \omega t + \theta(0)$ , and for the balanced steady-state conditions (3.6-5) and (3.6-6) may be expressed as

$$\begin{aligned} F_{qs} &= \sqrt{2}F_s \cos[(\omega_e - \omega)t + \theta_{ef}(0) - \theta(0)] \\ &= \text{Re}[\sqrt{2}F_s e^{j[\theta_{ef}(0) - \theta(0)]} e^{j(\omega_e - \omega)t}] \end{aligned} \quad (3.7-4)$$

$$\begin{aligned} F_{ds} &= -\sqrt{2}F_s \sin[(\omega_e - \omega)t + \theta_{ef}(0) - \theta(0)] \\ &= \text{Re}[j\sqrt{2}F_s e^{j[\theta_{ef}(0) - \theta(0)]} e^{j(\omega_e - \omega)t}] \end{aligned} \quad (3.7-5)$$

From (3.7-1), the phasor representing the *as* variables is

$$\tilde{F}_{as} = F_s e^{j\theta_{ef}(0)} \quad (3.7-6)$$

If  $\omega$  is not equal to  $\omega_e$ , then  $F_{qs}$  and  $F_{ds}$  are sinusoidal quantities, and from (3.7-4) and (3.7-5), we have

$$\tilde{F}_{qs} = F_s e^{j[\theta_{ef}(0) - \theta(0)]} \quad (3.7-7)$$

$$\tilde{F}_{ds} = j\tilde{F}_{qs} \quad (3.7-8)$$

It is necessary to consider negative frequencies since  $\omega$  can be greater than  $\omega_e$ . The phasors rotate in the counterclockwise direction for  $\omega < \omega_e$  and in the clockwise direction for  $\omega > \omega_e$ .

In the analysis of steady-state operation, we are free to select time zero. It is often convenient to set  $\theta(0) = 0$ . Then from (3.7-6) and (3.7-7)

$$\tilde{F}_{as} = \tilde{F}_{qs} \quad (3.7-9)$$

Thus, in all asynchronously rotating reference frames ( $\omega \neq \omega_e$ ) with  $\theta(0) = 0$ , the phasor representing the *as* quantities is equal to the phasor representing the *qs* quantities. For balanced steady-state conditions, the phasor representing the variables of one phase need only be shifted in order to represent the variables in the other phases.

In the synchronously rotating reference frame,  $\omega = \omega_e$  and  $\theta_e(0)$  is the zero position of the arbitrary reference frame. Recall  $\theta_{ef}(0)$  is the zero position of the *abc* quantities. If we continue to use uppercase letters to denote the steady-state quantities, then from (3.7-4) and (3.7-5), we obtain

$$F_{qs}^e = \text{Re}[\sqrt{2}F_s e^{j[\theta_{ef}(0) - \theta_e(0)]}] \quad (3.7-10)$$

$$F_{ds}^e = \text{Re}[j\sqrt{2}F_s e^{j[\theta_{ef}(0) - \theta_e(0)]}] \quad (3.7-11)$$

If we select the time-zero position of the synchronously rotating reference frame to be zero, then,  $\theta_e(0) = 0$  in (3.7-10) and (3.7-11) and

$$F_{qs}^e = \sqrt{2}F_s \cos \theta_{ef}(0) \quad (3.7-12)$$

$$F_{ds}^e = -\sqrt{2}F_s \sin \theta_{ef}(0) \quad (3.7-13)$$

Thus, we see from a comparison of (3.7-6) with (3.7-12) and (3.7-13) that

$$\sqrt{2}\tilde{F}_{as} = F_{qs}^e - jF_{ds}^e \quad (3.7-14)$$

Since  $\tilde{F}_{as} = \tilde{F}_{qs}$ , (3.7-14) is important in that it relates the synchronously rotating reference-frame variables to a phasor in all other reference frames.  $\tilde{F}_{as}$  is a phasor that

represents a sinusoidal quantity; however,  $F_{qs}^e$  and  $F_{ds}^e$  are not phasors. They are real quantities representing the constant steady-state variables of the synchronously rotating reference frame.

**EXAMPLE 3B** It is helpful to discuss the difference between the directions of  $f_{as}$ ,  $f_{bs}$ , and  $f_{cs}$ , as shown in Figure 3.3-1 and phasors. The relationships shown in Figure 3.3-1 trigonometrically illustrate the transformation defined by (3.3-1)–(3.3-6). Figure 3.3-1 is not a phasor diagram and should not be interpreted as such. It simply depicts the relationships between the directions of  $f_{as}$ ,  $f_{bs}$ ,  $f_{cs}$ ,  $f_{qs}$ , and  $f_{ds}$  as dictated by the equations of transformation regardless of the instantaneous values of these variables. On the other hand, phasors provide an analysis tool for steady-state, sinusoidal variables. The magnitude and phase angle of the phasor are directly related to the amplitude of the sinusoidal variation and its phase position relative to a reference. The balanced set given by (3.6-1)–(3.6-3) may be written as (3.7-1)–(3.7-3) for steady-state conditions. The phasor representation for  $as$  variables is given by (3.7-6). The phasor representation for the balanced set is

$$\tilde{F}_{as} = F_s e^{j\theta_{ef}(0)} \quad (3B-1)$$

$$\tilde{F}_{bs} = F_s e^{j[\theta_{ef}(0) - 2\pi/3]} \quad (3B-2)$$

$$\tilde{F}_{cs} = F_s e^{j[\theta_{ef}(0) + 2\pi/3]} \quad (3B-3)$$

The phasor diagram is shown in Figure 3B-1. For balanced conditions, the phasors that form an *abc* sequence are displaced from each other by  $120^\circ$  and each with a phase angle of  $\theta_{ef}(0)$ . The directions of  $f_{as}$ ,  $f_{bs}$ , and  $f_{cs}$  in Figure 3.3-1, that are fixed by the transformation, are such that  $f_{cs}$  is directed  $-120^\circ$  from  $f_{as}$ . However,  $\tilde{F}_{cs}$  is  $+120^\circ$  from  $\tilde{F}_{as}$  for balanced conditions (Fig. 3B-1). Another important difference is that the phasor diagram must be rotated at  $\omega_e$  in the counterclockwise direction and the real part of the phasors is related to the instantaneous values of the three-phase set. However, the diagram of  $f_{as}$ ,  $f_{bs}$ , and  $f_{cs}$  shown in Figure 3.3-1 is always stationary for stationary circuits.

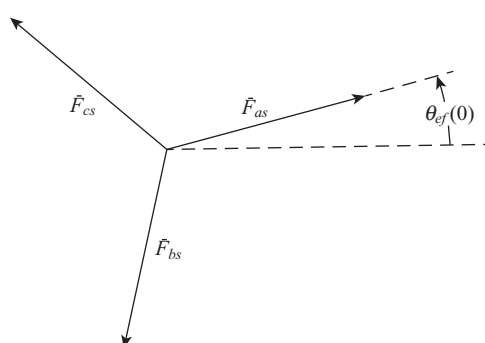


Figure 3B-1. Phasor representation for a three-phase balanced set.

### 3.8. BALANCED STEADY-STATE VOLTAGE EQUATIONS

If the three-phase system is symmetrical and if the applied voltages form a balance set as given by (3.6-1)–(3.6-3), then the steady-state currents will also form a balanced set. For equal resistance in each phase, the steady-state voltage equation in terms of the *as* variables is

$$\tilde{V}_{as} = r_s \tilde{I}_{as} \quad (3.8-1)$$

For linear, symmetrical inductive elements and since  $p = j\omega_e$ , the steady-state voltage equation may be written as

$$\tilde{V}_{as} = j\omega_e \tilde{\Lambda}_{as} \quad (3.8-2)$$

where  $\tilde{\Lambda}_{as}$  is an inductance times  $\tilde{I}_{as}$ . For linear, symmetrical capacitive elements, the steady-state current equation becomes

$$\tilde{I}_{as} = j\omega_e \tilde{Q}_{as} \quad (3.8-3)$$

where  $\tilde{Q}_{as}$  is a capacitance times  $\tilde{V}_{as}$ . It is clear that for any combination of linear symmetrical circuit elements, the steady-state voltage equation may be expressed in phasor form as

$$\tilde{V}_{as} = Z_s \tilde{I}_{as} \quad (3.8-4)$$

where  $Z_s$  is the impedance of each phase of the symmetrical three-phase system.

For equal resistance in each phase of the circuit, the balanced steady-state voltage equation for the *qs* variables in all asynchronously rotating reference frames can be written from (3.4-2) as

$$\tilde{V}_{qs} = r_s \tilde{I}_{qs} \quad (3.8-5)$$

For linear symmetrical inductive elements, the steady-state *qs* voltage equation in all asynchronously rotating reference frames may be written from (3.4-11) as

$$\tilde{V}_{qs} = \omega \tilde{\Lambda}_{ds} + j(\omega_e - \omega) \tilde{\Lambda}_{qs} \quad (3.8-6)$$

the  $(\omega_e - \omega)$  factor comes about due to the fact that the steady-state variables in all asynchronously rotating reference frames vary at the frequency corresponding to  $(\omega_e - \omega)$ . From (3.7-8),  $\tilde{\Lambda}_{ds} = j\tilde{\Lambda}_{qs}$ , thus (3.8-6) becomes

$$\tilde{V}_{qs} = j\omega_e \tilde{\Lambda}_{qs} \quad (3.8-7)$$

Similarly, for a linear symmetrical capacitive circuit, the steady-state *qs* current phasor equation in all asynchronously rotating reference frames may be written from (3.4-24) as

$$\tilde{I}_{qs} = j\omega_e \tilde{Q}_{qs} \quad (3.8-8)$$

Thus, for any combination of linear symmetrical circuit elements, the steady-state voltage equation in all asynchronously rotating reference frames may be expressed in phasor form as

$$\tilde{V}_{qs} = Z_s \tilde{I}_{qs} \quad (3.8-9)$$

where, for a given three-phase system,  $Z_s$  is the same complex impedance as in (3.8-4).

The fact that the steady-state phasor voltage equations are identical for the  $as$  and  $qs$  variables was actually known beforehand, since (3.7-9) tells us that for  $\theta(0) = 0$ , the phasors representing the  $as$  variables are equal to the phasors representing the  $qs$  variables in all asynchronously rotating reference frames; therefore, the  $as$  and  $qs$  circuits must have the same impedance.

**EXAMPLE 3C** It is instructive to derive the phasor voltage equation for an RL system with the inductance described in (3.4-17) for balanced steady-state conditions. Three methods of deriving this equation are described in the previous section. We will use all three approaches to arrive at the same steady-state, phasor voltage equation. As the first approach, the  $as$  voltage equation may be written from (3.4-1) and (3.4-4) using steady-state notation as

$$V_{as} = r_s I_{as} + L_s p I_{as} + M p I_{bs} + M p I_{cs} \quad (3C-1)$$

For balanced conditions

$$F_{as} + F_{bs} + F_{cs} = 0 \quad (3C-2)$$

Thus, (3C-1) may be written as

$$V_{as} = r_s I_{as} + (L_s - M) p I_{as} \quad (3C-3)$$

For steady-state conditions,  $p$  is replaced by  $j\omega_e$ , whereupon (3C-3) can be written in phasor form as

$$\tilde{V}_{as} = [r_s + j\omega_e (L_s - M)] \tilde{I}_{as} \quad (3C-4)$$

Comparing (3C-4) with (3.8-2) and (3.8-4), we see that

$$\tilde{\Lambda}_{as} = (L_s - M) \tilde{I}_{as} \quad (3C-5)$$

and

$$Z_s = r_s + j\omega_e (L_s - M) \quad (3C-6)$$

In the two remaining derivations, we will make use of the  $qs$  and  $ds$  voltage equations in the arbitrary reference frame. Thus, from (3.4-2), (3.4-11), and (3.4-12)

$$v_{qs} = r_s i_{qs} + \omega \lambda_{ds} + p \lambda_{qs} \quad (3C-7)$$

$$v_{ds} = r_s i_{ds} - \omega \lambda_{qs} + p \lambda_{ds} \quad (3C-8)$$

where

$$\lambda_{qs} = (L_s - M) i_{qs} \quad (3C-9)$$

$$\lambda_{ds} = (L_s - M) i_{ds} \quad (3C-10)$$

For the second method, we will start with either the  $qs$  or  $ds$  voltage equation in the asynchronously rotating reference frame. Thus, using steady-state notation, (3C-7) may be written as

$$V_{qs} = r_s I_{qs} + \omega \Lambda_{ds} + p \Lambda_{qs} \quad (3C-11)$$

For balanced steady-state conditions,  $p$  may be replaced by  $j(\omega_e - \omega)$ , and from (3.7-8),  $\Lambda_{ds} = j\Lambda_{qs}$ . Hence

$$\tilde{V}_{qs} = r_s \tilde{I}_{qs} + j\omega_e \tilde{\Lambda}_{qs} \quad (3C-12)$$

Clearly, (3.8-5) and (3.8-7) combine to give (3C-12). Substituting for  $\tilde{\Lambda}_{qs}$  yields

$$\tilde{V}_{qs} = [r_s + j\omega_e (L_s - M)] \tilde{I}_{qs} \quad (3C-13)$$

Since in all asynchronously rotating reference frames with  $\theta(0) = 0$

$$\tilde{F}_{as} = \tilde{F}_{qs} \quad (3C-14)$$

we have arrived at the same result as in the first case where we started with the  $as$  voltage equation.

For the third approach, let us write the voltage equations in the synchronously rotating reference frame. Thus, using steady-state notation, (3C-7) and (3C-8) may be written in the synchronously rotating reference frame as

$$V_{qs}^e = r_s I_{qs}^e + \omega_e \Lambda_{ds}^e + p \Lambda_{qs}^e \quad (3C-15)$$

$$V_{ds}^e = r_s I_{ds}^e - \omega_e \Lambda_{qs}^e + p \Lambda_{ds}^e \quad (3C-16)$$

For balanced steady-state conditions, the variables in the synchronously rotating reference frame are constants, therefore  $p \Lambda_{qs}^e$  and  $p \Lambda_{ds}^e$  are zero, whereupon (3C-15) and (3C-16) may be written as

$$V_{qs}^e = r_s I_{qs}^e + \omega_e (L_s - M) I_{ds}^e \quad (3C-17)$$

$$V_{ds}^e = r_s I_{ds}^e - \omega_e (L_s - M) I_{qs}^e \quad (3C-18)$$

wherein  $\Lambda_{qs}^e$  and  $\Lambda_{ds}^e$  have been written as a product of inductance and current. Now, (3.7-14) is

$$\sqrt{2} \tilde{F}_{as} = F_{qs}^e - j F_{ds}^e \quad (3C-19)$$

Thus

$$\sqrt{2} \tilde{V}_{as} = r_s I_{qs}^e + \omega_e (L_s - M) I_{ds}^e - j[r_s I_{ds}^e - \omega_e (L_s - M) I_{qs}^e] \quad (3C-20)$$

Now

$$\sqrt{2} \tilde{I}_{as} = I_{qs}^e - j I_{ds}^e \quad (3C-21)$$

and

$$j \sqrt{2} \tilde{I}_{as} = I_{ds}^e + j I_{qs}^e \quad (3C-22)$$

Substituting (3C-21) and (3C-22) into (3C-20) yields the desired equation:

$$\tilde{V}_{as} = [r_s + j \omega_e (L_s - M)] \tilde{I}_{as} \quad (3C-23)$$

### 3.9. VARIABLES OBSERVED FROM SEVERAL FRAMES OF REFERENCE

It is instructive to observe the waveform of the variables of a stationary three-phase series RL circuit in the arbitrary reference frame and in commonly used reference frames. For this purpose, we will assume that both  $\mathbf{r}_s$  and  $\mathbf{L}_s$  are diagonal matrices, each with equal nonzero elements, and the applied voltages are of the form

$$v_{as} = \sqrt{2} V_s \cos \omega_e t \quad (3.9-1)$$

$$v_{bs} = \sqrt{2} V_s \cos \left( \omega_e t - \frac{2\pi}{3} \right) \quad (3.9-2)$$

$$v_{cs} = \sqrt{2} V_s \cos \left( \omega_e t + \frac{2\pi}{3} \right) \quad (3.9-3)$$

where  $\omega_e$  is an unspecified constant. The currents, which are assumed to be zero at  $t = 0$ , may be expressed as

$$i_{as} = \frac{\sqrt{2} V_s}{|Z_s|} [-e^{-t/\tau} \cos \alpha + \cos(\omega_e t - \alpha)] \quad (3.9-4)$$

$$i_{bs} = \frac{\sqrt{2}V_s}{|Z_s|} \left[ -e^{-t/\tau} \cos\left(\alpha + \frac{2\pi}{3}\right) + \cos\left(\omega_e t - \alpha - \frac{2\pi}{3}\right) \right] \quad (3.9-5)$$

$$i_{cs} = \frac{\sqrt{2}V_s}{|Z_s|} \left[ -e^{-t/\tau} \cos\left(\alpha - \frac{2\pi}{3}\right) + \cos\left(\omega_e t - \alpha + \frac{2\pi}{3}\right) \right] \quad (3.9-6)$$

where

$$Z_s = r_s + j\omega_e L_s \quad (3.9-7)$$

$$\tau = \frac{L_s}{r_s} \quad (3.9-8)$$

$$\alpha = \tan^{-1} \frac{\omega_e L_s}{r_s} \quad (3.9-9)$$

It may at first appear necessary to solve the voltage equations in the arbitrary reference frame in order to obtain the expression for the currents in the arbitrary reference frame. This is unnecessary, since once the solution is known in one reference frame, it is known in all reference frames. In the example at hand, this may be accomplished by transforming (3.9-4)–(3.9-6) to the arbitrary reference frame. For illustrative purposes, let  $\omega$  be an unspecified constant with  $\theta(0) = 0$ , then  $\theta = \omega t$ , and in the arbitrary reference frame, we have

$$i_{qs} = \frac{\sqrt{2}V_s}{|Z_s|} \{ -e^{-t/\tau} \cos(\omega t - \alpha) + \cos[(\omega_e - \omega)t - \alpha] \} \quad (3.9-10)$$

$$i_{ds} = \frac{\sqrt{2}V_s}{|Z_s|} \{ e^{-t/\tau} \sin(\omega t - \alpha) - \sin[(\omega_e - \omega)t - \alpha] \} \quad (3.9-11)$$

Clearly, the state of the electric system is independent of the frame of reference from which it is observed. Although the variables will appear differently in each reference frame, they will exhibit the same mode of operation (transient or steady state) regardless of the reference frame. In general, (3.9-10) and (3.9-11) contain two balanced sets. One, which represents the electric transient, decays exponentially at a frequency corresponding to the instantaneous angular velocity of the arbitrary reference frame. In this set, the  $qs$  variable leads the  $ds$  variable by  $90^\circ$  when  $\omega > 0$  and lags by  $90^\circ$  when  $\omega < 0$ . The second balanced set, which represents the steady-state response, has a constant amplitude with a frequency corresponding to the difference in the angular velocity of the voltages applied to the stationary circuits and the angular velocity of the arbitrary reference frame. In this set, the  $qs$  variable lags the  $ds$  by  $90^\circ$  when  $\omega < \omega_e$  and leads by  $90^\circ$  when  $\omega > \omega_e$ . This, of course, leads to the concept of negative frequency when relating phasors that represent  $qs$  and  $ds$  variables by (3.7-8).

There are two frames of reference that do not contain both balanced sets. In the stationary reference frame  $\omega = 0$  and  $i_{qs}^s = i_{as}$ . The exponentially decaying balanced set becomes an exponential decay, and the constant amplitude balanced set varies at  $\omega_e$ . In the synchronously rotating reference frame where  $\omega = \omega_e$ , the electric transients are

represented by an exponentially decaying balanced set varying at  $\omega_e$ , and the constant amplitude balanced set becomes constants.

The waveforms of the system variables in various reference frames are shown in Figure 3.9-1, Figure 3.9-2, and Figure 3.9-3. The voltages of the form given by (3.9-1)–(3.9-3) are applied to the three-phase system with  $V_s = 10/\sqrt{2}$  V,  $r_s = 0.216$   $\Omega$ ,  $\omega_e L_s = 1.09$   $\Omega$  with  $\omega_e = 377$  rad/s. The response, for  $t > 0$ , of the electric system in the stationary reference frame is shown in Figure 3.9-1. Since we have selected  $\theta(0) = 0$ ,  $f_{as} = f_{qs}^s$  and the plots of  $v_{qs}^s$  and  $i_{qs}^s$  are  $v_{as}$  and  $i_{as}$ , respectively. The variables for the

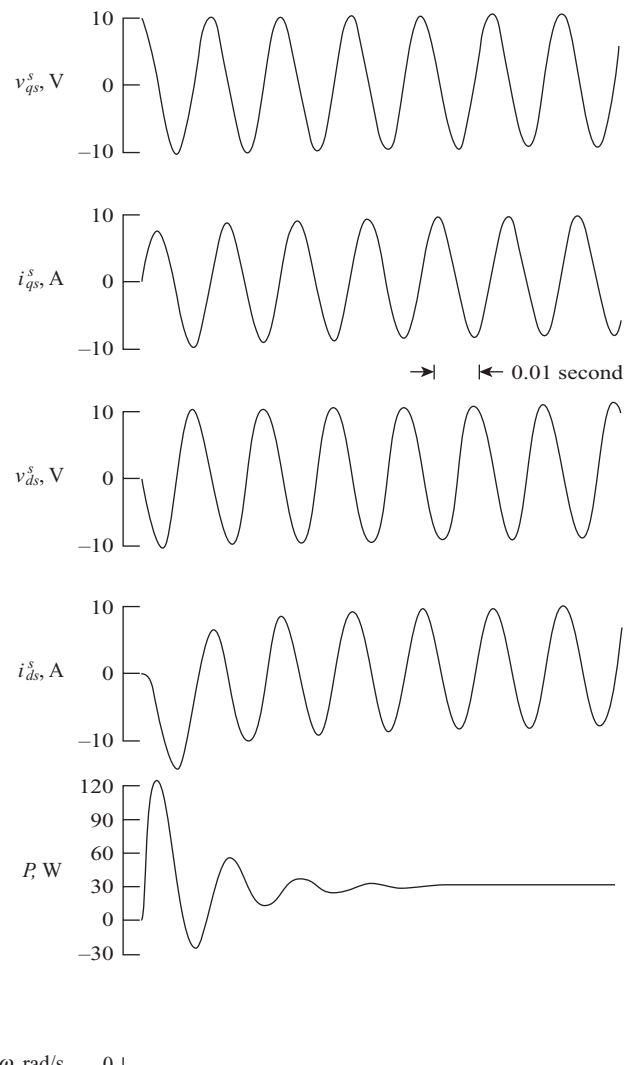


Figure 3.9-1. Variables of stationary three-phase system in the stationary reference frame.

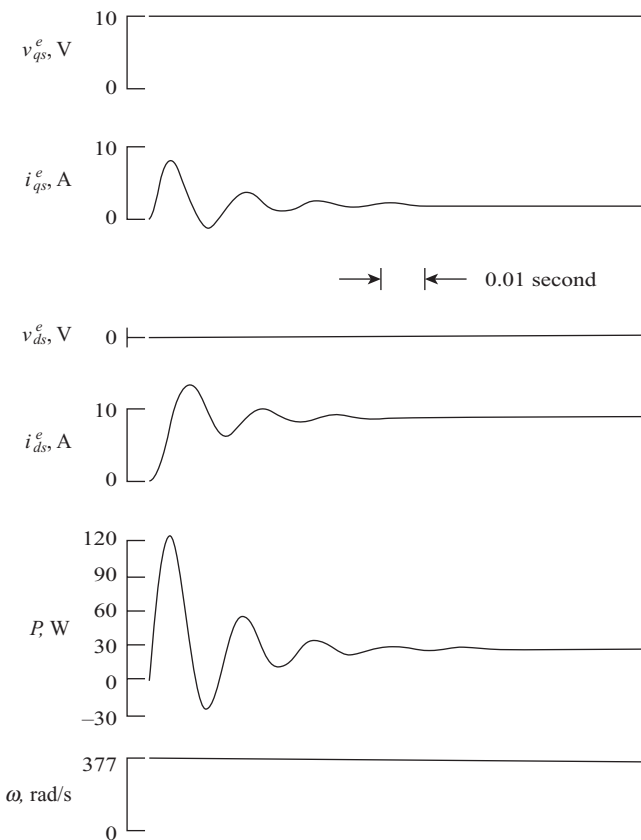
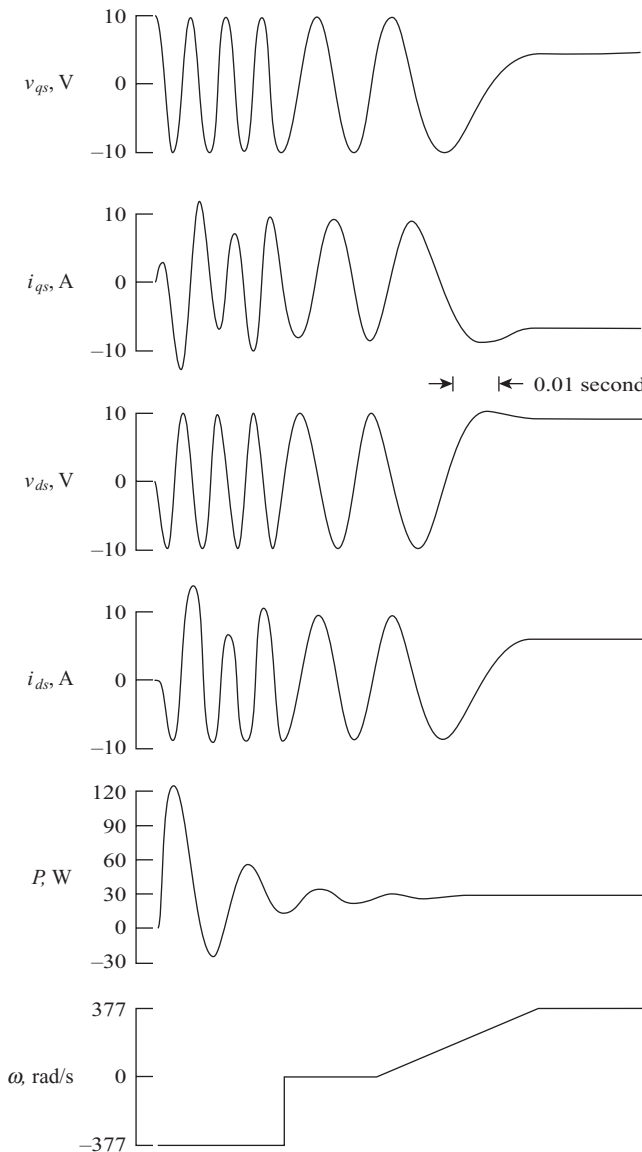


Figure 3.9-2. Variables of stationary three-phase system in synchronously rotating reference frame.

same mode of operation are shown in the synchronously rotating reference frame in Figure 3.9-2. Note from (3.9-1) that we have selected  $\theta_{ev}(0) = 0$ , thus, from (3.6-5) and (3.6-6) with  $\theta(0) = 0$ ,  $v_{qs}^e = 10$  V and  $v_{ds}^e = 0$ . In Figure 3.9-3, with  $\theta(0) = 0$  the speed of the reference frame is switched from its original value of  $-377$  rad/s to zero and the ramped to  $377$  rad/s.

There are several features worthy of note. The waveform of the instantaneous electric power is the same in all cases. The electric transient is very evident in the waveforms of the instantaneous electric power and the currents in the synchronously rotating reference frame (Fig. 3.9-2) and since  $v_{ds}^e$  is zero  $i_{qs}^e$  is related to the power by a constant ( $v_{qs}^e$ ). In Figure 3.9-3, we selected  $\theta_{ev}(0) = 0$  and  $\theta(0) = 0$ . The voltages were applied, and we observed the solution of the differential equations in the reference frame rotating clockwise at  $\omega_e$  ( $\omega = -\omega_e$ ). The reference-frame speed was then stepped from  $-377$  rad/s to 0, whereupon the differential equations were solved in the stationary reference frame. However, when switching from one reference frame to another the variables must be continuous. Therefore, after the switching occurs the solution



**Figure 3.9-3.** Variables of stationary three-phase system. First with  $\omega = -\omega_e$ , then  $\omega = 0$ , followed by a ramp change in reference-frame speed to  $\omega = \omega_e$ .

continues using the stationary reference-frame differential equations with the initial values determined by the instantaneous values of the variables in the previous reference frame ( $\omega = -\omega_e$ ) at the time of switching. It is important to note the change in frequency of the variables as the reference-frame speed is ramped from zero to  $\omega_e$ . Here, the differential equations being solved are continuously changing while the variables remain

continuous. When the reference-frame speed reaches synchronous speed, the variables have reached steady state, therefore they will be constant corresponding to their values at the instant  $\omega$  becomes equal to  $\omega_e$ . In essence, we have applied a balanced three-phase set of voltages to a symmetrical RL circuit, and in Figure 3.9-3, we observed the actual variables from various reference frames by first “jumping” and then “running” from one reference frame to another.

### 3.10. TRANSFORMATION BETWEEN REFERENCE FRAMES

In some derivations and analyses, it is convenient to relate variables in one reference frame to variables in another reference frame directly, without involving the  $abc$  variables in the transformation. In order to establish this transformation between any two frames of reference, let  $x$  denote the reference frame from which the variables are being transformed and  $y$  the reference frame to which the variables are being transformed, then

$$\mathbf{f}_{qd0s}^y = {}^x\mathbf{K}^y \mathbf{f}_{qd0s}^x \quad (3.10-1)$$

From (3.3-1), we obtain

$$\mathbf{f}_{qd0s}^x = \mathbf{K}_s^x \mathbf{f}_{abcs} \quad (3.10-2)$$

Substituting (3.10-2) into (3.10-1) yields

$$\mathbf{f}_{qd0s}^y = {}^x\mathbf{K}^y \mathbf{K}_s^x \mathbf{f}_{abcs} \quad (3.10-3)$$

However, from (3.3-1), we obtain

$$\mathbf{f}_{qd0s}^y = \mathbf{K}_s^y \mathbf{f}_{abcs} \quad (3.10-4)$$

Thus

$${}^x\mathbf{K}^y \mathbf{K}_s^x = \mathbf{K}_s^y \quad (3.10-5)$$

from which

$${}^x\mathbf{K}^y = \mathbf{K}_s^y (\mathbf{K}_s^x)^{-1} \quad (3.10-6)$$

The desired transformation is obtained by substituting the appropriate transformations into (3.10-6). Hence

$${}^x\mathbf{K}^y = \begin{bmatrix} \cos(\theta_y - \theta_x) & -\sin(\theta_y - \theta_x) & 0 \\ \sin(\theta_y - \theta_x) & \cos(\theta_y - \theta_x) & 0 \\ 0 & 0 & 1 \end{bmatrix} \quad (3.10-7)$$

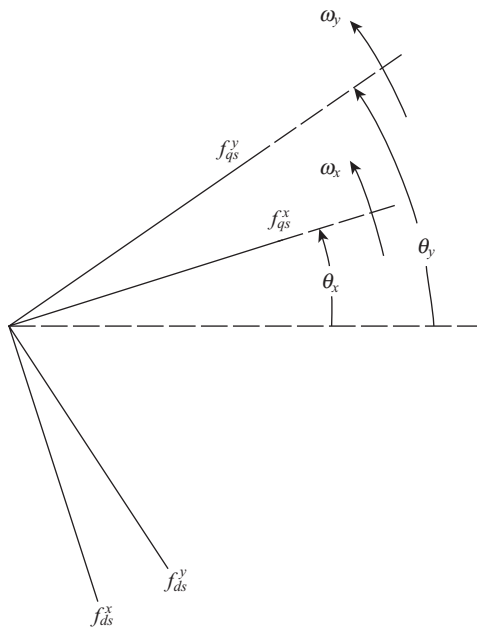


**Figure 3.10-1.** Transformation between two reference frames portrayed by trigonometric relationships.

Several of the trigonometric identities given in Appendix A are useful in obtaining (3.10-7). This transformation, which is sometimes referred to as a “vector rotator” or simply “rotator,” can also be visualized from the trigonometric relationship between two sets of rotating, orthogonal quantities, as shown in Figure 3.10-1. Resolving  $f_{qs}^x$  and  $f_{ds}^x$  into  $f_{qs}^y$  yields the first row of (3.10-7), and resolving  $f_{qs}^x$  and  $f_{ds}^x$  into  $f_{ds}^y$  yields the second row. It is left for the reader to show that

$$({}^x \mathbf{K}^y)^{-1} = ({}^x \mathbf{K}^y)^T \quad (3.10-8)$$

### 3.11. SPECIALTY TRANSFORMATIONS

The transformations that have been set forth are valid for any three-phase connection. In many cases, the three-phase voltages, currents, and flux linkages must sum to zero. This is common, although not the case if a third harmonic is present in the back-emf as in some permanent magnet ac machines. There are cases where the neutral is not accessible and only the line-to-line voltages are available, and yet it is desirable to express the  $v_{qs}$  and  $v_{ds}$ . If

$$f_{as} + f_{bs} + f_{cs} = 0 \quad (3.11-1)$$

we can express any one of the three variables in terms of the other two; let us start with expressing  $f_{cs}$  in (3.3-1) as

$$f_{cs} = -f_{as} - f_{bs} \quad (3.11-2)$$

After some trigonometric manipulation, (3.3-1) may be written as

$$\begin{bmatrix} f_{qs} \\ f_{ds} \end{bmatrix} = \begin{bmatrix} \cos \theta & \sin \theta \\ \sin \theta & -\cos \theta \end{bmatrix} \begin{bmatrix} f_{as} \\ \frac{1}{\sqrt{3}} f_{as} + \frac{2}{\sqrt{3}} f_{bs} \end{bmatrix} \quad (3.11-3)$$

This is the two-phase transformation to the arbitrary reference frame. Since we have reduced the three-wire connection to a two-phase system, we should not be too surprised by this. In a problem at the end of this chapter, you are asked to express the voltage vector in the right hand side of (3.11-3) in terms of  $f_{as}$  and  $f_{cs}$  and in terms of  $f_{bs}$  and  $f_{cs}$ .

It is left to the reader to show that (3.11-3) can be written

$$\begin{bmatrix} f_{qs} \\ f_{ds} \end{bmatrix} = \frac{2}{\sqrt{3}} \begin{bmatrix} \cos\left(\theta - \frac{\pi}{6}\right) & \sin \theta \\ \sin\left(\theta - \frac{\pi}{6}\right) & -\cos \theta \end{bmatrix} \begin{bmatrix} f_{as} \\ f_{bs} \end{bmatrix} \quad (3.11-4)$$

It is clear that  $f_{as}$ ,  $f_{bs}$ , and  $f_{cs}$  can be voltages, currents, or flux linkages and that the variables can be of any form. The variables need not form a balanced set. The only constraint is that  $f_{0s}$  is zero.

In a wye-connected system, if the neutral is not available then  $v_{as}$ ,  $v_{bs}$ , and  $v_{cs}$  are not available, however, we are still dealing with a three-wire, wye connection. If  $v_{0s}$  is zero, we can express  $v_{qs}$  and  $v_{ds}$  in terms of line-to-line voltages. This, of course, is important when it is necessary for control or analysis purposes to be able to determine  $v_{qs}$  and  $v_{ds}$  when the phase voltages are not physically available. The line-to-line voltages may be expressed in terms of phase voltages as

$$\begin{bmatrix} v_{abs} \\ v_{bcs} \\ v_{cas} \end{bmatrix} = \begin{bmatrix} v_{as} - v_{bs} \\ v_{bs} - v_{cs} \\ v_{cs} - v_{as} \end{bmatrix} \quad (3.11-5)$$

Solving (3.11-5) for  $v_{as}$ ,  $v_{bs}$ , and  $v_{cs}$  and substituting into (3.3-1) yields

$$\begin{bmatrix} v_{qs} \\ v_{ds} \end{bmatrix} = \frac{2}{3} \begin{bmatrix} \cos \theta & \cos\left(\theta - \frac{2\pi}{3}\right) & \cos\left(\theta + \frac{2\pi}{3}\right) \\ \sin \theta & \sin\left(\theta - \frac{2\pi}{3}\right) & \sin\left(\theta + \frac{2\pi}{3}\right) \end{bmatrix} \begin{bmatrix} v_{abs} + v_{bs} \\ v_{bcs} + v_{cs} \\ v_{cas} + v_{as} \end{bmatrix} \quad (3.11-6)$$

Since  $v_{0s}$  is zero, (3.11-6) may be written as

$$\begin{bmatrix} v_{qs} \\ v_{ds} \end{bmatrix} = \frac{2}{3} \begin{bmatrix} \cos \theta & \cos\left(\theta + \frac{2\pi}{3}\right) \\ \sin \theta & \sin\left(\theta + \frac{2\pi}{3}\right) \end{bmatrix} \begin{bmatrix} v_{abs} \\ v_{cbs} \end{bmatrix} \quad (3.11-7)$$

### 3.12. SPACE-PHASOR NOTATION

In the early 1900s, Fortescue [8] developed the method of symmetrical components to analyze the steady-state performance of induction machines during unbalanced operation. This theory is set forth later in Chapter 9; however, it is sufficient here to mention that this method of analysis, for a three-phase system, involves a balanced three-phase set of positive *abc* sequence phasors, a balanced three-phase set of negative *acb* sequence phasors, and a single-phase zero-sequence phasor. It is most convenient for the analysis of steady-state unbalanced operation of symmetrical two- or three-phase machines where in the case of a two-phase system the zero sequence is not present.

In a critical discussion of Park's hallmark paper [1], W.V. Lyon mentioned that Fortescue's work could be extended to the transient case. Twenty-five years later, Lyon published a book wherein he used instantaneous or time-varying symmetrical components (phasors) to analyze the transient operation of electric machines [9]. This approach was considered an alternative to Park's work; however, it did not gain wide acceptance primarily because it was inconvenient when analyzing systems with unsymmetrical components, such as a synchronous machine. Moreover, using Lyon's approach it is not possible to define circuits that carry complex time-varying currents and a negative-sequence instantaneous symmetrical component is necessary in the analysis even when the actual two- or three-phase variables are balanced [9, 10]. Nevertheless, Lyon's work appears to be the first use of instantaneous phasors in machine analysis.

Later, machine analysts began to combine the *qd* equations into a single complex expression [11–13]. That is, since the *q*- and *d*-axes are orthogonal, we can write

$$\vec{f}_{qds} = f_{qs} - jf_{ds} \quad (3.12-1)$$

where the over arrow is used to denote the instantaneous phasor, which is often referred to as the space vector or space phasor. Here, the  $f_{qs}$  and  $f_{ds}$  variables are arbitrary reference-frame variables. Using this space-phasor formulation, the *qd*-voltage equations given by (3A-3) and (3A-4) for an *rL*-circuit become

$$\begin{aligned} \vec{v}_{qds} &= v_{qs} - jv_{ds} \\ &= r_s \vec{i}_{qds} + p \vec{\lambda}_{qds} + j\omega \vec{\lambda}_{qds} \end{aligned} \quad (3.12-2)$$

Recall from Section 3.7, when we considered the form of the reference-frame variables during balanced steady-state operation, we found that the steady-state *q* and *d* variables

are sinusoidal in all reference frames except the synchronously rotating. Therefore, even for transient conditions during balanced conditions, the components of the complex expression (3.12-2) will be varying amplitude, sinusoidal quantities in all reference frames except the synchronously rotating reference frame where the components will be constant in the steady state but vary in amplitude during a transient. Although introducing the space phasor provides a means of expressing the  $q$  and  $d$  equations more compactly, it does not provide an analytical advantage. In fact, the complex expression is separated into its real and imaginary expressions before solving for the  $q$  and  $d$  variables. Therefore, the advantage of the space-phasor expression is primarily compactness; it does not offer any analytical advantage. In fact, it would be a disadvantage if an attempt was made to solve the complex space-phasor expression analytically except perhaps in the synchronous reference frame.

It is important to mention that the phasor expression given by (3.7-14), which relates the physical variables to  $f_{qs}^e$  and  $f_{ds}^e$  quantities during steady-state balanced conditions, is not a space phasor. This is a standard phasor that has been used in steady-state ac circuit theory since developed by Steinmetz [14].

There is one last space-phasor expression that warrants mentioning. In Section 3.10, we introduced the transformation between reference frames, which is given by (3.10-7). Therein it was mentioned that this is sometimes referred to as a “rotator” or “vector rotator.” If the zero-sequence quantities are assumed to be nonexistent then (3.10-1) may be written

$$\begin{bmatrix} f_{qs}^y \\ f_{ds}^y \end{bmatrix} = \begin{bmatrix} \cos(\theta_y - \theta_x) & \sin(\theta_y - \theta_x) \\ -\sin(\theta_y - \theta_x) & \cos(\theta_y - \theta_x) \end{bmatrix} \begin{bmatrix} f_{qs}^x \\ f_{ds}^x \end{bmatrix} \quad (3.12-3)$$

where  $x$  is the reference frame from which variables are being transformed and  $y$  the reference frame to which the variables are being transformed. If we expand (3.12-3) and express  $f_{qds}^y$  and  $f_{qds}^x$  as space phasors, we have

$$\begin{aligned} f_{qs}^y - jf_{ds}^y &= (f_{qs}^x - jf_{ds}^x)[\cos(\theta_y - \theta_x) + j\sin(\theta_y - \theta_x)] \\ &= (f_{qs}^x - jf_{ds}^x)e^{j(\theta_y - \theta_x)} \end{aligned} \quad (3.12-4)$$

Equation (3.12-4) may be written as

$$\vec{f}_{qds}^y = \vec{f}_{qds}^x e^{j(\theta_y - \theta_x)} \quad (3.12-5)$$

For a transformation between the stationary and synchronous reference frames, the rotator  $e^{j(\theta_y - \theta_x)}$  becomes  $e^{j\omega_{et}}$  when all time-zero displacements are selected as zero [12].

Although the space-phasor notation has advantages in providing a compact means of expressing the machine equations and portraying converter operation, this notation is not used in this text, as it offers no advantage other than compactness. Nevertheless, once the student has mastered the  $qd0$ -analysis, incorporating the space-phasor notation is straightforward. This is presented in Reference 11.

## REFERENCES

- [1] R.H. Park, "Two-Reaction Theory of Synchronous Machines—Generalized Method of Analysis—Part I," *AIEE Trans.*, Vol. 48, July 1929, pp. 716–727.
- [2] H.C. Stanley, "An Analysis of the Induction Motor," *AIEE Trans.*, Vol. 57 (Suppl), 1938, pp. 751–755.
- [3] G. Kron, *Equivalent Circuits of Electric Machinery*, John Wiley & Sons, New York, 1951.
- [4] D.S. Brereton, D.G. Lewis, and C.G. Young, "Representation of Induction Motor Loads During Power System Stability Studies," *AIEE Trans.*, Vol. 76, August 1957, pp. 451–461.
- [5] P.C. Krause and C.H. Thomas, "Simulation of Symmetrical Induction Machinery," *IEEE Trans. Power Apparatus Syst.*, Vol. 84, November 1965, pp. 1038–1053.
- [6] P.C. Krause, F. Nozari, T.L. Skvarenina, and D.W. Olive, "The Theory of Neglecting Stator Transients," *IEEE Trans. Power Apparatus Syst.*, Vol. 98, January/February 1979, pp. 141–148.
- [7] E. Clarke, *Circuit Analysis of A-C Power Systems*, Vol. I—*Symmetrical and Related Components*, John Wiley & Sons., New York, 1943.
- [8] C.L. Fortescue, "Method of Symmetrical Co-ordinates Applied to the Solution of Polyphase Networks," *AIEE Trans.*, Vol. 37, 1918, pp. 1027–1115.
- [9] W.V. Lyon, *Transient Analysis of Alternating-Current Machinery*, The Technology Press of Massachusetts Institute of Technology and John Wiley & Sons, New York, 1954.
- [10] D.C. White and H.H. Woodson, *Electromechanical Energy Conversion*, John Wiley & Sons, New York, 1959, pp. 316–317.
- [11] D.W. Novotny and T.A. Lipo, *Vector Control and Dynamics of AC Drives*, Oxford University Press, New York, 1997.
- [12] R.D. Lorenz, T.A. Lipo, and D.W. Novotny, "Motion Control with Induction Motors," *Proc. IEEE*, Vol. 82, No. 8, August 1994, pp. 1215–1240.
- [13] P. Vas, *Sensorless Vector and Direct Torque Control*, Oxford University Press, Oxford; New York; Tokyo, 1998.
- [14] C.P. Steinmetz, *Theory and Calculation of Alternating Current Phenomena*, W.J. Johnston, New York, 1897.

## PROBLEMS

1. The transformation for a two-phase set to the arbitrary reference frame is

$$\mathbf{f}_{qds} = \mathbf{K}_s \mathbf{f}_{abs}$$

where

$$(\mathbf{f}_{qds})^T = [f_{qs} \quad f_{ds}]$$

$$(\mathbf{f}_{abs})^T = [f_{as} \quad f_{bs}]$$

$$\mathbf{K}_s = \begin{bmatrix} \cos \theta & \sin \theta \\ \sin \theta & -\cos \theta \end{bmatrix}$$

where  $\theta$  is defined by (3.3-5).

(a) Determine  $(\mathbf{K}_s)^{-1}$ .

(b) Depict the transformation similar to that shown in Figure 3.3-1.

2. Using the transformation given in Problem 1, express the voltage and flux linkage equations in the arbitrary reference frame for a system

$$v_{as} = r_a i_{as} + p\lambda_{as}$$

$$v_{bs} = r_b i_{bs} + p\lambda_{bs}$$

$$\lambda_{as} = L_a i_{as}$$

$$\lambda_{bs} = L_b i_{bs}$$

where  $r_a = r_b = r_s$  and  $L_a = L_b = L_s$ . Then express the voltage and flux linkage equations for the case in which  $r_a \neq r_b$  and  $L_a \neq L_b$ .

3. Using the transformation given in Problem 1, express the current equations in the arbitrary reference frame for a two-phase capacitive circuit that is described by

$$C_s p v_{as} + \frac{v_{as}}{r_s} = i_{as}$$

$$C_s p v_{bs} + \frac{v_{bs}}{r_s} = i_{bs}$$

4. The phases of a three-phase circuit consist of equal resistances, equal inductances, and equal capacitances connected in series. The phases are not coupled. Write the voltage equations in the arbitrary reference frame and draw the equivalent circuit.
5. Repeat Problem 4 for the circuit elements in each phase connected in parallel.
6. In a reference frame  $x$ , the  $q$ - and  $d$ -axis voltages of a wye-connected RL circuit may be expressed as

$$v_{qs}^x = 0.1i_{qs}^x - 100i_{ds}^x + 5pi_{qs}^x$$

$$v_{ds}^x = 0.1i_{ds}^x + 100i_{qs}^x + 5pi_{ds}^x$$

Determine the resistance and inductance of the circuit, as well as the speed of the reference frame.

7. Show that for a two-phase set

$$f_{as}^2 + f_{bs}^2 = f_{qs}^2 + f_{ds}^2$$

8. Clarke's transformation may be written as

$$\mathbf{f}_{\alpha\beta 0} = \mathbf{C}\mathbf{f}_{abcs}$$

where

$$(\mathbf{f}_{\alpha\beta 0})^T = [f_\alpha \quad f_\beta \quad f_0]$$

$$\mathbf{C} = \frac{2}{3} \begin{bmatrix} 1 & -\frac{1}{2} & -\frac{1}{2} \\ 0 & -\frac{\sqrt{3}}{2} & \frac{\sqrt{3}}{2} \\ \frac{1}{2} & \frac{1}{2} & \frac{1}{2} \end{bmatrix}$$

Relate  $f_{qs}^s$ ,  $f_{ds}^s$ , and  $f_{0s}$  to  $f_\alpha$ ,  $f_\beta$ , and  $f_0$ , respectively.

9. A transformation that is sometimes used in the case of synchronous machines is one where  $f_{ds}$  leads  $f_{qs}$  in Figure 3.3-1 by  $90^\circ$  with  $\omega = \omega_r$ .
- Express the transformation.
  - Using this transformation, write the voltage equations for a three-phase inductive circuit.
10. The inductance matrix that describes the self- and mutual inductances between the stator windings of a salient-pole synchronous machine with mutual leakage terms neglected is given in the following equation:

$$\mathbf{L}_s = \begin{bmatrix} L_{ss} + L_A - L_B \cos 2\theta_r & -\frac{1}{2}L_A - L_B \cos 2\left(\theta_r - \frac{\pi}{3}\right) & -\frac{1}{2}L_A - L_B \cos 2\left(\theta_r + \frac{\pi}{3}\right) \\ -\frac{1}{2}L_A - L_B \cos 2\left(\theta_r - \frac{\pi}{3}\right) & L_{ss} + L_A - L_B \cos 2\left(\theta_r - \frac{2\pi}{3}\right) & -\frac{1}{2}L_A - L_B \cos 2(\theta_r + \pi) \\ -\frac{1}{2}L_A - L_B \cos 2\left(\theta_r + \frac{\pi}{3}\right) & -\frac{1}{2}L_A - L_B \cos 2(\theta_r + \pi) & L_{ss} + L_A - L_B \cos 2\left(\theta_r + \frac{2\pi}{3}\right) \end{bmatrix}$$

Evaluate  $\mathbf{K}'_s \mathbf{L}_s (\mathbf{K}'_s)^{-1}$  for this case. Repeat the evaluation for the case in which mutual leakage terms (refer to Chapter 2) are included.

- If  $A$  is one reference frame and  $B$  another, show that  $({}^A\mathbf{K}^B)^{-1} = {}^B\mathbf{K}^A$ .
- Equations (3.7-1)–(3.7-3) form an  $abc$  sequence. Express an  $acb$  sequence and transform this set to the arbitrary reference frame using (3.3-1). Express  $\mathbf{f}_{qd0s}^e$  ( $\omega = \omega_e$ ) and  $\mathbf{f}_{qd0s}^{-e}$  ( $\omega = -\omega_e$ ).
- Devise a transformation which yields only constants when  $\omega = \omega_e$  for a balanced three-phase set with a phase sequence of  $acb$ .
- Relate  $\tilde{F}_{bs}$  and  $\tilde{F}_{cs}$  to  $\tilde{F}_{qs}$  and  $\tilde{F}_{ds}$  for a balanced three-phase set with a time sequence of  $abc$ .
- For steady-state balanced conditions, the total three-phase power and reactive power may be expressed

$$P = 3V_s I_s \cos[\theta_{ev}(0) - \theta_{ei}(0)]$$

$$Q = 3V_s I_s \sin[\theta_{ev}(0) - \theta_{ei}(0)]$$

Show that the following expressions are equal to those given above.

$$P = \frac{3}{2}(V_{qs}I_{qs} + V_{ds}I_{ds})$$

$$Q = \frac{3}{2}(V_{qs}I_{ds} - V_{ds}I_{qs})$$

16. Write the expressions for the currents in Figure 3.9-1 and Figure 3.9-2.

17. Assume the steady-state *abc* variables are of the form

$$F_{as} = \sqrt{2}F_a \cos \omega_e t$$

$$F_{bs} = \sqrt{2}F_b \cos \left( \omega_e t - \frac{2\pi}{3} \right)$$

$$F_{cs} = \sqrt{2}F_c \cos \left( \omega_e t + \frac{2\pi}{3} \right)$$

where  $F_a$ ,  $F_b$ , and  $F_c$  are unequal constants. Show that this unbalanced set of *abc* variables forms two-phase balanced sets of *qs* and *ds* variables in the arbitrary reference frame with the arguments of  $(\omega_e t - \theta)$  and  $(\omega_e t + \theta)$ . Note the form of the *qs* and *ds* variables when  $\omega = \omega_e$  and  $\omega = -\omega_e$ .

18. Repeat Problem 17 with

$$F_{as} = \sqrt{2}F_s \cos(\omega_e t + \phi_a)$$

$$F_{bs} = \sqrt{2}F_s \cos(\omega_e t + \phi_b)$$

$$F_{cs} = \sqrt{2}F_s \cos(\omega_e t + \phi_c)$$

where  $\phi_a$ ,  $\phi_b$ , and  $\phi_c$  are unequal constants.

19. It is often suggested that  $\mathbf{K}_s$  should be changed so that  $(\mathbf{K}_s)^T = (\mathbf{K}_s)^{-1}$ . For example, if

$$\mathbf{K}_s = \sqrt{\frac{2}{3}} \begin{bmatrix} \cos \theta & \cos \left( \theta - \frac{2\pi}{3} \right) & \cos \left( \theta + \frac{2\pi}{3} \right) \\ \sin \theta & \sin \left( \theta - \frac{2\pi}{3} \right) & \sin \left( \theta + \frac{2\pi}{3} \right) \\ \frac{1}{\sqrt{2}} & \frac{1}{\sqrt{2}} & \frac{1}{\sqrt{2}} \end{bmatrix}$$

then  $(\mathbf{K}_s)^T = (\mathbf{K}_s)^{-1}$ . Show that this is true. Also, show that in this case

$$\mathbf{f}_{as}^2 + \mathbf{f}_{bs}^2 + \mathbf{f}_{cs}^2 = \mathbf{f}_{qs}^2 + \mathbf{f}_{ds}^2 + \mathbf{f}_{0s}^2$$

20. A system is described by the following equations:

$$p v_{as} - \frac{v_{bs}}{2} - \frac{v_{cs}}{2} + v_{as} = i_{as}$$

$$p v_{bs} - \frac{v_{as}}{2} - \frac{v_{cs}}{2} + v_{bs} = i_{bs}$$

$$p v_{cs} - \frac{v_{bs}}{2} - \frac{v_{as}}{2} + v_{cs} = i_{cs}$$

If the currents are a balanced (*abc*) sequence with  $I_{as} = \cos(t)$ , determine  $V_{qs}^e$ ,  $V_{as}$ , and  $V_{qs}^s$ .

21. A system is described as

$$0 = \mathbf{v}_{abcs} - \mathbf{i}_{abcs} - \begin{bmatrix} 1 & -\frac{1}{2} & -\frac{1}{2} \\ -\frac{1}{2} & 1 & -\frac{1}{2} \\ -\frac{1}{2} & -\frac{1}{2} & 1 \end{bmatrix} p \mathbf{i}_{abcs} - \mathbf{v}_{Cabcs}$$

$$p \mathbf{v}_{Cabcs} = \mathbf{i}_{abcs}$$

Determine  $I_{qs}^e$ ,  $I_{ds}$ , and,  $I_{as}$  if  $V_{as} = \cos 10t$ . Assume balanced voltages.

22. A system is described by the following:

$$v_{as} = i_{as} + p \lambda_{as}$$

$$v_{bs} = i_{bs} + p \lambda_{bs}$$

$$v_{cs} = i_{cs} + p \lambda_{cs}$$

$$\lambda_{as} = (0.1 + 1)i_{as} - 0.5i_{bs} - 0.5i_{cs}$$

$$\lambda_{bs} = -0.5i_{as} + (0.1 + 1)i_{bs} - 0.5i_{cs}$$

$$\lambda_{cs} = -0.5i_{as} - 0.5i_{bs} + (0.1 + 1)i_{cs}$$

If  $\tilde{\lambda}_{as} = 1 - j$ ,  $\omega_e = 10$  rad/s, use reference-frame theory to determine  $\tilde{V}_{as}$ .

23. A system is described as

$$\mathbf{v}_{abcs} = \mathbf{r}_s \mathbf{i}_{abcs} + p \boldsymbol{\lambda}_{abcs}$$

$$\boldsymbol{\lambda}_{abcs} = \begin{bmatrix} 0.1 + 1 - 0.25 \cos 2\theta_r & -\frac{1}{2} - 0.25 \cos 2\left(\theta_r - \frac{\pi}{3}\right) & -\frac{1}{2} - 0.25 \cos 2\left(\theta_r + \frac{\pi}{3}\right) \\ -\frac{1}{2} - 0.25 \cos 2\left(\theta_r - \frac{\pi}{3}\right) & 0.1 + 1 - 0.25 \cos 2\left(\theta_r - \frac{2\pi}{3}\right) & -\frac{1}{2} - 0.25 \cos 2(\theta_r + \pi) \\ -\frac{1}{2} - 0.25 \cos 2\left(\theta_r + \frac{\pi}{3}\right) & -\frac{1}{2} - 0.25 \cos 2(\theta_r + \pi) & 0.1 + 1 - 0.25 \cos 2\left(\theta_r + \frac{2\pi}{3}\right) \end{bmatrix} \mathbf{i}_{abcs}$$

If  $\lambda_{qs}^r = \lambda_{ds}^r = 1$  V·s, determine  $|\tilde{I}_{as}|$ .

24. A system is described as:

$$\mathbf{v}'_{12r} = \mathbf{r}'_r \mathbf{i}'_{12r} + p \boldsymbol{\lambda}'_{12r}$$

$$\boldsymbol{\lambda}'_{12r} = L_m \begin{bmatrix} \cos(\theta_r) & -\sin(\theta_r) \\ -\sin(\theta_r) & -\cos(\theta_r) \end{bmatrix} \mathbf{i}_{12s}$$

Using the definitions

$$\begin{bmatrix} f_{qs}^s \\ f_{ds}^s \end{bmatrix} = \mathbf{K}_s^s \begin{bmatrix} f_{1s} \\ f_{2s} \end{bmatrix}, \quad \text{where } \mathbf{K}_s^s = \begin{bmatrix} 1 & 0 \\ 0 & -1 \end{bmatrix}$$

$$\begin{bmatrix} f_{qr}^s \\ f_{dr}^s \end{bmatrix} = \mathbf{K}_r^s \begin{bmatrix} f_{1r} \\ f_{2r} \end{bmatrix}, \quad \text{where } \mathbf{K}_r^s = \begin{bmatrix} -\sin(\theta_r) & -\cos(\theta_r) \\ -\cos(\theta_r) & \sin(\theta_r) \end{bmatrix}, \quad \omega_r = \frac{d\theta_r}{dt}$$

transform the voltage and flux linkage equations into the stationary reference frame. Assuming the input voltages  $\mathbf{v}'_{12r}$  are balanced and have a frequency of  $337 - \omega_r$ , determine the frequency of the currents, voltages, and flux linkages in the stationary frame of reference.

25. A balanced three-phase system can be described in the stationary reference frame as:

$$p\dot{i}_{qs}^s + i_{qs}^s = v_{qs}^s$$

$$p\dot{i}_{ds}^s + i_{ds}^s = v_{ds}^s$$

$$p\dot{i}_{0s} + i_{0s} = v_{0s}$$

If the system is operating with  $\omega_e = 1$  rad/s,  $V_{qs}^e = \sqrt{2}$  V,  $V_{ds}^e = -\sqrt{2}$  V, use the steady-state equations to determine  $\tilde{I}_{as}$ . In addition, express the physical *abc* variables.

26. Consider a two-phase machine with the flux linkage equations:

$$\boldsymbol{\lambda}_{abs} = \begin{bmatrix} 8 - 4\cos(2\theta_r) & -2\sin(2\theta_r) \\ -2\sin(2\theta_r) & 2 + \cos(2\theta_r) \end{bmatrix} \mathbf{i}_{abs}$$

Where  $\theta_r$  is the electrical rotor position. Determine a set of *qd* flux linkage equations that are rotor position invariant. To do this, you will need to establish a suitable reference-frame transformation.

---

# PERMANENT-MAGNET AC MACHINES

---

## 4.1. INTRODUCTION

The permanent-magnet ac machine supplied from a controlled voltage or current source inverter is becoming widely used. This is attributed to a relatively high torque density (torque/mass or torque/volume) and ease of control relative to alternative machine architectures. Depending upon the control strategies, the performance of this inverter-machine combination can be made, for example, to (1) emulate the performance of a permanent-magnet dc motor, (2) operate in a maximum torque per ampere mode, (3) provide a “field weakening” technique to increase the speed range for constant power operation, and (4) shift the phase of the stator applied voltages to obtain the maximum possible torque at any given rotor speed. Fortunately, we are able to become quite familiar with the basic operating features of the permanent-magnet ac machine without getting too involved with the actual inverter or the control strategies. In particular, if we assume that the stator variables (voltages and currents) are sinusoidal and balanced with the same angular velocity as the rotor speed, we are able to predict the predominant operating features of all of the above mentioned modes of operation without becoming involved with the actual switching or control of the inverter. Therefore, in this chapter,

we will focus on the performance of the inverter-machine combination assuming that the inverter is designed and controlled appropriately and leave how this is done to Chapter 14.

## 4.2. VOLTAGE AND TORQUE EQUATIONS IN MACHINE VARIABLES

A two-pole, permanent-magnet ac machine, which is also called a permanent-magnet synchronous machine, is depicted in Figure 4.2-1. It has three-phase, wye-connected stator windings and a permanent-magnet rotor. The stator windings are identical windings displaced at 120°, each with  $N_s$  equivalent turns and resistance  $r_s$ . For our analysis, we will assume that the stator windings are sinusoidally distributed. The three sensors shown in Figure 4.2-1 are Hall effect devices. When the north pole is under a sensor, its output is nonzero; with a south pole under the sensor, its output is zero. During steady-state operation, the stator windings are supplied from an inverter that is switched at a frequency corresponding to the rotor speed. The states of the three sensors are used to determine the switching logic for the inverter. In the actual machine, the sensors are not positioned over the rotor, as shown in Figure 4.2-1. Instead, they are often placed over a ring that is mounted on the shaft external to the stator windings and magnetized in the same direction as the rotor magnets. We will return to these sensors and the role they play later.

The voltage equations in machine variables are

$$\mathbf{v}_{abcs} = \mathbf{r}_s \mathbf{i}_{abcs} + p \boldsymbol{\lambda}_{abcs} \quad (4.2-1)$$

where

$$(\mathbf{f}_{abcs})^T = [f_{as} \quad f_{bs} \quad f_{cs}] \quad (4.2-2)$$

$$\mathbf{r}_s = \text{diag}[r_s \quad r_s \quad r_s] \quad (4.2-3)$$

The flux linkages may be written as

$$\boldsymbol{\lambda}_{abcs} = \mathbf{L}_s \mathbf{i}_{abcs} + \boldsymbol{\lambda}'_m \quad (4.2-4)$$

where, neglecting mutual leakage terms and assuming that due to the permanent magnet the  $d$ -axis reluctance of the rotor is larger than the  $q$ -axis reluctance,  $\mathbf{L}_s$  may be written as

$$\mathbf{L}_s = \begin{bmatrix} L_{ls} + L_A + L_B \cos 2\theta_r & -\frac{1}{2}L_A + L_B \cos 2\left(\theta_r - \frac{\pi}{3}\right) & -\frac{1}{2}L_A + L_B \cos 2\left(\theta_r + \frac{\pi}{3}\right) \\ -\frac{1}{2}L_A + L_B \cos 2\left(\theta_r - \frac{\pi}{3}\right) & L_{ls} + L_A + L_B \cos 2\left(\theta_r - \frac{2\pi}{3}\right) & -\frac{1}{2}L_A + L_B \cos 2(\theta_r + \pi) \\ -\frac{1}{2}L_A + L_B \cos 2\left(\theta_r + \frac{\pi}{3}\right) & -\frac{1}{2}L_A + L_B \cos 2(\theta_r + \pi) & L_{ls} + L_A + L_B \cos 2\left(\theta_r + \frac{2\pi}{3}\right) \end{bmatrix} \quad (4.2-5)$$

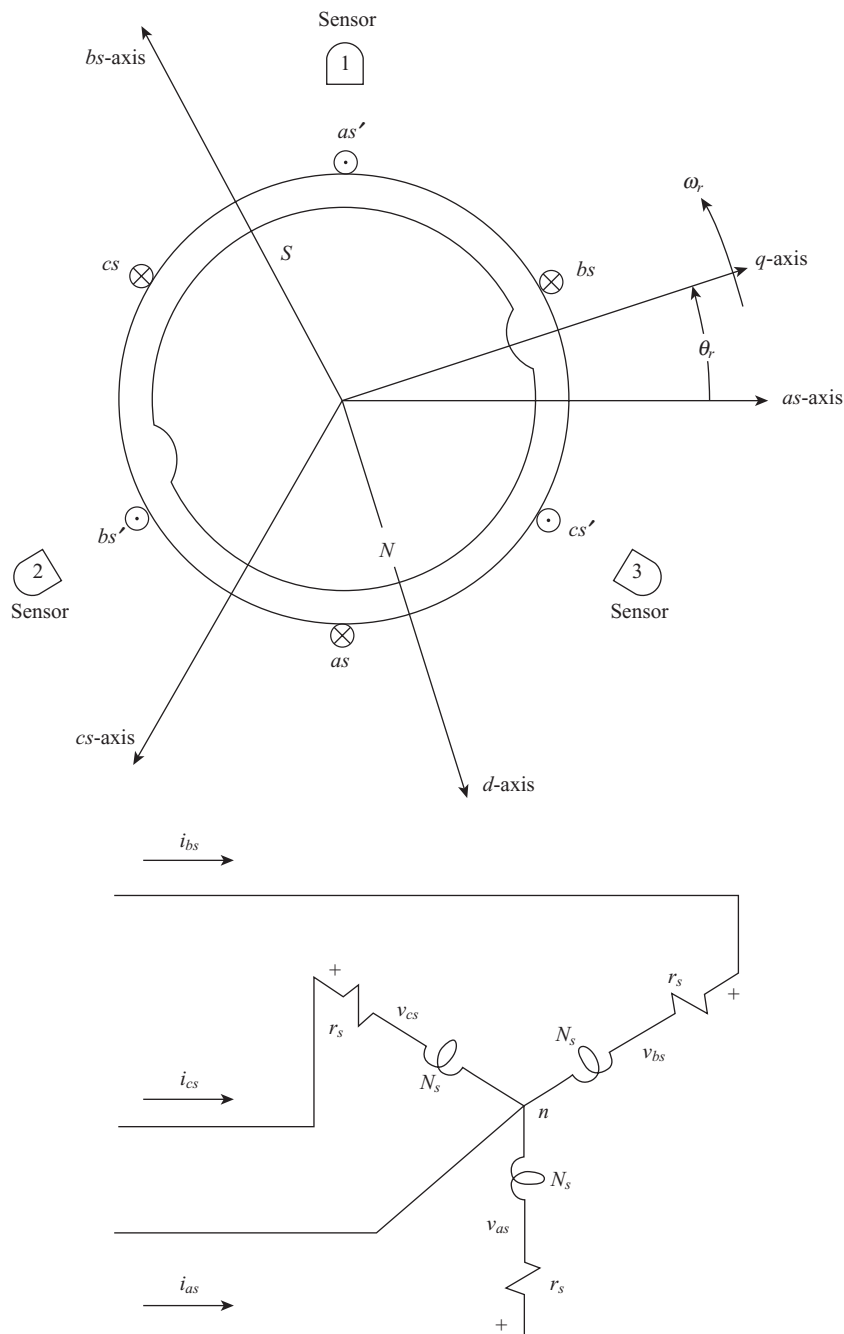


Figure 4.2-1. Two-pole, three-phase permanent-magnet ac machine.

The flux linkage  $\lambda'_m$  may be expressed as

$$\lambda'_m = \lambda'_m \begin{bmatrix} \sin \theta_r \\ \sin \left( \theta_r - \frac{2\pi}{3} \right) \\ \sin \left( \theta_r + \frac{2\pi}{3} \right) \end{bmatrix} \quad (4.2-6)$$

where  $\lambda'_m$  is the amplitude of the flux linkages established by the permanent magnet as viewed from the stator phase windings. In other words,  $p\lambda'_m$  would be the open-circuit voltage induced in each stator phase winding. Damper windings are neglected since the permanent magnets are typically relatively poor electrical conductors, and the eddy currents that flow in the nonmagnetic materials securing the magnets are small. Hence, in general large armature currents can be tolerated without significant demagnetization. We have assumed by (4.2-6) that the voltages induced in the stator windings by the permanent magnet are constant amplitude sinusoidal voltages. A derivation of (4.2-5) and (4.2-6) is provided in Chapter 15.

The expression for the electromagnetic torque may be written in machine variables using

$$T_e = \left( \frac{P}{2} \right) \frac{\partial W_c}{\partial \theta_r} \quad (4.2-7)$$

where

$$W_c = \frac{1}{2} \mathbf{i}_{abcs}^T \mathbf{L}_s \mathbf{i}_{abcs} + \mathbf{i}_{abcs}^T \lambda'_m + W_{pm} \quad (4.2-8)$$

In (4.2-8),  $W_{pm}$  is the energy in the coupling field due to the presence of the permanent magnet. Substituting (4.2-8) into (4.2-7) and neglecting any change in  $W_{pm}$  with rotor position, the electromagnetic torque is expressed

$$\begin{aligned} T_e = & \left( \frac{P}{2} \right) \left\{ \left( \frac{(L_{md} - L_{mq})}{3} \right) \left[ \left( i_{as}^2 - \frac{1}{2} i_{bs}^2 - \frac{1}{2} i_{cs}^2 - i_{as}i_{bs} - i_{as}i_{cs} + 2i_{bs}i_{cs} \right) \sin 2\theta_r \right. \right. \\ & \left. \left. + \frac{\sqrt{3}}{2} (i_{bs}^2 - i_{cs}^2 - 2i_{as}i_{bs} + 2i_{as}i_{cs}) \cos 2\theta_r \right] \right. \\ & \left. + \lambda'_m \left[ \left( i_{as} - \frac{1}{2} i_{bs} - \frac{1}{2} i_{cs} \right) \cos \theta_r + \frac{\sqrt{3}}{2} (i_{bs} - i_{cs}) \sin \theta_r \right] \right\} \end{aligned} \quad (4.2-9)$$

where  $L_{mq}$  and  $L_{md}$  are

$$L_{mq} = \frac{3}{2}(L_A + L_B) \quad (4.2-10)$$

$$L_{md} = \frac{3}{2}(L_A - L_B) \quad (4.2-11)$$

The above expression for torque is positive for motor action. The torque and speed may be related as

$$T_e = J \left( \frac{2}{P} \right) p \omega_r + B_m \left( \frac{2}{P} \right) \omega_r + T_L \quad (4.2-12)$$

where  $J$  is the inertia of the rotor and the connected load is in  $\text{kg}\cdot\text{m}^2$ . Since we will be concerned primarily with motor action, the torque  $T_L$  is positive for a torque load. The constant  $B_m$  is a damping coefficient associated with the rotational system of the machine and the mechanical load. It has the units  $\text{N}\cdot\text{m}\cdot\text{s}$  per radian of mechanical rotation, and it is generally small and often neglected. Derivations of  $L_{mq}$ ,  $L_{md}$ , and  $\lambda'_m$  based on the geometry, material properties, and stator winding configuration are provided in Chapter 15.

### 4.3. VOLTAGE AND TORQUE EQUATIONS IN ROTOR REFERENCE-FRAME VARIABLES

The voltage equations in the rotor reference frame may be written directly from (3.4-3) and (3.4-9) with  $\omega = \omega_r$ .

$$\mathbf{v}_{qd0s}^r = \mathbf{r}_s \mathbf{i}_{qd0s}^r + \omega_r \boldsymbol{\lambda}_{dqs}^r + p \boldsymbol{\lambda}_{qd0s}^r \quad (4.3-1)$$

where

$$(\boldsymbol{\lambda}_{dqs}^r)^T = [\lambda_{ds}^r \quad -\lambda_{qs}^r \quad 0] \quad (4.3-2)$$

$$\boldsymbol{\lambda}_{qd0s}^r = \begin{bmatrix} L_{ls} + L_{mq} & 0 & 0 \\ 0 & L_{ls} + L_{md} & 0 \\ 0 & 0 & L_{ls} \end{bmatrix} \begin{bmatrix} i_{qs}^r \\ i_{ds}^r \\ i_{0s} \end{bmatrix} + \lambda'_m \begin{bmatrix} 0 \\ 1 \\ 0 \end{bmatrix} \quad (4.3-3)$$

To be consistent with our previous notation, we have added the superscript  $r$  to  $\lambda'_m$ . In expanded form, we have

$$v_{qs}^r = r_s i_{qs}^r + \omega_r \lambda_{ds}^r + p \lambda_{qs}^r \quad (4.3-4)$$

$$v_{ds}^r = r_s i_{ds}^r - \omega_r \lambda_{qs}^r + p \lambda_{ds}^r \quad (4.3-5)$$

$$v_{0s} = r_s i_{0s} + p \lambda_{0s} \quad (4.3-6)$$

where

$$\lambda_{qs}^r = L_q i_{qs}^r \quad (4.3-7)$$

$$\lambda_{ds}^r = L_d i_{ds}^r + \lambda_m'' \quad (4.3-8)$$

$$\lambda_{0s} = L_{ls} i_{0s} \quad (4.3-9)$$

where  $L_q = L_{ls} + L_{mq}$  and  $L_d = L_{ls} + L_{md}$ . It is readily shown that if mutual leakage between stator windings shown in Chapter 2 is included in (4.2-5), the form of the  $q$ - and  $d$ -axis flux linkages remains unchanged. Indeed, the only impact will be on the respective leakage terms in  $L_q$  and  $L_d$ .

Substituting (4.3-7)–(4.3-9) into (4.3-4)–(4.3-6), and since  $p\lambda_m'' = 0$ , we can write

$$v_{qs}^r = (r_s + pL_q)i_{qs}^r + \omega_r L_d i_{ds}^r + \omega_r \lambda_m'' \quad (4.3-10)$$

$$v_{ds}^r = (r_s + pL_d)i_{ds}^r - \omega_r L_q i_{qs}^r \quad (4.3-11)$$

$$v_{0s} = (r_s + pL_{ls})i_{0s} \quad (4.3-12)$$

The expression for electromagnetic torque in terms of  $q$  and  $d$  variables may be obtained by substituting the expressions for the machine currents in terms of  $q$ - and  $d$ -currents into (4.2-9). This procedure is quite labor intensive; however, once we have expressed the voltage equations in terms of reference-frame variables, a more direct approach is possible [1]. In particular, the expression for input power is given by (3.3-8), and the electromagnetic torque multiplied by the rotor mechanical angular velocity is the power output. Thus we have

$$T_e \left( \frac{2}{P} \right) \omega_r = \frac{3}{2} (v_{qs}^r i_{qs}^r + v_{ds}^r i_{ds}^r + 2v_{0s} i_{0s}) \quad (4.3-13)$$

Substituting (4.3-4)–(4.3-6) into (4.3-13) gives us

$$\begin{aligned} T_e \left( \frac{2}{P} \right) \omega_r = & \frac{3}{2} r_s (i_{qs}^{r^2} + i_{ds}^{r^2} + 2i_{0s}^2) + \frac{3}{2} (\lambda_{ds}^r i_{qs}^r - \lambda_{qs}^r i_{ds}^r) \omega_r \\ & + \frac{3}{2} (i_{qs}^r p \lambda_{qs}^r + i_{ds}^r p \lambda_{ds}^r + 2i_{0s} p \lambda_{0s}) \end{aligned} \quad (4.3-14)$$

The first term on the right-hand side of (4.3-14) is the ohmic power loss in the stator windings, and the last term is the change of stored magnetic energy. If we equate the coefficients of  $\omega_r$ , we have

$$T_e = \left( \frac{3}{2} \right) \left( \frac{P}{2} \right) (\lambda_{ds}^r i_{qs}^r - \lambda_{qs}^r i_{ds}^r) \quad (4.3-15)$$

Substituting (4.3-7) and (4.3-8) into (4.3-15) yields

$$T_e = \left( \frac{3}{2} \right) \left( \frac{P}{2} \right) [\lambda_m'' i_{qs}^r + (L_d - L_q) i_{qs}^r i_{ds}^r] \quad (4.3-16)$$

The electromagnetic torque is positive for motor action.

When the machine is supplied from an inverter, it is possible, by controlling the firing of the inverter, to change the values of  $v_{qs}^r$  and  $v_{ds}^r$ . Recall that

$$\frac{d\theta_r}{dt} = \omega_r \quad (4.3-17)$$

Mathematically,  $\theta_r$  is obtained by integrating (4.3-17). In practice,  $\theta_r$  is estimated using Hall sensors or a position observer, or measured directly using an inline position encoder. For purposes of discussion, let us assume that the applied stator voltages are sinusoidal so that

$$v_{as} = \sqrt{2} v_s \cos \theta_{ev} \quad (4.3-18)$$

$$v_{bs} = \sqrt{2} v_s \cos \left( \theta_{ev} - \frac{2\pi}{3} \right) \quad (4.3-19)$$

$$v_{cs} = \sqrt{2} v_s \cos \left( \theta_{ev} + \frac{2\pi}{3} \right) \quad (4.3-20)$$

When the machine is supplied from an inverter, the stator voltages are controlled such that

$$\theta_{ev} = \theta_r + \phi_v \quad (4.3-21)$$

With power electronics, the voltages will generally have a waveform with switching harmonics included. Nevertheless, as a first approximation, (4.3-18)–(4.3-20) may be considered as the fundamental components of these stepped phase voltages.

Transforming (4.3-18)–(4.3-20) to the rotor reference frame yields

$$v_{qs}^r = \sqrt{2} v_s \cos \phi_v \quad (4.3-22)$$

$$v_{ds}^r = -\sqrt{2} v_s \sin \phi_v \quad (4.3-23)$$

## 4.4. ANALYSIS OF STEADY-STATE OPERATION

For steady-state operation with balanced, sinusoidal applied stator voltages, (4.3-10) and (4.3-11) may be written as

$$V_{qs}^r = r_s I_{qs}^r + \omega_r L_d I_{ds}^r + \omega_r \lambda_m'^r \quad (4.4-1)$$

$$V_{ds}^r = r_s I_{ds}^r - \omega_r L_q I_{qs}^r \quad (4.4-2)$$

where uppercase letters denote steady-state (constant) quantities. Assuming no demagnetization,  $\lambda_m'^r$  is always constant. The steady-state torque is expressed from (4.3-16) as

$$T_e = \left( \frac{3}{2} \right) \left( \frac{P}{2} \right) [\lambda_m'^r I_{qs}^r + (L_d - L_q) I_{qs}^r I_{ds}^r] \quad (4.4-3)$$

It is possible to establish a phasor voltage equation from (4.4-1) and (4.4-2). For steady-state operation,  $\phi_v$  is constant and represents the angular displacement between the peak value of the fundamental component of  $v_{as}$  and the  $q$ -axis fixed in the rotor. If we reference the phasors to the  $q$ -axis and let it be along the positive real axis of the “stationary” phasor diagram, then  $\phi_v$  becomes the phase angle of  $\tilde{V}_{as}$ , and we can write

$$\begin{aligned} \tilde{V}_{as} &= V_s e^{j\phi_v} \\ &= V_s \cos \phi_v + j V_s \sin \phi_v \end{aligned} \quad (4.4-4)$$

Comparing (4.4-4) with (4.3-22) and (4.3-23), we see that

$$\sqrt{2} \tilde{V}_{as} = V_{qs}^r - j V_{ds}^r \quad (4.4-5)$$

If we write the three-phase currents similar to (4.3-18)–(4.3-20) in terms of  $\theta_{ei}$ , then (4.3-21) would be in terms of  $\theta_{ei}$  and  $\phi_i$  rather than  $\theta_{ev}$  and  $\phi_v$  and we would arrive at a similar relation for current as (4.4-5). In particular,

$$\sqrt{2} \tilde{I}_{as} = I_{qs}^r - j I_{ds}^r \quad (4.4-6)$$

and

$$j \sqrt{2} \tilde{I}_{as} = I_{ds}^r + j I_{qs}^r \quad (4.4-7)$$

Substituting (4.4-1) and (4.4-2) into (4.4-5) and using (4.4-6) and (4.4-7) yields

$$\tilde{V}_{as} = (r_s + j \omega_r L_q) \tilde{I}_{as} + \tilde{E}_a \quad (4.4-8)$$

where

$$\tilde{E}_a = \frac{1}{\sqrt{2}} [\omega_r (L_d - L_q) I_{ds}^r + \omega_r \lambda_m'^r] e^{j0} \quad (4.4-9)$$

It is noted that  $\tilde{E}_a$  for the permanent-magnet ac machine, (4.4-9), is along the reference (real) axis.

## 4.5. BRUSHLESS DC MOTOR

The permanent-magnet ac machine is often referred to as a “brushless dc motor.” This is not because it has the physical configuration of a dc machine, but because by appropriate control of the driving inverter, its terminal characteristics may be made to resemble those of a dc motor. In order to show this, it is necessary to give a brief discussion of the dc machine that will be a review for most; however, a more detailed analysis is given in Chapter 14.

The voltages induced in the armature (rotating) windings of a dc machine are sinusoidal. These induced voltages are full-wave rectified as a result of the windings being mechanically switched by the action of the brushes sliding on the surface of the commutator mounted on the armature. This “dc voltage,” which is often called the counter electromotive force or back voltage, is proportional to the strength of the stationary field, in which the armature windings rotate, and the armature speed. This stationary field is established by either a winding on the stationary member of the machine or a permanent magnet. The steady-state armature voltage equation may be written

$$V_a = r_a I_a + \omega_r k_v \quad (4.5-1)$$

where  $V_a$  is the armature terminal voltage,  $r_a$  is the resistance of the armature windings between brushes,  $I_a$  is the armature current,  $\omega_r$  is the rotor speed in rad/s,  $k_v$  is proportional to the field strength, and  $\omega_r k_v$  is the counter electromotive force. If a field winding is used to establish the stationary field,  $k_v$  will vary with the winding current; if the field is established by a permanent magnet,  $k_v$  is constant. In either case,  $k_v$  has the units of V·s/rad. It is clear from (4.5-1) that the voltage  $\omega_r k_v$  is the open-circuit ( $I_a = 0$ ) armature voltage.

The commutation of the armature windings is designed so that the magnetic field established by the current following in the armature windings is stationary and orthogonal to the stationary magnetic field established by the field winding or the permanent magnet. With the two fields stationary and always in quadrature, the maximum possible torque is produced for any given strength of the magnetic fields. We will find that this optimum torque characteristic is the objective of many of the advanced control techniques for ac machines. The expression for torque may be obtained by multiplying (4.5-1) by  $I_a$  and recognizing that  $V_a I_a$  is the power input,  $I_a^2 r_a$  is the ohmic power loss, and  $\omega_r k_v I_a$  is the power output. Since the torque times rotor speed is the power output, the electromagnetic torque may be expressed as

$$T_e = k_v I_a \quad (4.5-2)$$

Let us now return to the permanent-magnet ac machine. From our earlier discussion, we are aware that the values of  $V_{qs}^r$  and  $V_{ds}^r$  are determined by the firing of the drive inverter. When the inverter is switched so that  $\phi_v = 0$ ,  $V_{qs}^r = \sqrt{2}V_s$  and  $V_{ds}^r = 0$ . In this case, (4.4-2) may be solved for  $I_{ds}^r$  in terms of  $I_{qs}^r$ .

$$I_{ds}^r = \frac{\omega_r L_q}{r_s} I_{qs}^r \quad \text{for } \phi_v = 0 \quad (4.5-3)$$

Substituting (4.5-3) into (4.4-1) yields

$$V_{qs}^r = \left( \frac{r_s^2 + \omega_r^2 L_q L_d}{r_s} \right) I_{qs}^r + \omega_r \lambda_m'^r \quad \text{for } \phi_v = 0 \quad (4.5-4)$$

We now start to see a similarity between the voltage equation for the permanent-magnet ac machine operated in this mode ( $\phi_v = 0$ ) and the dc machine. If we neglect  $\omega_r^2 L_q L_d$  in (4.5-4), then (4.5-1) and (4.5-4) would be identical in form. Let us note another similarity. If  $L_q = L_d$ , then the expression for the torque given by (4.4-3) is identical in form to (4.5-2). We now see why the permanent-magnet ac motor is called a brushless dc motor when  $\phi_v = 0$ , since the terminal characteristics appear to resemble those of a dc motor. We must be careful, however, since in order for (4.5-1) and (4.5-4) to be identical in form, the term  $\omega_r^2 L_q L_d$  must be significantly less than  $r_s$ . Let us see what effects this term has upon the torque versus speed characteristics. To do this, let us first let  $L_q = L_d = L_s$ , and if we then solve (4.5-4) for  $I_{qs}^r$ , and if we take that result along with (4.5-3) for  $I_{ds}^r$  and substitute these expressions into the expression for  $T_e$  (4.4-3), we obtain the following expression

$$T_e = \left( \frac{3}{2} \right) \left( \frac{P}{2} \right) \frac{r_s \lambda_m'^r}{r_s^2 + \omega_r^2 L_s^2} (V_{qs}^r - \omega_r \lambda_m'^r) \quad \text{for } \phi_v = 0 \quad (4.5-5)$$

The steady-state, torque-speed characteristics for a brushless dc motor are shown in Figure 4.5-1. Therein  $L_q = L_d$  and  $\phi_v = 0$ ; hence, Figure 4.5-1 is a plot of (4.5-5). If  $\omega_r^2 L_s^2$  is neglected, then (4.5-5) yields a straight line  $T_e$  versus  $\omega_r$  characteristic for a constant  $V_{qs}^r$ . Thus, if  $\omega_r^2 L_s^2$  could be neglected, the plot shown in Figure 4.5-1 would be a straight line as in the case of a dc motor. Although the  $T_e$  versus  $\omega_r$  is approximately linear over the region of motor operation where  $T_e \geq 0$  and  $\omega_r \geq 0$ , it is not linear over the complete speed range. In fact, we see from Figure 4.5-1 that there appears to be a maximum and

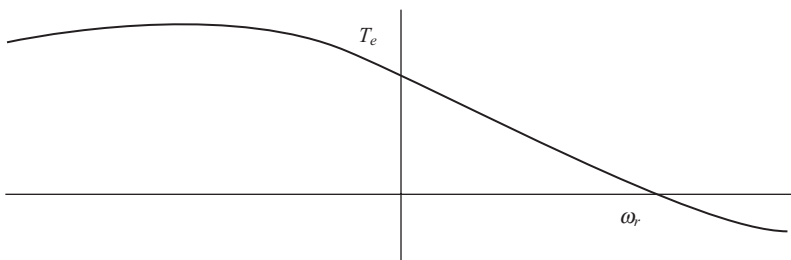


Figure 4.5-1. Torque-speed characteristics of a brushless dc motor with  $L_q = L_d$ ,  $\phi_v = 0$ ,  $V_{qs}^r = \sqrt{2}V_s$ , and  $V_{ds}^r = 0$ .

minimum torque. Let us take the derivative of (4.5-5) with respect to  $\omega_r$  and set the result to zero and solve for  $\omega_r$ . Thus, zero slope of the torque versus speed characteristics for  $L_q = L_d$ ,  $V_{qs}' = \sqrt{2}V_s$ , and  $V_{ds}' = 0$  ( $\phi_v = 0$ ) occurs at

$$\omega_{rMT} = \frac{V_{qs}^r}{\lambda_m^{rr}} \pm \sqrt{\left(\frac{V_{qs}^r}{\lambda_m^{rr}}\right)^2 + \left(\frac{r_s}{L_s}\right)^2} \quad \text{for } \phi_v = 0 \quad (4.5-6)$$

Due to the high reluctance of the magnetic material in the  $d$ -axis,  $L_d$  is generally smaller than  $L_q$ . In most cases, whether  $L_q > L_d$  or  $L_q < L_d$ , saliency has only secondary effects upon the torque-speed characteristics over the region of interest ( $T_e \geq 0$  and  $\omega_r \geq 0$ ). This is shown in Figure 4.5-2, where  $L_{md} = 0.6L_{mq}$  for the machine considered in Figure 4.5-1. The machine parameters for the characteristics shown in Figure 4.5-1 are  $r_s = 3.4\Omega$ ,  $L_{ls} = 1.1\text{ mH}$ , and  $L_{mq} = L_{md} = 11\text{ mH}$ , thus  $L_q = L_d = L_s = 12.1\text{ mH}$ . The device is a four-pole machine, and when it is driven at 1000 r/min, the open-circuit winding-to-winding voltage is sinusoidal with a peak-to-peak value of 60V. From this,  $\lambda_m^{rr}$  is calculated to be 0.0827 V·s. (The reader should verify this calculation.)

It is instructive to observe the machine variables during free acceleration and step changes in load torque with  $\phi_v = 0$ . In this case,  $J = 5 \times 10^{-4} \text{ kg} \cdot \text{m}^2$ , which represents the inertia of the machine and connected mechanical load. The dynamic performance is shown for applied stator phase voltages that are sinusoidal and stepped, as would be the case if a typical six-step voltage source inverter were used to supply the machine.

The free acceleration characteristics with sinusoidal phase voltages are shown in Figure 4.5-3. The applied stator phase voltages are of the form given by (4.3-18)–(4.3-20) with  $v_s = 11.25\text{ V}$ . The phase voltage  $v_{as}$ , phase current  $i_{as}$ ,  $q$ -axis voltage  $v_{qs}^r$ ,  $q$ -axis current  $i_{qs}^r$ ,  $d$ -axis current  $i_{ds}^r$ , electromagnetic torque  $T_e$ , and rotor speed  $\omega_r$  in electrical rad/s, are plotted. It is clear that since  $\phi_v = 0$ ,  $v_{ds}^r = 0$ . The device is a four-pole machine, thus 200 electrical rad/s is 955 r/min. A plot of  $T_e$  versus  $\omega_r$  is shown in

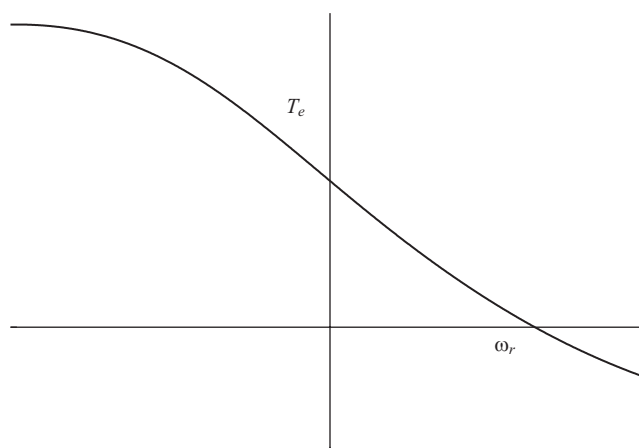


Figure 4.5-2. Same as Figure 4.5-1 with  $L_{md} = 0.6L_{mq}$ .

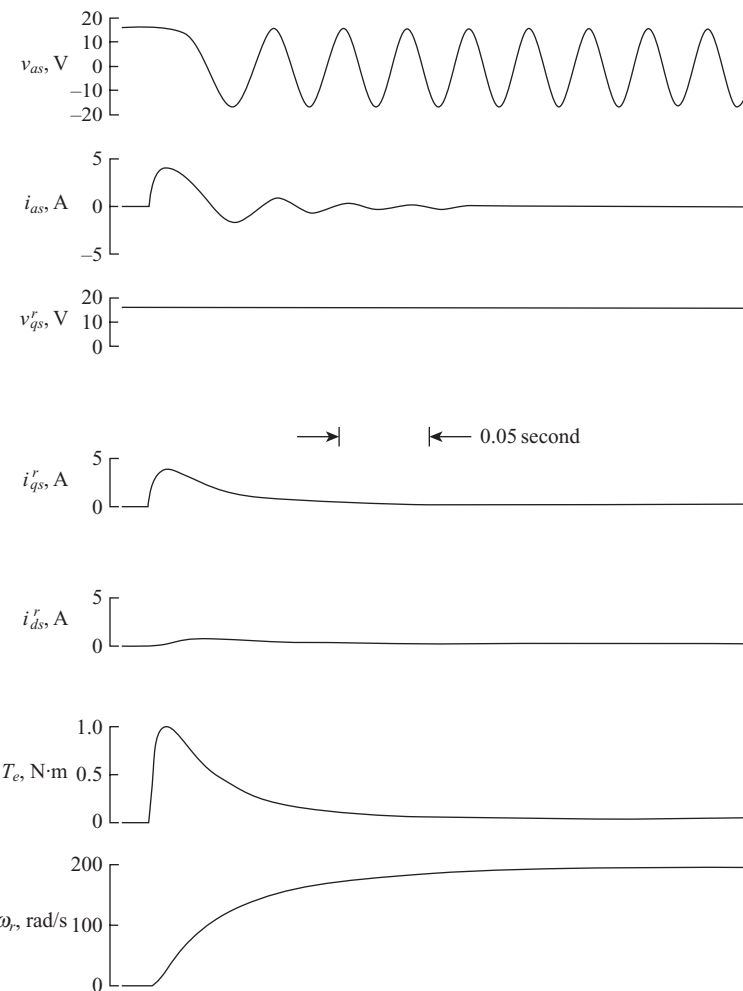
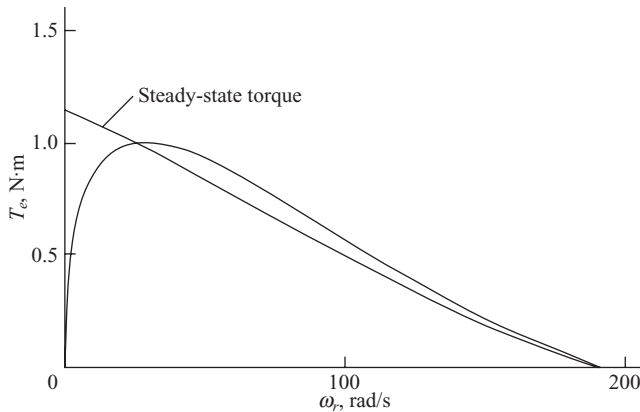


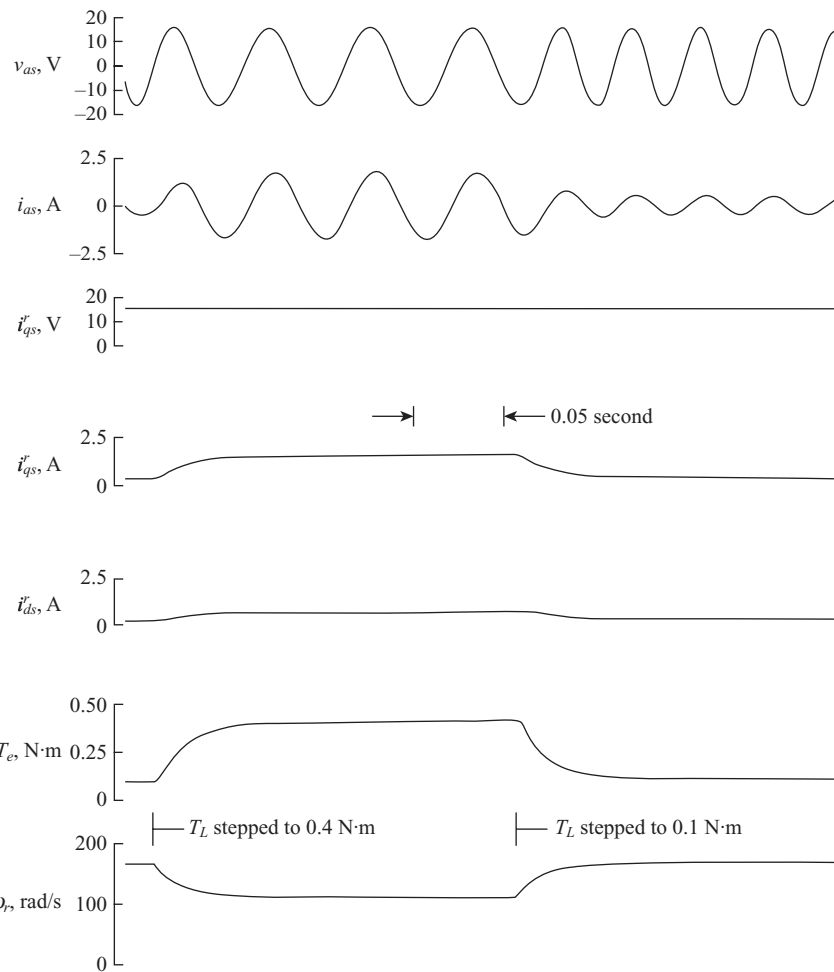
Figure 4.5-3. Free-acceleration characteristics of a brushless dc motor ( $\phi_v = 0$ ).

Figure 4.5-4 for the free acceleration depicted in Figure 4.5-3. The steady-state, torque-speed characteristic is superimposed for purposes of comparison. It is important to note that the dynamic torque-speed characteristics shown in Figure 4.5-4 differ from the steady-state, torque-speed characteristics. One must be aware of this discrepancy, which can be significant for small inertia drives, if one chooses to use the expression for the steady-state torque in a transfer function formulation describing the dynamic characteristics of a brushless dc motor.

The performance during step changes in load torque is illustrated in Figure 4.5-5. Initially the machine is operating with  $T_L = 0.1 \text{ N}\cdot\text{m}$ . The load torque is suddenly stepped to  $0.4 \text{ N}\cdot\text{m}$ . The machine slows down, and once steady-state operation is established,



**Figure 4.5-4.** Torque-speed characteristics for free acceleration shown in Figure 4.5-3.



**Figure 4.5-5.** Dynamic performance of a brushless dc motor ( $\phi_v = 0$ ) during step changes in load torque with  $J = 2 \times 10^{-4} \text{ kg} \cdot \text{m}^2$ .

the load torque is stepped back to  $0.1 \text{ N}\cdot\text{m}$ . In these studies, the inertia is  $2 \times 10^{-4} \text{ kg}\cdot\text{m}^2$ , which is 40% of the inertia used in Figure 4.5-3 and Figure 4.5-4.

The free-acceleration characteristics with the machine supplied from a typical voltage source inverter are shown in Figure 4.5-6 with  $J = 5 \times 10^{-4} \text{ kg}\cdot\text{m}^2$  so that a direct comparison can be made with Figure 4.5-3. Although this may seem inappropriate since we have yet to discuss the operation of the inverter, it does provide a first look at the machine variables in a drive application and, most important, it provides a justification of the sinusoidal approximation of the actual six-step phase voltages. The voltage  $v_{ds}^r$  is plotted in addition to the variables shown in Figure 4.5-3. It is recalled that with the sinusoidal approximation,  $v_{ds}^r$  is zero for  $\phi_v = 0$ . We see in Figure 4.5-6 that the average value of  $v_{ds}^r$  is zero. The torque versus speed characteristics for this free acceleration are shown in Figure 4.5-7.

In order to compare with the sinusoidal approximation, the inverter voltage was selected so that the constant component of  $v_{qs}^r$  is equal to the value used in the case of ac applied stator voltages. It is interesting to note that during the initial acceleration period, in Figure 4.5-6, before the first step (switching) occurs in  $v_{as}$ , the torque is slightly larger than with ac voltages applied (Fig. 4.5-3). This is due to the fact that a constant voltage is applied to the phases until the first switching occurs, and this constant voltage is larger than the effective value of the ac voltage during the same interval.

## 4.6. PHASE SHIFTING OF APPLIED VOLTAGES OF A PERMANENT-MAGNET AC MACHINE

Let us return to the voltage and torque equations for balanced steady-state operation given by (4.4-1)–(4.4-3). From (4.4-2)

$$I_{ds}^r = \frac{V_{ds}^r + \omega_r L_q I_{qs}^r}{r_s} \quad (4.6-1)$$

Substituting (4.6-1) into (4.4-1) yields

$$V_{qs}^r = \frac{r_s^2 + \omega_r^2 L_q L_d}{r_s} I_{qs}^r + \frac{\omega_r L_d}{r_s} V_{ds}^r + \omega_r \lambda_m'^r \quad (4.6-2)$$

Let us again set  $L_q = L_d = L_s$ , which simplifies our work. In this case,  $T_e$  and  $I_{qs}^r$  differ only by a constant multiplier. Solving (4.6-2) for  $I_{qs}^r$  yields

$$I_{qs}^r = \frac{r_s}{r_s^2 + \omega_r^2 L_s^2} \left( V_{qs}^r - \frac{L_s}{r_s} V_{ds}^r \omega_r - \lambda_m'^r \omega_r \right) \quad (4.6-3)$$

We see from (4.3-22) and (4.3-23) that if we consider only the fundamental component of the three-phase applied stator voltages

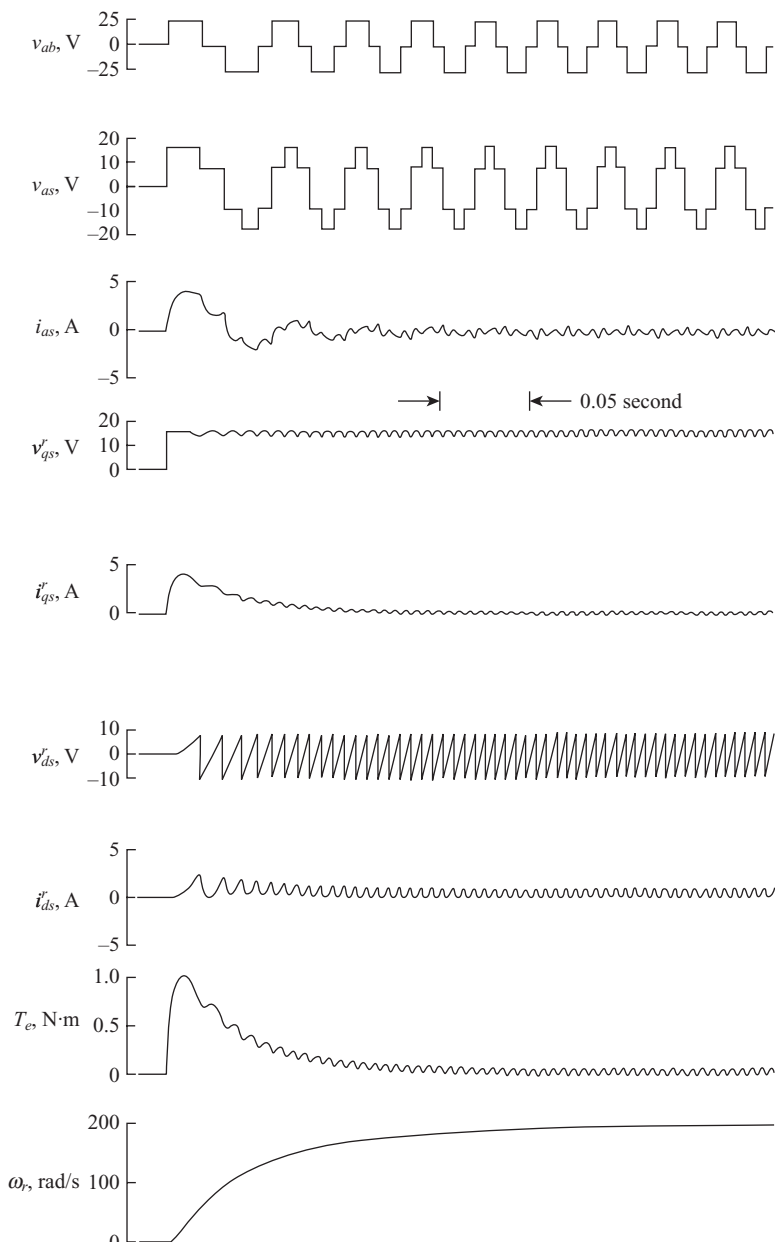


**Figure 4.5-6.** Free-acceleration characteristics of a brushless dc motor supplied from a typical six-step voltage source inverter ( $\phi_v = 0$ ). Compare with Figure 4.5-3.

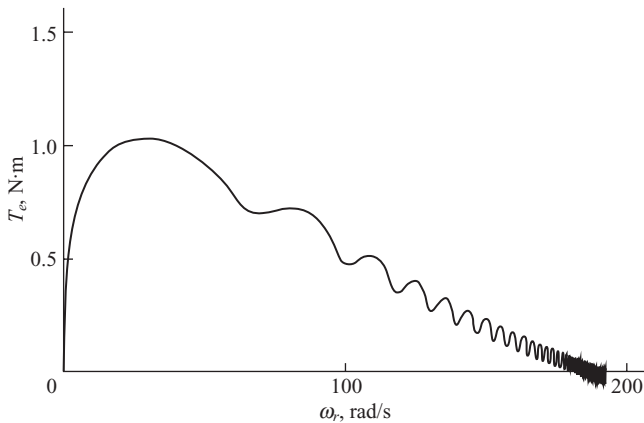


Figure 4.5-7. Torque-speed characteristics for free acceleration shown in Figure 4.5-6.

$$V_{qs}^r = \sqrt{2}V_s \cos \phi_v \quad (4.6-4)$$

$$V_{ds}^r = -\sqrt{2}V_s \sin \phi_v \quad (4.6-5)$$

wherein  $\phi_v$  is determined by the switching of the inverter. Substituting (4.6-4) and (4.6-5) into (4.6-3) yields

$$I_{qs}^r = \frac{\sqrt{2}r_s V_s}{r_s^2 + \omega_r^2 L_s^2} [\cos \phi_v + (\tau_s \sin \phi_v - \tau_v) \omega_r] \quad (4.6-6)$$

Here, we are using time constants, or what appear to be time constants, in a steady-state equation. This is not normally done; however, it allows us to work more efficiently. The constant  $\tau_s$  is  $L_s/r_s$ . It is the stator time constant. The quantity  $\tau_v$  is defined here as

$$\tau_v = \frac{\lambda_m'' r}{\sqrt{2}V_s} \quad (4.6-7)$$

It is introduced for our convenience. Be careful; although  $\tau_v$  has the units of seconds, it is not a constant; it will change with  $V_s$ . In speed control systems, the inverter supplying the permanent-magnet ac machine often provides a means to change the magnitude of  $V_s$ .

Equation (4.6-6) is an expression for  $I_{qs}^r$ , and thus  $T_e$ , in terms of the angle  $\phi_v$ , which is the phase shift of the fundamental component of the voltage  $v_{as}$  ahead of the  $q$ -axis of the rotor. There are several pieces of information that can be gained from this equation. First, let us find the maximum and minimum with respect to  $\phi_v$ . This may be accomplished by taking the derivative of (4.6-6) with respect to  $\phi_v$  and setting the result equal to zero. This yields

$$0 = -\sin \phi_v + \tau_s \omega_r \cos \phi_v \quad (4.6-8)$$

Thus, for a given rotor speed, a maximum or minimum value of  $I_{qs}^r(T_e)$  occurs when

$$\phi_{vMT} = \tan^{-1}(\tau_s \omega_r) \quad (4.6-9)$$

Hence, the maximum or minimum steady-state electromagnetic torque, with  $\phi_{vMT}$  given by (4.6-9), may be determined by substituting (4.6-9) into (4.6-6) and then substituting the results into (4.3-16) with  $L_q = L_d = L_s$ . Thus, the maximum or minimum steady-state electromagnetic torque for a given rotor speed may be expressed as

$$T_{eM} = \left( \frac{3}{2} \right) \left( \frac{P}{2} \right) \frac{\sqrt{2} V_s r_s \lambda_m'^r}{r_s^2 + \omega_r^2 L_s^2} \left[ \frac{(r_s^2 + \omega_r^2 L_s^2)^{1/2}}{r_s} - \frac{\lambda_m'^r \omega_r}{\sqrt{2} V_s} \right] \quad (4.6-10)$$

which may also be written as

$$T_{eM} = \left( \frac{3}{2} \right) \left( \frac{P}{2} \right) \frac{2 V_s^2 \tau_v}{r_s (1 + \tau_s^2 \omega_r^2)} [(1 + \tau_s^2 \omega_r^2)^{1/2} - \tau_v \omega_r] \quad (4.6-11)$$

Although (4.6-9)–(4.6-11) are valid for any speed, we are generally concerned with positive  $\omega_r$  for steady-state operation. With this in mind, let us look back to (4.6-6) and assume that the speed is positive. With this assumption,  $T_e$  is positive if

$$\cos \phi_v + \tau_s \omega_r \sin \phi_v > \tau_v \omega_r \quad (4.6-12)$$

Let us assume that  $\phi_v$  is  $\pi/2$ , which means that  $V_{qs}^r = 0$  and  $V_{ds}^r = -\sqrt{2} V_s$ . With  $\phi_v = \pi/2$ , (4.6-12) becomes

$$\tau_s > \tau_v \quad (4.6-13)$$

Equation (4.6-13) tells us that if  $\phi_v = \pi/2$  and if  $\tau_s > \tau_v$ , the torque will always be positive for  $\omega_r > 0$ . It follows that if  $\phi_v = \pi/2$  and if  $\tau_s = \tau_v$ , the torque will be zero regardless of the speed of the rotor, or if  $\tau_s < \tau_v$ , the torque will be negative for  $\omega_r > 0$ .

We will derive one more relationship from (4.6-6). For a fixed value of  $\phi_v$ , the speeds at which the maximum and minimum torques occur may be determined by taking the derivative of (4.6-6) with respect to  $\omega_r$  and setting the result to zero. This yields

$$\omega_{rMT} = \frac{1}{\tau_s \sin \phi_v - \tau_v} \left[ -\cos \phi_v \pm \frac{1}{\tau_s} \sqrt{\tau_s^2 + \tau_v^2 - 2 \tau_s \tau_v \sin \phi_v} \right] \quad (4.6-14)$$

It is left to the reader to show that (4.6-14), with  $\phi_v = 0$ , is (4.5-6).

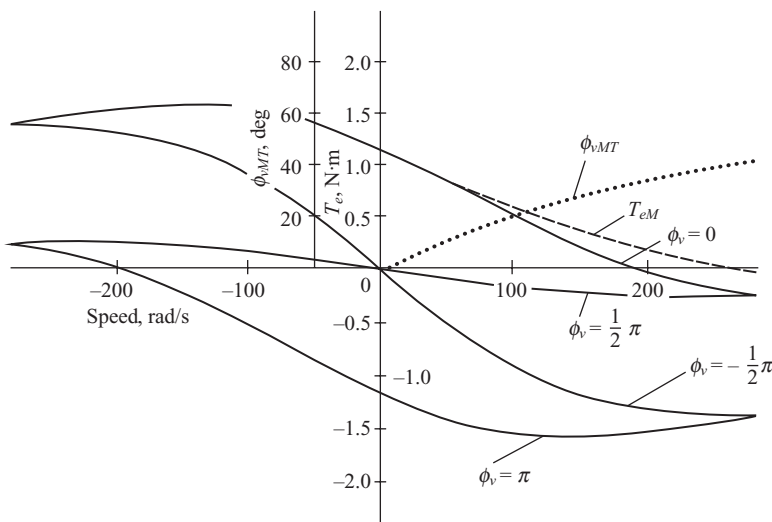


Figure 4.6-1. Torque-speed characteristics of a permanent-magnet ac machine with  $L_q = L_d$ .

The steady-state, torque-speed characteristics for the permanent-magnet ac machine with the parameters given in Section 4.5 are shown in Figure 4.6-1 for  $L_q = L_d$ . The value of  $V_s$  is 11.25 V. In order to illustrate the limits of the torque-speed characteristics for the various possible values of  $\phi_v$  plots of torque are shown for  $\phi_v = 0, \pm(\pi/2), \pi$  and  $\phi_{vMT}$  (4.6-9). The maximum torque for  $\omega_r > 0$  is also plotted.

We see that this machine, which is commercially available, yields negative  $T_e$  for  $\phi_v = \pi/2$  with  $\omega_r > 0$ . Therefore  $\tau_s$  must be less than  $\tau_v$ . Let us see;  $\tau_s = (12.1 \times 10^{-3})/3.4 = 3.56 \text{ ms}$ ;  $\tau_v = 0.0827 / (\sqrt{2} \times 11.25) = 5.2 \text{ ms}$ . In References 2 and 3, it was experimentally verified that advancing  $\phi_v$  from zero increased the torque at rotor speeds greater than zero. Therein, it is suggested that this might be a means of increasing the torque at high speeds. The parameters of the machine used in Reference 3 are given, and  $\tau_s > \tau_v$ . The influence of  $\tau_s$  upon the steady-state torque-speed characteristics is illustrated by Figure 4.6-2 and Figure 4.6-3. In Figure 4.6-2,  $\tau_s$  is increased by a factor of 3 ( $\tau_s = 3 \times 3.56 \text{ ms}$ ) by decreasing  $r_s$ . In Figure 4.6-3,  $\tau_s$  is increased by a factor of 3 by increasing  $L_s$ .

## 4.7. CONTROL OF STATOR CURRENTS

An alternative to controlling stator voltages is to use the inverter to control the stator phase currents. Under such control, a commanded phase current is issued to the inverter, and the switches are gated to track the commanded currents. Provided that the inverter is able to track the commanded currents, the phase currents are of the form

$$i_{as} = \sqrt{2}i_s \cos(\theta_r + \phi_i) \quad (4.7-1)$$

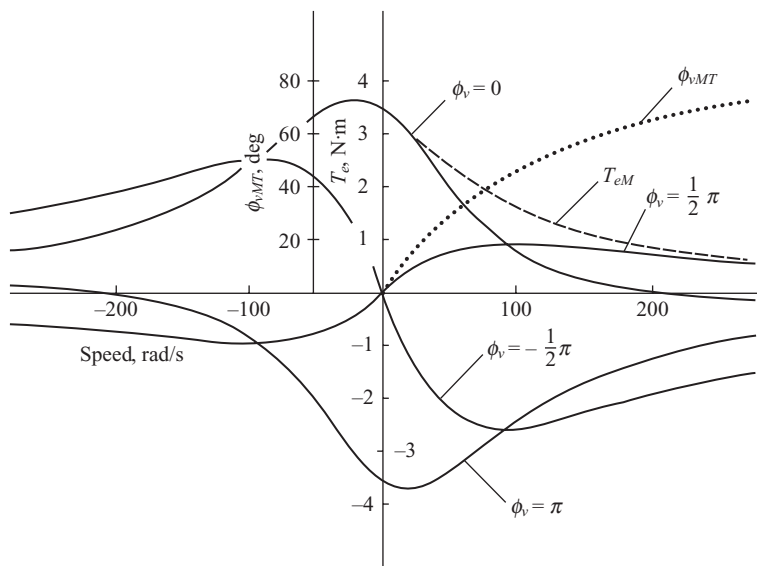


**Figure 4.6-2.** Torque-speed characteristics of permanent-magnet ac machine with  $\tau_s$  increased by a factor of 3 by decreasing  $r_s$ .

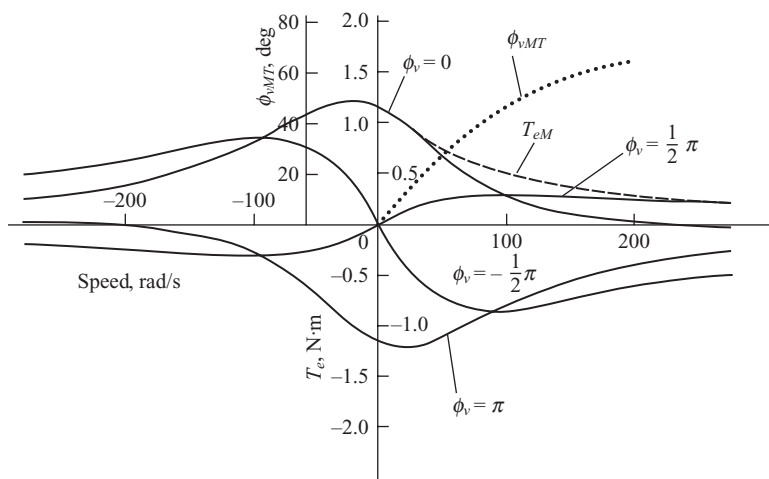


**Figure 4.6-3.** Torque-speed characteristics of permanent-magnet ac machine with  $\tau_s$  increased by a factor of 3 by increasing  $L_s$ .

$$i_{bs} = \sqrt{2}i_s \cos\left(\theta_r + \phi_i - \frac{2\pi}{3}\right) \quad (4.7-2)$$

$$i_{cs} = \sqrt{2}i_s \cos\left(\theta_r + \phi_i + \frac{2\pi}{3}\right) \quad (4.7-3)$$

The resulting  $q$ - and  $d$ -axis currents are of the form

$$i_{qs}^r = \sqrt{2}i_s \cos \phi_i \quad (4.7-4)$$

$$i_{ds}^r = -\sqrt{2}i_s \sin \phi_i \quad (4.7-5)$$

Direct control of the stator phase current can provide a relatively straightforward, yet high bandwidth control of the electromagnetic torque. As an example, if  $L_q = L_d$ , the electromagnetic torque is proportional to the  $q$ -axis current. Setting  $\phi_i$  to zero, electromagnetic torque can be adjusted directly through the value of  $i_s$ . In general, voltage constraints limit the speed over which  $\phi_i$  can be set to zero and one can track rated stator current. Above these speeds, the  $d$ -axis current is used to reduce stator winding voltage in what is generally referred to as field weakening. Details of current control strategies for surface and buried magnet machines are provided in Chapter 14.

## REFERENCES

- [1] R.H. Park, "Two-Reaction Theory of Synchronous Machines—Generalized Method of Analysis, Part I," *AIEE Trans.*, Vol. 48, July 1929, pp. 716–727.
- [2] T.W. Nehl, F.A. Fouad, and N.A. Demerdash, "Digital Simulation Power Conditioner—Machine Interaction for Electronically Commutated DC Permanent Magnet Machines," *IEEE Trans. Magn.*, Vol. 17, November 1981, pp. 3284–3286.
- [3] T.M. Jahns, "Torque Production in Permanent-Magnet Synchronous Motor Drives with Rectangular Current Excitations," *IAS Conf. Rec.*, October 1983, pp. 476–487.

## PROBLEMS

1. Verify (4.3-3).
2. Write the voltage equations given by (4.3-10)–(4.3-12) and the torque equation given by (4.3-15) in terms of flux linkages rather than currents.
3. Starting with the appropriate equations set forth in Section 4.3, develop a time-domain block diagram for the permanent-magnet ac machine. Consider  $v_{qs}^r$ ,  $v_{ds}^r$ , and  $T_L$  as inputs.
4. Starting with the appropriate equations set forth in Section 4.3, develop the equations of state with  $v_{qs}^r$ ,  $v_{ds}^r$ , and  $T_L$  as inputs.
5. Repeat Problems 3 and 4 with  $v_s$ ,  $\phi_v$ , and  $T_L$  as inputs.
6. Note in Figure 4.6-1 that the steady-state torque versus speed plots for  $\phi_v = 0$  and for  $\phi_v = \pi/2$  intersect. Calculate the rotor speed where this intersection occurs.

7. Show that the maximum torque plotted in Figure 4.6-2 is three times the maximum torque plotted in Figure 4.6-3.
8. Show that for  $\phi_{vMT}$  (4.6-9) set for maximum torque, the phase current leads the phase voltage when

$$\omega_r > \frac{\sqrt{2}V_s}{2\cos\phi_v\lambda_m'^r}$$

9. A four-pole, three-phase, permanent-magnet ac machine has  $r_s = 1 \Omega$ ,  $L_q = L_d = 1 \text{ mH}$ ,  $\lambda_m'^r = 0.1 \text{ V}\cdot\text{s}$ . The machine is operating in steady state with  $I_{as} = -\sqrt{2}100\sin(\theta_r - 135^\circ)$  and  $\phi_v = 0$ . Determine  $V_{as}$ . Determine a value of  $\phi_v$  to provide the same torque and speed, but with maximum efficiency.
10. A permanent-magnet ac machine has  $r_s = 0.1 \Omega$ ,  $L_q = L_d = 1 \text{ mH}$ ,  $\lambda_m'^r = 0.1 \text{ V}\cdot\text{s}$ ,  $P = 4$ . A torque of  $3 \text{ N}\cdot\text{m}$  is desired at a speed of  $\omega_r = 100 \text{ rad/s}$ . Determine the value of  $\phi_i$  that will minimize the stator current amplitude needed to achieve the desired torque. Determine the resulting  $V_{as}$ .
11. For the machine in Problem 10, assume that  $L_d = 0.7L_q$ . Determine the  $q$ - and  $d$ -axis currents that will minimize the stator current amplitude needed to achieve the desired torque. Determine the resulting  $V_{as}$ .
12. A permanent-magnet ac machine is operating with  $\lambda_{as} = 0.1\cos(100t) \text{ V}\cdot\text{s}$ .  $T_L = k\omega_r^2$ .  $P = 4$ ,  $L_q = 5 \text{ mH}$ ,  $L_d = 3 \text{ mH}$ ,  $r_s = 1 \Omega$ ,  $\lambda_m'^r = 0.1 \text{ V}\cdot\text{s}$ . Determine  $k$  and  $V_{as}$ .
13. A three-phase permanent-magnet ac machine is operating with  $I_{qs}' = 100 \text{ A}$  and  $I_{ds}' = -10 \text{ A}$ . The load is a fan with  $T_L = 0.1\omega_r^2$ . The parameters of the machine are  $P = 4$ ,  $r_s = 0.01 \Omega$ ,  $L_q = L_d = 1 \text{ mH}$ ,  $\lambda_m'^r = 0.133 \text{ V}\cdot\text{s}$ . Determine  $V_{as}$  and the machine efficiency.
14. A six-pole permanent-magnet ac machine has  $\lambda_{qs}^r = L_q i_{qs}^r$ ,  $\lambda_{ds}^r = L_d i_{qs}^r - \lambda_m'^r$ . Draw a cross sectional view of the machine that shows the phase- $a$  winding, the rotor, the magnets, and the relative position between the stator and rotor that would lead to such expressions for flux linkages. Express  $T_e$  in terms of  $q$ - and  $d$ -axis stator currents for this case. Label the  $q$ - and  $d$ -axis.
15. For the machine considered to create the plot in Figure 4.5-1, plot the torque versus speed and amplitude of stator current versus speed over the motoring region of operation assuming a rated voltage is applied and  $\phi_v = 0$ . For this machine, assume thermal constraints limit the continuous stator current to  $0.5 \text{ A}$ . Explain what impact the thermal constraints have on the torque versus speed curve that was plotted.

# SYNCHRONOUS MACHINES

## 5.1. INTRODUCTION

The electrical and electromechanical behavior of most synchronous machines can be predicted from the equations that describe the three-phase salient-pole synchronous machine. In particular, these equations can be used directly to predict the performance of synchronous motors, hydro, steam, combustion, or wind turbine driven synchronous generators, and, with only slight modifications, reluctance motors.

The rotor of a synchronous machine is equipped with a field winding and one or more damper windings and, in general, each of the rotor windings has different electrical characteristics. Moreover, the rotor of a salient-pole synchronous machine is magnetically unsymmetrical. Due to these rotor asymmetries, a change of variables for the rotor variables offers no advantage. However, a change of variables is beneficial for the stator variables. In most cases, the stator variables are transformed to a reference frame fixed in the rotor (Park's equations) [1]; however, the stator variables may also be expressed in the arbitrary reference frame, which is convenient for some computer simulations.

In this chapter, the voltage and electromagnetic torque equations are first established in machine variables. Reference-frame theory set forth in Chapter 3 is then used

to establish the machine equations with the stator variables in the rotor reference frame. The equations that describe the steady-state behavior are then derived using the theory established in Chapter 3. The machine equations are arranged convenient for computer simulation wherein a method for accounting for saturation is given. Computer traces are given to illustrate the dynamic behavior of a synchronous machine during motor and generator operation and a low-power reluctance motor during load changes and variable frequency operation.

Nearly all of the electric power used throughout the world is generated by synchronous generators driven either by hydro, steam, or wind turbines or combustion engines. Just as the induction motor is the workhorse when it comes to converting energy from electrical to mechanical, the synchronous machine is the principal means of converting energy from mechanical to electrical. In the power system or electric grid environment, the analysis of the synchronous generator is often carried out assuming positive currents out of the machine. Although this is very convenient for the power systems engineer, it tends to be somewhat confusing for beginning machine analysts and inconvenient for engineers working in the electric drives area. In an effort to make this chapter helpful in both environments, positive stator currents are assumed into the machine as done in the analysis of the induction machine, and then in Section 5.10, the sense of the stator currents is reversed, and high-power synchronous generators that would be used in a power system are considered. The changes in the machine equations necessary to accommodate positive current out of the machine are described. Computer traces are then given to illustrate the dynamic behavior of typical hydro and steam turbine-driven generators during sudden changes in input torque and during and following a three-phase fault at the terminals. These dynamic responses, which are calculated using the detailed set of nonlinear differential equations, are compared with those predicted by an approximate method of calculating the transient torque–angle characteristics, which was widely used before the advent of modern computers and which still offer an unequalled means of visualizing the transient behavior of synchronous generators in a power system.

## 5.2. VOLTAGE EQUATIONS IN MACHINE VARIABLES

A two-pole, three-phase, wye-connected, salient-pole synchronous machine is shown in Figure 5.2-1. The stator windings are identical sinusoidally distributed windings, displaced  $120^\circ$ , with  $N_s$  equivalent turns and resistance  $r_s$ . The rotor is equipped with a field winding and three damper windings. The field winding ( $fd$  winding) has  $N_{fd}$  equivalent turns with resistance  $r_{fd}$ . One damper winding has the same magnetic axis as the field winding. This winding, the  $kd$  winding, has  $N_{kd}$  equivalent turns with resistance  $r_{kd}$ . The magnetic axis of the second and third damper windings, the  $kq1$  and  $kq2$  windings, is displaced  $90^\circ$  ahead of the magnetic axis of the  $fd$  and  $kd$  windings. The  $kq1$  and  $kq2$  windings have  $N_{kq1}$  and  $N_{kq2}$  equivalent turns, respectively, with resistances  $r_{kq1}$  and  $r_{kq2}$ . It is assumed that all rotor windings are sinusoidally distributed.

In Figure 5.2-1, the magnetic axes of the stator windings are denoted by the  $as$ ,  $bs$ , and  $cs$  axes. This notation was also used for the stator windings of the induction

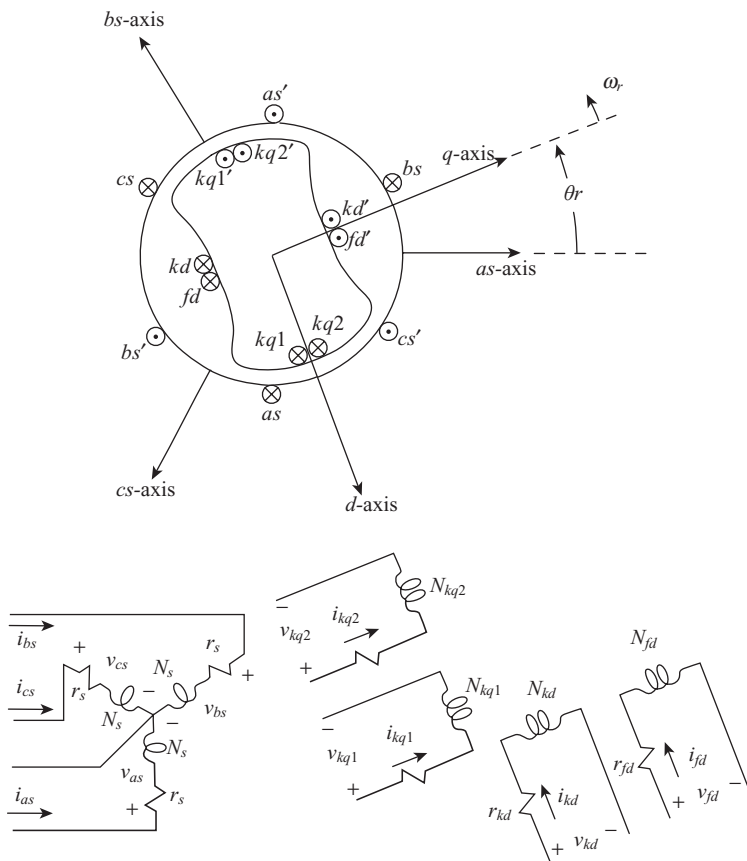


Figure 5.2-1. Two-pole, three-phase, wye-connected salient-pole synchronous machine.

machine. The quadrature axis ( $q$ -axis) and direct axis ( $d$ -axis) are introduced in Figure 5.2-1. The  $q$ -axis is the magnetic axis of the  $kq1$  and  $kq2$  windings, while the  $d$ -axis is the magnetic axis of the  $fd$  and  $kd$  windings. The use of the  $q$ - and  $d$ -axes was in existence prior to Park's work [1], and as mentioned in Chapter 3, Park used the notation of  $f_q$ ,  $f_d$ , and  $f_0$  in his transformation. Perhaps he made this choice of notation since, in effect, this transformation referred the stator variables to the rotor where the traditional  $q$ -and  $d$ -axes are located.

We have used  $f_{qs}$ ,  $f_{ds}$ , and  $f_{0s}$ , and  $f'_{qs}$ ,  $f'_{ds}$ , and  $f'_{0s}$  to denote transformed induction machine variables without introducing the connotation of a  $q$ - or  $d$ -axis. Instead, the  $q$ - and  $d$ -axes have been reserved to denote the rotor magnetic axes of the synchronous machine where they have an established physical meaning quite independent of any transformation. For this reason, one may argue that the  $q$  and  $d$  subscripts should not be used to denote the transformation to the arbitrary reference frame. Indeed, this line of reasoning has merit; however, since the transformation to the arbitrary reference

frame is in essence a generalization of Park's transformation, the  $q$  and  $d$  subscripts have been selected for use in the transformation to the arbitrary reference primarily out of respect for Park's work, which is the basis of it all.

Although the damper windings are shown with provisions to apply a voltage, they are, in fact, short-circuited windings that represent the paths for induced rotor currents. Currents may flow in either cage-type windings similar to the squirrel-cage windings of induction machines or in the actual iron of the rotor. In salient-pole machines at least, the rotor is laminated, and the damper winding currents are confined, for the most part, to the cage windings embedded in the rotor. In the high-speed, two- or four-pole machines, the rotor is cylindrical, made of solid iron with a cage-type winding embedded in the rotor. Here, currents can flow either in the cage winding or in the solid iron.

The performance of nearly all types of synchronous machines may be adequately described by straightforward modifications of the equations describing the performance of the machine shown in Figure 5.2-1. For example, the behavior of low-speed hydro turbine generators, which are always salient-pole machines, is generally predicted sufficiently by one equivalent damper winding in the  $q$ -axis. Hence, the performance of this type of machine may be described from the equations derived for the machine shown in Figure 5.2-1 by eliminating all terms involving one of the  $kq$  windings. The reluctance machine, which has no field winding and generally only one damper winding in the  $q$ -axis, may be described by eliminating the terms involving the  $fd$  winding and one of the  $kq$  windings. In solid iron rotor, steam turbine generators, the magnetic characteristics of the  $q$ - and  $d$ -axes are identical, or nearly so, hence the inductances associated with the two axes are essentially the same. Also, it is necessary, in most cases, to include all three damper windings in order to portray adequately the transient characteristics of the stator variables and the electromagnetic torque of solid iron rotor machines [2].

The voltage equations in machine variables may be expressed in matrix form as

$$\mathbf{v}_{abcs} = \mathbf{r}_s \mathbf{i}_{abcs} + p\boldsymbol{\lambda}_{abcs} \quad (5.2-1)$$

$$\mathbf{v}_{qdr} = \mathbf{r}_r \mathbf{i}_{qdr} + p\boldsymbol{\lambda}_{qdr} \quad (5.2-2)$$

where

$$(\mathbf{f}_{abcs})^T = [f_{as} \quad f_{bs} \quad f_{cs}] \quad (5.2-3)$$

$$(\mathbf{f}_{qdr})^T = [f_{kq1} \quad f_{kq2} \quad f_{fd} \quad f_{kd}] \quad (5.2-4)$$

In the previous equations, the  $s$  and  $r$  subscripts denote variables associated with the stator and rotor windings, respectively. Both  $\mathbf{r}_s$  and  $\mathbf{r}_r$  are diagonal matrices, in particular

$$\mathbf{r}_s = \text{diag}[r_s \quad r_s \quad r_s] \quad (5.2-5)$$

$$\mathbf{r}_r = \text{diag}[r_{kq1} \quad r_{kq2} \quad r_{fd} \quad r_{kd}] \quad (5.2-6)$$

The flux linkage equations for a linear magnetic system become

$$\begin{bmatrix} \lambda_{abcs} \\ \lambda_{qdr} \end{bmatrix} = \begin{bmatrix} \mathbf{L}_s & \mathbf{L}_{sr} \\ (\mathbf{L}_{sr})^T & \mathbf{L}_r \end{bmatrix} \begin{bmatrix} \mathbf{i}_{abcs} \\ \mathbf{i}_{qdr} \end{bmatrix} \quad (5.2-7)$$

From the work in Chapters 1 and 2, neglecting mutual leakage between stator windings, we can write  $\mathbf{L}_s$  as

$$\mathbf{L}_s = \begin{bmatrix} L_{ls} + L_A - L_B \cos 2\theta_r & -\frac{1}{2}L_A - L_B \cos 2\left(\theta_r - \frac{\pi}{3}\right) & -\frac{1}{2}L_A - L_B \cos 2\left(\theta_r + \frac{\pi}{3}\right) \\ -\frac{1}{2}L_A - L_B \cos 2\left(\theta_r - \frac{\pi}{3}\right) & L_{ls} + L_A - L_B \cos 2\left(\theta_r - \frac{2\pi}{3}\right) & -\frac{1}{2}L_A - L_B \cos 2(\theta_r + \pi) \\ -\frac{1}{2}L_A - L_B \cos 2\left(\theta_r + \frac{\pi}{3}\right) & -\frac{1}{2}L_A - L_B \cos 2(\theta_r + \pi) & L_{ls} + L_A - L_B \cos 2\left(\theta_r + \frac{2\pi}{3}\right) \end{bmatrix} \quad (5.2-8)$$

By a straightforward extension of the work in Chapters 1 and 2, we can express the self- and mutual inductances of the damper windings. The inductance matrices  $\mathbf{L}_{sr}$  and  $\mathbf{L}_r$  may then be expressed as

$$\mathbf{L}_{sr} = \begin{bmatrix} L_{skq1} \cos \theta_r & L_{skq2} \cos \theta_r & L_{sfd} \sin \theta_r & L_{skd} \sin \theta_r \\ L_{skq1} \cos\left(\theta_r - \frac{2\pi}{3}\right) & L_{skq2} \cos\left(\theta_r - \frac{2\pi}{3}\right) & L_{sfd} \sin\left(\theta_r - \frac{2\pi}{3}\right) & L_{skd} \sin\left(\theta_r - \frac{2\pi}{3}\right) \\ L_{skq1} \cos\left(\theta_r + \frac{2\pi}{3}\right) & L_{skq2} \cos\left(\theta_r + \frac{2\pi}{3}\right) & L_{sfd} \sin\left(\theta_r + \frac{2\pi}{3}\right) & L_{skd} \sin\left(\theta_r + \frac{2\pi}{3}\right) \end{bmatrix} \quad (5.2-9)$$

$$\mathbf{L}_r = \begin{bmatrix} L_{lkq1} + L_{mkq1} & L_{kq1kq2} & 0 & 0 \\ L_{kq1kq2} & L_{lkq2} + L_{mkq2} & 0 & 0 \\ 0 & 0 & L_{lfd} + L_{mfd} & L_{fdkd} \\ 0 & 0 & L_{fdkd} & L_{lkd} + L_{mkd} \end{bmatrix} \quad (5.2-10)$$

In (5.2-8),  $L_A > L_B$  and  $L_B$  is zero for a round rotor machine. Also in (5.2-8) and (5.2-10), the leakage inductances are denoted with  $l$  in the subscript. The subscripts  $skq1$ ,  $skq2$ ,  $sfd$ , and  $skd$  in (5.2-9) denote mutual inductances between stator and rotor windings.

The magnetizing inductances are defined as

$$L_{mq} = \frac{3}{2}(L_A - L_B) \quad (5.2-11)$$

$$L_{md} = \frac{3}{2}(L_A + L_B) \quad (5.2-12)$$

It can be shown that

$$L_{skq1} = \left( \frac{N_{kq1}}{N_s} \right) \left( \frac{2}{3} \right) L_{mq} \quad (5.2-13)$$

$$L_{skq2} = \left( \frac{N_{kq2}}{N_s} \right) \left( \frac{2}{3} \right) L_{mq} \quad (5.2-14)$$

$$L_{sfd} = \left( \frac{N_{fd}}{N_s} \right) \left( \frac{2}{3} \right) L_{md} \quad (5.2-15)$$

$$L_{skd} = \left( \frac{N_{kd}}{N_s} \right) \left( \frac{2}{3} \right) L_{md} \quad (5.2-16)$$

$$L_{mkq1} = \left( \frac{N_{kq1}}{N_s} \right)^2 \left( \frac{2}{3} \right) L_{mq} \quad (5.2-17)$$

$$L_{mkq2} = \left( \frac{N_{kq2}}{N_s} \right)^2 \left( \frac{2}{3} \right) L_{mq} \quad (5.2-18)$$

$$L_{mfd} = \left( \frac{N_{fd}}{N_s} \right)^2 \left( \frac{2}{3} \right) L_{md} \quad (5.2-19)$$

$$L_{mkd} = \left( \frac{N_{kd}}{N_s} \right)^2 \left( \frac{2}{3} \right) L_{md} \quad (5.2-20)$$

$$\begin{aligned} L_{kq1kq2} &= \left( \frac{N_{kq2}}{N_{kq1}} \right) L_{mkq1} \\ &= \left( \frac{N_{kq1}}{N_{kq2}} \right) L_{mkq2} \end{aligned} \quad (5.2-21)$$

$$\begin{aligned} L_{fdkd} &= \left( \frac{N_{kd}}{N_{fd}} \right) L_{mfd} \\ &= \left( \frac{N_{fd}}{N_{kd}} \right) L_{mkd} \end{aligned} \quad (5.2-22)$$

It is convenient to incorporate the following substitute variables, which refer the rotor variables to the stator windings.

$$i'_j = \left( \frac{2}{3} \right) \left( \frac{N_j}{N_s} \right) i_j \quad (5.2-23)$$

$$v'_j = \left( \frac{N_s}{N_j} \right) v_j \quad (5.2-24)$$

$$\lambda'_j = \left( \frac{N_s}{N_j} \right) \lambda_j \quad (5.2-25)$$

where  $j$  may be  $kq1$ ,  $kq2$ ,  $fd$ , or  $kd$ .

The flux linkages may now be written as

$$\begin{bmatrix} \lambda_{abcs} \\ \lambda'_{qdr} \end{bmatrix} = \begin{bmatrix} \mathbf{L}_s & \mathbf{L}'_{sr} \\ \frac{2}{3}(\mathbf{L}'_{sr})^T & \mathbf{L}'_r \end{bmatrix} \begin{bmatrix} \mathbf{i}_{abcs} \\ \mathbf{i}'_{qdr} \end{bmatrix} \quad (5.2-26)$$

where  $\mathbf{L}_s$  is defined by (5.2-8) and

$$\mathbf{L}'_{sr} = \begin{bmatrix} L_{mq} \cos \theta_r & L_{mq} \cos \theta_r & L_{md} \sin \theta_r & L_{md} \sin \theta_r \\ L_{mq} \cos \left( \theta_r - \frac{2\pi}{3} \right) & L_{mq} \cos \left( \theta_r - \frac{2\pi}{3} \right) & L_{md} \sin \left( \theta_r - \frac{2\pi}{3} \right) & L_{md} \sin \left( \theta_r - \frac{2\pi}{3} \right) \\ L_{mq} \cos \left( \theta_r + \frac{2\pi}{3} \right) & L_{mq} \cos \left( \theta_r + \frac{2\pi}{3} \right) & L_{md} \sin \left( \theta_r + \frac{2\pi}{3} \right) & L_{md} \sin \left( \theta_r + \frac{2\pi}{3} \right) \end{bmatrix} \quad (5.2-27)$$

$$\mathbf{L}'_r = \begin{bmatrix} L'_{lkq1} + L_{mq} & L_{mq} & 0 & 0 \\ L_{mq} & L'_{lkq2} + L_{mq} & 0 & 0 \\ 0 & 0 & L'_{ifd} + L_{md} & L_{md} \\ 0 & 0 & L_{md} & L'_{lkd} + L_{md} \end{bmatrix} \quad (5.2-28)$$

The voltage equations expressed in terms of machine variables referred to the stator windings are

$$\begin{bmatrix} \mathbf{v}_{abcs} \\ \mathbf{v}'_{qdr} \end{bmatrix} = \begin{bmatrix} \mathbf{r}_s + p\mathbf{L}_s & p\mathbf{L}'_{sr} \\ \frac{2}{3}p(\mathbf{L}'_{sr})^T & \mathbf{r}'_r + p\mathbf{L}'_r \end{bmatrix} \begin{bmatrix} \mathbf{i}_{abcs} \\ \mathbf{i}'_{qdr} \end{bmatrix} \quad (5.2-29)$$

In (5.2-28) and (5.2-29)

$$r'_j = \left( \frac{3}{2} \right) \left( \frac{N_s}{N_j} \right)^2 r_j \quad (5.2-30)$$

$$L'_{lj} = \left( \frac{3}{2} \right) \left( \frac{N_s}{N_j} \right)^2 L_{lj} \quad (5.2-31)$$

where, again,  $j$  may be  $kq1$ ,  $kq2$ ,  $fd$ , or  $kd$ .

### 5.3. TORQUE EQUATION IN MACHINE VARIABLES

The energy stored in the coupling field of a synchronous machine may be expressed as

$$W_f = \frac{1}{2}(\mathbf{i}_{abcs})^T \mathbf{L}_s \mathbf{i}_{abcs} + (\mathbf{i}_{abcs})^T \mathbf{L}'_{sr} \mathbf{i}'_{qdr} + \left(\frac{1}{2}\right) \left(\frac{3}{2}\right) (\mathbf{i}'_{qdr})^T \mathbf{L}'_{sr} \mathbf{i}'_{qdr} \quad (5.3-1)$$

Since the magnetic system is assumed to be linear,  $W_f = W_c$ , the second entry of Table 1.3-1 may be used, keeping in mind that the derivatives in Table 1.3-1 are taken with respect to mechanical rotor position. Using the fact that  $\theta_r = \frac{P}{2}\theta_{rm}$ , the torque is expressed in terms of electrical rotor position as

$$T_e = \left(\frac{P}{2}\right) \left\{ \frac{1}{2}(\mathbf{i}_{abcs})^T \frac{\partial}{\partial \theta_r} [\mathbf{L}_s] \mathbf{i}_{abcs} + (\mathbf{i}_{abcs})^T \frac{\partial}{\partial \theta_r} [\mathbf{L}'_{sr}] \mathbf{i}'_{qdr} \right\} \quad (5.3-2)$$

In expanded form (5.3-2) becomes

$$\begin{aligned} T_e = & \left(\frac{P}{2}\right) \left\{ \left( \frac{(L_{md} - L_{mq})}{3} \right) \left[ \left( i_{as}^2 - \frac{1}{2}i_{bs}^2 - \frac{1}{2}i_{cs}^2 - i_{as}i_{bs} - i_{as}i_{cs} + 2i_{bs}i_{cs} \right) \sin 2\theta_r \right. \right. \\ & + \frac{\sqrt{3}}{2} (i_{bs}^2 - i_{cs}^2 - 2i_{as}i_{bs} + 2i_{as}i_{cs}) \cos 2\theta_r \left. \right] \\ & + L_{mq} (i'_{kq1} + i'_{kq2}) \left[ \left( i_{as} - \frac{1}{2}i_{bs} - \frac{1}{2}i_{cs} \right) \sin \theta_r - \frac{\sqrt{3}}{2} (i_{bs} - i_{cs}) \cos \theta_r \right] \\ & \left. \left. - L_{md} (i'_{fd} + i'_{kd}) \left[ \left( i_{as} - \frac{1}{2}i_{bs} - \frac{1}{2}i_{cs} \right) \cos \theta_r + \frac{\sqrt{3}}{2} (i_{bs} - i_{cs}) \sin \theta_r \right] \right\} \quad (5.3-3) \end{aligned}$$

The above expression for torque is positive for motor action. The torque and rotor speed are related by

$$T_e = J \left(\frac{2}{P}\right) p \omega_r + T_L \quad (5.3-4)$$

where  $J$  is the inertia expressed in kilogram meters<sup>2</sup> (kg·m<sup>2</sup>) or Joule seconds<sup>2</sup> (J·s<sup>2</sup>). Often, the inertia is given as  $WR^2$  in units of pound mass feet<sup>2</sup> (lbm·ft<sup>2</sup>). The load torque  $T_L$  is positive for a torque load on the shaft of the synchronous machine.

### 5.4. STATOR VOLTAGE EQUATIONS IN ARBITRARY REFERENCE-FRAME VARIABLES

The voltage equations of the stator windings of a synchronous machine can be expressed in the arbitrary reference frame. In particular, by using the results presented in Chapter

3, the voltage equations for the stator windings may be written in the arbitrary reference frame as [3]

$$\mathbf{v}_{qd0s} = \mathbf{r}_s \mathbf{i}_{qd0s} + \omega \boldsymbol{\lambda}_{dqs} + p \boldsymbol{\lambda}_{qd0s} \quad (5.4-1)$$

where

$$(\boldsymbol{\lambda}_{dqs})^T = [\lambda_{ds} \quad -\lambda_{qs} \quad 0] \quad (5.4-2)$$

The rotor windings of a synchronous machine are asymmetrical; therefore, a change of variables offers no advantage in the analysis of the rotor circuits. Since the rotor variables are not transformed, the rotor voltage equations are expressed only in the rotor reference frame. Hence, from (5.2-2), with the appropriate turns ratios included and raised index  $r$  used to denote the rotor reference frame, the rotor voltage equations are

$$\mathbf{v}'^r_{qdr} = \mathbf{r}'_r \mathbf{i}'^r_{qdr} + p \boldsymbol{\lambda}'^r_{qdr} \quad (5.4-3)$$

For linear magnetic systems, the flux linkage equations may be expressed from (5.2-7) with the transformation of the stator variables to the arbitrary reference frame incorporated

$$\begin{bmatrix} \boldsymbol{\lambda}_{qd0s} \\ \boldsymbol{\lambda}'^r_{qdr} \end{bmatrix} = \begin{bmatrix} \mathbf{K}_s \mathbf{L}_s (\mathbf{K}_s)^{-1} & \mathbf{K}_s \mathbf{L}'_{sr} \\ \frac{2}{3} (\mathbf{L}'_{sr})^T (\mathbf{K}_s)^{-1} & \mathbf{L}'_r \end{bmatrix} \begin{bmatrix} \mathbf{i}_{qd0s} \\ \mathbf{i}'^r_{qdr} \end{bmatrix} \quad (5.4-4)$$

It can be shown that all terms of the inductance matrix of (5.4-4) are sinusoidal in nature except  $\mathbf{L}'_r$ . For example, by using trigonometric identities given in Appendix A

$$\mathbf{K}_s \mathbf{L}'_{sr} = \begin{bmatrix} L_{mq} \cos(\theta - \theta_r) & L_{mq} \cos(\theta - \theta_r) & -L_{md} \sin(\theta - \theta_r) & -L_{md} \sin(\theta - \theta_r) \\ L_{mq} \sin(\theta - \theta_r) & L_{mq} \sin(\theta - \theta_r) & L_{md} \cos(\theta - \theta_r) & L_{md} \cos(\theta - \theta_r) \\ 0 & 0 & 0 & 0 \end{bmatrix} \quad (5.4-5)$$

The sinusoidal terms of (5.4-5) are constant, independent of  $\omega$  and  $\omega_r$  only if  $\omega = \omega_r$ . Similarly,  $\mathbf{K}_s \mathbf{L}_s (\mathbf{K}_s)^{-1}$  and  $(2/3)(\mathbf{L}'_{sr})^T (\mathbf{K}_s)^{-1}$  are constant only if  $\omega = \omega_r$ . Therefore, the position-varying inductances are eliminated from the voltage equations only if the reference frame is fixed in the rotor. Hence, it would appear that only the rotor reference frame is useful in the analysis of synchronous machines. Although this is essentially the case, there are situations, especially in computer simulations, where it is convenient to express the stator voltage equations in a reference frame other than the one fixed in the rotor. For these applications, it is necessary to relate the arbitrary reference-frame variables to the variables in the rotor reference frame. This may be accomplished by using (3.10-1), from which

$$\mathbf{f}_{qd0s}^r = \mathbf{K}^r \mathbf{f}_{qd0s} \quad (5.4-6)$$

From (3.10-7)

$$\mathbf{K}^r = \begin{bmatrix} \cos(\theta_r - \theta) & -\sin(\theta_r - \theta) & 0 \\ \sin(\theta_r - \theta) & \cos(\theta_r - \theta) & 0 \\ 0 & 0 & 1 \end{bmatrix} \quad (5.4-7)$$

Here we must again recall that the arbitrary reference frame does not carry a raised index.

## 5.5. VOLTAGE EQUATIONS IN ROTOR REFERENCE-FRAME VARIABLES

R.H. Park was the first to incorporate a change of variables in the analysis of synchronous machines [1]. He transformed the stator variables to the rotor reference frame, which eliminates the position-varying inductances in the voltage equations. Park's equations are obtained from (5.4-1) and (5.4-3) by setting the speed of the arbitrary reference frame equal to the rotor speed ( $\omega = \omega_r$ ). Thus

$$\mathbf{v}_{qd0s}^r = \mathbf{r}_s \mathbf{i}_{qd0s}^r + \omega_r \boldsymbol{\lambda}_{dqs}^r + p \boldsymbol{\lambda}_{qd0s}^r \quad (5.5-1)$$

$$\mathbf{v}_{qdr}^r = \mathbf{r}_r' \mathbf{i}_{qdr}^r + p \boldsymbol{\lambda}_{qdr}^r \quad (5.5-2)$$

where

$$(\boldsymbol{\lambda}_{dqs}^r)^T = [\lambda_{ds}^r \quad -\lambda_{qs}^r \quad 0] \quad (5.5-3)$$

For a magnetically linear system, the flux linkages may be expressed in the rotor reference frame from (5.4-4) by setting  $\theta = \theta_r$ .  $\mathbf{K}_s$  becomes  $\mathbf{K}_s^r$ , with  $\theta$  set equal to  $\theta_r$  in (3.3-4). Thus,

$$\begin{bmatrix} \boldsymbol{\lambda}_{qd0s}^r \\ \boldsymbol{\lambda}_{qdr}^r \end{bmatrix} = \begin{bmatrix} \mathbf{K}_s^r \mathbf{L}_s (\mathbf{K}_s^r)^{-1} & \mathbf{K}_s^r \mathbf{L}'_{sr} \\ \frac{2}{3} (\mathbf{L}'_{sr})^T (\mathbf{K}_s^r)^{-1} & \mathbf{L}'_r \end{bmatrix} \begin{bmatrix} \mathbf{i}_{qd0s}^r \\ \mathbf{i}_{qdr}^r \end{bmatrix} \quad (5.5-4)$$

Using trigonometric identities from Appendix A, it can be shown that

$$\mathbf{K}_s^r \mathbf{L}_s (\mathbf{K}_s^r)^{-1} = \begin{bmatrix} L_{ls} + L_{mq} & 0 & 0 \\ 0 & L_{ls} + L_{md} & 0 \\ 0 & 0 & L_{ls} \end{bmatrix} \quad (5.5-5)$$

$$\mathbf{K}_s^r \mathbf{L}'_{sr} = \begin{bmatrix} L_{mq} & L_{mq} & 0 & 0 \\ 0 & 0 & L_{md} & L_{md} \\ 0 & 0 & 0 & 0 \end{bmatrix} \quad (5.5-6)$$

$$\frac{2}{3}(\mathbf{L}'_{sr})^T (\mathbf{K}_s^r)^{-1} = \begin{bmatrix} L_{mq} & 0 & 0 \\ L_{mq} & 0 & 0 \\ 0 & L_{md} & 0 \\ 0 & L_{md} & 0 \end{bmatrix} \quad (5.5-7)$$

In expanded form, (5.5-1) and (5.5-2) may be written as

$$v_{qs}^r = r_s i_{qs}^r + \omega_r \lambda_{ds}^r + p \lambda_{qs}^r \quad (5.5-8)$$

$$v_{ds}^r = r_s i_{ds}^r - \omega_r \lambda_{qs}^r + p \lambda_{ds}^r \quad (5.5-9)$$

$$v_{0s} = r_s i_{0s} + p \lambda_{0s} \quad (5.5-10)$$

$$v'_{kq1}^r = r'_{kq1} i'_{kq1}^r + p \lambda'_{kq1}^r \quad (5.5-11)$$

$$v'_{kq2}^r = r'_{kq2} i'_{kq2}^r + p \lambda'_{kq2}^r \quad (5.5-12)$$

$$v'_{fd}^r = r'_{fd} i'_{fd}^r + p \lambda'_{fd}^r \quad (5.5-13)$$

$$v'_{kd}^r = r'_{kd} i'_{kd}^r + p \lambda'_{kd}^r \quad (5.5-14)$$

Substituting (5.5-5)–(5.5-7) and (5.2-28) into (5.5-4) yields the expressions for the flux linkages. In expanded form

$$\lambda_{qs}^r = L_{ls} i_{qs}^r + L_{mq} (i_{qs}^r + i'_{kq1}^r + i'_{kq2}^r) \quad (5.5-15)$$

$$\lambda_{ds}^r = L_{ls} i_{ds}^r + L_{md} (i_{ds}^r + i'_{fd}^r + i'_{kd}^r) \quad (5.5-16)$$

$$\lambda_{0s} = L_{ls} i_{0s} \quad (5.5-17)$$

$$\lambda'_{kq1}^r = L'_{lkq1} i'_{kq1}^r + L_{mq} (i_{qs}^r + i'_{kq1}^r + i'_{kq2}^r) \quad (5.5-18)$$

$$\lambda'_{kq2}^r = L'_{lkq2} i'_{kq2}^r + L_{mq} (i_{qs}^r + i'_{kq1}^r + i'_{kq2}^r) \quad (5.5-19)$$

$$\lambda'_{fd}^r = L'_{lfd} i'_{fd}^r + L_{md} (i_{ds}^r + i'_{fd}^r + i'_{kd}^r) \quad (5.5-20)$$

$$\lambda'_{kd}^r = L'_{lkd} i'_{kd}^r + L_{md} (i_{ds}^r + i'_{fd}^r + i'_{kd}^r) \quad (5.5-21)$$

The voltage and flux linkage equations suggest the equivalent circuits shown in Figure 5.5-1.

As in the case of the induction machine, it is often convenient to express the voltage and flux linkage equations in terms of reactances rather than inductances. Hence, (5.5-8)–(5.5-14) are often written as

$$v_{qs}^r = r_s i_{qs}^r + \frac{\omega_r}{\omega_b} \psi_{ds}^r + \frac{p}{\omega_b} \psi_{qs}^r \quad (5.5-22)$$

$$v_{ds}^r = r_s i_{ds}^r - \frac{\omega_r}{\omega_b} \psi_{qs}^r + \frac{p}{\omega_b} \psi_{ds}^r \quad (5.5-23)$$

$$v_{0s} = r_s i_{0s} + \frac{p}{\omega_b} \psi_{0s} \quad (5.5-24)$$

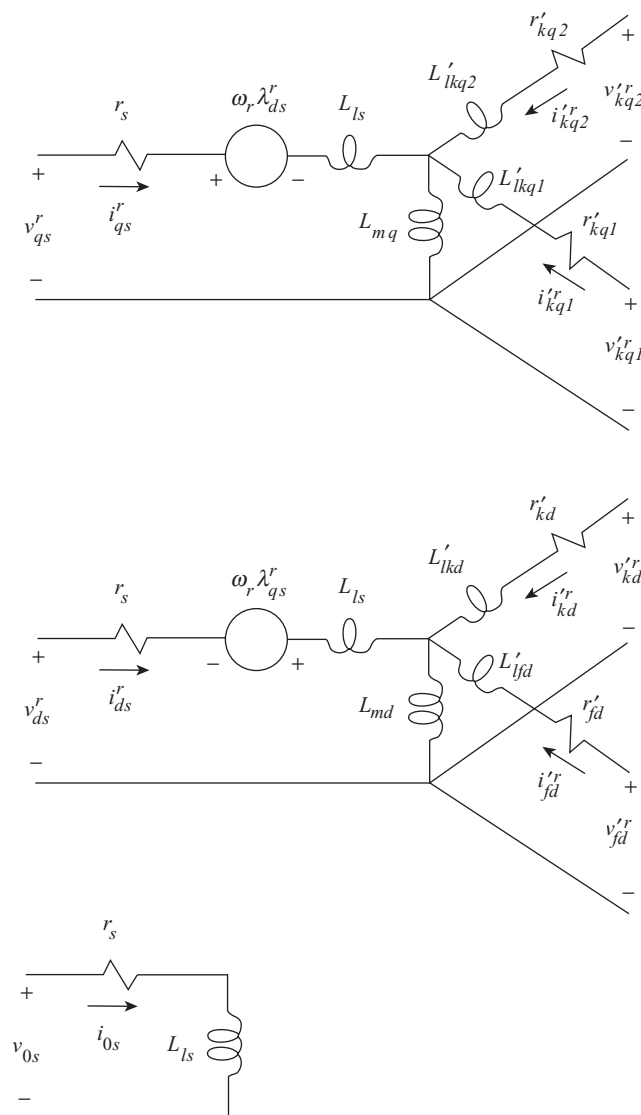


**Figure 5.5-1.** Equivalent circuits of a three-phase synchronous machine with the reference frame fixed in rotor: Park's equations.

$$v'_{kq1} = r'_{kq1} i'_{kq1} + \frac{p}{\omega_b} \psi'_{kq1} \quad (5.5-25)$$

$$v'_{kq2} = r'_{kq2} i'_{kq2} + \frac{p}{\omega_b} \psi'_{kq2} \quad (5.5-26)$$

$$v'_{fd} = r'_{fd} i'_{fd} + \frac{p}{\omega_b} \psi'_{fd} \quad (5.5-27)$$

$$v'_{kd} = r'_{kd} i'_{kd} + \frac{p}{\omega_b} \psi'_{kd} \quad (5.5-28)$$

where  $\omega_b$  is the base electrical angular velocity used to calculate the inductive reactances. The flux linkages per second are

$$\psi^r_{qs} = X_{ls} i^r_{qs} + X_{mq} (i^r_{qs} + i'_{kq1} + i'_{kq2}) \quad (5.5-29)$$

$$\psi^r_{ds} = X_{ls} i^r_{ds} + X_{md} (i^r_{ds} + i'_{fd} + i'_{kd}) \quad (5.5-30)$$

$$\psi_{0s} = X_{ls} i_{0s} \quad (5.5-31)$$

$$\psi'_{kq1} = X'_{lkq1} i'_{kq1} + X_{mq} (i^r_{qs} + i'_{kq1} + i'_{kq2}) \quad (5.5-32)$$

$$\psi'_{kq2} = X'_{lkq2} i'_{kq2} + X_{mq} (i^r_{qs} + i'_{kq1} + i'_{kq2}) \quad (5.5-33)$$

$$\psi'_{fd} = X'_{fd} i'_{fd} + X_{md} (i^r_{ds} + i'_{fd} + i'_{kd}) \quad (5.5-34)$$

$$\psi'_{kd} = X'_{lkd} i'_{kd} + X_{md} (i^r_{ds} + i'_{fd} + i'_{kd}) \quad (5.5-35)$$

Park's equations are generally written without the superscript  $r$ , the subscript  $s$ , and the primes, which denote referred quantities. Also, we will later find that it is convenient to define

$$e'_{xfd} = v'_{fd} \frac{X_{md}}{r'_{fd}} \quad (5.5-36)$$

and to substitute this relationship into the expression for field voltage so that (5.5-27) becomes

$$e'_{xfd} = \frac{X_{md}}{r'_{fd}} \left( r'_{fd} i'_{fd} + \frac{p}{\omega_b} \psi'_{fd} \right) \quad (5.5-37)$$

As we have pointed out earlier, the current and flux linkages are related and both cannot be independent or state variables. We will need to express the voltage equations in terms of either currents or flux linkages (flux linkages per second) when formulating transfer functions and implementing a computer simulation.

If we select the currents as independent variables, the flux linkages (flux linkages per second) are replaced by currents and the voltage equations given by (5.5-22)–(5.5-28), with (5.5-37) used instead of (5.5-27), become

$$\begin{bmatrix} \psi_{qs}^r \\ \psi_{ds}^r \\ \psi_{0s} \\ \psi_{kq1}^r \\ \psi_{kq2}^r \\ \psi_{fd}^r \\ \psi_{kd}^r \end{bmatrix} = \begin{bmatrix} r_s + \frac{p}{\omega_b} X_q & \frac{\omega_r}{\omega_b} X_d & 0 & \frac{p}{\omega_b} X_{mq} & \frac{p}{\omega_b} X_{mq} & \frac{\omega_r}{\omega_b} X_{md} & \frac{\omega_r}{\omega_b} X_{md} \\ -\frac{\omega_r}{\omega_b} X_q & r_s + \frac{p}{\omega_b} X_d & 0 & -\frac{\omega_r}{\omega_b} X_{mq} & -\frac{\omega_r}{\omega_b} X_{mq} & \frac{p}{\omega_b} X_{md} & \frac{p}{\omega_b} X_{md} \\ 0 & 0 & r_s + \frac{p}{\omega_b} X_{ls} & 0 & 0 & 0 & 0 \\ \frac{p}{\omega_b} X_{mq} & 0 & 0 & r'_{kq1} + \frac{p}{\omega_b} X'_{kq1} & \frac{p}{\omega_b} X_{mq} & 0 & 0 \\ \frac{p}{\omega_b} X_{mq} & 0 & 0 & \frac{p}{\omega_b} X_{mq} & r'_{kq2} + \frac{p}{\omega_b} X'_{kq2} & 0 & 0 \\ 0 & \frac{X_{md}}{r'_{fd}} \left( \frac{p}{\omega_b} X_{md} \right) & 0 & 0 & 0 & \frac{X_{md}}{r'_{fd}} \left( r'_{fd} + \frac{p}{\omega_b} X'_{fd} \right) \frac{X_{md}}{r'_{fd}} \left( \frac{p}{\omega_b} X_{md} \right) & 0 \\ 0 & \frac{p}{\omega_b} X_{md} & 0 & 0 & 0 & \frac{p}{\omega_b} X_{md} & r'_{kd} + \frac{p}{\omega_b} X'_{kd} \end{bmatrix} \begin{bmatrix} i_{qs}^r \\ i_{ds}^r \\ i_{0s} \\ i'_{kq1}^r \\ i'_{kq2}^r \\ i'_{fd}^r \\ i'_{kd}^r \end{bmatrix} \quad (5.5-38)$$

where

$$X_q = X_{ls} + X_{mq} \quad (5.5-39)$$

$$X_d = X_{ls} + X_{md} \quad (5.5-40)$$

$$X'_{kq1} = X'_{lkq1} + X_{mq} \quad (5.5-41)$$

$$X'_{kq2} = X'_{lkq2} + X_{mq} \quad (5.5-42)$$

$$X'_{fd} = X'_{lf} + X_{md} \quad (5.5-43)$$

$$X'_{kd} = X'_{lk} + X_{md} \quad (5.5-44)$$

The reactances  $X_q$  and  $X_d$  are generally referred to as  $q$ - and  $d$ -axis reactances, respectively. The flux linkages per second may be expressed from (5.5-29)–(5.5-35) as

$$\begin{bmatrix} \psi_{qs}^r \\ \psi_{ds}^r \\ \psi_{0s} \\ \psi_{kq1}^r \\ \psi_{kq2}^r \\ \psi_{fd}^r \\ \psi_{kd}^r \end{bmatrix} = \begin{bmatrix} X_q & 0 & 0 & X_{mq} & X_{mq} & 0 & 0 \\ 0 & X_d & 0 & 0 & 0 & X_{md} & X_{md} \\ 0 & 0 & X_{ls} & 0 & 0 & 0 & 0 \\ X_{mq} & 0 & 0 & X'_{kq1} & X_{mq} & 0 & 0 \\ X_{mq} & 0 & 0 & X_{mq} & X'_{kq2} & 0 & 0 \\ 0 & X_{md} & 0 & 0 & 0 & X'_{fd} & X_{md} \\ 0 & X_{md} & 0 & 0 & 0 & X_{md} & X'_{kd} \end{bmatrix} \begin{bmatrix} i_{qs}^r \\ i_{ds}^r \\ i_{0s} \\ i'_{kq1}^r \\ i'_{kq2}^r \\ i'_{fd}^r \\ i'_{kd}^r \end{bmatrix} \quad (5.5-45)$$

If the flux linkages or flux linkages per second are selected as independent variables, it is convenient to first express (5.5-45) as

$$\begin{bmatrix} \psi_{qs}^r \\ \psi_{kq1}^r \\ \psi_{kq2}^r \end{bmatrix} = \begin{bmatrix} X_q & X_{mq} & X_{mq} \\ X_{mq} & X'_{kq1} & X_{mq} \\ X_{mq} & X_{mq} & X'_{kq2} \end{bmatrix} \begin{bmatrix} i_{qs}^r \\ i'_{kq1}^r \\ i'_{kq2}^r \end{bmatrix} \quad (5.5-46)$$

$$\begin{bmatrix} \psi_{qs}^r \\ \psi_{fd}^r \\ \psi_{kd}^r \end{bmatrix} = \begin{bmatrix} X_d & X_{md} & X_{md} \\ X_{md} & X'_{fd} & X_{md} \\ X_{md} & X_{md} & X'_{kd} \end{bmatrix} \begin{bmatrix} i_{ds}^r \\ i_{fd}^r \\ i_{kd}^r \end{bmatrix} \quad (5.5-47)$$

$$\psi_{0s} = X_{ls} i_{0s} \quad (5.5-48)$$

Solving the above equations for currents yields

$$\begin{bmatrix} i_{qs}^r \\ i_{kq1}^r \\ i_{kq2}^r \end{bmatrix} = \frac{1}{D_q} \begin{bmatrix} X'_{kq1} X'_{kq2} - X_{mq}^2 & -X_{mq} X'_{kq2} + X_{mq}^2 & -X_{mq} X'_{kq1} + X_{mq}^2 \\ -X_{mq} X'_{kq2} + X_{mq}^2 & X_q X'_{kq2} - X_{mq}^2 & -X_q X_{mq} + X_{mq}^2 \\ -X_{mq} X'_{kq1} + X_{mq}^2 & -X_q X_{mq} + X_{mq}^2 & X_q X'_{kq1} - X_{mq}^2 \end{bmatrix} \begin{bmatrix} \psi_{qs}^r \\ \psi_{kq1}^r \\ \psi_{kq2}^r \end{bmatrix} \quad (5.5-49)$$

$$\begin{bmatrix} i_{ds}^r \\ i_{fd}^r \\ i_{kd}^r \end{bmatrix} = \frac{1}{D_d} \begin{bmatrix} X'_{fd} X'_{kd} - X_{md}^2 & -X_{md} X'_{kd} + X_{md}^2 & -X_{md} X'_{fd} + X_{md}^2 \\ -X_{md} X'_{kd} + X_{md}^2 & X_d X'_{kd} - X_{md}^2 & -X_d X_{md} + X_{md}^2 \\ -X_{md} X'_{fd} + X_{md}^2 & -X_d X_{md} + X_{md}^2 & X_d X'_{fd} - X_{md}^2 \end{bmatrix} \begin{bmatrix} \psi_{ds}^r \\ \psi_{fd}^r \\ \psi_{kd}^r \end{bmatrix} \quad (5.5-50)$$

$$i_{0s} = \frac{1}{X_{ls}} \psi_{0s} \quad (5.5-51)$$

where

$$D_q = -X_{mq}^2 (X_q - 2X_{mq} + X'_{kq1} + X'_{kq2}) + X_q X'_{kq1} X'_{kq2} \quad (5.5-52)$$

$$D_d = -X_{md}^2 (X_d - 2X_{md} + X'_{fd} + X'_{kd}) + X_d X'_{fd} X'_{kd} \quad (5.5-53)$$

Substituting (5.5-49)–(5.5-51) for the currents into the voltage equations (5.5-22)–(5.5-26), (5.5-37), and (5.5-38) yields

$$\begin{bmatrix} r_s a_{11} + \frac{p}{\omega_b} & \frac{\omega_r}{\omega_b} & 0 & -r_s a_{12} & -r_s a_{13} & 0 & 0 \\ -\frac{\omega_r}{\omega_b} & r_s a_{11} + \frac{p}{\omega_b} & 0 & 0 & 0 & -r_s b_{12} & -r_s b_{13} \\ 0 & 0 & \frac{r_s}{X_{ls}} + \frac{p}{\omega_b} & 0 & 0 & 0 & 0 \\ v_{qs}^r & v_{ds}^r & v_{0s} & v_{kq1}^r & v_{kq2}^r & e_{fd}^r & v_{kd}^r \end{bmatrix} = \begin{bmatrix} r'_{kq1} a_{21} & 0 & 0 & r'_{kq1} a_{22} + \frac{p}{\omega_b} & r'_{kq1} a_{23} & 0 & 0 \\ r'_{kq2} a_{31} & 0 & 0 & r'_{kq2} a_{32} & r'_{kq2} a_{33} + \frac{p}{\omega_b} & 0 & 0 \\ 0 & X_{md} b_{21} & 0 & 0 & 0 & X_{md} b_{22} + \frac{X_{md}}{r'_{fd}} \frac{p}{\omega_b} & X_{md} b_{23} \\ 0 & r'_{kd} b_{31} & 0 & 0 & 0 & r'_{kd} b_{32} & r'_{kd} b_{33} + \frac{p}{\omega_b} \end{bmatrix} \begin{bmatrix} \psi_{qs}^r \\ \psi_{ds}^r \\ \psi_{0s} \\ \psi_{kq1}^r \\ \psi_{kq2}^r \\ \psi_{fd}^r \\ \psi_{kd}^r \end{bmatrix} \quad (5.5-54)$$

In (5.5-54),  $a_{ij}$  and  $b_{ij}$  are the elements of the  $3 \times 3$  matrices given in (5.5-49) and (5.5-50), respectively.

## 5.6. TORQUE EQUATIONS IN SUBSTITUTE VARIABLES

The expression for the positive electromagnetic torque for motor action in terms of rotor reference-frame variables may be obtained by substituting the equation of transformation into (5.3-2). Hence

$$T_e = \left( \frac{P}{2} \right) [(\mathbf{K}_s^r)^{-1} \mathbf{i}_{qd0s}^r]^T \left\{ \frac{1}{2} \frac{\partial}{\partial \theta_r} [\mathbf{L}_s] (\mathbf{K}_s^r)^{-1} \mathbf{i}_{qd0s}^r + \frac{\partial}{\partial \theta_r} [\mathbf{L}'_{sr}] \mathbf{i}_{qdr}^r \right\} \quad (5.6-1)$$

After considerable work, the above equation reduces to

$$T_e = \left( \frac{3}{2} \right) \left( \frac{P}{2} \right) [L_{md} (i_{ds}^r + i_{fd}^r + i_{kd}^r) i_{qs}^r - L_{mq} (i_{qs}^r + i_{kq1}^r + i_{kq2}^r) i_{ds}^r] \quad (5.6-2)$$

Equation (5.6-2) is equivalent to

$$T_e = \left( \frac{3}{2} \right) \left( \frac{P}{2} \right) (\lambda_{ds}^r i_{qs}^r - \lambda_{qs}^r i_{ds}^r) \quad (5.6-3)$$

In terms of flux linkages per second and currents

$$T_e = \left( \frac{3}{2} \right) \left( \frac{P}{2} \right) \left( \frac{1}{\omega_b} \right) (\psi_{ds}^r i_{qs}^r - \psi_{qs}^r i_{ds}^r) \quad (5.6-4)$$

It is left to the reader to show that in terms of flux linkages per second, the electromagnetic torque may be expressed as

$$T_e = \left( \frac{3}{2} \right) \left( \frac{P}{2} \right) \left( \frac{1}{\omega_b} \right) [(a_{11} - b_{11}) \psi_{qs}^r \psi_{ds}^r + \psi_{ds}^r (a_{12} \psi_{kq1}^r + a_{13} \psi_{kq2}^r) - \psi_{qs}^r (b_{12} \psi_{fd}^r + b_{13} \psi_{kd}^r)] \quad (5.6-5)$$

where  $a_{ij}$  and  $b_{ij}$  are the elements of the  $3 \times 3$  matrices given in (5.5-49) and (5.5-50), respectively.

In Chapter 1, we derived an expression for torque starting with the energy balance

$$W_f = W_e + W_m \quad (5.6-6)$$

where  $W_f$  is the energy stored in the coupling field,  $W_e$  is the energy entering the coupling field from the electrical system, and  $W_m$  is the energy entering the coupling field from the mechanical system. We can turn (5.6-6) into a power balance equation by taking the total derivative with respect to time. Thus

$$pW_f = pW_e + pW_m \quad (5.6-7)$$

where

$$pW_m = -T_e \omega_{rm} \quad (5.6-8)$$

Since  $\omega_{rm} = (2/P)\omega_r$ , we can express  $pW_e$  as

$$pW_e = pW_f + T_e \left( \frac{2}{P} \right) \omega_r \quad (5.6-9)$$

The power entering the coupling field is  $pW_e$ , which can be expressed by multiplying the voltage equations of each winding (5.5-8)–(5.5-14) by the respective winding currents. Thus using (3.3-8)

$$\begin{aligned} \frac{2}{3} pW_e = & i_{qs}^r p \lambda_{qs}^r + i_{ds}^r p \lambda_{ds}^r + 2i_{0s} p \lambda_{0s} + i_{kq1}^r p \lambda_{kq1}^r + i_{kq2}^r p \lambda_{kq2}^r \\ & + i_{fd}^r p \lambda_{fd}^r + i_{kd}^r p \lambda_{kd}^r + (\lambda_{ds}^r i_{qs}^r - \lambda_{qs}^r i_{ds}^r) \omega_r \end{aligned} \quad (5.6-10)$$

We have extracted the  $i^2r$  terms. Although this is not necessary, it makes this derivation consistent with that given in Chapter 1. If we compare (5.6-10) with (5.6-9) and if we equate the coefficients of  $\omega_r$ , we have (5.6-3).

It is important to note that we obtained (5.6-3) by two different approaches. First, we used the field energy or coenergy and assumed a linear magnetic system; however, in the second approach, we used neither the field energy nor the coenergy. Therefore, we have shown that (5.6-3) is valid for linear or nonlinear magnetic systems. Park used the latter approach [1]. It is interesting that this latter approach helps us to identify situations, albeit relatively rare, that yields (5.6-3) invalid. In order to arrive at (5.6-3) from (5.6-10), it was necessary to equate coefficients of  $\omega_r$ . If, however, either  $\mathbf{v}_{qds}^r$  or  $\mathbf{i}_{qds}^r$  is an unsymmetrical or unbalanced function of  $\theta_r$ , then other coefficients of  $\omega_r$  could arise in addition to (5.6-3). In addition, in cases where a machine has a concentrated stator winding (low number of slots/pole/phase), magnetomotive force (MMF) harmonics lead to additional terms in the inductance matrix of (5.2-8). When Park's transformation is applied, the  $q$ - and  $d$ -axis inductances remain functions of  $\theta_r$ . Under these conditions, (5.6-3) has been shown to provide in experiments to be a reasonable approximation to the average torque, but does not accurately predict instantaneous torque [4].

## 5.7. ROTOR ANGLE AND ANGLE BETWEEN ROTORS

Except for isolated operation, it is convenient for analysis and interpretation purposes to relate the position of the rotor of a synchronous machine to a system voltage. If the machine is in a system environment, the electrical angular displacement of the rotor relative to its terminal (system) voltage is defined as the rotor angle. In particular, the rotor angle is the displacement of the rotor generally referenced to the maximum positive value of the fundamental component of the terminal (system) voltage of phase  $a$ . Therefore, the rotor angle expressed in radians is

$$\delta = \theta_r - \theta_{ev} \quad (5.7-1)$$

The electrical angular velocity of the rotor is  $\omega_r$ ;  $\omega_e$  is the electrical angular velocity of the terminal voltages. The definition of  $\delta$  is valid regardless of the mode of operation (either or both  $\omega_r$  and  $\omega_e$  may vary). Since a physical interpretation is most easily visualized during balanced steady-state operation, we will defer this explanation until the steady-state voltage and torque equations have been written in terms of  $\delta$ .

It is important to note that the rotor angle is often used as the argument in the transformation between the rotor and synchronously rotating reference frames since  $\omega_e$  is the speed of the synchronously rotating reference frame and it is also the angular velocity of  $\theta_{ev}$ . From (3.10-1)

$$\mathbf{f}_{qd0s}^r = {}^e\mathbf{K}^r \mathbf{f}_{qd0s}^e \quad (5.7-2)$$

where

$${}^e\mathbf{K}^r = \begin{bmatrix} \cos \delta & -\sin \delta & 0 \\ \sin \delta & \cos \delta & 0 \\ 0 & 0 & 1 \end{bmatrix} \quad (5.7-3)$$

The rotor angle is often used in relating torque and rotor speed. In particular, if  $\omega_e$  is constant, then (5.3-4) may be written as

$$T_e = J \left( \frac{2}{P} \right) p^2 \delta + T_L \quad (5.7-4)$$

where  $\delta$  is expressed in electrical radians.

## 5.8. PER UNIT SYSTEM

The equations for a synchronous machine may be written in per unit where base voltage is generally selected as the rms value of the rated phase voltage for the  $abc$  variables and the peak value for the  $qd0$  variables. However, we will often use the same base value when comparing  $abc$  and  $qd0$  variables. When considering the machine separately, the power base is selected as its volt-ampere rating. When considering power systems, a system power base (system base) is selected that is generally different from the power base of the machine (machine base).

Once the base quantities are established, the corresponding base current and base impedance may be calculated. Park's equations written in terms of flux linkages per second and reactances are readily per unitized by dividing each term by the peak of the base voltage (or the peak value of the base current times base impedance). The form of these equations remains unchanged as a result of per unitizing. When per unitizing

the voltage equation of the field winding ( $fd$  winding), it is convenient to use the form given by (5.5-37) involving  $e''_{fd}$ . The reason for this choice is established later.

Base torque is the base power divided by the synchronous speed of the rotor. Thus

$$\begin{aligned} T_B &= \frac{P_B}{(2/P)\omega_b} \\ &= \frac{\left(\frac{3}{2}\right)V_{B(qd0)}I_{B(qd0)}}{(2/P)\omega_b} \end{aligned} \quad (5.8-1)$$

where  $\omega_b$  corresponds to rated or base frequency,  $P_B$  is the base power,  $V_{B(qd0)}$  is the peak value of the base phase voltage, and  $I_{B(qd0)}$  is the peak value of the base phase current. Dividing the torque equations by (5.8-1) yields the torque expressed in per unit. For example, (5.6-4) with all quantities expressed in per unit becomes

$$T_e = \psi'_{ds}i'_{qs} - \psi'_{qs}i'_{ds} \quad (5.8-2)$$

Equation (5.3-4), which relates torque and speed, is expressed in per unit as

$$T_e = 2H_p \frac{\omega_r}{\omega_b} + T_L \quad (5.8-3)$$

If  $\omega_e$  is constant, then this relationship becomes

$$T_e = \frac{2H}{\omega_b} p^2 \delta + T_L \quad (5.8-4)$$

where  $\delta$  is in electrical radians. The inertia constant  $H$  is in seconds. It is defined as

$$\begin{aligned} H &= \left(\frac{1}{2}\right)\left(\frac{2}{P}\right) \frac{J\omega_b}{T_B} \\ &= \left(\frac{1}{2}\right)\left(\frac{2}{P}\right)^2 \frac{J\omega_b^2}{P_B} \end{aligned} \quad (5.8-5)$$

where  $J$  is often the combined inertia of the rotor and prime mover expressed in  $\text{kg}\cdot\text{m}^2$  or given as the quantity  $WR^2$  in  $\text{lbm}\cdot\text{ft}^2$ .

## 5.9. ANALYSIS OF STEADY-STATE OPERATION

Although the voltage equations that describe balanced steady-state operation of synchronous machines may be derived using several approaches, it is convenient to use Park's equations in this derivation. For balanced conditions, the 0s quantities are zero. For balanced steady-state conditions, the electrical angular velocity of the rotor

is constant and equal to  $\omega_e$ , whereupon the electrical angular velocity of the rotor reference frame becomes the electrical angular velocity of the synchronously rotating reference frame. In this mode of operation, the rotor windings do not experience a change of flux linkages, hence current is not flowing in the short-circuited damper windings. Thus, with  $\omega_r$  set equal to  $\omega_e$  and the time rate of change of all flux linkages set equal to zero, the steady-state versions of (5.5-22), (5.5-23), and (5.5-27) become

$$V_{qs}^r = r_s I_{qs}^r + \frac{\omega_e}{\omega_b} X_d I_{ds}^r + \frac{\omega_e}{\omega_b} X_{md} I_{fd}^r \quad (5.9-1)$$

$$V_{ds}^r = r_s I_{ds}^r - \frac{\omega_e}{\omega_b} X_q I_{qs}^r \quad (5.9-2)$$

$$V_{fd}^r = r_{fd}^r I_{fd}^r \quad (5.9-3)$$

Here, the  $\omega_e$  to  $\omega_b$  ratio is again included to accommodate analysis when the operating frequency is other than rated. It is recalled that all machine reactances used in this text are calculated using base or rated frequency.

The reactances  $X_q$  and  $X_d$  are defined by (5.5-39) and (5.5-40), that is,  $X_q = X_{ls} + X_{mq}$  and  $X_d = X_{ls} + X_{md}$ . As mentioned previously, Park's equations are generally written with the primes and the  $s$  and  $r$  indexes omitted. The uppercase letters are used here to denote steady-state quantities.

Equations (3.6-5) and (3.6-6) express the instantaneous variables in the arbitrary reference frame for balanced conditions. In the rotor reference frame, these expressions become

$$f_{qs}^r = \sqrt{2} f_s \cos(\theta_{ef} - \theta_r) \quad (5.9-4)$$

$$f_{ds}^r = -\sqrt{2} f_s \sin(\theta_{ef} - \theta_r) \quad (5.9-5)$$

For steady-state balanced conditions, (5.9-4) and (5.9-5) may be expressed

$$F_{qs}^r = \text{Re}[\sqrt{2} F_s e^{j(\theta_{ef} - \theta_r)}] \quad (5.9-6)$$

$$F_{ds}^r = \text{Re}[j\sqrt{2} F_s e^{j(\theta_{ef} - \theta_r)}] \quad (5.9-7)$$

It is to our advantage to express (5.9-6) and (5.9-7) in terms of  $\delta$  given by (5.7-1). Hence, if we multiply each equation by  $e^{j\theta_{ev}(1-1)}$  and since  $\theta_{ef}$  and  $\theta_{ev}$  are both functions of  $\omega_e$ , the earlier equations may be written as

$$F_{qs}^r = \text{Re}[\sqrt{2} F_s e^{j[\theta_{ef}(0) - \theta_{ev}(0)]} e^{-j\delta}] \quad (5.9-8)$$

$$F_{ds}^r = \text{Re}[j\sqrt{2} F_s e^{j[\theta_{ef}(0) - \theta_{ev}(0)]} e^{-j\delta}] \quad (5.9-9)$$

It is important to note that

$$\tilde{F}_{as} = F_s e^{j[\theta_{ef}(0) - \theta_{ev}(0)]} \quad (5.9-10)$$

is a phasor that represents the  $as$  variables referenced to the time-zero position of  $\theta_{ev}$ , which we will select later so that maximum  $v_{as}$  occurs at  $t = 0$ .

From (5.9-8) and (5.9-9)

$$F_{qs}^r = \sqrt{2}F_s \cos[\theta_{ef}(0) - \theta_{ev}(0) - \delta] \quad (5.9-11)$$

$$F_{ds}^r = -\sqrt{2}F_s \sin[\theta_{ef}(0) - \theta_{ev}(0) - \delta] \quad (5.9-12)$$

From which

$$\sqrt{2}\tilde{F}_{as}e^{-j\delta} = F_{qs}^r - jF_{ds}^r \quad (5.9-13)$$

where  $\tilde{F}_{as}$  is defined by (5.9-10). Hence

$$\sqrt{2}\tilde{V}_{as}e^{-j\delta} = V_{qs}^r - jV_{ds}^r \quad (5.9-14)$$

Substituting (5.9-1) and (5.9-2) into (5.9-14) yields

$$\sqrt{2}\tilde{V}_{as}e^{-j\delta} = r_s I_{qs}^r + \frac{\omega_e}{\omega_b} X_d I_{ds}^r + \frac{\omega_e}{\omega_b} X_{md} I_{fd}^r - j \left( r_s I_{ds}^r - \frac{\omega_e}{\omega_b} X_q I_{qs}^r \right) \quad (5.9-15)$$

If  $(\omega_e / \omega_b)X_q I_{ds}^r$  is added to and subtracted from the right-hand side of (5.9-15) and if it is noted that

$$j\sqrt{2}\tilde{I}_{as}e^{-j\delta} = I_{ds}^r + jI_{qs}^r \quad (5.9-16)$$

then (5.9-15) may be written as

$$\tilde{V}_{as} = \left( r_s + j \frac{\omega_e}{\omega_b} X_q \right) \tilde{I}_{as} + \frac{1}{\sqrt{2}} \left[ \frac{\omega_e}{\omega_b} (X_d - X_q) I_{ds}^r + \frac{\omega_e}{\omega_b} X_{md} I_{fd}^r \right] e^{j\delta} \quad (5.9-17)$$

It is convenient to define the last term on the right-hand side of (5.9-17) as

$$\tilde{E}_a = \frac{1}{\sqrt{2}} \left[ \frac{\omega_e}{\omega_b} (X_d - X_q) I_{ds}^r + \frac{\omega_e}{\omega_b} X_{md} I_{fd}^r \right] e^{j\delta} \quad (5.9-18)$$

which is sometimes referred to as the excitation voltage. Thus, (5.9-17) becomes

$$\tilde{V}_{as} = \left( r_s + j \frac{\omega_e}{\omega_b} X_q \right) \tilde{I}_{as} + \tilde{E}_a \quad (5.9-19)$$

The  $\omega_e$  to  $\omega_b$  ratio is included so that the equations are valid for the analysis of balanced steady-state operation at a frequency other than rated.

If (5.9-1) and (5.9-2) are solved for  $I_{qs}^r$  and  $I_{ds}^r$ , and the results substituted into (5.6-2), the expression for the balanced steady-state electromagnetic torque for a linear magnetic system can be written as

$$T_e = \left( \frac{3}{2} \right) \left( \frac{P}{2} \right) \left( \frac{1}{\omega_b} \right) \left\{ \frac{r_s X_{md} I'_{fd}^r}{r_s^2 + (\omega_e / \omega_b)^2 X_q X_d} \left( V_{qs}^r - \frac{\omega_e}{\omega_b} X_{md} I'_{fd}^r - \frac{\omega_e}{\omega_b} \frac{X_d}{r_s} V_{ds}^r \right) \right. \\ \left. + \frac{X_d - X_q}{[r_s^2 + (\omega_e / \omega_b)^2 X_q X_d]^2} \left[ r_s \frac{\omega_e}{\omega_b} X_q \left( V_{qs}^r - \frac{\omega_e}{\omega_b} X_{md} I'_{fd}^r \right)^2 \right. \right. \\ \left. \left. + \left[ r_s^2 - \left( \frac{\omega_e}{\omega_b} \right)^2 X_q X_d \right] V_{ds}^r \left( V_{qs}^r - \frac{\omega_e}{\omega_b} X_{md} I'_{fd}^r \right) - r_s \frac{\omega_e}{\omega_b} X_d (V_{ds}^r)^2 \right] \right\} \quad (5.9-20)$$

where  $P$  is the number of poles and  $\omega_b$  is the base electrical angular velocity used to calculate the reactances, and  $\omega_e$  corresponds to the operating frequency.

For balanced operation, the stator voltages may be expressed in the form given by (3.6-1)–(3.6-3). Thus

$$v_{as} = \sqrt{2} v_s \cos \theta_{ev} \quad (5.9-21)$$

$$v_{bs} = \sqrt{2} v_s \cos \left( \theta_{ev} - \frac{2\pi}{3} \right) \quad (5.9-22)$$

$$v_{cs} = \sqrt{2} v_s \cos \left( \theta_{ev} + \frac{2\pi}{3} \right) \quad (5.9-23)$$

where

$$\theta_{ev} = \omega_e t + \theta_{ev}(0) \quad (5.9-24)$$

These voltages may be expressed in the rotor reference frame by replacing  $\theta$  with  $\theta_r$  in (3.6-5) and (3.6-6).

$$v_{qs}^r = \sqrt{2} v_s \cos(\theta_{ev} - \theta_r) \quad (5.9-25)$$

$$v_{ds}^r = -\sqrt{2} v_s \sin(\theta_{ev} - \theta_r) \quad (5.9-26)$$

If the rotor angle from (5.7-1) is substituted into (5.9-25) and (5.9-26), we obtain

$$v_{qs}^r = \sqrt{2} v_s \cos \delta \quad (5.9-27)$$

$$v_{ds}^r = \sqrt{2} v_s \sin \delta \quad (5.9-28)$$

The only restriction on (5.9-27) and (5.9-28) is that the stator voltages form a balanced set. These equations are valid for transient and steady-state operation, that is,  $v_s$  and  $\delta$  may both be functions of time.

The torque given by (5.9-20) is for balanced steady-state conditions. In this mode of operation, (5.9-27) and (5.9-28) are constants, since  $v_s$  and  $\delta$  are both constants. Before proceeding, it is noted that from (5.5-37) that for balanced steady-state operation

$$E'_{xf} = X_{md} I'_{fd} \quad (5.9-29)$$

Although this expression is sometimes substituted into the above steady-state voltage equations, it is most often used in the expression for torque. In particular, if (5.9-29) and the steady-state versions of (5.9-27) and (5.9-28) are substituted in (5.9-20), and if  $r_s$  is neglected, the torque may be expressed as

$$T_e = -\left(\frac{3}{2}\right)\left(\frac{P}{2}\right)\left(\frac{1}{\omega_b}\right)\left[\frac{E'_{xfd}\sqrt{2}V_s}{(\omega_e / \omega_b)X_d}\sin\delta + \left(\frac{1}{2}\right)\left(\frac{\omega_e}{\omega_b}\right)^{-2}\left(\frac{1}{X_q} - \frac{1}{X_d}\right)(\sqrt{2}V_s)^2\sin 2\delta\right] \quad (5.9-30)$$

In per unit, (5.9-30) becomes

$$T_e = -\frac{E'_{xfd}V_s}{(\omega_e / \omega_b)X_d}\sin\delta - \left(\frac{1}{2}\right)\left(\frac{\omega_e}{\omega_b}\right)^{-2}\left(\frac{1}{X_q} - \frac{1}{X_d}\right)V_s^2\sin 2\delta \quad (5.9-31)$$

Neglecting  $r_s$  is justified if  $r_s$  is small relative to the reactances of the machine. In variable-frequency drive systems, this may not be the case at low frequencies, whereupon (5.9-20) must be used to calculate torque rather than (5.9-30). With the stator resistance neglected, steady-state power and torque are related by rotor speed, and if torque and power are expressed in per unit, they are equal during steady-state operation.

Although (5.9-30) is valid only for balanced steady-state operation and if the stator resistance is small relative to the magnetizing reactances ( $X_{mq}$  and  $X_{md}$ ) of the machine, it permits a quantitative description of the nature of the steady-state electromagnetic torque of a synchronous machine. The first term on the right-hand side of (5.9-30) is due to the interaction of the magnetic system produced by the currents flowing in the stator windings and the magnetic system produced by the current flowing in the field winding. The second term is due to the saliency of the rotor. This component is commonly referred to as the reluctance torque. The predominate torque is the torque due to the interaction of the stator and rotor magnetic fields. The amplitude of this component is proportional to the magnitudes of the stator voltage  $V_s$ , and the voltage applied to the field,  $E'_{xfd}$ . In power systems, it is desirable to maintain the stator voltage near rated. This is achieved by automatically adjusting the voltage applied to the field winding. Hence, the amplitude of this torque component varies as  $E'_{xfd}$  is varied to maintain the terminal voltage at or near rated and/or to control reactive power flow. The reluctance torque component is generally a relatively small part of the total torque. In power systems where the terminal voltage is maintained nearly constant, the amplitude of the reluctance torque would also be nearly constant, a function only of the parameters of the machine. A steady-state reluctance torque does not exist in round or cylindrical rotor synchronous machines since  $X_q = X_d$ . On the other hand, a reluctance machine is a device that is not equipped with a field winding, hence, the only torque produced is reluctance torque. Reluctance machines are used as motors especially in variable-frequency drive systems.

Let us return for a moment to the steady-state voltage equation given by (5.9-19). With  $\theta_{ev}(0) = 0$ ,  $\tilde{V}_{as}$  lies along the positive real axis of a phasor diagram. Since  $\delta$  is the angle associated with  $\tilde{E}_a$ , (5.9-18), its position relative to  $\tilde{V}_{as}$  is also the position of the

*q*-axis of the machine relative to  $\tilde{V}_{as}$  if  $\theta_e(0) = 0$ . With these time-zero conditions, we can superimpose the *q*- and *d*-axes of the synchronous machine upon the phasor diagram.

If  $T_L$  is assumed zero and if we neglect friction and windage losses along with the stator resistance, then  $T_e$  and  $\delta$  are also zero and the machine will theoretically run at synchronous speed without absorbing energy from either the electrical or mechanical system. Although this mode of operation is not feasible in practice since the machine will actually absorb some small amount of energy to satisfy the ohmic and friction and windage losses, it is convenient for purposes of explanation. With the machine “floating on the line,” the field voltage can be adjusted to establish the desired terminal conditions. Three situations may exist: (1)  $|\tilde{E}_a| = |\tilde{V}_{as}|$ , whereupon  $\tilde{I}_{as} = 0$ ; (2)  $|\tilde{E}_a| > |\tilde{V}_{as}|$ , whereupon  $\tilde{I}_{as}$  leads  $\tilde{V}_{as}$ ; the synchronous machine appears as a capacitor supplying reactive power to the system; or (3)  $|\tilde{E}_a| < |\tilde{V}_{as}|$ , with  $\tilde{I}_{as}$  lagging  $\tilde{V}_{as}$ , whereupon the machine is absorbing reactive power appearing as an inductor to the system.

In order to maintain the voltage in a power system at rated value, the synchronous generators are normally operated in the overexcited mode with  $|\tilde{E}_a| > |\tilde{V}_{as}|$ , since they are the main source of reactive power for the inductive loads throughout the system. In the past, some synchronous machines were often placed in the power system for the sole purpose of supplying reactive power without any provision to provide real power. During peak load conditions when the system voltage is depressed, these so-called “synchronous condensers” were brought online and the field voltage adjusted to help increase the system voltage. In this mode of operation, the synchronous machine behaves like an adjustable capacitor. Although the synchronous condenser is not used as widely as in the past, it is an instructive example. On the other hand, it may be necessary for a generator to absorb reactive power in order to regulate voltage in a high-voltage transmission system during light load conditions. This mode of operation is, however, not desirable and should be avoided since machine oscillations become less damped as the reactive power required is decreased. This will be shown in Chapter 8 when we calculate eigenvalues.

**EXAMPLE 5A** A three-phase, two-pole, 835 MVA, 0.85 pf, steam turbine generator is connected to a 26 kV (line-line rms) bus. The machine parameters at 60 Hz in ohms are  $X_q = X_d = 1.457$ ,  $X_{ls} = 0.1538$ . Plot the phasor diagram for the cases in which the generator is supplying rated power to a load at 0.85 power factor leading, unity, and 0.85 power factor lagging. Then, plot the amplitude of the stator phase current (rms) as a function of the field winding current. Assume resistance of the stator winding is negligible.

The rated real power being delivered under all conditions is  $P = -835 \cdot 0.85$  MW. For generator operation (assuming  $t = 0$  is defined such that  $\theta_{ev}(0) = 0$ ),

$$I_s \cos \theta_{ei}(0) = \frac{P}{3V_s} = \frac{-835 \cdot 0.85}{\sqrt{3} \cdot 26} \text{ kA} \quad (5A-1)$$

is fixed regardless of power factor. In addition, one can equate the imaginary components in (5.9-17) to establish the relationship (with stator resistance neglected):

$$E_s \sin \delta = -\frac{\omega_e}{\omega_b} X_q I_s \cos \theta_{ei}(0) = 1.457 \cdot \frac{835 \cdot 0.85}{\sqrt{3} \cdot 26} \text{ kV} \quad (5A-2)$$

which also holds under all power factors. It is assumed that the supplying of a load at 0.85 power factor leading implies that the load current leads the bus voltage. For phase currents that are defined as positive into the machine, this means that the phase winding currents of the synchronous machine lag the bus voltage. Thus

$$I_s \sin \theta_{ei}(0) = -\frac{835 \sqrt{1-0.85^2}}{\sqrt{3} \cdot 26} \text{ kA} \quad (5A-3)$$

The phase current can therefore be expressed as

$$\tilde{I}_{as} = \frac{-835 \cdot 0.85}{\sqrt{3} \cdot 26} - j \frac{835 \sqrt{1-0.85^2}}{\sqrt{3} \cdot 26} \text{ kA} \quad (5A-4)$$

To determine the real component of  $\tilde{E}_a$ , the real components in (5.9-17) are equated, yielding

$$E_s \cos \delta = V_s + \frac{\omega_e}{\omega_b} X_d I_s \sin \theta_{ei}(0) = \frac{26}{\sqrt{3}} - 1.457 \cdot \frac{835 \sqrt{1-0.85^2}}{\sqrt{3} \cdot 26} \text{ kV} \quad (5A-5)$$

From which

$$\tilde{E}_a = \frac{26}{\sqrt{3}} - 1.457 \cdot \frac{835 \cdot \sqrt{1-0.85^2}}{\sqrt{3} \cdot 26} + j 1.457 \cdot \frac{835 \cdot 0.85}{\sqrt{3} \cdot 26} \text{ kV} \quad (5A-6)$$

For the case in which rated power is delivered at unity power factor,

$$\tilde{I}_{as} = \frac{-835 \cdot 0.85}{\sqrt{3} \cdot 26} \text{ kA} \quad (5A-7)$$

$$E_s \cos \delta = V_s = \frac{26}{\sqrt{3}} \text{ kV} \quad (5A-8)$$

which yields

$$\tilde{E}_a = \frac{26}{\sqrt{3}} + j 1.457 \cdot \frac{835 \cdot 0.85}{\sqrt{3} \cdot 26} \text{ kV} \quad (5A-9)$$

Delivering 0.85 power factor lagging implies that the load current lags the bus voltage. For phase currents that are defined as positive into the synchronous machine, this means that the phase winding currents of the synchronous machine lead the bus voltage. Thus,

$$I_s \sin \theta_{ei}(0) = \frac{835\sqrt{1-0.85^2}}{\sqrt{3} \cdot 26} \text{ kA} \quad (5A-10)$$

and

$$E_s \cos \delta = V_s + \frac{\omega_e}{\omega_b} X_q I_s \sin \theta_{ei}(0) = \frac{26}{\sqrt{3}} + 1.457 \cdot \frac{835\sqrt{1-0.85^2}}{\sqrt{3} \cdot 26} \text{ kV} \quad (5A-11)$$

Thus

$$\tilde{E}_a = \frac{26}{\sqrt{3}} + 1.457 \cdot \frac{835\sqrt{1-0.85^2}}{\sqrt{3} \cdot 26} + j1.457 \cdot \frac{835 \cdot 0.85}{\sqrt{3} \cdot 26} \text{ kV} \quad (5A-12)$$

The phasor diagrams for the three load conditions are shown in Figure 5A-1. The amplitude of the stator phase current is plotted versus field current for a range of power factors in Figure 5A-2. This curve is the classic *V*-curve of the synchronous machine.

The manner in which torque is produced in a synchronous machine may now be further explained with a somewhat more detailed consideration of the interaction of the resulting air-gap MMF established by the stator currents and the field current with (1) the MMF established by the field current and with (2) the minimum reluctance path of the rotor. With the machine operating with  $T_L$  equal zero and  $|\tilde{E}_a| > |\tilde{V}_{as}|$ , the stator currents are

$$I_{as} = \sqrt{2} I_s \cos\left(\omega_e t + \frac{\pi}{2}\right), \text{ etc.} \quad (5.9-32)$$

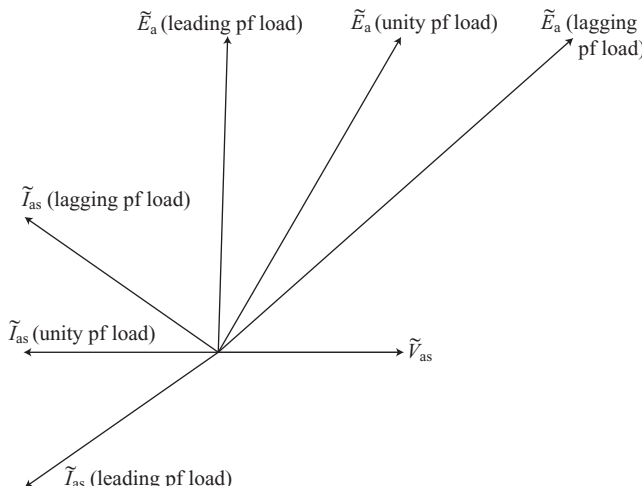


Figure 5A-1. Phasor diagram for conditions in Example 5A.

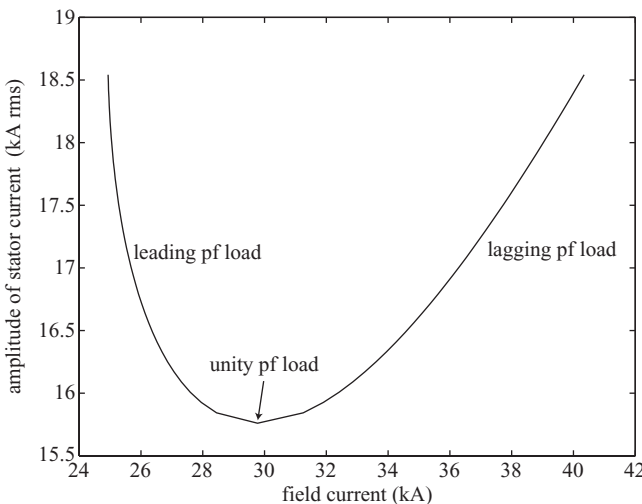


Figure 5A-2. Amplitude of stator current versus field current for conditions in Example 5A.

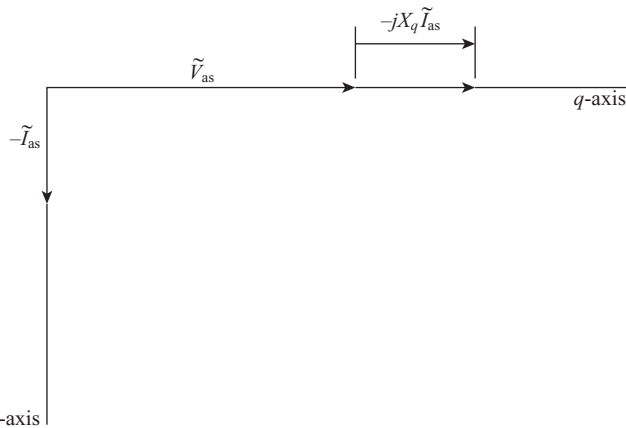


Figure 5.9-1. Phasor diagram with all losses neglected and zero power transfer.

The rotor angle is zero and the  $q$ -axis of the machine coincides with the real axis of a phasor diagram and  $d$ -axis with the negative imaginary axis as shown in Figure 5.9-1. With the time-zero conditions imposed, the rotor angle  $\delta$  is zero, and the  $q$ -axis of the machine coincides with the real axis of a phasor diagram and the  $d$ -axis with the negative imaginary axis. Electromagnetic torque is developed so as to align the poles or the MMF created by the field current with the resultant air-gap MMF produced by the stator currents. In this mode of operation, the MMF due to the field current is downward in the direction of the positive  $d$ -axis at the instant  $v_{as}$  is maximum. At this time,  $i_{as}$  is zero, while  $i_{bs}$  and  $i_{cs}$  are equal and opposite. Hence, the MMF produced by the stator currents is directed upward in the direction of the negative  $d$ -axis. The resultant of these

two MMFs must be in the direction of the positive  $d$ -axis since it was the increasing of the field MMF, by increasing the field current, which caused the stator current to lead the voltage thus causing the MMF produced by the stator currents to oppose the MMF produced by the field current. Therefore, the resultant air-gap MMF and the field MMF are aligned. Moreover, the resultant air-gap MMF and the minimum reluctance path of the rotor ( $d$  axis) are also aligned. It follows that zero torque is produced and the rotor and MMFs will rotate while maintaining this alignment. If, however, the rotor tries to move from this alignment by either speeding up or slowing down ever so slightly, there will be both a torque due to the interaction of stator and field currents and a reluctance torque to bring the rotor back into alignment.

Let us now consider the procedure by which generator action is established. A prime mover is mechanically connected to the shaft of the synchronous generator. This prime mover can be a steam turbine, a hydro turbine, a wind turbine, or a combustion engine. If, initially, the torque input on the shaft due to the prime mover is zero, the synchronous machine is essentially floating on the line. If now the input torque is increased to some value ( $T_L$  negative) by supplying steam to the turbine blades, for example, a torque imbalance occurs since  $T_e$  must remain at its original value until  $\delta$  changes. Hence the rotor will temporarily accelerate slightly above synchronous speed, whereupon  $\delta$  will increase in accordance with (5.7-1). Thus,  $T_e$  increases negatively, and a new operating point will be established with a positive  $\delta$  where  $T_L$  is equal to  $T_e$  plus torque due to losses. The rotor will again rotate at synchronous speed with a torque exerted on it in an attempt to align the field MMF with the resultant air-gap MMF. The actual dynamic response of the electrical and mechanical systems during this loading process is illustrated by computer traces in the following section. If, during generator operation, the magnitude of torque input from the prime mover is increased to a value greater than the maximum possible value of  $T_e$ , the machine will be unable to maintain steady-state operation since it cannot transmit the power supplied to the shaft. In this case, the device will accelerate above synchronous speed theoretically without bound, however, protection is normally provided that disconnects the machine from the system and reduces the input torque to zero by closing the steam valves of the steam turbine, for example, when it exceeds synchronous speed by generally 3–5%.

Normal steady-state generator operation is depicted by the phasor diagram shown in Figure 5.9-2. Here,  $\theta_{ei}(0)$  is the angle between the voltage and the current since the time-zero position is  $\theta_{ev}(0) = 0$  after steady-state operation is established. Since the phasor diagram and the  $q$ - and  $d$ -axes of the machine may be superimposed, the rotor reference-frame voltages and currents are also shown in Figure 5.9-2. For example,  $V_{qs}^r$  and  $I_{qs}^r$  are shown directed along the  $q$ -axis. If we wish to show each component of  $V_{qs}^r$ , it can be broken up according to (5.9-1) and each term added algebraically along the  $q$ -axis. Care must be taken, however, when interpreting the diagram.  $\tilde{V}_{as}$ ,  $\tilde{I}_{as}$ , and  $\tilde{E}_a$  are phasors representing sinusoidal quantities. On the other hand, all rotor reference-frame quantities are constants. They do not represent phasors in the rotor reference frame even though they are displayed on the phasor diagram.

There is one last detail to clear up. In (5.5-36), we defined  $e''_{xfd}$  ( $E''_{xfd}$  for steady-state operation) and indicated we would later find a convenient use for this term. If we assume that the stator of the synchronous machine is open-circuited and the rotor is being driven at synchronous speed then, from (5.9-19)

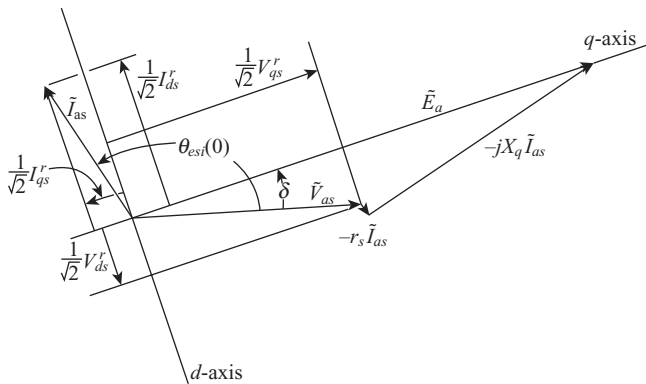


Figure 5.9-2. Phasor diagram for generator operation.

$$\tilde{V}_{as} = \tilde{E}_a \quad (5.9-33)$$

Substituting (5.9-18) for  $\tilde{E}_a$  with  $I_{ds}^r$  equal to zero yields

$$\sqrt{2} |\tilde{V}_{as}| = \frac{\omega_e}{\omega_b} X_{md} I_{fd}^r \quad (5.9-34)$$

However, as given by (5.9-29) for balanced steady-state operation

$$E_{xfd}^r = X_{md} I_{fd}^r \quad (5.9-35)$$

hence

$$\sqrt{2} |\tilde{V}_{as}| = \frac{\omega_e}{\omega_b} E_{xfd}^r \quad (5.9-36)$$

Now let us per unitize the previous equation. To do so, we must divide each side of (5.9-36) by  $V_{B(qd0)}$  or  $\sqrt{2} V_{B(abc)}$ , since  $E_{xfd}^r$  is a rotor reference-frame quantity. Thus

$$\frac{\sqrt{2} |\tilde{V}_{as}|}{\sqrt{2} V_{B(abc)}} = \frac{(\omega_e / \omega_b) E_{xfd}^r}{V_{B(qd0)}} \quad (5.9-37)$$

Therefore, when  $|\tilde{V}_{as}|$  is one per unit,  $(\omega_e / \omega_b) E_{xfd}^r$  is one per unit. During steady-state rated speed operation,  $(\omega_e / \omega_b)$  is unity, and therefore one per unit  $E_{xfd}^r$  produces one per unit open-circuit terminal voltage. Since this provides a convenient relationship,  $E_{xfd}^r$  is used extensively to define the field voltage rather than the actual voltage applied to the field winding.

## 5.10. STATOR CURRENTS POSITIVE OUT OF MACHINE: SYNCHRONOUS GENERATOR OPERATION

The early power system engineers and analysts chose to assume positive stator currents out of the synchronous machine perhaps because the main application was generator action. This notation is still used predominately in power system analysis and therefore warrants consideration. The synchronous machine shown in Figure 5.10-1 and the equivalent circuits shown in Figure 5.10-2 depict positive stator currents out of the machine. It is important to note that the field and damper winding currents are positive into the machine. It may at first appear that it would be a huge task to modify the analysis used thus far in this chapter to accommodate this change in the assumed direction of positive current. We would hope not to be forced to repeat the entire derivation. Fortunately, we will not have to do this. First, let us consider the changes

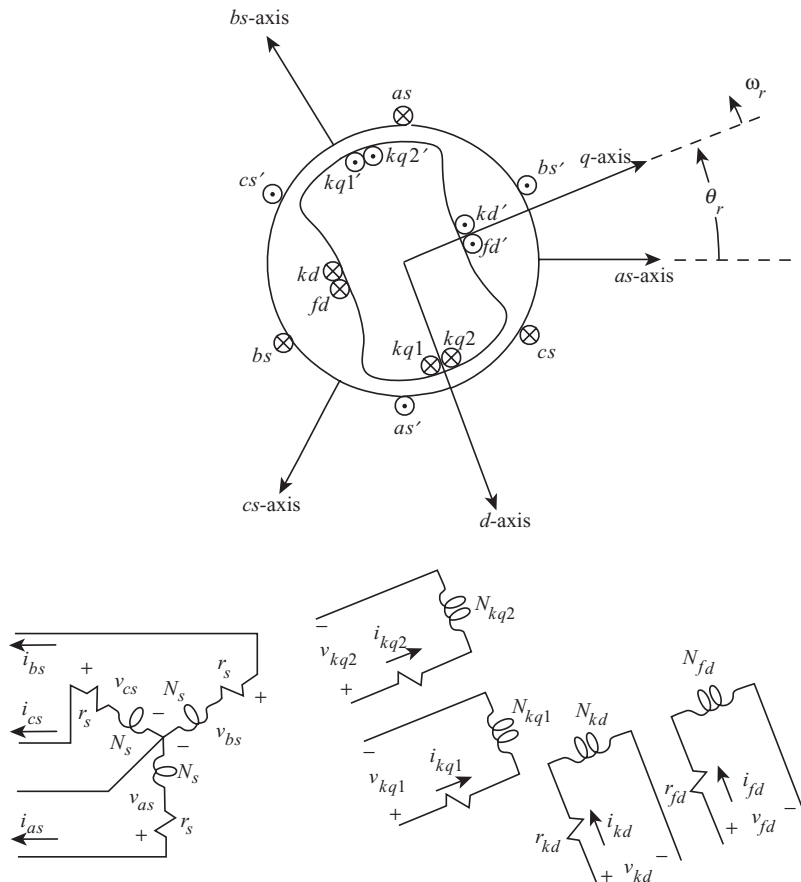


**Figure 5.10-1.** Two-pole, three-phase, wye-connected salient-pole synchronous machine with currents defined positive out of the stator phase windings.

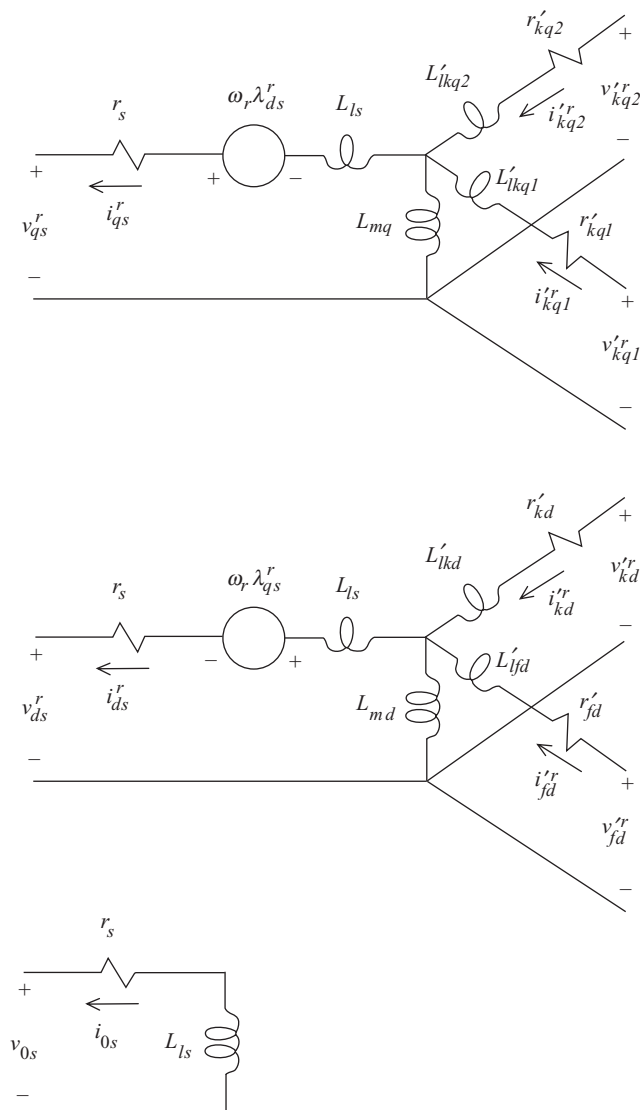


**Figure 5.10-2.** Equivalent circuits of a three-phase synchronous machine with the reference frame fixed in rotor: Park's equations with currents defined positive out of the phase windings.

necessary in order to make the steady-state equations compatible with assumed positive stator currents out of the machine.

The steady-state voltage and torque equations for positive stator currents out of the machine are obtained by simply changing the sign of stator current,  $\tilde{I}_{as}$ , or the substitute variables,  $I_{qs}^r$  and  $I_{ds}^r$ . From Section 5.9,

$$\tilde{V}_{as} = - \left( r_s + j \frac{\omega_e}{\omega_b} X_q \right) \tilde{I}_{as} + \tilde{E}_a \quad (5.10-1)$$

$$\tilde{E}_a = \frac{1}{\sqrt{2}} \left[ - \left( \frac{\omega_e}{\omega_b} \right) (X_d - X_q) I_{ds}^r + \frac{\omega_e}{\omega_b} X_{md} I_{fd}^{tr} \right] e^{j\delta} \quad (5.10-2)$$

The steady-state torque, positive for generator action, is the negative of (5.9-20), (5.9-30), or (5.9-31).

We realize that this changes the sense of the torque–angle plot from a negative sine to a positive sine. Along with this change is the change of the concept of stable operation. In particular, when we assumed positive currents into the machine, stable operation occurred on the negative slope part of the torque–angle plot; now stable operation is on the positive slope portion.

For generator action, the torque and rotor speed relationship is generally written

$$T_e = -J \left( \frac{2}{P} \right) p \omega_r + T_l \quad (5.10-3)$$

where  $T_e$  is positive for generator action and  $T_l$  is the input torque, which is positive for a torque input, to the shaft of the synchronous generator. Torque–speed relationships expressed in per unit are

$$T_e = -2H_p \frac{\omega_r}{\omega_b} + T_l \quad (5.10-4)$$

If  $\omega_e$  is constant, then (5.10-4) may be written as

$$T_e = - \frac{2H}{\omega_b} p^2 \delta + T_l \quad (5.10-5)$$

where  $H$  is in seconds, (5.8-5), and  $\delta$  is in electrical radians. A typical phasor diagram for generator action with positive stator currents out of the machine is shown in Figure 5.10-3.

It appears that we are now prepared to consider generator operation compatible with the convention used in power system analysis.

**EXAMPLE 5B** A three-phase, 64-pole, hydro turbine generator is rated at 325 MVA, with 20 kV line-to-line voltage and a power factor of 0.85 lagging. The machine parameters in ohms at 60 Hz are:  $r_s = 0.00234$ ,  $X_q = 0.5911$ , and  $X_d = 1.0467$ . For balanced, steady-state rated conditions, calculate (a)  $\tilde{E}_a$ , (b)  $E_{xfd}^{tr}$ , and (c)  $T_e$ .

The apparent power  $|S|$  is

$$|S| = 3 |\tilde{V}_{as}| |\tilde{I}_{as}| \quad (5B-1)$$

Thus

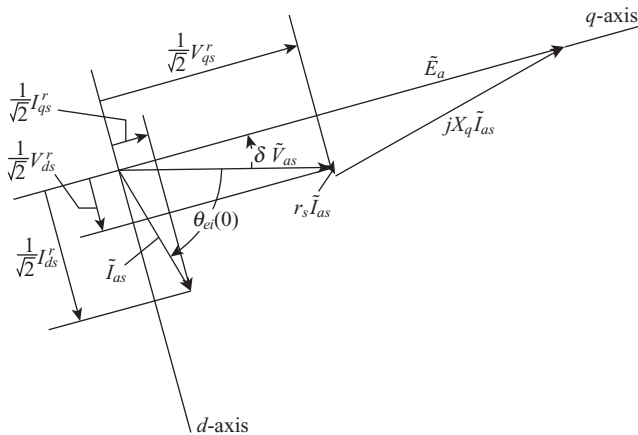


Figure 5.10-3. Phasor diagram for generator operation with currents defined positive out of the phase windings.

$$\begin{aligned}
 |\tilde{I}_{as}| &= \frac{|S|}{3|\tilde{V}_{as}|} \\
 &= \frac{325 \times 10^6}{(3 \times 20 \times 10^3) / \sqrt{3}} \\
 &= 9.37 \text{ kA}
 \end{aligned} \tag{5B-2}$$

The power factor angle is  $\cos^{-1} 0.85 = 31.8^\circ$ . Since current is positive out of the terminals of the generator, reactive power is delivered by the generator when the current is lagging the terminal voltage. Thus,  $\tilde{I}_{as} = 9.37 \angle -31.8^\circ$  kA. Therefore, from (5.10-1), we can obtain the answer to part (a).

$$\begin{aligned}
 \tilde{E}_a &= \tilde{V}_{as} + \left( r_s + j \frac{\omega_e}{\omega_b} X_q \right) \tilde{I}_{as} \\
 &= \frac{20 \times 10^3}{\sqrt{3}} \angle 0^\circ + [0.00234 + j(1)(0.5911)] 9.37 \times 10^3 \angle -31.8^\circ \\
 &= 15.2 \angle 18^\circ \text{ kV}
 \end{aligned} \tag{5B-3}$$

Hence  $\delta = 18^\circ$ .

We can solve for  $E''_{xd}$  by first substituting (5.9-29) into (5.10-1); however,  $I_{ds}^r$  is required before  $E''_{xd}$  can be evaluated. Thus from (5.9-12)

$$\begin{aligned}
 I_{ds}^r &= -\sqrt{2} I_s \sin[\theta_{ei}(0) - \theta_{ev}(0) - \delta] \\
 &= -\sqrt{2} |\tilde{I}_{as}| \sin[-31.8^\circ - 0 - 18^\circ] \\
 &= -\sqrt{2} (9.37 \times 10^3) \sin(-49.8^\circ) \\
 &= 10.12 \text{ kA}
 \end{aligned} \tag{5B-4}$$

From (5.9-29) and (5.10-2)

$$\begin{aligned}
 E'_{xfd} &= \frac{\omega_b}{\omega_e} \left[ \sqrt{2} |\tilde{E}_a| + \frac{\omega_e}{\omega_b} (X_d - X_q) I_{ds}^r \right] \\
 &= \sqrt{2} (15.2 \times 10^3) + (1.0467 - 0.5911) 10.12 \times 10^3 \\
 &= 26.1 \text{ kV}
 \end{aligned} \tag{5B-5}$$

Since  $r_s$  is small,  $T_e$  may be calculated by substitution into the negative of (5.9-30)

$$\begin{aligned}
 T_e &= \left( \frac{3}{2} \right) \left( \frac{P}{2} \right) \left( \frac{1}{\omega_b} \right) \left[ \frac{E'_{xfd} \sqrt{2} |\tilde{V}_{as}|}{(\omega_e / \omega_b) X_d} \sin \delta + \left( \frac{1}{2} \right) \left( \frac{\omega_e}{\omega_b} \right)^{-2} \left( \frac{1}{X_q} - \frac{1}{X_d} \right) (\sqrt{2} |\tilde{V}_{as}|)^2 \sin 2\delta \right] \\
 &= \left( \frac{3}{2} \right) \left( \frac{64}{2} \right) \left( \frac{1}{377} \right) \left\{ \frac{(26.1 \times 10^3) (\sqrt{2}) [(20 \times 10^3) / (\sqrt{3})]}{1.0467} \sin 18^\circ \right. \\
 &\quad \left. + \left( \frac{1}{2} \right) \left( \frac{1}{0.5911} - \frac{1}{1.0467} \right) \left[ \sqrt{2} \left( \frac{20 \times 10^3}{\sqrt{3}} \right)^2 \right] \sin 36^\circ \right\} \\
 &= 23.4 \times 10^6 \text{ N} \cdot \text{m}
 \end{aligned} \tag{5B-6}$$

## Dynamic Performance During a Sudden Change in Input Torque

It is instructive to observe the dynamic performance of a synchronous machine during a step change in input torque. For this purpose, the differential equations that describe the synchronous machine were programmed on a computer and a study was performed [5]. Two large machines are considered, a low-speed hydro turbine generator and a high-speed steam turbine generator. Information regarding each machine is given in Table 5.10-1 and Table 5.10-2. In the case of hydro turbine generators, parameters are given for only one damper winding in the  $q$ -axis. The reason for denoting this winding as the  $kq2$  winding rather than the  $kq1$  winding will become clear in Chapter 7.

The computer traces shown in Figure 5.10-4 and Figure 5.10-5 illustrate the dynamic behavior of the hydro turbine generator following a step change in input torque from zero to  $27.6 \times 10^6 \text{ N} \cdot \text{m}$  (rated for unity power factor). The dynamic behavior of the steam turbine generator is depicted in Figure 5.10-6 and Figure 5.10-7. In this case, the step change in input torque is from zero to  $1.11 \times 10^6 \text{ N} \cdot \text{m}$  (50% rated). In Figure 5.10-4 and Figure 5.10-5, the following variables are plotted:  $i_{as}$ ,  $v_{qs}^r$ ,  $i_{qs}^r$ ,  $v_{ds}^r$ ,  $i_{ds}^r$ ,  $i_{fd}^r$ ,  $T_e$ ,  $\omega_r$ , and  $\delta$ , where  $\omega_r$  is in electrical radians per second and  $\delta$  in electrical degrees. Figure 5.10-5 and Figure 5.10-7 illustrate the dynamic torque versus rotor angle characteristics. In all figures, the scales of the voltages and currents are given in multiples of peak rated values.

In each study, it is assumed that the machine is connected to a bus whose voltage and frequency remain constant, at the rated values, regardless of the stator current. This is commonly referred to as an infinite bus, since its characteristics do not change

TABLE 5.10-1. Hydro Turbine Generator

---

Rating: 325 MVA
Line to line voltage: 20 kV
Power factor: 0.85
Poles: 64
Speed: 112.5 r/min
Combined inertia of generator and turbine
$J = 35.1 \times 10^6 \text{ J} \cdot \text{s}^2$ , or $WR^2 = 833.1 \times 10^6 \text{ lbm} \cdot \text{ft}^2$ $H = 7.5$ seconds
Parameters in ohms and per unit
$r_s = 0.00234 \Omega$ , 0.0019 pu
$X_{ls} = 0.1478 \Omega$ , 0.120 pu
$X_q = 0.5911 \Omega$ , 0.480 pu $X_d = 1.0467 \Omega$ , 0.850 pu
$r'_{fd} = 0.00050 \Omega$ , 0.00041 pu
$X'_{fd} = 0.2523 \Omega$ , 0.2049 pu
$r'_{kq2} = 0.01675 \Omega$ , 0.0136 pu $r'_{kd} = 0.01736 \Omega$ , 0.0141 pu
$X'_{lkq2} = 0.1267 \Omega$ , 0.1029 pu $X'_{lkd} = 0.1970 \Omega$ , 0.160 pu

---

TABLE 5.10-2. Steam Turbine Generator

---

Rating: 835 MVA
Line to line voltage: 26 kV
Power factor: 0.85
Poles: 2
Speed: 3600 r/min
Combined inertia of generator and turbine
$J = 0.0658 \times 10^6 \text{ J} \cdot \text{s}^2$ , or $WR^2 = 1.56 \times 10^6 \text{ lbm} \cdot \text{ft}^2$ $H = 5.6$ seconds
Parameters in ohms and per unit
$r_s = 0.00243 \Omega$ , 0.003 pu
$X_{ls} = 0.1538 \Omega$ , 0.19 pu
$X_q = 1.457 \Omega$ , 1.8 pu $X_d = 1.457 \Omega$ , 1.8 pu
$r'_{kq1} = 0.00144 \Omega$ , 0.00178 pu $r'_{fd} = 0.00075 \Omega$ , 0.000929 pu
$X'_{lkq1} = 0.6578 \Omega$ , 0.8125 pu $X'_{fd} = 0.1145 \Omega$ , 0.1414 pu
$r'_{kq2} = 0.00681 \Omega$ , 0.00841 pu $r'_{kd} = 0.01080 \Omega$ , 0.01334 pu
$X'_{lkq2} = 0.07602 \Omega$ , 0.0939 pu $X'_{lkd} = 0.06577 \Omega$ , 0.08125 pu

---

regardless of the power supplied or consumed by any device connected to it. Although an infinite bus cannot be realized in practice, its characteristics are approached if the power delivery capability of the system, at the point where the machine is connected, is much larger than the rating of the machine.

Initially, each machine is operating with zero input torque with the excitation held fixed at the value that gives rated open-circuit terminal voltage at synchronous speed. It is instructive to observe the plots of  $T_e$ ,  $\omega_r$ , and  $\delta$  following the step change input torque. In particular, consider the response of the hydro turbine generator (Fig. 5.10-4) where the machine is subjected to a step increase in input torque from zero to  $27.6 \times 10^6 \text{ N} \cdot \text{m}$ . The rotor speed begins to increase immediately following the step

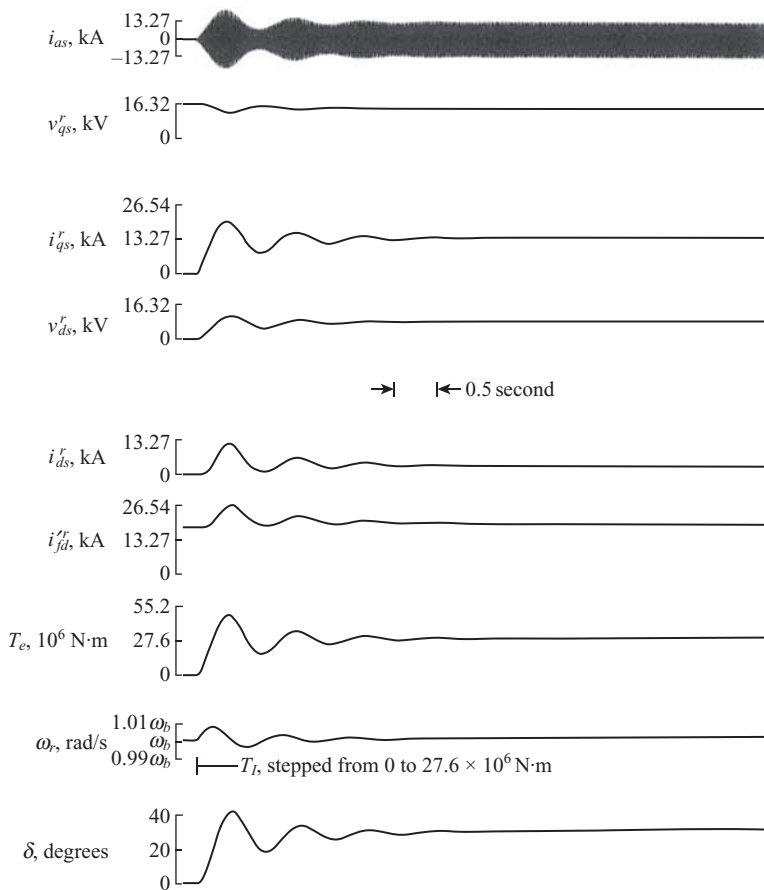


**Figure 5.10-4.** Dynamic performance of a hydro turbine generator during a step increase in input torque from zero to rated.

increase in input torque as predicted by (5.10-5), whereupon the rotor angle increases in accordance with (5.7-1). The rotor speeds up until the accelerating torque on the rotor is zero. As noted in Figure 5.10-4, the speed increases to approximately 380 electrical radians per second, at which time  $T_e$  is equal to  $T_l$  since the change of  $\omega_r$  is zero and hence the inertial torque ( $T_{II}$ ) is zero. Even though the accelerating torque is zero at this time, the rotor is running above synchronous speed, hence  $\delta$ , and thus  $T_e$ , will continue to increase. The increase in  $T_e$ , which is an increase in the power output of the machine, causes the rotor to decelerate toward synchronous speed. However, when synchronous speed is reached, the magnitude of  $\delta$  has become larger than necessary to satisfy the input torque. Note that at the first synchronous speed crossing of  $\omega_r$  after the change in input torque,  $\delta$  is approximately 42 electrical degrees and  $T_e$  approximately  $47 \times 10^6 \text{ N}\cdot\text{m}$ . Hence, the rotor continues to decelerate below synchronous speed and consequently  $\delta$  begins to decrease, which in turn decreases  $T_e$ . Damped oscillations

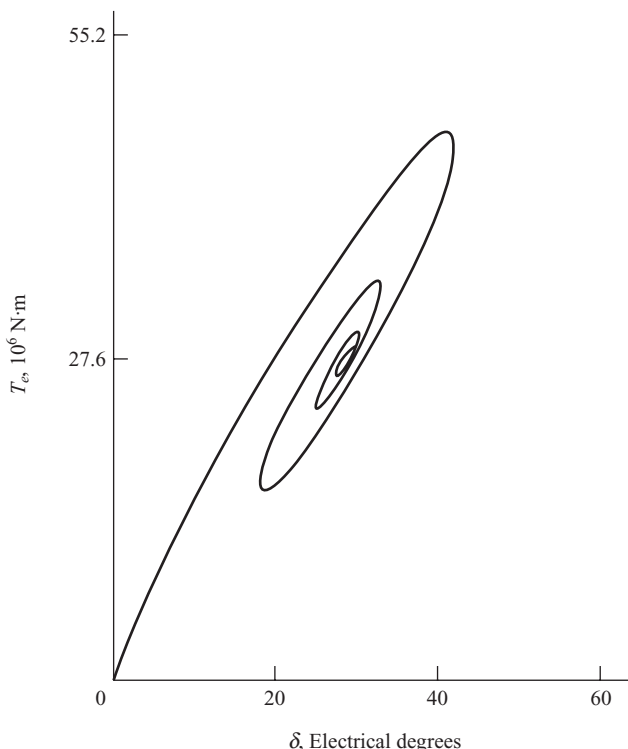


**Figure 5.10-5.** Torque versus rotor angle characteristics for the study shown in Figure 5.10-4.

of the machine variables continue and a new steady-state operating point is finally attained.

In the case of the hydro turbine generator (Fig. 5.10-4), the oscillations in machine variables subside in a matter of 2 or 3 seconds, and the machine establishes the new steady-state operating point within 8 or 10 seconds. In the case of the steam turbine generator (Fig. 5.10-6), the oscillations subside rapidly, but the new steady-state operating point is slowly approached. The damping is of course a function of the damper windings and can be determined from an eigenvalue analysis that will be discussed in Chapter 8. The point of interest here is the time required for the machine variables to reestablish steady-state operation after the torque disturbance. This rather slow approach to the new steady-state operating point in the case of the steam turbine generator is also apparent from the plot of  $T_e$  versus  $\delta$  (Fig. 5.10-7).

Let us consider, for a moment, the expression for steady-state torque, (5.9-30) (remember to change the sign). For the hydro turbine generator with  $E'_{xfd} = \sqrt{(2/3)}20$  kV

$$T_e = (32.5 \sin \delta + 12.5 \sin 2\delta) \times 10^6 \text{ N} \cdot \text{m} \quad (5.10-6)$$

and for the steam turbine generator with  $E'_{xfd} = \sqrt{(2/3)}26$  kV

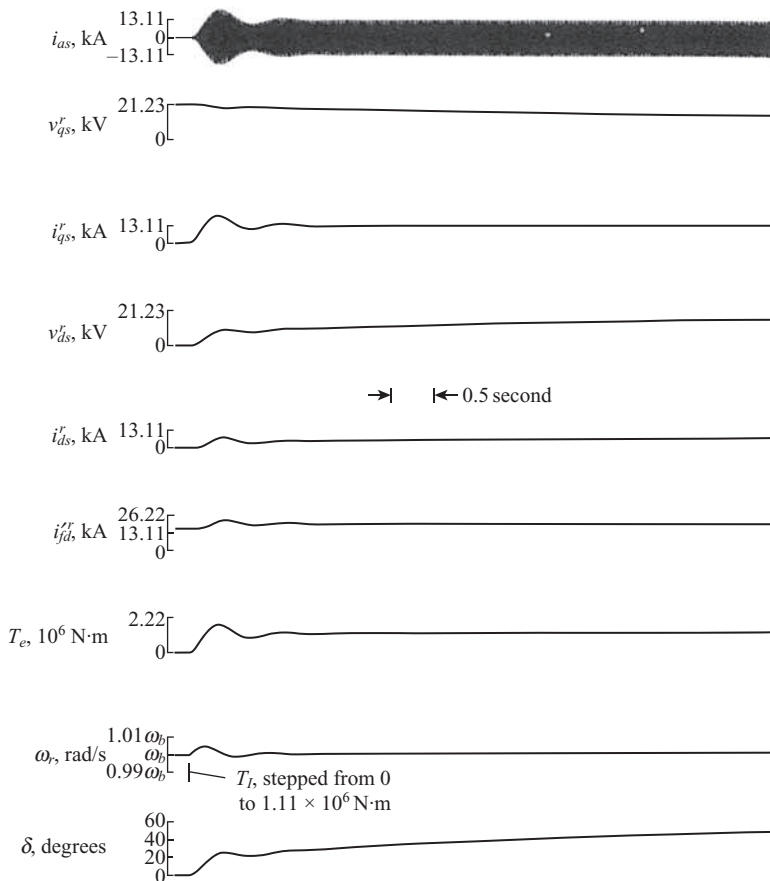


**Figure 5.10-6.** Dynamic performance of a steam turbine generator during a step increase in input torque from 0% to 50% rated.

$$T_e = 1.23 \times 10^6 \sin \delta \text{ N} \cdot \text{m} \quad (5.10-7)$$

If (5.10-6) and (5.10-7) are plotted on Figure 5.10-5 and Figure 5.10-7 respectively, the steady-state  $T_e$  versus  $\delta$  curves will pass through the final value of dynamic  $T_e$  versus  $\delta$  plots. However, the dynamic torque-angle characteristics immediately following the input torque disturbance yields a much larger  $T_e$  for a given value of  $\delta$  than does the steady-state characteristic. In other words, the dynamic or transient torque-angle characteristic is considerably different from the steady-state characteristic and the steady-state  $T_e$  versus  $\delta$  curve applies only after all transients have subsided. Although the computation of the transient torque during speed variations requires the solution of nonlinear differential equations, it can be approximated quite simply. This is the subject of a following section.

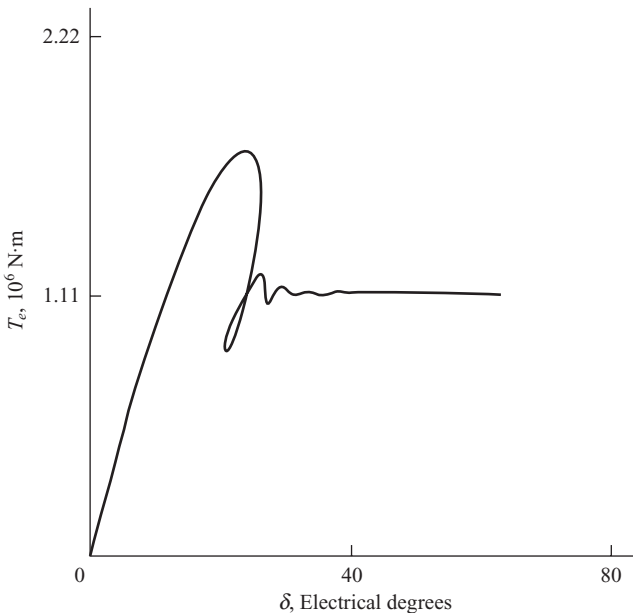


**Figure 5.10-7.** Torque versus rotor angle characteristics for the study shown in Figure 5.10-6.

### Dynamic Performance During a Three-Phase Fault at the Machine Terminals

The stability of synchronous machines throughout a power system following a fault is of major concern. A three-phase fault or short-circuit rarely occurs and a three-phase fault at the machine terminals is even more uncommon; nevertheless, it is instructive to observe the dynamic performance of a synchronous machine during this type of a fault.

The computer traces shown in Figure 5.10-8 and Figure 5.10-9 illustrate the dynamic behavior of the hydro turbine generator during and following a three-phase fault at the terminals. The dynamic behavior of the steam turbine generator as a result of a three-phase terminal fault is shown in Figure 5.10-10 and Figure 5.10-11. The parameters of the machines are those given previously. In Figure 5.10-8 and Figure 5.10-10, the following variables are plotted:  $i_{as}$ ,  $v_{qs}'$ ,  $i_{qs}'$ ,  $v_{ds}'$ ,  $i_{ds}'$ ,  $i_{fd}'$ ,  $T_e$ ,  $\omega_r$ , and  $\delta$ . Figure 5.10-9 and Figure 5.10-11 illustrate the dynamic torque-angle characteristics during and following the three-phase fault. In each case, the machine is initially connected to an infinite bus delivering rated MVA at rated power factor. In the case of the hydro turbine generator, the input torque is held constant at  $(0.85) 27.6 \times 10^6 \text{ N}\cdot\text{m}$ , with  $E_{xfd}'$  fixed at  $(1.6)\sqrt{(2/3)}20 \text{ kV}$ ; for the steam turbine generator,  $T_I = (0.85) 2.22 \times 10^6 \text{ N}\cdot\text{m}$  and  $E_{xfd}' = (2.48)\sqrt{(2/3)}26 \text{ kV}$ . (Rated operating conditions for the hydro turbine generator are calculated in Example 5B.) With the machines operating in these steady-state conditions, a three-phase terminal fault is simulated by setting  $v_{as}$ ,

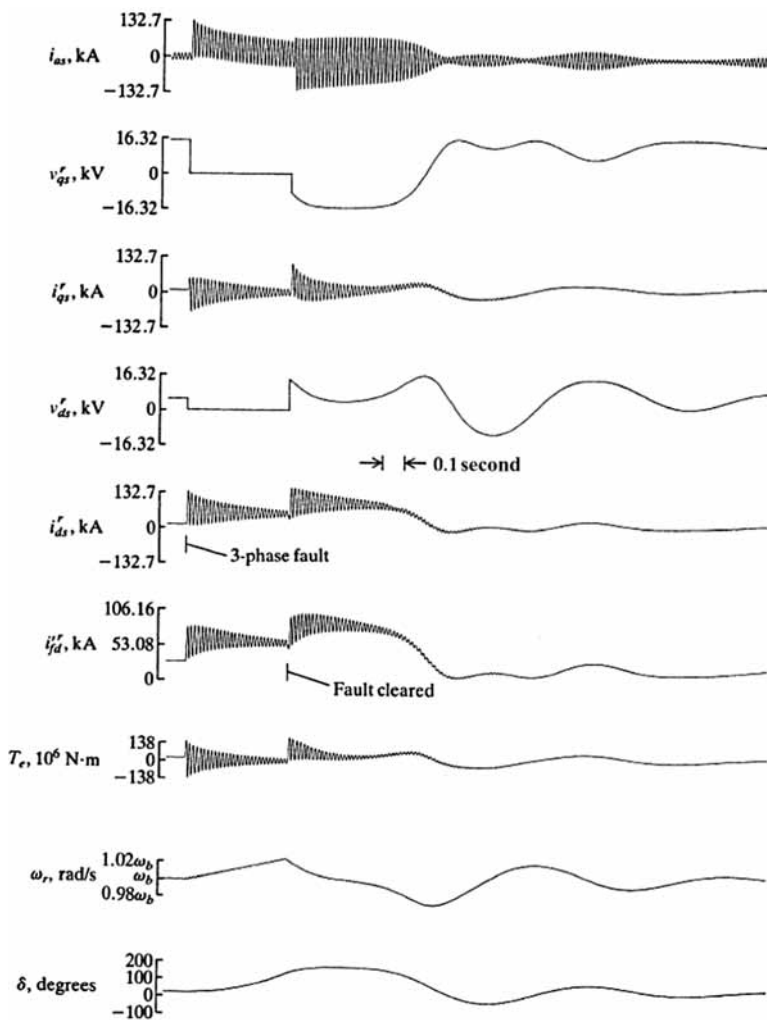


**Figure 5.10-8.** Dynamic performance of a hydro turbine generator during a three-phase fault at the terminals.

$v_{bs}$ , and  $v_{cs}$  to zero, in the simulation, at the instant  $v_{as}$  passes through zero going positive. The transient offset in the phase currents is reflected into the rotor reference-frame variables and the instantaneous torque as a decaying 60 Hz pulsation. Since the terminal voltage is zero during the three-phase fault, the machine is unable to transmit power to the system. Hence, all of the input torque, with the exception of the ohmic losses, accelerates the rotor.

In the case of the hydro turbine generator, the fault is removed in 0.466 seconds; 0.362 seconds in the case of the steam turbine generator. If the fault had been allowed to remain on the machines slightly longer, the machines would have become unstable,

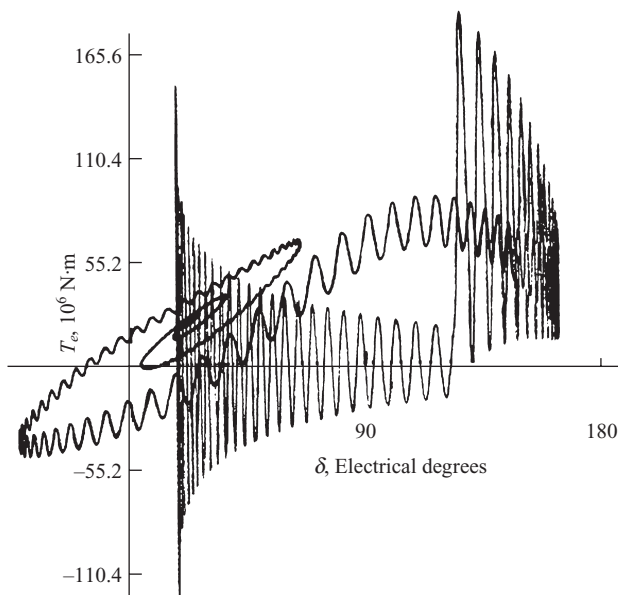


**Figure 5.10-9.** Torque versus rotor angle characteristics for the study shown in Figure 5.10-8.

that is, they would either not have returned to synchronous speed after removal of the fault or slipped poles before returning to synchronous speed. Asynchronous operation (pole slipping) is discussed in Chapter 10 of Reference 6.

When the fault is cleared, the system voltages are reapplied to the machine; offsets again occur in the phase currents, giving rise to the decaying 60Hz oscillations in the rotor reference-frame variables and the instantaneous torque. The dynamic torque-angle characteristics shown in Figure 5.10-9 and Figure 5.10-11 yield a very lucid illustration of the fault and switching sequence, and the return of the machine to its original operating condition after the fault is cleared. The torque-angle plots of the steam turbine generator are shown in Figure 8.9-1 and Figure 8.9-2 with the stator electric transients neglected, which eliminates the 60Hz pulsating electromagnetic torque and permits the average torque to be more clearly depicted.

The expression for the steady-state torque-angle characteristic for the hydro turbine generator is

$$T_e = (52.1 \sin \delta + 12.5 \sin 2\delta) \times 10^6 \text{ N} \cdot \text{m} \quad (5.10-8)$$

For the steam turbine generator

$$T_e = 3.05 \times 10^6 \sin \delta \text{ N} \cdot \text{m} \quad (5.10-9)$$

If these steady-state torque-angle characteristics are plotted on Figure 5.10-9 and Figure 5.10-11, respectively, they would pass through only the initial or final steady-

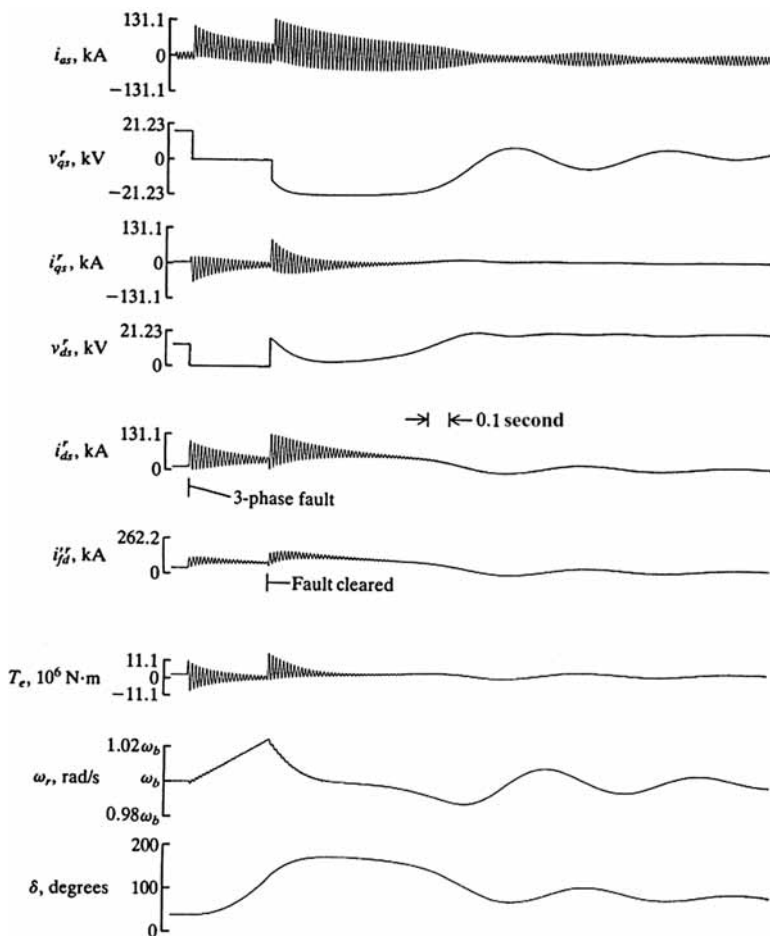


**Figure 5.10-10.** Dynamic performance of a steam turbine generator during a three-phase fault at the terminals.

state operating point. As in the case of a sudden change in input torque, the instantaneous and/or average value of the dynamic or transient torque-angle characteristic differs markedly from the steady-state torque-angle characteristics.

It is perhaps appropriate to mention that this example is somewhat impractical. In the case of a 3-phase fault close to a fully loaded machine, the circuit breakers would likely remove the machine from the system and reclosing would be prohibited since the machine would accelerate beyond speed limits before it would be physically possible to reclose the circuit breakers. A practical situation which is approximated by the example might be a three-phase fault on a large radial transmission line close to the machine terminals. Clearing or “switching out” of this line would then remove the fault from the system.

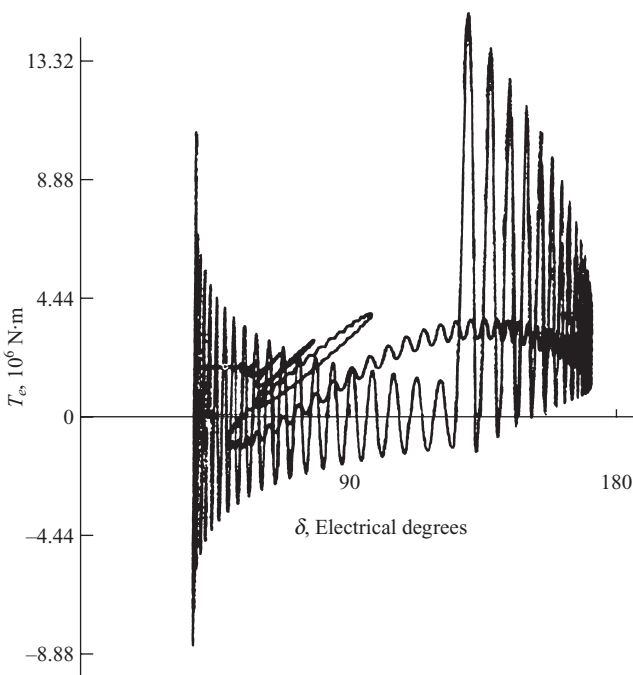


**Figure 5.10-11.** Torque versus rotor angle characteristics for the study shown in Figure 5.10-10.

### Approximate Transient Torque versus Rotor Angle Characteristics

As pointed out previously, the transient and steady-state torque versus rotor angle characteristics are quite different. Since the transient characteristics will determine if the machine remains in synchronism after a disturbance, it is necessary to calculate these characteristics accurately whenever determining the transient stability of a synchronous machine. With present-day computers, the calculation of the transient electromagnetic torque is a straightforward procedure. Consequently, it is difficult to appreciate the complex computational problems faced by machine and power system analysts before the advent of the computer and the techniques that they devised to simplify these problems.

In the late 1920s, R.E. Dorherty and C.A. Nickle [7] described a simple method of approximating the transient torque-angle characteristics. This method, combined with the concept of equal-area criterion, which is discussed later, formed the basis for transient stability studies of power systems until the 1960s. Although it is not the purpose here to dwell on techniques that have long been replaced, it is interesting to look back for a moment, not only to gain some appreciation of this early work, but to become acquainted with an approximate method that still remains invaluable in visualizing machine stability.

The method of approximating the transient torque-angle characteristics set forth by Doherty and Nickle [7] is based on the fact that the flux linkages will tend to remain constant in circuits that are largely inductive with a relative small resistance. Therefore, since the field winding has a small resistance with a large self-inductance, it is generally assumed that the field flux linkages will remain constant during the early part of the transient period. Moreover, it is assumed that all electric transients can be neglected and the action of the damper windings ignored, whereupon the steady-state voltage and flux linkage equations apply. With these assumptions, the steady-state versions of (5.5-30) and (5.5-34) may be written with a negative  $I_{ds}^r$  as

$$\psi_{ds}^r = -X_d I_{ds}^r + X_{md} I_{fd}^{r*} \quad (5.10-10)$$

$$\psi_{fd}^{r*} = X_{fd}^{r*} I_{fd}^{r*} - X_{md} I_{ds}^r \quad (5.10-11)$$

where  $X_d$  is defined by (5.5-40) and  $X_{fd}^{r*}$  by (5.5-43). Solving (5.10-10) for  $I_{fd}^{r*}$  and substituting the result into (5.10-11), we can write

$$\frac{X_{md}}{X_{fd}^{r*}} \psi_{fd}^{r*} = \psi_{ds}^r + \left( X_d - \frac{X_{md}^2}{X_{fd}^{r*}} \right) I_{ds}^r \quad (5.10-12)$$

Let us now define

$$X_d' = X_d - \frac{X_{md}^2}{X_{fd}^{r*}} \quad (5.10-13)$$

and

$$E_q' = \frac{X_{md}}{X_{fd}^{r*}} \psi_{fd}^{r*} \quad (5.10-14)$$

Equation (5.10-12) may now be written as

$$\psi_{ds}^r = -X_d' I_{ds}^r + E_q' \quad (5.10-15)$$

The reactance  $X_d'$  is referred to as the *d*-axis transient reactance. If the field flux linkages are assumed constant, then  $E_q'$ , which is commonly referred to as the voltage behind transient reactance, is also constant.

The quantities  $X_d'$  and  $E_q'$ , which are specifically related to the transient period, are each denoted by a prime. Heretofore, we have used the prime to denote rotor variables and rotor parameters referred to the stator windings by a turns ratio. As mentioned, the prime or any other distinguishing notation is seldom used in literature to denote referred quantities; on the other hand, the primes are always used to denote transient quantities. We will use the prime to denote both; the double meaning should not be confusing, since the primed quantities which pertain to the transient period are few in number and readily recognized.

Let us now return to the method used to obtain the steady-state voltage and torque equations. The steady-state voltage equations in the rotor reference frame, (5.9-1) and (5.9-2), were obtained from (5.5-22) and (5.5-23) with the time rate of change of all flux linkages neglected and  $\omega_r$  set equal to  $\omega_e$ . These equations could have also been written (note the sign change)

$$V_{qs}^r = -r_s I_{qs}^r + \frac{\omega_e}{\omega_b} \psi_{qs}^r \quad (5.10-16)$$

$$V_{ds}^r = -r_s I_{ds}^r - \frac{\omega_e}{\omega_b} \psi_{ds}^r \quad (5.10-17)$$

where, since damper winding currents are neglected

$$\begin{aligned} \psi_{ds}^r &= -X_d I_{ds}^r + X_{md} I_{fd}^{rr} \\ &= -X_d I_{ds}^r + \frac{X_{md}}{X'_{fd}} \psi_{fd}^{rr} \end{aligned} \quad (5.10-18)$$

$$\psi_{qs}^r = -X_q I_{qs}^r \quad (5.10-19)$$

If we compare (5.10-18) and (5.10-15), we see that the two equations have the same form. Therefore if, in our previous derivation, we replace  $X_d$  with  $X'_d$  and  $X_{md} I_{fd}^{rr}$  or  $E'_{fd}$  with  $E'_q$ , we will obtain voltage and torque expressions that should approximate the behavior of the synchronous machine during the early part of transient period, assuming the field flux linkages remain initially constant. In particular, the so-called transient torque-angle characteristic is expressed as

$$T_e = \left( \frac{3}{2} \right) \left( \frac{P}{2} \right) \left( \frac{1}{\omega_b} \right) \left[ \frac{E'_q \sqrt{2} V_s}{(\omega_e / \omega_b) X'_d} \sin \delta + \left( \frac{1}{2} \right) \left( \frac{\omega_e}{\omega_b} \right)^{-2} \left( \frac{1}{X_q} - \frac{1}{X'_d} \right) (\sqrt{2} V_s)^2 \sin 2\delta \right] \quad (5.10-20)$$

In per unit

$$T_e = \frac{E'_q V_s}{(\omega_e / \omega_b) X'_d} \sin \delta + \left( \frac{V_s^2}{2} \right) \left( \frac{\omega_e}{\omega_b} \right)^{-2} \left( \frac{1}{X_q} - \frac{1}{X'_d} \right) \sin 2\delta \quad (5.10-21)$$

Equations (5.10-20) and (5.10-21) are valid only if  $r_s$  can be neglected. Also, it is interesting to note that the coefficient of  $\sin 2\delta$  is zero if  $X_q = X'_d$ , which is seldom if ever the case. Actually,  $X_q > X'_d$  and the coefficient of  $\sin 2\delta$  is negative. In other words, the transient electromagnetic torque-angle curve is a function of  $\sin 2\delta$  even if  $X_q = X_d$  (round rotor).

We have yet to determine  $E'_q$  from a readily available quantity. If we substitute  $X'_d$  for  $X_d$  and  $E'_q$  for  $X_d I_{fd}^{rr}$  in (5.10-2), we have

$$\tilde{E}_a = \frac{1}{\sqrt{2}} \left( \frac{\omega_e}{\omega_b} \right) [-(X'_d - X_q) I_{ds}^r + E'_q] e^{j\delta} \quad (5.10-22)$$

Hence, the phasor voltage equation given by (5.10-1) can be used to calculate the predisturbance  $\tilde{E}_a$ , whereupon we can use (5.10-22) to determine  $E'_q$ , which is assumed to remain constant during the early part of the transient period.

### Comparison of Actual and Approximate Transient Torque-Angle Characteristics During a Sudden Change in Input Torque: First Swing Transient Stability Limit

In the studies involving a step increase in input torque, which were reported in a previous section, the machines were initially operating with essentially zero stator current and zero input torque. Hence,  $\tilde{E}_a = \tilde{V}_{as}$  and  $E'_q = \sqrt{2}V_s$ . The steady-state torque angle curve is given by (5.10-8) for the hydro unit and (5.10-9) for the steam unit. For the hydro turbine generator,  $X'_d = 0.3448 \Omega$  and the transient torque angle characteristic is

$$T_e = (98.5 \sin \delta - 20.5 \sin 2\delta) \times 10^6 \text{ N} \cdot \text{m} \quad (5.10-23)$$

For the steam turbine generator, where  $X'_d = 0.2591 \Omega$

$$T_e = (6.92 \sin \delta - 2.84 \sin 2\delta) \times 10^6 \text{ N} \cdot \text{m} \quad (5.10-24)$$

Figure 5.10-12 and Figure 5.10-13 show the approximate transient and steady-state torque-angle curves plotted along with the actual dynamic torque-angle characteristics obtained from the studies involving a step increase in input torque (Fig. 5.10-5 and Fig. 5.10-7). During the initial swing of the rotor, the dynamic torque-angle characteristic follows the approximate transient torque-angle curve more closely than the steady-state curve even though the approximation is rather crude, especially in the case of the steam turbine generator. As the transients subside, the actual torque-angle characteristic moves toward the steady-state torque-angle curve.

The approximate transient torque-angle characteristics is most often used along with equal-area criterion to predict the maximum change in input torque possible without the machine becoming unstable (transient stability limit) rather than the dynamic performance during a relatively small step increase in input torque as portrayed in Figure 5.10-12 and Figure 5.10-13. In order to compare the results obtained here with the transient stability limit, which we will calculate in a later section using equal-area criterion, it is necessary to define the “first swing” transient stability limit as the maximum value of input torque that can be suddenly applied and the rotor just returns to synchronous speed at the end of the first acceleration above synchronous speed. By trial and error, the transient stability limit, with initially zero input torque, for the hydro turbine generator was found to be  $76.7 \times 10^6 \text{ N} \cdot \text{m}$  and  $5.2 \times 10^6 \text{ N} \cdot \text{m}$  for the steam turbine generator. The computer traces shown in Figure 5.10-14, Figure 5.10-15, Figure 5.10-16, and Figure 5.10-17 show the transient response of the machine variables with the step input torque equal to the value at the “first swing” transient stability limit. Figure 5.10-14 and Figure 5.10-15 are for the hydro turbine generator and steam turbine generator, respectively, with the same variables shown as in Figure 5.10-4 and Figure 5.10-6. The machine flux linkages per second are shown in Figure

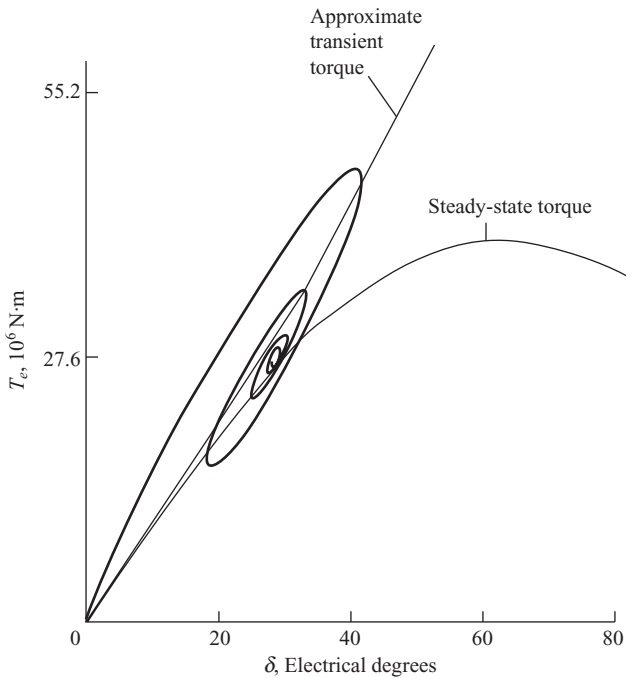


Figure 5.10-12. Comparison of the dynamic torque-angle characteristic during a step increase in input torque from zero to rated with the calculated steady-state and approximate transient torque-angle characteristics—hydro turbine generator.

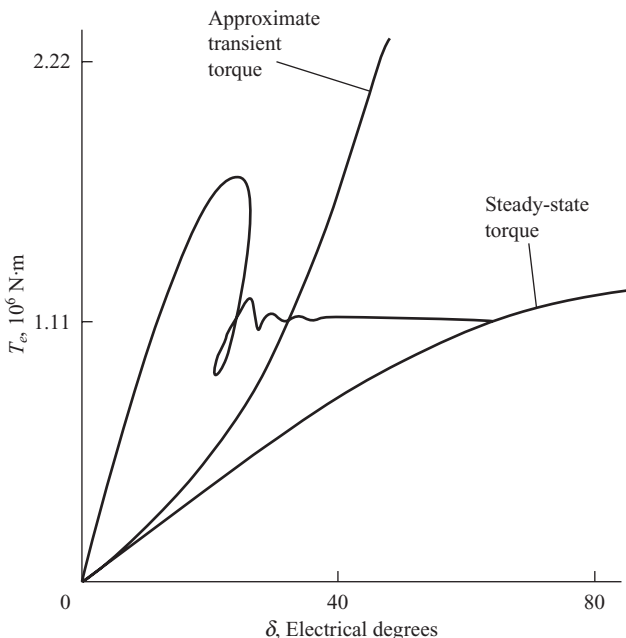


Figure 5.10-13. Same as Figure 5.10-12 for a steam turbine generator with input torque stepped from 0 to 50% rated.

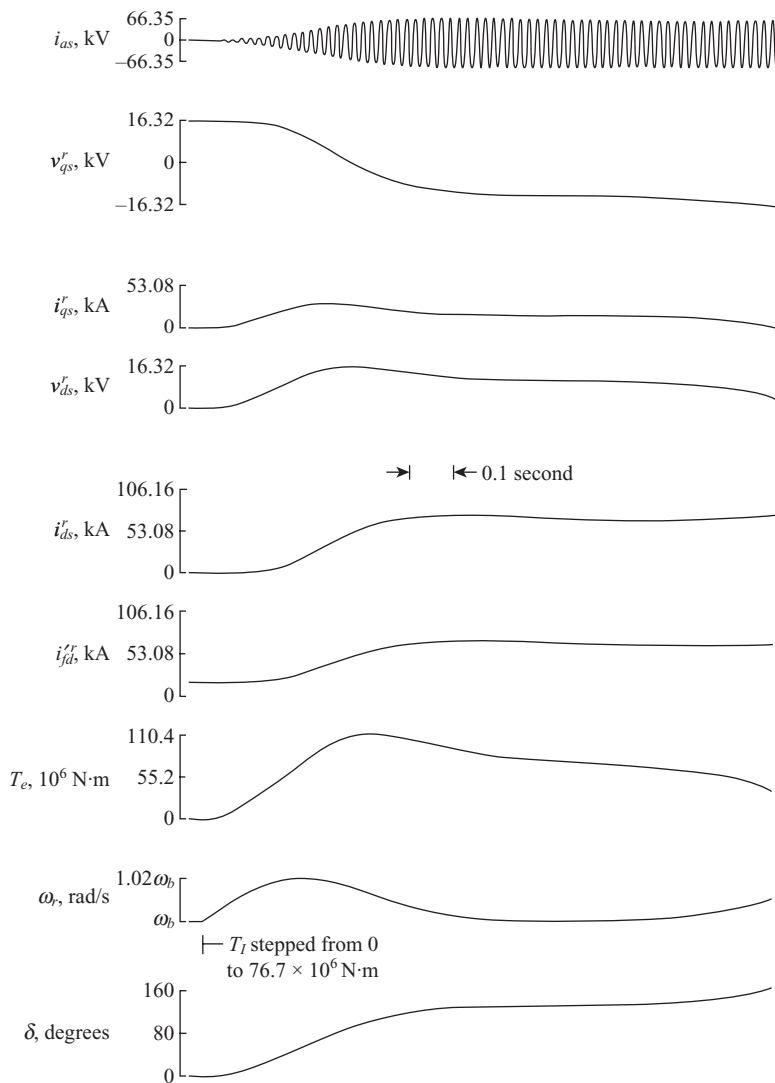


Figure 5.10-14. Dynamic performance of a hydro turbine generator at the "first swing" transient stability limit.

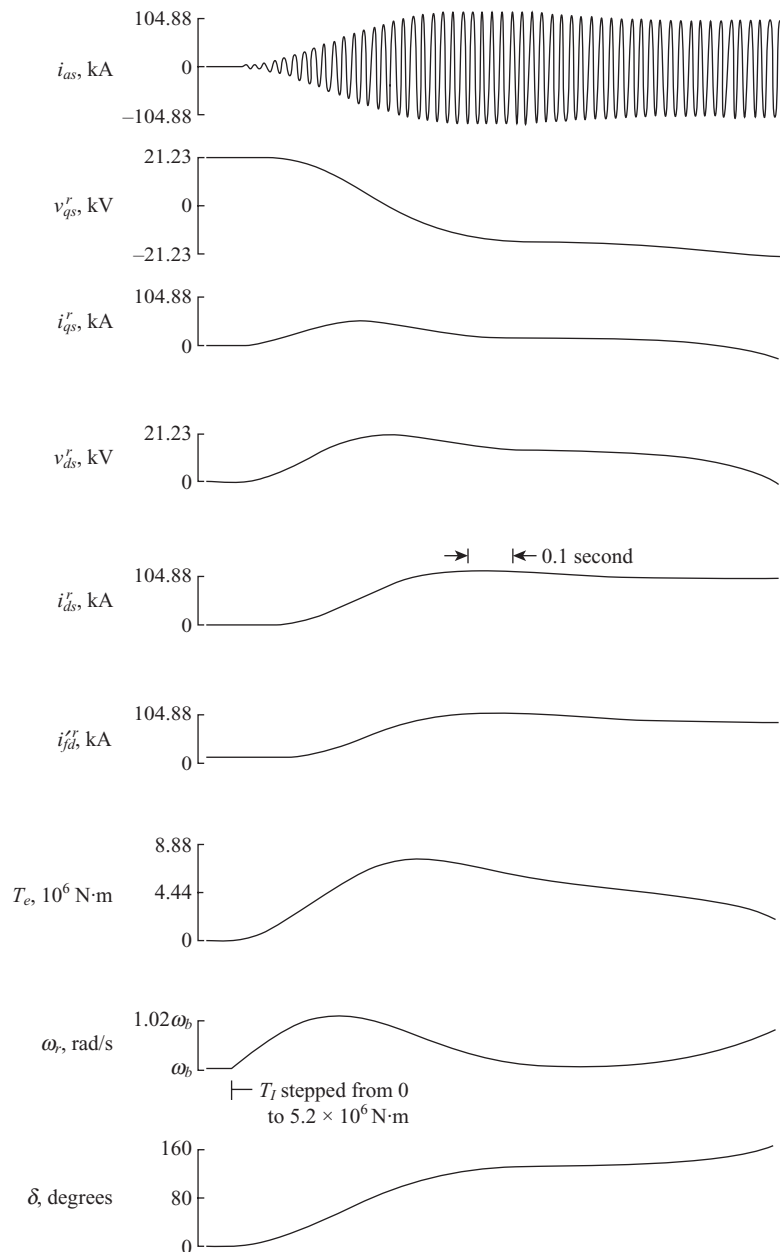


Figure 5.10-15. Same as Figure 5.10-14 for a steam turbine generator.

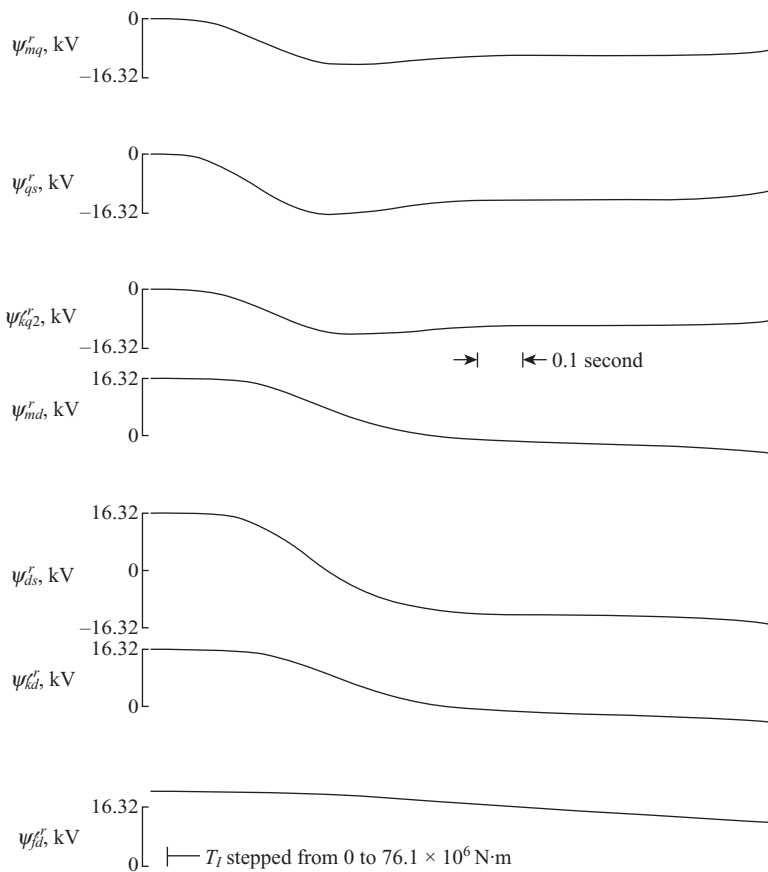


Figure 5.10-16. Traces of flux linkages per second for a hydro turbine generator at the “first swing” transient stability limit.

5.10-16 for the hydro turbine generator and in Figure 5.10-17 for the steam turbine generator.

In case of the hydro unit, the field flux linkages are relatively constant during the first swing of the machine varying approximately 17% from the original value (Fig. 5.10-16); however, the field flux linkages for the steam unit (Fig. 5.10-17) vary approximately 40% during the first swing. This is due to the fact that the field circuit of the hydro unit has a higher reactance to resistance ratio than the field circuit of the steam unit. This observation casts doubt on the accuracy of the approximate transient torque-angle characteristics, especially for the steam unit, as we have already noted in Figure 5.10-13. It is also important to note from Figure 5.10-17 that the change in  $\psi_{kq1}^r$  is much less than in the case of  $\psi_{fd}^r$ . The reactance to resistance ratios of the two circuits gives an indication of this result. In particular, the reactance to resistance ratio of the field circuit of the steam unit is 1333, while this ratio for the  $kq1$  winding is 1468.

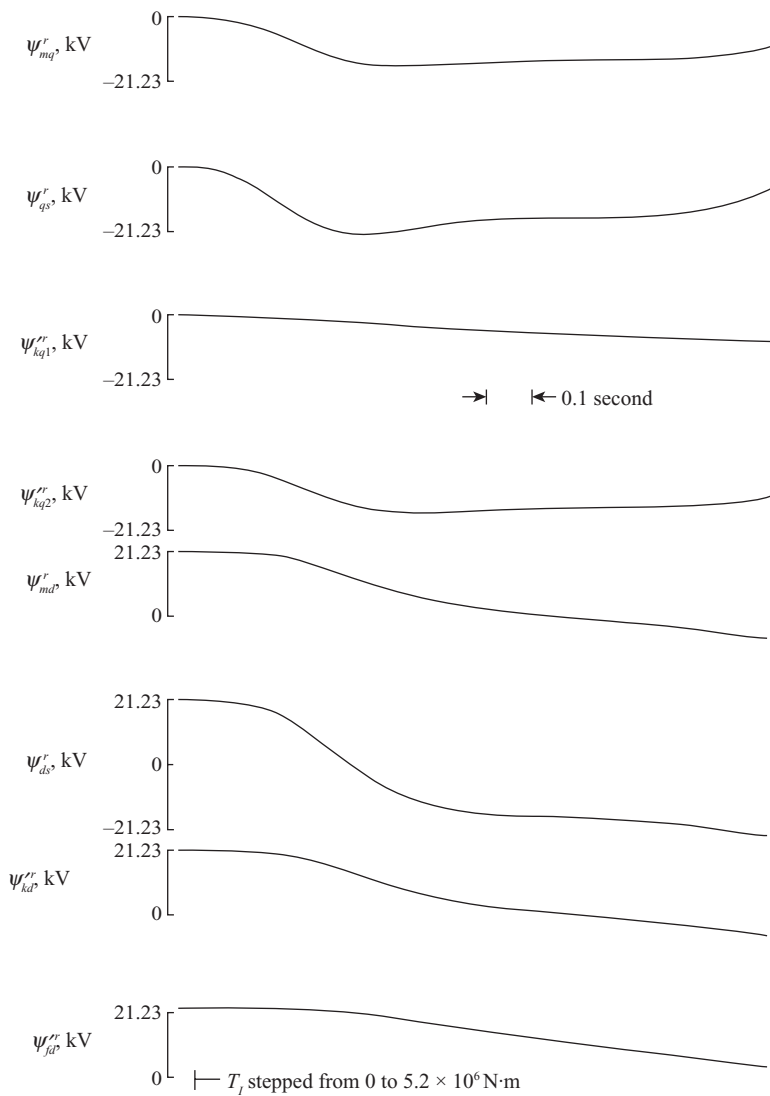
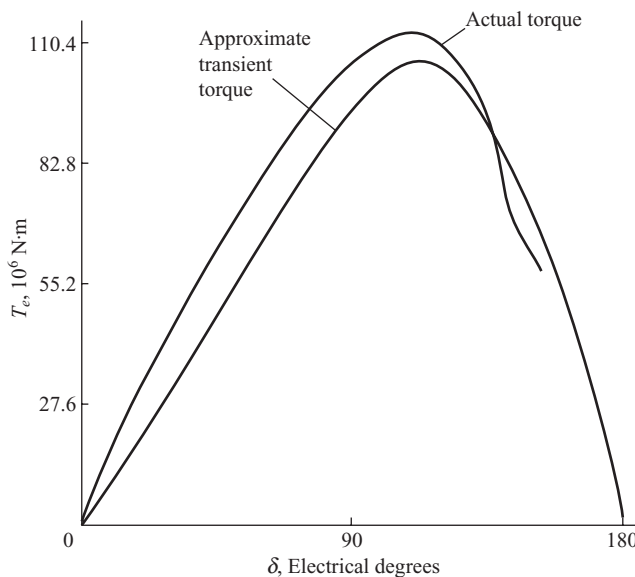
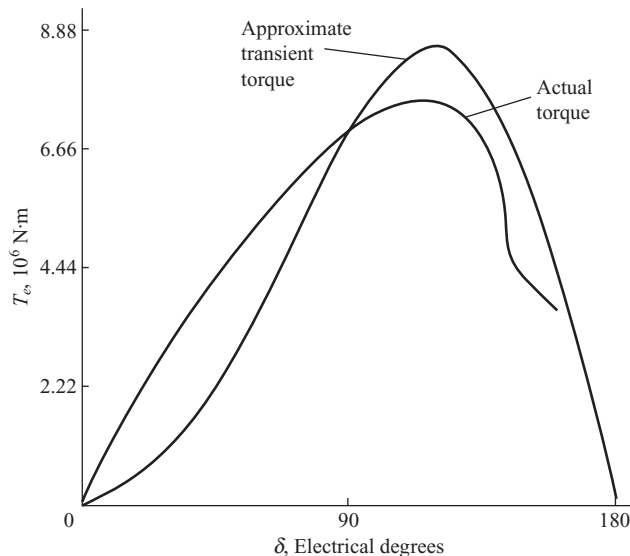


Figure 5.10-17. Same as Figure 5.10-16 for a steam turbine generator.

The actual dynamic torque-angle characteristics obtained from the computer study are shown in Figure 5.10-18 and Figure 5.10-19, with the approximate transient torque-angle curve calculated using constant flux linkages superimposed thereon. In the computer study, the machines went unstable at the transient stability limit. Nevertheless, the transient stability limit has been defined here as the “first swing” transient stability limit in an attempt to duplicate the conditions for which the equal-area criterion is to predict. The facility of the approximate transient torque-angle curve in predicting this transient stability must be deferred until we have described this criterion.



**Figure 5.10-18.** Comparison of the dynamic torque-angle characteristic at the "first swing" transient stability limit with the approximate transient torque-angle curve: hydro turbine generator.



**Figure 5.10-19.** Same as Figure 5.10-18 for a steam turbine generator.

### Comparison of Actual and Approximate Transient Torque-Angle Characteristics During a Three-Phase Fault at the Terminals: Critical Clearing Time

In the studies involving a three-phase fault at the terminals (Fig. 5.10-8, Fig. 5.10-9, Fig. 5.10-10, and Fig. 5.10-11), each machine is initially operating at rated conditions. In the case of the hydro turbine generator, the steady-state torque-angle curve is given by (5.10-8) and for the steam turbine generator by (5.10-9). For rated conditions,  $E'_q = (1.16)\sqrt{(2/3)}20$  kV for the hydro unit and the approximate transient torque-angle characteristic is

$$T_e = (114.3 \sin \delta - 20.5 \sin 2\delta) \times 10^6 \text{ N}\cdot\text{m} \quad (5.10-25)$$

For the steam turbine generator,  $E'_q = (1.09)\sqrt{(2/3)}26$  kV and the approximate transient torque-angle characteristic is

$$T_e = (7.53 \sin \delta - 2.84 \sin 2\delta) \times 10^6 \text{ N}\cdot\text{m} \quad (5.10-26)$$

Figure 5.10-20 and Figure 5.10-21 show the approximate transient and steady-state torque-angle curves for the hydro and steam units, respectively, plotted along with the actual dynamic torque-angle characteristics shown previously in Figure 5.10-9 and Figure 5.10-11. It is important to note that the approximate transient and steady-state torque-angle curves both pass through the steady-state operating point. The flux

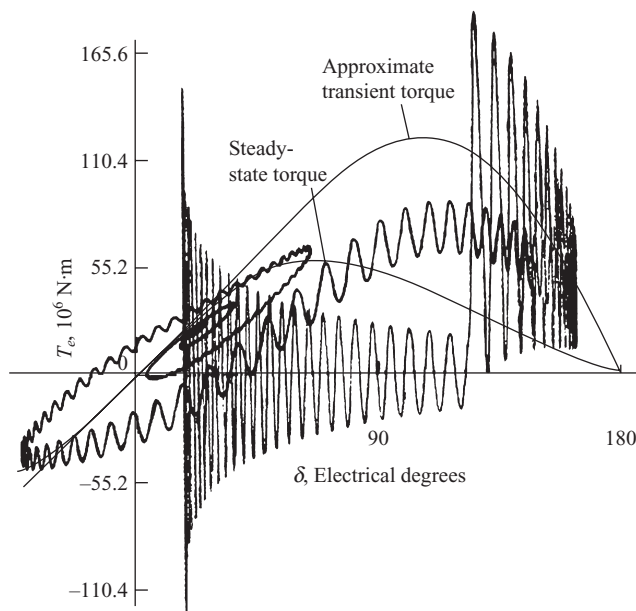
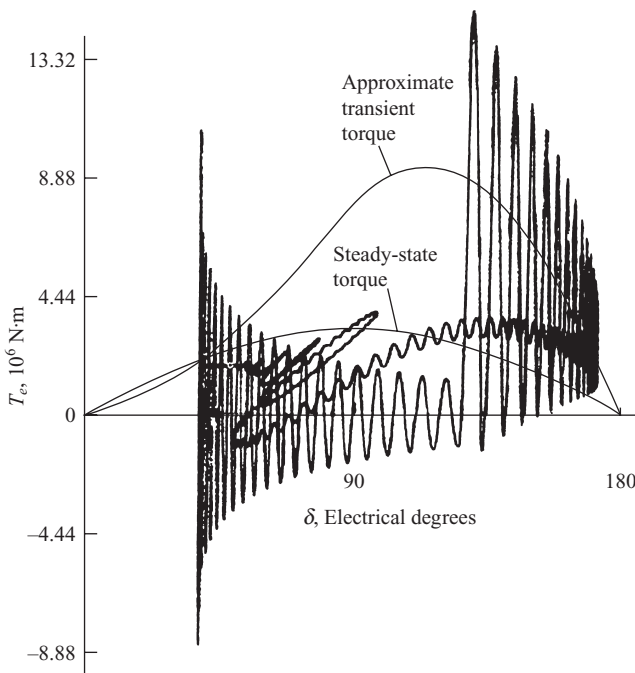


Figure 5.10-20. Comparison of the dynamic torque-angle characteristic during a three-phase fault with the calculated steady-state and approximate transient torque-angle characteristics: hydro turbine generator.



**Figure 5.10-21.** Same as Figure 5.10-20 for a steam turbine generator.

linkages per second during a three-phase fault and subsequent clearing are shown in Figure 5.10-22 for the hydro turbine generator and in Figure 5.10-23 for the steam turbine generator. The corresponding plots of voltages, currents, torque, speed, and rotor angle are shown in Figure 5.10-8 and Figure 5.10-10.

As mentioned earlier, the situation portrayed in this study (Fig. 5.10-8, Fig. 5.10-9, Fig. 5.10-10, Fig. 5.10-11, Fig. 5.10-22, and Fig. 5.10-23) is one where only a slight increase in the fault time would cause the machines to slip poles before returning to synchronous speed. This limiting condition is commonly referred to as the *critical clearing time*, and the corresponding maximum rotor angle attained is called the *critical clearing angle*. In the case of the hydro turbine generator, the critical clearing time and angle were found by trial and error to be 0.466 second and 123°. For the steam turbine generator, these values were found to be 0.362 second and 128°.

During the fault, the average value of the electromagnetic torque is essentially zero since the ohmic losses are small. The approximate transient torque–angle curve during this period is zero since the ohmic losses are neglected. The approximate transient torque–angle curve plotted in Figure 5.10-20 and Figure 5.10-21 applies only before the three-phase fault and after it is cleared. If the approximate transient torque–angle curve accurately portrayed the electromagnetic torque following the fault, the average of the instantaneous torque would traverse back and forth on this torque–angle characteristic until the initial operating condition was reestablished. The approximate characteristic appears to be adequate immediately following the fault when the rotor has reached the maximum angle. Thereafter, the approximation is quite inadequate

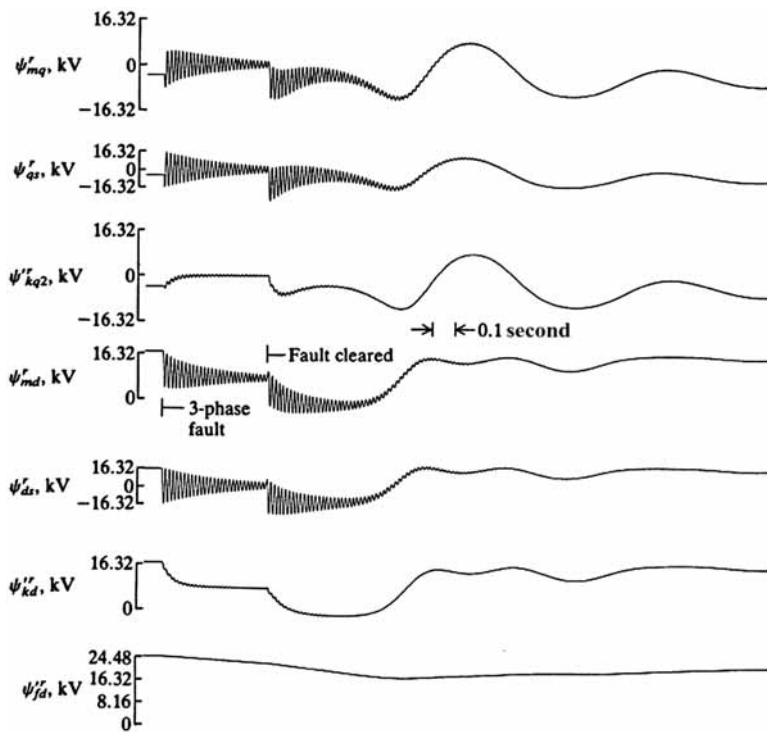


Figure 5.10-22. Traces of flux linkages per second for a hydro turbine generator during a three-phase fault at the terminals.

especially in the case of the steam turbine generator (Fig. 5.10-21). This inaccuracy can of course be contributed primarily to the fact that the average value of the field flux linkages does not remain constant during and following the fault. The change in field flux linkages is less in the case of the hydro unit, and the approximation is more accurate than in the case of the steam unit.

As in the case of a step increase in input torque, the damper winding flux linkages,  $\psi'_{kq1}$ , of the steam unit remains more nearly constant than any of the other machine flux linkages. Although the assumption of constant field flux linkages is by far the most common, there are refinements that can be made to yield the approximate transient torque-angle characteristic more accurately. In particular, it is sometimes assumed that the flux linkages of a  $q$ -axis damper winding also remains constant along with the field flux linkages. A voltage, different from  $E'_q$ , is then calculated behind a transient impedance. We will not consider this or other refinements in this text.

### Equal-Area Criterion

As mentioned previously, the approximate transient torque-angle characteristics along with the equal-area method were used extensively to predict the transient response of

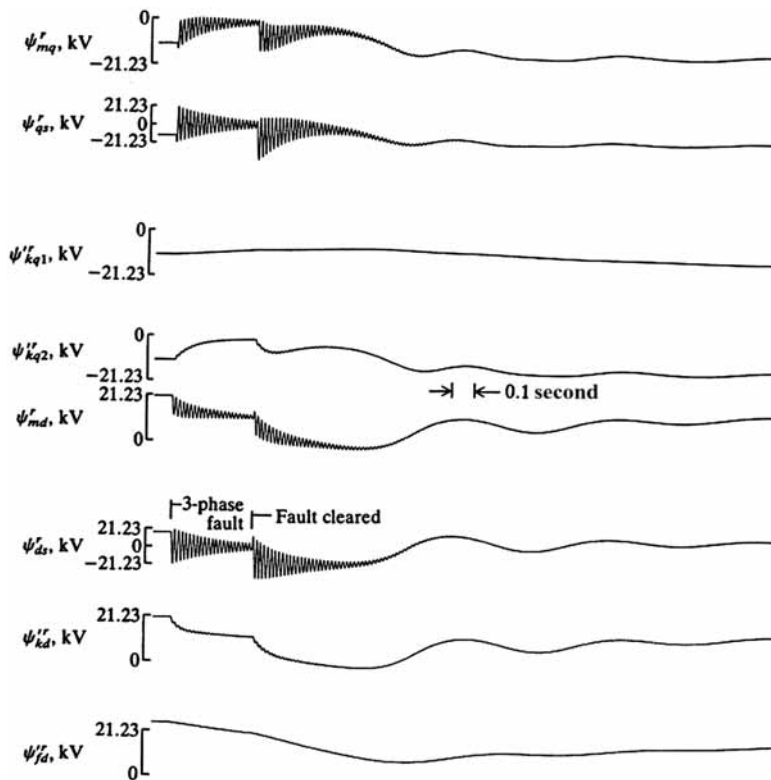


Figure 5.10-23. Same as Figure 5.10-22 for a steam turbine generator.

synchronous machines. In most cases, these concepts were used to determine the transient stability limit and the critical clearing time. The theory underlying the equal-area method as applied to an input torque disturbance or a system fault can be readily established. Regardless of discrepancies or questions that might arise as to the validity of the results, the approximate method of determining the transient torque and the application of the equal-area criterion to predict stability are very useful in understanding the overall dynamic behavior of synchronous machines.

For this development, let us consider the approximate transient torque-angle curve for the hydro turbine generator shown in Figure 5.10-18 and given again in Figure 5.10-24. Consider a sudden step increase in input torque of  $T_I$  from an initial value of zero so as to correspond with our earlier work. This torque level of  $T_I$  is identified by a horizontal line in Figure 5.10-24. At the instant the input torque is applied, the accelerating torque is  $T_I$ , since  $T_e$  is initially zero and the losses are neglected. We see that the accelerating torque on the rotor is positive when  $T_I > T_e$ , where here  $T_e$  is the approximate transient torque-angle curve.

Work or energy is the integral of force times a differential distance or, in the case of a rotational system, the integral of torque times a differential angular displacement. Hence, the energy stored in the rotor during the initial acceleration is

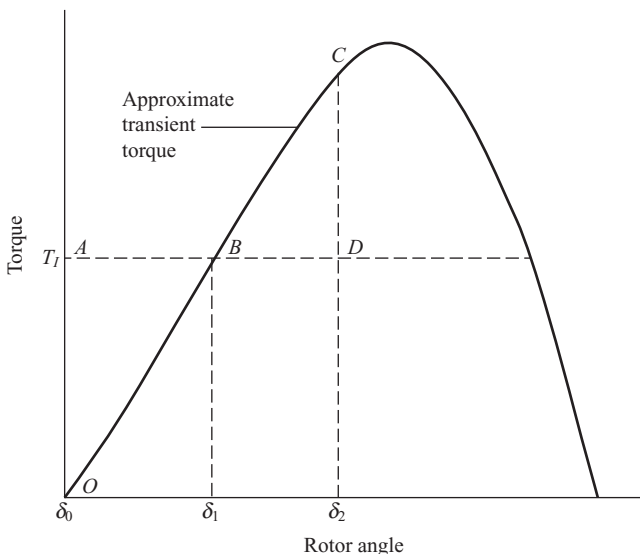


Figure 5.10-24. Equal-area criterion for sudden change in input torque.

$$\int_{\delta_0}^{\delta_1} (T_I - T_e) d\delta = \text{area } OABO \quad (5.10-27)$$

The energy given up by the rotor as it decelerates back to synchronous speed is

$$\int_{\delta_1}^{\delta_2} (T_I - T_e) d\delta = \text{area } BDCB \quad (5.10-28)$$

The maximum angle is reached and the rotor will return to synchronous speed after the application of the input torque when

$$|\text{area } OABO| = |\text{area } BDCB| \quad (5.10-29)$$

It follows that the rotor angle of the synchronous machine would then oscillate back and forth between  $\delta_0$  and  $\delta_2$ . We know, however, that the action of the damper windings will cause these oscillations to subside. One might then be led to believe that the new steady-state operating point would be established at point B. We, of course, know that this is not the case; instead, the new operating point is reestablished on the steady-state torque-angle curve, as illustrated in Figure 5.10-5 and Figure 5.10-7 or Figure 5.10-12 and Figure 5.10-13. We are aware of the limitations of the approximate transient torque-angle curve, and thus any method utilizing this approximation will, at best, be adequate only for the first swing of the rotor from synchronous speed. It is left to the reader to show that the application of equal-area criterion, which involves a graphical solution, gives a transient stability limit of  $T_I = 68.1 \times 10^6 \text{ N}\cdot\text{m}$  for the hydro turbine generator and  $T_I = 4.65 \times 10^6 \text{ N}\cdot\text{m}$  for the steam turbine generator.

It is instructive to compare the “first swing” transient stability limit obtained by means of a computer study for the two machines under consideration with the limits

obtained by applying equal-area criterion. It is recalled that the actual dynamic torque-angle characteristics, which are shown in Figure 5.10-18 and Figure 5.10-19 with the transient torque-angle curve calculated using constant flux linkages superimposed thereon, gave a “first swing” transient stability limit for the hydro turbine generator of  $76.7 \times 10^6 \text{ N}\cdot\text{m}$  and  $5.2 \times 10^6 \text{ N}\cdot\text{m}$  for the steam turbine generator. The maximum torques obtained using the equal-area criterion are approximately 10% less than those obtained from the computer study.

It should also be mentioned that the term involving the  $\sin 2\delta$  is often ignored, and only the  $\sin \delta$  term of (5.10-20) is used to calculate the approximate torque-angle curve. This enables a trial-and-error analytical solution, and in this case, it is a closer approximation. In particular, this method yields a transient stability limit of  $71.2 \times 10^6 \text{ N}\cdot\text{m}$  for the hydro turbine generator and  $5.03 \times 10^6 \text{ N}\cdot\text{m}$  for the steam turbine generator.

The approximate transient torque-angle curve along with the equal-area criterion is most often used to predict the large excursion dynamic behavior of a synchronous machine during a system fault. The application of the equal-area method during a three-phase system fault can be described by considering the approximate transient torque-angle curve of the hydro unit given in Figure 5.10-25. Assume that the input torque  $T_I$  is constant and the machine is operating steadily, delivering power to the system with a rotor angle  $\delta_0$ . When the three-phase fault occurs at the terminals, the power output drops to zero and thus the approximate  $T_e$  is zero since the resistances are neglected. The machine accelerates with the total input torque as the accelerating torque. The fault is cleared at  $\delta_1$  and, in this case, the torque immediately becomes the value of the

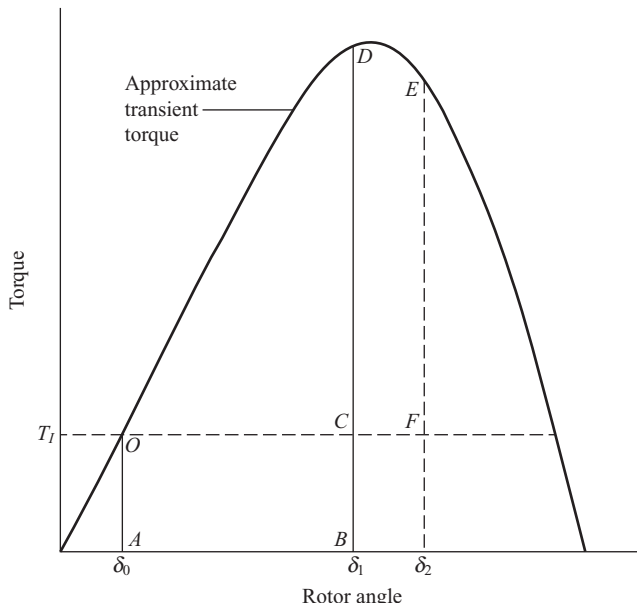


Figure 5.10-25. Equal-area criterion for a three-phase fault at the terminals.

approximate transient torque (point  $D$  in Fig. 5.10-25). The energy stored in the rotor during the acceleration or advance in angle from  $\delta_0$  to  $\delta_1$  is

$$\int_{\delta_0}^{\delta_1} (T_I - T_e) d\delta = \text{area } OABCO \quad (5.10-30)$$

where  $T_e$  is zero and  $T_I$  is constant.

After the clearing of the fault, the rotor decelerates back to synchronous speed. The energy given up by the rotor during this time is

$$\int_{\delta_1}^{\delta_2} (T_I - T_e) d\delta = \text{area } CDEF \quad (5.10-31)$$

The maximum rotor angle is reached when

$$|\text{area } OABCO| = |\text{area } CDEF| \quad (5.10-32)$$

The critical clearing angle is reached when any future increase in  $\delta_1$  causes the total area representing decelerating energy to become less than the area representing the accelerating energy. This occurs when  $\delta_2$ , or point  $F$ , is at the intersection of  $T_I$  and  $T_e$ .

The clearing time may be calculated from the clearing angle by using (5.10-5), which may be written

$$\delta_1 - \delta_0 = \frac{\omega_b}{2H} \int_{t_0}^{t_1} \int_{t_0}^{\tau} (T_I - T_e) dt d\tau \quad (5.10-33)$$

If, as in this example,  $T_e = 0$  and  $T_I$  is a constant during the fault and with  $t_0 = 0$ , the clearing time  $T_I$  becomes

$$t_1 = \sqrt{\frac{(\delta_1 - \delta_2)4H}{\omega_b T_I}} \quad (5.10-34)$$

It is recalled that the critical clearing times and angles obtained by computer study were 0.466 seconds and  $123^\circ$  for the hydro unit and 0.362 seconds and  $128^\circ$  for the steam unit. These values compare with 0.41 seconds and  $122^\circ$  for the hydro unit and 0.33 seconds and  $128^\circ$  for the steam unit, obtained by a graphical application of the method of equal area. Since the critical clearing angles were found to be essentially the same by both methods, the larger critical clearing times can be attributed to the power lost in the resistance during the fault. The accuracy of the approximate method is indeed surprising; a result that should not be taken as an indication that the approximate method is highly accurate in general.

As mentioned previously, the  $\sin 2\delta$  terms are often ignored in the approximate transient torque-angle characteristics. With the machine operating under load, ignoring the  $\sin 2\delta$  term yields a fictitious initial rotor angle. Although this leads to a simplified method of solution and even though it was used widely in the past, we will not consider it in this text. Actually, sufficient background has been established so that the reader can readily develop this technique if the need arises.

## 5.11. COMPUTER SIMULATION

There are two general types of computer simulations of a synchronous machine that we will consider. The simulation used most widely is derived from the voltage equations expressed in the rotor reference frame with the equations with stator and rotor flux linkages as state variables. This simulation was first developed by C.H. Thomas [8]. The second type of simulation that we will develop is one wherein the stator flux linkages per second are calculated in the arbitrary reference frame with the rotor flux linkages per second computed in the rotor reference frame. The simulation derivation is performed assuming that the positive direction of stator current is into the machine. For positive current assumed out of the machine, one could change the sign of the currents within the computer simulation. However, it would be much easier to follow the method of simulation given for positive current into the machine and simply change the sign of the stator currents when simulating the connection of the machine to the network. Similarly, the sign of  $T_e$  would simply be reversed when calculating rotor speed from (5.10-3)–(5.10-5).

### Simulation in Rotor Reference Frame

The voltage equations expressed in the rotor reference frame are given by (5.5-22)–(5.5-28) with the equations defining the flux linkages per second given by (5.5-29)–(5.5-35). Defining  $q$ - and  $d$ -axis magnetizing flux linkages

$$\psi_{mq}^r = X_{mq}(i_{qs}^r + i_{kq1}^r + i_{kq2}^r) \quad (5.11-1)$$

$$\psi_{md}^r = X_{md}(i_{ds}^r + i_{fd}^r + i_{kd}^r) \quad (5.11-2)$$

and using (5.11-1) and (5.11-2) in (5.5-29)–(5.5-35), the winding currents can be expressed in terms of winding and magnetizing flux linkages as

$$i_{qs}^r = \frac{1}{X_{ls}}(\psi_{qs}^r - \psi_{mq}^r) \quad (5.11-3)$$

$$i_{ds}^r = \frac{1}{X_{ls}}(\psi_{ds}^r - \psi_{md}^r) \quad (5.11-4)$$

$$i_{0s} = \frac{1}{X_{ls}}\psi_{0s} \quad (5.11-5)$$

$$i_{kq1}^r = \frac{1}{X'_{lkq1}}(\psi'_{kq1}^r - \psi_{mq}^r) \quad (5.11-6)$$

$$i_{kq2}^r = \frac{1}{X'_{lkq2}}(\psi'_{kq2}^r - \psi_{mq}^r) \quad (5.11-7)$$

$$i'_{fd} = \frac{1}{X'_{lfd}} (\psi'_{fd} - \psi_{md}^r) \quad (5.11-8)$$

$$i'_{kd} = \frac{1}{X'_{lkd}} (\psi'_{kd} - \psi_{md}^r) \quad (5.11-9)$$

Substituting (5.11-3)–(5.11-9) into (5.5-22)–(5.5-28) yields the state equations of the stator and rotor windings:

$$\psi_{qs}^r = \frac{\omega_b}{p} \left[ v_{qs}^r - \frac{\omega_r}{\omega_b} \psi_{ds}^r + \frac{r_s}{X_{ls}} (\psi_{mq}^r - \psi_{qs}^r) \right] \quad (5.11-10)$$

$$\psi_{ds}^r = \frac{\omega_b}{p} \left[ v_{ds}^r + \frac{\omega_r}{\omega_b} \psi_{qs}^r + \frac{r_s}{X_{ls}} (\psi_{md}^r - \psi_{ds}^r) \right] \quad (5.11-11)$$

$$\psi_{0s} = \frac{\omega_b}{p} \left[ v_{0s} - \frac{r_s}{X_{ls}} \psi_{0s} \right] \quad (5.11-12)$$

$$\psi'_{kq1} = \frac{\omega_b}{p} \left[ v'_{kq1} + \frac{r'_{kq1}}{X'_{lkq1}} (\psi_{mq}^r - \psi'_{kq1}) \right] \quad (5.11-13)$$

$$\psi'_{kq2} = \frac{\omega_b}{p} \left[ v'_{kq2} + \frac{r'_{kq2}}{X'_{lkq2}} (\psi_{mq}^r - \psi'_{kq2}) \right] \quad (5.11-14)$$

$$\psi'_{fd} = \frac{\omega_b}{p} \left[ \frac{r'_{fd}}{X_{md}} e'_{xfd} + \frac{r'_{fd}}{X'_{lfd}} (\psi_{md}^r - \psi'_{fd}) \right] \quad (5.11-15)$$

$$\psi'_{kd} = \frac{\omega_b}{p} \left[ v'_{kd} + \frac{r'_{kd}}{X'_{lkd}} (\psi_{md}^r - \psi'_{kd}) \right] \quad (5.11-16)$$

It is noted that to have a proper state model, the magnetizing flux linkages are expressed in terms of winding flux linkages (states) by substituting (5.11-3)–(5.11-9) into (5.11-1) and (5.11-2), which after manipulating, yields

$$\psi_{mq}^r = X_{aq} \left( \frac{\psi_{qs}^r}{X_{ls}} + \frac{\psi'_{kq1}}{X'_{lkq1}} + \frac{\psi'_{kq2}}{X'_{lkq2}} \right) \quad (5.11-17)$$

$$\psi_{md}^r = X_{ad} \left( \frac{\psi_{ds}^r}{X_{ls}} + \frac{\psi'_{fd}}{X'_{lfd}} + \frac{\psi'_{kd}}{X'_{lkd}} \right) \quad (5.11-18)$$

where

$$X_{aq} = \left( \frac{1}{X_{mq}} + \frac{1}{X_{ls}} + \frac{1}{X'_{lkq1}} + \frac{1}{X'_{lkq2}} \right)^{-1} \quad (5.11-19)$$

$$X_{ad} = \left( \frac{1}{X_{md}} + \frac{1}{X_{ls}} + \frac{1}{X'_{lfd}} + \frac{1}{X'_{lkd}} \right)^{-1} \quad (5.11-20)$$

If saturation is to be taken into account, the torque equation, which may be used in the simulation, is (5.6-4) or the per unitized version given by (5.8-2). The per unit rotor speed is obtained from (5.10-4) as

$$\omega_r = -\frac{\omega_b}{2H_p}(T_e - T_I) \quad (5.11-21)$$

Block diagrams showing the computer simulation of a synchronous machine in the rotor reference frame are shown in Figure 5.11-1. The equations used to perform

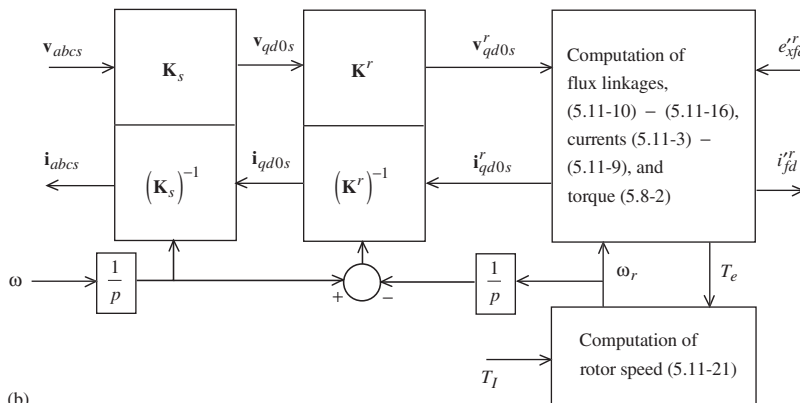
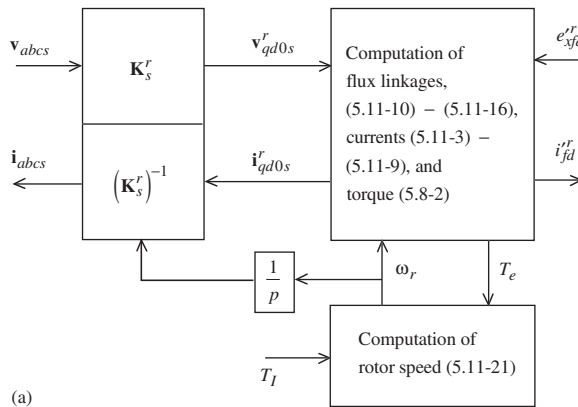


**Figure 5.11-1.** Simulation of a synchronous machine in the rotor reference frame shown in block diagram form. (a)  $abc$  variables transformed directly to the rotor reference frame; (b)  $abc$  variables transformed to arbitrary reference frame then to rotor reference frame.

the computations are indicated by number. The voltages applied to the damper windings are not shown since these windings are always short-circuited and the voltages are zero. The two simulations shown in Figure 5.11-1 differ only in the way that  $\mathbf{v}_{qd0s}^r$  is obtained. In Figure 5.11-1a,  $\mathbf{v}_{abcs}$  is transformed directly to  $\mathbf{v}_{qd0s}^r$ ; in Figure 5.11-1b,  $\mathbf{v}_{abcs}$  is first transformed to the arbitrary reference frame and then to the rotor reference frame.

### Simulation with Stator Voltage Equations in Arbitrary Reference Frame

A synchronous machine simulation that has found some use is one where the stator voltage equations are simulated in a reference frame other than the rotor reference frame. Either the stationary or synchronous reference frame is used; however, we will develop the simulation of stator equations in the arbitrary reference frame which, of course, encompasses all reference frames. The stator voltage equations in the arbitrary reference frame are given by (5.4-1). The integral equations in terms of flux linkages per second may be written as

$$\psi_{qs} = \frac{\omega_b}{p} \left[ v_{qs} - \frac{\omega}{\omega_b} \psi_{ds} - r_s i_{qs} \right] \quad (5.11-22)$$

$$\psi_{ds} = \frac{\omega_b}{p} \left[ v_{ds} + \frac{\omega}{\omega_b} \psi_{qs} - r_s i_{ds} \right] \quad (5.11-23)$$

$$\psi_{0s} = \frac{\omega_b}{p} (v_{0s} - r_s i_{0s}) \quad (5.11-24)$$

Here, we have not substituted for the currents as in the previous formulation. Instead,  $\psi_{qs}$  and  $\psi_{ds}$  are computed and transformed to the rotor reference frame, whereupon  $i_{qs}^r$  and  $i_{ds}^r$  are calculated and transformed back to the arbitrary reference frame. It is clear that

$$i_{0s} = \frac{\psi_{0s}}{X_{ls}} \quad (5.11-25)$$

This type of computer simulation is depicted in Figure 5.11-2. Only the rotor flux linkage equations are calculated in the rotor reference frame; (5.11-10)–(5.11-12) are not used. The transformation from the arbitrary reference frame to the rotor reference frame is performed by implementing (3.10-7) with the zero quantities omitted. As mentioned, the stator equations are generally simulated either in the stationary reference frame or in the synchronously rotating reference frame. The transformation between the synchronous reference frame and the rotor reference frame may be written in terms of the rotor angle  $\delta$ . This transformation may be obtained from (3.10-7) or it is given by (5.7-3).

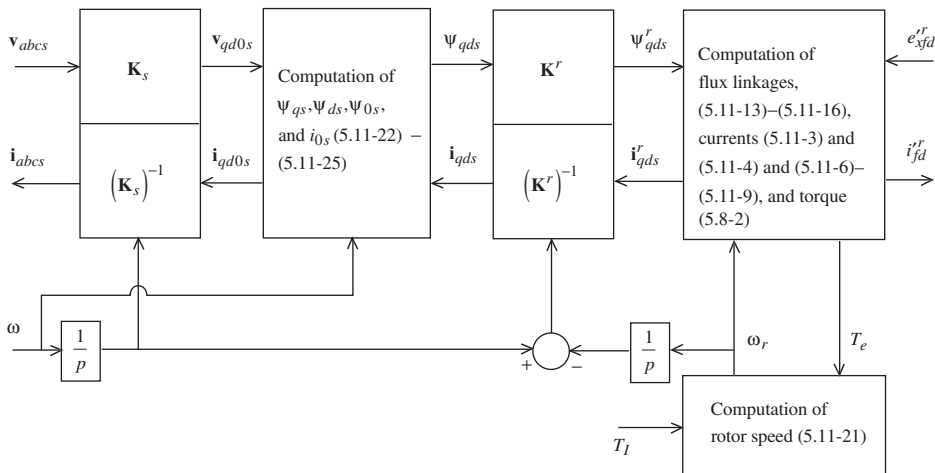


**Figure 5.11-2.** Block diagram of the simulation of a synchronous machine with stator voltage equations in the arbitrary reference frame.

## Simulation of Saturation

A method of simulating the effects of saturation in the direct axis of a synchronous machine was developed by C.H. Thomas [8]. In the case of salient pole machines, it is often sufficient to represent saturation only in the direct axis; however, in the case of round rotor machines (induction or synchronous), saturation should be represented in both axes. Thomas' method will be presented and then extended to include saturation in both axes of a round rotor machine.

The open-circuit test of a synchronous machine gives us a plot of the open-circuit terminal voltage versus field current as shown in Figure 5.11-3a. Therein the straight-line relation between the stator terminal voltage and field current is referred to as the air-gap line. Since the terminals are open-circuited, the stator currents are zero, therefore  $\psi_{qs}^r$  and  $v_{ds}^r$  are zero. Hence,  $v_{qs}^r$  is equal to the peak value of the line-to-neutral open-circuit stator voltage. Moreover,  $v_{qs}^r$  is equal to  $\psi_{ds}^r$ , which is  $\psi_{md}^r$ , since the stator currents are zero. Thus,  $V_t$  in Figure 5.11-3a may be replaced by  $\psi_{md}^r$ . Now, the current along the  $x$ -axis of the open-circuit characteristics is  $i_{fd}^{rr}$ ; however, this same characteristic would occur regardless of the current flowing in the magnetizing reactance. Hence,  $i_{fd}^{rr}$  may be replaced by the sum of  $i_{ds}^{rr} + i_{fd}^{rr} + i_{kd}^{rr}$ , which are the  $d$ -axis currents. It follows that Figure 5.11-3a,b are identical.

It is convenient to plot the saturation curve shown in Figure 5.11-3b with the scale in the  $x$ -axis selected so that the air-gap line is at a  $45^\circ$  angle as shown in Figure 5.11-4. The point that 1.0 per unit  $\psi_{md}^r$  intersects the air-gap line is 1.0 per unit  $X_{md}(i_{ds}^r + i_{fd}^r + i_{kd}^r)$ . Note from Figure 5.11-4 that we can write

$$X_{md}(i_{ds}^r + i_{fd}^r + i_{kd}^r) - f(\psi_{md}^r) \quad (5.11-26)$$

where  $f(\psi_{md}^r)$  is defined in Figure 5.11-4. Therefore, saturation may be simulated by replacing (5.11-18) with (5.11-26) in the computer simulation. However, before this

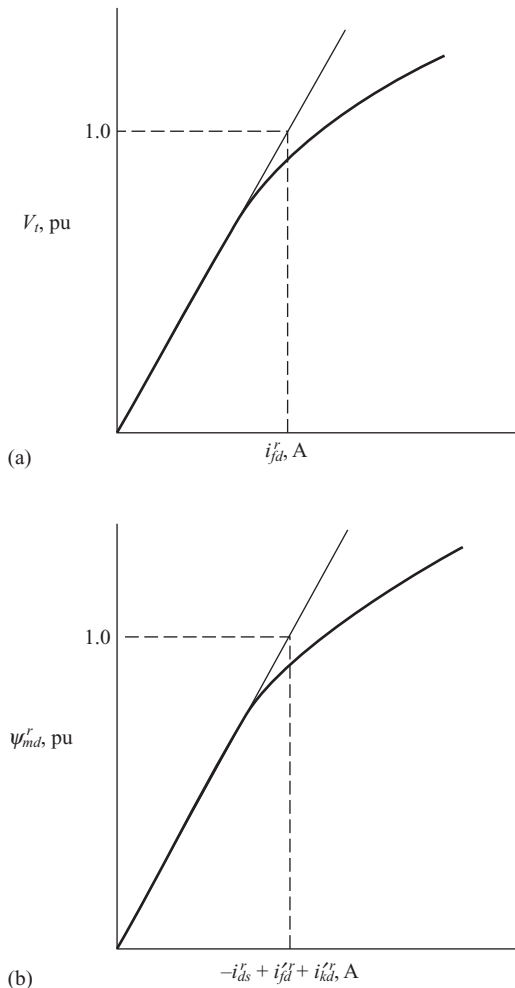


Figure 5.11-3. Saturation characteristics of a synchronous machine. (a) Open-circuited terminal voltage versus field current; (b) equivalent to characteristics shown in (a).

can be done, we must first obtain  $f(\psi_{md}^r)$ . This, of course, can be accomplished directly from Figure 5.11-4, and it is shown in Figure 5.11-5. Next, the currents in (5.11-26) must be replaced by flux linkages per second. This leads to

$$\psi_{md}^r = X_{ad} \left( \frac{\psi_{ds}^r}{X_{ls}} + \frac{\psi_{fd}^r}{X_{lfd}'} + \frac{\psi_{kd}^r}{X_{lkd}'} \right) - \frac{X_{ad}}{X_{md}} f(\psi_{md}^r) \quad (5.11-27)$$

where  $X_{ad}$  is defined by (5.11-20). Therefore, saturation in the direct axis of a synchronous machine is simulated by using a means of function generation to generate  $f(\psi_{md}^r)$  and replacing (5.11-18) with (5.11-27).

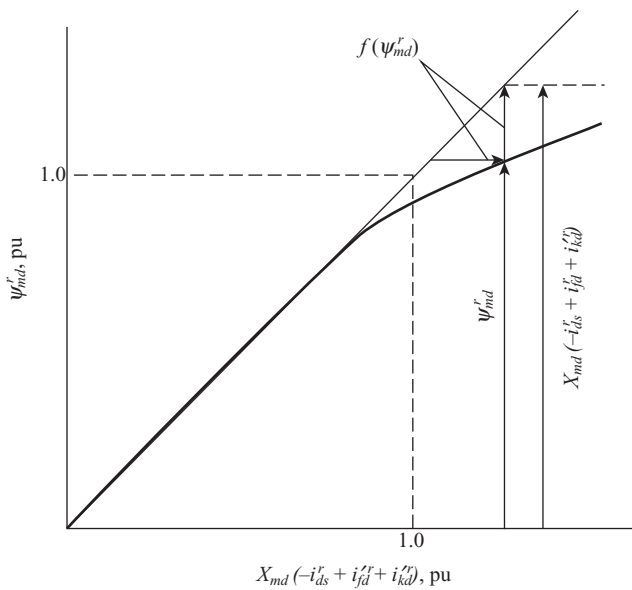


Figure 5.11-4. Saturation curve with flux linkages per second as variables.

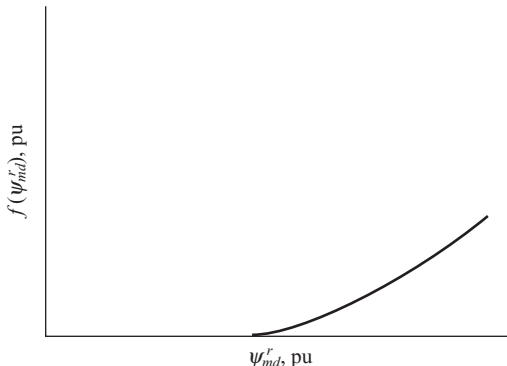


Figure 5.11-5. Plot of  $\Delta\psi_{md}^r$  obtained from Figure 5.11-4.

A computer simulation of saturation in both axes of a round rotor machine, synchronous or induction, has been set forth by D.M. Triezenberg [9]. For this development, let us consider the diagram shown in Figure 5.11-6. The values of the variables shown are for a given instant of time. From Figure 5.11-6

$$\psi_m^r = [(\psi_{mq}^r)^2 + (\psi_{md}^r)^2]^{1/2} \quad (5.11-28)$$

$$f(\psi_{mq}^r) = \frac{\psi_{mq}^r}{\psi_m^r} f(\psi_m^r) \quad (5.11-29)$$

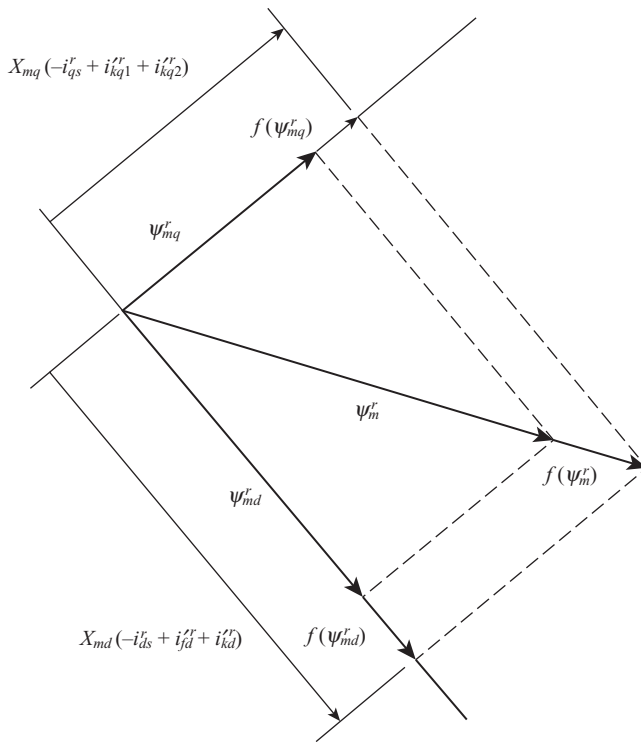


Figure 5.11-6. Saturation in both axes of a synchronous machine.

$$f(\psi_{md}^r) = \frac{\psi_{md}^r}{\psi_m^r} f(\psi_m^r) \quad (5.11-30)$$

If, in the case of a round rotor synchronous machine, the open-circuit saturation curve approximates the magnetic characteristics of the rotor regardless if the MMF is directed along the  $q$ - or  $d$ -axis or anywhere in between, then Figure 5.11-5 also describes the relationship between  $f(\psi_m^r)$  and  $\psi_m^r$ . Actually, it is convenient to use  $f(\psi_m^r) / \psi_m^r$  rather than  $f(\psi_m^r)$  as the ordinate when representing saturation in both axes. Also, it is convenient to plot  $f(\psi_m^r) / \psi_m^r$  versus  $(\psi_m^r)^2$ , which eliminates the need to perform the square root of (5.11-28) in order to obtain  $\psi_m^r$ . A block diagram depicting this method of representing saturation in both axes is shown in Figure 5.11-7. The expression for  $\psi_{md}^r$  is given by (5.11-27);  $\psi_{mq}^r$  now becomes

$$\psi_{mq}^r = X_{aq} \left( \frac{\psi_{qs}^r}{X_{ls}} + \frac{\psi'_{kq1}^r}{X'_{lkq1}} + \frac{\psi'_{kq2}^r}{X'_{lkq2}} \right) - \frac{X_{aq}}{X_{mq}} f(\psi_{mq}^r) \quad (5.11-31)$$

where  $X_{aq}$  is defined by (5.11-19).

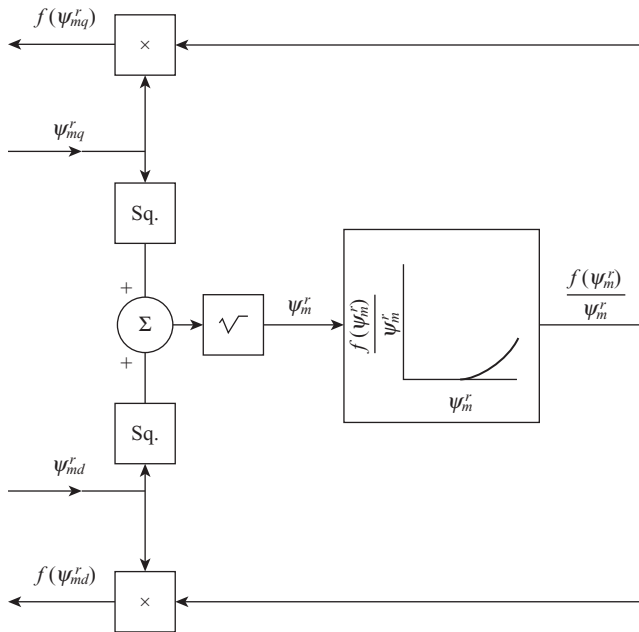


Figure 5.11-7. Simulation of saturation in both axes of a round rotor synchronous machine.

### Simulation of Balanced Conditions

Any of the simulations given in Figure 5.11-1 and Figure 5.11-2 may be used to represent balanced or symmetrical conditions. However, a simplified version of Figure 5.11-1b is probably most widely used. If it is necessary to have the stator phase variables available, then the synchronously rotating reference frame ( $\omega = \omega_e$ ) is convenient especially in the simulation of large power systems. The transformation of the variables from the synchronously rotating reference frame to the rotor reference frame is performed using the rotor angle  $\delta$  in the transformation given by (3.10-7) or (5.7-3). It is clear that the simulation given in Figure 5.11-2 may also be used in a similar manner; the only difference is that  $\psi_{qs}^e$  and  $\psi_{ds}^e$  would be computed in the synchronously rotating reference frame and transformed to the rotor reference frame rather than transforming voltages as in Figure 5.11-1b.

### Simulation of Unbalanced Stator Conditions

Since the rotor flux linkages are computed in the rotor reference frame, the simulation of various modes of operation of a synchronous machine is somewhat more difficult than in the case of the induction machine, which may be simulated in any reference frame. This is especially true when it is desirable to represent unbalanced or discontinuous stator operation, and in some cases, approximations are helpful in order to make the simulation manageable.

Perhaps the simulations shown in Figure 5.11-1a and Figure 5.11-2 offer the most convenient means of representing a synchronous machine during unbalanced stator conditions. It is generally advantageous to represent unbalanced or discontinuous stator conditions in *abc* variables. If the simulation given in Figure 5.11-1a is used, the stator voltages and currents are transformed between the stationary and rotor reference frames. If the simulation given in Figure 5.11-2 is used,  $\omega$  is set equal to zero, and the flux linkages per second  $\psi_{qs}^s$  and  $\psi_{ds}^s$  are computed in the stationary reference frame and then transformed to the rotor reference frame. Asynchronous and unbalanced operation, including motor starting and pole slipping, as well as line-to-neutral, line-to-line, and line-to-line-to-neutral faults, are all demonstrated and simulated in chapters 10 and 12 of Reference 6.

## REFERENCES

- [1] R.H. Park, "Two-Reaction Theory of Synchronous Machines—Generalized Method of Analysis—Part I," *AIEE Trans.*, Vol. 48, July 1929, pp. 716–727.
- [2] D.R. Brown and P.C. Krause, "Modeling of Transient Electrical Torques in Solid Iron Rotor Turbogenerators," *IEEE Trans. Power Apparatus Syst.*, Vol. 98, September/October 1979, pp. 1502–1508.
- [3] P.C. Krause, F. Nozari, T.L. Skvarenina, and D.W. Olive, "The Theory of Neglecting Stator Transients," *IEEE Trans. Power Apparatus Syst.*, Vol. 98, January/February 1979, pp. 141–148.
- [4] H. Bai, S.D. Pekarek, J. Tichenor, W. Eversman, D.J. Buening, G.R. Holbrook, and R.J. Krefta, "Incorporating the Effects of Magnetic Saturation in a Coupled-Circuit Model of a Claw–Pole Alternator," *IEEE Trans. Energy Convers.*, Vol. 22, No. 2, June 2007, pp. 290–298.
- [5] C.M. Ong, *Dynamic Simulation of Electric Machinery*, Prentice-Hall, PTR, Upper Saddle River, NJ, 1998.
- [6] P.C. Krause, O. Waszczuk, and S.D. Sudhoff, *Analysis of Electric Machinery*, IEEE Press, Piscataway, NJ, 1995.
- [7] R.E. Doherty and C.A. Nickle, "Synchronous Machines—III, Torque-Angle Characteristics Under Transient Conditions," *AIEE Trans.*, Vol. 46, January 1927, pp. 1–8.
- [8] C.H. Thomas, "Discussion of 'Analogue Computer Representations of Synchronous Generators in Voltage-Regulation Studies'," *Trans. AIEE Power Apparatus Syst.*, Vol. 75, December 1956, pp. 1182–1184.
- [9] D.M. Triezenberg, Private Communications with Authors, 1977.

## PROBLEMS

1. A two-pole, two-phase, salient-pole synchronous machine is shown in Figure 5P-1. In case of a two-phase machine, the magnetizing inductances are defined as

$$L_{mq} = L_A - L_B$$

$$L_{md} = L_A + L_B$$

Derive the voltage equations in machine variables similar in form to (5.2-29). Express all resistance and inductance matrices.

2. In the case of a three-phase synchronous machine,  $L_{mq}$  and  $L_{md}$  are defined with a  $3/2$  factor. This factor is unity in the case of the two-phase machine. Why?
3. Modify (5.2-29) to describe a three-phase round rotor synchronous machine.
4. Modify (5.2-29) to describe a three-phase reluctance machine. Assume the  $fd$  and  $kq1$  windings are not present and denote the  $kq2$  winding as simply the  $kq$  winding. Also, assume positive stator currents flow into the machine.
5. Justify that (5.3-3) will be positive for positive currents assumed out of the machine if the sign of the coefficients of  $\sin 2\theta_r$  and  $\cos 2\theta_r$  are changed.
6. Derive the expression for electromagnetic torque in machine variables for the two-phase synchronous machine shown in Figure 5P-1.
7. Determine  $\mathbf{K}_s \mathbf{L}_s (\mathbf{K}_s)^{-1}$  given in (5.4-4). Show that it is independent of  $\theta$  and  $\theta_r$  only if  $\theta = \theta_r$ .
8. Repeat Problem 7 for  $(\mathbf{L}'_{sr})^T (\mathbf{K}_s)^{-1}$ .
9. Show that if the arbitrary reference-frame variables given in (5.4-4) are transformed to the rotor reference frame, (5.5-4) results if  $\theta = \theta_r$ . Is this also true if only  $\omega = \omega_r$ ? Why?
10. Verify (5.5-5)–(5.5-7).
11. Derive Park's equation for the two-pole, two-phase, salient-pole synchronous machine shown in Figure 5P-1. Express the final equations in terms of flux linkages per second in a form similar to (5.5-22)–(5.5-35).
12. Modify Park's equations, (5.5-22)–(5.5-35), to describe a three-phase reluctance machine with the rotor winding arrangement as indicated in Problem 4. Assume positive stator currents flow into the machine.
13. Derive (5.6-1).
14. Using the results of Problem 6, derive the expression for the electromagnetic torque for a two-pole, two-phase salient-pole synchronous machine (Fig. 5P-1) in the form similar to (5.6-4).
15. Consider the hydro turbine generator given in Section 5.10. Select the rated MVA as the base power. Determine the base voltage, base current, and base impedance. Check the parameters given in per unit.
16. Repeat Problem 15 for the steam turbine generator given in Section 5.10.
17. Derive the steady-state voltage equation for the synchronous machine (5.9-19). In the derivation, use the stator voltage equations expressed in the arbitrary reference frame.
18. A four-pole, three-phase, salient-pole synchronous machine is supplied from a 440 volt (rms) line-to-line, 60Hz source. The machine is operated as a motor with the total input power of 40kW at the terminals. The parameters are

$$r_s = 0.3 \Omega \quad L_{md} = 0.015 \text{ H}$$

$$L_{ls} = 0.001 \text{ H} \quad L_{mq} = 0.008 \text{ H}$$

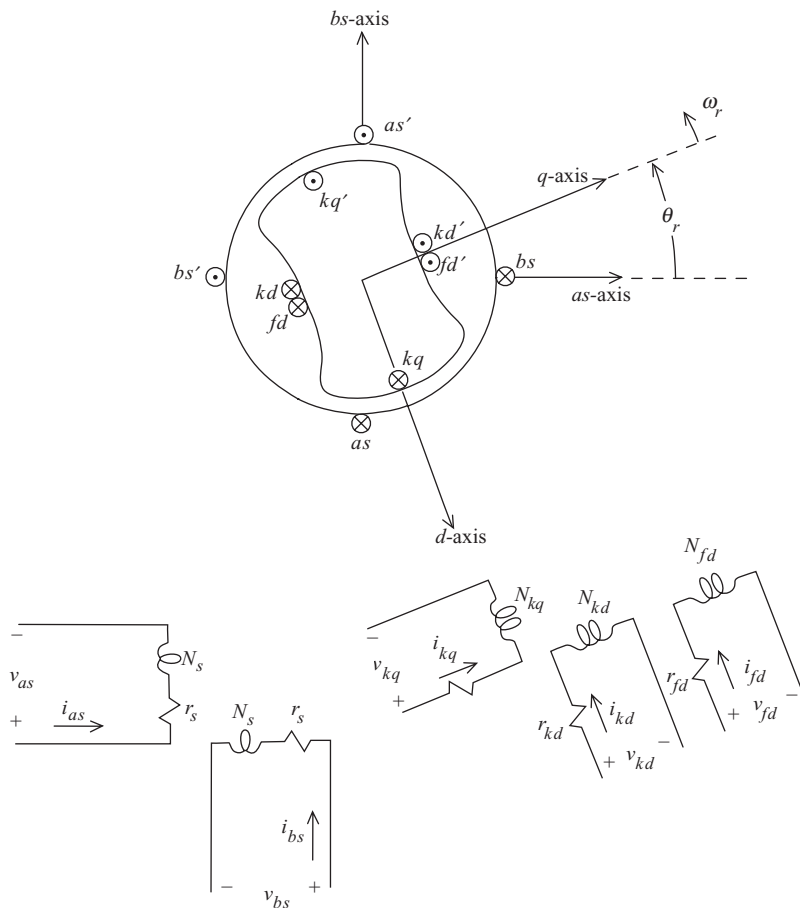


**Figure 5P-1.** Two-pole, two-phase, salient-pole synchronous machine.

Assume the positive direction of current is into the stator terminals.

- The excitation is adjusted so that  $\tilde{I}_{as}$  lags  $\tilde{V}_{as}$  by  $30^\circ$ . Calculate  $\tilde{E}_a$  and the reactive power  $Q$ . Draw the phasor diagram.
  - Repeat *a* with the excitation adjusted so that  $\tilde{I}_{as}$  is in phase with  $\tilde{V}_{as}$ .
  - Repeat *a* with the excitation adjusted so that  $\tilde{I}_{as}$  leads  $\tilde{V}_{as}$  by  $30^\circ$ .
19. A two-pole, 220-V(rms, line-to-line), 5-hp, three-phase reluctance machine has the following parameters

$$r_s = 1 \Omega \quad L_{md} = 0.10 \text{ H} \\ L_{ls} = 0.005 \text{ H} \quad L_{mq} = 0.02 \text{ H}$$

- The machine is supplied from 60-Hz, 220-V source with zero load torque. Calculate  $\delta$  and  $\tilde{I}_{as}$ .
- Repeat *a* with the machine connected to a 6-Hz, 22-V source.

20. The line-to-neutral voltage of phase  $a$  at one end of a three-phase transmission line is  $\tilde{V}_{a1} = V_1/\theta_1$ . At the other end,  $\tilde{V}_{a2} = V_2/\theta_2$ . The per phase impedance of the transmission line is  $X_l$ . Derive an expression for the steady-state power flowing over the transmission line in terms of  $V_1$ ,  $V_2$ ,  $\theta_1$ ,  $\theta_2$ , and  $X_l$ .
21. The stator terminals of two synchronous machines are connected in a phase-to-phase arrangement. Let  $\tilde{E}_{a1} = E_{a1}/\delta_1$  and  $\tilde{E}_{a2} = E_{a2}/\delta_2$ . Derive an expression for the steady-state power flowing between the two machines in terms of  $E_{a1}$ ,  $E_{a2}$ ,  $\delta_1$ ,  $\delta_2$ , and the appropriate reactances of each machine. Neglect the stator resistance of both machines.
22. Calculate the steady-state  $\tilde{I}_{as}$  and  $\delta$  for the hydro turbine generator for the final operating condition depicted in Figure 5.10-4 and Figure 5.10-5.
23. Repeat Problem 22 for the final operating conditions for the steam turbine generator depicted in Figure 5.10-6 and Figure 5.10-7.
24. Calculate the maximum steady-state torque that the steam turbine generator can deliver to an infinite bus with the excitation adjusted to produce rated open-circuit terminal voltage. Sketch the torque versus rotor angle response if a torque slightly larger than this maximum value is suddenly applied to the unloaded machine when connected to an infinite bus.
25. Calculate the initial, prefault values of all variables of the hydro turbine generator for the condition shown in Figure 5.10-8.
26. Calculate the initial, prefault values of all variables of the steam turbine generator for the condition shown in Figure 5.10-10.
27. Show that the rotor angle at which maximum steady-state torque occurs is

$$\cos \delta = -\frac{X_q E'_{xd}'}{4(X_d - X_q)V_s} \pm \sqrt{\left[ \frac{X_q E'_{xd}'}{4(X_d - X_q)V_s} \right]^2 + \frac{1}{2}}$$

where all values are in per unit and generally only the positive value of the radical is used.

28. Derive an expression similar to that given in Problem 27 for the rotor angle at which maximum transient torque occurs as predicted by the approximate transient torque-angle characteristic. Check the values of rotor angle at maximum transient torque for the hydro turbine generator shown in Figure 5.10-18 and for the steam turbine generator shown in Figure 5.10-19.
29. Calculate the prefault values of the flux linkages per second for the hydro turbine generator shown in Figure 5.10-22.
30. Calculate the prefault values of the flux linkages per second for the steam turbine generator shown in Figure 5.10-23.
31. Check the values given in Section 5.10 for the “first swing” transient stability limit of the hydro and steam units using both the  $\sin \delta$  and  $\sin 2\delta$  terms of the approximate transient torque-angle curve.
32. Repeat Problem 31 with the  $\sin 2\delta$  terms omitted.

33. Check the values of critical clearing time and critical clearing angle given in Section 5.10 for the hydro and steam units using the approximate transient torque–angle curve.
34. Determine the critical clearing time and critical clearing angle for the hydro and steam units using only the  $\sin\delta$  terms of the approximate transient torque–angle curve.

---

# 6

---

# SYMMETRICAL INDUCTION MACHINES

---

## 6.1. INTRODUCTION

The induction machine is used in a wide variety of applications as a means of converting electric power to mechanical work. It is without doubt the workhorse of the electric power industry. Pump, steel mill, and hoist drives are but a few applications of large multiphase induction motors. On a smaller scale, induction machines are used as the controlled drive motor in vehicles, air conditioning systems, and in wind turbines, for example. Single-phase induction motors are widely used in household appliances, as well as in hand and bench tools.

In the beginning of this chapter, classical techniques are used to establish the voltage and torque equations for a symmetrical induction machine expressed in terms of machine variables. Next, the transformation to the arbitrary reference frame presented in Chapter 3 is modified to accommodate rotating circuits. Once this groundwork has been laid, the machine voltage equations are written in the arbitrary reference frame directly without a laborious exercise in trigonometry that one faces when substituting the equations of transformations into the voltage equations expressed in machine variables. The equations may then be expressed in any reference frame by appropriate assignment of the reference-frame speed in the arbitrary reference-frame

---

*Analysis of Electric Machinery and Drive Systems*, Third Edition. Paul Krause, Oleg Waszynczuk, Scott Sudhoff, and Steven Pekarek.

© 2013 Institute of Electrical and Electronics Engineers, Inc. Published 2013 by John Wiley & Sons, Inc.

voltage equations. Although the stationary reference frame, the reference frame fixed in the rotor, and the synchronously rotating reference frame are the most frequently used, the arbitrary reference frame offers a direct means of obtaining the voltage equations in these and all other reference frames.

The steady-state voltage equations for an induction machine are obtained from the voltage equations in the arbitrary reference frame by direct application of the material presented in Chapter 3. Computer solutions are used to illustrate the dynamic performance of typical induction machines and to depict the variables in various reference frames during free acceleration. Finally, the equations for an induction machine are arranged appropriate for computer simulation. The material presented in this chapter forms the basis for solution of more advanced problems. In particular, these basic concepts are fundamental to the analysis of induction machines in most power system and controlled electric drive applications.

## 6.2. VOLTAGE EQUATIONS IN MACHINE VARIABLES

The winding arrangement for a two-pole, three-phase, wye-connected, symmetrical induction machine is shown in Figure 6.2-1 (which is Fig. 1.4-3 repeated here for convenience). The stator windings are identical, sinusoidally distributed windings, displaced 120°, with  $N_s$  equivalent turns and resistance  $r_s$ . For the purpose at hand, the rotor windings will also be considered as three identical sinusoidally distributed windings, displaced 120°, with  $N_r$  equivalent turns and resistance  $r_r$ . The positive direction of the magnetic axis of each winding is shown in Figure 6.2-1. It is important to note that the positive direction of the magnetic axes of the stator windings coincides with the direction of  $f_{as}$ ,  $f_{bs}$ , and  $f_{cs}$  as specified by the equations of transformation and shown in Figure 3.3-1.

The voltage equations in machine variables may be expressed

$$\mathbf{v}_{abcs} = \mathbf{r}_s \mathbf{i}_{abcs} + p \boldsymbol{\lambda}_{abcs} \quad (6.2-1)$$

$$\mathbf{v}_{abcr} = \mathbf{r}_r \mathbf{i}_{abcr} + p \boldsymbol{\lambda}_{abcr} \quad (6.2-2)$$

where

$$(\mathbf{f}_{abcs})^T = [f_{as} \quad f_{bs} \quad f_{cs}] \quad (6.2-3)$$

$$(\mathbf{f}_{abcr})^T = [f_{ar} \quad f_{br} \quad f_{cr}] \quad (6.2-4)$$

In the above equations, the  $s$  subscript denotes variables and parameters associated with the stator circuits, and the  $r$  subscript denotes variables and parameters associated with the rotor circuits. Both  $\mathbf{r}_s$  and  $\mathbf{r}_r$  are diagonal matrices each with equal nonzero elements. For a magnetically linear system, the flux linkages may be expressed as

$$\begin{bmatrix} \boldsymbol{\lambda}_{abcs} \\ \boldsymbol{\lambda}_{abcr} \end{bmatrix} = \begin{bmatrix} \mathbf{L}_s & \mathbf{L}_{sr} \\ (\mathbf{L}_{sr})^T & \mathbf{L}_r \end{bmatrix} \begin{bmatrix} \mathbf{i}_{abcs} \\ \mathbf{i}_{abcr} \end{bmatrix} \quad (6.2-5)$$

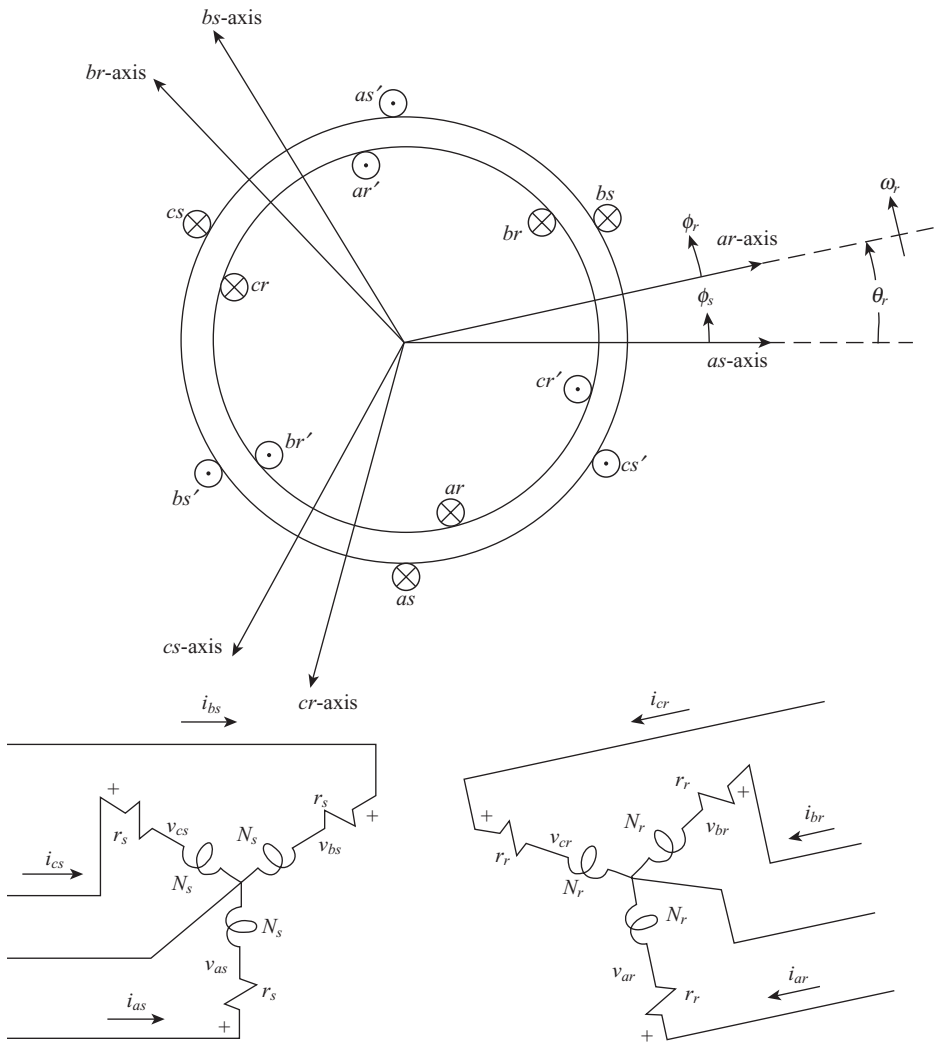


Figure 6.2-1. Two-pole, three-phase, wye-connected symmetrical induction machine.

The winding inductances are derived Chapter 2. Neglecting mutual leakage between the stator windings and also between the rotor windings, they can be expressed as

$$\mathbf{L}_s = \begin{bmatrix} L_{ls} + L_{ms} & -\frac{1}{2}L_{ms} & -\frac{1}{2}L_{ms} \\ -\frac{1}{2}L_{ms} & L_{ls} + L_{ms} & -\frac{1}{2}L_{ms} \\ -\frac{1}{2}L_{ms} & -\frac{1}{2}L_{ms} & L_{ls} + L_{ms} \end{bmatrix} \quad (6.2-6)$$

$$\mathbf{L}_r = \begin{bmatrix} L_{lr} + L_{mr} & -\frac{1}{2}L_{mr} & -\frac{1}{2}L_{mr} \\ -\frac{1}{2}L_{mr} & L_{lr} + L_{mr} & -\frac{1}{2}L_{mr} \\ -\frac{1}{2}L_{mr} & -\frac{1}{2}L_{mr} & L_{lr} + L_{mr} \end{bmatrix} \quad (6.2-7)$$

$$\mathbf{L}_{sr} = L_{sr} \begin{bmatrix} \cos \theta_r & \cos \left( \theta_r + \frac{2\pi}{3} \right) & \cos \left( \theta_r - \frac{2\pi}{3} \right) \\ \cos \left( \theta_r - \frac{2\pi}{3} \right) & \cos \theta_r & \cos \left( \theta_r + \frac{2\pi}{3} \right) \\ \cos \left( \theta_r + \frac{2\pi}{3} \right) & \cos \left( \theta_r - \frac{2\pi}{3} \right) & \cos \theta_r \end{bmatrix} \quad (6.2-8)$$

In the above inductance equations,  $L_{ls}$  and  $L_{ms}$  are, respectively, the leakage and magnetizing inductances of the stator windings;  $L_{lr}$  and  $L_{mr}$  are for the rotor windings. The inductance  $L_{sr}$  is the amplitude of the mutual inductances between stator and rotor windings.

A majority of induction machines are not equipped with coil-wound rotor windings; instead, the current flows in copper or aluminum bars that are uniformly distributed and are embedded in a ferromagnetic material with all bars terminated in a common ring at each end of the rotor. This type of rotor configuration is referred to as a squirrel-cage rotor. It may at first appear that the mutual inductance between a uniformly distributed rotor winding and a sinusoidally distributed stator winding would not be of the form given by (6.2-8). However, in most cases, a uniformly distributed winding is adequately described by its fundamental sinusoidal component and is represented by an equivalent three-phase winding. Generally, this representation consists of one equivalent winding per phase; however, the rotor construction of some machines is such that its performance is more accurately described by representing each phase with two equivalent windings connected in parallel. This type of machine is commonly referred to as a double-cage rotor machine.

Another consideration is that in a practical machine, the rotor conductors are often skewed. That is, the conductors are not placed in the plane of the axis of rotation of the rotor. Instead, the conductors are skewed slightly (typically one slot width) with the axis of rotation. This type of conductor arrangement helps to reduce the magnitude of harmonic torques that result from harmonics in the MMF waves. Such design features are not considered here. Instead, it is assumed that all effects upon the amplitude of the fundamental component of the MMF waveform due to skewing and uniformly distributed rotor windings are accounted for in the value of  $N_r$ . The assumption that the induction machine is a linear (no saturation) and MMF harmonic-free device is an oversimplification that cannot describe the behavior of induction machines in all modes of operation. However, in the majority of applications, its behavior can be adequately predicted with this simplified representation.

When expressing the voltage equations in machine variable form, it is convenient to refer all rotor variables to the stator windings by appropriate turns ratios.

$$\mathbf{i}'_{abcr} = \frac{N_r}{N_s} \mathbf{i}_{abcr} \quad (6.2-9)$$

$$\mathbf{v}'_{abcr} = \frac{N_s}{N_r} \mathbf{v}_{abcr} \quad (6.2-10)$$

$$\lambda'_{abcr} = \frac{N_s}{N_r} \lambda_{abcr} \quad (6.2-11)$$

The magnetizing and mutual inductances are associated with the same magnetic flux path; therefore  $L_{ms}$ ,  $L_{mr}$ , and  $L_{sr}$  are related as set forth by (1.2-21) with 1 and 2 replaced by  $s$  and  $r$ , respectively, or by (2.8-57)–(2.8-59). In particular

$$L_{ms} = \frac{N_s}{N_r} L_{sr} \quad (6.2-12)$$

Thus, we will define

$$\begin{aligned} \mathbf{L}'_{sr} &= \frac{N_s}{N_r} \mathbf{L}_{sr} \\ &= L_{ms} \begin{bmatrix} \cos \theta_r & \cos \left( \theta_r + \frac{2\pi}{3} \right) & \cos \left( \theta_r - \frac{2\pi}{3} \right) \\ \cos \left( \theta_r - \frac{2\pi}{3} \right) & \cos \theta_r & \cos \left( \theta_r + \frac{2\pi}{3} \right) \\ \cos \left( \theta_r + \frac{2\pi}{3} \right) & \cos \left( \theta_r - \frac{2\pi}{3} \right) & \cos \theta_r \end{bmatrix} \end{aligned} \quad (6.2-13)$$

Also, from (1.2-18) or (2.8-57) and (2.8-58),  $L_{mr}$  may be expressed as

$$L_{mr} = \left( \frac{N_r}{N_s} \right)^2 L_{ms} \quad (6.2-14)$$

and if we let

$$\mathbf{L}'_r = \left( \frac{N_s}{N_r} \right)^2 \mathbf{L}_r \quad (6.2-15)$$

then, from (6.2-7)

$$\mathbf{L}'_r = \begin{bmatrix} L'_{lr} + L_{ms} & -\frac{1}{2}L_{ms} & -\frac{1}{2}L_{ms} \\ -\frac{1}{2}L_{ms} & L'_{lr} + L_{ms} & -\frac{1}{2}L_{ms} \\ -\frac{1}{2}L_{ms} & -\frac{1}{2}L_{ms} & L'_{lr} + L_{ms} \end{bmatrix} \quad (6.2-16)$$

where

$$L'_{lr} = \left( \frac{N_s}{N_r} \right)^2 L_{lr} \quad (6.2-17)$$

The flux linkages may now be expressed as

$$\begin{bmatrix} \lambda_{abcs} \\ \lambda'_{abcr} \end{bmatrix} = \begin{bmatrix} \mathbf{L}_s & \mathbf{L}'_{sr} \\ (\mathbf{L}'_{sr})^T & \mathbf{L}'_r \end{bmatrix} \begin{bmatrix} \mathbf{i}_{abcs} \\ \mathbf{i}'_{abcr} \end{bmatrix} \quad (6.2-18)$$

The voltage equations expressed in terms of machine variables referred to the stator windings may now be written as

$$\begin{bmatrix} \mathbf{v}_{abcs} \\ \mathbf{v}'_{abcr} \end{bmatrix} = \begin{bmatrix} \mathbf{r}_s + p\mathbf{L}_s & p\mathbf{L}'_{sr} \\ p(\mathbf{L}'_{sr})^T & \mathbf{r}'_r + p\mathbf{L}'_r \end{bmatrix} \begin{bmatrix} \mathbf{i}_{abcs} \\ \mathbf{i}'_{abcr} \end{bmatrix} \quad (6.2-19)$$

where

$$\mathbf{r}'_r = \left( \frac{N_s}{N_r} \right)^2 \mathbf{r}_r \quad (6.2-20)$$

### 6.3. TORQUE EQUATION IN MACHINE VARIABLES

Evaluation of the energy stored in the coupling field by (1.3-51) yields the familiar expression for energy stored in a magnetically linear system. In particular, the stored energy is the sum of the self-inductance of each winding times one-half the square of its current and all mutual inductances, each times the currents in the two windings coupled by the mutual inductance. Thus, the energy stored in the coupling field may be written

$$\begin{aligned} W_f = & \frac{1}{2} (\mathbf{i}_{abcs})^T \mathbf{L}_s \mathbf{i}_{abcs} + (\mathbf{i}_{abcs})^T \mathbf{L}'_{sr} \mathbf{i}'_{abcr} \\ & + \frac{1}{2} (\mathbf{i}'_{abcr})^T \mathbf{L}'_r \mathbf{i}'_{abcr} \end{aligned} \quad (6.3-1)$$

Since the machine is assumed to be magnetically linear, the field energy  $W_f$  is equal to the coenergy  $W_c$ .

Before using the second entry of Table 1.3-1 to express the electromagnetic torque, it is necessary to modify the expressions given in Table 1.3-1 to account for a  $P$ -pole machine. The change of mechanical energy in a rotational system with one mechanical input may be written from (1.3-71) as

$$dW_m = -T_e d\theta_{rm} \quad (6.3-2)$$

where  $T_e$  is the electromagnetic torque positive for motor action (torque output) and  $\theta_{rm}$  is the actual angular displacement of the rotor. The flux linkages, currents,  $W_f$ , and  $W_c$ , are all expressed as functions of the electrical angular displacement  $\theta_r$ . Since

$$\theta_r = \left( \frac{P}{2} \right) \theta_{rm} \quad (6.3-3)$$

where  $P$  is the number of poles in the machine, then

$$dW_m = -T_e \left( \frac{2}{P} \right) d\theta_r \quad (6.3-4)$$

Therefore, to account for a  $P$ -pole machine, all terms on the right-hand side of Table 1.3-1 should be multiplied by  $P/2$ . Therefore, the electromagnetic torque may be evaluated from

$$T_e(\mathbf{i}, \theta_r) = \left( \frac{P}{2} \right) \frac{\partial W_c(\mathbf{i}, \theta_r)}{\partial \theta_r} \quad (6.3-5)$$

The abbreviated functional notation, as used in Table 1.3-1, is also used here for the currents. Since  $\mathbf{L}_s$  and  $\mathbf{L}'_r$  are not functions of  $\theta_r$ , substituting  $W_f$  from (6.3-1) into (6.3-5) yields the electromagnetic torque in Newton meters (N·m)

$$T_e = \left( \frac{P}{2} \right) (\mathbf{i}_{abcs})^T \frac{\partial}{\partial \theta_r} [\mathbf{L}'_{sr}] \mathbf{i}'_{abcr} \quad (6.3-6)$$

In expanded form, (6.3-6) becomes

$$T_e = -\left( \frac{P}{2} \right) L_{ms} \left[ \left[ i_{as} \left( i'_{ar} - \frac{1}{2} i'_{br} - \frac{1}{2} i'_{cr} \right) + i_{bs} \left( i'_{br} - \frac{1}{2} i'_{ar} - \frac{1}{2} i'_{cr} \right) \right. \right. \\ \left. \left. + i_{cs} \left( i'_{cr} - \frac{1}{2} i'_{br} - \frac{1}{2} i'_{ar} \right) \right] \sin \theta_r + \frac{\sqrt{3}}{2} [i_{as}(i'_{br} - i'_{cr}) + i_{bs}(i'_{cr} - i'_{ar}) + i_{cs}(i'_{ar} - i'_{br})] \cos \theta_r \right] \quad (6.3-7)$$

The torque and rotor speed are related by

$$T_e = J \left( \frac{2}{P} \right) p \omega_r + T_L \quad (6.3-8)$$

where  $J$  is the inertia of the rotor and in some cases the connected load. The first term on the right-hand side is the inertial torque. In (6.3-8), the units of  $J$  are kilogram·meter<sup>2</sup> (kg·m<sup>2</sup>) or Joules·second<sup>2</sup> (J·s<sup>2</sup>). Often the inertia is given as a quantity called  $WR^2$ , expressed in units of pound mass·feet<sup>2</sup> (lbm·ft<sup>2</sup>). The load torque  $T_L$  is positive for a torque load on the shaft of the induction machine.

## 6.4. EQUATIONS OF TRANSFORMATION FOR ROTOR CIRCUITS

In Chapter 3, the concept of the arbitrary reference frame was introduced and applied to stationary circuits. However, in the analysis of induction machines, it is necessary to transform the variables associated with the symmetrical rotor windings to the arbitrary reference frame. A change of variables that formulates a transformation of the three-phase variables of the rotor circuits to the arbitrary reference frame is

$$\mathbf{f}'_{qd0r} = \mathbf{K}_r \mathbf{f}'_{abcr} \quad (6.4-1)$$

where

$$(\mathbf{f}'_{qd0r})^T = [f'_{qr} \quad f'_{dr} \quad f'_{0r}] \quad (6.4-2)$$

$$(\mathbf{f}'_{abcr})^T = [f'_{ar} \quad f'_{br} \quad f'_{cr}] \quad (6.4-3)$$

$$\mathbf{K}_r = \frac{2}{3} \begin{bmatrix} \cos \beta & \cos \left( \beta - \frac{2\pi}{3} \right) & \cos \left( \beta + \frac{2\pi}{3} \right) \\ \sin \beta & \sin \left( \beta - \frac{2\pi}{3} \right) & \sin \left( \beta + \frac{2\pi}{3} \right) \\ \frac{1}{2} & \frac{1}{2} & \frac{1}{2} \end{bmatrix} \quad (6.4-4)$$

$$\beta = \theta - \theta_r \quad (6.4-5)$$

The angular displacement  $\theta$  is defined by (3.3-5)–(3.3-8), and  $\theta_r$  is defined by

$$\frac{d\theta_r}{dt} = \omega_r \quad (6.4-6)$$

The inverse of (6.4-4) is

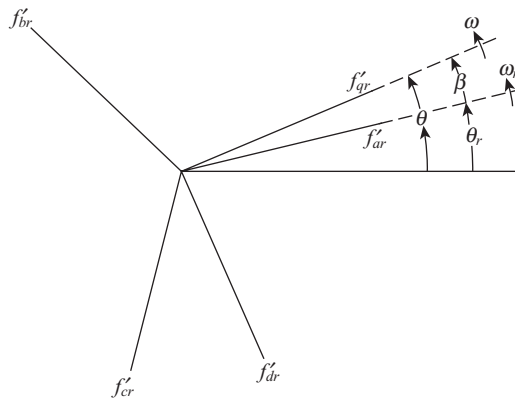


Figure 6.4-1. Transformation for rotating circuits portrayed by trigonometric relationships.

$$(\mathbf{K}_r)^{-1} = \begin{bmatrix} \cos \beta & \sin \beta & 1 \\ \cos\left(\beta - \frac{2\pi}{3}\right) & \sin\left(\beta - \frac{2\pi}{3}\right) & 1 \\ \cos\left(\beta + \frac{2\pi}{3}\right) & \sin\left(\beta + \frac{2\pi}{3}\right) & 1 \end{bmatrix} \quad (6.4-7)$$

The  $r$  subscript indicates the variables, parameters, and transformation associated with rotating circuits. Although this change of variables needs no physical interpretation, it is convenient, as in the case of stationary circuits, to visualize these transformation equations as trigonometric relationships between vector quantities, as shown in Figure 6.4-1.

It is clear that the above transformation equations for rotor circuits are the transformation equations for stationary circuits, with  $\beta$  used as the angular displacement of the arbitrary reference frame rather than  $\theta$ . In fact, the equations of transformation for stationary and rotor circuits are special cases of a transformation for all circuits, stationary or rotating. In particular, if in  $\beta$ ,  $\theta_r$  is replaced by  $\theta_c$ , where

$$\frac{d\theta_c}{dt} = \omega_c \quad (6.4-8)$$

then  $\omega_c$ , the angular velocity of the circuits, may be selected to correspond to the circuits being transformed, that is,  $\omega_c = 0$  for stationary circuits and  $\omega_c = \omega_r$  for rotor circuits. Although this more general approach could have been used in Chapter 3, it does add to the complexity of the transformation, making it somewhat more difficult to follow without deriving any advantage from the generality of the approach, since only two types of circuits, stationary or fixed in the rotor, are considered in this chapter.

It follows that all equations for stationary circuits in Section 3.3 and Section 3.4 are valid for rotor circuits if  $\theta$  is replaced by  $\beta$  and  $\omega$  by  $\omega - \omega_r$ . The phasor and steady-state relations for stationary circuits, given in Section 3.7, Section 3.8, and Section 3.9, also apply to rotor circuits of an induction machine if we realize that the rotor variables, during balanced, steady-state operation are of the form

$$F'_{ar} = \sqrt{2}F'_r \cos[(\omega_e - \omega_r)t + \theta_{erf}(0)] \quad (6.4-9)$$

$$F'_{br} = \sqrt{2}F'_r \cos\left[(\omega_e - \omega_r)t + \theta_{erf}(0) - \frac{2\pi}{3}\right] \quad (6.4-10)$$

$$F'_{cr} = \sqrt{2}F'_r \cos\left[(\omega_e - \omega_r)t + \theta_{erf}(0) + \frac{2\pi}{3}\right] \quad (6.4-11)$$

where  $\theta_{erf}(0)$  is the phase angle of  $F'_{ar}$  at time zero.

## 6.5. VOLTAGE EQUATIONS IN ARBITRARY REFERENCE-FRAME VARIABLES

Using the information set forth in Chapter 3 and in the previous section, we know the form of the voltage equations in the arbitrary reference frame without any further analysis [1]. In particular

$$\mathbf{v}_{qd0s} = \mathbf{r}_s \mathbf{i}_{qd0s} + \omega \boldsymbol{\lambda}_{dqs} + p \boldsymbol{\lambda}_{qd0s} \quad (6.5-1)$$

$$\mathbf{v}'_{qd0r} = \mathbf{r}'_r \mathbf{i}'_{qd0r} + (\omega - \omega_r) \boldsymbol{\lambda}'_{dqr} + p \boldsymbol{\lambda}'_{qd0r} \quad (6.5-2)$$

where

$$(\boldsymbol{\lambda}_{dqs})^T = [\lambda_{ds} \quad -\lambda_{qs} \quad 0] \quad (6.5-3)$$

$$(\boldsymbol{\lambda}'_{dqr})^T = [\lambda'_{dr} \quad -\lambda'_{qr} \quad 0] \quad (6.5-4)$$

The set of equations is complete once the expressions for the flux linkages are determined. Substituting the equations of transformation, (3.3-1) and (6.4-1), into the flux linkage equations expressed in *abc* variables (6.2-18), yields the flux linkage equations for a magnetically linear system

$$\begin{bmatrix} \boldsymbol{\lambda}_{qd0s} \\ \boldsymbol{\lambda}'_{qd0r} \end{bmatrix} = \begin{bmatrix} \mathbf{K}_s \mathbf{L}_s (\mathbf{K}_s)^{-1} & \mathbf{K}_s \mathbf{L}'_{sr} (\mathbf{K}_r)^{-1} \\ \mathbf{K}_r (\mathbf{L}'_{sr})^T (\mathbf{K}_s)^{-1} & \mathbf{K}_r \mathbf{L}'_r (\mathbf{K}_r)^{-1} \end{bmatrix} \begin{bmatrix} \mathbf{i}_{qd0s} \\ \mathbf{i}'_{qd0r} \end{bmatrix} \quad (6.5-5)$$

We know from Chapter 3 that for  $\mathbf{L}_s$  of the form given by (6.2-6)

$$\mathbf{K}_s \mathbf{L}_s (\mathbf{K}_s)^{-1} = \begin{bmatrix} L_{ls} + L_M & 0 & 0 \\ 0 & L_{ls} + L_M & 0 \\ 0 & 0 & L_{ls} \end{bmatrix} \quad (6.5-6)$$

where

$$L_M = \frac{3}{2} L_{ms} \quad (6.5-7)$$

Since  $\mathbf{L}'_r$  is similar in form to  $\mathbf{L}_s$ , it follows that

$$\mathbf{K}_r \mathbf{L}'_r (\mathbf{K}_r)^{-1} = \begin{bmatrix} L'_{lr} + L_M & 0 & 0 \\ 0 & L'_{lr} + L_M & 0 \\ 0 & 0 & L'_{lr} \end{bmatrix} \quad (6.5-8)$$

It can be shown that

$$\mathbf{K}_s \mathbf{L}'_{sr} (\mathbf{K}_r)^{-1} = \mathbf{K}_r (\mathbf{L}'_{sr})^T (\mathbf{K}_s)^{-1} = \begin{bmatrix} L_M & 0 & 0 \\ 0 & L_M & 0 \\ 0 & 0 & 0 \end{bmatrix} \quad (6.5-9)$$

Similar forms to (6.5-6) and (6.5-8) are obtained if the mutual leakage terms shown in Chapter 2 are included in the stator and rotor inductance matrices in (6.5-5). Proving this is left as a homework exercise at the end of the chapter. The voltage equations are often written in expanded form. From (6.5-1) and (6.5-2)

$$v_{qs} = r_s i_{qs} + \omega \lambda_{ds} + p \lambda_{qs} \quad (6.5-10)$$

$$v_{ds} = r_s i_{ds} - \omega \lambda_{qs} + p \lambda_{ds} \quad (6.5-11)$$

$$v_{0s} = r_s i_{0s} + p \lambda_{0s} \quad (6.5-12)$$

$$v'_{qr} = r_r i'_{qr} + (\omega - \omega_r) \lambda'_{dr} + p \lambda'_{qr} \quad (6.5-13)$$

$$v'_{dr} = r_r i'_{dr} - (\omega - \omega_r) \lambda'_{qr} + p \lambda'_{dr} \quad (6.5-14)$$

$$v'_{0r} = r_r i'_{0r} + p \lambda'_{0r} \quad (6.5-15)$$

Substituting (6.5-6), (6.5-8), and (6.5-9) into (6.5-5) yields the expressions for the flux linkages. In expanded form

$$\lambda_{qs} = L_{ls} i_{qs} + L_M (i_{qs} + i'_{qr}) \quad (6.5-16)$$

$$\lambda_{ds} = L_{ls} i_{ds} + L_M (i_{ds} + i'_{dr}) \quad (6.5-17)$$

$$\lambda_{0s} = L_{ls} i_{0s} \quad (6.5-18)$$

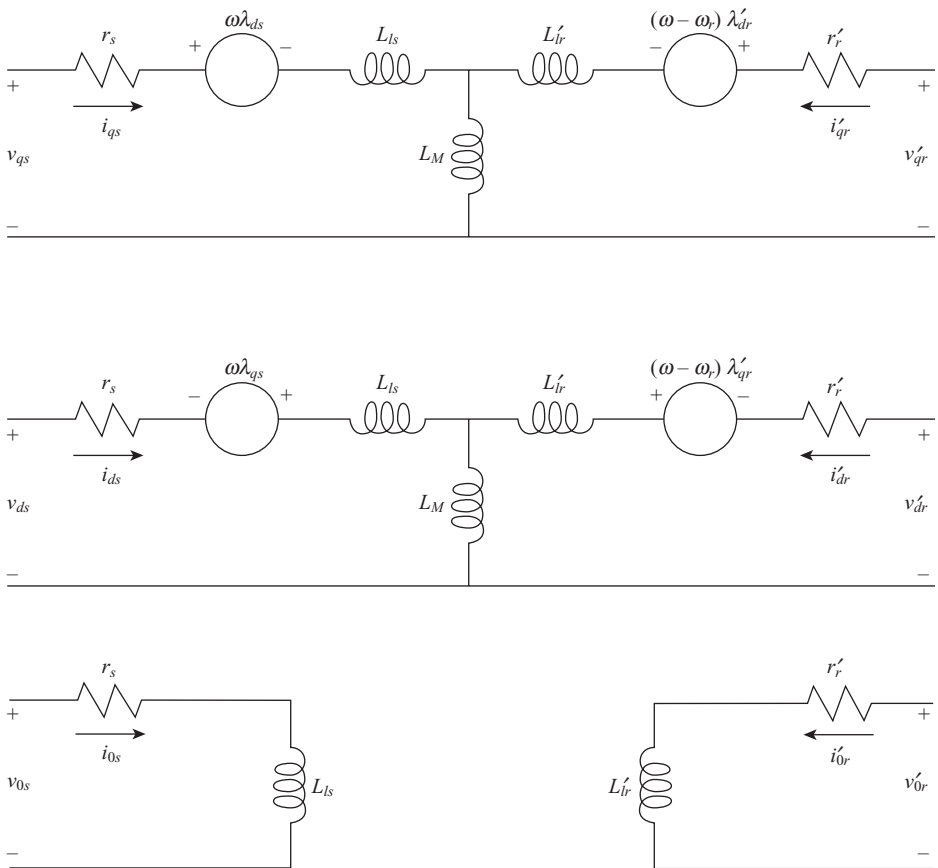


Figure 6.5-1. Arbitrary reference-frame equivalent circuits for a three-phase, symmetrical induction machine.

$$\lambda'_{qr} = L'_{lr} i'_{qr} + L_M (i_{qs} + i'_{qr}) \quad (6.5-19)$$

$$\lambda'_{dr} = L'_{lr} i'_{dr} + L_M (i_{ds} + i'_{dr}) \quad (6.5-20)$$

$$\lambda'_{0r} = L'_{lr} i'_{0r} \quad (6.5-21)$$

The voltage and flux linkage equations suggest the equivalent circuits shown in Figure 6.5-1.

Since machine and power system parameters are generally given in ohms or in per unit of a base impedance, it is convenient to express the voltage and flux linkage equations in terms of reactances rather than inductances. Hence, (6.5-10)–(6.5-15) are often written as

$$v_{qs} = r_s i_{qs} + \frac{\omega}{\omega_b} \psi_{ds} + \frac{p}{\omega_b} \psi_{qs} \quad (6.5-22)$$

$$v_{ds} = r_s i_{ds} - \frac{\omega}{\omega_b} \psi_{qs} + \frac{p}{\omega_b} \psi_{ds} \quad (6.5-23)$$

$$v_{0s} = r_s i_{0s} + \frac{p}{\omega_b} \psi_{0s} \quad (6.5-24)$$

$$v'_{qr} = r'_r i'_{qr} + \left( \frac{\omega - \omega_r}{\omega_b} \right) \psi'_{dr} + \frac{p}{\omega_b} \psi'_{qr} \quad (6.5-25)$$

$$v'_{dr} = r'_r i'_{dr} - \left( \frac{\omega - \omega_r}{\omega_b} \right) \psi'_{qr} + \frac{p}{\omega_b} \psi'_{dr} \quad (6.5-26)$$

$$v'_{0r} = r'_r i'_{0r} + \frac{p}{\omega_b} \psi'_{0r} \quad (6.5-27)$$

where  $\omega_b$  is the base electrical angular velocity used to calculate the inductive reactances. Flux linkages (6.5-16)–(6.5-21) now become flux linkages per second with the units of volts

$$\psi_{qs} = X_{ls} i_{qs} + X_M (i_{qs} + i'_{qr}) \quad (6.5-28)$$

$$\psi_{ds} = X_{ls} i_{ds} + X_M (i_{ds} + i'_{dr}) \quad (6.5-29)$$

$$\psi_{0s} = X_{ls} i_{0s} \quad (6.5-30)$$

$$\psi'_{qr} = X'_{lr} i'_{qr} + X_M (i_{qs} + i'_{qr}) \quad (6.5-31)$$

$$\psi'_{dr} = X'_{lr} i'_{dr} + X_M (i_{ds} + i'_{dr}) \quad (6.5-32)$$

$$\psi'_{0r} = X'_{lr} i'_{0r} \quad (6.5-33)$$

In the above equations, the reactances are obtained by multiplying  $\omega_b$  times inductance. It is left to the reader to modify the equivalent circuits shown in Figure 6.5-1 to accommodate the use of reactances rather than inductances in the voltage equations.

The voltage equations (6.5-10)–(6.5-15) or (6.5-22)–(6.5-27) are written in terms of currents and flux linkages (flux linkages per second). Clearly, the currents and flux linkages are related and both cannot be independent or state variables. In transfer function formulation and computer simulation of induction machines, we will find it desirable to express the voltage equations in terms of either currents or flux linkages (flux linkages per second).

If the currents are selected as independent variables and the flux linkages or flux linkages per second are replaced by the currents, the voltage equations become

$$\begin{bmatrix} v_{qs} \\ v_{ds} \\ v_{0s} \\ v'_{qr} \\ v'_{dr} \\ v'_{0r} \end{bmatrix} = \begin{bmatrix} r_s + \frac{p}{\omega_b} X_{ss} & \frac{\omega}{\omega_b} X_{ss} & 0 & \frac{p}{\omega_b} X_M & \frac{\omega}{\omega_b} X_M & 0 \\ -\frac{\omega}{\omega_b} X_{ss} & r_s + \frac{p}{\omega_b} X_{ss} & 0 & -\frac{\omega}{\omega_b} X_M & \frac{p}{\omega_b} X_M & 0 \\ 0 & 0 & r_s + \frac{p}{\omega_b} X_{ls} & 0 & 0 & 0 \\ \frac{p}{\omega_b} X_M & \left(\frac{\omega - \omega_r}{\omega_b}\right) X_M & 0 & r'_r + \frac{p}{\omega_b} X'_{rr} & \left(\frac{\omega - \omega_r}{\omega_b}\right) X'_{rr} & 0 \\ -\left(\frac{\omega - \omega_r}{\omega_b}\right) X_M & \frac{p}{\omega_b} X_M & 0 & -\left(\frac{\omega - \omega_r}{\omega_b}\right) X'_{rr} & r'_r + \frac{p}{\omega_b} X'_{rr} & 0 \\ 0 & 0 & 0 & 0 & 0 & r'_r + \frac{p}{\omega_b} X'_{lr} \end{bmatrix} \begin{bmatrix} i_{qs} \\ i_{ds} \\ i_{0s} \\ i'_{qr} \\ i'_{dr} \\ i'_{0r} \end{bmatrix} \quad (6.5-34)$$

where

$$X_{ss} = X_{ls} + X_M \quad (6.5-35)$$

$$X'_{rr} = X'_{lr} + X_M \quad (6.5-36)$$

The flux linkages per second may be expressed from (6.5-28)–(6.5-33) as

$$\begin{bmatrix} \psi_{qs} \\ \psi_{ds} \\ \psi_{0s} \\ \psi'_{qr} \\ \psi'_{dr} \\ \psi'_{0r} \end{bmatrix} = \begin{bmatrix} X_{ss} & 0 & 0 & X_M & 0 & 0 \\ 0 & X_{ss} & 0 & 0 & X_M & 0 \\ 0 & 0 & X_{ls} & 0 & 0 & 0 \\ X_M & 0 & 0 & X'_{rr} & 0 & 0 \\ 0 & X_M & 0 & 0 & X'_{rr} & 0 \\ 0 & 0 & 0 & 0 & 0 & X'_{lr} \end{bmatrix} \begin{bmatrix} i_{qs} \\ i_{ds} \\ i_{0s} \\ i'_{qr} \\ i'_{dr} \\ i'_{0r} \end{bmatrix} \quad (6.5-37)$$

If flux linkages or flux linkages per second are selected as independent variables, then (6.5-37) may be solved for currents and written as

$$\begin{bmatrix} i_{qs} \\ i_{ds} \\ i_{0s} \\ i'_{qr} \\ i'_{dr} \\ i'_{0r} \end{bmatrix} = \frac{1}{D} \begin{bmatrix} X'_{rr} & 0 & 0 & -X_M & 0 & 0 \\ 0 & X'_{rr} & 0 & 0 & -X_M & 0 \\ 0 & 0 & \frac{D}{X_{ls}} & 0 & 0 & 0 \\ -X_M & 0 & 0 & X_{ss} & 0 & 0 \\ 0 & -X_M & 0 & 0 & X_{ss} & 0 \\ 0 & 0 & 0 & 0 & 0 & \frac{D}{X'_{lr}} \end{bmatrix} \begin{bmatrix} \psi_{qs} \\ \psi_{ds} \\ \psi_{0s} \\ \psi'_{qr} \\ \psi'_{dr} \\ \psi'_{0r} \end{bmatrix} \quad (6.5-38)$$

where

$$D = X_{ss}X'_{rr} - X_M^2 \quad (6.5-39)$$

Substituting (6.5-38) for the currents into (6.5-22)–(6.5-27) yields the voltage equations in terms of flux linkages per second as given by (6.5-40)

$$\begin{bmatrix} v_{qs} \\ v_{ds} \\ v_{0s} \\ v'_{qr} \\ v'_{dr} \\ v'_{0r} \end{bmatrix} = \begin{bmatrix} \frac{r_s X'_{rr}}{D} + \frac{p}{\omega_b} & \frac{\omega}{\omega_b} & 0 & -\frac{r_s X_M}{D} & 0 & 0 \\ -\frac{\omega}{\omega_b} & \frac{r_s X'_{rr}}{D} + \frac{p}{\omega_b} & 0 & 0 & -\frac{r_s X_M}{D} & 0 \\ 0 & 0 & \frac{r_s}{X_{ls}} + \frac{p}{\omega_b} & 0 & 0 & 0 \\ -\frac{r'_r X_M}{D} & 0 & 0 & \frac{r'_r X_{ss}}{D} + \frac{p}{\omega_b} & \frac{\omega - \omega_r}{\omega_b} & 0 \\ 0 & -\frac{r'_r X_M}{D} & 0 & -\frac{\omega - \omega_r}{\omega_b} & \frac{r'_r X_{ss}}{D} + \frac{p}{\omega_b} & 0 \\ 0 & 0 & 0 & 0 & 0 & \frac{r'_r}{X'_{lr}} + \frac{p}{\omega_b} \end{bmatrix} \begin{bmatrix} \psi_{qs} \\ \psi_{ds} \\ \psi_{0s} \\ \psi'_{qr} \\ \psi'_{dr} \\ \psi'_{0r} \end{bmatrix} \quad (6.5-40)$$

It is interesting to note that each *q*- and *d*-voltage equation contains two derivatives of current when currents are selected as independent or state variables, (6.5-34). When flux linkages are selected as independent variables, (6.5-40), each *q*- and *d*-voltage equation contains only one derivative of flux linkage. This property makes it more convenient to implement a computer simulation of an induction machine with flux linkages as state variables rather than with currents.

## 6.6. TORQUE EQUATION IN ARBITRARY REFERENCE-FRAME VARIABLES

The expression for the electromagnetic torque in terms of arbitrary reference-frame variables may be obtained by substituting the equations of transformation into (6.3-6). Thus

$$T_e = \left( \frac{P}{2} \right) \left[ (\mathbf{K}_s)^{-1} \mathbf{i}_{qd0s} \right]^T \frac{\partial}{\partial \theta_r} [\mathbf{L}'_{sr}] (\mathbf{K}_r)^{-1} \mathbf{i}'_{qd0r} \quad (6.6-1)$$

This expression yields the torque expressed in terms of current as

$$T_e = \left( \frac{3}{2} \right) \left( \frac{P}{2} \right) L_M (i_{qs} i'_{dr} - i_{ds} i'_{qr}) \quad (6.6-2)$$

where  $T_e$  is positive for motor action. Other equivalent expressions for the electromagnetic torque of an induction machine are

$$T_e = \left( \frac{3}{2} \right) \left( \frac{P}{2} \right) (\lambda'_{qr} i'_{dr} - \lambda'_{dr} i'_{qr}) \quad (6.6-3)$$

$$T_e = \left( \frac{3}{2} \right) \left( \frac{P}{2} \right) (\lambda_{ds} i_{qs} - \lambda_{qs} i_{ds}) \quad (6.6-4)$$

Equations (6.6-3) and (6.6-4) may be somewhat misleading since they seem to imply that the leakage inductances are involved in the energy conversion process. This, however, is not the case. Even though the flux linkages in (6.6-3) and (6.6-4) contain the leakage inductances, they are eliminated by the algebra within the parentheses.

It is interesting and instructive to take a moment to return to Chapter 1 and to begin the derivation of torque using arbitrary reference-frame variables. From (1.3-21)

$$dW_e = dW_f - dW_m \quad (6.6-5)$$

where  $dW_e$  is the change of energy entering the coupling field via the electric inputs,  $dW_f$  is the change of energy stored in the coupling field, and  $dW_m$  is the change of energy entering the coupling field via the mechanical input. We can turn the energy balance equation given by (6.6-5) into a power balance equation by dividing (6.6-5) by  $dt$ . Thus,

$$pW_e = pW_f - pW_m \quad (6.6-6)$$

where  $p$  is the operator  $d/dt$ . The power input to the coupling field may be expressed from the voltage equations (6.5-10)–(6.5-15) by multiplying each voltage equation by the appropriate current and removing the  $i^2r$  terms. Thus, with  $e_{qs} = v_{qs} - i_{qs}r_s$ , and so on, we can write from (6.5-10)–(6.5-15) and (3.3-8)

$$\left( \frac{2}{3} \right) pW_e = e_{qs} i_{qs} + e_{ds} i_{ds} + 2e_{0s} i_{0s} + e'_{qr} i'_{qr} + e'_{dr} i'_{dr} + 2e'_{0r} i'_{0r} \quad (6.6-7)$$

Removing the  $ir$  voltage drop is not necessary; we have done this to be consistent with the work in Chapter 1. Appropriate substitution of (6.5-10)–(6.5-15) yields

$$\begin{aligned} \left( \frac{2}{3} \right) pW_e &= i_{qs} p\lambda_{qs} + i_{ds} p\lambda_{ds} + i_{0s} p\lambda_{0s} + i'_{qr} p\lambda'_{qr} + i'_{dr} p\lambda'_{dr} + i'_{0r} p\lambda'_{0r} \\ &+ \omega(\lambda_{ds} i_{qs} - \lambda_{qs} i_{ds} + \lambda'_{dr} i'_{qr} - \lambda'_{qr} i'_{dr}) - (\lambda'_{dr} i'_{qr} - \lambda'_{qr} i'_{dr}) p\theta_r \end{aligned} \quad (6.6-8)$$

Comparing (6.6-8) with (6.6-6), it is clear that the right-hand side of (6.6-4) is  $pW_f - pW_m$ . Now

$$pW_m = -T_e p\theta_{rm} \quad (6.6-9)$$

where  $\theta_{rm}$  is the actual angular displacement of the rotor and

$$\theta_r = \left( \frac{P}{2} \right) \theta_{rm} \quad (6.6-10)$$

where  $\theta_r$  is the electrical angular displacement and  $P$  is the number of poles. Therefore, (6.6-9) can be expressed in terms of the electrical angular velocity of the rotor as

$$pW_m = -T_e \left( \frac{2}{P} \right) p\theta_r \quad (6.6-11)$$

Therefore, (6.6-6) can be written as

$$\left( \frac{2}{3} \right) pW_e = pW_f + T_e \left( \frac{2}{P} \right) p\theta_r \quad (6.6-12)$$

If we compare (6.6-12) with (6.6-8), and if we equate coefficients of  $p\theta_r$ , we can express torque, positive for motor action, as

$$T_e = \left( \frac{3}{2} \right) \left( \frac{P}{2} \right) (\lambda'_{qr} i'_{dr} - \lambda'_{dr} i'_{qr}) \quad (6.6-13)$$

It is important to note that this expression for torque is valid for linear or nonlinear magnetic systems and that it was arrived at without evaluating field or coenergy. It would appear that since we are working in the arbitrary reference frame that (6.6-13) would be valid in all reference frames. This is not the case; there is one exception. In the rotor reference frame where  $p\theta = p\theta_r$ , the  $qr'$  and  $dr'$  variables disappear as coefficients of  $p\theta_r$  and the expression for torque becomes

$$T_e = \left( \frac{3}{2} \right) \left( \frac{P}{2} \right) (\lambda_{ds}^r i_{qs}^r - \lambda_{qs}^r i_{ds}^r) \quad (6.6-14)$$

where the raised  $r$  is used to denote variables in the rotor reference frame. It is interesting that this approach for deriving an expression for torque was used by Park in his 1929 paper [2]; however, his expression was the negative of (6.6-14) since he was dealing with a synchronous generator and considered power output as positive where we are considering power input as positive. There is another slight difference; Park did not consider a “complete” power balance since he did not include the field or damper circuits in his derivation. However, since, in the rotor reference frame, the voltage equations associated with these circuits do not contain a  $p\theta_r$  term; therefore, the expression for torque given by Park is consistent with the power balance approach.

It would seem that if in any reference frame where terms other than  $\lambda'_{dr}i'_{qr}$  and  $\lambda'_{qr}i'_{dr}$  products are coefficients of  $p\theta_r$ , then (6.6-13) would not be valid. We found that this was true when  $p\theta = p\theta_r$ . Now, the rotor circuits of a synchronous machine are unsymmetrical since the field winding and the damper windings do not form a symmetrical two- or three-phase set. Let us backup for a moment, (6.6-8) is valid for a machine with symmetrical stator windings and symmetrical rotor windings and can be used to obtain an expression for torque in any reference frame regardless if the magnetic system is linear or nonlinear. If either the stator or rotor windings are unsymmetrical, then (6.6-8) can still be used to obtain an expression for torque (linear or nonlinear magnet system) if we select the reference frame to be where the asymmetry exists;  $p\theta = p\theta_r$ , for rotor asymmetry and  $p\theta = 0$  for stator asymmetry.

It is also interesting that in the case of a linear magnetic system, the coefficient of  $p\theta$  in (6.6-8) becomes zero. Whereupon, (6.6-13) becomes valid in all reference frames. This would seem to fly in the face of (6.6-14). However, for a linear magnetic system, (6.6-13) and (6.6-14) are equal. Moreover,

$$T_e = \left( \frac{3}{2} \right) \left( \frac{P}{2} \right) L_M (i_{qs}i'_{dr} - i_{ds}i'_{qr}) \quad (6.6-15)$$

is also a valid expression for torque if the magnetic system is linear. Therefore, in the case of a linear magnetic system we have identified three expressions for torque in terms of arbitrary reference-frame variables that are identical; (6.6-13), (6.6-14) with the raised  $r$  removed, and (6.6-15). The reader may wish to verify these statements.

Also, the above expressions for torque are often written in terms of flux linkages per second and currents. For example, (6.6-13) can be written as

$$T_e = \left( \frac{3}{2} \right) \left( \frac{P}{2} \right) \left( \frac{1}{\omega_b} \right) (\psi'_{qr}i'_{dr} - \psi'_{dr}i'_{qr}) \quad (6.6-16)$$

It is left to the reader to show that in terms of flux linkages per second the electromagnetic torque may be expressed as

$$T_e = \left( \frac{3}{2} \right) \left( \frac{P}{2} \right) \left( \frac{X_M}{D\omega_b} \right) (\psi_{qs}\psi'_{dr} - \psi'_{qr}\psi_{ds}) \quad (6.6-17)$$

where  $D$  is defined by (6.5-39).

## 6.7. COMMONLY USED REFERENCE FRAMES

Although the behavior of a symmetrical induction machine may be described in any frame of reference, there are three that are commonly employed. Namely, the stationary reference frame first employed by H.C. Stanley [3], the rotor reference frame that is Park's transformation [2] applied to induction machines (Brereton et al. [4]), and

the synchronously rotating reference frame [5]. The voltage equations for each of these reference frames may be obtained from the voltage equations in the arbitrary reference frame by assigning the appropriate speed to  $\omega$ . That is,  $\omega = 0$  for the stationary,  $\omega = \omega_r$  for the rotor, and  $\omega = \omega_e$  for the synchronously rotating reference frame.

Generally, the conditions of operation will determine the most convenient reference frame for analysis and/or simulation purposes [1]. If, for example, the stator voltages are unbalanced or discontinuous and the rotor applied voltages are balanced or zero; the stationary reference frame should be used to simulate the performance of the induction machine. If, on the other hand, the external rotor circuits are unbalanced but the applied stator voltages are balanced, then the reference frame fixed in the rotor is most convenient. Either the stationary or synchronously rotating reference frame is generally used to analyze balanced or symmetrical conditions. Linearized machine equations that are used to determine eigenvalues and to express linearized transfer functions for use in control system analysis are obtained from the voltage equations expressed in the synchronously rotating reference frame. The synchronously rotating reference frame is also particularly convenient when incorporating the dynamic characteristics of an induction machine into a digital computer program used to study the transient and dynamic stability of large power systems. The synchronously rotating reference frame may also be useful in variable frequency applications if it is permissible to assume that the stator voltages are a balanced sinusoidal set. In this case, variable frequency operation may be analyzed by varying the speed of the arbitrary reference frame to coincide with the electrical angular velocity of the applied stator voltages. A word of caution is perhaps appropriate. Regardless of the reference frame being used, the stator and rotor voltages and currents must be properly transformed to and from this reference frame. In most cases, these transformations are straightforward and can be accomplished implicitly. However, it may be necessary to actually include or implement a transformation in the analysis or computer simulation of an induction machine whereupon special care must be taken.

## 6.8. PER UNIT SYSTEM

It is often convenient to express machine parameters and variables as per unit quantities. Base power and base voltage are selected, and all parameters and variables are normalized using these base quantities. When the machine is being considered separately, the base power is generally selected as the horsepower rating of the machine in volt-amperes (i.e., horsepower times 746). If, on the other hand, the machine is a part of a power system and if it is desirable to convert the entire system to per unit quantities, then only one power base (VA base) is selected that would most likely be different from the rating of any machine in the system. Here we will consider the machine separately with the rating of the machine taken as base power.

Although we will violate this convention from time to time when dealing with instantaneous quantities, the rms value of the rated phase voltage is generally selected as base voltage for the *abc* variables while the peak value is generally selected as base

voltage for the  $qd0$  variables. That is, if  $V_{B(abc)}$  is the rms voltage selected as base voltage for the  $abc$  variables, then  $V_{B(qd0)} = \sqrt{2}V_{B(abc)}$ . The base power may be expressed

$$P_B = 3V_{B(abc)}I_{B(abc)} \quad (6.8-1)$$

or

$$P_B = \left(\frac{3}{2}\right)V_{B(qd0)}I_{B(qd0)} \quad (6.8-2)$$

Therefore, since base voltage and base power are selected, base current can be calculated from either (6.8-1) or (6.8-2). It follows that the base impedance may be expressed

$$\begin{aligned} Z_B &= \frac{V_{B(abc)}}{I_{B(abc)}} \\ &= \frac{3V_{B(abc)}^2}{P_B} \end{aligned} \quad (6.8-3)$$

or

$$\begin{aligned} Z_B &= \frac{V_{B(qd0)}}{I_{B(qd0)}} \\ &= \left(\frac{3}{2}\right)\frac{V_{B(qd0)}^2}{P_B} \end{aligned} \quad (6.8-4)$$

The  $qd0$  equations written in terms of reactances, (6.5-22)–(6.5-33) can be readily converted to per unit by dividing the voltages by  $V_{B(qd0)}$ , the currents by  $I_{B(qd0)}$ , and the resistances and reactances by  $Z_B$ . Note that since a flux linkage per second is a volt, it is per unitized by dividing by the base voltage.

Although the voltage and flux linkage per second equations do not change form when per unitized, the torque equation is modified by the per unitizing process. For this purpose, the base torque may be expressed as

$$T_B = \frac{P_B}{(2/P)\omega_b} \quad (6.8-5)$$

where  $\omega_b$  corresponds to rated or base frequency of the machine. A word of caution is appropriate. If, in (6.8-5),  $P_B$  is the rated power of the machine, then base torque  $T_B$  will not be rated torque. We will find that in the case of an induction machine, rated power generally occurs at rated speed that is less than synchronous. Hence,  $T_B$  will be less than rated torque by the ratio of rated speed to synchronous speed.

If the torque expression given by (6.6-16) is divided by (6.8-5), with (6.8-2) substituted for  $P_B$ , the multiplier  $(\frac{3}{2})(P/2)(1/\omega_b)$  is eliminated, and with all quantities expressed in per unit, the per unit torque becomes

$$T_e = \psi'_{qr}i'_{dr} - \psi'_{dr}i'_{qr} \quad (6.8-6)$$

If the electrical variables are expressed in volts, amperes, and watts, then the inertia of the rotor is expressed in mks units. If, however, the per unit system is used the inertia is expressed in seconds. This can be shown by first recalling from (6.3-8) that the inertial torque  $T_{IT}$  for a  $P$ -pole machine may be expressed

$$T_{IT} = J\left(\frac{2}{P}\right)p\omega_r \quad (6.8-7)$$

where  $\omega_r$  is the electrical angular velocity of the rotor and  $J$  is the inertia of the rotor and connected mechanical load expressed in  $\text{kg}\cdot\text{m}^2$ . In order to express (6.8-7) in per unit, it is divided by base torque, and the rotor speed is normalized to base speed. Thus

$$T_{IT} = \frac{J(2/P)\omega_b}{T_B} p \frac{\omega_r}{\omega_b} \quad (6.8-8)$$

By definition, the inertia constant expressed in seconds is

$$\begin{aligned} H &= \left(\frac{1}{2}\right)\left(\frac{2}{P}\right)\frac{J\omega_b}{T_B} \\ &= \left(\frac{1}{2}\right)\left(\frac{2}{P}\right)^2 \frac{J\omega_b^2}{P_B} \end{aligned} \quad (6.8-9)$$

Thus, in per unit (6.3-8) becomes

$$T_e = 2Hp \frac{\omega_r}{\omega_b} + T_L \quad (6.8-10)$$

It is important to become familiar with both systems of units and to be able to convert readily from one to the other. We will use both systems interchangeably throughout the text.

## 6.9. ANALYSIS OF STEADY-STATE OPERATION

The voltage equations that describe the balanced steady-state operation of an induction machine may be obtained in several ways. For balanced conditions, the zero quantities of the stator and rotor are zero, and from our work in Chapter 3, we know that for balanced steady-state conditions, the  $q$  and  $d$  variables are sinusoidal in all reference

frames except the synchronously rotating reference frame wherein they are constant. Hence, one method of obtaining the steady-state voltage equations for balanced conditions is to first recall that in an asynchronously rotating reference frame the steady-state voltages are related by

$$\tilde{F}_{ds} = j\tilde{F}_{qs} \quad (6.9-1)$$

and with  $\theta(0) = 0$

$$\tilde{F}_{qs} = \tilde{F}_{as} \quad (6.9-2)$$

Since the induction machine is a symmetrical device, (6.9-1) and (6.9-2) also apply to the stator currents and flux linkages. Likewise, the steady-state rotor variables are related by

$$\tilde{F}'_{dr} = j\tilde{F}'_{qr} \quad (6.9-3)$$

and with  $\theta(0)$  and  $\theta_r(0)$  both selected equal to zero

$$\tilde{F}'_{qr} = \tilde{F}'_{ar} \quad (6.9-4)$$

Appropriate substitution of these equations into either (6.5-22) and (6.5-25) or (6.5-23) and (6.5-26) yields the standard steady-state voltage equations in phasor form. A second method is to express (6.5-22), (6.5-23), (6.5-25), and (6.5-26) in the synchronously rotating reference frame. Since for balanced steady-state operation the variables are constants, the time rate of change of all flux linkages is zero. Therefore, the phasor voltage equations may be derived by employing the relationships

$$\sqrt{2}\tilde{F}_{as} = F_{qs}^e - jF_{ds}^e \quad (6.9-5)$$

$$\sqrt{2}\tilde{F}'_{ar} = F'_{qr}^e - jF'_{dr}^e \quad (6.9-6)$$

We will proceed using the first approach and leave the latter as an exercise for the reader.

If, in (6.5-22) and (6.5-25),  $p$  is replaced by  $j(\omega_e - \omega)$ , the equations may be written in phasor form as

$$\tilde{V}_{qs} = r_s \tilde{I}_{qs} + \frac{\omega}{\omega_b} \tilde{\psi}_{ds} + j \left( \frac{\omega_e - \omega}{\omega_b} \right) \tilde{\psi}_{qs} \quad (6.9-7)$$

$$\tilde{V}'_{qr} = r'_r \tilde{I}'_{qr} + \left( \frac{\omega - \omega_r}{\omega_b} \right) \tilde{\psi}'_{dr} + j \left( \frac{\omega_e - \omega}{\omega_b} \right) \tilde{\psi}'_{qr} \quad (6.9-8)$$

Substituting (6.9-1) and (6.9-3) into the above equations yields

$$\tilde{V}_{qs} = r_s \tilde{I}_{qs} + j \frac{\omega_e}{\omega_b} \tilde{\psi}_{qs} \quad (6.9-9)$$

$$\tilde{V}'_{qr} = r'_r \tilde{I}'_{qr} + j \left( \frac{\omega_e - \omega_r}{\omega_b} \right) \tilde{\psi}'_{qr} \quad (6.9-10)$$

The well-known steady-state phasor voltage equations, which are actually valid in all asynchronously rotating reference frames, are obtained by substituting the phasor form of (6.5-28) and (6.5-31) for  $\tilde{\psi}_{qs}$  and  $\tilde{\psi}'_{qr}$ , respectively, into (6.9-9) and (6.9-10), and employing (6.9-2) and (6.9-4) to replace  $qs$  and  $qr$  variables with  $as$  and  $ar$  variables, respectively.

$$\tilde{V}_{as} = \left( r_s + j \frac{\omega_e}{\omega_b} X_{ls} \right) \tilde{I}_{as} + j \frac{\omega_e}{\omega_b} X_M (\tilde{I}_{as} + \tilde{I}'_{ar}) \quad (6.9-11)$$

$$\frac{\tilde{V}'_{ar}}{s} = \left( \frac{r'_r}{s} + j \frac{\omega_e}{\omega_b} X'_{lr} \right) \tilde{I}'_{ar} + j \frac{\omega_e}{\omega_b} X_M (\tilde{I}_{as} + \tilde{I}'_{ar}) \quad (6.9-12)$$

where the slip  $s$  is defined as

$$s = \frac{\omega_e - \omega_r}{\omega_e} \quad (6.9-13)$$

Equations (6.9-11) and (6.9-12) suggest the equivalent circuit shown in Figure 6.9-1.

All voltage equations are valid regardless of the frequency of operation in that  $\omega_e$  and  $\omega_b$  are both given explicitly. Since  $\omega_b$  corresponds to rated frequency, it is generally used to calculate and per unitize the reactances. Although the ratio of  $\omega_e$  to  $\omega_b$  is generally not included in the steady-state voltage equations, this ratio makes (6.9-11) and (6.9-12) valid for applied voltages of any constant frequency. It should be clear that all products of the ratio of  $\omega_e$  to  $\omega_b$  times a reactance may be replaced by  $\omega_e$  times the appropriate inductance.

The steady-state electromagnetic torque can be expressed in terms of currents in phasor form by first writing the torque in terms of currents in the synchronously rotating

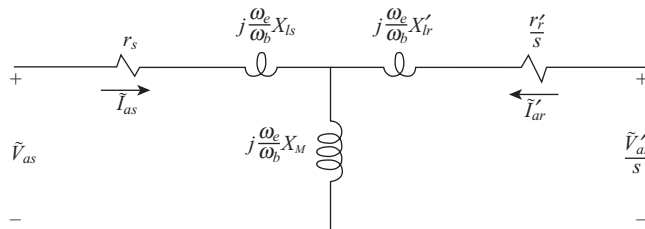


**Figure 6.9-1.** Equivalent circuit for steady-state operation of a symmetrical induction machine.

reference frame and then utilizing (6.9-5) and (6.9-6) to relate synchronously rotating reference frame and phasor quantities. The torque expression becomes

$$T_e = 3\left(\frac{P}{2}\right)\left(\frac{X_M}{\omega_b}\right)\text{Re}[j\tilde{I}_{as}^*\tilde{I}'_{ar}] \quad (6.9-14)$$

where  $\tilde{I}_{as}^*$  is the conjugate of  $\tilde{I}_{as}$ .

The balanced steady-state torque-speed or torque-slip characteristics of a singly excited (singly fed) induction machine warrants discussion. The vast majority of induction machines in use today are singly excited, wherein electric power is transferred to or from the induction machine via the stator circuits with the rotor windings short-circuited. Moreover, a vast majority of the singly excited induction machines are of the squirrel-cage rotor type. For singly fed machines,  $\tilde{V}'_{ar}$  is zero, whereupon

$$\tilde{I}'_{ar} = -\frac{j(\omega_e / \omega_b)X_M}{r'_r/s + j(\omega_e / \omega_b)X'_{rr}}\tilde{I}_{as} \quad (6.9-15)$$

where  $X'_{rr}$  is defined by (6.5-36). Substituting (6.9-15) into (6.9-14) yields

$$T_e = \frac{3\left(\frac{P}{2}\right)\left(\frac{\omega_e}{\omega_b}\right)\left(\frac{X_M^2}{\omega_b}\right)\left(\frac{r'_r}{s}\right)|\tilde{I}_{as}|^2}{\left(\frac{r'_r}{s}\right)^2 + \left(\frac{\omega_e}{\omega_b}\right)^2 X'^2_{rr}} \quad (6.9-16)$$

Now, the input impedance of the equivalent circuit shown in Figure 6.9-1, with  $\tilde{V}'_{ar}$  equal to zero, is

$$Z = \frac{\frac{r_s r'_r}{s} + \left(\frac{\omega_e}{\omega_b}\right)^2 (X_M^2 - X_{ss}X'_{rr}) + j \frac{\omega_e}{\omega_b} \left(\frac{r'_r}{s} X_{ss} + r_s X'_{rr}\right)}{\frac{r'_r}{s} + j \frac{\omega_e}{\omega_b} X'_{rr}} \quad (6.9-17)$$

where  $X_{ss}$  is defined by (6.5-35). Since

$$|\tilde{I}_{as}| = \frac{|\tilde{V}_{as}|}{|Z|} \quad (6.9-18)$$

the torque for a singly fed induction machine may be expressed as

$$T_e = \frac{3\left(\frac{P}{2}\right)\frac{\omega_e}{\omega_b}\left(\frac{X_M^2}{\omega_b}\right)r'_r s |\tilde{V}_{as}|^2}{\left[r'_r r'_r + s\left(\frac{\omega_e}{\omega_b}\right)^2 (X_M^2 - X_{ss}X'_{rr})\right]^2 + \left(\frac{\omega_e}{\omega_b}\right)^2 (r'_r X_{ss} + s r'_r X'_{rr})^2} \quad (6.9-19)$$

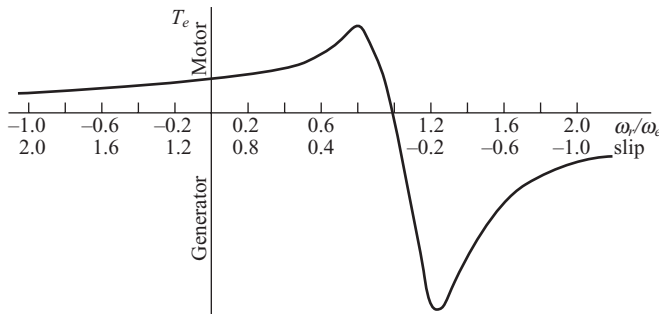


Figure 6.9-2. Steady-state torque–speed characteristics of a singly excited induction machine.

In per unit, (6.9-19) becomes

$$T_e = \frac{\frac{\omega_e}{\omega_b} X_M^2 r'_s |\tilde{V}_{as}|^2}{\left[ r_s r'_s + s \left( \frac{\omega_e}{\omega_b} \right)^2 (X_M^2 - X_{ss} X'_{rr}) \right]^2 + \left( \frac{\omega_e}{\omega_b} \right)^2 (r'_s X_{ss} + s r_s X'_{rr})^2} \quad (6.9-20)$$

The steady-state torque–speed or torque–slip characteristics typical of many singly excited multiphase induction machines are shown in Figure 6.9-2. Therein,  $\omega_e = \omega_b$ . Generally, the parameters of the machine are selected so that maximum torque occurs near synchronous speed, and the maximum torque output (motor action) is two or three times the rated torque of the machine.

An expression for the slip at maximum torque may be obtained by taking the derivative of (6.9-19) with respect to slip and setting the result equal to zero. Thus

$$s_m = r'_s G \quad (6.9-21)$$

where

$$G = \pm \left[ \frac{(\omega_e / \omega_b)^{-2} r_s^2 + X_{ss}^2}{(X_M^2 - X_{ss} X'_{rr})^2 \left( \frac{\omega_e}{\omega_b} \right)^2 + r_s^2 X'_{rr}^2} \right]^{\frac{1}{2}} \quad (6.9-22)$$

Two values of slip at maximum torque are obtained, one for motor action and one for generator action. It is important to note that  $G$  is not a function of  $r'_s$ ; thus the slip at maximum torque is directly proportional to  $r'_s$ . Consequently, with all other machine parameters constant, the speed at which maximum steady-state torque occurs may be varied by inserting external rotor resistance. This feature is often used when starting

large motors that have coil-wound rotors with slip rings. In this application, balanced external rotor resistances are inserted so that maximum torque occurs near stall. As the machine speeds up, the external resistors are reduced to zero. On the other hand, two-phase induction machines are often designed with high-resistance rotor windings to achieve a large starting torque.

It may at first appear that the magnitude of the maximum torque would be influenced by  $r'_r$ . However, if (6.9-21) is substituted in (6.9-19), the maximum torque is expressed as

$$T_{e(max)} = \frac{3\left(\frac{P}{2}\right)\left(\frac{\omega_e}{\omega_b}\right)\left(\frac{X_M^2}{\omega_b}\right)G|\tilde{V}_{as}|^2}{\left[r_s + G\left(\frac{\omega_e}{\omega_b}\right)^2(X_M^2 - X_{ss}X'_{rr})\right]^2 + \left(\frac{\omega_e}{\omega_b}\right)^2(X_{ss} + Gr_sX'_{rr})^2} \quad (6.9-23)$$

Equation (6.9-23) is independent of  $r'_r$ . Thus the maximum torque remains constant if only  $r'_r$  is varied. The effect of changing  $r'_r$  is illustrated in Figure 6.9-3; therein  $r'_{r3} > r'_{r2} > r'_{r1}$ .

In variable frequency drive systems, the operating speed of the electric machine (reluctance, synchronous, or induction) is changed by changing the frequency of the applied voltages by either an inverter or a cycloconverter arrangement. As mentioned previously, the phasor voltage equations are applicable regardless of the frequency of operation. It is only necessary to keep in mind that the reactances given in the steady-state equivalent circuits, Figure 6.9-1, are defined by the product of  $\omega_b$  and the inductances. As frequency is decreased, the time rate of change of the steady-state variables is decreased proportionally. Thus, the reactances, or  $(\omega_e/\omega_b)X$  in the equivalent circuit,

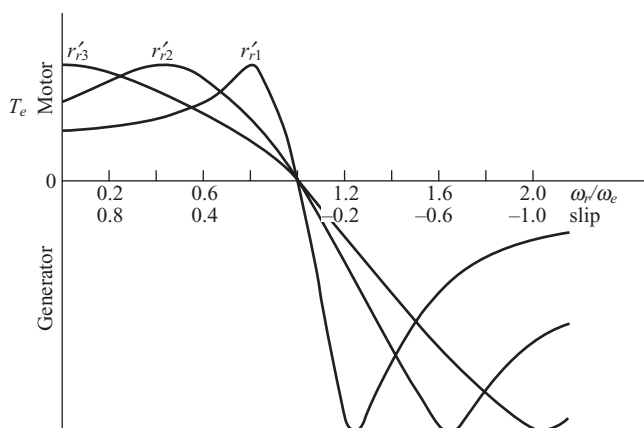


Figure 6.9-3. Steady-state torque-speed characteristics of a singly excited induction machine for various values of rotor resistance.

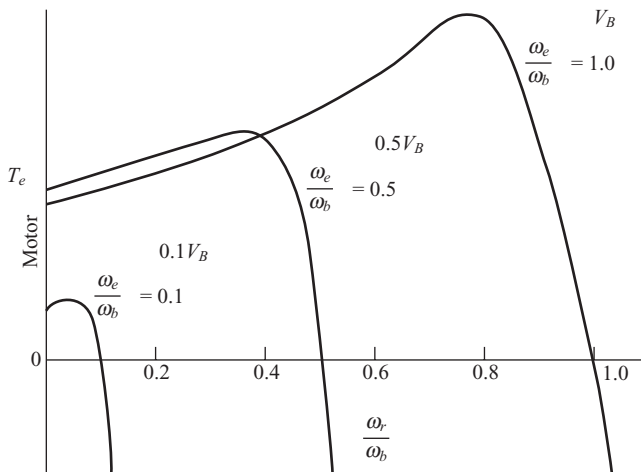


Figure 6.9-4. Steady-state torque–speed characteristics of a singly excited symmetrical induction machine for various operating frequencies.

decrease linearly with frequency. If the amplitude of the applied voltages is maintained at the rated value, the current will become excessive since the magnitude of the impedance decreases as frequency decreases. In order to prevent large currents, the magnitude of the stator voltages is decreased as the frequency is decreased. In many applications, the voltage magnitude is reduced linearly with frequency until a low frequency is reached, whereupon the decrease in voltage is programmed in a manner to compensate for the effects of the stator resistance.

The influence of frequency upon the steady-state torque–speed characteristics is illustrated in Figure 6.9-4. These characteristics are for a linear relationship between the magnitude of the applied voltages and frequency. The machine is designed to operate at  $\omega_e = \omega_b$ , where  $\omega_b$  corresponds to the base or rated frequency. Rated voltage is applied at rated frequency, that is, when  $\omega_e = \omega_b$ ,  $|\tilde{V}_{as}| = V_B$ , where  $V_B$  is the rated or base voltage. The maximum torque is reduced markedly at  $\omega_e/\omega_b = 0.1$ . At this frequency, the voltage would probably be increased somewhat so as to obtain a higher torque. Perhaps a voltage of say  $0.15V_B$  or  $0.2V_B$  would be used rather than  $0.1V_B$ . Saturation may, however, cause the current to be excessive at this higher voltage. These practical considerations of variable frequency drives are of major importance but beyond the scope of this chapter.

**EXAMPLE 6A** The parameters for the equivalent circuit shown in Figure 6.9-1 may be calculated using electric field theory or determined from tests [6]. The tests generally performed are a dc test, a no-load test, and a blocked-rotor test. The following test data are given for a 5-hp, four-pole, 220-V, three-phase, 60-Hz induction machine [7] where all ac voltages and currents are rms values

DC Test	No-Load Test	Blocked-Rotor Test
$V_{dc} = 13.8 \text{ V}$	$V_{nl} = 220 \text{ V}$	$V_{br} = 23.5 \text{ V}$
$I_{dc} = 13.0 \text{ A}$	$I_{nl} = 3.86 \text{ A}$	$I_{br} = 12.9 \text{ A}$
	$P_{nl} = 200 \text{ W}$	$P_{br} = 469 \text{ W}$
	$f = 60 \text{ Hz}$	$f = 15 \text{ Hz}$

During the dc test, a dc voltage is applied across two terminals while the machine is at standstill. Thus, assuming the stator windings are wye connected,

$$r_s = \frac{1}{2} \frac{V_{dc}}{I_{dc}} = \frac{13.8}{2 \times 13} = 0.531 \Omega \quad (6A-1)$$

The no-load test, which is analogous to the transformer open-circuit test, is performed with balanced three-phase, 60Hz voltages applied to the stator windings without mechanical load on the machine (no load). The power input during this test is the sum of the stator ohmic losses, the core losses due to hysteresis and eddy current losses, and rotational losses due to friction and windage. The stator ohmic losses are ( $I_{nl}$  is a phase current)

$$P_{I^2 r_s} = 3I_{nl}^2 r_s = 3 \times (3.86)^2 \times 0.531 = 23.7 \text{ W} \quad (6A-2)$$

Therefore, the power loss due to friction and windage losses and core losses is

$$P_{FWC} = P_{nl} - P_{I^2 r_s} = 200 - 23.7 = 176.3 \text{ W} \quad (6A-3)$$

In the equivalent circuit shown in Figure 6.9-1, this loss is neglected. It is generally small, and in most cases, little error is introduced by neglecting it. It can be taken into account by placing a resistor in shunt with the magnetizing reactance  $X_M$  or by applying a small mechanical load (torque) to the shaft of the machine.

It is noted from the no-load test data that the power factor is very small since the apparent power is ( $V_{nl}$  is a line-to-line voltage)

$$|S_{nl}| = \sqrt{3}V_{nl}I_{nl} = \sqrt{3} \times 220 \times 3.86 = 1470.9 \text{ VA} \quad (6A-4)$$

Therefore, the no-load impedance is highly inductive and its magnitude is assumed to be the sum of the stator leakage reactance and the magnetizing reactance since the rotor speed is essentially synchronous, whereupon  $r'_r/s$  is much larger than  $X_M$ . Thus

$$\begin{aligned}
 X_{ls} + X_M &= \frac{V_{nl}}{\sqrt{3}I_{nl}} \\
 &= \frac{220}{\sqrt{3} \times 3.86} = 32.9 \Omega
 \end{aligned} \tag{6A-5}$$

During the blocked-rotor test, which is analogous to the transformer short-circuit test, the rotor is locked by some external means and balanced three-phase stator voltages are applied. The frequency of the applied voltage is often less than rated in order to obtain a representative value of  $r'_r$  since, during normal operation, the frequency of the rotor currents is low and the rotor resistances of some induction machines vary considerably with frequency [6]. During stall, the impedance  $r'_r + jX'_{lr}$  is much smaller in magnitude than  $X_M$ , whereupon the current flowing in the magnetizing reactance may be neglected. Hence

$$P_{br} = 3I_{br}^2(r_s + r'_r) \tag{6A-6}$$

From that

$$\begin{aligned}
 r'_r &= \frac{P_{br}}{3I_{br}^2} - r_s \\
 &= \frac{469}{3 \times (12.9)^2} - 0.531 = 0.408 \Omega
 \end{aligned} \tag{6A-7}$$

The magnitude of the blocked-rotor input impedance is ( $V_{br}$  is a line-to-line voltage)

$$\begin{aligned}
 |Z_{br}| &= \frac{V_{br}}{\sqrt{3}I_{br}} \\
 &= \frac{23.5}{\sqrt{3} \times 12.9} = 1.052 \Omega
 \end{aligned} \tag{6A-8}$$

Now

$$\left| (r_s + r'_r) + j \frac{15}{60} (X_{ls} + X'_{lr}) \right| = 1.052 \Omega \tag{6A-9}$$

From that

$$\begin{aligned}
 \left[ \frac{15}{60} (X_{ls} + X'_{lr}) \right]^2 &= (1.052)^2 - (r_s + r'_r)^2 \\
 &= (1.052)^2 - (0.531 + 0.408)^2 \\
 &= 0.225 \Omega
 \end{aligned} \tag{6A-10}$$

Thus

$$X_{ls} + X'_{lr} = 1.9 \Omega \quad (6A-11)$$

Generally  $X_{ls}$  and  $X'_{lr}$  are assumed equal; however, in some types of induction machines, a different ratio is suggested [6]. We will assume that  $X_{ls} = X'_{lr}$ , whereupon we have determined the machine parameters. In particular, for  $\omega_b = 377$  rad/s, the parameters are

$$\begin{aligned} r_s &= 0.531 \Omega & X_M &= 31.95 \Omega & r'_r &= 0.408 \Omega \\ X_{ls} &= 0.95 \Omega & & & X'_{lr} &= 0.95 \Omega \end{aligned}$$

## 6.10. FREE ACCELERATION CHARACTERISTICS

It is instructive to observe the variables of several induction machines during free (no-load) acceleration from stall. For this purpose, the nonlinear differential equations that describe the induction machine were simulated on a computer and studies were performed. The parameters of the machines are from Reference 8 and given here in Table 6.10-1. Each machine is a four-pole, 60 Hz, three-phase induction motor. The parameters are expressed in ohms using the 60 Hz value of the reactances. In Table 6.10-1, the voltage is the rated rms line-to-line voltage, the speed is rated speed, and  $J$  includes the inertia of the load that is assumed to be equal to the inertia of the rotor. Base torque, as calculated from (6.8-5), and base or rated current (rms) are also given.

The torque-versus-speed characteristics during free acceleration are shown for each machine in Figure 6.10-1, Figure 6.10-2, Figure 6.10-3, Figure 6.10-4, Figure 6.10-5, and Figure 6.10-6. In each case, the machine is initially stalled when rated balanced voltage is applied with  $v_{as} = \sqrt{2}V_s \cos \omega_e t$ . The machine currents along with the electromagnetic torque and speed for the 3- and 2250-hp machines during free acceleration are shown in Figure 6.10-5 and Figure 6.10-6. Since friction and windage losses are not represented, the machines accelerate to synchronous speed. In all figures, the scales of the currents are given in multiples of rated peak values. The scale of the torque is given in multiples of base torque.

At stall, the input impedance of the induction machine is essentially the stator resistance and leakage reactance in series with the rotor resistance and leakage

TABLE 6.10-1. Induction Machine Parameters

Machine Rating			$T_B$	$I_{B(abc)}$	$r_s$	$X_{ls}$	$X_M$	$X'_{lr}$	$r'_r$	$J$
hp	volts	rpm	N·m	amps	ohms	ohms	ohms	ohms	ohms	kg·m <sup>2</sup>
3	220	1710	11.9	5.8	0.435	0.754	26.13	0.754	0.816	0.089
50	460	1705	198	46.8	0.087	0.302	13.08	0.302	0.228	1.662
500	2300	1773	$1.98 \times 10^3$	93.6	0.262	1.206	56.02	1.206	0.187	11.06
2250	2300	1786	$8.9 \times 10^3$	421.2	0.029	0.226	13.04	0.226	0.022	63.87

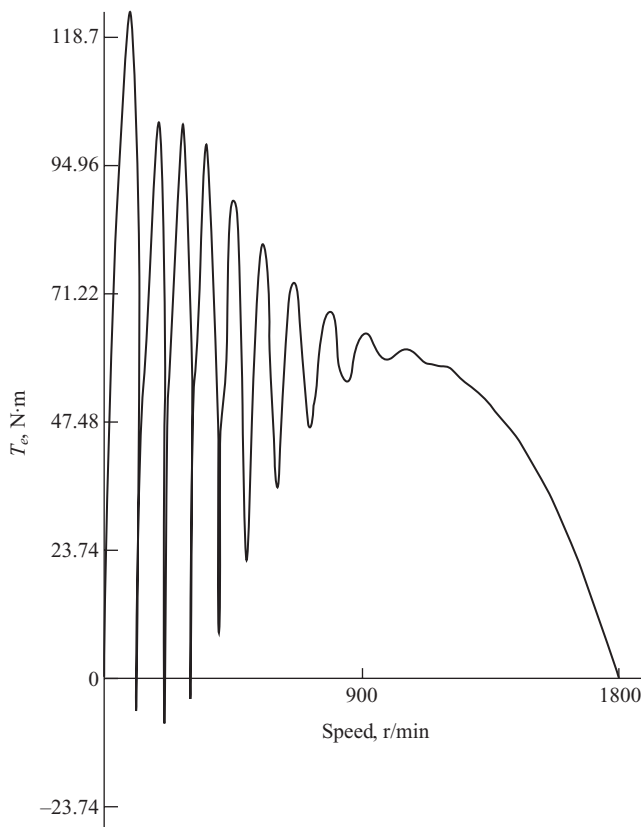
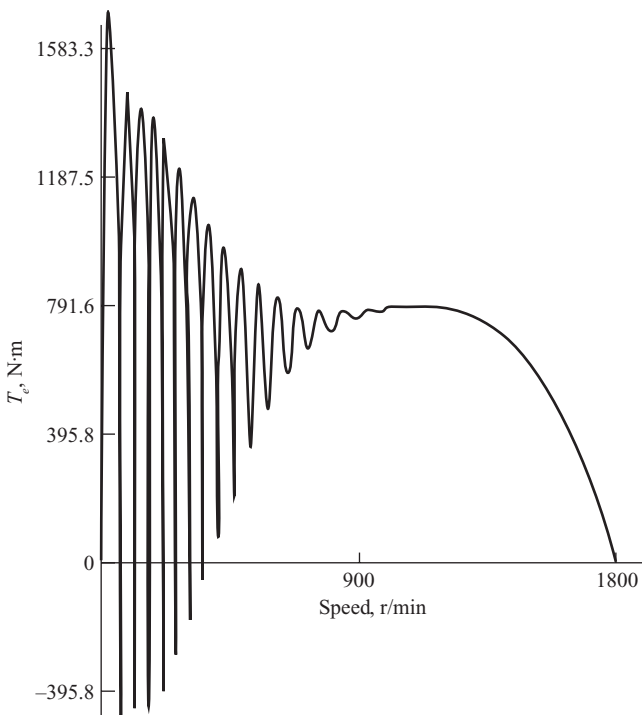


Figure 6.10-1. Torque–speed characteristics during free acceleration: 3-hp induction motor.

reactance. Consequently, with rated voltage applied, the starting current is large, in some cases, in the order of 10 times the rated value. Therefore, in practice, a compensator (transformer) is generally used to start large horsepower machines with reduced voltage until the machine has reached 60–80% of synchronous speed whereupon full voltage is applied.

The 3- and 50-hp machines are relatively high-slip machines, that is, rated torque is developed at a speed considerably less than synchronous speed. On the other hand, the 500- and 2250-hp machines are low-slip machines. These characteristics are evident in the torque–speed characteristics shown in Figure 6.10-1, Figure 6.10-2, Figure 6.10-3, Figure 6.10-4, Figure 6.10-5, and Figure 6.10-6.

The transient torque–speed characteristics are different from the steady-state torque–speed characteristics in several respects. The instantaneous electromagnetic torque, immediately following the application of the stator voltages, varies at 60 Hz, about an average positive value. This decaying, 60 Hz variation in the instantaneous torque is due to the transient offset in the stator currents. Although the offset in each



**Figure 6.10-2.** Torque-speed characteristics during free acceleration: 50-hp induction motor.

of the stator currents depends upon the values of the source voltages at the time of application, the instantaneous torque is independent of the initial values of balanced source voltages since the machine is symmetrical. We also note from the current traces in Figure 6.10-5 and Figure 6.10-6 that the envelope of the machine currents varies during the transient period. It is shown in a subsequent chapter that this is due to the interaction of the stator and rotor electric transients.

Another noticeable difference between the dynamic and steady-state torque-speed characteristics occurs in the case of the 500- and 2250-hp machines. In particular, the rotor speed overshoots synchronous speed and the instantaneous torque and speed demonstrate decayed oscillations about the final operating point. This characteristic is especially evident in the larger horsepower machines; however, in the case of the 3- and 50-hp machines, the rotor speed is highly damped and the final operating condition is attained without oscillations. It is noted from Table 6.10-1 that the ratio of rotor leakage reactance to rotor resistance is much higher for the larger horsepower machines than for the smaller. In a later chapter, we find that the complex conjugate pair of eigenvalues, associated with the rotor circuits, are much less damped in the case of the 500- and 2250-hp machines than in the case of the 3- and 50-hp machines.

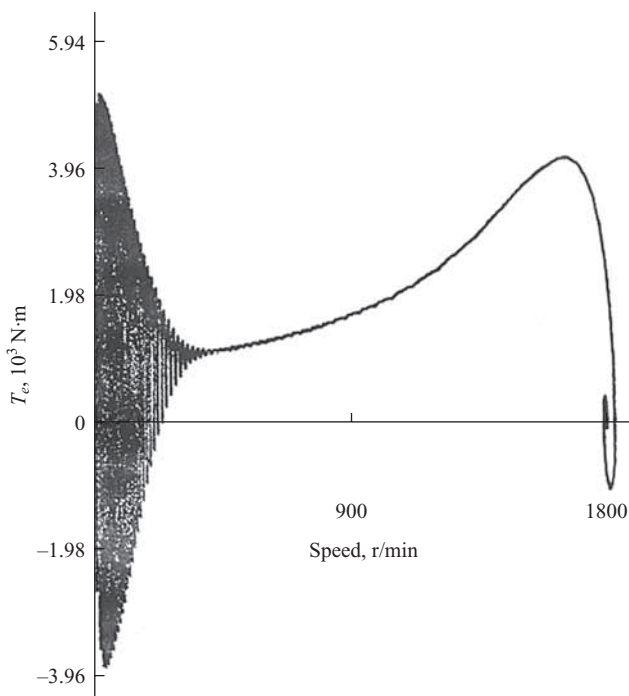


**Figure 6.10-3.** Torque-speed characteristics during free acceleration: 500-hp induction motor.

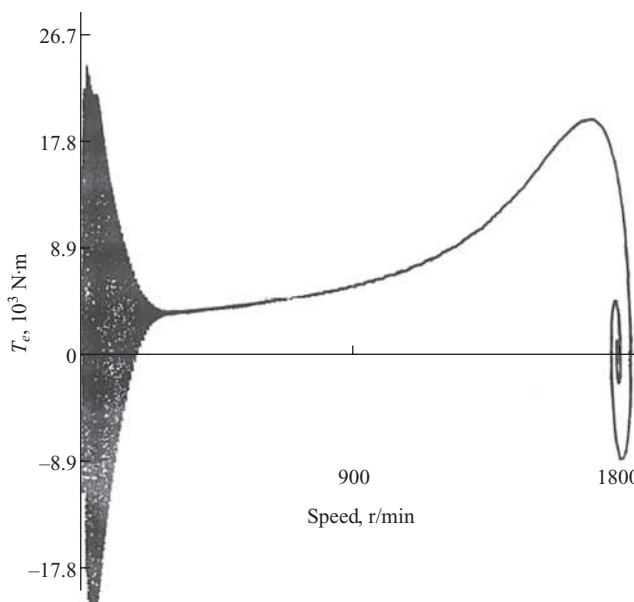


**Figure 6.10-4.** Torque-speed characteristics during free acceleration: 2250-hp induction motor.

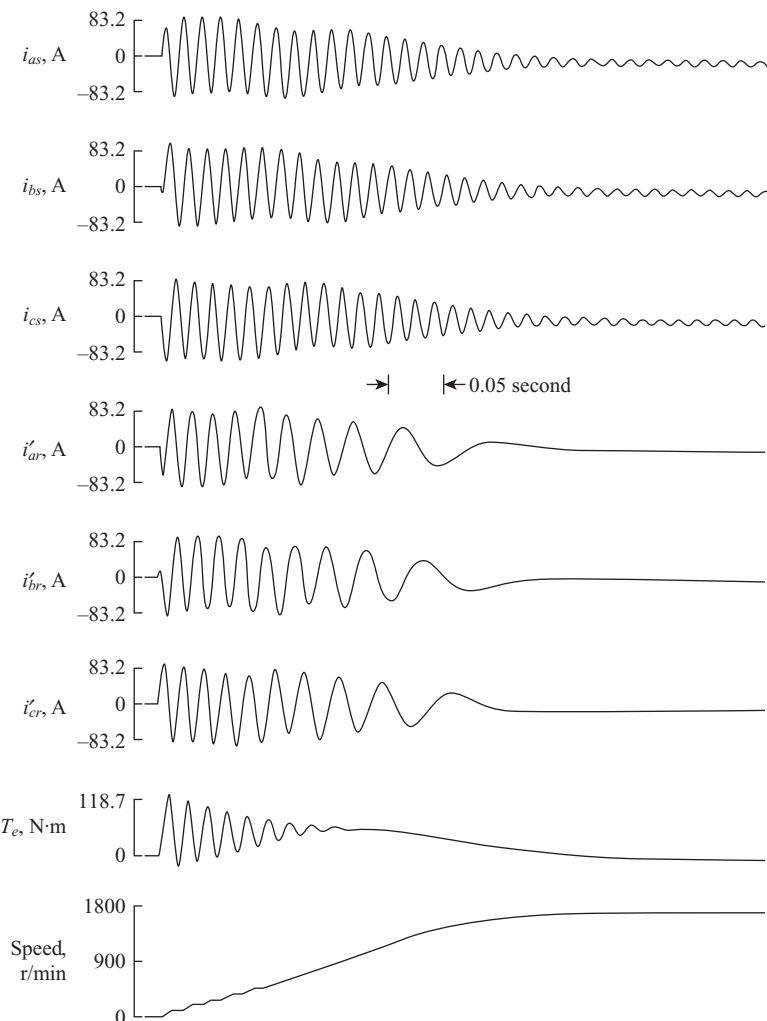


Figure 6.10-5. Machine variables during free acceleration of a 3-hp induction motor.

If we were to plot the steady-state torque–speed characteristics of the 3- and 50-hp machines upon the free acceleration torque–speed characteristics, we would find that the steady-state torque corresponds very closely to the average of the transient torque. This, however, is not the case for the 500- and 2250-hp machines where the steady-state value of maximum torque is much larger than that observed from the free acceleration characteristics. This is illustrated in Figure 6.10-7 and Figure 6.10-8 where the steady-state torque–speed characteristic is superimposed upon the free acceleration characteristic for the 500- and 2250-hp machines. In a later chapter, this difference is shown to be due primarily to the electric transients in the rotor circuits.

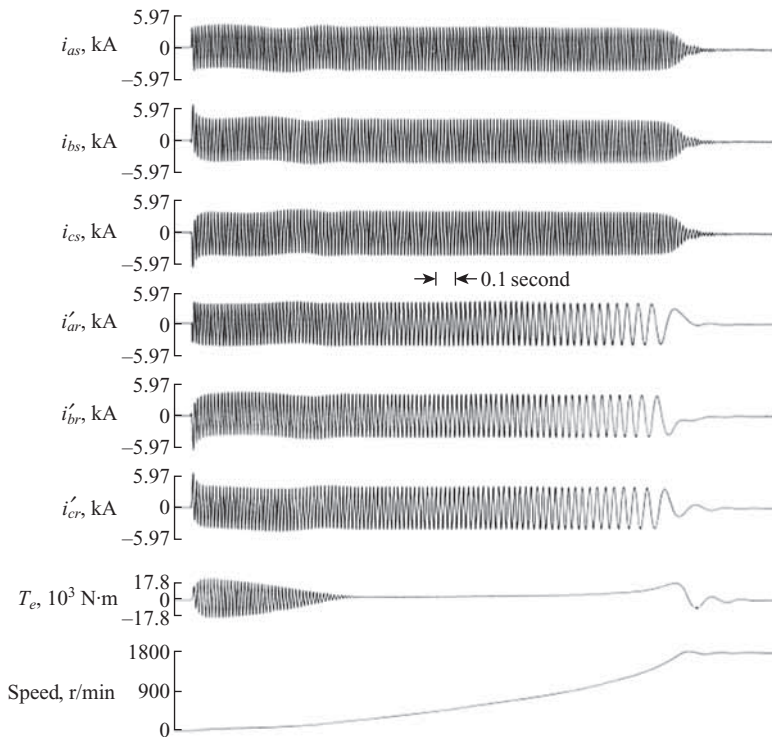


Figure 6.10-6. Machine variables during free acceleration of a 2250-hp induction motor.

**EXAMPLE 6B** Let us calculate the steady-state torque and current at stall for the 3-hp machine given in Table 6.10-1 and compare these values to those shown in Figure 6.10-1 and Figure 6.10-5. From (6.9-19) and Table 6.10-1 with  $s = 1$

$$\begin{aligned}
 T_e &= \frac{(3)(4/2)(1)[(26.13)^2 / 377](0.816)(1)(220 / \sqrt{3})^2}{[(0.435)(0.816) + (1)(1)^2(26.13^2 - 26.884 \times 26.884)]^2} \\
 &\quad + (1)^2(0.816 \times 26.884 + 1 \times 0.435 \times 26.884)^2 \\
 &= 51.9 \text{ N} \cdot \text{m}
 \end{aligned} \tag{6B-1}$$

This is approximately the average of the pulsating torque at  $\omega_r = 0$  depicted in Figure 6.10-1 and Figure 6.10-5.

The stall, steady-state current may be calculated from

$$\begin{aligned}
 \tilde{I}_{as} &= \frac{\tilde{V}_{ds}}{(r_s + r'_r) + j(X_{ls} + X'_{lr})} \\
 &= \frac{(220 / \sqrt{3}) / 0^\circ}{(0.435 + 0.816) + j(0.754 + 0.754)} \\
 &= 64.8 / -50.3^\circ \text{A}
 \end{aligned} \tag{6B-2}$$

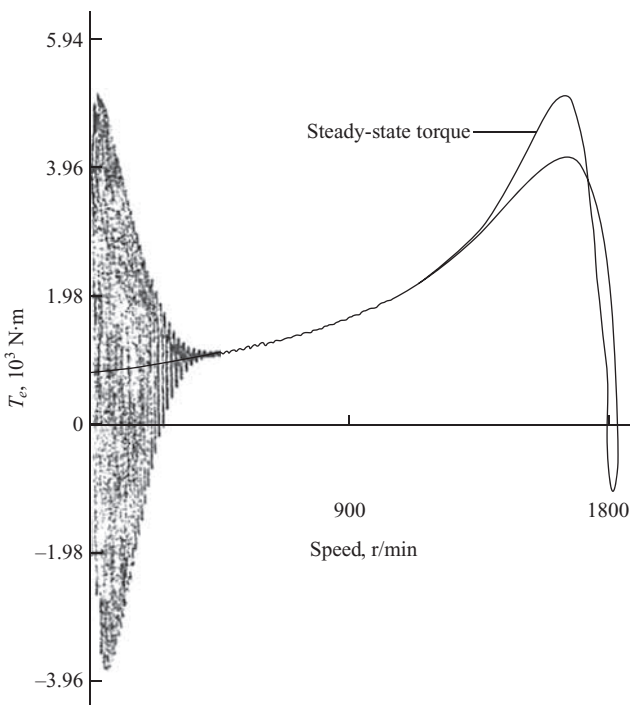


**Figure 6.10-7.** Comparison of steady-state and free acceleration torque–speed characteristics: 500-hp induction motor.

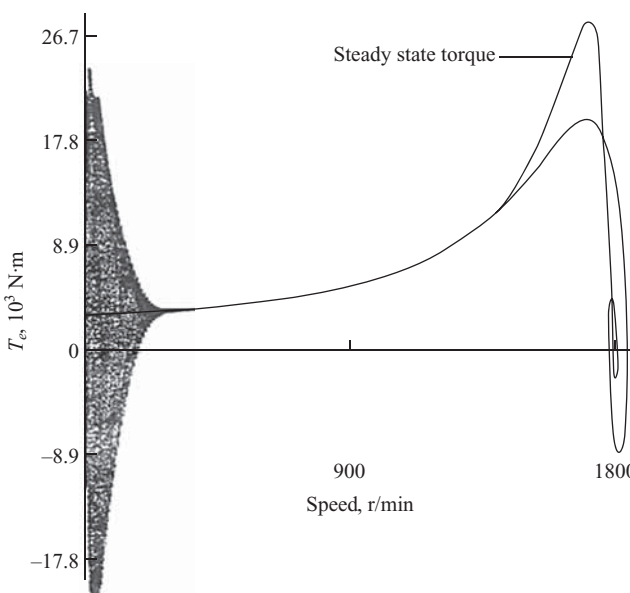


**Figure 6.10-8.** Comparison of steady-state and free acceleration torque–speed characteristics: 2250-hp induction motor.

This value is the steady-state current that would occur if the rotor is locked and after all electric transients have subsided. It is somewhat difficult to compare this value with that shown in Figure 6.10-5 since the electric transients cause the currents to be offset in Figure 6.10-5. However,  $i_{bs}$  in Figure 6.10-5 contains the least offset and it compares quite well. In particular, the rms value of the first cycle of  $i_{bs}$  is approximately 69A, that is, on the order of 12 times rated current.

## 6.11. FREE ACCELERATION CHARACTERISTICS VIEWED FROM VARIOUS REFERENCE FRAMES

It is also instructive to observe the variables of an induction machine in various reference frames during free acceleration from stall. The machine simulated on the computer, for this purpose, is a singly excited, six-pole, three-phase, 220-V (line-to-line), 10-hp, 60-Hz induction motor with the following parameters expressed in per unit.

$$\begin{array}{lll} r_s = 0.0453 & X_M = 2.042 & r'_r = 0.0222 \\ X_{ls} = 0.0775 & & X'_{lr} = 0.0322 \end{array}$$

The inertia of the rotor is  $H = 0.5$  s.

The machine variables during free acceleration are shown in Figure 6.11-1. All variables are plotted in per unit with the peak value of the base sinusoidal quantities given as 1.0pu. If we were to follow the convention set forth in Section 6.8, we would use the rms value as 1.0pu. However, the selection of peak values as 1.0pu allows a more direct comparison with the  $qd0s$  variables shown later. Also, base torque rather than rated torque is taken as one per unit torque. At  $t = 0$ , rated voltage, with  $v_{as}$  a cosine, is applied to the machine. As in the studies reported in the previous section, the rotor accelerates from stall with zero load torque and since friction and windage losses are not taken into account, the machine accelerates to synchronous speed.

The same free acceleration characteristics are shown in different reference frames in Figure 6.11-2, Figure 6.11-3, Figure 6.11-4, and Figure 6.11-5. In these computer studies all variables are held at their initial values prior to  $t = 0$ . The stationary reference-frame variables during free acceleration are shown in Figure 6.11-2. With the reference frame fixed in the stator, the  $qs$  and  $ds$  variables are arithmetically related to the  $abc$  variables. In particular, the time zero position of the reference frame is zero, therefore  $f_{as} = f_{qs}^s$ . Thus,  $v_{qs}^s$  and  $i_{qs}^s$  are identical to  $v_{as}$  and  $i_{as}$  of Figure 6.11-1. The rotor variables are referred to the stationary reference frame and vary therein at 60Hz.

The free acceleration characteristics with the reference frame fixed in the rotor is given in Figure 6.11-3. Here the zero position of the rotor and the reference frame are both zero, therefore  $f'_{ar} = f'_{qr}^r$ . Hence,  $i'_{qr}^r$  in Figure 6.11-3 is identical to  $i'_{ar}$  of Figure 6.11-1 and, since the stator variables are referred to the rotor, they vary at slip frequency. At stall, the rotor reference frame coincides with the stationary reference frame. At synchronous speed, the rotor reference frame becomes the synchronously rotating

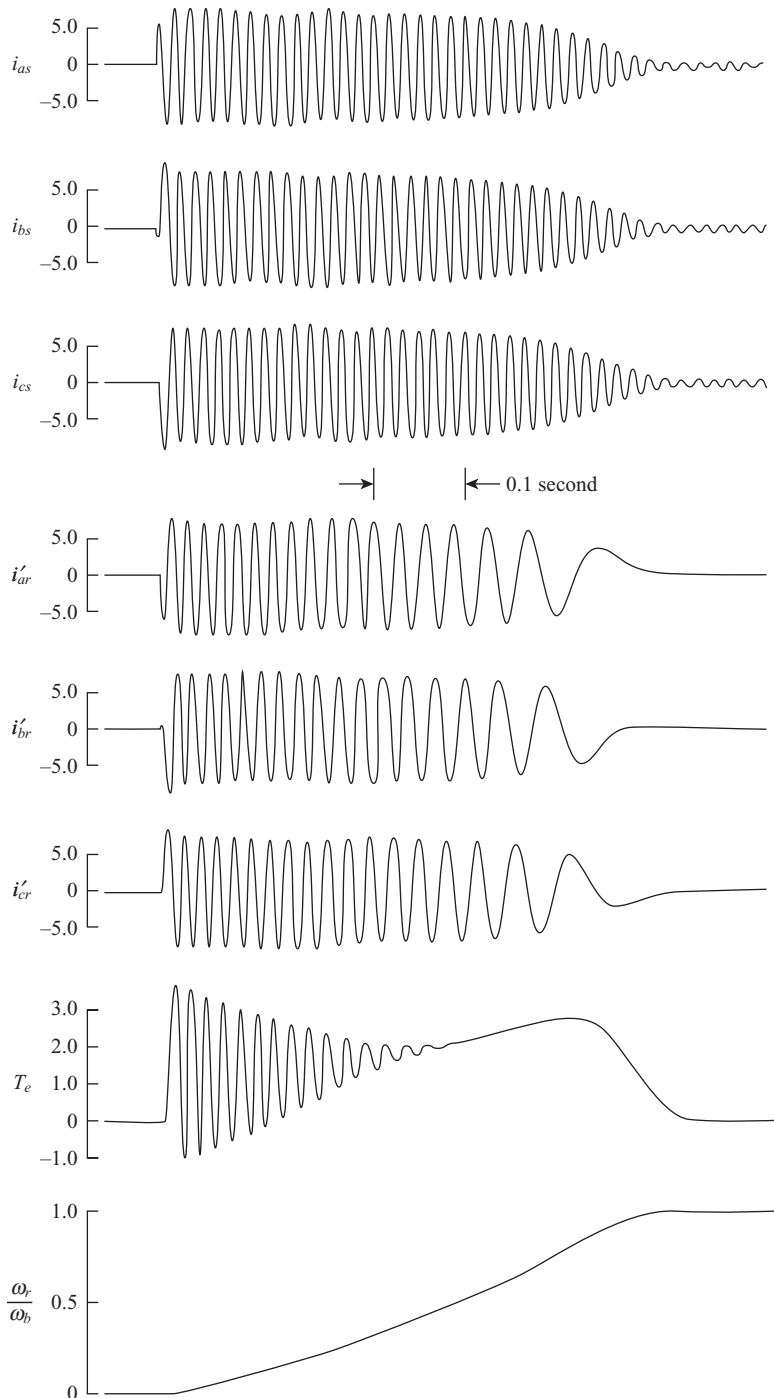
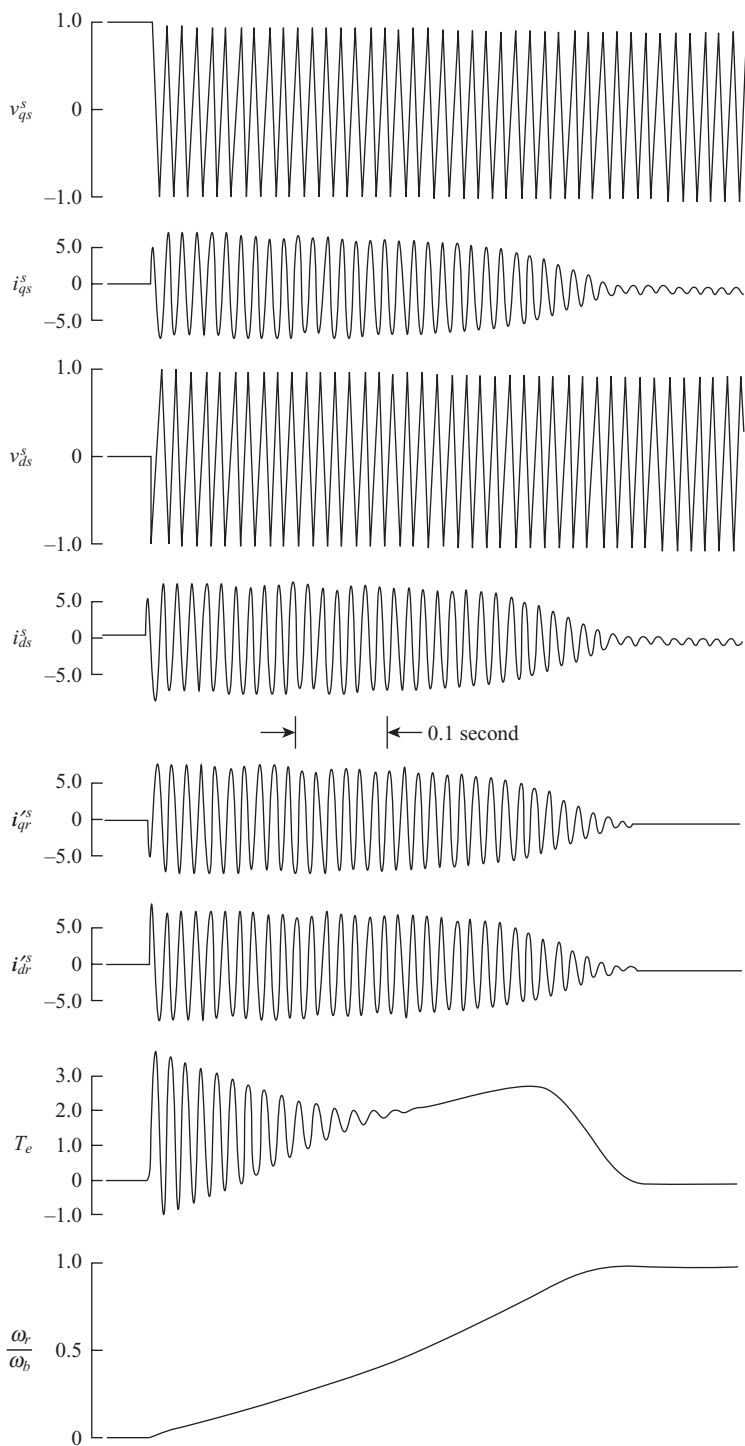
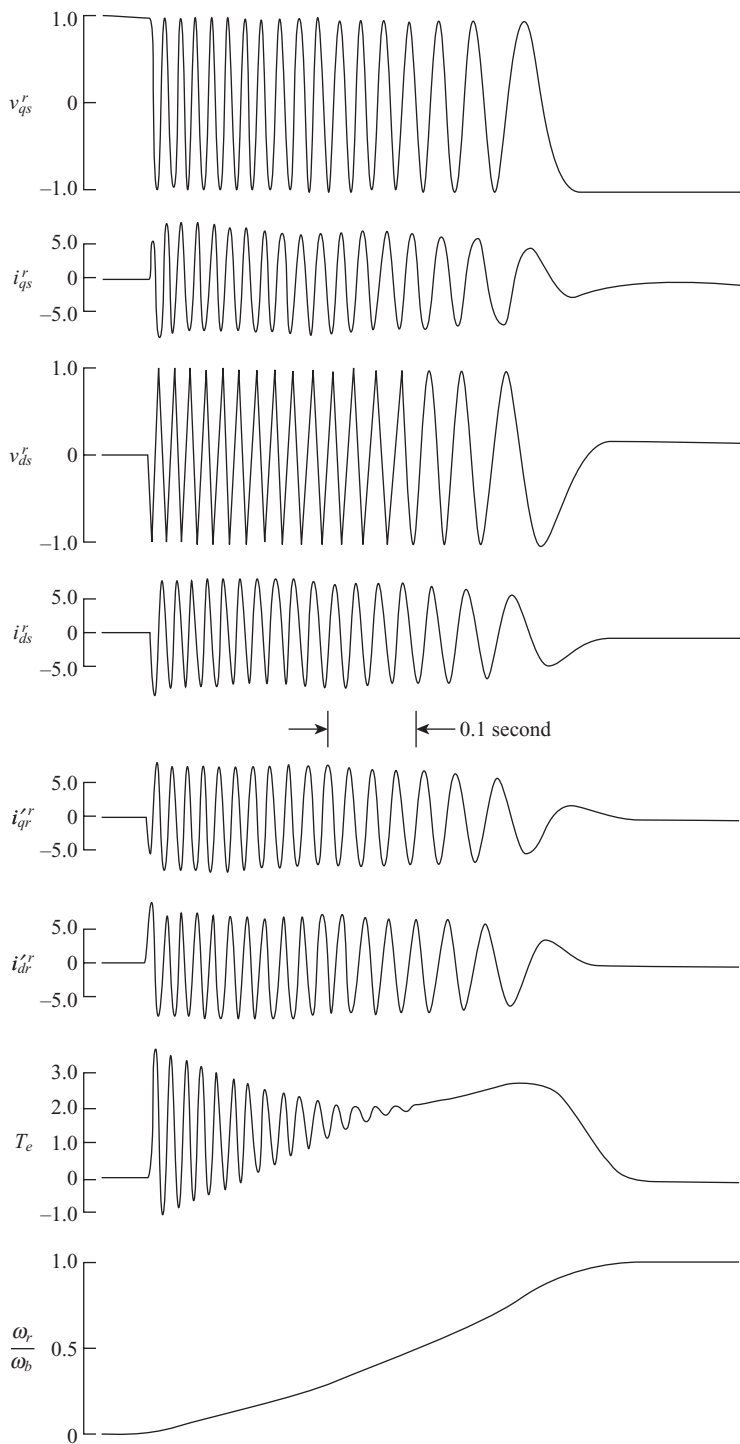


Figure 6.11-1. Free acceleration characteristics of a 10-hp induction motor in machine variables.



**Figure 6.11-2.** Free acceleration characteristics of a 10-hp induction motor in the stationary reference frame. ( $v_{qs}^s$  is set to  $v_{qs}^s(0)$  prior to  $t = 0$ .)



**Figure 6.11-3.** Free acceleration characteristics of a 10-hp induction motor in a reference frame fixed in rotor. ( $v_{qs}^r$  is set to  $v_{qs}^r(0)$  prior to  $t = 0$ .)

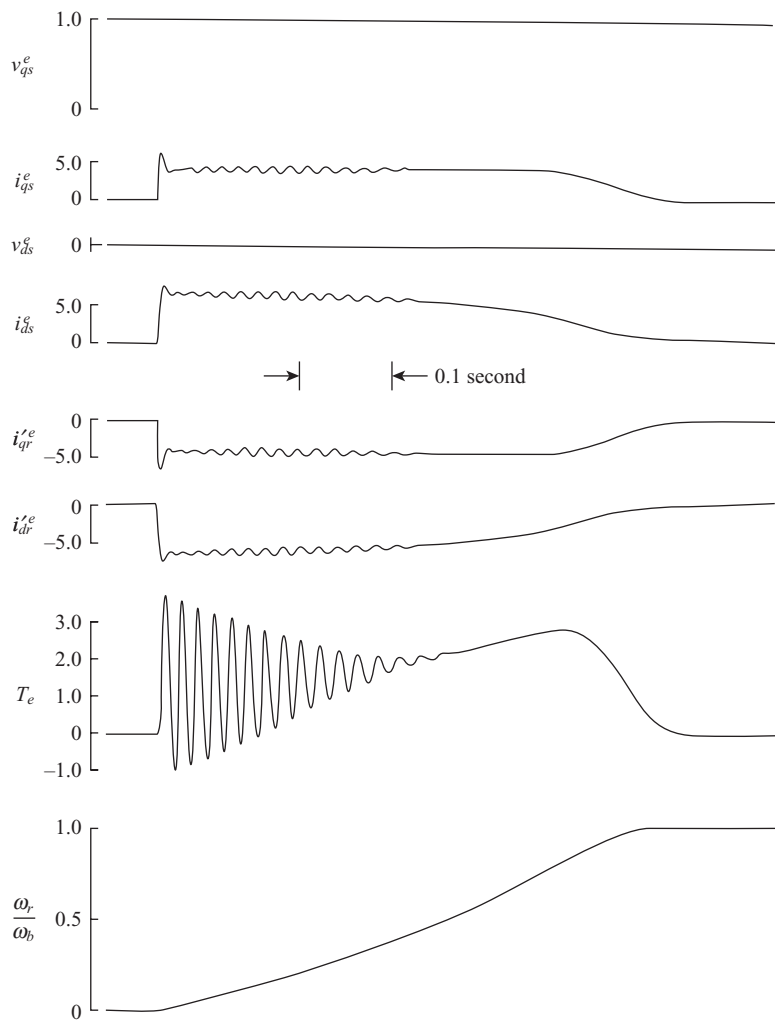


**Figure 6.11-4.** Free acceleration characteristics of a 10-hp induction motor in the synchronously rotating reference frame. ( $v_{qs}^e$  is set to  $v_{qs}^e(0)$  prior to  $t = 0$ .)

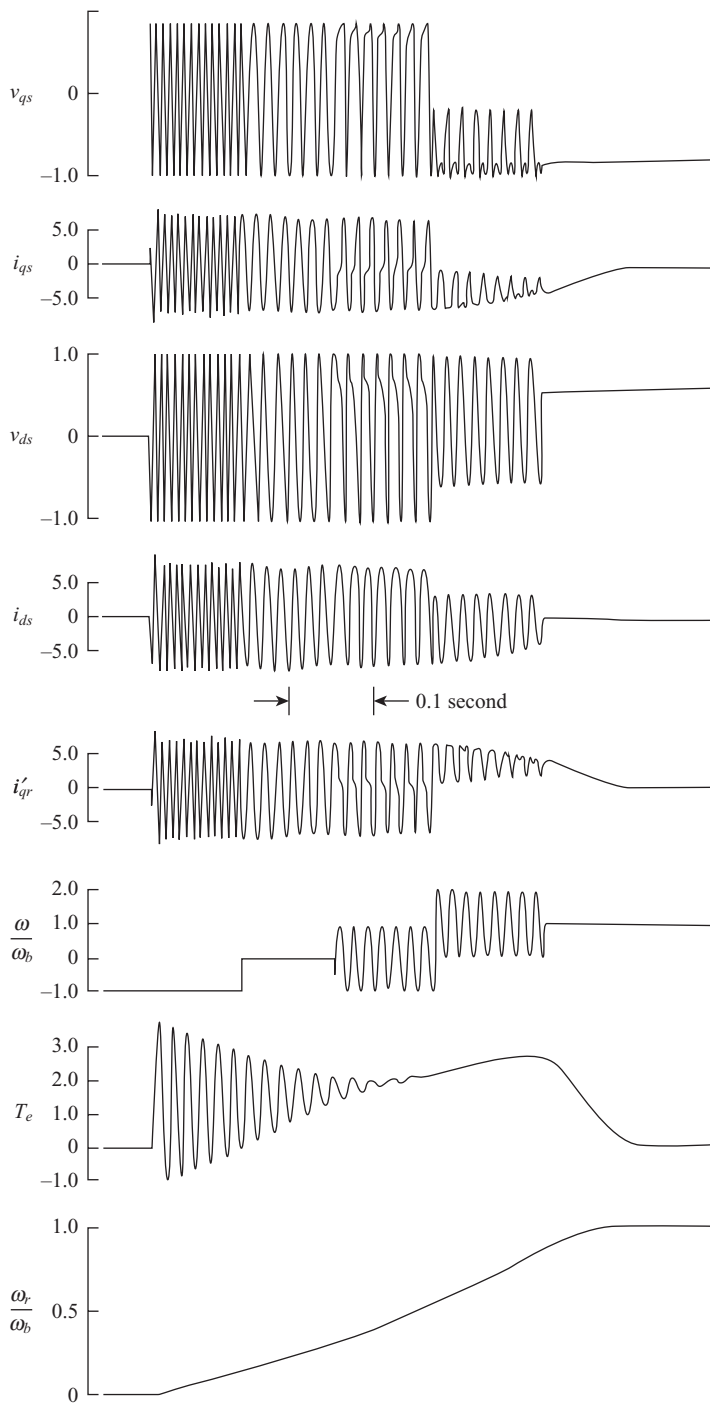


**Figure 6.11-5.** Free acceleration characteristics of a 10-hp induction motor in the arbitrary reference frame. First,  $\omega = -\omega_e$ , then  $\omega = 0$ ; followed by a sinusoidal variation about zero of  $\omega$  with amplitude  $\omega_e$  and frequency  $\omega_e$ , then the same variation about  $\omega_e$ . Finally,  $\omega$  is set equal to  $\omega_e$ .

reference frame. It is important to note that since the machine essentially operates in the steady-state mode upon reaching synchronous speed, the variables become constants corresponding to their instantaneous values at the time the rotor speed becomes equal to synchronous speed.

Free acceleration with the reference frame rotating in synchronism with the electrical angular velocity of the applied voltages is shown in Figure 6.11-4. Here, the zero position of the reference frame is selected so that  $v_{qs}^e$  is the amplitude of the stator applied phase voltages and  $v_{ds}^e = 0$ .

The fact that the reference frame may rotate at any speed, constant or varying, is depicted in Figure 6.11-5. During free acceleration from stall, the reference-frame speed is initially rotating at synchronous speed opposite to the direction of rotation of the rotating magnetic field established by the stator currents. The reference-frame speed is then stepped to zero, whereupon it becomes a stationary reference frame and the variables correspond to those in Figure 6.11-2. The speed of the reference frame is then varied sinusoidally at base frequency and finally it is held fixed at synchronous speed. It is interesting to note that the waveform of the torque is the same regardless of the speed or the change in the speed of the reference frame.

## 6.12. DYNAMIC PERFORMANCE DURING SUDDEN CHANGES IN LOAD TORQUE

The dynamic behavior of the 3- and 2250-hp induction motors during step changes in load torque is shown in Figure 6.12-1 and Figure 6.12-2, respectively. Initially, each machine is operating at synchronous speed. The load torque is first stepped from zero to base torque (slightly less than rated) and the machine allowed to establish this new operating point. Next, the load torque is stepped from base torque back to zero whereupon the machine reestablishes its original operating condition.

The variables of the 3-hp machine approach each new operating condition in an overdamped manner. This is characteristic of the 3- and 50-hp machines given in Table 6.10-1. We previously found that for these machines, the steady-state torque-speed characteristic nearly duplicates the free acceleration characteristic once the electrical transient associated with the stator circuits has subsided; therefore, we are not surprised to find that the dynamics during load torque changes can be predicted adequately by the steady-state torque-speed characteristics. Indeed, this is the case; the plot of torque versus speed during the load torque changes depicted in Figure 6.12-1 follows nearly exactly the steady-state torque-speed curve. Therefore, the dynamic behavior of most smaller induction machines during normal load torque changes can be predicted by using the steady-state voltage and torque equations to calculate the currents and torque, and (6.3-8) or (6.8-10) to relate torque to the inertia and rotor speed.

The dynamic performance of the 2250-hp machine during load torque changes is strongly influenced by the rotor electric transients. This influence of the rotor circuit

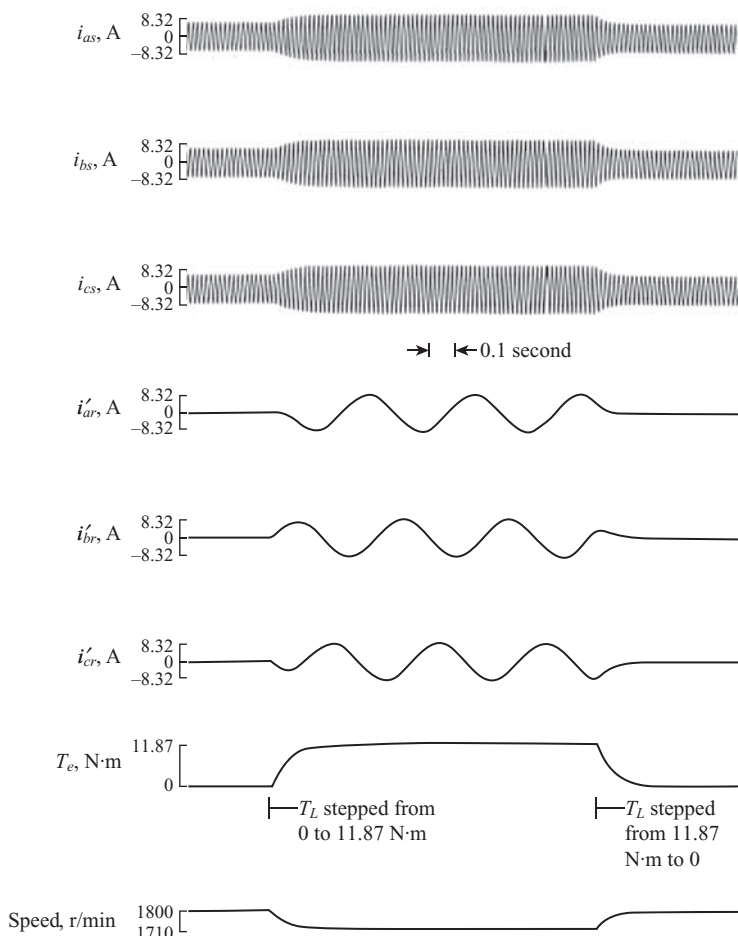


**Figure 6.12-1.** Dynamic performance of a 3-hp induction motor during step changes in load torque from 0 to 11.87 N·m to 0.

transients, which is illustrated more clearly in a later chapter, causes the 2250-hp machine to exhibit damped oscillations about the new operating point. At best, the steady-state torque–speed characteristics could approximate the average of this dynamic response; it could not predict the complete dynamics during normal load torque changes for the larger machines. This fact is further emphasized by the plot of torque versus speed for the 2250-hp machine in Figure 6.12-3. The steady-state torque–speed characteristic would be nearly a straight line drawn between the two operating points. We, of course, expected this from the previous comparison of the steady-state torque–speed curve with the free acceleration characteristics (Figure 6.10-8).

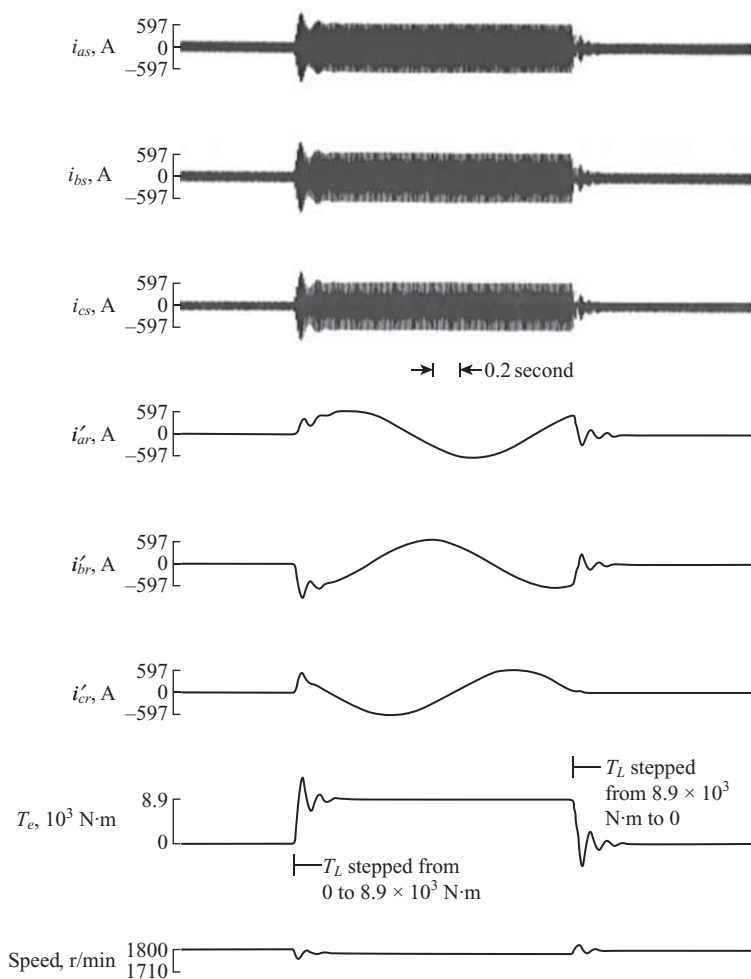


**Figure 6.12-2.** Dynamic performance of a 2250-hp induction motor during step changes in load torque from 0 to  $8.9 \times 10^3 \text{ N}\cdot\text{m}$  to 0.

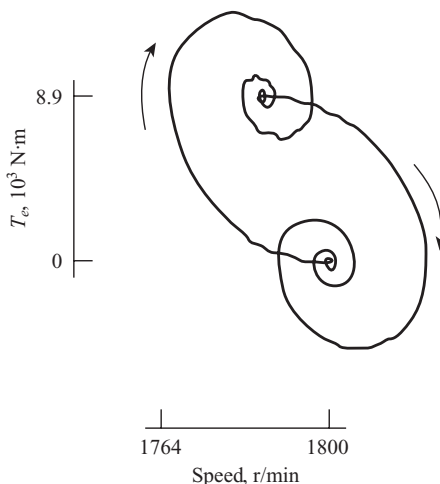


**Figure 6.12-3.** Torque versus speed for 2250-hp induction motor during load torque changes shown in Figure 6.12-2.

### 6.13. DYNAMIC PERFORMANCE DURING A THREE-PHASE FAULT AT THE MACHINE TERMINALS

The dynamic performance of the 3- and 2250-hp induction machines is shown, respectively, in Figure 6.13-1 and Figure 6.13-2 during and following a three-phase fault at the terminals. Initially, each motor is operating at essentially rated conditions with a load torque equal to base torque. The three-phase fault at the terminals is simulated by setting  $v_{as}$ ,  $v_{bs}$ , and  $v_{cs}$  to zero at the instant  $v_{as}$  passes through zero going positive. After six cycles, the source voltages are reapplied.

The stepping of the terminal voltages to zero at the time of the fault gives rise to decaying offsets in both the stator and rotor currents. These transient offsets in the stator currents appear in the rotor circuits as decaying oscillations of near 60 Hz (since the rotor speed is slightly less than synchronous) that are superimposed upon the transients of the rotor circuits. Similarly, the transient offsets in the rotor currents appear as decaying oscillations in the stator currents at a frequency corresponding to the rotor speed. In the case of the 3-hp machine, both the stator and rotor transients are highly damped and subside before the fault is removed and the voltages reapplied. With all machine currents equal to zero, the electromagnetic torque is, of course, zero; therefore, full load torque decelerates the machine.

In the case of the 2250-hp machine, which has a higher leakage reactance to resistance ratio in both the stator and rotor than the 3-hp machine, the stator and rotor transients are still present when the fault is removed and the voltages reapplied. Hence,  $T_e$  has an average value throughout the fault period corresponding to the ohmic losses.

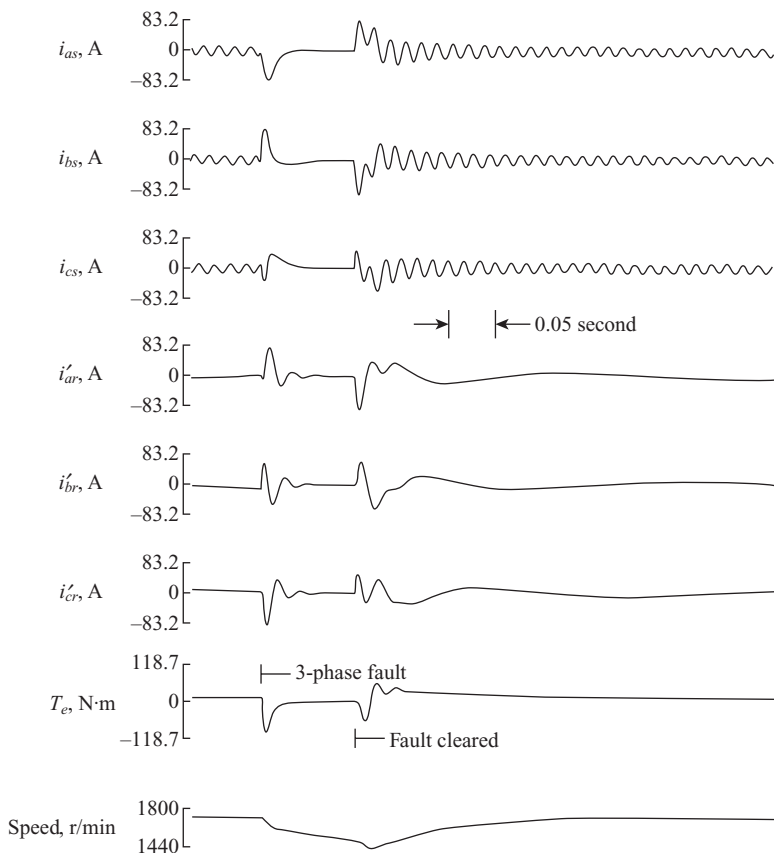


**Figure 6.13-1.** Dynamic performance of a 3-hp induction motor during a three-phase fault at the terminals.

When the voltages are reapplied, the offsets again occur in the stator currents. The machine reestablishes the original operating condition in a well-damped manner in the case of the 3-hp machine and in an oscillatory manner in the case of the 2250-hp machine. The decaying oscillations in the stator and rotor circuits, due to the transient offsets, are very apparent in Figure 6.13-2. We will discuss the performance of an induction motor during a three-phase fault at the terminals later when calculating eigenvalues and when considering reduced-order equations.

## 6.14. COMPUTER SIMULATION IN THE ARBITRARY REFERENCE FRAME

There are numerous ways of formulating the equations of an induction machine for the purposes of computer simulation. The form that we will use is that reported in

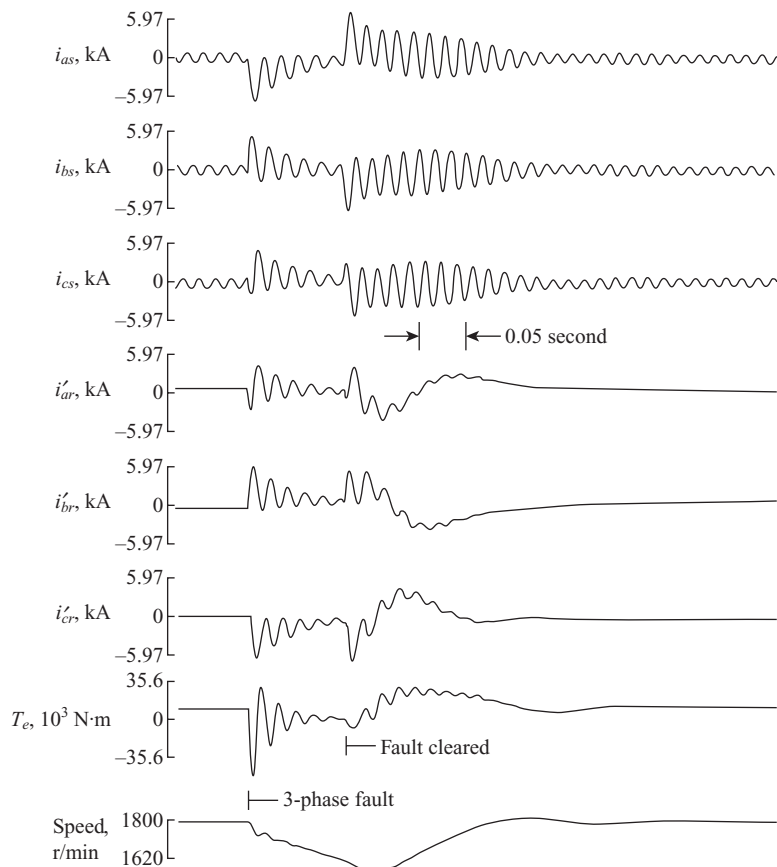


Figure 6.13-2. Dynamic performance of a 2250-hp induction motor during a three-phase fault at the terminals.

Reference 1. In particular, the computer representation of the symmetrical induction machine in the arbitrary reference frame will be used as the basis from which various modes of operation are represented. This simulation is quite convenient not only from the standpoint of representing all practical modes of operation, but this form also permits the effects of saturation to be readily simulated. The simulation of saturation is covered in Section 5.11 for synchronous machines. This method may also be used to simulate the saturation of an induction machine.

The equations convenient for simulating the symmetrical induction machine in the arbitrary reference frame may be established by first solving the flux linkage equations or flux linkage per second equations for the currents. Thus, from (6.5-28)–(6.5-33), we can write

$$i_{qs} = \frac{1}{X_{ls}}(\psi_{qs} - \psi_{mq}) \quad (6.14-1)$$

$$i_{ds} = \frac{1}{X_{ls}}(\psi_{ds} - \psi_{md}) \quad (6.14-2)$$

$$i_{0s} = \frac{1}{X_{ls}}\psi_{0s} \quad (6.14-3)$$

$$i'_{qr} = \frac{1}{X'_{lr}}(\psi'_{qr} - \psi_{mq}) \quad (6.14-4)$$

$$i'_{dr} = \frac{1}{X'_{lr}}(\psi'_{dr} - \psi_{md}) \quad (6.14-5)$$

$$i'_{0r} = \frac{1}{X'_{lr}}\psi'_{0r} \quad (6.14-6)$$

where  $\psi_{mq}$  and  $\psi_{md}$ , which are useful when representing saturation, are defined

$$\psi_{mq} = X_M(i_{qs} + i'_{qr}) \quad (6.14-7)$$

$$\psi_{md} = X_M(i_{ds} + i'_{dr}) \quad (6.14-8)$$

If (6.14-1)–(6.14-6) are used to eliminate the currents in (6.14-7) and (6.14-8), as well as in the voltage equations in the arbitrary reference frame given by (6.5-22)–(6.5-27), and if the resulting voltage equations are solved for the flux linkages per second, we can write the following integral equations

$$\psi_{qs} = \frac{\omega_b}{p} \left[ v_{qs} - \frac{\omega}{\omega_b} \psi_{ds} + \frac{r_s}{X_{ls}} (\psi_{mq} - \psi_{qs}) \right] \quad (6.14-9)$$

$$\psi_{ds} = \frac{\omega_b}{p} \left[ v_{ds} + \frac{\omega}{\omega_b} \psi_{qs} + \frac{r_s}{X_{ls}} (\psi_{md} - \psi_{ds}) \right] \quad (6.14-10)$$

$$\psi_{0s} = \frac{\omega_b}{p} \left[ v_{0s} - \frac{r_s}{X_{ls}} \psi_{0s} \right] \quad (6.14-11)$$

$$\psi'_{qr} = \frac{\omega_b}{p} \left[ v'_{qr} - \left( \frac{\omega - \omega_r}{\omega_b} \right) \psi'_{dr} + \frac{r'_r}{X'_{lr}} (\psi_{mq} - \psi'_{qr}) \right] \quad (6.14-12)$$

$$\psi'_{dr} = \frac{\omega_b}{p} \left[ v'_{dr} + \left( \frac{\omega - \omega_r}{\omega_b} \right) \psi'_{qr} + \frac{r'_r}{X'_{lr}} (\psi_{md} - \psi'_{dr}) \right] \quad (6.14-13)$$

$$\psi'_{0r} = \frac{\omega_b}{p} \left[ v'_{0r} - \frac{r'_r}{X'_{lr}} \psi'_{0r} \right] \quad (6.14-14)$$

Equations (6.14-7) and (6.14-8) are now expressed as

$$\psi_{mq} = X_{aq} \left( \frac{\psi_{qs}}{X_{ls}} + \frac{\psi'_{qr}}{X'_{lr}} \right) \quad (6.14-15)$$

$$\psi_{md} = X_{ad} \left( \frac{\psi_{ds}}{X_{ls}} + \frac{\psi'_{dr}}{X'_{lr}} \right) \quad (6.14-16)$$

in that

$$\begin{aligned} X_{aq} &= X_{ad} \\ &= \left( \frac{1}{X_M} + \frac{1}{X_{ls}} + \frac{1}{X'_{lr}} \right)^{-1} \end{aligned} \quad (6.14-17)$$

In the computer simulation, (6.14-9)–(6.14-16) are used to solve for the flux linkages per second, and (6.14-1)–(6.14-8) are used to obtain the currents from the flux linkages per second. It is clear that in the case of the zero quantities,  $i_{qs}$  and  $i'_{qr}$  may be solved for directly from (6.14-11) and (6.14-14), respectively, by substituting (6.14-3) for  $\psi_{qs}$  and (6.14-6) for  $\psi'_{qr}$  into these integral equations.

With saturation (nonlinear magnetic systems), the electromagnetic torque must be expressed by (6.6-13) when simulating in reference frames other than the rotor and (6.6-14) when the simulation is in the rotor reference frame. Thus, except for  $p\theta = p\theta_r$

$$T_e = \left( \frac{3}{2} \right) \left( \frac{P}{2} \right) \left( \frac{1}{\omega_b} \right) (\psi'_{qr} i'_{dr} - \psi'_{dr} i'_{qr}) \quad (6.14-18)$$

For  $p\theta = p\theta_r$ ,

$$T_e = \left( \frac{3}{2} \right) \left( \frac{P}{2} \right) \left( \frac{1}{\omega_b} \right) (\psi_{ds}^r i_{qs}^r - \psi_{qs}^r i_{ds}^r) \quad (6.14-19)$$

Equations (6.14-18) and (6.14-19) are positive for motor action. Equation (6.3-8) can be used to calculate rotor speed unless the equations are in per unit, whereupon (6.8-10) should be used. Often, per unit rotor speed  $\omega/\omega_b$  is used rather than  $\omega_r$ , since it is conveniently incorporated into the integral flux linkage equations.

A block diagram illustrating the computer representation of a symmetrical three-phase induction machine in the arbitrary reference frame is given in Figure 6.14-1. The machine equations that are used in the computer simulation are indicated by number in the block diagram. The transformations are defined by (3.3-1) for the stator variables and (6.4-1) for the rotor variables. The sinusoidal functions involved in the transformations are generated from  $\omega$  in the case of  $\mathbf{K}_s$  and  $\omega - \omega_r$  for  $\mathbf{K}_r$ . Although saturation

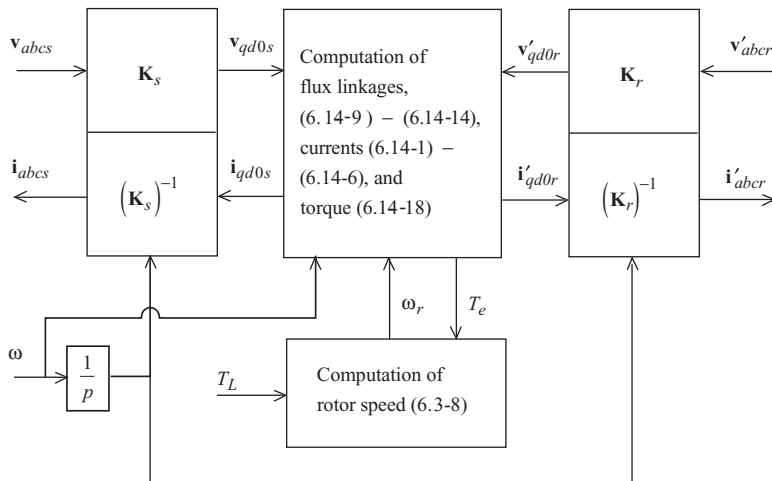


**Figure 6.14-1.** Simulation of a symmetrical three-phase induction machine in the arbitrary reference frame shown in block diagram form.

may be included in the flux linkage equations, the method of representing saturation is given in the computer simulation of the synchronous machine in Section 5.11. The programming of the equations is left to the reader. Our purpose is to set forth the computer equations and to discuss the procedures for representing various modes of operation.

The representation of the symmetrical induction machine in the arbitrary reference frame forms a general simulation from which the simulation for any practical mode of operation may be derived. Although the representation in the arbitrary reference frame may be used as depicted in Figure 6.14-1 for all modes of operation, the simulation in this form is more involved than is generally necessary. Depending upon the mode of operation, the computer simulation is implemented either in the stationary, rotor, or synchronous reference frames.

Often, there is little or no advantage in using one reference frame over another when simulating balanced conditions and disturbances such as a change in load torque, a symmetrical change in voltage, or a symmetrical three-phase fault. However, there are situations where it may be desirable to represent the stator phase variables (*abc* variables). In this case, the stationary reference frame ( $\omega = 0$ ) would offer advantage especially when simulating a singly fed induction machine, whereupon it would not be necessary to implement the transformations  $\mathbf{K}_s$  and  $(\mathbf{K}_s)^{-1}$ . On the other hand, if the machine is doubly fed, it may be advantageous to use the rotor reference frame ( $\omega = \omega_r$ ). If, in this case, the stator is supplied from a balanced source and if it is not necessary to have the stator currents available in the form of *abc* variables, then it is possible to reduce the transformation of the stator variables from that shown in Figure 6.14-1. In particular, for balanced stator conditions, we can write  $v_{qs}^r$  and  $v_{ds}^r$  directly from (3.6-5) and (3.6-6) as

$$v_{qs}^r = \sqrt{2}v_s \cos(\theta_{ev} - \theta_r) \quad (6.14-20)$$

$$v_{ds}^r = -\sqrt{2}v_s \sin(\theta_{ev} - \theta_r) \quad (6.14-21)$$

Perhaps the most widely used reference frame for the simulation of balanced operation of symmetrical induction machines is the synchronously rotating reference frame ( $\omega = \omega_e$ ). This reference frame is particularly convenient for simulation purposes since the variables are constant during steady-state operation and vary only when a system disturbance occurs. Moreover, if the system the stator of the induction machine is connected to is symmetrical and if it can also be represented in the synchronously rotating reference frame, then it is unnecessary to program the transformation of stator variables on the computer since both the network and machine are represented in the same reference frame.

Unbalanced conditions may be simulated by appropriate modification of the simulation block diagram shown in Figure 6.14-1. Unbalanced conditions, such as unbalanced stator voltages, unsymmetrical stator impedances, opening of a stator phase, and unsymmetrical rotor resistors, are all analyzed, and the procedures for simulation are set forth in chapters 9 and 12 of Reference 9. Therein, a method of representing magnetic saturation, which is a straightforward extension of that shown for synchronous machines in Chapter 5, is also presented.

## REFERENCES

- [1] P.C. Krause and C.H. Thomas, "Simulation of Symmetrical Induction Machinery," *IEEE Trans. Power App. Syst.*, Vol. 84, November 1965, pp. 1038–1053.
- [2] R.H. Park, "Two-Reaction Theory of Synchronous Machines—Generalized Method of Analysis—Part I," *AIEE Trans.*, Vol. 48, July 1929, pp. 716–727.
- [3] H.C. Stanley, "An Analysis of the Induction Motor," *AIEE Trans.*, Vol. 57 (Supplement), 1938, pp. 751–755.
- [4] D.S. Brereton, D.G. Lewis, and C.G. Young, "Representation of Induction Motor Loads During Power System Stability Studies," *AIEE Trans.*, Vol. 76, August 1957, pp. 451–461.
- [5] G. Kron, *Equivalent Circuits of Electric Machinery*, John Wiley and Sons, New York, 1951.
- [6] IEEE Std. 112-1978, IEEE Standard Test Procedure for Polyphase Induction Motors and Generators, IEEE, New York, 1978.
- [7] G. McPherson, *An Introduction to Electrical Machines and Transformers*, John Wiley and Sons, New York, 1981.
- [8] J.J. Cathey, R.K. Calvin III, and A.K. Ayoub, "Transient Load Model of an Induction Machine," *IEEE Trans. Power App. Syst.*, Vol. 92, July/August 1973, pp. 1399–1406.
- [9] P.C. Krause, O. Waszczuk, and S. Sudhoff, *Analysis of Electric Machinery*, IEEE Press, Piscataway, NJ, 1995.

## PROBLEMS

1. Consider the symmetrical two-pole, two-phase symmetrical induction machine shown in Figure 1.4-1. Derive the voltage equations in machine variables.
2. Repeat Problem 1 for the four-pole, two-phase symmetrical induction machine shown in Figure 1.4-2. Extend this development to show that if the electrical displacement and angular velocity of the rotor are defined as

$$\theta_r = \frac{P}{2} \theta_{rm}$$

$$\omega_r = \frac{P}{2} \omega_{rm}$$

then the voltage equations are identical to those obtained in Problem 1.

3. Prove that for a three-wire, wye-connected, stator winding  $\lambda_{as} + \lambda_{bs} + \lambda_{cs} = 0$ . For this to be true, is it necessary for the rotor windings to also be connected in a three-wire wye arrangement?
4. During balanced steady-state conditions, the total energy stored in the coupling field is constant. Therefore, show that (6.3-1) is constant for these conditions.
5. Derive an expression for the torque between the *as* and *bs* windings of the three-phase machine shown in Figure 6.2-1 with all other windings open-circuited.
6. Derive the expression for electromagnetic torque similar in form to (6.3-7) for a P-pole, two-phase induction machine.
7. Using the equations of transformation given in Problem 1 of Chapter 3, derive the voltage equations of a two-phase symmetrical induction machine in the arbitrary reference frame. Compare with those for a three-phase machine given by (6.5-10)–(6.5-21).
8. Write the voltage equations derived in Problem 7 with (a) currents as state variables and (b) flux linkages as state variables.
9. A two-phase induction machine has two sets of two-phase windings on the rotor. The *a* phases of the two-phase sets are tightly coupled and have the same magnetic axis; similarly for the *b* phases. The parameters of one set are  $r'_{r1}$  and  $X'_{lr1}$  and  $r'_{r2}$  and  $X'_{lr2}$  for the other. Draw the equivalent circuits in the arbitrary reference frame. Express all flux linkages per second and label all components and variables necessary to completely define the equivalent circuit of this double-cage rotor machine.
10. An induction machine has a 3-phase stator winding as shown in Figure 6.2-1 and a two-phase rotor winding as shown in Figure 1.4-1. Develop the equivalent circuits for this machine in the arbitrary reference frame.
11. The stator windings of a three-phase induction machine are connected in delta. By equations of transformation, relate the line currents and line-to-line voltages to the *qd0* variables in the arbitrary reference frame.

12. Derive an expression for electromagnetic torque in arbitrary reference-frame variables for a two-phase machine similar in form to (a) (6.6-2) and (b) (6.6-16).
13. Derive an expression for the electromagnetic torque in the arbitrary reference-frame variables for the machine in Problem 9.
14. Derive an expression for the electromagnetic torque in the arbitrary reference-frame variables for the machine in Problem 10.
15. Show that the inertia constant  $H$  is equivalent to the stored energy of the rotor at synchronous speed normalized to the base power.
16. Devise a relationship that can be used to convert a per unit impedance from one VA base to another.
17. Per unitize the machine parameters given in Table 6.10-1.
18. Convert the per unit parameters given for the 10-hp machine in Section 6.11 to ohms and henrys and with the inertia in  $\text{kg}\cdot\text{m}^2$ .
19. Verify (6.9-9) and (6.9-10).
20. In Section 6.9, two methods of deriving the steady-state voltage equations for an induction machine are discussed. The first method involves relating asynchronously rotating reference-frame variables to phasors; the second involves relating synchronously rotating reference-frame variables to phasors. The first method was used to obtain the steady-state voltage equations. Obtain these same equations using the second method.
21. Derive (6.9-14). What would this expression be in per unit?
22. A four-pole, 7.5-hp, three-phase induction motor has the following parameters

$$\begin{array}{lll} r_s = 0.3 \Omega & L_{ms} = 0.035 \text{ H} & r'_r = 0.15 \Omega \\ L_{ls} = 0.0015 \text{ H} & & L'_{lr} = 0.0007 \text{ H} \end{array}$$

The machine is supplied from a 110-V line-to-neutral 60-Hz source.

- (a) Calculate the steady-state starting torque and current.
- (b) Calculate the no-load current. Neglect friction and windage losses.
- (c) Plot the torque versus speed and efficiency versus speed curves from 0 to 2500 rpm.
- (d) If the rotor is driven mechanically to -500 rpm, determine the mechanical power at the shaft and electrical power at the stator terminals. From these, explain the power flow in this region of operation.
23. Repeat Problem 22 with the machine supplied from an 11-V line to neutral 6-Hz source.
24. An induction machine is connected to a 60-Hz supply. The no-load rotor speed is 1200 rpm. The machine is driven mechanically to a speed of 1250 rpm. Under this condition, determine the frequency of the stator and rotor currents in the stationary, rotor, and synchronous reference frames. Determine the speed and direction of the stator and rotor MMF when viewed from an observer positioned on (1) the stator and (2) the rotor.
25. Repeat Problem 24 assuming the rotor shaft speed is 1150 rpm.

- 26.** A four-pole, three-phase induction machine is operating with  $\omega_e = 377 \text{ rad/s}$ ,  $\omega_r = 350 \text{ rad/s}$ ,  $\tilde{I}_{qr}^{s*} = 100/150^\circ$ .  $L_{ls} = L'_{lr} = 1 \text{ mH}$ ,  $L_M = 30 \text{ mH}$ ,  $r_s = 0.3 \Omega$ , and  $r'_r = 0.2 \Omega$ . Assuming mechanical losses are negligible, determine  $\tilde{I}_{ar}^s$ ,  $T_L$ , and  $I_{qs}^e$ .
- 27.** An induction machine is operating with an applied peak stator voltage of 200 V (line-neutral) and  $\omega_e = 377 \text{ rad/s}$ .  $\omega_r = 360 \text{ rad/s}$ . At  $t = 0.1$  second,  $V_{qr}^{s*} = 10 \text{ V}$ . Determine the value of  $V_{qr}^{r*}$  and  $V_{qr}^{e*}$  at  $t = 0.1$  second. State any approximations made.
- 28.** Calculate the maximum steady-state torque (motor and generator action) for the 500-hp induction machine given in Table 6.10-1.
- 29.** Calculate the speed at maximum torque (motor action) for the 50-hp machine given in Table 6.10-1 when connected to a source of (a) 120 Hz, (b) 60 Hz, (c) 30 Hz, and (d) 6 Hz.
- 30.** The 3-hp induction machine given in Table 6.10-1 is operating at no load. The sequence of the applied voltages is suddenly reversed. Assume the electrical system establishes steady-state operation before the speed of the rotor has changed appreciably. Calculate the torque.
- 31.** Select three identical capacitors so that when they are connected in parallel with the 500-hp induction machine given in Table 6.10-1, the capacitor-induction machine combination operates at a 0.95 lagging power factor at rated power output.
- 32.** Per unitize the variables given in Figure 6.10-5 and Figure 6.10-6.
- 33.** Use the steady-state torque-speed characteristics and graphical integration to determine the time required to reach synchronous speed from stall for the 3- and 2250-hp machines. Compare with the acceleration time shown in Figure 6.10-5 and Figure 6.10-6.
- 34.** Use the steady-state torque-speed characteristics and graphical integration to determine the time required for the 3- and 2250-hp machines to slow down from synchronous speed to the new operating speed when the base load torque is applied. Compare with the time required in Figure 6.12-1 and Figure 6.12-2.
- 35.** Consider a three-phase machine with the following parameters:  $r_s = 72.5 \text{ m}\Omega$ ,  $L_{ls} = L'_{lr} = 1.32 \text{ mH}$ ,  $L_M = 20.1 \text{ mH}$ ,  $r'_r = 41.3 \text{ m}\Omega$ , and  $P = 4$ . The load torque varies with the speed cubed, and is such that 50-hp is required to spin the load at 1800 rpm. A balanced three-phase voltage source with a 460-V line-to-line rms amplitude and 60-Hz frequency is applied to the machine. Taking the a-phase voltage to be the zero reference for phase, find the rotor speed, the phasor representation of the a-phase current, the input power, the output power, and the efficiency.
- 36.** Consider the machine and load described in Problem 35. The machine is connected to a current source that sets the stator radian frequency to be

$$\omega_e = \omega_r + \frac{r'_r}{L'_{rr}}$$

and the rms amplitude of the a-phase current  $I_s$  to be whatever is required to satisfy the load at a given speed. Plot the efficiency of the machine versus speed for a speed range of 0 to 1800 rpm. Note that this particular control law can be shown to yield the most torque for a given stator current.

37. Repeat Problem 36 using

$$\omega_e = \omega_r + 0.5 \frac{r'_r}{L'_{rr}}$$

and

$$\omega_e = \omega_r + 1.5 \frac{r'_r}{L'_{rr}}$$

Compare results by superimposing the results of this exercise on top of those obtained from Problem 36.

---

# MACHINE EQUATIONS IN OPERATIONAL IMPEDANCES AND TIME CONSTANTS

---

## 7.1. INTRODUCTION

In Chapter 5, we assumed that the electrical characteristics of the rotor of a synchronous machine could be portrayed by two windings in each axis. This type of a representation is sufficient for most applications; however, there are instances where a more refined model may be necessary. For example, when representing solid iron rotor machines, it may be necessary to use three or more rotor windings in each axis so that transient dynamics are accurately represented. This may also be required to accurately capture switching dynamics when modeling machine/rectifier systems.

R.H. Park [1], in his original paper, did not specify the number of rotor circuits. Instead, he expressed the stator flux linkages in terms of operational impedances and a transfer function relating stator flux linkages to field voltage. In other words, Park recognized that, in general, the rotor of a synchronous machine appears as a distributed parameter system when viewed from the stator. The fact that an accurate, equivalent lumped parameter circuit representation of the rotor of a synchronous machine might require two, three, or four damper windings was more or less of academic interest until digital computers became available. Prior to the 1970s, the damper windings were seldom considered in stability studies; however, as the capability of computers increased, it became desirable to represent the machine in more detail.

The standard short-circuit test, which involves monitoring the stator short-circuit currents, provides information from which the parameters of the field winding and one damper winding in the  $d$ -axis can be determined. The parameters for the  $q$ -axis damper winding are calculated from design data. Due to the need for more accurate parameters, frequency-response data are now being used as means of measuring the operational impedances from which the parameters can be obtained for any number of rotor windings in both axes.

In this chapter, the operational impedances as set forth by Park [1] are described. The standard and derived synchronous machine time constants are defined and their relationship to the operational impedances established. Finally, a method of approximating the measured operational impedances by lumped parameter rotor circuits is presented.

## 7.2. PARK'S EQUATIONS IN OPERATIONAL FORM

R.H. Park [1] published the original  $qd0$ -voltage equations in the form

$$v'_{qs} = -r_s i'_{qs} + \frac{\omega_r}{\omega_b} \psi'_{ds} + \frac{p}{\omega_b} \psi'_{qs} \quad (7.2-1)$$

$$v'_{ds} = -r_s i'_{ds} - \frac{\omega_r}{\omega_b} \psi'_{qs} + \frac{p}{\omega_b} \psi'_{ds} \quad (7.2-2)$$

$$v_{0s} = -r_s i_{0s} + \frac{p}{\omega_b} \psi_{0s} \quad (7.2-3)$$

where

$$\psi'_{qs} = -X_q(p) i'_{qs} \quad (7.2-4)$$

$$\psi'_{ds} = -X_d(p) i'_{ds} + G(p) v'_{fd} \quad (7.2-5)$$

$$\psi_{0s} = -X_{ls} i_{0s} \quad (7.2-6)$$

In these equations, positive stator current is assumed out of the machine, the operator  $X_q(p)$  is referred to as the  $q$ -axis operational impedance,  $X_d(p)$  is the  $d$ -axis operational impedance, and  $G(p)$  is a dimensionless transfer function relating stator flux linkages per second to field voltage.

With the equations written in this form, the rotor of a synchronous machine can be considered as either a distributed or lumped parameter system. Over the years, the electrical characteristics of the rotor have often been approximated by three lumped parameter circuits, one field winding and two damper windings, one in each axis. Although this type of representation is generally adequate for salient-pole machines, it does not suffice for a solid iron rotor machine. It now appears that for dynamic and transient stability considerations, at least two and perhaps three damper windings should be used in the  $q$ -axis for solid rotor machines with a field and two damper windings in the  $d$ -axis [2].

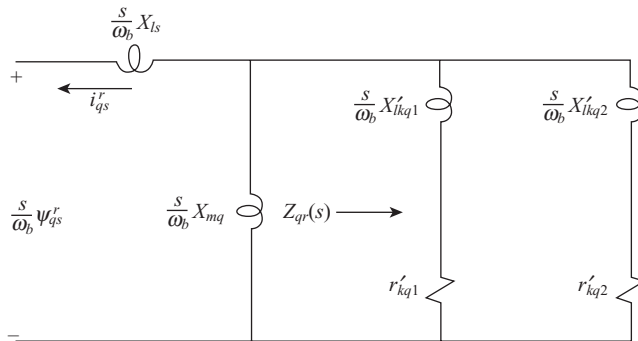


Figure 7.3-1. Equivalent circuit with two damper windings in the quadrature axis.

### 7.3. OPERATIONAL IMPEDANCES AND $G(p)$ FOR A SYNCHRONOUS MACHINE WITH FOUR ROTOR WINDINGS

In Chapter 5, the synchronous machine was represented with a field winding and one damper winding in the  $d$ -axis and with two damper windings in the  $q$ -axis. It is helpful to determine  $X_q(p)$ ,  $X_d(p)$ , and  $G(p)$  for this type of rotor representation before deriving the lumped parameter approximations from measured frequency-response data. For this purpose, it is convenient to consider the network shown in Figure 7.3-1. It is helpful in this and in the following derivations to express the input impedance of the rotor circuits in the form

$$Z_{qr}(s) = R_{eq} \frac{(1 + \tau_{qa}s)(1 + \tau_{qb}s)}{(1 + \tau_{Qa}s)} \quad (7.3-1)$$

Since it is customary to use the Laplace operator  $s$  rather than the operator  $p$ , Laplace notation will be employed hereafter. In (7.3-1)

$$R_{eq} = \frac{r'_{kq1} r'_{kq2}}{r'_{kq1} + r'_{kq2}} \quad (7.3-2)$$

$$\tau_{qa} = \frac{X'_{lkq1}}{\omega_b r'_{kq1}} \quad (7.3-3)$$

$$\tau_{qb} = \frac{X'_{lkq2}}{\omega_b r'_{kq2}} \quad (7.3-4)$$

$$\begin{aligned} \tau_{Qa} &= \frac{X'_{lkq1} + X'_{lkq2}}{\omega_b (r'_{kq1} + r'_{kq2})} \\ &= R_{eq} \left( \frac{\tau_{qa}}{r'_{kq2}} + \frac{\tau_{qb}}{r'_{kq1}} \right) \end{aligned} \quad (7.3-5)$$

From Figure 7.3-1

$$\frac{sX_q(s)}{\omega_b} = \frac{sX_{ls}}{\omega_b} + \frac{(sX_{mq}/\omega_b)Z_{qr}(s)}{Z_{qr}(s) + (sX_{mq}/\omega_b)} \quad (7.3-6)$$

Solving the above equation for  $X_q(s)$  yields the operational impedance for two damper windings in the  $q$ -axis, which can be expressed

$$X_q(s) = X_q \frac{1 + (\tau_{q4} + \tau_{q5})s + \tau_{q4}\tau_{q6}s^2}{1 + (\tau_{q1} + \tau_{q2})s + \tau_{q1}\tau_{q3}s^2} \quad (7.3-7)$$

where

$$\tau_{q1} = \frac{1}{\omega_b r'_{kq1}} (X'_{lkq1} + X_{mq}) \quad (7.3-8)$$

$$\tau_{q2} = \frac{1}{\omega_b r'_{kq2}} (X'_{lkq2} + X_{mq}) \quad (7.3-9)$$

$$\tau_{q3} = \frac{1}{\omega_b r'_{kq2}} \left( X'_{lkq2} + \frac{X_{mq}X'_{lkq1}}{X'_{lkq1} + X_{mq}} \right) \quad (7.3-10)$$

$$\tau_{q4} = \frac{1}{\omega_b r'_{kq1}} \left( X'_{lkq1} + \frac{X_{mq}X_{ls}}{X_{ls} + X_{mq}} \right) \quad (7.3-11)$$

$$\tau_{q5} = \frac{1}{\omega_b r'_{kq2}} \left( X'_{lkq2} + \frac{X_{mq}X_{ls}}{X_{ls} + X_{mq}} \right) \quad (7.3-12)$$

$$\tau_{q6} = \frac{1}{\omega_b r'_{kq2}} \left( X'_{lkq2} + \frac{X_{mq}X_{ls}X'_{lkq1}}{X_{mq}X_{ls} + X_{mq}X'_{lkq1} + X_{ls}X'_{lkq1}} \right) \quad (7.3-13)$$

The  $d$ -axis operational impedance  $X_d(s)$  may be calculated for the machine with a field and a damper winding by the same procedure. In particular, from Figure 7.3-2a

$$Z_{dr}(s) = R_{ed} \frac{(1 + \tau_{da}s)(1 + \tau_{db}s)}{(1 + \tau_{Da}s)} \quad (7.3-14)$$

where

$$R_{ed} = \frac{r'_{fd}r'_{kd}}{r'_{fd} + r'_{kd}} \quad (7.3-15)$$

$$\tau_{da} = \frac{X'_{bfd}}{\omega_b r'_{fd}} \quad (7.3-16)$$

$$\tau_{db} = \frac{X'_{bkd}}{\omega_b r'_{kd}} \quad (7.3-17)$$

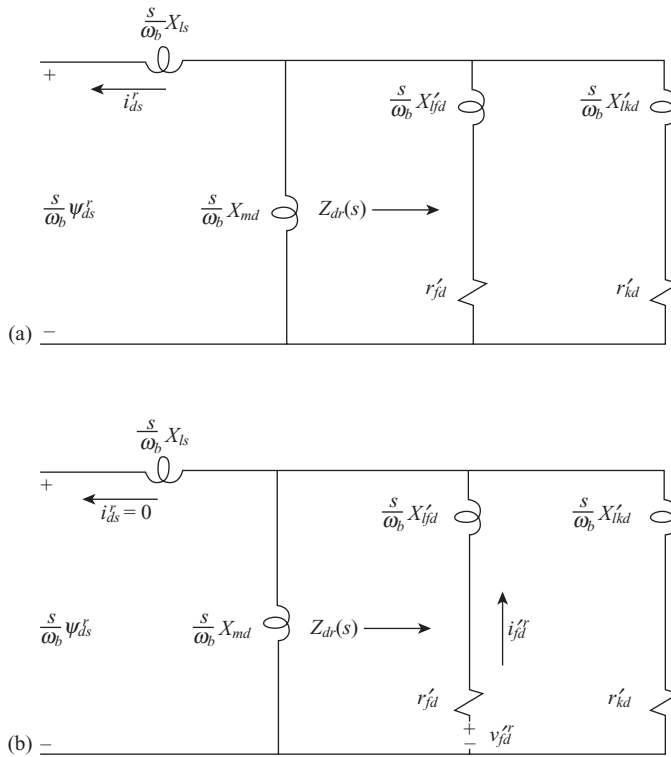


**Figure 7.3-2.** Calculation of  $X_d(s)$  and  $G(s)$  for two rotor windings in direct axis. (a) Calculation of  $X_d(s)$ ;  $v'_{fd} = 0$ ; (b) calculation of  $G(s)$ ;  $i'_{ds} = 0$ .

$$\begin{aligned} \tau_{D_d} &= \frac{X'_{fd} + X'_{lkd}}{\omega_b (r'_{fd} + r'_{kd})} \\ &= R_{ed} \left( \frac{\tau_{da}}{r'_{kd}} + \frac{\tau_{db}}{r'_{fd}} \right) \end{aligned} \quad (7.3-18)$$

The operational impedance for a field and damper winding in the  $d$ -axis can be obtained by setting  $v'_{fd}$  to zero and following the same procedure, as in the case of the  $q$ -axis. The final expression is

$$X_d(s) = X_d \frac{1 + (\tau_{d4} + \tau_{d5})s + \tau_{d4}\tau_{d6}s^2}{1 + (\tau_{d1} + \tau_{d2})s + \tau_{d1}\tau_{d3}s^2} \quad (7.3-19)$$

where

$$\tau_{d1} = \frac{1}{\omega_b r'_{fd}} (X'_{fd} + X_{md}) \quad (7.3-20)$$

$$\tau_{d2} = \frac{1}{\omega_b r'_{kd}} (X'_{lkd} + X_{md}) \quad (7.3-21)$$

$$\tau_{d3} = \frac{1}{\omega_b r'_{kd}} \left( X'_{lkd} + \frac{X_{md} X'_{lfd}}{X'_{lfd} + X_{md}} \right) \quad (7.3-22)$$

$$\tau_{d4} = \frac{1}{\omega_b r'_{fd}} \left( X'_{lfd} + \frac{X_{md} X_{ls}}{X_{ls} + X_{md}} \right) \quad (7.3-23)$$

$$\tau_{d5} = \frac{1}{\omega_b r'_{kd}} \left( X'_{lkd} + \frac{X_{md} X_{ls}}{X_{ls} + X_{md}} \right) \quad (7.3-24)$$

$$\tau_{d6} = \frac{1}{\omega_b r'_{kd}} \left( X'_{lkd} + \frac{X_{md} X_{ls}}{X_{md} X_{ls} + X_{md} X'_{lfd} + X_{ls} X'_{lfd}} \right) \quad (7.3-25)$$

The transfer function  $G(s)$  may be evaluated by expressing the relationship between stator flux linkages per second to field voltage,  $v'_{fd}$ , with  $i'_{ds}$  equal to zero. Hence, from (7.2-5)

$$G(s) = \frac{\psi'_{ds}}{v'_{fd}} \Bigg|_{i'_{ds}=0} \quad (7.3-26)$$

From Figure 7.3-2b, this yields

$$G(s) = \frac{X_{md}}{r'_{fd}} \frac{1 + \tau_{db}s}{1 + (\tau_{d1} + \tau_{d2})s + \tau_{d1}\tau_{d3}s^2} \quad (7.3-27)$$

where  $\tau_{db}$  is defined by (7.3-17).

## 7.4. STANDARD SYNCHRONOUS MACHINE REACTANCES

It is instructive to set forth the commonly used reactances for the four-winding rotor synchronous machine and to relate these reactances to the operational impedances whenever appropriate. The  $q$ - and  $d$ -axis reactances are

$$X_q = X_{ls} + X_{mq} \quad (7.4-1)$$

$$X_d = X_{ls} + X_{md} \quad (7.4-2)$$

These reactances were defined in Section 5.5. They characterize the machine during balanced steady-state operation whereupon variables in the rotor reference frame are constants. The zero frequency value of  $X_q(s)$  or  $X_d(s)$  is found by replacing the operator  $s$  with zero. Hence, the operational impedances for balanced steady-state operation are

$$X_q(0) = X_q \quad (7.4-3)$$

$$X_d(0) = X_d \quad (7.4-4)$$

Similarly, the steady-state value of the transfer function is

$$G(0) = \frac{X_{md}}{r'_{fd}} \quad (7.4-5)$$

The  $q$ - and  $d$ -axis transient reactances are defined as

$$X'_q = X_{ls} + \frac{X_{mq} X'_{lkq1}}{X'_{lkq1} + X_{mq}} \quad (7.4-6)$$

$$X'_d = X_{ls} + \frac{X_{md} X'_{lfd}}{X'_{lfd} + X_{md}} \quad (7.4-7)$$

Although  $X'_q$  has not been defined previously, we did encounter the  $d$ -axis transient reactance in the derivation of the approximate transient torque-angle characteristic in Chapter 5.

The  $q$ - and  $d$ -axis subtransient reactances are defined as

$$X''_q = X_{ls} + \frac{X_{mq} X'_{lkq1} X'_{lkq2}}{X_{mq} X'_{lkq1} + X_{mq} X'_{lkq2} + X'_{lkq1} X'_{lkq2}} \quad (7.4-8)$$

$$X''_d = X_{ls} + \frac{X_{md} X'_{lfd} X'_{lkd}}{X_{md} X'_{lfd} + X_{md} X'_{lkd} + X'_{lfd} X'_{lkd}} \quad (7.4-9)$$

These reactances are the high-frequency asymptotes of the operational impedances. That is

$$X_q(\infty) = X''_q \quad (7.4-10)$$

$$X_d(\infty) = X''_d \quad (7.4-11)$$

The high-frequency response of the machine is characterized by these reactances. It is interesting that  $G(\infty)$  is zero, which indicates that the stator flux linkages are essentially insensitive to high frequency changes in field voltage. Primes are used to denote transient and subtransient quantities, which can be confused with rotor quantities referred to the stator windings by a turns ratio. Hopefully, this confusion is minimized by the fact that  $X'_d$  and  $X'_q$  are the only single-primed parameters that are not referred impedances.

Although the steady-state and subtransient reactances can be related to the operational impedances, this is not the case with the transient reactances. It appears that the  $d$ -axis transient reactance evolved from Doherty and Nickle's [3] development of an approximate transient torque-angle characteristic where the effects of  $d$ -axis damper windings are neglected. The  $q$ -axis transient reactance has come into use when it became desirable to portray more accurately the dynamic characteristics of the solid iron rotor machine in transient stability studies. In many of the early studies, only one damper winding was used to describe the electrical characteristics of the  $q$ -axis, which is generally adequate in the case of salient-pole machines. In our earlier

development, we implied a notational correspondence between the  $kq1$  and the  $fd$  windings and between the  $kq2$  and the  $kd$  windings. In this chapter, we have associated the  $kq1$  winding with the transient reactance (7.4-6), and the  $kq2$  winding with the subtransient reactance (7.4-8). Therefore, it seems logical to use only the  $kq2$  winding when one damper winding is deemed adequate to portray the electrical characteristics of the  $q$  axis. It is recalled that in Chapter 5, we chose to use the  $kq2$  winding rather than the  $kq1$  winding in the case of the salient-pole hydro turbine generator.

It is perhaps apparent that the subtransient reactances characterize the equivalent reactances of the machine during a very short period of time following an electrical disturbance. After a period, of perhaps a few milliseconds, the machine equivalent reactances approach the values of the transient reactances, and even though they are not directly related to  $X_q(s)$  and  $X_d(s)$ , their values lie between the subtransient and steady-state values. As more time elapses after a disturbance, the transient reactances give way to the steady state reactances. In Chapter 5, we observed the impedance of the machine "changing" from transient to steady state following a system disturbance. Clearly, the use of the transient and subtransient quantities to portray the behavior of the machine over specific time intervals was a direct result of the need to simplify the machine equations so that precomputer computational techniques could be used.

## 7.5. STANDARD SYNCHRONOUS MACHINE TIME CONSTANTS

The standard time constants associated with a four-rotor winding synchronous machine are given in Table 7.5-1. These time constants are defined as

$\tau'_{qo}$  and  $\tau'_{do}$  are the  $q$ - and  $d$ -axis transient open-circuit time constants.

$\tau''_{qo}$  and  $\tau''_{do}$  are the  $q$ - and  $d$ -axis subtransient open-circuit time constants.

$\tau'_q$  and  $\tau'_d$  are the  $q$ - and  $d$ -axis transient short-circuit time constants.

$\tau''_q$  and  $\tau''_d$  are the  $q$ - and  $d$ -axis subtransient short-circuit time constants.

In the above definitions, open and short circuit refers to the conditions of the stator circuits. All of these time constants are approximations of the actual time constants, and when used to determine the machine parameters, they can lead to substantial errors in predicting the dynamic behavior of a synchronous machine. More accurate expressions for the time constants are derived in the following section.

## 7.6. DERIVED SYNCHRONOUS MACHINE TIME CONSTANTS

The open-circuit time constants, which characterize the duration of transient changes of machine variables during open-circuit conditions, are the reciprocals of the roots of the characteristic equation associated with the operational impedances, which, of course, are the poles of the operational impedances. The roots of the denominators of  $X_q(s)$  and  $X_d(s)$  can be found by setting these second-order polynomials equal to zero. From  $X_q(s)$ , (7.3-7)

TABLE 7.5-1. Standard Synchronous Machine Time Constants

## Open-Circuit Time Constants

$$\tau'_{qo} = \frac{1}{\omega_b r'_{kq1}} (X'_{lkq1} + X_{mq})$$

$$\tau'_{do} = \frac{1}{\omega_b r'_{fd}} (X'_{lfd} + X_{md})$$

$$\tau''_{qo} = \frac{1}{\omega_b r'_{kq2}} \left( X'_{lkq2} + \frac{X_{mq} X'_{lkq1}}{X_{mq} + X'_{lkq1}} \right)$$

$$\tau''_{do} = \frac{1}{\omega_b r'_{kd}} \left( X'_{lkd} + \frac{X_{md} X'_{lfd}}{X_{md} + X'_{lfd}} \right)$$

## Short-Circuit Time Constants

$$\tau'_q = \frac{1}{\omega_b r'_{kq1}} \left( X'_{lkq1} + \frac{X_{mq} X_{ls}}{X_{mq} + X_{ls}} \right)$$

$$\tau'_d = \frac{1}{\omega_b r'_{fd}} \left( X'_{lfd} + \frac{X_{md} X_{ls}}{X_{md} + X_{ls}} \right)$$

$$\tau''_q = \frac{1}{\omega_b r'_{kq2}} \left( X'_{lkq2} + \frac{X_{mq} X_{ls} X'_{lkq1}}{X_{mq} X_{ls} + X_{mq} X'_{lkq1} + X_{ls} X'_{lkq1}} \right)$$

$$\tau''_d = \frac{1}{\omega_b r'_{kd}} \left( X'_{lkd} + \frac{X_{md} X_{ls} X'_{lfd}}{X_{md} X_{ls} + X_{md} X'_{lfd} + X_{ls} X'_{lfd}} \right)$$

$$s^2 + \frac{\tau_{q1} + \tau_{q2}}{\tau_{q1} \tau_{q3}} s + \frac{1}{\tau_{q1} \tau_{q3}} = 0 \quad (7.6-1)$$

From  $X_d(s)$ , (7.3-19)

$$s^2 + \frac{\tau_{d1} + \tau_{d2}}{\tau_{d1} \tau_{d3}} s + \frac{1}{\tau_{d1} \tau_{d3}} = 0 \quad (7.6-2)$$

The roots are of the form

$$s = -\frac{b}{2} \pm \frac{b}{2} \sqrt{1 - \frac{4c}{b^2}} \quad (7.6-3)$$

The exact solution of (7.6-3) is quite involved. It can be simplified, however, if the quantity  $4c/b^2$  is much less than unity [4]. In the case of the  $q$ -axis

$$\frac{4c}{b^2} = \frac{4\tau_{q1}\tau_{q3}}{(\tau_{q1} + \tau_{q2})^2} \quad (7.6-4)$$

It can be shown that

$$\frac{4\tau_{q1}\tau_{q3}}{(\tau_{q1} + \tau_{q2})^2} \approx \frac{4r'_{kq1}r'_{kq2}(X'_{lkq1} + X'_{lkq2})}{X_{mq}(r'_{kq1} + r'_{kq2})^2} \quad (7.6-5)$$

In the case of the *d*-axis

$$\frac{4\tau_{d1}\tau_{d3}}{(\tau_{d1} + \tau_{d2})^2} \approx \frac{4r'_{fd}r'_{kd}(X'_{lfd} + X'_{lkd})}{X_{md}(r'_{fd} + r'_{kd})^2} \quad (7.6-6)$$

In most cases, the right-hand side of (7.6-5) and (7.6-6) is much less than unity. Hence, the solution of (7.6-3) with  $4c/b^2 \ll 1$  and  $c/b \ll b$  is obtained by employing the binomial expansion, from which

$$s_1 = -\frac{c}{b} \quad (7.6-7)$$

$$s_2 = -b \quad (7.6-8)$$

Now, the reciprocals of the roots are the time constants, and if we define the transient open-circuit time constant as the largest time constant and the subtransient open-circuit time constant as the smallest, then

$$\begin{aligned} \tau'_{qo} &= \frac{b}{c} \\ &= \tau_{q1} + \tau_{q2} \end{aligned} \quad (7.6-9)$$

and

$$\begin{aligned} \tau''_{qo} &= \frac{1}{b} \\ &= \frac{\tau_{q3}}{1 + \tau_{q2} / \tau_{q1}} \end{aligned} \quad (7.6-10)$$

Similarly, the *d*-axis open-circuit time constants are

$$\tau'_{do} = \tau_{d1} + \tau_{d2} \quad (7.6-11)$$

$$\tau''_{do} = \frac{\tau_{d3}}{1 + \tau_{d2} / \tau_{d1}} \quad (7.6-12)$$

The above derived open-circuit time constants are expressed in terms of machine parameters in Table 7.6-1.

TABLE 7.6-1. Derived Synchronous Machine Time Constants

## Open-Circuit Time Constants

$$\tau'_{qo} = \frac{1}{\omega_b r'_{kq1}} (X'_{lkq1} + X_{mq}) + \frac{1}{\omega_b r'_{kq2}} (X'_{lkq2} + X_{mq})$$

$$\tau'_{do} = \frac{1}{\omega_b r'_{fd}} (X'_{lfd} + X_{md}) + \frac{1}{\omega_b r'_{kd}} (X'_{lkd} + X_{md})$$

$$\tau''_{qo} = \frac{\frac{1}{\omega_b r'_{kq2}} \left( X'_{lkq2} + \frac{X_{mq} X'_{lkq1}}{X'_{lkq1} + X_{mq}} \right)}{1 + \frac{1}{\omega_b r'_{kq2}} (X'_{lkq2} + X_{mq})}$$

$$\tau''_{do} = \frac{\frac{1}{\omega_b r'_{kd}} \left( X'_{lkd} + \frac{X_{md} X'_{lfd}}{X'_{lfd} + X_{md}} \right)}{1 + \frac{1}{\omega_b r'_{kd}} (X'_{lkd} + X_{md})}$$

## Short-Circuit Time Constants

$$\tau'_q = \frac{1}{\omega_b r'_{kq1}} \left( X'_{lkq1} + \frac{X_{mq} X_{ls}}{X_{ls} + X_{mq}} \right) + \frac{1}{\omega_b r'_{kq2}} \left( X'_{lkq2} + \frac{X_{mq} X_{ls}}{X_{ls} + X_{mq}} \right)$$

$$\tau'_d = \frac{1}{\omega_b r'_{fd}} \left( X'_{lfd} + \frac{X_{md} X_{ls}}{X_{ls} + X_{md}} \right) + \frac{1}{\omega_b r'_{kd}} \left( X'_{lkd} + \frac{X_{md} X_{ls}}{X_{ls} + X_{md}} \right)$$

$$\tau''_q = \frac{\frac{1}{\omega_b r'_{kq2}} \left( X'_{lkq2} + \frac{X_{mq} X_{ls} X'_{lkq1}}{X_{mq} X_{ls} + X_{mq} X'_{lkq1} + X_{ls} X'_{lkq1}} \right)}{1 + \frac{1}{\omega_b r'_{kq2}} \left( X'_{lkq2} + \frac{X_{mq} X_{ls}}{X_{ls} + X_{mq}} \right)}$$

$$\frac{1}{\omega_b r'_{kq1}} \left( X'_{lkq1} + \frac{X_{mq} X_{ls}}{X_{ls} + X_{mq}} \right)$$

$$\tau''_d = \frac{\frac{1}{\omega_b r'_{kd}} \left( X'_{lkd} + \frac{X_{md} X_{ls} X'_{lfd}}{X_{md} X_{ls} + X_{md} X'_{lfd} + X_{ls} X'_{lfd}} \right)}{1 + \frac{1}{\omega_b r'_{kd}} \left( X'_{lkd} + \frac{X_{md} X_{ls}}{X_{ls} + X_{md}} \right)}$$

$$\frac{1}{\omega_b r'_{fd}} \left( X'_{lfd} + \frac{X_{md} X_{ls}}{X_{ls} + X_{md}} \right)$$

The short-circuit time constants are defined as the reciprocals of the roots of the numerator of the operational impedances. Although the stator resistance should be included in the calculation of the short-circuit time constants; its influence is generally small. From  $X_q(s)$ , (7.3-7)

$$s^2 + \frac{\tau_{q4} + \tau_{q5}}{\tau_{q4} \tau_{q6}} s + \frac{1}{\tau_{q4} \tau_{q6}} = 0 \quad (7.6-13)$$

From  $X_d(s)$ , given by (7.3-19)

$$s^2 + \frac{\tau_{d4} + \tau_{d5}}{\tau_{d4} \tau_{d6}} s + \frac{1}{\tau_{d4} \tau_{d6}} = 0 \quad (7.6-14)$$

The roots are of the form given by (7.6-3) and, as in the case of the open-circuit time constants,  $4c/b^2 \ll 1$  and  $c/b \ll b$ . Hence

$$\tau'_q = \tau_{q4} + \tau_{q5} \quad (7.6-15)$$

$$\tau''_q = \frac{\tau_{q6}}{1 + \tau_{q5} / \tau_{q4}} \quad (7.6-16)$$

$$\tau'_d = \tau_{d4} + \tau_{d5} \quad (7.6-17)$$

$$\tau''_d = \frac{\tau_{d6}}{1 + \tau_{d5} / \tau_{d4}} \quad (7.6-18)$$

The above derived synchronous machine time constants are given in Table 7.6-1 in terms of machine parameters. It is important to note that the standard machine time constants given in Table 7.5-1 are considerably different from the more accurate derived time constants. The standard time constants are acceptable approximations of the derived time constants if

$$r'_{kq2} \gg r'_{kq1} \quad (7.6-19)$$

and

$$r'_{kd} \gg r'_{jd} \quad (7.6-20)$$

In the lumped parameter approximation of the rotor circuits,  $r'_{kd}$  is generally much larger than  $r'_{jd}$ , and therefore the standard  $d$ -axis time constants are often good approximations of the derived time constants. This is not the case for the  $q$ -axis lumped parameter approximation of the rotor circuits. That is,  $r'_{kq2}$  is seldom if ever larger than  $r'_{kq1}$ , hence the standard  $q$ -axis time constants are generally poor approximations of the derived time constants.

## 7.7. PARAMETERS FROM SHORT-CIRCUIT CHARACTERISTICS

For much of the twentieth century, results from a short-circuit test performed on an unloaded synchronous machine were used to establish the  $d$ -axis parameters [5]. Alternative techniques have for the most part replaced short-circuit characterization. Despite being replaced, many of the terms, such as the short-circuit time-constants, have roots in the analytical derivation of the short circuit response of a machine. Thus, it is useful to briefly describe the test herein.

If the speed of the machine is constant, then (7.2-1)–(7.2-6) form a set of linear differential equations that can be solved using linear system theory. Prior to the short circuit of the stator terminals, the machine variables are in the steady state and the stator terminals are open-circuited. If the field voltage is held fixed at its prefault value, then the Laplace transform of the change in  $v_{fd}^r$  is zero. Hence, if the terms involving  $r_s^2$  are neglected, the Laplace transform of the fault currents (defined positive out of the machine), for the constant speed operation ( $\omega_r = \omega_b$ ), may be expressed

$$i_{qs}^r(s) = -\frac{1/X_q(s)}{s^2 + 2\alpha s + \omega_b^2} \left[ \frac{\omega_b^2 r_s v_{qs}^r(s)}{X_d(s)} + \omega_b s v_{qs}^r(s) - \omega_b^2 v_{ds}^r(s) \right] \quad (7.7-1)$$

$$i_{ds}^r(s) = -\frac{1/X_d(s)}{s^2 + 2\alpha s + \omega_b^2} \left[ \frac{\omega_b^2 r_s v_{ds}^r(s)}{X_q(s)} + \omega_b s v_{ds}^r(s) + \omega_b^2 v_{qs}^r(s) \right] \quad (7.7-2)$$

where

$$\alpha = \frac{\omega_b r_s}{2} \left( \frac{1}{X_q(s)} + \frac{1}{X_d(s)} \right) \quad (7.7-3)$$

It is clear that the 0 quantities are zero for a three-phase fault at the stator terminals. It is also clear that  $\omega_r$ ,  $\omega_b$ , and  $\omega_e$  are all equal in this example.

Initially, the machine is operating open-circuited, hence

$$v_{qs}^r = \sqrt{2}V_s \quad (7.7-4)$$

$$v_{ds}^r = 0 \quad (7.7-5)$$

The three-phase fault appears as a step decrease in  $v_{qs}^r$  to zero. Therefore, the Laplace transform of the change in the voltages from the prefault to fault values are

$$v_{qs}^r(s) = -\frac{\sqrt{2}V_s}{s} \quad (7.7-6)$$

$$v_{ds}^r(s) = 0 \quad (7.7-7)$$

If (7.7-6) and (7.7-7) are substituted into (7.7-1) and (7.7-2), and if the terms involving  $r_s$  are neglected except for  $\alpha$ , wherein the operational impedances are replaced by their high-frequency asymptotes, the Laplace transform of the short-circuit currents becomes

$$i_{qs}^r(s) = \frac{1/X_q(s)}{s^2 + 2\alpha s + \omega_b^2} (\omega_b \sqrt{2} V_s) \quad (7.7-8)$$

$$i_{ds}^r(s) = \frac{1/X_d(s)}{s^2 + 2\alpha s + \omega_b^2} \left( \frac{\omega_b^2 \sqrt{2} V_s}{s} \right) \quad (7.7-9)$$

where

$$\alpha = \frac{\omega_b r_s}{2} \left( \frac{1}{X_q(\infty)} + \frac{1}{X_d(\infty)} \right) \quad (7.7-10)$$

Replacing the operational impedances with their high frequency asymptotes in  $\alpha$  is equivalent to neglecting the effects of the rotor resistances in  $\alpha$ .

If we now assume that the electrical characteristics of the synchronous machine can be portrayed by two rotor windings in each axis, then we can express the operational impedances in terms of time constants. It is recalled that the open- and short-circuit time constants are respectively the reciprocals of the roots of the denominator and numerator of the operational impedances. Therefore, the reciprocals of the operational impedances may be expressed

$$\frac{1}{X_q(s)} = \frac{1}{X_q} \frac{(1 + \tau'_{q0}s)(1 + \tau''_{q0}s)}{(1 + \tau'_q s)(1 + \tau''_q s)} \quad (7.7-11)$$

$$\frac{1}{X_d(s)} = \frac{1}{X_d} \frac{(1 + \tau'_{d0}s)(1 + \tau''_{d0}s)}{(1 + \tau'_d s)(1 + \tau''_d s)} \quad (7.7-12)$$

These expressions may be written as [6]

$$\frac{1}{X_q(s)} = \frac{1}{X_q} \left( 1 + \frac{As}{1 + \tau'_q s} + \frac{Bs}{1 + \tau''_q s} \right) \quad (7.7-13)$$

$$\frac{1}{X_d(s)} = \frac{1}{X_d} \left( 1 + \frac{Cs}{1 + \tau'_d s} + \frac{Ds}{1 + \tau''_d s} \right) \quad (7.7-14)$$

where

$$A = -\frac{\tau'_q (1 - \tau'_{q0} / \tau'_q) (1 - \tau''_{q0} / \tau'_q)}{1 - \tau''_q / \tau'_q} \quad (7.7-15)$$

$$B = -\frac{\tau''_q (1 - \tau'_{q0} / \tau'_q) (1 - \tau''_{q0} / \tau''_q)}{1 - \tau'_q / \tau''_q} \quad (7.7-16)$$

The constants  $C$  and  $D$  are identical to  $A$  and  $B$ , respectively, with the  $q$  subscript replaced by  $d$  in all time constants.

Since the subtransient time constants are considerably smaller than the transient time constants, (7.7-13) and (7.7-14) may be approximated by

$$\frac{1}{X_q(s)} = \frac{1}{X_q} + \left( \frac{\tau'_{qo}}{\tau'_q} \frac{1}{X_q} - \frac{1}{X_q} \right) \frac{\tau'_q s}{1 + \tau'_q s} + \left( \frac{1}{X''_q} - \frac{\tau'_{qo}}{\tau'_q} \frac{1}{X_q} \right) \frac{\tau''_q s}{1 + \tau''_q s} \quad (7.7-17)$$

$$\frac{1}{X_d(s)} = \frac{1}{X_d} + \left( \frac{\tau'_{do}}{\tau'_d} \frac{1}{X_d} - \frac{1}{X_d} \right) \frac{\tau'_d s}{1 + \tau'_d s} + \left( \frac{1}{X''_d} - \frac{\tau'_{do}}{\tau'_d} \frac{1}{X_d} \right) \frac{\tau''_d s}{1 + \tau''_d s} \quad (7.7-18)$$

Although the assumption that the subtransient time constants are much smaller than the transient time constants is appropriate in the case of the  $d$ -axis time constants, the difference is not as large in the case of the  $q$ -axis time constants. Hence, (7.7-17) is a less acceptable approximation than is (7.7-18). This inaccuracy will not influence our work in this section, however. Also, since we have not restricted the derivation as far as time constants are concerned, either the standard or derived time constants can be used in the equations given in this section. However, if the approximate standard time constants are used,  $(\tau'_{qo} / \tau'_q)(1/X_q)$  and  $(\tau'_{do} / \tau'_d)(1/X_d)$  can be replaced by  $1/X'_q$  and  $1/X'_d$ , respectively.

If (7.7-17) and (7.7-18) are appropriately substituted into (7.7-8) and (7.7-9), the fault currents in terms of the Laplace operator become

$$i_{qs}^r(s) = \left( \frac{\sqrt{2}V_s}{s} \right) \left( \frac{\omega_b s}{s^2 + 2\alpha s + \omega_b^2} \right) \left[ \frac{1}{X_q} + \left( \frac{\tau'_{qo}}{\tau'_q} \frac{1}{X_q} - \frac{1}{X_q} \right) \frac{\tau'_q s}{1 + \tau'_q s} \right. \\ \left. + \left( \frac{1}{X''_q} - \frac{\tau'_{qo}}{\tau'_q} \frac{1}{X_q} \right) \frac{\tau''_q s}{1 + \tau''_q s} \right] \quad (7.7-19)$$

$$i_{ds}^r(s) = \left( \frac{\sqrt{2}V_s}{s} \right) \left( \frac{\omega_b^2}{s^2 + 2\alpha s + \omega_b^2} \right) \left[ \frac{1}{X_d} + \left( \frac{\tau'_{do}}{\tau'_d} \frac{1}{X_d} - \frac{1}{X_d} \right) \frac{\tau'_d s}{1 + \tau'_d s} \right. \\ \left. + \left( \frac{1}{X''_d} - \frac{\tau'_{do}}{\tau'_d} \frac{1}{X_d} \right) \frac{\tau''_d s}{1 + \tau''_d s} \right] \quad (7.7-20)$$

Equations (7.7-19) and (7.7-20) may be transformed to the time domain by the following inverse Laplace transforms. If  $a$  and  $\alpha$  are much less than  $\omega_b$ , then

$$L^{-1} \left[ \frac{\omega_b s}{(s+a)(s^2 + 2\alpha s + \omega_b^2)} \right] = e^{-\alpha t} \sin \omega_b t \quad (7.7-21)$$

$$L^{-1} \left[ \frac{\omega_b^2}{(s+a)(s^2 + 2\alpha s + \omega_b^2)} \right] = e^{-\alpha t} - e^{-\alpha t} \cos \omega_b t \quad (7.7-22)$$

If (7.7-21) is applied term by term to (7.7-19) with  $a$  set equal to zero for the term  $1/X_q$  and then  $1/\tau'_q$  and  $1/\tau''_q$  for successive terms, and if (7.7-22) is applied in a similar manner to (7.7-20), we obtain [6]

$$i_{qs}^r = \frac{\sqrt{2}V_s}{X''_q} e^{-\alpha t} \sin \omega_b t \quad (7.7-23)$$

$$i_{ds}^r = \sqrt{2}V_s \left[ \frac{1}{X_d} + \left( \frac{\tau'_{do}}{\tau'_d} \frac{1}{X_d} - \frac{1}{X_d} \right) e^{-t/\tau'_d} + \left( \frac{1}{X_d''} - \frac{\tau'_{do}}{\tau'_d} \frac{1}{X_d} \right) e^{-t/\tau_d''} \right] - \frac{\sqrt{2}V_s}{X_d''} e^{-\alpha t} \cos \omega_b t \quad (7.7-24)$$

It is clear that  $\omega_b$  may be replaced by  $\omega_e$  in the above equations.

Initially, the machine is operating open-circuited with the time zero position of the  $q$ - and  $d$ -axis selected so that the  $a$ -phase voltage is maximum at the time the  $q$ -axis coincides with the axis of the  $a$  phase. If we now select time zero at the instant of the short-circuit, and if the speed of the rotor is held fixed at synchronous speed then

$$\theta_r = \omega_b t + \theta_r(0) \quad (7.7-25)$$

where  $\theta_r(0)$  is the position of the rotor relative to the magnetic axis of the  $as$  winding at the time of the fault. In other words, the point on the  $a$ -phase sinusoidal voltage relative to its maximum value. Substituting (7.7-25) into the transformation given by (3.3-6) yields the  $a$ -phase short-circuit current

$$i_{as} = \sqrt{2}V_s \left[ \frac{1}{X_d} + \left( \frac{\tau'_{do}}{\tau'_d} \frac{1}{X_d} - \frac{1}{X_d} \right) e^{-t/\tau'_d} + \left( \frac{1}{X_d''} - \frac{\tau'_{do}}{\tau'_d} \frac{1}{X_d} \right) e^{-t/\tau_d''} \right] \sin[\omega_b t + \theta_r(0)] - \frac{\sqrt{2}V_s}{2} \left( \frac{1}{X_d''} + \frac{1}{X_q''} \right) e^{-\alpha t} \sin \theta_r(0) - \frac{\sqrt{2}V_s}{2} \left( \frac{1}{X_d''} + \frac{1}{X_q''} \right) e^{-\alpha t} \sin[2\omega_b t + \theta_r(0)] \quad (7.7-26)$$

The short-circuit currents in phases  $b$  and  $c$  may be expressed by displacing each term of (7.7-26) by  $-2\pi/3$  and  $2\pi/3$  electrical degrees, respectively.

Let us take a moment to discuss the terms of (7.7-26) and their relationship to the terms of (7.7-23) and (7.7-24). Since the rotor speed is held fixed at synchronous, the rotor reference frame is the synchronously rotating reference frame. In Section 3.6, we showed that a balanced three-phase set appears in the synchronously rotating reference frame as variables proportional to the amplitude of the three-phase balanced set, (3.6-8) and (3.6-9), which may be time varying. Therefore, we would expect that all terms on the right-hand side of (7.7-24), except the cosine term, would be the amplitude of the fundamental frequency-balanced three-phase set. We see from (7.7-26) that this is indeed the case. The amplitude of the balanced three-phase set contains the information necessary to determine the  $d$ -axis parameters. Later, we will return to describe the technique of extracting this information.

From the material presented in Section 3.9, we would expect the exponentially decaying offset occurring in the  $abc$  variables to appear as an exponentially decaying balanced two-phase set in the synchronously rotating reference frame as illustrated by (3.9-10) and (3.9-11). In particular, if we consider only the exponentially decaying term of the  $abc$  variables, then

$$i_{as}^* = -\frac{\sqrt{2}V_s}{2} \left( \frac{1}{X_d''} + \frac{1}{X_q''} \right) e^{-\alpha t} \sin \theta_r(0) \quad (7.7-27)$$

$$i_{bs}^* = -\frac{\sqrt{2}V_s}{2} \left( \frac{1}{X_d''} + \frac{1}{X_q''} \right) e^{-\alpha t} \sin \left[ \theta_r(0) - \frac{2\pi}{3} \right] \quad (7.7-28)$$

$$i_{cs}^* = -\frac{\sqrt{2}V_s}{2} \left( \frac{1}{X_d''} + \frac{1}{X_q''} \right) e^{-\alpha t} \sin \left[ \theta_r(0) + \frac{2\pi}{3} \right] \quad (7.7-29)$$

where the asterisk is used to denote the exponentially decaying component of the short-circuit stator currents. If these currents are transformed to the rotor (synchronous) reference frame by (3.3-1), the following *q*- and *d*-axis currents are obtained:

$$i_{qs}^{r*} = \frac{\sqrt{2}V_s}{2} \left( \frac{1}{X_d''} + \frac{1}{X_q''} \right) e^{-\alpha t} \sin \omega_b t \quad (7.7-30)$$

$$i_{ds}^{r*} = -\frac{\sqrt{2}V_s}{2} \left( \frac{1}{X_d''} + \frac{1}{X_q''} \right) e^{-\alpha t} \cos \omega_b t \quad (7.7-31)$$

These expressions do not appear in this form in (7.7-23) and (7.7-24); however, before becoming too alarmed, let us consider the double-frequency term occurring in the short-circuit stator currents. In particular, from (7.7-26)

$$i_{as}^{**} = -\frac{\sqrt{2}V_s}{2} \left( \frac{1}{X_d''} - \frac{1}{X_q''} \right) e^{-\alpha t} \sin [2\omega_b t + \theta_r(0)] \quad (7.7-32)$$

Therefore

$$i_{bs}^{**} = -\frac{\sqrt{2}V_s}{2} \left( \frac{1}{X_d''} - \frac{1}{X_q''} \right) e^{-\alpha t} \sin \left[ 2\omega_b t + \theta_r(0) - \frac{2\pi}{3} \right] \quad (7.7-33)$$

$$i_{cs}^{**} = -\frac{\sqrt{2}V_s}{2} \left( \frac{1}{X_d''} - \frac{1}{X_q''} \right) e^{-\alpha t} \sin \left[ 2\omega_b t + \theta_r(0) + \frac{2\pi}{3} \right] \quad (7.7-34)$$

where the superscript *\*\** denotes the double-frequency components of the short-circuit stator currents. These terms form a double-frequency, balanced three-phase set in the *abc* variables. We would expect this set to appear as a balanced two-phase set of fundamental frequency in the synchronously rotating reference frame ( $\omega = \omega_b$  or  $\omega_e$ ) and as decaying exponentials in a reference frame rotating at  $2\omega_b$ . Thus

$$i_{qs}^{r**} = -\frac{\sqrt{2}V_s}{2} \left( \frac{1}{X_d''} - \frac{1}{X_q''} \right) e^{-\alpha t} \sin \omega_b t \quad (7.7-35)$$

$$i_{ds}^{r**} = -\frac{\sqrt{2}V_s}{2} \left( \frac{1}{X_d''} - \frac{1}{X_q''} \right) e^{-\alpha t} \cos \omega_b t \quad (7.7-36)$$

We now see that if we add  $i_{qs}^{r*}$ , (7.7-30), and  $i_{qs}^{r**}$ , (7.7-35), we obtain (7.7-23). Similarly, if we add  $i_{ds}^{r*}$ , (7.7-31), and  $i_{ds}^{r**}$ , (7.7-36), we obtain the last term of (7.7-24). In other words, (7.7-23) and (7.7-24) can be written as

$$i_{qs}^r = \frac{\sqrt{2}V_s}{2} \left( \frac{1}{X_d''} + \frac{1}{X_q''} \right) e^{-\alpha t} \sin \omega_b t - \frac{\sqrt{2}V_s}{2} \left( \frac{1}{X_d''} - \frac{1}{X_q''} \right) e^{-\alpha t} \sin \omega_b t \quad (7.7-37)$$

$$i_{ds}^r = \sqrt{2}V_s \left[ \frac{1}{X_d} + \left( \frac{\tau'_{do}}{\tau'_d} \frac{1}{X_d} - \frac{1}{X_d} \right) e^{-t/\tau'_d} + \left( \frac{1}{X_d''} - \frac{\tau'_{do}}{\tau'_d} \frac{1}{X_d} \right) e^{-t/\tau''_d} \right] - \frac{\sqrt{2}V_s}{2} \left( \frac{1}{X_d''} + \frac{1}{X_q''} \right) e^{-\alpha t} \cos \omega_b t - \frac{\sqrt{2}V_s}{2} \left( \frac{1}{X_d''} - \frac{1}{X_q''} \right) e^{-\alpha t} \cos \omega_b t \quad (7.7-38)$$

If (7.7-23) and (7.7-24) had originally been written in this form, perhaps we could have written  $i_{as}$  by inspection or at least accepted the resulting form of  $i_{as}$  without questioning the theory that we had established in Chapter 3.

Let us now return to the expression for the short-circuit current  $i_{as}$  given by (7.7-26). In most machines,  $X_d''$  and  $X_q''$  are comparable in magnitude, hence the double-frequency component of the short-circuit stator currents is small. Consequently, the short-circuit current is predominately the combination of a decaying fundamental frequency component and a decaying offset. We first observed the waveform of the short-circuit current in Figure 5.10-8 and Figure 5.10-10. Although the initial conditions were different in that the machine was loaded and the speed of the machine increased slightly during the three-phase fault, the two predominate components of (7.7-26) are evident in these traces.

As mentioned previously, the amplitude or the envelope of the fundamental frequency component of each phase current contains the information necessary to determine the  $d$ -axis parameters. For purposes of explanation, let

$$i_{sc} = \sqrt{2}V_s \left[ \frac{1}{X_d} + \left( \frac{\tau'_{do}}{\tau'_d} \frac{1}{X_d} - \frac{1}{X_d} \right) e^{-t/\tau'_d} + \left( \frac{1}{X_d''} - \frac{\tau'_{do}}{\tau'_d} \frac{1}{X_d} \right) e^{-t/\tau''_d} \right] \quad (7.7-39)$$

where  $i_{sc}$  is the envelope of the fundamental component of the short-circuit stator currents. This can be readily determined from a plot of any one of the instantaneous phase currents.

Now, at the instant of the fault

$$i_{sc}(t = 0^+) = \frac{\sqrt{2}V_s}{X_d''} \quad (7.7-40)$$

At the final or steady state value

$$i_{sc}(t \rightarrow \infty) = \frac{\sqrt{2}V_s}{X_d} \quad (7.7-41)$$

Hence, if we know the prefault voltage and if we can determine the initial and final values of the current envelope,  $X_d''$  and  $X_d$  can be calculated.

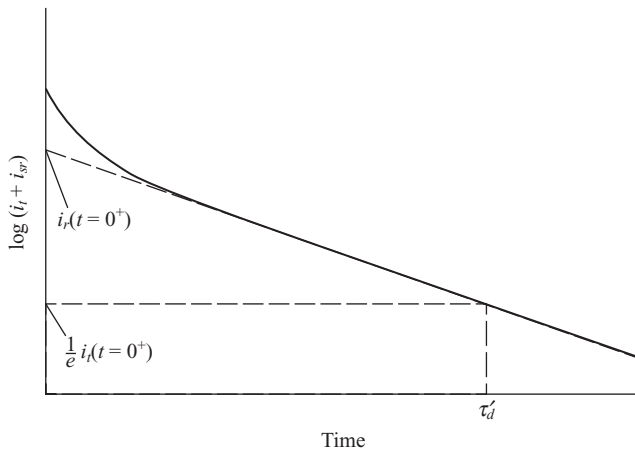


**Figure 7.7-1.** Plot of transient and subtransient components of the envelope of the short-circuit stator current.

It is helpful to break up  $i_{sc}$  into three components

$$i_{sc} = i_{ss} + i_t + i_{st} \quad (7.7-42)$$

where  $i_{ss}$  is the steady-state component,  $i_t$  is the transient component that decays according to  $\tau'_d$ , and  $i_{st}$  is the subtransient component with the time constant  $\tau''_d$ . It is customary to subtract the steady-state component  $i_{ss}$  from the envelope and plot  $(i_t + i_{st})$  on semilog paper as illustrated in Figure 7.7-1. Since  $\tau'_d > \tau''_d$ , the plot of  $(i_t + i_{st})$  is determined by  $i_t$  as time increases, and since the plot is on the semi-log paper, this decay is a straight line. If the transient component is extended to the y-axis as shown by the dashed line in Figure 7.7-1, the initial value of the transient component is obtained

$$i_t(t = 0^+) = \sqrt{2}V_s \left( \frac{\tau'_{do}}{\tau'_d} \frac{1}{X_d} - \frac{1}{X_d} \right) \quad (7.7-43)$$

Since  $X_d$  is determined from (7.7-41), we can now determine  $(\tau'_{do} / \tau'_d)(1/X_d)$ , or if we choose to use the standard time constants,  $(\tau'_{do} / \tau'_d)(1/X_d)$  is replaced by  $1/X'_d$ .

The time constant  $\tau'_d$  can also be determined from the plot shown in Figure 7.7-1. In particular,  $\tau'_d$  is the time it takes for  $i_t$  to decrease to  $1/e$  (0.368) of its original value. Thus, we now know  $X''_d$ ,  $X_d$ , and  $\tau'_d$ . Also,  $X'_d$  is known if we wish to use the standard, approximate time constants for  $\tau'_{do}$  if we wish to use the derived time constants to calculate the  $d$ -axis parameters.

We can now extract the subtransient component from Figure 7.7-1 by subtracting the dashed-line extension of the straight-line portion, which is  $i_t$ , from the plot of  $(i_t + i_{st})$ . This difference will also yield a straight line when plotted on semilog paper from which the initial value of the subtransient component,  $i_{st}(t = 0^+)$ , and the time constant  $\tau''_d$  can be determined.

Thus we have determined  $X'_d$ ,  $X_d$ ,  $\tau'_d$ ,  $\tau''_d$ , and  $\tau'_{do}$ . The stator leakage reactance  $X_{ls}$  can be calculated from the winding arrangement or from tests, or a reasonable value can be assumed. Hence, with a value of  $X_{ls}$ , we can determine the  $d$ -axis parameters. If  $r'_{jd} \ll r'_{kd}$ , it is generally sufficient to use  $X'_d$  and the standard time constants which, of course, markedly reduces the calculations involved.

## 7.8. PARAMETERS FROM FREQUENCY-RESPONSE CHARACTERISTICS

Toward the end of the twentieth century, a transition was made to determine the machine parameters for dynamic and transient stability studies from measured frequency-response data rather than short-circuit tests [7–10]. These tests are generally performed by applying a low voltage across two terminals of the stator windings, with the rotor at standstill and either the  $q$ - or  $d$ -axis aligned with the resultant magnetic axis established by the two stator windings. The frequency of the applied voltage is varied from a very low value of the order of  $10^{-3}$  Hz up to approximately 100 Hz. From these data  $X_q(s)$ ,  $X_d(s)$ , and  $G(s)$  are determined. An advantage of this method is that one can gain information regarding both the  $q$ - and  $d$ -axes, unlike the short-circuit test, which provides information on the parameters of only the  $d$ -axis. Moreover, the frequency-response test provides data from which the rotor can be represented by as many rotor windings in each axis as is required to obtain an acceptable match of the measured operational impedances and  $G(s)$ . Although popular, it has been shown that a number of issues can hinder the frequency response testing [11–13]. These include that minor hysteresis loops are traversed in the machine core under the small signal injection. As a result, the measured magnetizing inductances correspond to incremental permeability values, which lead to lower inductance than that predicted by the slope of an anhysteretic magnetizing curve. In addition, the low-level currents do not provide typical rotor heating or magnetic biasing, so that respective damper winding resistance and leakage inductances do not correspond to what would be experienced under load. These issues, along with techniques to characterize models that include saturation and an arbitrary rotor network representation using a combination of magnetization and frequency response testing, are described in Reference 14. Existing industry standards, which rely heavily on frequency response testing, are detailed in Reference 15.

To gain understanding of frequency response methods, plots of measured  $X_q(s)$  and  $X_d(s)$  versus frequency similar to those given in Reference 10 are shown in Figure 7.8-1 for a solid iron rotor machine. Figure 7.8-2 and Figure 7.8-3 show, respectively, a two-rotor winding and a three-rotor winding approximation of  $X_q(s)$ . It is recalled from (7.7-11) that for two rotor windings

$$X_q(s) = X_q \frac{(1 + \tau'_q s)(1 + \tau''_q s)}{(1 + \tau'_{qo} s)(1 + \tau''_{qo} s)} \quad (7.8-1)$$

As illustrated in Figure 7.8-2 and Figure 7.8-3, the asymptotic approximation of  $(1 + \tau s)$  is used to match the plot of the magnitude of  $X_q(s)$  versus frequency. Although a computer program could be used to perform curve fitting, the asymptotic approximation is

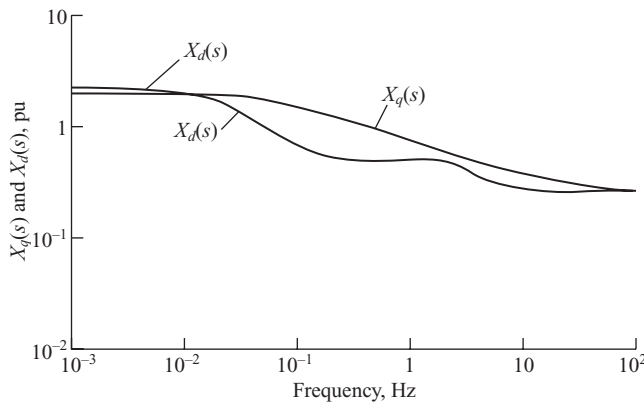


Figure 7.8-1. Plot of  $X_q(s)$  and  $X_d(s)$  versus frequency for a solid iron synchronous machine.

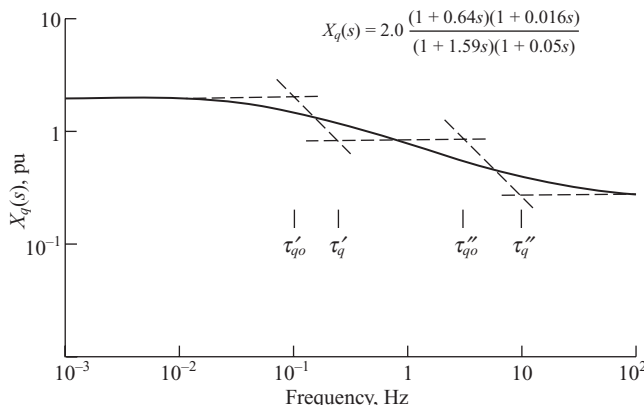


Figure 7.8-2. Two-rotor winding approximation of  $X_q(s)$ .

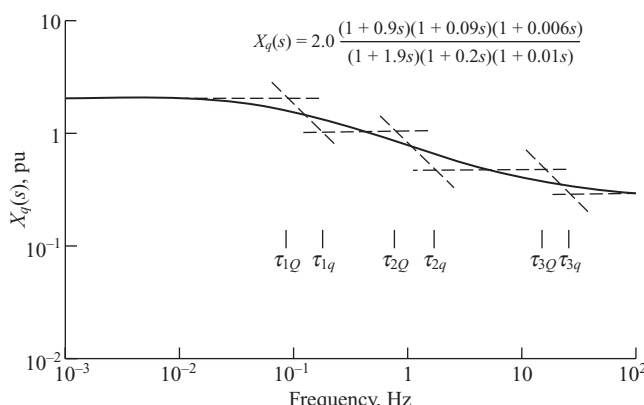


Figure 7.8-3. Three-rotor winding approximation of  $X_q(s)$ .

sufficient for our purposes. It is important, however, that regardless of the matching procedure employed, care must be taken to match the operational impedances as closely as possible over the frequency range from 0.05 to 5 Hz, since it has been determined that matching over this range is critical in achieving accuracy in dynamic and transient stability studies [10].

The asymptotic approximation of  $(1 + j\omega\tau)$ , where  $s$  has been replaced by  $j\omega$ , is that for  $\omega\tau < 1$ ,  $(1 + j\omega\tau)$  is approximated by 1, and for  $\omega\tau > 1$ ,  $(1 + j\omega\tau)$  is approximated by  $j\omega\tau$ . The corner frequency or “breakpoint” is at  $\omega\tau = 1$ , from which the time constant may be determined. At the corner frequency, the slope of the asymptotic approximation of  $(1 + j\omega\tau)$  changes from zero to a positive value increasing by one decade in amplitude (a gain of 20 dB) for every decade increase in frequency. It follows that the asymptotic approximation of  $(1 + j\omega\tau)^{-1}$  is a zero slope line to the corner frequency whereupon the slope becomes negative, decreasing in amplitude by one decade for every decade increase in frequency.

To obtain a lumped parameter approximation of  $X_q(s)$  by using this procedure, we start at the low-frequency asymptote, extending this zero slope line to a point where it appears that a breakpoint and thus a negative slope should occur in order to follow the measured value of  $X_q(s)$ . Since it is necessary that a negative slope occur after the breakpoint, a  $(1 + \tau s)$  factor must be present in the denominator. Hence, this corner frequency determines the largest time constant in the denominator, which is  $\tau'_{qo}$  in the case of the two-rotor winding approximation. We now continue on the negative slope asymptote until it is deemed necessary to again resume a zero slope asymptote in order to match the  $X_q(s)$  plot. This swing back to a zero slope line gives rise to a  $(1 + \tau s)$  factor in the numerator. This corner frequency determines the largest time constant in the numerator,  $\tau'_q$  in the case of the two-rotor winding approximation. It follows that  $\tau'_{qo}$  and  $\tau''_q$  are determined by the same procedure.

The phase angle of  $X_q(s)$  can also be measured at the same time that the magnitude of  $X_q(s)$  is measured. However, the phase angle was not made use of in the curve-fitting process. Although the measured phase angle does provide a check on the asymptotic approximation of  $X_q(s)$ , it is not necessary in this “minimum phase” system, where the magnitude of  $X_q(s)$  as a function of frequency is sufficient to determine the phase  $X_q(s)$  [9]. Hence, the asymptotic approximation provides an approximation of the magnitude and phase of  $X_q(s)$ .

The stator leakage reactance,  $X_{ls}$ , can be determined by tests or taken as the value recommended by the manufacturer that is generally calculated or approximated from design data. The value of  $X_{ls}$  should not be larger than the subtransient reactances since this choice could result in negative rotor leakage reactances that are not commonly used. For the machine under consideration,  $X_{ls}$  of 0.15 per unit is used. Once a value of  $X_{ls}$  is selected, the parameters may be determined from the information gained from the frequency-response tests. In particular, from Figure 7.8-2

$$\begin{array}{ll} X_q = 2 \text{ pu} & X''_q = 0.25 \text{ pu} \\ \tau'_{qo} = 1.59 \text{ second} & \tau''_{qo} = 0.05 \text{ second} \\ \tau'_q = 0.64 \text{ second} & \tau''_q = 0.016 \text{ second} \end{array}$$

with  $X_{ls}$  selected as 0.15 pu,  $X_{mq}$  becomes 1.85 pu. Four parameters remain to be determined  $r'_{kq1}$ ,  $X'_{lkq1}$ ,  $r'_{kq2}$ , and  $X'_{lkq2}$ . These may be determined from the expressions of the derived  $q$ -axis time constants given in Table 7.6-1.

There is another approach by which the parameters of the lumped-circuit approximation of  $X_q(s)$  may be determined that is especially useful when it is necessary to represent the rotor with more than two windings in an axis. By a curve-fitting procedure, such as illustrated in Figure 7.8-2 and Figure 7.8-3, it is possible to approximate  $X_q(s)$  by

$$X_q(s) = X_q \frac{N_x(s)}{D_x(s)} \quad (7.8-2)$$

where in general

$$N_x(s) = (1 + \tau_{1q}s)(1 + \tau_{2q}s) \dots \quad (7.8-3)$$

$$D_x(s) = (1 + \tau_{1Q}s)(1 + \tau_{2Q}s) \dots \quad (7.8-4)$$

The input impedance for a two-rotor winding circuit is expressed by (7.3-1). For any number of rotor circuits

$$Z_{qr}(s) = R_{eq} \frac{N_z(s)}{D_z(s)} \quad (7.8-5)$$

where

$$\frac{1}{R_{eq}} = \frac{1}{R_{qa}} + \frac{1}{R_{qb}} + \dots \quad (7.8-6)$$

$$N_z(s) = (1 + \tau_{qa}s)(1 + \tau_{qb}s) \dots \quad (7.8-7)$$

$$D_z(s) = (1 + \tau_{Qa}s) \dots \quad (7.8-8)$$

It is clear that (7.3-6) is valid regardless of the number of rotor windings. Thus, if we substitute (7.8-2) into (7.3-6) and solve for  $Z_{qr}(s)$ , we obtain [7]

$$Z_{qr}(s) = \frac{sX_{mq} / \omega_b [N_x(s) - (X_{ls} / X_q)D_x(s)]}{D_x(s) - N_x(s)} \quad (7.8-9)$$

Since the time constants of (7.8-3) and (7.8-4) can be obtained by a curve-fitting procedure, and since  $X_q$  is readily obtained from  $X_q(s)$ , all elements of (7.8-9) are known once  $X_{ls}$  is selected. Hence, values can be substituted into (7.8-9), and after some algebraic manipulation, it is possible to put (7.8-9) in the form of (7.8-5), whereupon  $R_{eq}$  and the time constants of (7.8-7) and (7.8-8) are known. The parameters of the lumped circuit approximation can then be determined. For example, in the case of the two-winding approximation

$$\begin{bmatrix} 1 & 1 \\ \tau_{qb} & \tau_{qa} \end{bmatrix} \begin{bmatrix} \frac{1}{r'_{kq1}} \\ \frac{1}{r'_{kq2}} \end{bmatrix} = \frac{1}{R_{eq}} \begin{bmatrix} 1 \\ \tau_{Qa} \end{bmatrix} \quad (7.8-10)$$

where the second row of (7.8-10) is (7.3-5). Thus,  $r'_{kq1}$  and  $r'_{kq2}$  can be evaluated from (7.8-10), and then  $X'_{lkq1}$  and  $X'_{lkq2}$  from (7.3-3), and (7.3-4), respectively.

In the case of the three-rotor winding approximation in the  $q$ -axis [7], (7.8-10) becomes

$$\begin{bmatrix} 1 & 1 & 1 \\ \tau_{qb} + \tau_{qc} & \tau_{qa} + \tau_{qc} & \tau_{qa} + \tau_{qb} \\ \tau_{qb} \tau_{qc} & \tau_{qa} \tau_{qc} & \tau_{qa} \tau_{qb} \end{bmatrix} \begin{bmatrix} \frac{1}{r'_{kq1}} \\ \frac{1}{r'_{kq2}} \\ \frac{1}{r'_{kq3}} \end{bmatrix} = \frac{1}{R_{eq}} \begin{bmatrix} 1 \\ \tau_{Qa} + \tau_{Qb} \\ \tau_{Qa} \tau_{Qb} \end{bmatrix} \quad (7.8-11)$$

It is left to the reader to express  $Z_{qr}(s)$  for three-rotor windings.

In the development of the lumped parameter circuit approximation, there is generally no need to preserve the identity of a winding that might physically exist in the  $q$ -axis of the rotor, since the interest is to portray the electrical characteristics of this axis as viewed from the stator. However, in the  $d$ -axis, we view the characteristics of the rotor from the stator by the operation impedance  $X_d(s)$  and the transfer function  $G(s)$ . If a lumped parameter circuit approximation is developed from only  $X_d(s)$ , the stator electrical characteristics may be accurately portrayed; however, the field-induced voltage during a disturbance could be quite different from that which occurs in the actual machine, especially if the measured  $G(s)$ , and the  $G(s)$  which results when using only  $X_d(s)$ , do not correspond. A representation of this type, wherein only  $X_d(s)$  is used to determine the lumped parameter approximation of the  $d$ -axis and the winding with the largest time constant is designated as the field winding, is quite adequate when the electrical characteristics of the field have only secondary influence upon the study being performed. Most dynamic and transient stability studies fall into this category. It has been shown that if the electrical characteristics of the stator are accurately portrayed, then the electromagnetic torque is also accurately portrayed even though the simulated field variables may be markedly different from those which actually occur [16]. In Reference 16, it is shown that this correspondence still holds even when a high initial response excitation system is used.

When the induced field voltage is of interest, as in the rating and control of solid-state switching devices that might be used in fast response excitation systems, it may be necessary to represent more accurately the electrical characteristics of the field circuit. Several researchers have considered this problem [9, 17, 18]. I.M. Canay [17] suggested the use of an additional rotor leakage inductance whereupon the  $d$ -axis circuit for a two-rotor winding approximation would appear as shown in Figure 7.8-4. The

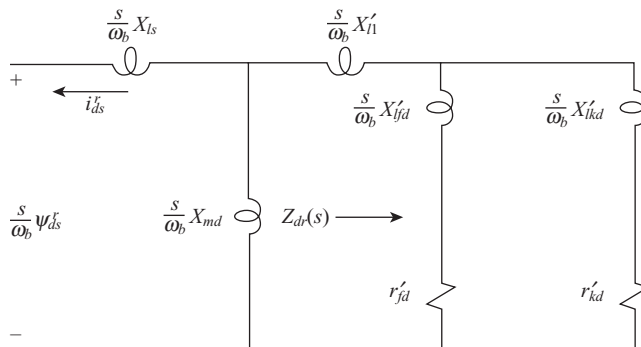


Figure 7.8-4. Two-rotor winding direct-axis circuit with unequal coupling.

additional rotor leakage reactance or the “cross-mutual” reactance provides a means to account for the fact that the mutual inductance between the rotor and the stator windings is not necessarily the same as that between the rotor field winding and equivalent damper windings [10]. I.M. Canay [17] showed that with additional rotor leakage reactance, both the stator and the field electrical variables could be accurately portrayed. However, in order to determine the parameters for this type of *d*-axis lumped parameter approximation, both  $X_d(s)$  and  $G(s)$  must be used [6, 9].

There are several reasons for not considering the issue of the additional rotor leakage reactance further at this time. Instead, we will determine the lumped parameter circuit approximation for the *d*-axis from only  $X_d(s)$  using the same techniques as in the case of  $X_q(s)$  and designate the rotor winding with the largest time constant as the field winding. There are many cases where the measured  $X_d(s)$  yields a winding arrangement that results in a  $G(s)$  essentially the same as the measured  $G(s)$ , hence the additional rotor leakage reactance is small. Also, most studies do not require this degree of refinement in the machine representation, that is, the accuracy of the simulated field variables is of secondary or minor importance to the system performance of interest. In cases in which this refinement is necessary, an attractive approach is to forego the use of lumped parameters and use the arbitrary rotor network representation proposed in Reference 19. For those who have a need to develop a model of a power system without having access to machine parameter values, Kimbark [20] provides a typical range of per-unit values of synchronous machine parameters and time constants that can be a helpful place to start an analysis.

## REFERENCES

- [1] R.H. Park, “Two-Reaction Theory of Synchronous Machines—Generalized Method of Analysis—Part I,” *AIEE Trans.*, Vol. 48, July 1929, pp. 716–727.
- [2] R.P. Schulz, W.D. Jones, and D.W. Ewart, “Dynamic Models of Turbine Generators Derived from Solid Rotor Equivalent Circuits,” *IEEE Trans. Power App. Syst.*, Vol. 92, May/June 1973, pp. 926–933.

- [3] R.E. Doherty and C.A. Nickle, "Synchronous Machines—III, Torque-Angle Characteristics under Transient Conditions," *AIEE Trans.*, Vol. 46, January 1927, pp. 1–8.
- [4] G. Shackshaft, "New Approach to the Determination of Synchronous Machine Parameters from Tests," *Proc. IEE*, Vol. 121, November 1974, pp. 1385–1392.
- [5] *IEEE Standard Dictionary of Electrical and Electronic Terms*, 2nd ed., John Wiley and Sons, New York, 1978.
- [6] B. Adkins and R.G. Harley, *The General Theory of Alternating Current Machines*, Chapman and Hall, London, 1975.
- [7] W. Watson and G. Manchur, "Synchronous Machine Operational Impedance from Low Voltage Measurements at the Stator Terminals," *IEEE Trans. Power App. Syst.*, Vol. 93, May/June 1974, pp. 777–784.
- [8] P.L. Dandeno and P. Kundur, "Stability Performance of 555 MVA Turboalternators—Digital Comparisons with System Operating Tests," *IEEE Trans. Power App. Syst.*, Vol. 93, May/June 1974, pp. 767–776.
- [9] S.D. Umans, J.A. Malleck, and G.L. Wilson, "Modeling of Solid Rotor Turbogenerators—Parts I and II," *IEEE Trans. Power App. Syst.*, Vol. 97, January/February 1978, pp. 269–296.
- [10] IEEE Committee Report, "Supplementary Definitions and Associated Test Methods for Obtaining Parameters for Synchronous Machine Stability and Study Simulations," *IEEE Trans. Power App. Syst.*, Vol. 99, July/August 1980, pp. 1625–1633.
- [11] F.P. de Mello and L.N. Hannett, "Determination of Synchronous Machine Electrical Characteristics by Test," *IEEE Trans. Power App. Syst.*, Vol. 102, December 1983, pp. 1625–1633.
- [12] S.H. Minnich, "Small Signals, Large Signals, and Saturation in Generator Modeling," *IEEE Trans. Energy Convers.*, Vol. 1, March 1986, pp. 94–102.
- [13] A.G. Jack and T.J. Bedford, "A Study of the Frequency Response of Turbogenerators with Special Reference to Nanticoke G. S.," *IEEE Trans. Energy Convers.*, Vol. EC-2, September 1987, pp. 496–505.
- [14] D.C. Aliprantis, S.D. Sudhoff, and B.T. Kuhn, "Experimental Characterization Procedure for a Synchronous Machine Model with Saturation and Arbitrary Rotor Network Representation," *IEEE Trans. Energy Convers.*, Vol. 20, September 2005, pp. 595–603.
- [15] IEEE Standard 115, Test Procedure for Synchronous Machines Part 2: Test Procedures and Parameter Determination for Dynamic Analysis, 2009.
- [16] D.R. Brown and P.C. Krause, "Modeling of Transient Electrical Torques in Solid Iron Rotor Turbogenerators," *IEEE Trans. Power App. Syst.*, Vol. 98, September/October 1979, pp. 1502–1508.
- [17] I.M. Canay, "Causes of Discrepancies on Calculation of Rotor Quantities and Exact Equivalent Diagrams of the Synchronous Machine," *IEEE Trans. Power App. Syst.*, Vol. 88, July 1969, pp. 1114–1120.
- [18] Y. Tabeda and B. Adkins, "Determination of Synchronous Machine Parameters Allowing for Unequal Mutual Inductances," *Proc. IEE*, Vol. 121, December 1974, pp. 1501–1504.
- [19] D.C. Aliprantis, S.D. Sudhoff, and B.T. Kuhn, "A Synchronous Machine Model with Saturation and Arbitrary Rotor Network Representation," *IEEE Trans. Energy Convers.*, Vol. 20, September 2005, pp. 584–594.
- [20] E.W. Kimbark, *Power System Stability: Synchronous Machines*, Vol. 3, Dover Publications, New York, 1968.

## PROBLEMS

- Derive expressions for the short-circuit time constants with the stator resistance included.
- Calculate and compare the standard and derived time constants for the hydro turbine generator given in Chapter 5.
- Repeat Problem 2 for the steam turbine generator given in Chapter 5.
- Derive an expression for the instantaneous electromagnetic torque during a three-phase short circuit at the terminals. Assume the stator terminals of the machine are initially open-circuited and the speed does not change during the fault.
- Derive an expression for the instantaneous field current for a three-phase short circuit at the terminals. As in Problem 4, assume that the machine is initially operating with the stator open-circuited and that the speed remains constant during the fault.
- Consider the short-circuit stator currents shown in Figure 7P-1. The machine is originally operating open-circuited at rated voltage. The speed is fixed during the fault. Assume  $r_s = 0.0037$  pu,  $X_d = 1.7$  pu, and  $X_{ls} = 0.19$  pu. Determine the remaining  $d$ -axis circuit parameters using (a) the derived time constants and (b) the standard time constants.
- For two-rotor windings in the  $d$ -axis, show that  $i_{fd}^{''r} = pG(p)i_{ds}^r$  for  $v_{fd}^{''r} = 0$ .

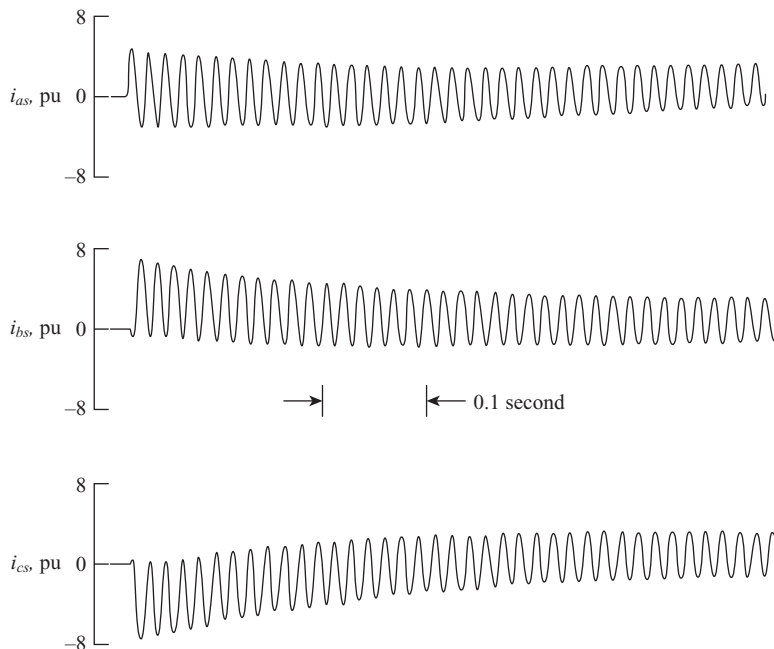


Figure 7P-1. Short-circuit stator currents.

8. Determine  $r'_{kq1}$ ,  $X'_{lkq1}$ ,  $r'_{kq2}$ , and  $X'_{lkq2}$  for the two-rotor winding approximation of  $X_q(s)$  given in Figure 7.8-2 by using (a) the derived time constants and (b) (7.8-10), (7.3-3), and (7.3-4).
9. Determine the parameters of a two-rotor winding approximation of  $X_d(s)$  given in Figure 7.8-1.
10. Express  $Z_{qr}(s)$  for a three-rotor winding approximation. Compare the terms in the denominator to the last two rows of (7.8-11).
11. Determine the time constants of  $X_d(s)$  given in Figure 7.8-1 for a three-rotor winding approximation.
12. Determine the parameters of a three-rotor winding approximation of  $X_q(s)$  shown in Figure 7.8-2.
13. Repeat Problem 12 for  $X_d(s)$  in Figure 7.8-1.
14. Write Park's equations for a synchronous machine represented by three damper windings in the  $q$ -axis and two damper windings and a field winding in the  $d$ -axis.
15. Derive  $X_d(s)$  and  $G(s)$  for the  $d$ -axis circuit with the additional rotor leakage reactance shown in Figure 7.8-4. Show that both have the same denominator.
16. Write the voltage equations in the rotor reference frame for the  $d$ -axis circuit with the additional rotor leakage reactance shown in Figure 7.8-4.
17. Plot the  $X_d(s)$  and  $X_q(s)$  for the steam and hydroturbine generators whose parameters are given in Chapter 5.

# ALTERNATIVE FORMS OF MACHINE EQUATIONS

## 8.1. INTRODUCTION

There are alternative formulations of induction and synchronous machine equations that warrant consideration since each has a specific useful purpose. In particular, (1) linearized or small-displacement formulation for operating point stability issues; (2) neglecting stator electric transients for large-excursion transient stability studies; and (3) voltage-behind reactances (VBRs) formulation convenient for machine-converter analysis and simulation. These special formulations are considered in this chapter.

Although standard computer algorithms may be used to automatically linearize machine equations, it is important to be aware of the steps necessary to perform linearization. This procedure is set forth by applying Taylor expansion about an operating point. The resulting set of linear differential equations describe the dynamic behavior during small displacements or small excursions about an operating point, whereupon basic linear system theory can be used to calculate eigenvalues. In the first sections of this chapter, the nonlinear equations of induction and synchronous machines are linearized and the eigenvalues are calculated. Although these equations are valid for operation with stator voltages of any frequency, only rated frequency operation is considered in detail.

Over the years, there has been considerable attention given to the development of simplified models primarily for the purpose of predicting the dynamic behavior of electric machines during large excursions in some or all of the machine variables.

Before the 1960s, the dynamic behavior of induction machines was generally predicted using the steady-state voltage equations and the dynamic relationship between rotor speed and torque. Similarly, the large-excitation behavior of synchronous machines was predicted using a set of steady-state voltage equations with modifications to account for transient conditions, as presented in Chapter 5, along with the dynamic relationship between rotor angle and torque. With the advent of the computer, these models have given way to more accurate representations. In some cases, the machine equations are programmed in detail; however, in the vast majority of cases, a reduced-order model is used in computer simulations of power systems. In particular, it is standard to neglect the electric transients in the stator voltage equations of all machines and in the voltage equations of all power system components connected to the stator (transformers, transmission lines, etc.). By using a static representation of the power grid, the required number of integrations is drastically reduced. Since “neglecting stator electric transients” is an important aspect of machine analysis especially for the power system engineer, the theory of neglecting electric transients is established and the voltage equations for induction and synchronous machines are given with the stator electric transients neglected. The large-excitation behavior of these machines as predicted by these reduced-order models is compared with the behavior predicted by the complete equations given in Chapter 5 and Chapter 6. From these comparisons, not only do we become aware of the inaccuracies involved when using the reduced-order models, but we are also able to observe the influence that the electric transients have on the dynamic behavior of induction and synchronous machines.

Finally, in an increasing number of applications, electric machines are coupled to power electronic circuits. In Chapter 4, Chapter 5, and Chapter 6, a great deal of the focus was placed upon utilizing reference-frame theory to eliminate rotor-dependent inductances (or flux linkage in the case of the permanent magnet machine). Although reference-frame theory enables analytical evaluation of steady-state performance and provides the basis for most modern electric drive controls, it can be difficult to apply a transformation to some power system components, particularly power electronic converters. In such cases, one is forced to establish a coupling between a machine modeled in a reference frame and a power converter modeled in terms of physical variables. As an alternative, it can be convenient to represent a machine in terms of physical variables using a VBR model. In this chapter, the derivation of a physical variable VBR model of the synchronous machine is provided, along with explanation of its potential application and advantages over alternative model structures. In addition, approximate forms of the VBR model are described in which rotor position-dependent inductances are eliminated, which greatly simplifies the modeling of machines in physical variables.

## 8.2. MACHINE EQUATIONS TO BE LINEARIZED

The linearized machine equations are conveniently derived from voltage equations expressed in terms of constant parameters with constant driving forces, independent of

time. During steady-state balanced conditions, these requirements are satisfied, in the case of the induction machine, by the voltage equations expressed in the synchronously rotating reference frame, and by the voltage equations in the rotor reference frame in the case of the synchronous machine. Since the currents and flux linkages are not independent variables, the machine equations can be written using either currents or flux linkages, or flux linkages per second, as state variables. The choice is generally determined by the application. Currents are selected here. Formulating the small-displacement equations in terms of flux linkages per second is left as an exercise for the reader.

## Induction Machine

The voltage equations for the induction machine with currents as state variables may be written in the synchronously rotating reference frame from (6.5-34) by setting  $\omega = \omega_e$  as

$$\begin{bmatrix} v_{qs}^e \\ v_{ds}^e \\ v_{qr}^e \\ v_{dr}^e \end{bmatrix} = \begin{bmatrix} r_s + \frac{p}{\omega_b} X_{ss} & \frac{\omega_e}{\omega_b} X_{ss} & \frac{p}{\omega_b} X_M & \frac{\omega_e}{\omega_b} X_M \\ -\frac{\omega_e}{\omega_b} X_{ss} & r_s + \frac{p}{\omega_b} X_{ss} & -\frac{\omega_e}{\omega_b} X_M & \frac{p}{\omega_b} X_M \\ \frac{p}{\omega_b} X_M & s \frac{\omega_e}{\omega_b} X_M & r'_r + \frac{p}{\omega_b} X'_{rr} & s \frac{\omega_e}{\omega_b} X'_{rr} \\ -s \frac{\omega_e}{\omega_b} X_M & \frac{p}{\omega_b} X_M & -s \frac{\omega_e}{\omega_b} X'_{rr} & r'_r + \frac{p}{\omega_b} X'_{rr} \end{bmatrix} \begin{bmatrix} i_{qs}^e \\ i_{ds}^e \\ i_{qr}^e \\ i_{dr}^e \end{bmatrix} \quad (8.2-1)$$

where  $s$  is the slip defined by (6.9-13) and the zero quantities have been omitted since only balanced conditions are considered. The reactances  $X_{ss}$  and  $X'_{rr}$  are defined by (6.5-35) and (6.5-36), respectively.

Since we have selected currents as state variables, the electromagnetic torque is most conveniently expressed as

$$T_e = X_M (i_{qs}^e i_{dr}^e - i_{ds}^e i_{qr}^e) \quad (8.2-2)$$

Here, the per unit version of (6.6-2) is selected for compactness. The per unit relationship between torque and speed is (6.8-10), which is written here for convenience

$$T_e = 2H_p \frac{\omega_r}{\omega_b} + T_L \quad (8.2-3)$$

## Synchronous Machine

The voltage equations for the synchronous machine in the rotor reference frame may be written from (5.5-38) for balanced conditions as

$$\begin{bmatrix} v'_{qs} \\ v'_{ds} \\ v'_{kq1} \\ v'_{kq2} \\ e'_{fd} \\ v'_{kd} \end{bmatrix} = \begin{bmatrix} r_s + \frac{p}{\omega_b} X_q & \frac{\omega_r}{\omega_b} X_d & \frac{p}{\omega_b} X_{mq} & \frac{p}{\omega_b} X_{mq} & \frac{\omega_r}{\omega_b} X_{md} & \frac{\omega_r}{\omega_b} X_{md} \\ -\frac{\omega_r}{\omega_b} X_q & r_s + \frac{p}{\omega_b} X_d & -\frac{\omega_r}{\omega_b} X_{mq} & -\frac{\omega_r}{\omega_b} X_{mq} & \frac{p}{\omega_b} X_{md} & \frac{p}{\omega_b} X_{md} \\ \frac{p}{\omega_b} X_{mq} & 0 & r'_{kq1} + \frac{p}{\omega_b} X'_{kq1} & \frac{p}{\omega_b} X_{mq} & 0 & 0 \\ \frac{p}{\omega_b} X_{mq} & 0 & \frac{p}{\omega_b} X_{mq} & r'_{kq2} + \frac{p}{\omega_b} X'_{kq2} & 0 & 0 \\ 0 & \frac{X_{md}}{r'_{fd}} \left( \frac{p}{\omega_b} X_{md} \right) & 0 & 0 & \frac{X_{md}}{r'_{fd}} \left( r'_{fd} + \frac{p}{\omega_b} X'_{fd} \right) & \frac{X_{md}}{r'_{fd}} \left( \frac{p}{\omega_b} X_{md} \right) \\ 0 & \frac{p}{\omega_b} X_{md} & 0 & 0 & \frac{p}{\omega_b} X_{md} & r'_{kd} + \frac{p}{\omega_b} X'_{kd} \end{bmatrix} \begin{bmatrix} i'_{qs} \\ i'_{ds} \\ i'_{kq1} \\ i'_{kq2} \\ i'_{fd} \\ i'_{kd} \end{bmatrix} \quad (8.2-4)$$

where positive currents are assumed into the machine and the reactances are defined by (5.5-39)–(5.5-44).

With the currents as state variables, the per unit electromagnetic torque positive for motor action is expressed from (5.6-2) as

$$T_e = X_{md}(i'_{ds} + i'_{fd} + i'_{kd})i'_{qs} - X_{mq}(i'_{qs} + i'_{kq1} + i'_{kq2})i'_{ds} \quad (8.2-5)$$

The per unit relationship between torque and rotor speed is given by (5.8-3), which is

$$T_e = 2H_p \frac{\omega_r}{\omega_b} + T_L \quad (8.2-6)$$

The rotor angle is expressed from (5.7-1) as

$$\delta = \frac{\omega_b}{p} \left( \frac{\omega_r - \omega_e}{\omega_b} \right) \quad (8.2-7)$$

It is necessary, in the following analysis, to relate variables in the synchronously rotating reference frame to variables in the rotor reference frame. This is accomplished by using (5.7-2) with the zero quantities omitted. Thus

$$\begin{bmatrix} f'_{qs} \\ f'_{ds} \end{bmatrix} = \begin{bmatrix} \cos \delta & -\sin \delta \\ \sin \delta & \cos \delta \end{bmatrix} \begin{bmatrix} f^e_{qs} \\ f^e_{ds} \end{bmatrix} \quad (8.2-8)$$

### 8.3. LINEARIZATION OF MACHINE EQUATIONS

There are two procedures that can be followed to obtain the linearized machine equations. One is to employ Taylor's expansion about a fixed value or operating point. That is, any machine variable  $f_i$  can be written in terms of a Taylor expansion about its fixed value,  $f_{io}$ , as

$$g(f_i) = g(f_{io}) + g'(f_{io})\Delta f_i + \frac{g''(f_{io})}{2!} \Delta f_i^2 + \dots \quad (8.3-1)$$

where

$$f_i = f_{io} + \Delta f_i \quad (8.3-2)$$

If only a small excursion from the fixed point is experienced, all terms higher than the first-order may be neglected, and  $g(f_i)$  may be approximated by

$$g(f_i) \approx g(f_{io}) + g'(f_{io})\Delta f_i \quad (8.3-3)$$

Hence, the small-displacement characteristics of the system are given by the first-order terms of Taylor's series,

$$\Delta g(f_i) = g'(f_{io})\Delta f_i \quad (8.3-4)$$

For functions of two variables, the same argument applies

$$g(f_1, f_2) \approx g(f_{1o}, f_{2o}) + \frac{\partial}{\partial f_1} g(f_{1o}, f_{2o})\Delta f_1 + \frac{\partial}{\partial f_2} g(f_{1o}, f_{2o})\Delta f_2 \quad (8.3-5)$$

where  $\Delta g(f_1, f_2)$  is the last two terms of (8.3-5).

If, for example, we apply this method to the expression for induction machine torque, (8.2-2), then

$$T_e(i_{qs}^e, i_{ds}^e, i_{qr}^e, i_{dr}^e) \approx T_e(i_{qso}^e, i_{dso}^e, i_{qro}^e, i_{dro}^e) + \frac{\partial T_e(i_{qso}^e, i_{dso}^e, i_{qro}^e, i_{dro}^e)}{\partial i_{qs}^e} \Delta i_{qs}^e + \text{etc.} \quad (8.3-6)$$

whereupon the small-displacement expression for torque becomes

$$\Delta T_e = X_M (i_{qso}^e \Delta i_{dr}^e + i_{dro}^e \Delta i_{qs}^e - i_{dso}^e \Delta i_{qr}^e - i_{qro}^e \Delta i_{ds}^e) \quad (8.3-7)$$

where the added subscript  $o$  denotes steady-state quantities.

An equivalent method of linearizing nonlinear equations is to write all variables in the form given by (8.3-2). If all multiplications are then performed and the steady-state expressions cancelled from both sides of the equations and if all products of small displacement terms ( $\Delta f_1 \Delta f_2$ , for example) are neglected, the small-displacement equations are obtained. It is left to the reader to obtain (8.3-7) by this technique.

## Induction Machine

If either of the above-described methods of linearization is employed to (8.2-1)–(8.2-3), the linear differential equations of an induction machine become

$$\begin{bmatrix} \Delta v_{qs}^e \\ \Delta v_{ds}^e \\ \Delta v_{qr}^e \\ \Delta v_{dr}^e \\ \Delta T_L \end{bmatrix} = \begin{bmatrix} r_s + \frac{p}{\omega_b} X_{ss} & \frac{\omega_e}{\omega_b} X_{ss} & \frac{p}{\omega_b} X_M & \frac{\omega_e}{\omega_b} X_M & 0 \\ -\frac{\omega_e}{\omega_b} X_{ss} & r_s + \frac{p}{\omega_b} X_{ss} & -\frac{\omega_e}{\omega_b} X_M & \frac{p}{\omega_b} X_M & 0 \\ \frac{p}{\omega_b} X_M & s_o \frac{\omega_e}{\omega_b} X_M & r'_r + \frac{p}{\omega_b} X'_{rr} & s_o \frac{\omega_e}{\omega_b} X'_{rr} & -X_M i_{ds0}^e - X'_{rr} i'_{dro}^e \\ -s_o \frac{\omega_e}{\omega_b} X_M & \frac{p}{\omega_b} X_M & -s_o \frac{\omega_e}{\omega_b} X'_{rr} & r'_r + \frac{p}{\omega_b} X'_{rr} & X_M i_{qso}^e + X'_{rr} i'_{qro}^e \\ X_M i'_{dro}^e & -X_M i'_{qro}^e & -X_M i_{ds0}^e & X_M i_{qso}^e & -2H_p \end{bmatrix} \begin{bmatrix} \Delta i_{qs}^e \\ \Delta i_{ds}^e \\ \Delta i_{qr}^e \\ \Delta i_{dr}^e \\ \frac{\Delta \omega_r}{\omega_b} \end{bmatrix} \quad (8.3-8)$$

where

$$s_o = \frac{\omega_e - \omega_{ro}}{\omega_e} \quad (8.3-9)$$

It is clear that with applied voltages of rated frequency, the ratio of  $\omega_e$  to  $\omega_b$  is unity. However, (8.3-8) and (8.3-9) are written with  $\omega_e$  included explicitly so as to accommodate applied voltages of a constant frequency other than rated as would occur in variable-speed drive systems. The frequency of the applied stator voltages in variable-speed drive systems is varied by controlling the firing of the source converter. Therefore, in some applications, the frequency of the stator voltages may be a controlled variable. It is recalled from Chapter 3 that variable-frequency operation may be investigated in the synchronously rotating reference frame by simply changing the speed of the reference frame corresponding to the change in frequency. Therefore, if frequency is a system input variable, then a small displacement in frequency may be taken into account by allowing the reference-frame speed to change by replacing  $\omega_e$  with  $\omega_{eo} + \Delta\omega_e$ .

It is convenient to separate out the derivative terms and write (8.3-8) in the form

$$Epx = \mathbf{Fx} + \mathbf{u} \quad (8.3-10)$$

where

$$(\mathbf{x})^T = \begin{bmatrix} \Delta i_{qs}^e & \Delta i_{ds}^e & \Delta i_{qr}^e & \Delta i_{dr}^e & \frac{\Delta \omega_r}{\omega_b} \end{bmatrix} \quad (8.3-11)$$

$$(\mathbf{u})^T = \begin{bmatrix} \Delta v_{qs}^e & \Delta v_{ds}^e & \Delta v_{qr}^e & \Delta v_{dr}^e & \Delta T_L \end{bmatrix} \quad (8.3-12)$$

$$\mathbf{E} = \frac{1}{\omega_b} \begin{bmatrix} X_{ss} & 0 & X_M & 0 & 0 \\ 0 & X_{ss} & 0 & X_M & 0 \\ X_M & 0 & X'_{rr} & 0 & 0 \\ 0 & X_M & 0 & X'_{rr} & 0 \\ 0 & 0 & 0 & 0 & -2H\omega_b \end{bmatrix} \quad (8.3-13)$$

$$\mathbf{F} = - \begin{bmatrix} r_s & \frac{\omega_e}{\omega_b} X_{ss} & 0 & \frac{\omega_e}{\omega_b} X_M & 0 \\ -\frac{\omega_e}{\omega_b} X_{ss} & r_s & -\frac{\omega_e}{\omega_b} X_M & 0 & 0 \\ 0 & s_o \frac{\omega_e}{\omega_b} X_M & r'_r & s_o \frac{\omega_e}{\omega_b} X'_{rr} & -X_M i_{dso}^e - X'_{rr} i_{dro}^e \\ -s_o \frac{\omega_e}{\omega_b} X_M & 0 & -s_o \frac{\omega_e}{\omega_b} X'_{rr} & r'_r & X_M i_{qso}^e + X'_{rr} i_{qro}^e \\ X_M i_{dro}^e & -X_M i_{qro}^e & -X_M i_{dso}^e & X_M i_{qso}^e & 0 \end{bmatrix} \quad (8.3-14)$$

In the analysis of linear systems, it is convenient to express the linear differential equations in the form

$$p\mathbf{x} = \mathbf{Ax} + \mathbf{Bu} \quad (8.3-15)$$

Equation (8.3-15) is the fundamental form of the linear differential equations. It is commonly referred to as the state equation.

Equation (8.3-10) may be written as

$$p\mathbf{x} = (\mathbf{E})^{-1} \mathbf{Fx} + (\mathbf{E})^{-1} \mathbf{u} \quad (8.3-16)$$

which is in the form of (8.3-15) with

$$\mathbf{A} = (\mathbf{E})^{-1} \mathbf{F} \quad (8.3-17)$$

$$\mathbf{B} = (\mathbf{E})^{-1} \quad (8.3-18)$$

## Synchronous Machines

Linearizing (8.2-4)–(8.2-8) yields (8.3-19). Since the steady-state damper winding currents ( $i_{kdo}^r$ ,  $i_{kq1o}^r$ , and  $i_{kq2o}^r$ ) are zero, they are not included in (8.3-19). Since the synchronous machine is generally connected to an electric system, such as a power system, and since it is advantageous to linearize the system voltage equations in the synchronously rotating reference frame, it is convenient to include the relationship between  $\Delta\omega_r$  and  $\Delta\delta$  in (8.3-19). As in the case of linearized equations for the induction machine,  $\omega_e$  is included explicitly in (8.3-19) so that the equations are in a form convenient for voltages of any constant frequency. Small controlled changes in the

frequency of the applied stator voltages, as is possible in variable-speed drive systems, may be taken into account analytically by replacing  $\omega_e$  with  $\omega_{eo} + \Delta\omega_e$  in the expression for  $\delta$  given by (8.2-7).

$$\begin{bmatrix} \Delta v_{qs}^r \\ \Delta v_{ds}^r \\ \Delta v_{kq1}^r \\ \Delta v_{kq2}^r \\ \Delta e_{qfd}^r \\ \Delta v_{kd}^r \\ \Delta T_L \\ 0 \end{bmatrix} = \begin{bmatrix} r_s + \frac{p}{\omega_b} X_q & \frac{\omega_e}{\omega_b} X_d & \frac{p}{\omega_b} X_{mq} & \frac{p}{\omega_b} X_{mq} & \frac{\omega_e}{\omega_b} X_{md} & \frac{\omega_e}{\omega_b} X_{md} & -X_d i_{dso}^r + X_{md} i_{fdo}^r & 0 \\ -\frac{\omega_e}{\omega_b} X_q & r_s + \frac{p}{\omega_b} X_d & -\frac{\omega_e}{\omega_b} X_{mq} & -\frac{\omega_e}{\omega_b} X_{mq} & \frac{p}{\omega_b} X_{md} & \frac{p}{\omega_b} X_{md} & X_q i_{qso}^r & 0 \\ \frac{p}{\omega_b} X_{mq} & 0 & r'_{kq1} + \frac{p}{\omega_b} X'_{kq1} & \frac{p}{\omega_b} X_q & 0 & 0 & 0 & 0 \\ \frac{p}{\omega_b} X_{mq} & 0 & \frac{p}{\omega_b} X_{mq} & r'_{kq2} + \frac{p}{\omega_b} X'_{kq2} & 0 & 0 & 0 & 0 \\ 0 & \frac{X_{md}}{r'_{fd}} \left( \frac{p}{\omega_b} X_{md} \right) & 0 & 0 & \frac{X_{md}}{r'_{fd}} \left( r'_{fd} + \frac{p}{\omega_b} X'_{fd} \right) \frac{X_{md}}{r'_{fd}} \left( \frac{p}{\omega_b} X_{md} \right) & 0 & 0 & 0 \\ 0 & \frac{p}{\omega_b} X_{md} & 0 & 0 & \frac{p}{\omega_b} X_{md} & r'_{kd} + \frac{p}{\omega_b} X'_{kd} & 0 & 0 \\ -X_{mq} i_{dso}^r + X_{md} (i_{dso}^r - i_{fdo}^r) X_{md} i_{qso}^r - X_{mq} i_{qso}^r & -X_{mq} i_{dso}^r & -X_{mq} i_{dso}^r & X_{md} i_{qso}^r & X_{md} i_{qso}^r & X_{md} i_{qso}^r & -2H_p & 0 \\ 0 & 0 & 0 & 0 & 0 & 0 & -\omega_b & p \end{bmatrix} \begin{bmatrix} \Delta i_{qs}^r \\ \Delta i_{ds}^r \\ \Delta i_{kq1}^r \\ \Delta i_{kq2}^r \\ \Delta i_{qfd}^r \\ \Delta i_{kd}^r \\ \Delta \omega_r \\ \Delta \delta \end{bmatrix} \quad (8.3-19)$$

In most cases, the synchronous machine is connected to a power system whereupon the voltage  $v_{qs}^r$  and  $v_{ds}^r$ , which are functions of the state variable  $\delta$ , will vary as the rotor angle varies during a disturbance. It is of course necessary to account for the dependence of the driving forces upon the state variables before expressing the linear differential equations in fundamental form. In power system analysis, it is often assumed that in some place in the system, there is a balanced source that can be considered a constant amplitude, constant frequency, and zero impedance source (infinite bus). This would be a balanced independent driving force that would be represented as constant voltages in the synchronously rotating reference frame. Hence, it is necessary to relate the synchronously rotating reference-frame variables, where the independent driving force exists, to the variables in the rotor reference frame. The transformation given by (8.2-8) is nonlinear. In order to incorporate it into a linear set of differential equations, it must be linearized. By employing the approximations that  $\cos \Delta\delta = 1$  and  $\sin \Delta\delta = \Delta\delta$ , the linearized version of (8.2-8) is

$$\begin{bmatrix} \Delta f_{qs}^r \\ \Delta f_{ds}^r \end{bmatrix} = \begin{bmatrix} \cos \delta_o & -\sin \delta_o \\ \sin \delta_o & \cos \delta_o \end{bmatrix} \begin{bmatrix} \Delta f_{qs}^e \\ \Delta f_{ds}^e \end{bmatrix} + \begin{bmatrix} -f_{dso}^r \\ f_{qso}^r \end{bmatrix} \Delta \delta \quad (8.3-20)$$

Linearizing the inverse transformation yields

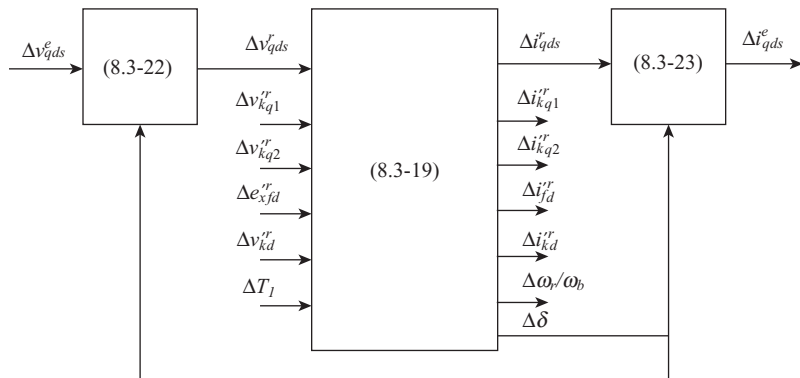


**Figure 8.3-1.** Interconnection of small-displacement equations of a synchronous machine: Park's equations.

$$\begin{bmatrix} \Delta f_{qs}^e \\ \Delta f_{ds}^e \end{bmatrix} = \begin{bmatrix} \cos \delta_o & \sin \delta_o \\ -\sin \delta_o & \cos \delta_o \end{bmatrix} \begin{bmatrix} \Delta f_{qs}^r \\ \Delta f_{ds}^r \end{bmatrix} + \begin{bmatrix} f_{dso}^e \\ -f_{aso}^e \end{bmatrix} \Delta \delta \quad (8.3-21)$$

It is convenient to write the above equations in the form

$$\Delta \mathbf{f}_{qds}^r = \mathbf{T} \Delta \mathbf{f}_{qds}^e + \mathbf{F}^r \Delta \boldsymbol{\delta} \quad (8.3-22)$$

$$\Delta \mathbf{f}_{qds}^e = (\mathbf{T})^{-1} \Delta \mathbf{f}_{qds}^r + \mathbf{F}^e \Delta \boldsymbol{\delta} \quad (8.3-23)$$

It is instructive to view the interconnections of the above relationships as shown in Figure 8.3-1. With the equations as shown in Figure 8.3-1, a change in  $\Delta v_{qds}^e$  is reflected through the transformation to the voltage equations in the rotor reference frame and finally back to the synchronously rotating reference-frame currents  $\Delta i_{qds}$ . The detail shown in Figure 8.3-1 is more than is generally necessary. If, for example, the objective is to study the small-displacement dynamics of a synchronous machine with its terminals connected to an infinite bus, then  $\Delta v_{qds}^e$  is zero and  $\Delta v_{qds}^r$  changes due only to  $\Delta \delta$ . Also, in this case, it is unnecessary to transform the rotor reference-frame currents to the synchronously rotating reference frame since the source (infinite bus) has zero impedance.

If the machine is connected through a transmission line to a large system (infinite bus), the small-displacement dynamics of the transmission system must be taken into account. If only the machine is connected to the transmission line and if it is not equipped with a voltage regulator, then it is convenient to transform the equations of the transmission line to the rotor reference frame. In such a case, the machine and transmission line can be considered in much the same way as a machine connected to an infinite bus. If, however, the machine is equipped with a voltage regulator or more than one machine is connected to the same transmission line, it is generally preferable to express the dynamics of the transmission system in the synchronously rotating reference frame and transform to and from the rotor reference frame of each machine as depicted in Figure 8.3-1.

If the machine is equipped with a voltage regulator, the dynamic behavior of the regulator will affect the dynamic characteristics of the machine. Therefore, the small-displacement dynamics of the regulator must be taken into account. When regulators are employed, the change in field voltage  $\Delta e_{fd}^r$  is dynamically related to the change in terminal voltage, which is a function of  $\Delta \mathbf{v}_{qds}^r$  (or  $\Delta \mathbf{v}_{qds}^r$ ), the change in field current  $\Delta \mathbf{i}_{fd}^r$ , and perhaps the change in rotor speed  $\Delta \omega_r / \omega_b$  if the excitation system is equipped with a control to help damp rotor oscillations by means of field voltage control. This type of damping control is referred to as a power system stabilizer (PSS).

In some investigations, it is necessary to incorporate the small-displacement dynamics of the prime mover system. The change of input torque (negative load torque) is a function of the change in rotor speed  $\Delta \omega_r / \omega_b$ , which in turn is a function of the dynamics of the masses, shafts, and damping associated with the mechanical system and, if long-term transients are of interest, the steam or hydro dynamics and associated controls.

Although a more detailed discussion of the dynamics of the excitation and prime mover systems would be helpful, it is clear from the earlier discussion that the equations that describe the operation and control of a synchronous machine equipped with a voltage regulator and a prime mover system are very involved. This becomes readily apparent when it is necessary to arrange the small-displacement equations of the complete system into the fundamental form. Rather than performing this task by hand, it is preferable to take advantage of analytical techniques, which involves formulating the equations of each component (machine, excitation system, prime mover system, etc.) in fundamental form. A computer routine can be used to arrange the small-displacement equations along with the interconnecting transformations of the complete system into the fundamental form.

## 8.4. SMALL-DISPLACEMENT STABILITY: EIGENVALUES

With the linear differential equations written in state variable form, the  $\mathbf{u}$  vector represents the forcing functions. If  $\mathbf{u}$  is set equal to zero, the general solution of the homogeneous or force-free linear differential equations becomes

$$\mathbf{x} = e^{\mathbf{A}t} \mathbf{K} \quad (8.4-1)$$

where  $\mathbf{K}$  is a vector formed by an arbitrary set of initial conditions. The exponential  $e^{\mathbf{A}t}$  represents the unforced response of the system. It is called the state transition matrix. Small-displacement stability is assured if all elements of the transition matrix approach zero asymptotically as time approaches infinity. Asymptotic behavior of all elements of the matrix occurs whenever all of the roots of the characteristic equation of  $\mathbf{A}$  have negative real parts where the characteristic equation of  $\mathbf{A}$  is defined

$$\det(\mathbf{A} - \lambda \mathbf{I}) = 0 \quad (8.4-2)$$

In (8.4-2),  $\mathbf{I}$  is the identity matrix and  $\lambda$  are the roots of the characteristic equation of  $\mathbf{A}$  referred to as characteristic roots, latent roots, or eigenvalues. Herein, we will use

the latter designation. One should not confuse the  $\lambda$  used here to denote eigenvalues with the same notation used to denote flux linkages.

The eigenvalues provide a simple means of predicting the behavior of an induction or synchronous machine at any balanced operating condition. Eigenvalues may either be real or complex, and when complex, they occur as conjugate pairs signifying a mode of oscillation of the state variables. Negative real parts correspond to state variables or oscillations of state variables that decrease exponentially with time. Positive real parts indicate an exponential increase with time, an unstable condition.

## 8.5. EIGENVALUES OF TYPICAL INDUCTION MACHINES

The eigenvalues of an induction machine can be obtained by using a standard eigenvalue computer routine to calculate the roots of  $\mathbf{A}$  given by (8.3-17). The eigenvalues given in Table 8.5-1 are for the machines listed in Table 6.10-1. The induction machine, as we have perceived it, is described by five state variables and hence five eigenvalues. Sets of eigenvalues for each machine at stall, rated, and no-load speeds are given in Table 8.5-1 for rated frequency operation. Plots of the eigenvalues (real part and only the positive imaginary part) for rotor speeds from stall to synchronous are given in Figure 8.5-1 and Figure 8.5-2 for the 3- and 2250-hp induction motors, respectively.

At stall, the two complex conjugate pairs of eigenvalues both have a frequency (imaginary part) corresponding to  $\omega_b$ . The frequency of one complex conjugate pair decreases as the speed increases from stall, while the frequency of the other complex conjugate pair remains at approximately  $\omega_b$ —in fact, nearly equal to  $\omega_b$  for the larger horsepower machines. The eigenvalues are dependent upon the parameters of the machine and it is difficult to relate analytically a change in an eigenvalue with a change in a specific machine parameter. It is possible, however, to identify an association between eigenvalues and the machine variables. For example, the complex conjugate pair that remains at a frequency close to  $\omega_b$  is primarily associated with the transient

TABLE 8.5-1. Induction Machine Eigenvalues

Rating, hp	Stall	Rated Speed	No Load
3	$-4.57 \pm j377$	$-85.6 \pm j313$	$-89.2 \pm j316$
	$-313 \pm j377$	$-223 \pm j83.9$	$-218 \pm j60.3$
	1.46	-16.8	-19.5
50	$-2.02 \pm j377$	$-49.4 \pm j356$	$-50.1 \pm j357$
	$-198 \pm j377$	$-142 \pm j42.5$	$-140 \pm j18.2$
	1.18	-14.4	-17.0
500	$-0.872 \pm j377$	$-41.8 \pm j374$	$-41.8 \pm j374$
	$-70.3 \pm j377$	$-15.4 \pm j41.5$	$-14.3 \pm j42.8$
	0.397	-27.5	-29.6
2250	$-0.428 \pm j377$	$-24.5 \pm j376$	$-24.6 \pm j376$
	$-42.6 \pm j377$	$-9.36 \pm j41.7$	$-9.05 \pm j42.5$
	0.241	-17.9	-18.5

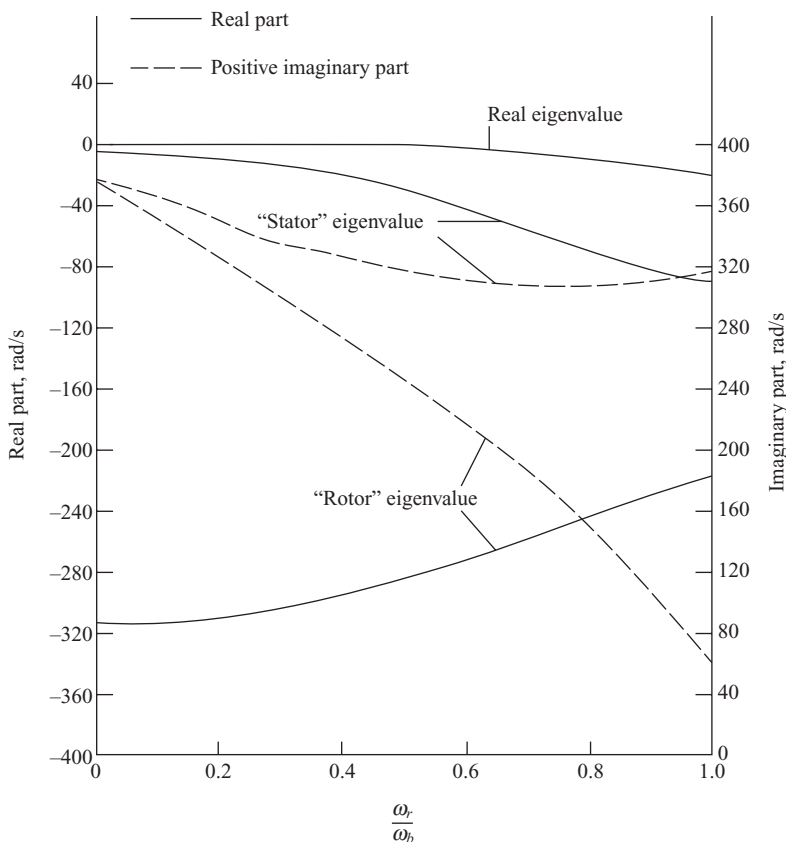


Figure 8.5-1. Plot of eigenvalues for a 3-hp induction motor.

offset currents in the stator windings, which reflects into the synchronously rotating reference as a decaying 60-Hz variation. This complex conjugate pair, which is denoted as the “stator” eigenvalues in Figure 8.5-1 and Figure 8.5-2, is not present when the electric transients are neglected in the stator voltage equations. It follows that the transient response of the machine is influenced by this complex conjugate eigenvalue pair whenever a disturbance causes a transient offset in the stator currents. It is recalled that in Chapter 6, we noted a transient pulsation in the instantaneous torque of 60 Hz during free acceleration and following a three-phase fault at the terminals with the machine initially operating at near rated conditions. We also noted that the pulsations were more damped in the case of the smaller horsepower machines than for the larger horsepower machines. It is noted in Table 8.5-1 that the magnitudes of the real part of the complex eigenvalues with a frequency corresponding to  $\omega_b$  are larger, signifying more damping, for the smaller horsepower machine than for the larger machines.

The complex conjugate pair which changes in frequency as the rotor speed varies is associated primarily with the electric transients in the rotor circuits and denoted in

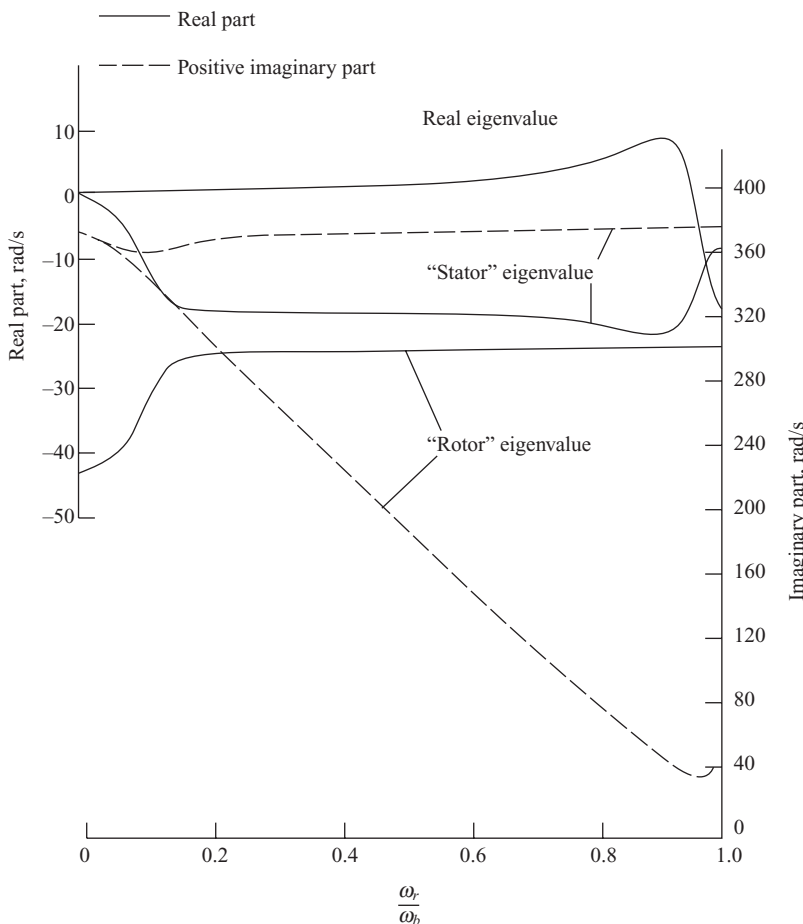


Figure 8.5-2. Plot of eigenvalues for a 2250-hp induction motor.

Figure 8.5-1 and Figure 8.5-2 as the “rotor” eigenvalue. This complex conjugate pair is not present when the rotor electric transients are neglected. The damping associated with this complex conjugate pair is less for the larger horsepower machines than the smaller machines. It is recalled that during free acceleration, the 3- and 50-hp machines approached synchronous speed in a well-damped manner, while the 500- and the 2250-hp machines demonstrated damped oscillations about synchronous speed. Similar behavior was noted as the machines approached their final operating point following a load torque change or a three-phase terminal fault. This behavior corresponds to that predicted by this eigenvalue. It is interesting to note that this eigenvalue is reflected noticeably into the rotor speed, whereas the higher-frequency “stator” eigenvalue is not. This, of course, is due to the fact that for a given inertia and torque amplitude, a low-frequency torque component will cause a larger amplitude variation in rotor speed than a high-frequency component.

The real eigenvalue signifies an exponential response. It would characterize the behavior of the induction machine equations if all electric transients are mathematically neglected or if, in the actual machine, the electric transients are highly damped, as in the case of the smaller horsepower machines. Perhaps the most interesting feature of this eigenvalue, which is denoted as the real eigenvalue in Figure 8.5-1 and Figure 8.5-2, is that it can be related to the steady-state torque-speed curve. If we think for a moment about the torque-speed characteristics, we realize that an induction machine can operate stably only in the negative-slope portion of the torque-speed curve. If we were to assume an operating point on the positive-slope portion of the torque-speed curve we would find that a small disturbance would cause the machine to move away from this operating point, either accelerating to the negative-slope region or decelerating to stall and perhaps reversing direction of rotation depending upon the nature of the load torque. A positive eigenvalue signifies a system that would move away from an assumed operating point. Note that this eigenvalue is positive over the positive-slope region of the torque-speed curve, becoming negative after maximum steady-state torque.

## 8.6. EIGENVALUES OF TYPICAL SYNCHRONOUS MACHINES

The linearized transformations, (8.3-22) and (8.3-23), and the machine equations (8.3-19) may each be considered as components as shown in Figure 8.3-1. The eigenvalues of the two synchronous machines, each connected to an infinite bus, studied in Section 5.10, are given in Table 8.6-1 for rated operation.

The complex conjugate pair with the frequency (imaginary part) approximately equal to  $\omega_b$  is associated with the transient offset currents in the stator windings, which cause the 60 Hz pulsation in electromagnetic torque. This pulsation in torque is evident in the computer traces of a three-phase fault at the machine terminals shown in Figure 5.10-8 and Figure 5.10-10. Although operation therein is initially at rated conditions, the three-phase fault and subsequent switching causes the operating condition to change significantly from rated conditions. Nevertheless, we note that the 60 Hz pulsation is damped slightly more in the case of the steam turbine generator than in the case of the hydro turbine generator. Correspondingly, the relative values of the real parts of the "stator" eigenvalues given in Table 8.6-1 indicate that the stator electric transients of the steam unit are damped more than the stator transients of the hydro unit.

TABLE 8.6-1. Synchronous Machine Eigenvalues for Rated Conditions

Hydro Turbine Generator	Steam Turbine Generator
$-3.58 \pm j377$	$-4.45 \pm j377$
$-133 \pm j8.68$	$-1.70 \pm j10.5$
-24.4	-32.2
-22.9	-11.1
-0.453	-0.349
	-0.855

The remaining complex conjugate pair is similar to the “rotor” eigenvalue in the case of the induction machine. However, in the case of the synchronous machine, this mode of oscillation is commonly referred to as the hunting or swing mode, which is the principal mode of oscillation of the rotor of the machine relative to the electrical angular velocity of the electrical system (the infinite bus in the case of studies made in Chapter 5). This mode of oscillation is apparent in the machine variables, especially the rotor speed, in Figure 5.10-8 and Figure 5.10-10 during the “settling out” period following reclosing. As indicated by this complex conjugate eigenvalue, the “settling out” rotor oscillation of the steam unit (Fig. 5.10-10) is more damped and of higher frequency than the corresponding rotor oscillation of the hydro unit.

The real eigenvalues are associated with the decay of the offset currents in the rotor circuits and therefore associated with the inverse of the effective time constant of these circuits. It follows that since the field winding has the largest time constant it gives rise to the smallest of the real eigenvalues. In Reference 1, it is shown that the “stator” eigenvalue and the real eigenvalues do not change significantly in value as the real and reactive power loading conditions change.

## 8.7. NEGLECTING ELECTRIC TRANSIENTS OF STATOR VOLTAGE EQUATIONS

In the case of the induction machine, there are two reduced-order models commonly employed to calculate the electromagnetic torque during large transient excursions. The most elementary of these is the one wherein the electric transients are neglected in both the stator and rotor circuits. We are familiar with this steady-state model from the information presented in Chapter 6. The reduced-order model of present interest is the one wherein the electric transients are neglected only in the stator voltage equations.

In the case of the synchronous machine, there are a number of reduced-order models used to predict its large-excursion dynamic behavior. Perhaps the best known is the voltage behind transient reactance reduced-order model that was discussed in Chapter 5. The reduced-order model that is widely used for power grid studies is the one wherein the electric transients of the stator voltage equations are neglected.

The theory of neglecting electric transients is set forth in Reference 2. To establish this theory, let us return for a moment to the work in Section 3.4, where the variables associated with stationary resistive, inductive, and capacitive elements were transformed to the arbitrary reference frame. It is obvious that the instantaneous voltage equations for the three-phase resistive circuit are the same form for either transient or steady-state conditions. However, it is not obvious that the equations describing the behavior of linear symmetrical inductive and capacitive elements with the electric transients neglected (steady-state behavior) may be arranged so that the instantaneous voltages and currents are related algebraically without the operator  $d/dt$ . Since the derivation to establish these equations is analogous for inductive and capacitive elements, it will be carried out only for an inductive circuit.

First, let us express the voltage equations of the three-phase inductive circuit in the synchronously rotating reference frame. From (3.4-11) and (3.4-12) with  $\omega = \omega_e$  and for balanced conditions

$$v_{qs}^e = \omega_e \lambda_{ds}^e + p \lambda_{qs}^e \quad (8.7-1)$$

$$v_{ds}^e = -\omega_e \lambda_{qs}^e + p \lambda_{ds}^e \quad (8.7-2)$$

For balanced steady-state conditions, the variables in the synchronously rotating reference frame are constants. Hence, we can neglect the electric transients by neglecting  $p\lambda_{qs}^e$  and  $p\lambda_{ds}^e$ . Our purpose is to obtain algebraically related instantaneous voltage equations in the arbitrary reference frame that may be used to portray the behavior with the electric transients neglected (steady-state behavior). To this end, it is helpful to determine the arbitrary reference-frame equivalent of neglecting  $p\lambda_{qs}^e$  and  $p\lambda_{ds}^e$ . This may be accomplished by noting from (3.10-1) that the synchronous rotating and arbitrary reference-frame variables are related by

$$\mathbf{f}_{qd0s} = {}^e \mathbf{K} \mathbf{f}_{qd0s}^e \quad (8.7-3)$$

From (3.10-7)

$${}^e \mathbf{K} = \begin{bmatrix} \cos(\theta - \theta_e) & -\sin(\theta - \theta_e) & 0 \\ \sin(\theta - \theta_e) & \cos(\theta - \theta_e) & 0 \\ 0 & 0 & 1 \end{bmatrix} \quad (8.7-4)$$

It is recalled that the arbitrary reference-frame variables do not carry a raised index. If (8.7-1) and (8.7-2) are appropriately substituted in (8.7-3), the arbitrary reference-frame voltage equations may be written as

$$v_{qs} = -(\omega_e - \omega) \lambda_{ds} + \omega_e \lambda_{ds} + p \lambda_{qs} \quad (8.7-5)$$

$$v_{ds} = (\omega_e - \omega) \lambda_{qs} - \omega_e \lambda_{qs} + p \lambda_{ds} \quad (8.7-6)$$

These equations are identical to (3.4-11) and (3.4-12) but written in a form that preserves the identity of  $p\lambda_{qs}^e$  and  $p\lambda_{ds}^e$ . In particular, the first and third terms on the right-hand side of (8.7-5) and (8.7-6) result from transforming  $p\lambda_{qs}^e$  and  $p\lambda_{ds}^e$  to the arbitrary reference frame. Thus, for balanced conditions, neglecting the electric transients in the arbitrary reference frame is achieved by neglecting these terms. The resulting equations are

$$v_{qs} = \omega_e \lambda_{ds} \quad (8.7-7)$$

$$v_{ds} = -\omega_e \lambda_{qs} \quad (8.7-8)$$

These equations, taken as a set, describe the behavior of linear symmetrical inductive circuits in any reference frame with the electric transients neglected. They could not

be deduced from the equations written in the form of (3.4-11) and (3.4-12), and at first glance, one might question their validity. Although one recognizes that these equations are valid for neglecting the electric transients in the synchronously rotating reference frame, it is more difficult to accept the fact that these equations are also valid in an asynchronously rotating reference frame where the balanced steady-state variables are sinusoidal. However, these steady-state variables form orthogonal balanced sinusoidal sets for a symmetrical system. Therefore, the  $\lambda_{ds}(\lambda_{qs})$  appearing in the  $v_{qs}(v_{ds})$  equation provides the reactance voltage drop. It is left to the reader to show that the linear algebraic equations in the arbitrary reference frame for a linear symmetrical capacitive circuit are

$$i_{qs} = \omega_e q_{ds} \quad (8.7-9)$$

$$i_{ds} = -\omega_e q_{qs} \quad (8.7-10)$$

Let us consider what we have done; the arbitrary reference-frame voltage equations have been established for inductive circuits with the electric transients neglected, by neglecting the change of flux linkages in the synchronously rotating reference frame. This is the same as neglecting the offsets that occur in the actual currents as a result of a system disturbance. However, during unbalanced conditions, such as unbalanced voltages applied to the stator circuits, the voltages in the synchronously rotating reference frame will vary with time. For example, 60 Hz unbalanced stator voltages give rise to a constant and a double-frequency voltage in the synchronously rotating reference frame. Therefore, the flux linkages in the synchronously rotating reference frame will also contain a double-frequency component. It follows that during unbalanced conditions, neglecting the change in the synchronously rotating reference-frame flux linkages results in neglecting something more than just the electric transients. Therefore, the voltage equations, which have been derived by neglecting the change in the flux linkages in the synchronously rotating reference frame apply for balanced or symmetrical conditions, such as simultaneous application of balanced voltages, a change in either load or input torque and a three-phase fault. Consequently, the zero sequence quantities are not included in the machine equations given in this chapter.

## Induction Machine

The voltage equations written in the arbitrary reference frame for an induction machine with the electric transients of the stator voltage equations neglected may be written from (6.5-22)–(6.5-33), with the zero quantities eliminated and (8.7-7) and (8.7-8) appropriately taken into account.

$$v_{qs} = r_s i_{qs} + \frac{\omega_e}{\omega_b} \psi_{ds} \quad (8.7-11)$$

$$v_{ds} = r_s i_{ds} - \frac{\omega_e}{\omega_b} \psi_{qs} \quad (8.7-12)$$

$$v'_{qr} = r'_r i'_{qr} + \left( \frac{\omega - \omega_r}{\omega_b} \right) \psi'_{dr} + \frac{p}{\omega_b} \psi'_{qr} \quad (8.7-13)$$

$$v'_{dr} = r'_r i'_{dr} - \left( \frac{\omega - \omega_r}{\omega_b} \right) \psi'_{qr} + \frac{p}{\omega_b} \psi'_{dr} \quad (8.7-14)$$

where

$$\psi_{qs} = X_{ls} i_{qs} + X_M (i_{qs} + i'_{qr}) \quad (8.7-15)$$

$$\psi_{ds} = X_{ls} i_{ds} + X_M (i_{ds} + i'_{dr}) \quad (8.7-16)$$

$$\psi'_{qr} = X'_{ls} i'_{qr} + X_M (i_{qs} + i'_{qr}) \quad (8.7-17)$$

$$\psi'_{dr} = X'_{ls} i'_{dr} + X_M (i_{ds} + i'_{dr}) \quad (8.7-18)$$

Although the reference-frame speed appears in the speed voltages in the rotor voltage equations, it does not appear in the stator voltage equations.

The voltage equations may be expressed in terms of currents by appropriately replacing the flux linkages per second in (8.7-11)–(8.7-14) with (8.7-15)–(8.7-18) or directly from (6.5-34) with the 0s and 0r quantities, and all derivatives in the  $v_{qs}$  and  $v_{ds}$  voltage equations eliminated and with  $\omega$  set equal to  $\omega_e$ . Hence

$$\begin{bmatrix} v_{qs} \\ v_{ds} \\ v'_{qr} \\ v'_{dr} \end{bmatrix} = \begin{bmatrix} r_s & \frac{\omega_e}{\omega_b} X_{ss} & 0 & \frac{\omega_e}{\omega_b} X_M \\ -\frac{\omega_e}{\omega_b} X_{ss} & r_s & -\frac{\omega_e}{\omega_b} X_M & 0 \\ \frac{p}{\omega_b} X_M & \left( \frac{\omega - \omega_r}{\omega_b} \right) X_M & r'_r + \frac{p}{\omega_b} X'_{rr} & \left( \frac{\omega - \omega_r}{\omega_b} \right) X'_{rr} \\ -\left( \frac{\omega - \omega_r}{\omega_b} \right) X_M & \frac{p}{\omega_b} X_M & -\left( \frac{\omega - \omega_r}{\omega_b} \right) X'_{rr} & r'_r + \frac{p}{\omega_b} X'_{rr} \end{bmatrix} \begin{bmatrix} i_{qs} \\ i_{ds} \\ i'_{qr} \\ i'_{dr} \end{bmatrix} \quad (8.7-19)$$

where  $X_{ss}$  and  $X'_{rr}$  are defined by (6.5-35) and (6.5-36), respectively. It is important to note that a derivative of  $i_{qs}(i_{ds})$  appears in  $v'_{qr}(v'_{dr})$ ; however,  $i_{qs}$  and  $i_{ds}$  are algebraically related to  $i'_{qr}$  and  $i'_{dr}$  by the equations for  $v_{qs}$  and  $v_{ds}$ . Hence, one might conclude that  $i'_{qr}$  and  $i'_{dr}$  may be selected as independent or state variables. This is not the case, since it can be shown that all currents are both algebraically and dynamically related to the stator voltages. Thus, if  $i'_{qr}$  and  $i'_{dr}$  are selected as state variables, the state equation must be written in a nonstandard form, which is not the most convenient form for computer simulation [1].

## Synchronous Machine

The stator voltage equations of the synchronous machine written in the arbitrary reference frame are given by (5.4-1). As illustrated by (8.7-7) and (8.7-8), the electric

transients are neglected in the stator voltage equations in the arbitrary reference frame by neglecting the derivative of flux linkages and setting  $\omega = \omega_e$ . Thus, in terms of flux linkages per second and with the electric transients neglected, the stator voltage equations of the synchronous machine expressed in the arbitrary reference frame are of the same form as (8.7-11) and (8.7-12) with the exception that positive current is assumed out of the terminals of the synchronous machine. This is done since reduced-order models have traditionally been used in power system analysis, where current is usually defined as positive out of the machine. It follows that the voltage equations for the synchronous machine in the rotor reference frame with the stator electric transients neglected are obtained by neglecting the derivative of the flux linkages in Park's equations and setting  $\omega_r = \omega_e$ . Thus, with the 0s quantities omitted

$$v_{qs}^r = -r_s i_{qs}^r + \frac{\omega_e}{\omega_b} \psi_{ds}^r \quad (8.7-20)$$

$$v_{ds}^r = -r_s i_{ds}^r - \frac{\omega_e}{\omega_b} \psi_{qs}^r \quad (8.7-21)$$

$$v_{kq1}^{\prime r} = r'_{kq1} i_{kq1}^{\prime r} + \frac{p}{\omega_b} \psi_{kq1}^{\prime r} \quad (8.7-22)$$

$$v_{kq2}^{\prime r} = r'_{kq2} i_{kq2}^{\prime r} + \frac{p}{\omega_b} \psi_{kq2}^{\prime r} \quad (8.7-23)$$

$$v_{fd}^{\prime r} = r'_{fd} i_{fd}^{\prime r} + \frac{p}{\omega_b} \psi_{fd}^{\prime r} \quad (8.7-24)$$

$$v_{kd}^{\prime r} = r'_{kd} i_{kd}^{\prime r} + \frac{p}{\omega_b} \psi_{kd}^{\prime r} \quad (8.7-25)$$

where

$$\psi_{qs}^r = -X_{ls} i_{qs}^r + X_{mq} (-i_{qs}^r + i_{kq1}^{\prime r} + i_{kq2}^{\prime r}) \quad (8.7-26)$$

$$\psi_{ds}^r = -X_{ls} i_{ds}^r + X_{md} (-i_{ds}^r + i_{fd}^{\prime r} + i_{kd}^{\prime r}) \quad (8.7-27)$$

$$\psi_{kq1}^{\prime r} = X'_{lkq1} i_{kq1}^{\prime r} + X_{mq} (-i_{qs}^r + i_{kq1}^{\prime r} + i_{kq2}^{\prime r}) \quad (8.7-28)$$

$$\psi_{kq2}^{\prime r} = X'_{lkq2} i_{kq2}^{\prime r} + X_{mq} (-i_{qs}^r + i_{kq1}^{\prime r} + i_{kq2}^{\prime r}) \quad (8.7-29)$$

$$\psi_{fd}^{\prime r} = X'_{lfd} i_{fd}^{\prime r} + X_{md} (-i_{ds}^r + i_{fd}^{\prime r} + i_{kd}^{\prime r}) \quad (8.7-30)$$

$$\psi_{kd}^{\prime r} = X'_{lkd} i_{kd}^{\prime r} + X_{md} (-i_{ds}^r + i_{fd}^{\prime r} + i_{kd}^{\prime r}) \quad (8.7-31)$$

As in the case of the induction machine, the voltage equations for the synchronous machine may be written in terms of the currents. Hence, (8.7-32) results from the substitution of (8.7-26)–(8.7-31) into (8.7-20)–(8.7-25) or directly from (5.5-38) with the 0s quantities and derivatives in the  $v_{qs}^r$  and  $v_{ds}^r$  voltage equations eliminated and with  $\omega_r$  set equal to  $\omega_e$  in the  $v_{qs}^r$  and  $v_{ds}^r$  voltage equations.

$$\begin{bmatrix} v_{qs}^r \\ v_{ds}^r \\ v_{kq1}^r \\ v_{kq2}^r \\ e_{fd}^r \\ v_{kd}^r \end{bmatrix} = \begin{bmatrix} r_s & \frac{\omega_e}{\omega_b} X_d & 0 & 0 & \frac{\omega_e}{\omega_b} X_{md} & \frac{\omega_e}{\omega_b} X_{md} \\ -\frac{\omega_e}{\omega_b} X_q & r_s & -\frac{\omega_e}{\omega_b} X_{mq} & -\frac{\omega_e}{\omega_b} X_{mq} & 0 & 0 \\ \frac{p}{\omega_b} X_{mq} & 0 & r'_{kq1} + \frac{p}{\omega_b} X'_{kq1} & \frac{p}{\omega_b} X_{mq} & 0 & 0 \\ \frac{p}{\omega_b} X_{mq} & 0 & \frac{p}{\omega_b} X_{mq} & r'_{kq2} + \frac{p}{\omega_b} X'_{kq2} & 0 & 0 \\ 0 & \frac{X_{md}}{r'_{fd}} \left( \frac{p}{\omega_b} X_{md} \right) & 0 & 0 & \frac{X_{md}}{r'_{fd}} \left( r'_{fd} + \frac{p}{\omega_b} X'_{fd} \right) & \frac{X_{md}}{r'_{fd}} \left( \frac{p}{\omega_b} X_{md} \right) \\ 0 & \frac{p}{\omega_b} X_{md} & 0 & 0 & \frac{p}{\omega_b} X_{md} & r'_{kd} + \frac{p}{\omega_b} X'_{kd} \end{bmatrix} \begin{bmatrix} -i'_{qs} \\ -i'_{ds} \\ i'_{kq1} \\ i'_{kq2} \\ i'_{fd} \\ i'_{kd} \end{bmatrix} \quad (8.7-32)$$

The reactances given in (8.7-32) are defined by (5.5-39)–(5.5-44). As in the case of the induction machine, the formulation of the voltage equations in terms of currents, with the stator electric transients neglected, results in equations in which all machine currents are both algebraically and dynamically related to the stator voltages. This gives rise to an inconvenient (nonstandard) form of the state equation [1].

## 8.8. INDUCTION MACHINE PERFORMANCE PREDICTED WITH STATOR ELECTRIC TRANSIENTS NEGLECTED

It is instructive to compare the large-excitation induction machine behavior predicted with stator electric transients neglected with that predicted by the detailed equations given in Chapter 6. The material presented in Chapter 6 has already made us aware of the inaccuracies involved when both the stator and rotor transients are neglected. Additional information regarding the large-excitation accuracy of the reduced-order models with only stator electric transients neglected and with both stator and rotor electric transients neglected is given by T.L. Skvarenina [3].

### Free Acceleration Characteristics

The free acceleration characteristics predicted for the 2250-hp induction motor with the electric transients neglected in the stator voltage equations are given in Figure 8.8-1. The parameters and operating conditions are identical to those used in Chapter 6. A comparison with Figure 6.10-6 reveals that the only significant difference is in the initial starting transient. Although a transient occurs in the instantaneous starting torque, it is much less pronounced when the stator electric transients are neglected. Our first reaction is to assume that the transient that remains is due to the rotor circuits. Although this is essentially the case, we must be careful with such an interpretation since we are imposing a condition upon the voltage equations that could not be realized in practice. We are aware from our earlier analysis that the stator electric transient gives rise to a 60 Hz pulsating torque and a complex

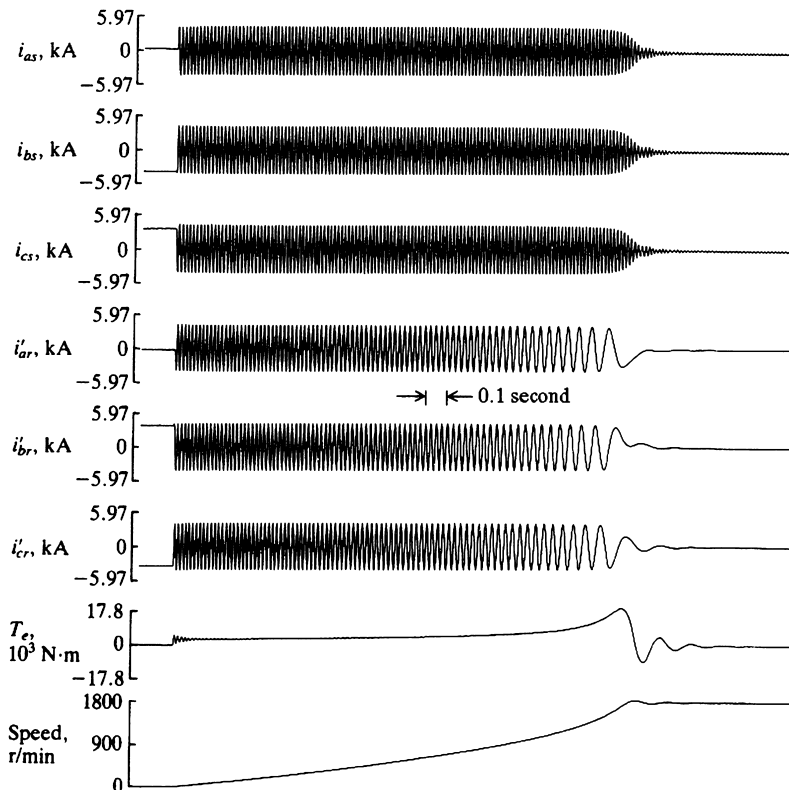


**Figure 8.8-1.** Machine variables during free acceleration of a 2250-hp induction motor predicted with stator electric transients neglected.

conjugate eigenvalue pair with a frequency (imaginary part) of approximately  $\omega_e$ . Since we are neglecting the electric transients in the stator voltage equations, we would expect discrepancies to occur whenever this transient is excited and whenever it influences the behavior of the machine. Once the stator electric transient subsides, the torque-speed characteristics are identical for all practical purposes. For the machine studied, the speed is not significantly influenced by the 60-Hz transient torque during free acceleration. If the inertia were relatively small or if the stator voltages were of frequency considerably less than rated, as occurs in variable speed drive systems, the pulsating electromagnetic torque could have a significant influence upon the behavior of the machine.

The oscillation about synchronous speed, which is determined primarily by the rotor circuits, is still present, as is clearly illustrated in the case of the 2250-hp machine. This oscillation does not occur when the electric transients of the rotor circuits are neglected. Another interesting feature regarding the transient characteristics of the induction machine is that the varying envelope of the machine currents during free acceleration does not occur when the stator electric transients are neglected. Therefore,

we must conclude that the varying current envelope depicted in Figure 6.10-5 and Figure 6.10-6 occurs due to the interaction of stator and rotor electric transients.

A word of explanation is necessary. In the computer simulation, the terminal voltages are applied in the initial condition mode. Although this has no influence upon the solution which follows, we can see the ambiguity which occurs when imposing impossible restrictions upon the behavior of electric circuits. Here we see that the stator voltages are algebraically related to all machine currents since the stator and rotor currents change instantaneously when the stator voltages are applied in the initial condition mode. It is interesting that this situation, which is impossible practically, does not give rise to an initial torque.

### Changes in Load Torque

As noted in Chapter 6, the steady-state voltage equations, along with the dynamic relationship between torque and speed, can generally be used to predict the dynamic response to changes in load torque for small horsepower induction machines. However, this reduced model, wherein both the stator and rotor electric transients are neglected, cannot adequately predict the dynamic response of large horsepower induction machines to load torque disturbances. On the other hand, studies reported in Reference 3 reveal that with only the stator electric transients neglected, the predicted dynamic response to load torque changes in the vicinity of rated torque is, for all practical purposes, identical to that predicted by the detailed model. We would expect this since, due to the inertia of the mechanical system, a change in load torque would normally excite a negligibly small transient offset in the stator currents.

### Three-Phase Fault at Machine Terminals

The dynamic behavior of the 2250-hp induction machine during and following a three-phase fault at the terminals, predicted with the stator electric transients neglected, is given in Figure 8.8-2. An indication of the accuracy of this reduced-order model can be ascertained by comparing these plots with those given in Figure 6.13-2. The same parameters and operating conditions are used. Initially, the machine is operating at base torque. A three-phase fault at the terminals is simulated by setting  $v_{as}$ ,  $v_{bs}$ , and  $v_{cs}$  to zero at the instant  $v_{as}$  passes through zero going positive. After six cycles, the source voltages are reapplied. Note the step change in all machine currents and torque at the instant the fault is applied and again at the instant the fault is removed and the stator voltages are reapplied. The algebraic relationship between the machine currents and stator voltages is clear.

With the electric transients neglected in the stator voltage equations, transient offset currents will appear only in the rotor circuits. At the beginning of the three-phase fault and following the reapplication of the terminal voltages, the rotor offset currents will reflect to the stator as balanced decaying sinusoidal currents with a frequency corresponding to the rotor speed. However, since transient offsets are neglected in the stator circuits, the rotor currents will not contain a sinusoidal component due to the reflection of the stator offset currents into the rotor circuits.

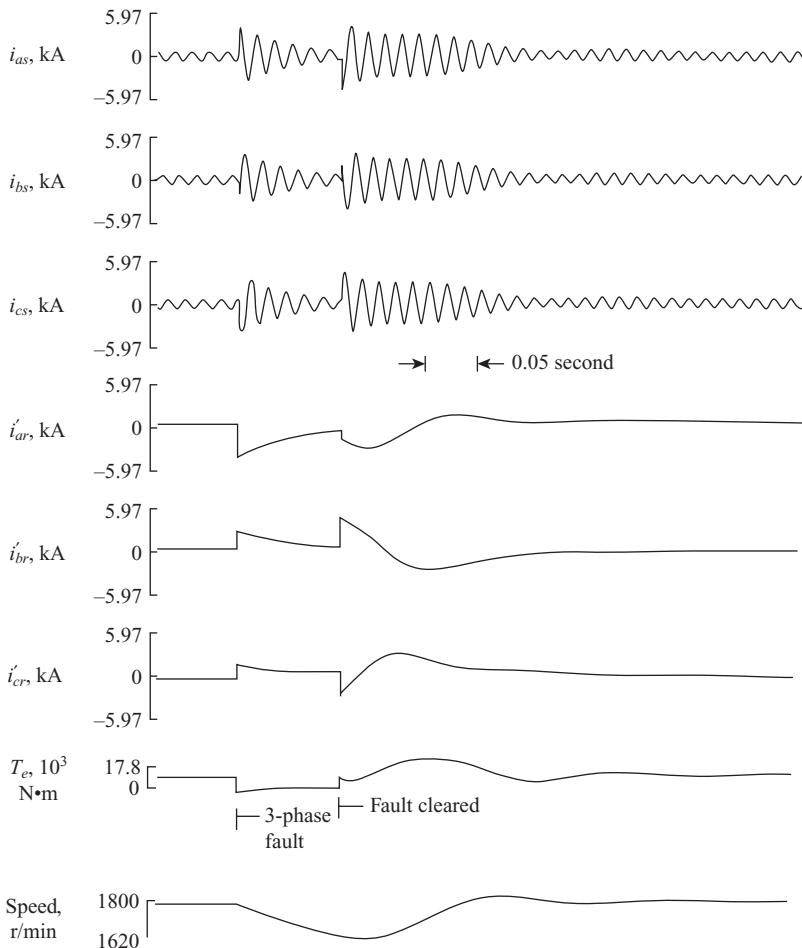


**Figure 8.8-2.** Dynamic performance of a 2250-hp induction motor during a three-phase fault at the terminals predicted with stator electric transients neglected.

With the stator electric transients absent, a decaying 60 Hz pulsating electromagnetic torque does not occur. A comparison of the response predicted with the stator electric transients neglected and that predicted by the detailed model reveals the error, which can occur in rotor speed when the 60 Hz torque is neglected. In most power system applications, this error would not be sufficient to warrant the use of the detailed model; however, for investigations of speed control of variable-speed drive systems this simplified model would probably not suffice. Also, if instantaneous shaft torques are of interest, the detailed model must be used.

If the reduced-order model with both stator and rotor electric transients neglected is used, the machine currents, and thus the torque, would instantaneously become zero at the time of the fault. The calculated speed would decrease, obeying the dynamic

relationship between the load torque and rotor speed. The currents and torque would instantaneously assume their steady-state values for the specific rotor speed at the time the stator voltages are reapplied.

## 8.9. SYNCHRONOUS MACHINE PERFORMANCE PREDICTED WITH STATOR ELECTRIC TRANSIENTS NEGLECTED

The reduced-order model of the synchronous machine obtained by neglecting the stator electric transients is used widely in the power industry as an analysis tool. Therefore, it is important to compare the performance of the synchronous machine predicted by the reduced-order equations with that predicted by the detailed model (Chapter 5), especially for disturbances common in transient stability studies. Since this comparison is of most interest to the power systems engineer, positive currents are assumed out of the machine terminals, which allows direct comparison with the performance characteristics in Section 5.10. Additional information regarding the large-excursion accuracy of the reduced-order model is found in References 1 and 3.

### Changes in Input Torque

A change in input torque would not normally excite an appreciable transient offset in the stator currents. Therefore, neglecting the electric transients in the stator voltage equations has negligible effect upon the accuracy in predicting the dynamic behavior of the typical synchronous machine during normal input torque disturbances.

### Three-Phase Fault at Machine Terminals

The dynamic behavior of the steam turbine generator during and following a three-phase fault at the terminals, predicted with the electric transients neglected in the stator voltage equations, is shown in Figure 8.9-1 and Figure 8.9-2. An indication of the accuracy of this reduced-order model can be obtained by comparing the behavior depicted in these figures to that shown in Figure 5.10-10 and Figure 5.10-11. The machine and operating conditions are identical. Initially, the machine is connected to an infinite bus delivering rated MVA at rated power factor. (Machine data are given in Section 5.10.) The input torque of the steam turbine generator is held constant at  $(0.85) 2.22 \times 10^6$  N·m and  $E'_{xd} = (2.48)\sqrt{(2/3)}26$  kV. With the machine operating in this steady-state condition, a three-phase fault at the terminals is simulated by setting  $v_{as}$ ,  $v_{bs}$ , and  $v_{cs}$  to zero at the instant  $v_{as}$  passes through zero going positive. The instantaneous changes in the machine currents and torque at the initiation and removal of the fault demonstrate the algebraic relationship between stator voltages and machine currents. With the stator electric transients neglected, the offset transients do not appear, and consequently, the 60 Hz pulsating electromagnetic torque is not present during and following the three-phase fault. The absence of the 60 Hz transient torque is especially apparent in the torque versus rotor angle characteristics given Figure 8.9-2.

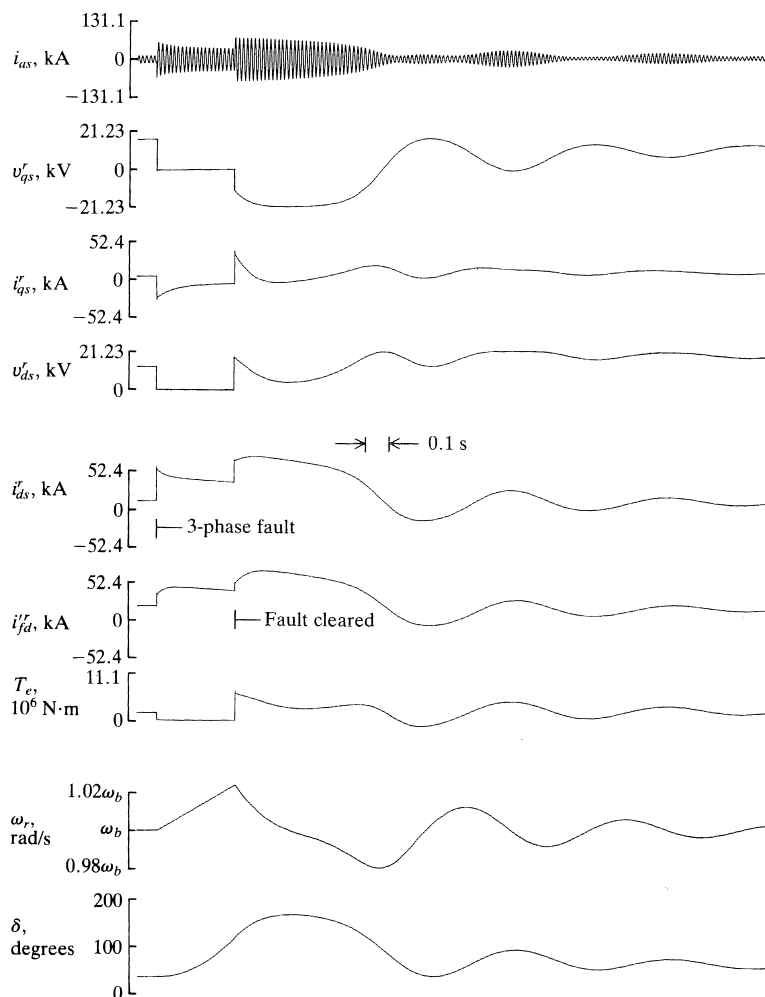


**Figure 8.9-1.** Dynamic performance of a steam turbine generator during a three-phase fault at the terminals predicted with stator electric transients neglected.

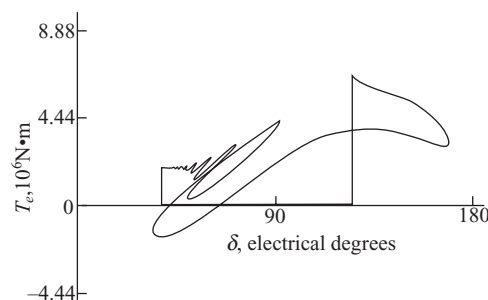


**Figure 8.9-2.** Torque versus rotor angle characteristics for the study shown in Figure 8.9-1.

From all outward appearances, it would seem that other than the pulsating electromagnetic torque, there is little difference between the behaviors predicted using the reduced-order or detailed models. Therefore, one would expect the reduced-order model to be sufficiently accurate in predicting this performance during and following a three-phase fault. There is, however, a difference that occurs when determining the critical clearing time. The situation portrayed in Figure 5.10-10 and Figure 5.10-11 and likewise in Figure 8.9-1 and Figure 8.9-2 is one where only a slight increase in the fault time would cause the machines to become unstable. That is, if the three-phase fault were allowed to persist slightly longer, the rotor speed would not return to synchronous after the fault is cleared. Using the detailed model in Chapter 5, this critical clearing time was determined to be 0.466 second for the hydro unit and 0.362 second for the steam unit. For the reduced-order model, the critical clearing time for the hydro unit is 0.424 and 0.334 second for the steam unit. The longer critical clearing times predicted by the detailed models is due primarily to the pulsating 60-Hz torque, which occurs immediately following the occurrence of the fault. The initial torque pulsation causes the rotor to slow down very slightly, which has the effect of delaying the increase in the "average" rotor speed. This effect can be observed in Figure 5.10-10. With the stator electric transients neglected, the 60-Hz pulsating torque is absent and hence the initial "backswing" does not occur [4]. There are two points which warrant mentioning in defense of this apparent inaccuracy of the reduced-order model. First, it will always yield conservative results. Second, a three-phase fault seldom if ever occurs instantaneously. That is, a fault generally starts as a single line-to-ground or as a phase-to-phase fault, and then it may progress rapidly to a three-phase fault. Hence, the instantaneous pulsation in electromagnetic torque is generally not sufficient in the practical case to cause the slowing down of the rotor as depicted in Figure 5.10-8 and Figure 5.10-10. In this regard, the effects of the 60-Hz pulsating torque resulting from an instantaneous three-phase fault is perhaps more of academic than of practical interest.

Although the reduced-order model obtained by neglecting stator electric transients is generally quite adequate for transient stability studies of large-scale power systems subjected to symmetrical disturbances, we are imposing impossible electrical conditions upon the voltage equations. When we attempt to "fool Mother nature" in this way, we should proceed with caution. In particular, using the reduced-order models for induction and synchronous machines in low-power, small-system applications may not be advisable. If the machines are small in horsepower or if the machines are operated over a relatively wide frequency range, one should not use the reduced-order model without first comparing its predication of system response to that of the detailed model. This is perhaps the most reasonable guideline to offer since it would be nearly impossible and certainly inappropriate to establish the accuracy of the reduced-order model obtained by neglecting the stator electric transients for all conceivable applications.

In computer programs used for transient stability studies of power systems, it is standard to neglect the electric transients in the stator voltage equations of all machines and in the voltage equations of all power system components connected to the machines. It is important to realize that once it is decided to neglect the electric transients in the representation of any part of the network, the electric transients should be neglected in the complete network, otherwise erroneous electric transients will appear in the

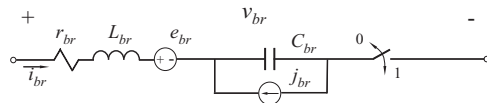


Figure 8.10-1. Example canonical branch circuit element.

solution. The computer simulation of induction and synchronous machines with stator electric transients is covered in Reference 1.

## 8.10. DETAILED VOLTAGE BEHIND REACTANCE MODEL

Many software packages exist to simulate the performance of electric machines within power systems. Examples of state-variable-based solvers include ACSL [5], Easy5 [6], Eurostag [7], and MATLAB/Simulink [8]. Specialized packages, such as SimPower-Systems [9], RT-Lab [10], PLECS [11], and ASMG [12], come with circuit interfaces that enable relatively straightforward assembly of system models using canonical branch circuits, such as the one shown in Figure 8.10-1 [12].

The creation of such tools has enabled the simulation of complicated systems; however, their optimal use requires some thought as to model structure and implementation. In Chapter 5 and Chapter 6, a great deal of the focus is to apply reference-frame theory to simplify the models of electric machinery by eliminating rotor position-dependent inductances. A key result of applying the respective transformations are the  $q$ - and  $d$ -circuit representations of wound rotor synchronous and induction machines shown in Figure 5.5-1 and Figure 6.5-1. Both have constant inductances and are readily implemented within circuit simulators using the branch element form of Figure 8.10-1. However, when simulating systems in which electric machines are coupled to power electronic circuits, a challenge arises. Specifically, it is difficult to apply the reference-frame transformation to the models of most power electronic circuits. As a result, coupling the  $q$ - and  $d$ -model of a machine to a power electronic circuit represented in terms of physical variables requires one to create a  $q$ - and  $d$ - to  $abc$  circuit interface. A similar challenge is encountered in power system models in which a transmission line/network is represented in terms of phase quantities, as is common, for example, in electromagnetic transient program EMTP-type solvers. In general, the interface that is utilized is software dependent. For example, in PSCAD/EMTDC, the machine model is coupled to the network model using a Norton current source/impedance [13].

An alternative is to model a respective machine using a physical-variable coupled-circuit (PVCC) form, that is, machine variables. The PVCC model of the induction machine is provided in (6.2-19) and (6.3-7). The PVCC model of the synchronous machine is given by (5.2-1), (5.2-2), (5.2-7), and (5.3-4). An example of the use of the PVCC of the synchronous machine is shown in Figure 8.10-2, wherein a machine is coupled to a diode rectifier using the branch elements of Figure 8.10-1. Both the stator and rotor circuits are represented using inductive branches whose elements are the terms in the matrices in (5.2-26). The stator branches are directly connected to those of the

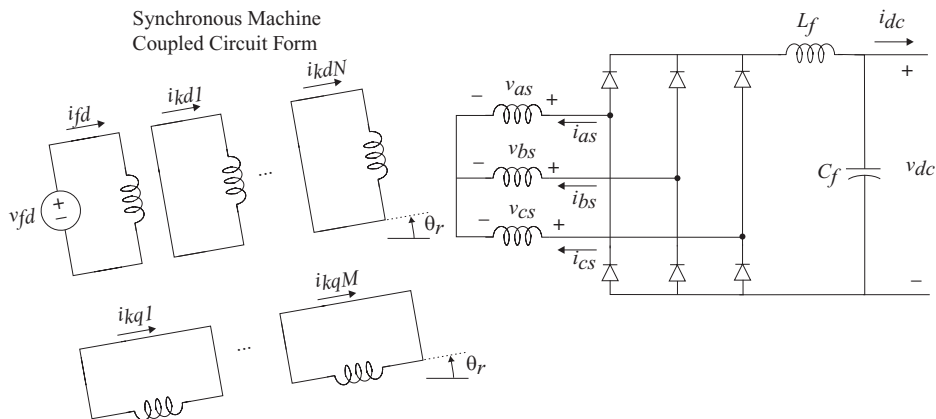


Figure 8.10-2. Machine/rectifier model using PVCC form.

diode circuit. The field winding branch is connected to a voltage source. The damper windings are short circuited. The  $\theta_r$  in Figure 8.10-2 is used to denote that the coupling between windings is rotor position-dependent. In the case of a salient-pole synchronous machine the stator inductances are also rotor position-dependent. Although application of the PVCC model eliminates the need to establish a  $q$ - and  $d$ - to  $abc$  coupling, the position-dependent inductances and the additional branches/elements of the PVCC model add computational cost.

An alternative to the PVCC is a physical-variable voltage-behind-reactance (PVVBR) formulation that was initially shown to provide advantages in modeling synchronous machines in state-model-based solvers in Reference 14. The PVVBR model was subsequently shown to have advantages in EMTP-type solvers in Reference 15. In this section, the PVVBR model is derived. A similar derivation is readily applied to the model of the induction machine, and has been documented in References 16 and 17.

Prior to deriving the PVVBR model, a few details of notation are necessary. In Chapters 5–7, a prime notation (') is used to denote a rotor variable that had been referred to the stator through an appropriate turns ratio. However, it is common in analyzing synchronous machines that a primed quantity is used to denote a time constant, or inductance associated with the “transient” interval. This is used, for example, in Chapters 5 and 7. Along the same line, a double prime (") is often used to denote a “subtransient” inductance or time constant. Subtransient inductances and time constants are typically expressed, assuming there are two damper windings in the  $q$ -axis and a single damper winding in the  $d$ -axis. During the “subtransient” interval, all damper windings are active. In this section, all rotor variables are indeed referred to the stator quantities through the turns ratios defined in Chapter 5. However, since here we have introduced additional primed variables, the prime notation for the turns ratio is dropped to avoid confusion, and the double-prime (") is applied to denote a dynamic inductance for a machine with arbitrary damper windings in each axis. In the case in which a machine is modeled using a single damper in the  $d$ -axis and two in the  $q$ -axis, the dynamic

inductances are the traditional subtransient inductances. Finally, since this model is often applied in drive system applications, we take positive stator currents into the machine.

Interestingly, the derivation of the PVVBR for the synchronous machine begins in the rotor frame of reference. Specifically, the  $q$ - and  $d$ -axis magnetizing flux linkages

$$\lambda_{mq} = L_{mq} \left( i_{qs}^r + \sum_{j=1}^M i_{kqj} \right) \quad (8.10-1)$$

$$\lambda_{md} = L_{md} \left( i_{ds}^r + i_{fd} + \sum_{j=1}^N i_{kdf} \right) \quad (8.10-2)$$

for a machine with  $M$  damper windings in the  $q$ -axis and  $N$  damper windings in the  $d$ -axis are first expressed in terms of rotor flux linkages using the relationship that

$$i_{kqj} = (\lambda_{kqj} - \lambda_{mq}) / L_{lkqj} \quad j = kq1, \dots, kqM \quad (8.10-3)$$

$$i_{kdf} = (\lambda_{kdf} - \lambda_{md}) / L_{lkdf} \quad j = kd1, \dots, kdN \quad (8.10-4)$$

$$i_{fd} = (\lambda_{fd} - \lambda_{md}) / L_{lfd} \quad (8.10-5)$$

Substituting (8.10-3)–(8.10-5) into (8.10-1) and (8.10-2) with some rearrangement results in

$$\lambda_{mq} = L''_{mq} i_{qs}^r + \lambda_q'' \quad (8.10-6)$$

$$\lambda_{md} = L''_{md} i_{ds}^r + \lambda_d'' \quad (8.10-7)$$

where

$$L''_{mq} = \frac{1}{L_{mq}} + \sum_{j=1}^M \frac{1}{L_{lkqj}} \quad (8.10-8)$$

$$L''_{md} = \frac{1}{L_{md}} + \frac{1}{L_{lfd}} + \sum_{j=1}^N \frac{1}{L_{lkdf}} \quad (8.10-9)$$

Using, (8.10-6) and (8.10-7), the stator flux linkages are then expressed as

$$\lambda_{qs}^r = L''_q i_{qs}^r + \lambda_q'' \quad (8.10-10)$$

$$\lambda_{ds}^r = L''_d i_{ds}^r + \lambda_d'' \quad (8.10-11)$$

where  $L''_q = L_{ls} + L''_{mq}$  and  $L''_d = L_{ls} + L''_{md}$  are the dynamic inductances. The dynamic flux linkages are given by

$$\lambda''_q = L''_{mq} \left( \sum_{j=1}^M \frac{\lambda_{kqj}}{L_{lkqj}} \right) \quad (8.10-12)$$

$$\lambda''_d = L''_{md} \left( \frac{\lambda_{fd}}{L_{lfd}} + \sum_{j=1}^N \frac{\lambda_{kqd}}{L_{lkdj}} \right) \quad (8.10-13)$$

Using (8.10-10) and (8.10-11), the  $q$ - and  $d$ -axis stator voltage equations of (5.5-8) and (5.5-9) can be written as

$$v_{qs}^r = r_s i_{qs}^r + \omega_r (L''_d i_{ds}^r + \lambda''_d) + p(L''_q i_{qs}^r + \lambda''_q) \quad (8.10-14)$$

$$v_{ds}^r = r_s i_{ds}^r - \omega_r (L''_q i_{qs}^r + \lambda''_q) + p(L''_d i_{ds}^r + \lambda''_d) \quad (8.10-15)$$

The terms

$$p\lambda''_q = -L''_{mq} \sum_{j=1}^M \frac{r_{kqj} i_{kqj}}{L_{lkqj}} \quad (8.10-16)$$

$$p\lambda''_d = L''_{md} \left( \frac{v_{fd} - r_{fd} i_{fd}}{L_{lfd}} - \sum_{j=1}^N \frac{r_{kqd} i_{kqd}}{L_{lkdj}} \right) \quad (8.10-17)$$

are then expressed in terms of stator current and rotor flux linkages by substituting (8.10-3)–(8.10-5) into (8.10-16) and (8.10-17) and applying the relation (8.10-6) and (8.10-7) to the result. The stator voltage equations are then expressed in a form

$$v_{qs}^r = r''_q i_{qs}^r + \omega_r L''_d i_{ds}^r + pL''_q i_{qs}^r + e''_q \quad (8.10-18)$$

$$v_{ds}^r = r''_d i_{ds}^r - \omega_r L''_q i_{qs}^r + pL''_d i_{ds}^r + e''_d \quad (8.10-19)$$

where

$$r''_q = r_s + L''_{mq}^2 \left( \sum_{j=1}^M \frac{r_{kqj}}{L_{lkqj}^2} \right) \quad (8.10-20)$$

$$r''_d = r_s + L''_{md}^2 \frac{r_{fd}}{L_{lfd}^2} + L''_{md}^2 \left( \sum_{j=1}^N \frac{r_{kqd}}{L_{lkdj}^2} \right) \quad (8.10-21)$$

and

$$e''_q = \omega_r \lambda''_d + \sum_{j=1}^M \left( \frac{L''_{mq} r_{kqj}}{L_{lkqj}^2} (\lambda''_q - \lambda_{kqj}) \right) \quad (8.10-22)$$

$$e_d'' = -\omega_r \lambda_q'' + \sum_{j=1}^N \left( \frac{L_{md}'' r_{k dj}}{L_{k dj}^2} (\lambda_d'' - \lambda_{k dj}) \right) + \frac{L_{md}''}{L_{fd}} v_{fd} + \frac{L_{md}'' r_{fd}}{L_{fd}^2} (\lambda_d'' - \lambda_{fd}) \quad (8.10-23)$$

Applying the inverse Park's transformation to (8.10-18), (8.10-19), and the zero sequence voltage equation of (5.5-10), yields

$$\mathbf{v}_{abcs} = \mathbf{r}_{abcs}''(\theta_r) \mathbf{i}_{abcs} + p[\mathbf{L}_{abcs}''(\theta_r) \mathbf{i}_{abcs}] + \mathbf{e}_{abcs}'' \quad (8.10-24)$$

where  $\mathbf{L}_{abcs}''$  is an inductance matrix containing dynamic inductances defined as

$$\mathbf{L}_{abcs}''(\theta_r) = \begin{bmatrix} L_S''(2\theta_r) & L_M''\left(2\theta_r - \frac{2\pi}{3}\right) & L_M''\left(2\theta_r + \frac{2\pi}{3}\right) \\ L_M''\left(2\theta_r - \frac{2\pi}{3}\right) & L_S''\left(2\theta_r - \frac{4\pi}{3}\right) & L_M''(2\theta_r) \\ L_M''\left(2\theta_r + \frac{2\pi}{3}\right) & L_M''(2\theta_r) & L_S''\left(2\theta_r + \frac{4\pi}{3}\right) \end{bmatrix} \quad (8.10-25)$$

The entries are expressed using  $\cdot$  to denote  $2\theta_r$ ,  $2\theta_r - (2\pi/3)$ ,  $2\theta_r + (2\pi/3)$ , respectively as

$$L_S''(\cdot) = L_{ls} + L_a'' - L_b'' \cos(\cdot) \quad (8.10-26)$$

$$L_M''(\cdot) = -\frac{L_a''}{2} - L_b'' \cos(\cdot) \quad (8.10-27)$$

$$L_a'' = \frac{(L_{ma}'' + L_{mq}'')}{3} \quad (8.10-28)$$

$$L_b'' = \frac{(L_{ma}'' - L_{mq}'')}{3} \quad (8.10-29)$$

The resistance matrix is

$$\mathbf{r}_{abcs}''(\theta_r) = \begin{bmatrix} r_S''(2\theta_r) & r_M''\left(2\theta_r - \frac{2\pi}{3}\right) & r_M''\left(2\theta_r + \frac{2\pi}{3}\right) \\ r_M''\left(2\theta_r - \frac{2\pi}{3}\right) & r_S''\left(2\theta_r - \frac{4\pi}{3}\right) & r_M''(2\theta_r) \\ r_M''\left(2\theta_r + \frac{2\pi}{3}\right) & r_M''(2\theta_r) & r_S''\left(2\theta_r + \frac{4\pi}{3}\right) \end{bmatrix} \quad (8.10-30)$$

where the entries are defined as follows

$$r_S''(\cdot) = r_s + r_a'' - r_b'' \cos(\cdot) \quad (8.10-31)$$

$$r_M''(\cdot) = \frac{-r_a''}{2} - r_b'' \cos(\cdot) \quad (8.10-32)$$

$$r_a'' = \frac{r_d'' + r_q''}{3} - \frac{2}{3} r_s \quad (8.10-33)$$

$$r_b'' = \frac{r_d'' - r_q''}{3} \quad (8.10-34)$$

The stator voltage equations given in (8.10-24), along with the rotor state equations

$$p\lambda_{kaj} = -\frac{r_{kaj}}{L_{lkaj}}(\lambda_{kaj} - \lambda_{mq}); \quad j = 1, \dots, M \quad (8.10-35)$$

$$p\lambda_{kdj} = -\frac{r_{kdj}}{L_{lkdj}}(\lambda_{kdj} - \lambda_{md}); \quad j = 1, \dots, N \quad (8.10-36)$$

$$p\lambda_{fd} = -\frac{r_{fd}}{L_{lfd}}(\lambda_{fd} - \lambda_{md}) + v_{fd} \quad (8.10-37)$$

where  $\lambda_{mq}$  and  $\lambda_{md}$  are given by (8.10-6) and (8.10-7), defines a detailed PVVBR model of the synchronous machine. When implementing the PVVBR model, the stator windings are included in defining the circuit topology using the canonical branch circuit elements of Figure 8.10-1. The rotor voltage equations are expressed explicitly in state model form with flux linkages as state variables. The subtransient voltages  $e_q''$  and  $e_d''$  represent outputs of the rotor model and are incorporated into the stator circuit as dependent sources. The stator branch currents are transformed to the rotor reference frame and represent inputs to the rotor state model. This is shown pictorially in Figure 8.10-3.

A few comments are in order regarding the PVVBR model. First, the assumptions upon which the model is based are identical to those of the traditional  $q$ - and  $d$ -model

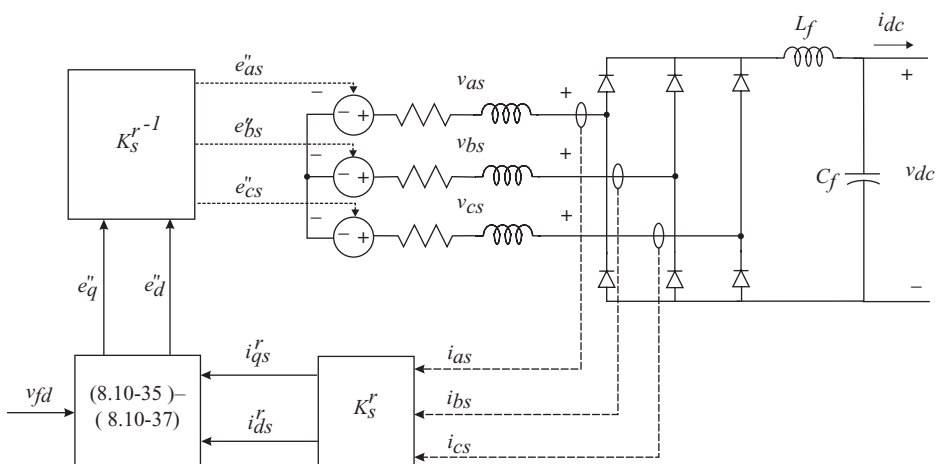


Figure 8.10-3. Machine/rectifier model using PVVBR model.

and the PVCC model. Thus, neglecting numerical error, the responses predicted using all three models should be the same. In addition, no assumptions have been made in regard to winding configuration. The windings may be connected in wye and delta, or the individual windings may be supplied by isolated converter circuits. Among the advantages of the PVVBR form has over a PVCC form is the reduced computation burden, due to a reduction in the number of nodes/branches required to characterize the stator windings. In addition, the eigenstructure of the PVVBR yields improved numerical accuracy, which is highlighted in Reference 14 and explained in further detail in Reference 15. Of course, each application and computer language presents its own challenges, and thus the choice of the model structure, state variables, and reference frame often requires experience and engineering judgment.

Among the challenges that can be faced when implementing the PVVBR model are the rotor-dependent resistances and inductances. The rotor-dependent resistances can be eliminated by restructuring the model slightly. Specifically, the terms

$$\left( \sum_{j=1}^M \left( r_{kqj} / L_{lkqj}^2 \right) \right) L_{mq}''^2 i_{qs}^r \text{ and } \left( \left( r_{fd} / L_{lfd}^2 \right) + \sum_{j=1}^N \left( r_{kqj} / L_{lkqj}^2 \right) \right) L_{md}''^2 i_{ds}^r$$

which are represented using resistances in (8.10-18) and (8.10-19), can be incorporated into the back-emf expressions in any simulation packages that allows current-based voltage sources in series with inductive branches. Doing so also eliminates resistive coupling between windings. An alternative that has been applied in the derivation of average-value models of machine-rectifier systems [18] is to neglect the  $p\lambda_q''$  and  $p\lambda_d''$  in (8.10-14) and (8.10-15). The justification is that the rotor flux linkages are relatively constant over a switching interval. Particular care must be applied in making such an approximation in that it has been shown in Reference 19, that the resulting model can be unstable.

Eliminating the rotor dependent inductances represents a more unique challenge and is related to the neglect of dynamic saliency in transient stability formulations. In the PVVBR model, the rotor position-dependent inductances are eliminated if the assumption

$$L_b'' = \frac{(L_{md}'' - L_{mq}''_3)}{3} \approx 0 \quad (8.10-38)$$

is made. Determining mathematical bounds for the error resulting from such an approximation is a tedious, if not intractable, task. In Reference 20, the effect of applying the approximation of (8.10-38) was considered in the frequency domain by comparing the  $q$ - and  $d$ -axis operational impedance of the PVVBR models with/without the approximation. Example results are shown in Figure 8.10-4. Comparing the impedances of the PVVBR and approximate PVVBR models shows the frequency domain errors associated with making the approximation of (8.10-38). In particular, the curves are both shifted by  $|X_d'' - X_q''|/2$  over the entire frequency range. An alternative to the approximation of (8.10-38) was proposed in Reference 20. Therein an additional damper winding is placed along the  $q$ -axis. The additional damper winding is used to fit machine parameters to approximate impedance curves that have equal dynamic reactances but

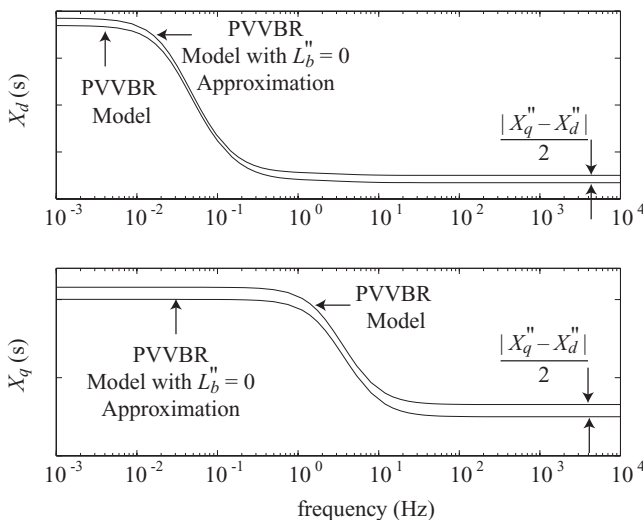


**Figure 8.10-4.** Operational impedance of PVVBR model and PVVBR model with approximation of  $L_b'' \equiv 0$ .

match the original operational impedances for frequencies less than a user specified fit frequency,  $f_r$ . The impact of doing so is shown in the frequency domain in Figure 8.10-5. In applying such an approximation, the user must balance between error and numerical stiffness. Specifically, as  $f_r$  is increased, the error between the salient and nonsalient versions of the PVVBR model reduces. However, the time constant associated with the additional damper winding increases. In Reference 20, it is shown that a reasonable balance between error and stiffness can be made, and that the resulting model yields much less error in the time-domain responses compared with a model in which (8.10-38) is applied.

A question that often arises is how to model saturation in the physical variable models. Specifically, at first glance it appears to be a challenge, since all stator self- and mutual inductances are impacted. A relatively straightforward method of incorporating  $d$ -axis saturation within the PVVBR model has been shown in Reference 21. A more general approach in which saturation is modeled in both axis and transfer functions to represent rotor dynamics is presented in Reference 22.

## 8.11. REDUCED ORDER VOLTAGE BEHIND REACTANCE MODEL

As indicated in Section 8.7, a common practice in modeling power systems is to neglect electric transients of the stator voltage equations. The resulting reduced-order model can be represented in a voltage behind reactance model form. Specifically, by expressing (8.7-20) and (8.7-21) in terms of dynamic inductances and flux linkages, the reduced order stator voltage equations can be written as

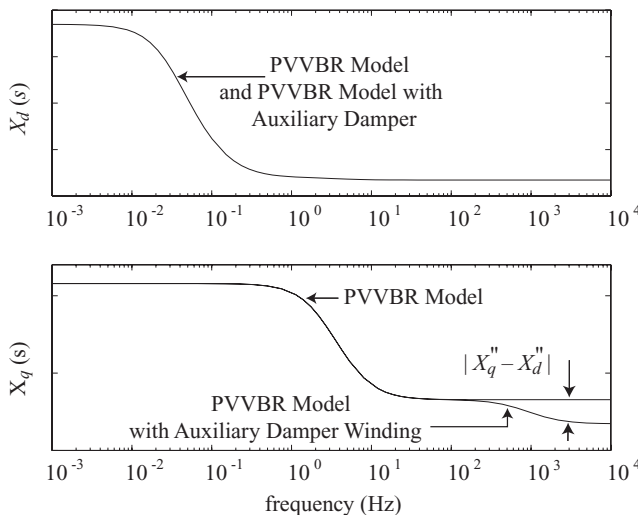


**Figure 8.10-5.** Operational impedance of PVVBR model and PVVBR model with auxiliary damper winding to force  $L_b'' = 0$ .

$$v_{qs}^r = -r_s i_{qs}^r - \omega_e L_d'' i_{ds}^r + e_q'' \quad (8.11-1)$$

$$v_{ds}^r = -r_s i_{ds}^r + \omega_e L_q'' i_{qs}^r + e_d'' \quad (8.11-2)$$

where

$$e_q'' = \omega_e \lambda_d'' \quad (8.11-3)$$

$$e_d'' = -\omega_e \lambda_q'' \quad (8.11-4)$$

Equations (8.11-1) and (8.11-2), together with the state equations of the rotor flux linkages of (8.10-35)–(8.10-37) form a reduced-order voltage behind reactance model with stator transients neglected.

## REFERENCES

- [1] P.C. Krause, O. Wasynczuk, and S.D. Sudhoff, *Analysis of Electric Machinery*, 1st ed., IEEE Press, New York, 1995.
- [2] P.C. Krause, F. Nozari, T.L. Skvarenina, and D.W. Olive, “The Theory of Neglecting Stator Transients,” *IEEE Trans. Power App. Syst.*, Vol. 98, January/February 1979, pp. 141–148.
- [3] T.L. Skvarenina, The Theory and Effects of Neglecting Stator and Network Transients, PhD Thesis, Purdue University, December 1979.
- [4] R.G. Harley and B. Adkins, “Calculations of the Angular Back Swing Following a Short-Circuit of a Loaded Alternator,” *Proc. IEE*, Vol. 117, No. 2, February 1970, pp. 377–386.

- [5] *acslX, Advanced Continuous Simulation Language, User's Guide*, Version 2.4, The AEgis Technologies Group, Inc., March 2008. Available at: <http://www.acslsim.com> (accessed on January 21, 2013).
- [6] *EASY5 Engineering Software for the Design, Analysis and Simulation*, MSC SimEnterprise, Inc. Available at: <http://www.mscsoftware.com> (accessed on January 21, 2013).
- [7] *EUROSTAG: Software for Simulation of Large Electric Power Systems*, Tractebel Energy Engineering. Available at: <http://www.eurostag.be> and <http://www.tractebel-engineering.com> (accessed on January 21, 2013).
- [8] *Simulink Dynamic System Simulation Software—Users Manual*, MathWorks, Inc., Natick, MA, 2009. Available at: <http://www.mathworks.com> (accessed on January 21, 2013).
- [9] *Simulink Dynamic System Simulation Software—SymPowerSystems Manual*, The Math-Works, Inc., Natick, MA, 2009.
- [10] *RT-Lab User's Manual*, Opal-RT Technologies, Montréal, QC. Available at: <http://www.opal-rt.com> (accessed on January 21, 2013).
- [11] *Piecewise Linear Electrical Circuit Simulation (PLECS) User Manual*, Version 1.5, Plexim GmbH, 2006. Available at: <http://www.plexim.com> (accessed on January 21, 2013).
- [12] *Automated State Model Generator (ASMG), Reference Manual*, Version 2, PC Krause and Associates Inc., 2002. Available at: <http://www.pcka.com> (accessed on January 21, 2013).
- [13] *EMTDC User's Guide*, Manitoba HVDC Research Center Inc., Winnipeg, MB, 2004.
- [14] S.D. Pekarek, O. Wasynczuk, and H.J. Hegner, "An Efficient and Accurate Model for the Simulation and Analysis of Synchronous Machine/Converter Systems," *IEEE Trans. Energy Convers.*, Vol. 13, No. 1, March 1998, pp. 42–48.
- [15] L. Wang and J. Jatskevich, "A Voltage-Behind-Reactance Synchronous Machine Model for the EMTP-type Solution," *IEEE Trans. Power Syst.*, Vol. 21, No. 4, November 2006, pp. 1539–1549.
- [16] L. Wang, J. Jatskevich, and S.D. Pekarek, "Modeling of Induction Machines Using a Voltage-Behind-Reactance Formulation," *IEEE Trans. Energy Convers.*, Vol. 23, No. 2, June 2008, pp. 382–392.
- [17] L. Wang, J. Jatskevich, C. Wang, and P. Li, "A Voltage-Behind-Reactance Induction Machine Model for the EMTP-type solution," *IEEE Trans. Power Syst.*, Vol. 23, No. 3, August 2008, pp. 1226–1238.
- [18] S.D. Sudhoff and O. Wasynczuk, "Analysis and Average-Value Modeling of Line-Commutated Converter Synchronous Machine Systems," *IEEE Trans. Energy Convers.*, Vol. 8, No. 1, March 1993, pp. 92–99.
- [19] S.D. Pekarek, A Partitioned State Model of Synchronous Machines for Simulation/Analysis of Power/Drive Systems, PhD Thesis, Purdue University, 1996.
- [20] S.D. Pekarek and E.A. Walters, "An Accurate Method of Neglecting Dynamic Saliency of Synchronous Machines in Power Electronic Based Systems," *IEEE Trans. Energy Convers.*, Vol. 14, No. 4, December 1999, pp. 1177–1183.
- [21] S.D. Pekarek, E.A. Walters, and B.T. Kuhn, "An Efficient and Accurate Method of Representing Saturation in Physical-Variable Models of Synchronous Machines," *IEEE Trans. Energy Convers.*, Vol. 14, No. 1, March 1999, pp. 72–79.
- [22] D.C. Aliprantis, O. Wasynczuk, and C.D. Rodriguez Valdez, "A Voltage-Behind-Reactance Synchronous Machine Model with Saturation and Arbitrary Rotor Network Representation," *IEEE Trans. Energy Convers.*, Vol. 23, No. 2, June 2008, pp. 499–508.

**PROBLEMS**

1. Derive the small-displacement equations of an induction machine with flux linkages per second as state variables. Express the equations in fundamental form.
2. Repeat Problem 1 for a synchronous machine.
3. Write the small-displacement equations for an induction machine with currents as state variables and with a small displacement in  $\omega_e$  where  $\Delta\omega_e$  is an input variable. It is clear that the resulting equations are valid for small changes in the frequency of the applied stator voltages.
4. Repeat Problem 3 for a synchronous machine.
5. Express the rotor voltage equations of an induction machine in the arbitrary reference frame with the electric transients neglected. Appropriately combine these equations with (8.7-11) and (8.7-12) to obtain the standard steady-state equivalent circuit given in Figure 6.9-1.
6. Neglect the electric transients in the stator and rotor of a synchronous machine. From these voltage equations, derive the familiar steady-state voltage equation given by (5.9-19).
7. Determine the initial condition currents for Figure 8.8-1. Show that the initial condition torque is zero.
8. Derive the PVVBR model of the three-phase induction machine.
9. Assume that the stator windings of an induction machine are connected in wye. Simplify the PVVBR model derived in Problem 8 using the fact that  $i_{0s} = 0$ .

# UNBALANCED OPERATION AND SINGLE-PHASE INDUCTION MACHINES

## 9.1. INTRODUCTION

The method of symmetrical components, as developed by Fortescue [1], has been used to analyze unbalanced operation of symmetrical induction machines since the early 1900s. This technique, which has been presented by numerous authors [2–5], is described in its traditional form in the first sections of this chapter. The extension of symmetrical components to analyze unbalanced conditions, such as an open-circuited stator phase, is generally achieved by revolving field theory. This approach is not used here; instead, reference-frame theory is used to establish the method of symmetrical components and to apply it to various types of unbalanced conditions [6]. In particular, it is shown that unbalanced phase variables can be expressed as a series of balanced sets in the arbitrary reference frame with coefficients that may be constant or time varying. This feature of the transformation to the arbitrary reference frame permits the theory of symmetrical components to be established analytically and it provides a straightforward means of applying the concept of symmetrical components to various types of unbalanced conditions.

In this chapter, unbalanced applied stator voltages, unbalanced stator impedances, open-circuited stator phase, and unbalanced rotor resistors of the three-phase induction

machine are considered. Single-phase induction motors are analyzed, and several unbalanced and fault modes of synchronous machine operation are illustrated.

## 9.2. SYMMETRICAL COMPONENT THEORY

In 1918, C.L. Fortescue [1] set forth the method of symmetrical components for the purpose of analyzing the steady-state behavior of power system apparatus during unbalanced operation. Fortescue showed that the phasors representing an unbalanced set of steady-state multiphase variables could be expressed in terms of balanced sets of phasors. For example, the phasors representing an unbalanced three-phase set can be expressed in terms of (1) a balanced set of phasors with an *abc* sequence (the positive sequence), (2) a balanced set of phasors with an *acb* sequence (the negative sequence), and (3) a set of three equal phasors (the zero sequence). Although the method of symmetrical components is widely used in the analysis of unbalanced static networks [2], it is perhaps most appropriate for the analysis of symmetrical induction machines during unbalanced operations.

Fortescue's change of variables is a complex transformation that may be written for three-phase stationary circuits in phasor form as

$$\tilde{\mathbf{F}}_{+-0s} = \mathbf{S} \tilde{\mathbf{F}}_{abcs} \quad (9.2-1)$$

where the symmetrical components are

$$(\tilde{\mathbf{F}}_{+-0s})^T = \begin{bmatrix} \tilde{F}_{+s} & \tilde{F}_{-s} & \tilde{F}_{0s} \end{bmatrix} \quad (9.2-2)$$

The unbalanced phasors are

$$(\tilde{\mathbf{F}}_{abcs})^T = \begin{bmatrix} \tilde{F}_{as} & \tilde{F}_{bs} & \tilde{F}_{cs} \end{bmatrix} \quad (9.2-3)$$

and the transformation is expressed

$$\mathbf{S} = \frac{1}{3} \begin{bmatrix} 1 & a & a^2 \\ 1 & a^2 & a \\ 1 & 1 & 1 \end{bmatrix} \quad (9.2-4)$$

The quantity  $a$  is complex, denoting a counterclockwise rotation of  $2\pi/3$  rad. That is

$$a = e^{j(2\pi/3)} = -\frac{1}{2} + j\frac{\sqrt{3}}{2} \quad (9.2-5)$$

$$a^2 = e^{j(4\pi/3)} = -\frac{1}{2} - j\frac{\sqrt{3}}{2} \quad (9.2-6)$$

The inverse transformation is

$$(\mathbf{S})^{-1} = \begin{bmatrix} 1 & 1 & 1 \\ a^2 & a & 1 \\ a & a^2 & 1 \end{bmatrix} \quad (9.2-7)$$

The +, -, and 0 subscripts denote the positive, negative, and zero sequences, respectively. Hence, for the induction machine shown in Figure 4.2-1,  $\tilde{F}_{+s}$ ,  $a^2\tilde{F}_{+s}$ , and  $a\tilde{F}_{+s}$  make up the positive sequence set of phasors, which we will denote as,  $\tilde{F}_{as+}$ ,  $\tilde{F}_{bs+}$ , and  $\tilde{F}_{cs+}$ , respectively. Similarly,  $\tilde{F}_{-s}$ ,  $a\tilde{F}_{-s}$ , and  $a^2\tilde{F}_{-s}$  are the negative sequence set, here denoted as  $\tilde{F}_{as-}$ ,  $\tilde{F}_{bs-}$ , and  $\tilde{F}_{cs-}$ . The zero sequence is the steady-state version of the zero quantities introduced in Chapter 3. Although we will assume that only one frequency is present, the method of symmetrical components can be applied to each frequency present in the system [6].

In order to compute the total instantaneous, steady-state power, it is first necessary to convert the phasors to the variables in sinusoidal form and then multiply phase voltage times phase current. Thus

$$\begin{aligned} P_{abc} &= V_{as}I_{as} + V_{bs}I_{bs} + V_{cs}I_{cs} \\ &= (V_{as+} + V_{as-} + V_{0s})(I_{as+} + I_{as-} + I_{0s}) + (V_{bs+} + V_{bs-} + V_{0s})(I_{bs+} + I_{bs-} + I_{0s}) \\ &\quad + (V_{cs+} + V_{cs-} + V_{0s})(I_{cs+} + I_{cs-} + I_{0s}) \end{aligned} \quad (9.2-8)$$

Uppercase letters are used to denote steady-state sinusoidal quantities. We will show that the instantaneous power consists of an average value and time-varying components.

### 9.3. SYMMETRICAL COMPONENT ANALYSIS OF INDUCTION MACHINES

Although the method of symmetrical components can be used to analyze unbalanced conditions other than unbalanced stator voltages, this application of symmetrical components is perhaps the most common. Once the unbalanced applied stator voltages are known, (9.2-1) can be used to determine  $\tilde{V}_{as+}$ ,  $\tilde{V}_{as-}$ , and  $\tilde{V}_{0s}$ . It is clear that the currents due to the positive-sequence balanced set can be determined from the voltage equations given by (6.9-11)–(6.9-13). These equations are rewritten here with the + added to the subscript to denote positive-sequence phasors.

$$\tilde{V}_{as+} = \left( r_s + j \frac{\omega_e}{\omega_b} X_{ls} \right) \tilde{I}_{as+} + j \frac{\omega_e}{\omega_b} X_M (\tilde{I}_{as+} + \tilde{I}'_{ar+}) \quad (9.3-1)$$

$$\frac{\tilde{V}'_{ar+}}{s} = \left( \frac{r'_r}{s} + j \frac{\omega_e}{\omega_b} X'_{lr} \right) \tilde{I}'_{ar+} + j \frac{\omega_e}{\omega_b} X_M (\tilde{I}_{as+} + \tilde{I}'_{ar+}) \quad (9.3-2)$$

where  $\omega_b$  is the base electrical angular velocity generally selected as rated and

$$s = \frac{\omega_e - \omega_r}{\omega_e} \quad (9.3-3)$$

As mentioned earlier, the method of symmetrical components can be applied to all frequencies present in the system. For example, the unbalanced applied voltages could be of any arbitrary periodic waveform whereupon the frequencies that exist in the Fourier series expression of these voltages could each be broken up into positive, negative, and zero sequences.

It is customary to obtain the voltage equations for the negative-sequence quantities by reasoning. In particular, slip is the normalized difference between the speed of the rotating air-gap MMF and the rotor speed. The negative-sequence currents establish an air-gap MMF that rotates a  $\omega_e$  in the clockwise direction. Hence, the normalized difference between the air-gap MMF and rotor speed is  $(\omega_e + \omega_r)/\omega_e$  which can be written as  $(2 - s)$ , where  $s$  is defined by (9.3-3). Therefore, the voltage equations for the negative-sequence quantities can be obtained by replacing  $s$  by  $(2 - s)$  in (9.3-1) and (9.3-2). In particular,

$$\tilde{V}_{as-} = \left( r_s + j \frac{\omega_e}{\omega_b} X_{ls} \right) \tilde{I}_{as-} + j \frac{\omega_e}{\omega_b} X_M (\tilde{I}_{as-} + \tilde{I}'_{ar-}) \quad (9.3-4)$$

$$\frac{\tilde{V}'_{ar-}}{2 - s} = \left( \frac{r'_r}{2 - s} + j \frac{\omega_e}{\omega_b} X'_{lr} \right) \tilde{I}'_{ar-} + j \frac{\omega_e}{\omega_b} X_M (\tilde{I}_{as-} + \tilde{I}'_{ar-}) \quad (9.3-5)$$

If the zero-sequence quantities exist in a three-phase induction machine, the steady-state variables may be determined from the phasor equivalent of (6.5-24) and (6.5-27). The electromagnetic torque may be calculated using sequence quantities; however, the derivation of the torque expression is deferred until later.

## 9.4. UNBALANCED STATOR CONDITIONS OF INDUCTION MACHINES: REFERENCE-FRAME ANALYSIS

The theory of symmetrical components set forth in the previous sections can be used to analyze most unbalanced steady-state operating conditions. However, one tends to look for a more rigorous development of this theory and straightforward procedures for applying it to unbalanced conditions, such as an open stator phase or unbalanced rotor resistors. Reference-frame theory can be useful in achieving these goals [6]. Although simultaneous stator and rotor unbalanced conditions can be analyzed, the notation necessary to formulate such a generalized method of analysis becomes quite involved. Therefore, we will consider stator and rotor unbalances separately.

In Reference 6, the stator variables are expressed as a series of sinusoidal functions with time-varying coefficients. Such an analysis is notationally involved and somewhat difficult to follow. We will not become that involved because the concept can be established by assuming a single-stator (rotor) frequency for stator (rotor) unbalances with constant coefficients. We will discuss the restrictions imposed by these assumptions as we go along.

## Unbalanced Machine Variables in the Arbitrary Reference Frame

If we assume that the rotor is a three-wire symmetrical system and the stator applied voltages are single frequency, then unbalanced steady-state stator variables may be expressed as

$$\begin{bmatrix} F_{as} \\ F_{bs} \\ F_{cs} \end{bmatrix} = \begin{bmatrix} F_{as\alpha} & F_{as\beta} \\ F_{bs\alpha} & F_{bs\beta} \\ F_{cs\alpha} & F_{cs\beta} \end{bmatrix} \begin{bmatrix} \cos \omega_e t \\ \sin \omega_e t \end{bmatrix} \quad (9.4-1)$$

Transforming the stator variables as expressed by (9.4-1) to the arbitrary reference frame by (3.3-1) reveals an interesting property. In particular, we have

$$\begin{bmatrix} F_{qs} \\ F_{ds} \end{bmatrix} = \begin{bmatrix} \cos(\omega_e t - \theta) & \sin(\omega_e t - \theta) & \cos(\omega_e t + \theta) & \sin(\omega_e t + \theta) \\ -\sin(\omega_e t - \theta) & \cos(\omega_e t - \theta) & \sin(\omega_e t + \theta) & -\cos(\omega_e t + \theta) \end{bmatrix} \begin{bmatrix} F_{qsA} \\ F_{qsB} \\ F_{qsC} \\ F_{qsD} \end{bmatrix} \quad (9.4-2)$$

and

$$F_{0s} = F_{abcs\alpha} \cos \omega_e t + F_{abcs\beta} \sin \omega_e t \quad (9.4-3)$$

where

$$\begin{aligned} F_{qsA} &= \frac{1}{3} \left[ F_{as\alpha} - \frac{1}{2} F_{bs\alpha} - \frac{1}{2} F_{cs\alpha} + \frac{\sqrt{3}}{2} (F_{bs\beta} - F_{cs\beta}) \right] \\ &= -F_{dsB} \end{aligned} \quad (9.4-4)$$

$$\begin{aligned} F_{qsB} &= \frac{1}{3} \left[ F_{as\beta} - \frac{1}{2} F_{bs\beta} - \frac{1}{2} F_{cs\beta} - \frac{\sqrt{3}}{2} (F_{bs\alpha} - F_{cs\alpha}) \right] \\ &= F_{dsA} \end{aligned} \quad (9.4-5)$$

$$\begin{aligned} F_{qsC} &= \frac{1}{3} \left[ F_{as\alpha} - \frac{1}{2} F_{bs\alpha} - \frac{1}{2} F_{cs\alpha} - \frac{\sqrt{3}}{2} (F_{bs\beta} - F_{cs\beta}) \right] \\ &= F_{dsD} \end{aligned} \quad (9.4-6)$$

$$\begin{aligned} F_{qsD} &= \frac{1}{3} \left[ F_{as\beta} - \frac{1}{2} F_{bs\beta} - \frac{1}{2} F_{cs\beta} + \frac{\sqrt{3}}{2} (F_{bs\alpha} - F_{cs\alpha}) \right] \\ &= -F_{dsC} \end{aligned} \quad (9.4-7)$$

$$F_{abcs\alpha} = \frac{1}{3} (F_{as\alpha} + F_{bs\alpha} + F_{cs\alpha}) \quad (9.4-8)$$

$$F_{abcs\beta} = \frac{1}{3}(F_{as\beta} + F_{bs\beta} + F_{cs\beta}) \quad (9.4-9)$$

It is recalled that

$$\frac{d\theta}{dt} = \omega \quad (9.4-10)$$

where  $\omega$  is the electrical angular velocity of the arbitrary reference frame.

It is interesting that the  $qs$  and  $ds$  variables form two, two-phase balanced sets in the arbitrary reference frame. In order to emphasize this, (9.4-2) is written with sinusoidal functions of  $(\omega_e t - \theta)$  separated from those with the argument of  $(\omega_e t + \theta)$ . It is possible to relate these balanced sets to the positive- and negative-sequence variables. For this purpose, let us consider the induction machine in Figure 6.2-1. A balanced three-phase set of currents of  $abc$  sequence will produce an air-gap MMF that rotates counterclockwise at an angular velocity of  $\omega_e$ . By definition, the positive sequence is the  $abc$  sequence, and it is often referred to as the positively rotating balanced set. The negative sequence, which has the time sequence of  $acb$ , produces an air-gap MMF that rotates in the clockwise direction. It is commonly referred to as the negatively rotating balanced set. Let us think of the  $qs$  and  $ds$  variables as being associated with windings with their magnetic axes positioned relative to the magnetic axis of the stator windings as shown in Figure 6.2-1. Now consider the series of balanced sets formed by the  $qs$  and  $ds$  variables in (9.4-2). The two balanced sets of currents formed by the first and second column of the  $2 \times 4$  matrix produce an air-gap MMF that rotates counterclockwise relative to the arbitrary reference frame whenever  $\omega < \omega_e$  and always counterclockwise relative to the actual stator winding. Hence, the balanced sets with the argument  $(\omega_e t - \theta)$  may be considered as positive sequence or positively rotating sets because they produce counterclockwise rotating air-gap MMFs relative to the stator windings. It follows that the balanced sets formed by the third and fourth columns with the argument  $(\omega_e t + \theta)$  can be thought of as negative sequence or negatively rotating sets. Therefore, we can express (9.4-2) as

$$F_{qs} = F_{qs+} + F_{qs-} \quad (9.4-11)$$

$$F_{ds} = F_{ds+} + F_{ds-} \quad (9.4-12)$$

The zero-sequence variables are expressed by (9.4-3). It is important to note that  $F_{qs+}$  ( $F_{ds+}$ ) is the positive-sequence terms of  $F_{qs}$  ( $F_{ds}$ ), and that together  $I_{qs+}$  with  $I_{ds+}$  produce the positive-sequence rotating air-gap MMF. Similarly,  $I_{qs-}$  with  $I_{ds-}$ , produce the negative-sequence rotating air-gap MMF.

It is understood that the  $qs$  and  $ds$  variables may be expressed in any reference frame by setting  $\omega$ , in (9.4-2), equal to the angular velocity of the reference frame of interest. For example,  $\omega = 0$  for the stationary reference frame and  $\omega = \omega_r$  for the rotor reference frame. It is also clear that the instantaneous sequence sets may be identified in these reference frames. In particular, when  $\omega$  is set equal to zero, the frequency of the variables is  $\omega_e$ ; however, the positive and negative sequence are immediately

identifiable. When  $\omega = \omega_r$ , we see that there are two electrical angular frequencies present;  $\omega_e - \omega_r$  and  $\omega_e + \omega_r$ . The latter occurs due to the air-gap MMF established by negative-sequence stator variables. Because we have assumed that the rotor circuits form a three-wire symmetrical system only one positive and one negative sequence set will be present in the rotor. However, the balanced negative-sequence set of rotor variables will appear in the arbitrary reference frame with the same frequency ( $\omega_e t + \theta$ ) as the negative sequence set established by the stator unbalance.

It follows that for stator unbalances and the assumption that the rotor is a three-wire symmetrical system, (9.4-2)–(9.4-9) can be used to identify the positive- and negative-sequence rotor variables. We only need to (1) replace all  $s$  subscripts with  $r$  in (9.4-2)–(9.4-7), (2) add a prime to all quantities associated with the rotor variables and (3) set  $\theta$  in (9.4-2) equal to  $\omega_r t$ . Recall that the rotor variables are transformed to the arbitrary reference frame by (6.4-1), wherein  $\beta$  is defined by (6.4-5). Please don't confuse the  $\beta$  given by (6.4-5) and the  $\beta$  used in the subscripts starting with (9.4-1)–(9.4-9).

The instantaneous electromagnetic torque may be expressed in arbitrary reference-frame variables as

$$T_e = \left(\frac{3}{2}\right) \left(\frac{P}{2}\right) \left(\frac{X_M}{\omega_b}\right) (I_{qs} I'_{dr} - I_{ds} I'_{qr}) \quad (9.4-13)$$

If we use (9.4-2) to express  $I_{qs}$  and  $I_{ds}$  and the equivalent expression for  $I'_{qr}$  and  $I'_{dr}$ , the torque, for a stator unbalance, may be expressed as

$$\begin{aligned} T_e = & \left(\frac{3}{2}\right) \left(\frac{P}{2}\right) \left(\frac{X_M}{\omega_b}\right) (I_{qsA} I'_{qrB} - I_{qsB} I'_{qrA} - I_{qsC} I'_{qrD} + I_{qsD} I'_{qrC}) \\ & + (-I_{qsA} I'_{qrD} + I_{qsC} I'_{qrB} - I_{qsB} I'_{qrC} + I_{qsD} I'_{qrA}) \cos 2\omega_e t \\ & + (I_{qsA} I'_{qrC} - I_{qsB} I'_{qrD} - I_{qsC} I'_{qrA} + I_{qsD} I'_{qrB}) \sin 2\omega_e t \end{aligned} \quad (9.4-14)$$

Torque may be expressed in per unit by expressing  $X_M$  in per unit and eliminating the factor  $(3/2)(P/2)(1/\omega_b)$ .

## Phasor Relationships

The phasors representing the instantaneous sequence quantities  $F_{qs}$  and  $F_{ds}$  for a stator unbalance given in (9.4-2)–(9.4-7) may be written as

$$\sqrt{2} \tilde{F}_{qs+} = F_{qsA} - jF_{qsB} \quad (9.4-15)$$

$$\begin{aligned} \sqrt{2} \tilde{F}_{ds+} &= F_{qsB} + jF_{qsA} \\ &= j\sqrt{2} \tilde{F}_{qs+} \end{aligned} \quad (9.4-16)$$

$$\sqrt{2}\tilde{F}_{qs-} = F_{qsC} - jF_{qsD} \quad (9.4-17)$$

$$\begin{aligned} \sqrt{2}\tilde{F}_{ds-} &= -F_{qsD} - jF_{qsC} \\ &= -j\sqrt{2}\tilde{F}_{qs-} \end{aligned} \quad (9.4-18)$$

If (9.4-15)–(9.4-18) are used to express (9.4-11) and (9.4-12) in phasor form, we have

$$\begin{bmatrix} \tilde{F}_{qs} \\ \tilde{F}_{ds} \end{bmatrix} = \begin{bmatrix} 1 & 1 \\ j & -j \end{bmatrix} \begin{bmatrix} \tilde{F}_{qs+} \\ \tilde{F}_{qs-} \end{bmatrix} \quad (9.4-19)$$

Solving (9.4-19) for  $\tilde{F}_{qs+}$  and  $\tilde{F}_{qs-}$  yields

$$\begin{bmatrix} \tilde{F}_{qs+} \\ \tilde{F}_{qs-} \end{bmatrix} = \frac{1}{2} \begin{bmatrix} 1 & -j \\ 1 & j \end{bmatrix} \begin{bmatrix} \tilde{F}_{qs} \\ \tilde{F}_{ds} \end{bmatrix} \quad (9.4-20)$$

Equation (9.4-20) is the symmetrical component transformation for a two-phase system and (9.4-19) is the inverse. The zero sequence may be expressed in phasor form from (9.4-3) as

$$\sqrt{2}\tilde{F}_{0s} = F_{abcs\alpha} - jF_{abcs\beta} \quad (9.4-21)$$

If we add the zero sequence to (9.4-20), we can write

$$\begin{bmatrix} \tilde{F}_{qs+} \\ \tilde{F}_{qs-} \\ \tilde{F}_{0s} \end{bmatrix} = \frac{1}{2} \begin{bmatrix} 1 & -j & 0 \\ 1 & j & 0 \\ 0 & 0 & 2 \end{bmatrix} \begin{bmatrix} \tilde{F}_{qs} \\ \tilde{F}_{ds} \\ \tilde{F}_{0s} \end{bmatrix} \quad (9.4-22)$$

Recall from our work in Chapter 3 that for balanced sets, the phasors are the same in all asynchronously rotating reference frames. The frequency of the balance set in a specific reference frame need to be considered only when expressing the instantaneous balanced set. Therefore, except for  $\tilde{F}_{0s}$ , all phasors in (9.4-22) are valid in any asynchronous reference frame, and it is not necessary to use a superscript, although we will for clarity.

Let us write (9.4-22) as

$$\begin{bmatrix} \tilde{F}_{qs+}^s \\ \tilde{F}_{qs-}^s \\ \tilde{F}_{0s}^s \end{bmatrix} = \frac{1}{2} \begin{bmatrix} 1 & -j & 0 \\ 1 & j & 0 \\ 0 & 0 & 2 \end{bmatrix} \mathbf{K}_s^s \begin{bmatrix} \tilde{F}_{as} \\ \tilde{F}_{bs} \\ \tilde{F}_{cs} \end{bmatrix} \quad (9.4-23)$$

What have we done? Well, first we added a superscript to the variables given in (9.4-22) to give us the sense of being in the stationary reference frame. Next, we transformed  $\tilde{F}_{qs}^s$ ,  $\tilde{F}_{ds}^s$ , and  $\tilde{F}_{0s}^s$  to  $\tilde{F}_{as}$ ,  $\tilde{F}_{bs}$ , and  $\tilde{F}_{cs}$  by  $\mathbf{K}_s^s$ . With  $\theta = 0$ ,  $\mathbf{K}_s^s$  becomes

$$\mathbf{K}_s^s = \frac{2}{3} \begin{bmatrix} 1 & -\frac{1}{2} & -\frac{1}{2} \\ 0 & -\frac{\sqrt{3}}{2} & \frac{\sqrt{3}}{2} \\ \frac{1}{2} & \frac{1}{2} & \frac{1}{2} \end{bmatrix} \quad (9.4-24)$$

Because  $\mathbf{K}_s^s$  is not a function of time, it is permissible to use it to transform phasors. It can be shown that

$$\mathbf{S} = \frac{1}{2} \begin{bmatrix} 1 & -j & 0 \\ 1 & j & 0 \\ 0 & 0 & 2 \end{bmatrix} \mathbf{K}_s^s \quad (9.4-25)$$

Thus (9.4-23) may be written as

$$\tilde{\mathbf{F}}_{qs \pm 0s}^s = \mathbf{S} \tilde{\mathbf{F}}_{abcs} \quad (9.4-26)$$

where  $\mathbf{S}$  is the symmetrical component transformation given by (9.2-4). Therefore, (9.4-26) is (9.2-1), and we have

$$\tilde{F}_{qs+}^s = \tilde{F}_{+s} \quad (9.4-27)$$

$$\tilde{F}_{qs-}^s = \tilde{F}_{-s} \quad (9.4-28)$$

Now that we are working in the stationary reference frame, let us rewrite (9.4-20) as

$$\begin{bmatrix} \tilde{F}_{qs+}^s \\ \tilde{F}_{qs-}^s \end{bmatrix} = \frac{1}{2} \begin{bmatrix} 1 & -j \\ 1 & j \end{bmatrix} \begin{bmatrix} \tilde{F}_{qs}^s \\ \tilde{F}_{ds}^s \end{bmatrix} \quad (9.4-29)$$

For stator unbalances with symmetrical three-wire rotor circuits, (9.4-29) also applies to rotor phasors in the stationary reference frame. That is

$$\begin{bmatrix} \tilde{F}_{qr+}^s \\ \tilde{F}_{qr-}^s \end{bmatrix} = \frac{1}{2} \begin{bmatrix} 1 & -j \\ 1 & j \end{bmatrix} \begin{bmatrix} \tilde{F}_{qr}^s \\ \tilde{F}_{dr}^s \end{bmatrix} \quad (9.4-30)$$

The steady-state voltage equations in the stationary reference frame may be obtained from (6.5-34) by setting  $\omega = 0$  and  $p = j\omega_e$ . Thus

$$\begin{bmatrix} \tilde{V}_{qs}^s \\ \tilde{V}_{ds}^s \\ \tilde{V}_{qr}^s \\ \tilde{V}_{dr}^s \end{bmatrix} = \begin{bmatrix} r_s + j \frac{\omega_e}{\omega_b} X_{ss} & 0 & j \frac{\omega_e}{\omega_b} X_M & 0 \\ 0 & r_s + j \frac{\omega_e}{\omega_b} X_{ss} & 0 & j \frac{\omega_e}{\omega_b} X_M \\ j \frac{\omega_e}{\omega_b} X_M & -\frac{\omega_r}{\omega_b} X_M & r_r + j \frac{\omega_e}{\omega_b} X'_{rr} & -\frac{\omega_r}{\omega_b} X'_{rr} \\ \frac{\omega_r}{\omega_b} X_M & j \frac{\omega_e}{\omega_b} X_M & \frac{\omega_r}{\omega_b} X'_{rr} & r_r' + j \frac{\omega_e}{\omega_b} X'_{rr} \end{bmatrix} \begin{bmatrix} \tilde{I}_{qs}^s \\ \tilde{I}_{ds}^s \\ \tilde{I}_{qr}^s \\ \tilde{I}_{dr}^s \end{bmatrix} \quad (9.4-31)$$

If we now incorporate (9.4-29) and (9.4-30) into (9.4-31), the sequence voltage equations become

$$\begin{bmatrix} \tilde{V}_{qs+}^s \\ \tilde{V}_{qr+}^s \\ \tilde{V}_{qs-}^s \\ \tilde{V}_{qr-}^s \\ 2-s \end{bmatrix} = \begin{bmatrix} r_s + j \frac{\omega_e}{\omega_b} X_{ss} & j \frac{\omega_e}{\omega_b} X_M & 0 & 0 \\ j \frac{\omega_e}{\omega_b} X_M & \frac{r'_r}{s} + j \frac{\omega_e}{\omega_b} X'_{rr} & 0 & 0 \\ 0 & 0 & r_s + \frac{\omega_e}{\omega_b} X_{ss} & j \frac{\omega_e}{\omega_b} X_M \\ 0 & 0 & j \frac{\omega_e}{\omega_b} X_M & \frac{r'_r}{2-s} + j \frac{\omega_e}{\omega_b} X'_{rr} \end{bmatrix} \begin{bmatrix} \tilde{I}_{qs+}^s \\ \tilde{I}_{qr+}^s \\ \tilde{I}_{qs-}^s \\ \tilde{I}_{qr-}^s \end{bmatrix} \quad (9.4-32)$$

where

$$s = \frac{\omega_e - \omega_r}{\omega_e} \quad (9.4-33)$$

The steady-state electromagnet torque, for a stator unbalance, may be expressed

$$T_e = 3 \left( \frac{P}{2} \right) \frac{X_M}{\omega_b} \operatorname{Re} \left[ j \left( \tilde{I}_{qs+}^s \tilde{I}_{qr+}^{*s} - \tilde{I}_{qs-}^s \tilde{I}_{qr-}^{*s} \right) \right] + \operatorname{Re} \left[ j \left( -\tilde{I}_{qs+}^s \tilde{I}_{qr-}^s + \tilde{I}_{qs-}^s \tilde{I}_{qr+}^s \right) \right] \cos 2\omega_e t + \operatorname{Re} \left[ \tilde{I}_{qs+}^s \tilde{I}_{qr-}^s - \tilde{I}_{qs-}^s \tilde{I}_{qr+}^s \right] \sin 2\omega_e t \quad (9.4-34)$$

where the asterisk denotes the conjugate.

Steady-state instantaneous stator variables,  $F_{as}$ ,  $F_{bs}$ , and  $F_{qs}$ , may be obtained from the phasors  $\tilde{F}_{as}$ ,  $\tilde{F}_{bs}$ , and  $\tilde{F}_{qs}$  determined from (9.4-23). With the assumption of a symmetrical rotor, the frequency of the stator variables is  $\omega_e$ ; however, as has been mentioned the rotor variables  $F'_{ar}$ ,  $F'_{br}$ , and  $F'_{cr}$  each contain two frequencies ( $\omega_e - \omega_r$ ) and ( $\omega_e + \omega_r$ ). The instantaneous rotor variables can be obtained by using the rotor equivalent of (9.4-15)–(9.4-18) to identify  $F'_{qrA}$  through  $F'_{qrD}$ , which can be substituted into the rotor equivalent of (9.4-2). To obtain  $F''_{qr}$  and  $F''_{dr}$ ,  $\theta$  in (9.4-2) must be set to  $\omega_r t$ , whereupon  $\mathbf{K}'_r$  may be used to obtain  $F'_{ar}$ ,  $F'_{br}$ , and  $F'_{cr}$ . Since we have assumed symmetrical three-wire stator and rotor circuits, neither  $F_{0s}$  nor  $F'_{0r}$  exist; however, we have included the zero-sequence notation in order to show the equivalence to the symmetrical component transformation. If a zero sequence were present in the rotor circuits, it would consist of two frequencies, unlike the stator zero sequence, which would contain only  $\omega_e$ .

## 9.5. TYPICAL UNBALANCED STATOR CONDITIONS OF INDUCTION MACHINES

Although it is not practical to consider all stator unbalanced conditions that might occur, the information given in this section should serve as a guide to the solution of a large class of problems. Unbalanced source voltages, unbalanced phase impedances, and an open-circuited stator phase are considered, and the method of calculating the steady-state performance is set forth in each case.

### Unbalanced Source Voltages

Perhaps the most common unbalanced stator condition is unbalanced source voltages. This can occur in a power system due to a fault or a switching malfunction that may cause unbalanced conditions to exist for a considerable period of time. The stator circuit of an induction machine for the purpose of analysis is given in Figure 9.5-1. From Figure 9.5-1, we can write

$$e_{ga} = v_{as} + v_{ng} \quad (9.5-1)$$

$$e_{gb} = v_{bs} + v_{ng} \quad (9.5-2)$$

$$e_{gc} = v_{cs} + v_{ng} \quad (9.5-3)$$

In a symmetrical three-wire system, the zero sequence is not present, and it can be shown that in the steady state, we have

$$\tilde{V}_{qs}^s = \frac{2}{3} \left( \tilde{E}_{ga} - \frac{1}{2} \tilde{E}_{gb} - \frac{1}{2} \tilde{E}_{gc} \right) \quad (9.5-4)$$

$$\tilde{V}_{ds}^s = \frac{1}{\sqrt{3}} \left( -\tilde{E}_{gb} + \tilde{E}_{gc} \right) \quad (9.5-5)$$

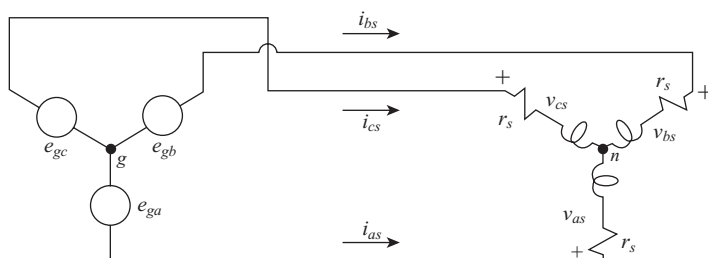


Figure 9.5-1. Stator circuit of induction machine.

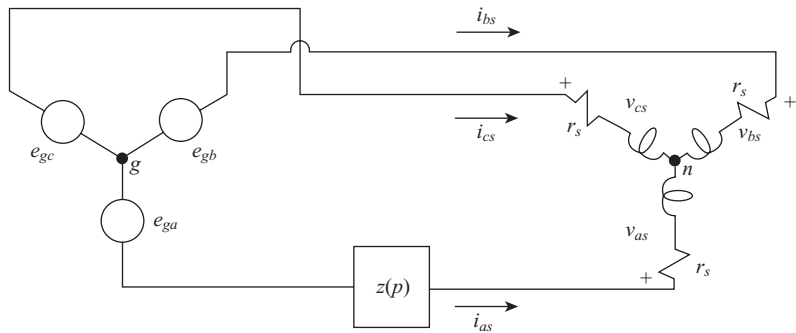


Figure 9.5-2. Stator circuit with impedance in series with *as* winding.

Substituting (9.5-4) and (9.5-5) into (9.4-29) yields

$$\tilde{V}_{qs+}^s = \frac{1}{3} \left( \tilde{E}_{ga} - \frac{1}{2} \tilde{E}_{gb} - \frac{1}{2} \tilde{E}_{gc} \right) - j \frac{1}{2\sqrt{3}} (-\tilde{E}_{gb} + \tilde{E}_{gc}) \quad (9.5-6)$$

$$\tilde{V}_{qs-}^s = \frac{1}{3} \left( \tilde{E}_{ga} - \frac{1}{2} \tilde{E}_{gb} - \frac{1}{2} \tilde{E}_{gc} \right) + j \frac{1}{2\sqrt{3}} (-\tilde{E}_{gb} + \tilde{E}_{gc}) \quad (9.5-7)$$

The steady-state phasor currents can be calculated from (9.4-32). The torque may then be calculated using (9.4-34).

### Unbalanced Stator Impedances

For this unbalanced condition, let us consider the stator circuit shown in Figure 9.5-2, wherein an impedance  $z(p)$  is placed in series with the *as* winding. The following equations may be written as

$$e_{ga} = i_{as}z(p) + v_{as} + v_{ng} \quad (9.5-8)$$

$$e_{gb} = v_{bs} + v_{ng} \quad (9.5-9)$$

$$e_{gc} = v_{cs} + v_{ng} \quad (9.5-10)$$

In a three-wire system,  $i_{0s}$  is zero, therefore  $v_{0s}$  is zero because the stator circuits are symmetrical. Let us now assume that the source voltages are balanced; hence, we can add (9.5-8)–(9.5-10), and we have

$$v_{ng} = -\frac{1}{3} i_{as}z(p) \quad (9.5-11)$$

Equation (9.5-11) is valid as long as  $e_{ga} + e_{gb} + e_{gc}$  is zero. Substituting (9.5-11) into (9.5-8)–(9.5-10) and solving for the phase voltages yields

$$v_{as} = e_{ga} - \frac{2}{3}i_{as}z(p) \quad (9.5-12)$$

$$v_{bs} = e_{gb} + \frac{1}{3}i_{as}z(p) \quad (9.5-13)$$

$$v_{cs} = e_{gc} + \frac{1}{3}i_{as}z(p) \quad (9.5-14)$$

In a problem at the end of the chapter, you are asked to write  $v_{as}$ ,  $v_{bs}$ , and  $v_{cs}$  assuming  $e_{ga}$ ,  $e_{gb}$ , and  $e_{gc}$  are not balanced. Substituting the steady-state phasor equivalents of (9.5-12)–(9.5-14) into (9.4-29) yields

$$\tilde{V}_{qs+}^s = \tilde{E}_{ga} - \frac{1}{3}\tilde{I}_{as}Z \quad (9.5-15)$$

$$\tilde{V}_{qs-}^s = -\frac{1}{3}\tilde{I}_{as}Z \quad (9.5-16)$$

From the inverse of (9.4-29) and because  $\tilde{I}_{0s}$  is zero, we have

$$\tilde{I}_{as} = \tilde{I}_{qs+}^s + \tilde{I}_{qs-}^s \quad (9.5-17)$$

If we now substitute (9.5-17) into (9.5-15) and (9.5-16) and then substitute the results into (9.4-32), we obtain

$$\begin{bmatrix} \tilde{E}_{ga} \\ \tilde{V}_{qr+}^s \\ 0 \\ 0 \end{bmatrix} = \begin{bmatrix} \frac{1}{3}Z + r_s + j\frac{\omega_e}{\omega_b}X_{ss} & j\frac{\omega_e}{\omega_b}X_M & \frac{1}{3}Z & 0 \\ j\frac{\omega_e}{\omega_b}X_M & \frac{r'_r}{s} + j\frac{\omega_e}{\omega_b}X'_{rr} & 0 & 0 \\ \frac{1}{3}Z & 0 & \frac{1}{3}Z + r_s + j\frac{\omega_e}{\omega_b}X_{ss} & j\frac{\omega_e}{\omega_b}X_M \\ 0 & 0 & j\frac{\omega_e}{\omega_b}X_M & \frac{r'_r}{2-s} + j\frac{\omega_e}{\omega_b}X'_{rr} \end{bmatrix} \begin{bmatrix} \tilde{I}_{qs+}^s \\ \tilde{I}_{qr+}^s \\ \tilde{I}_{qs-}^s \\ \tilde{I}_{qr-}^s \end{bmatrix} \quad (9.5-18)$$

The above equation, which can be reduced to a  $3 \times 3$  matrix, may be used to solve for the currents in phasor form and the torque may then be determined from (9.4-34). It is important to note that unbalanced external stator impedances cause the positive- and negative-sequence voltage equations to be coupled.

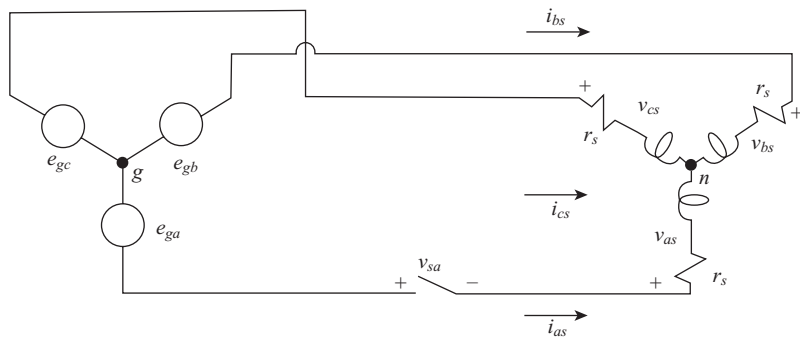


Figure 9.5-3. Stator circuit with provisions for switching  $i_{as}$ .

### Open-Circuited Stator Phase

For the purpose of analyzing an open-circuited stator phase, which is equivalent to single-phase operation, let us consider the stator circuits of a three-phase, wye-connected induction machine as shown in Figure 9.5-3, where phase  $a$  is open-circuited. Because the stator circuit is a three-wire symmetrical system,  $i_{0s}$  and  $v_{0s}$  are zero. Therefore, with  $\theta = 0$ ,  $f_{qs}^s = f_{as}$  and

$$v_{as} = v_{qs}^s = \frac{p}{\omega_b} \psi_{qs}^s \quad (9.5-19)$$

From (6.5-28) with  $i_{qs}^s = 0$

$$\psi_{qs}^s = X_M i_{qr}^s \quad (9.5-20)$$

Thus

$$v_{as} = \frac{p}{\omega_b} X_M i_{qr}^s \quad (9.5-21)$$

Therefore, if  $i_{as}$  is zero and the voltage  $(p/\omega_b)X_M i_{qr}^s$  is applied to phase  $a$ , the current  $i_{as}$  will be forced to remain at zero [7]. From Figure 9.5-3

$$v_{bs} = e_{gb} - v_{ng} \quad (9.5-22)$$

$$v_{cs} = e_{gc} - v_{ng} \quad (9.5-23)$$

In this system,  $v_{0s}$  is zero; therefore, adding (9.5-21)–(9.5-23) and solving the result for  $v_{ng}$  yields

$$v_{ng} = \frac{1}{2}(e_{gb} + e_{gc}) + \frac{1}{2}v_{as} \quad (9.5-24)$$

Substituting (9.5-24) into (9.5-22) and (9.5-23) gives

$$v_{bs} = \frac{1}{2}e_{gb} - \frac{1}{2}e_{gc} - \frac{1}{2}v_{as} \quad (9.5-25)$$

$$v_{cs} = -\frac{1}{2}e_{gb} + \frac{1}{2}e_{gc} - \frac{1}{2}v_{as} \quad (9.5-26)$$

The above relationships are valid for transient and steady-state conditions. It is assumed that the source voltages contain only one frequency, therefore, if we substitute the steady-state phasor equivalent of (9.5-21), (9.5-25), and (9.5-26) into (9.4-26), we obtain

$$\tilde{V}_{qs+}^s = j \frac{1}{2} \frac{\omega_e}{\omega_b} X_M \tilde{I}_{qr}^s + \tilde{E} \quad (9.5-27)$$

$$\tilde{V}_{qs-}^s = j \frac{1}{2} \frac{\omega_e}{\omega_b} X_M \tilde{I}_{qr}^s - \tilde{E} \quad (9.5-28)$$

where

$$\tilde{E} = j \frac{1}{2\sqrt{3}} (\tilde{E}_{gb} - \tilde{E}_{gc}) \quad (9.5-29)$$

We can write

$$\tilde{I}_{qr}^s = \tilde{I}_{qr+}^s + \tilde{I}_{qr-}^s \quad (9.5-30)$$

Also,  $\tilde{I}_{qs}^s$  may also be expressed in terms of its symmetrical components as

$$\tilde{I}_{qs}^s = \tilde{I}_{qs+}^s + \tilde{I}_{qs-}^s \quad (9.5-31)$$

However,  $\tilde{I}_{as}$  is zero, and since  $\theta$  and  $\tilde{I}_{0s}$  are both zero, then  $\tilde{I}_{qs}^s$ , which is  $\tilde{I}_{as}$ , is zero. Thus

$$\tilde{I}_{qs-}^s = -\tilde{I}_{qs+}^s \quad (9.5-32)$$

If we substitute (9.5-30) into (9.5-27) and (9.5-28), and then substitute the results into (9.4-32), and if we incorporate (9.5-32), we can write

$$\begin{bmatrix} \tilde{E} \\ \frac{\tilde{V}_{qr+}^s}{s} \\ 0 \end{bmatrix} = \begin{bmatrix} r_s + j \frac{\omega_e}{\omega_b} X_{ss} & j \frac{1}{2} \frac{\omega_e}{\omega_b} X_M & -j \frac{1}{2} \frac{\omega_e}{\omega_b} X_M \\ j \frac{\omega_e}{\omega_b} X_M & \frac{r'_r}{s} + j \frac{\omega_e}{\omega_b} X'_{rr} & 0 \\ -j \frac{\omega_e}{\omega_b} X_M & 0 & \frac{r'_r}{2-s} + j \frac{\omega_e}{\omega_b} X'_{rr} \end{bmatrix} \begin{bmatrix} \tilde{I}_{qs+}^s \\ \tilde{I}_{qr+}^s \\ \tilde{I}_{qr-}^s \end{bmatrix} \quad (9.5-33)$$

## 9.6. UNBALANCED ROTOR CONDITIONS OF INDUCTION MACHINES

In the analysis of unbalanced rotor conditions, it will be assumed that the stator circuits are symmetrical and the stator applied voltages are balanced and have only one frequency. Since the analysis of steady-state operation during unbalanced rotor conditions is similar in many respects to the analysis for unbalanced stator conditions, the relationships will be given without a lengthy discussion. The principal difference is the reference frame, in which the analysis is carried out. It is convenient, in the case of rotor unbalanced conditions with symmetrical stator circuits, to conduct the analysis in the rotor reference frame since therein the variables are of one frequency.

### Unbalanced Machine Variables in the Arbitrary Reference Frame

Assuming only one rotor frequency is present, the rotor variables may be expressed as

$$\begin{bmatrix} F'_{ar} \\ F'_{br} \\ F'_{cr} \end{bmatrix} = \begin{bmatrix} F'_{ar\alpha} & F'_{ar\beta} \\ F'_{br\alpha} & F'_{br\beta} \\ F'_{cr\alpha} & F'_{cr\beta} \end{bmatrix} \begin{bmatrix} \cos(\omega_e - \omega_r)t \\ \sin(\omega_e - \omega_r)t \end{bmatrix} \quad (9.6-1)$$

Transforming the rotor variables as expressed by (9.6-1) to the arbitrary reference frame by (6.4-1) yields

$$\begin{bmatrix} F'_{qr} \\ F'_{dr} \end{bmatrix} \begin{bmatrix} \cos(\omega_e t - \theta) & \sin(\omega_e t - \theta) & \cos[(\omega_e - 2\omega_r)t + \theta] & \sin[(\omega_e - 2\omega_r)t + \theta] \\ -\sin(\omega_e t - \theta) & \cos(\omega_e t - \theta) & \sin[(\omega_e - 2\omega_r)t + \theta] & -\cos[(\omega_e - 2\omega_r)t + \theta] \end{bmatrix} \begin{bmatrix} F'_{qrA} \\ F'_{qrB} \\ F'_{qrC} \\ F'_{qrD} \end{bmatrix} \quad (9.6-2)$$

and

$$F'_{0r} = F'_{abcr\alpha} \cos(\omega_e - \omega_r)t + F'_{abcr\beta} \sin(\omega_e - \omega_r)t \quad (9.6-3)$$

where

$$\begin{aligned} F'_{qrA} &= \frac{1}{3} \left[ F'_{ar\alpha} - \frac{1}{2} F'_{br\alpha} - \frac{1}{2} F'_{cr\alpha} + \frac{\sqrt{3}}{2} (F'_{br\beta} - F'_{cr\beta}) \right] \\ &= -F'_{drB} \end{aligned} \quad (9.6-4)$$

$$\begin{aligned} F'_{qrB} &= \frac{1}{3} \left[ F'_{ar\beta} - \frac{1}{2} F'_{br\beta} - \frac{1}{2} F'_{cr\beta} - \frac{\sqrt{3}}{2} (F'_{br\alpha} - F'_{cr\alpha}) \right] \\ &= F'_{drA} \end{aligned} \quad (9.6-5)$$

$$\begin{aligned} F'_{qrC} &= \frac{1}{3} \left[ F'_{ar\alpha} - \frac{1}{2} F'_{br\alpha} - \frac{1}{2} F'_{cr\alpha} - \frac{\sqrt{3}}{2} (F'_{br\beta} - F'_{cr\beta}) \right] \\ &= F'_{drD} \end{aligned} \quad (9.6-6)$$

$$\begin{aligned} F'_{qrD} &= \frac{1}{3} \left[ F'_{qr\beta} - \frac{1}{2} F'_{br\beta} - \frac{1}{2} F'_{cr\beta} + \frac{\sqrt{3}}{2} (F'_{br\alpha} - F'_{cr\alpha}) \right] \\ &= -F'_{drC} \end{aligned} \quad (9.6-7)$$

$$F'_{abcr\alpha} = \frac{1}{3} (F'_{ar\alpha} + F'_{br\alpha} + F'_{cr\alpha}) \quad (9.6-8)$$

$$F'_{abcr\beta} = \frac{1}{3} (F'_{ar\beta} + F'_{br\beta} + F'_{cr\beta}) \quad (9.6-9)$$

Also, in (6.4-1), we have substituted for  $\beta$ , where

$$\frac{d\beta}{dt} = (\omega - \omega_r) \quad (9.6-10)$$

Note that in (9.6-2), the positive sequence variables again have the argument of  $(\omega_e t - \theta)$ ; however, the argument of the negative sequence is  $[(\omega_e - 2\omega_r)t + \theta]$ . It follows that

$$F'_{qr} = F'_{qr+} + F'_{qr-} \quad (9.6-11)$$

$$F'_{dr} = F'_{dr+} + F'_{dr-} \quad (9.6-12)$$

We have assumed that the stator is a symmetrical, three-wire system and the applied voltages are balanced, containing only one frequency,  $\omega_e$ . Therefore, we can use (9.6-2)–(9.6-7) to express the stator variables by (1) replacing all  $r$  subscripts with  $s$ , (2) removing the primes, and (3) setting  $\theta = 0$  in (9.6-2). This gives rise to two stator frequencies;  $\omega_e$  and  $(\omega_e - 2\omega_r)$ . It is assumed that the source voltages are of the frequency  $\omega_e$ , and we will also assume a zero impedance source. Thus, the stator currents and the phase voltages of the stator windings will contain  $\omega_e$  and  $(\omega_e - 2\omega_r)$ . The  $(\omega_e - 2\omega_r)$  frequency, which is the stator negative sequence, is induced into the stator windings due to the

rotor unbalance. It is interesting to note that the stator negative sequence currents are not present when  $\omega_r = (1/2)\omega_e$ . Therefore, because  $\tilde{I}_{qs-}^r$  is zero at  $\omega_r = (1/2)\omega_e$ , we would expect the negative sequence torque to also be zero.

The instantaneous steady-state electromagnetic torque for a rotor unbalance may be expressed as

$$\begin{aligned} T_e = & \left(\frac{3}{2}\right)\left(\frac{P}{2}\right)\left(\frac{X_M}{\omega_b}\right)\left(I_{qsA}I'_{qrB} - I_{qsB}I'_{qrA} - I_{qsC}I'_{qrD} + I_{qsD}I'_{qrC}\right) \\ & + \left(-I_{qsA}I'_{qrD} + I_{qsC}I'_{qrB} - I_{qsB}I'_{qrC} + I_{qsD}I'_{qrA}\right)\cos 2(\omega_e - \omega_r)t \\ & + \left(I_{qsA}I'_{qrC} - I_{qsB}I'_{qrD} - I_{qsC}I'_{qrA} + I_{qsD}I'_{qrB}\right)\sin 2(\omega_e - \omega_r)t \end{aligned} \quad (9.6-13)$$

The pulsing component in (9.6-13) is commonly referred to as the “twice slip-frequency” torque.

## Phasor Relationships

It is convenient to conduct the steady-state analysis of unbalanced rotor conditions much the same as unbalanced stator conditions. The phasor expressions from (9.6-2) are

$$\sqrt{2}\tilde{F}'_{qr+} = F'_{qrA} - jF'_{qrB} \quad (9.6-14)$$

$$\begin{aligned} \sqrt{2}\tilde{F}'_{dr+} &= F'_{qrB} + jF'_{qrA} \\ &= j\sqrt{2}\tilde{F}'_{qr+} \end{aligned} \quad (9.6-15)$$

$$\sqrt{2}\tilde{F}'_{qr-} = F'_{qrC} - jF'_{qrD} \quad (9.6-16)$$

$$\begin{aligned} \sqrt{2}\tilde{F}'_{dr-} &= -F'_{qrD} - jF'_{qrC} \\ &= -j\sqrt{2}\tilde{F}'_{qr-} \end{aligned} \quad (9.6-17)$$

Following a procedure identical to that in the case of stator unbalance, we can write

$$\tilde{\mathbf{F}}'_{qr\pm 0r} = \mathbf{S}\tilde{\mathbf{F}}'_{abcr} \quad (9.6-18)$$

and

$$\tilde{\mathbf{F}}'_{qs\pm 0s} = \mathbf{S}\tilde{\mathbf{F}}'_{abcs} \quad (9.6-19)$$

We can write (6.5-34) in the rotor reference frame by setting  $\omega = \omega_r$ , and then, by setting  $p = j(\omega_e - \omega_r)$ , we can obtain the voltage equations for steady-state conditions. If we then substitute (9.4-29) and (9.4-30) for stator variables and similar relationships for rotor variables from (9.6-15) and (9.6-16) into the steady-state equations, we will obtain

$$\begin{bmatrix} \tilde{V}_{qs+}^r \\ \tilde{V}_{qr+}^r \\ \frac{\tilde{V}_{qs-}^r}{s} \\ \frac{\tilde{V}_{qr-}^r}{s} \end{bmatrix} = \begin{bmatrix} r_s + j \frac{\omega_e}{\omega_b} X_{ss} & j \frac{\omega_e}{\omega_b} X_M & 0 & 0 \\ j \frac{\omega_e}{\omega_b} X_M & \frac{r'_r}{s} + j \frac{\omega_e}{\omega_b} X'_{rr} & 0 & 0 \\ 0 & 0 & r_s + j \left( \frac{\omega_e - 2\omega_r}{\omega_b} \right) X_{ss} & j \left( \frac{\omega_e - 2\omega_r}{\omega_b} \right) X_M \\ 0 & 0 & j \frac{\omega_e}{\omega_b} X_M & \frac{r'_r}{s} + j \frac{\omega_e}{\omega_b} X'_{rr} \end{bmatrix} \begin{bmatrix} \tilde{I}_{qs+}^r \\ \tilde{I}_{qr+}^r \\ \tilde{I}_{qs-}^r \\ \tilde{I}_{qr-}^r \end{bmatrix} \quad (9.6-20)$$

where

$$s = \frac{\omega_e - \omega_r}{\omega_e} \quad (9.6-21)$$

Since we are dealing with symmetrical three-wire systems,  $F_{0s}$  and  $F'_{0r}$  are zero.

The steady-state electromagnetic torque for a rotor unbalance may be expressed

$$T_e = 3 \left( \frac{P}{2} \right) \frac{X_M}{\omega_b} \operatorname{Re} \left[ j \left( \tilde{I}_{qs+}^{r*} \tilde{I}_{qr+}^r - \tilde{I}_{qs-}^{r*} \tilde{I}_{qr-}^r \right) \right] + \operatorname{Re} \left[ j \left( -\tilde{I}_{qs+}^r \tilde{I}_{qr+}^r + \tilde{I}_{qs-}^r \tilde{I}_{qr+}^r \right) \right] \cos(\omega_e - 2\omega_r)t + \operatorname{Re} \left( \tilde{I}_{qs+}^r \tilde{I}_{qr-}^r - \tilde{I}_{qs-}^r \tilde{I}_{qr+}^r \right) \sin(\omega_e - 2\omega_r)t \quad (9.6-22)$$

where the asterisk denotes the conjugate. As we have mentioned, the negative sequence torque is zero when  $\omega_r = (1/2)\omega_e$ , since  $\tilde{I}_{qs-}^r$  becomes zero; however, the pulsating torque component is still present.

## 9.7. UNBALANCED ROTOR RESISTORS

In some applications where it is necessary to accelerate a large-inertia mechanical load, a wound-rotor induction machine equipped with variable external rotor resistors is often used. As the speed of the machine increases, the value of the external rotor resistors is decreased proportionally so as to maintain nearly maximum electromagnetic torque during most of the acceleration period. Care must be taken, however, in order not to unbalance the external rotor resistors during this process, otherwise a torque pulsation of twice slip frequency occurs as noted in (9.6-13) and (9.6-22), which may cause low-frequency oscillations in the connected mechanical system. For the purpose of analyzing unbalanced rotor resistors, we will consider the rotor circuit given in Figure 9.7-1. The rotor phase voltages may be written as

$$v'_{ar} = v_{pm} - i'_{ar} R'_{ar} \quad (9.7-1)$$

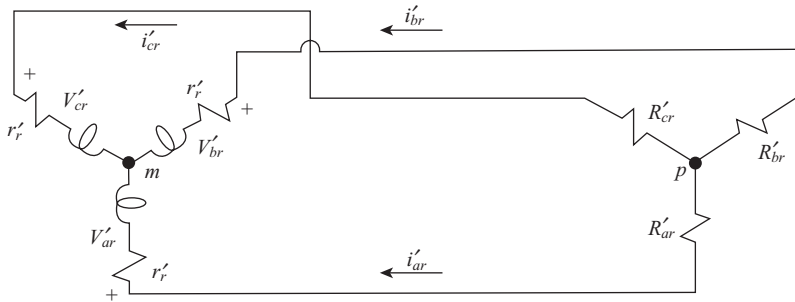


Figure 9.7-1. Rotor circuits with unbalanced external resistors.

$$v'_{br} = v_{pm} - i'_{br} R'_{br} \quad (9.7-2)$$

$$v'_{cr} = v_{pm} - i'_{cr} R'_{cr} \quad (9.7-3)$$

Since the rotor is assumed to be a three-wire system,  $i'_{0r} = 0$ , and hence  $v'_{0r} = 0$ , therefore, if we add (9.7-1)–(9.7-3) and solve for  $v_{pm}$ , we obtain

$$v_{pm} = \frac{1}{3}(i'_{ar} R'_{ar} + i'_{br} R'_{br} + i'_{cr} R'_{cr}) \quad (9.7-4)$$

Substituting (9.7-4) into (9.7-1)–(9.7-3) yields

$$\begin{bmatrix} v'_{ar} \\ v'_{br} \\ v'_{cr} \end{bmatrix} = \frac{1}{3} \begin{bmatrix} -2R'_{ar} & R'_{br} & R'_{cr} \\ R'_{ar} & -2R'_{br} & R'_{cr} \\ R'_{ar} & R'_{br} & -2R'_{cr} \end{bmatrix} \begin{bmatrix} i'_{ar} \\ i'_{br} \\ i'_{cr} \end{bmatrix} \quad (9.7-5)$$

For the analysis of steady-state operation, it is convenient to express (9.7-5) as

$$\tilde{\mathbf{V}}'_{abc} = \mathbf{R} \tilde{\mathbf{I}}'_{abc} \quad (9.7-6)$$

where the terms of (9.7-6) can be determined by comparison with (9.7-5). If we substitute (9.7-6) into (9.6-18), we obtain

$$\tilde{\mathbf{V}}''_{qr \pm 0r} = \mathbf{S} \mathbf{R} \tilde{\mathbf{I}}'_{abc} \quad (9.7-7)$$

If we now substitute the inverse of (9.6-18) for  $\tilde{\mathbf{I}}'_{abc}$ , we can write

$$\tilde{\mathbf{V}}''_{qr \pm 0r} = \mathbf{S} \mathbf{R} (\mathbf{S})^{-1} \tilde{\mathbf{I}}'_{qr \pm 0r} \quad (9.7-8)$$

It is clear that  $\tilde{V}'_{0r}$  is zero, therefore, if we solve (9.7-8), we obtain

$$\tilde{V}''_{qr+} = -R_{abc} \tilde{I}''_{qr+} + (R'_{ABC} + jR'_{BCr}) \tilde{I}''_{qr-} \quad (9.7-9)$$

$$\tilde{V}_{qr-}'' = (R'_{ABCr} - jR'_{bcr})\tilde{I}_{qr+}'' - R'_{abcr}\tilde{I}_{qr-}'' \quad (9.7-10)$$

where

$$R'_{abcr} = \frac{1}{3}(R'_{ar} + R'_{br} + R'_{cr}) \quad (9.7-11)$$

$$R'_{ABCr} = \frac{1}{3}(-R'_{ar} + \frac{1}{2}R'_{br} + \frac{1}{2}R'_{cr}) \quad (9.7-12)$$

$$R'_{bcr} = \frac{1}{2\sqrt{3}}(R'_{br} - R'_{cr}) \quad (9.7-13)$$

Substituting (9.7-9) and (9.7-10) into (9.6-20) yields

$$\begin{bmatrix} \tilde{V}_{qs+}^r \\ 0 \\ \tilde{V}_{qs-}^r \\ 0 \end{bmatrix} = \begin{bmatrix} r_s + j\frac{\omega_e}{\omega_b}X_{ss} & j\frac{\omega_e}{\omega_b}X_M & 0 & 0 \\ j\frac{\omega_e}{\omega_b}X_M & \frac{r'_r + R'_{abcr}}{s} + j\frac{\omega_e}{\omega_b}X'_{rr} & 0 & \frac{-R'_{ABCr} - jR'_{bcr}}{s} \\ 0 & 0 & r_s + j\left(\frac{\omega_e - 2\omega_r}{\omega_b}\right)X_{ss} & j\left(\frac{\omega_e - 2\omega_r}{\omega_b}\right)X_M \\ 0 & \frac{-R'_{ABCr} + jR'_{bcr}}{s} & j\frac{\omega_e}{\omega_b}X_M & \frac{r'_r + R'_{abcr}}{s} + j\frac{\omega_e}{\omega_b}X'_{rr} \end{bmatrix} \begin{bmatrix} \tilde{I}_{qs+}^r \\ \tilde{I}_{qr+}^r \\ \tilde{I}_{qs-}^r \\ \tilde{I}_{qr-}^r \end{bmatrix} \quad (9.7-14)$$

Because the stator is assumed to be balanced,  $\tilde{V}_{qs-}^r$  in the above equation is zero and  $\tilde{V}_{qs+}^r$  is  $\tilde{V}_{as}$ . Because  $\tilde{V}_{qs-}^r$  is zero, then at  $\omega_r = (1/2)\omega_e$ ,  $\tilde{I}_{qs-}^r$  must be zero.

The acceleration characteristics of an induction machine with unbalanced rotor resistors and a constant load torque are illustrated in Figure 9.7-2. The values of the external rotor resistors are  $R'_{ar} = 0.2$  pu,  $R'_{br} = 0.1$  pu, and  $R'_{cr} = 0.05$  pu. The machine is a six-pole, three-phase, 220-V (line-to-line), 10-hp, 60-Hz machine. The parameters expressed in per unit are

$$r_s = 0.0453 \quad X_M = 2.042 \quad r'_r = 0.0222$$

$$X_{ls} = 0.0775 \quad H = 0.05 \text{ s} \quad X'_{lr} = 0.0322$$

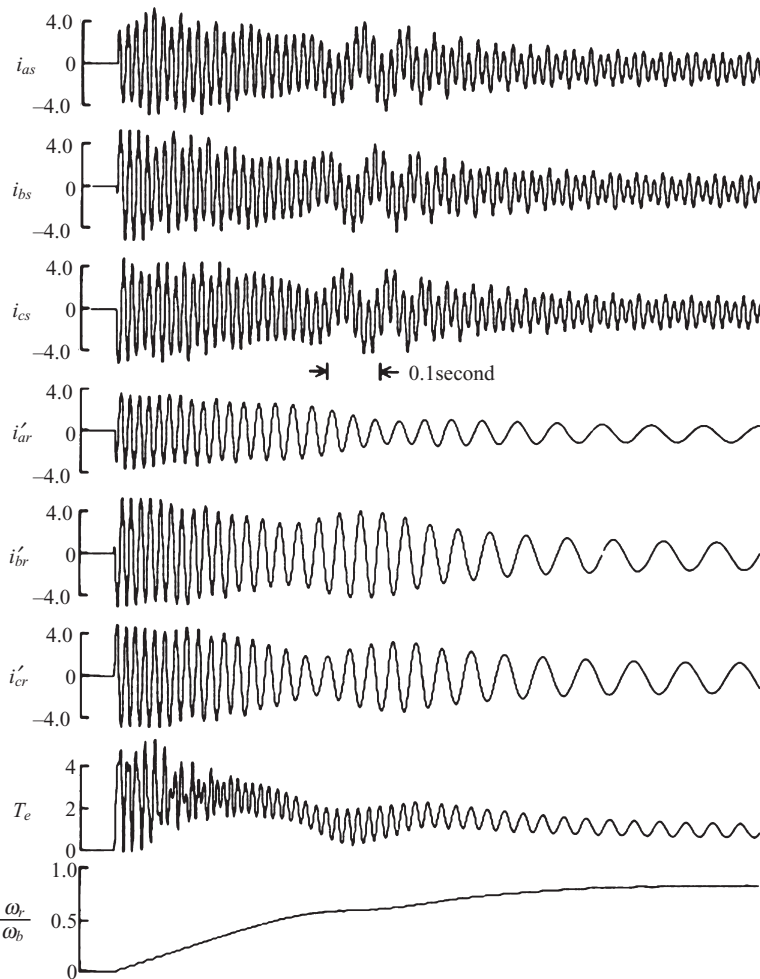


**Figure 9.7-2.** Starting characteristics of a 10-hp induction motor with unbalanced rotor resistors and 1.0 pu torque load;  $R'_{ar} = 0.2$  pu,  $R'_{br} = 0.1$  pu, and  $R'_{cr} = 0.05$  pu.

Balanced, rated stator voltages are applied, and the torque load is maintained constant at 1.0 pu.

The steady-state torque versus speed characteristics are shown in Figure 9.7-3 for balanced, rated stator voltages with the same rotor unbalance. The average torque,  $T_{e(+)}$ ,  $T_{e(-)}$ , and the zero to peak amplitude of the instantaneous, steady-state torque are plotted. The “dip” in the average torque, which occurs soon after  $\omega_r = (1/2)\omega_e$  and  $T_{e(-)}$  has become negative, is commonly referred to as “Goerges phenomenon,” named after Hans Goerges who, in the late 1800s, explained the reason why loaded induction motors

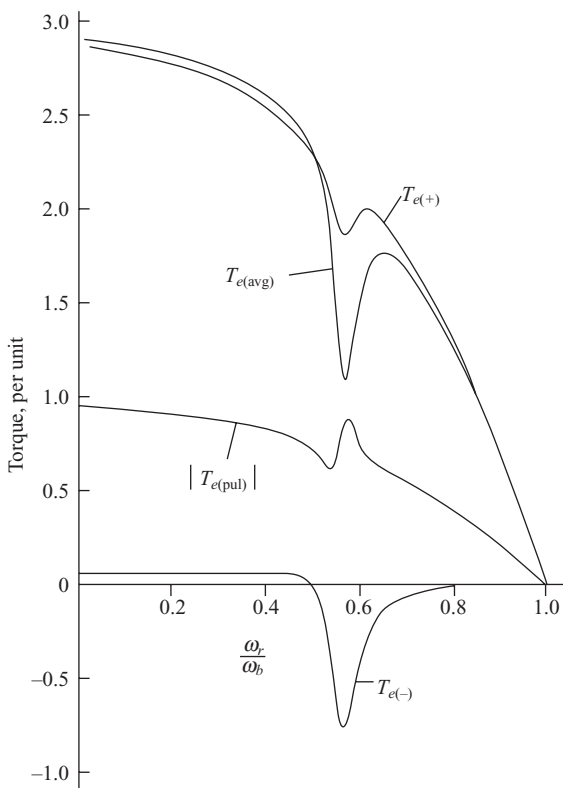


Figure 9.7-3. Steady-state torque-speed characteristics of a 10-hp induction motor with unbalanced rotor resistors as given in Figure 9.7-2.

with unbalanced rotor impedances often accelerated only to approximately half synchronous speed. This phenomenon is described in Reference 8.

## 9.8. SINGLE-PHASE INDUCTION MACHINES

The single-phase induction machine is used widely in household applications: refrigerator, washing machine, clothes dryer, furnace fan, garbage disposal, air conditioner, and so on. Although the brushless dc machine is starting to be used in some of these applications, the single-phase induction motor remains in wide use.

As we have mentioned, the single-phase induction machine cannot develop a starting torque. This is overcome by causing the currents in the stator windings of a two-phase induction machine to be out of phase. To accomplish this the impedances of the stator windings are made unequal. For example, the split-phase machine is a two-phase induction motor with the impedance of the start winding larger than that of the run winding. The asymmetry of the stator windings causes the winding currents to be

out of phase when the phases are connected to the same single-phase source. This provides a starting torque, and the start winding is generally mechanically disconnected once the rotor speed has reached 60–80% of rated speed. The starting torque may be increased by placing a capacitor in series with the start winding. This is called a capacitor-start machine. The capacitor with the start winding can be switched-out at 60–80% of rated speed or the start winding may remain connected to the source and the value of the series capacitance changed by switching out one branch of a parallel arrangement of capacitors, thus increasing the average torque at rated speed. This is referred to as a capacitor-start capacitor-run machine.

Although we may have made it appear that the split-phase machine is the type of two-phase machine that is used in single-phase applications, this is not the case. In fact, symmetrical two-phase induction machines are often used, whereupon the sizing of the series capacitor becomes the means by which starting torque is produced.

It is appropriate that we consider the analysis of the single-phase machines at this time because it is always operated in an unbalanced mode. In particular, the work we have done involving unbalanced stator voltages, unbalanced stator impedances, and open-circuited stator phase for the three-phase induction machine can, with minor modifications, be used to analyze the operating modes of single-phase machines. We will follow closely to the development for three-phase unbalanced case; however, we will limit our work to the symmetrical, two-phase induction machine. The unsymmetrical or split-phase induction machine will not be considered. It is covered in extensive detail in Reference 7.

## Voltage Equations in Arbitrary Reference Frame

Before considering single-phase operation, it is necessary to set forth the voltage equations in the arbitrary reference frame for the symmetrical two-phase induction machine. Most readers will find this a review; therefore, the equations are given with a minimum of explanation. The two-phase symmetrical induction machine is shown in Figure 9.8-1.

The change of variables that formulates a transformation of a two-phase set of variables associated with a stationary circuit to the arbitrary reference frame may be expressed as

$$\mathbf{f}_{qds} = \mathbf{K}_s \mathbf{f}_{abs} \quad (9.8-1)$$

where

$$(\mathbf{f}_{qds})^T = [f_{qs} \ f_{ds}] \quad (9.8-2)$$

$$(\mathbf{f}_{abs})^T = [f_{as} \ f_{bs}] \quad (9.8-3)$$

$$\mathbf{K}_s = \begin{bmatrix} \cos \theta & \sin \theta \\ \sin \theta & -\cos \theta \end{bmatrix} \quad (9.8-4)$$

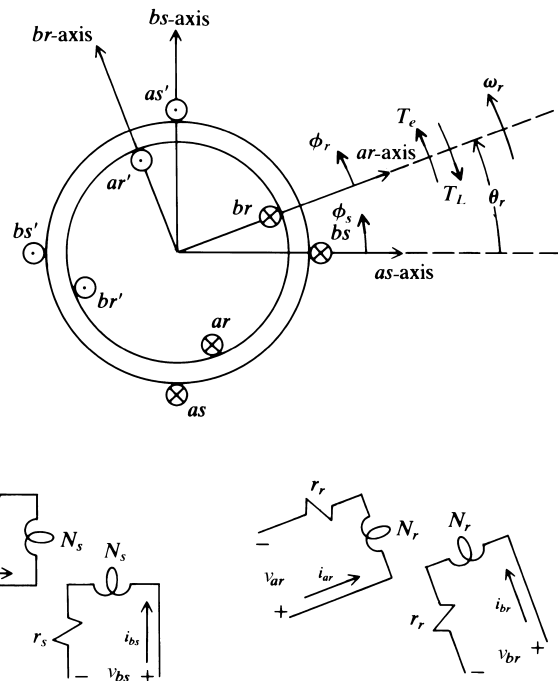


Figure 9.8-1. A two-pole two-phase symmetrical induction machine.

where  $\mathbf{K}_s = (\mathbf{K}_s)^{-1}$  and the superscript  $T$  denotes the transpose of a matrix, and the angular position may be expressed as

$$\frac{d\theta}{dt} = \omega \quad (9.8-5)$$

The change of variables that transforms the rotor variables to the arbitrary reference frame is

$$\mathbf{f}'_{qdr} = \mathbf{K}_r \mathbf{f}'_{abr} \quad (9.8-6)$$

where

$$(\mathbf{f}'_{qdr})^T = [f'_{qr} \ f'_{dr}] \quad (9.8-7)$$

$$(\mathbf{f}'_{abr})^T = [f'_{ar} \ f'_{br}] \quad (9.8-8)$$

$$\mathbf{K}_r = \begin{bmatrix} \cos \beta & \sin \beta \\ \sin \beta & -\cos \beta \end{bmatrix} \quad (9.8-9)$$

where  $\mathbf{K}_s = (\mathbf{K}_s)^{-1}$  and

$$\frac{d\beta}{dt} = \omega - \omega_r \quad (9.8-10)$$

The voltage equations in the arbitrary reference frame are

$$v_{qs} = r_s i_{qs} + \omega \lambda_{ds} + p \lambda_{qs} \quad (9.8-11)$$

$$v_{ds} = r_s i_{ds} - \omega \lambda_{qs} + p \lambda_{ds} \quad (9.8-12)$$

$$v'_{qr} = r'_r i'_{qr} + (\omega - \omega_r) \lambda'_{dr} + p \lambda'_{qr} \quad (9.8-13)$$

$$v'_{dr} = r'_r i'_{dr} - (\omega - \omega_r) \lambda'_{qr} + p \lambda'_{dr} \quad (9.8-14)$$

where

$$\lambda_{qs} = L_{ls} i_{qs} + L_{ms} (i_{qs} + i'_{qr}) \quad (9.8-15)$$

$$\lambda_{ds} = L_{ls} i_{ds} + L_{ms} (i_{ds} + i'_{dr}) \quad (9.8-16)$$

$$\lambda'_{qr} = L'_{lr} i'_{qr} + L_{ms} (i_{qs} + i'_{qr}) \quad (9.8-17)$$

$$\lambda'_{dr} = L'_{lr} i'_{dr} + L_{ms} (i_{ds} + i'_{dr}) \quad (9.8-18)$$

## Unbalanced Machine Variables in Arbitrary Reference Frame

Unbalanced steady-state, two-phase stator variables may be written as

$$\begin{bmatrix} F_{as} \\ F_{bs} \end{bmatrix} = \begin{bmatrix} F_{as\alpha} & F_{as\beta} \\ F_{bs\alpha} & F_{bs\beta} \end{bmatrix} \begin{bmatrix} \cos \omega_e t \\ \sin \omega_e t \end{bmatrix} \quad (9.8-19)$$

Transforming to the arbitrary reference frame by substituting (9.8-19) into (9.8-1) yields an equation of the same form as (9.4-2). Thus

$$\begin{bmatrix} F_{qs} \\ F_{ds} \end{bmatrix} = \begin{bmatrix} \cos(\omega_e t - \theta) & \sin(\omega_e t - \theta) & \cos(\omega_e t + \theta) & \sin(\omega_e t + \theta) \\ -\sin(\omega_e t - \theta) & \cos(\omega_e t - \theta) & \sin(\omega_e t + \theta) & -\cos(\omega_e t + \theta) \end{bmatrix} \begin{bmatrix} F_{qsA} \\ F_{qsB} \\ F_{qsC} \\ F_{qsD} \end{bmatrix} \quad (9.8-20)$$

where

$$\begin{aligned} F_{qsA} &= \frac{1}{2} (F_{as\alpha} - F_{bs\beta}) \\ &= -F_{dsB} \end{aligned} \quad (9.8-21)$$

$$\begin{aligned} F_{qsB} &= \frac{1}{2} (F_{as\beta} - F_{bs\alpha}) \\ &= F_{dsA} \end{aligned} \quad (9.8-22)$$

$$\begin{aligned} F_{qsC} &= \frac{1}{2}(F_{as\alpha} + F_{bs\beta}) \\ &= F_{dsD} \end{aligned} \quad (9.8-23)$$

$$\begin{aligned} F_{qsD} &= \frac{1}{2}(F_{as\beta} + F_{bs\alpha}) \\ &= -F_{dsC} \end{aligned} \quad (9.8-24)$$

The sinusoidal variations with the argument of  $(\omega_e t - \theta)$  are the positive-sequence variables; the negative-sequence variables have the argument  $(\omega_e t + \theta)$ . We can write (9.8-20) as

$$F_{qs} = F_{qs+} + F_{qs-} \quad (9.8-25)$$

$$F_{ds} = F_{ds+} + F_{ds-} \quad (9.8-26)$$

The torque equations given by (9.4-13) and (9.4-14) can be used to calculate the torque for a two-phase machine if the  $(3/2)$  factor is eliminated, and  $X_M$  is replaced by  $X_{ms}$ , and  $\omega_b$  is generally the rated angular velocity.

## Phasor Relationships

If we express the variables in the stationary reference frame in phasor form wherein  $\theta$  is set equal to zero; then  $\tilde{F}_{as} = \tilde{F}_{qs}^s$  and  $\tilde{F}_{bs} = -\tilde{F}_{ds}^s$ , and we can write from (9.4-20)

$$\begin{bmatrix} \tilde{F}_{qs+}^s \\ \tilde{F}_{qs-}^s \end{bmatrix} = \frac{1}{2} \begin{bmatrix} 1 & j \\ 1 & -j \end{bmatrix} \begin{bmatrix} \tilde{F}_{as} \\ \tilde{F}_{bs} \end{bmatrix} \quad (9.8-27)$$

where the symmetrical component transformation for a two-phase system is

$$\mathbf{S} = \frac{1}{2} \begin{bmatrix} 1 & j \\ 1 & -j \end{bmatrix} \quad (9.8-28)$$

$$(\mathbf{S})^{-1} = \begin{bmatrix} 1 & 1 \\ -j & j \end{bmatrix} \quad (9.8-29)$$

Following a similar procedure, we can write

$$\tilde{F}_{qr}^s = \tilde{F}_{qr+}^s + \tilde{F}_{qr-}^s \quad (9.8-30)$$

$$\tilde{F}_{dr}^s = \tilde{F}_{dr+}^s + \tilde{F}_{dr-}^s \quad (9.8-31)$$

and

$$\tilde{F}_{dr+}^s = j \tilde{F}_{qr+}^s \quad (9.8-32)$$

$$\tilde{F}_{dr-}^s = -j \tilde{F}_{qr-}^s \quad (9.8-33)$$

The steady-state torque may be calculated using (9.4-34) if the three multiplier is replaced by two and  $X_M$  with  $X_{ms}$ .

### Unbalanced Stator Impedances

During the capacitor-start and capacitor-start, capacitor-run modes of operation, a capacitor is placed in series with one of the stator windings. For this purpose, let

$$e_{ga} = i_{as}z(p) + v_{as} \quad (9.8-34)$$

$$e_{gb} = v_{bs} \quad (9.8-35)$$

where  $v_{as}$  and  $v_{bs}$  are the voltages across the stator phases and  $e_{ga}$  and  $e_{gb}$  are source voltages, and  $z(p)$  is the operational impedance in series with the  $as$ -winding. In phasor form, we have

$$\tilde{V}_{as} = \tilde{E}_{ga} - \tilde{I}_{as}Z \quad (9.8-36)$$

$$\tilde{V}_{bs} = \tilde{E}_{gb} \quad (9.8-37)$$

where  $Z$  is the impedance. Following a procedure similar to that for the three-phase induction machine, we can write

$$\begin{bmatrix} \tilde{E}_1 \\ 0 \\ \tilde{E}_2 \\ 0 \end{bmatrix} = \begin{bmatrix} \frac{1}{2}Z + r_s + j\frac{\omega_e}{\omega_b}X_{ss} & j\frac{\omega_e}{\omega_b}X_{ms} & \frac{1}{2}Z & 0 \\ j\frac{\omega_e}{\omega_b}X_{ms} & \frac{r'_r}{s} + j\frac{\omega_e}{\omega_b}X'_{rr} & 0 & 0 \\ \frac{1}{2}Z & 0 & \frac{1}{2}Z + r_s + j\frac{\omega_e}{\omega_b}X_{ss} & j\frac{\omega_e}{\omega_b}X_{ms} \\ 0 & 0 & j\frac{\omega_e}{\omega_b}X_{ms} & \frac{r'_r}{2-s} + j\frac{\omega_e}{\omega_b}X'_{rr} \end{bmatrix} \begin{bmatrix} \tilde{I}_{qs+}^s \\ \tilde{I}_{qr+}^s \\ \tilde{I}_{qs-}^s \\ \tilde{I}_{qr-}^s \end{bmatrix} \quad (9.8-38)$$

where

$$\tilde{E}_1 = \frac{1}{2}(\tilde{E}_{ga} + j\tilde{E}_{gb}) \quad (9.8-39)$$

$$\tilde{E}_2 = \frac{1}{2}(\tilde{E}_{ga} - j\tilde{E}_{gb}) \quad (9.8-40)$$

## Open-Circuited Stator Phase

In the capacitor-start mode of operation, the induction machine operates with only one winding energized once the rotor has reached 60–80% of rated speed. If we assume it is the *as*-winding, which is open-circuited then because  $v_{as}$  is  $v_{qs}^s$  with  $\theta = 0$

$$v_{qs}^s = p\lambda_{qs}^s \quad (9.8-41)$$

Because  $i_{as}$  is zero,  $i_{qs}^s$  is zero, and from (9.8-15), we can write

$$\lambda_{qs}^s = L_{ms}i_{qr}^s \quad (9.8-42)$$

Thus, during open-circuit operation, we have

$$v_{as} = \frac{X_{ms}}{\omega_b} pi_{qr}^s \quad (9.8-43)$$

$$v_{bs} = e_{gb} \quad (9.8-44)$$

Substituting into (9.8-27) yields

$$\tilde{V}_{qs+}^s = \frac{1}{2} j \frac{X_{ms}}{\omega_b} \tilde{I}_{qr}^s + \frac{1}{2} j \tilde{E}_{gb} \quad (9.8-45)$$

$$\tilde{V}_{qs-}^s = \frac{1}{2} j \frac{X_{ms}}{\omega_b} \tilde{I}_{qr}^s - \frac{1}{2} j \tilde{E}_{gb} \quad (9.8-46)$$

and because  $\tilde{I}_{as} = 0$ , we have

$$\tilde{I}_{qs-} = -\tilde{I}_{qs+} \quad (9.8-47)$$

Following a procedure similar to that for the three-phase machine, we can write

$$\begin{bmatrix} -\frac{1}{2} j \tilde{E}_{gb} \\ 0 \\ 0 \end{bmatrix} = \begin{bmatrix} r_s + j \frac{\omega_e}{\omega_b} X_{ss} & j \frac{1}{2} \frac{\omega_e}{\omega_b} X_{ms} & -j \frac{1}{2} \frac{\omega_e}{\omega_b} X_{ms} \\ j \frac{\omega_e}{\omega_b} X_{ms} & \frac{r'_r}{s} + j \frac{\omega_e}{\omega_b} X'_{rr} & 0 \\ -j \frac{\omega_e}{\omega_b} X_{ms} & 0 & \frac{r'_r}{2-s} + j \frac{\omega_e}{\omega_b} X'_{rr} \end{bmatrix} \begin{bmatrix} \tilde{I}_{qs+}^s \\ \tilde{I}_{qr+}^s \\ \tilde{I}_{qr-}^s \end{bmatrix} \quad (9.8-48)$$

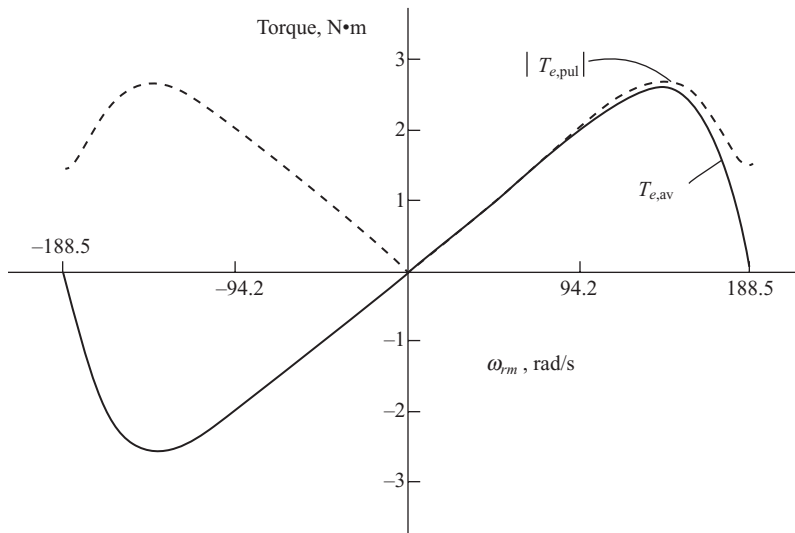


Figure 9.8-2. Steady-state torque versus speed characteristics for a single-phase induction motor.

### Operating Characteristics of Single-Phase Induction Motors

The steady-state torque versus speed characteristics are shown in Figure 9.8-2 for a symmetrical two-phase induction motor with rated voltage applied to one phase and the other phase open circuited. The symmetrical two-phase induction machine is a four-pole, (1/4)-hp, 110-V, 60-Hz motor with the following parameters:  $r_s = 2.02\Omega$ ,  $X_{ls} = 2.79\Omega$ ,  $X_{ms} = 66.8\Omega$ ,  $r'_s = 4.12\Omega$ , and  $X'_{ls} = 2.12\Omega$ . The total inertia is  $J = 1.46 \times 10^{-2}\text{ kg} \cdot \text{m}^2$ .

The average steady-state electromagnetic torque  $T_{e,av} = T_{e+} - T_{e-}$  and the magnitude of the double-frequency component of the torque  $|T_{e,pul}|$  are plotted in Figure 9.8-2. There are at least two features worth mentioning. First, the plot of the average torque  $T_{e,av}$  for  $\omega_{rm} < 0$  is the negative mirror image of that for  $\omega_{rm} > 0$ . Second, the plot of the pulsating torque  $|T_{e,pul}|$  is symmetrical about the zero speed axis. Finally, we see that the torque is zero at  $\omega_{rm} = 0$ .

If we take a two-phase symmetrical induction motor and apply the same single-phase voltage to both phases, the net torque at stall will be zero because the winding currents will be instantaneously equal and the air-gap MMF will pulsate along an axis midway between the *as*- and *bs*-axes. Consequently, two equal and oppositely rotating air-gap MMFs result. If, however, we cause the current in one of the phases to be different instantaneously from that in the other phase, a starting torque can be developed because this would make one of the rotating air-gap MMFs larger than the other. One way of doing this is to place a capacitor in series with one of the windings of a two-phase symmetrical induction motor. This will cause the current in the phase with the

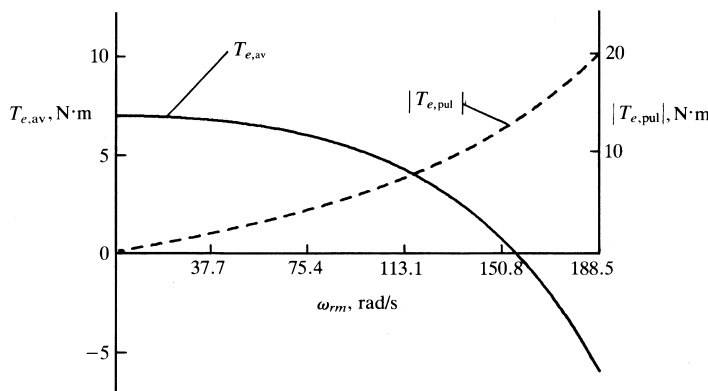


**Figure 9.8-3.** Steady-state torque versus speed characteristics with a capacitor in series with one winding of the two-phase induction machine.

series capacitor to lead the current in the other winding when the same voltage is applied to both.

We have already derived the equations necessary to calculate the component currents with an impedance in series with the *as* winding. In particular, (9.8-38) can be used to calculate the component currents with a capacitor in series with the *as* winding. If we set  $Z = -j1/\omega_e C$ , and let  $\tilde{E}_{ga} = \tilde{E}_{gb}$ , the single-phase source voltage, counterclockwise rotation will occur because  $\tilde{I}_{as}$  will lead  $\tilde{I}_{bs}$ . Recall that for the assumed positive direction of the magnetic axes and for a balanced two-phase set, we have had  $\tilde{I}_{as}$  leading  $\tilde{I}_{bs}$  by  $90^\circ$  for counterclockwise rotation of the air-gap MMF. These steady-state torque versus speed characteristics are shown in Figure 9.8-3 for  $C = 530.5 \mu\text{F}$ .

In capacitor-start, single-phase induction motors, the winding with the series capacitor is disconnected from the source after the rotor has reached 60–80% of synchronous speed. This is generally accomplished by a centrifugal switching mechanism located inside the housing of the motor. Once the winding with the series capacitor is disconnected, the device then operates as a single-phase induction motor. In Figure 9.8-4, the plot of average torque versus speed with a series capacitor in one phase (Fig. 9.8-3) is superimposed upon the plot of average torque versus speed with a single-phase winding (Fig. 9.8-2). The transition from capacitor-start to single-phase operation at 75% of synchronous speed is illustrated.

The free acceleration characteristics of the example capacitor-start single-phase induction motor are shown in Figure 9.8-5. The variables  $v_{as}$ ,  $i_{as}$ ,  $v_{bs}$ ,  $i_{bs}$ ,  $v_c$ ,  $T_e$ , and  $\omega_{rm}$  are plotted. The voltage  $v_c$  is the instantaneous voltage across the capacitor that is connected in series with the *bs* winding, which is disconnected from the source at a normal current zero once the rotor reaches 75% of synchronous speed. The voltage across the capacitor is shown to remain constant at its value when the *bs* winding is disconnected from the source. In practice, this voltage would slowly decay owing to leakage currents within the capacitor, which are not considered in this analysis. The

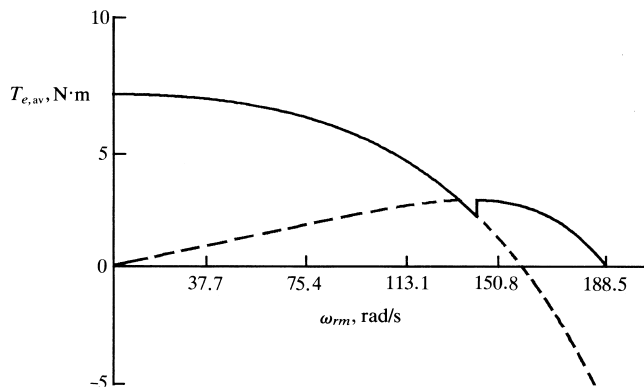


Figure 9.8-4. Average steady-state torque versus speed characteristics of a capacitor-start single-phase induction motor.

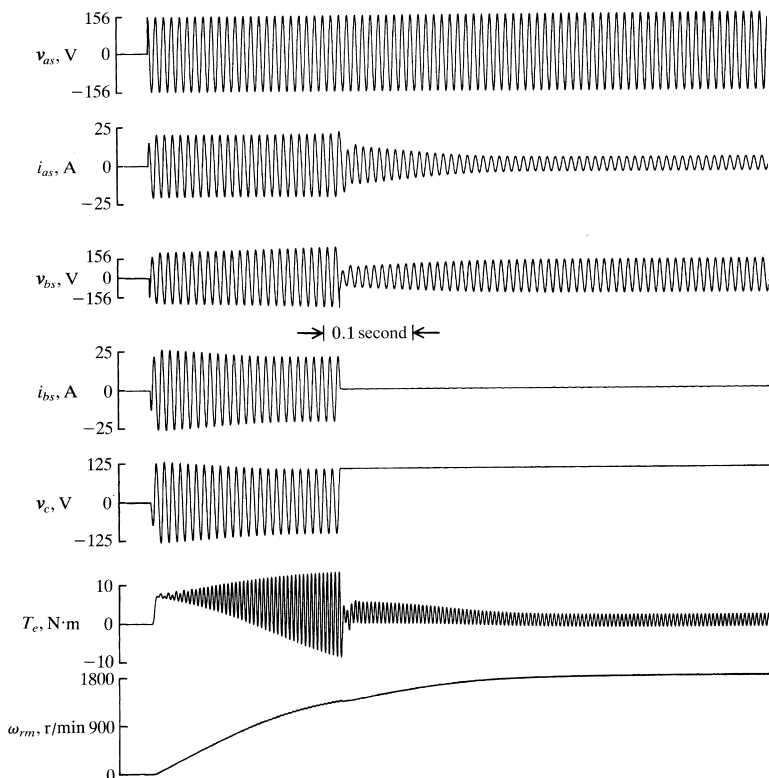


Figure 9.8-5. Free-acceleration characteristics of a capacitor-start single-phase induction motor.

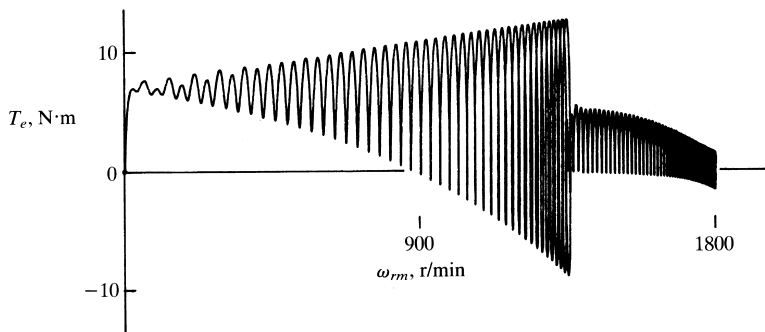


Figure 9.8-6. Torque versus speed characteristics for Figure 9.8-5.

torque versus speed characteristics given in Figure 9.8-6 are for the free acceleration shown in Figure 9.8-5.

## 9.9. ASYNCHRONOUS AND UNBALANCED OPERATION OF SYNCHRONOUS MACHINES

The analysis of unbalanced operation of synchronous machines is quite involved, requiring manipulation of a large number of equations to calculate even steady-state performance. This complexity is actually anticipated because the machine is electrically unsymmetrical in the rotor, and when a stator unbalance occurs, such as a line-to-ground fault, a series of harmonic voltages is induced due to the asymmetry of the rotor circuits and the network external to the machine. Although the transient performance of a synchronous machine during unbalanced stator conditions is of interest, the analysis of steady-state performance is of limited value, since in practice, an unbalanced condition due to a system fault is generally removed before the machine reaches steady-state operation. On the other hand, the analysis of steady-state performance of a synchronous machine during asynchronous operation (pole slipping) is of importance.

Over the years, there have been several approximate methods set forth to analyze unbalanced operation of synchronous machines [3, 9]. For the most part, this work has been directed toward simplified representations of a synchronous machine to approximate its dynamic performance during unbalanced faults in the same way that the voltage behind transient reactance representation (Chapter 5) is used to approximate the dynamic behavior during symmetrical disturbances. We will not become involved in a lengthy analyses because, as we have mentioned, the solutions are of limited value. Instead, we will use computer solutions to demonstrate various modes of unbalanced operation.

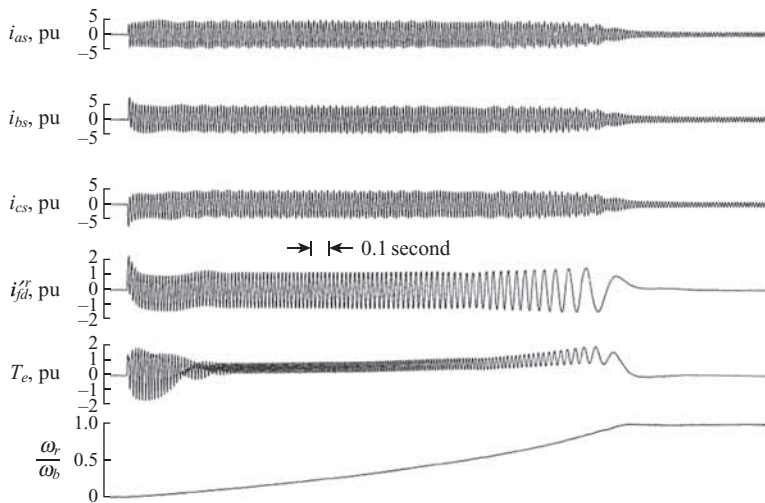


Figure 9.9-1. Free acceleration of synchronous motor with  $H = 1.0$  second and no load.

## Motor Starting

The free acceleration characteristics of a synchronous motor with the field winding short circuited are shown in Figure 9.9-1. The per unit parameters of this 60-Hz, eight-pole, 4-kV, 6000-hp machine are

$$\begin{aligned}
 r_s &= 0.0121 & X_{md} &= 1.03 & r'_{kd} &= 0.0302 \\
 X_{ls} &= 0.140 & X_{mq} &= 0.75 & X'_{lkq} &= 0.092 \\
 r'_{kq} &= 0.039 & H &= 1 \text{ s} & r'_{fd} &= 0.00145 \\
 X'_{lkq} &= 0.115 & & & X'_{ifd} &= 0.267
 \end{aligned}$$

In Figure 9.9-1,  $i_{as}$ ,  $i_{bs}$ ,  $i_{cs}$ ,  $i'_{fd}$ ,  $T_e$ , and  $\omega_r/\omega_b$  are plotted with the peak value of rated stator current taken as 1.0 pu. The voltages applied to the stator windings are balanced, and  $i_{as}$  is assumed positive into the machine and  $T_e$  is positive for motor action. During the acceleration period shown in Figure 9.9-1, the field winding is short-circuited through a discharge resistor, making the total field circuit resistance 0.3 pu. The friction and windage losses are neglected, and since there is no mechanical load on the shaft of the machine, it accelerates to synchronous speed without applying a voltage to the field winding as the machine approaches synchronous speed. The steady-state torque speed characteristics of this machine are shown in Figure 9.9-2. Therein the average torque  $T_{e,av}$  and the zero-to-peak amplitude of the pulsating torque  $|T_{e,pul}|$  are plotted. These plots are calculated using a procedure similar to that in the case of unbalanced rotor resistors of an induction machine. It is interesting to compare the plot of average

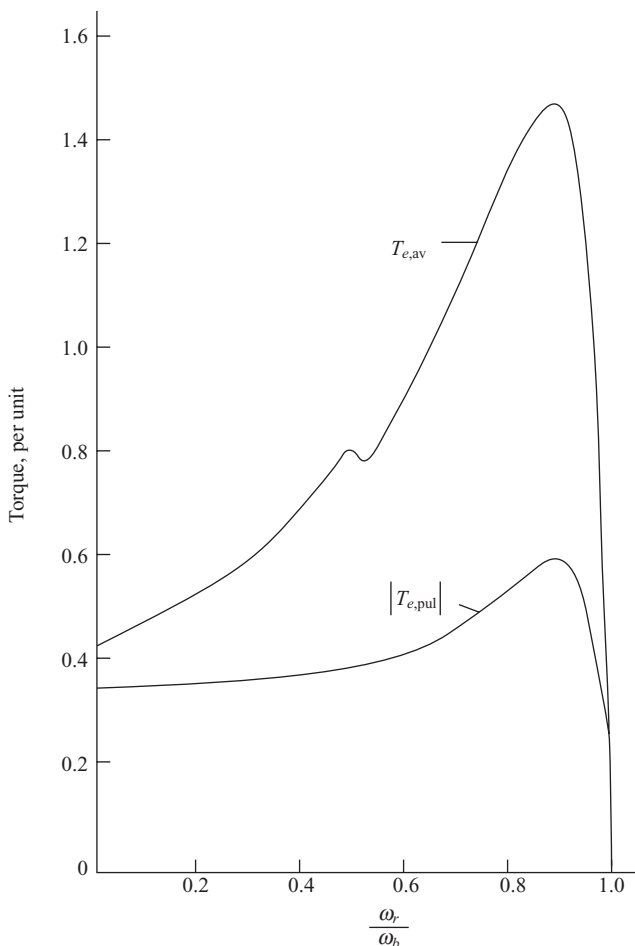


**Figure 9.9-2.** Steady-state torque-speed characteristics of the same synchronous motor depicted in Figure 9.9-1.

torque with that in Figure 9.7-3 where the “one-half speed dip” is more pronounced. The pulling into step after applying the field voltage is illustrated in Figure 9.9-3. In this case, the machine is loaded with a small shaft load (0.2 pu) to simulate friction and windage losses and/or a small external mechanical load. The total shaft inertia, including the mechanical load, is 4 seconds. The machine fails to pull into synchronism and instead operates as an induction motor at a speed slightly less than synchronous. Only the very last portion of the acceleration period is shown. At a normal field current zero, the discharge resistor is disconnected or bypassed and simultaneously, 1.0 pu field voltage ( $E'_{xd}^r$ ) is applied to the field winding. The machine pulls into step and operates as a synchronous motor.

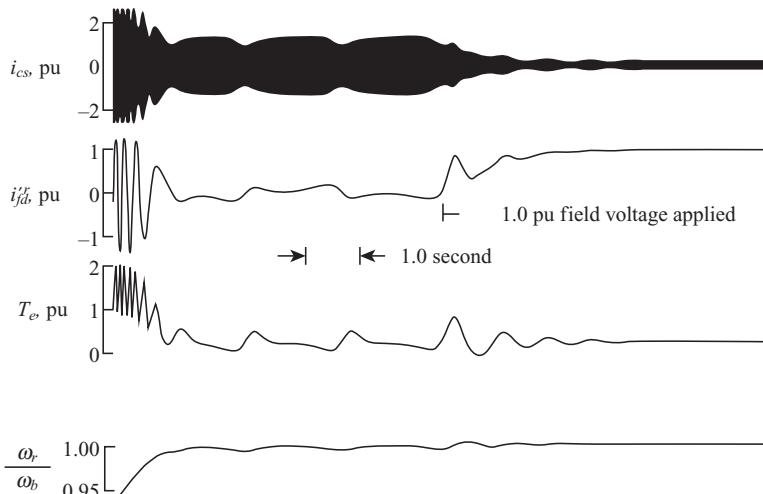


**Figure 9.9-3.** Pulling into step after applying 1.0 pu field voltage with  $H = 4.0$  seconds and  $T_L = 0.2$  pu.

### Pole Slipping

Asynchronous operation of a hydro turbine generator is demonstrated in Figure 9.9-4. The parameters for the hydro turbine generator are given in Section 5.10. The machine is initially operating steadily at rated conditions as in Figure 5.10-8. In particular, the input torque is constant at 0.85 pu and  $E_{sfd}''$  fixed at 1.6 pu. The stator and field currents are plotted along with  $T_e$ ,  $\omega_r/\omega_b$ , and  $\delta$ . A three-phase fault occurs at the terminals, which reduces the voltages instantaneously to zero at the instant  $v_{as}$  passes through zero going positive. In Figure 5.10-8, the fault was removed in 0.466 seconds; the machine returned to synchronous speed with the rotor speed and angle reaching maximum of approximately 2.2% (above synchronous speed) and  $164^\circ$ , respectively. In Figure 9.9-4, the three-phase fault remains on the terminals of the machine for approximately 0.8 second. When the fault is removed, the rotor speed is approximately 4% above synchronous speed and the rotor angle is approximately  $400^\circ$ . In other words, the rotor has advanced more than one revolution ahead of the system. Here, it is helpful to recall the definition of  $\delta$  given by (5.7-1). When the rotor advances  $360^\circ$  from its original operating point, it is said to have “slipped a pole.” In Figure 9.9-4, the machine slips a pole before returning to synchronous speed. If the fault had remained for only slightly longer, the machine would not have been able to return to synchronous speed.

Due to the possibility of damage to the mechanical system resulting from large average torques (in excess of 3 pu in Fig. 9.9-4), and due to the large stator currents that occur during pole slipping, power systems are generally designed to protect against its occurrence. In particular, overspeed protection would prevent reclosing the machine back onto the system if the rotor speed exceeds a predetermined value of generally between 3% and 5% of synchronous speed of the rotor.

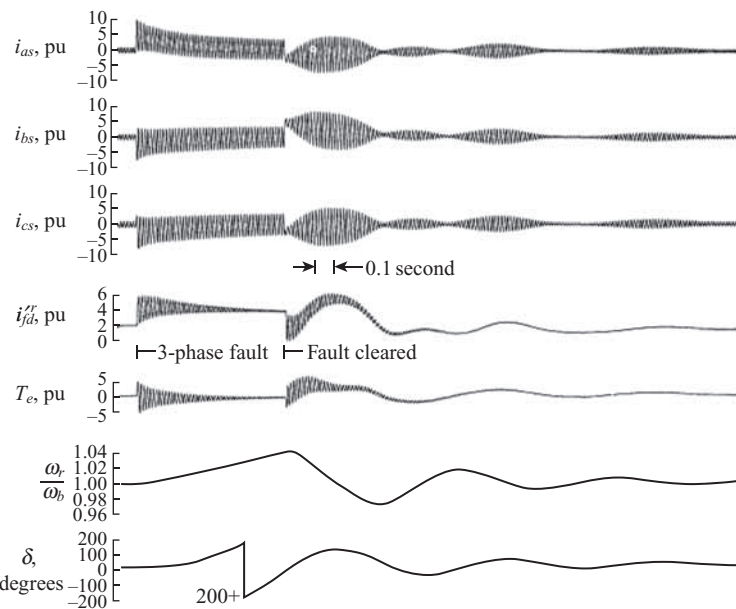


Figure 9.9-4. Pole slipping of hydro turbine generator.

### Line-to-Neutral Fault

The behavior of the steam turbine generator during a line-to-neutral fault is shown in Figure 9.9-5. The parameters are given in Section 5.10. The machine is initially operating at rated conditions with the input torque equal to 2.48 pu for the steam turbine generator. The line-to-neutral fault was applied to phase  $a$  at the instant  $v_{as}$  passed through zero going positive. It was assumed that the neutral of the wye-connected source voltage is connected to the neutral of the wye-connected stator windings. Thus, during the fault

$$v_{as} = 0 \quad (9.9-1)$$

$$v_{bs} = e_{gb} \quad (9.9-2)$$

$$v_{cs} = e_{gc} \quad (9.9-3)$$

where  $e_{gb}$  and  $e_{gc}$  are the source voltages. After 0.25 second, the fault was removed and the source voltage ( $e_{ga}$ ) instantaneously reapplied. The currents  $i_{as}$ ,  $i_{bs}$ ,  $i_{cs}$ , and  $i_{fd}'$  are plotted along with  $T_e$ ,  $\omega_r/\omega_b$  and  $\delta$ . Following the fault, the initial steady-state operating condition is reestablished. With the exception of the high value of  $i_{as}$ , this fault is not severe; in fact, the machine would remain in synchronism during a sustained line-to-neutral fault of this type.

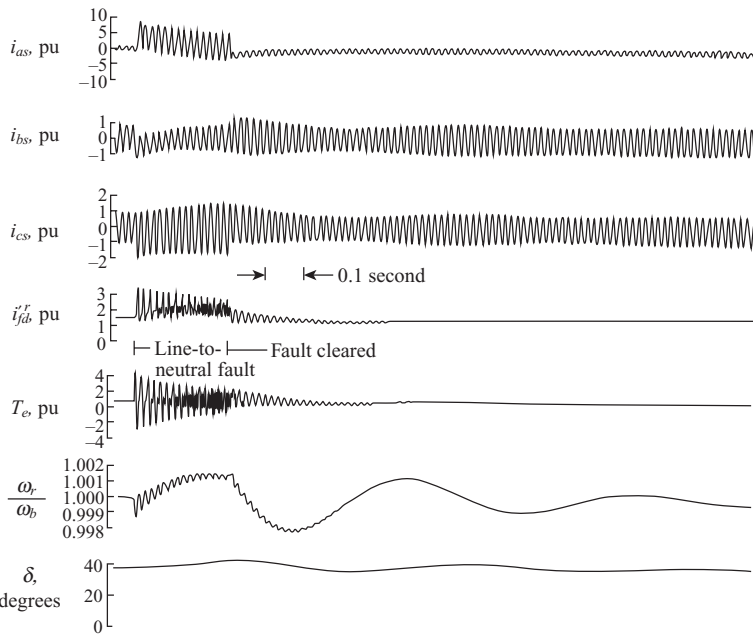


**Figure 9.9-5.** Dynamic performance of a steam turbine generator during a line-to-neutral fault at the terminals.

### Line-to-Line Fault

The performance of the steam turbine generator during and following a line-to-line fault is shown in Figure 9.9-6. Again, the machine was initially operating at rated conditions. Phases *a* and *b* were short-circuited at the terminals at the instant  $v_{as}$  passed through zero going positive. The fault was removed and the voltages reapplied after 0.25 second. In each case, the neutral of the machine and source were connected, therefore, during the fault, we have

$$v_{as} = v_{bs} \quad (9.9-4)$$

$$v_{cs} = e_{gc} \quad (9.9-5)$$

### Line-to-Line-to-Neutral Fault

The behavior of the steam generator during and following a line-to-line-to-neutral (double line-to neutral) fault is demonstrated in Figure 9.9-7. With the machine operating at rated conditions, the terminals of phases *a* and *b* are short circuited to the neutral at the instant  $v_{as}$  passes through zero going positive. It is again assumed that the neutrals of the source voltages and the stator windings are connected. Thus, during the fault we have

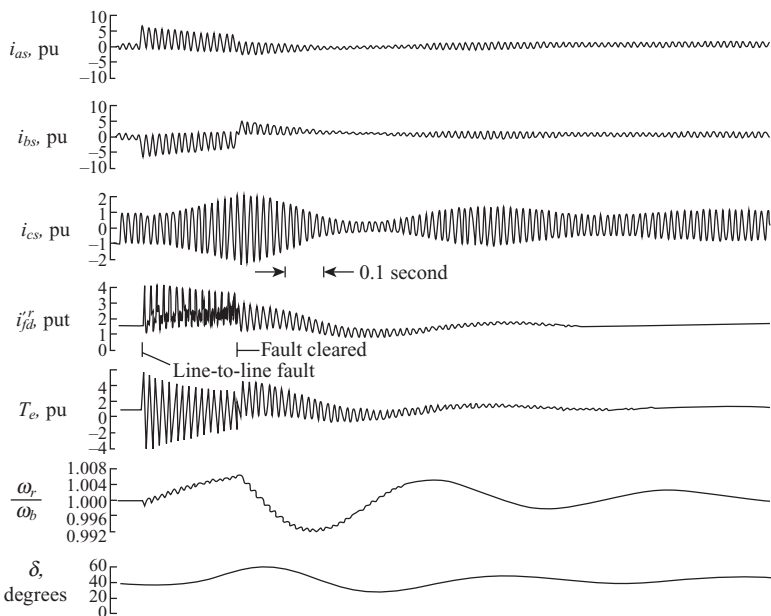


Figure 9.9-6. Dynamic performance of a steam turbine generator during a line-to-line fault at the terminals.

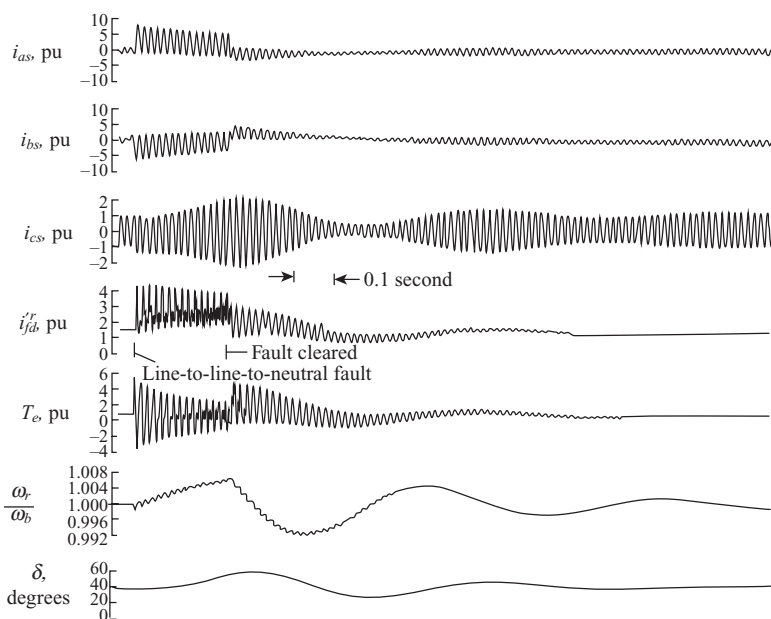


Figure 9.9-7. Dynamic performance of a steam turbine generator during a line-to-line-to-neutral fault at the terminals.

$$v_{as} = v_{bs} = 0 \quad (9.9-6)$$

$$v_{cs} = e_{gc} \quad (9.9-7)$$

## REFERENCES

- [1] C.L. Fortescue, "Method of Symmetrical Co-ordinates Applied to the Solution of Polyphase Networks," *AIEE Trans.*, Vol. 37, 1918, pp. 1027–1115.
- [2] E. Clarke, *Circuit Analysis of A-C Power Systems*, Vols. I and II, John Wiley and Sons, New York, 1943 and 1950.
- [3] W.V. Lyon, *Transient Analysis of Alternating-Current Machinery*, Technology Press of MIT and John Wiley and Sons, New York, 1954.
- [4] D.C. White and H.H. Woodson, *Electromechanical Energy Conversion*, John Wiley and Sons, New York, 1959.
- [5] Y.H. Ku, *Electric Energy Conversion*, Ronald Press, New York, 1959.
- [6] P.C. Krause, "The Method of Symmetrical Components Derived by Reference Frame Theory," *IEEE Trans. Power App. Syst.*, Vol. 104, June 1985, pp. 1492–1499.
- [7] P.C. Krause, O. Waszczuk, and S. Sudhoff, *Analysis of Electric Machinery and Drive Systems*, 2nd ed., IEEE Press, Piscataway, NJ, and John Wiley & Sons, New York, 2002.
- [8] H.L. Garbarino and E.T.B. Gross, "The Goerges Phenomenon—Induction Motors with Unbalanced Rotor Impedances," *AIEE Trans.*, Vol. 69, 1950, pp. 1569–1575.
- [9] C. Concordia, *Synchronous Machines*, John Wiley and Sons, New York, 1951.

## PROBLEMS

1. Show that, for a given source frequency,  $|T_{e,pul}|$  is zero for  $\omega_r = 0$  when the stator voltages are unbalanced and the induction machine is singly fed.
2. Consider the stator circuit shown in Figure 9.5-1. Assume

$$e_{ga} = \sqrt{2} \cos 377t$$

$$e_{gb} = \frac{\sqrt{2}}{2} \cos \left( 377t - \frac{2\pi}{3} \right)$$

$$e_{gc} = \sqrt{2} \cos \left( 377t + \frac{\pi}{2} \right)$$

The induction machine is the 10-hp machine given in Section 9.7. Calculate the torque for  $\omega_r/\omega_b$  of 0, 0.1, 0.2, . . . , 1.0. Plot  $T_{e+}$ ,  $T_{e-}$ , and  $|T_{e,pul}|$ .

3. A dc voltage of 1.0 pu is applied across two stator terminals of the 10-hp machine given in Section 9.7. Plot the steady-state torque-speed characteristics for  $-1.0 \leq \omega_r / \omega_b \leq 1.0$ .

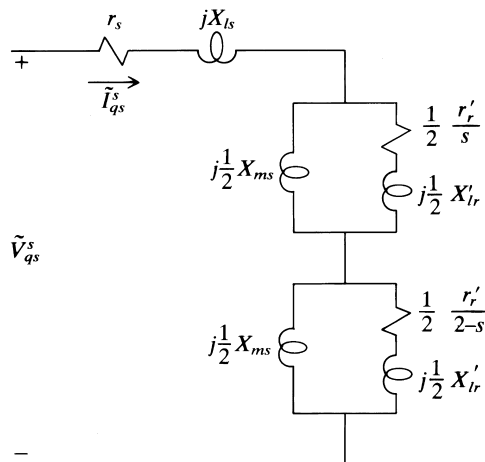


Figure 9P-1. Equivalent circuit for single-phase winding.

4. Determine the set of voltage equations similar to (9.5-18) that can be used to analyze the steady-state performance of an induction machine with an impedance  $z(p)$  in series with (a) the bs winding and (b) the cs winding.
5. Determine the set of voltage equations similar to (9.5-18) that can be used to analyze the steady-state performance of an induction machine with an impedance  $z(p)$  in series with the *as* winding and supplied from an unbalanced set of source voltages.
6. Express  $v_{sa}$  in Figure 9.5-3 in terms of the source voltages and  $v_{as}$ , then write a phasor expression for  $\tilde{V}_{sa}$ .
7. Derive the voltage equations in a form similar to (9.8-48) for (a)  $i_{bs} = 0$  and (b)  $i_{cs} = 0$ .
8. Derive the voltage equations for a three-phase induction machine with  $i'_{ar} = 0$ .
9. What modifications must be made to (9.4-32) in order to analyze unbalanced stator voltages of a two-phase symmetrical induction motor.
10. The equivalent circuit given in Figure 9P-1 is for an induction motor with only one stator winding. Show that this equivalent circuit is the same as (9.8-48).

# DC MACHINES AND DRIVES

## 10.1. INTRODUCTION

The direct-current (dc) machine is not as widely used today as it was in the past. For the most part, the dc generator has been replaced by solid-state rectifiers. Nevertheless, it is still desirable to devote some time to the dc machine since it is still used as a drive motor, especially at the low-power level. Numerous textbooks have been written over the last century on the design, theory, and operation of dc machines. One can add little to the analytical approach that has been used for years. In this chapter, the well-established theory of dc machines is set forth, and the dynamic characteristics of the shunt and permanent-magnet machines are illustrated. The time-domain block diagrams and state equations are then developed for these two types of motors.

## 10.2. ELEMENTARY DC MACHINE

It is instructive to discuss the elementary machine shown in Figure 10.2-1 prior to a formal analysis of the performance of a practical dc machine. The two-pole elementary machine is equipped with a field winding wound on the stator poles, a rotor coil ( $a-a'$ ),

---

*Analysis of Electric Machinery and Drive Systems*, Third Edition. Paul Krause, Oleg Wasenczuk, Scott Sudhoff, and Steven Pekarek.

© 2013 Institute of Electrical and Electronics Engineers, Inc. Published 2013 by John Wiley & Sons, Inc.

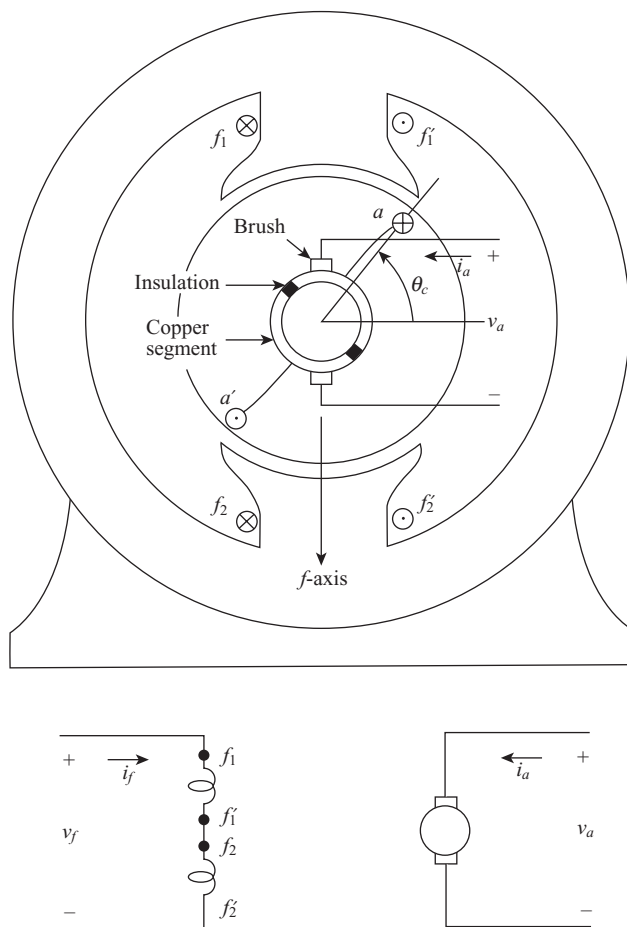


Figure 10.2-1. Elementary two-pole dc machine.

and a commutator. The commutator is made up of two semicircular copper segments mounted on the shaft at the end of the rotor and insulated from one another as well as from the iron of the rotor. Each terminal of the rotor coil is connected to a copper segment. Stationary carbon brushes ride upon the copper segments whereby the rotor coil is connected to a stationary circuit.

The voltage equations for the field winding and rotor coil are

$$v_f = r_f i_f + \frac{d\lambda_f}{dt} \quad (10.2-1)$$

$$v_{a-a'} = r_a i_{a-a'} + \frac{d\lambda_{a-a'}}{dt} \quad (10.2-2)$$

where  $r_f$  and  $r_a$  are the resistance of the field winding and armature coil, respectively. The rotor of a dc machine is commonly referred to as the *armature*; rotor and armature will be used interchangeably. At this point in the analysis, it is sufficient to express the flux linkages as

$$\lambda_f = L_{ff}i_f + L_{fa}i_{a-a'} \quad (10.2-3)$$

$$\lambda_{a-a'} = L_{af}i_f + L_{aa}i_{a-a'} \quad (10.2-4)$$

As a first approximation, the mutual inductance between the field winding and an armature coil may be expressed as a sinusoidal function of  $\theta_r$  as

$$L_{af} = L_{fa} = -L \cos \theta_r \quad (10.2-5)$$

where  $L$  is a constant. As the rotor revolves, the action of the commutator is to switch the stationary terminals from one terminal of the rotor coil to the other. For the configuration shown in Figure 10.2-1, this switching or commutation occurs at  $\theta_r = 0, \pi, 2\pi, \dots$ . At the instant of switching, each brush is in contact with both copper segments, whereupon the rotor coil is short-circuited. It is desirable to commutate (short-circuit) the rotor coil at the instant the induced voltage is a minimum. The waveform of the voltage induced in the open-circuited armature coil during constant-speed operation with a constant field winding current may be determined by setting  $i_{a-a'} = 0$  and  $i_f$  equal to a constant. Substituting (10.2-4) and (10.2-5) into (10.2-2) yields the following expression for the open-circuit voltage of coil  $a-a'$  with the field current  $i_f$  a constant:

$$v_{a-a'} = \omega_r L I_f \sin \theta_r \quad (10.2-6)$$

where  $\omega_r = d\theta_r/dt$  is the rotor speed. The open-circuit coil voltage  $v_{a-a'}$  is zero at  $\theta_r = 0, \pi, 2\pi, \dots$ , which is the rotor position during commutation. Commutation is illustrated in Figure 10.2-2. The open-circuit terminal voltage,  $v_a$ , corresponding to the rotor positions denoted as  $\theta_{ra}$ ,  $\theta_{rb}$  ( $\theta_{rb} = 0$ ), and  $\theta_{rc}$  are indicated. It is important to note that during one revolution of the rotor, the assumed positive direction of armature current  $i_a$  is down coil side  $a$  and out coil side  $a'$  for  $0 < \theta_r < \pi$ . For  $\pi < \theta_r < 2\pi$ , positive current is down coil side  $a'$  and out of coil side  $a$ . Previously, we let positive current flow into the winding denoted without a prime and out the winding denoted with a prime. We will not be able to adhere to this relationship in the case of the armature windings of a dc machine since commutation is involved.

The machine shown in Figure 10.2-1 is not a practicable machine. Although it could be operated as a generator supplying a resistive load, it could not be operated effectively as a motor supplied from a voltage source owing to the short-circuiting of the armature coil at each commutation. A practicable dc machine, with the rotor equipped with an  $a$  winding and an  $A$  winding, is shown schematically in Figure 10.2-3. At the rotor position depicted, coils  $a_4 - a'_4$  and  $A_4 - A'_4$  are being commutated. The bottom brush short-circuits the  $a_4 - a'_4$  coil while the top brush short-circuits the  $A_4 - A'_4$  coil. Figure 10.2-3 illustrates the instant when the assumed direction of positive current

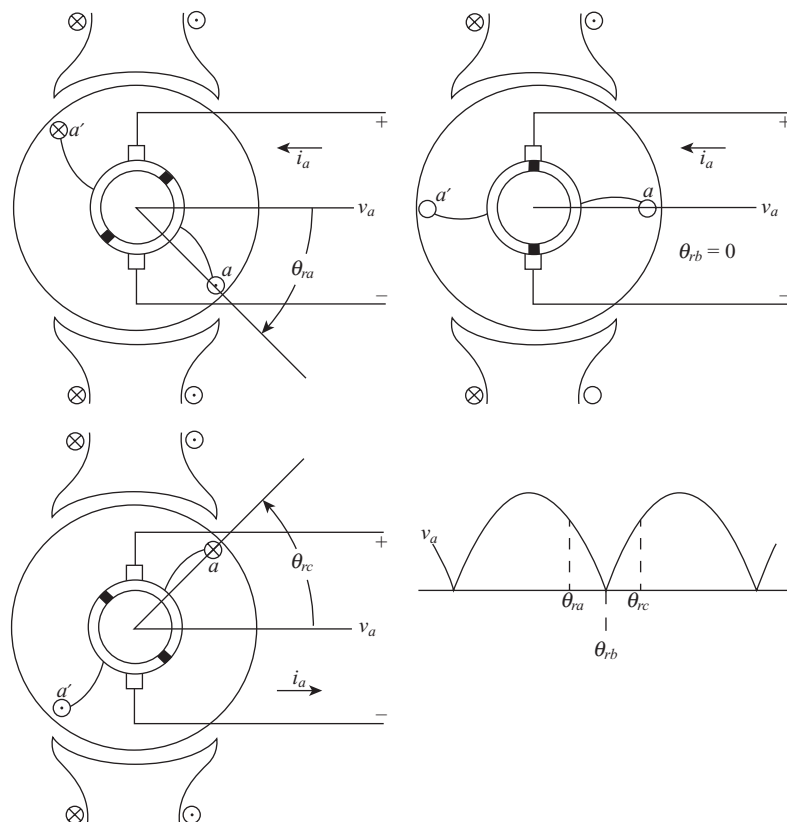


Figure 10.2-2. Commutation of the elementary dc machine.

is into the paper in coil sides  $a_1, A_1$ ;  $a_2, A_2$ ; . . . , and out in coil sides  $a'_1, A'_1$ ;  $a'_2, A'_2$ ; . . . It is instructive to follow the path of current through one of the parallel paths from one brush to the other. For the angular position shown in Figure 10.2-3, positive currents enter the top brush and flow down the rotor via  $a_1$  and back through  $a'_1$ ; down  $a_2$  and back through  $a'_2$ ; down  $a_3$  and back through  $a'_3$  to the bottom brush. A parallel current path exists through  $A_3 - A'_3$ ,  $A_2 - A'_2$ , and  $A_1 - A'_1$ . The open-circuit or induced armature voltage is also shown in Figure 10.2-3; however, these idealized waveforms require additional explanation. As the rotor advances in the counterclockwise direction, the segment connected to  $a_1$  and  $A_4$  moves from under the top brush, as shown in Figure 10.2-4. The top brush then rides only on the segment connecting  $A_3$  and  $A'_4$ . At the same time, the bottom brush is riding on the segment connecting  $a_4$  and  $a'_3$ . With the rotor so positioned, current flows in  $A_3$  and  $A'_4$  and out  $a_4$  and  $a'_3$ . In other words, current flows down the coil sides in the upper one half of the rotor and out of the coil sides in the bottom one half. Let us follow the current flow through the parallel paths of the armature windings shown in Figure 10.2-4. Current now flows through the top brush into  $A'_4$  out  $A_4$ , into  $a_1$  out  $a'_1$ , into  $a_2$ , out  $a'_2$ , into  $a_3$  out  $a'_3$  to the bottom brush. The

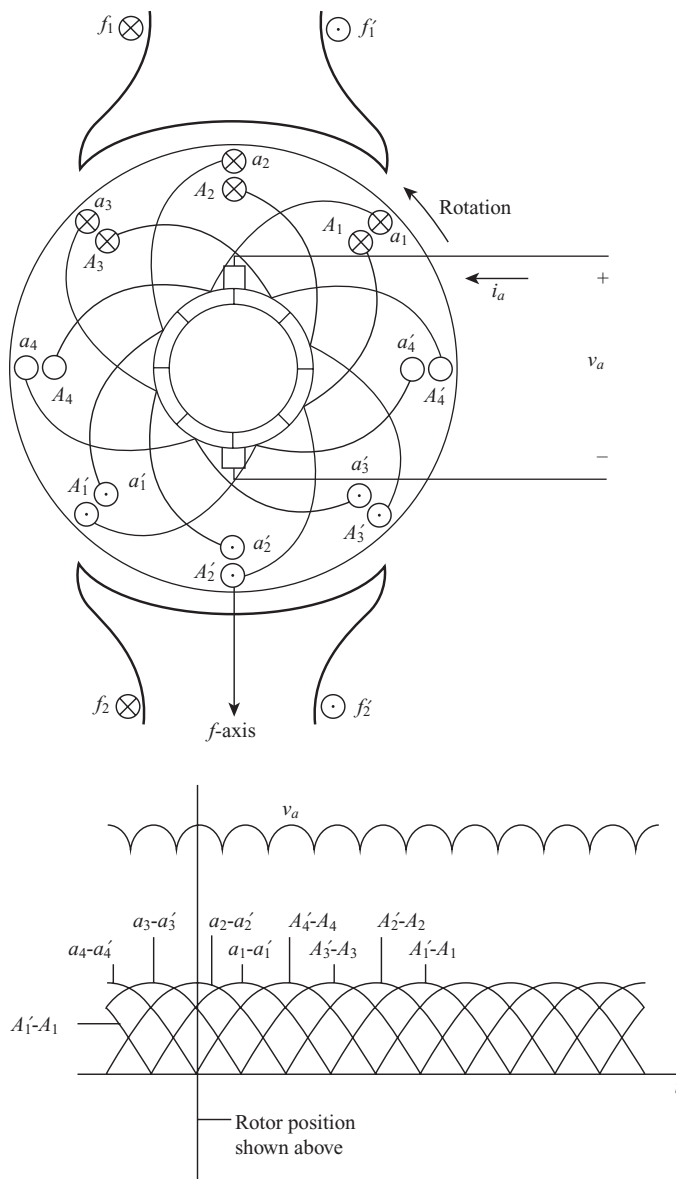


Figure 10.2-3. A dc machine with parallel armature windings.

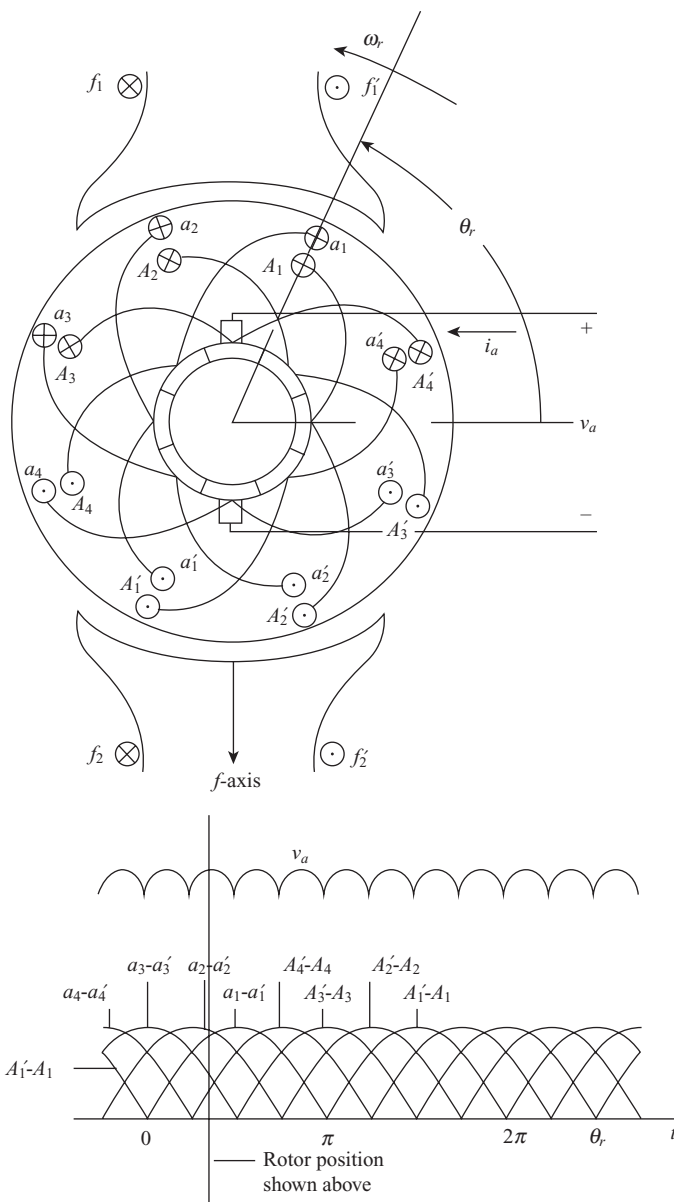


Figure 10.2-4. Same as Figure 10.2-3, with rotor advanced approximately  $22.5^\circ$  counterclockwise.

parallel path beginning at the top brush is  $A_3 - A'_3$ ,  $A_2 - A'_2$ , and  $A_1 - A'_1$ , and  $a'_4 - a_4$  to the bottom brush. The voltage induced in the coils is shown in Figure 10.2-3 and Figure 10.2-4 for the first parallel path described. It is noted that the induced voltage is plotted only when the coil is in this parallel path.

In Figure 10.2-3 and Figure 10.2-4, the parallel windings consist of only four coils. Usually, the number of rotor coils is substantially more than four, thereby reducing the harmonic content of the open-circuit armature voltage. In this case, the rotor coils may be approximated as a uniformly distributed winding, as illustrated in Figure 10.2-5. Therein, the rotor winding is considered as current sheets that are fixed in space due to the action of the commutator and which establish a magnetic axis positioned orthogonal to the magnetic axis of the field winding. The brushes are shown positioned on the current sheet for the purpose of depicting commutation. The small angular

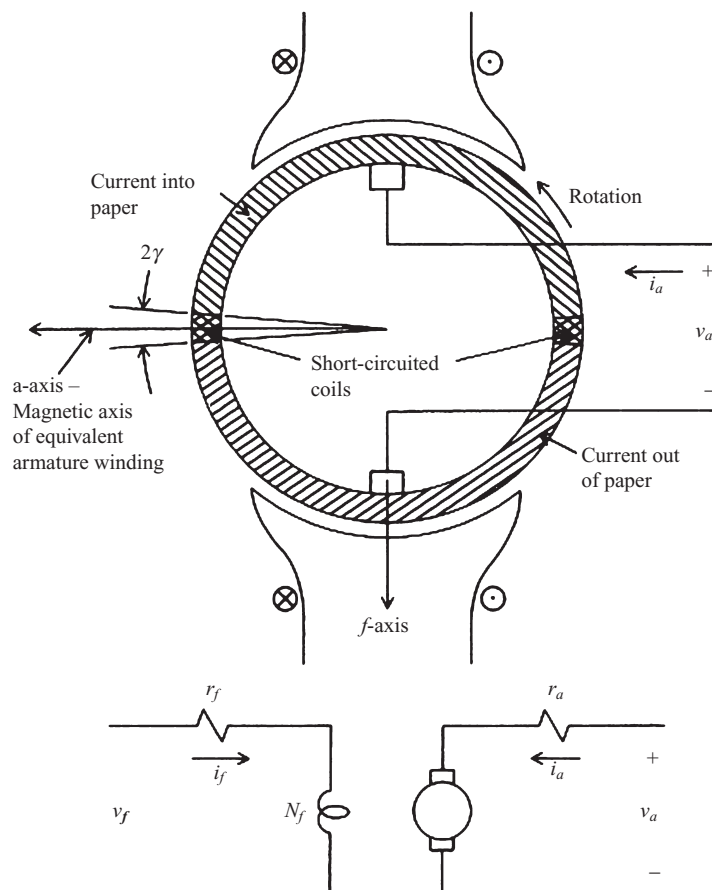


Figure 10.2-5. Idealized dc machine with uniformly distributed rotor winding.

displacement, denoted by  $2\gamma$ , designates the region of commutation wherein the coils are short-circuited. However, commutation cannot be visualized from Figure 10.2-5; one must refer to Figure 10.2-3 and Figure 10.2-4.

In our discussion of commutation, it was assumed that the armature current was zero. With this constraint, the sinusoidal voltage induced in each armature coil crosses through zero when the coil is orthogonal to the field flux. Hence, the commutator was arranged so that the commutation would occur when an armature coil was orthogonal to field flux. When current flows in the armature winding, the flux established therefrom is in an axis orthogonal to the field flux. Thus, a voltage will be induced in the armature coil that is being commutated as a result of “cutting” the flux established by the current flowing in the other armature coils. Arcing at the brushes will occur, and the brushes and copper segments may be damaged with even a relatively small armature current. Although the design of dc machines is not a subject of this text, it is important to mention that brush arcing may be substantially reduced by mechanically shifting the position of the brushes as a function of armature current or by means of interpoles. Interpoles or commutating poles are small stator poles placed over the coil sides of the winding being commutated, midway between the main poles of large horsepower machines. The action of the interpole is to oppose the flux produced by the armature current in the region of the short-circuited coil. Since the flux produced in this region is a function of the armature current, it is desirable to make the flux produced by the interpole a function of the armature current. This is accomplished by winding the interpole with a few turns of the conductor carrying the armature current. Electrically, the interpole winding is between the brush and the terminal. It may be approximated in the voltage equations by increasing slightly the armature resistance and inductance ( $r_a$  and  $L_{AA}$ ).

### 10.3. VOLTAGE AND TORQUE EQUATIONS

Although rigorous derivation of the voltage and torque equations is possible, it is rather lengthy and little is gained since these relationships may be deduced. The armature coils revolve in a magnetic field established by a current flowing in the field winding. We have established that voltage is induced in these coils by virtue of this rotation. However, the action of the commutator causes the armature coils to appear as a stationary winding with its magnetic axis orthogonal to the magnetic axis of the field winding. Consequently, voltages are not induced in one winding due to the time rate of change of the current flowing in the other (transformer action). Mindful of these conditions, we can write the field and armature voltage equations in matrix form as

$$\begin{bmatrix} v_f \\ v_a \end{bmatrix} = \begin{bmatrix} r_f + pL_{FF} & 0 \\ \omega_r L_{AF} & r_a + pL_{AA} \end{bmatrix} \begin{bmatrix} i_f \\ i_a \end{bmatrix} \quad (10.3-1)$$

where  $L_{FF}$  and  $L_{AA}$  are the self-inductances of the field and armature windings, respectively, and  $p$  is the short-hand notation for the operator  $d/dt$ . The rotor speed is denoted as  $\omega_r$ , and  $L_{AF}$  is the mutual inductance between the field and the rotating armature

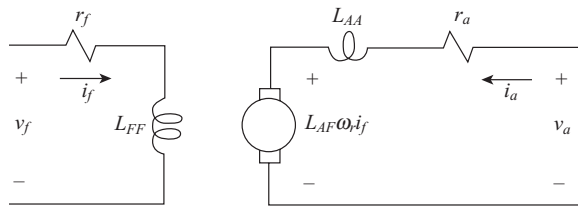


Figure 10.3-1. Equivalent circuit of dc machine.

coils. The above equation suggests the equivalent circuit shown in Figure 10.3-1. The voltage induced in the armature circuit,  $\omega L_{AF} i_f$ , is commonly referred to as the counter or back emf. It also represents the open-circuit armature voltage.

A substitute variable often used is

$$k_v = L_{AF} i_f \quad (10.3-2)$$

We will find this substitute variable is particularly convenient and frequently used. Even though a permanent-magnet dc machine has no field circuit, the constant field flux produced by the permanent magnet is analogous to a dc machine with a constant  $k_v$ . For a dc machine with a field winding, the electromagnetic torque can be expressed

$$T_e = L_{AF} i_f i_a \quad (10.3-3)$$

Here again the variable  $k_v$  is often substituted for  $L_{AF} i_f$ . In some instances,  $k_v$  is multiplied by a factor less than unity when substituted into (10.3-5) so as to approximate the effects of rotational losses. It is interesting that the field winding produces a stationary MMF and, owing to commutation, the armature winding also produces a stationary MMF that is displaced  $(1/2)\pi$  electrical degrees from the MMF produced by the field winding. It follows then that the interaction of these two MMF's produces the electromagnetic torque.

The torque and rotor speed are related by

$$T_e = J \frac{d\omega_r}{dt} + B_m \omega_r + T_L \quad (10.3-4)$$

where  $J$  is the inertia of the rotor and, in some cases, the connected mechanical load. The units of the inertia are  $\text{kg}\cdot\text{m}^2$  or  $\text{J}\cdot\text{s}^2$ . A positive electromagnetic torque  $T_e$  acts to turn the rotor in the direction of increasing  $\theta_r$ . The load torque  $T_L$  is positive for a torque, on the shaft of the rotor, which opposes a positive electromagnetic torque  $T_e$ . The constant  $B_m$  is a damping coefficient associated with the mechanical rotational system of the machine. It has the units of  $\text{N}\cdot\text{m}\cdot\text{s}$  and it is generally small and often neglected.

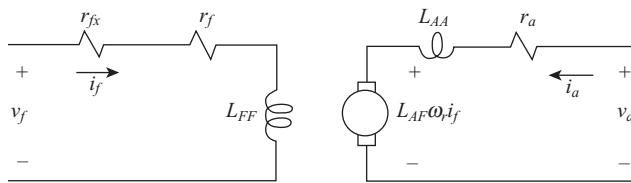


Figure 10.4-1. Equivalent circuit for separate field and armature excitation.

## 10.4. BASIC TYPES OF DC MACHINES

The field and armature windings may be excited from separate sources or from the same source with the windings connected differently to form the basic types of dc machines, such as the shunt-connected, the series-connected, and the compound-connected dc machines. The equivalent circuits for each of these machines are given in this section along with an analysis and discussion of their steady-state operating characteristics.

### Separate Winding Excitation

When the field and armature windings are supplied from separate voltage sources, the device may operate as either a motor or a generator; it is a motor if it is driving a torque load and a generator if it is being driven by some type of prime mover. The equivalent circuit for this type of machine is shown in Figure 10.4-1. It differs from that shown in Figure 10.3-1 in that external resistance  $r_{fx}$  is connected in series with the field winding. This resistance, which is often referred to as a *field rheostat*, is used to adjust the field current if the field voltage is supplied from a constant source.

The voltage equations that describe the steady-state performance of this device may be written directly from (10.3-1) by setting the operator  $p$  to zero ( $p = d/dt$ ), whereupon

$$V_f = R_f I_f \quad (10.4-1)$$

$$V_a = r_a I_a + \omega_r L_{AF} I_f \quad (10.4-2)$$

where  $R_f = r_{fx} + r_f$  and capital letters are used to denote steady-state voltages and currents. We know from the torque relationship given by (10.3-6) that during steady-state operation  $T_e = T_L$  if  $B_m$  is assumed to be zero. Analysis of steady-state performance is straightforward.

A permanent-magnet dc machine fits into this class of dc machines. As we have mentioned, the field flux is established in these devices by a permanent magnet. The voltage equation for the field winding is eliminated, and  $L_{AF} i_f$  is replaced by a constant  $k_v$ , which can be measured if it is not given by the manufacturer. Most small, hand-held, fractional-horsepower dc motors are of this type, and speed control is achieved by controlling the amplitude of the applied armature voltage.

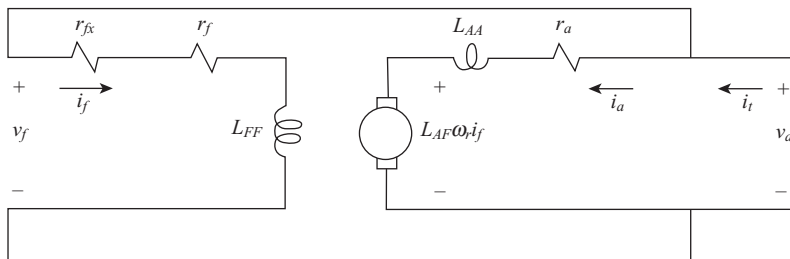


Figure 10.4-2. Equivalent circuit of a shunt-connected dc machine.

### Shunt-Connected dc Machine

The field and armature windings may be connected as shown schematically in Figure 10.4-2. With this connection, the machine may operate either as a motor or a generator. Since the field winding is connected between the armature terminals,  $V_a = V_f$ . This winding arrangement is commonly referred to as a *shunt-connected dc machine* or simply a shunt machine. During steady-state operation, the armature circuit voltage equation is (10.4-2) and, for the field circuit,

$$V_a = I_f R_f \quad (10.4-3)$$

The total current  $I_t$  is

$$I_t = I_f + I_a \quad (10.4-4)$$

Solving (10.4-2) for  $I_a$  and (10.4-3) for  $I_f$  and substituting the results in (10.3-3) yields the following expression for the steady-state electromagnetic torque, positive for motor action, for this type of dc machine:

$$T_e = \frac{L_{AF} V_a^2}{r_a R_f} \left( 1 - \frac{L_{AF}}{R_f} \omega_r \right) \quad (10.4-5)$$

The shunt-connected dc machine may operate as either a motor or a generator when connected to a dc source. It may also operate as an isolated self-excited generator, supplying an electric load, such as a dc motor or a static load. When the shunt machine is operated from a constant-voltage source, the steady-state operating characteristics are those shown in Figure 10.4-3. Several features of these characteristics warrant discussion. At stall ( $\omega_r = 0$ ), the steady-state armature current  $I_a$  is limited only by the armature resistance. In the case of small, permanent-magnet motors, the armature resistance is quite large so that the starting armature current, which results when rated voltage is applied, is generally not damaging. However, larger-horsepower machines are designed with a small armature resistance. Therefore, an excessively high armature current will occur during the starting period if rated voltage is applied to the armature terminals.

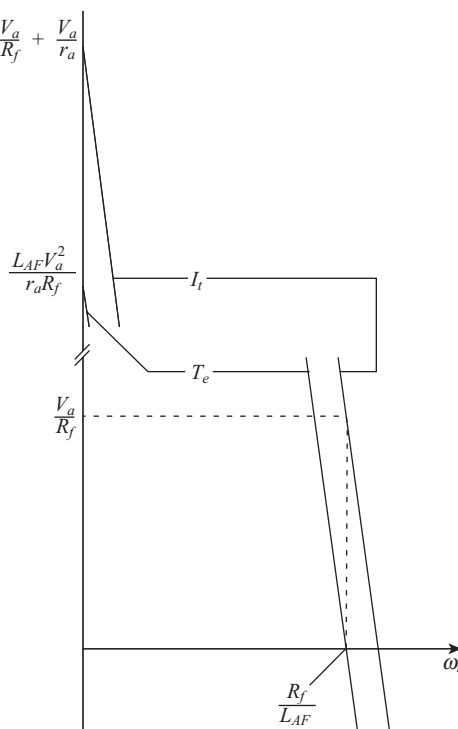


Figure 10.4-3. Steady-state operating characteristics of a shunt-connected dc machine with constant source voltage.

To prevent high starting current, resistance may be inserted into the armature circuit at stall and decreased either manually or automatically to zero as the machine accelerates to normal operating speed. When silicon-controlled rectifiers (SCR's) or thyristors are used to convert an ac source voltage to dc to supply the dc machine, they may be controlled to provide a reduced voltage during the starting period, thereby preventing a high starting current and eliminating the need to insert resistance into the armature circuit. Other features of the shunt machine with a small armature resistance are the steep torque-versus-speed characteristics. In other words, the speed of the shunt machine does not change appreciably as the load torque is varied from zero to rated.

### Series-Connected dc Machine

When the field is connected in series with the armature circuit, as shown in Figure 10.4-4, the machine is referred to as a *series-connected dc machine* or a series machine. It is convenient to add the subscript *s* to denote quantities associated with the series field. It is important to mention the physical difference between the field winding of a shunt machine and that of a series machine. If the field winding is to be a shunt-connected winding, it is wound with a large number of turns of small-diameter wire,

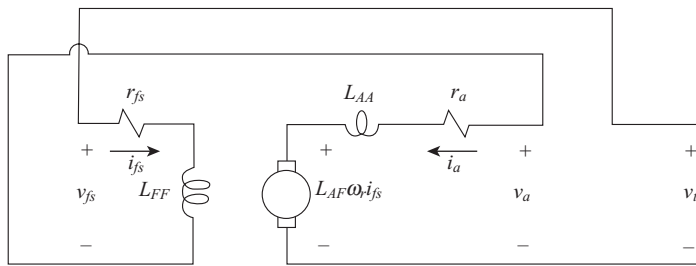


Figure 10.4-4. Equivalent circuit for a series-connected dc machine.

making the resistance of the field winding quite large. However, since the series-connected field winding is in series with the armature, it is designed so as to minimize the voltage drop across it. Thus, the winding is wound with a few turns of low-resistance wire.

Although the series machine does not have wide application, a series field is often used in conjunction with a shunt field to form a compound-connected dc machine, which is more common. In the case of a series machine (Fig. 10.4-4),

$$v_t = v_{fs} + v_a \quad (10.4-6)$$

$$i_a = i_{fs} \quad (10.4-7)$$

where  $v_{fs}$  and  $i_{fs}$  denote the voltage and current associated with the series field. The subscript  $s$  is added to avoid confusion with the shunt field when both fields are used in a compound machine.

If the constraints given by (10.4-6) and (10.4-7) are substituted into the armature voltage equation, the steady-state performance of the series-connected dc machine may be described by

$$V_t = (r_a + r_{fs} + L_{AFs}\omega_r)I_a \quad (10.4-8)$$

From (10.3-5),

$$\begin{aligned} T_e &= L_{AFs}I_a^2 \\ &= \frac{L_{AFs}V_t^2}{(r_a + r_{fs} + L_{AFs}\omega_r)^2} \end{aligned} \quad (10.4-9)$$

The steady-state torque-speed characteristic for a typical series machine is shown in Figure 10.4-5. The stall torque is quite high since it is proportional to the square of the armature current for a linear magnetic system. However, saturation of the magnetic system due to large armature currents will cause the torque to be less than that calculated from (10.4-9). At high rotor speeds, the torque decreases less rapidly with increasing speed. In fact, if the load torque is small, the series motor may accelerate to speeds large enough to cause damage to the machine. Consequently, the series motor is used

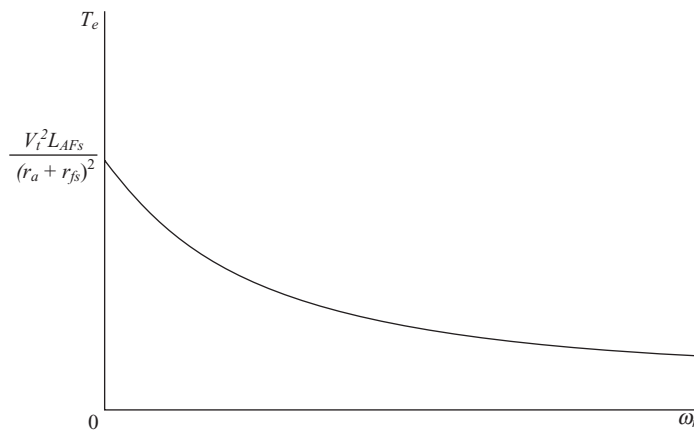


Figure 10.4-5. Steady-state torque–speed characteristics of a series-connected dc machine.

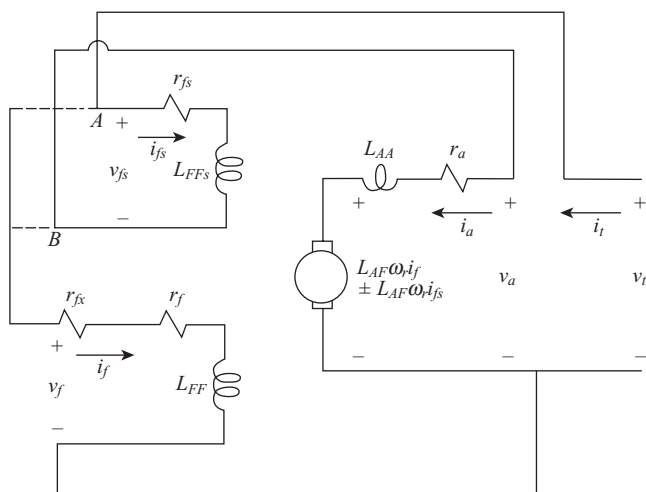


Figure 10.4-6. Equivalent circuit of a compound dc machine.

in applications such as traction motors for trains and buses or in hoists and cranes where high starting torque is required and an appreciable load torque exists under normal operation.

### Compound-Connected dc Machine

A compound-connected or compound dc machine, which is equipped with both a shunt and a series field winding, is illustrated in Figure 10.4-6. In most compound machines, the shunt field dominates the operating characteristics while the series field, which consists of a few turns of low-resistance wire, has a secondary influence. It may be

connected so as to aid or oppose the flux produced by the shunt field. If the compound machine is to be used as a generator, the series field is connected so to aid the shunt field (cumulative compounding). Depending upon the strength of the series field, this type of connection can produce a “flat” terminal-voltage-versus-load-current characteristic, whereupon a near-constant terminal voltage is achieved from no load to full load. In this case, the machine is said to be “flat compounded.” An “overcompounded” machine occurs when the strength of the series field causes the terminal voltage at full load to be larger than at no load. The meaning of the “undercompound” machine is obvious. In the case of compound dc motors, the series field is often connected to oppose the flux produced by the shunt field (differential compounding). If properly designed, this type of connection can provide a near-constant speed from no-load to full-load torque.

The voltage equations for a compound dc machine may be written as

$$\begin{bmatrix} v_f \\ v_t \end{bmatrix} = \begin{bmatrix} R_f + pL_{FF} & \pm pL_{FS} & 0 \\ \omega_r L_{AF} \pm pL_{FS} & \pm \omega_r L_{AFs} + r_{fs} + pL_{FFs} & r_a + pL_{AA} \end{bmatrix} \begin{bmatrix} i_f \\ i_{fs} \\ i_a \end{bmatrix} \quad (10.4-10)$$

where  $L_{FS}$  is the mutual inductance between the shunt and the series fields. The plus and minus signs are used so that either a cumulative or a differential connection may be described.

The shunt field may be connected ahead of the series field (long-shunt connection) or behind the series field (short-shunt connection), as shown by *A* and *B*, respectively, in Figure 10.4-6. The long-shunt connection is commonly used. In this case

$$v_t = v_f = v_{fs} + v_a \quad (10.4-11)$$

$$i_t = i_f + i_{fs} \quad (10.4-12)$$

where

$$i_{fs} = i_a \quad (10.4-13)$$

The steady-state performance of a long shunt-connected compound machine may be described by the following equations:

$$V_t = \left[ \frac{r_a + r_{fs} \pm L_{AFs}\omega_r}{1 - (L_{AF} / R_f)\omega_r} \right] I_a \quad (10.4-14)$$

The torque for the long-shunt connection may be obtained by employing (10.3-3) for each field winding. In particular,

$$\begin{aligned} T_e &= L_{AF} I_f I_a \pm L_{AFs} I_{fs} I_a \\ &= \frac{L_{AF} V_t^2 [1 - (L_{AF} / R_f)\omega_r]}{R_f (r_a + r_{fs} \pm L_{AFs}\omega_r)} \pm \frac{L_{AFs} V_t^2 [1 - (L_{AF} / R_f)\omega_r]^2}{(r_a + r_{fs} \pm L_{AFs}\omega_r)^2} \end{aligned} \quad (10.4-15)$$

**EXAMPLE 10A** A permanent-magnet dc motor is rated at 6V with the following parameters:  $r_a = 7\Omega$ ,  $L_{AA} = 120\text{mH}$ ,  $k_T = 2\text{oz}\cdot\text{in}/\text{A}$ ,  $J = 150\mu\text{oz}\cdot\text{in}\cdot\text{s}^2$ . According to the motor information sheet, the no-load speed is approximately 3350 r/min, and the no-load armature current is approximately 0.15A. Let us attempt to interpret this information.

First, let us convert  $k_T$  and  $J$  to units that we have been using in this book. In this regard, we will convert the inertia to  $\text{kg}\cdot\text{m}^2$ , which is the same as  $\text{N}\cdot\text{m}\cdot\text{s}^2$ . To do this, we must convert ounces to newtons and inches to meters (Appendix A). Thus,

$$J = \frac{150 \times 10^{-6}}{(3.6)(39.37)} = 1.06 \times 10^{-6} \text{ kg}\cdot\text{m}^2 \quad (10A-1)$$

We have not seen  $k_T$  before. It is the torque constant and, if expressed in the appropriate units, it is numerically equal to  $k_v$ . When  $k_v$  is used in the expression for  $T_e$  ( $T_e = k_v i_a$ ), it is often referred to as the *torque constant* and denoted as  $k_T$ . When used in the voltage equation, it is always denoted as  $k_v$ . Now we must convert ounce-in into newton-meter, whereupon  $k_T$  equals our  $k_v$ ; hence,

$$k_v = \frac{2}{(16)(0.225)(39.37)} = 1.41 \times 10^{-2} \text{ N}\cdot\text{m}/\text{A} = 1.41 \times 10^{-2} \text{ V}\cdot\text{s}/\text{rad} \quad (10A-2)$$

What do we do about the no-load armature current? What does it represent? Well, probably it is a measure of the friction and windage losses. We could neglect it, but we will not. Instead, let us include it as  $B_m$ . First, however, we must calculate the no-load speed. We can solve for the no-load rotor speed from the steady-state armature voltage equation for the shunt machine, (10.4-2), with  $L_{AF}i_f$  replaced by  $k_v$ :

$$\begin{aligned} \omega_r &= \frac{V_a - r_a I_a}{k_v} = \frac{6 - (7)(0.15)}{1.41 \times 10^{-2}} = 351.1 \text{ rad/s} \\ &= \frac{(351.1)(60)}{2\pi} = 3353 \text{ r/min} \end{aligned} \quad (10A-3)$$

Now at this no-load speed,

$$T_e = k_v i_a = (1.41 \times 10^{-2})(0.15) = 2.12 \times 10^{-3} \text{ N}\cdot\text{m} \quad (10A-4)$$

Since  $T_L$  and  $J(d\omega_r/dt)$  are zero for this steady-state no-load condition, (10.3-4) tells us that (10A-4) is equal to  $B_m \omega_r$ ; hence,

$$B_m = \frac{2.12 \times 10^{-3}}{\omega_r} = \frac{2.12 \times 10^{-3}}{351.1} = 6.04 \times 10^{-6} \text{ N}\cdot\text{m}\cdot\text{s} \quad (10A-5)$$

**EXAMPLE 10B** The permanent-magnet dc machine described in Example 10A is operating with rated applied armature voltage and load torque  $T_L$  of 0.5 oz·in. Our task is to determine the efficiency where percent eff = (power output/power input) 100.

First let us convert ounce·in into newton·meter:

$$T_L = \frac{0.5}{(16)(0.225)(39.37)} = 3.53 \times 10^{-3} \text{ N} \cdot \text{m} \quad (10B-1)$$

In Example 10A, we determined  $k_v$  to be  $1.41 \times 10^{-2}$  V s/rad and  $B_m$  to be  $6.04 \times 10^{-6}$  N·m·s.

During steady-state operation, (10.3-6) becomes

$$T_e = B_m \omega_r + T_L \quad (10B-2)$$

From (10.3-5), with  $L_{AF}i_f$  replaced by  $k_v$ , the steady-state electromagnetic torque is

$$T_e = k_v I_a \quad (10B-3)$$

Substituting (10B-3) into (10B-2) and solving for  $\omega_r$  yields

$$\omega_r = \frac{k_v}{B_m} I_a - \frac{1}{B_m} T_L \quad (10B-4)$$

From (10.4-2) with  $L_{AF}i_f = k_v$ ,

$$V_a = r_a I_a + k_v \omega_r \quad (10B-5)$$

Substituting (10B-4) into (10B-5) and solving for  $I_a$  yields

$$\begin{aligned} I_a &= \frac{V_a + (k_v / B_m) T_L}{r_a + (k_v^2 / B_m)} \\ &= \frac{6 + [(1.41 \times 10^{-2}) / (6.04 \times 10^{-6})] (3.53 \times 10^{-3})}{7 + (1.41 \times 10^{-2})^2 / (6.04 \times 10^{-6})} = 0.357 \text{ A} \end{aligned} \quad (10B-6)$$

From (10B-4),

$$\begin{aligned} \omega_r &= \frac{1.41 \times 10^{-2}}{6.04 \times 10^{-6}} 0.357 - \frac{1}{6.04 \times 10^{-6}} (3.53 \times 10^{-3}) \\ &= 249 \text{ rad/s} \end{aligned} \quad (10B-7)$$

The power input is

$$P_{\text{in}} = V_a I_a = (6)(0.357) = 2.14 \text{ W} \quad (10B-8)$$

The power output is

$$P_{\text{out}} = T_L \omega_r = (3.53 \times 10^{-3})(249) = 0.8 \text{ W} \quad (10\text{B}-9)$$

The efficiency is

$$\begin{aligned} \eta &= \frac{P_{\text{out}}}{P_{\text{in}}} 100 \\ &= \frac{0.88}{2.14} 100 = 41.1\% \end{aligned} \quad (10\text{B}-10)$$

The low efficiency is characteristic of low-power dc motors due to the relatively large armature resistance. In this regard, it is interesting to determine the losses due to  $i^2r$ , friction, and windage.

$$P_{i^2r} = r_a I_a^2 = (7)(0.357)^2 = 0.89 \text{ W} \quad (10\text{B}-11)$$

$$P_{fw} = (B_m \omega_r) \omega_r = (6.04 \times 10^{-6})(249)^2 = 0.37 \text{ W} \quad (10\text{B}-12)$$

Let us check our work:

$$P_{\text{in}} = P_{i^2r} + P_{fw} + P_{\text{out}} = 0.89 + 0.37 + 0.88 = 2.14 \text{ W} \quad (10\text{B}-13)$$

which is equal to (10B-8).

## 10.5. TIME-DOMAIN BLOCK DIAGRAMS AND STATE EQUATIONS

Although the analysis of control systems is not our intent, it is worthwhile to set the stage for this type of analysis by means of a “first look” at time-domain block diagrams and state equations. In this section, we will consider only the shunt and permanent-magnet dc machines. The series and compound machines are treated in problems at the end of the chapter.

### Shunt-Connected dc Machine

Block diagrams, which portray the interconnection of the system equations, are used extensively in control system analysis and design. Although block diagrams are generally depicted by using the Laplace operator, we shall work with the time-domain equations for now, using the  $p$  operator to denote differentiation with respect to time and the operator  $1/p$  to denote integration

Arranging the equations of a shunt machine into a block diagram representation is straightforward. The field and armature voltage equations, (10.3-1), and the relationship between torque and rotor speed, (10.3-4), may be written as

$$v_f = R_f(1 + \tau_f p)i_f \quad (10.5-1)$$

$$v_a = r_a(1 + \tau_a p)i_a + \omega_r L_{AF}i_f \quad (10.5-2)$$

$$T_e - T_L = (B_m + Jp)\omega_r \quad (10.5-3)$$

where the field time constant  $\tau_f = L_{FF}/R_f$  and the armature time constant  $\tau_a = L_{AA}/r_a$ . Here, again,  $p$  denotes  $d/dt$  and  $1/p$  will denote integration. Solving (10.5-1) for  $i_f$ , (10.5-2) for  $i_a$ , and (10.5-3) for  $\omega_r$  yields

$$i_f = \frac{1/R_f}{\tau_f p + 1} v_f \quad (10.5-4)$$

$$i_a = \frac{1/r_a}{\tau_a p + 1} (v_a - \omega_r L_{AF} i_f) \quad (10.5-5)$$

$$\omega_r = \frac{1}{Jp + B_m} (T_e - T_L) \quad (10.5-6)$$

The time-domain block diagram portraying (10.5-4) through (10.5-6) with  $T_e = L_{AF} i_f i_a$  is shown in Figure 10.5-1. This diagram consists of a set of linear blocks, wherein the relationship between the input and corresponding output variable is depicted in transfer function form and a pair of multipliers that represent nonlinear blocks.

The state equations of a system represent the formulation of the state variables into a matrix form convenient for computer implementation, particularly for linear systems. The state variables of a system are defined as a minimal set of variables such that knowledge of these variables at any initial time  $t_0$  plus information on the input excitation subsequently applied is sufficient to determine the state of the system at any time  $t > t_0$  [1]. In the case of dc machines, the field current  $i_f$ , the armature current  $i_a$ , the rotor speed  $\omega_r$ , and the rotor position  $\theta_r$  are chosen as state variables. The rotor position  $\theta_r$  can be established from  $\omega_r$  by

$$\omega_r = \frac{d\theta_r}{dt} \quad (10.5-7)$$

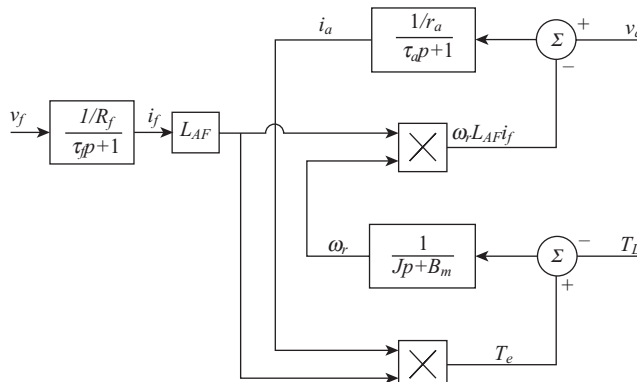


Figure 10.5-1. Time-domain block diagram of a shunt-connected dc machine.

Since  $\theta_r$  is considered a state variable only when the shaft position is a controlled variable, we will omit  $\theta_r$  from consideration in this development.

The formulation of the state equations for the shunt machine can be readily achieved by straightforward manipulation of the field and armature voltage equations given by (10.3-1) and the equation relating torque and rotor speed given by (10.3-4). In particular, solving the field voltage equation (10.3-1) for  $di_f/dt$  yields

$$\frac{di_f}{dt} = -\frac{R_f}{L_{FF}} i_f + \frac{1}{L_{FF}} v_f \quad (10.5-8)$$

Solving the armature voltage equation, (10.3-1), for  $di_a/dt$  yields

$$\frac{di_a}{dt} = -\frac{r_a}{L_{AA}} i_a - \frac{L_{AF}}{L_{AA}} i_f \omega_r + \frac{1}{L_{AA}} v_a \quad (10.5-9)$$

If we wish, we could use  $k_v$  for  $L_{AF}i_f$ ; however, we shall not make this substitution. Solving (10.3-4) for  $d\omega_r/dt$  with  $T_e = L_{AF}i_f i_a$  yields

$$\frac{d\omega_r}{dt} = -\frac{B_m}{J} \omega_r + \frac{L_{AF}}{J} i_f i_a - \frac{1}{J} T_L \quad (10.5-10)$$

All we have done here is to solve the equations for the highest derivative of the state variables while substituting (10.3-3) for  $T_e$  into (10.3-4). Now let us write the state equations in matrix (or vector matrix) form as

$$p \begin{bmatrix} i_f \\ i_a \\ \omega_r \end{bmatrix} = \begin{bmatrix} -\frac{R_f}{L_{FF}} & 0 & 0 \\ 0 & -\frac{r_a}{L_{AA}} & 0 \\ 0 & 0 & -\frac{B_m}{J} \end{bmatrix} \begin{bmatrix} i_f \\ i_a \\ \omega_r \end{bmatrix} + \begin{bmatrix} 0 \\ -\frac{L_{AF}}{L_{AA}} i_f \omega_r \\ \frac{L_{AF}}{J} i_f i_a \end{bmatrix} + \begin{bmatrix} \frac{1}{L_{FF}} & 0 & 0 \\ 0 & \frac{1}{L_{AA}} & 0 \\ 0 & 0 & -\frac{1}{J} \end{bmatrix} \begin{bmatrix} v_f \\ v_a \\ T_L \end{bmatrix} \quad (10.5-11)$$

where  $p$  is the operator  $d/dt$ . Equation (10.5-11) is the state equation(s); however, note that the second term (vector) on the right-hand side contains the products of state variables causing the system to be nonlinear.

## Permanent-Magnet dc Machine

As we have mentioned previously, the equations that describe the operation of a permanent-magnet dc machine are identical to those of a shunt-connected dc machine with the field current constant. Thus, the work in this section applies to both. For the permanent-magnet machine,  $L_{AF}i_f$  is replaced by  $k_v$ , which is a constant determined by

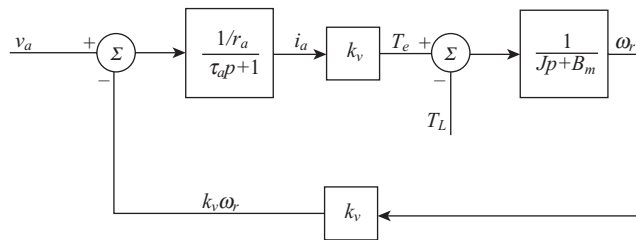


Figure 10.5-2. Time-domain block diagram of a permanent-magnet dc machine.

the strength of the magnet, the reluctance of the iron and air gap, and the number of turns of the armature winding. The time-domain block diagram may be developed for the permanent-magnet machine by using (10.5-2) and (10.5-3), with  $k_v$  substituted for  $L_{AF}i_f$ . The time-domain block diagram for a permanent-magnet dc machine is shown in Figure 10.5-2.

Since  $k_v$  is constant, the state variables are now  $i_a$  and  $\omega_r$ . From (10.5-9), for a permanent-magnet machine,

$$\frac{di_a}{dt} = -\frac{r_a}{L_{AA}} i_a - \frac{k_v}{L_{AA}} \omega_r + \frac{1}{L_{AA}} v_a \quad (10.5-12)$$

From (10.5-10),

$$\frac{d\omega_r}{dt} = -\frac{B_m}{J} \omega_r + \frac{k_v}{J} i_a - \frac{1}{J} T_L \quad (10.5-13)$$

The system is described by a set of linear differential equations. In matrix form, the state equations become

$$p \begin{bmatrix} i_a \\ \omega_r \end{bmatrix} = \begin{bmatrix} -\frac{r_a}{L_{AA}} & -\frac{k_v}{L_{AA}} \\ \frac{k_v}{J} & -\frac{B_m}{J} \end{bmatrix} \begin{bmatrix} i_a \\ \omega_r \end{bmatrix} + \begin{bmatrix} \frac{1}{L_{AA}} & 0 \\ 0 & -\frac{1}{J} \end{bmatrix} \begin{bmatrix} v_a \\ T_L \end{bmatrix} \quad (10.5-14)$$

The form in which the state equations are expressed in (10.5-14) is called the fundamental form. In particular, the previous matrix equation may be expressed symbolically as

$$p\mathbf{x} = \mathbf{Ax} + \mathbf{Bu} \quad (10.5-15)$$

which is called the fundamental form, where  $p$  is the operator  $d/dt$ ,  $\mathbf{x}$  is the state vector (column matrix of state variables), and  $\mathbf{u}$  is the input vector (column matrix of inputs to the system). We see that (10.5-14) and (10.5-15) are identical in form. Methods of

solving equations of the fundamental form given by (10.5-15) are well known. Consequently, it is used extensively in control system analysis [1].

## 10.6. SOLID-STATE CONVERTERS FOR DC DRIVE SYSTEMS

Numerous types of ac/dc and dc/dc converters are used in variable-speed drive systems to supply an adjustable dc voltage to the dc drive machine. In the case of ac/dc converters, half-wave, semi-, full and dual converters are used depending upon the amount of power being handled and the application requirements; such as fast response time, regeneration, and reversible or nonreversible drives. In the case of dc/dc converters, one-, two-, and four-quadrant converters are common. Obviously, we cannot treat all types of converters and all important applications; instead, it is our objective in this section to present the widely used converters and to set the stage for the following sections wherein the analysis and performance of several common dc drive systems are set forth.

### Single-Phase ac/dc Converters

Several types of single-phase phase-controlled ac/dc converters are shown in Figure 10.6-1. Therein, the converters consist of SCRs and diodes. The dc machine is illustrated in abbreviated form without showing the field winding and the resistance and inductance of the armature winding. The dc machines that are generally used with ac/dc converters are the permanent magnet, shunt, or series machines. Half-wave, semi-, full, and dual converters are shown in Figure 10.6-1.

The half-wave converter yields discontinuous armature current in all modes of operation, and only positive current flows on the ac side of the converter. Analysis of the operation of a dc drive with discontinuous armature current is quite involved [2] and not considered. The other converters shown in Figure 10.6-1 can operate with either a continuous or discontinuous armature current. The half-wave and the semi-converters allow a positive dc voltage and unidirectional armature current; however, the semi-converter may be equipped with a diode connected across the terminals of the machine (free-wheeling diode) to dissipate energy stored in the armature inductance when the converter blocks current flow. The full and dual converters can regenerate, that is, the polarity of the motor voltage may be reversed. However, the current of the full converter is unidirectional. Although a reversing switch may be used to change the connection of the full converter to the machine and thereby reverse the current flow through the armature, bidirectional current flow is generally achieved with a dual converter. Consequently, dual converters are used extensively in variable-speed drives wherein it is necessary for the machine to rotate in both directions as in rolling mills and crane applications.

### Three-Phase ac/dc Converters

For drive applications requiring over 20–30 hp, three-phase converters are generally used. Typical three-phase converters are illustrated in Figure 10.6-2. The machine

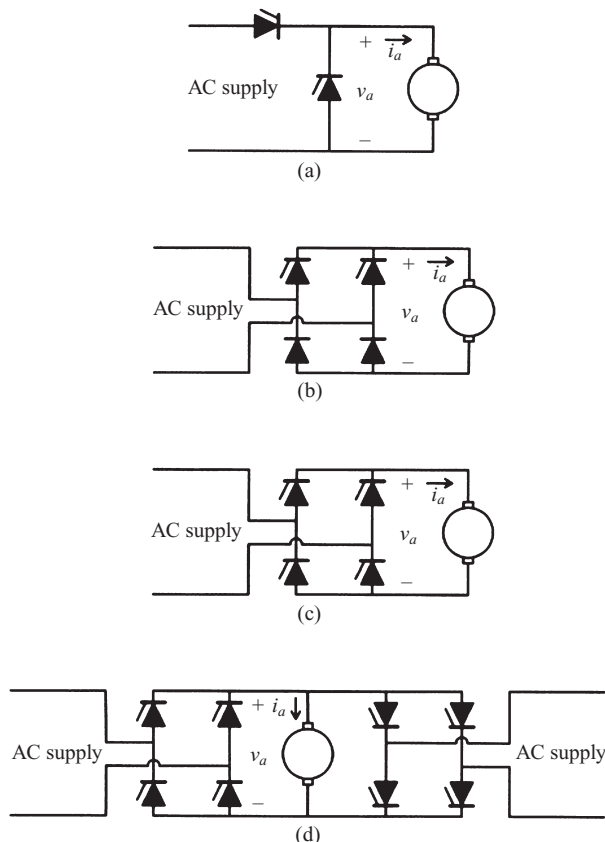
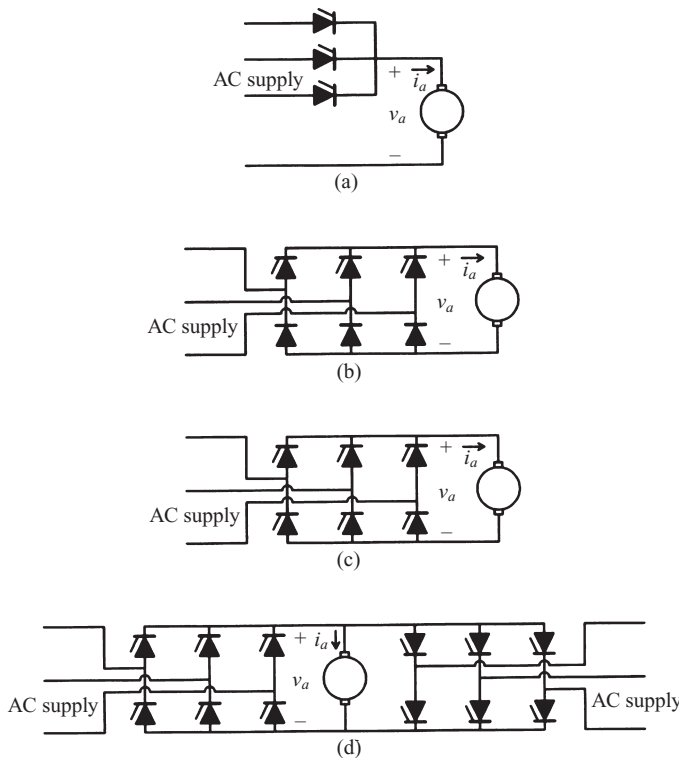


Figure 10.6-1. Typical single-phase phase-controlled ac/dc converters. (a) Half-wave converter; (b) semi-converter; (c) full converter; and (d) dual converter.

current is continuous in most modes of operation of dc drives with three-phase converters. The semi- and full-bridge converters are generally used except in reversible drives where the dual converter is more appropriate. Continuous-current operation of a three-phase, full-bridge converter is analyzed in Chapter 11 and several modes of operation illustrated.

## dc/dc Converters

The commonly used dc/dc converters in dc drive systems are shown in Figure 10.6-3. Therein the SCR or transistor is represented by a switch that can carry positive current only in the direction of the arrow. The one-quadrant converter (Fig. 10.6-3a) is used extensively in low power applications. Since the armature current will become discontinuous in some modes of operation, the analysis of the one-quadrant converter is



**Figure 10.6-2.** Typical three-phase, phase-controlled ac/dc converters. (a) Half-wave converter; (b) semi-converter; (c) full converter; and (d) dual converter.

somewhat involved. This analysis is set forth later in this chapter. The two- and four-quadrant converters are bidirectional in regard to current. In case of the four-quadrant converter, the polarity of the armature voltage can be reversed. All of these dc/dc converters will be considered later in this chapter.

## 10.7. ONE-QUADRANT DC/DC CONVERTER DRIVE

In this section, we will analyze the operation and establish the average-value model for a one-quadrant chopper drive. A brief word regarding nomenclature: dc/dc converter and chopper will be used interchangeable throughout the text.

### One-Quadrant dc/dc Converter

A one-quadrant dc/dc converter is depicted in Figure 10.7-1. The switch  $S$  is either a SRC with auxiliary turn-off circuitry or a transistor. It is assumed to be ideal. That is,

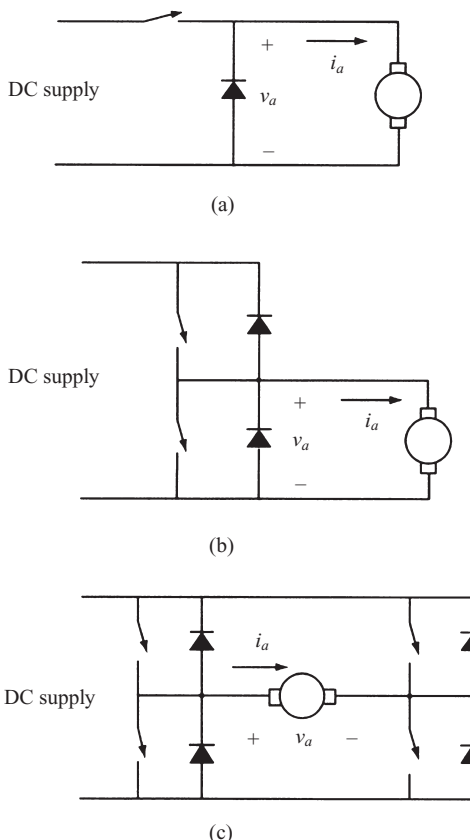


Figure 10.6-3. Typical dc/dc converters. (a) One quadrant; (b) two quadrant; and (c) four quadrant.

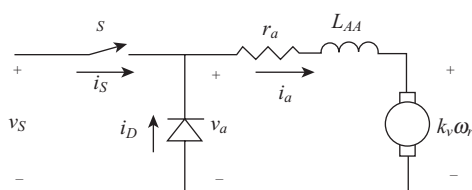
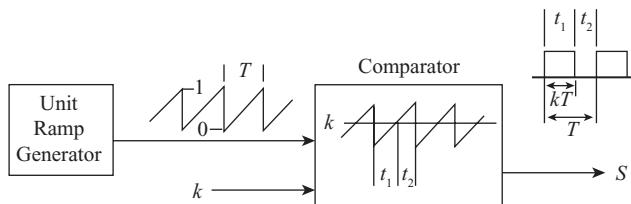


Figure 10.7-1. One-quadrant chopper drive system.

if the switch  $S$  is closed, current is allowed to flow in the direction of the arrow; current is not permitted to flow opposite to the arrow. If  $S$  is open, current is not allowed to flow in either direction regardless of the voltage across the switch. If  $S$  is closed and the current is positive, the voltage drop across the switch is assumed to be zero. Similarly, the diode  $D$  is ideal. Therefore, if the diode current  $i_D$  is greater than zero, the voltage across the diode,  $v_a$ , is zero. The diode current can never be less than zero. In



**Figure 10.7-2.** Switching logic for voltage control of one-quadrant chopper drive shown in Figure 10.7-1.

in this analysis, it will be assumed that the dc machine is either a permanent magnet or a shunt with constant field current. Hence,  $k_v$  is used rather than  $L_{AF}i_f$ , and the field circuit will not show in any of the illustrations.

A voltage control scheme which is often used in dc drives is shown in Figure 10.7-2. As illustrated in Figure 10.7-2, a ramp generator provides a sawtooth waveform of period  $T$ , which ramps from zero to one. This ramp is compared with  $k$ , which is referred to as the duty cycle control signal. As the name implies,  $k$  is often the output variable of an open- or closed-loop control. The switch  $S$  is controlled by the output of the comparator. The duty cycle control signal may vary between zero and one, ( $0 \leq k \leq 1$ ). From Figure 10.7-2, we see that whenever  $k$  is greater than the ramp signal, the logic output of the comparator is high and  $S$  is closed. This corresponds to the time interval  $t_1$  in Figure 10.7-2. Now, since the ramp signal (sawtooth waveform) varies between zero and one, and since  $0 \leq k \leq 1$ , we can relate  $k$ ,  $T$ , and  $t_1$  as

$$t_1 = kT \quad (10.7-1)$$

which may be written as

$$t_1 = \frac{k}{f_s} \quad (10.7-2)$$

where  $f_s$  is the switching or chopping frequency of the chopper ( $f_s = 1/T$ ).

When  $k$  is less than the ramp signal, the logic output is low and  $S$  is open. This corresponds to the time interval  $t_2$ , thus, since

$$t_1 + t_2 = T \quad (10.7-3)$$

we can write

$$\begin{aligned} t_2 &= (1-k)T \\ &= (1-k) \frac{1}{f_s} \end{aligned} \quad (10.7-4)$$

It follows that if  $k$  is fixed at one,  $S$  is always closed, and if  $k$  is fixed at zero,  $S$  is always open.

The one-quadrant chopper is unidirectional, and as its name implies, the armature voltage  $v_a$  and the armature current  $i_a$  can only be positive or zero, ( $0 \leq v_a$ ,  $0 \leq i_a$ ). In the continuous-current mode of operation,  $i_a > 0$ . The discontinuous-current mode of operation occurs when  $i_a$  becomes zero either periodically or during a transient following a system disturbance.

### Continuous-Current Operation

The continuous-current mode of operation for the one-quadrant dc drive is shown in Figure 10.7-3. The armature current varies periodically between  $I_1$  and  $I_2$ . This is considered steady-state operation since  $v_s$ ,  $k_v$ , or  $\omega L_A i_r$ , and  $\omega$ , are all considered constant. It may at first appear that  $\omega$ , cannot be constant since the armature current and thus the electromagnetic torque varies periodically. The rotor speed; however, is essentially constant since the switching frequency of the chopper is generally high so that the change in rotor speed due to the current switching is very small.

The period  $T$  in Figure 10.7-3 is divided into interval A and interval B. During interval A or  $t_1$  ( $0 \leq t \leq kT$ ), switch  $S$  is closed, and the source voltage is applied to the armature circuit. During interval B or  $t_2$  ( $kT \leq t \leq T$ ), switch  $S$  is open and the armature winding is short-circuited through the diode D.

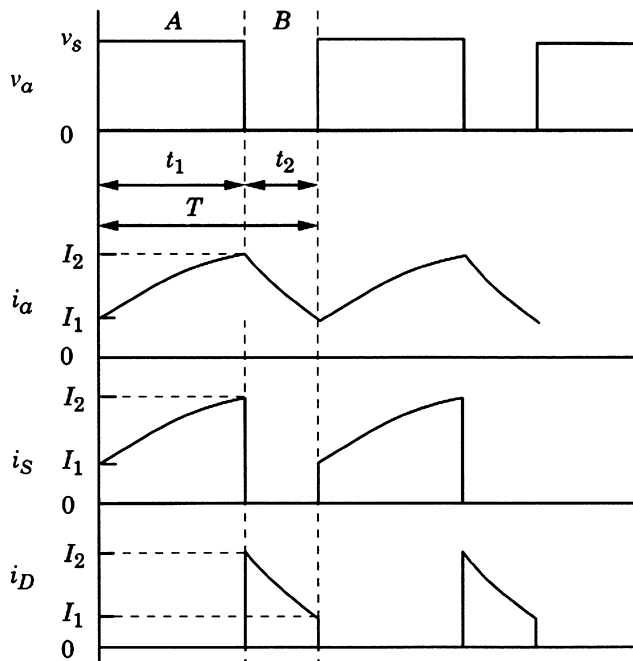


**Figure 10.7-3.** Typical waveforms for continuous-current steady-state operation of a one-quadrant chopper drive.

During interval A,  $v_a = v_S$ ,  $i_a = i_S$ , and  $i_D = 0$ . The armature voltage during this interval is

$$v_S = r_a i_a + L_{AA} \frac{di_a}{dt} + k_v \omega_r \quad (10.7-5)$$

where  $r_a$  and  $L_{AA}$  are the resistance and inductance of the armature circuit, respectively. In (10.7-5),  $k_v$  is used to emphasize that the following analysis is for a permanent magnet or a shunt machine with a constant field current. During interval B,  $v_a = 0$ ,  $i_S = 0$ , and  $i_a = i_D$ . For this interval

$$0 = r_a i_a + L_{AA} \frac{di_a}{dt} + k_v \omega_r \quad (10.7-6)$$

Let us solve for the armature current for intervals A and B. From (10.7-5), for interval A

$$L_{AA} \frac{di_a}{dt} + r_a i_a = v_S - k_v \omega_r \quad (10.7-7)$$

Since  $v_S$  and  $\omega_r$  are assumed constant, the solution of (10.7-7) may be expressed in the form

$$i_a(t) = i_{a,ss} + i_{a,tr} \quad (10.7-8)$$

where  $i_{a,ss}$  is the steady-state current that would flow if the given interval were to last indefinitely. This current can be calculated by assuming  $di_a/dt = 0$ , whereupon from (10.7-7)

$$i_{a,ss} = \frac{v_s - k_v \omega_r}{r_a} \quad (10.7-9)$$

The transient component ( $i_{a,tr}$ ) of (10.7-7) is the solution of the homogeneous or force-free equation

$$L_{AA} \frac{di_a}{dt} + r_a i_a = 0 \quad (10.7-10)$$

Thus,

$$i_{a,tr} = K e^{-t/\tau_a} \quad (10.7-11)$$

where  $\tau_a = L_{AA}/r_a$ . Thus, during interval A, where  $0 \leq t \leq t_1$ , or  $0 \leq t \leq kT$ , the armature current may be expressed as

$$i_a = \frac{1}{r_a} (v_s - k_v \omega_r) + K e^{-t/\tau_a} \quad (10.7-12)$$

At  $t = 0$  for interval A,  $i_a(0) = I_1$  (Fig. 10.7-3), thus

$$I_1 = \frac{1}{r_a} (v_s - k_v \omega_r) + K \quad (10.7-13)$$

Solving for  $K$  and substituting the result into (10.7-12) yields the following expression for  $i_a$ , which is valid for interval A

$$i_a = I_1 e^{-t/\tau_a} + \frac{(v_s - k_v \omega_r)}{r_a} (1 - e^{-t/\tau_a}) \quad (10.7-14)$$

If  $T \ll \tau_a$ , which is generally the case in most practical dc drives, we can approximate (10.7-14) by using the first two terms of the Taylor series  $e^x = 1 + x + (1/2)x^2 + \dots$ . In particular, (10.7-14) may be written as

$$i_a \approx I_1 \left( 1 - \frac{t}{\tau_a} \right) + \frac{v_s - k_v \omega_r}{L_{AA}} t \quad \text{for } T \ll \tau_a \quad (10.7-15)$$

At  $t = t_1$  or  $kT$ ,  $i_a = I_2$ ; from (10.7-14)

$$I_2 = I_1 e^{-kT/\tau_a} + \frac{(v_s - k_v \omega_r)}{r_a} (1 - e^{-kT/\tau_a}) \quad (10.7-16)$$

Equation (10.7-16) relates  $I_2$ , the current at the end of interval A, to  $I_1$ , the current at the beginning of interval A.

During interval B

$$L_{AA} \frac{di_a}{dt} + r_a i_a = -k_v \omega_r \quad (10.7-17)$$

which is (10.7-6) rewritten. Solving for the steady-state current yields

$$i_{a,ss} = \frac{k_v \omega_r}{r_a} \quad (10.7-18)$$

and  $i_{a,tr}$  is still (10.7-11). Thus

$$i_a = -\frac{k_v \omega_r}{r_a} + K e^{-t/\tau_a} \quad (10.7-19)$$

For convenience of analysis, we will define a “new” time zero at the beginning of interval B, thus at this new  $t = 0$ ,  $i_a = I_2$  and

$$I_2 = -\frac{k_v \omega_r}{r_a} + K \quad (10.7-20)$$

Therefore, during interval B, with  $t = 0$  at the start of interval B,

$$i_a = I_2 e^{-t/\tau_a} - \frac{k_v \omega_r}{r_a} (1 - e^{-t/\tau_a}) \quad (10.7-21)$$

If  $T \ll \tau_a$ , then (10.7-21) may be approximated as

$$i_a \approx I_2 \left(1 - \frac{t}{\tau_a}\right) - \frac{k_v \omega_r}{L_{AA}} t \quad \text{for } T \ll \tau_a \quad (10.7-22)$$

Equation (10.7-14) defines the current during interval A, assuming the initial current,  $I_1$ , for this interval is known while (10.7-21) defines the current during interval B, assuming the initial current,  $I_2$ , for interval B is known. How can we establish these currents? Well, the initial current during interval B is the final current in interval A. That is,  $I_2$  is calculated from (10.7-14) by setting  $t = kT$ , giving an expression for  $I_2$  in terms of  $I_1$  (10.7-16). But what determines the value of  $I_1$ ? At the end of interval B, when  $t = t_2$  in (10.7-21), the current  $i_a$  must return to  $I_1$  for steady-state operation. Now, from (10.7-4),  $t_2 = (1 - K)T$ . In other words,  $i_a = I_1$  when  $t$  in (10.7-21) is  $(1 - K)T$ . Thus,

$$I_1 = I_2 e^{-(1-k)T/\tau_a} - \frac{k_v \omega_r}{r_a} (1 - e^{-(1-k)T/\tau_a}) \quad (10.7-23)$$

Equation (10.7-16) and Equation (10.7-23) can be used to solve for  $I_1$  and  $I_2$  in terms of  $v_s$ ,  $k$ ,  $T$ ,  $\omega_r$ , and the machine parameters. In particular, with some work, we can write

$$I_1 = \frac{v_s}{r_a} \left[ \frac{e^{-T/\tau_a} (e^{kT/\tau_a} - 1)}{1 - e^{-T/\tau_a}} \right] - \frac{k_v \omega_r}{r_a} \quad (10.7-24)$$

$$I_2 = \frac{v_s}{r_a} \left[ \frac{1 - e^{-kT/\tau_a}}{1 - e^{-T/\tau_a}} \right] - \frac{k_v \omega_r}{r_a} \quad (10.7-25)$$

The current ripple is defined as

$$\Delta I = I_2 - I_1 \quad (10.7-26)$$

Substituting (10.7-24) and (10.7-25) into (10.7-28) yields

$$\Delta I = \frac{v_s}{r_a} \left[ \frac{1 - e^{-kT/\tau_a} + e^{-T/\tau_a} - e^{-(1-k)T/\tau_a}}{1 - e^{-T/\tau_a}} \right] \quad (10.7-27)$$

The value of  $k$ , which produces maximum ripple in the current, occurs when  $\frac{d(\Delta I)}{dk} = 0$ . This yields

$$e^{-kT/\tau_a} - e^{-(1-kT)/\tau_a} = 0 \quad (10.7-28)$$

Solving (10.7-28) for  $k$  gives  $k = 0.5$  for maximum ripple; an expected result. With  $k = 0.5$

$$\Delta I_{\max} = \frac{v_s}{r_a} \left[ \frac{1 - 2e^{-T/2\tau_a} + e^{-T/\tau_a}}{1 - e^{-T/\tau_a}} \right] \quad (10.7-29)$$

After considerable work, (10.7-29) can be expressed as

$$\Delta I_{\max} = \frac{v_s}{r_a} \tanh \frac{T}{4\tau_a} \quad (10.7-30)$$

Note that when the switching period is much less than the armature time constant ( $T \ll \tau_a$ ),  $e^{-T/\tau_a}$  approaches unity, and  $\Delta I$  from (10.7-29) approaches zero.

## Discontinuous-Current Operation

Steady-state discontinuous-current operation of a one-quadrant chopper is shown in Figure 10.7-4. In this case, the period  $T$  is divided into three intervals. In interval A, where  $0 \leq t \leq t_1$ , or  $0 \leq t \leq kT$ , the switch  $S$  is closed, and the source voltage is applied to the armature circuit. The armature current increases from zero ( $I_1 = 0$ ) to  $I_2$  at which time the ramp signal (Fig. 10.7-2) becomes larger than  $k$  and  $S$  is opened. The armature current is instantaneously diverted through the diode. During interval B, the armature voltage  $v_a$  is zero and the armature current decays to zero whereupon the diode stops conducting. As in the case of continuous operation, we will select a “new” time zero for analysis purposes at the beginning of interval B. Interval B continues for the time  $t_2$ . Thus, measuring from the new time zero, interval B occurs from  $0 \leq t \leq t_2$  or  $0 \leq t \leq \beta T$ , where  $t_2 = \beta T$ . Interval C begins at the instant  $i_a$  becomes zero and it continues to the end of the period  $T$ . This time interval is denoted  $t_3$  in Figure 10.7-4. During interval C, the armature winding is open-circuited, and the counter emf ( $k_v \omega_r$ ) appears at the terminals. That is, during interval C,  $v_a = k_v \omega_r$ . From Figure 10.7-4, it is clear that  $T = t_1 + t_2 + t_3$ . Since  $t_1 = kT$  and  $t_2 = \beta T$ ,  $t_3$  may be expressed as  $(1-k-\beta)T$ .

The armature current over the interval A can be expressed from (10.7-14) with  $I_1 = 0$ . Thus

$$i_a = \frac{(v_s - k_v \omega_r)}{r_a} (1 - e^{-t/\tau_a}) \quad (10.7-31)$$

If  $T \ll \tau_a$ , (10.7-31) may be approximated as

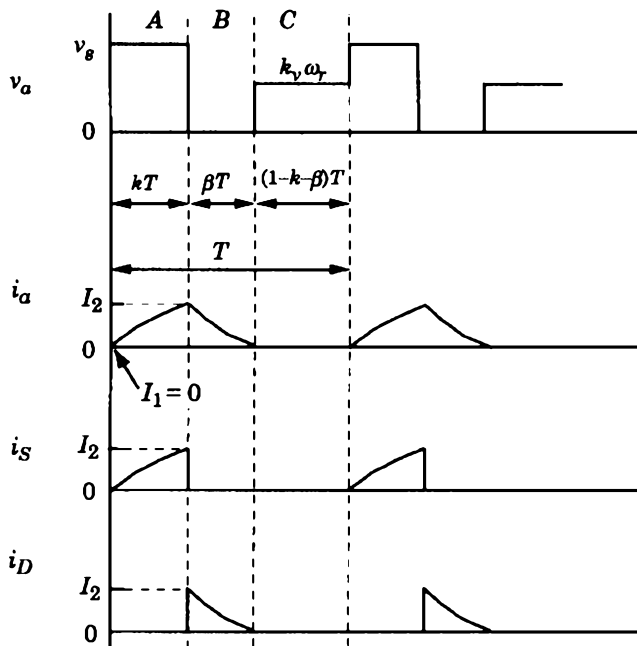


**Figure 10.7-4.** Typical waveforms for discontinuous-current steady-state operation of a one-quadrant chopper drive.

$$i_a \approx \frac{v_s - k_v \omega_r}{L_{AA}} t \quad \text{for } T \ll \tau_a \quad (10.7-32)$$

During interval B, where, with our new time zero,  $0 \leq t \leq \beta T$

$$i_a = I_2 e^{-t/\tau_a} - \frac{k_v \omega_r}{r_a} (1 - e^{-t/\tau_a}) \quad (10.7-33)$$

If  $T \ll \tau_a$ , (10.7-33) may be approximated as

$$i_a \approx I_2 \left( 1 - \frac{t}{\tau_a} \right) - \frac{k_v \omega_r}{L_{AA}} t \quad \text{for } T \ll \tau_a \quad (10.7-34)$$

When  $t = kT$  in (10.7-31)  $i_a = I_2$

$$I_2 = \frac{(v_s - k_v \omega_r)}{r_a} (1 - e^{-kT/\tau_a}) \quad (10.7-35)$$

When  $t = \beta T$  in (10.7-33)  $i_a = 0$

$$0 = I_2 e^{-\beta T / \tau_a} - \frac{k_v \omega_r}{r_a} (1 - e^{-\beta T / \tau_a}) \quad (10.7-36)$$

Substituting (10.7-35) into (10.7-36) and solving for  $\beta$  yields

$$\beta = \frac{\tau_a}{T} \ln \left[ \frac{(v_s - k_v \omega_r)}{k_v \omega_r} (1 - e^{-kT / \tau_a}) + 1 \right] \quad (10.7-37)$$

If  $T \ll \tau_a$ , (10.7-37) may be approximated as

$$\beta \approx \frac{(v_s - k_v \omega_r)k}{k_v \omega_r} \quad \text{for } T \ll \tau_a \quad (10.7-38)$$

Recall that  $t_3 = (1 - k - \beta)T$ ; therefore, discontinuous-current operation occurs only if

$$1 - k - \beta > 0 \quad (10.7-39)$$

If (10.7-38) is substituted into (10.7-39), discontinuous-current operation will occur approximately when

$$k_v \omega_r > k v_s \quad \text{for } T \ll \tau_a \quad (10.7-40)$$

At first glance, we might be led to believe from (10.7-40) that the occurrence of discontinuous-current operation is independent of the switching period  $T$ . Clearly, this is not the case since increasing  $T$  will tend to increase the time of discontinuous-current operation. In this approximation, we have made  $T$  very small, whereupon (10.7-40) can be used to approximate when discontinuous-current operation will occur if  $T \ll \tau_a$ . Actually, (10.7-40) is quite logical once we realize that  $k v_s$  is the average armature voltage over a period  $T$  if the current is continuous.

## Average-Value Analysis

It may at first appear that the harmonics introduced by the switching of the chopper would drastically complicate the analysis of dc/dc converter drive systems. Fortunately, this is generally not the case. Since the switching period ( $T$ ) of the chopper is generally much smaller than the time constant of the armature circuit ( $\tau_a$ ) and always much smaller than the time constant of the mechanical system ( $\tau_m$ ), it is possible to describe the performance of a dc/dc converter drive system with average-value variables. This can be accomplished by establishing a continuous average-value equivalent of the armature voltage  $v_a$ . Once this continuous average value of  $v_a$ , which we will denote as  $\hat{v}_a$ , is determined, we will show that the voltage and torque equations that have previously been derived may be used directly to predict the average-value dynamic and steady-state response of the dc drive system.

The goal of the “average valuing” is to establish continuous averages of the waveforms ( $v_a$ ,  $i_a$ , and  $\omega_r$ ) that predict the average-value performance of the dc drive during dynamic and steady-state operation. Our first step in establishing justification for replacing the switched and discontinuous variables with average-value equivalents is to follow a procedure similar to that used in Reference 3. In particular, we will define the dynamic average of a variable as

$$\hat{f}(t) = \frac{1}{T} \int_{t-T}^t f(\xi) d\xi \quad (10.7-41)$$

where  $\xi$  is a dummy variable and, for our purpose,  $T$  is the switching period of the chopper and  $f$  can represent either  $v_a$ ,  $i_a$ , or  $\omega_r$ . The averaging process is achieved by continuously performing (10.7-41) on all variables as the averaging interval,  $(t - T)$ , moves or slides with time. Therefore, the result of this process is often referred to as the moving or sliding average rather than the dynamic average which we will use here.

Our next step is to derive the dynamic average value of the armature voltage, which would be valid for period-to-period changes in the duty cycle  $k$  with  $v_s$  constant. For this purpose, the change in  $k$  is depicted in Figure 10.7-5 for continuous-current operation of a one-quadrant chopper. Therein,  $t_i$  is the beginning of the  $i^{th}$  interval wherein the duty cycle is  $k_i$ . During the next interval, the  $i^{th} + 1$  interval, which begins at  $t_{i+1}$ , the duty cycle is denoted  $k_{i+1}$ . In Figure 10.7-5, we see that  $k_{i+1} < k_i$ , hence the switch  $S$  in Figure 10.7-1 is closed longer during the  $i^{th}$  interval than during the  $i+1$  interval. Superimposed upon the plot of  $v_a$  is the averaging interval, which is equal in length to the switching period  $T$  and which begins at  $t - T$  and ends at  $t$ . In order to establish the dynamic average of  $v_a$ , we will let this averaging interval move from  $t = t_{i+1}$  to  $t = t_{i+1} + T$ .

The averaging interval will yield the same dynamic average for  $v_a$  as it is moved to the right from  $t = t_{i+1}$  until  $t = t_{i+1} + k_{i+1}T$ . This dynamic average of the armature voltage may be expressed as

$$\begin{aligned} \hat{v}_a &= \frac{1}{T} \left[ \int_{t-T}^{t_i+k_iT} v_s d\xi + \int_{t_{i+1}}^t v_s d\xi \right] \\ &= \frac{1}{T} [v_s(t_i - k_i T - t + T) + v_s(t - t_{i+1})] \\ &= k_i v_s \quad \text{for } t_{i+1} \leq t \leq t_{i+1} + k_{i+1}T \end{aligned} \quad (10.7-42)$$

where  $\xi$  is a dummy variable of integration. In the evaluation of (10.7-42), we use the fact that  $t_i + T = t_{i+1}$ . The result that  $\hat{v}_a = k_i v_s$  for  $t_{i+1} \leq t \leq t_{i+1} + k_{i+1}T$  is expected. This of course would be the average taking over the interval  $T$  from  $t_i$  to  $t_{i+1}$ . Clearly, this average will not change as the averaging interval is moved to the right until a change is encountered at  $t$  that is not encountered at  $t - T$ , as is the case at  $t = t_{i+1} + k_{i+1}T$ .

Once  $t$  becomes larger than  $t_{i+1} + k_{i+1}T$ , the averaging interval is positioned as shown in Figure 10.7-6. The leading edge of the sliding averaging interval includes  $v_a = 0$  in the  $i+1$  interval; the trailing edge value is  $v_s$  until  $t - T = t_i + k_i T$ , which may

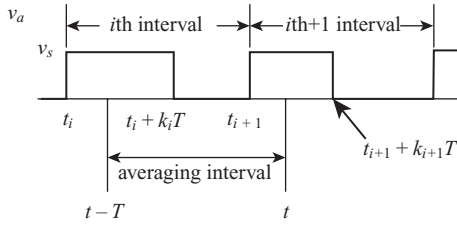


**Figure 10.7-5.** Averaging interval for  $t_{i+1} \leq t \leq t_{i+1} + k_{i+1}T$ ; continuous-current operation of one-quadrant chopper drive.

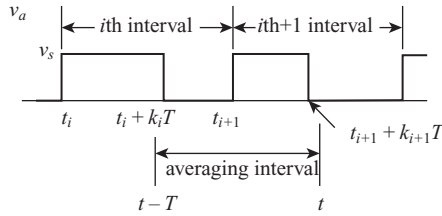


**Figure 10.7-6.** Averaging interval for  $t_{i+1} + k_{i+1}T \leq t \leq t_{i+1} + k_i T$ ; continuous-current operation of one-quadrant chopper drive.

be written as  $t = t_{i+1} + k_i T$ . Thus, for the time interval from  $t_{i+1} + k_{i+1}T \leq t \leq t_{i+1} + k_i T$  the dynamic average of  $v_a$  may be expressed as

$$\begin{aligned}\hat{v}_a &= \frac{1}{T} \left[ \int_{t-T}^{t_{i+1} + k_i T} v_s d\xi + \int_{t_{i+1}}^{t_{i+1} + k_{i+1} T} v_s d\xi + \int_{t_{i+1} + k_{i+1} T}^t 0 d\xi \right] \\ &= \frac{1}{T} [v_s(t_i + k_i T - t + T) + v_s(t_{i+1} + k_{i+1} T - t_{i+1})] \\ &= v_s \left[ \frac{t_{i+1} - t}{T} + (k_i + k_{i+1}) \right] \quad \text{for } t_{i+1} + k_{i+1} T \leq t \leq t_{i+1} + k_i T \quad (10.7-43)\end{aligned}$$

As the trailing edge of the averaging interval slides past  $t - T = t_i + k_i T$ , only the  $v_s$ , which appears in the  $i + 1$  interval, is within the averaging interval. Thus, for  $t_{i+1} + k_i T \leq t \leq t_{i+1} + T$ , the dynamic average of  $v_a$  is  $k_{i+1} v_s$ . Let us show this

$$\begin{aligned}\hat{v}_a &= \frac{1}{T} \int_{t-T}^{t_{i+1}} 0 d\xi + \frac{1}{T} \int_{t_{i+1}}^{t_{i+1} + k_{i+1} T} v_s d\xi + \frac{1}{T} \int_{t_{i+1} + k_{i+1} T}^t 0 d\xi \\ &= \frac{1}{T} [v_s(t_{i+1} + k_{i+1} T - t_{i+1})] \\ &= k_{i+1} v_s \quad \text{for } t_{i+1} + k_i T \leq t \leq t_{i+1} + T \quad (10.7-44)\end{aligned}$$

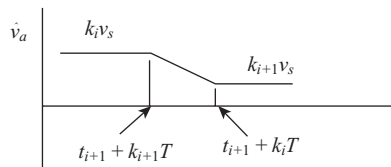


Figure 10.7-7.  $\dot{v}_a$  versus  $t$  for  $v_a$  shown in Figure 10.7-5 and Figure 10.7-6.

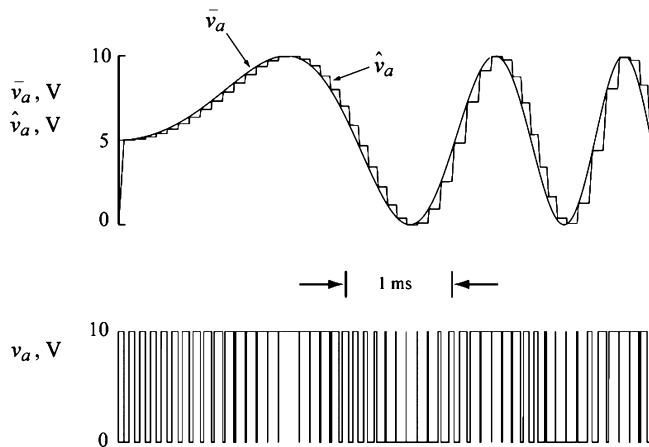


Figure 10.7-8. Comparison of  $\hat{v}_a$  and  $\bar{v}_a$  for  $k = 0.5 + 0.5 \sin[r(t)t]$ .

After we have gone through the dynamic averaging process, we realize that we could have written the results given in (10.7-42) and in (10.7-44) by inspection and concern ourselves only with finding the dynamic average during the transition interval  $t_{i+1} + k_{i+1}T \leq t \leq t_{i+1} + kT$ .

A plot of the dynamic average of  $v_a$  as a function of time is piecewise linear, as shown in Figure 10.7-7. In general,  $\hat{v}_a$  is a staircase-like function with ramp changes occurring once per switching cycle due to changes in  $k$ . If the change in duty cycle is small from one period to the next,  $\hat{v}_a$  will be approximately equal to the continuous signal  $kv_s$ , which we will denote as  $\bar{v}_a$ . That is,

$$\hat{v}_a \approx \bar{v}_a = kv_s \quad (10.7-45)$$

provided the change in  $k$  is small from one period to the next, which is generally the case. Let us look more closely at this. For this purpose, it is interesting to compare  $\bar{v}_a$  and the dynamic average,  $\hat{v}_a$ , obtained by continuously performing the moving average (10.7-41).

This is illustrated in Figure 10.7-8. Here,  $v_a$ ,  $\hat{v}_a$ , and  $\bar{v}_a$  are shown for  $v_s = 10\text{V}$ ,  $T = 0.1\text{ ms}$ , and  $k$  is expressed as

$$k = 0.5 + 0.5 \sin[r(t)t] \quad (10.7-46)$$

where  $r(t)$  is a ramp signal. In particular,  $r(t) = k_r t$ ; it is left to the reader to determine  $k_r$ . Before proceeding, it is important to note the difference between  $\hat{v}_a$  and  $\bar{v}_a$  at near time zero. At  $t = 0$ ,  $\bar{v}_a$  is 0.5  $v_s$ ; however,  $\hat{v}_a$  is 0. Recall that at time zero, the averaging interval is over the period before time zero ( $t - T$  to  $t$ ). Therefore,  $\hat{v}_a$  is zero until  $t$  increases from zero and the interval begins its slide with  $t$ , whereupon  $\hat{v}_a$  ramps to slightly larger than 5 V in the first period  $T$ .

When the frequency of  $k$  (10.7-46) is small, changing slow relative to the switching,  $\bar{v}_a$  is an excellent approximation of  $\hat{v}_a$ . However, when the frequency of the variation in  $k$  approaches the switching frequency, the duty cycle  $k$  can change significantly from one switching interval to the next, and  $\bar{v}_a$  is less accurate in approximating  $\hat{v}_a$ . In most applications,  $k$  and  $v_s$  do not change significantly from one switching period to the next, and  $\hat{v}_a$  is sufficiently approximated by  $\bar{v}_a$ . Therefore, we need not use the sliding averaging interval to determine  $\hat{v}_a$  for a given mode of converter operation. Instead, we will evaluate the  $\bar{v}_a$  over one period and assume that it will be a valid approximation for slow changes in  $k$  and  $v_s$  relative to the switching frequency. Let us apply this to determine  $\bar{v}_a$  for discontinuous-current operation (Fig. 10.7-4). Here

$$\begin{aligned}\bar{v}_a &= \frac{1}{T} \left[ \int_0^{kT} v_s d\xi + \int_{(k+\beta)T}^T k_v \bar{\omega}_r d\xi \right] \\ &= k v_s + (1 - k - \beta) k_v \bar{\omega}_r\end{aligned}\quad (10.7-47)$$

We have established that  $\bar{v}_a$  can be used for  $\hat{v}_a$ , and we will now assume that  $\hat{v}_a$  will give rise to  $\hat{i}_a(\hat{T}_e)$  and  $\hat{\omega}_r$ , which all together will portray the average-value dynamic and steady-state performance of the dc drive. This seems to be a logical assumption and we will omit its proof; however, for those who might question this, the details are given in Reference 3. We can now predict the average-value dynamic and steady-state performance of the one-quadrant drive for continuous- and discontinuous-current mode of operation using the average-value time-domain block diagram shown in Figure 10.7-9.

## Operating Characteristics

It is instructive to observe the performance of a dc drive supplied from a one-quadrant chopper and to compare the detailed system response with that predicted by

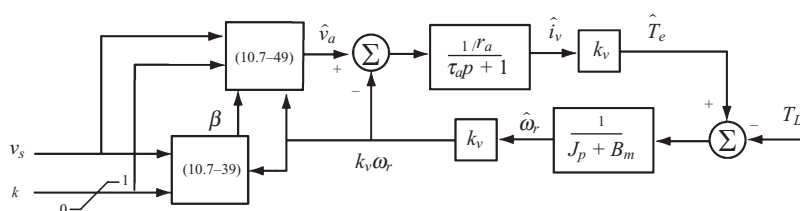


Figure 10.7-9. Average-value model for a one-quadrant chopper drive.

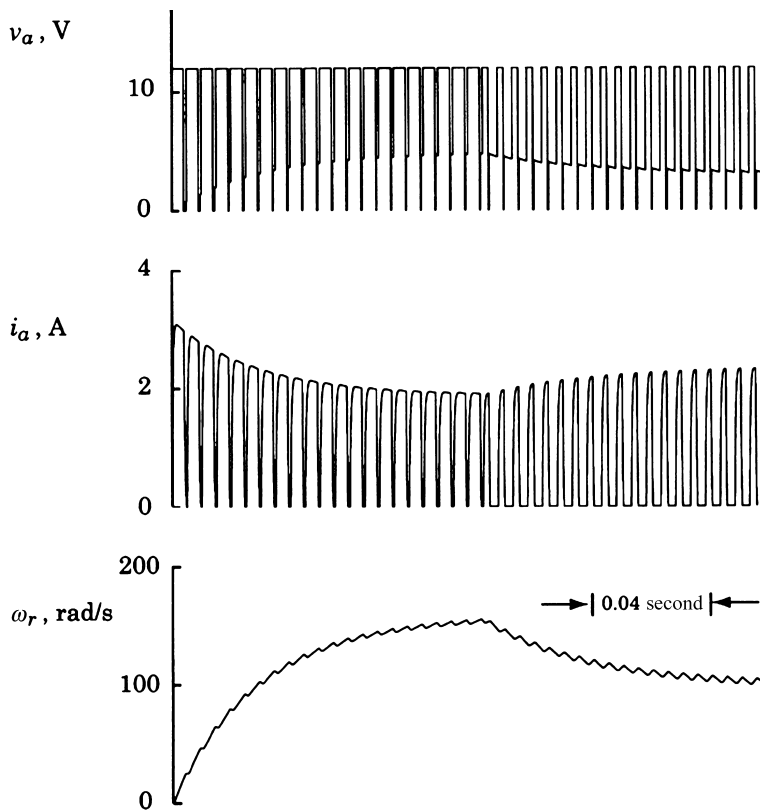


Figure 10.7-10. Operating characteristics of a one-quadrant chopper drive.

the average-value model that we have developed. The parameters of the fractional horsepower dc machine are  $r_a = 3.8\Omega$ ,  $L_{AA} = 1.14\text{mH}$ ,  $k_v = 0.031\text{V}\cdot\text{s}/\text{rad}$ ,  $J = 1.41 \times 10^{-5}\text{N}\cdot\text{m}\cdot\text{s}^2$ ,  $B_m = 2.82 \times 10^{-4}\text{ N}\cdot\text{m}\cdot\text{s}/\text{rad}$ , and  $T_L = 0$ . The source voltage  $v_s$  is 12 V. A computer study that depicts the one-quadrant chopper drive is shown in Figure 10.7-10, wherein  $v_a$ ,  $i_a$ , and  $\omega_r$  are plotted. Initially the rotor is stalled with  $k$  fixed at zero. The duty cycle is stepped to  $k = 0.8$ ; the machine accelerates and approaches steady-state operation. The duty cycle is then stepped to  $k = 0.4$ , the rotor speed decreases and again approaches steady-state operation. The last few cycles of this study are shown in Figure 10.7-11 with an expanded time scale.

It is noted that discontinuous operation occurs throughout this study. This was done intentionally by selecting a switching frequency of 200 Hz, which is at least an order of magnitude lower than normal. This makes the operation (switching) of the converter more clearly discerned and the discontinuous operation provides a difficult mode of operation for comparison purposes with the average-value model response, which is shown in Figure 10.7-12. This computer study was performed by simulating the

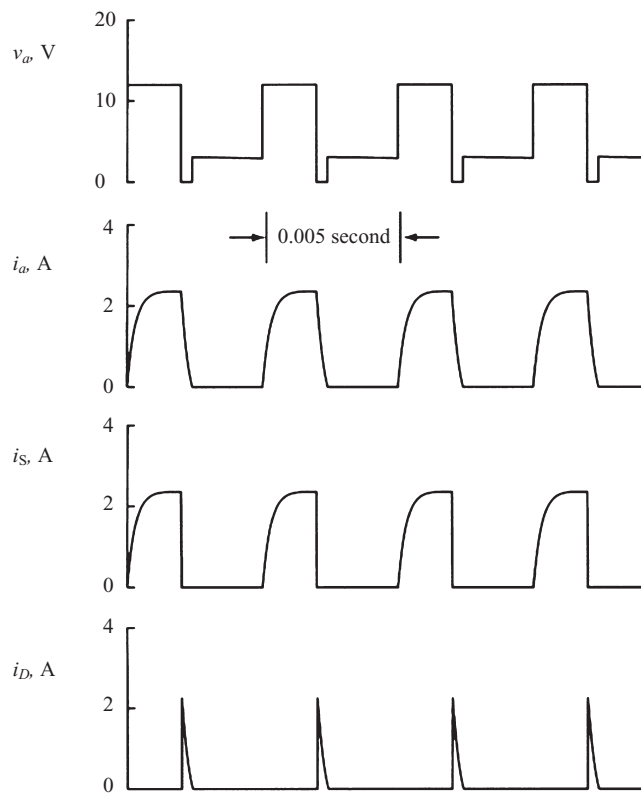


Figure 10.7-11. Part of Figure 10.7-10 with expanded time scale.

time-domain block diagram of the one-quadrant chopper drive shown in Figure 10.7-9. It appears that this average-value model adequately predicts the average performance of this system; however, there is something that can be done to make this comparison more meaningful. It is difficult to compare  $\hat{v}_a$  and  $\hat{i}_a$  (Fig. 10.7-12) with  $v_a$  and  $i_a$  (Fig. 10.7-10). The dynamic averaging process can be used to aid with this comparison. If we perform the dynamic averaging (moving or sliding averaging) process as described by (10.7-43) upon each of the variables ( $v_a$ ,  $i_a$ , and  $\omega_r$ ) shown in, we will obtain  $\hat{v}_a$ ,  $\hat{i}_a$  and  $\hat{\omega}_r$  as shown in Figure 10.7-13. The comparison of Figure 10.7-12 and Figure 10.7-13 clearly establishes the accuracy of the average-value model. Please realize that by selecting  $T$  much larger than normal to intentionally insure discontinuous-current operation for the machine parameters and load conditions, a very strict test has been imposed upon the accuracy of average-value modeling. From the comparison of Figure 10.7-10 and Figure 10.7-13, it is clear that the average-value model can be used without reservation to analyze and design a one-quadrant chopper drive system for most modes of operation.

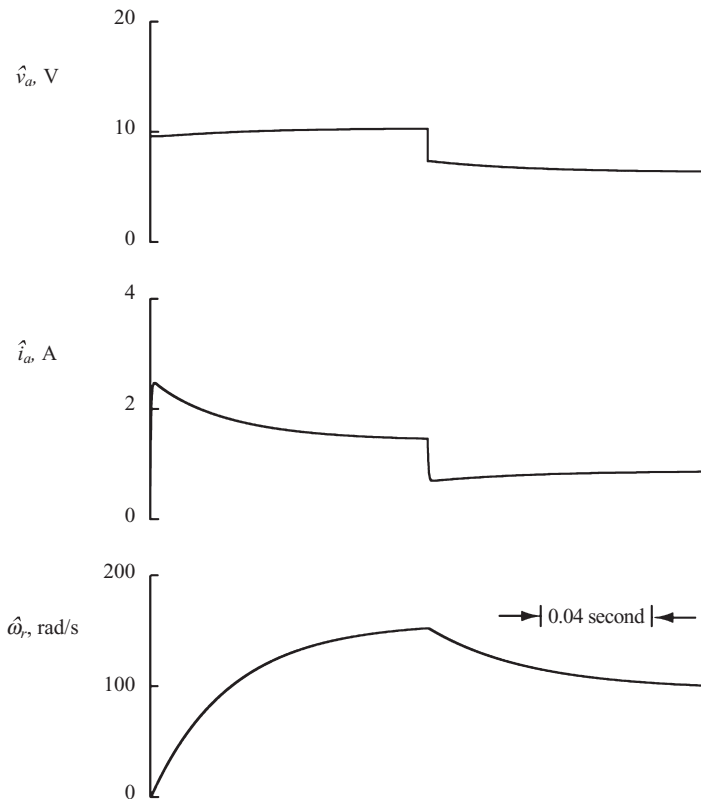


Figure 10.7-12. Same as Figure 10.7-10 using the average-value model shown in Figure 10.7-9.

**EXAMPLE 10C** A change in source voltage is depicted in Figure 10C-1. During the  $i$ th interval, the source voltage is  $v_{Si}$  and  $v_{S(i+1)}$  during the  $i^{\text{th}} + 1$  interval. The duty cycle  $k$  and the switching period are constant. Let us determine the dynamic average. We realize that for  $t \leq t_{i+1}$ , the dynamic average is  $kv_{Si}$  and for  $t - T \geq t_i + kT$  the dynamic average is  $kv_{S(i+1)}$ . During the interval for  $t_{i+1} \leq t \leq t_{i+1} + kT$ , the dynamic average is

$$\begin{aligned}
 \hat{v}_a &= \frac{1}{T} \left[ \int_{t-T}^{t_i+kT} v_{Si} d\xi + \int_{t_{i+1}}^t v_{S(i+1)} d\xi \right] \\
 &= \frac{1}{T} [v_{Si}(t_i + kT - t + T) + v_{S(i+1)}(t - t_{i+1})] \\
 &= kv_{Si} + (v_{Si} - v_{S(i+1)}) \left( \frac{t_{i+1} - t}{T} \right) \quad \text{for } t_{i+1} \leq t \leq t_{i+1} + kT
 \end{aligned} \tag{10C-1}$$

A plot of (10C-1) is shown in Figure 10C-2.

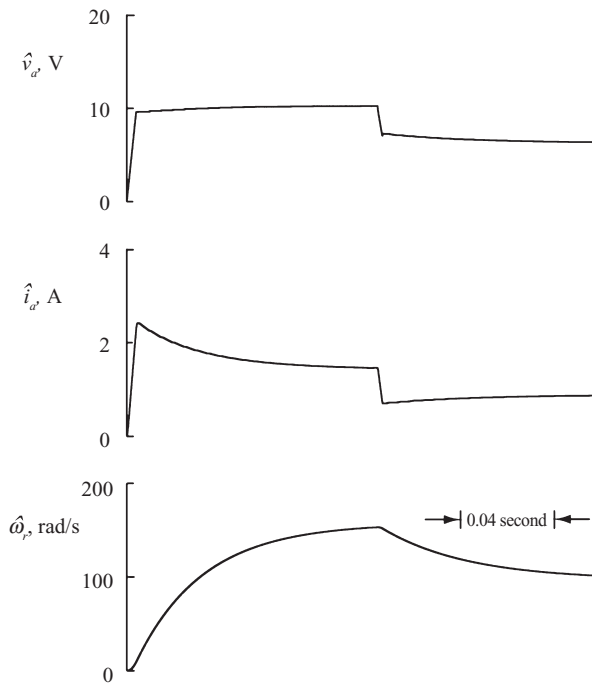


Figure 10.7-13. Dynamic average of variables shown in Figure 10.7-10.

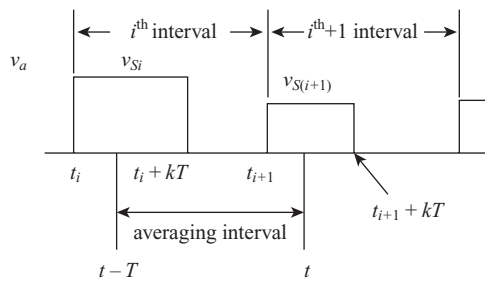


Figure 10C-1. Dynamic averaging of  $v_a$  for a change in source voltage  $v_s$ .

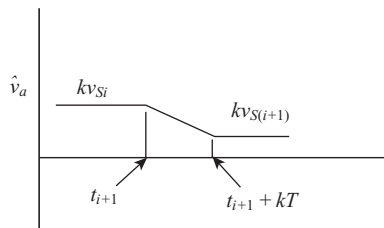


Figure 10C-2.  $\hat{v}_a$  versus  $t$  for  $v_a$  shown in Figure 10C-1.

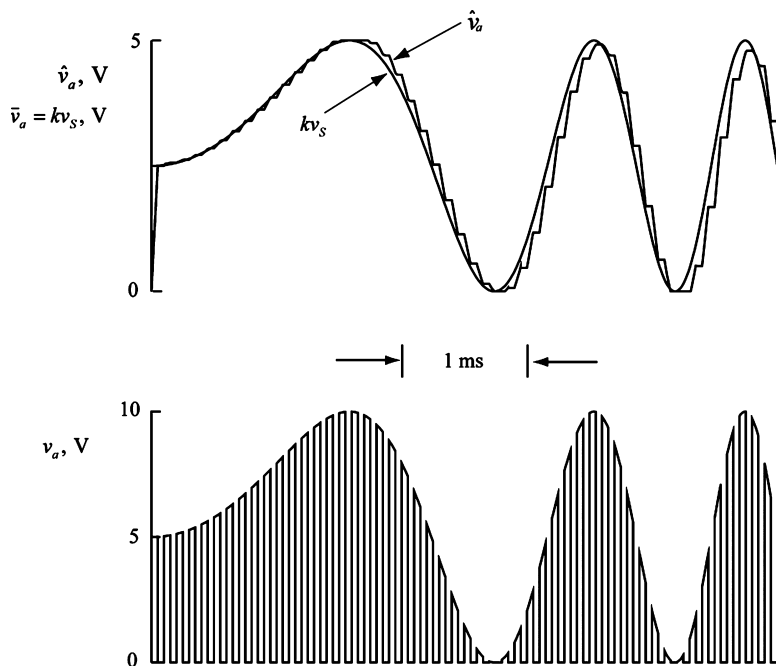


Figure 10C-3. Comparison of  $\hat{v}_a$  and  $\bar{v}_a$  for  $v_s = 5 + 5 \sin[r(t)t]$ .

It is interesting to compare  $\hat{v}_a$  and  $\bar{v}_a$  for

$$v_s = 5 + 5 \sin r(t)t \quad (10C-2)$$

The comparison is shown in Figure 10C-3, wherein  $T = 0.1$  ms and  $k = 0.6$ . The plots in Figure 10C-3 depict a comparison of  $\hat{v}_a$  and  $\bar{v}_a$  similar to that noted for a change in  $k$ . The signal  $\bar{v}_a = kv_s$  very closely approximates  $\hat{v}_a$  until the frequency of the change in  $v_s$  approaches the switching frequency.

## 10.8. TWO-QUADRANT DC/DC CONVERTER DRIVE

A simplified schematic diagram of a two-quadrant chopper supplying a dc machine is shown in Figure 10.8-1. Typical waveforms of the converter variables during steady-state operation are shown in Figure 10.8-2. With a two-quadrant chopper, the armature voltage cannot be negative ( $v_a \geq 0$ ); however, the armature current can be positive or negative. That is,  $I_1$  and  $I_2$  (Fig. 10.8-2) can both be positive, whereupon the two-quadrant chopper is operating as a continuous-current one-quadrant chopper, or  $I_1$  can be negative and  $I_2$  positive, or  $I_1$  and  $I_2$  can both be negative. The mode of operation where  $I_1$  is negative and  $I_2$  is positive is shown in Figure 10.8-2. The mode of operation depicted is motor operation since the average value of  $i_a$  is positive.

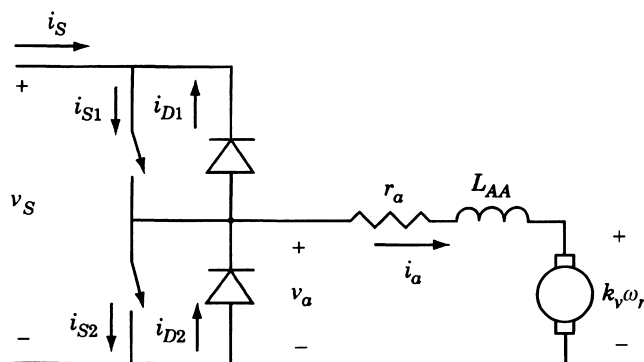


Figure 10.8-1. Two-quadrant chopper drive system.

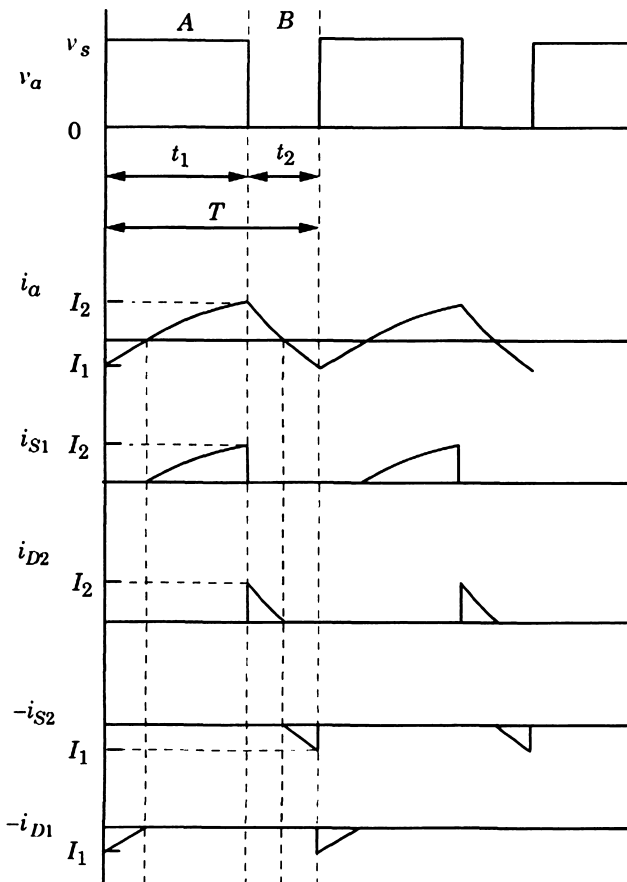


Figure 10.8-2. Typical waveforms for steady-state operation of a two-quadrant chopper drive.

In a two-quadrant chopper, there are two switches and two diodes arranged, as shown in Figure 10.8-1. As in the case of the one-quadrant chopper, we will assume that these devices are ideal. The switching logic is generated from the duty cycle  $k$ , as shown in Figure 10.7-2. When the comparator output signal is high,  $S1$  is closed and  $S2$  is open (interval A in Fig. 10.8-2); when it is low,  $S1$  is open and  $S2$  is closed (interval B in Fig. 10.8-2). There is a practical consideration that must be mentioned. Electronic switches have finite turn-off and turn-on times. The turn-off time is generally longer than the turn-on time. Therefore, the switching logic must be arranged so that the turn-on signal is delayed in order to prevent short-circuiting the source, causing "shoot-through." Although the delay is very short, it must be considered in the design; however, it does not make our analysis invalid wherein we will assume instant-on, instant-off operation.

It is important to discuss the mode of operation depicted in Figure 10.8-2. During interval A,  $S1$  is closed and  $S2$  is open and, at the start of interval A,  $i_a = I_1$ , which is negative in Figure 10.8-2. Since  $S2$  is open, a negative  $i_a$  ( $I_1$ ) can only flow through  $D1$ . It is important to note that  $-i_{D1}$  and  $-i_{S2}$  are plotted in Figure 10.8-2 to allow ready comparison with the waveform of  $i_a$ . Let us go back to the start of interval A. How did  $i_a$  become negative? Well, during the interval B, in the preceding period,  $S2$  was closed with  $S1$  open. With  $S2$  closed, the armature terminals are short-circuited, and the counter emf has driven the  $i_a$  negative. Therefore, when  $S1$  is closed and  $S2$  is opened at the start of interval A, the source voltage has to contend with this negative  $I_1$ . We see from Figure 10.8-2 that the average value of  $i_a$  is slightly positive, which indicates that the dc machine is operating as a motor. Therefore,  $v_s$  is larger than the counter emf, and at the start of interval A, when  $v_s$  is applied to the machine, the armature current begins to increase toward zero from the negative value of  $I_1$ . Once  $i_a$  reaches zero, the diode  $D1$  blocks the current flow. That is,  $i_{D1}$  cannot become negative; however,  $S1$  has been closed since the start of interval A, and since  $i_{S1}$  can only be positive,  $S1$  is ready to carry the positive  $i_a$ . The armature current, which is now  $i_{S1}$  continuous to increase until the end of interval A ( $I_2$ ).

At the beginning of interval B,  $S1$  is opened and  $S2$  is closed. However,  $S2$  cannot conduct a positive armature current. Therefore, the positive current ( $I_2$ ) is diverted to diode  $D2$ , which is short-circuiting the armature terminals. Now, the counter emf has the positive current ( $I_2$ ) with which to contend. It is clear that if the armature terminals were permanently short-circuited, the counter emf would drive  $i_a$  negative. At the start of interval B, the counter emf begins to do just that; however, when  $i_a$  becomes zero, diode  $D2$  blocks  $i_{D2}$  and the negative armature current is picked up by  $S2$ , which has been closed, since the beginning of interval B, waiting to be called upon to conduct a negative armature current. This continues until the end of interval B whereupon we are back to where we started.

It is apparent that if the mode of operation is such that  $I_1$  and  $I_2$  are both positive, then the machine is acting as a motor with a substantial load torque. In this mode, either  $S1$  or  $D2$  will carry current during a switching period  $T$ . If both  $I_1$  and  $I_2$  are negative, the machine is operating as a generator, delivering power to the source. In this case, either  $S2$  or  $D1$  will carry current during a switching period.

From Figure 10.8-2, we see that each switching period is divided into interval A and interval B. This is identical to that shown in Figure 10.7-3 for a one-quadrant

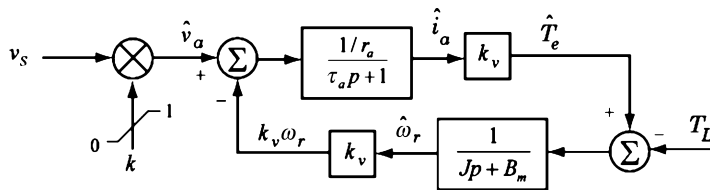


Figure 10.8-3. Average-value model of a two-quadrant chopper drive.

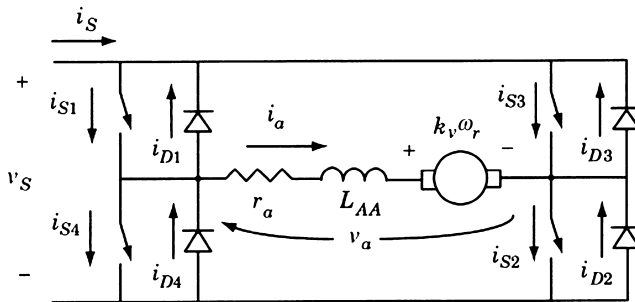


Figure 10.9-1. Four-quadrant chopper drive system.

chopper in the continuous-current mode of operation. Hence, the relationships developed in the previous section for continuous-current operation of a one-quadrant chopper apply directly to the two-quadrant chopper. The average-value time-domain block diagram for the two-quadrant chopper drive system is shown in Figure 10.8-3.

## 10.9. FOUR-QUADRANT DC/DC CONVERTER DRIVE

A simplified schematic diagram of a four-quadrant chopper drive system is shown in Figure 10.9-1. Typical steady-state waveforms that depict the operation of the converter are shown in Figure 10.9-2. As the name implies, four-quadrant operation (voltage vs. current) is possible. That is, the instantaneous armature current  $i_a$  and the instantaneous armature voltage may be positive or negative. Four-quadrant operation is depicted in Figure 10.9-2. Therein,  $I_1$  is negative and  $I_2$  is positive, and  $v_a$  is  $v_s$  during interval A and  $-v_s$  during interval B; however, the average  $v_a$  and the average  $i_a$  are positive. Therefore, from an average-value point of view, the dc drive system depicted in Figure 10.9-2 is operating as a motor with the rotor speed  $\omega_r$  positive (say ccw). This is first-quadrant operation of an average-current versus average-voltage plot even though four-quadrant operation occurs each switching period. In the fourth quadrant, the average  $v_a$  is positive, average  $i_a$  is negative, and  $\omega_r$  is positive (ccw); the machine is operating as a generator. In the second quadrant, average  $v_a$  is negative, average  $i_a$  is positive, and  $\omega_r$  is negative (cw)—generator operation. In the third quadrant, average

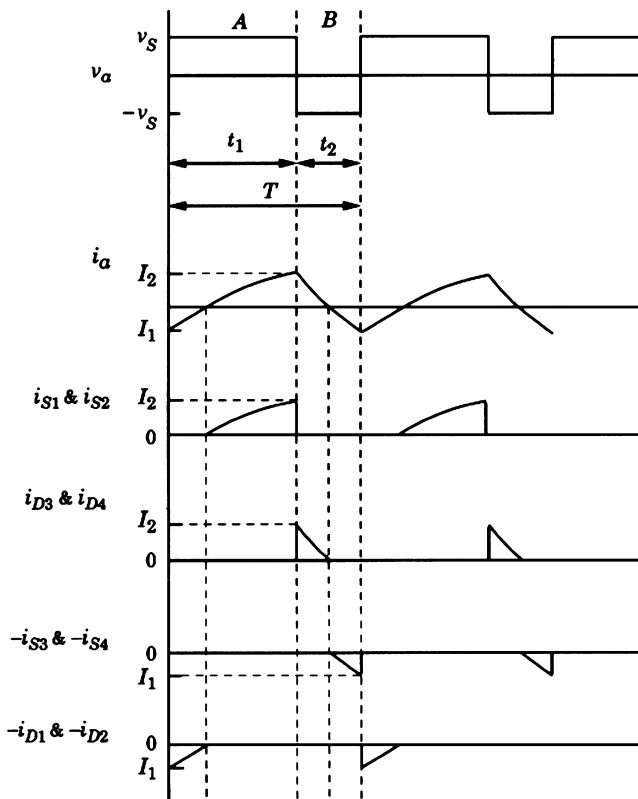


Figure 10.9-2. Typical waveforms for steady-state operation of a four-quadrant chopper drive.

$v_a$  is negative, average  $i_a$  is negative, and  $\omega_r$  is negative (cw)—motor operation. One must distinguish between four-quadrant operation during a period and four-quadrant average-value operation.

There are numerous switching strategies that might be used with a four-quadrant chopper. The switching depicted in Figure 10.9-2 is perhaps one of the least involved. In this case, there are only two states. In the first state, which occurs over interval A,  $S_1$  and  $S_2$  are closed and  $S_3$  and  $S_4$  are open. The second state occurs over interval B, wherein the  $S_3$  and  $S_4$  are closed and  $S_1$  and  $S_2$  are open. As in the case of the previous dc/dc converters, we will consider the switches and diodes as being ideal.

During interval A,  $S_1$  and  $S_2$  are closed and  $S_3$  and  $S_4$  are open. At the beginning of the interval,  $i_a$  is negative ( $I_1$ ) in Figure 10.9-2. Since  $S_1$  and  $S_2$  cannot carry negative armature current,  $I_1$  must flow through diodes  $D_1$  and  $D_2$ . Note in Figure 10.9-2 that  $-i_{D1}$ ,  $-i_{D2}$ ,  $-i_{S3}$ , and  $-i_{S4}$  are plotted for the purpose of a direct comparison with  $i_a$ . During interval A the armature voltage  $v_a$  is  $v_s$  and since  $v_s$  is larger than the counter emf, the armature current increases from the negative value of  $I_1$  toward

zero. During this part of interval, the source current is  $-i_{D1}$ , which is also  $-i_{D2}$ . When  $i_a$  reaches zero,  $D1$  and  $D2$  block positive armature current flow; however,  $S1$  and  $S2$  are closed ready to carry a positive  $i_a$ . Hence, the current increases from zero to  $I_2$  through  $S1$  and  $S2$ . During this part of interval, the source current  $i_s$  is  $i_{S1}$ , which is also  $i_{S2}$ .

During interval B,  $v_a$  is  $-v_s$  and  $S1$  and  $S2$  are open, with  $S3$  and  $S4$  closed. At the beginning of interval B,  $i_a$  is positive ( $I_2$ ); however,  $S3$  and  $S4$  cannot conduct a positive armature current. Hence, at the beginning of interval B, the positive  $I_2$  flows through diodes  $D3$  and  $D4$ . This continues until  $i_a$  is driven to zero by  $-v_s$ . During this part of interval B, the source current  $i_s$  is  $-i_{D3}$  or  $-i_{D4}$ . When  $i_a$  reaches zero, diodes  $D3$  and  $D4$  block negative  $i_a$ ; thus,  $S3$  and  $S4$  carry the negative armature current to the end of interval B, where  $i_a = I_1$  which is negative. During this part of interval B, the source current  $i_s$  is  $i_{S3}$  or  $i_{S4}$ . We have completed a switching cycle.

Expressions for  $I_1$  and  $I_2$  can be derived by a procedure similar to that used in the case of the previous choppers. It can be shown that

$$I_1 = \frac{v_s}{r_a} \left[ \frac{2e^{-(1-k)T/\tau_a} - e^{-T/\tau_a} - 1}{1 - e^{-T/\tau_a}} \right] - \frac{k_v \omega_r}{r_a} \quad (10.9-1)$$

$$I_2 = \frac{v_s}{r_a} \left[ \frac{1 - 2e^{-kT/\tau_a} + e^{-T/\tau_a}}{1 - e^{-T/\tau_a}} \right] - \frac{k_v \omega_r}{r_a} \quad (10.9-2)$$

If  $k$  and  $v_s$  do not change significantly from one switching period to the next, the average armature voltage may be expressed as

$$\begin{aligned} \bar{v}_a &= \frac{1}{T} \left[ \int_0^{kT} v_s d\xi + \int_{kT}^T -v_s d\xi \right] \\ &= \frac{1}{T} [kTv_s - (1-k)Tv_s] \\ &= (2k-1)v_s \end{aligned} \quad (10.9-3)$$

Note that when  $k = 0$ ,  $v_a = -v_s$ , and when  $k = 1$ ,  $v_a = v_s$ . It is clear that the time-domain block diagram for the four-quadrant chopper drive is the same as that shown in Figure 10.8-3 for the two-quadrant chopper drive, with  $v_a = kv_s$  replaced with  $v_a = (2k-1)v_s$ , which is (10.9-3).

## 10.10. MACHINE CONTROL WITH VOLTAGE-CONTROLLED DC/DC CONVERTER

Although we will not become involved in the design of closed-loop controls, it is important to discuss typical control systems and to set the stage for control design using the average-value models. When the dc/dc converter is used to control the voltage applied to the armature circuit,  $v_a$ , through the duty cycle,  $k$ , it is a voltage-controlled dc/dc converter. We will continue with this type of converter in this section; in the

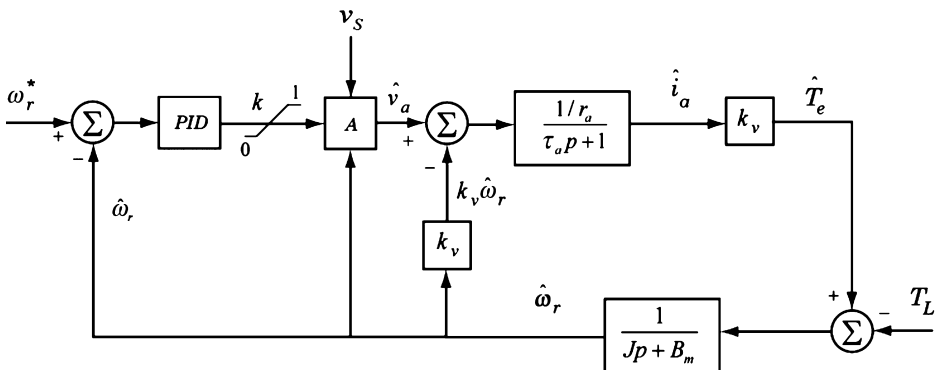


Figure 10.10-1. Speed control of dc machine with voltage-controlled dc/dc converter.

following section, we will introduce the so-called current-controlled dc/dc converter, which is generally implemented by appropriate control of a four-quadrant dc/dc converter.

### Speed Control: Voltage-Controlled dc/dc Converter

A block diagram of a machine speed control with a voltage-controlled chopper is shown in Figure 10.10-1. Therein,  $\omega_r^*$  is the reference or commanded speed. The error signal is supplied to a basic controller herein noted as a PID controller. The output of the PID controller is the duty cycle which, along with the source voltage and the rotor speed, are inputs to block A. The output of block A is the average armature voltage. The rest of the block diagram is self-explanatory.

It is clear that the calculation of the average armature voltage that occurs in block A will depend upon the type of chopper being used. For a one-quadrant chopper, the calculation performed in block A is

$$\hat{v}_a = kv_s + (1 - k - \beta)k_v \hat{\omega}_r \quad (10.10-1)$$

For a two-quadrant chopper, the calculation in block A is

$$\hat{v}_a = kv_s \quad (10.10-2)$$

For a four-quadrant chopper, the block A calculation is

$$\hat{v}_a = (2k - 1)v_s \quad (10.10-3)$$

The average rotor speed  $\hat{\omega}_r$  is shown as an input to block A. It is needed to calculate  $\beta$  for the one-quadrant chopper; however, it is not needed to calculate  $\hat{v}_a$  for the two- and four-quadrant choppers. It is clear that only the four-quadrant chopper can be used for bidirectional speed control.

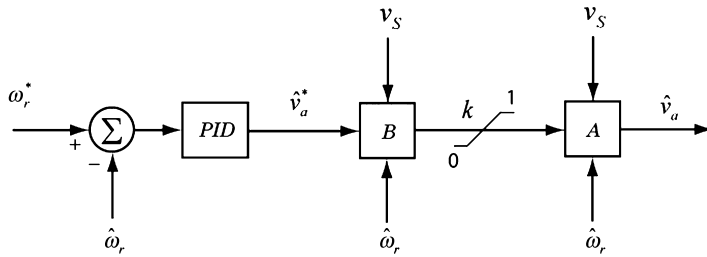


Figure 10.10-2. Feedforward voltage control.

### Speed Control: Voltage-Controlled dc/dc Converter with Voltage Feedforward Control

A block diagram of a machine speed control with a voltage-controlled chopper equipped with voltage feedforward control is shown in Figure 10.10-2. In this case, the PID controller establishes the desired or commanded  $\hat{v}_a^*$  from the speed error signal. The source voltage and average rotor speed are inputs to block B along with  $\hat{v}_a^*$ . The output of block B is the duty cycle that is an input to block A as in Figure 10.10-1.

The calculations to be performed in block B are obtained by applying (10.10-1), (10.10-2), and (10.10-3) and then solving each equation for the duty cycle  $k$ . In particular, for a one-quadrature chopper, the calculation performed in block B is

$$k = \frac{\hat{v}_a^* - k_v \bar{\omega}_r (1 - \beta)}{v_s - k_v \bar{\omega}_r} \quad \text{with } 0 \leq \hat{v}_a^* \leq v_s \quad (10.10-4)$$

For a two-quadrant chopper

$$k = \frac{\hat{v}_a^*}{v_s} \quad \text{with } 0 \leq \hat{v}_a^* \leq v_s \quad (10.10-5)$$

For the four-quadrant chopper

$$k = \frac{1}{2} + \frac{\hat{v}_a^*}{2v_s} \quad \text{with } -v_s \leq \hat{v}_a^* \leq v_s \quad (10.10-6)$$

As in the case of block A, the average rotor speed is not needed in block B for the two- and four-quadrant choppers.

The purpose of the feedforward (block B) is clear once we consider the response of the speed control shown in Figure 10.10-1 to a change in source voltage,  $v_s$ . If, for example,  $v_s$  decreases, then  $\hat{v}_a$ , the output of block A, decreases by the same amount since the duty cycle  $k$  will not change to compensate for the decrease in  $v_s$  until the rotor speed has decreased and the action of the PID controller increases  $k$ . With the voltage feedforward control, the calculation in block B is aware of the decrease in  $v_s$

and instantaneously increases  $k$  to compensate for this decrease. Hence,  $\hat{v}_a$  remains essentially unaware of a change in  $v_s$ ; consequently, the average torque and thus the speed are not affected by a change in source voltage.

## 10.11. MACHINE CONTROL WITH CURRENT-CONTROLLED DC/DC CONVERTER

Current-control of dc machines is very desirable since by controlling the current, the torque is controlled. Moreover, current control can be used to prevent large damaging armature currents during start-up. Some form of current control or limiting can be achieved using the one- and two-quadrant choppers; however, the four-quadrant chopper is the most appropriate for current control since the polarity of the armature voltage can be reversed, thereby allowing the maximum possible current-control capability. It is not our purpose to become involved in the design, operation, and application of current-controlled dc/dc converters. Nevertheless, we will set forth the operation of the four-quadrant current-controlled chopper from an ideal point of view, and, where appropriate, establish an average-value model that may be used for analysis and design purposes.

### Current-Controlled Four-Quadrant dc/dc Converter

It is recalled from our discussion of the four-quadrant chopper (Fig. 10.9-1) that the source current equals  $i_a$  ( $i_s = i_a$ ), where  $S1$  and  $S2$  are closed and  $i_s = -i_a$  when  $S3$  and  $S4$  are closed. Since we wish to control  $i_a$ , it is necessary to measure it directly or establish it from a measurement of  $i_s$ . The latter is generally done, as shown in Figure 10.11-1, by picking up a signal proportional to  $i_s$  from a resistive shunt placed in the  $i_s$  path on the low voltage (negative) side of the source voltage. That is, since the low side of the source voltage is grounded, the resistive shunt is connected in series with  $i_s$  between the bottom connection of  $S4$  and  $D4$  and ground. The demodulator shown in Figure 10.11-1 is used to obtain a signal proportional to  $i_a$  ( $Ki_a$ ) from  $i_s$  ( $Ki_s$ ). As indicated in Figure 10.11-1, this is achieved by switching low-power transistors with  $S1$  ( $S2$ ) and  $S3$  ( $S4$ ) unfolding  $Ki_s$  into  $Ki_a$ . The signal  $Ki_a$  is then compared with the commanded  $Ki_a^*$ , and the error signal is supplied to a comparator with hysteresis (Fig. 10.11-2). When the output of this comparator ( $L$ ) is high,  $S1$  and  $S2$  are closed and  $S3$  and  $S4$  are open; when  $L$  is low,  $S3$  and  $S4$  are closed and  $S1$  and  $S2$  are open.

The action of this type of current control is illustrated in Figure 10.11-3. Therein,  $i_a^*$  is stepped from zero to a positive value. At the instant of the step increase, the error signal, which is the input to the comparator with hysteresis, is positive and greater than  $\epsilon$ . The output of the comparator is high, and  $S1$  and  $S2$  are closed and  $S3$  and  $S4$  are open. The armature current increases until  $i_a = i_a^* + \epsilon$ , at which time the comparator output steps low and  $S1$  and  $S2$  are opened and  $S3$  and  $S4$  are closed. The armature current decreases until  $i_a = i_a^* - \epsilon$ , at which time the comparator output becomes high;  $S1$  and  $S2$  are closed and  $S3$  and  $S4$  are opened. This cycling will continue until the commanded current is changed. It is apparent from Figure 10.11-2 and Figure 10.11-3

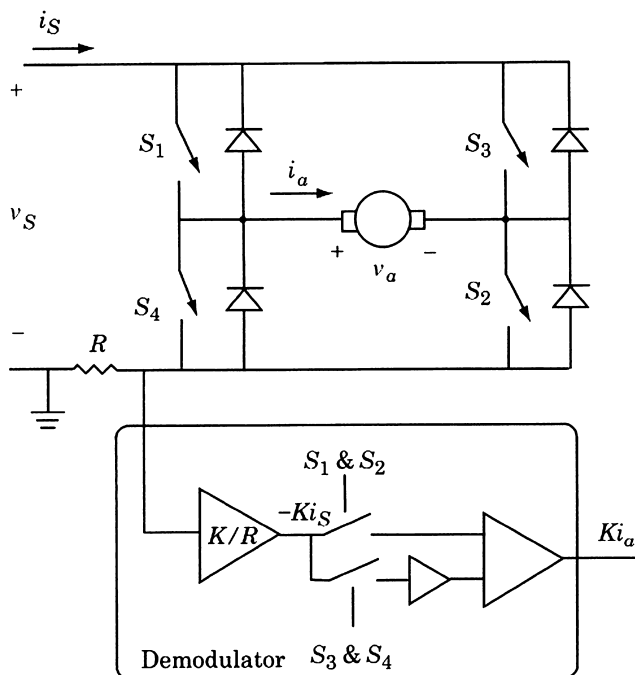


Figure 10.11-1. Demodulator:  $Ki_S$  to  $Ki_a$ .

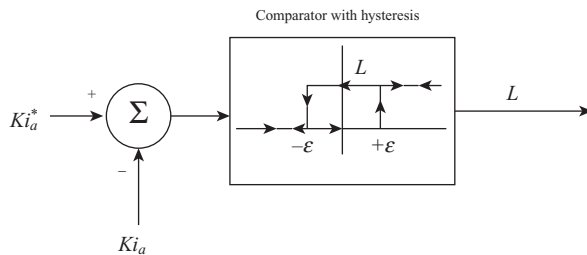


Figure 10.11-2. Hysteresis-type current controller of a current-controlled four-quadrant chopper.

that the period of this cycling or switching, which is denoted as  $T$  in Figure 10.11-3, is directly related to the bounds ( $\pm\epsilon$ ) within the hysteresis comparator.

For analysis purposes, the switching period is divided into two intervals,  $t_1$  and  $t_2$ . During  $t_1$ ,  $S1$  and  $S2$  are closed and  $v_S$  is applied to the armature circuit; during  $t_2$ ,  $S3$  and  $S4$  are closed and  $-v_S$  is applied to the armature circuit. The rise time is also shown in Figure 10.11-3. This is denoted by  $t_r$ , and it is defined as the time for the current to increase from zero to the commanded current with the rotor speed equal to zero. If we set  $I_1 = 0$  and  $\omega_r = 0$  in (10.7-14)

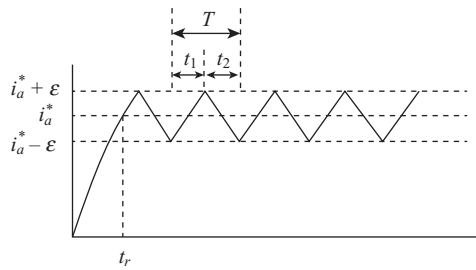


Figure 10.11-3. Typical response of a current-controlled four-quadrant chopper for step increase in  $i_a^*$  from zero.

$$i_a = \frac{v_s}{r_a} (1 - e^{t/\tau_a}) \quad (10.11-1)$$

If we now let  $i_a = i_a^*$  at  $t = t_r$ , (10.11-1) can be solved for  $t_r$

$$t_r = -\tau_a \ln \left( 1 - \frac{r_a i_a^*}{v_s} \right) \quad (10.11-2)$$

It is now of interest to obtain expressions for  $t_1$  and  $t_2$  in terms of  $v_s$ ,  $\epsilon$  (the hysteresis limits), and machine parameters. It is clear that  $\epsilon$  is generally made small in order to achieve minimum variation in  $i_a$  about  $i_a^*$ , and since  $r_a$  is generally small,  $i_a$  can be approximated by a straight line between  $i_a^* \pm \epsilon$ . The familiar voltage equation for the armature circuit is

$$v_a = r_a i_a + L_{AA} \frac{di_a}{dt} + \omega_r k_v \quad (10.11-3)$$

Our purpose is to obtain a straight-line approximation for  $i_a^* - \epsilon \leq i_a \leq i_a^* + \epsilon$ . If in (10.11-3) we let  $r_a i_a = r_a i_a^*$ , and if we assume  $v_s$  and  $\omega_r$  are constant over the switching period  $T$ , then with  $S1$  and  $S2$  closed

$$i_a = i_a^* - \epsilon + \frac{1}{L_{AA}} (v_s - r_a i_a^* - k_v \omega_r) t \quad \text{for } 0 \leq t < t_1 \quad (10.11-4)$$

Note that we have selected time zero at the beginning of the switching period  $T$ . During the interval when  $S3$  and  $S4$  are closed

$$i_a = i_a^* + \epsilon - \frac{1}{L_{AA}} (v_s + r_a i_a^* + k_v \omega_r) t \quad \text{for } t_1 \leq t < t_2 \quad (10.11-5)$$

If in (10.11-4) we set  $t = t_1$ , then  $i_a = i_a^* + \epsilon$  and  $t_1$  becomes

$$t_1 = \frac{2L_{AA}\epsilon}{v_s - r_a i_a^* - k_v \omega_r} \quad (10.11-6)$$

This expression for  $t_1$ , albeit an approximation, provides us with information which we would have expected if we would have thought about it. As  $v_s - r_a i_a^* - k_v \omega_r$  approaches zero,  $t_1$  approaches infinity. This says that as the rotor speed increases, the source voltage is not large enough ( $S1$  and  $S2$  fixed closed) to maintain the commanded current. In other words, the chopper is unable to provide the commanded current, and it has lost current tracking capability. We would expect this unless  $v_s$  could be increased without limit.

Now, what about  $t_2$ ? Well if, in (10.11-5), we set  $t = t_2$ ,  $i_a = i_a^* - \epsilon$  and solve for  $t_2$

$$t_2 = \frac{2L_{AA}\epsilon}{v_s + r_a i_a^* + k_v \omega_r} \quad (10.11-7)$$

Hence,  $t_2$  approaches zero as  $\omega_r$  approaches infinity. In other words, the higher the speed, the faster  $i_a$  decreases from  $i_a^* + \epsilon$  to  $i_a^* - \epsilon$ . That seems logical.

We can now express the switching period  $T$ . After some manipulation

$$T = t_1 + t_2 \\ = \frac{4L_{AA}v_s\epsilon}{v_s^2 - (r_a i_a^* + k_v \omega_r)^2} \quad (10.11-8)$$

Here we again see what (10.11-6) already told us;  $T$  approaches infinity as  $v_s - r_a i_a^* - k_v \omega_r$  approaches zero. In other words,  $T$  becomes larger as the rotor speed increases.

The operation of a four-quadrant current-controlled chopper during the starting of a dc machine is shown in Figure 10.11-4. Therein the current and rotor speed are plotted.

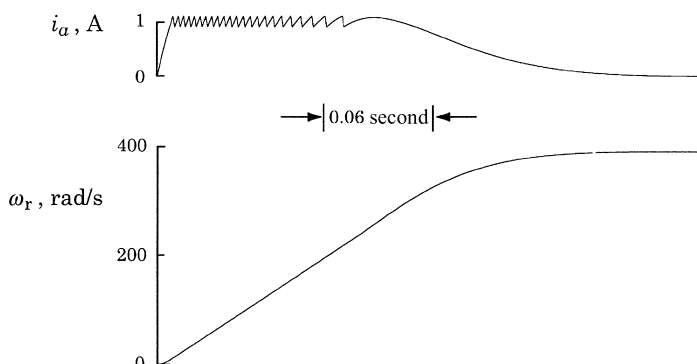


**Figure 10.11-4.** Acceleration from stall of dc drive with currents-controlled dc/dc converter.

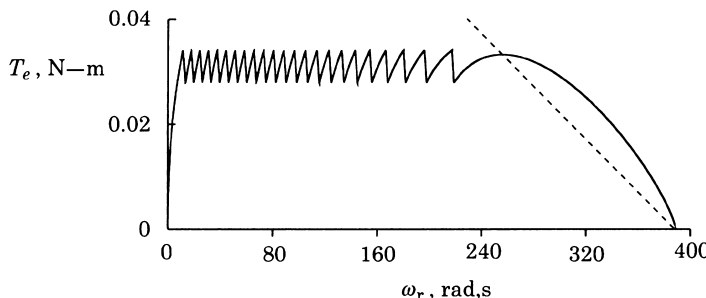


Figure 10.11-5. Torque versus speed for acceleration shown in Figure 10.11-4.

The dynamic torque versus speed characteristics for this acceleration period are shown in Figure 10.11-5. The steady-state torque speed characteristic is also shown in this figure by a dashed line. The parameters of the fractional horsepower dc machine and current controller are:  $r_a = 3.8 \Omega$ ,  $L_{AA} = 76 \text{ mH}$ ,  $k_v = 0.031 \text{ V}\cdot\text{s}/\text{rad}$ ,  $J = 1.41 \times 10^{-5} \text{ kg}\cdot\text{m}^2$ ,  $\varepsilon = 0.1 \text{ A}$ ,  $i_a^* = 1 \text{ A}$ , and  $v_S = 12 \text{ V}$ .

The plot of  $i_a$  (Fig. 10.11-4) illustrates the characteristics of the current control discussed earlier. In particular,  $t_1$  and  $T$  increase as the speed increases while  $t_2$  decreases. The commanded current  $i_a^*$  is set at 1 A. It appears from Figure 10.11-4 and Figure 10.11-5 that current tracking is lost when  $\omega_r$  is near 250 rad/s, after which the machine accelerates to the steady-state speed with  $v_a = v_S$  ( $S1$  and  $S2$  closed). Actually, we can approximate the speed at which current tracking will be lost. When  $S1$  and  $S2$  are closed, and if we let  $i_a = i_a^*$ , the armature voltage equations becomes

$$v_S = r_a i_a^* + L_{AA} \frac{di_a^*}{dt} + \omega_r k_v \quad (10.11-9)$$

Since  $di_a^* / dt$  is zero, we can approximate the maximum rotor speed at which  $v_S$  can maintain  $i_a^*$  with  $S1$  and  $S2$  fixed closed. In particular, for first-quadrant operation

$$\omega_r = \frac{1}{k_v} (v_S - r_a i_a^*) \quad (10.11-10)$$

This becomes  $(1/0.031)(12 - 3.8 \times 1) = 264.5 \text{ rad/s}$  for the conditions depicted in Figure 10.11-4 and Figure 10.11-5.

It is difficult to portray the action of a current-controlled converter with an average-value model when current tracking is lost. In Figure 10.11-4, current tracking occurs during most of the acceleration period; however, current tracking does not occur during the initial rise of the current and during the final acceleration period. It is clear that a single continuous average-value model cannot predict all modes of operation. Switching or high-gain clamping circuits must be incorporated. Such models are beyond the scope of this treatment of dc drives.

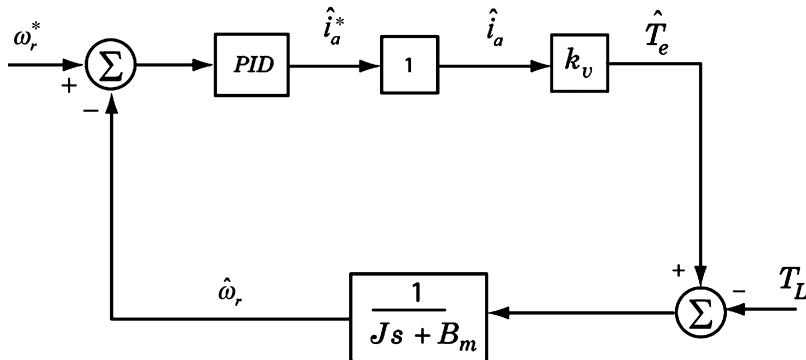


Figure 10.11-6. Speed control of dc machine with current-controlled dc/dc converter: current tracking operation.

### Speed Control: Current-Controlled dc/dc Converter

An average-value model that can be used for speed control of a dc machine being supplied from a current-controlled dc/dc converter is shown in Figure 10.11-6. This average-value model is valid only when  $i_a^*$  is being maintained. When current tracking is lost, this average-value model is not valid. It is clear that it may be appropriate to include a safeguard to prevent its use when current tracking is lost. Perhaps incorporating a version of (10.11-10) to limit  $\omega_r^*$  might be sufficient. In any event, the average-value model is valid for analysis and design purposes during current tracking.

### REFERENCES

- [1] B.C. Kuo, *Automatic Control Systems*, Prentice-Hall, Englewood Cliffs, NJ, 1987.
- [2] P.C. Sen, *Thyristor DC Drives*, John Wiley & Sons, New York, 1981.
- [3] J.G. Kassakian, M.F. Schlecht, and G.C. Verghese, *Principles of Power Electronics*, Addison-Wesley, Reading, MA, 1991.

### PROBLEMS

1. The parameters of a dc shunt machine are  $R_f = 240\Omega$ ,  $L_{FF} = 120\text{H}$ ,  $L_{AF} = 1.8\text{H}$ ,  $r_a = 0.6\Omega$ , and  $L_{AA} = 0$ . The load torque is  $5\text{N}\cdot\text{m}$  and  $V_a = V_f = 240\text{V}$ . Calculate the steady-state rotor speed.
2. The power input to a dc shunt motor during rated-load conditions is  $100\text{W}$ . The rotor speed is  $2000\text{r/min}$ , and the armature voltage is  $100\text{V}$ . The armature resistance is  $2\Omega$  and  $R_f = 200\Omega$ . Calculate the no-load rotor speed.
3. A permanent-magnet dc motor has the following parameters:  $r_a = 8\Omega$  and  $k_v = 0.01\text{Vs}/\text{rad}$ . The shaft load torque is approximated as  $T_L = K\omega_r$ , where

$K = 5 \times 10^{-6} \text{ N}\cdot\text{m}\cdot\text{s}$ . The applied voltage is 6V and  $B_m = 0$ . Calculate the steady-state rotor speed  $\omega_r$  in rad/s.

4. A 250-V, 600-r/min, 200-hp dc shunt motor is delivering rated horsepower at rated speed.  $R_f = 12 \Omega$ ,  $L_{AF} = 0.18 \text{ H}$ , and  $r_a = 0.012 \Omega$ .
  - (a) Calculate the terminal voltage that must be applied to this machine to satisfy this load condition.
  - (b) Calculate the full-load ohmic losses and determine the efficiency.
5. Losses in a dc machine include ohmic, no-load rotational, and stray-load losses. The no-load rotational losses range from approximately 2–14% of the rated output. These losses include windage, friction, and core losses. Stray-load losses include the increase in core losses due to load and eddy current losses induced by the armature current. These losses are generally taken to be 1% of the rating of the machine. Another loss in the machine is due to the brush voltage drop. This is accounted for by increasing the armature resistance or assuming a constant-voltage drop across the brushes regardless of load. Repeat Problem 4, assuming the machine has 5% rotational losses, 1% stray-load losses, and a total voltage drop across the brushes of 2V that should be added to that calculated in Problem 4a. Assume that the rotational and stray-load losses can be represented by a resistance connected across the terminals of the machine.
6. The parameters of a dc shunt machine are  $r_a = 10 \Omega$ ,  $R_f = 50 \Omega$ , and  $L_{AF} = 0.5 \text{ H}$ . Neglect  $B_m$  and  $V_a = V_f = 25 \text{ V}$ . Calculate (a) the steady-state stall torque, (b) the no-load speed, and (c) the steady-state rotor speed with  $T_L = 3.75 \times 10^{-3} \omega_r$ .
7. A permanent-magnet dc motor is driven by a mechanical source at 3820 r/min. The measured open-circuit armature voltage is 7V. The mechanical source is disconnected, and a 12-V electric source is connected to the armature. With zero-load torque,  $I_a = 0.1 \text{ A}$  and  $\omega_r = 650 \text{ rad/s}$ . Calculate  $k_v$ ,  $B_m$ , and  $r_a$ .
8. Express the maximum steady-state power output of a dc shunt motor ( $P_{out} = T_e \omega_r$ ) if the field current  $i_f$  and armature voltage  $v_a$  are held constant. Let  $B_m = 0$ . (Hint: First express the rotor speed for maximum power output.)
9. The parameters of a 5-hp dc shunt machine are  $r_a = 0.6 \Omega$ ,  $L_{AA} = 0.012 \text{ H}$ ,  $R_f = 120 \Omega$ ,  $L_{FF} = 120 \text{ H}$ ,  $L_{AF} = 1.8 \text{ H}$ .  $V_a = V_f = 240 \text{ V}$ . Calculate the steady-state rotor speed  $\omega_r$  for  $I_t = 0$ ; generator action.
10. A dc series motor requires 100W at full load. The full-load speed is 2000 r/min, and the terminal voltage is 100V,  $r_a = 2 \Omega$ , and  $r_{fs} = 1 \Omega$ . Calculate the stall torque of the motor ( $T_e$  with  $\omega_r = 0$ ).
11. The torque load of a dc series motor is  $T_L = 100 \text{ Nm}$ ,  $L_{AFs} = 0.6 \text{ H}$ ,  $r_a = 2 \Omega$ , and  $r_{fs} = 3 \Omega$ . The voltage applied to the motor is 200V. Calculate the steady-state rotor speed. Assume  $B_m = 0$ .
12. A dc compound motor requires 100W at full load. The full-load speed is 2000 r/min and the voltage applied to the terminals of the machine is 100V,  $r_a = 2 \Omega$ ,  $R_f = 200 \Omega$ , and  $r_{fs} = 1 \Omega$ . The series field is differentially connected. Calculate the steady-state no-load speed if  $L_{AFs} = 0.1 L_{AF}$ .
13. Modify the state equations given by (10.5-14) for a permanent-magnet dc machine to include  $\theta_r$  as a state variable.

14. Write the field voltage equation of a shunt dc machine in terms of  $k_v$  and express the transfer function between  $k_v$  and  $v_f$ .
15. A separately excited dc machine is operating with no load ( $T_L = 0$ ) and fixed field current. The armature resistance and inductance,  $r_a$  and  $L_{AA}$ , are small and can be neglected. Assume  $B_m = 0$ . Express the transfer function between  $i_a$  and  $v_a$ . Show that this motor appears as a capacitor to  $v_a$ .
16. Develop the time-domain block diagram for a series-connected dc machine.
17. Develop the time-domain block diagram for the compound machine with a long-shunt connection.
18. Construct the block diagram in terms of the Laplace operator for the permanent-magnet dc motor valid for load torque changes with the armature-applied voltage held constant. Write the transfer function  $\Delta\omega_r(s)/\Delta T_L(s)$ .
19. Consider the one-quadrant chopper shown in Figure 10.7-1. Let  $v_s = 100$  V,  $L_{AA} = 5$  mH,  $r_a = 10$   $\Omega$ ,  $k_v = 1$  V·s/rad,  $\omega_r = 0$ , and  $f_s = 10$  kHz. (a) Calculate  $I_1$  and  $I_2$  for steady-state operation at  $k = 0.5$ . Sketch  $i_a$ ,  $v_a$ ,  $i_s$ ,  $i_D$ , and the instantaneous electric power supplied to the motor,  $P_e = v_a i_a$ .
20. Calculate the average values for the plots of  $i_a$ ,  $v_a$ ,  $i_s$ ,  $i_D$ , and  $P_e$  shown in Problem 19. Make the simplifying approximation that the current waveform is made up of straight-line segments. Compare average  $P_e$  with average  $v_a$  times average  $i_a$  and the average power  $P_s$  supplied by the source.
21. Plot the source current  $i_s$  and the variables shown in Figure 10.8-2 for the two-quadrant chopper operating with (a)  $I_1$  and  $I_2$  positive and (b)  $I_1$  and  $I_2$  negative.
22. Consider the two-quadrant chopper shown in Figure 10.8-1. Let  $v_s = 12$  V,  $f_s = 10$  kHz,  $L_{AA} = 1.14$  mH,  $r_a = 3.8$   $\Omega$ , and  $k_v = 0.031$  V·s/rad. If  $\omega_r = 100$  rad/s and  $T_e = 2.82 \times 10^{-2}$  N·m, (a) calculate  $k$ , (b) determine  $I_1$  and  $I_2$ , and (c) sketch  $i_a$ ,  $v_a$ ,  $i_{s1}$ ,  $i_{D1}$ ,  $i_s$ . Also, sketch  $P_s$  and  $P_e$ , the instantaneous electric power supplied from the source and to the machine, respectively.
23. Refer to Problem 22. Make simplifying straight-line approximations to calculate the average  $i_a$ ,  $v_a$ ,  $i_{s1}$ ,  $i_{D1}$ ,  $i_s$ ,  $P_s$ , and  $P_e$ .

# SEMI-CONTROLLED BRIDGE CONVERTERS

## 11.1. INTRODUCTION

A brief analysis of single- and three-phase semi-controlled bridge converters is presented in this chapter. This type of converter is also commonly referred to as a line-commutated converter. The objective is to provide a basic background in converter operation without becoming overly involved. For this reason, only the constant-current operation is considered. A more detailed analysis of these and other converters can be found in References 1–4. Finally, to set the stage for the analysis of dc and ac drive systems in later chapters, an average-value model of the three-phase semi-controlled bridge converter is derived. This model can be used to predict the average-value performance during steady-state and transient operating conditions.

## 11.2. SINGLE-PHASE LOAD COMMUTATED CONVERTER

A single-phase line-commutated full-bridge converter is shown in Figure 11.2-1. The ac source voltage and current are denoted  $e_{ga}$  and  $i_{ga}$ , respectively. The series inductance (commutating inductance) is denoted  $l_c$ . The thyristors are numbered  $T1$  through  $T4$ , and the associated gating or firing signals are denoted  $e_{f1}$  through  $e_{f4}$ . The converter output voltage and current are  $v_d$  and  $i_d$ . The following simplifying assumptions are

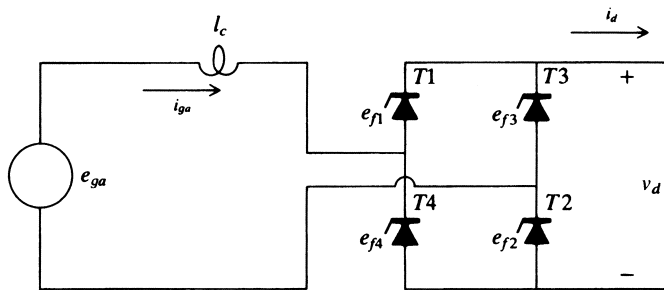


Figure 11.2-1. Single-phase full-bridge converter.

made in this analysis: (1) the ac source contains only one frequency, (2) the output current  $i_d$  is constant, (3) the thyristor is an infinite impedance device when in the reverse bias mode (cathode positive) or when the gating signal to allow current flow has not occurred, and (4) when conducting, the voltage drop across the thyristor is negligibly small.

### Operation without Commutating Inductance or Firing Delay

It is convenient to analyze converter operation in steps starting with the simplest case where the commutating inductance is not present and there is no firing delay. In this case, it can be assumed that the gating signals are always present, whereupon the thyristors will conduct whenever they become forward biased (anode positive) just as if they were diodes. Converter operation for constant  $i_d$  with  $l_c = 0$  and without firing delay is depicted in Figure 11.2-2. The thyristor in the upper part of the converter ( $T1$  or  $T3$ ) that conducts is the one with the greatest anode voltage. Similarly, the thyristor that conducts in the lower part of the converter ( $T2$  or  $T4$ ) is the one whose cathode voltage is the most negative. In this case, the converter operates as a full-wave rectifier.

Let us begin our analysis assuming that the source voltage may be described by

$$e_{ga} = \sqrt{2}E \cos \theta_g \quad (11.2-1)$$

where

$$\theta_g = \omega_g t + \phi_g \quad (11.2-2)$$

In (11.2-2),  $\omega_g$  and  $\phi_g$  are the radian frequency and phase of the source, respectively. We wish to compute the steady-state average-value of  $v_d$ , which is defined as

$$\bar{V}_d = \frac{1}{2\pi} \int_{-\pi}^{\pi} v_d d\theta_g \quad (11.2-3)$$

It is noted that the output voltage is made up of two identical  $\pi$  intervals per cycle of the source voltage. For the interval  $-\pi/2 \leq \theta_g \leq \pi/2$

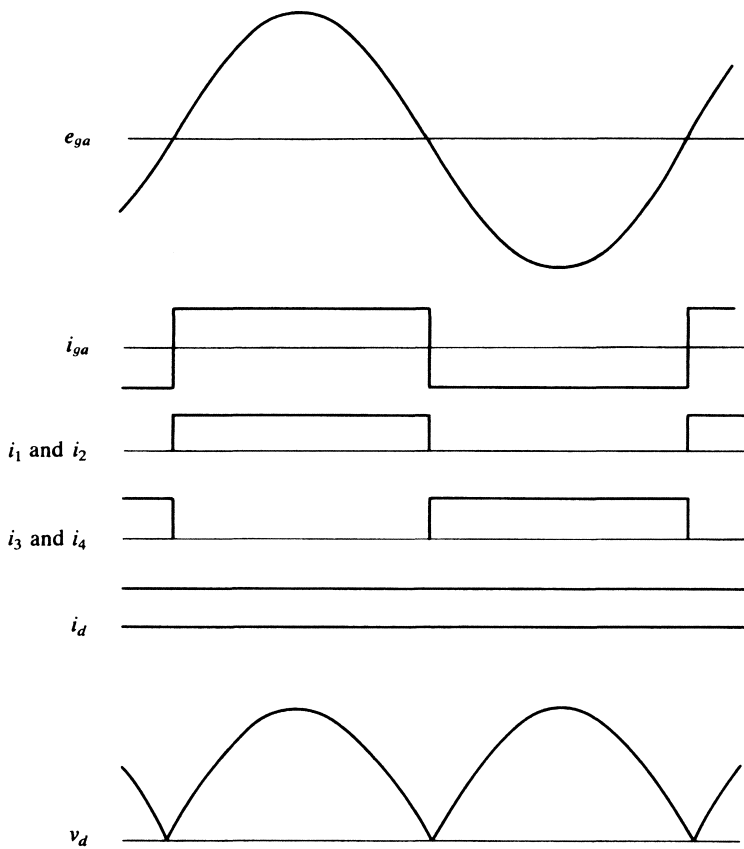


Figure 11.2-2. Single-phase, full-bridge converter operation for constant output current without  $i_c$  and firing delay.

$$v_d = e_{ga} \quad (11.2-4)$$

Using symmetry and (11.2-1)–(11.2-4), the average output voltage may be determined by finding the average of (11.2-3) over the interval  $-\pi/2 \leq \theta_g \leq \pi/2$ . Thus, the average-value of  $v_d$  may be expressed

$$\begin{aligned} \overline{V_d} &= V_{d0} = \frac{1}{\pi} \int_{-\pi/2}^{\pi/2} \sqrt{2}E \cos \theta_g d\theta_g \\ &= \frac{2\sqrt{2}}{\pi} E \end{aligned} \quad (11.2-5)$$

where  $E$  is the rms value of the source voltage. We will use  $V_{d0}$  to denote the average output voltage without commutation inductance and without firing delay.

## Operation with Commutating Inductance and without Firing Delay

When  $l_c$  is zero, the process of “current switching” from one thyristor to the other in either the upper or lower part of the converter ( $T_1$  to  $T_3$  to  $T_1$  to . . . , etc., and  $T_2$  to  $T_4$  to  $T_2$  to . . . , etc.) takes place instantaneously. Instantaneous commutation cannot occur in practice since there is always some inductance between the source and the converter. The operation of the converter with commutating inductance and without firing delay is shown in Figure 11.2-3. During commutation, the source is short-circuited simultaneously through  $T_1$  and  $T_3$  and through  $T_2$  and  $T_4$ . Hence, if we consider the commutation from  $T_1$  to  $T_3$  and  $T_2$  to  $T_4$  and if we assume that the short-circuit current during commutation is positive through  $T_3$ , then

$$e_{ga} = -l_c \frac{di_3}{dt} \quad (11.2-6)$$

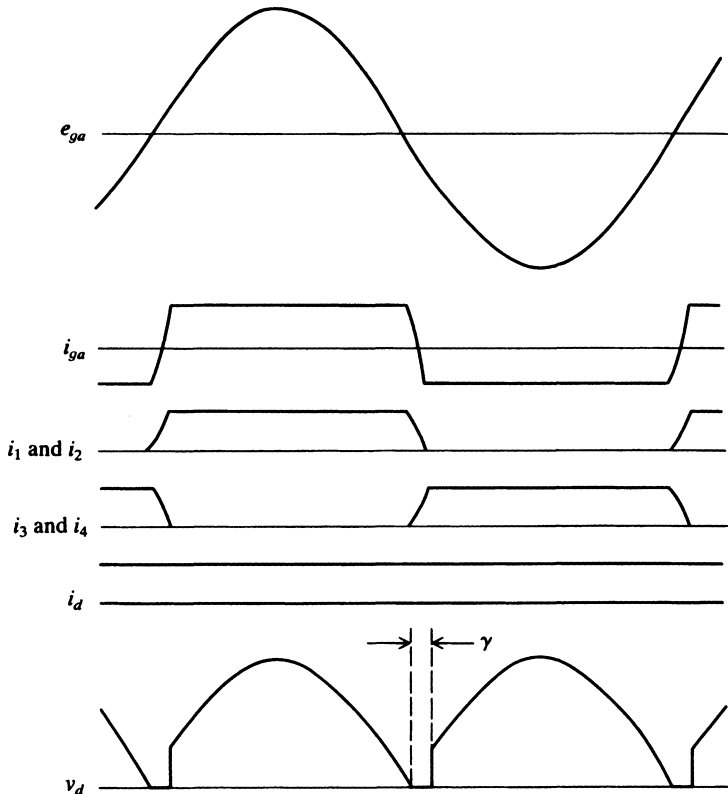


Figure 11.2-3. Single-phase, full-bridge converter operation for constant output current with  $l_c$  and without firing delay.

where  $i_3$  is the current in thyristor T3. Substituting (11.2-1) into (11.2-6) and solving for  $i_3$  yields

$$\begin{aligned} i_3 &= -\frac{1}{l_c} \int \sqrt{2}E \cos \theta_g dt \\ &= -\frac{\sqrt{2}E}{\omega_g l_c} \sin \theta_g + C \end{aligned} \quad (11.2-7)$$

At  $\theta_g = \pi/2$ ,  $i_3 = 0$ , therefore

$$C = \frac{\sqrt{2}E}{\omega_g l_c} \quad (11.2-8)$$

whereupon

$$i_3 = \frac{\sqrt{2}E}{\omega_g l_c} (1 - \sin \theta_g) \quad (11.2-9)$$

At the end of commutation  $\theta_g = \pi/2 + \gamma$  and  $i_3 = I_d$ , therefore

$$I_d = \frac{\sqrt{2}E}{\omega_g l_c} (1 - \cos \gamma) \quad (11.2-10)$$

where  $\gamma$  is the commutation angle (Fig. 11.2-3). The uppercase ( $I_d$ ) is used to denote constant or steady-state quantities. During commutation, the converter output voltage  $v_d$  is zero. Once commutation is completed, the short-circuit paths are broken, and the output voltage jumps to the value of the source voltage since  $i_d$ , and hence  $i_{ga}$ , are assumed constant after commutation. Since  $i_{ga}$  is constant, zero voltage is dropped across the inductance  $l_c$ . It is recalled that  $V_{d0}$  given by (11.2-5) is the average converter output voltage when  $l_c$  is zero. When  $l_c$  is considered, the output voltage is zero during commutation. Hence, the average output voltage decreases due to commutation. The average converter output voltage may be determined by

$$\begin{aligned} \bar{V}_d &= \frac{1}{\pi} \int_{-\pi/2+\gamma}^{\pi/2} \sqrt{2}E \cos \theta_g d\theta_g \\ &= \frac{V_{d0}}{2} (1 + \cos \gamma) \end{aligned} \quad (11.2-11)$$

If (11.2-10) is solved for  $\cos \gamma$  and the result substituted into (11.2-11), the average converter output voltage with commutating inductance but without firing delay becomes

$$\bar{V}_d = V_{d0} - \frac{\omega_g l_c}{\pi} I_d \quad (11.2-12)$$

It is interesting to note that commutation appears as a voltage drop as if the converter had an internal resistance of  $\omega_g l_c / \pi$ . However, this is not a resistance in the sense that it does not dissipate energy.

### Operation without Commutating Inductance and with Firing Delay

Thus far, we have considered the thyristor as a diode and hence have only considered rectifier operation of the converter. However, the thyristor will conduct only if the anode voltage is positive and it has received a gating signal. Hence, the conduction of a thyristor may be delayed after the anode has become positive by delaying the gating signal (firing signal). Converter operation with firing delay but without commutating inductance is shown in Figure 11.2-4.

We can determine the average output by

$$\begin{aligned}\bar{V}_d &= \frac{1}{\pi} \int_{-\pi/2+\alpha}^{\pi/2+\alpha} \sqrt{2}E \cos \theta_g d\theta_g \\ &= \frac{2\sqrt{2}}{\pi} E \cos \alpha \\ &= V_{d0} \cos \alpha\end{aligned}\quad (11.2-13)$$

where  $\alpha$  is the firing delay angle (Fig. 11.2-4). If the current is maintained constant, the average output voltage will become negative for  $\alpha$  greater than  $\pi/2$ . This is referred to as inverter operation, wherein average power is being transferred from the dc part of the circuit to the ac part of the circuit.

### Operation with Commutating Inductance and Firing Delay

Converter operation with both commutating inductance and firing delay is shown in Figure 11.2-5. The calculation of  $i_3$  and  $\bar{V}_d$  are identical to that given by (11.2-6)–(11.2-12), except that the intervals of evaluation are different. In particular, (11.2-7) applies, but it is at  $\theta_g = \pi/2 + \alpha$ , where  $i_3 = 0$ , thus

$$C = \frac{\sqrt{2}E}{\omega_g l_c} \cos \alpha \quad (11.2-14)$$

Commutation ends at  $\theta_g = \pi/2 + \alpha + \gamma$ , whereupon  $i_3 = I_d$ , thus

$$I_d = \frac{\sqrt{2}E}{\omega_g l_c} [\cos \alpha - \cos(\alpha + \gamma)] \quad (11.2-15)$$

From (11.2-13)

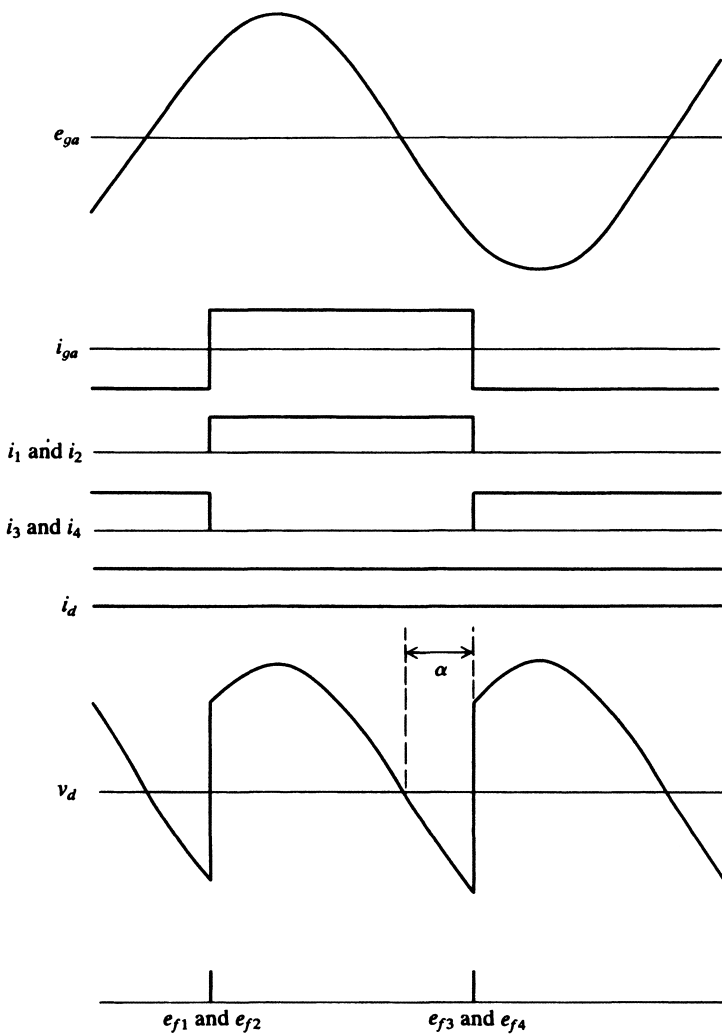


Figure 11.2-4. Single-phase, full-bridge converter operation for constant output current without  $I_c$  and with firing delay.

$$\begin{aligned}
 V_d &= \frac{1}{\pi} \int_{-\pi/2+\alpha+\gamma}^{\pi/2+\alpha} \sqrt{2}E \cos \theta_g d\theta_g \\
 &= \frac{V_{d0}}{2} [\cos \alpha + \cos(\alpha + \gamma)]
 \end{aligned} \tag{11.2-16}$$

Solving (11.2-15) for  $\cos(\alpha + \gamma)$  and substituting the results into (11.2-16) yields the following expression for the average output voltage with commutating inductance and firing delay.

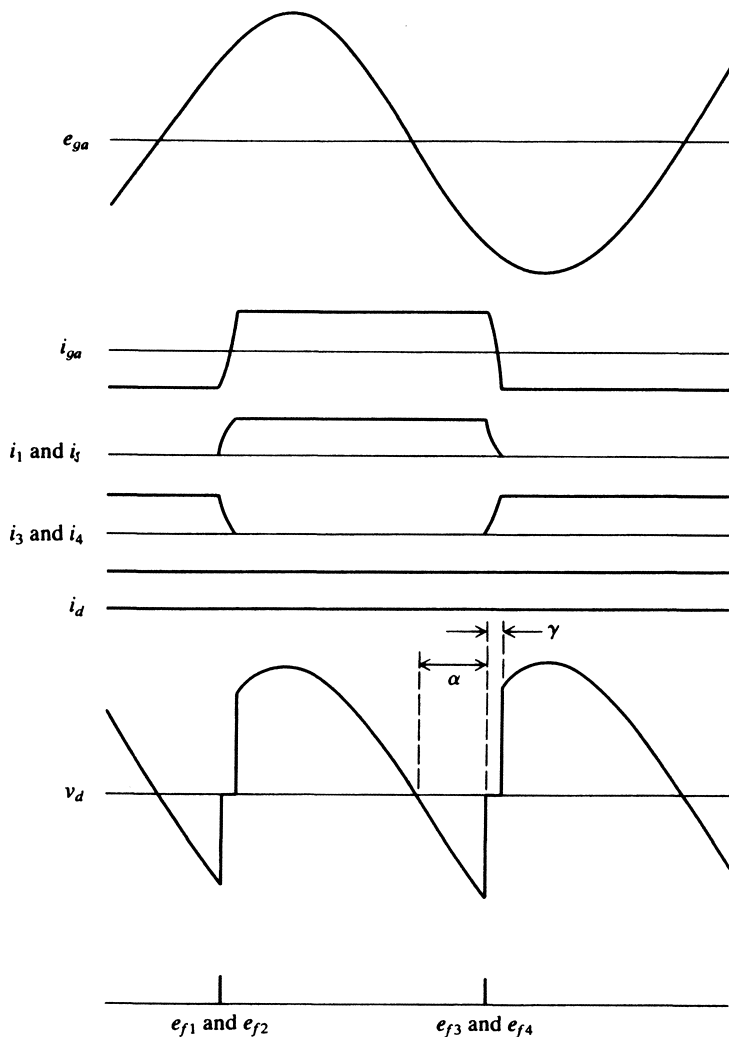


Figure 11.2-5. Single-phase, full-bridge converter operation for constant output current with  $i_c$  and firing delay.

$$\bar{V}_d = V_{d0} \cos \alpha - \frac{\omega_g l_c}{\pi} I_d \quad (11.2-17)$$

The equivalent circuit suggested by (11.2-17) is shown in Figure 11.2-6.

The average-value relations and corresponding equivalent circuit depicted in Figure 11.2-6 were developed based upon the assumptions that (1) the rms amplitude of the ac source voltage,  $E$ , is constant, and (2) the dc load current  $i_d$  is constant and hence denoted  $I_d$ . This equivalent circuit provides a reasonable approximation of the

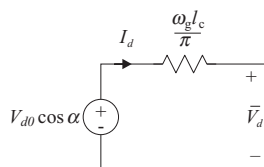


Figure 11.2-6. Average-value equivalent circuit for a single-phase full-bridge converter.

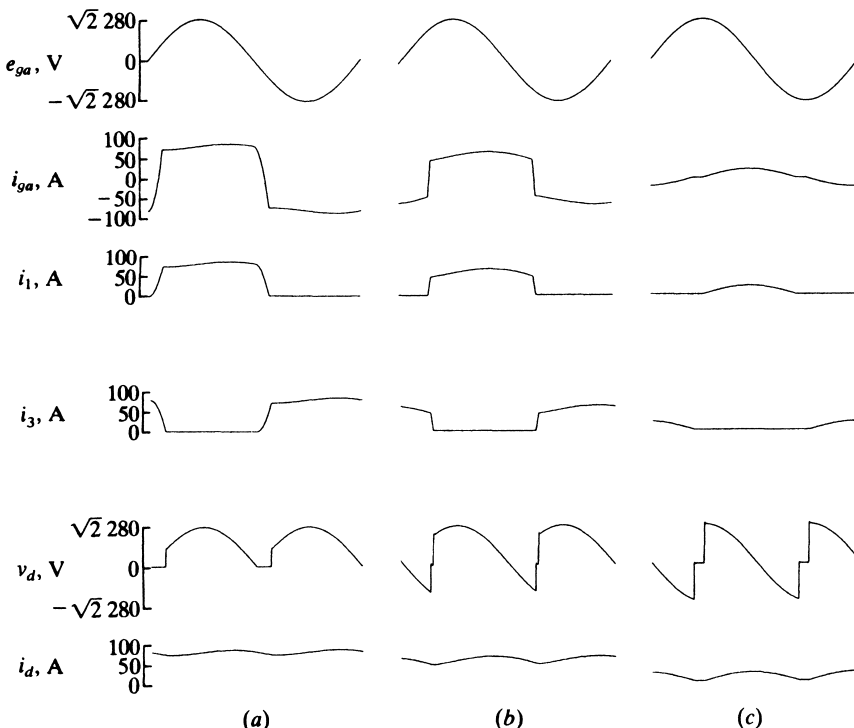


Figure 11.2-7. Single-phase, full-bridge converter operation with RL load. (a)  $\alpha = 0^\circ$ ; (b)  $\alpha = 45^\circ$ ; (c)  $\alpha \approx 90^\circ$ , discontinuous operation.

average dc voltage even if  $E$  and  $i_d$  vary with respect to time provided that the variations from one conduction interval to the next are small.

## Modes of Operation

Various modes of operation of a single-phase, full-bridge converter are illustrated by simulation results in Figure 11.2-7, Figure 11.2-8, and Figure 11.2-9. The source voltage is 280 V (rms) and the commutating inductance in 1.4 mH. In each case,  $e_{ga}$ ,  $i_{ga}$ ,  $i_1$ ,  $i_3$ ,  $v_d$ , and  $i_d$  are plotted, where  $i_1$  and  $i_3$  are the currents through thyristors  $T1$  and  $T3$ , respectively. In Figure 11.2-7, the converter is operating with a series RL load connected across the output terminals, where  $R = 3\Omega$  and  $L = 40$  mH. In Figure 11.2-7a,

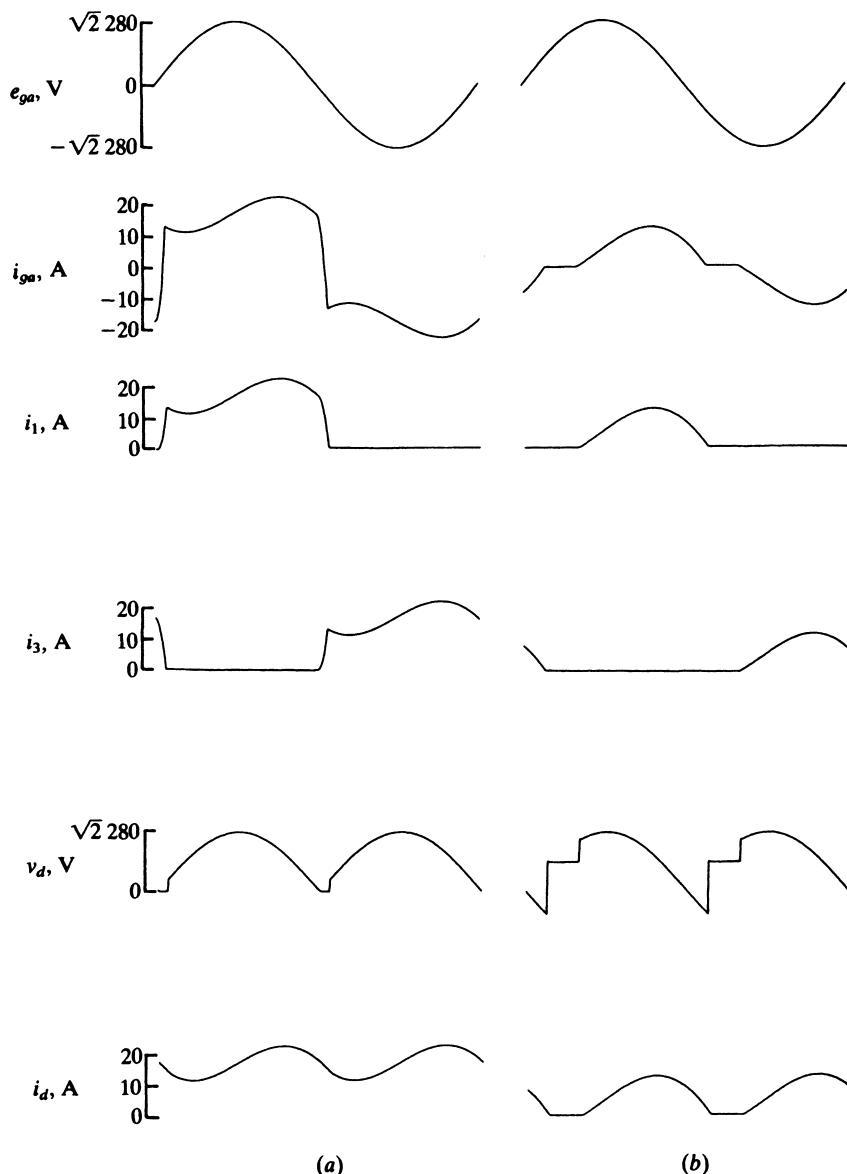


Figure 11.2-8. Single-phase, full-bridge converter operation with RL and an opposing dc source connected in series across the converter terminals. (a)  $\alpha = 0^\circ$ ; (b)  $\alpha = 60^\circ$ .

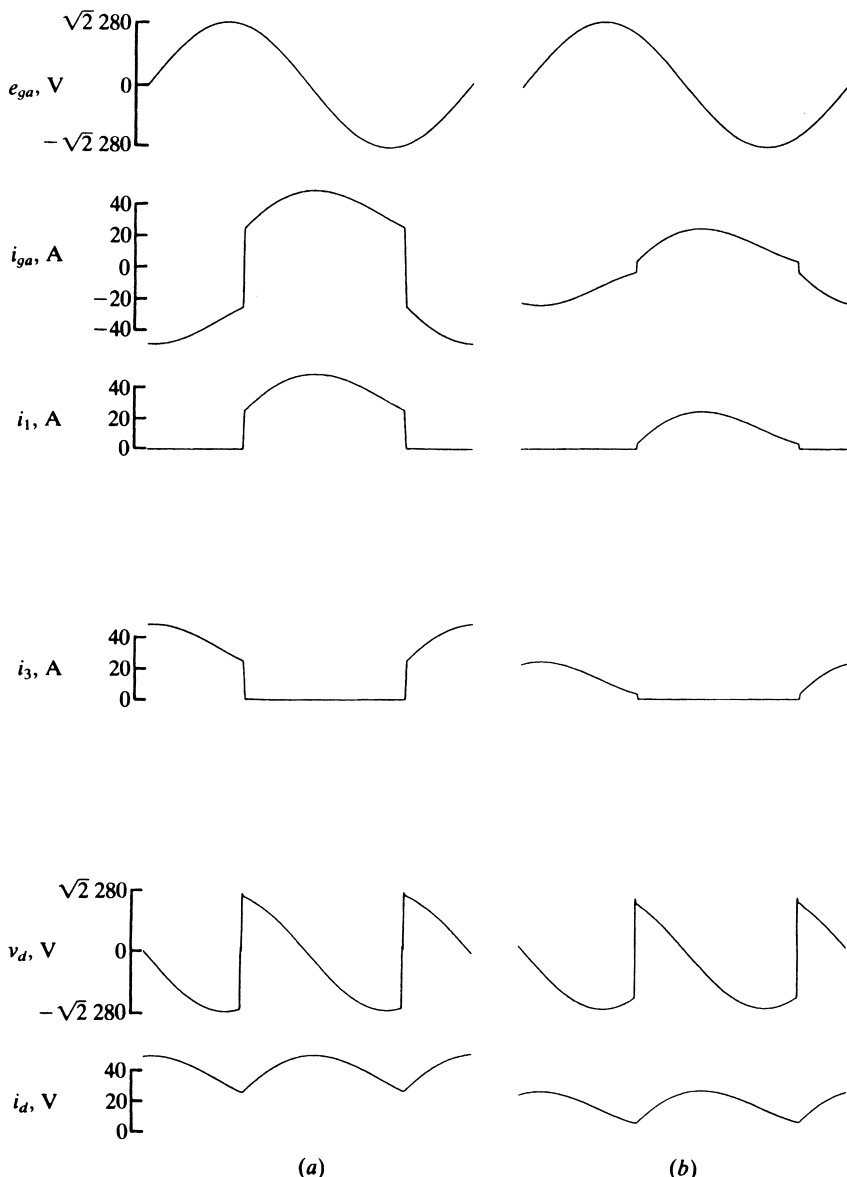


Figure 11.2-9. Single-phase, full-bridge converter operation with RL and an aiding dc source connected in series across the converter terminals. (a)  $\alpha = 108^\circ$ ; (b)  $\alpha = 126^\circ$ .

the converter is operating without firing delay. In Figure 11.2-7b, the firing delay angle is  $45^\circ$ . In Figure 11.2-7c, the firing delay is slightly less than  $90^\circ$ ; the current  $i_d$  is discontinuous. The output current is nearly constant when the converter is operating without firing delay due to the large-load inductance.

In the case shown in Figure 11.2-8, the combination of a series  $RL$  ( $R = 3\Omega$ ,  $L = 40\text{ mH}$ ) connected in series with a constant 200-V source is connected across the output terminals of the converter. The dc source is connected so that it opposes a positive  $v_d$ . In Figure 11.2-8a, the converter is operating without firing delay, while in Figure 11.2-8b, the firing delay angle is  $60^\circ$ . During the zero-current portion of operation,  $v_d$  is equal to 200 V, the magnitude of the series-connected dc source.

Inverter operation is depicted in Figure 11.2-9. In this case, the combination of the RL load and dc source is still connected across the output terminals of the converter, but the polarity of the dc source is reversed. In Figure 11.2-9a, the firing delay angle is  $108^\circ$ . In Figure 11.2-9b, the firing delay angle is  $126^\circ$ .

Although (11.2-17) was derived for a constant output current, it is quite accurate for determining the average values of converter voltage and current, especially if the current is not discontinuous. The reader should take the time to compare the calculated converter output voltage and current using (11.2-17) with the average-values shown in Figure 11.2-7, Figure 11.2-8, and Figure 11.2-9, and to qualitatively justify any differences that may occur.

### 11.3. THREE-PHASE LOAD COMMUTATED CONVERTER

A three-phase, line-commutated, full-bridge converter is shown in Figure 11.3-1. The voltages of the three-phase, ac source are denoted  $e_{ga}$ ,  $e_{gb}$ , and  $e_{gc}$ , and the phase currents  $i_{ag}$ ,  $i_{bg}$ , and  $i_{cg}$ . The ac source voltages may be expressed as

$$e_{ga} = \sqrt{2}E \cos \theta_g \quad (11.3-1)$$

$$e_{bg} = \sqrt{2}E \cos \left( \theta_g - \frac{2\pi}{3} \right) \quad (11.3-2)$$

$$e_{cg} = \sqrt{2}E \cos \left( \theta_g + \frac{2\pi}{3} \right) \quad (11.3-3)$$

where  $E$  is the rms magnitude of the source voltage,  $\theta_g$  is given by (11.2-2) and is the angular position of the source voltages, and the source frequency is  $\omega_g = p\theta_g$ . The ac side inductance (commutating inductance) is denoted as  $l_c$ . The thyristors are numbered  $T1$  through  $T6$  in the order in which they are turned on and the gating or firing signals for the thyristors are  $e_{f1}$  through  $e_{f6}$ . The converter output voltage and current are denoted  $v_d$  and  $i_d$ , respectively. This circuit also includes a dc inductor and resistor,  $L_{dc}$  and  $r_{dc}$ , that may represent the armature inductance and resistance of a dc machine or the inductance and resistance of a filtering circuit. Likewise, the voltage  $e_d$  may represent the back emf of a dc machine or the capacitor voltage in a dc filter.

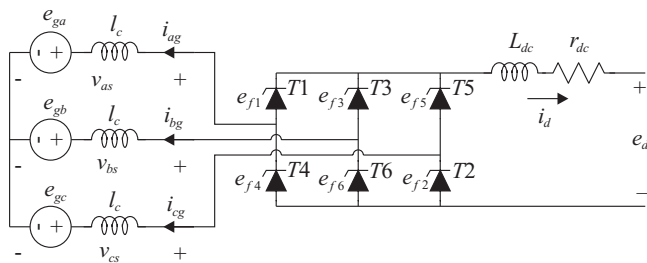
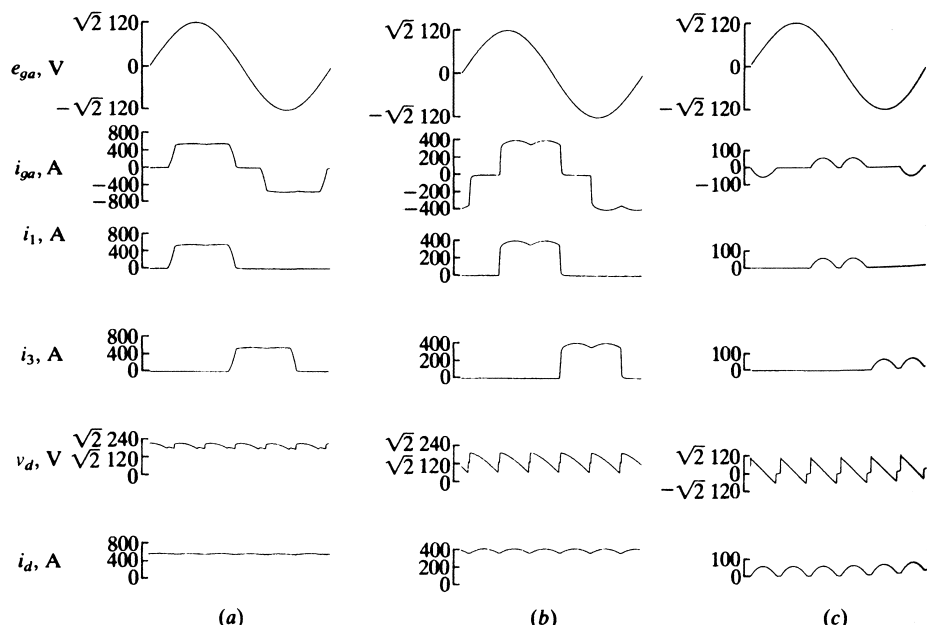


Figure 11.3-1. Three-phase full-bridge converter.

Figure 11.3-2. Three-phase, full-bridge converter operation with RL load. (a)  $\alpha = 0^\circ$ ; (b)  $\alpha = 45^\circ$ ; (c)  $\alpha = 90^\circ$ .

## Modes of Operation

Before analyzing the converter, it is instructive to consider several modes of operation of a three-phase, full-bridge converter illustrated in Figure 11.3-2, Figure 11.3-3, and Figure 11.3-4 by simulation results. The line-to-line ac source voltage is 208 V (rms) and the commuting inductance is  $45 \mu\text{H}$ . In each case,  $e_{ga}$ ,  $i_{ga} = -i_{ag}$ ,  $i_1$ ,  $i_3$ ,  $v_d$ , and  $i_d$  are plotted where the currents  $i_1$  and  $i_3$  are the currents through thyristors  $T1$  and  $T3$ , respectively.

In Figure 11.3-2, the converter is operating with  $r_{dc} = 0.5 \Omega$ ,  $L_{dc} = 1.33 \text{ mH}$ , and  $e_d = 0$ . In Figure 11.3-2a, the converter is operating without firing delay. It is interesting

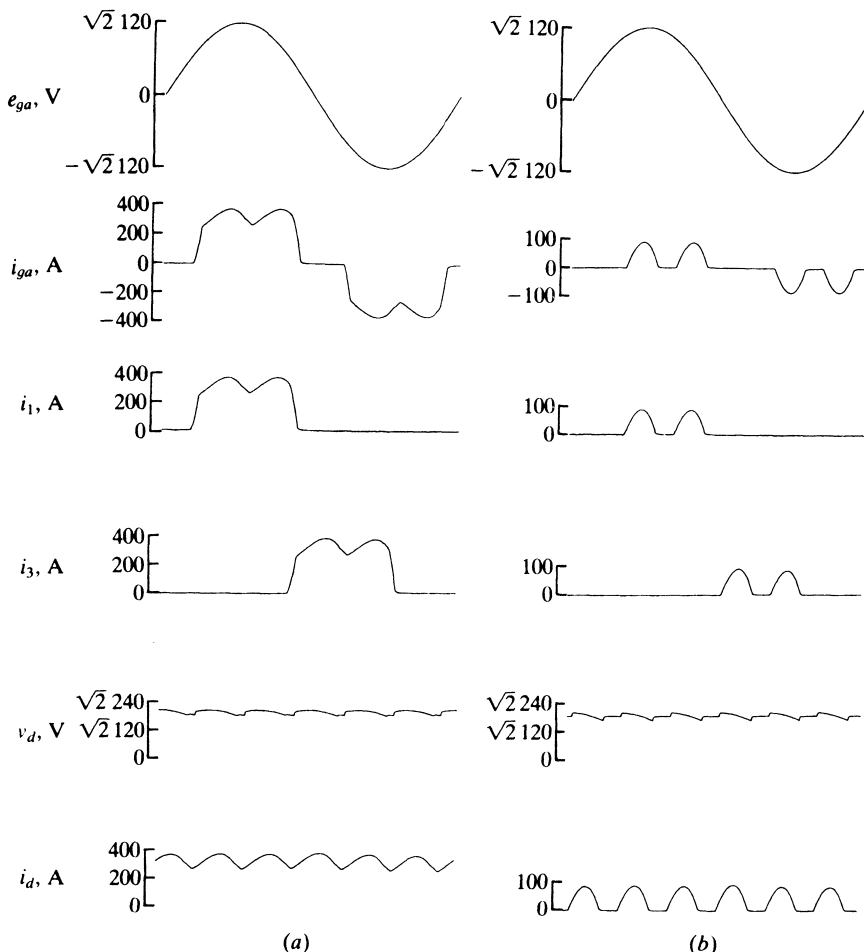


Figure 11.3-3. Three-phase, full-bridge converter operation with RL and an opposing dc source connected in series across the converter terminals. (a)  $\alpha = 0^\circ$ ; (b)  $\alpha = 35^\circ$ .

to note that the output current is nearly constant. In this study, there are alternately two or three thyristors conducting; hence, this will be referred to as 2-3 mode, which is the normal mode of operation. The firing delay angle is  $45^\circ$  in Figure 11.3-1b (again 2-3 mode) and  $90^\circ$  in Figure 11.3-1c where the output current  $i_d$  is discontinuous. Note, when  $i_d$  is zero,  $v_d$  is also zero. In this case, there are alternately 2 and 0 thyristors conducting; hence, this will be referred to as 2-0 mode.

In the case depicted in Figure 11.3-3, the combination of a  $r_{dc} = 50 \text{ m}\Omega$  and  $L_{dc} = 133 \mu\text{H}$  is connected in series with a  $e_d = 260 \text{ V}$  dc source is connected across the output terminals of the converter. In Figure 11.3-2a (2-3 mode), the converter is

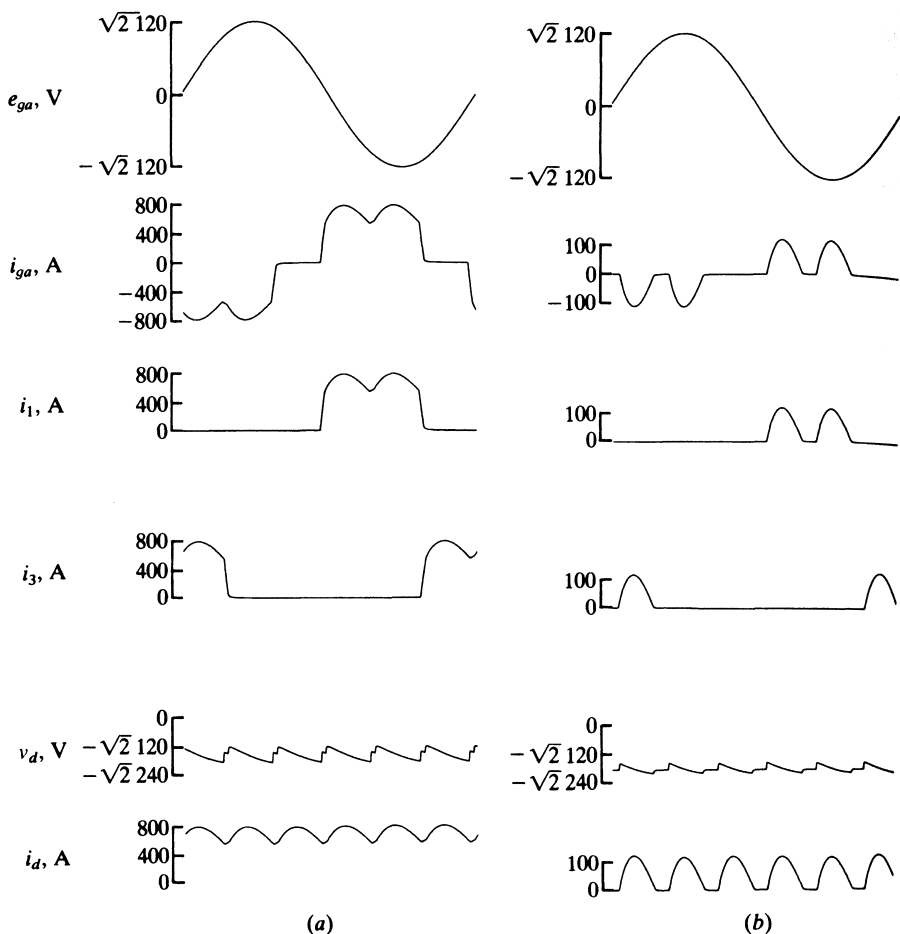


Figure 11.3-4. Three-phase, full-bridge converter operation with RL and an aiding dc source connected in series across the converter terminals. (a)  $\alpha = 140^\circ$ ; (b)  $\alpha = 160^\circ$ .

operating without firing delay. In Figure 11.3-2b, the firing delay angle is  $35^\circ$ , and the output current is discontinuous (2-0 Mode). Note that when  $i_d$  is zero,  $v_d$  is 260 V.

Inverter operation is illustrated in Figure 11.3-4. In this case,  $r_{dc} = 50 \text{ m}\Omega$ ,  $L_{dc} = 133 \mu\text{H}$ , and  $e_d = -260 \text{ V}$ . In Figure 11.3-4a, the firing delay angle is  $140^\circ$  (2-3 mode). The firing delay angle in Figure 11.3-4b is  $160^\circ$  where discontinuous output current occurs (2-0 mode). Clearly, when  $i_d$  is zero,  $v_d$  is  $-260 \text{ V}$ .

Note that while these studies depict 2-3 and 2-0 modes, other modes exist. In 3-3 mode, which we will consider later, there are always three thyristors conducting. In 3-4 mode, which occurs under heavy rectifier loads, there are alternately three and four thyristors conducting. In this case, the dc link becomes periodically shorted as in the single-phase case.

## Analysis and Average-Value Model

Unlike our work in Section 11.2, herein we use a  $qd$  framework for our analysis, and include the derivation for the ac currents (represented in terms of  $qd$  variables). The explicit consideration of a slowly varying  $i_d$  will yield a dynamic average-value model of the load-commutated inverter that more accurately predicts the average dc voltage during transients. The consideration of the average  $q$ - and  $d$ -axis components of the ac source currents allows the model to be used in a system context and to calculate the real, apparent, and/or reactive power supplied by the ac source using expressions developed in Chapter 3. The use of  $qd$  variables is desirable because by suitable choice of reference frame, the  $qd$  state variables will be constant in the steady-state, which facilitates a variety of analyses. The following simplifying assumptions are made herein: (1) the three-phase source is balanced, (2) the current  $i_d$  is varying slowly relative to the converter switching frequency, (3) the thyristor is an infinite impedance device when reverse biased or when the gating signal to allow current flow has not occurred, (4) when conducting the voltage drop across the thyristor is negligibly small and (5) operation is in the 2-3 or 3-3 modes.

In order to put our work into a  $qd$  framework, let us transform the source voltages (11.3-1)–(11.3-3) to  $qd$  variables using the reference-frame transformation. In particular,

$$\mathbf{v}_{qd}^g = \begin{bmatrix} v_{qg}^g \\ v_{dg}^g \end{bmatrix} = \mathbf{K}_s^g|_{utr} \begin{bmatrix} e_{ag} \\ e_{bg} \\ e_{cg} \end{bmatrix} \quad (11.3-4)$$

where the “g” superscript denotes a reference frame wherein  $\theta = \theta_g$  and “utr” denotes upper two rows. This yields

$$v_{qg}^g = \sqrt{2}E \quad (11.3-5)$$

$$v_{dg}^g = 0 \quad (11.3-6)$$

A goal of the model herein will be to accept  $q$ - and  $d$ -voltages in an arbitrary reference frame and then to find the currents in that same reference frame. For  $q$ - and  $d$ -voltages in an arbitrary reference frame (emphasized with a superscript “a” herein), in which (11.3-5) and (11.3-6) do not hold, we can utilize a frame-to-frame transformation. In particular, if the  $q$ - and  $d$ -axis components of the source voltages are given in the arbitrary reference frame, the transformation into the reference frame wherein (11.3-5) and (11.3-6) hold may be deduced from the frame-to-frame transformation

$$\mathbf{f}_{qd}^g = {}^a\mathbf{K}^g \mathbf{f}_{qd}^a \quad (11.3-7)$$

where, from Chapter 3,

$${}^a\mathbf{K}^g = \begin{bmatrix} \cos \theta_{ga} & -\sin \theta_{ga} \\ \sin \theta_{ga} & \cos \theta_{ga} \end{bmatrix} \quad (11.3-8)$$

and where  $\mathbf{f} = [f_q \ f_d]^T$  can be a voltage  $v$  or current  $i$ , and  $\theta_{ga} = \theta_g - \theta_a$ , where  $\theta_a$  is the position of the arbitrary reference frame. Manipulating (11.3-5) through (11.3-8),

$$\theta_{ga} = -\text{angle}(v_{qg}^a - jv_{dg}^a) \quad (11.3-9)$$

$$E = \frac{1}{\sqrt{2}} \sqrt{(v_{qg}^a)^2 + (v_{dg}^a)^2} \quad (11.3-10)$$

where  $v_{qg}^a$  and  $v_{dg}^a$  are the  $q$ - and  $d$ -axis voltages to the left of the ac side inductor  $l_c$  in Figure 11.3-1.

The next step is to derive an expression for the average dc voltage. All dc side and  $qd$  variables are periodic in  $\pi/3$  of  $\theta_g$ . Thus, the average-values may be established for any  $\pi/3$  interval of  $\theta_g$ . It is convenient to consider the  $\pi/3$  interval that begins when  $T3$  begins to conduct and ends when  $T4$  begins to conduct. The average dc voltage over this interval may be expressed

$$\hat{v}_d = \frac{3}{\pi} \int_{\frac{\pi}{3} + \alpha}^{\frac{2\pi}{3} + \alpha} (v_{bs} - v_{cs}) d\theta_g \quad (11.3-11)$$

In (11.3-11), the “ $\wedge$ ” is used to denote the average-value during dynamical conditions wherein the dc current  $i_d$  and/or the amplitude of the ac voltages  $E$  are allowed to vary, provided that the variation from one switching interval to the next is relatively small. In other words, the averaging interval in (11.3-11) is assumed to be small relative to the longer-term dynamics associated with the variations in  $E$  and/or  $i_d$ . Thus, (11.3-11) may be interpreted as the short-term average of  $v_d$ . Likewise, the short-term average of  $i_d$  (average of  $i_d$  over a  $\pi/3$  interval) will be denoted as  $\hat{i}_d$ . The firing delay angle  $\alpha$  in (11.3-11) is defined such that  $T3$  fires when

$$\theta_g = \frac{\pi}{3} + \alpha \quad (11.3-12)$$

The average dc voltage indicated in (11.3-11) may be evaluated by noting from Figure 11.3-1 that

$$v_{as} = e_{ga} + l_c \frac{di_{ag}}{dt} \quad (11.3-13)$$

$$v_{bs} = e_{gb} + l_c \frac{di_{bg}}{dt} \quad (11.3-14)$$

$$v_{cs} = e_{gc} + l_c \frac{di_{cg}}{dt} \quad (11.3-15)$$

Substituting (11.3-13)–(11.3-15) into (11.3-11) yields

$$\hat{v}_d = \frac{3}{\pi} \int_{\frac{\pi}{3}+\alpha}^{\frac{2\pi}{3}+\alpha} (e_{gb} - e_{gc}) d\theta_g + \frac{3}{\pi} l_c \omega_g (i_{bg} - i_{cg}) \Big|_{\frac{\pi}{3}+\alpha}^{\frac{2\pi}{3}+\alpha} \quad (11.3-16)$$

Substituting (11.3-2) and (11.3-3) into (11.3-16) and simplifying yields

$$\hat{v}_d = \frac{3\sqrt{6}}{\pi} E \cos \alpha + \frac{3}{\pi} l_c \omega_g (i_{bg} - i_{cg}) \Big|_{\frac{\pi}{3}+\alpha}^{\frac{2\pi}{3}+\alpha} \quad (11.3-17)$$

Further simplification can be obtained by observing that prior to the instant when  $T3$  begins to conduct, only  $T1$  and  $T2$  are conducting. Therefore,

$$\mathbf{i}_{abcg} \Big|_{\theta_g = \frac{\pi}{3}+\alpha} = \begin{bmatrix} -\hat{i}_d & 0 & \hat{i}_d \end{bmatrix}^T \quad (11.3-18)$$

Similarly, immediately prior to the instant when  $T4$  begins to conduct, only  $T2$  and  $T3$  are on, therefore

$$\mathbf{i}_{abcg} \Big|_{\theta_g = \frac{2\pi}{3}+\alpha} = \begin{bmatrix} 0 & -\hat{i}_d - \Delta\hat{i}_d & \hat{i}_d + \Delta\hat{i}_d \end{bmatrix}^T \quad (11.3-19)$$

In (11.3-19),  $\Delta\hat{i}_d$  represents the change in average dc current over the given conduction interval due to long-term dynamics. It follows from this definition that the derivative of the dynamic-average rectifier current may be approximated as

$$\frac{d\hat{i}_d}{dt} = \frac{\Delta\hat{i}_d}{\pi/3} \omega_g \quad (11.3-20)$$

Substituting (11.3-18)–(11.3-20) into (11.3-17) and simplifying yields

$$\hat{v}_d = \frac{3\sqrt{6}}{\pi} E \cos \alpha - \frac{3}{\pi} l_c \omega_g \hat{i}_d - 2l_c \frac{d\hat{i}_d}{dt} \quad (11.3-21)$$

From Figure 11.3-1,  $\hat{v}_d$  can be related to  $\hat{i}_d$  and  $e_d$  using

$$\hat{v}_d = r_{dc} \hat{i}_d + L_{dc} \frac{d\hat{i}_d}{dt} + e_d \quad (11.3-22)$$

Combining (11.3-21) and (11.3-22) yields

$$\frac{d\hat{i}_d}{dt} = \frac{\frac{3\sqrt{6}}{\pi} E \cos \alpha - \left( r_{dc} + \frac{3}{\pi} l_c \omega_g \right) \hat{i}_d - e_d}{L_{dc} + 2l_c} \quad (11.3-23)$$

To establish the average  $q$ - and  $d$ -axis components of the ac currents, it is assumed that the rectifier current is constant throughout the interval and equal to  $\hat{i}_d$ . It is convenient to divide the interval into two subintervals; the commutation interval during which the current is transferred from  $T1$  to  $T3$ , and the conduction interval during which only  $T2$  and  $T3$  are conducting. During the commutation interval,  $T1$ ,  $T2$ , and  $T3$  are conducting. Therefore, the current into the ac source must be of the form

$$\mathbf{i}_{abcg} = \begin{bmatrix} i_{ag} & -\hat{i}_d - i_{ag} & \hat{i}_d \end{bmatrix}^T \quad (11.3-24)$$

and

$$v_{as} = v_{bs} = 0 \quad (11.3-25)$$

Algebraically manipulating (11.2-2), (11.3-1), (11.3-2), (11.3-13), (11.3-14), (11.3-24), and (11.3-25), it is possible to show that

$$\frac{di_{ag}}{dt} = \frac{\sqrt{6}E}{2l_c\omega_g} \cos\left(\theta_g - \frac{5\pi}{6}\right) \quad (11.3-26)$$

From (11.3-26) and noting that at  $\theta_g = \alpha + \pi/3$ , we have that  $i_{ag} = -\hat{i}_d$ , we conclude that

$$i_{ag}(\theta_g) = -\hat{i}_d + \frac{\sqrt{6}}{2l_c\omega_g} E \left[ \cos(\alpha) - \cos\left(\theta_g - \frac{\pi}{3}\right) \right] \quad (11.3-27)$$

The commutation subinterval ends when the current in  $T1$ , which is the  $a$ -phase current, becomes zero. The angle from the time  $T3$  is turned on and  $T1$  is turned off is known as the commutation angle  $\gamma$ . It can be found by setting (11.3-27) equal to zero. In particular,

$$\gamma = -\alpha + \arccos\left(\cos \alpha - \frac{2l_c\omega_g \hat{i}_d}{\sqrt{6}E}\right) \quad (11.3-28)$$

For (11.3-27) to be applicable, several conditions need to be met. First, for (11.3-28) to be defined

$$\left| \cos \alpha - \frac{2l_c\omega_g \hat{i}_d}{\sqrt{6}E} \right| \leq 1 \quad (11.3-29)$$

However, this is not the only condition which must be met. Note that  $T3$  turns on at

$$\theta_g = \frac{\pi}{3} + \alpha \quad (11.3-30)$$

For  $T3$  to turn on, the time derivative of  $i_{ag}$  must be positive, so that the current in  $T3$  will increase. Substitution of (11.3-30) into (11.3-26), we conclude

$$\alpha \geq 0 \quad (11.3-31)$$

Similarly, the end of commutation occurs at

$$\theta_g = \frac{\pi}{3} + \alpha + \gamma \quad (11.3-32)$$

For commutation to complete, the time derivative of  $i_{ag}$  must be positive at the end of commutation as well. Substitution of (11.3-32) into (11.3-26) and requiring the time derivative to be positive,

$$\alpha + \gamma \leq \pi \quad (11.3-33)$$

This requirement is particularly relevant to inverter operation in which  $\alpha$  is large. Finally, for 2-3 mode, we must have

$$\gamma \leq \frac{\pi}{3} \quad (11.3-34)$$

Because of these restrictions, it is useful to differentiate between the actual firing delay  $\alpha$  and the intended (or commanded) firing delay angle  $\alpha^*$ . Suppose we take  $\alpha = \alpha^*$  in our analysis (11.3-28)–(11.3-34). If all constraints are met, then this is indeed the case. If the constraints are not met, then the converter is either in another mode or is not operating properly (and is, e.g., experiencing commutation failures). While our approach is not valid for these other modes, we can extend it to 3-3 mode. In this mode, the commutation angle is exactly  $\pi/3$ , and the firing delay is increased from the intended value to the value that corresponds to the aforementioned commutation angle. Setting  $\gamma = \pi/3$  in (11.3-28) and solving for the firing angle

$$\alpha = \frac{\pi}{3} - \arccos\left(\frac{2l_c \omega_g \hat{i}_d}{\sqrt{6}E}\right) \quad (11.3-35)$$

Note that mathematically, there is another solution with a change of sign on the  $\arccos()$  term; however, this alternate solution does not make sense physically since such a solution would yield a firing delay that decreases with increasing  $\hat{i}_d$ . Note that for (11.3-35) to be valid,

$$\frac{1}{2} \leq \frac{2l_c \omega_g \hat{i}_d}{\sqrt{6}E} \leq 1 \quad (11.3-36)$$

or  $\alpha$  will be negative or the argument to the  $\arccos()$  function will be out of range.

Summarizing, these results, we have

$$\alpha = \begin{cases} \alpha^* & \text{valid 2-3 mode} \\ \frac{\pi}{3} - \arccos\left(\frac{2l_c \omega_g \hat{i}_d}{\sqrt{6}E}\right) & \text{valid 3-3 mode} \end{cases} \quad (11.3-37)$$

In other words, if we assume  $\alpha = \alpha^*$  and it yields valid 2-3 mode of operation, then indeed  $\alpha = \alpha^*$ . If this does not yield valid operation, then we can find  $\alpha$  from (11.3-35). If this yields valid 3-3 mode, then this is the firing delay. If neither assumption yields a valid result, the operation is in another mode (e.g., 3-4 mode, wherein the converter operates between three and four thyristors on) or the converter is not operating in a periodic fashion.

The next step in our analysis is to determine an expression for the ac side currents. The average  $q$ - and  $d$ -axis components can be established using

$$\hat{i}_{qg}^g = \frac{3}{\pi} \int_{\frac{\pi}{3} + \alpha}^{\frac{2\pi}{3} + \alpha} i_{qg}^g(\theta_g) d\theta_g \quad (11.3-38)$$

$$\hat{i}_{dg}^g = \frac{3}{\pi} \int_{\frac{\pi}{3} + \alpha}^{\frac{2\pi}{3} + \alpha} i_{dg}^g(\theta_g) d\theta_g \quad (11.3-39)$$

Since the expressions for the ac currents are different during the conduction interval than in the commutation interval, it is convenient to break up (11.3-38) and (11.3-39) into components corresponding to these two intervals. In particular,

$$\hat{i}_{qg}^g = \hat{i}_{qg,com}^g + \hat{i}_{qg,cond}^g \quad (11.3-40)$$

$$\hat{i}_{dg}^g = \hat{i}_{dg,com}^g + \hat{i}_{dg,cond}^g \quad (11.3-41)$$

where

$$\hat{i}_{qg,com}^g = \frac{3}{\pi} \int_{\frac{\pi}{3} + \alpha}^{\frac{\pi}{3} + \alpha + \gamma} i_{qg}^g(\theta_g) d\theta_g \quad (11.3-42)$$

$$\hat{i}_{qg,cond}^g = \frac{3}{\pi} \int_{\frac{\pi}{3} + \alpha + \gamma}^{\frac{2\pi}{3} + \alpha} i_{qg}^g(\theta_g) d\theta_g \quad (11.3-43)$$

$$\hat{i}_{dg,com}^g = \frac{3}{\pi} \int_{\frac{\pi}{3}+\alpha}^{\frac{\pi}{3}+\alpha+\gamma} i_{dg}^g(\theta_g) d\theta_g \quad (11.3-44)$$

$$\hat{i}_{dg,cond}^g = \frac{3}{\pi} \int_{\frac{\pi}{3}+\alpha}^{\frac{2\pi}{3}+\alpha} i_{dg}^g(\theta_g) d\theta_g \quad (11.3-45)$$

The commutation component of the current may be found by substituting (11.3-27) into (11.3-24), applying the reference-frame transformation (3.3-1) with  $\theta = \theta_g$ , and integrating in accordance with (11.3-42) and (11.3-44). After considerable manipulation,

$$\begin{aligned} \hat{i}_{qg,com}^g &= \frac{2\sqrt{3}}{\pi} \hat{i}_d \left[ \sin\left(\gamma + \alpha - \frac{5\pi}{6}\right) - \sin\left(\alpha - \frac{5\pi}{6}\right) \right] \\ &+ \frac{3}{\pi} \frac{\sqrt{2}E}{l_c \omega_g} \cos(\alpha) [\cos(\gamma + \alpha) - \cos(\alpha)] \\ &+ \frac{1}{4} \frac{3}{\pi} \frac{\sqrt{2}E}{l_c \omega_g} [\cos(2\alpha) - \cos(2\alpha + 2\gamma)] \end{aligned} \quad (11.3-46)$$

$$\begin{aligned} \hat{i}_{dg,com}^g &= \frac{2\sqrt{3}}{\pi} \hat{i}_d \left[ -\cos\left(\gamma + \alpha - \frac{5\pi}{6}\right) + \cos\left(\alpha - \frac{5\pi}{6}\right) \right] \\ &+ \frac{3}{\pi} \frac{\sqrt{2}E}{l_c \omega_g} \cos(\alpha) [\sin(\gamma + \alpha) - \sin(\alpha)] \\ &+ \frac{1}{4} \frac{3}{\pi} \frac{\sqrt{2}E}{l_c \omega_g} [\sin(2\alpha) - \sin(2\alpha + 2\gamma)] - \frac{3}{\pi} \frac{\sqrt{2}E}{l_c \omega_g} \frac{1}{2} \gamma \end{aligned} \quad (11.3-47)$$

To compute the conduction component of the average currents, note that after commutation, the  $a$ -phase current remains at zero; therefore

$$\mathbf{i}_{abcg} = \begin{bmatrix} 0 & -\hat{i}_d & \hat{i}_d \end{bmatrix}^T \quad (11.3-48)$$

Transforming (11.3-48) to the  $\theta = \theta_g$  reference frame and utilizing (11.3-43) and (11.3-45),

$$\hat{i}_{qg,cond}^g = \frac{2\sqrt{3}}{\pi} \hat{i}_d \left[ \sin\left(\alpha + \frac{7\pi}{6}\right) - \sin\left(\alpha + \gamma + \frac{5\pi}{6}\right) \right] \quad (11.3-49)$$

$$\hat{i}_{dg,cond}^g = \frac{2\sqrt{3}}{\pi} \hat{i}_d \left[ -\cos\left(\alpha + \frac{7\pi}{6}\right) + \cos\left(\alpha + \gamma + \frac{5\pi}{6}\right) \right] \quad (11.3-50)$$

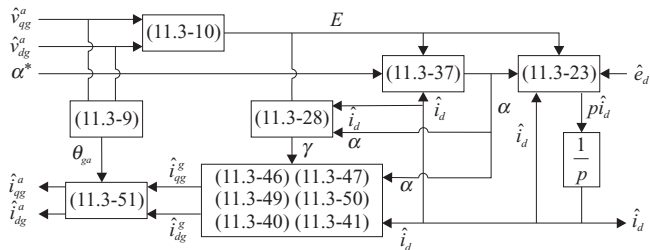


Figure 11.3-5. Average-value model of three-phase full-bridge converter.

At this point, the total  $q$ - and  $d$ -axis current may be found using (11.3-40) and (11.3-41). The resulting currents can then be transformed back to the desired reference frame using

$$\hat{\mathbf{i}}_{qd}^a = {}^s \mathbf{K}^a \hat{\mathbf{i}}_{qd}^g = [{}^s \mathbf{K}^a]^{-1} \hat{\mathbf{i}}_{qd}^g \quad (11.3-51)$$

The relationships between the previous equations are conveniently summarized in the block diagram illustrated in Figure 11.3-5, which represents an average-value model of the load commutated converter. The inputs to this model include the commanded firing delay  $\alpha^*$ , the  $q$ - and  $d$ -axis components of the source voltage in the arbitrary reference frame, and the dc source voltage  $e_d$ . The outputs of the model include the dynamic-average of the rectifier current  $\hat{i}_d$  and the dynamic-average of the  $q$ - and  $d$ -axis components of the ac currents in the arbitrary reference frame.

To illustrate the dynamic response that is established using the average-value model, it is assumed that the rated line-to-line source voltage is 208 V (rms). The commutating inductance  $l_c$  is 45  $\mu$ H. Also,  $r_{dc} = 0.5 \Omega$ ,  $L_{dc} = 1.33$  mH, and  $e_d = 0$ . In the following study, the dc and ac currents are initially zero, and rated voltages are suddenly applied at  $t = 0$  with the firing delay angle  $\alpha$  set to zero. The dynamic response is shown in Figure 11.3-6, wherein the following variables are plotted:  $i_d$ —the dc current,  $i_{qg}^g$ —the  $q$ -axis component of the ac current, and  $i_{dg}^g$ —the  $d$ -axis component of the ac current. The ac currents are expressed in the reference frame wherein  $v_{dg}^g = 0$ . The variables indicated with an “ $\hat{\cdot}$ ” correspond to the average-value model in Figure 11.3-5, while those that do not include the “ $\hat{\cdot}$ ” correspond to the actual response. At the instant of time indicated in Figure 11.3-6, the firing delay angle is stepped to 45°. As shown, the average-value model accurately portrays the dynamic-average dynamic response for the given study. The steady-state waveforms for  $\alpha = 0$  and  $\alpha = 45^\circ$  are shown in Figure 11.3-2a,b, respectively.

## 11.4. CONCLUSIONS AND EXTENSIONS

The focus of this chapter has been the development of average-value and dynamic average-value models of line-commutated converters connected to an ideal source. A natural extension of this work is the consideration of the connection of line-commutated

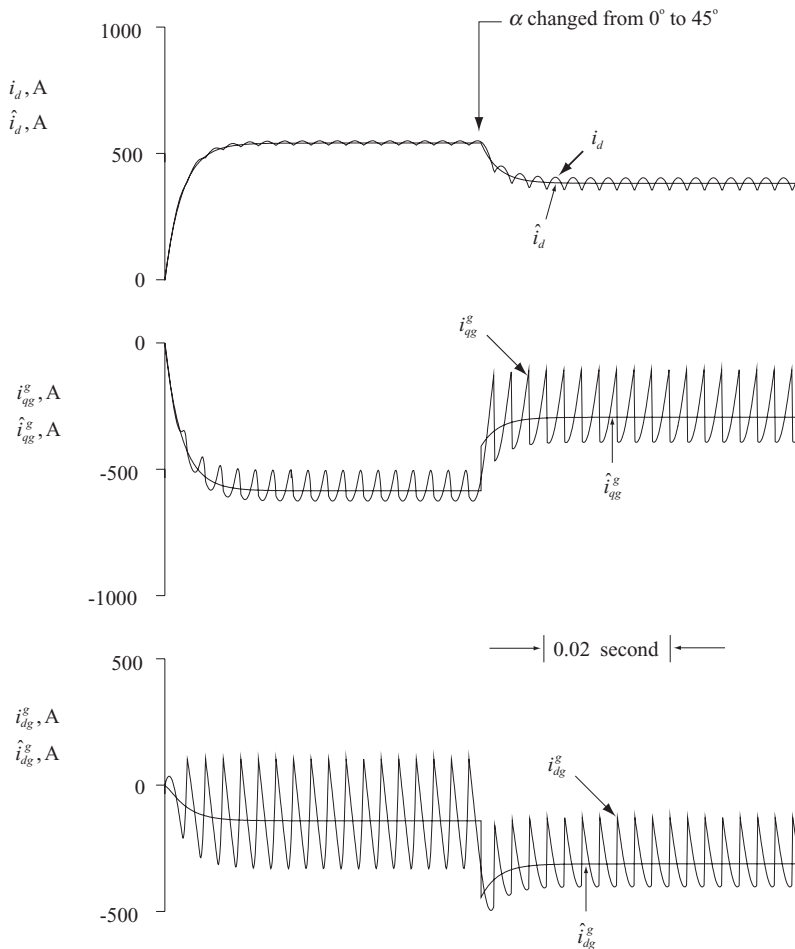


Figure 11.3-6. Comparison of average-value dynamic response with actual response.

converters to synchronous machines. One approach to doing this is set forth in References 5 and 6. An extension of the methodology to a six-phase rectifier connected to a six-phase machine is set forth in Reference 7. In Reference 8, a method of determining instantaneous waveforms from an average-value model is considered using a procedure referred to as waveform reconstruction. Throughout this work, it was assumed that enough dc link inductance was included so that the dc current could be considered constant. An analysis of line-commutated converter systems in which no dc-link is present is set forth in Reference 9. Finally, it is appropriate to consider methods for

the detailed simulation of line-commutated inverters. While the literature is rich in this subject, a particularly computationally efficient methodology is set forth in Reference 10.

## REFERENCES

- [1] C. Adamson and N.G. Hingarani, *High Voltage Direct Current Power Transmission*, Garroway Limited, London, 1960.
- [2] E.W. Kimbark, *Direct Current Transmission—Vol. 1*, John Wiley and Sons, New York, 1971.
- [3] S.B. Dewan and A. Straughen, *Power Semiconductor Circuits*, John Wiley and Sons, New York, 1975.
- [4] P. Wood, *Switching Power Converters*, Van Nostrand Reinhold Co., New York, 1981.
- [5] S.D. Sudhoff and O. Wasyczuk, “Analysis and Average-Value Modeling of Line-Commuted Converter—Synchronous Machine Systems,” *IEEE Trans. Energy Conversion*, Vol. 8, No. 1, March 1993, pp. 92–99.
- [6] S.D. Sudhoff, K.A. Corzine, H.J. Hegner, and D.E. Delisle, “Transient and Dynamic Average-Value Modeling of Synchronous Machine Fed Load-Commuted Converters,” *IEEE Trans. Energy Conversion*, Vol. 11, No. 3, September 1996, pp. 508–514.
- [7] S.D. Sudhoff, “Analysis and Average-Value Modeling of Dual Line-Commuted Converter—6-Phase Synchronous Machine Systems,” *IEEE Trans. Energy Conversion*, Vol. 8, No. 3, September 1993, pp. 411–417.
- [8] S.D. Sudhoff, “Waveform Reconstruction in the Average-Value Modeling of Line-Commuted Converter—Synchronous Machine Systems,” *IEEE Trans. Energy Conversion*, Vol. 8, No. 3, September 1993, pp. 404–410.
- [9] J.T. Alt, S.D. Sudhoff, and B.E. Ladd, “Analysis and Average-Value Modeling of an Inductorless Synchronous Machine Load Commutated Converter System,” *IEEE Trans. Energy Conversion*, Vol. 14, No. 1, March 1999, pp. 37–43.
- [10] O. Wasyczuk and S.D. Sudhoff, “Automated State Model Generation Algorithm for Power Circuits and Systems,” *IEEE Trans. Power Systems*, Vol. 11, No. 4, November 1996, pp. 1951–1956.

## PROBLEMS

1. Using the average-value equations derived in Section 11.2, calculate the average dc voltage and current for each of the conditions in Figure 11.2-7. Compare with the average-values plotted in Figure 11.2-7.
2. Using the average-value equations derived in Section 11.3, calculate the average dc voltage and current for each of the conditions in Figure 11.3-2. Compare with the average-values plotted in Figure 11.3-2.
3. Assume that the ac source voltage applied to the three-phase load commutated converter have an *acb* phase sequence. Indicate the sequence in which the thyristors should be fired.

- 4.** Derive (11.3-9) and (11.3-10).
- 5.** Starting with (11.3-26) obtain (11.3-27).
- 6.** Using (11.3-26) and (11.3-32), infer (11.3-33).
- 7.** Perform the detailed mathematical manipulation needed to obtain (11.3-46).
- 8.** Perform the detailed mathematical manipulation needed to obtain (11.3-47).
- 9.** Perform the detailed mathematical manipulation needed to obtain (11.3-49).
- 10.** Perform the detailed mathematical manipulation needed to obtain (11.3-50).

---

# 12

---

## FULLY CONTROLLED THREE-PHASE BRIDGE CONVERTERS

---

### 12.1. INTRODUCTION

In our study of induction, synchronous, and permanent-magnet ac machines, we set forth control strategies that assumed the machine was driven by a three-phase, variable-frequency voltage or current source without mention of how such a source is actually obtained, or what its characteristics might be. In this chapter, the operation of a three-phase fully controlled bridge converter is set forth. It is shown that by suitable control, this device can be used to achieve either a three-phase controllable voltage source or a three-phase controllable current source, as was assumed to exist in previous chapters.

### 12.2. THE THREE-PHASE BRIDGE CONVERTER

The converter topology that serves as the basis for many three-phase variable speed drive systems is shown in Figure 12.2-1. This type of converter is comprised of six controllable switches labeled T1–T6. Physically, bipolar junction transistors (BJTs),

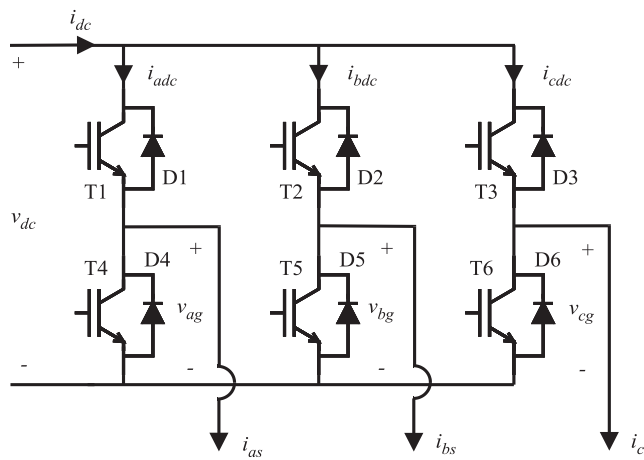


Figure 12.2-1. The three-phase bridge converter topology.

metal–oxide–semiconductor field-effect transistors (MOSFETs), insulated-gate bipolar junction transistors (IGBTs), and MOS controlled thyristors (MCTs) are just a few of the devices that can be used as switches. Across each switch is an antiparallel diode used to ensure that there is a path for inductive current in the event that a switch which would normally conduct current of that polarity is turned off. This type of converter is often referred to as an inverter when power flow is from the dc system to the ac system. If power flow is from the ac system to the dc system, which is also possible, the converter is often referred to as an active rectifier.

In Figure 12.2-1,  $v_{dc}$  denotes the dc voltage applied to the converter bridge, and  $i_{dc}$  designates the dc current flowing into the bridge. The bridge is divided into three legs, one for each phase of the load. The line-to-ground voltage of the  $a$ -,  $b$ -, and  $c$ -phase legs of the converter are denoted  $v_{ag}$ ,  $v_{bg}$ , and  $v_{cg}$  respectively. In this text, the load current will generally be the stator current into a synchronous, induction, or permanent-magnet ac machine; therefore,  $i_{as}$ ,  $i_{bs}$ , and  $i_{cs}$  are used to represent the current into each phase of the load. Finally, the dc currents from the upper rail into the top of each phase leg are designated  $i_{adc}$ ,  $i_{bdc}$ , and  $i_{cdc}$ .

To understand the operation of this basic topology, it must first be understood that none of the semiconductor devices shown are ever intentionally operated in the active region of their  $i$ – $v$  characteristics. Their operating point is either in the saturated region (on) or in the cutoff region (off). If the devices were operated in their active region, then by applying a suitable gate voltage to each device, the line-to-ground voltage of each leg could be continuously varied from 0 to  $v_{dc}$ . At first, such control appears advantageous, since each leg of the converter could be used as a controllable voltage source. The disadvantage of this strategy is that, if the switching devices are allowed to operate in their active region, there will be both a voltage across and current through each semiconductor device, resulting in power loss. On the other hand, if each semiconductor is either on or off, then either there is a current through the device but no voltage, or a voltage across the device but no current. Neither case results in power

loss. Of course, in a real device, there will be some power losses due to the small voltage drop that occurs even when the device is in saturation (on), and due to losses that are associated with turning the switching devices on or off (switching losses); nevertheless, inverter efficiencies greater than 95% are readily obtained.

In this study of the operation of the converter bridge, it will be assumed that either the upper switch or lower switch of each leg is gated on, except during switching transients (the result of turning one switch on while turning another off). Ideally, the leg-to-ground voltage of a given phase will be  $v_{dc}$  if the upper switch is on and the lower switch is turned off, or 0 if the lower switch is turned on and the upper switch is off. This assumption is often useful for analysis purposes, as well as for time-domain simulation of systems, in which the dc supply voltage is much greater than the semiconductor voltage drops. If a more detailed analysis or simulation is desired (and hence the voltage drops across the semiconductors are not neglected), then the line-to-ground voltage is determined both by the switching devices turned on and the phase current.

To illustrate this, consider the diagram of one leg of the bridge as is shown in Figure 12.2-2. Therein,  $x$  can be  $a$ ,  $b$ , or  $c$ , to represent the  $a$ -,  $b$ -, or  $c$ -phase, respectively. Figure 12.2-3a illustrates the effective equivalent circuit shown in Figure 12.2-2 if the upper transistor is on and the current  $i_{xs}$  is positive. For this condition, it can be seen that the line-to-ground voltage  $v_{xg}$  will be equal to the dc supply voltage  $v_{dc}$  less the voltage drop across the switch  $v_{sw}$ . The voltage drop across the switch is generally in the range of 0.7–3.0 V. Although the voltage drop is actually a function of the switch current, it can often be represented as a constant. From Figure 12.2-3a, the dc current into the bridge,  $i_{xdc}$ , is equal to the phase current  $i_{xs}$ .

If the upper transistor is on and the phase current is negative, then the equivalent circuit is as shown in Figure 12.2-3b. In this case, the dc current into the leg  $i_{xdc}$  is again equal to the phase current  $i_{xs}$ . However, since the current is now flowing through the diode, the line-to-ground voltage  $v_{xg}$  is equal to the dc supply voltage  $v_{dc}$  plus the diode forward voltage drop  $v_d$ . If the upper switch is on and the phase current is zero, it seems

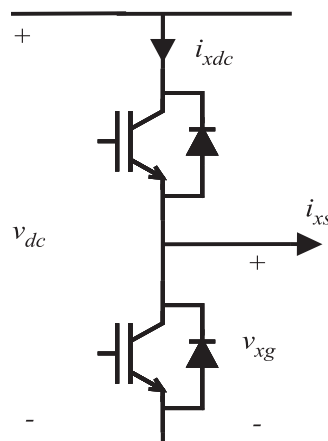
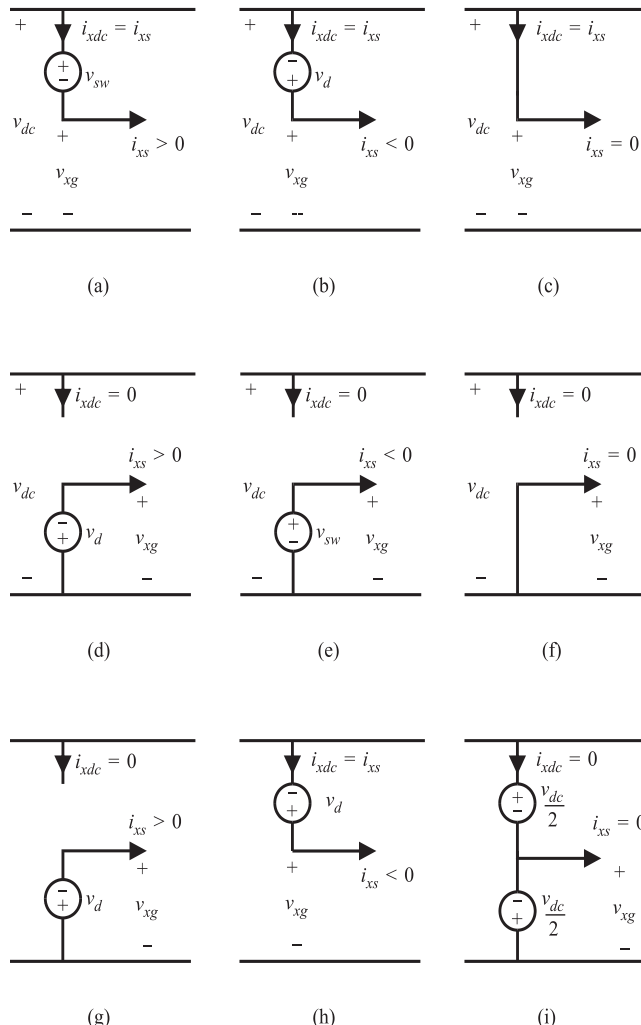


Figure 12.2-2. One phase leg.



**Figure 12.2-3.** Phase leg equivalent circuits. (a) Upper switch on;  $i_{xs} > 0$ . (b) Upper switch on;  $i_{xs} < 0$ . (c) Upper switch on;  $i_{xs} = 0$ . (d) Lower switch on;  $i_{xs} > 0$ . (e) Lower switch on;  $i_{xs} < 0$ . (f) Lower switch on;  $i_{xs} = 0$ . (g) Neither switch on;  $i_{xs} > 0$ . (h) Neither switch on;  $i_{xs} < 0$ . (i) Neither switch on;  $i_{xs} = 0$ .

reasonable to assume that the line-to-ground voltage is equal to the supply voltage as indicated in Figure 12.2-3c. Although other estimates could be argued (such as averaging the voltage from the positive and negative current conditions), it must be remembered that this is a rare condition, so a small inaccuracy will not have a perceptible effect on the results.

The positive, negative, and zero current equivalent circuits, which represent the phase leg when the lower switching device is on and the upper switching device is off,

are illustrated in Figure 12.2-3d,e,f, respectively. The situation is entirely analogous to the case in which the upper switch is on.

One final possibility is the case in which neither transistor is turned on. As stated previously, it is assumed that in the drives considered herein, either the upper or lower transistor is turned on. However, there is a delay between the time a switch is commanded to turn off and the time it actually turns off, as well as a delay between the time a switch is commanded to turn on and the time it actually turns on. Sophisticated semiconductor device models are required to predict the exact voltage and current waveforms associated with the turn-on and turn-off transients of the switching devices [1–5]. However, as an approximate representation, it can be assumed that a device turns on with a delay  $T_{on}$  after the control logic commands it to turn on, and turns off after a delay  $T_{off}$  after the control logic commands it to turn off. The turn-off time is generally longer than the turn-on time. Unless the turn-on time and turn-off time are identical, there will be an interval in which either no device in a leg is turned on or both devices in a leg are turned on. The latter possibility is known as “shoot-through” and is extremely undesirable; therefore, an extra delay is incorporated into the control logic such that the device being turned off will do so before the complementary device is turned on (see Problem 10). Therefore, it may be necessary to represent the condition in which neither device of a leg is turned on.

If neither device of a phase leg is turned on and the current is positive, then the situation is as in Figure 12.2-3g. Since neither switching device is conducting, the current must flow through the lower diode. Thus, the line-to-ground voltage  $v_{xg}$  is equal to  $-v_d$  and the dc current into the leg  $i_{xdc}$  is zero. Conversely, if the phase current is negative, then the upper diode must conduct as is indicated in Figure 12.2-3h. In this case, the line-to-ground voltage is  $v_{dc} + v_d$  and the dc current into the leg  $i_{xdc}$  is equal to phase current into the load  $i_{xx}$ . In the event that neither transistor is on, and that the phase current into the load is zero, it is difficult to identify what the line-to-ground voltage will be since it will become a function of the back emf of the machine to which the converter is connected. If, however, it is assumed that the period during which neither switching device is gated on is brief (on the order of a microsecond), then assuming that the line-to-ground voltage is  $v_{dc}/2$  is an acceptable approximation. Note that this approximation cannot be used if the period during which neither switching device is gated on is extended. An example of the type of analysis that must be conducted if both the upper and lower switching devices are off for an extended period appears in References [6–8].

Table 12.2-1 summarizes the calculation of line-to-ground voltage and dc current into each leg of the bridge for each possible condition. Once each of the line-to-ground voltages are found, the line-to-line voltages may be calculated. In particular,

$$v_{abs} = v_{ag} - v_{bg} \quad (12.2-1)$$

$$v_{bcs} = v_{bg} - v_{cg} \quad (12.2-2)$$

$$v_{cas} = v_{cg} - v_{ag} \quad (12.2-3)$$

and from Figure 12.2-1, the total dc current into the bridge is given by

TABLE 12.2-1. Converter Voltages and Currents

Switch On	Current Polarity	$v_{xg}$	$i_{xdc}$
Upper	Positive	$v_{dc} - v_{sw}$	$i_{xs}$
	Negative	$v_{dc} + v_d$	$i_{xs}$
	Zero	$v_{dc}$	$i_{xs}$
Lower	Positive	$-v_d$	0
	Negative	$v_{sw}$	0
	Zero	0	0
Neither	Positive	$-v_d$	0
	Negative	$v_{dc} + v_d$	$i_{xs}$
	Zero	$v_{dc}/2$	0

$$i_{dc} = i_{adc} + i_{bdc} + i_{cdc} \quad (12.2-4)$$

Since machines are often wye-connected, it is useful to derive equations for the line-to-neutral voltages produced by the three-phase bridge. If the converter of Figure 12.2-1 is connected to a wye-connected load, then the line-to-ground voltages are related to the line-to-neutral voltages and the neutral-to-ground voltage by

$$v_{ag} = v_{as} + v_{ng} \quad (12.2-5)$$

$$v_{bg} = v_{bs} + v_{ng} \quad (12.2-6)$$

$$v_{cg} = v_{cs} + v_{ng} \quad (12.2-7)$$

Summing (12.2-5)–(12.2-7) and rearranging yields

$$v_{ng} = \frac{1}{3}(v_{ag} + v_{bg} + v_{cg}) - \frac{1}{3}(v_{as} + v_{bs} + v_{cs}) \quad (12.2-8)$$

The final term in (12.2-8) is recognized as the zero-sequence voltage of the machine, thus

$$v_{ng} = \frac{1}{3}(v_{ag} + v_{bg} + v_{cg}) - v_{0s} \quad (12.2-9)$$

For a balanced, wye-connected machine, such as a synchronous machine, induction machine, or permanent-magnet ac machine, summing the line-to-neutral voltage equations indicates that the zero-sequence voltage is zero. However, if the machine is unbalanced, this would not be the case. Another practical example of a case in which the zero-sequence voltage is not identically equal to zero is a permanent-magnet ac machine with a square-wave or trapezoidal back emf, in which case the sum of the three-phase back emfs is not zero. However, for the machines considered in this text in which the zero-sequence voltage must be zero, (12.2-9) reduces to

$$v_{ng} = \frac{1}{3}(v_{ag} + v_{bg} + v_{cg}) \quad (12.2-10)$$

Substitution of (12.2-10) into (12.2-5)–(12.2-7) and solving for the line-to-neutral voltages yields

$$v_{as} = \frac{2}{3}v_{ag} - \frac{1}{3}v_{bg} - \frac{1}{3}v_{cg} \quad (12.2-11)$$

$$v_{bs} = \frac{2}{3}v_{bg} - \frac{1}{3}v_{ag} - \frac{1}{3}v_{cg} \quad (12.2-12)$$

$$v_{cs} = \frac{2}{3}v_{cg} - \frac{1}{3}v_{ag} - \frac{1}{3}v_{bg} \quad (12.2-13)$$

## 12.3. SIX-STEP OPERATION

In the previous section, the basic voltage and current relationships needed to analyze the three-phase bridge were set forth with no discussion as to how the bridge would enable operation of a three-phase ac machine from a dc supply. In this section, a basic method of accomplishing the dc to ac power conversion is set forth. This method will be referred to as six-step operation, and is also commonly referred to as  $180^\circ$  voltage-source operation. In this mode of operation, the converter appears as a three-phase voltage source to the ac system, and so six-step operation is classified as a voltage-source control scheme.

The operation of a six-stepped three-phase bridge is shown in Figure 12.3-1. Therein, the first three traces illustrate switching signals applied to the power electronic devices, which are a function of  $\theta_c$ , the converter angle. The definition of the converter angle is dependent upon the type of machine the given converter is driving. For the present, the converter angle can be taken to be  $\omega_c t$ , where  $t$  is time and  $\omega_c$  is the radian frequency of the three-phase output. In subsequent chapters, the converter angle will be related to the electrical rotor position or the position of the synchronous reference frame depending upon the type of machine. Referring to Figure 12.3-1, the logical complement of the switching command to the lower device of each leg is shown for convenience, since this signal is equal to the switch command of the upper device if switching times are neglected. For purposes of explanation, it is further assumed that the diode and switching devices are ideal—that is, that they are perfect conductors when turned on or perfect insulators when turned off. With these assumptions, the line-to-ground voltages are as shown in the central three traces of Figure 12.3-1. From the line-to-ground voltages, the line-to-line voltages may be calculated from (12.2-1)–(12.2-3), which are illustrated in the final three traces. Since the waveforms are square waves rather than sine waves, the three-phase bridge produces considerable harmonic content in the ac output when operated in this fashion. In particular, using Fourier series techniques, the  $a$ - to  $b$ -phase line-to-line voltage may be expressed as

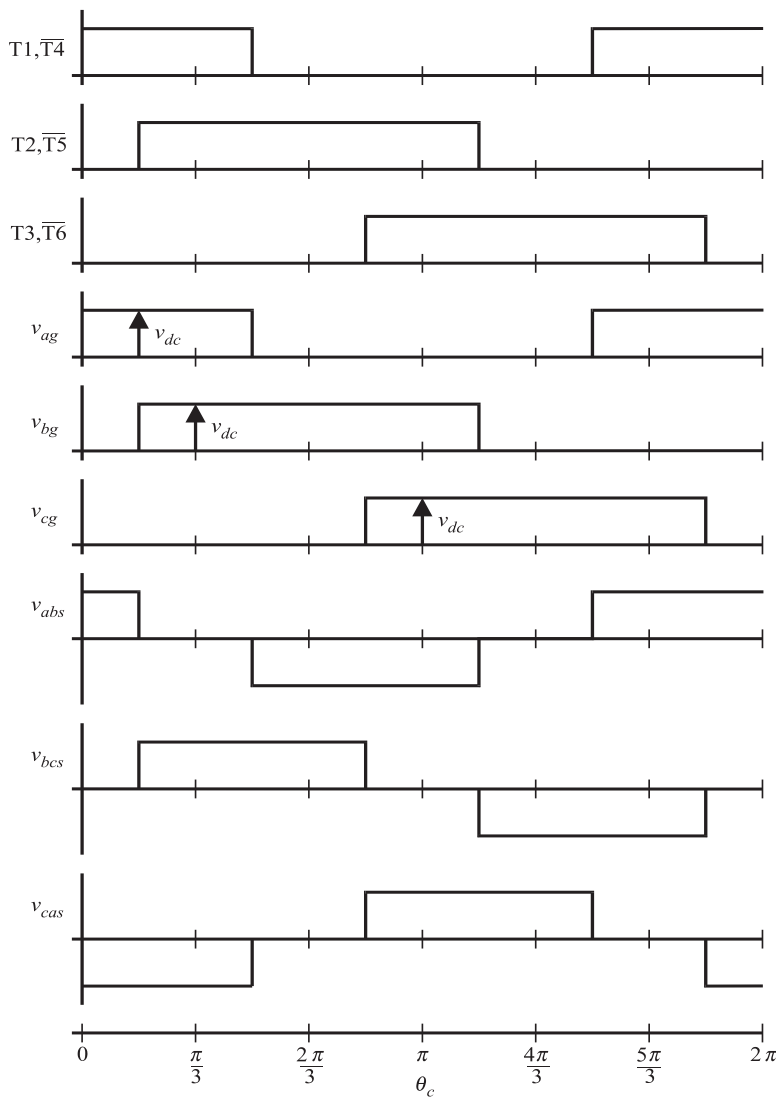


Figure 12.3-1. Line-to-line voltages for six-step operation.

$$\begin{aligned}
 v_{abs} = & \frac{2\sqrt{3}}{\pi} v_{dc} \cos\left(\theta_c + \frac{\pi}{6}\right) \\
 & + \frac{2\sqrt{3}}{\pi} v_{dc} \left( \sum_{j=1}^{\infty} \left( -\frac{1}{6j-1} \cos\left((6j-1)\left(\theta_c + \frac{\pi}{6}\right)\right) + \frac{1}{6j+1} \cos\left((6j+1)\left(\theta_c + \frac{\pi}{6}\right)\right) \right) \right)
 \end{aligned} \quad (12.3-1)$$

From (12.3-1), it can be seen that the line-to-line voltage contains a fundamental component, as well as the 5th, 7th, 9th, 11th, 13th, 17th, 19th . . . harmonic components. There are no even harmonics or odd harmonics that are a multiple of three. The effect of harmonics depends on the machine. In the case of a permanent-magnet ac machine with a sinusoidal back emf, the harmonics will result in torque harmonics but will not have any effect on the average torque. In the case of the induction motor, torque harmonics will again result; however, in this case the average torque will be affected. In particular, it can be shown that the  $6j - 1$  harmonics form an *acb* sequence that will reduce the average torque, while the  $6j + 1$  harmonics form an *abc* sequence that increases the average torque. The net result is usually a small decrease in average torque. In all cases, harmonics will result in increased machine losses.

Figure 12.3-2 again illustrates six-stepped operation, except that the formulation of the line-to-neutral voltages is considered. From the line-to-ground voltage, the neutral-to-ground voltage  $v_{ng}$  is calculated using (12.2-10). The line-to-neutral voltages are calculated using the line-to-ground voltages and line-to-neutral voltage from (12.2-5)–(12.2-7). From Figure 12.3-2, the *a*-phase line-to-neutral voltage may be expressed as a Fourier series of the form

$$v_{as} = \frac{2}{\pi} v_{dc} \cos \theta_c + \frac{2}{\pi} v_{dc} \sum_{j=1}^{\infty} \left( \frac{(-1)^{j+1}}{6j-1} \cos((6j-1)\theta_c) + \frac{(-1)^j}{6j+1} \cos((6j+1)\theta_c) \right) \quad (12.3-2)$$

Relative to the fundamental component, each harmonic component of the line-to-neutral voltage waveform has the same amplitude as in the line-to-line voltage. The frequency spectrum of both the line-to-line and line-to-neutral voltages is illustrated in Figure 12.3-3.

The effect of these harmonics on the current waveforms is illustrated in Figure 12.3-4. In this study, a three-phase bridge supplies a wye-connected load consisting of a  $2\Omega$  resistor in series with a  $1\text{-mH}$  inductor in each phase. The dc voltage is 100 V and the frequency is 100 Hz. The *a*-phase voltage has the waveshape depicted in Figure 12.3-2, and the impact of the *a*-phase voltage harmonics on the *a*-phase current is clearly evident. Because of the harmonic content of the waveforms, the power going into the three-phase load is not constant, which implies that the power into the converter, and hence the dc current into the converter, is not constant. As can be seen, the dc current waveform repeats every 60 electrical degrees; this same pattern will also be shown to be evident in *q*- and *d*-axis variables.

Since the analysis of electric machinery is based on reference-frame theory, it is convenient to determine *q*- and *d*-axis voltages produced by the converter. To do this,

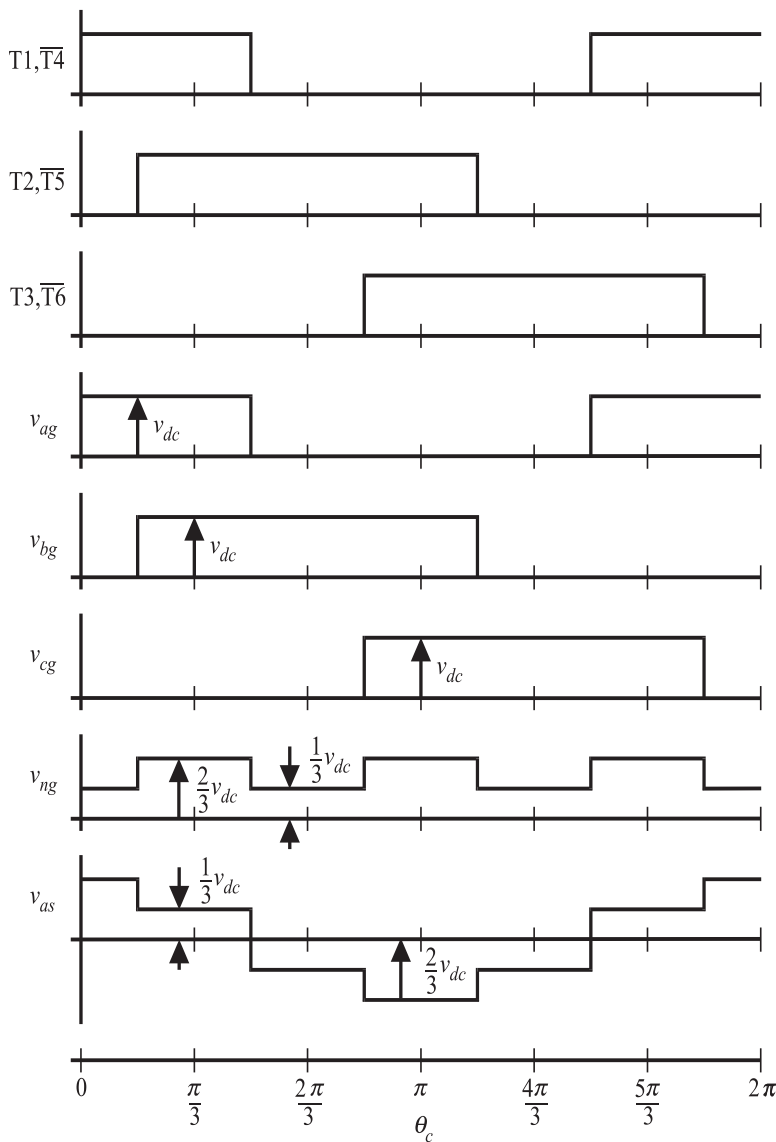


Figure 12.3-2. Line-to-neutral voltage for six-step operation.

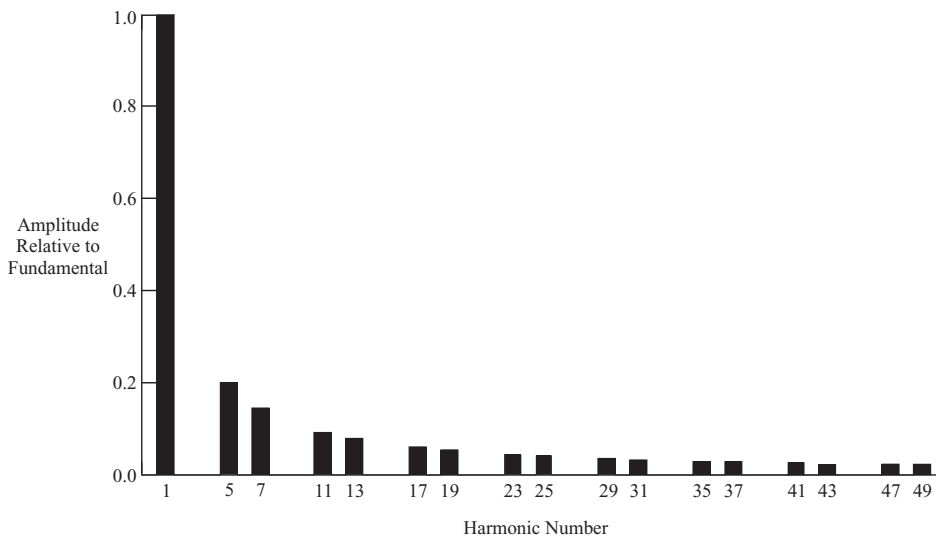


Figure 12.3-3. Frequency spectrum of six-step operation.

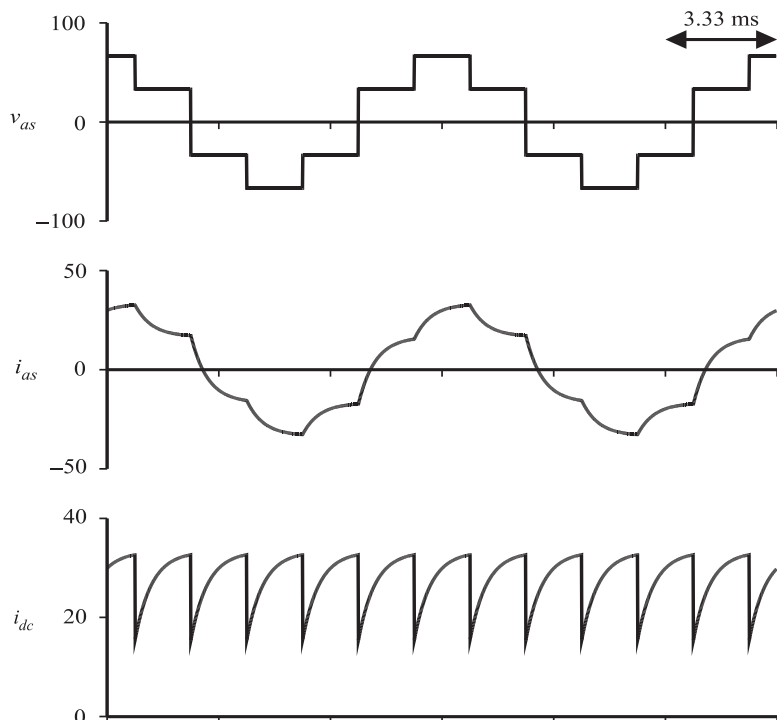


Figure 12.3-4. Voltage and current waveforms for a six-stepped converter feeding an RL load.

we will define the converter reference frame to be a reference frame in which  $\theta$  of (3.3-4) is equal to  $\theta_c$ . In this reference frame, the average  $q$ -axis voltage is equal to the peak value of the fundamental component of the applied line-to-neutral voltage and the average  $d$ -axis voltage is zero. This transformation will be designated  $\mathbf{K}_c^c$ . Usually, the converter reference frame will be the rotor reference frame in the case of a permanent magnet ac machine or the synchronously rotating reference frame in the case of an induction motor. Deriving expressions analogous to (12.3-2) for the  $b$ - and  $c$ -phase line-to-neutral voltages and transforming these voltages to the converter reference frame yields

$$v_{qs}^c = \frac{2}{\pi} v_{dc} - \frac{2}{\pi} v_{dc} \sum_{j=1}^{\infty} \frac{2(-1)^j}{36j^2 - 1} \cos(6j\theta_c) \quad (12.3-3)$$

$$v_{ds}^c = \frac{2}{\pi} v_{dc} \sum_{j=1}^{\infty} \frac{12j}{36j^2 - 1} \sin(6j\theta_c) \quad (12.3-4)$$

From (12.3-3) and (12.3-4), it can be seen that the  $q$ - and  $d$ -axis variables will contain a dc component in addition to multiples of the sixth harmonic. In addition to being evident in  $qd$  variables, the 6th harmonic is also apparent in the torque waveforms of machines connected to six-stepped converters.

For the purposes of machine analysis, it is often convenient to derive an average-value model of the machine in which harmonics are neglected. From (12.3-3) and (12.3-4), the average  $q$ - and  $d$ -axis voltage may be expressed

$$\bar{v}_{qs}^c = \frac{2}{\pi} v_{dc} \quad (12.3-5)$$

$$\bar{v}_{ds}^c = 0 \quad (12.3-6)$$

where the line above the variables denotes average value.

It is interesting to compare the line-to-neutral voltage to the  $q$ - and  $d$ -axis voltage. Such a comparison appears in Figure 12.3-5. As can be seen, the  $q$ - and  $d$ -axis voltages repeat every 60 electrical degrees, which is consistent with the fact that these waveforms only contain a dc component and harmonics that are a multiple of six. The  $qd$  currents,  $qd$  flux linkages, and electromagnetic torque also possess the property of repeating every 60 electrical degrees.

In order to calculate the average dc current into the inverter, note that the instantaneous power into the inverter is given by

$$P_m = i_{dc} v_{dc} \quad (12.3-7)$$

The power out of the inverter is given by

$$P_{out} = \frac{3}{2} (v_{qs} i_{qs} + v_{ds} i_{ds}) \quad (12.3-8)$$

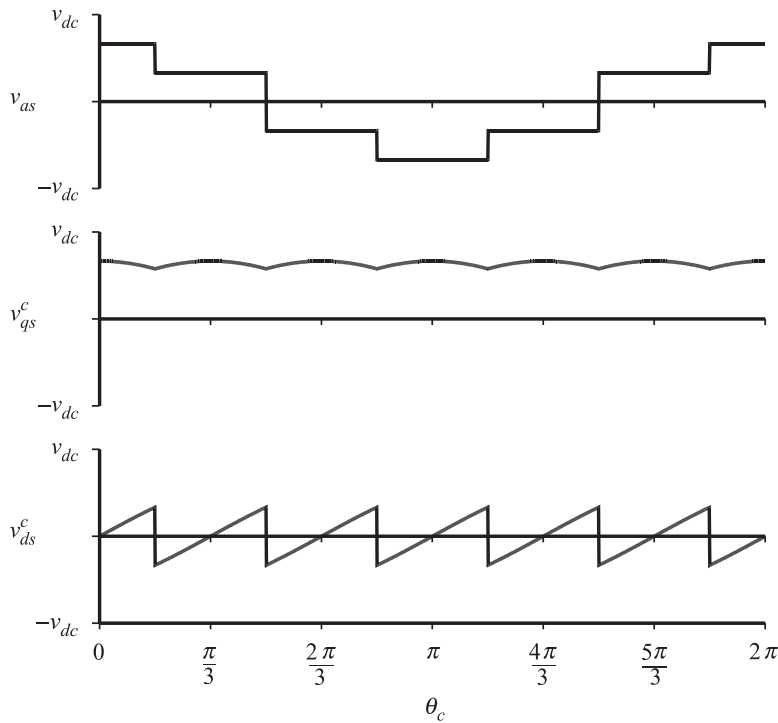


Figure 12.3-5. Comparison of  $a$ -phase voltage to  $q$ - and  $d$ -axis voltage.

Neglecting inverter losses, the input power must equal the output power, therefore

$$i_{dc} = \frac{3(v_{qs}i_{qs} + v_{ds}i_{ds})}{2v_{dc}} \quad (12.3-9)$$

Equation (12.3-9) is true on an instantaneous basis in any reference frame. Therefore, it is also true on average, thus

$$\bar{i}_{dc} = \frac{3}{2} \left( \frac{\bar{v}_{qs}i_{qs} + \bar{v}_{ds}i_{ds}}{v_{dc}} \right) \quad (12.3-10)$$

In a reference frame in which the fundamental components of the applied voltages are constant and if the power transmitted through the bridge via the harmonics of the voltage and current waveforms is neglected, (12.3-10) may be approximated as

$$\bar{i}_{dc} = \frac{3}{2} \frac{\bar{v}_{qs}\bar{i}_{qs} + \bar{v}_{ds}\bar{i}_{ds}}{\bar{v}_{dc}} \quad (12.3-11)$$

It should be emphasized that (12.3-11) is only valid in a reference frame in which the variables are constant in the steady state (the converter reference frame, rotor reference frame of a synchronous or permanent magnet ac machine, or the synchronous reference frame) and when the harmonic power can be neglected.

**EXAMPLE 3A** Suppose a six-step bridge converter drives a three-phase RL load. The system parameters are as follows:  $v_{dc} = 100$  V,  $r = 1.0$   $\Omega$ ,  $l = 1.0$  mH, and  $\omega_c = 2\pi 100$  rad/s. Estimate the average dc current into the inverter. From (12.3-5) and (12.3-6), we have that  $\bar{v}_{qs}^c = 63.7$  V and  $\bar{v}_{ds}^c = 0$  V. From the steady-state equations representing the RL circuit in the converter reference frame,

$$\begin{bmatrix} \bar{i}_{qs}^c \\ \bar{i}_{ds}^c \end{bmatrix} = \begin{bmatrix} r & \omega_c l \\ -\omega_c l & r \end{bmatrix}^{-1} \begin{bmatrix} \bar{v}_{qs}^c \\ \bar{v}_{ds}^c \end{bmatrix} \quad (3A-1)$$

from which we obtain  $\bar{i}_{qc} = 45.6$  A and  $\bar{i}_{dc} = 28.7$  A. From (12.3-11), we have that  $\bar{i}_{dc} = 43.6$  A. It is instructive to do this calculation somewhat more accurately by including the harmonic power. In particular, from (12.3-2), the harmonic content of the voltage waveform can be calculated, which can then be used to find the total power being supplied by the load as

$$P_{out} = \frac{3}{2} r \left( \left| \frac{\frac{2}{\pi} v_{dc}}{r + j\omega_c l} \right|^2 + \sum_{i=1}^{\infty} \left( \left| \frac{2}{r + j(6k-1)\omega_c l} v_{dc} \right|^2 + \left| \frac{2}{r + j(6k+1)\omega_c l} v_{dc} \right|^2 \right) \right) \quad (3A-2)$$

This yields  $P_{out} = 4389$  W, which requires an average dc current of 43.9 A. Thus, at least for this load, the approximations made in deriving (12.3-11) are valid.

Six-step operation is the simplest strategy for controlling the three-phase bridge topology so as to synthesize a three-phase ac voltage source from a single-phase dc voltage source. By varying  $\omega_c$ , variable frequency operation is readily achieved. Nevertheless, there are two distinct disadvantages of this type of operation. First, the only way that the amplitude of the fundamental component can be achieved is by varying  $v_{dc}$ . Although this is certainly possible by using a controllable dc source, appropriate control of the power electronic switches can also be used, which allows the use of a less expensive uncontrolled dc supply. Such a method is considered in the following section. Second, the harmonic content inevitably lowers the machine efficiency. An appropriate switching strategy can substantially alleviate this problem. Thus, although the control strategy just considered is simple, more sophisticated methods of control are generally preferred. The one advantage of the method besides its simplicity is that the amplitude of the fundamental component of the voltage is the largest possible with the topology considered. For this reason, many other control strategies effectively approach six-step operation as the desired output voltage increases.

## 12.4. SIX-STEP MODULATION

In this section, a refinement of six-step operation is presented. In particular, one of several pulse-width modulation (PWM) control strategies that allows the amplitude of the fundamental component of the voltage to be readily controlled is set forth in this section. As in the case of six-step operation, the converter will appear as a voltage-source to the system, and so six-step modulation is also described as a voltage-source modulation scheme.

Figure 12.4-1 illustrates the logic control strategy for six-step modulation. Therein, the logic signals  $S_1$ – $S_3$  are the same as the switching signals  $T_1$ – $T_3$  for six-step operation. The control input to the converter is the duty cycle  $d$ , which may be varied from 0 to 1. The signal  $w$  is a triangle waveform that also varies between 0 and 1. The duty cycle  $d$  and triangle wave  $w$  are inputs of a comparator, the output of which will be denoted  $c$ . The comparator output is logically added with  $S_1$ – $S_3$  to yield the control signals for the semiconductor devices.

The operation of this control circuit is illustrated in Figure 12.4-2. As alluded to previously, the signals  $S_1$ – $S_3$  are identical to  $T_1$ – $T_3$  in six-step operation. The duty cycle  $d$  is assumed to be constant or to vary slowly relative to the triangle wave. The frequency of the triangle wave is the switching frequency  $f_{sw}$  (the number of times each switching device is turned on per second), which should be much greater than the frequency of the fundamental component of the output. The output of the comparator  $c$  is a square wave whose average value is  $d$ . When  $c$  is high, the switching signals to the transistors  $T_1$ – $T_3$ , and hence the voltages, are all identical to those of six-step operation. When  $c$  is low, all the voltages are zero.

In order to analyze six-step modulation, it is convenient to make use of the fact that the voltages produced by this control strategy are equal to voltages applied in the six-step operation multiplied by the output of the comparator. Using Fourier series techniques, the comparator output may be expressed as

$$c = d + 2d \sum_{k=1}^{\infty} \text{sinc}(kd) \cos(k\theta_{sw}) \quad (12.4-1)$$

where  $\theta_{sw}$  is the switching angle defined by

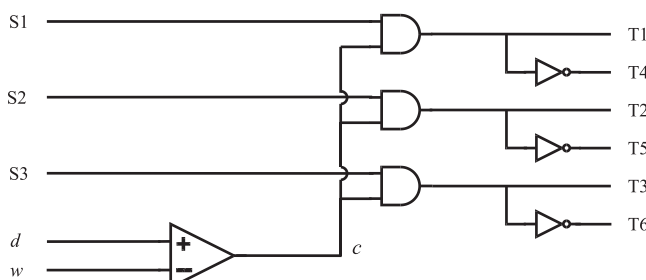


Figure 12.4-1. Six-step modulation control schematic (deadtime logic not shown).

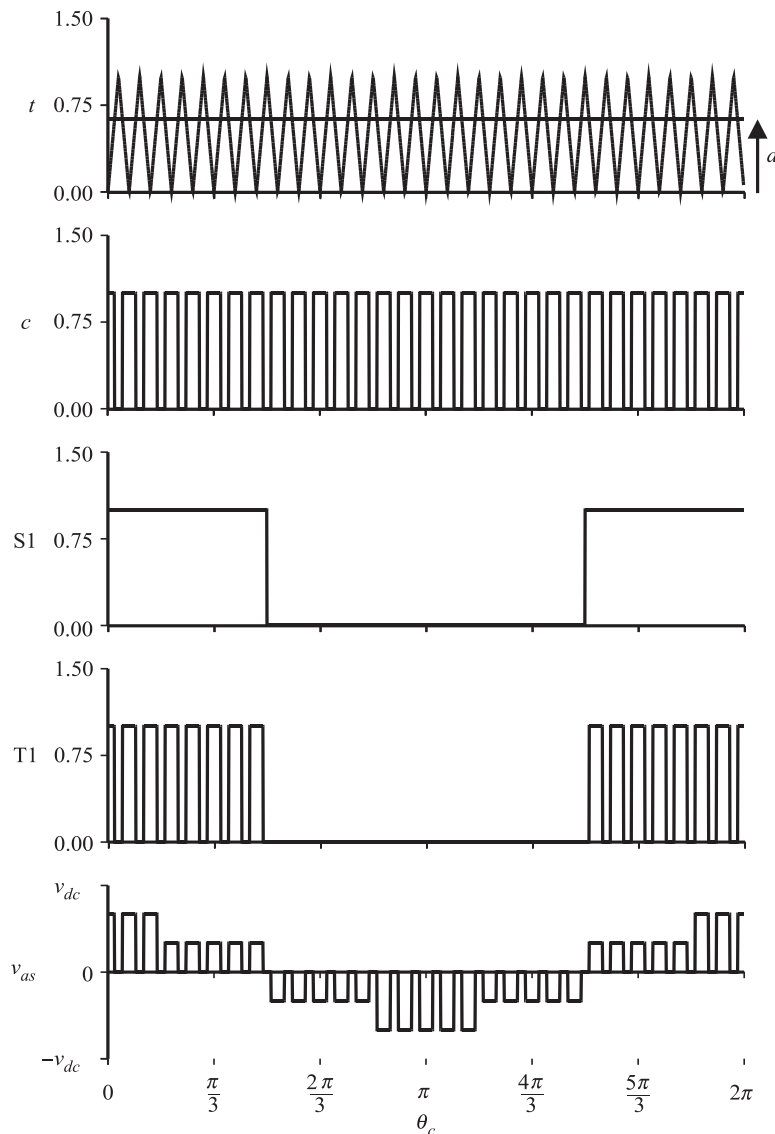


Figure 12.4-2. Six-step modulation control signals.

$$p\theta_{sw} = \omega_{sw} \quad (12.4-2)$$

where  $\omega_{sw} = 2\pi f_{sw}$ . Multiplying (12.4-1) by (12.3-2) yields a Fourier series expression for the *a*-phase line-to-neutral voltage:

$$\begin{aligned} v_{as} = & \frac{2dv_{dc}}{\pi} \left( \cos \theta_c + \sum_{j=1}^{\infty} \left( \frac{(-1)^{j+1}}{6j-1} \cos((6j-1)\theta_c) + \frac{(-1)^j}{6j+1} \cos((6j+1)\theta_c) \right) \right) \\ & + \frac{2dv_{dc}}{\pi} \sum_{k=1}^{\infty} \operatorname{sinc}(kd) \cos(k\theta_{sw} - \theta_c) \\ & + \frac{2dv_{dc}}{\pi} \sum_{k=1}^{\infty} \operatorname{sinc}(kd) \sum_{j=1}^{\infty} \left( \frac{(-1)^{j+1}}{6j-1} \cos(k\theta_{sw} - (6j-1)\theta_c) + \frac{(-1)^j}{6j+1} \cos(k\theta_{sw} - (6j+1)\theta_c) \right) \\ & + \frac{2dv_{dc}}{\pi} \sum_{k=1}^{\infty} \operatorname{sinc}(kd) \cos(k\theta_{sw} + \theta_c) \\ & + \frac{2dv_{dc}}{\pi} \sum_{k=1}^{\infty} \operatorname{sinc}(kd) \sum_{j=1}^{\infty} \left( \frac{(-1)^{j+1}}{6j-1} \cos(k\theta_{sw} + (6j-1)\theta_c) + \frac{(-1)^j}{6j+1} \cos(k\theta_{sw} + (6j+1)\theta_c) \right) \end{aligned} \quad (12.4-3)$$

As can be seen, (12.4-3) is quite involved. The first line indicates that the PWM drive will produce all the harmonics produced by six-step operation, except that all components, including the fundamental, will be scaled by the duty cycle. The next two lines represent the spectrum produced by six-step operation as projected onto the lower side band of the fundamental and harmonics of the switching frequency. The final two lines represent the spectrum produced by six-step operation as projected onto the upper side band of the fundamental and harmonics of the switching frequency. Although the high-frequency harmonic components are not of direct interest for machine analysis, the location of these harmonics is important in the identification of acoustic and electromagnetic noise.

From (12.4-3), it is apparent that the fundamental component of the applied voltage is given by

$$|v_{as}|_{\text{fund}} = d \frac{2}{\pi} v_{dc} \cos \theta_c \quad (12.4-4)$$

From (12.4-4), it follows that the average *q*- and *d*-axis voltage are given by

$$\bar{v}_{qs}^c = \frac{2}{\pi} dv_{dc} \quad (12.4-5)$$

$$\bar{v}_{ds}^c = 0 \quad (12.4-6)$$

Thus, by varying the duty-cycle, the amplitude of the fundamental component of the inverter voltage is readily achieved with a fixed dc supply voltage.

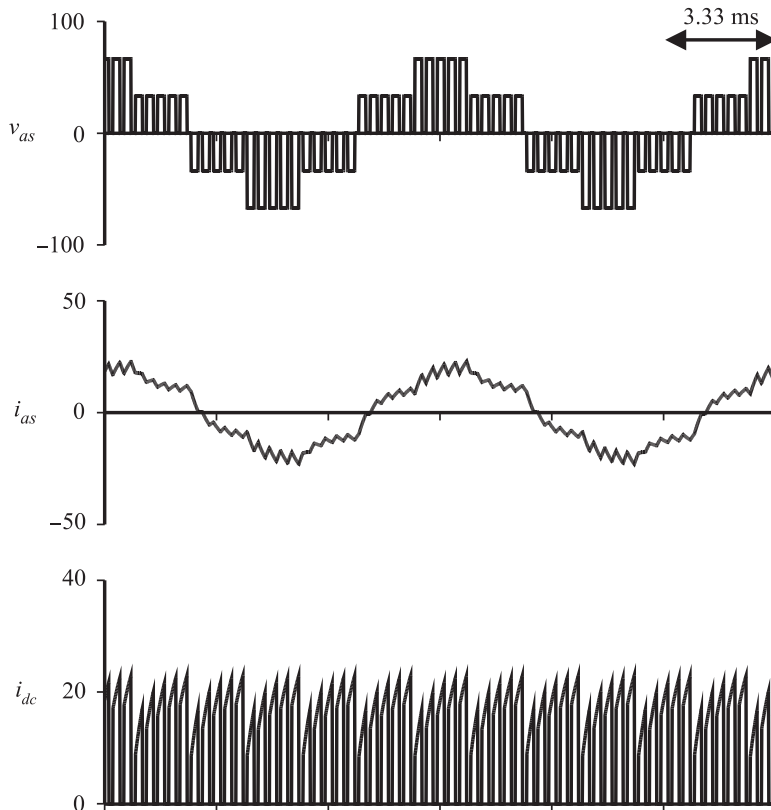


**Figure 12.4-3.** Voltage and current waveforms for six-step modulated converter feeding an RL load.

Figure 12.4.3 illustrates the voltage and current waveforms obtained using six-step modulation. The system parameters are the same as for Figure 12.3-4, except that the duty cycle is 0.628 and the switching frequency is 3000 Hz. As can be seen, the  $a$ -phase current waveform is approximately 0.628 times the current waveform in Figure 12.3-4 if the higher-frequency components of the  $a$ -phase current are neglected.

Although this control strategy allows the fundamental component of the applied voltage to be readily controlled, the disadvantage of this method is that the low-frequency harmonic content adversely affects the performance of the drive. The next modulation scheme considered, sine-triangle modulation, also allows for the control of the applied voltage. However, in this case, there is relatively little low-frequency harmonic content, resulting in nearly ideal machine performance.

## 12.5. SINE-TRIANGLE MODULATION

In the previous section, a method to control the amplitude of the applied voltages was set forth. Although straightforward, considerable low-frequency harmonics were

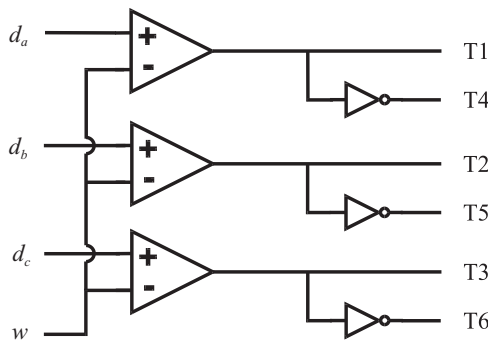


Figure 12.5-1. Sine-triangle modulation control schematic (deadtime logic not shown).

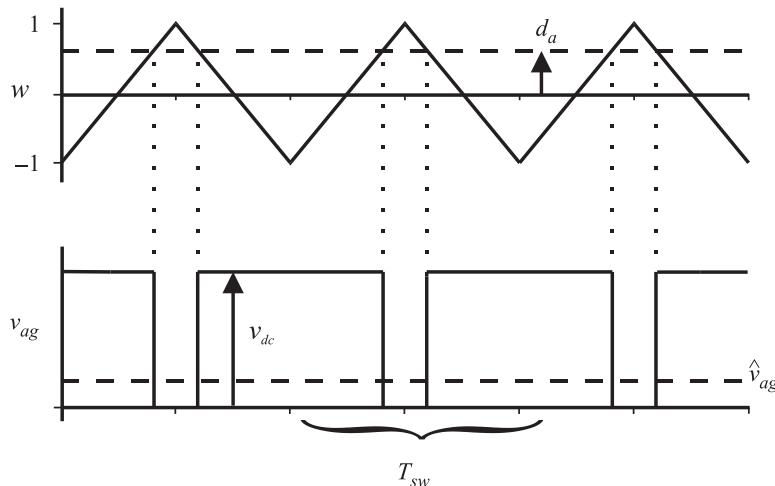


Figure 12.5-2. Operation of a sine-triangle modulator.

generated. The sine-triangle modulation strategy illustrated in Figure 12.5-1 does not share this drawback. Like six-step and six-step modulated operation, this control strategy again makes the converter appear as a voltage-source to the ac system, and so it is again classified as a voltage-source modulation strategy.

In Figure 12.5-1, the signals  $d_a$ ,  $d_b$ , and  $d_c$  represent duty cycles that vary in a sinusoidal fashion and  $w$  is a triangle wave that varies between  $-1$  and  $1$  with a period  $T_{sw}$ . In practice, each of these variables is typically scaled such that the actual voltage levels make the best use of the hardware on which they are implemented.

Figure 12.5-2 illustrates the triangle wave  $w$ ,  $a$ -phase duty cycle, and resulting  $a$ -phase line-to-ground voltage. Therein, the  $a$ -phase duty cycle is shown as being constant even though it is sinusoidal. This is because the triangle wave is assumed to be of a much higher switching frequency than the duty cycle signals, so that on the time scale shown, the  $a$ -phase duty cycle appears to be constant. For the purposes of

analysis, it is convenient to define the “dynamic average” of a variable—that is, the average value over of a period of time  $T_{sw}$ —as

$$\hat{x}(t) = \frac{1}{T_{sw}} \int_{t-T_{sw}}^t x(t) dt \quad (12.5-1)$$

From Figure 12.5-1 and (12.5-1), it can be shown that

$$\hat{v}_{ag} = \frac{1}{2}(1+d_a)v_{dc} \quad (12.5-2)$$

Similarly,

$$\hat{v}_{bg} = \frac{1}{2}(1+d_b)v_{dc} \quad (12.5-3)$$

$$\hat{v}_{cg} = \frac{1}{2}(1+d_c)v_{dc} \quad (12.5-4)$$

If  $d_a$ ,  $d_b$ , and  $d_c$  form a balanced three-phase set, then these three signals must sum to zero. Making use of this fact, substitution of (12.5-2)–(12.5-4) into (12.2-11)–(12.2-13) yields

$$\hat{v}_{as} = \frac{1}{2}d_a v_{dc} \quad (12.5-5)$$

$$\hat{v}_{bs} = \frac{1}{2}d_b v_{dc} \quad (12.5-6)$$

$$\hat{v}_{cs} = \frac{1}{2}d_c v_{dc} \quad (12.5-7)$$

Although it has been assumed that the duty cycles are sinusoidal, (12.5-5)–(12.5-7) hold whenever the sum of the duty cycles is zero. If the duty cycles are specified as

$$d_a = d \cos \theta_c \quad (12.5-8)$$

$$d_b = d \cos \left( \theta_c - \frac{2\pi}{3} \right) \quad (12.5-9)$$

$$d_c = d \cos \left( \theta_c + \frac{2\pi}{3} \right) \quad (12.5-10)$$

it follows from (12.5-5)–(12.5-7) that

$$\hat{v}_{as} = \frac{1}{2} dv_{dc} \cos \theta_c \quad (12.5-11)$$

$$\hat{v}_{bs} = \frac{1}{2} dv_{dc} \cos \left( \theta_c - \frac{2\pi}{3} \right) \quad (12.5-12)$$

$$\hat{v}_{cs} = \frac{1}{2} dv_{dc} \cos \left( \theta_c + \frac{2\pi}{3} \right) \quad (12.5-13)$$

Recall that the “ $\wedge$ ” denotes the dynamic-average value. Thus, assuming that the frequency of the triangle wave is much higher than the frequency of the desired waveform, the sine-triangle modulation strategy does not produce any low-frequency harmonics. Transforming (12.5-11)–(12.5-13) to the converter reference frame yields

$$\hat{v}_{qs}^c = \frac{1}{2} dv_{dc} \quad (12.5-14)$$

$$\hat{v}_{ds}^c = 0 \quad (12.5-15)$$

Equation (12.5-14) and Equation (12.5-15) serve as both steady-state average-value, and, since there are no low-frequency harmonics, dynamic-average-value expressions.

Figure 12.5-3 illustrates the performance of a sine-triangle modulated converter feeding an RL load. The system parameters are identical to the study in Figure 12.4-3, except that  $d = 0.4$ , which results in the voltage waveform with the same fundamental component as in Figure 12.4-3. Comparing Figure 12.5-3 with Figure 12.4-3, it is evident that the sine-triangle modulation strategy results in greatly reduced low-frequency current harmonics. This is even more evident as the switching frequency is increased.

From (12.5-11)–(12.5-13) or (12.5-14) and (12.5-15), it can be seen that if  $d$  is limited to values between 0 and 1, then the amplitude of the applied voltage varies from 0 to  $v_{dc}/2$ , whereas in the case of pulse width modulation, the amplitude varies between 0 and  $2v_{dc}/\pi$ . The maximum amplitude produced by the sine-triangle modulation scheme can be increased to the same value as for six-step modulation by increasing  $d$  to a value greater than 1, a mode of operation known as overmodulation.

Figure 12.5-4 illustrates overmodulated operation. In the upper trace, the two lines indicate the envelope of the triangle wave. The action of the comparators, given the value of the duty cycle relative the envelope of the triangle wave in the upper trace of Figure 12.5-4, results in the following description of the dynamic-average of the  $a$ -phase line-to-ground voltage

$$\hat{v}_{ag} = \begin{cases} v_{dc} & d_a > 1 \\ \frac{1}{2}(1+d_a)v_{dc} & -1 \leq d_a \leq 1 \\ 0 & d_a < 1 \end{cases} \quad (12.5-16)$$

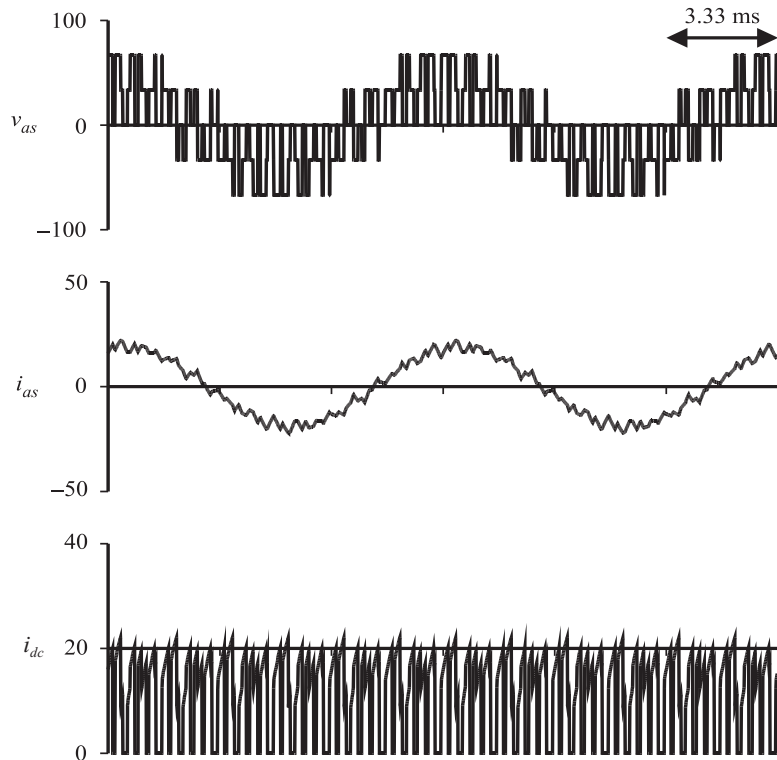


Figure 12.5-3. Voltage and current waveforms using sine-triangle modulation.

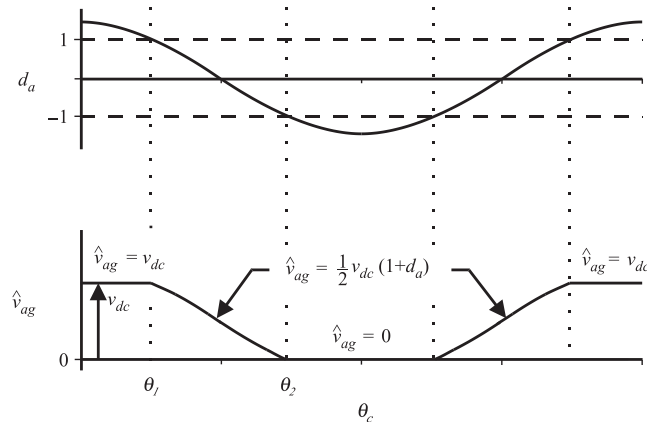


Figure 12.5-4. Overmodulation.

This is illustrated in the second trace of Figure 12.5-4, wherein the angles  $\theta_1$  and  $\theta_2$  mark the points at which the *a*-phase duty cycle is equal to 1 and  $-1$ , respectively. Using Fourier analysis,  $v_{ag}$  may be expressed in terms of its average-value and fundamental component as

$$|v_{ag}|_{avg+fund} = \frac{v_{dc}}{2} + \frac{2v_{dc}}{\pi} f(d) \cos \theta_c \quad (12.5-17)$$

where

$$f(d) = \frac{1}{2} \sqrt{1 - \left(\frac{1}{d}\right)^2 + \frac{1}{4} d \left(\pi - 2 \arccos\left(\frac{1}{d}\right)\right)} \quad (12.5-18)$$

and  $d$  must be greater than unity (overmodulated). The *b*- and *c*-phase voltages may be similarly expressed by subtracting and adding  $120^\circ$  from  $\theta_c$  in (12.5-17), respectively, whereupon (12.2-11)–(12.2-13) may be used to express the line-to-neutral voltages. This yields that

$$|v_{as}|_{fund} = \frac{2v_{dc}}{\pi} f(d) \cos(\theta_c) \quad (12.5-19)$$

As  $d$  varies from one to infinity,  $f(d)$  varies from  $\pi/4$  to 1. Thus, the amplitude of the fundamental component increases as the duty cycle becomes greater than 1. However, this increase is at a cost; low-frequency harmonics will be present and will increase with duty cycle. In particular, at a duty cycle of 1, no low-frequency harmonics will be present, but at  $d = \infty$ , the harmonics are equal to those produced by six-step operation.

Expressing the *b*- and *c*-phase voltages analogously to (12.5-19) and transforming to the converter reference frame yields

$$\bar{v}_{qs}^c = \frac{2v_{dc}}{\pi} f(d) \quad d \geq 1 \quad (12.5-20)$$

$$\bar{v}_{ds}^c = 0 \quad d \geq 0 \quad (12.5-21)$$

It is interesting to observe the performance of the overmodulated sine-triangle modulated bridge. Figure 12.5-5 illustrates system performance for the same conditions as illustrated in Figure 12.5-3, except that  $d$  has been increased to 2. As can be seen, the fundamental component of the voltage and current waveforms has increased; however, this is at the expense of a slight increase in the low-frequency harmonics. As the duty cycle is further increased, the voltage and current waveforms will approach those shown in Figure 12.3-4.

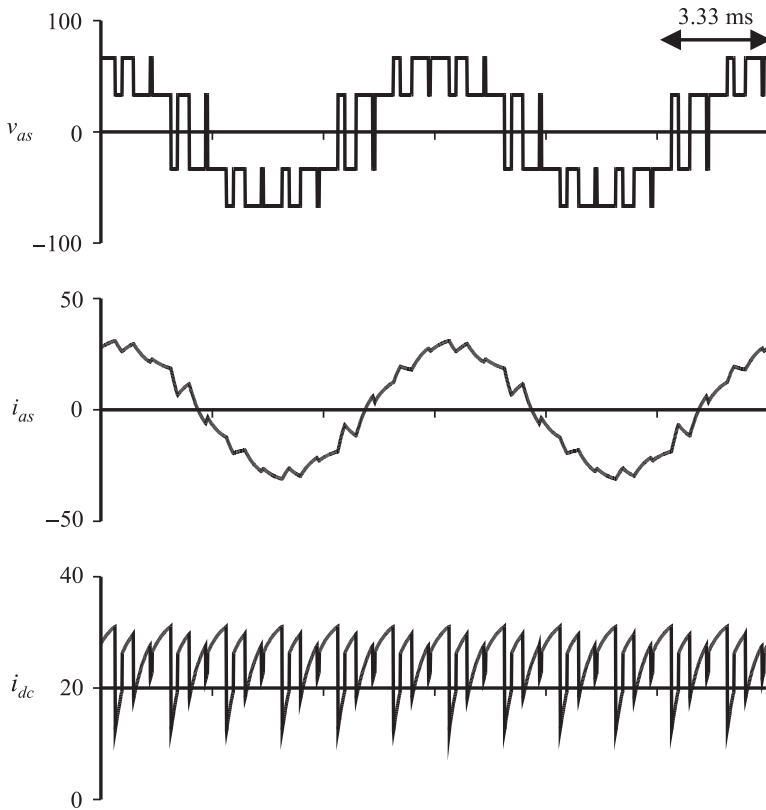


Figure 12.5-5. Voltage and current waveforms during overmodulated operation.

## 12.6. EXTENDED SINE-TRIANGLE MODULATION

One of the chief limitations of sine-triangle modulation is that the peak value of the fundamental component of the line-to-neutral voltage is limited to  $v_{dc}/2$ . As it turns out, this limit can be increased by changing the duty cycle waveforms from the expression given by (12.5-8)–(12.5-10) to the following:

$$d_a = d \cos \theta_c - d_3 \cos(3\theta_c) \quad (12.6-1)$$

$$d_b = d \cos\left(\theta_c - \frac{2\pi}{3}\right) - d_3 \cos(3\theta_c) \quad (12.6-2)$$

$$d_c = d \cos\left(\theta_c + \frac{2\pi}{3}\right) - d_3 \cos(3\theta_c) \quad (12.6-3)$$

Doing this will allow us to use values of  $d$  greater than 1. This scheme will be referred to as extended sine-triangle modulation, which is also classified as a voltage-source modulation scheme.

In order to understand why (12.6-1)–(12.6-3) can be used to increase the maximum fundamental component of the line-to-neutral voltage, note that applying the dynamic-average definition to (12.2-10) yields

$$\hat{v}_{ng} = \frac{1}{3}(\hat{v}_{ag} + \hat{v}_{bg} + \hat{v}_{cg}) \quad (12.6-4)$$

Applying the same dynamic-average definition to (12.2-5)–(12.2-7) and solving for the line-to-neutral voltage yields

$$\hat{v}_{as} = \hat{v}_{ag} - \hat{v}_{ng} \quad (12.6-5)$$

$$\hat{v}_{bs} = \hat{v}_{bg} - \hat{v}_{ng} \quad (12.6-6)$$

$$\hat{v}_{cs} = \hat{v}_{cg} - \hat{v}_{ng} \quad (12.6-7)$$

Substitution of (12.6-1)–(12.6-3) into (12.5-2)–(12.5-4), and then substituting the resulting expressions for  $\hat{v}_{ag}$ ,  $\hat{v}_{bg}$ , and  $\hat{v}_{cg}$  into (12.6-4) and then (12.6-5)–(12.6-7) yields

$$\hat{v}_{as} = \frac{1}{2}d\hat{v}_{dc} \cos \theta_c \quad (12.6-8)$$

$$\hat{v}_{bs} = \frac{1}{2}d\hat{v}_{dc} \cos\left(\theta_c - \frac{2\pi}{3}\right) \quad (12.6-9)$$

$$\hat{v}_{cs} = \frac{1}{2}d\hat{v}_{dc} \cos\left(\theta_c + \frac{2\pi}{3}\right) \quad (12.6-10)$$

This is the same result as was obtained for sine-triangle modulation in the previous section, (12.5-11), (12.5-12), and (12.5-13), and like the previous result is valid provided  $|d_a|$ ,  $|d_b|$ , and  $|d_c|$  are less than unity for all  $\theta_c$ . The difference is that this requirement on  $|d_a|$ ,  $|d_b|$ , and  $|d_c|$  is met. In particular, in the case of sine-triangle modulation, ensuring that  $|d_a|$ ,  $|d_b|$ , and  $|d_c|$  are all less than unity is met by requiring  $|d| < 1$ , which forces the fundamental component of the line-to-neutral voltage to be limited to  $v_{dc}/2$ . In the case of extended sine-triangle modulation, the requirement that  $|d_a|$ ,  $|d_b|$ , and  $|d_c|$  are all less than unity can be met with  $d > 1$ , because the third-harmonic term can be used to reduce the peak value of the phase duty cycle waveforms.

It remains to establish the maximum value of  $d$  and the value that should be used for  $d_3$ . Because of symmetry, these quantities can be determined by considering just the  $a$ -phase over the range  $0 \leq \theta_c \leq \pi/6$ . Note that over this range, the effect of the third-harmonic term is to reduce the magnitude of  $d_a$  (provided that  $d$  is positive). However, at  $\theta_c = \pi/6$ ,  $\cos 3\theta_c$  is zero and so the amount of the reduction is zero. Evaluating (12.6-1) at  $\theta_c = \pi/6$  leads to the requirement that

$$d \cos(\pi/6) \leq 1 \quad (12.6-11)$$

which means that

$$d \leq \frac{2}{\sqrt{3}} \quad (12.6-12)$$

for the strategy to work correctly. The next step is to establish the value of  $d_3$ . To derive this value, requiring that (12.6-1) has a peak value less than unity for all  $\theta_c$  when  $d$  is its maximum value of  $2/\sqrt{3}$  yields  $d_3 = 1/(3\sqrt{3})$ . For this reason, it is common to select  $d_3 = d/6$ . This answer is unique; any other value will result in overmodulation when  $d = 2/\sqrt{3}$ .

The primary advantage of this strategy is the increase in available voltage, which can be obtained. In particular, substituting  $d = 2/\sqrt{3}$  into (12.6-8), the fundamental component of the line-to-neutral voltage is increased to  $v_{dc}/\sqrt{3}$ , a 15% increase in amplitude over sine-triangle modulation. In regard to the average value modeling of this strategy, (12.5-14) and (12.5-15) are valid provided that  $d \leq 2/\sqrt{3}$ .

## 12.7. SPACE-VECTOR MODULATION

Another voltage-source PWM strategy for achieving three-phase voltage waveforms that are devoid of low-frequency harmonic content is space-vector modulation [9]. This modulation strategy is designed to work with voltage commands expressed in terms of  $qd$  variables. In particular, in this strategy, voltage commands expressed in a stationary reference frame ( $v_{qs}^{s*}$  and  $v_{ds}^{s*}$ ) are sampled at the beginning of each switching cycle, and then the inverter semiconductors are switched in such a way that the dynamic average of the actual  $q$ - and  $d$ -axis voltages in the stationary reference frame ( $\hat{v}_{qs}^s$  and  $\hat{v}_{ds}^s$ ) are obtained over the ensuing switching period.

When describing the space-vector modulator algorithm, it is convenient to define the  $q$ - and  $d$ -axis modulation indexes as the  $q$ - and  $d$ -axis voltages in the stationary reference frame normalized to the dc voltage

$$m_q^s = \hat{v}_q^s / v_{dc} \quad (12.7-1)$$

$$m_d^s = \hat{v}_d^s / v_{dc} \quad (12.7-2)$$

It is likewise convenient to define the commanded modulation indexes as

$$m_q^{s*} = v_q^{s*} / v_{dc} \quad (12.7-3)$$

$$m_d^{s*} = v_d^{s*} / v_{dc} \quad (12.7-4)$$

Assuming that the dc voltage is constant, or at least slowly varying compared with the switching frequency, it is apparent that the dynamic-average of the  $q$ - and  $d$ -axis voltage will be equal to the commanded voltages if the dynamic average of the  $q$ - and  $d$ -axis modulation index is equal to the commanded modulation index.

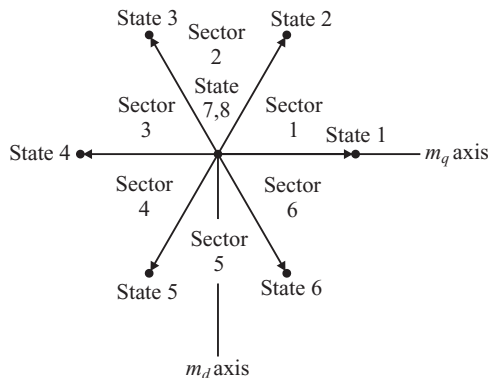


Figure 12.7-1. Space-vector diagram.

TABLE 12.7-1. Modulation Indices versus State

State	$T1/\bar{T4}$	$T2/\bar{T5}$	$T3/\bar{T6}$	$m_{q,x}$	$m_{d,x}$
1	1	0	0	$2/3 \cos(0^\circ)$	$-2/3 \sin(0^\circ)$
2	1	1	0	$2/3 \cos(60^\circ)$	$-2/3 \sin(60^\circ)$
3	0	1	0	$2/3 \cos(120^\circ)$	$-2/3 \sin(120^\circ)$
4	0	1	1	$2/3 \cos(180^\circ)$	$-2/3 \sin(180^\circ)$
5	0	0	1	$2/3 \cos(240^\circ)$	$-2/3 \sin(240^\circ)$
6	1	0	1	$2/3 \cos(300^\circ)$	$-2/3 \sin(300^\circ)$
7	1	1	1	0	0
8	0	0	0	0	0

The space-vector modulation strategy can now be explained in terms of the space-vector diagram illustrated in Figure 12.7-1. Therein, the  $q$ - and  $d$ -axis modulation index vector corresponding to each of the eight possible switching states of the converter is shown. The numerical values of the  $q$ - and  $d$ -axis modulation index corresponding to the  $i$ 'th state,  $m_{q,x}$  and  $m_{d,x}$ , respectively, along with the on/off status of the inverter transistors corresponding to that state, are listed in Table 12.7-1.

In order to determine the sequence of states required to achieve the desired modulation index for a switching cycle, the following steps are performed. First, given the  $q$ - and  $d$ -axis voltage command in the stationary reference frame, the  $q$ - and  $d$ -axis modulation index command is calculated using (12.7-3) and (12.7-4). The next step is to limit the magnitude of the modulation index command to reflect the voltage limitation applied to the converter. The magnitude of the modulation index command is defined as

$$m^* = \sqrt{(m_q^{*})^2 + (m_d^{*})^2} \quad (12.7-5)$$

In the stationary reference frame, the modulation index command vector has a magnitude of  $m^*$  and rotates in the  $qd$  plane at the desired electrical frequency. The largest

magnitude that can be achieved without introducing low-frequency harmonics corresponds to the radius of the largest circle that can be circumscribed within the boundaries of the hexagon connecting the switching state vectors in Figure 12.7-1. This radius is given by

$$m_{\max} = \frac{1}{\sqrt{3}} \quad (12.7-6)$$

The limited modulation index command is next found as follows. First, the magnitude of the raw command is computed using (12.7-5). Then the conditioned modulation index commands are calculated as follows:

$$m_q^{**} = \begin{cases} m_q^* & m^* \leq m_{\max} \\ m_{\max} \frac{m_q^*}{|m^*|} & m^* > m_{\max} \end{cases} \quad (12.7-7)$$

$$m_d^{**} = \begin{cases} m_d^* & m^* \leq m_{\max} \\ m_{\max} \frac{m_d^*}{|m^*|} & m^* > m_{\max} \end{cases} \quad (12.7-8)$$

The next step is to compute the sector of the conditioned modulation command. This is readily calculated from

$$\text{Sector} = \text{ceil}\left(\frac{\text{angle}(m_q^{**} - jm_d^{**})3}{\pi}\right) \quad (12.7-9)$$

where  $\text{angle}()$  returns the angle of its complex argument and has a range of  $0$ – $2\pi$  and  $\text{ceil}()$  returns the next greatest integer.

Once the sector has been determined, the sequence of states used in the ensuing switching cycle are as set forth in Table 12.7-2. This sequence consists of four states: the initial state denoted  $\alpha$ , the second state denoted  $\beta$ , the third state denoted  $\gamma$ , and the final state denoted  $\delta$ . The initial state is always 7 or 8, and the final state will be 8 if the initial state is 7 and will be 7 if the initial state is 8. Therefore, the switching state always begins and ends in a state in which the instantaneous modulation indexes are zero. Another property of the listed state sequence is that only the three states (with states 7 and 8 counted as a single state since they produce identical voltages) with modulation indexes spatially closest to the desired modulation index are used. It is also interesting to observe that with the state sequence listed, the transition between each state and the following state is always achieved by switching the semiconductors in a single converter leg. This is an important feature because it minimizes switching frequency.

After the state sequence has been determined, the time to be spent in each state has to be determined. It can be shown that the dynamic average of the modulation index is given by

TABLE 12.7-2. State Sequence

Sector	Initial State ( $\alpha$ )	2nd State ( $\beta$ )	3rd State ( $\gamma$ )	Final State ( $\delta$ )
1	7	2	1	8
2	7	2	3	8
3	7	4	3	8
4	7	4	5	8
5	7	6	5	8
6	7	6	1	8
1	8	1	2	7
2	8	3	2	7
3	8	3	4	7
4	8	5	4	7
5	8	5	6	7
6	8	1	6	7

$$\hat{m}_q = \frac{t_\beta}{T_{sw}} m_{q,\beta} + \frac{t_\gamma}{T_{sw}} m_{q,\gamma} \quad (12.7-10)$$

$$\hat{m}_d = \frac{t_\beta}{T_{sw}} m_{d,\beta} + \frac{t_\gamma}{T_{sw}} m_{d,\gamma} \quad (12.7-11)$$

where  $t_\beta$  and  $t_\gamma$  denote the amount of time spent in the second and third states of the sequence,  $\beta$  and  $\gamma$  denote index (1–6, see Table 12.7-1) of the second and third states of the sequence as determined from Table 12.7-2, and  $T_{sw}$  denotes the switching period. Setting the dynamic-average modulation indexes equal to the limited modulation index commands and solving (12.7-10) and (12.7-11) for the switching times yields

$$t_\beta = T_{sw} (m_{d,\gamma} m_q^{**} - m_{q,\gamma} m_d^{**}) / D \quad (12.7-12)$$

$$t_\gamma = T_{sw} (-m_{d,\beta} m_q^{**} + m_{q,\beta} m_d^{**}) / D \quad (12.7-13)$$

where

$$D = m_{q,\beta} m_{d,\gamma} - m_{q,\gamma} m_{d,\beta} \quad (12.7-14)$$

Once  $t_\beta$  and  $t_\gamma$  have been found, the last step is to determine the instants at which the state transitions will occur. To this end, it is convenient to define  $t = 0$  as the beginning of the switching cycle and to define  $t_A$ ,  $t_B$ , and  $t_C$  as the times at which the transition from state  $\alpha$  to  $\beta$ ,  $\beta$  to  $\gamma$ , and  $\gamma$  to  $\delta$ , respectively, are made. These times are determined in accordance with

$$t_A = (T_{sw} - t_\beta - t_\gamma) / 2 \quad (12.7-15)$$

$$t_B = t_A + t_\beta \quad (12.7-16)$$

$$t_C = t_B + t_\gamma \quad (12.7-17)$$

In summary, the space-vector modulator operates as follows. At the beginning of a switching cycle, the commanded modulation indexes are calculated using (12.7-3) and (12.7-4). Next, the conditioned modulation index commands are limited using (12.7-5)–(12.7-8) in order to reflect the voltage limitations of the converter. Next, the sector of the modulation command is determined using (12.7-9) from which the state sequence is established using Table 12.7-2. At this point, (12.7-12)–(12.7-14) are used to determine the amount of time spent in each state, and then (12.7-15)–(12.7-17) are used to calculate the actual transition times.

The modeling of this switching algorithm is quite straightforward. In particular, neglecting deadtime and voltage drops, it may be assumed that the output voltage in the stationary reference frame may be expressed as

$$\hat{v}_{qs}^s = m_q^{**} v_{dc} \quad (12.7-18)$$

$$\hat{v}_{ds}^s = m_d^{**} v_{dc} \quad (12.7-19)$$

It is interesting to note that because of the limitation on the magnitude of the modulation index (12.7-6), the limit on the peak value of the fundamental component of the line-to-neutral voltage that can be produced is  $v_{dc} / \sqrt{3}$ , which is identical to that of extended sine-triangle modulation.

## 12.8. HYSTERESIS MODULATION

Thus far, all the bridge control strategies considered have resulted in a three-phase voltage source. Thus, those strategies may all be described as voltage-source. However, it is also possible for the bridge to be controlled so as to appear to be, at some level, and for some conditions, as a current source. Hysteresis modulation is one of these current-source control schemes. In particular, let  $i_{as}^*$ ,  $i_{bs}^*$ , and  $i_{cs}^*$  denote the desired machine or load currents. In order that the actual  $a$ -phase current be maintained within a certain tolerance of the desired  $a$ -phase currents, the control strategy depicted in Figure 12.8-1, known as a hysteresis modulator, is used. As can be seen, if the  $a$ -phase current becomes greater than the reference current plus the hysteresis level  $h$ , the lower transistor of the  $a$ -phase leg is turned on, which tends to reduce the current. If the  $a$ -phase current becomes less than the reference current minus the hysteresis level  $h$ , the upper transistor is turned on, which tends to increase the  $a$ -phase current. The  $b$ - and  $c$ -phases are likewise controlled. The net effect is that the  $a$ -phase current is within the hysteresis level of the desired current, as is illustrated in Figure 12.8-2. As can be seen, the  $a$ -phase current tends to wander back and forth between the two error bands. However, the  $a$ -phase current has inflections even when the current is not against one of the error bands; these are due to the switching in the other phase legs.

The performance of the hysteresis modulator is illustrated in Figure 12.8-3 for the same conditions illustrated in Figure 12.4-3 and Figure 12.5-3. In this case, the commanded  $a$ -phase current is

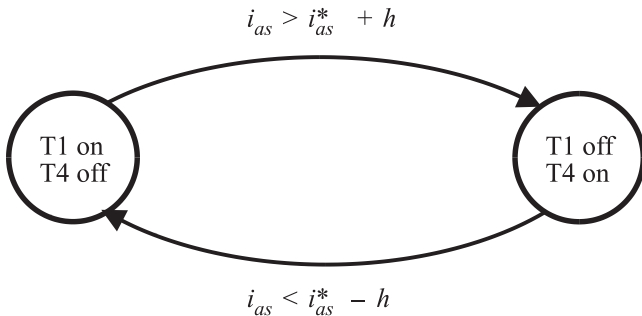


Figure 12.8-1. State transition diagram.

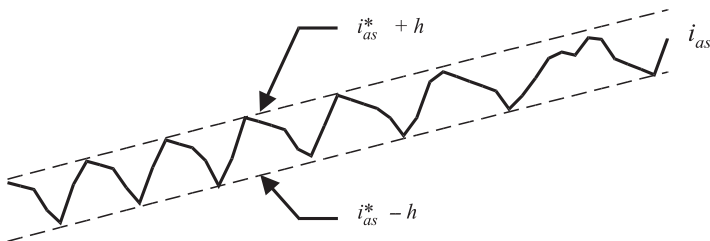


Figure 12.8-2. Allowable current band.

$$i_{as}^* = 19.1 \cos(\theta_c - 17.4^\circ)$$

and the *b*- and *c*-phase reference currents lag the *a*-phase reference currents by  $120^\circ$  and  $240^\circ$ , respectively. This current command is the fundamental component of the current obtained in Figure 12.4-3 and Figure 12.5-3. The hysteresis level is set at 2 A. As can be seen, as in the case of the sine-triangle modulated converter, relatively little low-frequency harmonic content is generated.

Although the concept of having a controllable current source is attractive in that it allows us to ignore the stator dynamics, there are several limitations of hysteresis modulation. First, there is a limit on the range of currents that can actually be commanded. In particular, assume that for a given current command, the peak line-to-neutral terminal voltage is  $v_{pk}$ . Since the peak line-to-neutral voltage the bridge can supply is  $2v_{dc}/3$ , it is apparent that  $v_{pk}$  must be less than  $2v_{dc}/3$  if the commanded current is to be obtained. There is another constraint, which is that the peak line-to-line voltage  $\sqrt{3}v_{pk}$  must be less than the peak line-to-line voltage the converter can achieve, which is equal to  $v_{dc}$ . This requirement is more restrictive and defines the steady-state range over which we can expect the currents to be tracked. In particular,

$$v_{pk} < \frac{v_{dc}}{\sqrt{3}} \quad (12.8-1)$$

Note that the maximum voltage achieved using hysteresis modulation is greater than that which is achieved using sine-triangle modulation, but equal to that of extended sine-triangle or space-vector modulation.

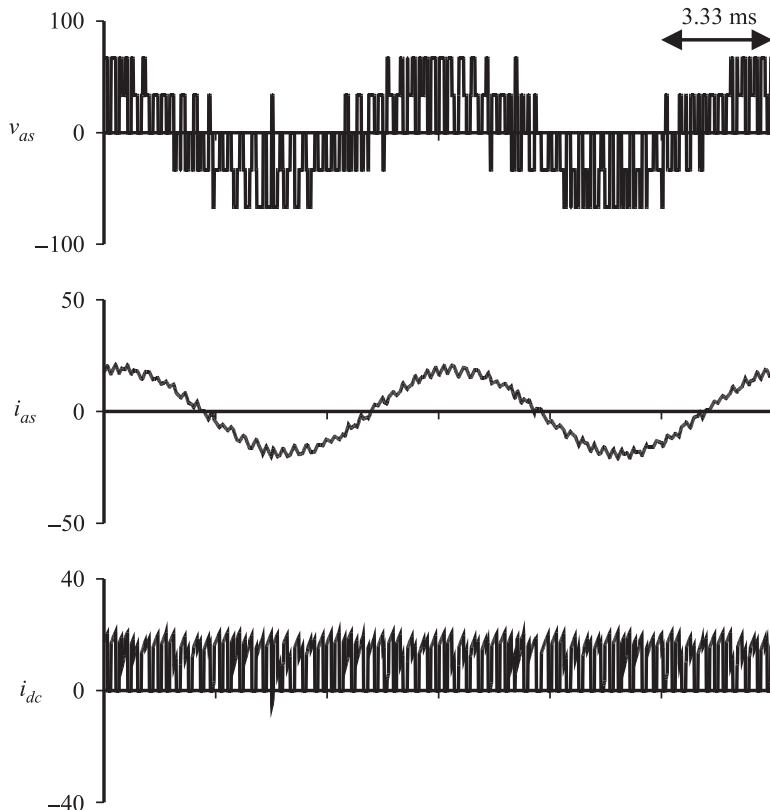


Figure 12.8-3. Voltage and current waveforms using a hysteresis modulator.

In addition to the steady-state limitation on whether the commanded currents will be tracked, there is also a dynamic limitation. In particular, since the stator currents of a machine are algebraically related to the state variables, they cannot be changed instantaneously. Therefore, current tracking will be lost during any step change in commanded currents. When the current command is being changed in a continuous fashion, then current tracking will be maintained provided the peak line-to-neutral voltage necessary to achieve the commanded currents does not exceed (12.8-1).

One disadvantage of the hysteresis-controlled modulation scheme is that the switching frequency cannot be directly controlled. Indirectly, it can be controlled by setting  $h$  to an appropriate level—making  $h$  smaller increases the switching frequency and making  $h$  larger decreases the switching frequency; however, once  $h$  is set, the switching frequency will vary depending on the machine parameters and the operating point. For this reason, current-regulated operation is sometimes synthesized by using suitable control of a voltage-regulated modulation scheme with current feedback.

In regard to average-value modeling, the most straightforward approach is to assume that the actual currents are equal to the commanded currents. Since this involves

neglecting the dynamics associated with the load, such an approach constitutes a reduced-order model. When taking this approach, a check should be conducted to make sure that sufficient voltage is available to actually achieve the current command because such a modeling approach is not valid if sufficient voltage is not present. In the event that a more sophisticated model is required, the reader is referred to References 10 and 11, which describe how to include dynamics of hysteresis modulation and how to model the effects of loss of current tracking due to insufficient inverter voltage, respectively.

## 12.9. DELTA MODULATION

Delta modulation is another current-source modulation strategy. This strategy has an advantage over hysteresis modulation in that a maximum switching frequency is set. The disadvantage is that there is no guarantee on how closely the actual current will track the commanded current.

In this strategy, the current error of each phase is calculated in accordance with

$$e_{xs} = i_{xs}^* - i_{xs} \quad (12.9-1)$$

Every  $T_{sw}$  seconds (the switching period), the current error is sampled. If the current error is positive, the upper switch is turned on; if it is negative, the lower switch is turned on. Clearly, as the switching period is decreased, the actual current will track the desired current more and more closely. It should be observed that since the sign of the error does not necessarily change from one sampling to the next, the phase leg involved will not necessarily switch at every sampling. In addition, since a semiconductor must be turned off before being turned back on, the switching frequency is less than  $1/(2T_{sw})$ .

There are two variations of this strategy. In the first, the three phase legs are sampled and switched simultaneously. In the second, the switching between phases is staggered. The second method is preferred because it provides slightly higher bandwidth and is more robust with respect to electromagnetic compatibility concerns since the switching in one phase will not interfere with the switching in another. This robustness, coupled with its extreme simplicity in regard to hardware implementation, make this strategy very attractive.

As in the case of hysteresis modulation, there are limitations on how well and under what conditions a current waveform can be achieved. The limitations arising from available voltage are precisely the same as for hysteresis modulation, and so no further discussion will be given in this regard. However, in the case of delta modulation, there is an additional limitation in that there is no guarantee on how closely the waveform will track the reference. This must be addressed through careful selection of the switching frequency. Trading off waveform quality versus the switching frequency, while keeping in mind that the actual switching frequency will be lower than the set switching frequency, is a trade-off best made through the use of a waveform-level simulation of the converter machine system.

## 12.10. OPEN-LOOP VOLTAGE AND CURRENT REGULATION

In the previous sections, a variety of modulation strategies were set forth that achieve voltages or currents of a certain magnitude and frequency. For each of these, a method to predict the dynamic average of the  $q$ - and  $d$ -axis voltages or currents in the converter reference frame was set forth. In this section, we examine the inverse problem—that of obtaining the appropriate duty cycle(s) and the converter reference-frame position in order to achieve a desired dynamic-average synchronous reference frame  $q$ - and  $d$ -axis voltage or current.

Six-step modulation, extended sine-triangle modulation, and space-vector modulation are all voltage-source modulation schemes. In our development, we will use these schemes to develop an open-loop voltage-regulated converter. Hysteresis modulation and delta modulation are both current source-based schemes. These will be used as the basis of developing an open-loop current-regulated converter.

The first modulation strategy considered in this chapter that was capable of achieving a  $q$ - and  $d$ -axis voltage command was six-step modulation. In order to see how the variables associated with this modulation strategy are related to a voltage command, observe that from (3.6-7), we have that

$$\begin{bmatrix} v_{qs}^e \\ v_{ds}^e \end{bmatrix} = \begin{bmatrix} \cos \theta_{ce} & \sin \theta_{ce} \\ -\sin \theta_{ce} & \cos \theta_{ce} \end{bmatrix} \begin{bmatrix} v_{qs}^c \\ v_{ds}^c \end{bmatrix} \quad (12.10-1)$$

where  $\theta_{ce}$  is angular displacement of the synchronous reference frame from the converter reference frame, that is,

$$\theta_{ce} = \theta_c - \theta_e \quad (12.10-2)$$

Replacing  $v_{qs}^e$  with the commanded value  $v_{qs}^{e*}$ ,  $v_{ds}^e$  with the commanded value  $v_{ds}^{e*}$ , and  $v_{qs}^c$  and  $v_{ds}^c$  with the average values expressions given by (12.4-5) and (12.4-6) in (12.10-1) yields

$$\begin{bmatrix} v_{qs}^{e*} \\ v_{ds}^{e*} \end{bmatrix} = \begin{bmatrix} \cos \theta_{ce} & \sin \theta_{ce} \\ -\sin \theta_{ce} & \cos \theta_{ce} \end{bmatrix} \begin{bmatrix} \frac{2}{\pi} dv_{dc} \\ 0 \end{bmatrix} \quad (12.10-3)$$

From (12.10-3), we obtain

$$d = \frac{\pi}{2v_{dc}} \sqrt{(v_{qs}^{e*})^2 + (v_{ds}^{e*})^2} \quad (12.10-4)$$

$$\theta_{ce} = \text{angle}(v_{qs}^{e*} - jv_{ds}^{e*}) \quad (12.10-5)$$

Together, (12.10-4) and (12.10-5) suggest the control strategy illustrated in Figure 12.10-1. Therein the inputs are the  $q$ - and  $d$ -axis voltage commands in the synchronous reference frame  $v_{qs}^{e*}$  and  $v_{ds}^{e*}$ , the dc input voltage to the inverter  $v_{dc}$ , and the position of

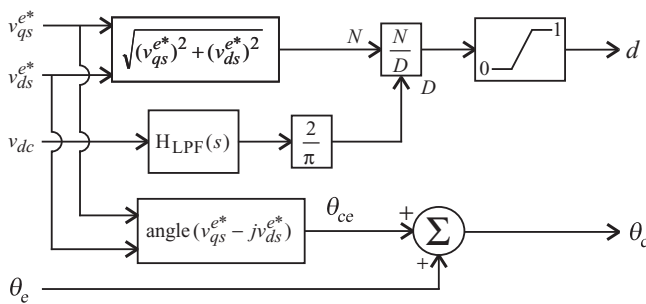


Figure 12.10-1. Voltage regulation using a six-step modulator.

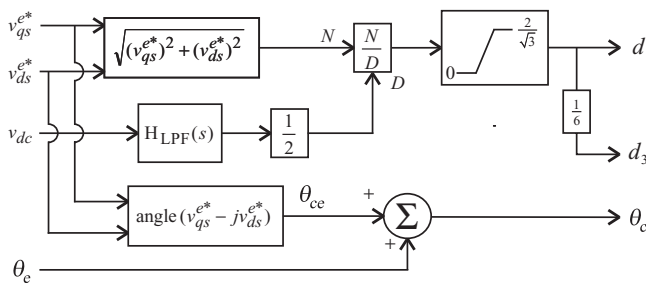


Figure 12.10-2. Voltage regulation using an extended sine-triangle modulator.

the synchronous reference frame  $\theta_e$ . The outputs are the duty cycle  $d$ , and the position of the converter reference frame  $\theta_c$ , as required by the switch level control defined by Figure 12.4-1 (in which S1, S2, and S3 are defined in the same way as T1, T2, and T3 in Fig. 12.3-1). As can be seen in Figure 12.10-1, the duty cycle is essentially calculated in accordance with (12.10-4) with the exception that the dc voltage is filtered through a transfer function  $H_{LPF}(s)$  to eliminate noise and for the purposes of stability. In addition, a limit is placed on the duty cycle  $d$ . The position of the converter reference frame is established by simply adding  $\theta_{ce}$  as set forth in (12.10-5) to the position of the synchronous reference frame  $\theta_e$ .

The next modulation strategy considered was sine-triangle modulation. However, sine-triangle modulation is rarely used in its pure form; it is normally utilized in conjunction with the extended sine-triangle modulation since this yields the potential for a greater ac voltage for a given dc voltage than sine-triangle modulation. The development of a strategy to generate the duty cycle and the position of the converter reference frame from the  $q$ - and  $d$ -axis voltage command is nearly identical to the case for six-step modulation except that (12.5-14) and (12.5-15) replace (12.4-5) and (12.4-6) in the development, which results in a change in the gain following the low-pass filter output from  $2/\pi$  to  $1/2$ , the change of the limit on the duty cycle from 1 to  $2/\sqrt{3}$ , and the introduction of the duty cycle  $d_3$ . These modifications are reflected in Figure 12.10-2. Using the output of this block, the gating of the transistors is readily determined as explained in Section 12.5 and Section 12.6.

In the case of space-vector modulation, the situation is more straightforward since this switching algorithm is based on a  $q$ - and  $d$ -axis voltage command, albeit in the stationary reference frame. In this case, the  $q$ - and  $d$ -axis voltage in the stationary reference frame is calculated from the  $q$ - and  $d$ -axis command in the stationary reference frame using the frame-to-frame transformation; in particular, this yields,

$$v_{qs}^{s*} = v_{qs}^{e*} \cos \theta_e + v_{ds}^{e*} \sin \theta_e \quad (12.10-6)$$

$$v_{ds}^{s*} = -v_{qs}^{e*} \sin \theta_e + v_{ds}^{e*} \cos \theta_e \quad (12.10-7)$$

Let us now consider the problem of obtaining an open-loop current-regulated converter using one of the current source-based modulation schemes. Both hysteresis and delta modulation are based on an  $abc$  variable current command, which is readily computed in terms of a  $q$ - and  $d$ -axis current command in the synchronous reference, and the position of the synchronous reference frame,  $\theta_e$ , using the inverse transformation. In particular, this yields

$$i_{abcs}^* = \mathbf{K}_s^{e^{-1}} i_{qd0s}^* \quad (12.10-8)$$

## 12.11. CLOSED-LOOP VOLTAGE AND CURRENT REGULATION

In the previous section, several strategies for obtaining  $q$ - and  $d$ -axis voltage and current commands were discussed. However, each of these methods was open-loop. In the case of the voltage control strategies, errors will arise because of logic propagation delays, switching deadtime, and the voltage drop across the semiconductors. In the case of current control, even if the inverter is operated in an ideal sense, there will still be a deviation between the actual and commanded current that will have the net effect that the average  $q$ - and  $d$ -axis current obtained will not be equal to the commanded values.

In this section, closed-loop methods of regulating  $q$ - and  $d$ -axis voltages and currents are set forth. These methods stem from the synchronous regulator concept set forth in Reference 12. This concept is based on the observation that integral feedback loop is most effective if implemented in the synchronous reference frame. Because of the integral feedback, there will be no error for dc terms provided the inverter can produce the required voltage. In other words, the average value of the voltages or currents (as expressed in the synchronous reference frame) will be exactly achieved. Since the average value in the synchronous reference frame corresponds to the fundamental component in  $abc$  variables, it can be seen that integral feedback loop implemented in a synchronous reference frame will ensure that the desired fundamental component of the applied voltages or currents is precisely achieved.

Figure 12.11-1 illustrates a method whereby integral feedback can be used to form a closed-loop voltage-regulated converter using a voltage-source modulator or a closed-loop current-regulated converter using a current-source modulator. Therein,  $f$  can denote either voltage  $v$  or current  $i$ . The superscript  $**$  designates a physically desired value, whereas the superscript  $*$  designates the inverter command (which will be used in accordance with one of the modulation strategies described in Section 12.10). Note that

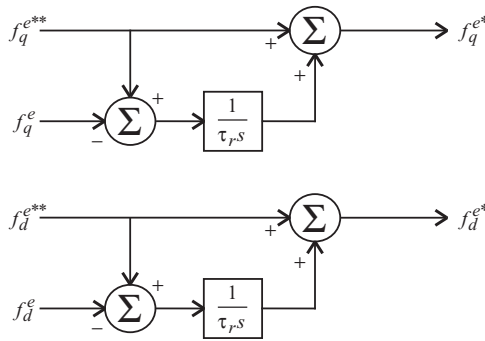


Figure 12.11-1. Synchronous regulator.

the strategy is dependent upon the measured value of voltage or current in the synchronous reference frame,  $f_q^e$  and  $f_d^e$ . These variables are obtained by measuring the *abc* voltages or currents and transforming them to the synchronous reference frame.

For the purposes of analysis, it is sufficient to consider the *q*-axis loop (as the *d*-axis will yield identical results), whereupon it is convenient to assume that *q*-axis quantity  $f_q^e$  will be equal to the *q*-axis inverter command  $f_q^{e*}$  plus an error term; in particular,

$$f_q^e = f_q^{e*} + f_{q,err} \quad (12.11-1)$$

Incorporating (12.11-1) into Figure 12.11-1, it is straightforward to show that the transfer function between the *q*-axis quantity  $f_q^e$ , the command  $f_q^{e**}$ , and the error  $f_{q,err}$  is given by

$$f_q^e = f_q^{e**} + \frac{\tau_r s}{\tau_r s + 1} f_{q,err} \quad (12.11-2)$$

From (12.11-2), it is readily seen that in the steady state, the average value of the *q*-axis quantity  $f_q^e$  will be equal to the *q*-axis command  $f_q^{e**}$ . It is also possible to see that from the perspective of (12.11-2), it is desirable to make time constant  $\tau_r$  as small as possible since this decreases the frequency range and extent to which  $f_{q,err}$  can corrupt  $f_q^e$ .

However, there is a constraint on how small  $\tau_r$  can be made. In particular, again using (12.11-1) in conjunction with Figure 12.11-1, it can be shown that

$$f_q^{e*} = f_q^{e**} + \frac{1}{\tau_r s + 1} f_{q,err} \quad (12.11-3)$$

As this point, it is important to keep in mind that  $f_{q,err}$  should be relatively free from harmonic content or otherwise distortions in the switching pattern will result. Since  $f_{q,err}$  contains considerable high-frequency switching components,  $\tau_r$  must be large enough so that significant switching harmonics are not present in  $f_q^{e*}$ .

The selection of  $\tau_r$  is a function of the modulation strategy. For example, if this strategy is used for current regulation using a current-source modulator, then selecting

$$\tau_r \approx \frac{5}{2\pi f_{sw,est}} \quad (12.11-4)$$

where  $f_{sw,est}$  is the estimated switching frequency (which can be determined through a waveform-level simulation), should normally produce adequate attenuation of the switching ripple in the inverter command.

However, if the scheme is being used for voltage-regulation in conjunction with a extended sine-triangle or space-vector voltage-source modulator, then there will be considerable voltage error ripple, whereupon selecting

$$\tau_r \approx \frac{20}{2\pi f_{sw}} \quad (12.11-5)$$

where  $f_{sw}$  is the switching frequency is more appropriate. Finally, for six-step modulation, the presence of low-frequency harmonics necessitates an even larger time constant, perhaps on the order of

$$\tau_r \approx \frac{20}{2\pi 6 f_{min}} \quad (12.11-6)$$

where  $f_{min}$  denotes the minimum frequency of the fundamental component of the applied waveform that will be used (this can require a very long time constant and implies poor transient performance).

The regulator shown in Figure 12.11-1 is designed as a trimming loop wherein a voltage-source modulation strategy (i.e., six-step, sine-triangle, extended sine-triangle, or space-vector modulators) is used to create a voltage-source converter, or in which a current-based modulation strategy (hysteresis or delta modulators) is used in a current-regulated inverter. However, it is sometimes the case that a voltage-based modulation strategy will be used to regulate current. The advantage of this approach to obtaining a current command is that it allows a fixed switching frequency modulation strategy to be used.

One approach to achieving a voltage-source-modulator-based current regulator is depicted in Figure 12.11-2. Inputs to this control are the  $q$ - and  $d$ -axis current commands  $i_{qs}^{e*}$  and  $i_{ds}^{e*}$ , the measured  $q$ - and  $d$ -axis currents  $i_{qs}^e$  and  $i_{ds}^e$  (obtained by measuring the  $abc$  currents and transforming to the synchronous reference frame), and finally the speed of the synchronous reference frame  $\omega_e$ . The outputs of the control are the  $q$ - and  $d$ -axis voltage commands in a synchronous reference frame  $v_{qs}^{e*}$  and  $v_{ds}^{e*}$ , which are achieved using one of the open-loop control strategies discussed in Section 12.10. Parameters associated with this strategy are the regulator gain  $K_r$ , time constant  $\tau_r$ , and a Thevenin equivalent inductance of the load  $L_T$ . The low-pass filter  $H_{LPF}(s)$  is designed to have unity gain at dc with a cut-off frequency somewhat below the switching frequency.

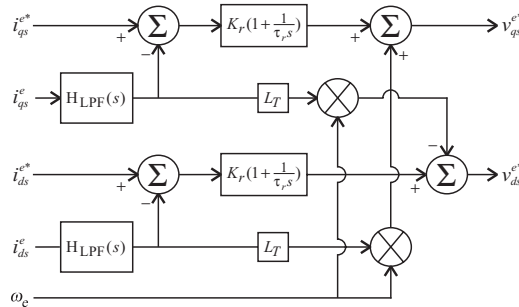


Figure 12.11-2. Voltage-source modulator based current regulator.

In order to gain insight into the operation of this control loop, let us assume that the actual  $q$ - and  $d$ -axis voltages  $v_{qs}^e$  and  $v_{ds}^e$  are equal to their commanded values  $v_{qs}^{e*}$  and  $v_{ds}^{e*}$ , that the low pass filter has dynamics that are appreciably faster than those of this regulator so that they may be ignored for the purpose of designing this control loop, and that on the time scale that this control loop operates (which is much faster than the typical fundamental component of the waveforms in  $abc$  variables but slower than the switching frequency), the load on the inverter may be approximated as

$$v_{qs}^e = \omega_e L_T i_{ds}^e + L_T p i_{qs}^e + e_{qt} \quad (12.11-7)$$

$$v_{ds}^e = -\omega_e L_T i_{qs}^e + L_T p i_{ds}^e + e_{dt} \quad (12.11-8)$$

where  $e_{qt}$  and  $e_{dt}$  are slowly varying quantities. In essence, this is the model of a voltage-behind-inductance load. Many machines, including permanent-magnet ac machines (see Problem 19) and induction machines (see Problem 20), can have their stator equation approximated by this form for fast transients. Incorporating these assumptions into Figure 12.11-2 yields

$$i_{qs}^e = \frac{K_r(\tau_r s + 1)i_{qs}^{e*} + \tau_r s e_{qt}^e}{L_T \tau_r \left( s^2 + \frac{K_r}{L_T} s + \frac{K_v}{L_T \tau_v} \right)} \quad (12.11-9)$$

A similar result can be derived for the  $d$ -axis. Inspection of (12.11-9) reveals that there will be no steady-state error and that there is no interaction between the  $q$ - and  $d$ -axis. This interaction was eliminated by the  $L_T$  term in the control. Of course, if this term is not used, or if the value used is not equal to the Thevenin equivalent inductance, then interaction between the  $q$ - and  $d$ -axis will exist and can be quite pronounced.

The gain  $K_r$  and time constant  $\tau_r$  may be readily chosen using pole-placement techniques. In particular, if it is desired that the pole locations be at  $s = -s_1$  and  $s = -s_2$ , wherein  $s_1$  and  $s_2$  are chosen to be as fast as possible, subject to the constraint that the two poles will be considerably slower than the low pass filter and the switching frequency, then the gain and time constant may be readily expressed as

$$K_r = L_T(s_1 + s_2) \quad (12.11-10)$$

$$\tau_r = \frac{1}{s_1} + \frac{1}{s_2} \quad (12.11-11)$$

In utilizing (12.11-10) and (12.11-11), one choice is to make the system critically damped and chose

$$s_1 = s_2 \approx \frac{\pi f_{sw}}{5} \quad (12.11-12)$$

where  $f_{sw}$  is the switching frequency. A numerical example in applying this design procedure to the design of the current control loops of a large induction motor drive is set forth in Reference 13, and the application of the same general technique to an ac power supply is set forth in Reference 14; this latter reference includes an excellent discussion of the decoupling mechanism.

Any of the techniques used in this section will guarantee that provided enough dc voltage is present, the desired fundamental component of the applied voltage or current will be exactly obtained. Of course, low levels of low frequency harmonics (including negative sequence terms, fifth and seventh harmonics, etc.) and high frequency switching harmonics will still be present. A method of eliminating low-frequency harmonics is set forth in References 15 and 16.

## REFERENCES

- [1] J.G. Kassakian, M.F. Schlecht, and G.C. Verghese, *Principals of Power Electronics*, Addison-Wesley, Reading, MA, 1991.
- [2] N. Mohan, T.M. Undeland, and W.P. Robbins, *Power Electronics*, 2nd ed., John Wiley & Sons/IEEE Press, New York, 1995.
- [3] M.H. Rashid, *Power Electronics*, 2nd ed., Prentice-Hall, Englewood Cliffs, NJ, 1993.
- [4] R.S. Ramshaw, *Power Electronics Semiconductor Switches*, 2nd ed., Chapman & Hall, London, 1993.
- [5] J.T. Tichenor, S.D. Sudhoff, and J.L. Drewniak, "Behavioral IGBT Modeling for Prediction of High Frequency Effects in Motor Drives," Proceedings of the 1997 Naval Symposium on Electric Machines, July 28–31, 1997, Newport, RI, pp. 69–75.
- [6] R.R. Nucera, S.D. Sudhoff, and P.C. Krause, "Computation of Steady-State Performance of an Electronically Commutated Motor," *IEEE Trans. Industry Applications*, Vol. 25, November/December 1989, pp. 1110–1117.
- [7] S.D. Sudhoff and P.C. Krause, "Average-Value Model of the Brushless DC 120° Inverter System," *IEEE Trans. Energy Conversion*, Vol. 5, September 1990, pp. 553–557.
- [8] S.D. Sudhoff and P.C. Krause, "Operating Modes of the Brushless DC Motor with a 120° Inverter," *IEEE Trans. Energy Conversion*, Vol. 5, September 1990, pp. 558–564.
- [9] H.W. Van Der Broek, H. Ch. Skudelny, and G. Stanke, "Analysis and Realization of a Pulse Width Modulator Based on Voltage Space Vectors," *IEEE Trans. Industry Applications*, Vol. 24, No. 1, January/February 1988, pp. 142–150.

- [10] S.F. Glover, S.D. Sudhoff, H.J. Hegner, and H.N. Robey, Jr., "Average Value Modeling of a Hysteresis Controlled DC/DC Converter for Use in Electrochemical System Studies," Proceedings of the 1997 Naval Symposium on Electric Machines, July 28–31, 1997, Newport, RI, pp. 77–84.
- [11] K.A. Corzine, S.D. Sudhoff, and H.J. Hegner, "Analysis of a Current-Regulated Brushless DC Drive," *IEEE Trans. Energy Conversion*, Vol. 10, No. 3, September 1995, pp. 438–445.
- [12] T.M. Rowan and R.J. Kerkman, "A New Synchronous Current Regulator and an Analysis of Current-Regulated Inverters," *IEEE Trans. Industry Applications*, Vol. IA-22, No. 4, 1986, pp. 678–690.
- [13] S.D. Sudhoff, J.T. Alt, H.J. Hegner, and H.N. Robey, Jr., "Control of a 15-Phase Induction Motor Drive System," Proceedings of the 1997 National Symposium on Electric Machines, July 28–31, 1997, Newport, RI, pp. 103–110.
- [14] O. Wasynczuk, S.D. Sudhoff, T.D. Tran, D.H. Clayton, and H.J. Hegner, "A Voltage Control Strategy for Current-Regulated PWM Inverters," *IEEE Trans. Power Electronics*, Vol. 11, No. 1, January 1996, pp. 7–15.
- [15] P.L. Chapman and S.D. Sudhoff, "A Multiple Reference Frame Synchronous Estimator/Regulator," *IEEE Trans. Energy Conversion*, Vol. 15, No. 2, June 2000, pp. 197–202.
- [16] P.L. Chapman and S.D. Sudhoff, "Optimal Control of Permanent-Magnet AC Drives with a Novel Multiple Reference Frame Synchronous Estimator/Regulator," Proceedings of the 34th Industry Applications Society Annual Meeting, 1999.

## PROBLEMS

1. Show that  $v_{0s}$  is zero for a balanced three-phase induction motor.
2. Show that  $v_{0s}$  is zero for a balanced three-phase synchronous machine.
3. Show that  $v_{0s}$  is zero for a balanced three-phase permanent magnet ac machine with a sinusoidal back emf.
4. Figure 12P-1 illustrates the  $a$ -phase line-to-ground voltage of a three-phase bridge converter. Determine the diode and transistor forward voltage drops.
5. From Figure 12.3-1, derive (12.3-1).
6. From (12.3-1), deduce analogous expressions for  $v_{bcs}$  and  $v_{cas}$ .
7. From Figure 12.3-2, derive (12.3-2).
8. From (12.3-2), deduce analogous expressions for  $v_{bs}$  and  $v_{cs}$ .
9. Consider a three-phase bridge supplying a wye-connected load in which the  $a$ -phase,  $b$ -phase, and  $c$ -phase resistances are 2, 4, and 4  $\Omega$ , respectively. Given that the dc supply voltage is 100 V and the control strategy is six-step operation, sketch the  $a$ -phase line-to-neutral voltage waveform.
10. Figure 12P-2 illustrates a circuit that can be used to avoid shoot-through. If 5 V logic is used, the gate threshold turn-on voltage is 3.4 V, and the resistor is 1 k $\Omega$ , compute the capacitance necessary to assure that gate turn-off will occur 1.5  $\mu$ s before the second transistor of the pair is gated on.

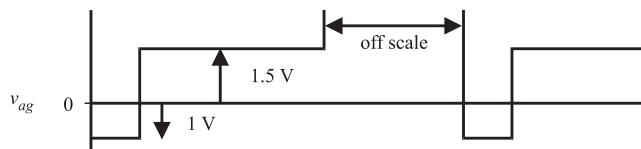


Figure 12P-1. The a-phase line-to-ground voltage of a three-phase bridge converter.

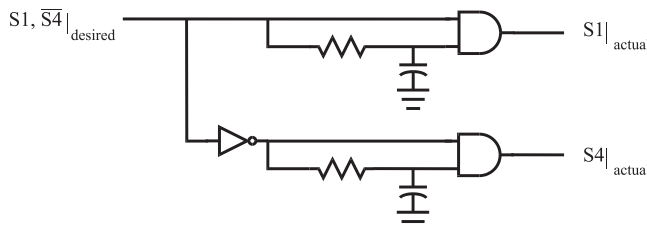


Figure 12P-2. Circuit than can be used to avoid shoot-through.

11. Consider the 3-hp induction motor whose parameters are listed in Table 6.10-1. Plot the torque-speed and dc current-speed curves if it is being fed from a three-phase bridge in six-step operation, assuming that the dc voltage is 560 V and the frequency is 120 Hz. Neglect harmonics.
12. Consider the system discussed in Problem 11. Compute the effect of the fifth and seventh harmonics on the average torque if the machine is operating at a slip of 0.025 relative to the fundamental component of the applied voltages.
13. A six-step modulated drive with a dc voltage of 600 V and a duty cycle of 0.75 is used to drive a permanent-magnet ac machine. At a certain operating speed, the fundamental component of the stator frequency is 300 Hz. If the switching frequency is 10 kHz, compute the amplitude of the strongest two harmonics in the region of 50 kHz.
14. A permanent magnet ac machine is to be operated from the six-step modulated three-phase bridge. The dc voltage is 100 V, and the desired  $q$ - and  $d$ -axis voltages are  $v_{qs}^r = 50$  V and  $v_{ds}^r = 10$  V. Specify the duty-cycle  $d$  and the relationship between  $\theta_c$  and  $\theta_r$  such that these voltages are obtained.
15. Derive (12.5-17) and (12.5-18) from Figure 12.5-4.
16. Consider the 3-hp induction motor in Table 6.10-1. The machine is being fed from a sine-triangle modulated three-phase bridge with  $v_{dc} = 280$  V. If the machine is being operated at a speed of 1710 rpm and the frequency of the fundamental component of the applied voltages is 60 Hz, plot the torque versus duty cycle as the duty-cycle  $d$  is varied from 0 to 5.
17. A three-phase four-pole permanent magnet ac machine has the parameters  $r_s = 2.99 \Omega$ ,  $L_{ss} = 11.35$  mH, and  $\lambda'_m = 0.156$  V·s/rad is operated from a current-source modulated inverter with  $v_{dc} = 140$  V. If it is being operated at 2670 rpm, plot the locus of points in the  $q$ -axis current command versus  $d$ -axis current

command plane that describes the limits of the region over which the current command can be expected to be obtained.

18. Rederive (12.11-9)–(12.11-11) if a resistive term is included in the load model (12.11-7) and (12.11-8).
19. Ignoring stator resistance, and taking the synchronous reference frame to be the rotor reference frame, express  $L_T$ ,  $e_{qT}$ , and  $e_{dT}$  in terms of electrical rotor speed for a surface mounted (nonsalient) permanent magnet ac machine.
20. Ignoring stator resistance, and assuming that the rotor flux linkages in the synchronous reference frame are constants, express  $L_T$ ,  $e_{qT}$ , and  $e_{dT}$  for an induction machine in terms of the  $q$ - and  $d$ -axis rotor flux linkages and the electrical rotor speed. As an aside, because the rotor winding are shorted, their time derivative tends to be small, which leads to this approximation—it is akin to putting the model in sub-transient form in the case of synchronous machines.

# INDUCTION MOTOR DRIVES

## 13.1. INTRODUCTION

The objective of this chapter is to explore the use of induction machines in variable-speed drive systems. Several strategies will be considered herein. The first, volts-per-hertz control, is designed to accommodate variable-speed commands by using the inverter to apply a voltage of correct magnitude and frequency so as to approximately achieve the commanded speed without the use of speed feedback. The second strategy is constant slip control. In this control, the drive system is designed so as to accept a torque command input—and therefore speed control requires an additional feedback loop. Although this strategy requires the use of a speed sensor, it has been shown to be highly robust with respect to changes in machine parameters and results in high efficiency of both the machine and inverter. One of the disadvantages of this strategy is that in closed-loop speed-control situations, the response can be somewhat sluggish. Another strategy considered is field-oriented control. In this method, nearly instantaneous control of torque can be obtained. A disadvantage of this strategy is that in its direct form, the sensor requirements are significant, and in its indirect form, it is sensitive to parameter measurements unless online parameter estimation or other steps are

taken. Another method of controlling torque, called direct torque control (DTC), is also described, and its performance illustrated by computer traces. Finally, slip energy recovery systems, such as those used in modern variable-speed wind turbines, are described.

### 13.2. VOLTS-PER-HERTZ CONTROL

Perhaps the simplest and least expensive induction motor drive strategy is constant volt-per-hertz control. This is a speed control strategy that is based on two observations. The first of these is that the torque speed characteristic of an induction machine is normally quite steep in the neighborhood of synchronous speed, and so the electrical rotor speed will be near to the electrical frequency. Thus, by controlling the frequency, one can approximately control the speed. The second observation is based on the  $a$ -phase voltage equation, which may be expressed

$$v_{as} = r_s i_{as} + p\lambda_{as} \quad (13.2-1)$$

For steady-state conditions at mid- to high speeds wherein the flux linkage term dominates the resistive term in the voltage equation, the magnitude of the applied voltage is related to the magnitude of the stator flux linkage by

$$V_s = \omega_e \Lambda_s \quad (13.2-2)$$

which suggests that in order to maintain constant flux linkage (to avoid saturation), the stator voltage magnitude should be proportional to frequency.

Figure 13.2-1 illustrates one possible implementation of a constant volts-per-hertz drive. Therein, the speed command, denoted by  $\omega_{rm}^*$ , acts as input to a slew rate limiter (SRL), which acts to reduce transients by limiting the rate of change of the speed command to values between  $\alpha_{min}$  and  $\alpha_{max}$ . The output of the SRL is multiplied by  $P/2$ , where  $P$  is the number of poles in order to arrive at the electrical rotor speed command  $\omega_r^*$  to which the radian electrical frequency  $\omega_e$  is set. The electrical frequency is then multiplied by the volts-per-hertz ratio  $V_b/\omega_b$ , where  $V_b$  is rated voltage, and  $\omega_b$  is rated radian frequency in order to form an rms voltage command  $V_s$ . The rms voltage command  $V_s$  is then multiplied by  $\sqrt{2}$  in order to obtain a  $q$ -axis voltage command  $v_{qs}^{e*}$  (the voltage is arbitrarily placed in the  $q$ -axis). The  $d$ -axis voltage command is set to zero. In a parallel path, the electrical frequency  $\omega_e$  is integrated to determine the position of a synchronous reference frame  $\theta_e$ . The integration to determine  $\theta_e$  is periodically reset by an integer multiple of  $2\pi$  in order to keep  $\theta_e$  bounded. Together, the  $q$ - and  $d$ -axis voltage commands may then be passed to any one of a number of modulation strategies in order to achieve the commanded voltage as discussed in Chapter 12. The advantages of this control are that it is simple, and that it is relatively inexpensive by virtue of being entirely open loop; speed can be controlled (at least to a degree) without feedback. The principal drawback of this type of control is that because it is open loop, some measure of error will occur, particularly at low speeds.

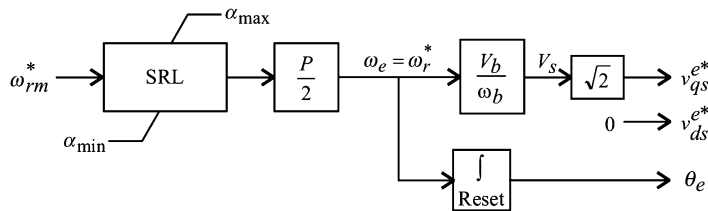


Figure 13.2-1. Elementary volts-per-hertz drive.

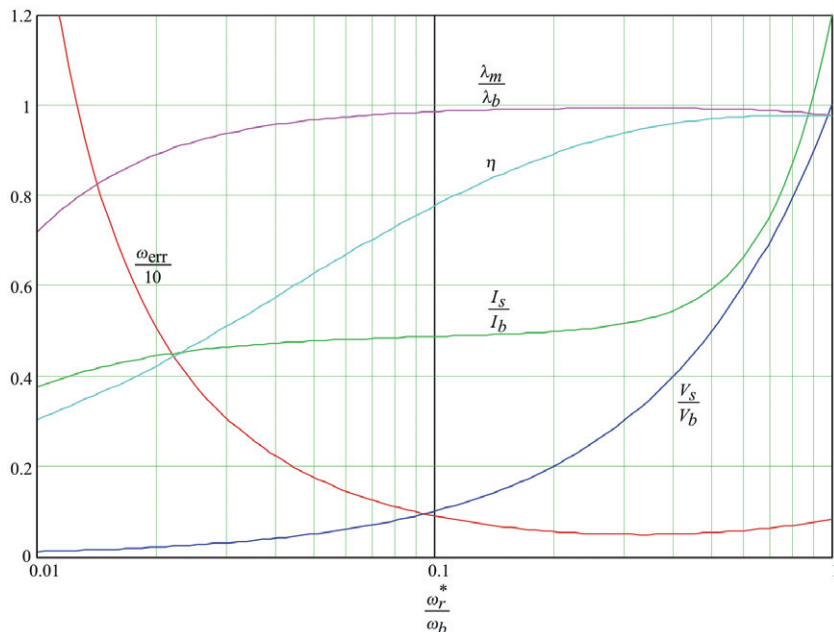


Figure 13.2-2. Performance of elementary volts-per-hertz drive.

Figure 13.2-2 illustrates the steady-state performance of the voltage-per-hertz drive strategy shown in Figure 13.2-1. In this study, the machine is a 50-hp, four-pole, 1800-rpm, 460-V (line-to-line, rms) with the following parameters:  $r_s = 72.5 \text{ mΩ}$ ,  $L_{ls} = 1.32 \text{ mH}$ ,  $L_M = 30.1 \text{ mH}$ ,  $L'_{lr} = 1.32 \text{ mH}$ ,  $r'_r = 41.3 \text{ mΩ}$ , and the load torque is assumed to be of the form

$$T_L = T_b \left( 0.1S(\omega_{rm}) + 0.9 \left( \frac{\omega_{rm}}{\omega_{bm}} \right)^2 \right) \quad (13.2-3)$$

where  $S(\omega_{rm})$  is a stiction function that varies from 0 to 1 as  $\omega_{rm}$  goes from 0 to  $0^+$ . Figure 13.2-2 illustrates the percent error in speed  $100(\omega_r^* - \omega_r)/\omega_r^*$ , normalized voltage  $V_s/V_b$ , normalized current  $I_s/I_b$ , efficiency  $\eta$ , and normalized air-gap flux linkage

$\lambda_m/\lambda_b$  versus normalized speed command  $\omega_{rm}^* / \omega_{bm}$ . The base for the air-gap flux linkage is taken to be the no-load air-gap flux linkage that is obtained at rated speed and rated voltage.

As can be seen, the voltage increases linearly with speed command, while the rms current remains approximately constant until about 0.5 pu and then rises to approximately 1.2 pu at a speed command of 1 pu. Also, it is evident that the percent speed error remains less than 1% for speeds from 0.1 to 1 pu; however, the speed error becomes quite large for speeds less than 0.1 pu. The reason for this is the fact that the magnetizing flux drops to zero as the speed command goes to zero due to the fact that the resistive term dominates the flux-linkage term in (13.2-1) at low speeds. As a result, the torque-speed curve loses its steepness about synchronous speed, resulting in larger percentage error between commanded and actual speed.

The low-speed performance of the drive can be improved by increasing the voltage command at low frequencies in such a way as to make up for the resistive drop. One method of doing this is based on the observation that the open-loop speed regulation becomes poorer at low speeds, because the torque-speed curve becomes decreasingly steep as the frequency is lowered if the voltage is varied in accordance with (13.2-2). To prevent this, it is possible to vary the rms voltage in such a way that the slope of the torque-speed curve at synchronous speed becomes independent of the electrical frequency. Taking the derivative of torque with respect to rotor speed in (6.9-20) about synchronous speed for an arbitrary electrical frequency and setting it equal to the same derivative about base electrical frequency yields

$$V_s = V_b \sqrt{\frac{r_{s,est}^2 + \omega_e^2 L_{ss,est}^2}{r_{s,est}^2 + \omega_b^2 L_{ss,est}^2}} \quad (13.2-4)$$

where  $r_{s,est}$  and  $L_{ss,est}$  are the estimated value of  $r_s$  and  $L_{ss}$ , respectively. The block diagram of this version of volts-per-hertz control is identical to that shown in Figure 13.2-1, with the exception that (13.2-4) replaces (13.2-2). Several observations are in order. First, it can be readily shown that varying the voltage in accordance with (13.2-4) will yield the same air-gap flux at zero frequency as is seen for no load conditions at rated frequency—thus the air-gap flux does not fall to zero at low frequency as it does when (13.2-2) is used. It is also interesting to observe that (13.2-4) reduces to (13.2-2) at a frequency such that  $\omega_e L_{ss,est} \gg r_{s,est}$ .

In order to further increase the performance of the drive, one possibility is to utilize the addition of current feedback in determining the electrical frequency command. Although this requires at least one (but more typically two) current sensor(s) that will increase cost, it is often the case that a current sensor(s) will be utilized in any case for overcurrent protection of the drive. In order to derive an expression for the correct feedback, first note that near synchronous speed, the electromagnetic torque may be approximated as

$$T_e = K_{tv}(\omega_e - \omega_r) \quad (13.2-5)$$

where

$$K_{tv} = -\left. \frac{\partial T_e}{\partial \omega_r} \right|_{\omega_r = \omega_e} \quad (13.2-6)$$

If (13.2-4) is used

$$K_{tv} = \frac{3 \left( \frac{P}{2} \right) L_M^2 r'_r V_b^2}{r'^2 (r_s^2 + \omega_b^2 L_{ss}^2)} \quad (13.2-7)$$

regardless of synchronous speed. Next, note that from (6.6-14), torque may be expressed as

$$T_e = \frac{3}{2} \frac{P}{2} (\lambda_{ds}^e i_{qs}^e - \lambda_{qs}^e i_{ds}^e) \quad (13.2-8)$$

From (6.5-10) and (6.5-11), for steady-state conditions, the stator flux linkage equations may be expressed as

$$\lambda_{ds}^e = \frac{v_{qs}^e - r_s i_{qs}^e}{\omega_e} \quad (13.2-9)$$

and

$$\lambda_{qs}^e = -\frac{v_{ds}^e - r_s i_{ds}^e}{\omega_e} \quad (13.2-10)$$

Approximating  $v_{qs}^e$  by its commanded value of  $v_{qs}^{e*}$  and  $v_{ds}^e$  by its commanded value of zero in (13.2-9) and (13.2-10) and substitution of the results into (13.2-8) yields

$$T_e = \frac{3}{2} \frac{P}{2} \frac{1}{\omega_e} (v_{qs}^{e*} i_{qs}^e - 2r_s I_s^2) \quad (13.2-11)$$

where

$$I_s = \frac{1}{\sqrt{2}} \sqrt{i_{qs}^{e2} + i_{ds}^{e2}} \quad (13.2-12)$$

Equating (13.2-7) and (13.2-11) and solving for  $\omega_e$  yields

$$\omega_e = \frac{\omega_r^* + \sqrt{\omega_r^{*2} + 3P(v_{qs}^{e*} i_{qs}^e - 2r_s I_s^2) / K_{tv}}}{2} \quad (13.2-13)$$

In practice, (13.2-13) is implemented as

$$\omega_e = \frac{\omega_r^* + \sqrt{\max(0, \omega_r^{*2} + X_{corr})}}{2} \quad (13.2-14)$$

where

$$X_{corr} = H_{LPF}(s) \chi_{corr} \quad (13.2-15)$$

and where

$$\chi_{corr} = 3P(v_{qs}^{*2} i_{qs}^e - 2r_s I_s^2) / K_{tv} \quad (13.2-16)$$

In (13.2-15),  $H_{LPF}(s)$  represents the transfer function of a low-pass filter, which is required for stability and to remove noise from the measured variables. This filter is often simply a first-order lag filter. The resulting control is depicted in Figure 13.2-3.

Figure 13.2-4 illustrates the steady-state performance of the compensated voltage-per-hertz drive for the same operating conditions as those of the study depicted in Figure 13.2-2. Although in many ways the characteristic shown in Figure 13.2-4 are similar to those of Figure 13.2-2, there are two important differences. First, the air-gap flux does not go to zero at low speed commands. Second, the speed error is dramatically reduced over the entire operating range of drive. In fact, the speed error using this strategy is less than 0.1% for speed commands ranging from 0.1 to 1.0 pu—without the use of a speed sensor.

In practice, Figure 13.2-4 is over optimistic for two reasons. First, the presence of a large amount of stiction can result in reduced low-speed performance (the machine will simply stall at some point). Second, it is assumed in the development that the

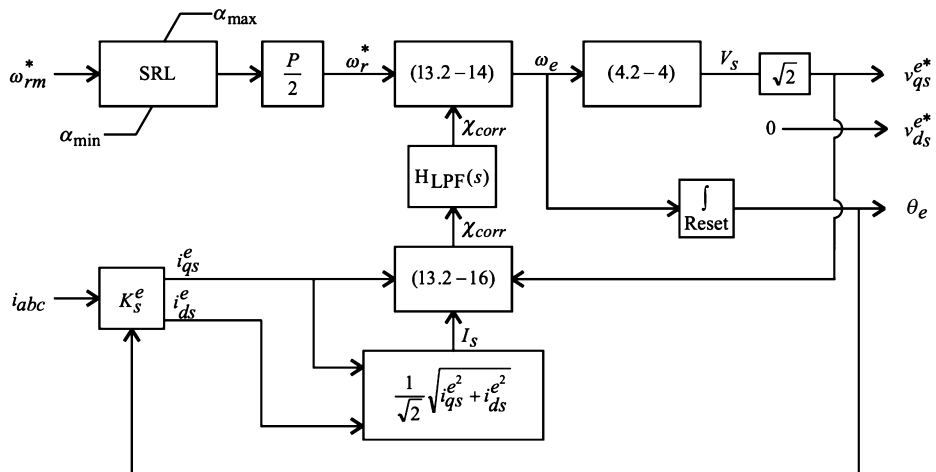


Figure 13.2-3. Compensated volts-per-hertz drive.

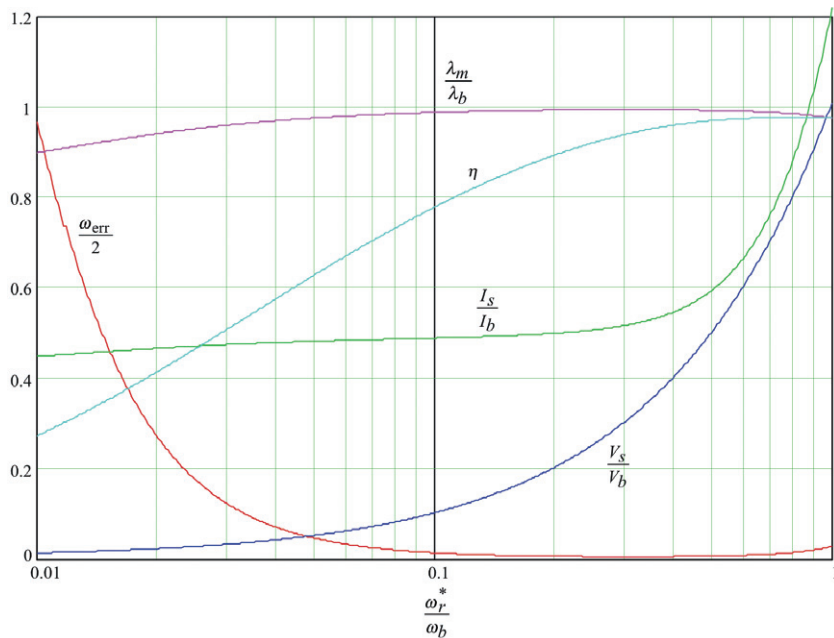


Figure 13.2-4. Performance of compensated volts-per-hertz drive.

desired voltage is applied. At extremely low commanded voltages, semiconductor voltage drops, and the effects of dead time can become important and result in reduced control fidelity. In this case, it is possible to use either closed loop (such as discussed in Section 13.11) or open-loop compensation techniques to help ensure that the desired voltages are actually obtained.

Figure 13.2-5 illustrates the start-up performance of the drive for the same conditions as Figure 13.2-2. In this study, the total mechanical inertia is taken to be  $8.2 \text{ N m s}^2$ , and the low-pass filter used to calculate  $X_{cor}$  was taken to be a first-order lag filter with a 0.1-second time constant. The acceleration limit,  $\alpha_{max}$ , was set to  $75.4 \text{ rad/s}^2$ . Variables depicted in Figure 13.2-5 include the mechanical rotor speed  $\omega_m$ , the electromagnetic torque  $T_e$ , the peak magnitude of the air-gap flux linkage  $\lambda_m = \sqrt{\lambda_{qm}^2 + \lambda_{dm}^2}$ , and finally the  $a$ -phase current  $i_{as}$ . Initially, the drive is completely off; approximately 0.6 second into the study, the mechanical rotor speed command is stepped from 0 to  $188.5 \text{ rad/s}$ . As can be seen, the drive comes to speed in roughly 3 seconds, and the build up in speed is essentially linear (following the output of the slew rate limit). The air-gap flux takes some time to reach rated value; however, after approximately 0.5 second, it is close to its steady state value. The  $a$ -phase current is very well behaved during start-up, with the exception of an initial (negative) peak—this was largely the result of the initial dc offset. Although the drive could be brought to rated speed more quickly by increasing the slew rate, this would have required a larger starting current and therefore a larger and more costly inverter. There are several other compensation techniques set forth in the literature [1, 2].

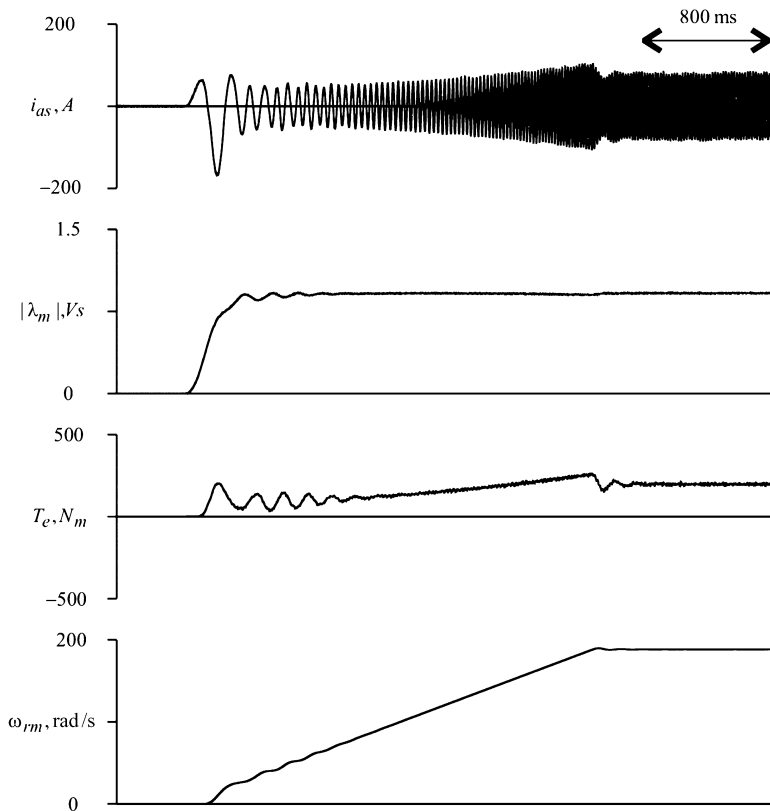


Figure 13.2-5. Start-up performance of compensated volts-per-hertz drive.

### 13.3. CONSTANT SLIP CURRENT CONTROL

Although the three-phase bridge inverter is fundamentally a voltage source device, by suitable choice of modulation strategy (such as be hysteresis or delta modulation), it is possible to achieve current source based operation. One of the primary disadvantages of this approach is that it requires phase current feedback (and its associated expense); however, at the same time, this offers the advantage that the current is readily limited, making the drive extremely robust, and, as a result, enabling the use of less conservatism when choosing the current ratings of the inverter semiconductors.

One of the simplest strategies for current control operation is to utilize a fixed-slip frequency, defined as

$$\omega_s = \omega_e - \omega_r \quad (13.3-1)$$

By appropriate choice of the radian slip frequency,  $\omega_s$ , several interesting optimizations of the machine performance can be obtained, including achieving the optimal torque

for a given value of stator current (maximum torque per amp), as well as the maximum efficiency [3, 4].

In order to explore these possibilities, it is convenient to express the electromagnetic torque as given by (6.9-16) in terms of slip frequency, which yields

$$T_e = \frac{3\left(\frac{P}{2}\right)\omega_s L_M^2 I_s^2 r'_s}{(r'_s)^2 + (\omega_s L'_{rr})^2} \quad (13.3-2)$$

From (13.3-2), it is apparent that in order to achieve a desired torque  $T_e^*$  utilizing a slip frequency  $\omega_s$ , the rms value of the fundamental component of the stator current should be set in accordance with

$$I_s = \sqrt{\frac{2|T_e^*|(r'_{s,est}^2 + (\omega_s L'_{rr,est})^2)}{3P|\omega_s|L_{M,est}^2 r'_{rr,est}}} \quad (13.3-3)$$

In (13.3-3), the parameter subscripts in (13.3-2) have been augmented with “est” in order to indicate that this relationship will be used in a control system in which the parameter values reflect estimates of the actual values.

As alluded to previously, the development here points toward control in which the slip frequency is held constant at a set value  $\omega_{s,est}$ . However, before deriving the value of slip frequency to be used, it is important to establish when it is reasonable to use a constant slip frequency. The fundamental limitation that arises in this regard is magnetic saturation. In order to avoid overly saturating the machine, a limit must be placed on the flux linkages. A convenient method of accomplishing this is to limit the rotor flux linkage. From the steady-state equivalent circuit, the a-phase rotor flux linkage may be expressed as

$$\tilde{\lambda}_{ar} = L_{lr} \tilde{I}_{ar} + L_M (\tilde{I}_{as} + \tilde{I}'_{ar}) \quad (13.3-4)$$

From the steady state equivalent circuit it is also clear that

$$\tilde{I}'_{ar} = -\tilde{I}_{as} \frac{j\omega_e L_M}{j\omega_e L'_{rr} + r'_s/s} \quad (13.3-5)$$

Substitution of (13.3-5) into (13.3-4) yields

$$\tilde{\lambda}'_{ar} = \tilde{I}_{as} L_M \frac{r'_s}{j\omega_s L'_{rr} + r'_s} \quad (13.3-6)$$

Taking the magnitude of both sides of (13.3-6) yields

$$\lambda_r = I_s L_M \frac{r'_s}{\sqrt{\omega_s^2 L'_{rr}^2 + r'^2_s}} \quad (13.3-7)$$

where  $\lambda_r$  and  $I_s$  are the rms value of the fundamental component of the referred  $a$ -phase rotor flux linkage and  $a$ -phase stator current, respectively. Combining (13.3-7) with (13.3-2) yields

$$T_e = 3 \frac{P}{2} \frac{\omega_s \lambda_r^2}{r'_r} \quad (13.3-8)$$

Now, if a constant slip frequency  $\omega_{s,set}$  is used, and the rotor flux is limited to  $\lambda_{r,max}$ , then the maximum torque that can be achieved in such an operating mode, denoted  $T_{e,thresh}$ , is

$$T_{e,thresh} = 3 \frac{P}{2} \frac{\omega_{s,set} \lambda_{r,max}^2}{r'_{r,est}} \quad (13.3-9)$$

From (13.3-8), for torque commands in which  $|T_e^*| > T_{e,thresh}$ , the slip must be varied in accordance with

$$\omega_s = \frac{2T_e^* r'_{r,est}}{3P\lambda_{r,max}^2} \quad (13.3-10)$$

Figure 13.3-1 illustrates the combination of the ideas into a coherent control algorithm. As can be seen, based on the magnitude of the torque command, the magnitude of the slip frequency  $\omega_s$  is either set equal to the set point value  $\omega_{s,set}$  or to the value arrived at from (13.3-10), and the result is given the sign of  $T_e^*$ . The slip frequency  $\omega_s$  and torque command  $T_e^*$  are together used to calculate the rms magnitude of the fundamental component of the applied current  $I_s$ , which is scaled by  $\sqrt{2}$  in order to arrive at a  $q$ -axis current command  $i_{qs}^*$ . The  $d$ -axis current command  $i_{ds}^*$  is set to zero. Of course, the placement of the current command into the  $q$ -axis was completely arbitrary; it could have just as well been put in the  $d$ -axis or any combination of the two provided the proper magnitude is obtained. In addition to being

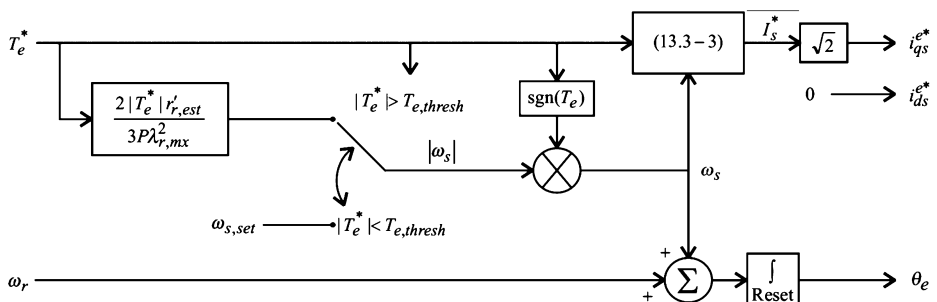


Figure 13.3-1. Constant slip frequency drive.

used to determine  $I_s$ , the slip frequency  $\omega_s$  is added to the electrical rotor speed  $\omega_r$  in order to arrive at the electrical frequency  $\omega_e$ , which is in turn integrated in order to yield the position of the synchronous reference frame  $\theta_e$ . There are a variety of ways to achieve the commanded  $q$ - and  $d$ -axis currents as discussed in Chapter 12. Finally, it should also be observed that the control depicted in Figure 13.3-1 is a torque rather than speed control system; speed control is readily achieved through a separate control loop in which the output is a torque command. Using this approach, it is important that the speed control loop is set to be slow relative to the torque controller, which can be shown to have a dynamic response on the order of the rotor time constant.

One remaining question is the selection of the slip frequency set point  $\omega_{s,sel}$ . Herein, two methods of selection are considered; the first will maximize torque for a given stator current and the second will maximize the machine efficiency. In order to maximize torque for a given stator current, note that by setting  $\omega_s = \omega_{s,sel}$  in (13.3-1), torque is maximized for a given stator current by maximizing the ratio

$$\frac{T_e}{I_s^2} = \frac{3\left(\frac{P}{2}\right)\omega_{s,sel}L_M^2r'_r}{(r'_r)^2 + (\omega_{s,sel}L'_r)^2} \quad (13.3-11)$$

Setting the derivative of the right-hand side of (13.3-11) with respect to  $\omega_{s,sel}$  equal to zero and solving for  $\omega_{s,sel}$  yields the value of  $\omega_{s,sel}$ , which maximizes the torque for a given stator current. This yields

$$\omega_{s,sel} = \frac{r'_{r,est}}{L'_{rr,est}} \quad (13.3-12)$$

In order to obtain an expression for slip frequency that will yield maximum efficiency, it is convenient to begin with an expression for the input power of the machine. With  $\tilde{I}_{as} = I_s$ , the input power may be expressed as

$$P_{in} = 3I_s \operatorname{Re}(\tilde{V}_{as}) \quad (13.3-13)$$

Using the induction motor equivalent circuit model, it is possible to expand (13.3-13) to

$$P_{in} = 3r_s I_s^2 + \frac{3I_s^2 \omega_e L_M^2 \omega_s r'_r}{r'^2 + (\omega_s L'_r)^2} \quad (13.3-14)$$

Comparison of (13.3-14) to (13.3-2) yields

$$P_{in} = 3r_s I_s^2 + \frac{2}{P} \omega_e T_e \quad (13.3-15)$$

Noting that  $\omega_e = \omega_s + \omega_r$ , and that

$$P_{out} = \frac{2}{P} \omega_r T_e \quad (13.3-16)$$

(13.3-15) may be expressed as

$$P_{in} - P_{out} = 3r_s I_s^2 + \frac{2}{P} T_e \omega_s \quad (13.3-17)$$

Substitution of (13.3-2) into (13.3-17) yields an expression for the power losses in terms of torque and slip frequency; in particular

$$P_{loss} = \frac{2}{P} T_e \left[ \frac{r'_r r_s}{\omega_s L_m^2} + \frac{\omega_s r_s L_{rr}^2}{r'_r L_m^2} + \omega_s \right] \quad (13.3-18)$$

Setting  $T_e = T_e^*$  and  $\omega_s = \omega_{s,est}$  in (13.3-18), then minimizing the right-hand side with respect to  $\omega_{s,est}$  yields a slip frequency set point of

$$\omega_{s,est} = \frac{r'_{s,est}}{L'_{rr,est}} \frac{1}{\sqrt{\frac{L_{m,est}^2}{L'_{rr,est}^2} \frac{r_{s,est}}{r'_{s,est}} + 1}} \quad (13.3-19)$$

Assuming that  $L_{m,est} \approx L'_{rr,est}$ , and that  $r_{s,est} \approx r'_{s,est}$ , it is apparent that the slip frequency for maximum efficiency is lower than the slip frequency for maximum torque per amp by a factor of roughly  $1/\sqrt{2}$ .

The steady-state performance of a constant slip control drive is depicted in Figure 13.3-2, wherein  $\omega_{s,est}$  is determined using (13.3-12), and Figure 13.3-3, wherein  $\omega_{s,est}$  is determined using (13.3-13). In these studies, the parameters are those of the 50-hp induction motor discussed in Section 13.2, the maximum rotor flux allowed is set to be the value obtained for no-load operation at rated speed and rated voltage, and the estimated values of the parameters are assumed to be correct. It is assumed that the speed in this study is equal to the commanded speed (the assumption being the drive is used in the context of a closed-loop speed control since rotor position feedback is present). As can be seen, this drive results in appreciably lower losses for low-speed operation than in the case of the volts-per-hertz drives discussed in the previous section. Because core losses are not included in Figure 13.3-2 and Figure 13.3-3, the fact that these strategies utilize reduced flux levels will further accentuate the difference between constant slip and volts-per-hertz controls. In comparing Figure 13.3-2 with Figure 13.3-3, it is interesting to observe that setting the slip frequency to achieve maximum torque per amp performance yields nearly the same efficiency as setting the slip frequency to minimize losses. Since inverter losses go up with current, this suggest that setting the slip to optimize torque per amp may yield higher overall efficiency than setting the slip to minimize machine losses—particularly in view of the fact that the lower flux level

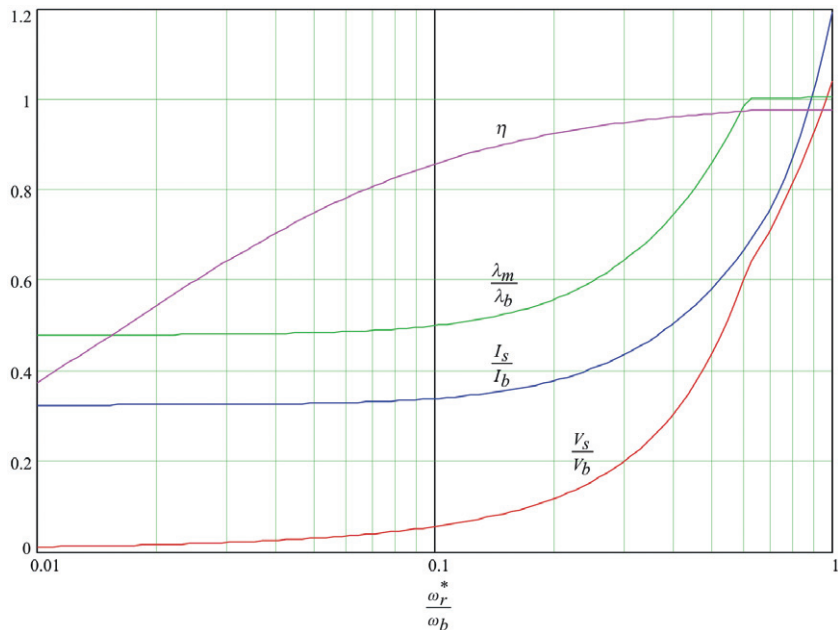


Figure 13.3-2. Performance of constant slip frequency drive (maximum torque-per-amp).

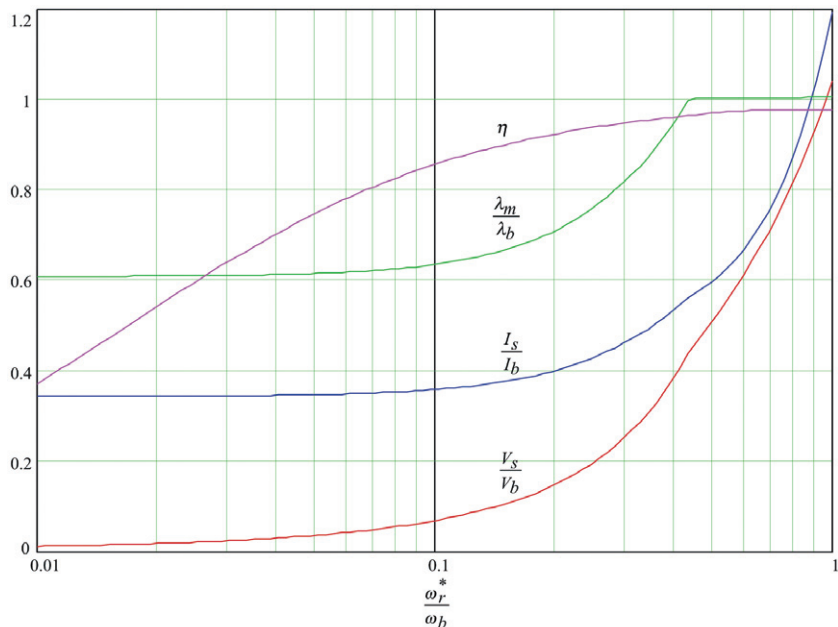


Figure 13.3-3. Performance of constant slip frequency drive (maximum efficiency).

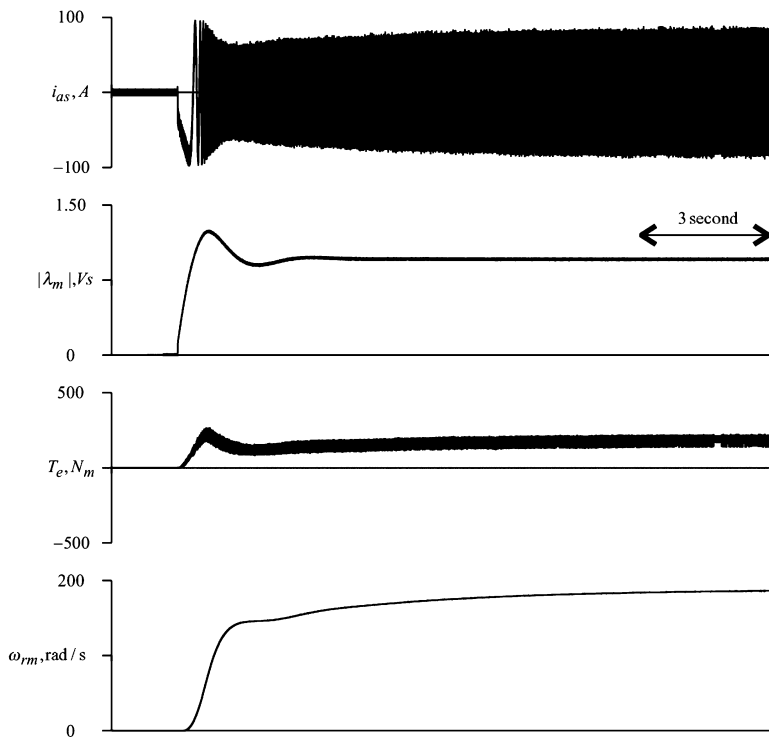


Figure 13.3-4. Start-up performance of constant slip controlled drive.

in maximum torque per amp control will reduce core losses relative to maximum efficiency control.

Another question that arises in regard to the control is the effect errors in the estimated value of the machine parameters will have on the effectiveness of the control. As it turns out, this algorithm is very robust with respect to parameter estimation, as the optimums being sought (maximum torque per amp or maximum efficiency) are broad. An extended discussion of this is set forth in References 3 and 4.

The use of the constant slip control in the context of a speed control system is depicted in Figure 13.3-4. Initially, the system is at zero speed. Approximately 2 seconds into the study, the speed command is stepped to 188.5 rad/s. In this study, the machine and load are identical to those in the study shown in Figure 13.2-4. However, since the constant-slip control is a torque input control, a speed control is necessary for speed regulation. For the study shown in Figure 13.3-4, the torque command is calculated in accordance with the speed control shown in Figure 13.3-5. This is a relatively simple PI control with a limited output, and antiwindup integration that prevents the integrator from integrating the positive (negative) speed error whenever the maximum (minimum) torque limit is invoked. For the purposes of this study, the maximum and minimum torque commands were taken to 218 N · m (1.1 pu) and 0 N · m, respectively while  $K_{sc}$  and  $\tau_{sc}$  were selected to be 1.64 N · m s/rad and 2 seconds, respectively. It

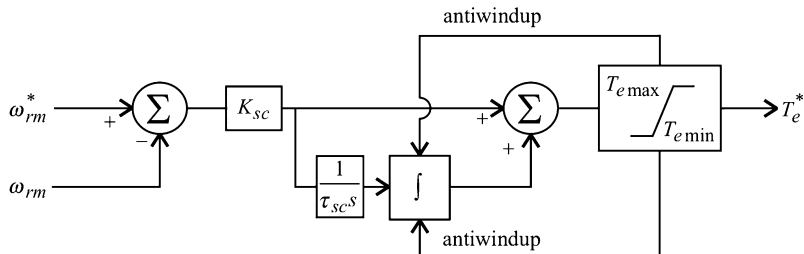


Figure 13.3-5. Speed control.

can be shown that if  $T_e = T_e^*$ , and if the machine were unloaded, this would result in a transfer function between the actual and commanded speeds with two critically damped poles with 1-second time constants. Also used in conjunction with the control system was a synchronous current regulator in order to precisely achieve the current command output of the constant slip control. To this end, the synchronous current regulator depicted in Figure 12.11-1 was used. The time constant of the regulator was set to 16.7 ms.

As can be seen, the start-up performance using the constant slip control is much slower than using the constant volts-per-hertz control; this is largely because of the fact that the speed control needed to be fairly slow in order to accommodate the sluggish torque response. However, one point of interest is that the stator current, by virtue of the tight current regulation, is very well behaved; in fact, the peak value is only slightly above the steady-state value.

### 13.4. FIELD-ORIENTED CONTROL

In many motor drive systems, it is desirable to make the drive act as a torque transducer wherein the electromagnetic torque can nearly instantaneously be made equal to a torque command. In such a system, speed or position control is dramatically simplified because the electrical dynamics of the drive become irrelevant to the speed or position control problem. In the case of induction motor drives, such performance can be achieved using a class of algorithms collectively known as field-oriented control. There are a number of permutations of this control—stator flux oriented, rotor flux oriented, and air-gap flux oriented, and of these types there are direct and indirect methods of implementation. This text will consider the most prevalent types, which are direct rotor flux-oriented control and indirect rotor flux-oriented control. For discussions of the other types, the reader is referred to texts entirely devoted to field-oriented control such as References 5 and 6.

The basic premise of field-oriented control may be understood by considering the current loop in a uniform flux field shown in Figure 13.4-1. From the Lorenze force equation, it is readily shown that the torque acting on the current loop is given by

$$T_e = -2BiNLr \sin \theta \quad (13.4-1)$$

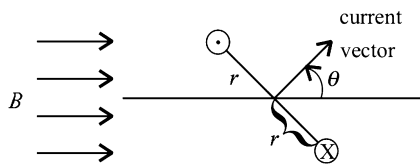


Figure 13.4-1. Torque on a current loop.

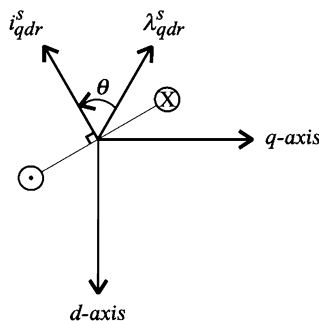


Figure 13.4-2. Torque production in an induction motor.

where  $B$  is the flux density,  $i$  is the current,  $N$  is the number of turns,  $L$  is the length of the coil into the page, and  $r$  is the radius of the coil. Clearly, the magnitude of the torque is maximized when the current vector (defined perpendicular to the surface of the winding forming the current loop and in the same direction as the flux produced by that loop) is orthogonal to the flux field. The same conclusion is readily applied to an induction machine. Consider Figure 13.4-2. Therein,  $qd$ -axis rotor current and flux linkage vectors  $i'_{qdr} = [i'_{qr} \ i'_{dr}]^T$  and  $\lambda'_{qdr} = [\lambda'_{qr} \ \lambda'_{dr}]^T$ , respectively, are shown at some instant of time. Repeating (6.6-3)

$$T_e = \frac{3}{2} \frac{P}{2} (\lambda'_{qr} i'_{dr} - \lambda'_{dr} i'_{qr}) \quad (13.4-2)$$

which may be expressed as

$$T_e = -\frac{3}{2} \frac{P}{2} |\lambda'_{qdr}| |i'_{qdr}| \sin \theta \quad (13.4-3)$$

which is analogous to (13.4-1). Again, for a given magnitude of flux linkage, torque is maximized when the flux linkage and current vectors are perpendicular.

Thus, it is desirable to keep the rotor flux linkage vector perpendicular to the rotor current vector. As it turns out, this is readily accomplished in practice. In particular, in the steady state, the rotor flux linkage vector and rotor current vector are always

perpendicular for all singly fed induction machines. To see this, consider the rotor voltage equations (6.5-13) and (6.5-14). With the rotor circuits short-circuited and using the synchronous reference frame, it can be shown that the rotor currents may be expressed as

$$i_{qr}^e = -\frac{1}{r_r'}(\omega_e - \omega_r)\lambda_{dr}^e \quad (13.4-4)$$

$$i_{dr}^e = \frac{1}{r_r'}(\omega_e - \omega_r)\lambda_{qr}^e \quad (13.4-5)$$

The dot product of the rotor flux linkage and rotor current vectors may be expressed as

$$\lambda_{qdr}^e \cdot i_{qdr}^e = \lambda_{qr}^e i_{qr}^e + \lambda_{dr}^e i_{dr}^e \quad (13.4-6)$$

Substitution of (13.4-4) and (13.4-5) into (13.4-6) reveals that this dot product is zero whereupon it may be concluded that the rotor flux and rotor current vectors, as expressed in the synchronous reference frame, are perpendicular. Furthermore, if they are perpendicular in the synchronous reference frame, they are perpendicular in every reference frame. In this sense, in the steady state, every singly excited induction machine operates with an optimal relative orientation of the rotor flux and rotor current vectors. However, the defining characteristic of a field-oriented drive is that this characteristic is maintained during transient conditions as well. It is this feature that results in the high transient performance capabilities of this class of drive.

In both direct and indirect field oriented drives, the method to achieve the condition that the rotor flux and rotor current vectors are always perpendicular is twofold. The first part of the strategy is to ensure that

$$\lambda_{qr}^e = 0 \quad (13.4-7)$$

and the second to is to ensure that

$$i_{dr}^e = 0 \quad (13.4-8)$$

Clearly, if (13.4-7) and (13.4-8) hold during transient conditions, then by (13.4-6), the rotor flux linkage and rotor current vectors are perpendicular during those same conditions. By suitable choice of  $\theta_e$  on an instantaneous basis, (13.4-7) can always be satisfied by choosing the position of the synchronous reference frame to put all of the rotor flux linkage in the  $d$ -axis. Satisfying (13.4-8) can be accomplished by forcing the  $d$ -axis stator current to remain constant. To see this, consider the  $d$ -axis rotor voltage equation (with zero rotor voltage):

$$0 = r_r' i_{dr}^e + (\omega_e - \omega_r)\lambda_{qr}^e + p\lambda_{dr}^e \quad (13.4-9)$$

By suitable choice of reference frame, (13.4-7) is achieved; therefore  $\lambda'_{qr}^e$  can be set to zero in (13.4-9) to yield

$$0 = r'_r i'_{dr} + p \lambda'_{dr}^e \quad (13.4-10)$$

Next, substitution of the *d*-axis rotor flux linkage equation (6.5-20) into (13.4-10) and rearranging yields

$$p i'_{dr} = -\frac{r'_r}{L_{rr}} i'_{dr} - \frac{L_M}{L_{rr}} p i_{ds}^e \quad (13.4-11)$$

Equation (13.4-11) can be viewed as a stable first-order differential equation in  $i'_{dr}^e$  with  $p i_{ds}^e$  as input. Therefore, if  $i_{ds}^e$  is held constant, then  $i'_{dr}^e$  will go to, and stay at, zero, regardless of other transients which may be taking place.

Before proceeding further, it is motivational to explore some of the other implications of (13.4-7) and (13.4-8) being met. First, combining (13.4-8) with (6.5-17) and (6.5-20), respectively, it is clear that

$$\lambda_{ds}^e = L_{ss} i_{ds}^e \quad (13.4-12)$$

and that

$$\lambda'_{dr}^e = L_M i_{ds}^e \quad (13.4-13)$$

Clearly, the *d*-axis flux levels are set solely by the *d*-axis stator current. Combining (13.4-2) with (13.4-7), it can be seen that torque may be expressed

$$T_e = -\frac{3}{2} \frac{P}{2} \lambda'_{dr}^e i'_{qr}^e \quad (13.4-14)$$

Furthermore, from (13.4-7) and (6.5-19), it can be shown that

$$i'_{qr}^e = -\frac{L_M}{L_{rr}} i_{qs}^e \quad (13.4-15)$$

Combining (13.4-14) and (13.4-15)

$$T_e = \frac{3}{2} \frac{P}{2} \frac{L_M}{L_{rr}} \lambda'_{dr}^e i_{qs}^e \quad (13.4-16)$$

Together, (13.4-13) and (13.4-16) suggest the “generic” rotor flux-oriented control depicted in Figure 13.4-3. Therein, variables of the form  $x^*$ ,  $\hat{x}$ , and  $\hat{x}$  denote commanded, measured, and estimated, respectively; in the case of parameters, an addition

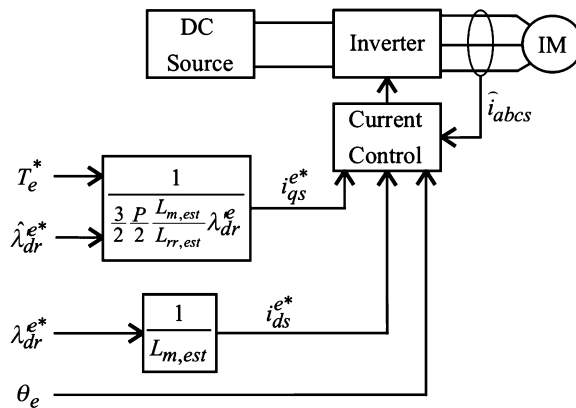


Figure 13.4-3. Generic rotor flux oriented control.

of a “,est” to the subscript indicates the assumed value. As can be seen, a dc source supplies an inverter driving an induction machine. Based on a torque command  $T_e^*$ , the assumed values of the parameters, and the estimated value of the  $d$ -axis rotor flux  $\hat{\lambda}_{dr}^{e*}$ , (13.4-16) is used to formulate a  $q$ -axis stator current command  $i_{qs}^{e*}$ . The  $d$ -axis stator current command  $i_{ds}^{e*}$  is calculated such as to achieve a rotor flux command (which is typically maintained constant or varied only slowly)  $\lambda_{dr}^{e*}$  based on (13.4-13). The  $q$ - and  $d$ -axis stator current command is then achieved using any one of a number of current-source current controls as discussed in Section 12.11. However, this diagram of the rotor flux-oriented field-oriented control is incomplete in two important details—the determination of  $\hat{\lambda}_{dr}^{e*}$  and the determination of  $\theta_e$ . The difference in direct and indirect field oriented control is in how these two variables are established.

### 13.5. DIRECT FIELD-ORIENTED CONTROL

In direct field-oriented control, the position of the synchronous reference is based on the value of the  $q$ - and  $d$ -axis flux linkages in the rotor reference frame. From (3.10-7), upon setting the position of the stationary reference frame to be zero, we have that

$$\begin{bmatrix} \lambda_{qr}^{e*} \\ \lambda_{dr}^{e*} \end{bmatrix} = \begin{bmatrix} \cos\theta_e & -\sin\theta_e \\ \sin\theta_e & \cos\theta_e \end{bmatrix} \begin{bmatrix} \lambda_{qr}^s \\ \lambda_{dr}^s \end{bmatrix} \quad (13.5-1)$$

In order to achieve  $\lambda_{qr}^{e*} = 0$ , from (13.5-1), it is sufficient to define the position of the synchronous reference frame in accordance with

$$\theta_e = \text{angle}(\lambda_{qr}^s - j\lambda_{dr}^s) + \frac{\pi}{2} \quad (13.5-2)$$

whereupon it can be shown that

$$\lambda'_{dr}^s = \sqrt{(\lambda'_{qr}^s)^2 + (\lambda'_{ds}^s)^2} \quad (13.5-3)$$

The difficulty in this approach is that  $\lambda'_{qr}^s$  and  $\lambda'_{ds}^s$  are not directly measurable quantities. However, they can be estimated using direct measurement of the air-gap flux. In this method, hall-effect sensors (or some other means) are placed in the air gap and used to measure the air-gap flux in the  $q$ - and  $d$ -axis of the stationary reference frame (since the position of the sensors is fixed in a stationary reference frame). The net effect is that  $\lambda_{qm}^s$  and  $\lambda_{dm}^s$  may be regarded as measurable. In order to establish  $\lambda'_{qr}^s$  and  $\lambda'_{ds}^s$  from  $\lambda_{qm}^s$  and  $\lambda_{dm}^s$ , note that

$$\lambda'_{qm}^s = L_M (i_{qs}^s + i'_{qr}^s) \quad (13.5-4)$$

Therefore,

$$i'_{qr}^s = \frac{\lambda'_{qm}^s - L_M i_{qs}^s}{L_M} \quad (13.5-5)$$

Recall that the  $q$ -axis rotor flux linkages may be expressed as

$$\lambda'_{qr}^s = L_{lr} i'_{qr}^s + L_M (i_{qs}^s + i'_{qr}^s) \quad (13.5-6)$$

Substitution of (13.5-5) into (13.5-6) yields

$$\lambda'_{qr}^s = \frac{L'_{rr}}{L_M} \lambda_{qm}^s - L_{lr} i_{qs}^s \quad (13.5-7)$$

Performing an identical derivation for the  $d$ -axis yields

$$\lambda'_{ds}^s = \frac{L'_{rr}}{L_M} \lambda_{dm}^s - L'_{lr} i_{ds}^s \quad (13.5-8)$$

This suggests the rotor flux calculator shown in Figure 13.5-1, which calculates both the position of the synchronous reference frame as well as the  $d$ -axis flux linkage. This is based directly on (13.5-7), (13.5-8), (13.5-2), and (13.5-3), with the addition of two low-pass filters in order to prevent switching frequency noise from effecting the control (the time constant  $\tau_{rfc}$  must be set small enough that this transfer function has no effect on the highest frequency fundamental component that will be utilized) and that, as in Figure 13.4-1, a more careful distinction is made between measured and estimated values. Figure 13.5-2 depicts the incorporation of the rotor flux calculator into the direct field-oriented control. This will be important in future analysis when the effects of using parameter values in the control algorithms which are not equal to the actual parameters of the machine (which are highly operating-point dependent).

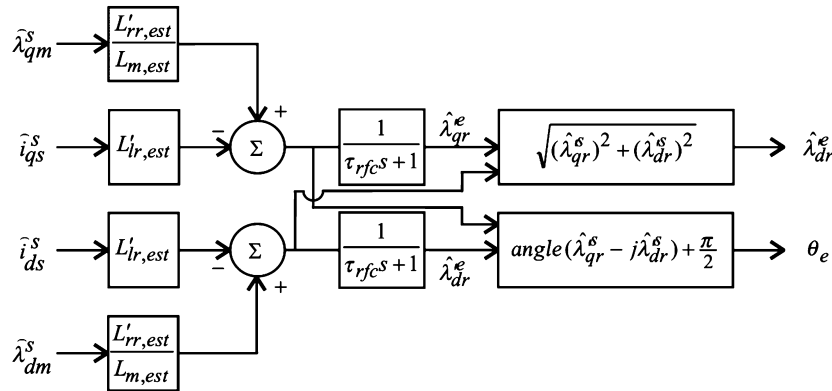


Figure 13.5-1. Rotor flux calculator.

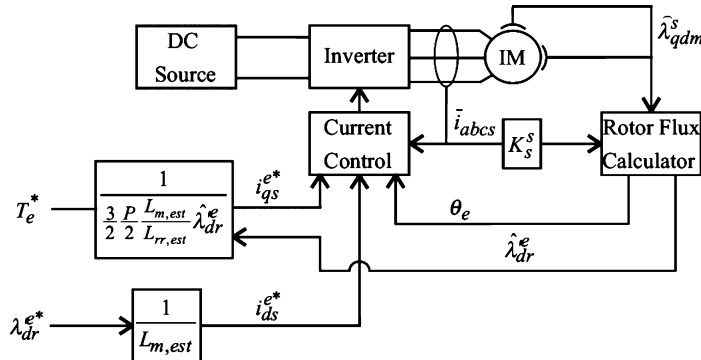


Figure 13.5-2. Direct field-oriented control.

### 13.6. ROBUST DIRECT FIELD-ORIENTED CONTROL

One of the problems of the control strategy presented is that it is a function of the parameters of the machine. Because of magnetic nonlinearities and the distributed nature of the machine windings, particularly the rotor windings—the model is not particularly accurate. The machine resistances and inductances are highly operating point dependent. In order to understand the potential sources of error, let us first consider the rotor flux observer. From Figure 13.5-1, recall the rotor flux vector is estimated as

$$\hat{\lambda}'_{qdr}^e = \frac{L'_{rr,est}}{L_{M,est}} \hat{\lambda}_{qd,m}^s - L'_{lr,est} \hat{i}_{qds}^s \quad (13.6-1)$$

Assuming that the measured flux and measured current are accurate, (13.6-1) is relatively insensitive to parameter variation. To see this, let us first consider the first term on the right-hand side of (13.6-1). The term is a function of  $L_{rr,est}/L_{M,est}$ . However, note that since the rotor leakage inductance is much less than the magnetizing inductance, this ratio will be close to unity regardless of the actual value of the parameters. Hence, this term will not be a strong function of the parameters of the machine. The second term in (13.6-1) is a strong function of the leakage inductance. However, the second term as a whole is considerably smaller than the first since the first term represents the air-gap flux and the second has a magnitude equal to the rotor leakage flux. Thus, as a whole, (13.6-1) and the rotor flux estimator are relatively insensitive to the machine parameters.

Another key relationship used in the direct field-oriented control which is a function of the parameters of the machine is the calculation of the  $q$ -axis current; in particular

$$i_{qs}^{e*} = \frac{T_e^*}{\frac{3}{2} \frac{P}{2} \frac{L_{M,est}}{L_{rr,est}} \hat{\lambda}_{dr}^{te*}} \quad (13.6-2)$$

Again, since the ratio of  $L_{M,est}$  to  $L_{rr,est}$  is close to unity for the normal range of parameters, this relationship is again relatively insensitive to parameters.

However, this is not the case for the calculation of the  $d$ -axis current, which is calculated in accordance with

$$i_{ds}^{e*} = \frac{\lambda_{dr}^{e*}}{L_{M,est}} \quad (13.6-3)$$

As can be seen, this relationship is highly sensitive to  $L_{M,est}$ . An error in the  $d$ -axis current command will result in an incorrect value of rotor flux linkages. Because the rotor flux linkages can be estimated using the rotor flux estimator shown in Figure 13.5-1, this error can be readily eliminated by introducing a rotor flux feedback loop shown in Figure 13.6-1. The basis of this loop is (13.6-3). However, integral feedback is utilized to force the  $d$ -axis rotor flux linkage to be equal to its commanded value. For the purposes of design of this feedback loop, it is convenient to assume that  $\lambda_{dr}^{e*} = L_M i_{ds}^{e*}$ , and that  $\hat{\lambda}_{dr}^{re} = \lambda_{dr}^{e*}$ , whereupon it can be shown that the transfer function between the actual and commanded flux linkages is given by

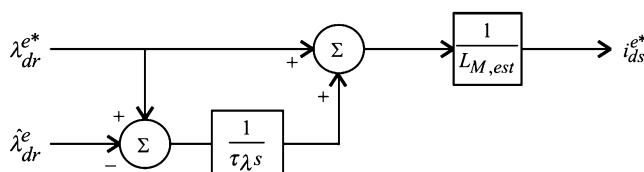


Figure 13.6-1. Flux control loop.

$$\frac{\lambda'_{dr}^e}{\lambda'_{dr}^{e*}} = \frac{\tau_\lambda s + 1}{\tau_\lambda \frac{L_{M,est}}{L_M} s + 1} \quad (13.6-4)$$

From the form of this transfer function, it can be seen that in the steady state, the rotor flux will be equal to the commanded value. Furthermore, note that if  $L_{M,est} = L_M$ , the transfer function between the commanded and actual rotor flux is unity. The value of  $\tau_f$  is chosen so that that  $\tau_f 2\pi f_{sw} L_{M,est} / L_M \gg 1$ ; as a worst case estimate,  $L_{M,est} = L_M$  can be taken to be 0.7 or so in this process.

Although this approach goes a long way in making the direct field-oriented control robust with respect to parameter variations, the design can be made even more robust by adding a torque calculator and feedback loop. From (6.6-4), recall that torque may be expressed as

$$T_e = \frac{3}{2} \frac{P}{2} (\lambda_{ds}^s i_{qs}^s - \lambda_{qs}^s i_{ds}^s) \quad (13.6-5)$$

Furthermore, the stator flux may be expressed as

$$\lambda_{qds}^s = L_{ls} i_{qds}^s + \lambda_{qdm}^s \quad (13.6-6)$$

Substitution of (13.6-6) into (13.6-5) yields

$$T_e = \frac{3}{2} \frac{P}{2} (\lambda_{dm}^s i_{qs}^s - \lambda_{qm}^s i_{ds}^s) \quad (13.6-7)$$

which suggests that an estimate for torque can be calculated as

$$\hat{T}_e = \frac{3}{2} \frac{P}{2} (\hat{\lambda}_{dm}^s \hat{i}_{qs}^s - \hat{\lambda}_{qm}^s \hat{i}_{ds}^s) \quad (13.6-8)$$

With the torque calculator present, it is possible to introduce a torque feedback loop shown in Figure 13.6-2. For the purposes of analysis of this loop, it is convenient to define

$$K_{t,est} = \frac{3}{2} \frac{P}{2} \frac{L_{M,est}}{L'_{rr}} \lambda'_{dr}^{e*} \quad (13.6-9)$$

which will be treated as a constant parameter for the purposes of torque loop design. For the purpose of gaining intuition about the performance of the flux loop, it is convenient to assume that

$$T_e = K_t i_{qs}^{e*} \quad (13.6-10)$$

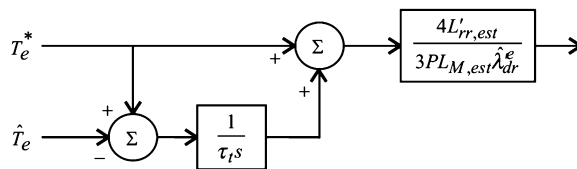


Figure 13.6-2. Torque control loop.

where

$$K_t = \frac{3}{2} \frac{P}{2} \frac{L_M}{L'_{rr}} \lambda'_{dr}^e \quad (13.6-11)$$

Under these conditions, it is readily shown that transfer function between actual and commanded torque is given by

$$\frac{T_e}{T_e^*} = \frac{\tau_t s + 1}{\tau_t \frac{K_{t,est}}{K_t} s + 1} \quad (13.6-12)$$

Upon inspection of (13.6-12), it is clear that at dc, there will be no error between the actual and commanded torque in the steady state (at least if the error in the current and flux sensors is ignored). Further, if  $K_t$  and  $K_{t,est}$  are equal, the transfer function will be unity, whereupon it would be expected that the actual torque would closely track the commanded torque even during transients. The time constant  $\tau_t$  is chosen as small as possible subject to the constraint that  $2\pi f_{sw} \tau_t K_{t,est} / K_t \gg 1$  so that switching frequency noise does not enter into the torque command.

Incorporating the rotor and torque feedback loops into the direct field oriented-control yields the robust field-oriented control depicted in Figure 13.6-3. Therein, the use of a flux estimator, torque calculator, and closed-loop torque and flux controls yields a drive that is highly robust with respect to deviations of the parameters from their anticipated values.

The start-up performance of the direct field-oriented control is depicted in Figure 13.6-4. Therein, the machine, load, and speed controls are the same as the study depicted in Figure 13.3-4, with the exception that the parameters of the speed control were changed to  $K_{sc} = 16.4 \text{ N}\cdot\text{m}\cdot\text{s}/\text{rad}$  and  $\tau_{sc} = 0.2$  second in order to take advantage of the nearly instantaneous torque response characteristic of field-oriented drives. Parameters of the field-oriented controller were:  $\tau_{rfc} = 100 \mu\text{s}$ ,  $\tau_\lambda = 50 \text{ ms}$ , and  $\tau_t = 50 \text{ ms}$ . The current commands were achieved using a synchronous current regulator (Fig. 12.11-1) in conjunction with a delta-modulated current control. The synchronous current regulator time constant  $\tau_{scr}$  and delta modulator switching frequency were set to 16.7 ms and 10 kHz, respectively. Initially, the drive is operating at zero speed, when, approximately 250 ms into the study, the mechanical speed command is stepped

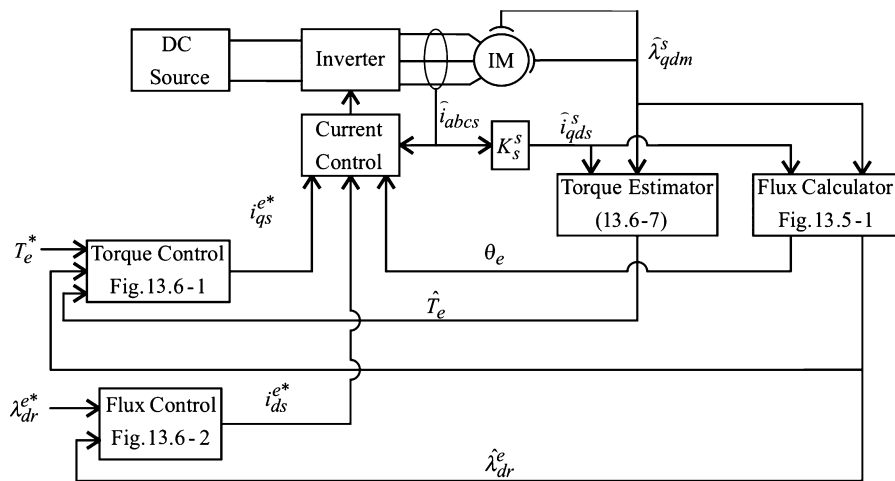


Figure 13.6-3. Robust direct rotor field oriented control.

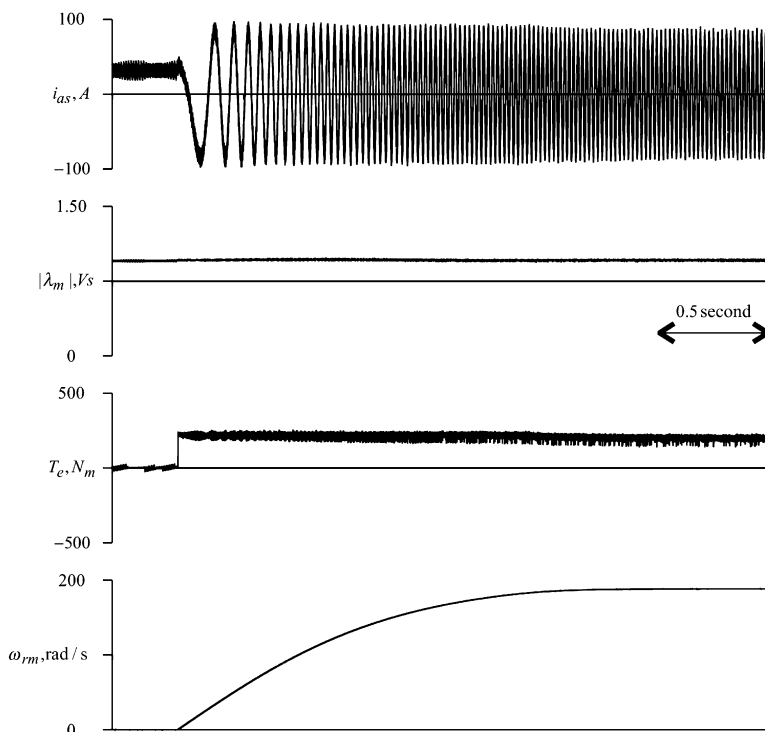


Figure 13.6-4. Start-up performance of robust direct field oriented drive.

from 0 to 188.5 rad/s. The electromagnetic torque steps to the torque limit (which was set to 218 N·m) for approximately 1.5 seconds, after which the torque command begins to decrease as the speed approaches the commanded value. The drive reaches steady-state conditions within 2 seconds, and at the same time, the peak current utilized was only slightly larger than the steady-state value. In this context, it can be seen that although the control is somewhat elaborate, it can be used to achieve a high-degree of dynamic performance with minimal inverter requirements. It is also interesting to observe that the magnitude of the air-gap flux was essentially constant throughout the entire study.

### 13.7. INDIRECT ROTOR FIELD-ORIENTED CONTROL

Although direct field-oriented control can be made fairly robust with respect to variation of machine parameters, the sensing of the air-gap flux linkage (typically) using hall-effect sensors is somewhat problematic (and expensive) in practice. This has led to considerable interest in indirect field-oriented control methods that are more sensitive to knowledge of the machine parameters but do not require direct sensing of the rotor flux linkages.

In order to establish an algorithm for implementing field-oriented control without knowledge of the rotor flux linkages, it is useful to first establish the electrical frequency that is utilized in direct field-oriented control. From the  $q$ -axis rotor voltage equation

$$0 = r'_{rr} i'^e_{qr} + (\omega_e - \omega_r) \lambda'^e_{dr} + p \lambda'^e_{qr} \quad (13.7-1)$$

Since  $\lambda'^e_{qr} = 0$  for the direct field-oriented control, (13.7-1) necessitates

$$\omega_e = \omega_r - r' \frac{i'^e_{qr}}{\lambda'^e_{dr}} \quad (13.7-2)$$

Using (13.4-12) to express  $i'^e_{qr}$  in terms of  $i^e_{qs}$ , and (13.4-10) to express  $\lambda'^e_{dr}$  in terms of  $i^e_{ds}$ , (13.7-2) becomes

$$\omega_e = \omega_r + \frac{r'}{L'_{rr}} \frac{i^e_{qs}}{i^e_{ds}} \quad (13.7-3)$$

This raises an interesting question. Suppose that instead of establishing  $\theta_e$  utilizing the rotor flux calculator in Figure 13.5-1, it is instead calculated by integrating  $\omega_e$ , where  $\omega_e$  is established by

$$\omega_e = \omega_r + \frac{r'}{L'_{rr}} \frac{i^{e*}_{qs}}{i^{e*}_{ds}} \quad (13.7-4)$$

As it turns out, this is sufficient to satisfy the conditions for field-oriented control  $\lambda'_{qr} = 0$  and  $i'_{dr} = 0$  provided that  $i'^{*}_{ds}$  is held constant. To show this, first consider the rotor voltage equations

$$0 = r'_r i'^{e*}_{qr} + (\omega_e - \omega_r) \lambda'_{dr} + p \lambda'_{qr} \quad (13.7-5)$$

$$0 = r'_r i'^{e*}_{dr} - (\omega_e - \omega_r) \lambda'_{qr} + p \lambda'_{dr} \quad (13.7-6)$$

Substitution of (13.7-4) into (13.7-5) and (13.7-6) yields

$$0 = r'_r i'^{e*}_{qr} + \frac{r'_r}{L'_{rr}} \frac{i'^{e*}_{qs}}{i'^{e*}_{de}} \lambda'_{dr} + p \lambda'_{qr} \quad (13.7-7)$$

$$0 = r'_r i'^{e*}_{dr} - \frac{r'_r}{L'_{rr}} \frac{i'^{e*}_{qs}}{i'^{e*}_{de}} \lambda'_{qr} + p \lambda'_{dr} \quad (13.7-8)$$

The next step is to utilize the rotor flux linkage equations into (13.4-7) and (13.4-8), which upon making the assumption the stator currents are equal to their commanded values yields

$$0 = r'_r \left[ \frac{\lambda'_{qr} - L_M i'^{e*}_{qs}}{L'_{rr}} \right] i'^{e*}_{qr} + \frac{r'_r}{L'_{rr}} \frac{i'^{e*}_{qs}}{i'^{e*}_{de}} [L'_{rr} i'^{e*}_{dr} + L_M i'^{e*}_{ds}] + p \lambda'_{qr} \quad (13.7-9)$$

$$0 = r'_r i'^{e*}_{dr} - \frac{r'_r}{L'_{rr}} \frac{i'^{e*}_{qs}}{i'^{e*}_{de}} \lambda'_{qr} + p [L'_{rr} i'^{e*}_{qr} + L_M i'^{e*}_{ds}] \quad (13.7-10)$$

Noting that  $p i'^{e*}_{ds} = 0$  and rearranging (13.7-9) and (13.7-10) yields

$$p \lambda'_{qr} = - \frac{r'_r}{L'_{rr}} \lambda'_{qr} - r'_r \frac{i'^{e*}_{qs}}{i'^{e*}_{ds}} i'^{e*}_{dr} \quad (13.7-11)$$

$$p i'^{e*}_{dr} = - \frac{r'_r}{L'_{rr}} i'^{e*}_{dr} + \frac{r'_r}{(L'_{rr})^2} \frac{i'^{e*}_{qs}}{i'^{e*}_{ds}} \lambda'_{qr} \quad (13.7-12)$$

Provided that  $p i'^{e*}_{ds} = 0$ , (13.7-11) and (13.7-12) constitute a set of asymptotically stable differential equations with an equilibrium point of  $\lambda'_{qr} = 0$  and  $i'^{e*}_{dr} = 0$ . The conclusion is that  $\lambda'_{qr}$  and  $i'^{e*}_{dr}$  will go to and stay at zero, thereby satisfying the conditions for field-oriented control.

Figure 13.7-1 depicts the block diagram of the indirect rotor field-oriented control, which is based on (13.6-2), (13.6-3), and (13.7-3). As can be seen, it is considerably simpler than the direct field-oriented control—though it is much more susceptible to performance degradation as a result of error in estimating the effective machine parameters.

The start-up performance of the indirect field-oriented drive is depicted in Figure 13.7-2. Therein, the parameters of the induction machine, speed control, inverter, and

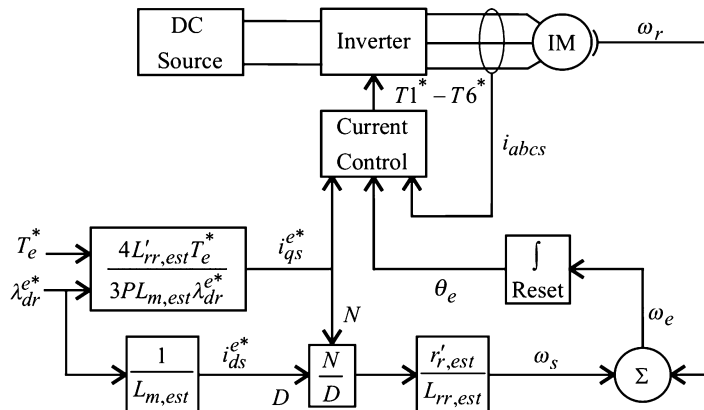


Figure 13.7-1. Indirect rotor field oriented control.

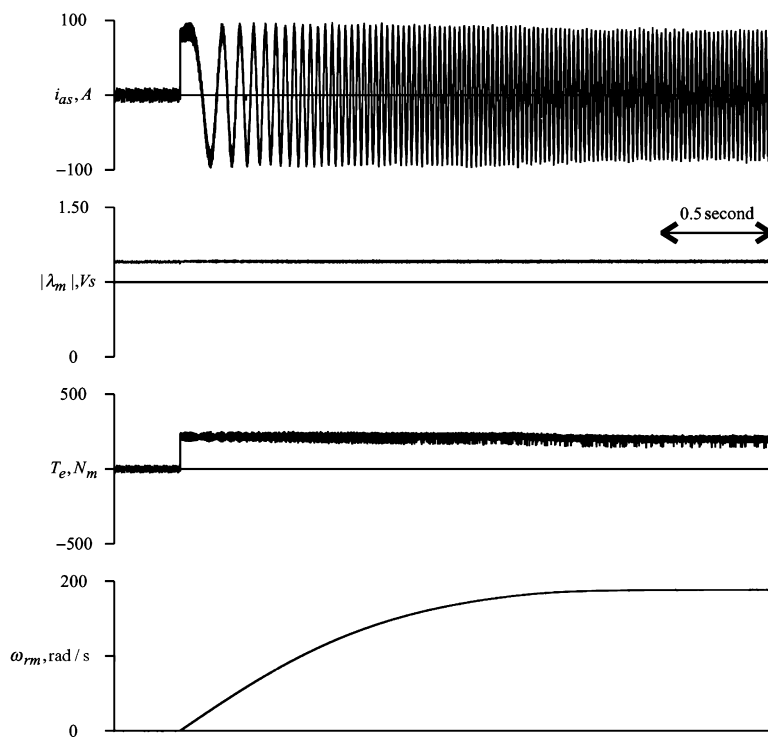
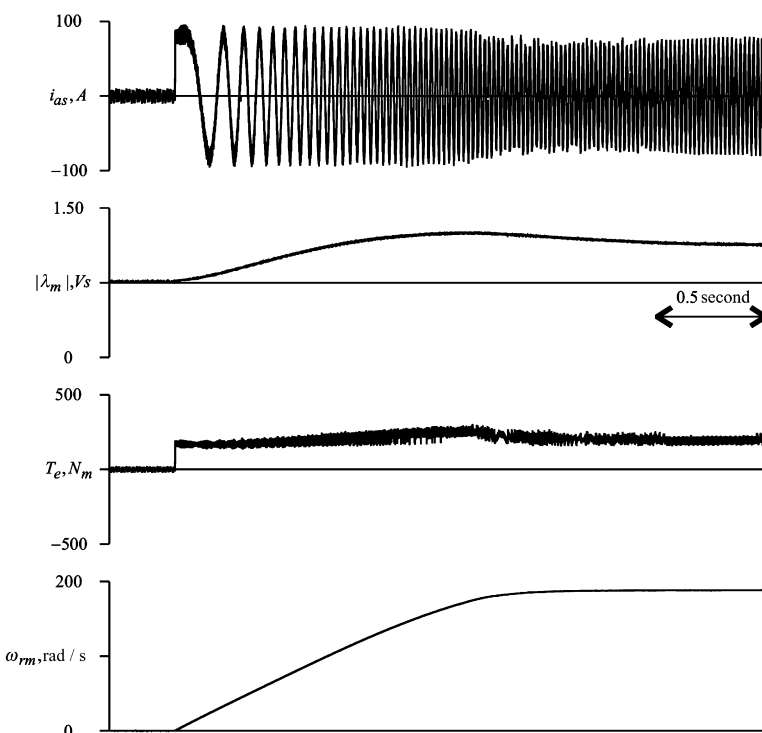


Figure 13.7-2. Start-up performance of indirect field oriented drive.

current regulator are all identical to those of the corresponding study shown in Figure 13.6-4. In fact, comparison of Figure 13.6-4 with Figure 13.7-2 reveals that the two controls give identical results. This is largely the result of the fact that the estimated parameters were taken to be the parameter of the machine, and that the machine was assumed to behave in accordance with the machine model described in Chapter 6. However, in reality, the machine parameter can vary significantly. Because of the feedback loops, in the case of the direct field-oriented control parameter, variations will have relatively little effect on performance. In the case of the indirect field oriented drive, significant degradation of the response can result. This is illustrated in Figure 13.7-3, which is identical to Figure 13.7-2, with the exception that an error in the estimated parameters is included in the analysis; in particular  $L_{M,est} = 1.25L_m$  and  $r'_{r,est} = 0.75r'_r$ . As can be seen, although the speed control still achieves the desired speed, the transient performance of the drive is compromised, as can be seen by the variation in air-gap flux linkages and electromagnetic torque. This degradation is particularly important at low speeds where instability in the speed or position controls can result.



**Figure 13.7-3.** Start-up performance of indirect field oriented drive with errors in estimated parameter values.

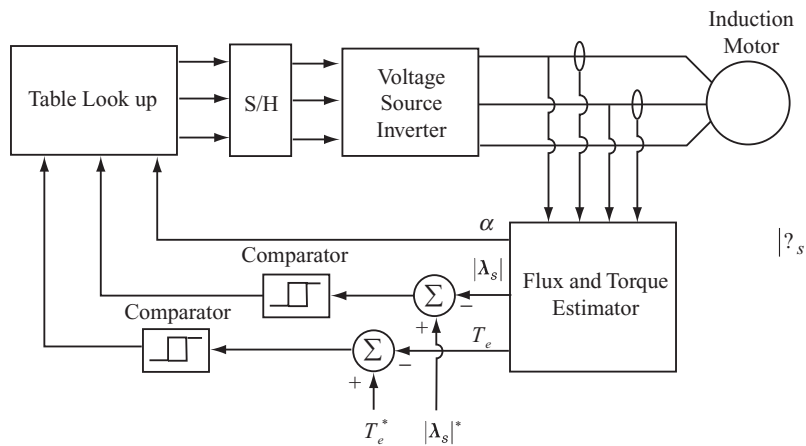


Figure 13.8-1. Direct torque control of an induction motor.

### 13.8. DIRECT TORQUE CONTROL

Another established method of controlling the torque in an induction machine is the method of DTC [6–9]. A block diagram of an induction motor drive using DTC is depicted in Figure 13.8-1, wherein it is assumed that a three-phase induction machine is supplied by a voltage source inverter (Chapter 12). As shown, the DTC includes a block that estimates the stator flux and torque based on measured voltages and currents, and a set of comparators that compare the estimated stator flux magnitude and electromagnetic torque with their commanded values (denoted with an asterisk), and a table look-up block that supplies the switching signals to the inverter through a sample/hold block that prevents the switching state from changing too fast.

In order to explain the underlying concepts behind DTC, it is helpful to define the stator space flux vector  $\lambda_s$  such that its horizontal component is  $\lambda_{qs}^s$  and vertical component is  $-\lambda_{ds}^s$ , as shown in Figure 13.8-2a. Likewise, it is convenient to define the inverter output voltage vectors  $V_0$  through  $V_7$ , corresponding to each of the inverter switching states, such that the horizontal component is  $v_{qs}^s$  and vertical component is  $-v_{ds}^s$ . These voltage vectors as summarized in Table 13.8-1 and plotted in Figure 13.8-2b.

In the steady state at constant torque and rotor speed, the stator flux vector  $\lambda_s$  ideally has a constant magnitude and rotates in the counterclockwise direction at an angular velocity of  $\omega_e$ . The steady-state stator flux trajectory for the desired torque is shown as a dashed line in Figure 13.8-2a. Utilizing the concept of north and south poles discussed in Chapter 2,  $\lambda_s$  points in the direction of the net south pole as it enters the inner periphery of the stator. If the north pole attributed to the rotor currents lags (leads)  $\lambda_s$ , the electromagnetic torque will be positive (negative). In either case, advancing  $\lambda_s$  in the counterclockwise direction will increase  $T_e$  and delaying  $\lambda_s$  will decrease  $T_e$ .

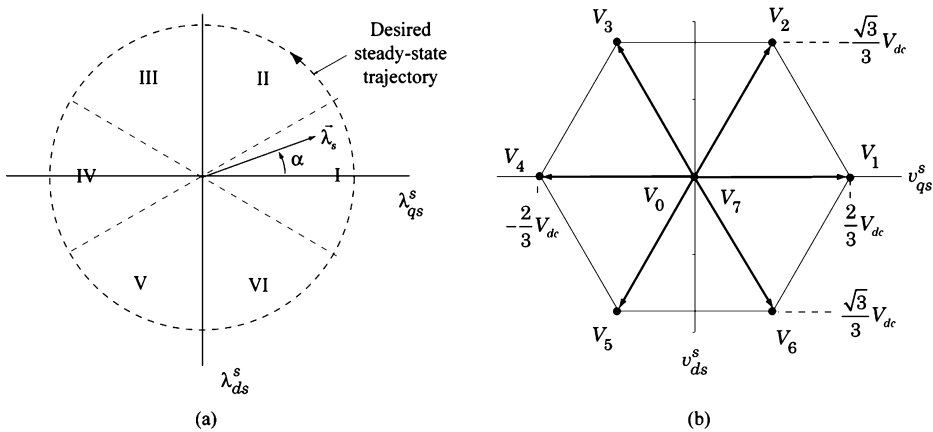


Figure 13.8-2. Stator flux and achievable voltage vectors.

TABLE 13.8-1. Achievable Voltage Vectors and Corresponding Switching State

Voltage Vector	Switching State		
	$T_1 / \bar{T}_4$	$T_2 / \bar{T}_5$	$T_3 / \bar{T}_6$
$V_0$	0	0	0
$V_1$	1	0	0
$V_2$	1	1	0
$V_3$	0	1	0
$V_4$	0	1	1
$V_5$	0	0	1
$V_6$	1	0	1
$V_7$	1	1	1

At this point, it is possible to explain the underlying concept behind DTC. For this purpose, it is assumed arbitrarily that, at a given instant of time,  $\lambda_s$  lies in Sector I (Fig. 13.8-2a) and its magnitude is smaller than the commanded  $|\lambda_s^*|$ . The control system should then select the inverter switching state that increases the magnitude of  $\lambda_s$  and, if  $T_e$  is smaller than  $T_e^*$ , advances  $\lambda_s$  in the counterclockwise direction. From Figure 13.8-2b, voltage vector  $V_2$  should be selected. Using Faraday's law, it can be argued that the subsequent change in  $\lambda_s$  will be in the direction of  $V_2$ . Specifically, combining the relations  $\Delta\lambda_{qs}^s \approx \Delta T v_{qs}^s$  and  $\Delta\lambda_{ds}^s \approx \Delta T v_{ds}^s$ , where  $\Delta T$  is the sample/hold interval, into a single vector relation yields the desired result. While the direction of the ensuing change in  $\lambda_s$  will be along  $V_2$ , the magnitude of the change,  $\Delta|\lambda_s|$ , will be proportional to  $\Delta T$ , which should be carefully selected so that  $\Delta|\lambda_s|$  is not too large or too small.

Using a similar argument with reference to Figure 13.8-2a,b, if it is necessary to increase flux and decrease torque, voltage vector  $\mathbf{V}_6$  should be selected. On the other hand, if  $\lambda_s$  lies outside the circle while still located in Sector I, and the torque is smaller (larger) than its commanded value, it is necessary to decrease the magnitude of  $\lambda_s$  while advancing (delaying) its counterclockwise rotation. Referring again to Figure 13.8-2a,b, voltage vector  $\mathbf{V}_3$  ( $\mathbf{V}_5$ ) should be selected. In Reference 9, voltage vector  $\mathbf{V}_7$  or  $\mathbf{V}_0$  is chosen if  $T_e > T_e^*$  irrespective of the magnitude of the stator flux, which results in zero voltages applied to the stator and only a small subsequent change in the stator flux vector (due to the ohmic voltage drop in the stator windings). The preceding switching states are summarized in the column corresponding to Sector I of Table 13.8-2. Therein,  $\Delta T_e$  and  $\Delta |\lambda_s|$  are the desired change in torque and flux, respectively. A similar argument can be applied if  $\lambda_s$  lies in any of the other sectors shown in Figure 13.8-2, resulting in a cyclic permutation of the subscripts as shown in Table 13.8-2.

To illustrate the dynamic performance of an induction motor drive with DTC, it is assumed that the motor described in Section 13.2 is operating at 200 N·m and 1800 rpm, whereupon the torque command is stepped to -200 N·m while holding the commanded stator flux magnitude at its rated value (1.0 V·s) throughout the study. The resulting electromagnetic torque and stator flux magnitude are depicted in Figure 13.8-3 wherein

TABLE 13.8-2. Switching Table for Direct Torque Control

$\Delta T_e$	$\Delta  \lambda_s $	Sector					
		I	II	III	IV	V	VI
1	1	$\mathbf{V}_2$	$\mathbf{V}_3$	$\mathbf{V}_4$	$\mathbf{V}_5$	$\mathbf{V}_6$	$\mathbf{V}_1$
0	1	$\mathbf{V}_7$	$\mathbf{V}_0$	$\mathbf{V}_7$	$\mathbf{V}_0$	$\mathbf{V}_7$	$\mathbf{V}_0$
-1	1	$\mathbf{V}_6$	$\mathbf{V}_1$	$\mathbf{V}_2$	$\mathbf{V}_3$	$\mathbf{V}_4$	$\mathbf{V}_5$
1	0	$\mathbf{V}_3$	$\mathbf{V}_4$	$\mathbf{V}_5$	$\mathbf{V}_6$	$\mathbf{V}_1$	$\mathbf{V}_2$
0	0	$\mathbf{V}_0$	$\mathbf{V}_7$	$\mathbf{V}_0$	$\mathbf{V}_7$	$\mathbf{V}_0$	$\mathbf{V}_7$
-1	0	$\mathbf{V}_5$	$\mathbf{V}_6$	$\mathbf{V}_1$	$\mathbf{V}_2$	$\mathbf{V}_3$	$\mathbf{V}_4$

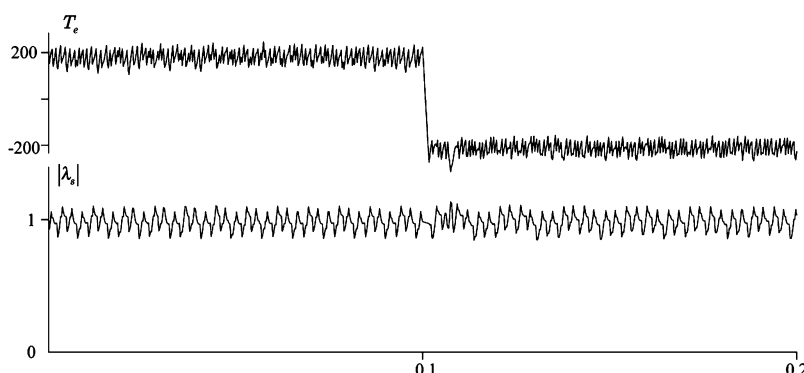


Figure 13.8-3. Step response of an induction motor with DTC.

it is assumed that over the time interval shown, the rotor speed does not change. For the given study, the sample/hold rate was set to 4 kHz. As shown, the torque response is very rapid and there is a negligible change in the magnitude of the stator flux. A key advantage of DTC is the fact that the machine parameters are not required to implement the control; however, a disadvantage is the potential for high torque ripple.

### 13.9. SLIP ENERGY RECOVERY DRIVES

If an induction machine is supplied by a fixed-frequency fixed-amplitude supply, it exhibits the well-known torque-versus-speed characteristic discussed in Section 6.9. Therein, it was mentioned that increasing the rotor resistance has the benefit of increasing the starting torque and concurrently reducing the reactive power drawn from the source during startup from zero speed. However, once the motor has accelerated to its final steady-state speed, the slip will be larger than with the original rotor resistance thereby increasing losses. With the advent of modern power electronics, it is possible to achieve the benefits of increasing rotor resistance without the associated power losses.

A typical slip energy recovery drive system is depicted in Figure 13.9-1. As shown, the stator is connected to a fixed-frequency, fixed-amplitude source, which also supplies an active bridge rectifier whose dc output is regulated to a fixed value. The dc voltage is then

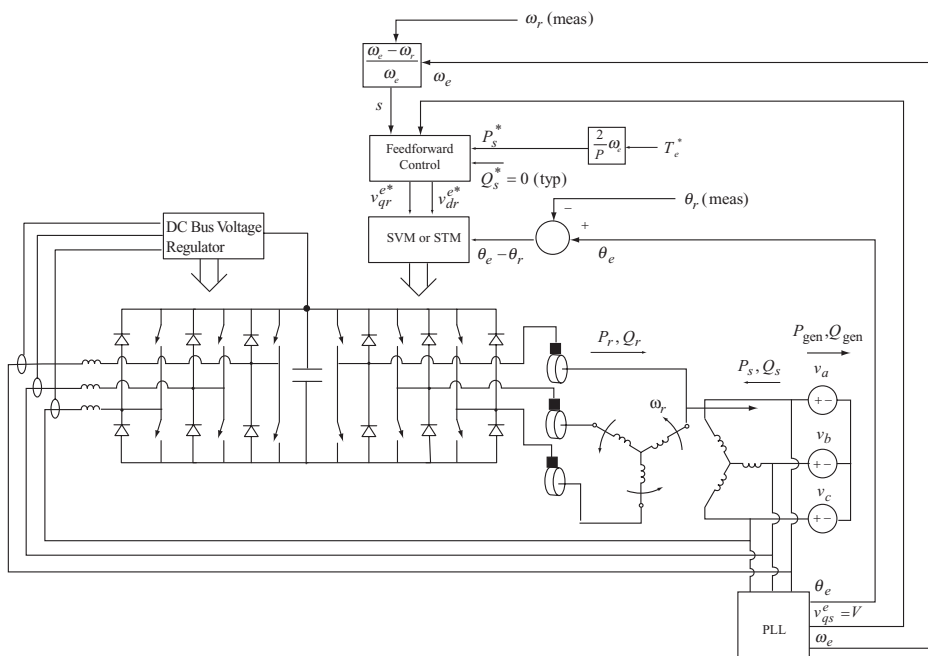


Figure 13.9-1. Circuit/block diagram of a slip energy recovery drive system.

converted to three-phase ac by a six-step inverter using, for example, a sine-triangle or space vector modulator (STM or SVM) as described in Section 12.7. Using this approach, it is possible to control both the amplitude and frequency of the voltages applied to the rotor windings. By doing so appropriately, it is possible to set the electromagnetic torque to any desired value within design limits over a range of rotor speeds. It is also possible to control the net reactive power supplied to or by the electric source. Such an arrangement is commonly used in modern wind turbine generators at the multimegawatt level where the rotor speed at which optimum power extraction occurs varies as a function of the wind speed.

A strategy that can be used to control the electromagnetic torque can be established by considering the steady-state relationships between the rotor and stator voltage and currents, which are repeated here for convenience. The steady-state real and reactive power supplied to the stator windings may be expressed as

$$P_s = \frac{3}{2}(V_{qs}I_{qs} + V_{ds}I_{ds}) \quad (13.9-1)$$

$$Q_s = \frac{3}{2}(V_{qs}I_{ds} - V_{ds}I_{qs}) \quad (13.9-2)$$

Likewise, the steady-state real and reactive power supplied to the rotor windings may be expressed as

$$P_r = \frac{3}{2}(V'_{qr}I'_{qr} + V'_{dr}I'_{dr}) \quad (13.9-3)$$

$$Q_r = \frac{3}{2}(V'_{qr}I'_{dr} - V'_{dr}I'_{qr}) \quad (13.9-4)$$

For analysis purposes, it is convenient to select the synchronous reference frame with its time-zero location set so that  $V_{ds}^e = 0$ . The steady-state stator voltage equations become

$$V_{qs}^e = r_s I_{qs}^e + \omega_e \Psi_{ds}^e \quad (13.9-5)$$

$$0 = r_s I_{ds}^e - \omega_e \Psi_{qs}^e \quad (13.9-6)$$

where  $\Psi = \omega_e \lambda$ . In terms of currents, the stator voltage equations become

$$V_{qs}^e = r_s I_{qs}^e + X_{ss} I_{ds}^e + X_M I_{dr}^e \quad (13.9-7)$$

$$V_{ds}^e = r_s I_{ds}^e - X_{ss} I_{qs}^e - X_M I_{qr}^e \quad (13.9-8)$$

The rotor voltage equations may be expressed similarly as

$$V'_{qr}^e = r' I_{dr}^e + s(X_M I_{ds}^e + X'_{rr} I_{dr}^e) \quad (13.9-9)$$

$$V'_{dr}^e = r' I_{dr}^e - s(X_M I_{qs}^e + X'_{rr} I_{qr}^e) \quad (13.9-10)$$

where  $s = (\omega_e - \omega_r)/\omega_e$  is the slip. To establish the voltages that should be applied to the rotor so as to produce the desired value of torque, we start with the established expression for torque

$$T_e = \frac{P}{2} \frac{3}{2} \frac{1}{\omega_e} (\Psi_{ds}^e I_{qs}^e - \Psi_{ds}^e I_{qs}^e) \quad (13.9-11)$$

If the stator resistance is small, then from (13.9-5) and (13.9-6),  $V_{qs}^e \approx \Psi_{qs}^e$  and  $V_{ds}^e \approx -\Psi_{ds}^e$ , whereupon

$$T_e \approx \frac{P}{2} \frac{3}{2} \frac{1}{\omega_e} (V_{qs}^e I_{qs}^e + V_{ds}^e I_{ds}^e) \quad (13.9-12)$$

Comparing (13.9-12) with (13.9-1),

$$T_e \approx \frac{P}{2} \frac{1}{\omega_e} P_s \quad (13.9-13)$$

The preceding steady-state relationships suggest the “feedforward” control strategy shown in Figure 13.9-2. Therein, the measured peak stator voltage is established using a phase-locked loop (PLL), which also determines the electrical frequency  $\omega_e$ .

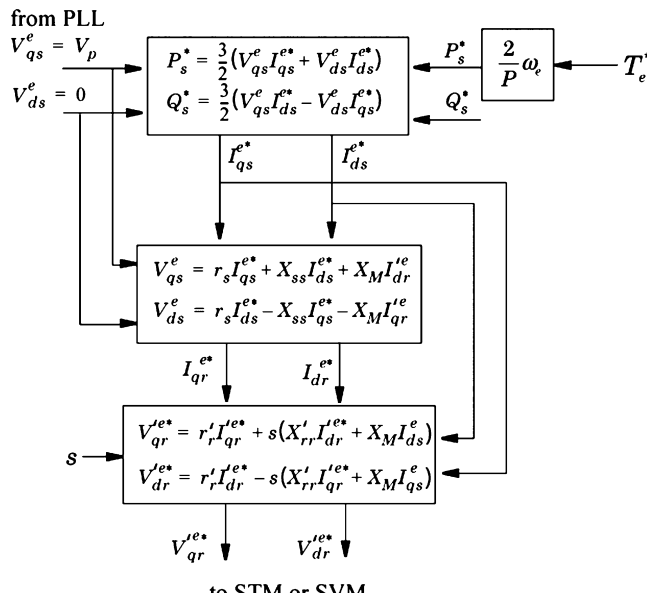


Figure 13.9-2. Feedforward control for a slip energy recovery drive system.

Based on the commanded electromagnetic torque and reactive power, the steady-state equations are used to establish, in sequence, the desired stator currents, the desired rotor currents, and finally the commanded rotor voltages, which are supplied to the inverter modulator (SVM or STM). If the calculated rotor currents and voltages are substituted into the expression for rotor power (13.9-3) and the stator losses are small,

$$P_r \approx -sP_s \quad (13.9-14)$$

If the converter losses are small, the net electrical power supplied to the drive system is

$$P_e \approx P_s + P_r \quad (13.9-15)$$

which is positive if the drive system is operating as a motor and negative if it is operating as a generator. The main advantage of a slip energy recovery drive can be seen from (13.9-14) and (13.9-15). If the rotor speeds  $\omega_r$  over which the drive system operates lie in a narrow range about the fixed electrical frequency  $\omega_e$ , the slip  $s$  will be small, and from (13.9-14) and (13.9-15), the power that needs to be supplied to the rotor windings, which determines the power rating of the associated rectifier and inverter, is a small fraction of the net electric power  $P_e$  supplied to or by the drive system.

## 13.10. CONCLUSIONS

In this chapter, a variety of induction motor drive schemes have been explored including volts-per-hertz, compensated volts-per-hertz, constant-slip, rotor flux oriented, and DTC. If the rotor speed is expected to vary inside a limited range near synchronous speed, slip energy recovery drive systems are shown to have an advantage. This chapter is intended to be an introduction to these diverse methods of control. For detailed aspects and refinements to the basic approaches described herein, the reader is referred to Reference 9.

## REFERENCES

- [1] A. Muñoz-García, T.A. Lipo, and D.W. Novotny, "A New Induction Motor V/f Control Method Capable of High-Performance Regulation at Low Speeds," *IEEE Trans. Ind. Appl.*, Vol. 34, No. 4, July/August 1998, pp. 813–821.
- [2] P.P. Waite and G. Pace, "Performance Benefits of Resolving Current in Open-Loop AC Drives," Proceedings of the 5th European Conference on Power Electronics and Applications, September 13–16, 1993, Brighton, UK, pp. 405–409.
- [3] O. Wasyczuk, S.D. Sudhoff, K.A. Corzine, J.L. Tichenor, P.C. Krause, I.G. Hansen, and L.M. Taylor, "A Maximum Torque per Ampere Control Strategy for Induction Motor Drives," *IEEE Trans. Energy Conversion*, Vol. 13, No. 2, June 1998, pp. 163–169.

- [4] O. Wasynczuk and S.D. Sudhoff, "Maximum Torque per Ampere Induction Motor Drives—An Alternative to Field-Oriented Control," *SAE Trans., J. Aerosp.*, Vol. 107, Section 1, 1998, pp. 85–93.
- [5] A.M. Trzynadlowski, *The Field Orientation Principle in Control of Induction Motors*, Kluwer Academic Publishers, Boston, 1994.
- [6] I. Boldea and S.A. Nasar, *Vector Control of AC Drives*, CRC Press, Boca Raton, FL, 1992.
- [7] I. Takahashi and T. Noguchi, "A New Quick-Response and High-Efficiency Control Strategy of an Induction Motor," *IEEE Trans. Ind. Appl.*, Vol. 22, September/October 1986, pp. 820–827.
- [8] I. Takahashi and Y. Ohmori, "High-Performance Direct Torque Control of an Induction Motor," *IEEE Trans. Ind. Appl.*, Vol. 25, No. 2, March/April 1989, pp. 257–264.
- [9] P. Vas, *Sensorless Vector and Direct Torque Control*, Oxford Science Publications, Oxford, 1998.
- [10] K. Rajashekara, A. Kawamura, and K. Matsuse, *Sensorless Control of AC Motor Drives—Speed and Position Sensorless Operation*, IEEE Press, Piscataway, NJ, 1996 (Selected Reprints).

## PROBLEMS

1. Derive (13.2-4) and (13.2-7).
2. Calculate the characteristics shown in Figure 13.2-4 if (a)  $r_{s,est} = 0.75r_s$  and (b)  $L_{ss,est} = 1.1L_{ss}$ .
3. Consider the 50-hp induction machine used in the studies in this chapter. Suppose the combined inertia of the machine and load is  $2 \text{ N}\cdot\text{m}\cdot\text{s}^2$ . Compute the minimum value of  $\alpha_{\max}$  of a slew rate limiter by assuming that there is no load torque and that the rated electrical torque is obtained.
4. Using the parameters of the 50-hp induction motor set forth in this chapter, plot the ratio of power loss divided by torque (see 13.3-18) and the corresponding value of the magnitude of the air-gap flux as a function of slip frequency  $\omega_s$ .
5. Repeat the study depicted in Figure 13.3-2 if (a)  $r'_{r,est} = 0.75r'_r$  and (b)  $r'_{r,est} = 1.25r'_r$ .
6. Derive the transfer function between commanded and actual speed if the control used in Figure 13.2-5 is used. Assume that the electromagnetic torque is equal to its commanded value, that the load torque is zero, and that the combined inertia of the electric machine and load is  $J$ .
7. Suppose it is desired that the rms value of the fundamental component of the rotor flux,  $\lambda_r$ , in the constant slip control is to be limited to the value that would be obtained at rated speed, rated frequency, and rated voltage for no-load conditions. Compute the numerical value of  $\lambda_r$ . If maximum torque per amp control is used, at what percentage of base torque does the control change from constant slip to constant flux?
8. Using the same criterion as in problem 6, compute  $\lambda_{dr}^{g*}$  for field oriented control.
9. At moderate and high speeds, it is possible to measure the applied voltages and currents, and based on this information, form an estimate of  $\lambda_{qs}^s$  and  $\lambda_{ds}^s$ . Draw a

block diagram of a control that could achieve this. Given  $\lambda_{qs}^s$  and  $\lambda_{ds}^s$ , devise flux and torque control loops that could be used to add robustness to the indirect field-oriented controller. Why would this method not work at low speeds?

10. Derive (13.6-4).
11. Derive (13.6-12).
12. Derive an indirect field oriented control strategy in which  $\lambda'_{dr}^e = 0$  and  $i'_{qr}^e = 0$ .

# PERMANENT-MAGNET AC MOTOR DRIVES

## 14.1. INTRODUCTION

There are a great variety of permanent-magnet ac motor drive configurations. Generally, these may be described by the block diagram in Figure 14.1-1. Therein, the permanent-magnet ac drive is seen to consist of four main parts, a power converter, a permanent-magnet ac machine (PMAM), sensors, and a control algorithm. The power converter transforms power from the source (such as the local utility or a dc supply bus) to the proper form to drive the PMAM, which, in turn, converts electrical energy to mechanical energy. One of the salient features of the permanent-magnet ac drive is the rotor position sensor (or at least an estimator or observer). Based on the rotor position, and a command signal(s), which may be a torque command, voltage command, speed command, and so on, the control algorithms determine the gate signal to each semiconductor in the power electronic converter.

In this chapter, the converter connected to the machine will be assumed to be a fully controlled three-phase bridge converter, as discussed in Chapter 12. Because we will primarily be considering motor operation, we will refer to this converter as an inverter throughout this chapter.

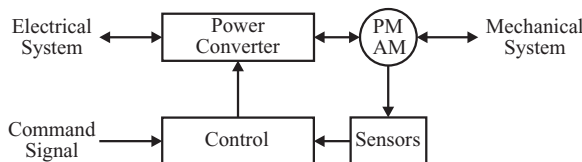


Figure 14.1-1. Permanent-magnet ac motor drive.

The structure of the control algorithms determines the type of permanent-magnet ac motor drive, of which there are two main classes, voltage-source-based drives and current-regulated drives. Both voltage-source and current-regulated drives may be used with PMAMs with either sinusoidal or nonsinusoidal back emf waveforms. Machines with sinusoidal back emfs may be controlled so as to achieve nearly constant torque; however, machines with a nonsinusoidal back emf may be less expensive to manufacture. The discussion in this chapter will focus on the machines with sinusoidal back emfs; for information on the nonsinusoidal drives, the reader is referred to References 1–3.

In this chapter, a variety of voltage-source and current-regulated drives featuring machines with sinusoidal back emf waveforms will be analyzed. For each drive considered, computer simulations will be used to demonstrate performance. Next, average-value models for each drive are set forth, along with a corresponding linearized model for control synthesis. Using these models, the steady-state, transient, and dynamic performance of each drive configuration considered will be set forth. Design examples will be used to illustrate the performance of the drive in the context of a control system.

## 14.2. VOLTAGE-SOURCE INVERTER DRIVES

Figure 14.2-1 illustrates a voltage-source-modulated inverter-based permanent-magnet ac motor drive. Here, voltage-source inverter refers to an inverter being controlled by a voltage-source modulation strategy (six-stepped, six-step modulated, sine-triangle modulated, etc.). Power is supplied from the utility through a transformer, which is depicted as an equivalent voltage behind inductance. The transformer output is rectified using a semi-controlled three-phase bridge converter, as discussed in Chapter 11. Since this converter is operated as a rectifier (i.e., converting power from the ac system to the dc system), it will be simply referred to as a rectifier herein. The rectifier output is connected to the dc link filter, which may be simply an LC filter ( $L_{dc}$ ,  $C_{dc}$ ), but which may include a stabilizing filter ( $L_{st}$ ,  $r_{st}$ ,  $C_{st}$ ) as well. The filtered rectifier output is used as a dc voltage source for the inverter, which drives the PMAM. This voltage is commonly referred to as the dc link voltage. As can be seen, rotor position is an input to the controller. Based on rotor position and other inputs, the controller determines the switching states of each of the inverter semiconductors. The command signal to the controller may be quite varied depending on the structure of the controls

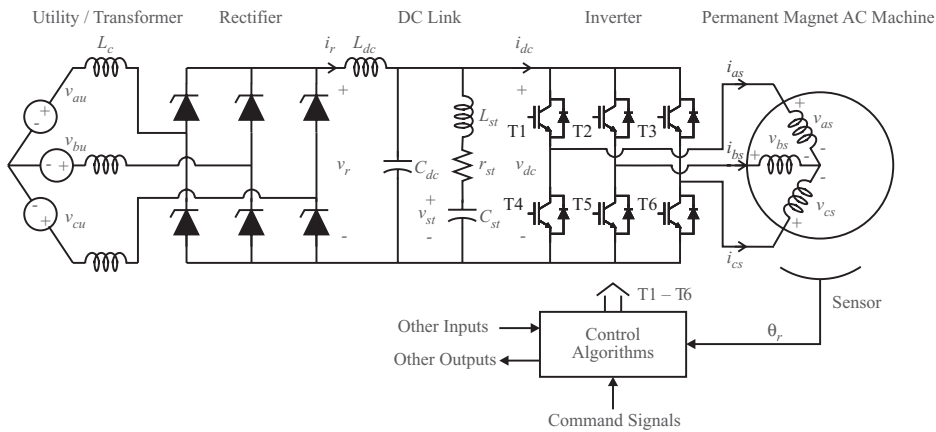


Figure 14.2-1. Permanent-magnet ac motor drive circuit.

in the system in which the drive will be embedded; it will often be a torque command. Other inputs to the control algorithms may include rotor speed and dc link voltage. Other outputs may include gate signals to the rectifier thyristors if the rectifier is phase-controlled.

Variables of particular interest in Figure 14.2-1 include the utility supply voltage,  $v_{au}$ ,  $v_{bu}$ , and  $v_{cu}$ , the utility current into the rectifier  $i_{au}$ ,  $i_{bu}$ , and  $i_{cu}$ , the rectifier output voltage,  $v_r$ , the rectifier current,  $i_r$ , the stabilizing filter current  $i_{st}$ , the stabilizing filter capacitor voltage  $v_{st}$ , the inverter voltage  $v_{dc}$ , the inverter current  $i_{dc}$ , the three-phase currents into the machine  $i_{as}$ ,  $i_{bs}$ , and  $i_{cs}$ , and the machine line-to-neutral voltages  $v_{as}$ ,  $v_{bs}$ , and  $v_{cs}$ .

Even within the context of the basic system shown in Figure 14.2-1, there are many possibilities for control, depending on whether or not the rectifier is phase-controlled and the details of the inverter modulation strategy. Regardless of the control strategy, it is possible to relate the operation of the converter back to the idealized machine analysis set forth in Chapter 4, which will be the starting point for our investigation into voltage-source inverter fed permanent-magnet ac motor drive systems.

### 14.3. EQUIVALENCE OF VOLTAGE-SOURCE INVERTERS TO AN IDEALIZED SOURCE

Voltage-source inverters are inverters with a voltage-source modulator. In order to make use of our analysis of the PMAM set forth in Chapter 4 when the voltage source is an inverter rather than an ideal source, it is necessary to relate the voltage-source inverter to an ideal source. This relationship is a function of the type of modulation strategy used. In this section, the equivalence of six-stepped, six-step-modulated, sine triangle-modulated, extended-sine triangle-modulated, or space-vector-modulated inverter to an idealized source is established.

The six-stepped inverter-based permanent-magnet ac motor drive is the simplest of all the strategies to be considered in terms of generating the signals required to control the inverter. It is based on the use of relatively inexpensive Hall effect rotor position sensors. For this reason, the six-stepped inverter drive is a relatively low-cost drive. Furthermore, since the frequency of the switching of the semiconductors corresponds to the frequency of the machine, fast semiconductor switching is not important, and switching losses will be negligible. However, the inverter does produce considerable harmonic content, which will result in increased machine losses.

In the six-stepped inverter, the on/off status of each of the semiconductors is directly tied to electrical rotor position, which is accomplished through the use of the Hall effect sensors. These sensors are configured to have a logical 1 output when they are under a south magnetic pole and a logic 0 when they are under a north magnetic pole of the permanent magnet, and are arranged on the stator of the PMAM as illustrated in Figure 14.3-1, where  $\phi_h$  denotes the position of the Hall effect sensors. The logical output of sensors H1, H2, and H3 are equal to the gate signals for T1, T2, and T3, respectively, so that the gating signals are as indicated in Figure 14.3-2. The gate signals T4, T5, and T6 are the logical complements of T1, T2, and T3, respectively.

Comparing the gating signals shown in Figure 14.3-2 with those illustrated in the generic discussion of six-step operation in Chapter 12 (see Fig. 12.3-1), it can be seen that the two sets of waveforms are identical provided the converter angle  $\theta_c$  is related to rotor position and the Hall effect position by

$$\theta_c = \theta_r + \phi_h \quad (14.3-1)$$

In Section 12.3, expressions for the average-value of the  $q$ - and  $d$ -axis voltages in the converter reference frame were derived. Taking these expressions as dynamic averages,

$$\hat{v}_{qs}^c = \frac{2}{\pi} \hat{v}_{dc} \quad (14.3-2)$$

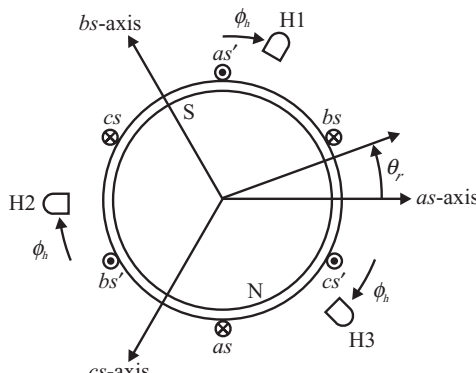


Figure 14.3-1. Electrical diagram of a permanent-magnet ac machine.

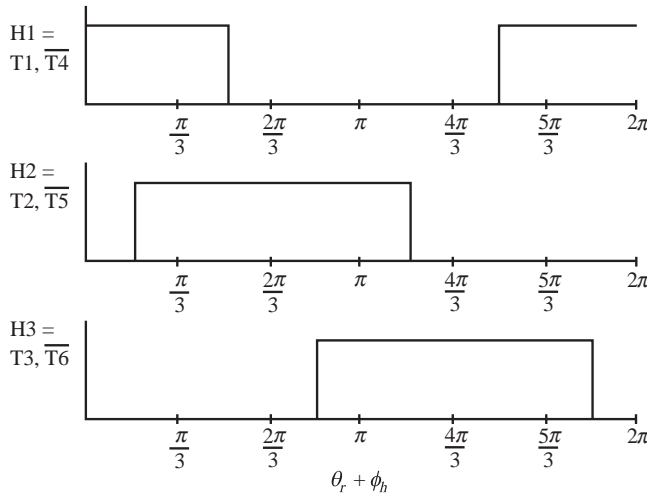


Figure 14.3-2. Semiconductor switching signals.

$$\hat{v}_{ds}^c = 0 \quad (14.3-3)$$

From (14.3-1), the difference in the angular position between the converter reference frame and rotor reference frame is the Hall effect position  $\phi_h$ . Using this information, the dynamic-average of the stator voltages may be determined in the rotor reference frame using the frame-to-frame transformation  ${}^c\mathbf{K}_s^r$ , which yields

$$\hat{v}_{qs}^r = \frac{2}{\pi} \hat{v}_{dc} \cos \phi_h \quad (14.3-4)$$

$$\hat{v}_{ds}^r = -\frac{2}{\pi} \hat{v}_{dc} \sin \phi_h \quad (14.3-5)$$

From (14.3-4) and (14.3-5), we conclude that at least in terms of the fundamental component, the operation of the PMAM from a six-stepped inverter is identical to a PMAM fed by ideal three-phase variable-frequency voltage source with an rms amplitude of

$$v_s = \frac{1}{\sqrt{2}} \frac{2}{\pi} \hat{v}_{dc} \quad (14.3-6)$$

and a phase advance of

$$\phi_v = \phi_h \quad (14.3-7)$$

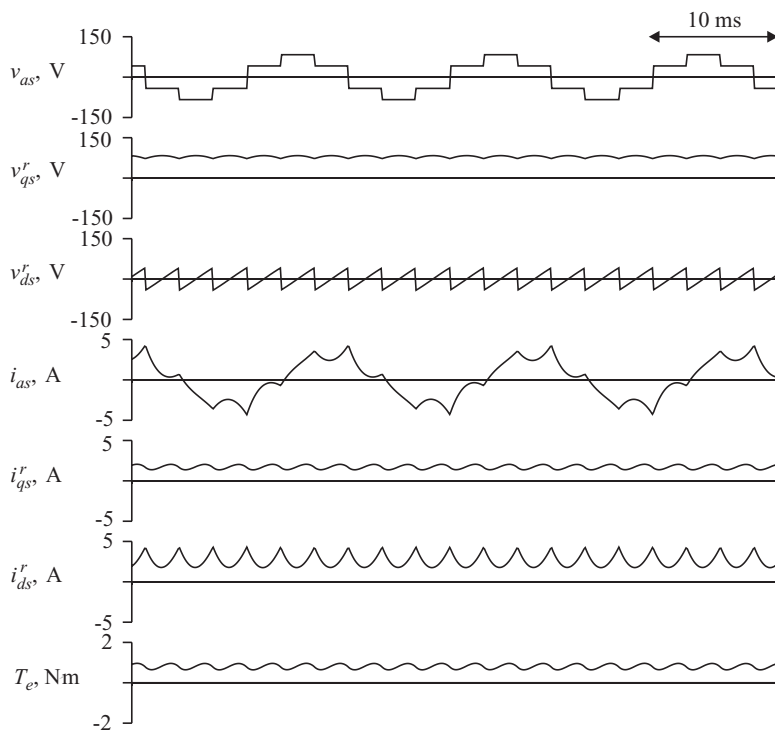


Figure 14.3-3. Steady-state performance of a six-stepped permanent-magnet ac motor drive.

Figure 14.3-3 illustrates the steady-state performance of a six-stepped inverter. In this study, the inverter voltage  $v_{dc}$  is regulated at 125 V and the mechanical rotor speed is 200 rad/s. The machine parameters are  $r_s = 2.98 \Omega$ ,  $L_q = L_d = 11.4 \text{ mH}$ ,  $\lambda'_m = 0.156 \text{ Vs}$ , and  $P = 4$ . There is no phase advance. As can be seen, the nonsinusoidal  $a$ -phase voltage results in time-varying  $q$ - and  $d$ -axis voltages. The effect of the harmonics is clearly evident in the  $a$ -phase current waveform, as well as the  $q$ - and  $d$ -axis current waveforms. Also apparent are the low-frequency torque harmonics (six times the fundamental frequency) that result. The current harmonics do not contribute to the average torque; therefore, the net effect of the harmonics is to increase machine losses. On the other hand, since the inverter is switching at a relatively low frequency (six times the electrical frequency of the fundamental component of the applied voltage), switching losses are extremely low.

This drive system is easy to implement in hardware; however, at the same time, it is difficult to utilize in a speed control system, since the fundamental component of the applied voltage cannot be adjusted unless a controlled rectifier is used. Although this is certainly possible, and has often been done in the past, it is generally advantageous

to control the applied voltages with the inverter rather than rectifier since this minimizes the total number of power electronics devices.

In order to control the amplitude of the fundamental component of the applied voltage, six-step modulation may be used, as is discussed in Section 12.4. In this case, the gate drive signals T1–T6 are modulated in order to control the amplitude of the applied voltage. Recall from Section 12.4 that for six-step modulation, the dynamic-average  $q$ - and  $d$ -axis voltages are given by

$$\hat{v}_{qs}^c = \frac{2}{\pi} d\hat{v}_{dc} \quad (14.3-8)$$

and

$$\hat{v}_{ds}^c = 0 \quad (14.3-9)$$

Using (14.3-1) to relate the positions of the converter and rotor reference frames, the frame-to-frame transformation may be used to express the  $q$ - and  $d$ -axis voltage in the rotor reference frame. In particular,

$$\hat{v}_{qs}^r = \frac{2}{\pi} d\hat{v}_{dc} \cos \phi_h \quad (14.3-10)$$

$$\hat{v}_{ds}^r = -\frac{2}{\pi} d\hat{v}_{dc} \sin \phi_h \quad (14.3-11)$$

From (14.3-10) and (14.3-11), it is clear that the effective rms amplitude of the applied voltage is

$$v_s = \frac{1}{\sqrt{2}} \frac{2}{\pi} d\hat{v}_{dc} \quad (14.3-12)$$

The phase advance given by (14.3-7) is applicable to the six-step modulated drive in addition to the six-stepped inverter.

Figure 14.3-4 illustrates the performance of a six-step modulated drive. For this study, the parameters are identical to those for the study depicted in Figure 14.3-3, with the exception of the modulation strategy, which is operating with a duty cycle of 0.9 at a frequency of 5 kHz, and the dc rail voltage is 138.9 V, which yields the same fundamental component of the applied voltage as in the previous study. As can be seen, the voltage waveforms posses an envelop similar in shape to that of the six-step case; however, they are rapidly switching within that envelope. Note that the current waveforms are similar to the previous study, although there is additional high-frequency harmonic content.

By utilizing six-step modulation, the amplitude of the applied voltage is readily varied. However, due to the increased switching frequency, the switching losses in the

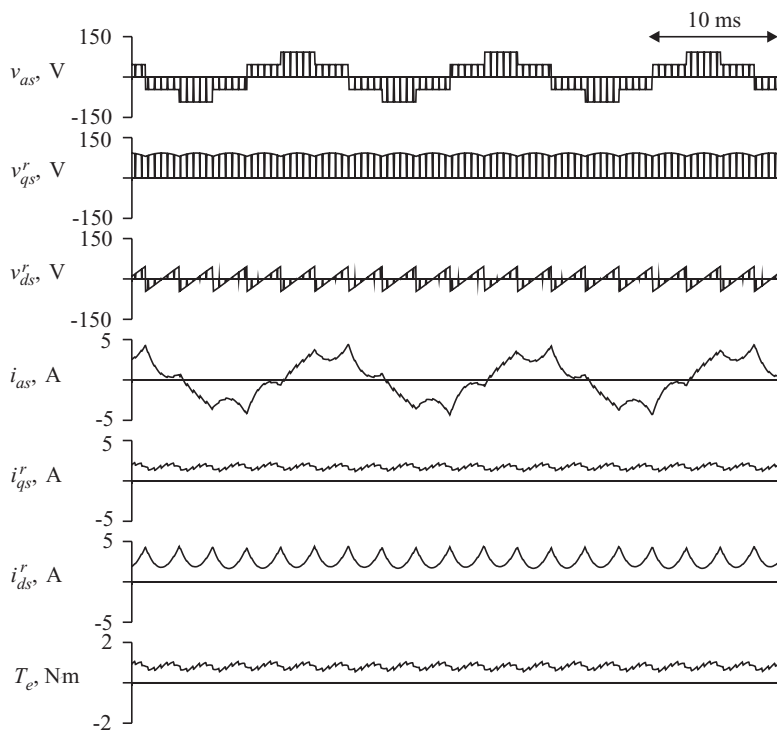


Figure 14.3-4. Steady-state performance of a six-step-modulated permanent-magnet ac motor drive.

converter are increased. The losses in the machine will be similar to those in the previous study.

Like six-step modulation, sine-triangle modulation may also be used to control the amplitude of the voltage applied to the PMAM. However, in this case, Hall effect sensors are generally not adequate to sense rotor position. Recall from Section 12.5 that phase-leg duty cycles are continuous function of converter angle, which implies that they will be continuous functions of rotor position. For this reason, a resolver or an optical encoder must be used as the rotor position sensor. Although this increases the cost of the drive, and also increases the switching losses of the power electronics devices, the sine-triangle modulated drive does have an advantage in that the low-frequency harmonic content of the machine currents are greatly reduced, thereby reducing machine losses in machines with a sinusoidal back emf and also reducing acoustic noise and torque ripple.

In the case of the sine-triangle modulated inverter, the angular position used to determine the phase-leg duty cycles, that is, the converter angle, is equal to the electric rotor position plus an offset, that is,

$$\theta_c = \theta_r + \phi_v \quad (14.3-13)$$

From Section 12.5,

$$\hat{v}_{qs}^c = \begin{cases} \frac{1}{2} d \hat{v}_{dc} & 0 < d \leq 1 \\ \frac{2}{\pi} \hat{v}_{dc} f(d) & d > 1 \end{cases} \quad (14.3-14)$$

$$\hat{v}_{ds}^c = 0 \quad (14.3-15)$$

where

$$f(d) = \frac{1}{2} \sqrt{1 - \left(\frac{1}{d}\right)^2} + \frac{1}{4} d \left(\pi - 2 \arccos\left(\frac{1}{d}\right)\right) \quad d > 1 \quad (14.3-16)$$

Using (14.3-13) to compute the angular difference of the locations of the converter and rotor reference frames, the dynamic averages of the  $q$ - and  $d$ -axis stator voltages may be expressed as

$$\hat{v}_{qs}^r = \begin{cases} \frac{1}{2} \hat{v}_{dc} d \cos \phi_v & d \leq 1 \\ \frac{2}{\pi} \hat{v}_{dc} f(d) \cos \phi_v & d > 1 \end{cases} \quad (14.3-17)$$

$$\hat{v}_{ds}^r = \begin{cases} -\frac{1}{2} \hat{v}_{dc} d \sin \phi_v & d \leq 1 \\ -\frac{2}{\pi} \hat{v}_{dc} f(d) \sin \phi_v & d > 1 \end{cases} \quad (14.3-18)$$

Figure 14.3-5 illustrates the performance of a sine-triangle modulated inverter drive. The parameters and operating conditions are identical to those in the previous study with a duty cycle is 0.9 and the switching frequency of 5 kHz, with the exception that the dc voltage has been increased to 176.8 V. This yields the same fundamental component of the applied voltage as in the previous two studies. Although on first inspection the voltage waveforms appear similar to the six-step modulated case, the harmonic content of the waveform has been significantly altered. This is particularly evident in the current waveforms which no longer contain significant harmonic content. As a result, the torque waveform is also devoid of low-frequency harmonics. Like six-step modulation, this strategy allows the fundamental component of the applied voltage to be changed. In addition, the phase can be readily changed, and low-frequency current and torque harmonics are eliminated. However, the price for these benefits is that rotor position must be known on a continuous basis, which requires either an optical encoder or resolver, which are considerably more expensive than Hall effect sensors. Several methods of eliminating the need for the encoder or resolver have been set forth in References 4 and 5.

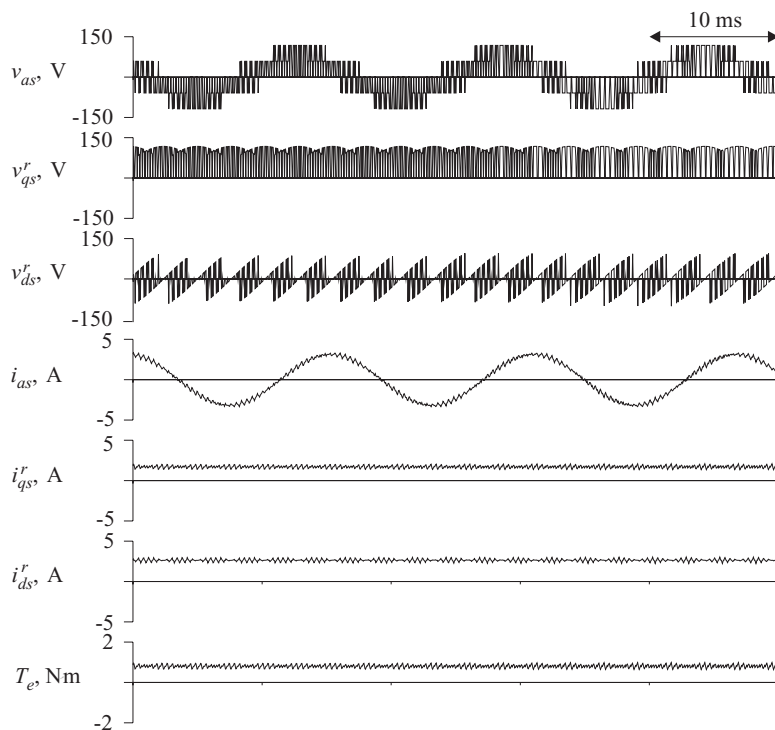


**Figure 14.3-5.** Steady-state performance of sine-triangle-modulated permanent-magnet ac motor drive.

In Chapter 12, the next modulation strategy considered was extended sine-triangle modulation. The analysis of this strategy is the same as for sine-triangle modulation, with the exception that the amplitude of the duty cycle  $d$  may be increased to  $2/\sqrt{3}$  before overmodulation occurs. Therefore, we have

$$\hat{v}_{qs}^r = \frac{1}{2} d \hat{v}_{dc} \cos \phi_v \quad 0 \leq d \leq 2/\sqrt{3} \quad (14.3-19)$$

$$\hat{v}_{ds}^r = -\frac{1}{2} d \hat{v}_{dc} \sin \phi_v \quad 0 \leq d \leq 2/\sqrt{3} \quad (14.3-20)$$

The final voltage-source modulation strategy considered in Chapter 12 was space-vector modulation. This strategy is designed to control the inverter semiconductors in such a way that the dynamic average of the  $q$ - and  $d$ -axis output voltages are equal to the  $q$ - and  $d$ -axis voltage command, provided that the peak commanded line-to-neutral input voltage magnitude is less than  $v_{dc}/\sqrt{3}$ . If this limit is exceeded, the  $q$ - and

*d*-output voltage vector retains its commanded direction, but its magnitude is limited. Thus, we have that

$$\hat{v}_{qs}^r = \begin{cases} v_{qs}^{r*} & v_{spk}^* < v_{dc} / \sqrt{3} \\ \frac{\hat{v}_{dc}}{\sqrt{3}} \frac{v_{qs}^{r*}}{v_{spk}^*} & v_{spk}^* \geq v_{dc} / \sqrt{3} \end{cases} \quad (14.3-21)$$

$$\hat{v}_{ds}^r = \begin{cases} v_{ds}^{r*} & v_{spk}^* < v_{dc} / \sqrt{3} \\ \frac{\hat{v}_{dc}}{\sqrt{3}} \frac{v_{ds}^{r*}}{v_{spk}^*} & v_{spk}^* \geq v_{dc} / \sqrt{3} \end{cases} \quad (14.3-22)$$

where

$$v_{spk}^* = \sqrt{(v_{qs}^{r*})^2 + (v_{ds}^{r*})^2} \quad (14.3-23)$$

In order to summarize the results of this section, notice that in each case, the dynamic-average *q*- and *d*-axis voltages may be expressed as

$$\hat{v}_{qs}^r = \hat{v}_{dc} m \cos \phi_v \quad (14.3-24)$$

$$\hat{v}_{ds}^r = -\hat{v}_{dc} m \sin \phi_v \quad (14.3-25)$$

where

$$m = \begin{cases} \frac{2}{\pi} & \text{six-step operation} \\ \frac{2}{\pi} d & \text{six-step modulation } (d \leq 1) \\ \frac{1}{2} d & \text{sine-triangle modulation } (d \leq 1) \\ \frac{2}{\pi} f(d) & \text{sine-triangle modulation } (1 < d) \\ \frac{1}{2} d & \text{extended sine-triangle modulation } (d \leq 2 / \sqrt{3}) \\ \frac{v_{spk}^*}{v_{dc}} & \text{space-vector modulation } (v_{spk}^* \leq v_{dc} / \sqrt{3}) \\ \frac{1}{\sqrt{3}} & \text{space-vector modulation } (v_{spk}^* > v_{dc} / \sqrt{3}) \end{cases} \quad (14.3-26)$$

In the case of space-vector modulation, observe that  $\phi_v$  is defined as

$$\phi_v = \text{angle}(v_{qs}^{r*} - j v_{ds}^{r*}) \quad (14.3-27)$$

#### 14.4. AVERAGE-VALUE ANALYSIS OF VOLTAGE-SOURCE INVERTER DRIVES

The average-value model of a voltage-source inverter drive consist of five parts, (1) the rectifier model, (2) the dc link and stabilizing filter model, (3) the inverter model, and (4) the machine model. From Chapter 11, recall that the dynamic-average rectifier voltage is given by

$$\hat{v}_r = v_{r0} \cos \alpha - r_r \hat{i}_r - l_r p \hat{i}_r \quad (14.4-1)$$

where  $v_{r0}$ ,  $r_r$ , and  $l_r$  are given by

$$v_{r0} = \begin{cases} \frac{3\sqrt{6}}{\pi} E & \text{three-phase rectifier} \\ \frac{2\sqrt{2}}{\pi} E & \text{single-phase rectifier} \end{cases} \quad (14.4-2)$$

$$r_r = \begin{cases} \frac{3}{\pi} \omega_{eu} L_c & \text{three-phase rectifier} \\ \frac{2}{\pi} \omega_{eu} L_c & \text{single-phase rectifier} \end{cases} \quad (14.4-3)$$

$$l_r = \begin{cases} 2L_c & \text{three-phase rectifier} \\ L_c & \text{single-phase rectifier} \end{cases} \quad (14.4-4)$$

In (14.4-2)–(14.4-4),  $\omega_{eu}$  is the radian electrical frequency of the source feeding the rectifier, not to be confused with the fundamental frequency being synthesized by the drive, and  $E$  is the rms line-to-neutral utility voltage (line-to-line voltage in single-phase applications), and  $L_c$  is the commuting inductance. In the typical case wherein a transformer/rectifier is used,  $E$  and  $L_c$  reflect the utility voltage and transformer leakage impedance referred to the secondary (drive) side of the transformer.

The electrical dynamics of the rectifier current may be expressed as

$$L_{dc} p \hat{i}_r = v_r - v_{dc} - r_{dc} \hat{i}_r \quad (14.4-5)$$

Treating the variables in (14.4-5) as dynamic-average values yields

$$L_{dc} p \hat{i}_r = \hat{v}_r - \hat{v}_{dc} - r_{dc} \hat{i}_r \quad (14.4-6)$$

In (14.4-6), the rectifier voltage is given by (14.4-1); however, that expression for the rectifier voltage involves the time derivative of  $\hat{i}_r$ . Hence, (14.4-1) and (14.4-6) should be combined into a single differential equation. In particular,

$$p\hat{i}_r = \frac{\hat{v}_{r0} \cos \alpha - \hat{v}_{dc} - r_{rl}\hat{i}_r}{L_{rl}} \quad (14.4-7)$$

where

$$r_{rl} = r_r + r_{dc} \quad (14.4-8)$$

$$L_{rl} = L_r + L_{dc} \quad (14.4-9)$$

Finally, using Kirchoff's laws, the dc voltage, stabilizing filter current, and stabilizing filter voltage are governed by

$$p\hat{v}_{dc} = \frac{\hat{i}_r - \hat{i}_{st} - \hat{i}_{dc}}{C_{dc}} \quad (14.4-10)$$

$$p\hat{i}_{st} = \frac{\hat{v}_{dc} - \hat{v}_{st} - r_{st}\hat{i}_{st}}{L_{st}} \quad (14.4-11)$$

and

$$p\hat{v}_{st} = \frac{\hat{i}_{st}}{C_{st}} \quad (14.4-12)$$

respectively. Because the rectifier current must be positive, (14.4-7) is only valid for this condition. If the rectifier current is zero and the derivative given by (14.4-7) is negative, then  $p\hat{i}_r$  should be set to zero since the diodes or thyristors will be reverse biased. From (12.3-11), the dc current into the converter may be approximated as

$$\hat{i}_{dc} = \frac{3}{2} \frac{\hat{v}_{qs}^r \hat{i}_{qs}^r + \hat{v}_{ds}^r \hat{i}_{ds}^r}{\hat{v}_{dc}} \quad (14.4-13)$$

Substitution of (14.3-24) and (14.3-25) into (14.4-13) and simplifying yields

$$\hat{i}_{dc} = \frac{3}{2} m (\hat{i}_{qs}^r \cos \phi_v - \hat{i}_{ds}^r \sin \phi_v) \quad (14.4-14)$$

The next step in developing the average-value model for the voltage-source inverter drive is the incorporation of the electrical dynamics of the machine in average-value form. Taking the dynamic-average of PMAM voltage equations (expressed in terms of currents) and rearranging yields

$$p\hat{i}_{qs}^r = \frac{\hat{v}_{qs}^r - r_s \hat{i}_{qs}^r - \omega_r L_d \hat{i}_{ds}^r - \omega_r \dot{\lambda}_m}{L_q} \quad (14.4-15)$$

$$p\hat{i}_{ds}^r = \frac{\hat{v}_{ds}^r - r_s\hat{i}_{ds}^r + \omega_r L_q \hat{i}_{ds}^r}{L_d} \quad (14.4-16)$$

Note that in (14.4-15) and (14.4-16), the electrical rotor speed is not given an average-value designation. Since the rotor speed varies slowly compared with the electrical variables, it can generally be considered a constant as far as the dynamic-averaging procedure is concerned. However, there are instances when this approximation may not be completely accurate—for example, in the case of six-stepped inverter-fed permanent-magnet ac motor drive with an exceptionally low inertia during the initial part of the start-up transient. Normally, however, the approximation works extremely well in practice.

From Chapter 4, the expression for instantaneous electromagnetic torque is given by

$$T_e = \frac{3}{2} \frac{P}{2} (\lambda'_m i_{qs}^r + (L_d - L_q) i_{qs}^r i_{ds}^r) \quad (14.4-17)$$

Upon neglecting the correlation between the  $q$ -axis current harmonics and the  $d$ -axis current harmonics, (14.4-17) may be averaged to yield

$$\hat{T}_e = \frac{3}{2} \frac{P}{2} (\lambda'_m \hat{i}_{qs}^r + (L_d - L_q) \hat{i}_{qs}^r \hat{i}_{ds}^r) \quad (14.4-18)$$

This approximation (i.e., assuming that the average of the products is equal to the product of the averages) works well in the case of sine-triangle modulation wherein there is relatively little low-frequency harmonic content. However, in the case of the six-step operation or six-step modulation, some error arises from this simplification in salient machines. In the case of nonsalient machines in which the  $q$ - and  $d$ -axis inductances are equal, (14.4-18) is exact regardless of the modulation scheme.

To complete the average-value model of the drive, it only remains to include the mechanical dynamics. In particular,

$$p\omega_r = \frac{P}{2} \frac{\hat{T}_e - \hat{T}_l}{J} \quad (14.4-19)$$

and, if rotor position is of interest,

$$p\theta_r = \omega_r \quad (14.4-20)$$

Equations (14.4-19) and (14.4-20) complete the average-value model of the voltage-source inverter drive. It is convenient to combine these relationships and express them in matrix-vector form. This yields

$$\begin{aligned}
 p \begin{bmatrix} \hat{i}_r \\ \hat{v}_{dc} \\ \hat{i}_{st} \\ \hat{v}_{st} \\ \hat{i}_{qs}^r \\ \hat{i}_{ds}^r \\ \omega_r \end{bmatrix} = & \begin{bmatrix} -\frac{r_{rl}}{L_{rl}} & -\frac{1}{L_{rl}} & 0 & 0 & 0 & 0 & 0 \\ \frac{1}{C_{dc}} & 0 & -\frac{1}{C_{dc}} & 0 & 0 & 0 & 0 \\ 0 & \frac{1}{L_{st}} & -\frac{r_{st}}{L_{st}} & -\frac{1}{L_{st}} & 0 & 0 & 0 \\ 0 & 0 & \frac{1}{C_{st}} & 0 & 0 & 0 & 0 \\ 0 & 0 & 0 & 0 & -\frac{r_s}{L_q} & 0 & -\frac{\lambda'_m}{L_q} \\ 0 & 0 & 0 & 0 & 0 & -\frac{r_s}{L_d} & 0 \\ 0 & 0 & 0 & 0 & \frac{3}{2} \left( \frac{P}{2} \right)^2 \frac{1}{J} \lambda'_m & 0 & 0 \end{bmatrix} \begin{bmatrix} \hat{i}_r \\ \hat{v}_{dc} \\ \hat{i}_{st} \\ \hat{v}_{st} \\ \hat{i}_{qs}^r \\ \hat{i}_{ds}^r \\ \omega_r \end{bmatrix} \\
 & + \begin{bmatrix} \frac{1}{L_{rl}} v_{r0} \cos \alpha \\ -\frac{3}{2} \frac{m}{C_{dc}} (\cos \phi_v \hat{i}_{qs}^r - \sin \phi_v \hat{i}_{ds}^r) \\ 0 \\ 0 \\ \frac{1}{L_q} \hat{v}_{dc} m \cos \phi_v - \frac{L_d}{L_q} \omega_r \hat{i}_{ds}^r \\ -\frac{1}{L_d} \hat{v}_{dc} m \sin \phi_v + \frac{L_q}{L_d} \omega_r \hat{i}_{qs}^r \\ \frac{P}{2} \frac{1}{J} \left( \frac{3}{2} \frac{P}{2} (L_d - L_q) \hat{i}_{qs}^r \hat{i}_{ds}^r - \hat{T}_L \right) \end{bmatrix} \quad (14.4-21)
 \end{aligned}$$

## 14.5. STEADY-STATE PERFORMANCE OF VOLTAGE-SOURCE INVERTER DRIVES

In the previous section, an average-value model of a voltage-source inverter fed PMAC motor drive was set forth. Before using this model to explore the transient behavior of the drive, it is appropriate to first consider the steady-state performance. Throughout this development, variables names will be uppercase, and averages are denoted with an overbar rather than a “ $\wedge$ ” since we are considering steady-state quantities. From the work presented in Chapter 12, it is clear that given the modulation strategy and  $\bar{V}_{dc}$  the average of the  $q$ - and  $d$ -axis voltages may be obtained, whereupon the work set forth in Chapter 4 may be used to calculate any quantity of interest. Therefore, the goal of this section will primarily be to establish an expression for  $\bar{V}_{dc}$ .

The differential equations that govern the dynamic-average value performance of the drive have inputs that are constants in the steady-state; therefore, the solution of these equations is also constant in the steady-state, assuming that a stable solution exists. Therefore, the steady-state solution may be found by setting the derivative terms equal to zero. Thus, for steady-state conditions, the rectifier voltage equation (14.4-7) necessitates that

$$0 = v_{r0} \cos \alpha - \bar{V}_{dc} - r_{rl} \bar{I}_r \quad (14.5-1)$$

Similarly, substitution of (14.4-14) into (14.4-10) and setting the time derivative to zero yields

$$0 = \bar{I}_r - \bar{I}_{st} - \frac{3}{2} m (\bar{I}_{qs}^r \cos \phi_v - \bar{I}_{ds}^r \sin \phi_v) \quad (14.5-2)$$

Due to the series capacitance in the stabilizing filter, the average of the stabilizing filter current must be equal to zero. Therefore, (14.5-2) reduces to

$$0 = \bar{I}_r - \frac{3}{2} m (\bar{I}_{qs}^r \cos \phi_v - \bar{I}_{ds}^r \sin \phi_v) \quad (14.5-3)$$

Combining (14.5-3) with (14.5-1) yields

$$\bar{V}_{dc} = v_{r0} \cos \alpha - \frac{3}{2} r_{rl} m (\bar{I}_{qs}^r \cos \phi_v - \bar{I}_{ds}^r \sin \phi_v) \quad (14.5-4)$$

The next step in the development is to eliminate the  $q$ - and  $d$ -axis stator currents from (14.5-4). To this end, setting the time derivatives in (14.4-15) and (14.4-16) to zero and replacing the  $q$ - and  $d$ -axis voltages with the expressions (14.3-24) and (14.3-25) yields

$$0 = \bar{V}_{dc} m \cos \phi_v - r_s \bar{I}_{qs}^r - \omega_r L_d \bar{I}_{ds}^r - \omega_r \lambda'_m \quad (14.5-5)$$

$$0 = -\bar{V}_{dc} m \sin \phi_v - r_s \bar{I}_{ds}^r + \omega_r L_q \bar{I}_{qs}^r \quad (14.5-6)$$

Solving for (14.5-5) and (14.5-6) simultaneously for  $\bar{I}_{qs}^r$  and  $\bar{I}_{ds}^r$  in terms of  $\bar{V}_{dc}$ ,  $m$ , and  $\omega_r$

$$\bar{I}_{qs}^r = \frac{r_s (\bar{V}_{dc} m \cos \phi_v - \omega_r \lambda'_m) + \omega_r L_d \bar{V}_{dc} m \sin \phi_v}{r_s^2 + \omega_r^2 L_d L_q} \quad (14.5-7)$$

$$\bar{I}_{ds}^r = \frac{\omega_r L_d (\bar{V}_{dc} m \cos \phi_v - \omega_r \lambda'_m) - r_s \bar{V}_{dc} m \sin \phi_v}{r_s^2 + \omega_r^2 L_d L_q} \quad (14.5-8)$$

Finally, substitution of (14.5-7) and (14.5-8) into (14.5-4) and solving for  $\bar{V}_{dc}$ , we have that

$$\bar{V}_{dc} = \frac{(r_s^2 + \omega_r^2 L_d L_q) v_{r0} \cos \alpha + \frac{3}{2} r_{rl} m \omega_r \lambda'_m (r_s \cos \phi_v - \omega_r L_q \sin \phi_v)}{r_s^2 + \omega_r^2 L_d L_q + \frac{3}{2} m^2 r_{rl} r_s + \frac{3}{4} r_{rl} \omega_r (L_d - L_q) m^2 \sin 2\phi_v} \quad (14.5-9)$$

Since (14.4-1) is only valid for rectifier currents greater than zero, it follows that (14.5-9) is only valid when it yields a dc supply voltage such that the rectifier current is positive. In the event that it is not, then the rectifier appears as an open-circuit, and all the diodes or thyristors are reverse biased. In this case, the average dc link current must be equal to zero. Thus, it follows from (14.4-14) that

$$\bar{I}_{qs}^r \cos \phi_v - \bar{I}_{ds}^r \sin \phi_v = 0 \quad (14.5-10)$$

Substitution of (14.5-7) and (14.5-8) into (14.5-10) yields

$$\bar{V}_{dc} \Big|_{\bar{I}_{dc}=0} = \frac{\omega_r \lambda'_m (r_s \cos \phi - \omega_r L_q \sin \phi_v)}{m \left( r_s + \frac{1}{2} \omega_r (L_d - L_q) \sin 2\phi_v \right)} \quad (14.5-11)$$

Thus, as long as (14.5-9) yields a positive rectifier current, it is a valid expression. In the event that (14.5-9) yields a negative rectifier current, (14.5-11) should be used.

The steady-state performance characteristics of a permanent-magnet ac motor drive are illustrated in Figure 14.5-1. Therein the dc inverter voltage, the peak amplitude of the fundamental component of stator current, defined by

$$\bar{I}_{spk} = \sqrt{\bar{I}_{qs}^r + \bar{I}_{ds}^r} \quad (14.5-12)$$

and the average electromagnetic torque are illustrated versus speed for the same parameters that were used in generating Figure 14.3-3. In this case, however, the machine is connected to a transformer rectifier such that  $v_{r0} = 35$  V and  $r_r = 3.0 \Omega$ . Superimposed on each characteristic is the trace that would be obtained if  $\bar{V}_{dc}$  were held constant (i.e., there was no voltage drop due to commutating inductance). As can be seen, the amplitude of the stator current, the electromagnetic torque, and dc voltage are all considerably reduced due to the voltage drop that occurs due to the commutating reactance, although the difference decreases with speed. It is interesting to observe that above 145 rad/s, the dc voltage increases. This is due to the fact that rectified machine voltage is greater than the voltage produced by the rectifier diodes, hence these diodes become reverse biased.

## 14.6. TRANSIENT AND DYNAMIC PERFORMANCE OF VOLTAGE-SOURCE INVERTER DRIVES

In this section, the transient (large disturbance) and dynamic (small disturbance) behavior of voltage-source inverter-based drives is examined. To this end, consider the drive system illustrated in Figure 14.2-1. The parameters for this drive system are  $E = 85.5$  V,

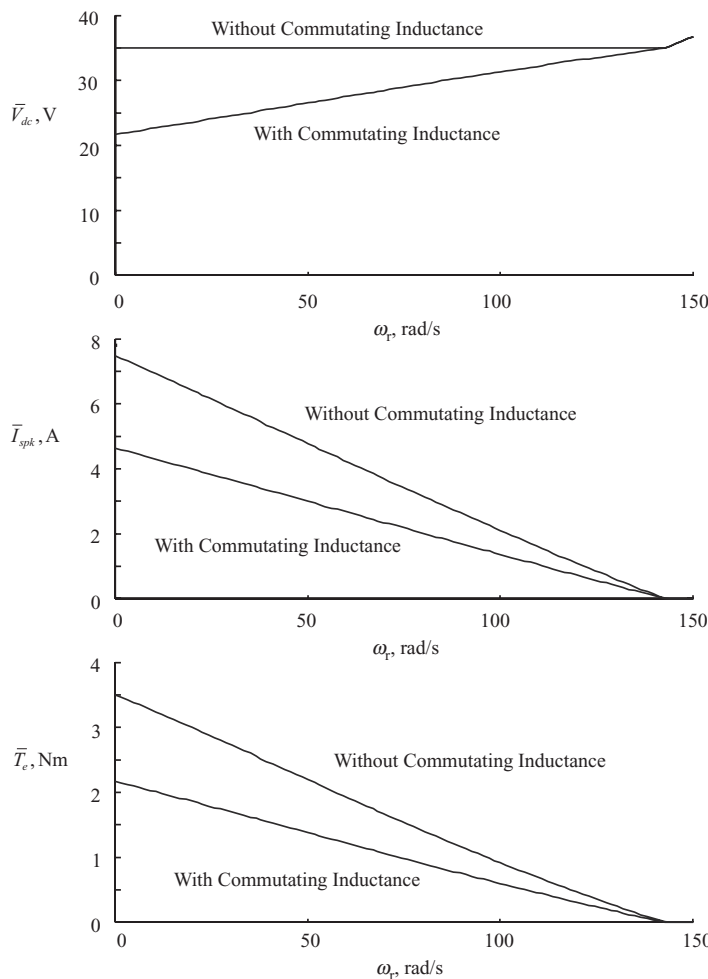
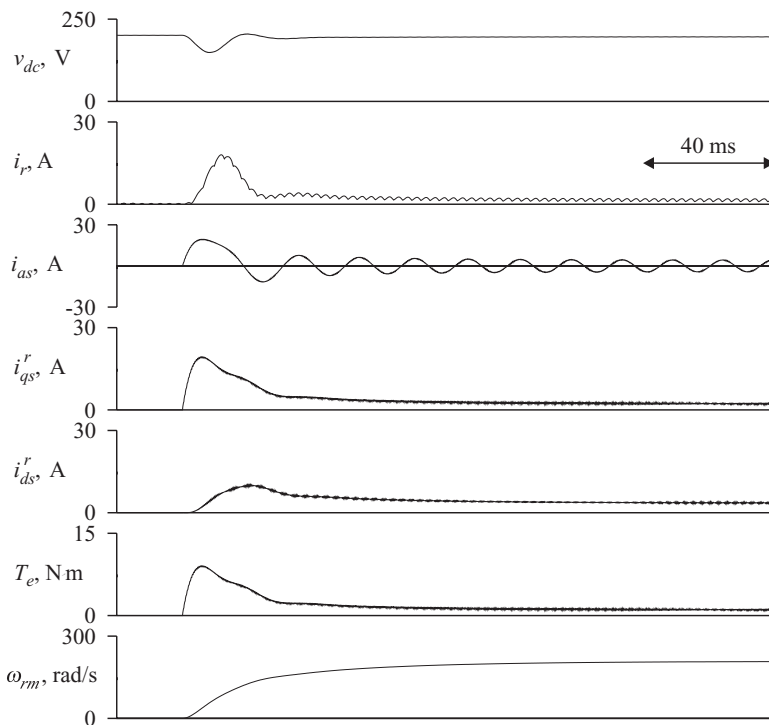


Figure 14.5-1. Steady-state voltage-source inverter-based permanent-magnet ac motor drive characteristics with and without commutating inductance.

$\omega_{eu} = 2\pi 60$  rad/s,  $L_c = 5$  mH,  $L_{dc} = 5$  mH, and  $C = 1000 \mu\text{F}$ . The rectifier is uncontrolled (diodes are used), and the inverter is sine-triangle modulated. The machine parameters are identical to those of the machine considered in Section 14.3, and the load torque is equal to  $0.005 \text{ N m s/rad}$  times the mechanical rotor speed.

Figure 14.6-1 illustrates the startup performance as the duty cycle is stepped from 0 to 0.9 as calculated by a waveform-level model in which the switching of each semiconductor is taken into account. As can be seen, there is a large inrush of current on startup since initially the impedance of the machine consists solely of the stator resistance, and since initially there is no back emf. This results in a large initial torque so the machine rapidly accelerates. Note that the large inrush current causes a significant drop in the dc voltage. Although the inrush current results in a large initial torque, this



**Figure 14.6-1.** Start-up performance of a sine-triangle-modulated permanent-magnet ac motor drive as calculated using a waveform-level model.

is generally an undesirable affect since the initial current is well over the rated current of the machine (3.68 A, peak). In addition, if provision is not made to avoid these overcurrents, then the inverter and rectifier will both have to be sized to insure that the semiconductors are not damaged. Since the cost of the semiconductors is roughly proportional to the voltage rating times the current rating, and since the overcurrent is five times rated current, the cost of the oversizing will be a fivefold increase in the cost of the semiconductors. Fortunately, by suitable control of the duty cycle, the overcurrent can be minimized.

It is interesting to compare the waveform-level portrayal of the drives start-up response to the portrayal predicted by the average-value model (14.4-21), which is illustrated in Figure 14.6-2. Comparing the two figures, it is evident that the average-value model captures the salient features of the start-up with the exception of the harmonics, which were neglected in the averaging procedure. In addition to being considerably easier to code, the computation time using the average-value representation is approximately 120 times faster than the computation time required by a detailed representation in which the switching of all the semiconductors is taken into account, making it an ideal formulation for control system analysis and synthesis.

Since many control algorithms are based on linear control theory, it is convenient to linearize the average-value model. Linearizing (14.4-21) yields

$$\begin{aligned}
 & P \begin{bmatrix} \Delta \hat{i}_r & \Delta \hat{v}_{dc} & \Delta \hat{i}_{st} & \Delta \hat{v}_{st} & \Delta \hat{i}_{qs}^r & \Delta \hat{i}_{ds}^r & \Delta \omega_r \end{bmatrix}^T = \\
 & \begin{bmatrix} -\frac{r_d}{L_{rl}} & -\frac{1}{L_{rl}} & 0 & 0 & 0 & 0 & 0 \\ \frac{1}{C_{dc}} & 0 & -\frac{1}{C_{dc}} & 0 & -\frac{3}{2} \frac{m_0}{C_{dc}} \cos \phi_{v0} & \frac{3}{2} \frac{m_0}{C_{dc}} \sin \phi_{v0} & 0 \\ 0 & \frac{1}{L_{st}} & -\frac{r_s}{L_{st}} & -\frac{1}{L_{st}} & 0 & 0 & 0 \\ 0 & 0 & \frac{1}{C_{st}} & 0 & 0 & 0 & 0 \\ 0 & \frac{m_0}{L_q} \cos \phi_{v0} & 0 & 0 & -\frac{r_s}{L_q} & -\frac{L_d}{L_q} \omega_{r0} & -\frac{L_d}{L_q} \bar{I}_{ds0}^r - \frac{\lambda'_m}{L_q} \\ 0 & -\frac{m_0}{L_d} \sin \phi_{v0} & 0 & 0 & +\frac{L_q}{L_d} \omega_{r0} & -\frac{r_s}{L_d} & \frac{L_d}{L_d} \bar{I}_{qs0}^r \\ 0 & 0 & 0 & 0 & \frac{3}{2} \left( \frac{P}{2} \right)^2 \frac{1}{J} (\lambda'_m + (L_d - L_q) \bar{I}_{ds0}^r) & \frac{3}{2} \left( \frac{P}{2} \right)^2 \frac{1}{J} (L_d - L_q) \bar{I}_{qs0}^r & 0 \end{bmatrix} \\
 & + \begin{bmatrix} \frac{v_{r0}}{L_{rl}} & \frac{\cos \alpha_0}{L_{rl}} & 0 & 0 & 0 & 0 & 0 \\ 0 & 0 & -\frac{3}{2} \frac{(\cos \phi_{v0} \bar{I}_{qs0}^r - \sin \phi_{v0} \bar{I}_{ds0}^r)}{C_{dc}} & \frac{3}{2} \frac{m_0 (\sin \phi_{v0} \bar{I}_{qs0}^r + \cos \phi_{v0} \bar{I}_{ds0}^r)}{C_{dc}} & 0 & 0 & 0 \\ 0 & 0 & 0 & 0 & 0 & 0 & 0 \\ 0 & 0 & 0 & 0 & 0 & 0 & 0 \\ 0 & 0 & \frac{\bar{V}_{dc0}}{L_q} \cos \phi_{v0} & -\frac{\bar{V}_{dc0} m_0}{L_q} \sin \phi_{v0} & 0 & 0 & 0 \\ 0 & 0 & -\frac{\bar{V}_{dc0}}{L_q} \sin \phi_{v0} & -\frac{\bar{V}_{dc0} m_0}{L_q} \cos \phi_{v0} & 0 & 0 & 0 \\ 0 & 0 & 0 & 0 & 0 & -\frac{P}{2} \frac{1}{J} & 0 \end{bmatrix} \begin{bmatrix} \Delta \hat{i}_r \\ \Delta \hat{v}_{dc} \\ \Delta \hat{i}_{st} \\ \Delta \hat{v}_{st} \\ \Delta \hat{i}_{qs}^r \\ \Delta \hat{i}_{ds}^r \\ \Delta \omega_r \end{bmatrix} \quad (14.6-1)
 \end{aligned}$$

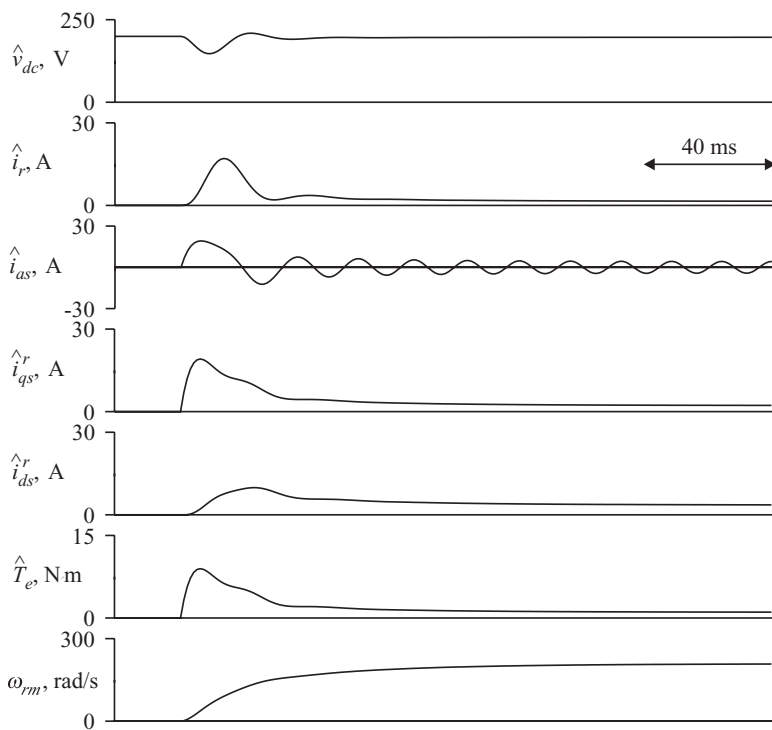
In (14.6-1), the addition of a subscript zero designates the initial equilibrium point about which the equations are linearized, and  $\Delta$  denotes a change in a variable. Thus

$$x = x_0 + \Delta x \quad (14.6-2)$$

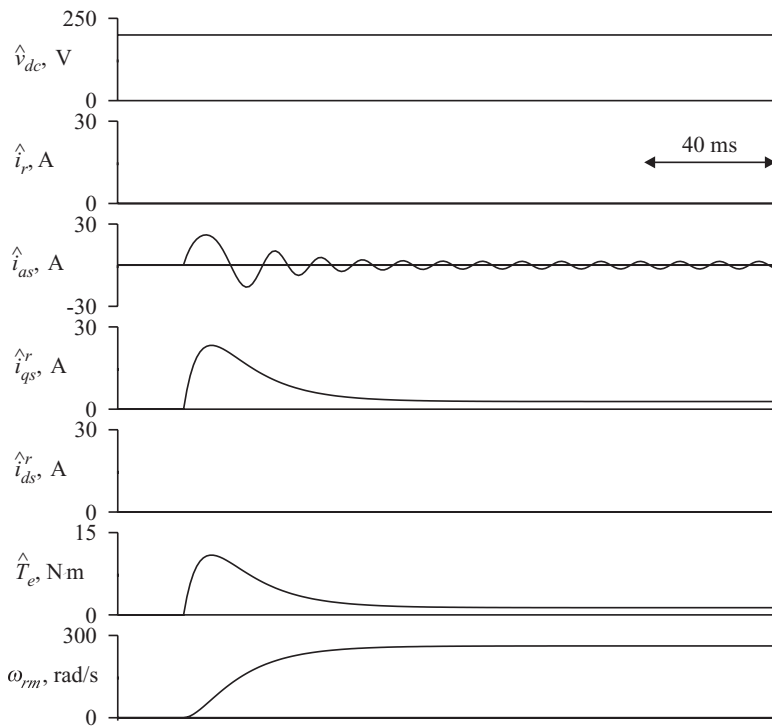
where  $x$  is any state, input variable, or output variable.

Figure 14.6-3 illustrates the startup response as predicted by the average-value model linearized about the initial operating point. In this figure, (14.6-2) has been used to determine each variable from its initial value and its excursion given by (14.6-1). As can be seen, there are many discrepancies between the prediction of the linearized model and the performance of the drive as illustrated in Figure 14.6-1. In particular, the linearized model does not predict any perturbation to the dc voltage or that there will be any rectifier current. In addition, the linearized model predicts a significantly higher  $q$ -axis current than is observed but fails to predict any  $d$ -axis current. The linearized model also significantly overestimates the peak torque and the final speed. Thus, this study illustrates the hazards involved in using the linearized model to predict large disturbance transients.

Although the linearized model cannot be used to predict large-signal transients, it can be used for dynamic analysis such as operating point stability. To illustrate this,



**Figure 14.6-2.** Start-up performance of a sine-triangle-modulated permanent-magnet ac motor drive as calculated using an average-value model.



**Figure 14.6-3.** Start-up performance of a sine-triangle-modulated permanent-magnet ac motor drive as calculated using a linearized model.

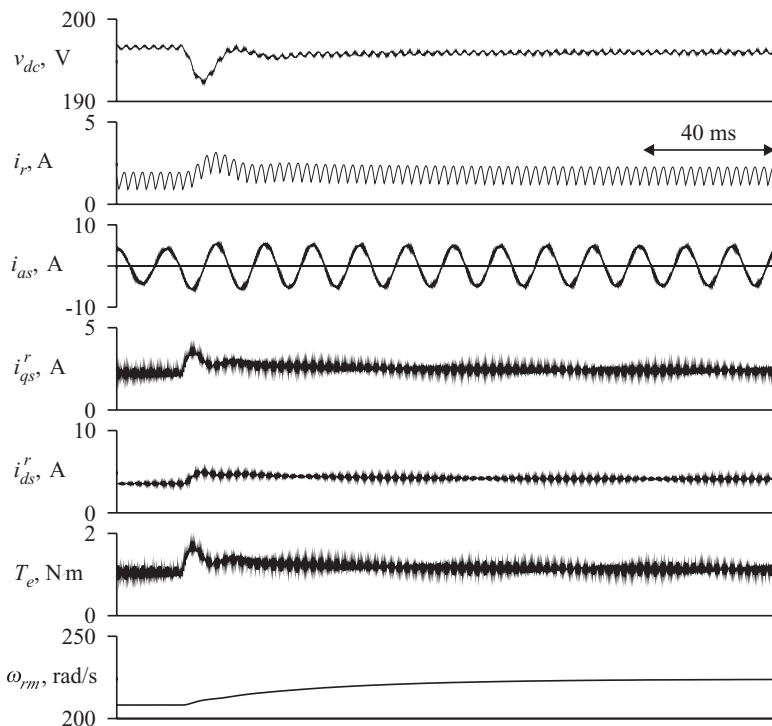


**Figure 14.6-4.** Response of a sine-triangle-modulated permanent-magnet ac motor drive to a step change in duty cycle as calculated using a waveform-level model.

Figure 14.6-4 and Figure 14.6-5 depict the performance of the drive as predicted by a waveform-level simulation and the linearized model (determined from the initial operating point) as the duty cycle is changed from 0.9 to 1. In this case, the linearized model accurately portrays the transient.

## 14.7. CASE STUDY: VOLTAGE-SOURCE INVERTER-BASED SPEED CONTROL

Now that the basic analytical tools to analyze voltage-source inverter based permanent-magnet ac motor drives have been set forth, it is appropriate to consider the use of these tools in control system synthesis. To this end, consider a sine-triangle modulated drive with the parameters listed in Table 14.7-1. It is desired to use this drive in order to achieve speed control of an inertial load. Design requirements are: (1) there shall be no steady-state error, and (2) the phase margin will be  $60^\circ$  when the drive is operated at the nominal operating speed of 200 rad/s (mechanical).

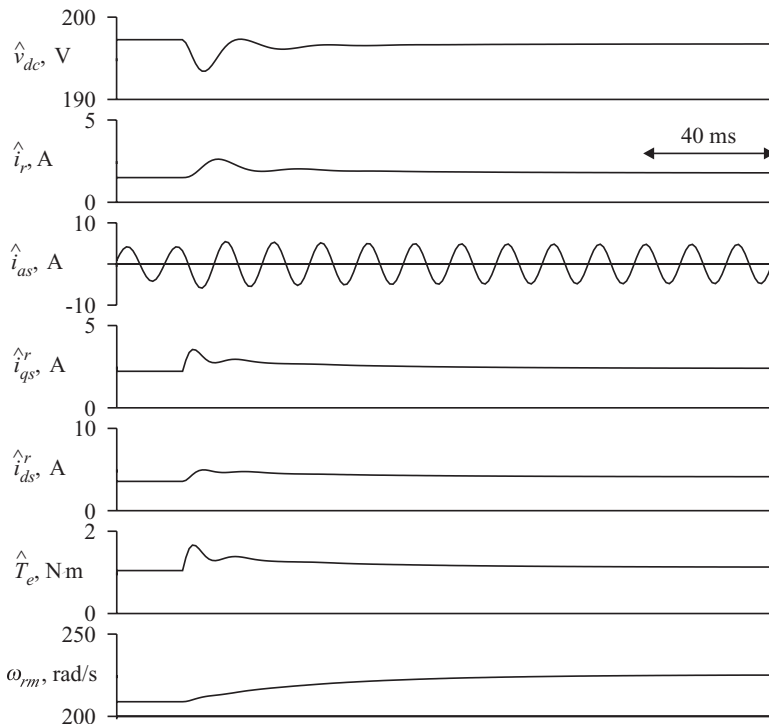


**Figure 14.6-5.** Response of a sine-triangle-modulated permanent-magnet ac motor drive to a step change in duty cycle as calculated using a linearized model.

TABLE 14.7-1. Drive System Parameters

$E$	85.5 V	$C_{dc}$	$1000 \mu\text{F}$	$L_d$	11.4 mH
$\omega_{eu}$	377 rad/s	$J$	$0.005 \text{ N}\cdot\text{ms}^2$	$\lambda'_m$	0.156 Vs
$L_c$	5 mH	$r_s$	2.98 $\Omega$	$P$	4
$L_{dc}$	5 mH	$L_q$	11.4 mH		

The design requirement of no steady-state error necessitates integral feedback. Thus, a proportional plus integral (PI) controller would be appropriate. A block diagram of this control in a system context is illustrated in Figure 14.7-1. In this figure, the  $s$  represents the time derivative operator in Laplace notation, which is typically used for control synthesis. In the time domain, the control law is of the form

$$d = K(\omega_{rm}^* - \omega_{rm}) + \frac{K}{\tau} \int (\omega_{rm}^* - \omega_{rm}) dt \quad (14.7-1)$$

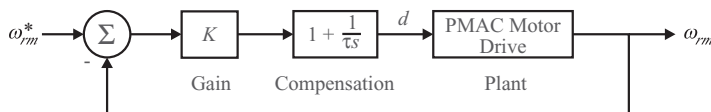


Figure 14.7-1. Speed control system.

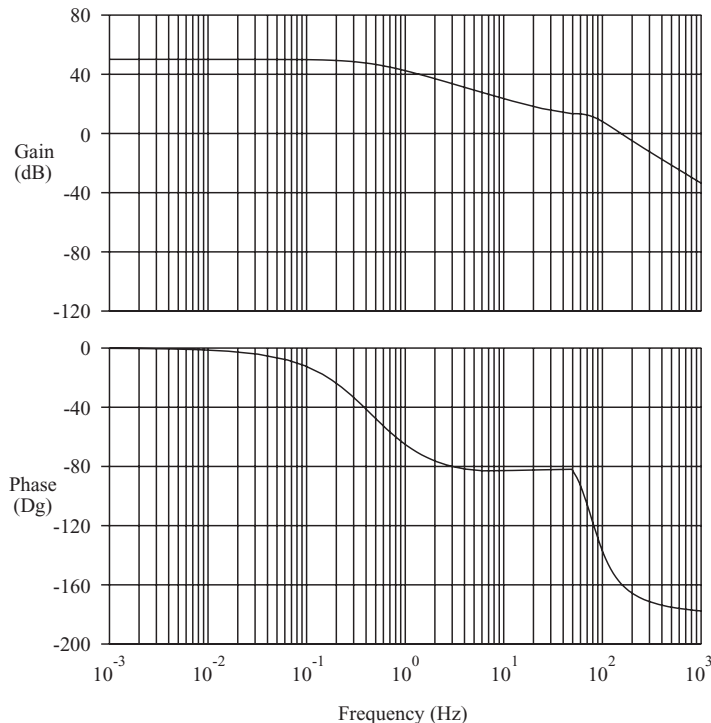


Figure 14.7-2. Frequency response of the open-loop permanent-magnet ac motor drive.

For the purpose of design, we will make use of a linearized model of the permanent-magnet ac motor drive, in which the system is linearized about at operating speed of 200 rad/s. The linearized model can either be calculated using (14.6-1), or it can be calculated by automatic linearization of a nonlinear average-value model, a feature common to many simulation languages.

Figure 14.7-2 illustrates the open-loop Bode plot of the permanent-magnet ac motor drive, wherein the output is the mechanical rotor speed and the input is the duty cycle. Since the Bode characteristic is based on a linearized model, strictly speaking, it is only valid about the operating point about which it was linearized (200 rad/s). From Figure 14.7-2, we see that although the gain margin is infinite, the phase margin is only 20°. A phase margin of 30° is often considered to be the minimum acceptable.

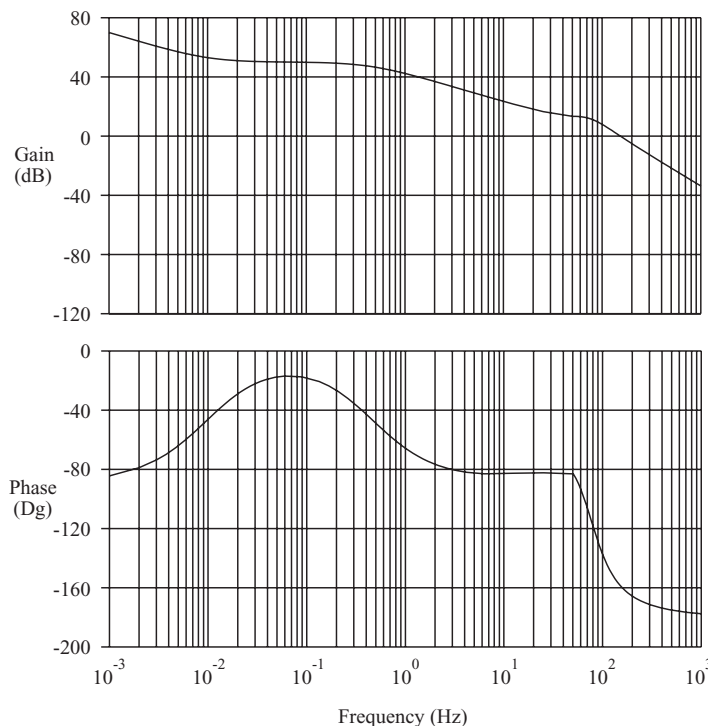
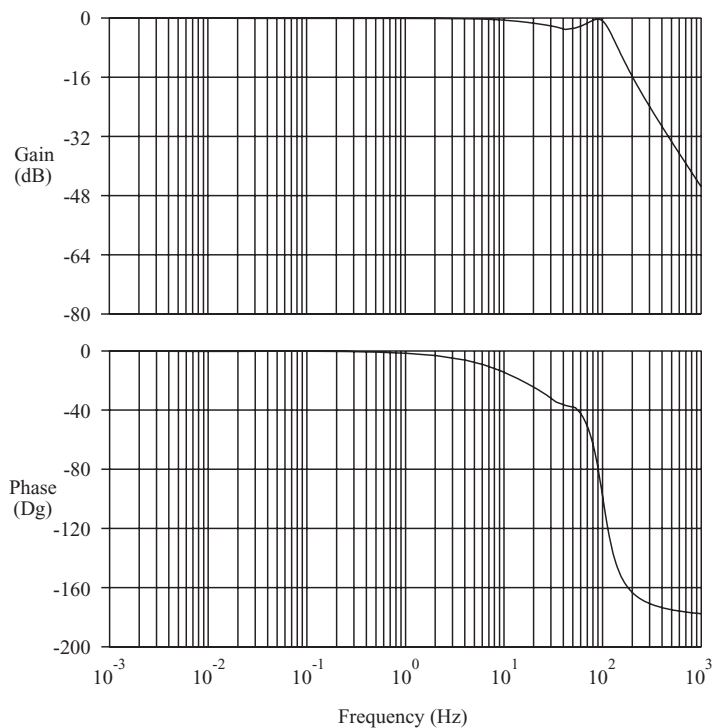


Figure 14.7-3. Frequency response of the compensated permanent-magnet ac motor drive.

The design process begins by selection of  $\tau$ . The integral feedback will decrease the phase by  $90^\circ$  at frequencies much less than  $1/(2\pi\tau)$ . Since this will decrease the already small phase margin, it is important to pick  $\tau$  so that the breakpoint frequency of the compensator is considerably less than the frequency at which the phase of the plant begins to decrease from zero. Selecting the breakpoint frequency of the compensator to be at 0.01 Hz yields  $\tau$  of 16 seconds.

The Bode characteristic of the compensated plant is depicted in Figure 14.7-3. As can be seen, the phase margin is still  $20^\circ$ . The next step is to select  $K$  so as to obtain the desired phase margin, which can be accomplished choosing the gain such that the phase at the gain crossover frequency is  $-120^\circ$ . From Figure 14.7-3, it can be seen that the phase of the compensated plant is  $-120^\circ$  when the gain of the compensated plant is 12 dB. Thus, choosing  $K = 0.25$  (-12 dB) will result in the desired phase margin.

Figure 14.7-4 illustrated the Bode characteristic of the closed-loop plant. As can be seen, the bandwidth of the system is on the order of 100 Hz, and the resonant peak is not overly pronounced. However, the closed-loop frequency response cannot be used as a sole judge of the systems performance since the actual system is nonlinear. For this, the simplest approach is to use a nonlinear average-value model. Figure



**Figure 14.7-4.** Frequency response of the closed-loop permanent-magnet ac motor drive.

14.7-5 illustrates the system performance during a step change in commanded speed from 0 to 200 rad/s. As can be seen, the transient performance in speed is quite well behaved. Nevertheless, the reader might be surprised by Figure 14.7-5 in several ways. First, it can be seen that the duty cycle, which is normally 0–1, is nearly 50 in the initial part of the study. Thus, the drive will be overmodulated and we can expect the current to exhibit considerable low-frequency harmonics on start-up (these are not apparent in Fig. 14.7-5 since an average-value model was used). Since the applied voltage was effectively much lower than expected, the bandwidth for this large disturbance is not nearly the 100 Hz indicated in Figure 14.7-4. Finally, the rated current for the machine in question is only 2.6 A, rms. Although the machine could probably withstand the temporary overcurrent, the inverter probably could not, and thus either the bandwidth should be reduced so as to alleviate the overcurrent or the duty cycle should be limited as a function of the current. Finally, close inspection reveals that at the end of the study, the speed is not 200 rad/s, and does not even appear to be rapidly increasing. This is because the bandwidth of the compensation was chosen to be quite low, and as a result, a small error in rotor speed will persist for some time, although it will eventually go to zero. A second design iteration in order to address these issues is left to the reader.

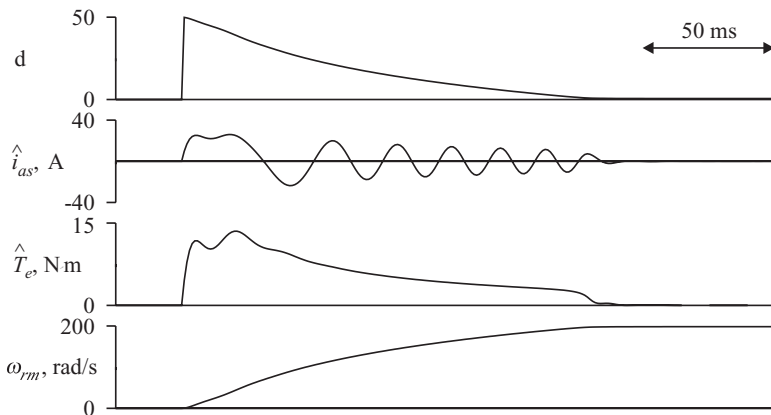


Figure 14.7-5. Start-up response of the closed-loop permanent-magnet ac motor drive.

## 14.8. CURRENT-REGULATED INVERTER DRIVES

Sections 14.1–14.7 explored the performance of drives in which the machine is controlled through suitable regulation of the applied voltages. In the remainder of this chapter, an alternate strategy is considered—control of the machine through the regulation of the stator currents. The hardware configuration for current-regulated inverter drives is identical to that of voltage-source inverter drives, as illustrated in Figure 14.2-1. The only difference is in the way in which the gate signals to the individual semiconductors are established.

Current-regulated inverters have several distinctive features. First, since torque is a function of the machine current, the torque may be controlled with the same bandwidth as to which the stator currents are controlled. In fact, it is often the case that for practical purposes, the torque control is essentially instantaneous. A second feature of current-regulated drives is that they are robust with regard to changes in machine parameters. For example, current-regulated drives are insensitive to parameter variations in the stator leakage inductance or the stator resistance. Current-regulated drives are also robust in regard to faults. In the event of a winding-to-winding short within the machine, the currents are automatically limited, which prevents damage to the inverter. The currents are also automatically limited during start-up.

Figure 14.8-1 illustrates the control of current-regulated drive. Therein, based on the commanded torque  $T_e^*$ , electrical rotor speed  $\omega_r$ , and the inverter voltage  $v_{dc}$ , the  $q$ - and  $d$ -axis current commands  $i_{qs}^*$  and  $i_{ds}^*$  are formulated. Using the inverse transformation, the corresponding  $abc$  variable current command  $i_{abc}^*$  is determined. Finally, based on the  $abc$  variable current command and the actual currents, the on and off status of each of the inverter semiconductors (T1–T6) is determined using hysteresis modulation as set forth in Section 12.8. An immediate question that arises is how the  $q$ - and

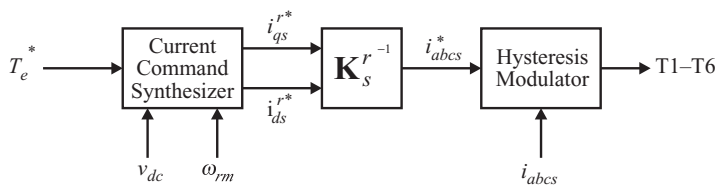


Figure 14.8-1. Hysteresis-modulated current-regulated drive control.

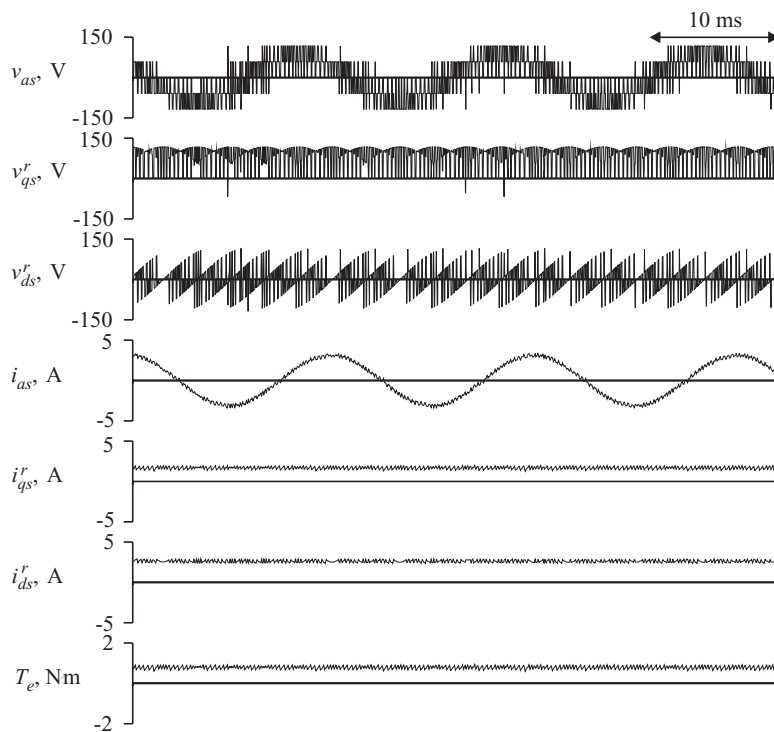


Figure 14.8-2. Steady-state performance of a hysteresis-modulated permanent-magnet ac motor drive.

*d*-axis current commands are generated to begin with; this question is addressed in detail in a following section. For the present, it suffices to say that the command is determined in such a way that if the commanded currents are obtained, the commanded torque will also be obtained.

Figure 14.8-2 illustrates the steady-state performance of a hysteresis modulated permanent-magnet ac motor drive. Therein the operating conditions are identical to

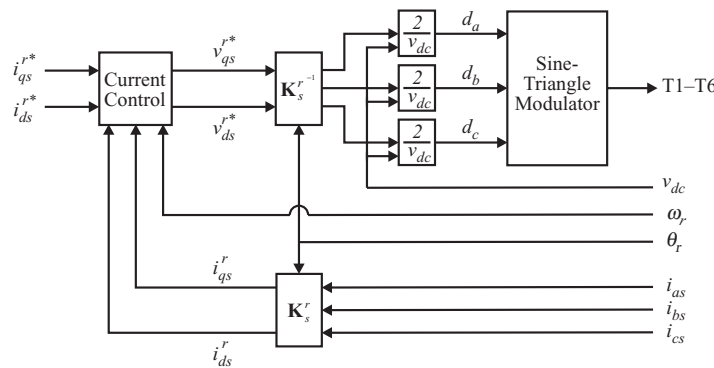


Figure 14.8-3. A sine-triangle-modulator based current regulator.

those portrayed in 14.3-5 except for the modulation strategy. The  $q$ - and  $d$ -axis current commands are set to 1.73 and 2.64 A, respectively, so that the fundamental component of the commanded current is identical to that in Figure 14.3-5. As can be seen, although the modulation strategies are different, the waveforms produced by the sine-triangle modulation and hysteresis modulation strategies are very similar.

A second method to implement a current-regulated inverter drive is to utilize a current-control loop on a voltage-source inverter drive. This is illustrated in Figure 14.8-3. Therein, the current command synthesizer serves the same function as in Figure 14.8-1. Based on the commanded  $q$ - and  $d$ -axis currents and the measured  $q$ - and  $d$ -axis currents (determined by transforming the measured  $abc$  variable currents), the  $q$ - and  $d$ -axis voltage commands ( $v_{qs}^*$  and  $v_{ds}^*$ ) are determined. The  $q$ - and  $d$ -axis voltage command is then converted to an  $abc$  variable voltage command  $v_{abc}^*$ , which is scaled in order to determine the instantaneous duty cycles  $d_a$ ,  $d_b$ , and  $d_c$  of the sine-triangle modulation strategy. Based on these duty cycles, T1-T6 are determined as described in Section 12.5. There are several methods of developing the current control, such as a synchronous current regulator [6]. An example of the design of a feedback linearization-based controller is considered in Example 14A.

**EXAMPLE 14A** Let us consider the design of a current regulator for a nonsalient permanent-magnet ac motor. The goal is to determine the  $q$ - and  $d$ -axis voltage command so that the actual currents become equal to the commanded currents. Let us attempt to accomplish this goal by specifying the voltage commands as

$$v_{qs}^* = \omega_r (L_{ss} i_{ds}^r + \lambda'_m) + \left( K_p + \frac{K_i}{s} \right) (i_{qs}^{r*} - i_{qs}^r) \quad (14A-1)$$

$$v_{ds}^{r*} = -\omega_r L_{ss} i_{qs}^{r*} + \left( K_p + \frac{K_i}{s} \right) (i_{ds}^{r*} - i_{ds}^r) \quad (14A-2)$$

where  $s$  denotes the Laplace operator. This control algorithm contains feedback terms that cancel the nonlinearities in the stator voltage equations, feedforward terms that cancel the effect of the back emf, and a PI control loop. Assuming that the actual  $q$ - and  $d$ -axis voltages are equal to the commanded  $q$ - and  $d$ -axis voltages, it can be shown that the transfer function between the commanded and actual  $q$ -axis currents is given by

$$\frac{i_{qs}^r(s)}{i_{qs}^{r*}(s)} = \frac{\frac{K_p}{L_{ss}} \left( s + \frac{K_i}{K_p} \right)}{s^2 + \frac{(r_s + K_p)}{L_{ss}} s + \frac{K_i}{L_{ss}}} \quad (14A-3)$$

The transfer function relating the  $d$ -axis current to the commanded  $d$ -axis current is identical. Assuming the same machine parameters as in the study illustrated in Figure

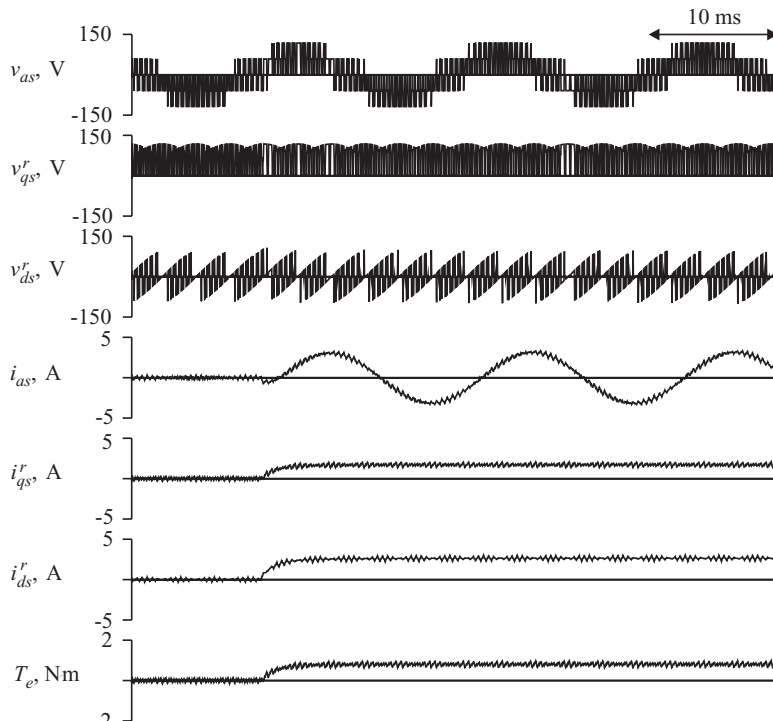


**Figure 14A-1.** Step response of a feedforward sine-triangle-modulated current-regulated permanent-magnet ac motor drive.

14.8-2, and selecting pole locations of  $s = -200$  and  $s = -2000$  (note that the poles may be arbitrarily placed), we have that

$$K_i = 2280 \Omega/\text{s} \quad (14\text{A}-4)$$

$$K_p = 10.7 \Omega \quad (14\text{A}-5)$$

Figure 14A-1 illustrates the response of the permanent-magnet ac drive as the current command is stepped from zero to  $i_{qs}^{r*} = 1.73$  A and  $i_{ds}^{r*} = 2.64$  A. All operating conditions are as in Figure 14.8-2. As can be seen, the machine performance is extremely well behaved and is dominated by the pole at  $s = -200$ .

## 14.9. VOLTAGE LIMITATIONS OF CURRENT-REGULATED INVERTER DRIVES

As alluded to previously, assuming that the current control loop is sufficiently fast, the current-regulated drive can be thought of as an ideal current source. However, there are some limitations on the validity of this approximation. In particular, eventually, the back emf of the machine will rise to the point where the inverter cannot achieve the current command due to the fact that the back emf of the machine becomes too large. Under such conditions, the machine is said to have lost current tracking.

In order to estimate the operating region over which current tracking is obtained, consider the case in which current tracking is obtained, that is

$$\hat{i}_{qs}^r = i_{qs}^{r*} \quad (14.9-1)$$

$$\hat{i}_{ds}^r = i_{ds}^{r*} \quad (14.9-2)$$

Substitution of (14.9-1) and (14.9-2) into the stator voltage equations and neglecting the stator dynamics

$$\hat{v}_{qs}^r = r_s \hat{i}_{qs}^r + \omega_r L_d \hat{i}_{ds}^r + \omega_r \lambda'_m \quad (14.9-3)$$

$$\hat{v}_{ds}^r = r_s \hat{i}_{ds}^r - \omega_r L_q \hat{i}_{qs}^r \quad (14.9-4)$$

Recall that the rms value of the fundamental component of the applied voltage is given by

$$v_s = \frac{1}{\sqrt{2}} \sqrt{(\hat{v}_{qs}^r)^2 + (\hat{v}_{ds}^r)^2} \quad (14.9-5)$$

Substitution of (14.9-3) and (14.9-4) into (14.9-5) yields

$$v_s = \frac{1}{\sqrt{2}} \sqrt{(r_s i_{qs}^{r*} + \omega_r L_d i_{ds}^{r*} + \lambda'_m \omega_r)^2 + (r_s i_{ds}^{r*} - \omega_r L_q i_{qs}^{r*})^2} \quad (14.9-6)$$

Recall from Section 12.8 that for the hysteresis-controlled current-regulated inverters, the maximum rms value of the fundamental component of the applied voltage that can be obtained without low-frequency harmonics is given by

$$v_s = \frac{1}{\sqrt{6}} \hat{v}_{dc} \quad (14.9-7)$$

If low-frequency harmonics are tolerable, and a synchronous regulator is used, then the maximum RMS value of the fundamental component becomes

$$v_s = \frac{\sqrt{2}}{\pi} \hat{v}_{dc} \quad (14.9-8)$$

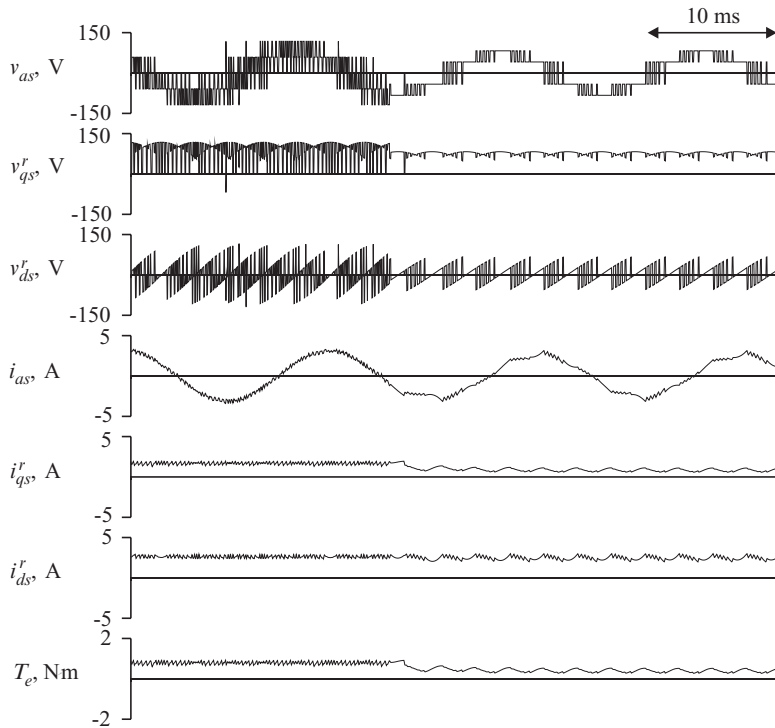
In the event that for a given current command and speed (14.9-8) cannot be satisfied, then it is not possible to obtain stator currents equal to the commanded current. If (14.9-8) can be satisfied, but (14.9-7) cannot be satisfied, then it is possible to obtain stator current that have the same fundamental component as the commanded currents provided that integral feedback in the rotor reference frame is present to drive the current error to zero; however, low-frequency harmonics will be present.

Figure 14.9-1 illustrates the effects of loss of current tracking. Initially, operating conditions are identical to those portrayed in Figure 14.8-2. However, approximately 20 ms into the study, the dc inverter voltage is stepped from 177 to 124 V, which results in a loss of current tracking. As can be seen, the switching of the hysteresis modulator is such that some compensation takes place; nevertheless, current tracking is lost. As a result, harmonics appear in the  $a$ -phase and  $q$ - and  $d$ -axis current waveforms, as well as in the electromagnetic torque.

## 14.10. CURRENT COMMAND SYNTHESIS

It is now appropriate to address the question as to how to determine the current command. Normally, when using a current-regulated inverter, the input to the controller is a torque command. Thus, the problem may be reformulated as the determination of the current command from the torque command. To answer this question, let us first consider a nonsalient machine in which  $L_{ss} \triangleq L_q = L_d$ . In this case, torque may be expressed as

$$T_e = \frac{3}{2} \frac{P}{2} \lambda'_m i_{qs}^r \quad (14.10-1)$$



**Figure 14.9-1.** Response of hysteresis-modulated current-regulated permanent-magnet ac motor drive to step decrease in dc inverter voltage.

Therefore, the commanded  $q$ -axis current may be expressed in terms of the commanded torque as

$$i_{qs}^{r*} = \frac{2}{3} \frac{2}{P} \frac{1}{\lambda'_m} T_e^* \quad (14.10-2)$$

Clearly, if the desired torque is to be obtained, then (14.10-2) must be satisfied. The  $d$ -axis current does not effect average torque, and so its selection is somewhat arbitrary. Since  $d$ -axis current does not affect the electromagnetic torque, but does result in additional stator losses, the  $d$ -axis current is often selected to be zero, that is,

$$i_{ds}^{r*} = 0 \quad (14.10-3)$$

This selection of  $d$ -axis current minimizes the current amplitude into the machine, thus maximizing torque per amp, and at the same time maximizes the efficiency of the machine by minimizing the stator resistive losses.

Although (14.10-3) has several distinct advantages, there is one reason to command a nonzero  $d$ -axis current. To see this, consider (14.9-6) for the nonsalient case:

$$v_s = \frac{1}{\sqrt{2}} \sqrt{(r_s i_{qs}^{r*} + \omega_r L_{ss} i_{ds}^{r*} + \lambda'_m \omega_r)^2 + (r_s i_{ds}^{r*} - \omega_r L_{ss} i_{qs}^{r*})^2} \quad (14.10-4)$$

From (14.10-4), we see that the required inverter voltage goes up with either speed or  $q$ -axis current (which is proportional to torque). However, examining the first squared term in (14.10-4), it can be seen that at positive speeds, the required inverter voltage can be reduced by injecting negative  $d$ -axis current. In fact, by solving (14.10-4) for  $d$ -axis current in terms of the  $q$ -axis current command and speed, we have that

$$i_{ds}^{r*} = \frac{-\lambda'_m L_{ss} \omega_r^2 + \sqrt{2z^2 v_s^2 - (r_s \omega_r \lambda'_m + z^2 i_{qs}^{r*})^2}}{z^2} \quad (14.10-5)$$

where

$$z = \sqrt{r_s^2 + \omega_r^2 L_{ss}^2} \quad (14.10-6)$$

Thus, a logical current control strategy is to command zero  $d$ -axis current as long as the inverter voltage requirements are not exceeded, and to inject the amount of  $d$ -axis current specified by (14.10-5) if they are. Note that there are limitations on  $d$ -axis current injection in that (1) (14.10-5) may not have a solution, (2) excessive  $d$ -axis current injection may result in demagnetization of the permanent magnet, and (3) excessive  $d$ -axis current injection can result in exceeding the current limit of the machine or inverter. In addition, the use of (14.10-5) requires accurate knowledge of the dc inverter voltage (to determine the peak  $v_s$ ), the rotor speed, and all of the machine parameters. A means of implementing such a control without knowledge of the dc inverter voltage, speed, and machine parameters is set forth in Reference 7.

The process for determining the current command in salient machines, which typically are constructed using buried magnet technology, is somewhat more involved than in the nonsalient case. Let us first consider the problem of computing the  $q$ - and  $d$ -axis current commands so as to maximize torque-per-amp performance. In the case of the nonsalient machine, from Chapter 4, the expression for electromagnetic torque is given by

$$T_e = \frac{3}{2} \frac{P}{2} (\lambda'_m i_{qs}^r + (L_d - L_q) i_{qs}^r i_{ds}^r) \quad (14.10-7)$$

Solving (14.10-7) for  $d$ -axis current command in terms of the  $q$ -axis current command and in terms of the commanded torque yields

$$i_{ds}^{r*} = \frac{4T_e}{3P(L_d - L_q)} \frac{1}{i_{qs}^{r*}} - \frac{\lambda'_m}{L_d - L_q} \quad (14.10-8)$$

In terms of the  $qd$  commanded currents, the rms value of the fundamental component of the commanded current is given by

$$i_s = \frac{1}{\sqrt{2}} \sqrt{(i_{qs}^{r*})^2 + (i_{ds}^{r*})^2} \quad (14.10-9)$$

Substitution of (14.10-8) into (14.10-9) yields an expression for the magnitude of the stator current in terms of the commanded torque and  $q$ -axis current. Setting the derivative of the resulting expression with respect to the  $q$ -axis current command equal to zero gives the following transcendental expression for the  $q$ -axis current command that maximizes torque per amp:

$$(i_{qs}^{r*})^4 + \frac{4T_e \lambda'_m i_{qs}^{r*}}{3P(L_d - L_q)^2} - \left( \frac{4T_e}{3P(L_d - L_q)} \right)^2 = 0 \quad (14.10-10)$$

Once the  $q$ -axis current command is determined by solving (14.10-10), the  $d$ -axis current command may be found by solving (14.10-8). From the form of (14.10-10), it is apparent that the solution of for the  $q$ -axis current must be accomplished numerically. For this reason, when implementing this control with a microprocessor, the  $q$ - and  $d$ -axis current commands are often formulated through a look-up table that has been constructed through offline solution to (14.10-8) and (14.10-10).

Once the  $q$ - and  $d$ -axis current commands have been formulated, it is necessary to check whether or not the inverter is capable of producing the required voltage. If it is not, it is necessary to recalculate the commanded  $q$ - and  $d$ -axis currents such that the required inverter voltage does not exceed that obtainable by the converter. This calculation can be conducted by solving (14.9-6) and (14.10-8) simultaneously for the  $q$ - and  $d$ -axis current command.

Figure 14.10-1 illustrates the graphical interpretation of the selection of the commanded  $q$ - and  $d$ -axis currents for a machine in which  $r = 0.2 \Omega$ ,  $L_q = 20 \text{ mH}$ ,  $L_d = 10 \text{ mH}$ , and  $\lambda'_m = 0.07 \text{ Vs}$ . The machine is operating at a speed of 500 rad/s (electrical) and  $v_s = 50 \text{ V}$ . Illustrated therein are the trajectory of the maximum torque-per-amp characteristic, the loci of points in the  $qd$  plane at which the electromagnetic torque of 5 Nm is obtained, and the loci of points representing the voltage limit imposed by (14.10-4). For a given electromagnetic torque command, the  $q$ - and  $d$ -axis current command is formulated using the maximum torque-per-amp trajectory, provided this point is inside the voltage limit. However,  $q$ - and  $d$ -axis currents on this trajectory corresponding to torques greater than that obtainable at Point A cannot be achieved. Suppose a torque of 5 Nm is desired. Point B represents the point on the maximum torque-per-amp trajectory, which has the desired torque. Unfortunately, Point B is well outside of the limit imposed by the available voltage. However, any point on the constant torque locus will satisfy the desired torque. Thus, in this case, the current command is chosen to correspond to Point C.

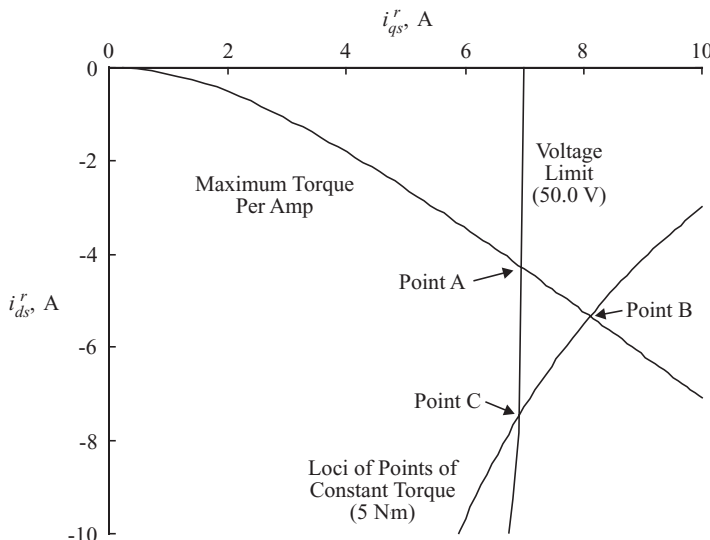


Figure 14.10-1. Selection of  $q$ - and  $d$ -axis currents.

## 14.11. AVERAGE-VALUE MODELING OF CURRENT-REGULATED INVERTER DRIVES

In this section, an average-value model of the current-regulated inverter drive is formulated in much the same way as the average-value model of the voltage-source inverter drive. Since the topology of the rectifier and inverter are the same, it follows that the expressions for the time derivatives of the rectifier current, the dc link voltage, the stabilizing filter current, and the stabilizing filter voltage given by (14.4-7) and (14.4-10)–(14.4-12) are valid. Furthermore, the change in control strategy does not affect the mechanical dynamics, thus (14.4-19) and (14.4-20) may still be used to represent the machine. However, the change in control strategy will change the formulation of the expression for the dc link currents, the stator dynamics, and the expression for electromagnetic torque.

In order to formulate an expression for the dc link current, it is convenient to assume that the actual machine currents are equal to the commanded machine currents, whereupon

$$\hat{i}_{qs}^r = i_{qs}^{r*} \quad (14.11-1)$$

$$\hat{i}_{ds}^r = i_{ds}^{r*} \quad (14.11-2)$$

Of course, this assumption is only valid when the dc link voltage is such that the desired current is actually obtained. An average-value model of a permanent-magnet ac motor drive in which current tracking is not obtained is set forth in Reference 8. Assuming that the actual currents are equal to the commanded currents, the stator currents are no longer state variables. Neglecting the stator dynamics, the  $q$ - and  $d$ - axis voltages may be expressed as

$$\hat{v}_{qs}^r = r_s i_{qs}^{r*} + \omega_r L_d i_{ds}^{r*} + \lambda'_m \omega_r \quad (14.11-3)$$

$$\hat{v}_{ds}^r = r_s i_{ds}^{r*} - \omega_r L_q i_{qs}^{r*} \quad (14.11-4)$$

The instantaneous power into the machine is given by

$$P = \frac{3}{2} [r_s (i_{qs}^{r*} + i_{ds}^{r*})^2 + \omega_r (L_d - L_q) i_{qs}^{r*} i_{ds}^{r*} + \omega_r \lambda'_m i_{qs}^r] \quad (14.11-5)$$

Assuming that no power is lost into the inverter, it follows that the dc link current is given by

$$\hat{i}_{dc} = \frac{P}{\hat{v}_{dc}} \quad (14.11-6)$$

Combining (14.11-5) with (14.11-6) yields

$$\hat{i}_{dc} = \frac{3}{2} \frac{1}{\hat{v}_{dc}} [r_s (i_{qs}^{r*} + i_{ds}^{r*})^2 + \omega_r (L_d - L_q) i_{qs}^{r*} i_{ds}^{r*} + \omega_r \lambda'_m i_{qs}^{r*}] \quad (14.11-7)$$

The other expression affected by the change from a voltage-source inverter to a current-regulated inverter will be the expression for torque. In particular, from (14.4-17) and again assuming that the actual stator currents are equal to the commanded currents

$$T_e = \frac{3}{2} \frac{P}{2} (\lambda'_m i_{qs}^{r*} + (L_d - L_q) i_{qs}^{r*} i_{ds}^{r*}) \quad (14.11-8)$$

As can be seen from (14.11-8), if it is assumed that the actual currents are equal to the commanded currents, then any desired torque may be instantaneously obtained.

Combining (14.4-7), (14.4-10)–(14.4-12), (14.4-19), (14.11-7), and (14.11-8) yields

$$\begin{aligned}
 p \begin{bmatrix} \hat{i}_r \\ \hat{v}_{dc} \\ \hat{i}_{st} \\ \hat{v}_{st} \\ \omega_r \end{bmatrix} = & \begin{bmatrix} -\frac{r_{rl}}{L_{rl}} & -\frac{1}{L_{rl}} & 0 & 0 & 0 \\ \frac{1}{C_{dc}} & 0 & -\frac{1}{C_{dc}} & 0 & 0 \\ 0 & \frac{1}{L_{st}} & -\frac{r_{st}}{L_{st}} & -\frac{1}{L_{st}} & 0 \\ 0 & 0 & \frac{1}{C_{st}} & 0 & 0 \\ 0 & 0 & 0 & 0 & 0 \end{bmatrix} \begin{bmatrix} \hat{i}_r \\ \hat{v}_{dc} \\ \hat{i}_{st} \\ \hat{v}_{st} \\ \omega_r \end{bmatrix} \\
 & + \begin{bmatrix} \frac{v_{r0} \cos \alpha}{L_{rl}} \\ -\frac{1}{C_{dc}} \frac{3}{2} \frac{1}{\hat{v}_{dc}} [r_s (i_{qs}^{r*} + i_{ds}^{r*})^2 + \omega_r (L_d - L_q) i_{qs}^{r*} i_{ds}^{r*} + \omega_r \lambda'_m i_{qs}^{r*}] \\ 0 \\ 0 \\ \frac{P}{2} \frac{1}{J} \left[ \frac{3}{2} \frac{P}{2} (\lambda'_m i_{qs}^{r*} + (L_d - L_q) i_{qs}^{r*} i_{ds}^{r*}) - T_L \right] \end{bmatrix} \quad (14.11-9)
 \end{aligned}$$

## 14.12. CASE STUDY: CURRENT-REGULATED INVERTER-BASED SPEED CONTROLLER

The control of current-regulated inverter drives is considerably simpler than for their voltage-source-based counterparts, due to the fact that when designing the speed or position control algorithms, the inverter and machine act as a nearly ideal torque transducer (neglecting the stator dynamics of the machine). To illustrate this, let us reconsider the speed control system discussed in Section 14.7. Assuming that a current command synthesizer and current regulator can be designed with sufficiently high bandwidth, the speed control algorithm may be designed by assuming that the drive will produce an electromagnetic torque equal to the desired torque, therefore

$$T_e = T_e^* \quad (14.12-1)$$

In order to ensure that there will be no steady-state error, let us consider a PI control law in accordance with

$$T_e^* = K_p \left( 1 + \frac{1}{\tau_s} \right) (\omega_{rm}^* - \omega_{rm}) \quad (14.12-2)$$

wherein  $\omega_{rm}^*$  represents the speed command. Combining (14.12-1), (14.12-2), and the inertial mechanical dynamics of the drive, it can be shown that the resulting transfer function between the actual and commanded rotor speed is given by

$$\frac{\omega_{rm}}{\omega_{rm}^*} = \frac{K(\tau s + 1)}{J\tau s^2 + K\tau s + K} \quad (14.12-3)$$

Since (14.12-3) is a second-order system and there are two free parameters, the poles of (14.12-3) may be arbitrarily placed. However, some restraint should be exercised since it is important that the current regulator be much faster than the mechanical system if (14.12-1) and hence (14.12-3) are valid. Placing the poles at  $s = -5$  and  $s = -50$  yields  $K = 0.257 \text{ N m s/rad}$  and  $\tau = 0.22 \text{ second}$ . The pole at  $s = -5$  will dominate the response.

In order to complete the design, a current command synthesizer (to determine what the current command should be to achieve the desired torque) and a current regulation control strategy need be designed. For this example, let us assume a simple current command synthesizer in which all of the current is injected into the  $q$ -axis, and let us use the sine-triangle-modulated voltage-source inverter based current regulator set forth in Example 14A as a current regulator. Recall that the poles of the current regulator are at  $s = -200$  and  $s = -1000$ , which are much faster than those of the mechanical system.

Practically speaking, there are two important refinements that can be made to this control system. First, the  $q$ -axis current command generated by the current command synthesizer should be limited to  $\pm 3.68$  A in order to limit the current to the rated value of the machine. However, limiting the  $q$ -axis current command may cause the integrator in the speed control to wind up. For this reason, the contribution of the  $K/(\tau_s)$  portion of the speed control (that is the integral portion of the control) should be limited to avoid excessive windup. Herein, the portion of the torque command contributed by the integral term will be limited to 0.861 Nm, which is 50% of the torque, which would be obtained if the  $q$ -axis current command is at its maximum value. This value is obtained so that the overshoot for worst-case conditions is limited to an acceptable value (some iteration using time-domain simulations would be used to determine the exact number).

Figure 14.12-1 illustrates the interactions of the various controllers. Based on the speed error, the PI speed control determines a torque command  $T_e^*$  (the limit on the integral feedback is not shown). Then the current command synthesizer determines

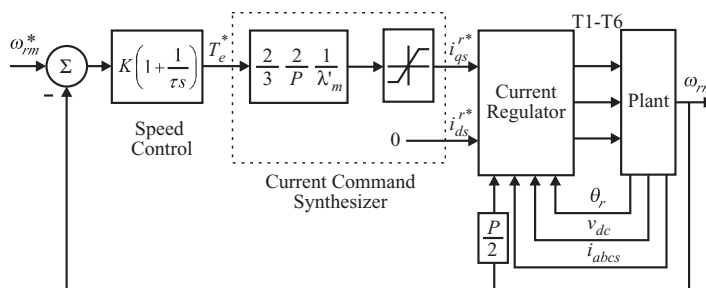


Figure 14.12-1. Current-regulated-inverter based speed control

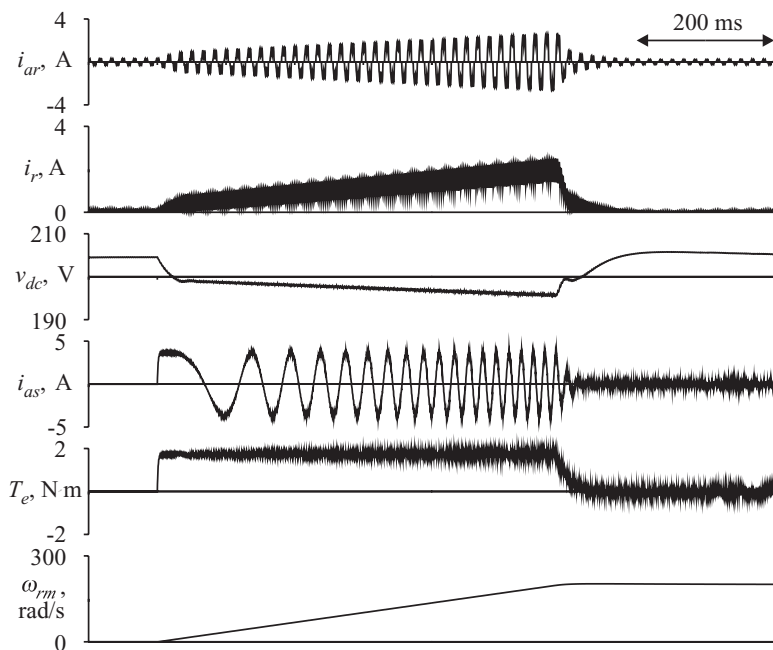


Figure 14.12-2. Start-up response of current-regulated-inverter based speed control system.

the  $q$ -axis current required to obtain the desired torque, subject to the  $q$ -axis current limit. In this controller, the  $d$ -axis current is set to zero. Based on the commanded  $q$ - and  $d$ -axis currents, the electrical rotor speed, the actual currents, and the dc supply voltage, the current regulator determines the on or off status of each of the semiconductors in the inverter (T1–T6).

Figure 14.12-2 illustrates the performance of the speed control system. Initially, the system is in the steady state. However, 50 ms into the study, the speed command is stepped from 0 to 200 rad/s. As can be seen, the torque command immediately jumps to the value that corresponds to the maximum  $q$ -axis current command. Since the electromagnetic torque is constant, the speed increases linearly with time. As can be seen, the magnitude of the ac current into the rectifier and the dc rectifier current both increase linearly with speed. This is due to the fact that the power going into the machine increases linearly with speed. The increasing rectifier current results in a dc link voltage that decreases linearly with time. Note that the dc link voltage initially undergoes a sudden dip of 5 V since the rectifier was initially under no-load condition, and hence it charged the dc link capacitor to peak rather than the average value of the rectifier voltage. Eventually, the machine reaches the desired speed. At this point, the torque command falls off since the load is inertial. As a result, the electromagnetic torque, stator current, and rectifier current all decrease to their original values, and the dc link voltage increases to its original value.

Comparing Figure 14.12-2 with Figure 14.7-5, the reader will observe that the current-regulated inverter based speed control system is considerably more sluggish than the voltage-source inverter based speed control system. However, this is a result of the fact that the machine currents in the current-regulated inverter based system did not exceed the current limits of the machine. In fact, the current-regulated inverter based system brought the machine to speed as fast as possible subject to the limitation of the stator current.

## REFERENCES

- [1] P.L. Chapman, S.D. Sudhoff, and C. Whitcomb, "Multiple Reference Frame Analysis of Non-Sinusoidal Brushless DC Drives," *IEEE Trans. Energy Conversion*, Vol. 14, No. 3, September 1999, pp. 440–446.
- [2] P.L. Chapman, S.D. Sudhoff, and C.A. Whitcomb, "Optimal Current Control Strategies for Non-Sinusoidal Permanent-Magnet Synchronous Machine Drives," *IEEE Trans. Energy Conversion*, Vol. 14, No. 3, December 1999, pp. 1043–1050.
- [3] P.L. Chapman and S.D. Sudhoff, "A Multiple Reference Frame Synchronous Estimator/Regulator," *IEEE Trans. Energy Conversion*, Vol. 15, No. 2, June 2000, pp. 197–202.
- [4] H.G. Yeo, C.S. Hong, J.Y. Yoo, H.G. Jang, Y.D. Bae, and Y.S. Park, "Sensorless Drive for Interior Permanent Magnet Brushless DC motors," IEEE International Electric Machines and Drives Conference Record, May 18–21, 1997, pp. TD1-3.1-4.3.
- [5] K.A. Corzine and S.D. Sudhoff, "A Hybrid Observer for High Performance Brushless DC Drives," *IEEE Trans. Energy Conversion*, Vol. 11, No. 2, June 1996, pp. 318–323.
- [6] T.M. Rowan and R.J. Kerkman, "A New Synchronous Current Regulator and an Analysis of Current-Regulated Inverters," *IEEE Trans. Industry Applications*, Vol. IA-22, No. 4, 1986, pp. 678–690.
- [7] S.D. Sudhoff, K.A. Corzine, and H.J. Hegner, "A Flux-Weakening Strategy for Current-Regulated Surface-Mounted Permanent-Magnet Machine Drives," *IEEE Trans. Energy Conversion*, Vol. 10, No. 3, September 1995, pp. 431–437.
- [8] K.A. Corzine, S.D. Sudhoff, and H.J. Hegner, "Analysis of a Current-Regulated Brushless DC Drive," *IEEE Trans. Energy Conversion*, Vol. 10, No. 3, September 1995, pp. 438–445.

## PROBLEMS

1. Consider the permanent-magnet ac motor drive whose characteristics are depicted in Figure 14.5-1. Plot the characteristics if  $\phi_v = \text{atan}(\omega_s L_{ss}/r_s)$ .
2. Consider the drive system whose parameters are given in Table 14.7-1. If  $\phi_v = 0$ , compute the turns ratio of the transformer with the minimum secondary voltage which would be required if the drive is to supply a 1.72 Nm load at a mechanical rotor speed of 200 rad/s. Assume that the primary of the transformer is connected to a 230 V source (rms, line-to-line) and that the effective series leakage reactance will be 0.05 pu. Further assume that the VA rating of the transformer is 1.5 times the mechanical output power.

3. Consider the speed control system considered in Section 14.8. Plot the closed-loop frequency response of the system about a nominal operating speed of 20 rad/s (mechanical).
4. Consider the speed-control system considered in Section 14.8. Estimate the bandwidth of the closed-loop plant that could be designed if the current is to be restricted to the rated value of 2.6 A, rms.
5. Assuming that the drive discussed in Example 14A is operating at an electrical rotor speed of 200 rad/s, compute the pole locations if the linearizing feedback terms are not used in making up the command voltages.
6. Consider a current-regulated buried permanent-magnet ac motor drive in which stator resistances is negligible. Sketch the locus of obtainable  $q$ - and  $d$ -axis currents in terms of the maximum fundamental component of the applied voltage, the electrical rotor speed, the  $q$ - and  $d$ -axis inductances, and  $\lambda'_m$ .
7. A four-pole permanent-magnet ac motor drive has the following parameters:  $r_s = 0.3 \Omega$ ,  $L_{ss} = 20 \text{ mH}$ , and  $\lambda'_m = 0.2 \text{ Vs}$ . The machine is to deliver 10 Nm at a mechanical rotor speed of 200 rad/s. Compute the  $q$ - and  $d$ -axis current commands such that the power factor is maximized. What is the rms voltage and current applied to the machine, and what is the efficiency?
8. Repeat Problem 7, except choose the current command so as to minimize the required dc voltage.
9. Repeat Problem 7, except choose the current command so as to minimize the commanded current.
10. Compute the locations of Points A, B, and C on Figure 14.10-1.

---

# INTRODUCTION TO THE DESIGN OF ELECTRIC MACHINERY

---

## 15.1. INTRODUCTION

The majority of this text concerns the analysis of electric machinery and drive systems. The focus of this chapter is the use of these concepts for design. In particular, the design of a permanent-magnet ac machine is considered. In doing this, the prevalent design approach based on design rules coupled with detailed numerical analysis and manual design iteration is not used. Instead, the machine design problem is posed in a rigorous way as a formal mathematical optimization problem, as in References 1–3.

The reader is forewarned that the approach has been simplified. Structural issues, thermal issues, and several loss mechanisms are neglected, and infinitely permeable magnetic steel is assumed, though saturation is considered. Even so, the design problem is nontrivial and provides an organized and systematic approach to machine design. This approach may be readily extended to include a wide variety of design considerations.

The machine design problem is made easier if given context. To this end, our problem is to design a three-phase, wye-connected, permanent-magnet ac machine to produce a desired torque  $T_e^*$  at a desired mechanical speed  $\omega_{rm}^*$ . It is assumed that the

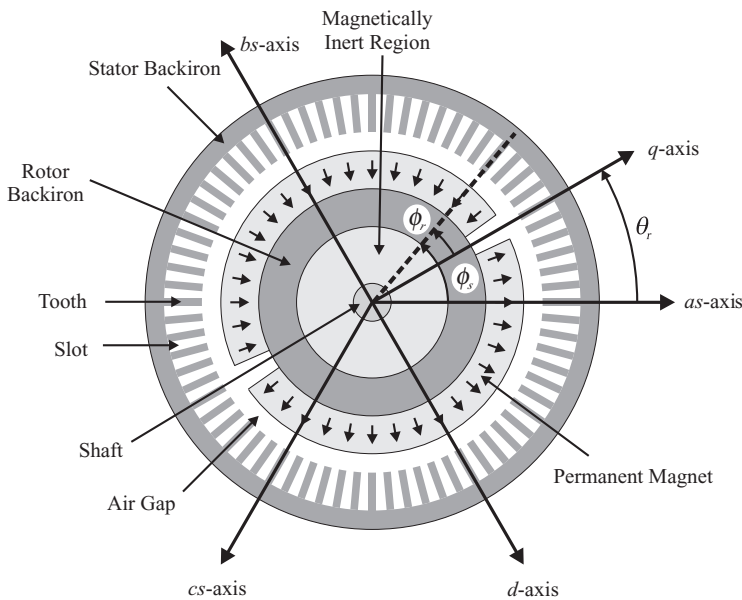


Figure 15.1-1. Surface-mounted permanent-magnet synchronous machine.

inverter driving the machine is current controlled as discussed in Sections 12.8–12.11, and operated from a dc bus voltage of  $v_{dc}$ . It is desired to minimize mass, to minimize loss, to restrict current density (since it is closely related to winding temperature), to avoid heavy magnetic saturation, and to avoid demagnetization of the magnet.

Figure 15.1-1 illustrates a diagram of a two-pole version of the machine (we will consider a  $P$ -pole design). The phase magnetic axes are shown, as well as the  $q$ - and  $d$ -axis. The stator is broken into two regions, the stator backiron and the slot/tooth region. The rotor includes a shaft, a magnetically inert region (which could be steel but need not be), a rotor backiron region, and permanent magnets. Arrows within the permanent magnet region indicate the direction of magnetization. Also shown in Figure 15.1-1 is the electrical rotor position,  $\theta_r$ , position measured from the stator,  $\phi_s$ , and position measured relative to the rotor  $\phi_r$ . Since a two-pole machine is shown, these angles are identical to their mechanical counterparts,  $\theta_{rm}$ ,  $\phi_{sm}$ , and  $\phi_{rm}$  for the device shown.

Again, our approach will be to formulate the design problem as a formal optimization problem. Hence, our goal will be to predict machine performance based on a geometrical machine description. The work will proceed as follows. First, Section 15.2 will set forth the details of the geometry. Next, the winding configuration will be discussed in Section 15.3. Needed material properties will be outlined in Section 15.4. The current control philosophy will be delineated in Section 15.5. At this point, attention will turn to finding an expression for the radial flux density of the machine in Section 15.6, and a derivation of expressions for the electrical parameters of the

machine in Section 15.7. The implications of the air-gap field on the field within the steel and permanent magnet is addressed in Section 15.8. As this point, the primary analytical results required for the machine design will have been put in place. Thus, in Section 15.9, the formulation of the design problem is considered. Section 15.10 provides a case study in multiobjective optimization-based machine design. Finally, Section 15.11 discusses extensions to the approach set forth herein.

## 15.2. MACHINE GEOMETRY

Figure 15.2-1 illustrates a cross-section of the machine. As can be seen, the machine is divided into regions. Proceeding from the exterior of the machine to the interior, the outermost region of the machine is the stator backiron, which extends from a radius of  $r_{sb}$  to  $r_{ss}$  from the center of the machine. In this region, flux enters and leaves from the teeth and predominantly travels in the tangential direction. The next region is the slot/tooth region, which contains the stator slots and teeth and stator conductors as discussed in Chapter 2. The slot/tooth region extends from  $r_{st}$  to  $r_{sb}$ . The next region is the air gap, which includes radii from  $r_{rg}$  to  $r_{st}$ . Proceeding inward, the permanent magnet includes points with radii between  $r_{rb}$  and  $r_{rg}$  and consists of one of two types of material, either a permanent magnet that will produce radial flux, or a magnetically inert spacer that may be air (as shown). The rotor backiron extends from  $r_{ri}$  to  $r_{rb}$ . Flux enters and leaves the rotor backiron predominantly in the radial direction; but the majority of the flux flow through the rotor backiron will be tangential. It serves a purpose similar to the stator backiron. The inert region (radii from  $r_{rs}$  to  $r_{ri}$ ) mechanically transfers torque from the rotor backiron to the shaft. It is often just a continuation of the rotor

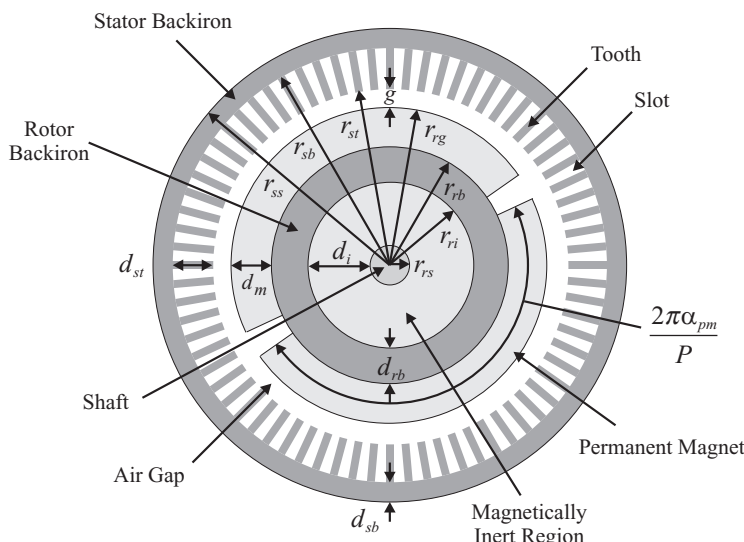


Figure 15.2-1. Dimensions of surface-mounted permanent-magnet synchronous machine.

backiron (possibly with areas removed to reduce mass) or could be a lightweight composite material. Material in this region does not serve a magnetic purpose, even if it is a magnetic material.

Variables depicted in Figure 15.2-1 include:  $d_{sb}$ —the stator backiron depth,  $d_{st}$ —the stator tooth depth,  $g$ —the air-gap depth,  $d_m$ —the permanent magnet depth,  $d_{rb}$ —the rotor backiron depth,  $d_i$ —the magnetically inert region depth, and  $r_{rs}$ —the rotor shaft radius. The active length of the machine (the depth of the magnetic steel into the page) is denoted as  $l$ . The quantity  $\alpha_{pm}$  is the angular fraction of a magnetic pole occupied by the permanent magnet. All of these variables, with the exception of the radius of the rotor shaft,  $r_{rs}$ , which is assumed to be known, will be determined as part of the design process.

In terms of the parameters identified in the previous paragraph, the following may be readily calculated:  $r_{ri}$ —the rotor inert region radius,  $r_{rb}$ —the rotor backiron radius,  $r_{rg}$ —the rotor air-gap radius,  $r_{st}$ —the stator tooth inner radius,  $r_{sb}$ —the stator backiron inner radius, and  $r_{ss}$ —the stator shell radius. A stator shell, if present, is used for protection, mechanical strength, and thermal transfer. It will not be considered in our design.

Figure 15.2-2 depicts a portion of the stator consisting of one tooth and one slot (with  $\frac{1}{2}$  of a slot on either side of the tooth). Variables depicted therein which have not been previously defined include:  $S_s$ —the number of stator slots,  $\theta_{ti}$ —the angle spanned by the tooth tip at radius  $r_{st}$ ,  $\theta_{si}$ —the angle spanned by the slot at radius  $r_{st}$ ,  $r_{si}$ —the radius to the inside tooth tip,  $\theta_{ti}$ —the angle spanned by the tooth at radius  $r_{si}$ ,  $\theta_{tb}$ —the angle spanned by the tooth at radius  $r_{sb}$ ,  $w_{tb}$ —the width of the tooth base,  $d_{tb}$ —the depth of the tooth base,  $d_{te}$ —the depth of the tooth tip edge, and  $d_{tc}$ —the depth of the tooth tip center at  $\theta_{ti}/2$ .

For the purposes of design, it will be convenient to introduce the tooth fraction  $\alpha_t$  and tooth tip fraction  $\alpha_{tt}$ . The tooth fraction is defined as the angular fraction of the slot/tooth region occupied by the tooth at radius  $r_{st}$ . Hence,

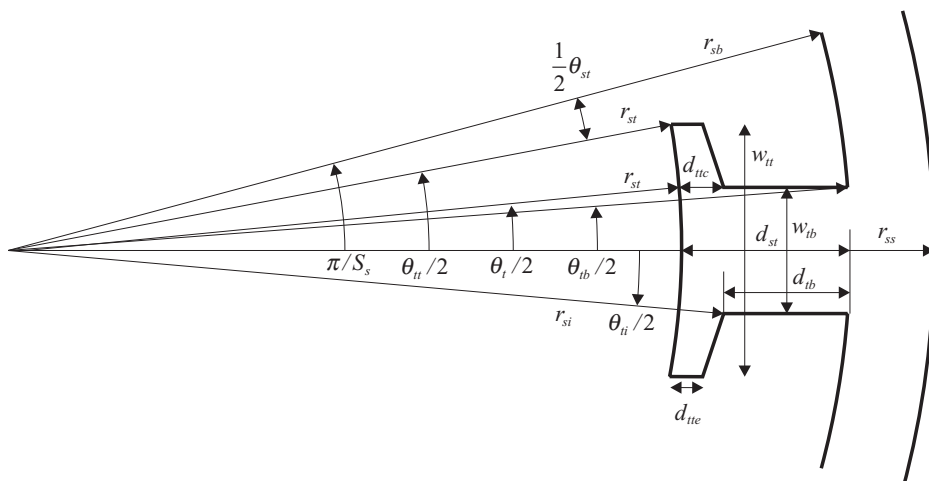


Figure 15.2-2. Slot and tooth dimensions.

$$\alpha_t = \frac{S_s \theta_t}{2\pi} \quad (15.2-1)$$

The tooth tip fraction is herein defined as the angular fraction of the slot/tooth region occupied by the tooth tip at radius  $r_{st}$ . It is defined as

$$\alpha_{tt} = \frac{S_s \theta_{tt}}{2\pi} \quad (15.2-2)$$

As previously noted, not all the variables in Figure 15.2-1 and Figure 15.2-2 are independent, being related by geometry. One choice of variables sufficient to define the geometry is given by

$$\mathbf{G}_x = [r_{rs} \ d_i \ d_{rb} \ d_m \ g \ d_{tb} \ d_{ttc} \ d_{tte} \ \alpha_t \ \alpha_{tt} \ d_{sb} \ \alpha_{pm} \ l \ P \ S_s \ \phi_{ss1}]^T \quad (15.2-3)$$

where a “G” is used to denote geometry and the subscript “x” serves as a reminder that these variables are considered independent. Note that we have not discussed the last element of  $\mathbf{G}_x$ , namely  $\phi_{ss1}$ , in this chapter; it is the center location of the first slot as discussed in Chapter 2. Given  $\mathbf{G}_x$ , the locations of the slots and teeth may be calculated using (2.2-8) and (2.2-9); next, the remaining quantities in Figure 15.2-1 and Figure 15.2-2 can be readily calculated as

$$r_{ri} = r_{rs} + d_i \quad (15.2-4)$$

$$r_{rb} = r_{ri} + d_{rb} \quad (15.2-5)$$

$$r_{rg} = r_{rb} + d_m \quad (15.2-6)$$

$$r_{st} = r_{rg} + g \quad (15.2-7)$$

$$r_{si} = r_{st} + d_{ttc} \quad (15.2-8)$$

$$\theta_t = 2\pi\alpha_t / S_s \quad (15.2-9)$$

$$\theta_{tt} = 2\pi\alpha_{tt} / S_s \quad (15.2-10)$$

$$\theta_{st} = 2\pi / S_s - \theta_{tt} \quad (15.2-11)$$

$$w_{tb} = 2r_{st} \sin(\theta_t / 2) \quad (15.2-12)$$

$$w_{tt} = 2r_{st} \sin(\theta_{tt} / 2) \quad (15.2-13)$$

$$r_{sb} = \sqrt{(w_{tb} / 2)^2 + (r_{st} \cos(\theta_t / 2) + d_{tb} + d_{ttc})^2} \quad (15.2-14)$$

$$\theta_{tb} = 2\arcsin\left(\frac{w_{tb}}{2r_{sb}}\right) \quad (15.2-15)$$

$$\theta_{ti} = 2\arcsin\left(\frac{w_{tb}}{2r_{si}}\right) \quad (15.2-16)$$

$$d_{st} = r_{sb} - r_{st} \quad (15.2-17)$$

$$r_{ss} = r_{sb} + d_{sb} \quad (15.2-18)$$

Another geometrical variable of interest, although not shown in Figure 15.2-2, is the slot opening, that is, the distance between teeth. This is readily expressed as

$$w_{so} = 2r_{st} \sin\left(\frac{\theta_{st}}{2}\right) \quad (15.2-19)$$

In addition to the computing the dependent geometrical variables, there are several other quantities of interest that will prove useful in the design of the machine. The first of these is the area of a tooth base, which is the portion of the tooth that falls within  $r_{si} \leq r \leq r_{sb}$  and is given by

$$a_{tb} = w_{tb}d_{tb} + \frac{r_{sb}}{2} \left( r_{sb}\theta_{tb} - w_{tb} \cos\left(\frac{\theta_{tb}}{2}\right) \right) - \frac{r_{si}}{2} \left( r_{si}\theta_{ti} - w_{tb} \cos\left(\frac{\theta_{ti}}{2}\right) \right) \quad (15.2-20)$$

The area of a tooth tip, which is the material at a radius  $r_{st} \leq r \leq r_{si}$  from the center of the machine, may be expressed as

$$a_{tt} = \frac{1}{2} \left( 2w_{tt}d_{te} + (w_{tb} + w_{tt})(r_{si} \cos(\theta_{ti}/2) - r_{st} \cos(\theta_{tt}/2) - d_{te}) \right) - \frac{1}{2} \left( -r_{si}^2\theta_{tt} + r_{st}w_{tt} \cos(\theta_{tt}/2) + r_{si}^2\theta_{ti} - r_{si}w_{tb} \cos(\theta_{ti}/2) \right) \quad (15.2-21)$$

The slot area is defined as the cross-sectional area of the slot between radii  $r_{sb}$  and  $r_{si}$ . This area is calculated as

$$a_{slt} = \frac{\pi}{S_s} (r_{sb}^2 - r_{si}^2) - a_{tb} \quad (15.2-22)$$

The total volume of all stator teeth,  $v_{st}$ , the back iron,  $v_{sb}$ , and the stator laminations,  $v_{sl}$ , may be formulated as

$$v_{st} = S_s(a_{tt} + a_{tb})l \quad (15.2-23)$$

$$v_{sb} = \pi(r_{ss}^2 - r_{sb}^2)l \quad (15.2-24)$$

$$v_{sl} = v_{st} + v_{sb} \quad (15.2-25)$$

The total volume of the rotor backiron, denoted as  $v_{rb}$ , rotor inert region,  $v_{ri}$ , and permanent magnet,  $v_{pm}$ , are readily found from

$$v_{rb} = \pi(r_{rb}^2 - r_{ri}^2)l \quad (15.2-26)$$

$$v_{ri} = \pi(r_{ri}^2 - r_{rs}^2)l \quad (15.2-27)$$

$$v_{pm} = \pi(r_{rg}^2 - r_{rb}^2)\alpha_{pm}l \quad (15.2-28)$$

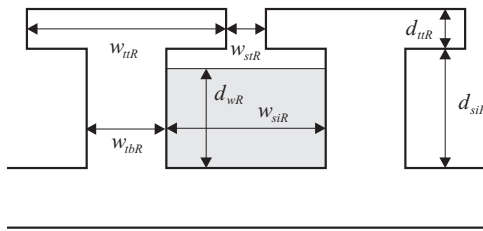


Figure 15.2-3. Rectangular slot approximation.

For purposes of leakage inductance calculations, it is convenient to approximate the slot geometry as being rectangular, as depicted in Figure 15.2-3.

There are many ways such an approximation can be accomplished. One approach is as follows. First, the width of the tooth tip is approximated as the circumferential length of the actual tooth tip

$$w_{ttR} = r_{st} \theta_{tt} \quad (15.2-29)$$

The depth of the rectangular approximation to the tooth tip is set so that the tooth tip has the same cross sectional area. In particular,

$$d_{ttR} = \frac{a_{tt}}{w_{ttR}} \quad (15.2-30)$$

Next, the width of the slot between the stator tooth tips is approximated by circumferential distance between the tooth. Thus

$$w_{stR} = r_{st} \theta_{st} \quad (15.2-31)$$

The width of slot between the base of the tips is taken as the average of the distance of the chord length of the inner corners of the tooth tips at the top of the tooth and the chord distance between the bottom corners of the teeth. This yields

$$w_{siR} = r_{si} \sin\left(\frac{\pi}{S_s} - \frac{\theta_{ti}}{2}\right) + r_{sb} \sin\left(\frac{\pi}{S_s} - \frac{\theta_{tb}}{2}\right) \quad (15.2-32)$$

Maintaining the area of the slot and the area of the tooth base, the depth of the slot (exclusive of the tooth tip) and width of the tooth base are set in accordance with

$$d_{siR} = \frac{a_{slt}}{w_{siR}} \quad (15.2-33)$$

$$w_{ibR} = \frac{a_{tb}}{d_{siR}} \quad (15.2-34)$$

Note that this approach is not consistent in that it does not require  $w_{siR} + w_{tbR} = w_{ttR} + w_{stR}$ . However, this does not matter in the primary use of the model—the calculation of the slot leakage permeance as discussed in Appendix C. The final parameter shown in Figure 15.2-3 is the depth of the winding within the slot,  $d_{wR}$ . This parameter will not be considered a part of the stator geometry, but rather as part of the winding.

Before concluding this section, it is appropriate to organize our calculations in order to support our design efforts. In (15.2-3), we defined a list of “independent” variables that define the machine geometry, and organized them into a vector  $\mathbf{G}_x$ . Based on this, we found a host of related variables which will also be of use. It is convenient to define these dependent variables as a vector

$$\mathbf{G}_y = [r_{ri} \ r_{rb} \ r_{rg} \ r_{st} \ r_{ri} \ \theta_t \ \theta_{tt} \ w_{tt} \ r_{sb} \ \theta_{tb} \ \theta_{ti} \ d_{st} \ r_{ss} \ w_{so} \cdots \\ a_{st} \ a_{tt} \ a_{tb} \ v_{st} \ v_{sb} \ v_{sl} \ v_{rb} \ v_{ri} \ v_{pm} \ w_{ttR} \ d_{ttR} \ w_{stR} \ w_{siR} \ d_{siR} \ w_{tbR}]^T \quad (15.2-35)$$

where again “ $\mathbf{G}$ ” denotes geometry and the “ $y$ ” indicates dependent variables. We may summarize our calculations (from 15.2-4 to 15.2-34) as a vector-valued function  $\mathbf{F}_G$  such that

$$\mathbf{G}_y = \mathbf{F}_G(\mathbf{G}_x) \quad (15.2-36)$$

This view of our geometrical calculations will be useful as we develop computer codes to support machine design, directly suggesting the inputs and outputs of a subroutine/function calls to make geometrical calculations. Finally, other calculations we will need to perform will require knowledge of both  $\mathbf{G}_x$  and  $\mathbf{G}_y$ ; it will therefore be convenient to define

$$\mathbf{G} = [\mathbf{G}_x^T \ \mathbf{G}_y^T]^T \quad (15.2-37)$$

### 15.3. STATOR WINDINGS

It is assumed herein that the conductor distribution is sinusoidal with the addition of a third harmonic term as discussed in Section 2.2, and given, in a slightly different but equivalent form, by (2.2-12). In particular, the assumed conductor density is given by

$$n_{as}(\phi_{sm}) = N_{s1}^* \left( \sin\left(\frac{P}{2}\phi_{sm}\right) - \alpha_3^* \sin\left(3\frac{P}{2}\phi_{sm}\right) \right) \quad (15.3-1)$$

$$n_{bs}(\phi_{sm}) = N_{s1}^* \left( \sin\left(\frac{P}{2}\phi_{sm} - \frac{2\pi}{3}\right) - \alpha_3^* \sin\left(3\frac{P}{2}\phi_{sm}\right) \right) \quad (15.3-2)$$

$$n_{cs}(\phi_{sm}) = N_{s1}^* \left( \sin\left(\frac{P}{2}\phi_{sm} + \frac{2\pi}{3}\right) - \alpha_3^* \sin\left(3\frac{P}{2}\phi_{sm}\right) \right) \quad (15.3-3)$$

where  $N_{s1}^*$  and  $\alpha_3^*$  are the desired fundamental amplitude of the conductor density, and ratio between the third harmonic component and fundamental component, respectively.

The goal of this chapter is to design a machine that can be constructed, which means that we need to specify the specific number of conductors of each phase to be placed in each slot. To this end, we can use the results from Section 2.2. Using (2.2-24) in conjunction with (15.3-1)–(15.3-3) yields

$$N_{as,i} = \text{round}\left(\frac{4N_{s1}^*}{P}\left(\sin\left(\frac{P}{2}\phi_{ss,i}\right)\sin\left(\frac{\pi P}{2S_s}\right) - \frac{\alpha_3^*}{3}\sin\left(\frac{3P}{2}\phi_{ss,i}\right)\sin\left(\frac{3P\pi}{2S_s}\right)\right)\right) \quad (15.3-4)$$

$$N_{bs,i} = \text{round}\left(\frac{4N_{s1}^*}{P}\left(\sin\left(\frac{P}{2}\phi_{ss,i} - \frac{2\pi}{3}\right)\sin\left(\frac{\pi P}{2S_s}\right) - \frac{\alpha_3^*}{3}\sin\left(\frac{3P}{2}\phi_{ss,i}\right)\sin\left(\frac{3P\pi}{2S_s}\right)\right)\right) \quad (15.3-5)$$

$$N_{cs,i} = \text{round}\left(\frac{4N_{s1}^*}{P}\left(\sin\left(\frac{P}{2}\phi_{ss,i} + \frac{2\pi}{3}\right)\sin\left(\frac{\pi P}{2S_s}\right) - \frac{\alpha_3^*}{3}\sin\left(\frac{3P}{2}\phi_{ss,i}\right)\sin\left(\frac{3P\pi}{2S_s}\right)\right)\right) \quad (15.3-6)$$

where  $N_{as,i}$ ,  $N_{bs,i}$ , and  $N_{cs,i}$  are the number of conductors of the respective phase in the  $i$ 'th slot and where  $\phi_{ss,i}$  denotes the mechanical location of the center of the  $i$ 'th stator slot, which is given by (2.2-8) in terms of  $\phi_{ss,1}$ , which is the location of the center of the first slot. This angle takes on a value of 0 if the  $a$ -phase magnetic axis is aligned with the first slot or  $\pi/S_s$  if it desired to align the  $a$ -phase magnetic axis with the first tooth.

The total number of conductors in the  $i$ th slot is given by

$$N_{s,i} = |N_{as,i}| + |N_{bs,i}| + |N_{cs,i}| \quad (15.3-7)$$

For some of our magnetic analysis, we will use the continuous rather than discrete description of the winding. Once the number of conductors in each slot are computed using (15.3-4)–(15.3-6), then from (2.2-12), (15.3-1), and (2.2-20), the effective value of  $N_{s1}$  and  $\alpha_3$  are given by

$$N_{s1} = \frac{1}{\pi} \sum_{i=1}^{S_s} N_{as,i} \cos(\phi_{ss,i}) \quad (15.3-8)$$

$$\alpha_3 = -\frac{1}{\pi N_{s1}} \sum_{i=1}^{S_s} N_{as,i} \cos(3\phi_{ss,i}) \quad (15.3-9)$$

It is also necessary to establish an expression to describe the end conductor distribution. The end conductor distribution for each winding may be calculated in terms of the slot conductor distribution using the methods of Section 2.2. In particular, repeating (2.2-25) for convenience, the net end conductor distribution for winding “x” is expressed

$$M_{x,i} = M_{x,i-1} + N_{x,i-1} \quad (15.3-10)$$

Using (15.3-10) requires knowledge of the net number of end conductors  $M_{x,1}$  on the end of tooth 1. This, and the number of cancelled conductors in each slot,  $C_{x,i}$  (see Section 2.2), determines the type of winding (lap, wave, or concentric). For the purposes of this chapter, let us take the number of canceled conductors to be zero and require the end winding conductor arrangement to be symmetric in the sense that for any end conductor count over tooth  $i$ , the end conductor count over the diametrically opposed tooth (in an electrical sense) has the opposite value. Mathematically,

$$M_{x,i} = -M_{x,S_s/P+i} \quad (15.3-11)$$

From (15.3-10) and (15.3-11), it can be shown that (Problem 4)

$$M_{x,1} = -\frac{1}{2} \sum_{i=1}^{S_s/P} N_{x,i} \quad (15.3-12)$$

Thus, once the slot conductor distribution is known, (15.3-12) and (15.3-10) can be used to find an end conductor distribution. The distribution chosen herein corresponds to a concentric winding. Note that (15.3-12) can yield a noninteger result. In this case, minor alterations to the end conductor arrangement can be used to provide proper connectivity with an integer number of conductors.

In addition to the distribution of the wire, it is also necessary to compute the wire cross-sectional area. To this end, the concept of packing factor is useful. The packing factor is defined as the maximum (over all slots) of the ratio of the total conductor cross-sectional area within the slot to the total slot area, and will be denoted by  $\alpha_{pf}$ . Typical packing factors for round wire range from 0.4 to 0.7. Assuming that it is advantageous not to waste the slot area, the conductor cross-sectional area and diameter may be expressed as

$$a_c = \frac{a_{slt} \alpha_{pf}}{\|\mathbf{N}_s\|_{\max}} \quad (15.3-13)$$

$$d_c = \sqrt{\frac{4a_c}{\pi}} \quad (15.3-14)$$

where  $\|\mathbf{N}_s\|_{\max}$  denotes the maximum element of the vector  $\mathbf{N}_s$ . If desired,  $a_c$  and  $d_c$  can be adjusted to match a standard wire gauge. In this case, the gauge selected should be the one with the largest conductor area that is smaller than that calculated using (15.3-13).

Finally, it will be necessary to compute the depth of the winding within the slot for the rectangular slot approximation. This may be readily expressed as

$$d_{wR} = \frac{\|\mathbf{N}_s\|_{\max} a_c}{\alpha_{pf} w_{siR}} \quad (15.3-15)$$

Another variable of interest is the dimension of the end winding bundle in the direction parallel to the rotor shaft. Assuming the same depth as calculated by (15.3-15), this dimension may be approximated as

$$l_{ew} = \frac{\|M_{as}| + |M_{bs}| + |M_{cs}\|_{\max} a_c}{\alpha_{pf} d_{wR}} \quad (15.3-16)$$

Another variable of interest is the total volume of stator conductor per phase,  $v_{cd}$ . From (2.7-1)–(2.7-3),

$$v_{cd} = (l + 2l_{eo})a_c \sum_{i=1}^{S_s} |N_{as,i}| + \frac{2\pi}{S_s} (r_{st} + r_{sb}) a_c \sum_{i=1}^{S_y} |M_{as,i}| \quad (15.3-17)$$

where  $l_{eo}$  is the end winding offset, which is the amount of overhang of the end winding between the end of the stator stack and the end winding bundle. The end winding offset is a function of the manufacturing process. In general, it is desirable to make this as small as possible, though extremely small values may increase leakage inductance and core loss somewhat.

As in the case of the stator geometry, it is convenient to organize the variables discussed into independent and dependent variables, which will show the relationship of the variables from a programming point of view. To this end, it is convenient to organize the independent variables of the winding description as

$$\mathbf{W}_x = [N_{s1}^* \alpha_3^* \alpha_{pf}^* l_{eo}]^T \quad (15.3-18)$$

The output of our winding calculations are encapsulated by the vector

$$\mathbf{W}_y = [N_{s1} \alpha_3 N_{as} N_{bs} N_{cs} N_s \mathbf{M}_{as} \mathbf{M}_{bs} \mathbf{M}_{cs} a_c d_{wR} l_{ew} v_{cd}]^T \quad (15.3-19)$$

Functionally, we have

$$\mathbf{W}_y = \mathbf{F}_W(\mathbf{W}_x, \mathbf{G}) \quad (15.3-20)$$

It will also prove convenient to define

$$\mathbf{W} = [\mathbf{W}_x^T \quad \mathbf{W}_y^T]^T \quad (15.3-21)$$

## 15.4. MATERIAL PARAMETERS

As part of the design process, we will also need to select materials for the stator steel, the rotor steel, the conductor, and the permanent magnet. We will use  $s_t$ ,  $r_t$ ,  $c_t$ , and  $m_t$  as integer variables denoting the stator steel type, the rotor steel type, the conductor

type, and the permanent magnet type. Based on these variables, the material parameters can be established using tabulated functions in accordance with

$$\mathbf{S} = F_{sc}(s_t) \quad (15.4-1)$$

$$\mathbf{R} = F_{sc}(r_t) \quad (15.4-2)$$

$$\mathbf{C} = F_{cc}(c_t) \quad (15.4-3)$$

$$\mathbf{M} = F_{mc}(m_t) \quad (15.4-4)$$

where “sc,” “cc,” and “mc” denote “steel catalog,” “conductor catalog,” and “magnet catalog,”, and where  $\mathbf{S}$ ,  $\mathbf{R}$ ,  $\mathbf{C}$ , and  $\mathbf{M}$  are vectors of material parameters for the stator steel, rotor steel, conductor, and magnet, and may be expressed as

$$\mathbf{S} = [\rho_s \ B_{s,lim}]^T \quad (15.4-5)$$

$$\mathbf{R} = [\rho_r \ B_{r,lim}]^T \quad (15.4-6)$$

$$\mathbf{C} = [\rho_c \ \sigma_c \ J_{lim}]^T \quad (15.4-7)$$

$$\mathbf{M} = [\rho_m \ B_r \ \chi_m \ H_{lim}]^T \quad (15.4-8)$$

In (15.4-5)–(15.4-8),  $\rho$  denotes volumetric mass density,  $B_{s,lim}$  and  $B_{r,lim}$  denote flux density limits on the stator and rotor steel so as to avoid saturation,  $\sigma_c$  is the conductor conductivity,  $J_{lim}$  is a recommended limit on current density, and  $B_r$ ,  $\chi_m$ , and  $H_{lim}$  are the permanent magnet parameters.

The permanent magnet parameters are illustrated in terms of the magnet  $B$ – $H$  and  $M$ – $H$  characteristic in Figure 15.4-1, where  $M$  is magnetization. In any material,  $B$ ,  $H$ , and  $M$  are related by

$$B = \mu_0 H + M \quad (15.4-9)$$

The  $B$ – $H$  relationship is often referred to as the material’s normal characteristic, while the  $M$ – $H$  relationship is referred to as the intrinsic characteristic. In Figure 15.4-1,  $B_r$  is the residual flux density of the material (the flux density or magnetization when the field intensity is zero),  $H_c$  is the coercive force (the point where the flux density goes to zero), and  $H_{ci}$  is the intrinsic coercive force (the point where the magnetization goes to zero), and  $\chi_m$  is the susceptibility of the material. Permanent magnet material is generally operated in the second quadrant if it is positively magnetized or fourth quadrant if it is negatively magnetized. It is important to make sure that

$$H \geq H_{lim} \quad (\text{positively magnetized}) \quad (15.4-10)$$

$$H \leq H_{lim} \quad (\text{negatively magnetized}) \quad (15.4-11)$$

in order to avoid demagnetization, where  $H_{lim}$  is a minimum allowed field intensity to avoid demagnetization, which is a negative number whose magnitude is less than that

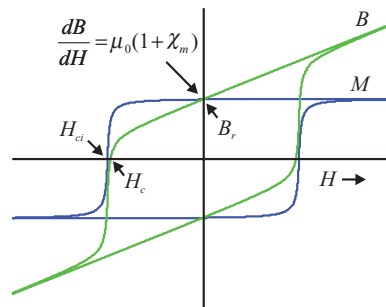
Figure 15.4-1.  $B$ - $H$  and  $M$ - $H$  characteristics of PM material.

TABLE 15.4-1. Magnetic Steels

Material	M19	M36	M43	M47
$s_t/r_t$	1	2	3	4
$B_{s,lim}/B_{r,lim}$ (T)	1.39	1.34	1.39	1.49
$\rho_s/\rho_r$ (kg/m <sup>3</sup> )	7400	7020	7290	7590

TABLE 15.4-2. Conductors

Material	Copper	Aluminum
$c_t$	1	2
$J_{c,lim}$ (MA/m <sup>2</sup> )	7.60	6.65
$\sigma_C$ (MΩ <sup>-1</sup> /m)	59.6	37.7
$\rho_c$ (kg/m <sup>3</sup> )	8890	2710

TABLE 15.4-3. Permanent Magnets

Material	SmCo5-R20	SmCo5-R25	SmCo17-R28	SmCo17-R32
$m_p$	1	2	3	4
$B_r$ (T)	0.9	1.0	1.1	1.15
$\chi_m$	0.023	0.027	0.094	0.096
$H_{lim}$ (kA/m)	-1200	-1200	-1000	-675
$\rho_m$ (kg/m <sup>3</sup> )	8400	8400	8300	8300

of  $H_{ci}$ , and which is a function of magnet material and often of operating temperature. It should also be noted that while the shape of the  $M$ - $H$  characteristic is fairly consistent between materials, the shape of the  $B$ - $H$  curve is not; indeed  $B$ - $H$  may take on the slanted shape shown in Figure 15.4-1, or appear relatively square.

Material data for a limited number of steels, conductors, and permanent magnets is given in Table 15.4-1, Table 15.4-2, and Table 15.4-3, respectively. Note that recommended saturation flux density limits are a “soft” recommendation since the  $B$ - $H$

characteristic of magnetic materials is a continuous function. Magnetic steel properties vary not only with grade, but also manufacturer. Further, the recommendation on maximum current density is a soft recommendation. All material parameters are a function of temperature though this aspect of the design is not treated in this introduction to the topic of machine design. Temperature dependence can have a particularly strong impact on permanent magnet characteristics.

## 15.5. STATOR CURRENTS AND CONTROL PHILOSOPHY

In our design, we will consider a machine connected to a current-regulated inverter, and that through the action of the inverter controls, the machine currents are regulated to be equal to the commanded  $q$ - and  $d$ -axis currents. This is reasonable, assuming the use of a synchronous current regulator (see Section 12.11) or a similar technique. The corresponding  $abc$  currents are readily found from the inverse rotor reference-frame transformation; alternately, they may be expressed

$$i_{as} = \sqrt{2}I_s \cos(\theta_r + \phi_i) \quad (15.5-1)$$

$$i_{bs} = \sqrt{2}I_s \cos(\theta_r + \phi_i - 2\pi/3) \quad (15.5-2)$$

$$i_{cs} = \sqrt{2}I_s \cos(\theta_r + \phi_i + 2\pi/3) \quad (15.5-3)$$

where  $I_s$  is the rms current, and  $\phi_i$  is the current phase advance. From our work in Chapter 3, these quantities are readily expressed as

$$I_s = \frac{1}{\sqrt{2}} \sqrt{(i_{qs}^r)^2 + (i_{ds}^r)^2} \quad (15.5-4)$$

$$\phi_i = \text{angle}(i_{qs}^r - j i_{ds}^r) \quad (15.5-5)$$

Although the calculations of this section are very straightforward, for the sake of consistency, they will be organized as in previous sections. We will define an input vector, and output vector, and a functional relationship as

$$\mathbf{I}_x = [i_{qs}^r \ i_{ds}^r]^T \quad (15.5-6)$$

$$\mathbf{I}_y = [I_s \ \phi_i]^T \quad (15.5-7)$$

and

$$\mathbf{I}_y = \mathbf{F}_I(\mathbf{I}_x) \quad (15.5-8)$$

respectively. The amalgamation of variables associated with the currents is

$$\mathbf{I} = [\mathbf{I}_x^T \ \mathbf{I}_y^T]^T \quad (15.5-9)$$

## 15.6. RADIAL FIELD ANALYSIS

The objective of this section is a magnetic analysis of the machine. A key assumption is that the MMF drop across the steel portions of the machine is negligible. Unless the steel becomes highly saturated, this is a reasonable assumption because relative permeability of most permanent magnet materials is very low compared with steel, and so the MMF drop across the permanent magnet and air-gap dominate that of the steel.

In performing our analysis, we will take the rotor position to be fixed. This may strike the reader as overly restrictive. However, as stated in the introduction, it will be our objective to produce a design that yields a constant torque  $T_e^*$ . In such a machine, except for the perturbation caused by slot effects, the flux and current densities are traveling waves that rotate but do not change in magnitude under steady-state conditions. Thus, ideally, it is only necessary to consider a single position, which could, for example, be taken to be zero. In practice, slot effects are a factor so we will consider several fixed rotor positions, although all positions will be within one slot/tooth pitch of zero.

In order to analyze the field in the machine, we note that from Section 2.4 that in the absence of rotor currents the air-gap MMF drop is equal to the stator MMF. In particular, from (2.4-20)

$$\mathbb{F}_g(\phi_{sm}) = \mathbb{F}_s(\phi_{sm}) \quad (15.6-1)$$

In the definition of air gap MMF used in defining (2.4-20), it is important to recall that the definition of air gap MMF drop given by (2.4-3) extended from the rotor steel to the stator steel. In particular, in terms of the dimensions of Figure 15.2-1,

$$\mathbb{F}_g(\phi_{sm}) = \int_{r_{rb}}^{r_{st}} H(r, \phi_{sm}) \cdot dr \quad (15.6-2)$$

where  $H(r, \phi_{sm})$  denotes the radial component of field intensity.

For the purposes at hand, it will be convenient to define

$$\mathbb{F}_{pm}(\phi_{sm}) = \int_{r_{rb}}^{r_{rg}} H(r, \phi_{sm}) dr \quad (15.6-3)$$

$$\mathbb{F}_a(\phi_{sm}) = \int_{r_{rg}}^{r_{st}} H(r, \phi_{sm}) dr \quad (15.6-4)$$

which describe the MMF drop across the range of radii spanned by the permanent magnet, and the MMF drop across the air gap, respectively. Comparing (15.6-1)–(15.6-4), it is clear that

$$\mathbb{F}_a(\phi_{sm}) + \mathbb{F}_{pm}(\phi_{sm}) = \mathbb{F}_s(\phi_{sm}) \quad (15.6-5)$$

In the following subsections, we will establish expression for each term in (15.6-5), and then use these to establish an expression for the radial flux density in the machine.

## Stator MMF

The first step in determining the stator MMF is to determine the winding functions. The conductor density distribution is given by (15.3-1)–(15.3-3) with the replacement of  $N_{s1}^*$  by  $N_{s1}$  and  $\alpha_3^*$  by  $\alpha_3$ . In particular, for the *a*-phase,

$$n_{as}(\phi_{sm}) = N_{s1} \left( \sin\left(\frac{P}{2}\phi_{sm}\right) - \alpha_3 \sin\left(3\frac{P}{2}\phi_{sm}\right) \right) \quad (15.6-6)$$

Applying (2.3-11) to (15.6-6) yields the *a*-phase winding function

$$w_{as}(\phi_{sm}) = \frac{2N_{s1}}{P} \left( \cos(P\phi_{sm}/2) - \frac{\alpha_3}{3} \cos(3P\phi_{sm}/2) \right) \quad (15.6-7)$$

Expressions of the *b*- and *c*-phases are similarly derived.

From (2.5-7), the stator MMF may be expressed as

$$\mathbb{F}_s = w_{as}i_{as} + w_{bs}i_{bs} + w_{cs}i_{cs} \quad (15.6-8)$$

Substitution of the winding functions and the expressions for currents (15.5-1)–(15.5-3) into (15.6-8) and simplifying yields the expression for stator MMF, namely

$$\mathbb{F}_s(\phi_{sm}) = \frac{3\sqrt{2}N_{s1}I_s}{P} \cos\left(\frac{P}{2}\phi_{sm} - \theta_r - \phi_i\right) \quad (15.6-9)$$

Alternately, in terms of *qd* variables,

$$\mathbb{F}_s(\phi_{sm}) = \frac{3N_{s1}}{P} \left( \cos\left(\frac{P}{2}\phi_{sm} - \theta_r\right) i_{qs}^r - \sin\left(\frac{P}{2}\phi_{sm} - \theta_r\right) i_{ds}^r \right) \quad (15.6-10)$$

## Radial Field Variation

Before establishing expressions for the permanent magnet and air-gap MMF drop, it is necessary to describe how the radial component of flux density varies with the radius from the center of the machine. In Chapter 2, we considered the flux density to be constant. However, in this case, the distance from the rotor steel to the stator steel is much larger than in a typical induction or synchronous machine, and so it is appropriate to take the radial variation of the flux density into account when determining MMF components.

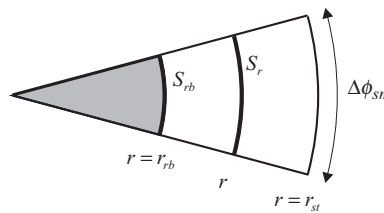


Figure 15.6-1. Thin sector of machine.

In order to establish the radial variation in the field, consider Figure 15.6-1. Therein, a cross section of an angular slice of the machine is shown. Assuming that the flux density is entirely radial for radii between the rotor backiron and the stator teeth, then the flux through surface  $S_{rb}$  at the rotor backiron radius must, by Gauss's law, be equal to the flux through the surface  $S_r$  at an arbitrary radius, whereupon it follows that the flux density of an arbitrary radius is given by

$$B(r, \phi_{sm}) = \frac{r_{rb}}{r} B_{rb}(\phi_{sm}) \quad r_{rb} \leq r \leq r_{st} \quad (15.6-11)$$

where  $B_{rb}$  is the radial flux density at the rotor backiron radius.

### Air-Gap MMF Drop

In the air gap, the field intensity and flux density are related by

$$B(r, \phi_{sm}) = \mu_0 H(r, \phi_{sm}) \quad r_{rg} \leq r \leq r_{st} \quad (15.6-12)$$

Manipulating (15.6-4), (15.6-11), and (15.6-12), one obtains

$$\mathbb{F}_a(\phi_{sm}) = B_{rb}(\phi_{sm}) R_g \quad (15.6-13)$$

where  $R_g$  is a quasi-reluctance which may be expressed as

$$R_g = \frac{r_{rb}}{\mu_0} \ln \left( 1 + \frac{g}{r_{rb} + d_m} \right) \quad (15.6-14)$$

Note that the accuracy of (15.6-14) can be improved by replacing  $g$  by  $g_{eff}$ , which is the effective air gap determined using Carter's coefficient, which compensates for the effect of the missing steel in the stator slots on the air gap MMF. It is discussed in Appendix B.

### Permanent-Magnet MMF

The next step in our development is to calculate the MMF across the permanent magnet region. Assuming that the knee of the magnetization curve is avoided (which will be a

design constraint), the relationship between flux density and field intensity for  $r_{rb} \leq r \leq r_{rg}$  may be expressed as

$$B = \begin{cases} \mu_0(1 + \chi_m)H + B_r & \text{positively magnetized} \\ \mu_0(1 + \chi_m)H - B_r & \text{negatively magnetized} \\ \mu_0 H & \text{inert region between magnets} \end{cases} \quad (15.6-15)$$

It is convenient to represent (15.6-15) as

$$B = \mu_0 \mu_{rm}(\phi_{rm})H + B_m(\phi_{rm}) \quad (15.6-16)$$

where  $B_m(\phi_{rm})$  is due to the residual flux density in the permanent magnet and  $\mu_{rm}(\phi_{rm})$  is the relative permeability of the permanent magnet region (including the inert material), and  $\phi_{rm}$  denotes position as measured from the  $q$ -axis of the rotor, and both  $B$  and  $H$  refer to the radial component of the field directed from the rotor to the stator. These functions are illustrated in Figure 15.6-2 in developed diagram form.

The spatial dependence of  $B_m(\phi_{rm})$  and  $\mu_{rm}(\phi_{rm})$  is illustrated in the second and third traces of Figure 15.6-2. From this figure, we may express  $\mu_{rm}(\phi_{rm})$  and  $B_m(\phi_{rm})$  as

$$B_m(\phi_{rm}) = -\text{sqw}_s\left(\frac{P}{2}\phi_{rm}, \alpha_{pm}\right)B_r \quad (15.6-17)$$

$$\mu_{rm}(\phi_{rm}) = 1 + \left| \text{sqw}_s\left(\frac{P}{2}\phi_{rm}, \alpha_{pm}\right) \right| \chi_m \quad (15.6-18)$$

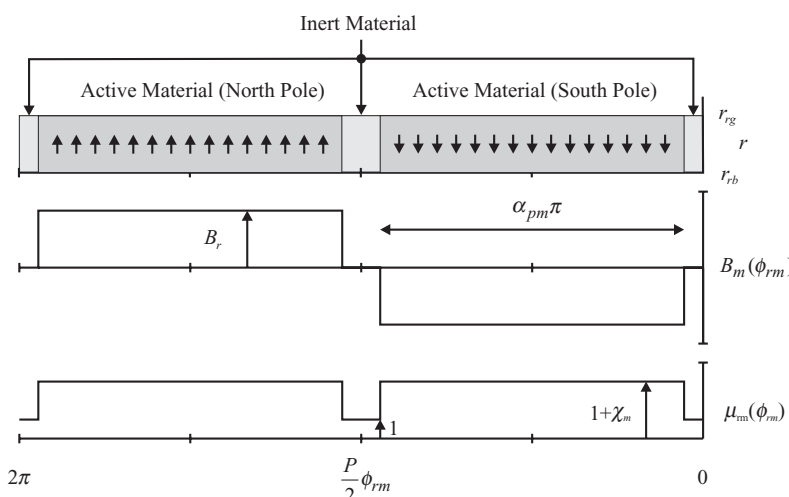


Figure 15.6-2. Radial magnetization.

where  $sqw_s(\cdot)$  is the square wave function with sine symmetry defined as

$$sqw_s(\theta, \alpha) = \begin{cases} 1 & \sin(\theta) \geq \sin(\pi(1-\alpha)/2) \\ -1 & \sin(\theta) \leq -\sin(\pi(1-\alpha)/2) \\ 0 & |\sin(\theta)| < \sin(\pi(1-\alpha)/2) \end{cases} \quad (15.6-19)$$

Manipulating (15.6-3), (15.6-11), and (15.6-16), one obtains the expression for the MMF drop across the permanent magnet region, in particular

$$\mathbb{F}_{pm}(\phi_{sm}) = R_m(\phi_{sm})B_{rb}(\phi_{sm}) - \mathbb{F}_m(\phi_{sm}) \quad (15.6-20)$$

where

$$R_m(\phi_{sm}) = \frac{r_{rb}}{\mu_0 \mu_m(\phi_{sm} - \theta_{rm})} \ln\left(1 + \frac{d_m}{r_{rb}}\right) \quad (15.6-21)$$

and

$$\mathbb{F}_m(\phi_{sm}) = \frac{d_m}{\mu_0 \mu_m(\phi_{sm} - \theta_{rm})} B_m(\phi_{sm} - \theta_{rm}) \quad (15.6-22)$$

It should be observed that  $R_m(\phi_{rm})$  is not a reluctance; however, it plays a similar role. It takes on two values depending upon stator and rotor position. For positions under the permanent magnet,

$$R_m(\phi_{sm}) = R_{pm} = \frac{r_{rb}}{\mu_0(1 + \chi_m)} \ln\left(1 + \frac{d_m}{r_{rb}}\right) \quad (15.6-23)$$

and for positions under the inert region

$$R_m(\phi_{sm}) = R_i = \frac{r_{rb}}{\mu_0} \ln\left(1 + \frac{d_m}{r_{rb}}\right) \quad (15.6-24)$$

$\mathbb{F}_m(\phi_{rm})$  can be thought of as an MMF source resulting from the permanent magnet.

## Solution for Radial Flux Density

At this point, it is possible to solve for the radial flux density. Manipulating (15.6-5), (15.6-11), (15.6-13), and (15.6-20), one obtains

$$B(r, \phi_{sm}) = \frac{r_{rb}}{r} \frac{\mathbb{F}_m(\phi_{sm}) + \mathbb{F}_s(\phi_{sm})}{R_m(\phi_{sm}) + R_g} \quad r_{rb} \leq r \leq r_{st} \quad (15.6-25)$$

We will use this result extensively in the sections to follow. It should be noted that  $\theta_{rm}$  is an implicit argument of  $\mathbb{F}_m(\phi_{sm})$ ,  $\mathbb{F}_s(\phi_{sm})$ , and  $R_m(\phi_{sm})$ . Because of this, we will sometimes denote the radial flux density given by (15.6-25) as  $B(r, \phi_{sm}, \theta_{rm})$  when it is important to remember this functional dependence.

## 15.7. LUMPED PARAMETERS

The goal of this section is to set forth the means to calculate the parameters of the lumped parameter model of the machine as used in Chapter 3—namely the stator resistance  $R_s$ , the leakage inductance  $L_{ls}$ , the magnetizing inductances  $L_{qm}$  and  $L_{dm}$ , and the flux linkage due to the permanent magnet  $\lambda_m$ . We will use these parameters in our calculation of electromagnetic torque, as well as to compute the required inverter voltage. Note that in a break with the notation of the rest of this text, stator resistance is denoted as  $R_s$  rather than  $r_s$ . This is done to avoid confusion with a machine radius.

Let us start with the calculation of the stator resistance. From (2.7-4) and (2.7-5),

$$R_s = \frac{v_{cd}}{a_c^2 \sigma_c} \quad (15.7-1)$$

We will next turn our attention to the parameters associated with the magnetizing flux linkage. From our work in Chapter 2, using (2.6-7), the magnetizing flux linkages of the three phases may be expressed in vector form as

$$\lambda_{abcm} = lr_{st} \int_0^{2\pi} \mathbf{w}_{abcs}(\phi_{sm}) \mathbf{B}(r_{st}, \phi_{sm}) d\phi_{sm} \quad (15.7-2)$$

In terms of  $q$ - and  $d$ -axis variables, (15.7-2) becomes

$$\lambda_{qdm} = lr_{st} \int_0^{2\pi} \mathbf{K}_s^r(\theta_r) \Big|_{\text{utr}} \mathbf{w}_{abcs}(\phi_{sm}) \mathbf{B}(r_{st}, \phi_{sm}) d\phi_{sm} \quad (15.7-3)$$

where “utr” denotes upper two rows. Evaluating (15.7-3) using Park’s transformation, the winding functions of the form (15.6-7), and the expression for flux density (15.6-25) along with its constituent relationships (15.6-10) and (15.6-22)–(15.6-24) yields

$$\lambda_{qm} = L_{qm} i_{qs}^r \quad (15.7-4)$$

$$\lambda_{dm} = L_{dm} i_{ds}^r + \lambda_m \quad (15.7-5)$$

where

$$L_{qm} = \frac{6lr_{rb}N_{sl}^2}{P^2} \left[ \frac{\pi(1-\alpha_{pm}) + \sin(\pi\alpha_{pm})}{R_i + R_g} + \frac{\pi\alpha_{pm} - \sin(\pi\alpha_{pm})}{R_{pm} + R_g} \right] \quad (15.7-6)$$

$$L_{dm} = \frac{6lr_{rb}N_{sl}^2}{P^2} \left[ \frac{\pi(1-\alpha_{pm}) - \sin(\pi\alpha_{pm})}{R_i + R_g} + \frac{\pi\alpha_{pm} + \sin(\pi\alpha_{pm})}{R_{pm} + R_g} \right] \quad (15.7-7)$$

$$\lambda_m = \frac{8r_{rb}lN_{sl}}{P(R_{pm} + R_g)} \frac{d_m}{\mu_0\mu_{rm}} B_r \sin\left(\frac{\pi\alpha_{pm}}{2}\right) \quad (15.7-8)$$

The accuracy of (15.7-6) and (15.7-7) may be improved by replacing the length of the machine,  $l$ , with the effective length  $l_{eff}$  as described in Reference 2. This accounts for end-flux paths in the machine. This improvement does not apply to the magnetizing flux linkage (15.7-8). Once the  $q$ - and  $d$ -magnetizing inductances have been found using (15.7-6) and (15.7-7), and the leakage inductance is computed using the methods of Appendix C based on geometrical and winding variables,  $\mathbf{G}$  and  $\mathbf{W}$ , the  $q$ - and  $d$ -axis inductances are calculated as

$$L_q = L_{ls} + L_{qm} \quad (15.7-9)$$

$$L_d = L_{ls} + L_{dm} \quad (15.7-10)$$

In order to organize our calculations for design, it is useful to specify the functional dependence. The calculation of the lumped parameter models does not require any inputs over those already defined. The outputs of this analysis are encapsulated into a vector of electrical parameters  $\mathbf{E}$  as

$$\mathbf{E} = [R_s \ L_q \ L_d \ \lambda_m]^T \quad (15.7-11)$$

Functionally, the outputs of this section may be described in the form

$$\mathbf{E} = \mathbf{F}_E(\mathbf{M}, \mathbf{C}, \mathbf{G}, \mathbf{W}) \quad (15.7-12)$$

## 15.8. FERROMAGNETIC FIELD ANALYSIS

In this section, the problem of determining the flux density waveforms in the ferromagnetic portions of the machine is considered. This is desirable for two reasons. First, we will place a limit on the maximum value of flux density so that we do not overly magnetically saturate the steel. Second, although not discussed in this chapter, the flux density waveforms in the stator backiron and teeth can be used to determine hysteresis and eddy current losses. Finally, the problem of computing the minimum field intensity in the positively magnetized portion of the permanent magnet is addressed. This is necessary in order to check for demagnetization.

We begin the development by assuming that all the radial flux density in the air gap within  $\pm\pi/N_s$  cumulates in the tooth. Thus, the flux in the  $i$ 'th tooth is expressed as

$$\Phi_{t(i)}(\theta_{rm}) = \int_{\phi_{t,i}-\pi/N_s}^{\phi_{t,i}+\pi/N_s} B(r_{st}, \phi_{sm}, \theta_{rm}) d\phi_{sm} \quad (15.8-1)$$

where the explicit dependence of the radial flux density on the rotor position is indicated as discussed after (15.6-25). Because of the slot and tooth structure of the machine, the field varies as the rotor moves over the angle occupied by a slot and tooth in a more involved way than a simple rotation. Thus, we will consider a number of discrete mechanical rotor positions as the rotor position varies over a sector of the machine consisting of one slot and one tooth. To this end, let  $\Theta_{rms}$  denote a vector of mechanical rotor position values over a sector. In particular, the elements of  $\Theta_{rms}$  are given by

$$\Theta_{rms(j)} = -\frac{\pi}{N_s} + \frac{2\pi}{N_s} \frac{j-1}{J} \quad j \in [1 \dots J] \quad (15.8-2)$$

where  $j$  is a rotor position index variable, and where  $J$  is the number of positions considered.

As a next step, let  $\Phi_{ts}$  denote a matrix of tooth flux values as the mechanical rotor position varies over the slot/tooth sector. In particular, define the elements of  $\Phi_{ts}$  as

$$\Phi_{ts(i,j)} = \Phi_{t(i)}(\Theta_{rms,j}) \quad i \in [1 \dots S_s 2 / P] \quad j \in [1 \dots J] \quad (15.8-3)$$

In (15.8-3),  $i$  is a tooth index and  $j$  is the rotor position index.

The operation of a permanent magnet ac machine is such that the flux in a tooth at a given rotor position is equal to the flux in the next tooth at that position plus a mechanical displacement of one slot plus one tooth. Thus,

$$\Phi_{t(i)}(\theta_{rm}) = \Phi_{t(i+1)}(\theta_{rm} + 2\pi / S_s) \quad (15.8-4)$$

Using (15.8-3) and (15.8-4), it is possible to synthesize a vector of tooth flux values for tooth 1 over a rotational cycle of rotor positions. In particular, this vector is denoted  $\Phi_{t1c}$  and has elements given by

$$\Phi_{t1c(j+J(i-1))} = \Phi_{ts(\text{mod}(S_s - i + 1, S_s) + 1, j)} \quad (15.8-5)$$

The elements in  $\Phi_{t1c}$  correspond to mechanical rotor positions over a cycle given by

$$\Theta_{rmc(j+J(i-1))} = \Theta_{rms,j} + \frac{2\pi}{S_s}(i-1) \quad i \in [1 \dots 2S_s / P] \quad j \in [1 \dots J] \quad (15.8-6)$$

We will use  $\Theta_{rmc}$  to denote the corresponding electrical rotor positions. From  $\Phi_{t1c}$  a vector of flux density values in the first tooth as the rotor position varies over one cycle is readily expressed

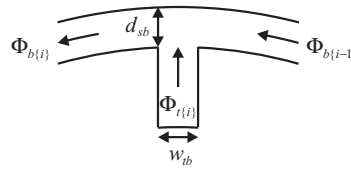


Figure 15.8-1. Backiron flux calculation.

$$\mathbf{B}_{r1c} = \frac{\Phi_{r1c}}{w_{rb}l} \quad (15.8-7)$$

and the maximum tooth flux density as

$$B_{tmx} = \|\mathbf{B}_{r1c}\|_{\max} \quad (15.8-8)$$

where  $\|\cdot\|_{\max}$  returns the absolute value of the element of its matrix or vector argument with the greatest absolute value.

The flux density in the stator backiron is also of interest. Let  $\Phi_{b\{i\}}$  denote the flux in backiron segment  $i$ . In order to calculate the flux density in the stator backiron, consider Figure 15.8-1. Clearly, the backiron flux in segment  $i$  of the machine is related to the flux in tooth  $i$  and the flux in segment  $i-1$  by

$$\Phi_{b\{i\}}(\theta_{rm}) = \Phi_{b\{i-1\}}(\theta_{rm}) + \Phi_{t\{i\}}(\theta_{rm}) \quad (15.8-9)$$

where the segment index operations are modulus  $S_s$ , so that  $\Phi_{b\{1-1\}} = \Phi_{b\{S_s\}}$ . Assuming the fields in the machine are odd-half wave symmetric, it follows that the flux in backiron segment  $S_s$  may be expressed

$$\Phi_{b,S_s}(\theta_{rm}) = -\frac{1}{2} \sum_{n=1}^{S_s/P} \Phi_{t\{n\}}(\theta_{rm}) \quad (15.8-10)$$

Thus, for a given rotor position, (15.8-9) and (15.8-10) may be used to determine the backiron fluxes from the tooth fluxes.

Using (15.8-9) and (15.8-10), a matrix of backiron segment fluxes  $\Phi_{bs}$  is created. Here the rows correspond to segment number and the columns to rotor position. Thus, the elements are assigned as

$$\Phi_{bs\{i,j\}} = \Phi_{b\{i\}}(\theta_{rms,j}) \quad (15.8-11)$$

Using  $\Phi_{bs}$ , it is possible to determine the flux in backiron segment 1 over a cycle of rotor position using an approach identical to that used in calculating the flux in tooth 1. In particular,

$$\Phi_{b1s\{j+J(i-1)\}} = \Phi_{bs\{\text{mod}(S_s-i+1,S_s)+1,j\}} \quad i \in [1 \cdots 2S_s / P] \quad j \in [1 \cdots J] \quad (15.8-12)$$

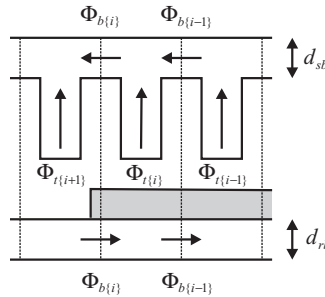


Figure 15.8-2. Backiron flux linkage.

whereupon the flux density in backiron segment 1 is calculated as

$$\mathbf{B}_{b1c} = \frac{\Phi_{b1c}}{d_{sb}l} \quad (15.8-13)$$

$$\mathbf{B}_{sbmx} = \|\mathbf{B}_{b1c}\|_{\max} \quad (15.8-14)$$

At this point, a means of calculating the stator flux density waveforms in tooth 1 and backiron segment 1 has been set forth. It is unnecessary to calculate these waveforms in other teeth, as they will simply be phase shifted from the waveform in tooth 1 and backiron segment 1. For the next step in our development, let us consider the problem of calculating the rotor fields. Since rotor field is essentially dc (viewed from the rotor), our focus will be on computing the extrema in the fields so that we can avoid heavy saturation and demagnetization.

Let us first consider the rotor backiron flux density, since it is closely related to the stator backiron flux density. Consider Figure 15.8-2. Therein a portion of the stator and rotor is shown in developed diagram form. The key point in this figure is that because the backiron rotor flux is governed by a relationship analogous to that governed by the stator backiron flux, the rotor flux at the indicated positions and directions will be equal to the stator flux at the corresponding segments. This conclusion can also be reached by consideration of Gauss's law. Considering all segments and all rotor positions, an estimate of the peak tangential flux density in the rotor is given by

$$B_{rbt,mx} = \frac{1}{d_{rb}l} \|\Phi_{bs}\|_{\max} \quad (15.8-15)$$

Now let us consider the peak radial flux density in the rotor. From (15.6-25), with  $r = r_{rb}$

$$B(r_{rb}, \phi_{sm}) = \frac{\mathbb{F}_m(\phi_{sm}) + \mathbb{F}_s(\phi_{sm})}{R_p(\phi_{sm}) + R_g} \quad (15.8-16)$$

In (15.8-16),  $\mathbb{F}_m(\phi_{sm})$  and  $R_p(\phi_{sm})$  are constant except for points of discontinuity. The maximum radial flux density must either be at an extrema of  $\mathbb{F}_s(\phi_{sm})$  or at one of the

points of discontinuity. Because of symmetry, it is sufficient to consider the maximum of  $\mathbb{F}_s(\phi_{sm})$  and the two points on the edges of positively magnetized permanent magnet regions. This yields

$$B_{rbr, mx} = \max \left( \left| \frac{\mathbb{F}_{st1}}{R_i + R_g} \right|, \left| \frac{\mathbb{F}_{m,pk} + \mathbb{F}_{st1}}{R_{pm} + R_g} \right|, \left| \frac{\mathbb{F}_{m,pk} + \mathbb{F}_{st2}}{R_{pm} + R_g} \right|, \left| \frac{\mathbb{F}_{st2}}{R_i + R_g} \right|, \left| \frac{\mathbb{F}_m(2\phi_i / P) + \mathbb{F}_{s,pk}}{R_p(2\phi_i / P) + R_g} \right| \right) \quad (15.8-17)$$

where  $\mathbb{F}_{st1}$  and  $\mathbb{F}_{st2}$  are the stator MMF at the edges of the positively magnetized permanent magnet regions (with the rotor position at zero), which are given by

$$\mathbb{F}_{st1} = \mathbb{F}_s \left( \frac{(3 - \alpha_{pm})\pi}{P} \right) \quad (15.8-18)$$

$$\mathbb{F}_{st2} = \mathbb{F}_s \left( \frac{(3 + \alpha_{pm})\pi}{P} \right) \quad (15.8-19)$$

and where  $\mathbb{F}_{m,pk}$  and  $\mathbb{F}_{s,pk}$  are the peak values of the permanent magnet and stator MMF, which are given by

$$\mathbb{F}_{m,pk} = \frac{d_m B_r}{\mu_0(1 + \chi_m)} \quad (15.8-20)$$

$$\mathbb{F}_{s,pk} = \frac{3\sqrt{2}N_{s1}I_s}{P} \quad (15.8-21)$$

At this point, we have developed expressions for the peak tangential flux density from (15.8-15) in the rotor backiron, as well as the peak radial flux density entering the outer edge of the backiron given by (15.8-17). The question arises about the interaction of these two field components, and whether this interaction could result in magnetic saturation even if the individual components are bounded. As it turns out, this is not the case. First, it should be remembered that the peak tangential flux density in the backiron and the peak radial flux density do not occur at the same spatial location. Indeed, they are spatially separated by 90 electrical degrees. Second, it should be remembered that the radial component of the flux density is only the radial component of the flux density at the outer surface of the rotor backiron. Consider Figure 15.8-3. Therein the backiron region of the machine is shown. Consider a radial component of the flux density  $B_r$  entering a region of cross sectional area  $S_r$ . Let  $B_{t1}$  and  $B_{t1}$  be the flux density through surfaces  $S_{t1}$  and  $S_{t2}$ . Now, suppose that  $|B_r| < B_{sat}$ ,  $|B_{t1}| < B_{sat}$ , and  $|B_{t2}| < B_{sat}$ , where  $B_{sat}$  is the flux density level considered to be saturated. Now consider the flux density  $B_i$ , which we will take to be uniform across an intermediate surface  $S_i$ . Given our limits on the input flux densities, and the fact that  $S_i \geq \min(S_r + S_{t1}, S_{t2})$ , it follows that  $|B_i| < B_{sat}$ —in other words, the flux could distribute itself so as to avoid saturation.

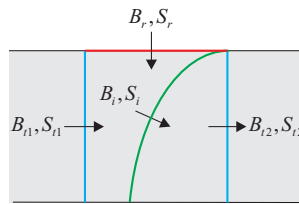


Figure 15.8-3. Flux density in rotor backiron.

Now let us consider the field intensity in the permanent magnet. Our interest is computing the minimum (most negative) field intensity in the positively magnetized region. Combining (15.6-15) with (15.6-25) in a region of positive magnetization yields

$$H = \frac{\frac{r_r}{r} \frac{\mathbb{F}_{m,pk} + \mathbb{F}_s}{R_{pm} + R_g} - B_r}{\mu_0(1 + \chi_m)} \quad (15.8-22)$$

Assuming that  $\mathbb{F}_{m,pk} + \mathbb{F}_s > 0$ , it follows that the minimum field intensity occurs where  $\mathbb{F}_s$  is a minimum and where the radius is a maximum. Thus

$$H_{mn} = \frac{\frac{r_r}{r_{rg}} \frac{\mathbb{F}_{m,pk} + \mathbb{F}_{s,mn}}{R_{pm} + R_g} - B_r}{\mu_0(1 + \chi_m)} \quad (15.8-23)$$

where the minimum stator flux density over the positively magnetized region of the permanent magnet can be shown to be

$$\mathbb{F}_{s,mn} = \begin{cases} -\mathbb{F}_{s,pk} & 3 - \alpha_{pm} \leq \text{mod}(2 + 2\phi_i / \pi, 4) \leq 3 + \alpha_{pm} \\ \min(\mathbb{F}_{st1}, \mathbb{F}_{st2}) & \text{otherwise} \end{cases} \quad (15.8-24)$$

At this point, it is convenient to define the functional dependence of our field calculations. These calculations require no inputs beyond those previously defined. The output of the analysis of this section is

$$\mathbf{F} = [\theta_{rm} \ B_{t1c} \ B_{b1s} \ B_{rbt,mx} \ B_{rbm,mx} \ H_{mn}]^T \quad (15.8-25)$$

The calculations of this section may thus be organized as

$$\mathbf{F} = \mathbf{F}_F(\mathbf{M}, \mathbf{G}, \mathbf{W}, \mathbf{I}) \quad (15.8-26)$$

## 15.9. FORMULATION OF DESIGN PROBLEM

At this point, we are ready to consider the design of the machine. There are many ways to formulate the design problem. Herein, an approach will be given that is readily tailored to a specific application and can be readily expanded to include a large variety of considerations. We will specifically consider the problem of designing a machine to produce a positive torque  $T_e^*$  at a mechanical speed  $\omega_{rm}^*$  using an inverter with a given dc bus voltage,  $v_{dc}$ . Our approach will be to formulate the design problem as an optimization problem in which we attempt to minimize mass and loss, and then to use an optimization algorithm to arrive at the best choice of parameters.

### Design Space

An important early step in the design process is to identify the parameters we are free to choose. We will use  $\Theta$  to denote the vector of free design parameters. One possible choice of a parameter vector is

$$\Theta = [s_t \ r_t \ c_t \ m_t \ \mathbf{G}_x \ \mathbf{W}_x \ \mathbf{I}_x]^T \quad (15.9-1)$$

Using this choice, every other quantity of the machine can be calculated. However, it is often the case that some of these parameters are fixed prior to the initiation of the design process. For our purposes, it is assumed that the shaft radius  $r_{sh}$  is known. Other variables that we will consider to be fixed include the number of poles  $P$  and the number of slots  $S_s$ . Generally speaking, if one neglects frequency dependent losses, increasing the number of poles of the machine will result in decreased mass and loss. Since we have not included these effects here, we will fix this parameter. The number of slots should be an integer multiple of the number of phases times the number of poles so that the machine can be constructed in a symmetric fashion. We will also assume a packing factor  $\alpha_{pf}$ , end winding offset  $l_{eo}$ , and the location of stator slot 1,  $\phi_{ss1}$ , to be fixed. In order to simplify the design problem further, we will assume that we will not have tooth tips. Thus,  $d_{tc} = d_{te} = 0$  and  $\theta_{tt} = \theta_t$ . This further reduces the design space. In our design process, we will also require the mass be less than  $m_{lim}$  and have a power less than  $P_{lim}$ . We will base our magnetic analysis on  $J$  rotor positions. Let us denote the vector of fixed design parameters as  $\mathbf{D}$ , where

$$\mathbf{D} = [v_{dc} \ T_e^* \ \omega_{rm}^* \ P \ S_s \ \alpha_{pf} \ l_{eo} \ r_{sh} \ v_{fs} \ J \ \phi_{ss1} \ m_{lim} \ P_{lim}]^T \quad (15.9-2)$$

With the variables associated with  $\mathbf{D}$  set *a priori*, and in the absence of a tooth tip, the parameter vector that we must find becomes

$$\Theta = [s_t \ r_t \ c_t \ m_t \ \hat{\mathbf{G}}_x \ \hat{\mathbf{W}}_x \ \mathbf{I}_x]^T \quad (15.9-3)$$

where

$$\hat{\mathbf{G}}_x = [d_i \ d_{rb} \ d_m \ g \ d_{tb} \ \alpha_t \ d_{sb} \ \alpha_{pm} \ l]^T \quad (15.9-4)$$

and

$$\hat{\mathbf{W}}_x = [N_{s1}^* \ \alpha_3^*]^T \quad (15.9-5)$$

Note that even with the fixed parameters, our design is left with four discrete variables (the material types) and 13 continuous variables for a total of 17 degrees of freedom.

## Design Metrics

While there are many possible design metrics of interest, herein we will focus on two—mass and loss. The mass may be readily expressed as

$$m = v_{sl}\rho_s + v_{rb}\rho_r + v_{pm}\rho_m + 3v_{cd}\rho_c \quad (15.9-6)$$

We will consider two components of the loss. First, we will consider the resistive loss in the machine, which is readily expressed as

$$P_r = 3R_s I_s^2 \quad (15.9-7)$$

Next, we will consider the semiconductor conduction loss. As an estimate of the loss, we will treat both the diode and transistor as having a forward voltage drop of  $v_{fs}$ . With this assumption, it can be shown that the total semiconductor power loss in the three phase bridge is given by

$$P_s = \frac{6\sqrt{2}}{\pi} v_{fs} I_s \quad (15.9-8)$$

The sum of these two loss components is given by

$$P_{loss} = P_s + P_r \quad (15.9-9)$$

We will attempt to select the parameter of the machine to minimize the total mass  $m$  and the power loss  $P_{loss}$ , subject to operating constraints. These constraints are our next topic.

## Design Constraints

In order to ensure proper operation of the machine, we will enforce a number of constraints on the design. As an example, one constraint will be that the machine must produce the desired torque. Let  $c_i$  denote a variable that describes whether the  $i$ 'th constraint is satisfied. We will formulate  $c_i$  in such a way that  $0 \leq c_i \leq 1$ , and that if

$c_i = 1$ , the constraint will be said to be satisfied. In order to evaluate the constraint variable, we will define less-than-or-equal-to and greater-than-or-equal-to functions as

$$\text{lte}(x, x_{mx}) = \begin{cases} 1 & x \leq x_{mx} \\ \frac{1}{1 + x - x_{mx}} & x > x_{mx} \end{cases} \quad (15.9-10)$$

$$\text{gte}(x, x_{mn}) = \begin{cases} 1 & x \geq x_{mn} \\ \frac{1}{1 + x_{mn} - x} & x < x_{mn} \end{cases} \quad (15.9-11)$$

Both of these functions have an appropriate range, and evaluate to 1 if their respective constraints are satisfied. As their respective constraints become further from being satisfied, they tend toward zero.

Our first two constraints will be related to the machine geometry and structural issues. First, it is desired to keep the length of the teeth reasonable compared with their width. Thus, we will require that

$$c_1 = \text{lte}(d_{st}, \alpha_{tar} w_{tb}) \quad (15.9-12)$$

where  $\alpha_{tar}$  is the allowed tooth aspect ratio (depth to width). In order to make the machine easier to wind, we will next require that the wire diameter multiplied by a slot opening factor  $\alpha_{so}$  (which is greater than one) be less than the width of the slot opening  $w_{so}$ . Thus

$$c_2 = \text{lte}(d_c \alpha_{so}, w_{so}) \quad (15.9-13)$$

The next five constraints are related to the field analysis, and in particular to ensuring that we do not overly saturate the material nor demagnetize the permanent magnet

$$c_3 = \text{lte}(\|B_{t1c}\|_{\max}, B_{s,lim}) \quad (15.9-14)$$

$$c_4 = \text{lte}(\|B_{b1s}\|_{\max}, B_{s,lim}) \quad (15.9-15)$$

$$c_5 = \text{lte}(B_{brt,mx}, B_{r,lim}) \quad (15.9-16)$$

$$c_6 = \text{lte}(B_{brb,mx}, B_{r,lim}) \quad (15.9-17)$$

$$c_7 = \text{gte}(H_{mn}, H_{lim}) \quad (15.9-18)$$

Another constraint is that the current density within the wire does not exceed an acceptable value. Thus we choose

$$c_8 = \text{lte}(I_s / a_c, J_{c,lim}^*) \quad (15.9-19)$$

where  $J_{c,mx}^*$  is the maximum allowable rms current density for the material,  $m_c$ . In essence, this is a thermal limit, which, if rigorously treated, should be a function of

how well the machine conducts heat away from the winding. However, the allowed current density will be treated as a constant herein.

Our next constraint will be that the desired torque is obtained. The torque is readily calculated from the lumped parameter model. From Chapter 4, torque may be expressed as

$$T_e = \frac{3}{2} \frac{P}{2} (\lambda_m i_{qs}^r + (L_d - L_q) i_{qs}^r i_{ds}^r) \quad (15.9-20)$$

Assuming motor operation at positive speed, the torque constraint may be expressed as

$$c_9 = \text{gte}(T_e, T_e^*) \quad (15.9-21)$$

The next constraint we will consider is designed to ensure that there is adequate dc link voltage. The *q*- and *d*-axis voltage at our operating point may be expressed as

$$v_{qs}^r = r_s i_{qs}^r + \omega_r^* (L_d i_{ds}^r + \lambda_m) \quad (15.9-22)$$

$$v_{ds}^r = r_s i_{ds}^r - \omega_r^* L_q i_{qs}^r \quad (15.9-23)$$

whereupon the peak line-to-line voltage may be expressed as

$$v_{pk,ll} = \sqrt{3} \sqrt{(v_{qs}^r)^2 + (v_{ds}^r)^2} \quad (15.9-24)$$

From our work in Chapter 12, the peak line-to-line voltage must be less than the dc voltage if the desired current is to be obtained. This leads to the constraint

$$c_{10} = \text{lte}(v_{ll,pk}, v_{dc}) \quad (15.9-25)$$

Our two final constraints will be designed to focus our attention to reasonable mass and loss. Thus, we will constrain the mass and loss as

$$c_{11} = \text{lte}(m, m_{lim}) \quad (15.9-26)$$

$$c_{12} = \text{lte}(P_{loss}, P_{lim}) \quad (15.9-27)$$

where  $m_{lim}$  and  $P_{lim}$  are limits on the allowed loss and mass, respectively.

Before concluding this section, it is convenient to define an aggregate constraint as

$$c_a = \frac{1}{N_c} \sum_{i=1}^{N_c} c_i \quad (15.9-28)$$

where  $N_c$  is the number of constraints, in this case 10. The aggregate constraint has properties similar to the individual constraints. It has a range of [0,1], and is 1 if all constraints are satisfied, and less than 1 if not.

## Design Fitness

The fitness of the design refers to a mathematical function to be maximized. It is desired to create the function so that when maximized, the resulting design finds the extrema of the desired metrics subject to all constraints being satisfied. In this case, the fitness will be a vector-valued function since we desired to minimize both mass and loss. A suitable choice in fitness function is given by

$$f(\boldsymbol{\theta}, \mathbf{D}) = \begin{cases} \varepsilon(c_a - 1)[1 \ 1]^T & c_a < 1 \\ \left[ \frac{1}{m} \ \frac{1}{P_{loss}} \right]^T & c_a = 1 \end{cases} \quad (15.9-29)$$

where the notation  $f(\boldsymbol{\theta}, \mathbf{D})$  is used as a reminder that although not explicitly indicated, the mass and constraints values are functions of the design parameters and design specifications, and where  $\varepsilon$  denotes a small positive number used for scaling purposes for plotting; its value does not affect the outcome of the optimization. If constraints are not met, then both elements of the fitness will be equal to a small negative number. As the constraints become closer to being satisfied, both elements of the fitness function will tend to zero (and will be equal). If all constraints are met, the elements of the fitness are the inverse of the mass and the inverse of the power loss. Note that maximizing  $f(\boldsymbol{\theta}, \mathbf{D})$  does not yield a single design, but rather a set of designs known as the Pareto-optimal front. The designs on this front have the property that it is impossible to improve one metric without sacrificing the other. In particular, maximizing  $f(\boldsymbol{\theta}, \mathbf{D})$  yields a set of designs, where each design in the set has the property that loss cannot be decreased without increasing mass.

Before concluding this section, let us consider the problem of evaluating the fitness function—something that is clearly required for optimization. Given  $\boldsymbol{\theta}$  as defined by (15.9-3) and the fixed parameters  $\mathbf{D}$  given by (15.9-2), then the material types  $s_t$ ,  $r_t$ ,  $c_t$ , and  $m_t$ , as well as all parameters associated with  $\mathbf{G}_x$ ,  $\mathbf{W}_x$ , and  $\mathbf{I}_x$  are known. Using  $s_t$ ,  $r_t$ ,  $c_t$ , and  $m_t$ , the material parameter vectors  $\mathbf{S}$ ,  $\mathbf{R}$ ,  $\mathbf{C}$ , and  $\mathbf{M}$  are readily determined using (15.4-1)–(15.4-4). Based on the parameters in  $\mathbf{G}_x$ , the remaining geometrical parameters are calculated using (15.2-35) and (15.2-36), which encapsulate the calculations of Section 15.2, whereupon of the geometry vector  $\mathbf{G}$  is known. From the input variables to the winding variable vector  $\mathbf{W}_x$ , the winding variable vector  $\mathbf{W}$  is readily calculated using (15.3-20) and (15.3-21) using the expressions in Section 15.3. Using the geometry and winding parameters  $\mathbf{G}$  and  $\mathbf{W}$ , as well as material parameters  $\mathbf{C}$ , and  $\mathbf{M}$ , the parameters of the lumped parameter machine model  $\mathbf{E}$  are readily calculated using (15.7-12) and the analysis of Section 15.6. The currents stored in  $\mathbf{I}_x$  can then be used to calculate the current vector  $\mathbf{I}$  using (15.5-8) and (15.5-9) and the analysis of Section 15.4. Finally, information in the field vector  $\mathbf{F}$  may be computed in accordance with (15.8-26) and the analysis of Section 15.8. At this point, all information needed to evaluate the design metrics and constraints is available. The fitness can thus be calculated by sequentially evaluating (15.9-6)–(15.9-9) and (15.9-12)–(15.9-29).

## 15.10. CASE STUDY

In this section, we will undertake a case study in machine design. The design requirements and fixed parameters of this design are enumerated in Table 15.10-1. Our goal is to determine a set of designs that define the performance possibilities in the trade-off between loss and mass. In order to solve this optimization problem, any optimization method can be used. However, in this work, we will use a genetic algorithm. Genetic algorithms use the principles of biological evolution to evolve a population of designs. The reader is referred to [4, 5] for introductions to genetic algorithms. The effectiveness to this technique relative to other for this class or problem is discussed in Reference 3.

When using genetic algorithms, the parameters are encoded into “genes.” In this problem, the public-domain open-source MATLAB-based GOSET package is used [6]. The encoding process consists of mapping the parameter values to normalized numbers between 0 and 1, where 0 corresponds to the minimum allowed parameter value and 1 corresponds to the maximum allowed parameter value. Thus, a minimum and maximum value for each parameter must be specified. In addition, each parameter has a type indicating how it is mapped; 1 denotes integer values that are linearly mapped to the range, 2 denotes real numbers, but that are also linearly mapped, and 3 denotes real numbers that are mapped in an logarithmic fashion. Each parameter is assigned to a gene, and each gene is assigned to a chromosome (though only one chromosome is used herein). The ranges and types of all parameters used in this example are listed in Table 15.10-2. The ranges are determined by experience and engineering judgment. Fortunately, only crude estimates of the ranges are needed.

The final step needed to perform the design using a genetic algorithm is to select a population size and the number of generations, both of which are set to 3000 in this study. Figure 15.10-1 illustrates the evolution of the design. Consider Figure 15.10-1a, which has an upper and lower trace. The upper trace depicts the parameter distribution of the final population. In this trace, each design is marked with a point in each of the 15 columns, each of which corresponds to a normalized parameter value (gene). The point placement along the width of the column is in order of the fitness of the first objective, in this case, mass; points on the left side of the column have relatively low fitness, while those at the right side have high fitness. The distribution of points gives an indication of the sensitivity of fitness to a parameter within its range and the appropriateness of the parameter limits. For example, if all point were clustered to the top of a column, it would indicate that the parameter range needs to be increased.

TABLE 15.10-1. Fixed Design Specifications

Parameter	Value	Parameter	Value	Parameter	Value
$v_{dc}$	400 V	$\alpha_{pf}$	0.5	$\phi_{ss1}$	$\pi/24$
$T_e^*$	20 Nm	$l_{eo}$	1 cm	$m_{lim}$	25 kg
$\omega_m^*$	2000 rpm	$r_{sh}$	2 cm	$P_{lim}$	500 W
$S_s$	24	$v_{js}$	2 V	$\alpha_{tar}$	10
$P$	4	$J$	3	$\alpha_{so}$	1.5

TABLE 15.10-2. Parameter Ranges

Parameter	Description	Type	Min	Max	Gene
$s_t$	Stator steel type	1	1	4	1
$r_t$	Rotor steel type	1	1	4	2
$c_t$	Conductor type	1	1	2	3
$m_t$	Magnet type	1	1	4	4
$d_i$	Depth of inert region (m)	2	0	$10^{-1}$	5
$d_{rb}$	Depth of rotor backiron (m)	3	$10^{-3}$	$5 \cdot 10^{-2}$	6
$d_m$	Magnet depth (m)	3	$10^{-3}$	$5 \cdot 10^{-2}$	7
$g$	Air gap (m)	3	$5 \cdot 10^{-4}$	$10^{-2}$	8
$d_{tb}$	Depth of tooth base (m)	3	$10^{-3}$	$5 \cdot 10^{-2}$	9
$\alpha_t$	Tooth fraction	2	0.05	0.95	10
$d_{sb}$	Depth of stator backiron (m)	3	$10^{-3}$	$5 \cdot 10^{-2}$	11
$\alpha_{pm}$	Magnet fraction	2	0.05	0.95	12
$l$	Length (m)	3	$10^{-2}$	0.5	13
$N_{s1}^*$	Pk. fund. cond. density (cond/rad)	3	10	$10^3$	14
$\alpha_3^*$	Coefficient 3rd harmonic cond. density	2	0.1	0.7	15
$i_{qs}^r$	$q$ -axis current (A)	3	0.1	50	16
$i_{ds}^*$	$d$ -axis current (A)	2	-50	0	17

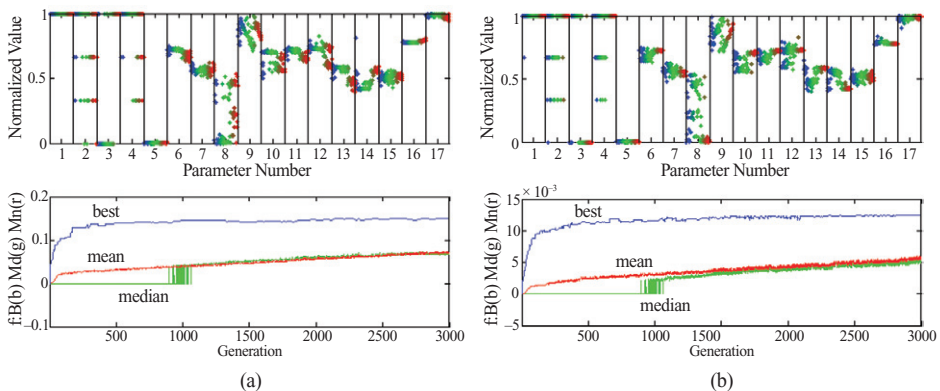


Figure 15.10-1. Design evolution. (a) Mass objective; (b) loss objective.

The lower trace depicts the fitness in terms of the first objective (reciprocal of mass) of the most fit individual versus generation, as well as the median and average inverse mass of the population versus generation. Figure 15.10-1b is similar, although in this case, the fitness being considered is the second objective, in particular the reciprocal of the loss.

As previously described, the output of a multiobjective optimization is not a single design, but a set of designs referred to as a Pareto-optimal front. For this case study, the Pareto-optimal front is shown in Figure 15.10-2. Therein, each “x” marks a specific design. Each design is better than all the others in terms of either mass or loss;

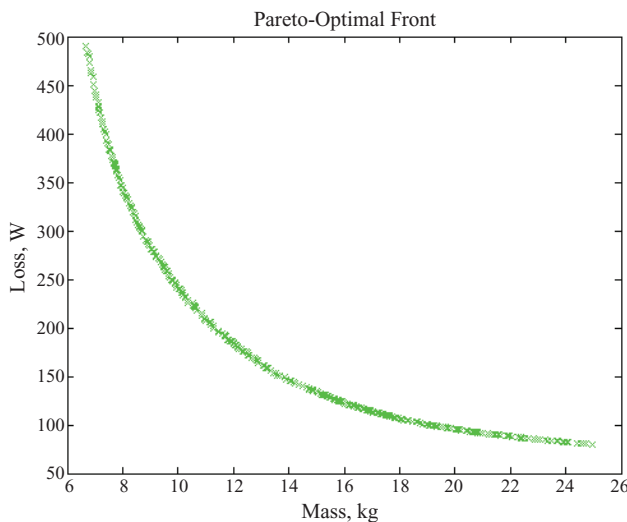


Figure 15.10-2. Mass-loss tradeoff.

however, no design is better than any of the others in both mass and loss. In optimization terms, the solutions are described as being “nondominated.” In terms of machine design, this set of designs defines the performance trade-offs between the competing objectives.

Again, each “x” in Figure 15.10-2 corresponds to an individual design. The parameters and some performance data for machine design 1, which corresponds to the leftmost “x” in Figure 15.10-2 and is the design with the least mass, is given in Table 15.10-3. Note that the mass does not include the machine housing, and the losses do not include core losses or windage. However, the basic approach may be readily extended to include these effects. There are many points of interest in Table 15.10-3. First, note that the conductor used is aluminum rather than copper. This may surprise the reader in that copper is normally considered a better conductor. However, this is only true on a volumetric basis. On a per-mass-basis aluminum is a superior conductor. This advantage is tempered, however, in that the increased volume requires an increase in steel to accommodate larger slots, so on some points on the front, copper is used. Looking at the electrical model parameters, it is noted that the machine is slightly salient. This is due to the fact that the permanent magnet has a susceptibility that is slightly larger than that of air. In the operating point performance data, it is interesting that a small  $d$ -axis current is being used, suggesting a slight amount of flux weakening. This is compatible with the fact that the peak line-to-line voltage is essentially equal to the maximum value allowed for the dc voltage of 400 V. It is also interesting to observe that the stator tooth, stator backiron, and rotor tangential flux densities are all at the maximum value allowed. Observe that the permanent magnet is not close to its demagnetization limit.

TABLE 15.10-3. Machine Design 1 from Pareto-Optimal Front

Design data	Electrical model
Outside diameter: 16.6 cm	Number of poles: 4
Total length: 11.5 cm	Nominal stator resistance: 1.54 $\Omega$
Active length: 5.33 cm	$q$ -axis inductance: 11.8 mH
Number of poles: 4	$d$ -axis inductance: 12.1 mH
Number of slots: 24	Flux linkage due to PM: 489 mVs
Stator material type: M47	
Rotor Material type: M36	
Conductor type: Aluminum	
Permanent magnet type: SmCo17-R28	
Permanent magnet fraction: 71.5%	
Permanent magnet depth: 0.896 cm	
Shaft radius: 2 cm	
Inert radius: 2 cm	
Rotor iron radius: 3.48 cm	
Air gap: 2.25 mm	
Slot depth: 2.38 cm	
Tooth fraction: 56.2%	
Stator backiron depth: 1.32 cm	
Rotor backiron depth: 1.48 cm	
Fundamental conductor density: 153 cond/rad	
3rd harmonic conductor density: 36.5%	
Conductor diameter: 1.38 mm	
Stator Iron mass: 4.12 kg	
Rotor iron mass: 0.953 kg	
Conductor mass: 0.914 kg	
Magnet mass: 0.7 kg	
Mass: 6.69 kg	
$a$ -phase winding pattern (1st pole): 0 18 49 49 18 0	
Minimum conductors per slot: 67	
Maximum conductors per slot: 67	
Packing factor: 50%	
Operating point performance data	
	Speed: 2000 rpm
	Frequency: 66.7 Hz
	$q$ -axis voltage: 220 V
	$d$ -axis voltage: -69.7 V
	Peak line-to-line voltage: 399 V
	$q$ -axis current: 13.7 A
	$d$ -axis current: -1.19 A
	Peak line current: 13.8 A
	Current density: 6.53 A rms/mm <sup>2</sup>
	Torque: 20.1 Nm
	Semiconductor conduction loss: 52.6 W
	Machine resistive losses: 438 W
	Total loss: 490 W
	Machine efficiency: 90.6%
	Inverter efficiency: 98.9%
	Machine/inverter efficiency: 89.6%
	Stator tooth flux density/limit: 98.6%
	Stator backiron flux density/limit: 99.6%
	Rotor peak tangential flux density/limit: 98.8%
	Rotor peak radial flux density/limit: 85%
	Permanent magnet demagnetization/limit: 36.1%

A cross section of the machine is depicted in Figure 15.10-3. Therein, the darkest region is the machine shaft. The stator and rotor steels shapes are also indicated. It is interesting that the machine used two different steels—M47 in the stator and M36 in the rotor. The M47 has a higher saturation flux density that is particularly advantageous in the stator where the flux becomes concentrated in the teeth. The M36 grade considered has a lower density that is advantageous in regions where the higher flux density is not needed.

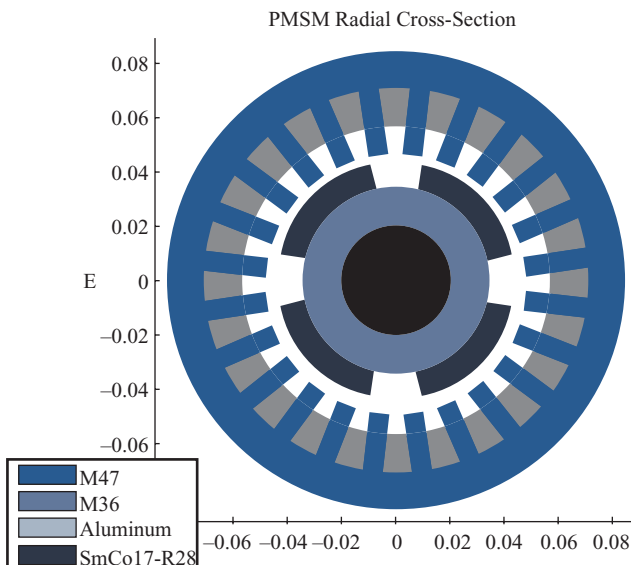


Figure 15.10-3. Machine design 1 cross section.

Figure 15.10-4 depicts the flux density in a tooth and in a backiron segment. It is interesting that although the machine will have a sinusoidal back emf waveform, neither of the flux density waveforms is sinusoidal. The tooth flux density waveform can be viewed as a trapezoidal contribution due to the permanent magnet added to a sinusoidal component due to the stator current. Nevertheless, the approximately sinusoidal conductor distribution yields a machine with a sinusoidal back emf waveform (at least in terms of line-to-line measurement).

It is interesting to compare this design with a second design from the front. Table 15.10-4 lists the parameters and performance data from machine design 100 (the 100th machine design in order of increasing mass). This machine has significantly lower loss than the first machine (252 W vs. 490 W), and significantly higher mass (9.71 kg vs. 6.69 kg). Although many features of the design have changed, one of the most significant changes is an increase in wire diameter from 1.38 to 1.87 mm. This lowers the machine resistance, but increases conductor mass from 0.914 to 1.64 kg and stator mass from 4.12 to 6.40 kg. The increase in stator mass is in order to accommodate larger slots for the larger diameter wire. The changes in magnet and rotor mass are less significant. As a result of the increased conductor size, the current density drops from 6.53 to 3.32 A rms/mm<sup>2</sup>.

## 15.11. EXTENSIONS

The objective of this chapter was to provide an introduction to the design of permanent-magnet ac machines. Although the approach considered was fairly detailed, several

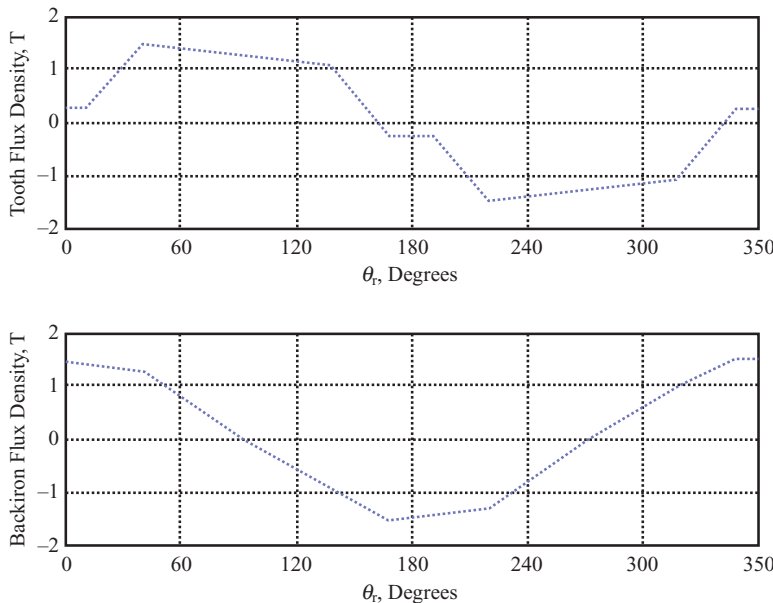


Figure 15.10-4. Flux density waveforms.

refinements are clearly necessary before using this approach for commercial designs. Shortcomings include addressing stator core loss, incorporating thermal analysis, and addressing structural issues, to name a few. Nevertheless, the general approach presented here may be readily extended to include these issues. Indeed, some of these extensions are described in References 2, 3, and 7–10. Another straightforward extension is the consideration of multiple operating points. This may be readily incorporated by requiring that all operational constraints be satisfied at every desired operating point and computing a weighted loss metric in terms of the individual operating points. Finally, it should be observed that there are many configurations of permanent-magnet ac machines. A discussion of many types, as well as other aspects that may be desirable to include in the design, such as core and proximity effect loss, are discussed in Reference 11.

## ACKNOWLEDGMENTS

The authors would like to thank the U.S. Office of Naval Research for supporting the development of this section as Grant N00014-08-1-0080. In addition, we would like to thank the Grainger Center for Electromechanics for support of numerous machine design grants.

TABLE 15.10-4. Machine Design 100 from Pareto-Optimal Front

Design data	Electrical model
Outside diameter: 18.3 cm	Number of poles: 4
Total length: 12.9 cm	Nominal stator resistance: 813 mΩ
Active length: 6.58 cm	$q$ -axis inductance: 12.3 mH
Number of poles: 4	$d$ -axis inductance: 12.7 mH
Number of slots: 24	Flux linkage due to PM: 526 mVs
Stator material type: M47	
Rotor material type: M47	
Conductor type: Aluminum	
Permanent magnet type: SmCo27-R32	
Permanent magnet fraction: 58.9%	
Permanent magnet depth: 0.866 cm	
Shaft radius: 2 cm	
Inert radius: 2.03 cm	
Rotor iron radius: 3.27 cm	
Air gap: 1 mm	
Slot depth: 3.68 cm	
Tooth fraction: 64%	
Stator backiron depth: 1.23 cm	
Rotor backiron depth: 1.23 cm	
Fundamental conductor density: 135 cond/rad	
3rd harmonic conductor density: 36.1%	
Conductor diameter: 1.87 mm	
Stator iron mass: 6.4 kg	
Rotor Iron mass: 1.02 kg	
Conductor mass: 1.64 kg	
Magnet mass: 0.647 kg	
Mass: 9.71 kg	
<i>a</i> -phase winding pattern (1st pole)	
0 16 43 43 16 0	
Minimum conductors per slot: 59	
Maximum conductors per slot: 59	
Packing factor: 50%	
	Operating point performance data
	Speed: 2000 rpm
	Frequency: 66.7 Hz
	$q$ -axis voltage: 219 V
	$d$ -axis voltage: -67.5 V
	Peak line-to-line voltage: 397 V
	$q$ -axis current: 12.7 A
	$d$ -axis current: -2.19 A
	Peak line current: 12.9 A
	Current density: 3.32 A rms/mm <sup>2</sup>
	Torque: 20 Nm
	Semiconductor conduction loss: 49.2 W
	Machine resistive losses: 203 W
	Total loss: 252 W
	Machine efficiency: 95.4%
	Inverter efficiency: 98.9%
	Machine/inverter efficiency: 94.3%
	Stator tooth flux density/limit: 99.4%
	Stator backiron flux density/limit: 99.9%
	Rotor peak tangential flux density/limit: 99.3%
	Rotor peak radial flux density/limit: 86%
	Permanent magnet demagnetization/limit: 42.4%

## REFERENCES

- [1] S.D. Sudhoff, J. Cale, B. Cassimere, and M. Swinney, "Genetic Algorithm Based Design of a Permanent Magnet Synchronous Machine," 2005 International Electric Machines and Drives Conference, San Antonio, TX, May 15–18, 2005.
- [2] B.N. Cassimere and S.D. Sudhoff, "Analytical Design Model for Surface Mounted Permanent Magnet Synchronous Machines," *IEEE Trans. Energy Conversion*, Vol. 24, No. 2, June 2009, pp. 338–346.

- [3] B.N. Cassimere and S.D. Sudhoff, "Population Based Design of Permanent Magnet Synchronous Machines," *IEEE Trans. Energy Conversion*, Vol. 24, No. 2, June 2009, pp. 347–357.
- [4] J.H. Holland, *Adaptation in Natural and Artificial Systems: An Introductory Analysis with Applications to Biology, Control, and Artificial Intelligence*, The MIT Press, Cambridge, MA, 1992.
- [5] K. Deb, *Multi-Objective Optimization Using Evolutionary Algorithms*, John Wiley & Sons, Chichester, UK, 2001.
- [6] S.D. Sudhoff, "Genetic Optimization Engineering Tool (GOSET)." Available at: <https://engineering.purdue.edu/ECE/Research/Areas/PEDS> (accessed on January 21, 2013).
- [7] M. Bash, S.D. Pekarek, S.D. Sudhoff, J. Whitmore, and M. Frantzen, "Comparing the Pareto-Optimal Fronts of Machine-Rectifier Systems," Proceedings of the Electric Machinery Technology Symposium, Philadelphia, PA, May 19–20, 2010.
- [8] M. Bash, S.D. Pekarek, S.D. Sudhoff, J. Whitmore, and M. Frantzen, "A Comparison of Permanent Magnet and Wound Rotor Synchronous Machines for Portable Power Generation," 2010 Power and Energy Conference and Illinois, Urbana, IL, February 12–13, 2010.
- [9] J. Krizan and S.D. Sudhoff, "Modeling Semiconductor Losses for Population Based Electric Machinery Design," 2012 Applied Power Electronics Conference, Orlando, FL, February 5–9, 2012.
- [10] J. Krizan and S.D. Sudhoff, "Theoretical Performance Boundaries for Permanent Magnet Machines as a Function of Magnet Type," 2012 Power Engineering Society General Meeting, San Diego, CA, July 22–26, 2012.
- [11] D.C. Hanselman, *Brushless Permanent-Magnet Motor Design*, McGraw-Hill, New York, 1994.

## PROBLEMS

1. Derive (15.2-4)–(15.2-18).
2. Derive (15.2-20) and (15.2-21).
3. Consider (15.2-32). Another approach that has been suggested [2] for this width is such that the reciprocal of  $w_{siR}$  is set to the average of the reciprocals of the chord lengths between inner corners of slot at the top of the slot (under the tooth tip) and the outer corners of the slot at the bottom of the tooth. Derive an expression similar to (15.2-32) using this approach.
4. From (15.3-10) and (15.3-11), derive (15.3-12).
5. Suppose round conductors are arranged in a grid such that center points are aligned with the vertices of the grid. What is the highest packing factor that can be obtained?
6. Suppose that round conductors could be placed arbitrarily. What is the theoretical limit on packing factor?

7. Derive an expression analogous to (15.6-14) and (15.6-21) if the radial variation in the field is neglected.
8. Derive (15.7-6).
9. Derive (15.7-7) and (15.7-8).
10. Assuming that the machine current is sinusoidal, derive (15.9-8).

---

# APPENDIX A

## TRIGONOMETRIC RELATIONS, CONSTANTS AND CONVERSION FACTORS, AND ABBREVIATIONS

---

### A.1. BASIC TRIGONOMETRIC RELATIONS

$$e^{jx} = \cos x + j \sin x$$
$$a \cos x + b \sin x = \sqrt{a^2 + b^2} \cos(x + \phi) \quad \phi = \text{angle}(a - jb)$$
$$\cos^2 x + \sin^2 x = 1$$
$$\sin 2x = 2 \sin x \cos x$$
$$\cos 2x = \cos^2 x - \sin^2 x = 2 \cos^2 x - 1 = 1 - 2 \sin^2 x$$
$$\cos x \cos y = \frac{1}{2} \cos(x + y) + \frac{1}{2} \cos(x - y)$$
$$\sin x \sin y = \frac{1}{2} \cos(x - y) - \frac{1}{2} \cos(x + y)$$
$$\sin x \cos y = \frac{1}{2} \sin(x + y) + \frac{1}{2} \sin(x - y)$$
$$\cos(x \pm y) = \cos x \cos y \mp \sin x \sin y$$
$$\sin(x \pm y) = \sin x \cos y \pm \cos x \sin y$$

## A.2. THREE-PHASE TRIGONOMETRIC RELATIONS

$$\cos x + \cos\left(x - \frac{2\pi}{3}\right) + \cos\left(x + \frac{2\pi}{3}\right) = 0$$

$$\sin x + \sin\left(x - \frac{2\pi}{3}\right) + \sin\left(x + \frac{2\pi}{3}\right) = 0$$

$$\cos^2 x + \cos^2\left(x - \frac{2\pi}{3}\right) + \cos^2\left(x + \frac{2\pi}{3}\right) = \frac{3}{2}$$

$$\sin^2 x + \sin^2\left(x - \frac{2\pi}{3}\right) + \sin^2\left(x + \frac{2\pi}{3}\right) = \frac{3}{2}$$

$$\sin x \cos x + \sin\left(x - \frac{2\pi}{3}\right) \cos\left(x - \frac{2\pi}{3}\right) + \sin\left(x + \frac{2\pi}{3}\right) \cos\left(x + \frac{2\pi}{3}\right) = 0$$

$$\sin x \cos y + \sin\left(x - \frac{2\pi}{3}\right) \cos\left(y - \frac{2\pi}{3}\right) + \sin\left(x + \frac{2\pi}{3}\right) \cos\left(y + \frac{2\pi}{3}\right) = \frac{3}{2} \sin(x - y)$$

$$\sin x \sin y + \sin\left(x - \frac{2\pi}{3}\right) \sin\left(y - \frac{2\pi}{3}\right) + \sin\left(x + \frac{2\pi}{3}\right) \sin\left(y + \frac{2\pi}{3}\right) = \frac{3}{2} \cos(x - y)$$

$$\cos x \cos y + \cos\left(x - \frac{2\pi}{3}\right) \cos\left(y - \frac{2\pi}{3}\right) + \cos\left(x + \frac{2\pi}{3}\right) \cos\left(y + \frac{2\pi}{3}\right) = \frac{3}{2} \cos(x - y)$$

$$\sin x \cos y + \sin\left(x + \frac{2\pi}{3}\right) \cos\left(y - \frac{2\pi}{3}\right) + \sin\left(x - \frac{2\pi}{3}\right) \cos\left(y + \frac{2\pi}{3}\right) = \frac{3}{2} \sin(x + y)$$

$$\sin x \sin y + \sin\left(x + \frac{2\pi}{3}\right) \sin\left(y - \frac{2\pi}{3}\right) + \sin\left(x - \frac{2\pi}{3}\right) \sin\left(y + \frac{2\pi}{3}\right) = -\frac{3}{2} \cos(x + y)$$

$$\cos x \cos y + \cos\left(x + \frac{2\pi}{3}\right) \cos\left(y - \frac{2\pi}{3}\right) + \cos\left(x - \frac{2\pi}{3}\right) \cos\left(y + \frac{2\pi}{3}\right) = \frac{3}{2} \cos(x + y)$$

## A.3. CONSTANTS AND CONVERSION FACTORS

Permeability of free space	$\mu_0 = 4\pi \times 10^{-7}$ Wb/At·m
Permittivity (capacititivity) of free space	$\epsilon_0 = 8.854 \times 10^{-12}$ C <sup>2</sup> /N·m <sup>2</sup>
Acceleration of gravity	$g = 9.807$ m/s <sup>2</sup>
Length	1 m = 3.281 ft = 39.37 in
Mass	1 kg = 0.0685 slug = 2.205 lb (mass)
Force	1 N = 0.225 lb = 7.23 pdl
Torque	1 N·m = 0.738 lb·ft

Energy	$1 \text{ J} (\text{W} \cdot \text{s}) = 0.738 \text{ lb} \cdot \text{ft}$		
Power	$1 \text{ W} = 1.341 \times 10^{-3} \text{ hp}$		
Moment of inertia	$1 \text{ kg} \cdot \text{m}^2 = 0.738 \text{ slug} \cdot \text{ft}^2$ $= 23.7 \text{ lb} \cdot \text{ft}^2$		
Magnetic flux	$1 \text{ Wb} = 10^8 \text{ Mx (lines)}$		
Magnetic flux density	$1 \text{ Wb/m}^2 = 10,000 \text{ G}$ $= 64.5 \text{ klines/in}^2$		
Magnetizing force	$1 \text{ At/m} = 0.0254 \text{ At/in}$ $= 0.0126 \text{ Oe}$		

#### A.4. ABBREVIATIONS

Alternating current	ac	Megawatt	MW
Ampere	A	Meter	m
Ampere-turn	At	Microfarad	$\mu\text{F}$
Coulomb	C	Millihenry	mH
Direct current	dc	Newton	N
Foot	ft	Newton meter	N·m
Gram	g	Oersted	Oe
Henry	H	Pound	lb
Hertz	Hz	Poundal	pdl
Horsepower	hp	Power factor	pf
Inch	in	Pulse-width modulation	PWM
Joule	J	Radian	rad
Kilogram	kg	Revolution per minute	r/min (rpm)
Kilovar	kvar	Second	s
Kilovolt	kV	Voltampere reactive	var
Kilovoltampere	kVA	Volt	V
Kilowatt	kW	Voltampere	VA
Magnetomotive force	MMF	Watt	W
Maxwell	Mx	Weber	Wb

---

# APPENDIX B

## CARTER'S COEFFICIENT

---

In our previous analysis, we neglected the effects of slots on the stator and rotor. As it turns out, the effects of slots can be readily incorporated into the analysis by replacing the air gap  $g$  with a modified air gap  $g'$ . In particular, for the case of the stator slots, the modified air gap is calculated as

$$g' = g c_s \quad (B-1)$$

where  $c_s$  is the stator Carter's coefficient. We will now derive this result as well as a value for  $c_s$ .

The derivation of (B-1) begins with consideration of Figure B-1. This figure depicts the developed diagram over a small range of position  $w$  corresponding to one-half of a stator slot width plus one-half of a stator tooth width. Thus

$$w = \frac{1}{2} w_{ss} + \frac{1}{2} w_{st} \quad (B-2)$$

where  $w_{ss}$  is the stator slot width and  $w_{st}$  is the stator tooth width, both measured at the stator/air-gap interface.

Let us first consider the situation if we ignore the slot. In this case, it can be shown that the flux flowing across the air gap in the interval  $w$  may be expressed as

$$\Phi = \frac{\mu_0 \mathbb{F} l}{2g} (w_{ss} + w_{st}) \quad (B-3)$$

where  $l$  is the length of the machine and  $\mathbb{F}$  is the magnetomotive force (MMF) drop between the stator and rotor at that point. Because the slot is unaccounted for in (B-3), this expression is in error, because part of the flux ( $\Phi_2$ ) will have to travel further. Our goal will be to establish a value  $g'$  such that

$$\Phi = \frac{\mu_0 \mathbb{F} l}{2g'} (w_{ss} + w_{st}) \quad (B-4)$$

is correct, or is at least a good approximation.

To this end, let us calculate the flux, including the effects of the slot. To this end, it is convenient to divide the flux into two components,

$$\Phi = \Phi_1 + \Phi_2 \quad (B-5)$$

The first term is readily expressed as

$$\Phi_1 = \frac{\mu_0 \mathbb{F} w_{st} l}{2g} \quad (B-6)$$

The second term is more involved. At a position  $z$  (see Fig. B-1), the distance from the rotor to the stator along the indicate path is  $g + \pi z / 2$ . Thus, the field intensity along this path may be estimated as

$$H = \frac{\mathbb{F}}{g + \pi z / 2} \quad (B-7)$$

The flux  $\Phi_2$  may be expressed as

$$\Phi_2 = \int_{z=0}^{w_{ss}/2} B l dz \quad (B-8)$$

Substitution of (B-7) into (B-8) and noting that the fields are in air yields

$$\Phi_2 = \frac{2\mu_0 \mathbb{F} l}{\pi} \ln \left( 1 + \frac{\pi w_{ss}}{4g} \right) \quad (B-9)$$

The final step is to add (B-6) and (B-8) and to equate the result to (B-4). The result is (B-1), where

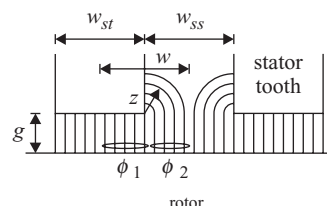


Figure B-1. Carter's coefficient.

$$c_s = \frac{w_{ss} + w_{st}}{w_{st} + \frac{4g}{\pi} \ln\left(1 + \frac{\pi w_{ss}}{4g}\right)} \quad (B-10)$$

Observe that  $g$ ,  $g'$ , and  $c_s$  can all be functions of position (as measured from the stator or the rotor) but this functional dependence is not explicitly shown.

The use of (B-1) and (B-10) is straightforward and very useful, because it allows us, with a simple substitution of  $g'$  for  $g$ , to account, albeit approximately, for the effects of the stator slots on magnetizing inductance calculations, as well as flux linkage due to permanent magnets.

For machines with both stator and rotor slots, the concept of Carter's coefficient can still be used; however, in this case

$$g' = g c_s c_r \quad (B-11)$$

where

$$c_r = \frac{w_{rs} + w_{rt}}{w_{rt} + \frac{4gc_s}{\pi} \ln\left(1 + \frac{\pi w_{rs}}{4g}\right)} \quad (B-12)$$

and where  $w_{rs}$  and  $w_{rt}$  are the width of the rotor slot and rotor tooth where it meets the air gap.

Before concluding, it should be noted that (B-10) and (B-12) are based on a geometry in which tooth tips do not exist or are neglected. In cases where this is not applicable, the same methods can be used to find an alternate expression for Carter's coefficient.

---

# APPENDIX C

## LEAKAGE INDUCTANCE

---

In this appendix, we consider the problem of the computation of leakage inductance of the stator winding. The method discussed herein is based on Reference 1, which uses some techniques presented in Reference 2. As discussed in Chapter 2, the leakage flux linkage is associated with flux that does not cross the air gap. In our development here, we will assume symmetry and magnetic linearity, whereupon the stator leakage flux linkage may be expressed in terms of the stator currents as

$$\lambda_{abcs,l} = \begin{bmatrix} L_{lp} & L_{lm} & L_{lm} \\ L_{lm} & L_{lp} & L_{lm} \\ L_{lm} & L_{lm} & L_{lp} \end{bmatrix} i_{abcs} \quad (C-1)$$

where  $L_{lp}$  is a self-leakage inductance, and  $L_{lm}$  is a mutual leakage inductance. Mutual leakage inductance is the result of flux that couples phases, but does not cross the air gap. Transforming (C-1) to  $qd$  variables in the arbitrary reference frame yields

$$\lambda_{qd0s,l} = \begin{bmatrix} L_{ls} & 0 & 0 \\ 0 & L_{ls} & 0 \\ 0 & 0 & L_{ls} + 3L_{lm} \end{bmatrix} i_{qd0s} \quad (C-2)$$

where

$$L_{ls} = L_{lp} - L_{lm} \quad (C-3)$$

is what we normally refer to as the leakage inductance. Thus, our primary task in this section is to find expressions for  $L_{lp}$  and  $L_{lm}$ .

To this end, let us consider Figure C-1, which illustrates the  $i$ 'th slot of the machine, and a group of conductors within the slot, which includes all phases. Superimposed on the slot and conductor region is a simple MEC of the slot. Therein,  $N_{as,i}$ ,  $N_{bs,i}$ , and  $N_{cs,i}$  are the number of conductors of each phase within the slot, and  $P_{sl}$  denotes the

---

*Analysis of Electric Machinery and Drive Systems*, Third Edition. Paul Krause, Oleg Waszynczuk, Scott Sudhoff, and Steven Pekarek.

© 2013 Institute of Electrical and Electronics Engineers, Inc. Published 2013 by John Wiley & Sons, Inc.

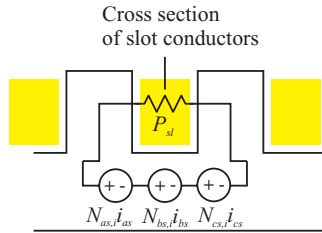


Figure C-1. Slot leakage inductance.

permeance of the flux path within the slot. Consideration of Figure C-1 yields that the contributions of the leakage inductance by the leakage flux in the  $i$ 'th slot may be expressed as

$$L_{lp,i} = P_{sl} N_{as,i} \quad (C-4)$$

$$L_{lmsl,i} = P_{sl} N_{as,i} N_{bs,i} \quad (C-5)$$

where the added “*sl*” subscript denotes the components of  $L_{lp}$  and  $L_{lm}$  due to slot leakage.

As it turns out, there is another component to the leakage inductance. This second component arises from the end conductors. Consider Figure C-2, which depicts part of a longitudinal cross section of the machine, including a cross section of the end conductors across the  $i$ 'th backiron segment. Superimposed on this is a simple MEC in which  $M_{as,i}$ ,  $M_{bs,i}$ , and  $M_{cs,i}$  are the *a*-, *b*-, and *c*-phase end conductors across this segment (as discussed in Chapter 2), and  $P_{el}$  is the permeance associated with the flux path associated with this segment. Considering this simple MEC yields the contribution of the  $i$ 'th end conductor segment to the leakage inductance

$$L_{lpe,i} = P_{el} M_{as,i} \quad (C-6)$$

$$L_{lme,i} = P_{el} M_{as,i} M_{bs,i} \quad (C-7)$$

where the “*el*” in the subscript denotes end leakage.

Adding the slot leakage and end leakage terms together, and adding the contribution over all slot and end segments yields

$$L_{lp} = P_{sl} \sum_{i=1}^{N_s} N_{as,i}^2 + P_{el} \sum_{i=1}^{N_s} M_{as,i}^2 \quad (C-8)$$

$$L_{lm} = P_{sl} \sum_{i=1}^{N_s} N_{as,i} N_{bs,i} + P_{el} \sum_{i=1}^{N_s} M_{as,i} M_{bs,i} \quad (C-9)$$

The next step is the calculation of the permeances  $P_{sl}$  and  $P_{el}$ . We will begin this endeavor with consideration of  $P_{sl}$ . This calculation will be based on a rectangular slot

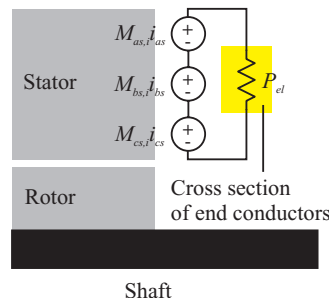


Figure C-2. End leakage inductance.

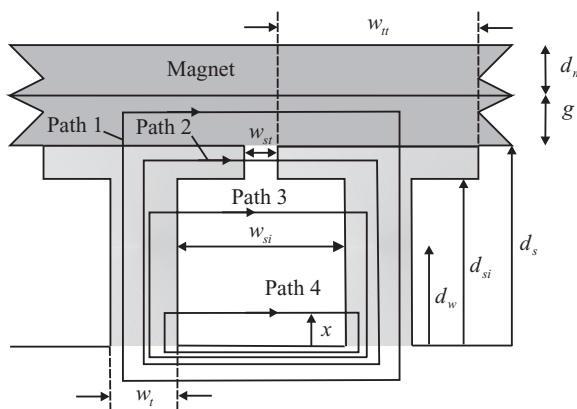


Figure C-3. Primary slot permeance (taken from Reference 1).

approximation, and assume that the steel has infinite permeability. We will break this permeance into a seven terms corresponding to seven flux paths depicted in Figure C-3 and Figure C-4.

The permeances associated of path  $i$  will be denoted  $P_{sl,i}$ . The first three permeances are based on treating the flux path as a rectangular block in which the field is uniform over a cross section. This yields

$$P_{sl,1} = \frac{lg\mu_0}{w_{st} + w_{tt}} \quad (C-10)$$

$$P_{sl,2} = ld_{tt}\mu_0 / w_{st} \quad (C-11)$$

$$P_{sl,3} = l(d_{si} - d_w)\mu_0 / w_{si} \quad (C-12)$$

In (C-10),  $g$  is the air gap used for slot leakage. In a synchronous or induction machine, this would be the actual air gap, and this term will be very small. In a PM machine,  $g$  will include the actual air gap and the magnet depth, since many magnet materials have a permeability similar to that of air.

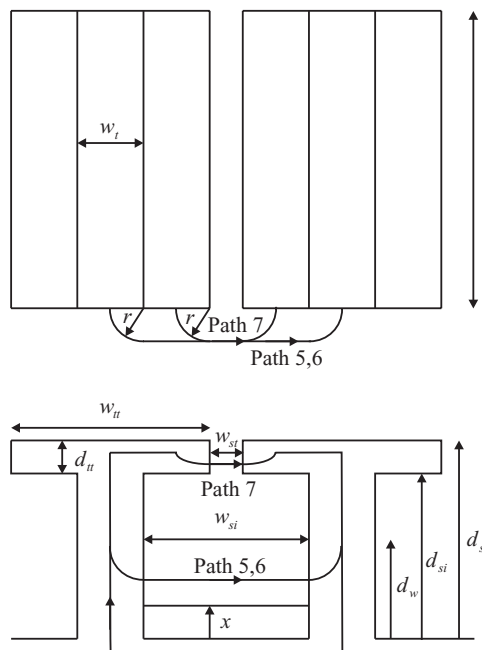


Figure C-4. End leakage permeance (taken from Reference 1).

The permeance of Path 4 is calculated using an energy-based approach, since not all the flux produced links the entire winding. In this approach, the energy stored in the path is found based on the field distribution and equated to the energy stored in an ideal inductance (permeance). In particular, the relationship,

$$\frac{1}{2} L_v i^2 = \frac{1}{2} P_v F^2 = \int_v B \cdot H \, dv \quad (C-13)$$

is used, where  $L_v(P_v)$  denotes the inductance (permeance) associated with some volume,  $F$  is the net MMF source, and  $B$  and  $H$  are the flux density and field intensity within that volume. Applying (C-12) to the volume of Path 4 yields

$$P_{sl,4} = \mu_0 l d_w / 3 w_{si} \quad (C-14)$$

The final three paths considered are illustrated in Figure C-4, and include an axial component. Again, using energy arguments, we obtain

$$P_{sl,5} = \frac{\mu_0 d_w}{3\pi} \log \left( 1 + \frac{\pi w_t}{w_{ci}} \right) \quad (C-15)$$

$$P_{sl,6} = \frac{\mu_0}{\pi} \log \left( 1 + \frac{\pi w_t}{w_{ci}} \right) (d_{si} - d_w) \quad (C-16)$$

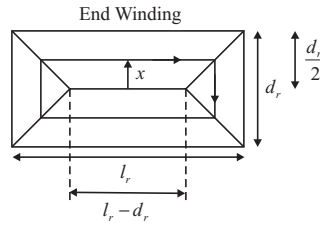


Figure C-5. End winding permeance: interior path (taken from Reference 1).

$$P_{sl,7} = \frac{\mu_0}{\pi} \log \left( 1 + \frac{\pi w_{tt}}{w_{st}} \right) d_{tt} \quad (\text{C-17})$$

Adding all components together yields

$$P_{sl} = P_{sl,1} + P_{sl,2} + P_{sl,3} + P_{sl,4} + 2P_{sl,5} + 2P_{sl,6} + 2P_{sl,7} \quad (\text{C-18})$$

The final step in our effort is the calculation of the end leakage permeance. This has two components, one associated with flux within the winding bundle, and the other with flux on the exterior of the winding bundle. Figure C-5 illustrates the flux path within the end winding bundle. Therein, a segment of end winding bundle is shown in cross-section. The assumed path of flux is rectangular—clearly a crude approximation. The field intensity is assumed to be uniform along this path and is only a function of the distance  $x$ .

Using energy arguments, the permeance associated with this path may be expressed as

$$P_{el,1} = \frac{\mu_0 L_{seg}}{d_r^2 l_r^2} \left[ \frac{d_r^4}{32} + \frac{d_r^3}{16} (l_r - d_r) + \frac{d_r^2}{64} (l_r - d_r)^2 - \frac{d_r}{64} (l_r - d_r)^3 + \frac{1}{128} (l_r - d_r)^4 \ln \left( 1 + \frac{2d_r}{l_r - d_r} \right) \right] \quad (\text{C-19})$$

where  $l_r$  and  $d_r$  are the length and depth of the end winding segment, respectively, and  $L_{seg}$  is the length of the segment of the end winding in the tangential direction. In particular,

$$L_{seg} = \frac{2\pi}{N_s} \left( r_s + d_s - \frac{d_w}{2} \right) \quad (\text{C-20})$$

In (C-19), it will be assumed that  $l_r \geq d_r$ , such that

$$l_r = \max(l_{ew}, d_{ew}) \quad (\text{C-21})$$

$$d_r = \min(l_{ew}, d_{ew}) \quad (\text{C-22})$$

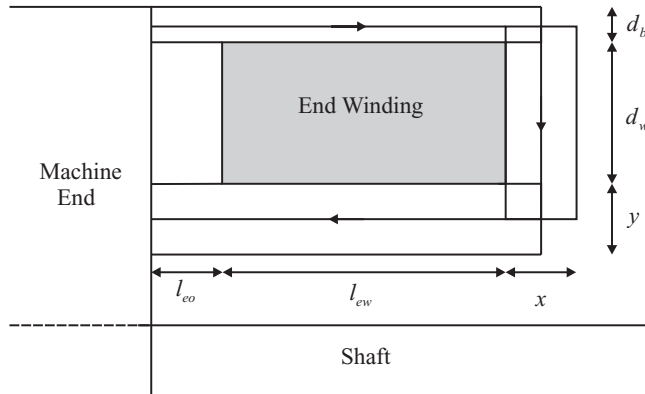


Figure C-6. End winding permeance: exterior path (taken from Reference 1).

where  $l_{ew}$  and  $w_{ew}$  are the dimensions of the end winding segment. If  $l_r = d_r$ , the expression of the permeance becomes

$$P_{el,1} = \frac{\mu_0 L_{seg}}{32} \quad (C-23)$$

Note that while this approach is rather crude, this term provides only a minor contribution to the overall leakage inductance, and so the sensitivity of the leakage inductance to the error in (C-19) is small.

The second contribution of the end leakage permeance is associated with wind flux flow around the end winding segment, as shown in Figure C-6.

Using the mean path approximation with rectangular elements, the reluctance of this path may be expressed as

$$R = \frac{(l_{eo} + l_{ew} + x)}{d_b L_{seg} \mu_0} + \frac{\left(d_w + \frac{d_b}{2} + y\right)}{2x L_{seg} \mu_0} + \frac{(l_{eo} + l_{ew} + x)}{2y L_{seg} \mu_0} \quad (C-24)$$

In order to determine the dimensions  $x$  and  $y$ , it is assumed that these are such that the reluctance of the path is minimized

$$P_{el,2} = 1 / R_{\min} \quad (C-25)$$

where  $R_{\min}$  is the minimum value of  $R$  for all  $x$  and  $y$  in (C-24).

At this point, the total end leakage permeance may be calculated as

$$P_{el} = 2P_{el,1} + 2P_{el,2} \quad (C-26)$$

## REFERENCES

- [1] B.N. Cassimere and S.D. Sudhoff, "Analytical Design Model for Surface Mounted Permanent Magnet Synchronous Machines," *IEEE Trans. Energy Conversion*, Vol. 24, No. 2, June 2009, pp. 338–346.
- [2] D.C. Hanselman, *Brushless Permanent-Magnet Motor Design*, McGraw-Hill, New York, 1994.

---

# INDEX

---

## Symbols

“ $\sim$ ” symbol, steady-state performance, 555–557  
“ $\wedge$ ” symbol, average-values, 450, 456, 480, 555

*abc* variables:  
base voltage, 159  
current command, 567  
exponential decay, 286  
hysteresis and delta modulation, 495  
permanent-magnet ac motor drives, 567  
per unit system, 233, 234  
*qs* and *ds* variables, 251  
stator conditions, unbalanced or discontinuous, 210  
stator currents, 265  
total instantaneous power, 89–90  
transformation, 203, 224  
voltage command, 569  
zero variables, 89  
Achievable, voltage vectors, 533  
Ac machines, *see* Alternating current (ac) machines  
Air gap, synchronous machines, 79, 205  
Air-gap flux density, 75  
Air-gap magnetomotive force (MMF), *see also* Poles  
distributed windings in, 83  
radial field analysis, 597, 599

rotating poles, 37  
single-phase induction machines, 365–366  
stator currents, 67–71, 167–168  
unbalanced machine variables, 341–342  
Alternating current (ac) machines:  
distributed windings in, 53–83  
air-gap magnetomotive force (MMF), 67–71  
common winding arrangements, 62–64  
conductor distributions, 58–59, 68  
continuous description of, 58  
developed diagram, 58  
discrete/continuous conversions, 59–60  
discrete description of, 56–57  
end conductors, 60–61  
flux linkage and inductance, 73–76  
goal of, 55  
induction machine, 81–83  
overview of, 53–56  
path of integration, 68  
position measurements, 54  
problems, 84–85  
resistance, 76–77  
rotating MMF, 71–73  
stator voltage equations, 77  
synchronous machines, 77–80  
winding functions, 64–67  
electromechanical energy conversion, 35–44

- permanent-magnet ac machine, 121–140  
as brushless dc motor, 129–134  
overview of, 121–122  
phase-shifting of applied  
voltages, 134–138  
problems, 140–141  
rotor reference frame variables, voltage  
and torque, 125–127  
stator current control, 138–140  
steady-state operation, 127–128  
variables, voltage and torque  
equations, 122–125
- Ampere's law, 4, 68
- Angular displacement:  
rotational system, 28, 197  
as rotor angle, 158  
steady-state operation, 128  
symmetrical induction machines, 231  
synchronous reference frame, 493  
transformation, rotor circuits, 221, 222,  
223  
two-pole vs. four-pole, 39
- Angular position:  
dc machines, 380  
distributed windings, 55  
Hall effect position, 545  
sine-triangle modulated inverter, 548  
speed voltage, 92  
synchronously rotating reference frame, 99  
three-phase commutated converter, 445  
transformation, change of variables, 89  
unbalanced operation analysis, 360
- Angular velocity:  
electrical vs. actual, 39  
induction motor drives, 532  
Park's equations, 87  
permanent-magnet ac machine, 126  
reference frames, 92, 94, 97, 99, 106  
symmetrical induction machines, 223, 227,  
233, 235, 338  
synchronous machines, 154, 159, 161, 163  
transformation, 89, 223  
unbalanced machine variables, 341, 362
- a*-phase conductors, 58, 62, 64  
*a*-phase current, 452, 455, 477, 489, 490,  
509, 512  
*a*-phase duty cycle, 478, 482, 489  
*a*-phase voltage, 286, 468, 472, 476, 480,  
501, 546
- Arbitrary reference frame:  
balanced steady-state phasor  
conditions, 99–101  
computer simulation  
symmetrical induction  
machines, 261–266  
synchronous machines, 204–205  
electric transients, neglecting, 313–318  
free acceleration characteristics, 256  
history of, 87  
single-phase induction machines, 359–362  
stationary circuit variables, 90–96  
stator voltage equations, 149–151  
subscripts, 144  
torque equation, 229–232  
transformation, 89, 144–145  
transformation, balanced set, 98–99  
two-phase transformation, 111  
unbalanced machine variables, 340–342,  
351–353  
voltage equations, 104, 106  
symmetrical induction  
machines, 224–229
- Armature terminal voltage, 129, 392
- Armature windings:  
continuous-current operation, one-quadrant  
dc drive, 403–407, 411  
dc machine, elementary two-pole,  
381–383, 384
- Asynchronous operation (pole slipping), 182,  
195, 368–375
- Asynchronous reference frame, 100,  
102–103
- Average-value analysis:  
dynamic vs. actual response, 457  
one-quadrant dc/dc converter drive,  
409–413, 416  
permanent-magnet ac motor drives  
current-regulated inverters, 576–578  
voltage-source inverters, 552–555, 561  
six-stepped three-phase bridge  
operation, 471–472  
three-phase load commutated  
converter, 449–456
- Average-valuing, *see* Average-value analysis
- Back electromotive force, 129, 385, 420  
Backiron flux calculation, 605  
Backiron flux linkage, 606

- Back voltage, 129  
 Balanced conditions simulation, 209  
 Balanced set transformation, 98–99  
 Balanced steady-state phasor conditions, 99–101  
 Base torque, 160  
*B-H* curve, 9  
 Block diagrams:  
     average-value time-domain, 413, 421, 423  
     computer simulation, 203, 205, 265  
     dc machine, speed control, 424, 425  
     elementary electromechanical system, 12  
     induction motor drives, 532  
     permanent-magnet ac motor drives, 542  
     semi-controlled bridge converters, 456  
     slip energy recovery drives, 535  
     slip energy recovery drive system, 535  
     time-domain, 394–398  
 Blocked-rotor test, 243  
 Bode characteristic, 564–565  
 Brereton, D.S., 87  
 Bridge control strategies:  
     delta modulation, 492  
     hysteresis modulation, 489–492  
     sine-triangle modulation, 477–483  
     space-vector modulation, 485–489  
 Bridge converters, *see* Semi-controlled bridge converters; Three-phase bridge converters  
 Brushless dc motor, 129–134, *see also* Permanent-magnet ac machine  
     dynamic performance of, 133  
     free-acceleration characteristics, 132, 135  
     torque-speed characteristics, 130, 131, 133, 136  
 Bus voltage, 166–167  
 Canay, I.M., 294  
 Capacitive circuit elements, 94–96  
 Carter's method, 75  
 Circuits:  
     coupled circuits  
         inductive circuit elements, 92–94  
         magnetic, 1–12  
         synchronous machines, 326  
     dc machine, elementary two-pole, 378  
     history of, 87  
     induction machine, voltage equations, 81  
     magnetically coupled, 1–12  
     Park's transformation, 87  
     rotor circuits  
         eigenvalues, 313  
         equations of transformation  
             for, 222–224  
         free acceleration characteristics, 318  
         induction machine, 81, 83  
         input impedance of, 273, 282  
         reference frame theory, 98  
         short-circuited, 519  
         symmetrical induction machines, 232, 233, 246, 248, 260–261  
         three-phase fault at terminals, 320  
         three-wire symmetrical system, 342, 343, 345  
         unbalanced rotor resistors, 354–355  
         semi-controlled bridge converters, 442  
     stationary circuits  
         arbitrary reference frame, 359  
         magnetically coupled circuits, 9, 20, 29, 31  
         phasor form, 337  
         reference frame theory, 88, 101  
         symmetrical induction machines, 222, 223, 224  
     stator circuits  
         induction machine, 238, 346, 347, 349, 351  
         machine equations, alternative forms, 315, 320, 330  
         subscript for, 216  
         time constants, standard, 278  
     three-phase bridge converters, 463  
     three-phase synchronous machine, 153  
     transformation, reference frames, 90–96  
     two damper windings in quadrature axis, 273  
 Clarke, E., 98  
 Closed-loop permanent-magnet ac motor drive, 565–567  
 Closed-loop voltage and current regulation, 495–499  
 Coenergy, 17, 18–19  
 Coils, *see also* Windings  
     defined, 12  
     distributed windings, 54  
     flux components, 2–3  
     magnetization curve, 10  
     magnetizing and demagnetizing, 3–6

- multiexcited system, 20–21  
reference, 7  
resistance, 76–77  
winding arrangements, 63–64
- Coil-wound rotor windings, 218
- Commutator and commutation:  
dc machines, 378, 379–380, 383–384  
semi-controlled bridge  
converters, 434–445  
three-phase load commutated  
converter, 451–453, 455
- Compound-connected dc machine, 389, 390–394
- Computer simulation:  
permanent-magnet ac motor drives, 542  
reference frames, 233  
stationary coupled coils, 9, 10, 12  
stator variables, arbitrary reference  
frame, 142, 143  
stator voltage equations, 316  
symmetrical induction machines  
arbitrary reference frame, 261–266  
free acceleration, in reference  
frames, 251–257  
induction machine, 216, 227
- synchronous machines, 201–210  
arbitrary reference frames, 204–205  
asynchronous and unbalanced operation  
of, 368–375  
balanced conditions, 209  
rotor reference frames, 201–204  
saturation, 205–209  
unbalanced conditions, 209–210  
voltage equations, 154
- voltage equations, reactance  
model, 325–332
- Concentric winding arrangement, 63
- Condition modulation index command, 487
- Conductor catalog, 594
- Conductors, *see also* Windings  
arrangements, 12. *see also* Coils;  
Windings  
canceled conductors, 61  
density, 590–591  
distribution of, 78–79  
end conductors, 60–61  
materials, 595  
number of, in slot, 57, 591  
placement of, 56–57
- skewed arrangement of, 218  
symmetry conditions of, 58–59  
winding functions, 65, 68
- Consequent pole winding arrangement, 63
- Constant slip current control, 510–517
- Continuous-current operation, one-quadrant  
dc drive, 403–407, 411
- Continuous description, windings, 58–60, 66–67
- Converter angle, defined, 466
- Converters, *see also* Inverters  
current-controlled dc/dc  
converter, 426–431  
dc drives, solid-state converters, 398–400  
four-quadrant dc/dc converter  
drive, 421–423  
inverter. *see also* Inverter  
one-quadrant dc/dc converter  
drive, 400–403  
permanent-magnet ac motor drives, 541, 542, 544, 549, 545548  
semi-controlled bridge converters. *see*  
Semi-controlled bridge converters  
single-phase load commutated  
converter, 434–445
- three-phase bridge converters, 460–466.  
*see also* Three-phase bridge  
converters
- three-phase load commutated  
converter, 445–456
- two-quadrant dc/dc converter drive, 401, 418–421
- voltage-controlled dc/dc  
converter, 423–426
- Counter electromotive force, 129, 385, 420, 542
- Coupled circuits:  
inductive circuit elements, 92–94  
magnetic, 1–12  
linear magnetic system, 3–8  
nonlinear magnetic system, 8–11  
synchronous machines, 326
- Coupling fields:  
block diagram of, 12  
electromechanical energy conversion, 23, 28–29, 33  
energy in, 16–22  
energy relationships, 12, 13, 14, 15, 16  
energy stored in, 16–22, 220, 230

- Coupling fields (*cont'd*)  
 force equation, 28  
 permanent-magnet ac machine, 24  
 symmetrical induction machines, 220  
 synchronous machines, 149, 157, 158
- Critical clearing angle, 195, 200
- Critical clearing time, 195, 197, 200
- Cumulative compounding, 391
- Current command synthesis, permanent-magnet ac motor drives, 572–576, 579
- Current-controlled dc/dc converter, 426–431
- Current control operation, fixed-slip frequency, 510
- Currents, *see also* Stators  
 arbitrary reference frames, simulation, 204–205  
 dc machine, elementary two-pole, 380, 383  
 flux linkage replacement, 154–155, 156  
 permanent-magnet ac machine, 128, 138–140  
 positive stator currents, synchronous machine, 171–200  
 dynamic performance of, 175–180  
 stator currents  
 electric machinery design, 596  
 permanent-magnet ac machine, 138–140  
 synchronous generator operation, positive, 171–200  
 symmetrical induction machines, 218, 227–229  
 synchronous machines, 145, 167–168  
 three-phase bridge converters, 465  
 three-phase load commutated converter, 452
- Current-source modulation strategy:  
 delta modulation, 492  
 hysteresis modulation, 489–492. *see also* Hysteresis modulation  
 permanent-magnet ac motor drives, 542, 567–581  
 average-value analysis, 576–578  
 current command synthesis, 572–576  
 features, 567–571  
 speed control study, 578–581  
 voltage limitations, 571–572
- Current tracking, 571–572
- Damper windings:  
 permanent-magnet ac machine, 124  
 synchronous machines, 44, 143
- Dc/dc converters, 399–400
- Dc machines, *see* Direct current (dc) machines
- Delta modulation, 492
- Demagnetization, 594–595
- Demodulator, 427
- Design, of electric machinery, 583–620  
 backiron flux calculation, 605  
 backiron flux linkage, 606  
 case study, 614–618  
 cross-section of, 618  
 design from pareto-optimal front, 617, 620  
 fixed design specs, 614  
 flux density waveforms, 619  
 mass and loss objectives, 615  
 mass-loss tradeoff, 616  
 parameter ranges, 615  
 control philosophy, 596  
 cross-section of, 585  
 extensions, 618–620  
 ferromagnetic field analysis, 603–608  
 flux density in rotor backiron, 608  
 formulation of design problem, 609–613  
 design constraints, 610–612  
 design metrics, 610  
 design space, 609–610  
 fitness, 613  
 lumped parameter model, 602–603  
 machine geometry, 585–590  
 material parameters, 593–596  
 overview of, 583–585  
 problems, 621–622  
 radial field analysis, 597–602  
 radial magnetization, 600  
 slot and tooth dimensions, 586  
 stator currents, 596  
 stator windings, 590–593  
 surface-mounted permanent-magnet synchronous machine, 584
- Dielectric losses, 12, 13
- Direct current (dc) machines, 377–431  
 block diagrams, time-domain, 394–398  
 permanent-magnet, 396–398  
 shunt-connected, 394–396  
 equivalent circuit of, 385

- four-quadrant dc/dc converter  
    drive, 421–423
- machine control  
    current-controlled dc/dc  
        converter, 426–431
- voltage-controlled dc/dc  
        converter, 423–426
- one-quadrant dc/dc converter drive, 400–418  
    average-value analysis, 409–413, 416
- continuous-current operation, 403–407,  
        411
- discontinuous-current  
        operation, 407–409
- operating characteristics, 413–418
- overview of, 400–403
- overview of, elementary  
    two-pole, 377–384
- parallel armature windings, 381, 382
- permanent-magnet ac machine, as  
    brushless dc motor, 129–134
- problems, 431–433
- solid-state converters for drives, 398–400
- two-quadrant dc/dc converter drive, 401,  
    418–421
- types of, 386–394  
    compound-connected, 389, 390–394
- permanent-magnet, 396–398
- separate winding excitation, 386
- series-connected, 388–390
- shunt-connected, 387–388, 394–396
- uniformly distributed rotor windings, 383
- use of, 377  
    voltage and torque equations, 384–386
- Direct field-oriented control, induction motor  
    drives, 521–523
- Direct torque control (DTC), induction motor  
    drives, 532–535
- Discontinuous-current operation, one-  
    quadrant dc/dc converter  
    drive, 407–409
- Discrete description, windings, 56–57,  
    59–60, 66–67
- Distributed windings, ac machinery, 53–83  
    air-gap MMF, 67–71
- common winding arrangements, 62–64
- conductor distributions, 58–59, 68
- continuous description of, 58
- developed diagram, 58
- discrete/continuous conversions, 59–60
- discrete description of, 56–57
- end conductors, 60–61
- flux linkage and inductance, 73–76
- goal of, 55
- induction machine, 81–83
- overview of, 53–56
- path of integration, 68
- position measurements, 54
- problems, 84–85
- resistance, 76–77
- rotating MMF, 71–73
- stator voltage equations, 77
- synchronous machines, 77–80
- winding functions, 64–67
- Doherty, R.H., 184–185
- Double-cage rotor machine, 218
- Drive motors:  
    direct current machines as, 377. *see also*  
        Direct current (dc) machines
- four-quadrant dc/dc converter  
        drive, 421–423
- induction motor drives. *see* Induction  
        motor drives
- one-quadrant dc/dc converter  
        drive, 400–403
- permanent-magnet ac motor drives. *see*  
        Permanent-magnet ac motor drives
- two-quadrant dc/dc converter drive, 401,  
        418–421
- Dual converters, 398, 399
- Dummy variable, 19
- Duty cycles:  
    open-loop voltage-regulated  
        converter, 493–495
- permanent-magnet ac motor drives,  
        548–550, 558, 562, 566
- sine-triangle modulation, 478–482
- Dynamic-average rectifier voltage, 552
- Dynamic averaging process:  
    one-quadrant dc/dc converter drive, 411,  
        412, 415
- open-loop voltage-regulated converter, 493
- other terms for, 410
- permanent-magnet ac motor drives, 544,  
        545, 549, 551, 553, 556
- sine-triangle modulation, 479, 480, 484
- space-vector modulation, 485, 487, 488
- three-phase load commutated  
        converter, 449, 451

- Dynamic performance:  
 electromechanical systems, 31, 32  
 permanent-magnet ac motor  
   drives, 557–562  
 prediction methods, 300  
 symmetrical induction machines  
   three-phase fault, 260–261, 262  
   torque changes, 257–260  
 three-phase fault  
   induction machine, 320–322  
   synchronous machines, 180–184,  
   260–261, 262  
 torque, step change in input, 175–180
- Eddy current:  
 electromechanical energy conversion, 12,  
 13, 17  
 ferromagnetic field analysis, 603  
 permanent-magnet ac machine, 124  
 symmetrical induction machines, 242
- Eigenvalues:  
 induction machines, 309–312  
 linearized machine equations, 233  
 overview of, 308–309  
 synchronous machines, 312–313
- Electrical angles, defining, 55–56
- Electrical angular displacement, of rotor, 39
- Electrical angular velocity, 341
- Electric machinery design, 583–620  
 backiron flux calculation, 605  
 backiron flux linkage, 606  
 case study, 614–618  
   cross-section of, 618  
   design from pareto-optimal front, 617,  
   620  
   fixed design specs, 614  
   flux density waveforms, 619  
   mass and loss objectives, 615  
   mass-loss tradeoff, 616  
   parameter ranges, 615  
 control philosophy, 596  
 cross-section of, 585  
 extensions, 618–620  
 ferromagnetic field analysis, 603–608  
 flux density in rotor backiron, 608  
 formulation of design problem,  
   609–613  
   constraints, 610–612  
   fitness, 613  
   metrics, 610  
   space, 609–610  
 lumped parameter model, 602–603  
 machine geometry, 585–590  
 material parameters, 593–596  
 overview of, 583–585  
 problems, 621–622  
 radial field analysis, 597–602  
 radial magnetization, 600  
 slot and tooth dimensions, 586  
 stator currents, 596  
 stator windings, 590–593  
 surface-mounted permanent-magnet  
   synchronous machine, 584
- Electric transients, neglecting, 313–318
- Electromagnetic forces, 14, 23–29
- Electromagnetic torque:  
 calculation of, 184, 186  
 dc machine with field winding, 385  
 free acceleration characteristics, 244, 245  
 induction motor drives, 528, 531, 532  
 linear magnetic system, balanced steady-  
   state, 162–163, 164, 301  
 lumped parameters, 602  
 in machine variables, 124  
 magnetomotive force, 168–169  
 motor action, 126–127, 157, 221, 302, 387  
 neglecting in voltage equations, 313–318  
 one-quadrant dc/dc converter drive, 403  
 permanent-magnet ac machine, 124, 126,  
   127, 137, 140  
 permanent-magnet ac motor drives, 554,  
   574–575, 578, 580  
 production of, 55  
 rotational system, 28  
 shunt-connected dc machine, 387  
 single-phase induction machines, 365  
 slip frequency, 511  
 symmetrical induction machines, 221,  
   229–230, 237–238, 264  
 synchronous machines, 164, 169, 195  
 three-phase fault, 195, 322  
 unbalanced machine variables, 342, 345  
 unbalanced rotor resistors, 354  
 volts-per-hertz drive strategy, 506, 509
- Electromechanical energy conversion:  
 ac machines, elementary, 35–44  
 electromagnetic and electrostatic  
   forces, 23–29

- energy balance, 13, 16  
energy in coupling fields, 16–22  
energy relationships, 12–16  
graphical interpretation of, 22–23, 24  
magnetically coupled circuits, 1–12  
    linear magnetic system, 3–8  
    nonlinear magnetic system, 8–11  
problems, 44–52  
steady-state and dynamic  
    performance, 29–35  
theory of, 1  
Electrostatic forces, 14, 23–29  
Emf, *see* Counter electromotive force  
End conductors:  
    importance of, 60–61  
    winding volume, 76–77  
End turns, 76–77  
Energy balance, 157–158  
    electromagnetic and electrostatic  
        forces, 23–29  
Energy conversion:  
    electromagnetic and electrostatic  
        forces, 23–29  
    graphical interpretation of, 22–23, 24  
Energy loss:  
    dielectric losses, 12, 13  
    hysteresis (core) losses. *see* Hysteresis  
    term for, 13, 15  
Energy relationships, electromechanical  
    systems, 12–16  
Equal-area criterion, 184, 196–200  
Equations, *see also* Torque; *specific types of*  
    equations; Voltage equations  
alternative forms, 299–333  
    eigenvalues, induction  
        machines, 309–312  
    eigenvalues, overview, 308–309  
    eigenvalues, synchronous  
        machines, 312–313  
    linearized machine equations,  
        300–308  
    performance prediction, induction  
        machine, 318–322  
    performance prediction, synchronous  
        machine, 322–325  
    voltage behind reactance  
        model, 325–333  
dc machines and drives, 394–398  
flux linkage. *see* Flux linkage  
operational impedance  
    derived synchronous machine, 278–282  
frequency-response  
    parameters, 290–295  
Park's equations, 272–273  
short-circuit characterization, 283–290  
standard synchronous machine, 278, 279  
synchronous machine, four-winding  
    rotor, 273–276  
synchronous machine, standard  
    reactance, 276–278  
operational impedances, 271–295  
permanent-magnet ac machine, 122–125  
time constants, steady-state equation, 136  
transformation, change of variables, 88–90  
transformation, rotor circuits, 222–224  
Excitation voltage, 162  
Exercises, *see* Problems  
Exponential decay, 106–107, 286–287  
Extended sine-triangle modulation, 551  
Faraday's law, 77, 78, 533  
Faults:  
    line-to-ground fault, 368  
    line-to-line fault, 373  
    line-to-line-to-neutral fault, 373–375  
    line-to-neutral fault, 372, 373  
    three-phase fault. *see* Three-phase fault  
Feedforward current control, 570  
Feedforward voltage control, 425–426, 537  
Ferromagnetic field analysis, 603–608  
Field energy, 20, 21–22, 25  
Field flux linkages, 78, 185, 186, 191–192,  
    196  
Field intensity of air gap, 71  
Field-oriented control, induction motor  
    drives, 517–521  
Field rheostat, 386  
Field voltage, 154  
Field weakening technique, 121  
Field winding:  
    dc machines  
        separate winding excitation, 386  
        series-connected, 388–390  
        shunt-connected, 387–388  
    machine variables, 143, 313, 326  
    Park's equations, 272  
    symmetrical induction machines, 232  
    synchronous machines, 164, 185, 369, 370

- Field winding (*cont'd*)  
 voltage equation for, 78, 160  
 voltage equations, 378
- Firing delay, 437–441, 445, 447, 448, 450, 453, 456
- “First swing” transient stability limit, 187–193, 198–200
- Fitness function, 613
- Fixed-slip frequency, 510
- Flat compounding, 391
- Flux:  
 air-gap flux density, 75  
 arbitrary reference frames, simulation, 204–205  
 components of, 2–3  
 electromagnetic systems, 25–26  
 as independent variables, 155–156  
 inductive circuit elements, 92–93  
 leakage vs. magnetizing, 73–76  
 linear magnetic system, 4–6, 146, 148, 150, 151–152  
 linkage and inductance, 73–76  
 magnetizing flux. *see* Magnetizing flux  
 permanent-magnet ac machine, 122–125  
 poles and, 55  
 rotational electromechanical device, 34–35  
 stator. *see* Stator flux  
 symmetrical induction machines, 225–228  
 three-phase fault at terminals, 196  
 three-phase induction machine, 39–41, 43–44  
 in a tooth, 604  
 transient torque-rotor angle characteristics, 185  
 two-phase induction machine, 36–37  
 winding functions, 66
- Flux control loop, 524
- Flux linkage:  
 ac machinery, distributed windings, 78  
 computer simulation, 201, 202, 203, 204, 205, 206  
 constant slip current control, 511  
 dc machines, 379  
 direct field-oriented control, 520, 521–522  
 field flux linkage, 78, 185, 186, 191–192, 196  
 as independent variable, 25–26  
 indirect field-oriented control, 524
- indirect rotor field-oriented control, 529–530
- linear magnetic system, 4, 5, 6, 18, 34
- lumped parameters, 602
- machine equations, alternative forms, 301, 315, 316, 317, 327, 328, 330, 333
- Park’s equations, 87
- permanent-magnet ac machine, 122, 125
- reference frames, 91, 92, 96
- symmetrical induction machines, 216, 220, 221, 224, 225, 227, 228, 229, 263, 265
- synchronous machines, 148, 151, 152, 154, 155, 157, 161
- term for, 3
- three-phase bridge converters, 471
- volts-per-hertz control, 504
- Formulas, *see* Equations
- Fortescue, C.L., 113, 337
- Fourier series:  
 conductor distributions, 59  
 sine-triangle modulation, 482  
 six-step operation, 476  
 six-stepped three-phase bridge operation, 468
- Four-pole, two-phase induction machine, 37–39
- Four-quadrant dc/dc converter drive, 421–423, 425, 426–431
- Four-winding rotor synchronous machine:  
 operational impedance, 273–276  
 time constants, derived, 278–282  
 time constants, standard, 278, 279
- Free acceleration:  
 brushless dc motor, 132, 135  
 performance prediction, induction machine, 318–322
- symmetrical induction machines, 244–251
- symmetrical induction machines, reference frames, 251–257
- synchronous motor, field winding short circuited, 369–370
- Frequency:  
 balanced steady-state phasor conditions, 99  
 dc machines and drives, 402, 413–414, 418  
 distributed windings, 55, 72, 83  
 energy relationships, 12

- fixed-slip frequency, 510–515  
induction motor drives, 504, 506, 507, 536  
machine equations  
    alternative forms, 304, 309, 310, 311, 319, 332, 333  
    operational impedances, 290–295  
negative frequency, 106  
permanent-magnet ac machine, 122  
permanent-magnet ac motor drives, 552, 564–566  
reference frames, 97  
symmetrical induction machines, 233, 234, 237, 240–241, 243, 251, 256  
synchronous machines, 160, 162, 163, 164  
three-phase bridge converters, 468, 473, 474, 476–478, 480, 492, 497–499  
twice slip-frequency, 353  
unbalanced operation analysis, 338, 340, 342, 351, 352  
Frequency-response parameters, operational impedance, 290–295  
Full converters, 398, 399, 400  
Fully controlled three-phase bridge converters, *see* Three-phase bridge converters  
Gauss's law, 599, 606  
Generator action:  
    energy conversion, 23, 29  
    positive stator currents, synchronous machine, 173  
    slip, at maximum torque, 239  
    synchronous machines, 169, 171, 173  
Generators:  
    dynamic performance of, torque changes, 175–180  
    hydro turbine generator, 145, 176–180  
        dynamic performance, torque changes, 176–180  
        equal-area criterion, 198–200  
        three-phase fault at terminals, 180–184  
        transient torque, actual vs.  
            approximate, 187, 188, 189, 191, 193  
        transient torque, three-phase fault, 194–196  
    positive stator currents, synchronous machine, 173–175  
    role of, 143  
steam turbine generator, 176–180, 312  
    dynamic performance, torque changes, 176–180  
    equal-area criterion, 198–200  
    three-phase fault at terminals, 181, 182–183  
    transient torque, actual vs.  
        approximate, 187, 188, 190, 191, 192–193  
        transient torque, three-phase fault, 194–196, 197  
wind turbine generator, 142, 143, 169, 215, 504, 536  
Genetic algorithms, 614  
Goerges, Hans, 357–358  
Goerges phenomenon, 357–358  
GOSET, 614  
Half-wave converters, 398, 399, 400  
Hall effect rotor position sensors, 544, 549  
Harmonics:  
    distributed windings, 67  
    magnetomotive force. *see* Magnetomotive force (MMF)  
    permanent-magnet ac motor drives, 546, 549, 554, 559, 572  
    sine-triangle modulation, 482  
    three-phase bridge converters, 468, 471, 472, 476, 480, 482, 499  
    waveforms. *see* Waveforms  
Hydro turbine generator:  
    dynamic performance, torque changes, 176–180  
    equal-area criterion, 198–200  
    three-phase fault at terminals, 180–184  
    transient torque, actual vs.  
        approximate, 187, 188, 189, 191, 193  
    transient torque, three-phase fault, 194–196  
Hysteresis:  
    (core) losses from, 8, 12, 13, 17, 242  
    frequency-response parameters, 290  
Hysteresis modulation, 489–492  
    abc variable current command, 495, 567  
    dc machines, 426, 428  
    vs. delta modulation, 492  
    flux density waveforms, 603  
    permanent-magnet ac motor drives, 568, 572, 573

- Impedance:
- circuits, magnetically coupled, 8, 10
  - infinite bus. *see* Infinite bus
  - operational impedances. *see* Operational impedances
  - per unit system, 159
  - of PVVBR models, 331, 332, 333
  - single-phase induction machine, 358, 359
  - on startup, 558
  - symmetrical induction machines, 234, 238, 241, 242, 243, 244, 266
  - symmetrical three-phase system, 102–103
  - thyristor, in reverse bias mode, 435, 449
  - unbalanced stator impedances, 347–349, 363
- Indirect rotor field-oriented control, 528–531
- Inductance:
- ac machines, 41, 79
  - electromechanical systems, 29, 34
  - flux linkage and, 73–76
  - induction machine, 81–83
  - leakage, 629–634. *see also* Leakage inductance
  - magnetizing inductance, 5, 37, 73–75, 96, 146, 218, 219, 290, 602–603, 628
  - mutual inductance. *see* Mutual inductance
  - self-inductance, 4, 34, 37, 42, 75, 79, 96, 220, 384
  - between two windings, 75
- Inductance matrix, 93, 329
- Induction machine:
- distributed windings, ac machines, 81–83
  - eigenvalues, 309–312
  - electromagnetic torque, neglecting, 313–316
  - linearized machine equations, 300–301, 302–305
  - performance prediction, 318–322
  - purpose of, 215
  - single-phase machines, 358–368
  - symmetrical component analysis, 338–339
  - symmetrical induction machines, 215–266
    - common reference frames, 232–233
    - dynamic performance, three-phase fault, 260–261, 262
    - dynamic performance, torque changes, 257–260
    - free acceleration, in reference frames, 251–257
  - free acceleration
    - characteristics, 244–251
    - overview of, 215–216
    - parameters, 244
    - per unit system, 233–235
    - problems, 267–270
    - simulation, arbitrary reference frame, 261–266
    - steady-state operation, 235–244
  - torque equation, arbitrary reference-frame variables, 229–232
  - torque equation, machine variables, 220–222
  - transformation equations, 222–224
  - voltage equations, arbitrary reference-frame variables, 224–229
  - voltage equations, machine variables, 216–220
- unbalanced rotor conditions, 351–354
- unbalanced stator conditions, 346–351
- unbalanced stator machines, 339–345
- voltage and flux, 152–153
- Induction motor drives, 503–538
- constant slip current control, 510–517
  - direct field-oriented control, 521–523
  - direct torque control, 532–535
  - field-oriented control, 517–521
  - indirect rotor field-oriented control, 528–531
  - overview of, 503–504
  - problems, 539–540
  - robust direct field-oriented control, 523–528
  - slip energy recovery drives, 535–538
  - volts-per-hertz control, 504–510
- Inductive circuit elements, 91–94
- Inertia constant, 160
- Infinite bus, 175–176, 180, 306, 307, 312, 313, 322
- Instantaneous phasor, 113–114
- Insulated-gate bipolar junction transistors (IGBTs), 461
- Interpoles, 384
- Intervals, three-phase load commutated converters, 452
- Inverters, *see also* Converters; Permanent-magnet ac motor drives
- design, electric machinery, 584, 596, 602, 609, 617, 620

- induction motor drives, 510, 514, 521, 528, 529, 532–533, 536, 538  
permanent-magnet ac machine, 121, 127, 131, 135–136, 138–140  
permanent-magnet ac motor drives, 541  
case study, 562–567  
current-regulated, 567–571  
transient and dynamic behavior, 557–562  
voltage-sourced, 552–557  
voltage-source inverter, 542–551  
semi-controlled bridge converters, 439, 445, 448, 453  
three-phase bridge converters, 461–462, 471, 476, 486, 492, 493, 495–499
- Kirchoff's law, 553  
Kron, G., 87
- Laplace notation, 273, 283, 285, 394, 563, 570  
Lap winding arrangement, 63  
Law of conservation of energy, 13  
Leakage flux, 2–3, 4, 73–76, 524, 629–630  
Leakage inductance:  
current-regulated inverter drives, 567  
defined, 5  
design, electric machinery, 589, 593, 602, 603  
distributed windings, 74, 79, 80, 83  
induction motor drives, 524  
machine equations, 290, 294  
of stator winding, 629–634  
symmetrical induction machines, 230  
synchronous machines, 146  
Linearized machine equations, 300–308  
Linearized model, 542, 560–564  
Linear magnetic system:  
dc machines, 389  
flux linkage equations, 224  
magnetically coupled circuits, 3–8, 18  
power balance approach, 232  
synchronous machines, 146, 150, 158, 162  
Line-commutated converter, *see* Semi-controlled bridge converters  
Line-to-line fault, 373  
Line-to-line-to-neutral fault, 373–375  
Line-to-line voltage, six-step operation, 467–468
- Line-to-neutral fault, 372, 373  
Line-to-neutral voltage, six-step operation, 470, 476  
Load torque, 320  
Long-shunt connection, 391  
Lorenze force equation, 517  
Loss components, 610  
Lumped circuit approximation, 292–294  
Lumped parameter model, 602–603  
Lyon, W.V., 113
- Machine control:  
current-controlled dc/dc converter, 426–431  
voltage-controlled dc/dc converter, 423–426
- Machine equations:  
alternative forms, 299–333  
eigenvalues, induction machines, 309–312  
eigenvalues, overview, 308–309  
eigenvalues, synchronous machines, 312–313  
linearized machine equations, 300–308  
performance prediction, induction machine, 318–322  
performance prediction, synchronous machine, 322–325  
problems, 335  
voltage behind reactance model, 325–333
- in operational impedances and time constraints, 271–295  
derived time constants, 278–282  
frequency-response parameters, 290–295  
overview of, 271–272
- Park's equations, operational form, 272–273  
problems, 297–298  
short-circuit characterization, 283–290  
standard time constants, 278, 279  
synchronous machine, four-winding rotor, 273–276  
synchronous machine, standard reactance, 276–278
- Machine terminal fault, 180  
Machine variables:  
free acceleration, 248–249, 252  
torque equation, 149

- Machine variables (*cont'd*)  
 symmetrical induction machines, 220–222  
 unbalanced, in arbitrary reference frame, 340–342, 351–353, 361–362  
 voltage equations  
   symmetrical induction machines, 216–220  
   synchronous machines, 143–149
- Magnet catalog, 594
- Magnetically coupled circuits, 1–12  
 linear magnetic system, 3–8  
 magnetization curve, 11  
 nonlinear magnetic system, 8–11
- Magnetic steels, 594–595
- Magnetizing flux:  
 design, electric machinery, 602, 603  
 induction motor drives, 506  
 vs. leakage flux, 73–76  
 linear magnetic system, 2–3, 4  
 machine equations, alternative forms, 327  
 in winding flux linkage terms, 201, 202
- Magnetizing inductance, 5, 37, 73–75, 96, 146, 218, 219, 290, 602–603, 628
- Magnetomotive force (MMF):  
 air-gap MMF. *see* Air-gap magnetomotive force (MMF)  
 dc machines, 385  
 ferromagnetic field analysis, 607  
 linear magnetic system, 4, 6, 9  
 radial field analysis, 597  
 rotating MMF, 71–73  
 rotating poles, 37  
 round rotor synchronous machine, 208  
 skewed conductor arrangement, 218  
 stator and rotor source, 71  
 sum of backiron and air-gap  
   MMFs, 70–71  
 synchronous machines, 158  
 unbalanced operation analysis, 339  
 waves, 73
- Mass-loss tradeoff, 616
- Material parameters, electric machinery design, 593–596
- MATLAB-based GOSET, 614
- Metal-oxide-semiconductor field-effect transistors (MOSFETs), 461
- Modulation index command, magnitude of, 486–487
- Modulation indices, vs. state, 486
- MOS controlled thyristors (MCTs), 461
- Motor action:  
 asynchronous operation of synchronous machines, 369–370  
 electromagnetic torque, 127, 221, 302, 387  
 electromechanical energy conversion, 23, 29, 44  
 permanent-magnet ac machine, 125  
 startup, 369  
 synchronous machines, torque equation, machine variables, 149  
 torque equation, 44, 149, 157, 230, 231, 239
- Motors, *see* Drive motors; Induction motor drives
- Moving average, *see* Dynamic averaging process
- Multiexcited electromagnetic system, 20, 22
- Mutual inductance:  
 ac machines, 34, 37, 41, 42, 80, 83  
 dc machines, 379, 384, 391  
 defined, 5  
 history of, 87  
 permanent-magnet ac machine, 122, 126  
 reference frames, 93, 94, 96  
 symmetrical induction machines, 218, 219, 220  
 synchronous machines, 146  
 between two windings, 75
- Newton's law, 15
- Nickle, C.A., 184–185
- No-load test, 242–243
- Nonlinear magnetic system, 8–11
- Ohm's law, 77, 78
- One-quadrant dc/dc converter drive:  
 average-value analysis, 409–413, 416  
 continuous-current operation, 403–407, 411  
 discontinuous-current operation, 407–409  
 operating characteristics, 413–418  
 overview of, 400–403
- Open-circuit coil voltage, 379
- Open-circuited stator phase, 349–351, 364
- Open-circuit test, 205, 206
- Open-circuit time constants, 279, 280, 281

- Open-loop permanent-magnet ac motor drive, 564
- Open-loop voltage and current regulation, 493–495
- Operational impedances, 271–295  
derived time constants, 278–282  
frequency-response parameters, 290–295  
overview of, 271–272  
Park's equations, operational form, 272–273  
problems, 297–298  
short-circuit characterization, 283–290  
standard time constants, 278, 279  
synchronous machine, four-winding rotor, 273–276  
synchronous machine, standard reactance, 276–278
- Overmodulation, 480, 481, 483, 485, 550, 566
- Parameter vector, 609
- Park, R.H., 87, 98, 113, 144, 145, 151, 271, 272
- Park's equations:  
linearized machine equations, 307  
lumped parameter model, 602  
machine equations, alternative forms, 317, 329  
in operational form, 272–273  
per unit equations, 159–160  
power balance approach, 231  
on rotor, as distributed parameter system, 271  
synchronous machines, 153, 154, 158, 159–160  
three-phase synchronous machine, 172  
voltage equations, reactance model, 327
- Path of integration, ac machinery, 68
- Peak radial flux density, 606
- Peak tangential flux density, 606, 607
- Periodicity, field distribution, 75–76
- Permanent-magnet ac machine (PMAM), 121–140  
ac machines, distributed. *see* Alternating current (ac) machines  
as brushless dc motor, 129–134  
overview of, 121–122  
phase-shifting of applied voltages, 134–138
- problems, 140–141  
rotor reference frame variables, voltage and torque, 125–127  
stator current control, 138–140  
steady-state operation, 127–128  
variables, voltage and torque equations, 122–125
- Permanent-magnet ac motor drives, 541–581  
block diagram, 542
- current-regulated inverter drives, 567–581  
average-value analysis, 576–578  
current command synthesis, 572–576  
features, 567–571  
speed control study, 578–581  
voltage limitations, 571–572  
overview of, 541–542  
parts of, 541  
problems, 581–582  
voltage-source inverter drives, 542–566  
average-value analysis, 552–555  
features, 542–543  
ideal source equivalence, 543–551  
speed control study, 562–567  
steady-state operation, 555–557  
transient and dynamic performance, 557–562
- Permanent-magnet dc machine, 386, 392–394  
block diagrams, time-domain, 396–398
- Permanent-magnet magnetomotive force (MMF), 599–601
- Permanent magnet material, 594, 595
- Per unit systems:  
symmetrical induction machines, 233–235  
synchronous machines, 159–160
- Phase-leg duty cycles, 548–549
- Phase-locked loop (PLL), 537
- Phase-shifting of applied voltages, permanent-magnet ac machine, 134–138
- Phasor conditions, steady-state:  
arbitrary reference frame, 99–101  
single-phase induction machines, 362–363  
symmetrical induction machines, 236–237  
synchronous machines, 167, 169–170  
unbalanced machine variables, 342–345, 353–354
- Physical-variable coupled-circuit (PVCC) model, 325–326, 331

- Physical-variable voltage-behind-reactance (PVVBR) model, 326–332, 333
- PID controller, 424, 425
- Plus integral (PI) controller, 563, 578, 579
- Poles, *see also* Air-gap magnetomotive force (MMF)
- design, electric machinery, 609, 617, 620
  - distributed windings, ac machines, 53, 55, 83
  - electromechanical energy conversion, 35, 37, 39
  - flux and, 55
  - induction motor drives, 504, 517, 532
  - permanent-magnet ac motor drives, 571, 579
  - symmetrical induction machines, 221, 231, 278
  - synchronous machines, 163, 169, 176, 182
  - two-pole vs. four-pole, 35–39. *see also* *Two-pole entries*
- Pole slipping, 371, *see also* Asynchronous operation
- Positive stator currents, synchronous machines, 171–200
- dynamic performance, three-phase fault, 180–184
- dynamic performance, torque changes, 175–180
- equal-area criterion, 196–200
- transient torque, actual vs. approximate, 187–193
- transient torque, three-phase fault, 194–196
- transient torque vs. rotor angle, 184–187
- Power balance approach, 230, 231
- Power factor, 166
- P*-pole machines, 55, 221
- Prime mover, torque from, 169
- Problems:
- ac machines, distributed windings, 84–85
  - dc machines, 431–433
  - design, electric machinery, 621–622
  - electromechanical energy conversion, 44–52
  - induction motor drives, 539–540
  - machine equations, alternative forms, 335
  - operational impedance, 297–298
  - permanent-magnet ac machine, 140–141
- permanent-magnet ac motor drives, 581–582
- reference frame theory, 115–120
- semi-controlled bridge converters, 458–459
- symmetrical induction machines, 267–270
- synchronous machines, 210–214
- three-phase bridge converters, 500–502
- unbalanced operation, 375–376
- Pulse-width modulation (PWM) control:
- modulation indices vs. state, 486
  - six-step operation, 474–477
  - space-vector modulation, 485–489
- qd* framework, 449
- Radial field analysis, 597–602
- Radial flux density, 601–602
- Radial magnetization, 600
- Rectifiers:
- induction motor drives, 535, 538
  - permanent-magnet ac motor drives, 542, 543, 546–547, 552–553, 556, 557–560, 580
  - PVCC form, 326
  - PVVBR form, 330
  - semi-controlled bridge converters, 435, 451, 452, 457, 461
  - silicon-controlled rectifiers (SCR's), 388
- Reduced-order model, 321, 324, 332–333
- Reference frames and theory, 86–114
- arbitrary reference frame, 87, 89, 90–96
  - balanced steady-state phasor conditions, 99–101
  - balance steady-state voltage equations, 102–105
  - field-oriented control, induction motor drives, 520
  - free acceleration, 251–257
  - history of, 87–88
  - overview of, 86–87
  - problems, 115–120
  - rotor reference frame variables, 97–98, 150–151
  - six-stepped three-phase bridge operation, 472–473
  - space-phasor notation, 113–114
  - stationary circuit variables and arbitrary reference frame, 90–96

- stator voltage equations, 149–151  
symmetrical induction machines, 232–233  
*synchronous reference frame. see  
Synchronous reference frame*  
transformation  
    balanced set, 98–99  
    change of variables, 88–90  
    between reference frames, 110–111  
    special cases, 111–113  
transformation between, 110–111  
types of, 97–98  
unbalanced stator conditions, 339–345  
variables from several frames of  
    reference, 105–110  
Reluctance machines, 164  
Resistance, ac machines, 76–77  
Resistance matrix, 91, 329  
Resistive circuit elements, 90–91  
Revolving field theory, 336  
Rms (root mean square) voltage, 159,  
    233–234, 244, 251, 436, 445, 506  
Robust direct field-oriented control, induction  
    motor drives, 523–528  
Rotating magnetomotive force, 71–73  
Rotational device, torque of, 33–34  
Rotor circuits:  
    eigenvalues, 313  
    equations of transformation for, 222–224  
    free acceleration characteristics, 318  
    induction machine, 81, 83  
    input impedance of, 273, 282  
    reference frame theory, 98  
    short-circuited, 519  
    symmetrical induction machines, 232, 233,  
        246, 248, 260–261  
    three-phase fault at terminals, 320  
    three-wire symmetrical system, 342, 343,  
        345  
    unbalanced rotor resistors, 354–355  
Rotor coil, 377–378, 379, 383  
Rotor-dependent resistances, 331  
Rotor flux calculator, 522–523  
Rotor flux observer, 523–524  
Rotor position:  
    dc machines and drives, 379, 381, 382,  
        395  
    design, electric machinery, 601, 604–607,  
        609  
    distributed windings, ac machines, 53, 80  
electromechanical energy conversion, 1,  
    37  
machine equations, alternative forms, 325,  
    326, 331  
permanent-magnet ac motor drives, 541,  
    542, 544, 548–549, 554  
permanent-magnet machine, 124  
reference frames, 87, 91  
synchronous machines, 149  
Rotor reference frame:  
    free acceleration characteristics, 254  
    physical-variable  
        voltage-behind-reactance, 327  
    reference frame theory, 97–98  
    simulation in, 201–204  
    synchronous machines, 150–151, 162  
Rtors:  
    ac machines, 35–37, 42  
    angle of, vs. transient torque, 184–187  
    angles of, 158–159  
    dc machine, elementary two-pole, 381,  
        382–383  
    diagram of, 34, 35  
    dynamic performance and torque  
        changes, 177, 178  
    eigenvalues, 310, 311  
    electrical angular displacement of, 39  
    electrical angular velocity of, 39  
    equal-area criterion, 199–200  
    leakage inductance, 74  
    mechanical speed of, 55  
    position dependence. *see* Rotor position  
    reference frame variables, 153  
    skewed arrangement of, 218  
    speed of. *see* Rotor speed  
    synchronous machines, 142  
    transformation equations, 222–224  
    unbalanced conditions, 351–354  
    unbalanced resistors, 354–358  
    unbalanced stator conditions, 339–345  
Rotor speed:  
    computer simulation, 201, 203, 205  
    dc machines and drives, 379, 384, 385,  
        395–396, 424, 425, 430  
    distributed windings in, 55, 83  
    dynamic vs. steady-state torque, 246, 300  
    eigenvalues, 309, 311  
    induction motor drives, 504, 506, 509,  
        513, 536, 538

- Rotor speed (*cont'd*)  
 Park's equations, 151  
 permanent-magnet ac machines, 122, 129, 137, 138  
 permanent-magnet ac motor drives, 543, 546, 554, 567, 574, 578–579  
 series-connected dc machine, 389  
 slip and, 339, 371  
 symmetrical induction machines, 264, 265  
 synchronous machines, 73  
 three-phase fault, 324  
 torque and, 149, 159, 164, 173, 222, 302, 322, 385, 394  
 Round rotor synchronous machine, saturation simulation, 207–209
- Saturation:  
 linear magnetic system, 3–4  
 nonlinear magnetic system, 9, 10  
 rotor reference frames, simulation, 203  
 simulation of, 205–209  
 symmetrical induction machines, 262
- Sector, conditioned modulation command, 487
- Self-inductance:  
 ac machines, 37, 42, 79, 83  
 arbitrary reference frame, 96  
 dc machines and drives, 384  
 electromechanical energy conversion, 34  
 linear magnetic system, 4  
 symmetrical induction machines, 220  
 between two windings, 75
- Semiconductor devices, 461, 464, 474, 544–545
- Semi-controlled bridge converters, 434–458  
 extensions, 456–458  
 problems, 458–459  
 single-phase load commutated converter, 434–445  
 basic operation of, 435–436  
 modes of operation, 442–445  
 operation with commuting inductance, 437–439  
 operation with commuting inductance and firing delay, 439–442  
 operation with firing delay, 439
- three-phase load commutated converter, 445–456
- analysis and average-value model, 449–456  
 modes of operation, 446–448
- Semi-converters, 398, 399, 400
- Separate winding excitation dc machine, 386
- Series-connected dc machines, 388–390  
 "Shoot-through," 464
- Short-circuit, *see also* Faults  
 dc machines, 379, 384  
 dynamic performance during, 180–184
- Short-circuit stator current, 289–290
- Short-circuit test, 243
- Short-circuit time constants, 279, 281, 281–282
- Short-shunt connection, 391
- Shunt-connected dc machine, 387–388, 394–396
- Silicon-controlled rectifiers (SCRs), 388
- Simulation, *see* Computer simulation:
- Sine-triangle modulation (STM):  
 induction motor drives, 536  
 permanent-magnet ac motor drives  
 current-regulated inverters, 569–571  
 voltage-source inverters, 548–550, 558–559, 561, 562–563
- three-phase bridge converters, 477–483  
 voltage regulation, 494
- Single-phase ac/dc converters, 398, 399
- Single-phase induction machines, 358–368  
 background and application of, 358–359  
 motor operating characteristics, 365–368  
 open-circuited stator phase, 364  
 phasor relationships, 362–363  
 unbalanced machine variables, arbitrary reference frame, 361–362
- unbalanced stator impedances, 363
- voltage equations, arbitrary reference frame, 359–361
- Single-phase load commutated converter, 434–445  
 basic operation of, 435–436  
 modes of operation, 442–445  
 operation with commuting inductance, 437–439  
 operation with commuting inductance and firing delay, 439–442  
 operation with firing delay, 439
- Single-phase rectifiers, 552

- Singly excited electric systems, 13, 28, 238, 240–241
- Six-step modulated permanent-magnet ac motor drive, 544–548
- Six-stepped three-phase bridge operation, 466–473
- average-value analysis, 471–472
  - closed-loop voltage and current regulation, 495–499
- delta modulation, 492
- example, find average dc current, 473
- frequency spectrum, 470
- hysteresis modulation, 489–492
- line-to-line voltages, 467–468
- line-to-neutral voltages, 469
- modulation control signals, 475
- open-loop voltage and current regulation, 493–495
- overmodulation, 481
- permanent-magnet ac motor drives. *see also* Permanent-magnet ac motor drives
- problems, 500–502
  - pulse-width modulation control, 474–477
  - sine-triangle modulation, 477–483
  - voltage and current waveforms, 470
- Slew rate limiter (SRL), 504
- Sliding average, *see* Dynamic averaging process
- Slip:
- constant slip current control, 510–517
  - defined, 237, 339
  - at maximum torque, 239–240
  - pole slipping. *see* Pole slipping
  - slip energy recovery drives, 535–538
  - steady-state torque, 239–240. *see also* Asynchronous operation
  - “twice slip-frequency,” 353
- Slip energy recovery drives, 535–538
- Slip frequency, 511, 512–515
- Slot leakage permeance, 590
- Slots:
- area, 588
  - conductor distributions, 591–592
  - locations of, 587
  - opening (distance between teeth), 588
  - rectangular approximation, 589, 592
  - volume of, 76–77
- Slot structure, 56
- Slot vs. end conductors, 60–61
- Small-displacement stability:
- induction machines, 309–312
  - overview of, 308–309
  - synchronous machines, 312–313
- Solid-state converters for dc drives, 398–400
- Source voltages, unbalanced, 346–347
- Space-phasor notation, 113–114
- Space-vector modulation, 551
- Space-vector modulation (SVM), 485–489, 495, 536
- Speed control, *see also* Rotor speed
- current-controlled dc/dc converter, 430
  - permanent-magnet ac motor drives
  - current-regulated inverters, 578–581
  - voltage-source inverters, 562–567
  - voltage-controlled dc/dc converter, 425–426
- Speed currents, 95
- Speed voltage, 92, 95
- Square wave function, 601
- Squirrel-cage rotor, 218, 238
- Stanley, H.C., 87, 232
- Start-up response, 559, 567, 580
- State sequence, determination of, 487, 488
- Stationary circuits:
- arbitrary reference frame, 359
  - magnetically coupled circuits, 2, 9, 20, 29, 31
  - phasor form, 337, 362
  - reference frame theory, 88, 90–98, 101
  - symmetrical induction machines, 222, 223, 224
- Stationary coupled coils, 9
- Stationary reference frame:
- direct field-oriented control, 521, 522
  - free acceleration characteristics, 253
  - overview of, 97–98
  - reference frame theory, 107, 109
  - three-phase bridge converters, 485, 486, 489, 495
  - unbalanced machine variables, 344
- Stator circuits:
- induction machine, 238, 346, 347, 349, 351
  - machine equations, alternative forms, 315, 320, 330
  - subscript for, 216
  - time constants, standard, 278

- Stator current control, permanent-magnet ac machines, 138–140, 577
- Stator currents:
- electric machinery design, 596
  - permanent-magnet ac machine, 138–140
  - synchronous generator operation, positive, 171–200
- Stator flux, 201, 271–272, 277, 327, 525, 532–535, 606, 608
- Stator magnetomotive force, 598
- Stators, *see also* Voltages and currents
- ac machines, 35–37, 41
  - backiron, 69, 71
  - conductors placement, 56
  - distributed winding, 54
  - eigenvalues, 310, 311
  - electromechanical energy conversion, 34, 35
  - flux. *see* Stator flux
  - leakage inductance, 74
  - MMF expression, 72
  - positive stator currents, synchronous machine. *see* Synchronous machines
  - stator windings, permanent-magnet ac machines, 122–125
  - unbalanced conditions, 339–345
  - unbalanced conditions simulation, 209–210
  - unbalanced impedances, 363
  - unbalanced stator impedances, 347–349
  - voltage equations, 77, 81
- Stator time constant, 136
- Stator voltage equations, 149–151, 163
- Stator windings, 590–593
- Steady-state conditions:
- armature voltage, 129
  - balanced steady-state phasor conditions, 99–101
  - brushless dc motor, 130
  - constant slip control drive, 514–516
  - dc machines
    - compound-connected, 391, 393
    - continuous-current operation, one-quadrant dc drive, 405
    - series-connected, 389–390
  - vs. dynamic performance and torque changes, 179
- electromechanical energy systems, 29–35
- permanent-magnet ac machine, 127–128
- permanent-magnet ac motor drives, 550
- current-regulated inverters, 568
  - voltage-source inverters, 546–548, 558
- PMAC voltage-source inverters, 555–557
- shunt-connected dc machine, 387–388
- slip energy recovery drives, 536
- symmetrical induction machines, 235–244
- synchronous machines, 160–170
- time constants in, 136
- transient torque, three-phase fault, 194–196
- unbalanced operation analysis, 337–338
- voltage equations, 102–105
- volts-per-hertz drive strategy, 505, 506
- Steady-state torque, 128, 130, 133, 182, 188, 195, 249, 250
- Steam turbine generator, 312
- dynamic performance, torque changes, 176–180
  - equal-area criterion, 198–200
  - three-phase fault at terminals, 181, 182–183
  - transient torque, actual vs. approximate, 187, 188, 190, 191, 192–193
  - transient torque, three-phase fault, 194–196, 197
- Steel catalog, 594
- Step response, induction motor DTC, 534
- Stiction, 505, 508
- Stored energy, 17, 18–19
- Surface-mounted permanent-magnet synchronous machine, 584, 585
- Switches, three-phase bridge converters, 461
- Switching frequency:
- dc machines and drives, 403, 413, 418
  - induction motor drives, 522, 526
  - permanent-magnet ac motor drives, 549
  - three-phase bridge converters, 474, 476, 477, 480, 491, 497, 499
- Switching losses, 462, 544, 546, 547, 548
- Switching state, achievable voltage vectors, 533
- Symmetrical component theory, 337–338
- Symmetrical systems:
- induction machine, 215–266. *see also* Induction machine
  - common reference frames, 232–233

- dynamic performance, three-phase fault, 260–261, 262
- dynamic performance, torque changes, 257–260
- free acceleration, in reference frames, 251–257
- free acceleration characteristics, 244–251
- overview of, 215–216
- per unit system, 233–235
- problems, 267–270
- simulation, arbitrary reference frame, 261–266
- steady-state operation, 235–244
- torque equation, arbitrary reference-frame variables, 229–232
- torque equation, machine variables, 220–222
- transformation equations, 222–224
- voltage equations, arbitrary reference-frame variables, 224–229
- voltage equations, machine variables, 216–220
- linear three-phase coupled systems, 93–94
- symmetrical analysis, induction machines, 338–339
- symmetrical component theory, 337–338
- unbalanced conditions. *see* Unbalanced operation
- Symmetrical three-wire system, 346–347, 352, 354–358
- Synchronous condensers, 165
- Synchronous machines, 142–210
- ac machines, distributed, 77–80
- ac machines, elementary, 41, 42, 43, 44
- asynchronous and unbalanced operation of, 368–375
- computer simulation, 201–210
- arbitrary reference frames, 204–205
- balanced conditions, 209
- rotor reference frames, 201–204
- saturation, 205–209
- unbalanced conditions, 209–210
- eigenvalues, 312–313
- electromagnetic torque, neglecting, 313, 316–318
- linearized machine equations, 300–302, 305–308
- operational impedances. *see* Operational impedances
- overview of, 142–143
- performance prediction, 322–325
- permanent-magnet ac machine, 122
- per unit system, 159–160
- positive stator currents, 171–200
- dynamic performance, three-phase fault, 180–184
- dynamic performance, torque changes, 175–180
- equal-area criterion, 196–200
- transient torque, actual vs. approximate, 187–193
- transient torque, three-phase fault, 194–196
- transient torque vs. rotor angle, 184–187
- prediction methods, 300
- problems, 210–214
- rotor angles, 158–159
- stator voltage equations, 149–151
- steady-state operation, 160–170
- torque equations
- machine variables, 149
- substitute variables, 157–158
- voltage equations
- machine variables, 143–149
- rotor reference frame variables, 151–156
- Synchronous reference frame:
- free acceleration characteristics, 255
- induction motor drives, 513, 519, 521, 522, 536
- overview of, 97–98, 114
- three-phase bridge converters, 493, 494–497
- variables of, 108
- Taylor's expansion, 299, 302–303
- Thomas, C.H., 201, 205
- 3/2 factor, 90
- Three-phase ac/dc converters, 398–399, 400
- Three-phase bridge converters, 460–499
- closed-loop voltage and current regulation, 495–499
- converter voltages and currents, 465
- delta modulation, 492
- hysteresis modulation, 489–492

- Three-phase bridge converters (*cont'd*)  
 modulation indices vs. state, 486  
 one phase leg, 462  
 open-loop voltage and current  
     regulation, 493–495  
 overmodulation, 481  
 overview of, 460–466  
 phase leg equivalent circuits, 463  
 problems, 500–502  
 sine-triangle modulation, 477–483  
 six-step operation, 466–473  
     average-value analysis, 471–472  
     example, find average dc current, 473  
     frequency spectrum, 470  
     line-to-line voltages, 467–468  
     line-to-neutral voltages, 469  
     modulation control signals, 475  
     pulse-width modulation  
         control, 474–477  
     voltage and current waveforms, 470  
 space-vector modulation, 485–489  
 topology of, 461
- Three-phase capacitive circuit, 94–96
- Three-phase fault:  
 asynchronous operation of synchronous  
     machines, 372  
 dynamic performance during  
     induction machine, 320–322  
     symmetrical induction machines, 260–  
         261, 262  
     synchronous machines, 180–184,  
         322–325  
 equal-area criterion, 198–200  
 transient torque, actual vs.  
     approximate, 194–196
- Three-phase induction machine, 39–43, 265,  
 349–351
- Three-phase inductive circuit, 91–94
- Three-phase load commutated  
 converter, 445–456  
 analysis and average-value  
 model, 449–456  
 modes of operation, 446–448
- Three-phase rectifiers, 552
- Three-phase stator winding, 72–73
- Three-phase synchronous machine, 153
- Three-phase winding, 218
- Three-wire system, symmetrical, 346–347,  
 352, 354–358
- Time constants:  
 derived synchronous machine, 278–282  
 standard synchronous machine, 278, 279  
 steady-state equation, 136
- Time-domain block diagrams, 394–398
- Tooth fraction, defined, 586
- Tooth tip area, 588
- Tooth tip fraction, 587
- Torque:  
 base torque, 160  
 brushless dc motor, 129–134, 136  
 constant slip current control, 513  
 dc machines  
     compound-connected, 391  
     current-controlled dc/dc converter,  
         430  
     equations, 384–386  
     series-connected, 389–390  
 design constraint, 610–612  
 direct field-oriented control, 525–526  
 dynamic performance  
     three-phase fault, 180–184  
     torque input changes, 175–180  
 electromagnetic systems, 25, 33, 35. *see also* Electromagnetic torque
- field-oriented control, induction motor  
 drives, 518, 520
- induction motor drives, direct  
 control, 532–535
- load torque, changes in, 320
- Lorenze force equation, 517
- permanent-magnet ac machine, 122–125,  
 137–138
- permanent-magnet ac motor drives,  
 572–573, 575
- positive stator currents, synchronous  
 machine, 172–173
- protection from, 371
- vs. rotor angle characteristics, 184–187
- rotor reference frame variables, 125–127
- rotor speed equations. *see* Rotor speed
- single-phase induction machines, 358
- steady-state conditions, 128
- steady-state torque, 128, 130, 133, 182,  
 188, 195, 249, 250
- substitute variables, 157–158
- symmetrical induction machines  
 arbitrary reference-frame  
 variables, 229–232

- dynamic performance, torque changes, 257–260  
machine variables, 220–222  
steady-state operation, 237–239
- synchronous machines  
equal-area criterion, 198  
machine variables, 149  
performance prediction, 322, 323  
steady-state operation, 164  
transient torque, actual vs. approximate, 187–193  
transient torque, three-phase fault, 194–196  
unbalanced rotor resistors, 357
- Torque constant, 392
- Torque-speed characteristics symmetrical induction machines, 245–250
- Transformations, *see also* Reference frame theory  
balanced set, 98–99  
defined, 264  
equations for rotor circuits, 222–224  
equations of change of variables, 88–90  
overview of, 86–88  
between reference frames, 110–111  
reference frame types, 97–98  
special cases, 111–113  
stationary circuits, 90  
stationary circuit variables and arbitrary reference frame, 90–96  
unbalanced operation analysis, 337–338
- Transformers, *see also* Magnetically coupled circuits  
linear magnetic system, 8  
permanent-magnet ac motor drives, 542  
silicon steel field strength curve, 9
- Transient performance, 368, 497, 519, 531, 557–562
- Transient torque-angle characteristics, 186, 187  
three-phase fault at terminals, 194–196
- Transmission line, 91, 93, 95, 307, 325
- Triezenberg, D.M., 207
- Turn-off time, 464
- Turn-on time, 464
- Twice slip-frequency, 353
- Two-phase induction machine:  
four-poles, 37–39  
two-poles, 35–37
- Two-pole, three-phase induction machine, 39–43, 216–220
- Two-pole, three-phase permanent-magnet ac machine, 122–125
- Two-pole, three-phase salient-pole synchronous machine, 143–145, 171–172
- Two-pole, two-phase induction machine, 35–37
- Two-pole elementary dc machine, 377–384
- Two-quadrant dc/dc converter drive, 401, 418–421, 425
- Unbalanced operation, 336–375  
asynchronous operation of synchronous machines, 368–375  
machine variables, arbitrary reference frame, 340–342  
overview of, 336–337  
phasor relationships, 342–345  
problems, 375–376  
reference-frame analysis, 339–345  
rotor conditions, induction machines, 351–354  
rotor resistors, 354–358  
single-phase induction machines, 358–368  
stator conditions, induction machines, 346–351  
stator conditions, reference-frame analysis, 339–345  
symmetrical analysis, induction machines, 338–339  
symmetrical component theory, 337–338
- Unbalanced source voltages, 346–347
- Unbalanced stator conditions simulation, 209–210
- Unbalanced stator impedances, 347–349, 363
- Undercompound machine, 391
- Variables:  
changes of, 86–88  
equations of, 88–90  
overview of. *see also* Reference frame theory  
reference frame types, 97–98  
stationary reference frame, 107, 109  
synchronously rotating reference frame, 108  
circuits, 216

- Variables (*cont'd*)  
 organizing, dependent vs.  
   independent, 593  
 $qd$  framework, 449  
 symmetrical induction machines  
   free acceleration  
     characteristics, 244–251  
   voltage equations, arbitrary reference-frame variables, 224–229  
 synchronous machines  
   flux linkage, 155–156  
   machine variables, 143–149  
   rotor reference frame variables, 151–156, 203  
   saturation simulation, 207–209  
   stator voltage equations, 150  
   torque equations, 157–158  
   torque equations, machine variables, 149  
 Vector rotator, 111, 114  
 Voltage behind reactance model, 325–333  
 Voltage-controlled dc/dc converter, 423–426  
 Voltage equations:  
   arbitrary reference frame, 96  
   balance steady-state set, 102–105  
   dc machines, 384–386  
     compound-connected, 391  
     current-controlled dc/dc converter, 428, 430  
     elementary two-pole, 378–379  
     separate winding excitation, 386  
     series-connected, 389  
     shunt-connected, 387–388, 396  
   electromagnetic torque,  
     neglecting, 313–318  
 electromechanical energy systems, 15  
 field-oriented control, induction motor drives, 519  
 linearized machine equations, 300–308  
 linear magnetic system, 6, 7  
 magnetically coupled circuits, 3  
 nonlinear magnetic system, 9  
 operational impedance, 272–273  
 permanent-magnet ac machine, 122–125  
 permanent-magnet ac motor  
   drives, 571–572  
 positive stator currents, synchronous machine, 172–173  
 reactance model, 325–332  
 rotor reference frame variables, 125–127  
 single-phase induction machines, 359–362  
 slip energy recovery drives, 536  
 space-phasor notation, 113–114  
 stator voltage equations, 77, 81  
 symmetrical induction machines  
   arbitrary reference-frame variables, 224–229  
   in machine variables, 216–220  
   simulation, arbitrary reference frame, 263–264  
   steady-state operation, 235–244  
 synchronous machines, 77–80  
   arbitrary reference frames,  
     simulation, 204–205  
   machine variables, 143–149  
   rotor reference frames,  
     simulation, 201–204  
   rotor reference frame  
     variables, 151–156  
   stator voltage equations, 149–151  
     steady-state operation, 160–170, 186  
   unbalanced source voltage, 346–347  
 Voltages and currents, converter, 465  
 Voltage-source modulation strategies:  
   current regulator, 498  
 permanent-magnet ac motor  
   drives, 542–566  
   average-value analysis, 552–555  
   description, 542–543  
   ideal source equivalence, 543–551  
   speed control study, 562–567  
   steady-state operation, 555–557  
   transient and dynamic  
     performance, 557–562  
   sine-triangle modulation, 477–483  
   six-step modulation, 474–477, 494  
   space-vector modulation, 485–489  
 Voltage vectors, achievable, 533  
 Volts-per-hertz control, induction motor drives, 504–510  
 Volume, of the winding, 76–77  
 Wave equation, 73  
 Waveform-level model, 558, 559, 562  
 Waveforms:  
   average-value analysis, one-quadrant dc drive, 410  
   continuous-current operation, one-quadrant dc drive, 403

- discontinuous-current operation, one-quadrant dc drive, 408  
ferromagnetic field analysis, 606  
four-quadrant dc/dc converter drive, 422  
hysteresis modulation, 491  
observed from different reference frames, 107–109  
one-quadrant dc/dc converter drive, 402  
permanent-magnet ac machines, 127  
permanent-magnet ac motor drives, 559  
rotor conductor placement, 218  
short-circuit stator current, 288  
sine-triangle modulation, 480, 483  
six-stepped three-phase bridge operation, 466, 470, 477  
three-phase load commutated converter, 446, 447  
two-quadrant dc/dc converter drive, 419  
Wave winding arrangement, 63  
Windings, *see also* Coils; Rotor; Stator  
ac machines, distributed, 53–83  
air-gap MMF, 67–71  
common arrangements, 62–64  
conductor distributions, 58–59, 68  
continuous description of, 58  
developed diagram, 58  
discrete/continuous conversions, 59–60  
end conductors, 60–61  
flux linkage and inductance, 73–76  
goal of, 55  
induction machine, 81–83  
overview of, 53–56  
position measurements, 54  
resistance, 76–77  
rotating MMF, 71–73  
synchronous machines, 77–80  
winding functions, 64–67  
air-gap flux density, 75  
damper windings. *see* Damper windings  
dc machines, 129, 381–383  
defined, 12  
state equations, stator and rotor windings, 202  
stator voltage equations, 77  
synchronous machines, 147, 148  
three-phase induction machine, 41  
two-phase induction machine, 36–37  
volume of, 76–77  
Wind turbine generator, 142, 143, 169, 215, 504, 536  
Wye configuration:  
line-to-neutral fault, 372  
open-circuited stator phase, 349  
reference frame theory, 111–112  
symmetrical induction machines, 217, 242  
synchronous machines, 144, 171  
three-phase bridge converters, 465  
three-phase RL circuit, 94  
Zero-sequence variables, 341, 343, 345, 346



# IEEE Press Series on Power Engineering

1. *Principles of Electric Machines with Power Electronic Applications, Second Edition*  
M. E. El-Hawary
2. *Pulse Width Modulation for Power Converters: Principles and Practice*  
D. Grahame Holmes and Thomas Lipo
3. *Analysis of Electric Machinery and Drive Systems, Second Edition*  
Paul C. Krause, Oleg Waszczuk, and Scott D. Sudhoff
4. *Risk Assessment of Power Systems: Models, Methods, and Applications*  
Wenyuan Li
5. *Optimization Principles: Practical Applications to the Operations of Markets of the Electric Power Industry*  
Narayan S. Rau
6. *Electric Economics: Regulation and Deregulation*  
Geoffrey Rothwell and Tomas Gomez
7. *Electric Power Systems: Analysis and Control*  
Fabio Saccomanno
8. *Electrical Insulation for Rotating Machines: Design, Evaluation, Aging, Testing, and Repair*  
Greg Stone, Edward A. Boulter, Ian Culbert, and Hussein Dhirani
9. *Signal Processing of Power Quality Disturbances*  
Math H. J. Bollen and Irene Y. H. Gu
10. *Instantaneous Power Theory and Applications to Power Conditioning*  
Hirofumi Akagi, Edson H. Watanabe, and Mauricio Aredes
11. *Maintaining Mission Critical Systems in a 24/7 Environment, Second Edition*  
Peter M. Curtis
12. *Elements of Tidal-Electric Engineering*  
Robert H. Clark
13. *Handbook of Large Turbo-Generator Operation Maintenance, Second Edition*  
Geoff Klempner and Isidor Kerszenbaum
14. *Introduction to Electrical Power Systems*  
Mohamed E. El-Hawary
15. *Modeling and Control of Fuel Cells: Disturbed Generation Applications*  
M. Hashem Nehrir and Caisheng Wang

16. *Power Distribution System Reliability: Practical Methods and Applications*  
Ali A. Chowdhury and Don O. Koval
17. *Introduction to FACTS Controllers: Theory, Modeling, and Applications*  
Kalyan K. Sen and Mey Ling Sen
18. *Economic Market Design and Planning for Electric Power Systems*  
James Momoh and Lamine Mili
19. *Operation and Control of Electric Energy Processing Systems*  
James Momoh and Lamine Mili
20. *Restructured Electric Power Systems: Analysis of Electricity Markets with Equilibrium Models*  
Xiao-Ping Zhang
21. *An Introduction to Wavelet Modulated Inverters*  
S.A. Saleh and M. Azizur Rahman
22. *Probabilistic Transmission System Planning*  
Wenyuan Li
23. *Control of Electric Machine Drive Systems*  
Seung-Ki Sul
24. *High Voltage and Electrical Insulation Engineering*  
Ravindra Arora and Wolfgang Mosch
25. *Practical Lighting Design with LEDs*  
Ron Lenk and Carol Lenk
26. *Electricity Power Generation: The Changing Dimensions*  
Digambar M. Tagare
27. *Electric Distribution Systems*  
Abdelhay A. Sallam and Om P. Malik
28. *Maintaining Mission Critical Systems in a 24/7 Environment, Second Edition*  
Peter M. Curtis
29. *Power Conversion and Control of Wind Energy Systems*  
Bin Wu, Yongqiang Lang, Navid Zargan, and Samir Kouro
30. *Integration of Distributed Generation in the Power System*  
Math Bollen and Fainan Hassan
31. *High Voltage Protection for Telecommunications*  
Steven W. Blume
32. *Doubly Fed Induction Machine: Modeling and Control for Wind Energy Generation*  
Gonzalo Abad, Jesús Lopéz, Miguel Rodríguez, Luis Marroyo, and Grzegorz Iwanski
33. *Smart Grid: Fundamentals of Design and Analysis*  
James Momoh

34. *Electromechanical Motion Devices, Second Edition*  
Paul Krause, Oleg Wasynczuk, and Steven Pekarek

35. *Arc Flash Hazard and Analysis and Mitigation*  
J. C. Das

36. *Electrical Energy Conversion and Transport: An Interactive Computer-Based Approach, Second Edition*  
George G. Karady and Keith E. Holbert

37. *Analysis of Electric Machinery and Drive Systems, Third Edition*  
Paul Krause, Oleg Wasynczuk, Scott Sudhoff, and Steven Pekarek